NASA/TM–1999-209579

Experimental Aerodynamic Characteristics of an Oblique Wing for the F-8 OWRA

Robert A. Kennelly, Jr., Ralph L. Carmichael, Stephen C. Smith, James M. Strong, and Ilan M. Kroo

September 1999

The NASA STI Program Office . . . in Profile

Since its founding, NASA has been dedicated to the advancement of aeronautics and space science. The NASA Scientific and Technical Information (STI) Program Office plays a key part in helping NASA maintain this important role.

The NASA STI Program Office is operated by Langley Research Center, the Lead Center for NASA's scientific and technical information. The NASA STI Program Office provides access to the NASA STI Database, the largest collection of aeronautical and space science STI in the world. The Program Office is also NASA's institutional mechanism for disseminating the results of its research and development activities. These results are published by NASA in the NASA STI Report Series, which includes the following report types:

- TECHNICAL PUBLICATION. Reports of completed research or a major significant phase of research that present the results of NASA programs and include extensive data or theoretical analysis. Includes compilations of significant scientific and technical data and information deemed to be of continuing reference value. NASA's counterpart of peer-reviewed formal professional papers but has less stringent limitations on manuscript length and extent of graphic presentations.

- TECHNICAL MEMORANDUM. Scientific and technical findings that are preliminary or of specialized interest, e.g., quick release reports, working papers, and bibliographies that contain minimal annotation. Does not contain extensive analysis.

- CONTRACTOR REPORT. Scientific and technical findings by NASA-sponsored contractors and grantees.

- CONFERENCE PUBLICATION. Collected papers from scientific and technical conferences, symposia, seminars, or other meetings sponsored or cosponsored by NASA.

- SPECIAL PUBLICATION. Scientific, technical, or historical information from NASA programs, projects, and missions, often concerned with subjects having substantial public interest.

- TECHNICAL TRANSLATION. English-language translations of foreign scientific and technical material pertinent to NASA's mission.

Specialized services that complement the STI Program Office's diverse offerings include creating custom thesauri, building customized databases, organizing and publishing research results . . . even providing videos.

For more information about the NASA STI Program Office, see the following:

- Access the NASA STI Program Home Page at *http://www.sti.nasa.gov*

- E-mail your question via the Internet to help@sti.nasa.gov

- Fax your question to the NASA Access Help Desk at (301) 621-0134

- Telephone the NASA Access Help Desk at (301) 621-0390

- Write to:
  NASA Access Help Desk
  NASA Center for AeroSpace Information
  7121 Standard Drive
  Hanover, MD 21076-1320

NASA/TM–1999-209579

Experimental Aerodynamic Characteristics of an Oblique Wing for the F-8 OWRA

Robert A. Kennelly, Jr., Ralph L. Carmichael, Stephen C. Smith, and James M. Strong
Ames Research Center, Moffett Field, California

Ilan M. Kroo
Department of Aeronautics and Astronautics, Stanford University, Stanford, California

National Aeronautics and
Space Administration

Ames Research Center
Moffett Field, California 94035-1000

September 1999

Acknowledgments

The authors wish to thank Robert E. Curry, NASA Dryden Flight Research Center, for his contributions during the planning of these tests and for assistance with the review of this report. We also thank Raul Mendoza for his help with the analysis of aileron effectiveness and preparation of some of the figures.

Available from:

NASA Center for AeroSpace Information
7121 Standard Drive
Hanover, MD 21076-1320
(301) 621-0390

National Technical Information Service
5285 Port Royal Road
Springfield, VA 22161
(703) 487-4650

Contents

Experimental Aerodynamic Characteristics of an Oblique Wing for the F-8 OWRA

ROBERT A. KENNELLY, JR., RALPH L. CARMICHAEL, STEPHEN C. SMITH, JAMES M. STRONG, AND ILAN M. KROO*

Ames Research Center

Summary

An experimental investigation was conducted during June–July 1987 in the NASA Ames 11-Foot Transonic Wind Tunnel to study the aerodynamic performance and stability and control characteristics of a 0.087-scale model of an F-8 airplane fitted with an oblique wing. This effort was part of the Oblique Wing Research Aircraft (OWRA) program performed in conjunction with Rockwell International. The Ames-designed, aspect ratio 10.47, tapered wing used specially designed supercritical airfoils with 0.14 thickness/chord ratio at the root and 0.12 at the 85% span location. The wing was tested at two different mounting heights above the fuselage.

Performance and longitudinal stability data were obtained at sweep angles of 0°, 30°, 45°, 60°, and 65° at Mach numbers ranging from 0.30 to 1.40. Reynolds number varied from 3.1×10^6 to 5.2×10^6, based on the reference chord length. Angle of attack was varied from –5° to 18°. The performance of this wing is compared with that of another oblique wing, designed by Rockwell International, which was tested as part of the same development program. Lateral-directional stability data were obtained for a limited combination of sweep angles and Mach numbers. Sideslip angle was varied from –5° to +5°.

Landing flap performance was studied, as were the effects of cruise flap deflections to achieve roll trim and tailor wing camber for various flight conditions. Roll-control authority of the flaps and ailerons was measured. A novel, deflected wing tip was evaluated for roll-control authority at high sweep angles.

The raised wing mounting position did not achieve the benefits anticipated by Rockwell International and degraded performance. Cruise flap deflection was moderately effective in achieving roll trim, but the limited deflections tested did not show any performance improvements. The maximum lift coefficient with landing flaps fell short of the value assumed during preliminary design, although the lowest Mach number tested was well above the expected landing approach Mach number. A "shark-fin" vortex generator was ineffective in modifying the stability characteristics.

The variable-sweep wing demonstrated good performance over a wide Mach number range. New, thick, high-lift transonic airfoils were specially designed for the F-8 OWRA. Both the wing dragrise characteristics and the overall envelope of the L/D (max) curves for the vehicle demonstrated that the airfoil design goals were met. Simple sweep theory and other approximations provided useful guidance for wing design and for interpreting the wind tunnel data.

Introduction

Research on the analysis and design of oblique wing aircraft was conducted at Ames Research Center in parallel with work at Rockwell International under contract to NASA during the Oblique Wing Research Aircraft (OWRA) program [Rockwell International 1984; Rockwell International 1987]. The objective of these efforts was the design of an oblique wing flight demonstrator to be based on the Vought F-8 Crusader. The results of testing the Rockwell-designed OWRA in July of 1988 were published by Kennelly et al. [1990]. This report presents the results of testing the Ames-designed wing for the OWRA in the Ames 11-Foot Transonic Wind Tunnel during June–July 1987.

A high-aspect-ratio oblique wing was mounted on a scale model of the F-8 airplane. The new wing was sized to represent a full-scale wing with 300 sq ft planform area. For comparison, the production F-8 has a 350 sq ft wing with AR 3.6 and quarter-chord sweep angle of 42°. The 0°-to-65° variable sweep

* Department of Aeronautics and Astronautics, Stanford University, Stanford, California.

wing was pivoted about an inclined axis so that the wing banked to the right as it was swept, right tip forward. Two wing pivot heights were considered for the wing; the wing could be mounted just above the fuselage or raised somewhat.

The primary test objectives were to examine the performance and stability characteristics of the Ames-designed wing and to provide timely information on the effects of the wing height and pivot axis inclination angle proposed by Rockwell. Flap and aileron effects were measured to provide a preliminary look at the performance of a 300 sq ft (full-scale) wing on the F-8 fuselage prior to final wind tunnel validation of the contractor's aerodynamic stability and control model.

Other test objectives included examination of the benefits of varying the wing camber with wing sweep for efficient roll trim and measurement of the effectiveness of deflected tips as an alternative to ailerons for roll control at high sweep angles. A simple fuselage-mounted vortex generator was also tested.

It should be noted that several other oblique wing tests using an F-8 model have been conducted at Ames Research Center. Some comparisons with results from the 300 sq ft Rockwell-designed wing [Kennelly et al. 1990] are presented here. (Indeed, some of the data for the Ames wing, the subject of this report, were actually obtained in July 1988 during this second test.) In his doctoral dissertation, Morris [1990] draws upon data presented here and in the report on the Rockwell wing, as well as upon unpublished results from tests of two smaller, 250 sq ft wings. Several other wings, including one with an 8:1 elliptical planform, were tested [Graham, Jones, and Summers 1973; Smith, Jones, and Summers 1975; Smith, Jones, and Summers 1976], but those data are not directly comparable because of differences in inlet fairing, tail incidence angle, presence of ventral fins, method of wing attachment, etc.

Nomenclature

The reference axis systems and sign conventions employed are illustrated in figure 1. Lift and drag are presented in the stability-axis system, and the other forces and moments are presented in the body-axis coordinate system.

Symbols

AR	aspect ratio, b^2/S
b	wing span
c	wing chord
c_{ref}	wing reference chord
c_{root}	wing root chord (unswept)
C_D	drag coefficient, (drag force)/qS
C_D (min)	minimum drag coefficient achieved as angle of attack is varied near zero degrees
c_d	airfoil section drag coefficient, (drag force)/qc
C_L	lift coefficient, (lift force)/qS
C_{L_α}	lift-curve slope, $d(C_L)/d\alpha$ (per deg)
C_L (max)	maximum lift coefficient as angle of attack is increased past stall
c_l	airfoil section lift coefficient, (lift force per unit span)/qc
C_l	rolling moment coefficient, (rolling moment)/qSb
C_{l_β}	lateral stability parameter, $d(C_l)/d\beta$
C_m	pitching moment coefficient, (pitching moment)/qSc_{ref} (see fig. 2 for location of moment-center)
C_{m_α}	derivative of pitching moment with angle of attack, $d(C_m)/d\alpha$ (per deg)
C_n	yawing moment coefficient, (yawing moment)/qSb
C_{n_β}	directional stability parameter, $d(C_n)/d\beta$
C_Y	side force coefficient, (side force)/qS
L/D	lift-drag ratio
L/D (max)	maximum lift-drag ratio achieved as angle of attack is varied (fixed Mach number and sweep angle)
Ma	free-stream Mach number
$Ma_\perp$	component of free-stream Mach number perpendicular to the 0.40c line of the wing
q	free-stream dynamic pressure

Re	Reynolds number
S	wing reference area
x	Cartesian coordinate along axis parallel to model centerline; positive downstream
y	Cartesian coordinate along wing span perpendicular to centerline; positive to right
z	Cartesian coordinate vertical from fuselage centerline; positive upward

Greek symbols

α	angle of attack (deg)
β	sideslip angle (deg)
Λ	sweep angle of the wing in a horizontal plane, measured between the 0.40c line of the wing and a perpendicular to the body axis; positive angles mean right tip forward (deg)

Configuration and control surface codes

HP	High pivot: wing raised above the fuselage, on bare cylindrical post
HPF	High pivot with fairing; same as HP but with addition of a fairing around the mount post
LP	Low pivot: wing mounted just above the fuselage
LA	Left aileron (+58% to +85% semispan)
LI	Left inboard flap (+9% to +34% semispan)
LO	Left outboard flap (+34% to + 58% semispan)
LT	Left tip (hinged along +85% semispan)
RA	Right aileron
RI	Right inboard flap (right-side controls same as left)
RO	Right outboard flap
RT	Right tip

Model Description

An aspect ratio 10.47 wing was mounted on a 0.087-scale model of an F-8 fighter-type aircraft as shown in figure 2. The fuselage, empennage, and ventral fins were based on the Ames–Dryden F-8C Digital-Fly-by-Wire testbed vehicle, but the model engine inlet was faired over. The wing was mounted above the fuselage on a pivot shaft, rather than submerged within it. The horizontal and vertical tail surfaces have NACA 65A006 airfoil sections and a 45° swept quarter-chord line. The horizontal tail was mounted at 0.0° incidence relative to the fuselage centerline. The oblique wing airfoils were modern, thick "supercritical" sections.

Lofting of the wing surface was linear from root to the planform break at 85% semispan. The wing leading edge was "sheared" rearward 4°. (The term "sweep" will be reserved for motion of the wing as a whole.) There were 2° of washout between wing root and the planform break, measured between the reference axes of the defining airfoil sections. (The airfoil reference axes do not correspond to the airfoil chord lines, but rather are arbitrary coordinate axes for defining the individual airfoils.) The wing was lofted with a small amount of dihedral such that the upper surface was flat along the 0.40c line. Pertinent dimensions of the wing, fuselage, and tail are given in table 1. Airfoil section OW 70-10-14, of 14% thickness, was used at the wing root and the 12% thick OW 70-10-12 from 85% semispan to the wing tip. Both airfoils were designed for efficient high lift, with c_l near 1.0 at Mach 0.70. The OW 70-10-12 was adapted from airfoil 70-10-13 [Bauer et al. 1975] using the airfoil manipulation program of Collins and Saunders [1984]. It has been evaluated in a two-dimensional wind tunnel test (unpublished). Airfoil OW 70-10-14 is new, designed using the method of Kennelly [1983] and with the aid of the analysis code described by Bauer et al. [1975]. Sketches and normalized coordinates of the airfoils are given in figure 3.

The wing pivot axis was inclined so that the wing banks as it sweeps (right tip forward and down). The wing bank angle was 10° at 65° sweep, viewed along the long axis of the fuselage. The pivot axis inclination was chosen by Rockwell International [1987] to be 7.894° forward and 5.0° to the right in order to counteract a sweep-dependent side force observed in previous tests. In addition to wing bank, this choice of axis tilt yields a wing root incidence (of the airfoil reference axis) of 0.0° at both the 0° and 65° sweep angles.

High and low mounting posts were used to simulate the two candidate wing heights. Each had a two-position locating pin that engaged one of five holes on the underside of the wing 15° apart to establish wing sweep settings. Wing sweep angles of 0°, 30°, 45°, 60°, and 65° were tested on the Ames OWRA configuration. As shown in figure 4, the high pivot had a removable fairing. Installation photographs of the model in the wind tunnel are shown in figure 5. The wing is in the low-pivot position with ailerons deflected.

The wing had flaps, ailerons, and deflectable tips that consisted of detachable segments machined at fixed deflection angles. The tips were "hinged" along a chord line at 85% semispan, and the trailing edge devices were hinged at 70% chord. The ailerons extended laterally from 58% to 85% semispan. The flaps were built in two segments to permit evaluation of the effectiveness of inboard vs. outboard location, and for testing their effect on cruise drag. The outboard flap segments covered 34% to 58% semispan, while the inboard flaps ran from 9% to 34%. The left, inboard flap could not be deployed in a positive sense, i.e., downwards, when the wing was swept. Left- and right-hand side control surfaces had the same chordwise and spanwise dimensions.

A 0.10-in.-wide strip of glass beads was placed at 10% x/c from the leading edge on the upper and lower wing and tail surfaces and in a ring 1.0 in. from the nose of the fuselage to ensure consistent boundary layer transition. The bead diameter was nominally 0.0058 in., calculated to induce transition with the wing unswept at tunnel Reynolds number 3.3×10^6/ft (corresponding to q = 700 psf, Mach 1.40) based on the criteria of Braslow and Knox [1958].

Test Facility

The test was conducted in the Ames Research Center 11-Foot Transonic Wind Tunnel, part of the Unitary Plan Wind Tunnel complex. It is a closed circuit, continuous flow facility capable of operation at stagnation pressures from 0.5 to 2.25 atm (corresponding to unit Reynolds numbers from 1.5×10^6/ft to 9.4×10^6/ft). The Mach number is variable from 0.30 to 1.45, with a flexible-wall nozzle forming an adjustable throat for supersonic flow in the test section. The slotted-wall test section permits testing through the transonic range. A 3-stage axial flow compressor powered by up to four 45,000 hp induction motors drives the wind tunnel.

Data acquisition and reduction tasks were performed by the NASA Ames Standardized Wind Tunnel System (SWTS), a distributed system consisting of signal conditioning hardware, minicomputers for device interfacing and real-time data monitoring, and a Digital Equipment Corporation VAX-11/780 computer for final computations, reporting, and archiving.

Test Procedure and Data Reduction

The model was supported on a sting through the base of the fuselage, and an internally mounted six-component strain-gauge balance selected for its high rolling moment capacity measured forces and moments. The Task "Mark XXXIV" balance capacities are 5000 in.-lb roll, 400 lb axial force, 3600 lb side force, and 7000 lb normal force (Able Corporation, Yorba Linda, CA). Using measured values of sting cavity pressure, the balance data were adjusted to a condition corresponding to free-stream static pressure on the base of the model. Due to accidental breakage of the sample tubes, many of the runs were inadvertently made without cavity pressure measurements. To allow base corrections, a look-up table based on Mach number and angle of attack was created using the results of earlier runs, which were unaffected by the mishap. These cavity pressure corrections were subsequently verified by comparison with data from other F-8 OWRA tests which used the same fuselage and sting arrangement. Several sets of repeat runs, discussed below under Error Analysis, also confirm the validity of this approach to the cavity correction.

The reference quantities used for data reduction are summarized in table 1. The moment center was located on the model centerline at the longitudinal position of the wing pivot (at $0.4c_{root}$), as shown in figure 2.

Most data were obtained at constant q = 700 psf, corresponding to Reynolds numbers between 2.5×10^6 and 3.9×10^6 based on the unswept reference chord. The initial investigation of pivot height effects consisted of a run series at each wing sweep angle over a range of Mach numbers centered on that value corresponding to $Ma_{\perp} = 0.70$, the design Mach number for the airfoils. Tunnel Mach number was held to within ±0.003 of the nominal value for each series of runs. Angle of attack ranged from –5° to +18° except where limited by model strength safety factors or balance rolling-moment capacity. Model configuration codes and angle-of-attack schedule designations are listed in table 2, and excerpts from the run schedule are presented diagrammatically in table 3. (Since some of the results to be discussed are taken from a later test of the same model, portions of that test schedule are shown in table 4.) Once the better pivot height was chosen, additional studies were made of aileron effectiveness (10° and 30° deflections), tip deflection effectiveness (5° and 10° deflections), low-speed C_L (max) for inboard, outboard, and combined flap segments (30° and 50° flap angles), and the effect of flap and aileron deflection on loiter and high-speed cruise performance. A small number of runs were devoted to looking at the interaction between sideslip (±5°) and sweep angle. Finally, a series of runs at q = 1200 psf examined Reynolds number sensitivity.

Attack and sideslip angles were measured by the angular "knuckle-sleeve" drive system of the model support strut located at the base of the sting, with corrections for balance and sting deflections based on pretest calibration. Angle of attack was further corrected for flow angularity using previously measured values ranging from 0.02°, for Mach 1.05 and above, to 0.10° for Mach numbers below 0.60.

As in previous OWRA project tests, no corrections for model blockage or buoyancy were applied. The small buoyancy does not affect the drag increment between various wing configurations tested on the same fuselage-sting arrangement. Furthermore, the balance capacity required to support the large (untrimmed) moments inherent to oblique wings precludes drag measurement with sufficient precision to make a buoyancy correction meaningful. For similar reasons, no corrections for "grit drag" or laminar run ahead of the transition strip were applied.

Results and Discussion

Effects of Wing Height

The first test runs of the Ames 300 sq ft wing were devoted to measuring forces and moments for two different wing mounting heights above the fuselage: a low pivot (denoted LP), with the wing nearly resting on the top of the fuselage, and a high pivot which had been suggested by contractor Rockwell International as a means of reducing wing/fuselage interference. This second wing position was tested both with and without a fairing around the mount post (configurations HPF and HP, respectively). The unfaired pivot was not envisioned as a practical mounting scheme, but was tested to help assess the impact of increased side area when the fairing was added. The force and moment results for these three pivot/fairing configurations are presented in figures 6(a)–(s), organized by sweep angle and Mach number. Summary plots of maximum L/D, minimum drag coefficient, lift-curve slope, and pitching moment–curve slope, grouped by sweep, are plotted vs. Mach number in figures 7(a)–(e).

The advantages of the high-pivot wing location appear to be outweighed by its disadvantages. As expected, the side force is somewhat reduced at 45° sweep for Mach = 0.95 and above. In addition, due to an unexpected trend in the data, side force is also reduced at high lift coefficients with 60° and 65° sweep at subsonic speeds. This behavior seems to be correlated with early breaks in the rolling, pitching, and yawing moments, as evident in figure 6, and thus is probably not due to any systematic reduction in wing/fuselage interference. But C_Y for the high pivot case is either larger or more variable than for the low configuration in the regime of subsonic speeds and moderate sweep, negating the advantage at supersonic conditions. In addition, the high pivot aggravates the transonic pitch-up observed at intermediate sweep angles (discussed later), and it adds a drag penalty at all flight conditions amounting to 5% to 10% in L/D. The remainder of the test was accordingly devoted to the low-pivot wing configuration.

Aerodynamic Characteristics of the Low-Pivot Configuration

The variation of the six force and moment coefficients with pitch are presented in figures 8 and 9; the data are presented with either sweep or Mach number as parameters. The effect of sweep angle at each Mach number is given in figure 8, while the effect of Mach number for the various sweep angles tested is presented in figure 9. Finally, a summary of derived aerodynamic characteristics (L/D (max), C_D (min), C_{L_α}, and C_{m_α}) is presented in figure 10 for sweep angles from 0° to 65° as a function of Mach number.

Some typical features of oblique wing aerodynamic characteristics exhibited by this model are described and interpreted briefly below. Note that these are rigid-wing results. The upward bend of a flexible wing under load can have a significant effect on the nonlinearities observed [Hopkins, Meriwether, and Pena 1973; Hopkins and Nelson 1976].

Lift (C_L)— The variation of lift with angle of attack depends on sweep angle. It is linear with a two-dimensional type stall at 0° sweep, while at 60° and 65° the lift curve is deceptively straight because the development of vortex lift at high angles of attack approximately compensates for the circulation lost when the flow separates. The 30°- and 45°-sweep configurations lie between these two cases. The "post-stall" lift curve is straight and indicates the presence of vortex lift, but with shallower slope than the low-α portion of the curve. When the contributions of the body and horizontal tail are properly accounted for, the lift curve slope in the linear regime is well modeled by handbook methods such as the USAF Datcom [United States Air Force 1978], developed for conventional, symmetrically swept wings. Experimental and theoretical results for C_{L_α} are presented in figure 11 as a function of Mach number for sweep angles of 0°, 30°, 45°, and 65°. As would be expected, the agreement deteriorates for $Ma_\perp$ greater than about 0.70, the design Mach number of the airfoils.

Drag (C_D)— The drag polars for low sweep angles are unusual only in that the variable sweep permits compressibility effects to be delayed, albeit at the cost of somewhat higher induced drag due to the reduction in aspect ratio. At higher sweep angles, additional drag emerges at moderate lift coefficients, apparently due to the onset of leading-edge flow separation. This additional drag is distinguished from compressibility drag rise because the lift coefficient corresponding to the onset of the additional drag decreases as the sweep is increased, opposite to the trend expected for classical buffet onset. Figure 12 provides comparisons of the drag polars at Ma = 0.8 for various sweep angles with two approximate drag models. The first drag model is a typical attached-flow model of C_D (min) plus induced drag, assuming an elliptic span loading. The second model is a high-α "flat-plate" model that assumes the drag grows roughly as $C_L \times \tan\alpha$. At 30° sweep, the drag departs from the attached-flow model at $C_L = 0.6$ and tracks the flat plate model. The same behavior begins at $C_L = 0.5$ for 45° sweep and at $C_L = 0.3$ for 65° sweep. These conditions all correspond to fairly high two-dimensional section lift coefficients (in relation to $Ma_\perp$) where a breakdown in lift would be expected (see also Jones and Cohen [1960], pp. 42–48). The resulting separated flow forms one or more leading-edge vortices.

With the wing sufficiently swept, the drag penalty for supersonic flight is due primarily to the F-8's fuselage, as illustrated in figure 13. The nose of the model, with its faired-over engine inlet, is not particularly slender. C_D (min) for the body and tail alone are compared with results for the wing at 30°, 45°, and 65° sweep. Unfortunately, measurements on a configuration consisting only of the fuselage and tail were made at lower Reynolds number corresponding to q = 500 psf, and with the ventral fins removed, so the increments in C_D (min) shown here are not precisely correct. Nonetheless, the wing's contribution to the drag at 65° sweep is nearly constant through Mach 1.0, about 0.0090, as it falls from 40% to 20% of the total, so the volume-dependent wave drag due to the wing must therefore be very small.

Side Force (C_Y)— A lift-dependent side force is one consequence of asymmetric wing sweep. The wing, by itself, experiences a lateral component of the lift vector, positive here, due to the wing bank angle. Model build-up studies performed during earlier oblique wing tests have shown that the vertical tail is a major contributor to the side force, in the negative direction. In addition, the effect of the wing's pressure field on the fuselage produces a negative side force since the aft-swept wing panel carries progressively more lift than the forward panel as angle of attack increases. According to Rockwell International [1987], this interference term is comparable to the wing-alone side force for 65° sweep at high angles of attack. These effects, and perhaps others, combine to form complex side-force behavior. At 30° sweep, C_Y tends to increase with α, indicating that the effect of bank angle is dominant, while at high sweep angles the side force decreases, becoming strongly negative at high angles of attack. The 45°-sweep case lies between these extremes.

Rolling Moment (C_l)— The nonlinearities in rolling and pitching moments arise from the interaction of at least two mechanisms. First is the more rapid growth of lift on the aft-swept wing panel compared with the forward panel followed by stall of the aft-swept wing, and second is the formation of a leading-edge vortex affecting primarily the forward-swept panel. Thus the initial response to increased α is faster growth of lift on the aft wing, hence positive rolling moment, followed by a reversal. For subsonic flight at intermediate sweep angles, a distinct break is observed, while at high sweeps the effect is milder but with the same ultimate tendency to roll to the left once the aft-swept wing stalls.

The rolling moment characteristics are further complicated by the fact that the wing is mounted above the moment reference axis. The wing sweep produces a side-force component of the total resultant force (sometimes thought of as “leading edge suction”) as a result of the induced flow field. For a symmetrical swept wing, the side force on the left and right sides balance, but on an oblique wing there is a net side force on the wing which produces a rolling moment if the wing is not located in the plane of the center of gravity. (See also the discussion by Morris [1990].)

Pitching Moment (C_m)— While the wing's contribution to the pitching moment follows the pattern described above for rolling moment, C_m is dominated by the effect of the horizontal tail, just as it is for conventional aircraft. The swept wing does appear to create a small pitch-up tendency at some transonic conditions, again like many airplanes with symmetrically swept wings. Note that there is little variation in pitching moment with wing sweep, and thus little change in trim or stability level, an advantage of oblique wings over other variable geometry designs.

Yawing Moment (C_n)— The nonlinear variation of yawing moment with angle of attack is somewhat Mach and sweep dependent, but the general pattern is for the zero-lift value to decrease initially and then reverse at an intermediate lift coefficient. Note the jump in the zero-lift C_n from sub- to supersonic Mach number; see figures 9(c) and (d) for sweeps 45° and 60°. (The under-swept case illustrated in figure 9(b) for Mach = 1.20, $\Lambda = 30°$ is probably too badly separated to be relevant.) As was the case with C_Y, discussed above, the vertical tail has been found to have an important effect, as does wing/body interference.

Effects of Sideslip

The low-pivot configuration (LP) was also tested at sideslip angles of ±5°. These data are presented in figure 14 for sweep angles of 0° (Mach 0.70), 30° (Mach 0.80), and 65° (Mach 0.80 and 1.20). Note that the forces and moments are plotted against angle of attack here rather than lift coefficient and that for the symmetric, 0°-sweep case, only positive sideslip was tested. The lift and drag data are presented in the stability axis system, so the drag coefficients plotted for non-zero β are actually C_{D_S} rather than C_D. C_{D_S} is the balance force resolved in the direction of the wind vector projected onto the body mid-plane (fig. 1). The effects of sideslip on lift and drag are consistent with small changes in sweep angle: increasing the sweep reduces both lift-curve slope and drag. Side force, C_Y, is dominated by the fuselage and tail; it responds linearly and symmetrically to sideslip.

The rolling and yawing moments of this asymmetrical configuration are somewhat more strongly affected by sideslip. C_{l_β}, the dihedral effect, was computed from the test data for both positive and negative β and is presented in figure 15. The zero-sweep value is negative, as expected for a high-wing configuration with small positive dihedral of the wing. For 30° sweep, C_{l_β} varies widely in the angle-of-attack region where the left-hand wing panel stalls. The behavior is more moderate at higher sweep angles, and is fairly symmetrical with respect to sideslip direction.

Yawing moment is well behaved for small angles but tends toward a β-independent positive value at high angles of attack. Directional stability parameter C_{n_β} is plotted in figure 16, where for the swept cases the derivative has been computed from the test data for both positive and negative β. C_{n_β} vanishes above about 12° angle of attack. This is evidently a feature of the F-8 fuselage and vertical tail, since it is present even for the zero-sweep case. When the wing is swept, the configuration's asymmetry does have an effect: C_{n_β} deteriorates somewhat earlier for positive β (fuselage nose to the left of the wind axis, corresponding to increased wing sweep angle). The early break in C_{n_β} for 30° sweep (at small positive α), which would appear to be the result of shock-induced stall, is dependent on the sweep-plus-sideslip angle of the wing. These effects are secondary to the behavior of the fuselage/vertical tail, and lead to only small shifts in the limiting angle of attack.

High-Speed Performance

Base configuration— Values of L/D (max) were determined by inspection of the data for each Mach number and sweep. The envelope of the L/D curves, presented in figure 17, is in reasonable agreement with the expectation, based on simple sweep theory, that the best performance will be obtained when the airfoils are operating at their design Mach number, about 0.70 for this configuration.

Thus, 30° sweep proves best at Mach 0.80 ($Ma_{\perp} = 0.69$), 45° sweep is superior at Mach 0.95 ($Ma_{\perp} = 0.67$), and 60° sweep is best at supersonic Mach numbers up to 1.40 ($Ma_{\perp} = 0.70$). The trend from Mach 1.20 to 1.40 suggests that the benefit of sweep angles above 60° will be modest. The agreement with the simple sweep theory prediction is noteworthy, since computational experiments have shown that it is a poor predictor of wing pressure distributions at high sweep angles, where the aspect ratio is so low that three-dimensional effects are significant over the whole span.

The maximum L/D results with the wing unswept show no sign of the transonic dip at Mach numbers below the airfoil's design point which has been observed for a "supercritical" wing [Jones 1977; Graham, Jones, and Summers 1973]. In that case, the subcritical performance of the wing section was compromised by the choice of a shock-free rather than a balanced, weak-shock design as in the present wing.

Lift/Drag ratio— More relevant to the flight vehicle is the relationship between L/D and Mach number for constant lift. At constant altitude, the lift coefficient varies inversely with the square of the Mach number. The aerodynamic efficiency for a representative constant value of $C_L \times Ma^2$ is plotted in figure 18, with a separate curve for each wing sweep angle. The flight condition corresponds to a 24,000 lb aircraft in level flight at 30,000 ft altitude. This figure illustrates typical aircraft performance with a variable-sweep oblique wing; note that the L/D envelope is broader than could be obtained with fixed wing sweep.

Dragrise— Because of its variable-sweep wing, the high-speed performance of the OWRA is not dependent on its dragrise characteristics at *constant* sweep. However, these results can provide some verification that the desired airfoil properties were achieved. The design conditions for the Ames sections were $c_l = 1.0$ at $Ma = 0.70$, for $Re = 20$ million. Only the 12%-thick tip section, OW 70-10-12, has been tested [Kennelly and Hicks, private communication]. The section's dragrise characteristics at constant lift coefficients from 0.60 to 1.20 are presented in figure 19. Looking ahead to figure 20, the OWRA configuration performs as well as or better than the tip airfoil with respect to dragrise. This suggests that OW 70-10-14, the more aggressive, but untested, 14%-thick center airfoil, is performing well.

A plot of zero-sweep drag coefficient vs. Mach number (fig. 20) for the Ames 300 sq ft wing at constant lift coefficient shows almost no "drag creep" for lift coefficients up to 1.0, and the break in the drag coefficient due to compressibility occurs at about Mach 0.70. Results from the Rockwell-designed 300 sq ft wing are also shown for comparison; the data from which these dragrise curves were derived was reported earlier [Kennelly et al. 1990]. The Ames wing sections were designed for higher lift coefficients and clearly perform better in this regime than does the (constant 14%-thick) section chosen by Rockwell.

High-speed cruise flaps and ailerons— Wing-alone flow calculations performed during the design phase of the OWRA project suggested that roll trim could be achieved along with improvements in chordwise pressure distribution and induced drag by using a combination of upward wing bend and variable camber. Trimming with upward bend alone led to excessively high leading edge suction peaks on the forward wing panel. Several antisymmetric flap and aileron deflections (somewhat larger than those predicted to be desirable) were tested at sweep angles of 45°, 60°, and 65°. The basic results, presented in figure 21 for 45°, 60°, and 65° sweep angles, show little or no drag reduction for any of the variations tested. While some configurations appear to offer a benefit for transonic conditions at high angle of attack, data reliability above about 10° is poor—see the Error Analysis discussion, below. Finer deflection increments and flow-aligned flap edges would probably be beneficial, but the limited set of deflected model flaps available precluded a more detailed investigation.

Antisymmetric flap deflection does provide some roll trim at 45° sweep. The combined (inboard and outboard) flaps with ±5° deflection provide about half the rolling-moment increment of the 10° aileron deflection. At higher sweep angles the flaps were ineffective; see below for further discussion of roll trim.

Flap Effectiveness and Low-Speed Performance

Clean configuration— Unswept OWRA characteristics (untrimmed) were presented in figure 6(a) for $Ma = 0.40$, and the effect of Mach number is also summarized in figure 9(a). Some additional data points and a comparison with the Rockwell wing are presented in figure 22, which shows C_L (max) vs. Mach for both wings.

Landing flaps— The 300 sq ft wing's plain flaps were deflected by 30° and 50° to study high-lift performance at Mach 0.40 with the wing unswept. The results are presented in figure 23. At 30° deflection, either inboard or outboard flap segment alone increased the maximum lift by about 4% over the clean wing C_L (max) of 1.47, while both together yielded 1.60, a 9% improvement. Slightly inferior results were obtained with the 50° deflection, achieving a C_L (max) of 1.56. The primary effect of the larger flap angle was a reduction in the angle of attack at which maximum lift occurred. C_L (max) occurs at 12° for the clean wing, 10° for the 30° setting, and 8° for the 50° setting.

At either deflection angle, the outboard flap segment increased the lift more efficiently than the inboard segment, while both segments combined (up to the stall angle) produced the lowest lift-drag ratio. In addition to causing less drag, the outboard flaps had a smaller effect on pitching moment than did the inboard segments (fig. 23).

A single run at Mach 0.30 demonstrated the variation of C_L (max) with Mach number. The chord Reynolds number for this run was 2.7×10^6. A lift coefficient of 1.68 was obtained at 10° angle of attack with the wing unswept and both inboard and outboard flap segments deflected 50°, compared with $C_L = 1.56$ for the same configuration at Mach 0.40, as shown in figure 24. These C_L (max) results are significantly lower than the values used in the OWRA design report, where C_L (max) was assumed to be greater than 2.0 [Rockwell International 1987]. Although the trend shown here of increasing C_L (max) with decreasing Mach number is encouraging, it is not clear that the assumed value can be obtained at landing conditions, where the full-scale OWRA chord Reynolds number would be about 6.3×10^6 and Mach number would be about 0.15.

Loiter— Since the promise of efficient loiter performance provided some of the motivation for the OWRA program, a series of runs was devoted to studying the effect on drag of several different inboard and outboard flap settings. Data were taken at Mach 0.40 and 0.60, with both positive and negative 5° flap angles. Figure 25 shows the results, including a close-up look at the drag polar using an expanded C_D scale. As was the case with the landing flaps, the inboard and outboard flap segments were about equally effective in augmenting lift at a given angle of attack, and the two combined had twice the effect of either one alone. At the lower Mach number, none of the loiter flap configurations were able to reduce drag over the normal operating range of lift coefficients. At Mach 0.60, the results for a combined flap setting of –5° (upward) flap angle were slightly better than the baseline wing for C_L below 0.35, showing a drag reduction of about 10 to 20 counts, and about equal to the baseline at higher C_L. Once again, the limited set of deflected model flaps precluded more detailed investigation.

Control Surface Effectiveness in Roll

Ailerons— Aileron effectiveness was measured for asymmetric deflections of 10° and 30°, in both roll directions (for the symmetric, zero-sweep case only right-hand roll deflections were evaluated). Force and moment results for these configurations are presented in figure 26, grouped by sweep angle. The low-sweep cases with 30° right-hand roll aileron deflection were run at a dynamic pressure of only 500 psf to reduce the rolling moment applied to the balance. Even at q = 500, some of these runs are incomplete because the large rolling moments generated at low angles of attack exceeded the balance capacity.

Rolling moment has been plotted against aileron deflection angle in figure 27 for three cases, with all data interpolated to a common lift coefficient of 0.30: sweep angles of 30° and 45° for Mach 0.80 and at the largest available sweep angle of 65° at Mach 1.20. The abscissa for these plots is the left aileron deflection, although both aileron surfaces are deflected. The aileron response is fairly linear and symmetrical, but aileron effectiveness evidently falls off rapidly beyond 45° sweep. If the OWRA is to be rolled using wing-mounted control surfaces, then a supplement to the ailerons that does not deteriorate with increasing sweep may be required. One such approach is discussed in the next section.

Deflected tips— While the effectiveness of conventional ailerons decreases with wing sweep, movable wing tip sections (here, hinged along the chord lines at ±85% semispan) provide superior roll control at high sweep angles. They have more surface area per unit of span and are located to take best advantage of the available moment arm. Forces and moments for the wing with individual deflections of the tips by 5° and 10° are presented in figure 28.

At a fixed lift coefficient of 0.30, rolling moment is plotted as a function of deflection angle in figure 29 for Mach 0.80 at 45° sweep and for Mach 1.20 at 65°. (Note that a downward tip deflection, labeled positive here, *decreases* the local angle of attack on a forward-swept wing panel but *increases* the angle of attack on the aft-swept panel.) The response is linear, with nearly equal effectiveness on left and right sides. Slopes derived from linear least-squares fits ranged from 0.0003 to 0.0006 per degree of tip deflection.

Comparing the results for ailerons and deflected tips for the 45° sweep, Mach 0.80 case, the summed effect of both tips together was somewhat less than the ailerons, with a rolling moment slope of roughly 0.00105/deg vs. 0.00175/deg for the ailerons. With 65° wing sweep, Mach 1.20, the relationship is reversed: the deflected tips are three times as effective in roll as the ailerons, producing about 0.00064/deg compared with 0.00020/deg for the ailerons.

The side effects of individual wing tip deflections include complex changes in yawing moment and a more easily understood shift in pitching moment. The yawing moment response was rather different for left and right surfaces: the right (upstream) tip had a much greater effect on the moment, particularly at 65° sweep. Upward deflection of the right tip produced a strong positive shift (aircraft nose right) in C_n beginning at 4° angle of attack, while similar deflection of the left tip had little effect, tracking the positive break in C_n at $\alpha = 8°$ exhibited by the clean wing. Figure 30 illustrates this left-right asymmetry for Mach 1.20 at 65° sweep.

The effect of tip deflection on pitching moment is simpler to understand: upward deflection of either left or right tip yields a positive increment which is only weakly dependent on angle of attack (see fig. 31). This may be interpreted geometrically since upward bend on the forward-swept wing panel adds to the local angle of attack, while the same bend on the rearward-swept surface reduces the angle. Either way, the effect is to shift the center of lift forward, increasing the nose-up moment.

The effects of tip deflection for transonic flow at intermediate sweep angles are not to be trusted. As for the cruise flaps, these data are corrupted by an insufficiently controlled test parameter for high angle of attack (above about 10°). This is discussed further below, in the Error Analysis section.

Pitch-up at Transonic Speeds

As often observed with conventional swept wing configurations, the wing exhibited a tendency to pitch up as the rear wing stalled. This effect, due to disproportionate loss of lift on the more highly loaded aft-swept panel, occurred at transonic Mach numbers, Ma = 0.80 to 0.95, and for moderate sweep angles, $\Lambda = 30°$ and 45°. The pitch-up occurs simultaneously with the breaks in the rolling and yawing moments. Low-pivot results for C_L vs. α, C_l, C_m, and C_n are presented in figure 32. Several special runs were made with finer angle-of-attack steps in the region of interest, and at Mach 0.85, which was not otherwise part of the test schedule. At 30° sweep, there was only a flattening of $d(C_m)/d(C_L)$ for Mach 0.70 and 0.80—no pitch-up was observed despite clear rolling moment breaks at $C_L = 0.70$ and 0.90, respectively. For higher Mach numbers neither rolling nor pitching moment showed these nonlinearities, presumably because the under-swept wing was always beyond stall onset. With 45° of sweep, the pitch-up was present from Mach = 0.85 to 0.95 and occurred at the same (Mach-dependent) values of lift coefficient as the break in the rolling moment. For supersonic speeds the pitch-up was not observed.

A pitch-up was also observed at subsonic Mach numbers with the wing swept 65°, as may be seen in figures 8(a) and (c) for Mach 0.60 and 0.80. These are not normal flight conditions except perhaps for penetration through turbulence. The mechanism is evidently different from the transonic case above, since the low speed and high sweep eliminate any aft-wing stall related to compressibility effects. The high sweep does cause excessive loading on the aft wing, though, and the effective section lift coefficient is well beyond C_L (max) of the airfoils, so this effect is probably caused by the progressive onset of ordinary stall coupled with boundary layer build-up on the downstream wing panel.

Fuselage-Mounted Vortex Generator

A small, triangular "shark-fin" vortex generator (approximately 1.375 in. high) mounted on the fuselage ahead of, and protruding slightly higher than, the wing was found to be ineffective in improving the nonlinear roll, pitch, and yaw characteristics associated with stall. The rolling moment, in particular, was unchanged except at those conditions where the pitch-up occurs. Over this narrow range, C_l became slightly more negative and the pitch-up was aggravated, suggesting that the stall on the rearward-swept left wing had been made worse. The yawing moment was also slightly affected by the vortex generator: C_n is shifted in the negative direction for the 45° sweep cases, and in the positive direction for 65° sweep. This approach to moderating undesirable characteristics associated with aft-wing stall probably deserves another look, perhaps augmented by surface flow visualization, and should include wing-mounted vortex generators.

Effects of Dynamic Pressure

Several run conditions were repeated at q = 1200 psf over a reduced range of angles limited by balance capacity constraints. Since the calculated effect of q on wing bend was small, this amounted to a study of Reynolds number sensitivity. For $\Lambda = 30°$, data were taken at Mach 0.80 and 1.20, and for $\Lambda = 65°$ at Mach 1.20 (fig. 33). Corresponding chord-based Reynolds numbers for Mach 0.80 were 3.1×10^6 (q = 700) and 5.2×10^6 (q = 1200), and 2.4×10^6 and 4.0×10^6 for Mach 1.20. The biggest differences were seen for the Mach 0.80, $\Lambda = 30°$ case ($Ma_{\perp} = 0.693$): both lift-curve slope and the force-break lift coefficient (the lift coefficient where a significant change in slope occurs) increase with Reynolds number while C_D (min) is reduced; the result was an 11% increase in L/D (max), typical of models tested at these Reynolds numbers. The other forces and moments were essentially unchanged below about $C_L = 0.80$, where the rear wing panel stalled. At 65° sweep, the data were unaffected by Reynolds number up to $C_L \approx 0.20$, except for a small reduction in C_D (min) at Mach 0.80.

Error Analysis

While no formal analysis of the accuracy or precision of these results has been performed, data from several repeat runs are presented (fig. 34). Note that these comparisons include data from Test #079-1-11 (the primary source of data for this report) and from Test #100-1-11 (conducted a year later). The data generally agree well—there was little run-to-run variation, except at very high angles of attack. All comparisons include either runs made before and after the base pressure sensor mishap (run number 28) or from both test entries, so the satisfactory drag repeatability confirms the base-pressure correction technique applied.

The poor repeatability of some transonic runs at high angle of attack has been alluded to in the discussion of cruise flaps and deflected tips, above. Among the repeat runs shown, this is evident in figure 34(c), sweep 30° at Mach 0.80; in figure 34(d), sweep 45° at Mach 0.80; and in figure 34(e), sweep 45° at Mach 1.20. We have concluded that this was not caused by model configuration errors, e.g., improperly recorded pivot height or sweep angle, and is not exclusively associated with the Test #079-1-11 data. A possible culprit is insufficient care in maintaining the grit strip intended to trip the boundary layer, coupled with a sensitivity of the configuration with respect to flow separation at high angle of attack (above about 10°). A clear lesson to be drawn from this is that future oblique wing testing will require closer attention to trip efficacy, including appropriate flow visualization to verify that transition occurs as intended, although some other cause may yet be discovered. In any event, these unreliable data lie well above the normal flight regime and do not affect the main conclusions from the test.

Concluding Remarks

The following remarks, presented in the order that the various points were discussed in the text, summarize the main conclusions of this study.

(1) As in the case of the previously reported Rockwell wing, the high pivot caused excessive drag with little reduction in wing/fuselage interference and was less stable in pitch for high angles of attack.

(2) Simple models of lift and drag based on airfoil characteristics and simple sweep theory, with extensions for separated flow, provide a useful characterization of oblique wing performance.

(3) The overall F-8 OWRA drag is rather high, but most of this is caused by the large, blunt fuselage with abruptly faired-over engine inlet.

(4) Side force and the three moments are complex functions of sweep, Mach number, and lift. The underlying flow mechanisms are similar to those observed on conventional, symmetrically swept wings, but they manifest themselves differently because of the asymmetric wing and its interactions with the fuselage.

(5) The directional stability of the F-8 OWRA with the wing swept is only slightly degraded in comparison to the zero-sweep configuration.

(6) The performance benefits of variable geometry were confirmed for sweep angles up to 60° at Mach 1.40; higher speed testing will be required to check whether higher sweeps are desirable.

(7) The thick, high-lift, supercritical airfoils designed for the Ames 300 sq ft wing appear to have achieved their design objectives. Both the wing dragrise characteristics and the performance envelope at the various sweep angles are in agreement with expectations based on simple sweep theory. No off-design penalty attributable to the use of supercritical sections was observed.

(8) Cruise and loiter flaps were found to be ineffective in reducing drag for the limited set of flap deflections tested. Asymmetrical deflection of cruise flaps can be useful for roll trim with negligible drag penalty.

(9) High lift performance with segmented plain flaps was measured. Although maximum lift was somewhat improved by flap deflection, the largest effects were an increase in drag and a shift of α for maximum lift to lower values. The maximum lift coefficient was strongly affected by Mach number.

(10) Deflected wing tips were found useful for roll control and are superior to ailerons at high sweep angles. Both deflected tips and ailerons have side effects on pitching and yawing moments.

(11) A pitch-up was observed for intermediate sweep angles at transonic Mach numbers. The pitch-up is associated with the increase in lift loading on the rear wing panel as angle of attack is increased, leading to buffet and/or stall of the rear wing panel. This pitch-up is typical of conventional swept wings except for the coupled nonlinearities in rolling and yawing moment due to the asymmetric configuration.

(12) A fuselage-mounted vortex generator positioned ahead of the center of the wing did not significantly affect the nonlinear characteristics of the oblique wing as various portions of the wing stalled.

(13) With the exception of drag, the forces and moments were not significantly affected by variation in Reynolds number. The decrease of drag with increasing Reynolds number was typical of models tested at these Reynolds numbers.

References

Bauer, Frances; Garabedian, Paul; Korn, David; and Jameson, Antony: Supercritical Wing Sections II. Springer-Verlag (Berlin), 1975.

Braslow, A. L.; and Knox, E. C.: Simplified Method for Determination of Critical Height of Distributed Roughness Particles for Boundary-Layer Transition at Mach Numbers From 0. to 5. NACA TN-4363, September 1958.

Collins, Leslie; and Saunders, David: PROFILE: Airfoil Geometry Manipulation and Display, User's Guide. NASA CR-177332, November 1984, revised February 1997.

Graham, Lawrence A.; Jones, Robert T.; and Boltz, Frederick W.: An Experimental Investigation of Three Oblique-Wing and Body Combinations at Mach Numbers Between 0.60 and 1.40. NASA TM X-62,256, April 1973.

Graham, Lawrence A.; Jones, Robert T.; and Summers, James L.: Wind Tunnel Tests of an F-8 Airplane Model Equipped with an Oblique Wing. NASA TM X-62,273, June 1973.

Harris, Charles D.: NASA Supercritical Airfoils: A Matrix of Family-Related Airfoils. NASA TP 2969, March 1990.

Hopkins, Edward J.; Meriwether, Frank D.; and Pena, Douglas F.: Experimental Aerodynamic Characteristics of Low Aspect Ratio Swept and Oblique Wings at Mach Numbers Between 0.6 and 1.4. NASA TM X-62,317, November 1973.

Hopkins, Edward J.; and Nelson, Edgar R.: Effect of Wing Bend on the Experimental Force and Moment Characteristics of an Oblique Wing. NASA TM X-3343, March 1976.

Jones, Robert T.: The Oblique Wing—Aircraft Design for Transonic and Low Supersonic Speeds. Acta Astronautica, vol. 4, 1977, pp. 99–109.

Jones, Robert T.; and Cohen, Doris: High Speed Wing Theory. Princeton University Press (Princeton, New Jersey), 1960.

Kennelly, Robert A., Jr.: Improved Method for Transonic Airfoil Design-by-Optimization. AIAA Paper 83-1864, July 1983.

Kennelly, Robert A., Jr.; Kroo, Ilan M.; Strong, James M.; and Carmichael, Ralph L.: Transonic Wind Tunnel Test of a 14% Thick Oblique Wing. NASA TM-102230, August 1990.

Morris, Stephen James: Integrated Aerodynamic and Control System Design of Oblique Wing Aircraft. Ph.D. dissertation, Stanford University, Jan. 1990.

Rockwell International: A Feasibility Design Study for an F-8 Oblique Wing Research Demonstrator: Final Report, Contract NAS-11409. Report NA-84-1135, July 1984.

Rockwell International: Oblique Wing Research Aircraft: Phase B, Preliminary Design, Contract NAS2-12229. Report NA-87-1033, April 1987, draft.

Smith, Ronald C.; Jones, Robert T.; and Summers, James L.: Transonic Wind-Tunnel Tests of an F-8 Airplane Model Equipped with 12- and 14-Percent-Thick Oblique Wings. NASA TM X-62,478, October 1975.

Smith, Ronald C.; Jones, Robert T.; and Summers, James L.: Transonic Lateral and Longitudinal Control Characteristics of an F-8 Airplane Model Equipped with an Oblique Wing. NASA TM X-73,103, March 1976.

United States Air Force: USAF Stability and Control Datcom. Air Force Flight Dynamics Laboratory (Wright-Patterson Air Force Base, Ohio), April 1978.

Table 1. F-8 OWRA model dimensions (Ames wing).

Fuselage		
Length		55.677 in.
Maximum depth (at station 11.850)		6.589 in.
Maximum width (at station 32.828 in.)		5.278 in.
Base diameter		3.750 in.
Wing		
Span		58.524 in.
Area		326.97 sq in.
Chord	Root	8.193 in.
	85% semi-span (planform break)	3.933 in.
	Tip	1.844 in.
	Reference	5.587 in.
Aspect ratio	Sweep 0°	10.47
Section (see table 2)	Root	OW 70-10-14
	85% semi-span	OW 70-10-12
Incidence	Root	0°
	85% semi-span	–2°
0.40-chord sweep		0°
Dihedral (due to straight upper surface 0.40 chord line)		0.67°
Horizontal tail		
Span		18.868 in.
Area		101.74 sq in.
Chord	Root (on centerline)	9.396 in.
	Tip	1.388 in.
Aspect ratio		3.50
Section		NACA 65A006
Incidence		0°
0.25-chord sweep		45°
Dihedral		6°
Vertical tail		
Span		12.608 in.
Area		107.85 sq in.
Chord	Root (on centerline)	13.570 in.
	Tip	3.539 in.
Aspect ratio		1.45
Section		NACA 65A006
Incidence		0°
0.25-chord sweep		45°

Table 2. Model configuration codes and angle-of-attack schedule.

Configuration codes

Config	Pivot	VG	LT	LA	LO	LI	RI	RO	RA	RT
1	LP		0	0	0	0	0	0	0	0
2	LP	on	0	0	0	0	0	0	0	0
3	HP		0	0	0	0	0	0	0	0
4	HPF		0	0	0	0	0	0	0	0
5	LP		0	10	0	0	0	0	-10	0
6	LP		0	30	0	0	0	0	-30	0
7	LP		0	-30	0	0	0	0	30	0
8	LP		0	-10	0	0	0	0	10	0
9	LP		+5	0	0	0	0	0	0	0
10	LP		0	0	0	0	0	0	0	+5
11	LP		-5	0	0	0	0	0	0	0
16	LP		0	0	0	+30	+30	0	0	0
17	LP		0	0	+30	0	0	+30	0	0
18	LP		0	0	+30	+30	+30	+30	0	0
19	LP		0	0	0	+50	+50	0	0	0
20	LP		0	0	+50	0	0	+50	0	0
21	LP		0	0	+50	+50	+50	+50	0	0
22	LP		0	-10	-5	-5	+5	+5	+10	0
23	LP		0	-10	-5	-5	+10	+10	+10	0
24	LP		0	0	-5	-5	+5	+5	0	0
26	LP		0	0	0	+5	+5	0	0	0
27	LP		0	0	+5	0	0	+5	0	0
28	LP		0	0	+5	+5	+5	+5	0	0
29	LP		0	0	0	-5	-5	0	0	0
30	LP		0	0	-5	0	0	-5	0	0
31	LP		0	0	-5	-5	-5	-5	0	0
32	LP		0	0	-5	-5	-5	-5	0	0
33	LP		0	0	-5	0	0	+5	0	0
34	LP		-10	0	0	0	0	0	0	0
35	LP		0	0	0	0	0	0	0	-10

Alpha schedules

A	-5, -4, -3, -2, -1, 0, +1, +2, +4, +6, +8, +10, +12, +14, +16, +18	
B	-4, -2, 0, +2, +4, +6, +8, +10, +12, +14, +16, +18	
C	+2, +3, +4, +5, +6	
D	+4, +5, +6, +7, +8, +9, +10	
E	-4, -2, 0, +2, +4, +6, +7, +8, +9, +10, +11, +12, +13, +14, +15, +16	(Test #100-1-11)
F	-4, -2, 0, +2, +4, +6	(Test #100-1-11)
G	-4, -2, 0, +1, +2, +3, +4, +5, +6, +8	(Test #100-1-11)

Table 3. Test #079-1-11 run conditions (excerpts).

Purpose Three candidate base configurations. Note that the M = .40 cases were run at reduced Q (about 440).

														Mach								
Sweep	**Pivot**	**LT**	**LA**	**LOF**	**LIF**	**RIF**	**ROF**	**RA**	**RT**	**Config**	**Alpha**	**Beta**	**Q**	**.40**	**.60**	**.70**	**.80**	**.90**	**.95**	**1.10**	**1.20**	**1.40**
0	LP	0	0	0	0	0	0	0	0	1	A	0	max	*12*								
0	LP	0	0	0	0	0	0	0	0	1	A	0	700		*11*	*10*	*9*					
15	LP	0	0	0	0	0	0	0	0	1	B	0	700			*248*	*251*					
30	LP	0	0	0	0	0	0	0	0	1	A	0	700			*15*	*14*	*13*	*238*		*235*	
45	LP	0	0	0	0	0	0	0	0	1	A	0	700				*20*	*19*	*18*	*17*	*16*	
60	LP	0	0	0	0	0	0	0	0	1	A	0	700						*35*	*34*	*33*	*32*
65	LP	0	0	0	0	0	0	0	0	1	A	0	700		*105*		*229*			*31*	*30*	*29*
0	HP	0	0	0	0	0	0	0	0	3	A	0	max	*54*								
0	HP	0	0	0	0	0	0	0	0	3	A	0	700		*53*	*52*	*51*					
30	HP	0	0	0	0	0	0	0	0	3	A	0	700			*50*	*49*	*48*				
30	HP	0	0	0	0	0	0	0	0	3	A	0	700				*47*	*46*	*45*	*44*	*43*	
60	HP	0	0	0	0	0	0	0	0	3	A	0	700						*42*	*41*	*40*	*39*
65	HP	0	0	0	0	0	0	0	0	3	A	0	700							*38*	*37*	*36*
0	HPF	0	0	0	0	0	0	0	0	4	A	0	max	*87*								
0	HPF	0	0	0	0	0	0	0	0	4	A	0	700		*88*	*89*	*90*					
15	HPF	0	0	0	0	0	0	0	0	4	A	0	700			*91*	*92*	*93*				
45	HPF	0	0	0	0	0	0	0	0	4	A	0	700				*98*	*97*	*96*	*95*	*94*	
60	HPF	0	0	0	0	0	0	0	0	4	A	0	700						*102*	*101*	*100*	*99*
65	HPF	0	0	0	0	0	0	0	0	4	A	0	700							*58*	*57*	*56*

Table 3. Continued.

Purpose Aileron effectiveness. For sweep = 0, only left-positive deflections were tested. Some runs which did not repeat well (against Test #100-1-11) have been dropped.

														Mach								
Sweep	**Pivot**	**LT**	**LA**	**LOF**	**LIF**	**RIF**	**ROF**	**RA**	**RT**	**Config**	**Alpha**	**Beta**	**Q**	**.40**	**.60**	**.70**	**.80**	**.90**	**.95**	**1.10**	**1.20**	**1.40**
0	LP	0	10	0	0	0	0	-10	0	5	B	0	700		*121*	*122*	*123*					
60	LP	0	10	0	0	0	0	-10	0	5	B	0	700							*111*	*110*	*109*
65	LP	0	10	0	0	0	0	-10	0	5	B	0	700							*108*	*107*	*106*

Note The first part of this group (config. 6) was run at Q = 500 to reduce the balance loads.

Sweep	**Pivot**	**LT**	**LA**	**LOF**	**LIF**	**RIF**	**ROF**	**RA**	**RT**	**Config**	**Alpha**	**Beta**	**Q**	**.40**	**.60**	**.70**	**.80**	**.90**	**.95**	**1.10**	**1.20**	**1.40**
0	LP	0	30	0	0	0	0	-30	0	6	B	0	500		*124*	*125*	*126*					
60	LP	0	-30	0	0	0	0	30	0	7	B	0	700							*144*	*143*	*142*
65	LP	0	-30	0	0	0	0	30	0	7	B	0	700							*148*	*147*	*146*
30	LP	0	-10	0	0	0	0	10	0	8	B	0	700			*159*	*158*	*157*				
45	LP	0	-10	0	0	0	0	10	0	8	B	0	700				*164*	*163*	*162*	*161*	*160*	
60	LP	0	-10	0	0	0	0	10	0	8	B	0	700							*167*	*166*	*165*
65	LP	0	-10	0	0	0	0	10	0	8	B	0	700							*170*	*169*	*168*

Table 3. Continued.

Purpose Tip deflection effectiveness.

Sweep	Pivot	LT	LA	LOF	LIF	RIF	ROF	RA	RT	Config	Alpha	Beta	Q	Mach .40	.60	.70	.80	.90	.95	1.10	1.20	1.40
45	LP	+5	0	0	0	0	0	0	0	9	B	0	700				*66*	*65*	*64*	*63*	*62*	
65	LP	+5	0	0	0	0	0	0	0	9	B	0	700							*70*	*69*	*68*
45	LP	0	0	0	0	0	0	0	+5	10	B	0	700				*78*	*77*	*76*	*75*	*74*	
65	LP	0	0	0	0	0	0	0	+5	10	B	0	700							*73*	*72*	*71*
45	LP	-5	0	0	0	0	0	0	0	11	B	0	700				*85*	*84*	*83*	*82*	*81*	
65	LP	-10	0	0	0	0	0	0	0	34	B	0	700								*264*	*263*
45	LP	0	0	0	0	0	0	0	-10	35	B	0	700				*268*				*267*	
65	LP	0	0	0	0	0	0	0	-10	35	B	0	700								*266*	*265*

Purpose Landing flap effectiveness. Mach .40 cases were run at reduced Q (about 440).

Swp	Pivot	LT	LA	LOF	LIF	RIF	ROF	RA	RT	Con	Alpha	Beta	Q	Mach .40	.60	.70	.80	.90	.95	1.10	1.20	1.40
0	LP	0	0	0	+30	+30	0	0	0	16	B	0	max	*175*								
0	LP	0	0	+30	0	0	+30	0	0	17	B	0	max	*176*								
0	LP	0	0	+30	+30	+30	+30	0	0	18	B	0	max	*177*								
0	LP	0	0	0	+50	+50	0	0	0	19	B	0	max	*174*								
0	LP	0	0	+50	0	0	+50	0	0	20	B	0	max	*173*								
0	LP	0	0	+50	+50	+50	+50	0	0	21	B	0	max	*172*								

Note The following run looked at the effect of Mach on CL-max.

Swp	Pivot	LT	LA	LOF	LIF	RIF	ROF	RA	RT	Con	Alpha	Beta	Q	Mach .30
0	LP	0	0	+50	+50	+50	+50	0	0	21	B	0	max	*171*

Table 3. Continued.

Purpose Cruise flap effectiveness (see also -10¡ / +10¡ aileron effectiveness runs, config. 8).

Sweep	Pivot	LT	LA	LOF	LIF	RIF	ROF	RA	RT	Config	Alpha	Beta	Q	.40	.60	.70	.80	.90	.95	1.10	1.20	1.40
60	LP	0	-10	-5	-5	+5	+5	+10	0	22	A	0	700						*189*	*188*	*187*	*186*
65	LP	0	-10	-5	-5	+5	+5	+10	0	22	A	0	700							*185*	*184*	*182*
45	LP	0	0	-5	-5	+5	+5	0	0	24	A	0	700				*199*	*198*	*197*	*196*	*195*	
60	LP	0	0	-5	-5	+5	+5	0	0	24	A	0	700						*203*	*202*	*201*	*200*
65	LP	0	0	-5	-5	+5	+5	0	0	24	A	0	700							*206*	*205*	*204*
65	LP	0	0	-5	-5	-5	-5	0	0	32	A	0	700								*208*	*207*
60	LP	0	0	-5	0	0	+5	0	0	33	A	0	700								*212*	*211*
65	LP	0	0	-5	0	0	+5	0	0	33	A	0	700								*210*	*209*

Purpose Loiter flap effectiveness. Maximum Q for M = .40 cases is about 440.

Sweep	Pivot	LT	LA	LOF	LIF	RIF	ROF	RA	RT	Config	Alpha	Beta	Q	.40	.60	.70	.80	.90	.95	1.10	1.20	1.40
0	LP	0	0	0	+5	+5	0	0	0	26	A	0	max	*215*								
0	LP	0	0	0	+5	+5	0	0	0	26	A	0	700		*216*							
0	LP	0	0	+5	+5	+5	+5	0	0	28	A	0	max	*213*								
0	LP	0	0	+5	+5	+5	+5	0	0	28	A	0	700		*214*							
0	LP	0	0	0	-5	-5	0	0	0	29	A	0	max	*217*								
0	LP	0	0	0	-5	-5	0	0	0	29	A	0	700		*218*							
0	LP	0	0	-5	0	0	-5	0	0	30	A	0	max	*223*								
0	LP	0	0	-5	0	0	-5	0	0	30	A	0	700		*224*							
0	LP	0	0	-5	-5	-5	-5	0	0	31	A	0	max	*221*								
0	LP	0	0	-5	-5	-5	-5	0	0	31	A	0	700		*222*							

Table 3. Continued.

Purpose Effect of sideslip.

Sweep	Pivot	LT	LA	LOF	LIF	RIF	ROF	RA	RT	Config	Alpha	Beta	Q	Mach .40	.60	.70	.80	.90	.95	1.10	1.20	1.40
0	LP	0	0	0	0	0	0	0	0	1	B	+5	700			*258*	*260*					
15	LP	0	0	0	0	0	0	0	0	1	B	-5	700			*249*	*252*					
15	LP	0	0	0	0	0	0	0	0	1	B	+5	700			*250*	*253*					
30	LP	0	0	0	0	0	0	0	0	1	B	-5	700				*246*	*242*	*239*		*236*	
30	LP	0	0	0	0	0	0	0	0	1	B	+5	700				*247*	*243*	*240*		*237*	
65	LP	0	0	0	0	0	0	0	0	1	B	-5	700				*230*				*227*	
65	LP	0	0	0	0	0	0	0	0	1	B	+5	700				*231*				*228*	

Purpose Pitch-up study. Limited range of alphas, Mach = .85 added.

Sweep	Pivot	LT	LA	LOF	LIF	RIF	ROF	RA	RT	Config	Alpha	Beta	Q	Mach .70	.80	.85	.90	.95
30	LP	0	0	0	0	0	0	0	0	1	C	0	700	*275*	*274*	*273*		
45	LP	0	0	0	0	0	0	0	0	1	D	0	700		*272*	*271*	*270*	*269*

Table 3. Concluded.

Purpose Miscellaneous.

Sweep	**Pivot**	**VG**	**LT**	**LA**	**LOF**	**LIF**	**RIF**	**ROF**	**RA**	**RT**	**Config**	**Alpha**	**Beta**	**Q**	**Mach .40**	**.60**	**.70**	**.80**	**.90**	**.95**	**1.10**	**1.20**	**1.40**
Note	Vortex generator. (Cavity pressure tubing apparently broke during run 28.)																						
45	LP	on	0	0	0	0	0	0	0	0	2	A	0	700				*25*	*24*	*23*	*22*	*21*	
65	LP	on	0	0	0	0	0	0	0	0	2	A	0	700							*28*	*27*	*26*
Note	Reynolds number sensitivity.																						
0	LP		0	0	0	0	0	0	0	0	1	B	0	1200				*255*					
30	LP		0	0	0	0	0	0	0	0	1	B	0	1200				*244*				*234*	
65	LP		0	0	0	0	0	0	0	0	1	B	0	1200				*232*				*233*	
Note	Repeat runs.																						
0	LP		0	0	0	0	0	0	0	0	1	B	0	max	*254*								
0	LP		0	0	0	0	0	0	0	0	1	B	0	700		*256*	*257*	*259*					
30	LP		0	0	0	0	0	0	0	0	1	B	0	700				*245*	*241*				
45	LP		0	0	0	0	0	0	0	0	1	B	0	700				*80*				*79*	
65	LP		0	0	0	0	0	0	0	0	1	B	0	700								*104*	
65	LP		0	0	0	0	0	0	0	0	1	B	0	700								*226*	

Table 4. Test #100-1-11 run conditions (excerpts).

Purpose Ames wing base configuration. Max. Q's for Mach .30 and .40 are about 250 and 440, respectively.

Note Repeat runs and flow angularity baseline at 0¡ and 65¡ sweep. 65¡ also permits double-checking CD correction used in test #079 . Several subsonic, high-sweep cases were added to look at the effect of sweep at constant Mach. The Mach .30, 0¡ case is also new.

														Mach									
Sweep	**Pivot**	**LT**	**LA**	**LOF**	**LIF**	**RIF**	**ROF**	**RA**	**RT**	**Config**	**Alpha**	**Beta**	**Q**	**.30**	**.40**	**.60**	**.70**	**.80**	**.90**	**.95**	**1.10**	**1.20**	**1.40**
0	LP	0	0	0	0	0	0	0	0	1	E	0	max	*16*	*17*								
0	LP	0	0	0	0	0	0	0	0	1	A	0	700			*15*	*14*						
30	LP	0	0	0	0	0	0	0	0	1	A	0	700			*133*	*132*						
45	LP	0	0	0	0	0	0	0	0	1	A	0	700			*21*	*20*	*19*				*18*	
60	LP	0	0	0	0	0	0	0	0	1	A	0	700			*137*	*136*	*135*				*134*	
65	LP	0	0	0	0	0	0	0	0	1	A	0	700			*29*	*28*	*27*	*26*	*25*	*24*	*23*	*22*

Note Ames wing, model inverted, for flow angularity measurement. The overlap at high subsonic Machs will permit a check of sweep sensitivity. Only a limited range of alphas is required.

														Mach									
Sweep	**Pivot**	**LT**	**LA**	**LOF**	**LIF**	**RIF**	**ROF**	**RA**	**RT**	**Config**	**Alpha**	**Beta**	**Q**	**.30**	**.40**	**.60**	**.70**	**.80**	**.90**	**.95**	**1.10**	**1.20**	**1.40**
0	LP	0	0	0	0	0	0	0	0	1	F	0	max	*42*	*43*								
0	LP	0	0	0	0	0	0	0	0	1	F	0	700			*41*	*40*						
65	LP	0	0	0	0	0	0	0	0	1	F	0	700			*39*	*38*	*37*	*36*	*35*	*34*	*33*	*32*

Table 4. Continued.

Purpose Ames wing base configuration, continued.

Note Repeats and some more-closely-spaced Machs for the Ames wing. Note special Mach and alpha schedules.

														Special Mach series								
Sweep	**Pivot**	**LT**	**LA**	**LOF**	**LIF**	**RIF**	**ROF**	**RA**	**RT**	**Config**	**Alpha**	**Beta**	**Q**	**.30**	**.50**	**.65**	**.68**	**.70**	**.72**	**.74**	**.76**	**.78**
0	LP	0	0	0	0	0	0	0	0	1	E	0	max	*115*								
0	LP	0	0	0	0	0	0	0	0	1	G	0	700		*114*	*113*	*112*	*111*	*110*	*109*	*108*	*107*
																.60		**.80**	**.85**			
30	LP	0	0	0	0	0	0	0	0	1	A	0	700					*233*	*232*			
65	LP	0	0	0	0	0	0	0	0	1	B	0	700			*187*						

Table 4. Continued.

Purpose Ames wing with aileron deflections. These are to replace the results from test #079, some of which had incorrect sweep labels. A few runs used Q = 500 to stay within balance limits.

																	Mach					
Sweep	**Pivot**	**LT**	**LA**	**LOF**	**LIF**	**RIF**	**ROF**	**RA**	**RT**	**Config**	**Alpha**	**Beta**	**Q**	**.30**	**.40**	**.60**	**.70**	**.80**	**.90**	**.95**	**1.10**	**1.20**	**1.40**
30	LP	0	+10	0	0	0	0	-10	0	5	B	0	700			*218*		*219*					
45	LP	0	+10	0	0	0	0	-10	0	5	B	0	700			*215*		*216*				*217*	
65	LP	0	+10	0	0	0	0	-10	0	5	B	0	700			*213*		*214*				*212*	
30	LP	0	+30	0	0	0	0	-30	0	6	B	0	500			*220*		*60*					
30	LP	0	+30	0	0	0	0	-30	0	6	B	0	700									*59*	
45	LP	0	+30	0	0	0	0	-30	0	6	B	0	700			*221*		*57*				*56*	
60	LP	0	+30	0	0	0	0	-30	0	6	B	0	700					*55*				*54*	
65	LP	0	+30	0	0	0	0	-30	0	6	B	0	700			*222*		*231*				*230*	
30	LP	0	-30	0	0	0	0	+30	0	7	B	0	500			*225*		*61*					
45	LP	0	-30	0	0	0	0	+30	0	7	B	0	700			*224*		*63*				*62*	
60	LP	0	-30	0	0	0	0	+30	0	7	B	0	700					*65*				*64*	
65	LP	0	-30	0	0	0	0	+30	0	7	B	0	700			*223*		*227*				*226*	
30	LP	0	-10	0	0	0	0	+10	0	8	B	0	700			*204*		*203*					
45	LP	0	-10	0	0	0	0	+10	0	8	B	0	700			*207*		*206*				*205*	
65	LP	0	-10	0	0	0	0	+10	0	8	B	0	700			*211*		*210*				*209*	

Table 4. Continued.

Purpose Landing flap effectiveness. Note switch to alpha schedule E, which emphasizes CL-max determination. Max. Q's are about 250 for Mach .30, and 440 for Mach .40.

Note Ames wing, adding Mach .30 to the data taken in the last test. The 50° deflections are of interest primarily because the angle at which CL-max occurs is reduced.

														Mach									
Sweep	**Pivot**	**LT**	**LA**	**LOF**	**LIF**	**RIF**	**ROF**	**RA**	**RT**	**Config**	**Alpha**	**Beta**	**Q**	**.30**	**.40**	**.60**	**.70**	**.80**	**.90**	**.95**	**1.10**	**1.20**	**1.40**
0	LP	0	0	0	+30	+30	0	0	0	16	E	0	max	*104*									
0	LP	0	0	+30	0	0	+30	0	0	17	E	0	max	*106*									
0	LP	0	0	+30	+30	+30	+30	0	0	18	E	0	max	*105*									
0	LP	0	0	0	+50	+50	0	0	0	19	E	0	max	*119*									
0	LP	0	0	+50	0	0	+50	0	0	20	E	0	max	*122*									
0	LP	0	0	+50	+50	+50	+50	0	0	21	E	0	max	*121*	*120*								

Table 4. Continued.

Purpose Vertical tail off, Ames wing. Model buildup data should shed light on side force and yawing moment.

																		Mach				
Sweep	**Pivot**	**LT**	**LA**	**LOF**	**LIF**	**RIF**	**ROF**	**RA**	**RT**	**Config**	**Alpha**	**Beta**	**Q**	**.30**	**.40**	**.60**	**.70**	**.80**	**.90**	**.95**	**1.10**	**1.20**	**1.40**
30	LP	0	0	0	0	0	0	0	0	36	B	0	700			*170*	*169*	*168*	*167*				
45	LP	0	0	0	0	0	0	0	0	36	B	0	700			*153*		*150*	*149*	*148*	*147*	*144*	
60	LP	0	0	0	0	0	0	0	0	36	B	0	700			*176*		*175*		*174*	*173*	*172*	*171*
65	LP	0	0	0	0	0	0	0	0	36	B	0	700			*164*		*161*			*160*	*157*	*156*
Note	Beta sweeps with vertical tail off.																						
45	LP	0	0	0	0	0	0	0	0	36	B	-5	700			*155*		*152*				*146*	
45	LP	0	0	0	0	0	0	0	0	36	B	+5	700			*154*		*151*				*145*	
65	LP	0	0	0	0	0	0	0	0	36	B	-5	700			*166*		*163*				*159*	
65	LP	0	0	0	0	0	0	0	0	36	B	+5	700			*165*		*162*				*158*	

Purpose Effect of beta, repeat Ames wing data from test #079 which used the wrong sweep and add subsonic Mach condition.

																		Mach				
Sweep	**Pivot**	**LT**	**LA**	**LOF**	**LIF**	**RIF**	**ROF**	**RA**	**RT**	**Config**	**Alpha**	**Beta**	**Q**	**.30**	**.40**	**.60**	**.70**	**.80**	**.90**	**.95**	**1.10**	**1.20**	**1.40**
45	LP	0	0	0	0	0	0	0	0	1	B	-5	700			*142*		*141*				*138*	
45	LP	0	0	0	0	0	0	0	0	1	B	+5	700			*143*		*140*				*139*	
65	LP	0	0	0	0	0	0	0	0	1	B	-5	700			*189*							
65	LP	0	0	0	0	0	0	0	0	1	B	+5	700			*188*							

Table 4. Continued.

Purpose Vortillons on aft-swept panel of Ames wing. Check for lessening of pitch-up in 45°, Mach 0.90 region.

														Mach										
Sweep	**Pivot**	**LT**	**LA**	**LOF**	**LIF**	**RIF**	**ROF**	**RA**	**RT**	**Config**	**Alpha**	**Beta**	**Q**	**.30**	**.40**	**.60**	**.70**	**.80**	**.90**	**.95**	**1.10**	**1.20**	**1.40**
45	LP	0	0	0	0	0	0	0	0	50	B	0	700			*242*		*241*	*240*	*239*	*238*	*237*	

Purpose Vortex generator, Ames wing. Fuselage mounted, overlapping wing LE (glued in place, so wing sweep is fixed).

														Mach									
Sweep	**Pivot**	**LT**	**LA**	**LOF**	**LIF**	**RIF**	**ROF**	**RA**	**RT**	**Config**	**Alpha**	**Beta**	**Q**	**.30**	**.40**	**.60**	**.70**	**.80**	**.90**	**.95**	**1.10**	**1.20**	**1.40**
65	LP	0	0	0	0	0	0	0	0	2	B	0	700			*244*							

Table 4. Continued.

Purpose Flow visualization using oil flow.

Note Ames wing, coated evenly with oil behind the transition strip.

																			Mach				
Sweep	**Pivot**	**LT**	**LA**	**LOF**	**LIF**	**RIF**	**ROF**	**RA**	**RT**	**Config**	**Alpha**	**Beta**	**Q**	**.30**	**.40**	**.60**	**.70**	**.80**	**.90**	**.95**	**1.10**	**1.20**	**1.40**
30	LP	0	0	0	0	0	0	0	0	1	10°	0	700				*run 248, seq*	*:1*					
30	LP	0	0	0	0	0	0	0	0	1	10°	0	700					*:2*					
30	LP	0	0	0	0	0	0	0	0	1	2°	0	700					*:3*					
30	LP	0	0	0	0	0	0	0	0	1	2°	0	700					*:4*					
30	LP	0	0	0	0	0	0	0	0	1	2°	0	700					*:5*					
30	LP	0	0	0	0	0	0	0	0	1	0°	0	700					*:6*					
30	LP	0	0	0	0	0	0	0	0	1	10°	0	700					*:7*					
45	LP	0	0	0	0	0	0	0	0	1	4°	0	700				*run 249, seq*	*:1*					
45	LP	0	0	0	0	0	0	0	0	1	4°	0	700					*:2*					
45	LP	0	0	0	0	0	0	0	0	1	4°	0	700					*:3*					
45	LP	0	0	0	0	0	0	0	0	1	2°	0	700				*run 250, seq*	*:1*					
45	LP	0	0	0	0	0	0	0	0	1	2°	0	700					*:2*					
45	LP	0	0	0	0	0	0	0	0	1	2°	0	700					*:3*					
45	LP	0	0	0	0	0	0	0	0	1	2°	0	700					*:4*					

Table 4. Concluded.

Purpose Flow visualization using oil flow, continued.

Note Vortex generator. Single row of oil dots on wing upper surface behind the transition strip.

														Mach									
Sweep	**Pivot**	**LT**	**LA**	**LOF**	**LIF**	**RIF**	**ROF**	**RA**	**RT**	**Config**	**Alpha**	**Beta**	**Q**	**.30**	**.40**	**.60**	**.70**	**.80**	**.90**	**.95**	**1.10**	**1.20**	**1.40**
65	LP	0	0	0	0	0	0	0	0	2	10°	0	700				*run 245, seq*	*:1*					
65	LP	0	0	0	0	0	0	0	0	2	10°	0	700					*:2*					
65	LP	0	0	0	0	0	0	0	0	2	2°	0	700					*:3*					
65	LP	0	0	0	0	0	0	0	0	2	2°	0	700					*:4*					

Note Vortex generator, three rows of oil dots.

65	LP	0	0	0	0	0	0	0	0	2	10°	0	700				*run 246, seq*	*:1*					
65	LP	0	0	0	0	0	0	0	0	2	10°	0	700					*:2*					
65	LP	0	0	0	0	0	0	0	0	2	2°	0	700					*:3*					
65	LP	0	0	0	0	0	0	0	0	2	2°	0	700					*:4*					

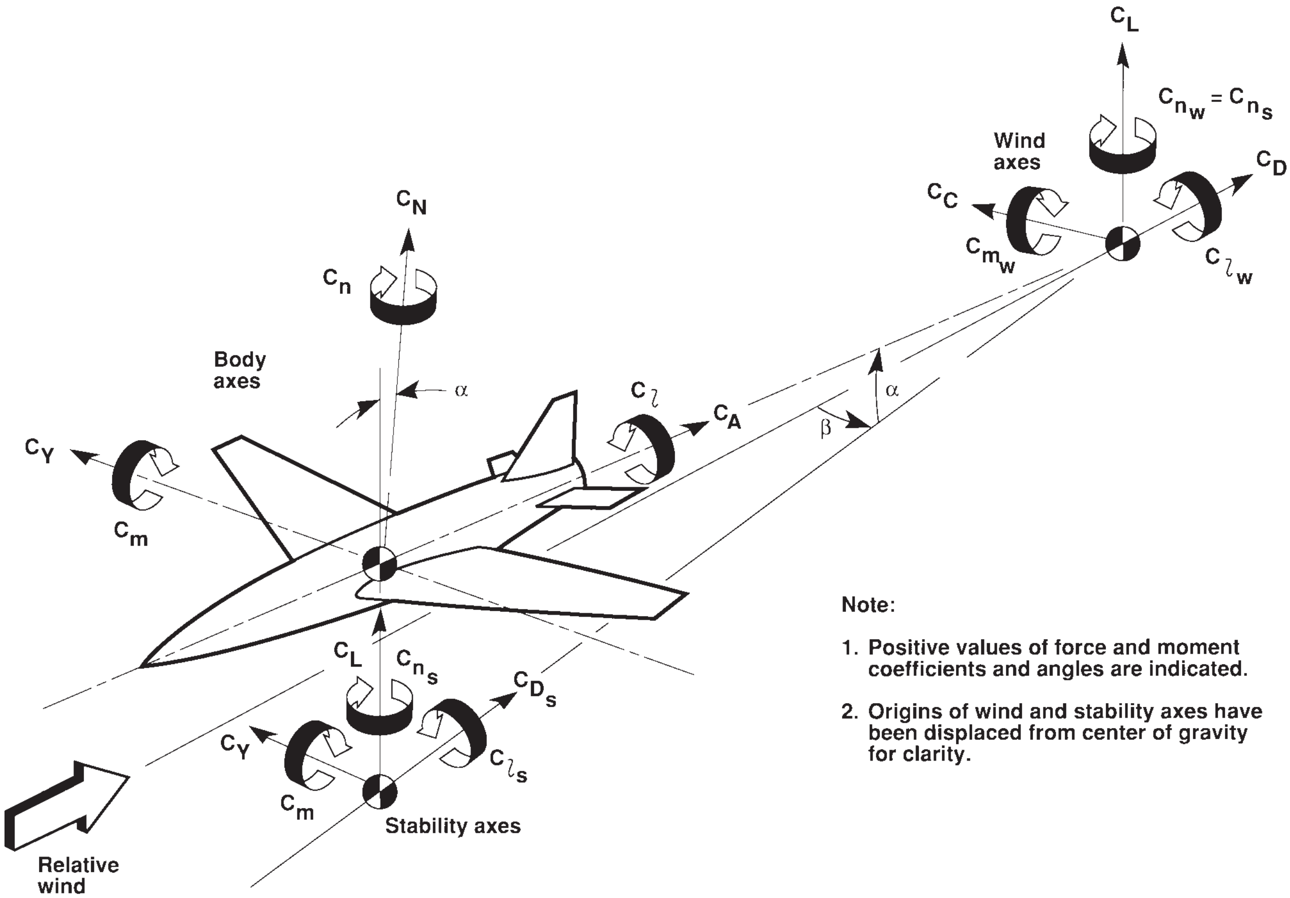

Figure 1. Reference axis systems.

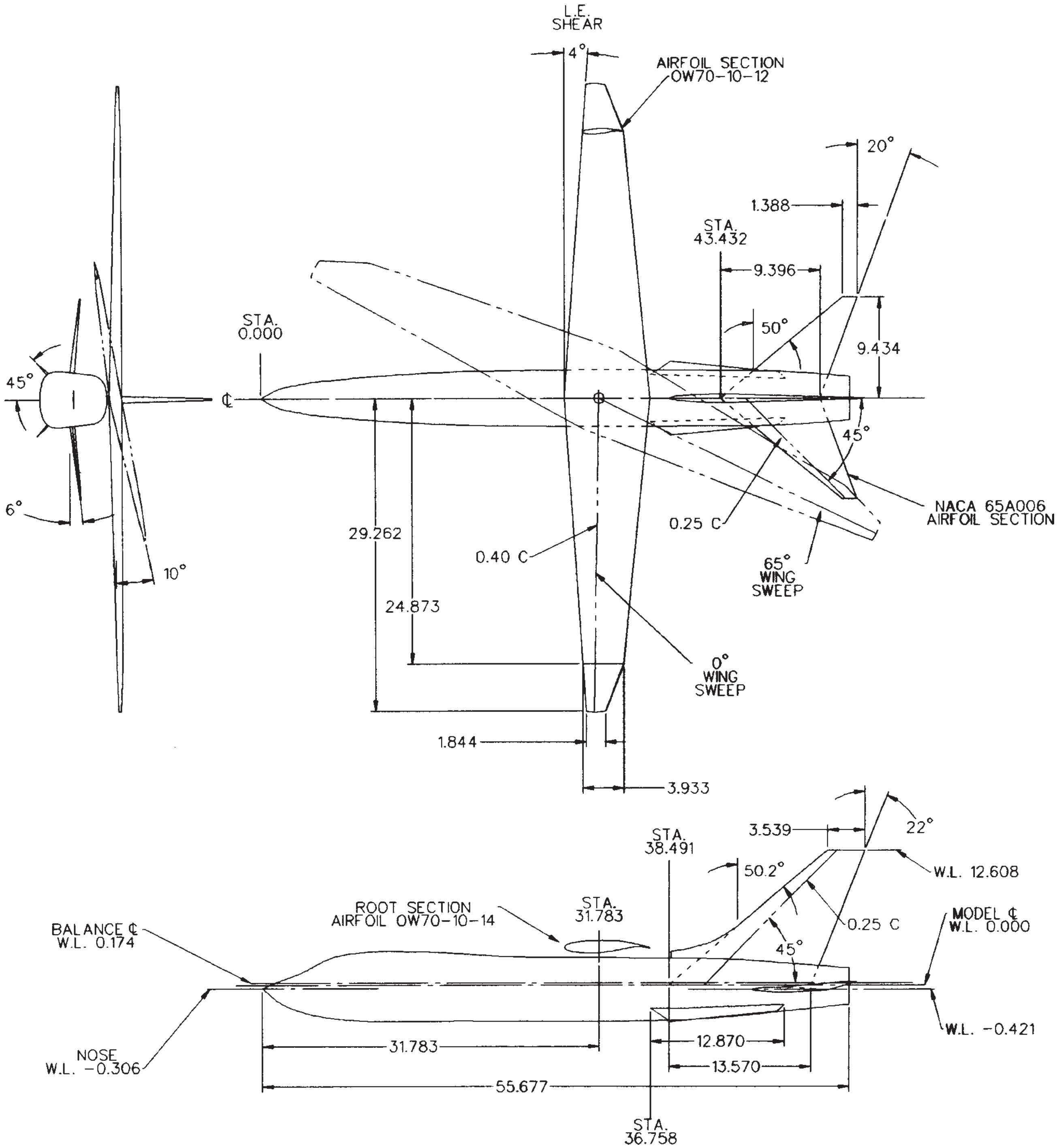

Figure 2. F-8 OWRA model, showing coordinate origin and moment reference center.

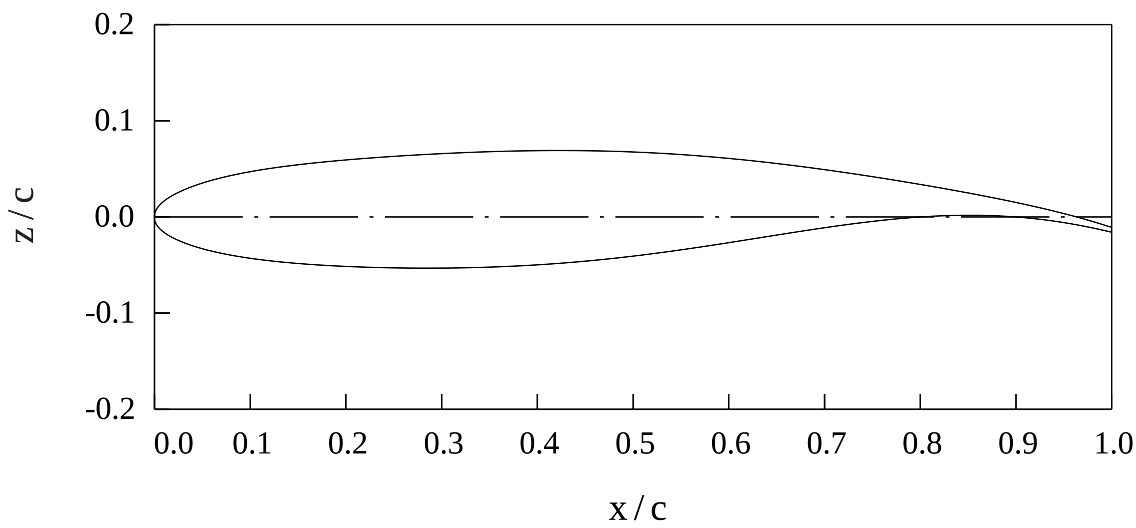

x/c	z/c upper	z/c lower	camber	thickness
0.000000	0.000000	0.000000	0.000000	0.000000
0.000200	0.002799	-0.002789	0.000005	0.005588
0.000500	0.004203	-0.004179	0.000012	0.008382
0.001000	0.005730	-0.005682	0.000024	0.011412
0.001500	0.006881	-0.006809	0.000036	0.013690
0.002000	0.007841	-0.007745	0.000048	0.015586
0.005000	0.011951	-0.011712	0.000120	0.023663
0.010000	0.016542	-0.016067	0.000238	0.032609
0.015000	0.020048	-0.019344	0.000352	0.039392
0.020000	0.022986	-0.022056	0.000465	0.045042
0.030000	0.027843	-0.026477	0.000683	0.054320
0.040000	0.031831	-0.030044	0.000893	0.061875
0.050000	0.035226	-0.033034	0.001096	0.068260
0.060000	0.038179	-0.035594	0.001293	0.073773
0.080000	0.043101	-0.039756	0.001673	0.082857
0.100000	0.047061	-0.042982	0.002040	0.090043
0.120000	0.050324	-0.045524	0.002400	0.095848
0.140000	0.053070	-0.047544	0.002763	0.100614
0.160000	0.055421	-0.049155	0.003133	0.104576
0.180000	0.057465	-0.050435	0.003515	0.107900
0.200000	0.059270	-0.051438	0.003916	0.110708
0.220000	0.060880	-0.052200	0.004340	0.113080
0.240000	0.062326	-0.052747	0.004790	0.115073
0.260000	0.063629	-0.053090	0.005270	0.116719
0.280000	0.064796	-0.053237	0.005780	0.118033

Figure 3(a). Ames oblique wing airfoil OW 70-10-12.

x/c	z/c upper	z/c lower	camber	thickness
0.300000	0.065838	-0.053188	0.006325	0.119026
0.320000	0.066746	-0.052937	0.006905	0.119683
0.340000	0.067519	-0.052481	0.007519	0.120000
0.360000	0.068145	-0.051812	0.008167	0.119957
0.380000	0.068616	-0.050921	0.008848	0.119537
0.400000	0.068918	-0.049803	0.009558	0.118721
0.420000	0.069044	-0.048454	0.010295	0.117498
0.440000	0.068979	-0.046869	0.011055	0.115848
0.460000	0.068713	-0.045052	0.011831	0.113765
0.480000	0.068241	-0.043006	0.012618	0.111247
0.500000	0.067554	-0.040741	0.013407	0.108295
0.520000	0.066648	-0.038267	0.014191	0.104915
0.540000	0.065525	-0.035607	0.014959	0.101132
0.560000	0.064183	-0.032778	0.015703	0.096961
0.580000	0.062624	-0.029812	0.016406	0.092436
0.600000	0.060857	-0.026738	0.017060	0.087595
0.620000	0.058887	-0.023594	0.017647	0.082481
0.640000	0.056724	-0.020421	0.018152	0.077145
0.660000	0.054379	-0.017264	0.018558	0.071643
0.680000	0.051866	-0.014173	0.018847	0.066039
0.700000	0.049193	-0.011198	0.018998	0.060391
0.720000	0.046374	-0.008394	0.018990	0.054768
0.740000	0.043421	-0.005819	0.018801	0.049240
0.760000	0.040341	-0.003528	0.018407	0.043869
0.780000	0.037139	-0.001578	0.017781	0.038717
0.800000	0.033818	-0.000027	0.016896	0.033845
0.820000	0.030374	0.001071	0.015723	0.029303
0.840000	0.026798	0.001663	0.014231	0.025135
0.860000	0.023075	0.001703	0.012389	0.021372
0.880000	0.019174	0.001149	0.010162	0.018025
0.900000	0.015061	-0.000032	0.007515	0.015093
0.920000	0.010688	-0.001869	0.004410	0.012557
0.940000	0.005991	-0.004376	0.000808	0.010367
0.960000	0.000893	-0.007560	-0.003334	0.008453
0.970000	-0.001835	-0.009402	-0.005619	0.007567
0.980000	-0.004698	-0.011410	-0.008054	0.006712
0.990000	-0.007716	-0.013577	-0.010647	0.005861
0.995000	-0.009286	-0.014720	-0.012003	0.005434
1.000000	-0.010901	-0.015901	-0.013401	0.005000

Figure 3(a), concluded. Ames oblique wing airfoil OW 70-10-12.

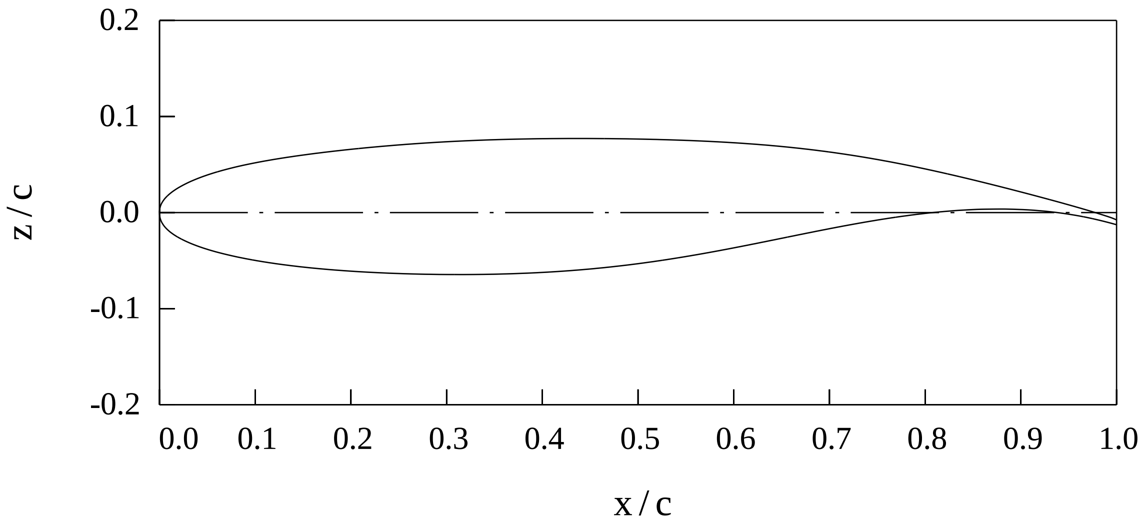

x/c	z/c upper	z/c lower	camber	thickness
0.000000	0.000000	0.000000	0.000000	0.000000
0.000200	0.003323	-0.003447	-0.000062	0.006770
0.000500	0.004974	-0.005160	-0.000093	0.010134
0.001000	0.006756	-0.007000	-0.000122	0.013756
0.001500	0.008086	-0.008370	-0.000142	0.016456
0.002000	0.009190	-0.009501	-0.000156	0.018691
0.005000	0.013847	-0.014217	-0.000185	0.028064
0.010000	0.018948	-0.019270	-0.000161	0.038218
0.015000	0.022791	-0.022998	-0.000104	0.045789
0.020000	0.025982	-0.026046	-0.000032	0.052028
0.030000	0.031224	-0.030973	0.000125	0.062197
0.040000	0.035498	-0.034933	0.000283	0.070431
0.050000	0.039123	-0.038268	0.000427	0.077391
0.060000	0.042271	-0.041147	0.000562	0.083418
0.080000	0.047525	-0.045931	0.000797	0.093456
0.100000	0.051792	-0.049788	0.001002	0.101580
0.120000	0.055375	-0.052953	0.001211	0.108328
0.140000	0.058471	-0.055572	0.001450	0.114043
0.160000	0.061200	-0.057740	0.001730	0.118940
0.180000	0.063640	-0.059526	0.002057	0.123166
0.200000	0.065837	-0.060986	0.002426	0.126823
0.220000	0.067816	-0.062160	0.002828	0.129976
0.240000	0.069589	-0.063077	0.003256	0.132666
0.260000	0.071158	-0.063759	0.003700	0.134917
0.280000	0.072530	-0.064220	0.004155	0.136750

Figure 3(b). Ames oblique wing airfoil OW 70-10-14.

x/c	z/c upper	z/c lower	camber	thickness
0.300000	0.073706	-0.064467	0.004620	0.138173
0.320000	0.074692	-0.064498	0.005097	0.139190
0.340000	0.075489	-0.064308	0.005591	0.139797
0.360000	0.076114	-0.063886	0.006114	0.140000
0.380000	0.076576	-0.063217	0.006680	0.139793
0.400000	0.076888	-0.062286	0.007301	0.139174
0.420000	0.077060	-0.061074	0.007993	0.138134
0.440000	0.077105	-0.059571	0.008767	0.136676
0.460000	0.077027	-0.057757	0.009635	0.134784
0.480000	0.076830	-0.055631	0.010600	0.132461
0.500000	0.076513	-0.053189	0.011662	0.129702
0.520000	0.076068	-0.050437	0.012816	0.126505
0.540000	0.075480	-0.047389	0.014046	0.122869
0.560000	0.074736	-0.044067	0.015335	0.118803
0.580000	0.073810	-0.040506	0.016652	0.114316
0.600000	0.072679	-0.036742	0.017969	0.109421
0.620000	0.071313	-0.032825	0.019244	0.104138
0.640000	0.069690	-0.028808	0.020441	0.098498
0.660000	0.067782	-0.024754	0.021514	0.092536
0.680000	0.065566	-0.020726	0.022420	0.086292
0.700000	0.063030	-0.016790	0.023120	0.079820
0.720000	0.060160	-0.013018	0.023571	0.073178
0.740000	0.056955	-0.009474	0.023741	0.066429
0.760000	0.053420	-0.006224	0.023598	0.059644
0.780000	0.049571	-0.003333	0.023119	0.052904
0.800000	0.045433	-0.000861	0.022286	0.046294
0.820000	0.041030	0.001129	0.021080	0.039901
0.840000	0.036399	0.002590	0.019495	0.033809
0.860000	0.031574	0.003455	0.017515	0.028119
0.880000	0.026586	0.003671	0.015129	0.022915
0.900000	0.021459	0.003174	0.012317	0.018285
0.920000	0.016202	0.001890	0.009046	0.014312
0.940000	0.010799	-0.000258	0.005271	0.011057
0.960000	0.005197	-0.003357	0.000920	0.008554
0.970000	0.002290	-0.005292	-0.001501	0.007582
0.980000	-0.000721	-0.007494	-0.004108	0.006773
0.990000	-0.003881	-0.009962	-0.006922	0.006081
0.995000	-0.005565	-0.011285	-0.008425	0.005720
1.000000	-0.007654	-0.012654	-0.010154	0.005000

Figure 3(b), concluded. Ames oblique wing airfoil OW 70-10-14.

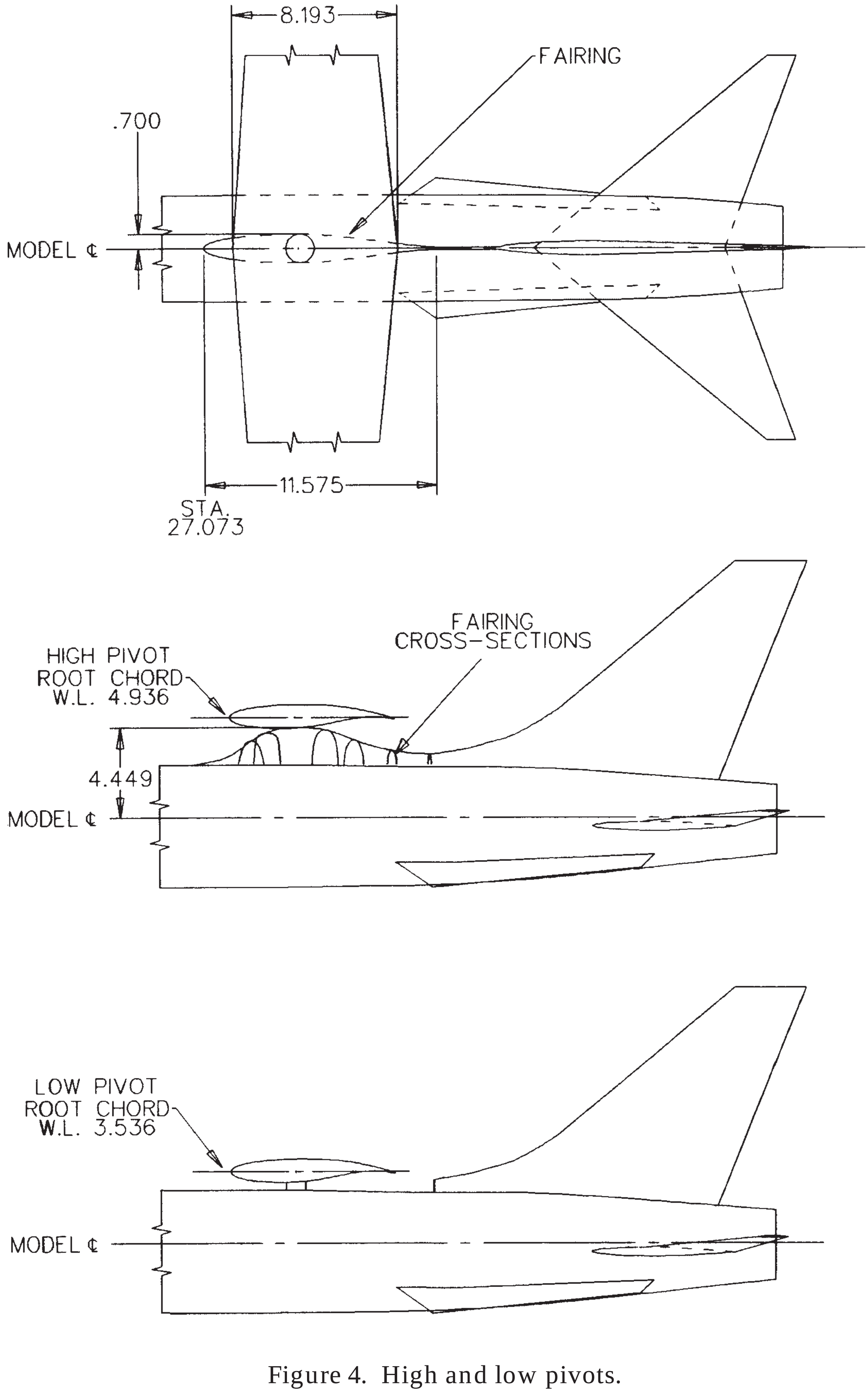

Figure 4. High and low pivots.

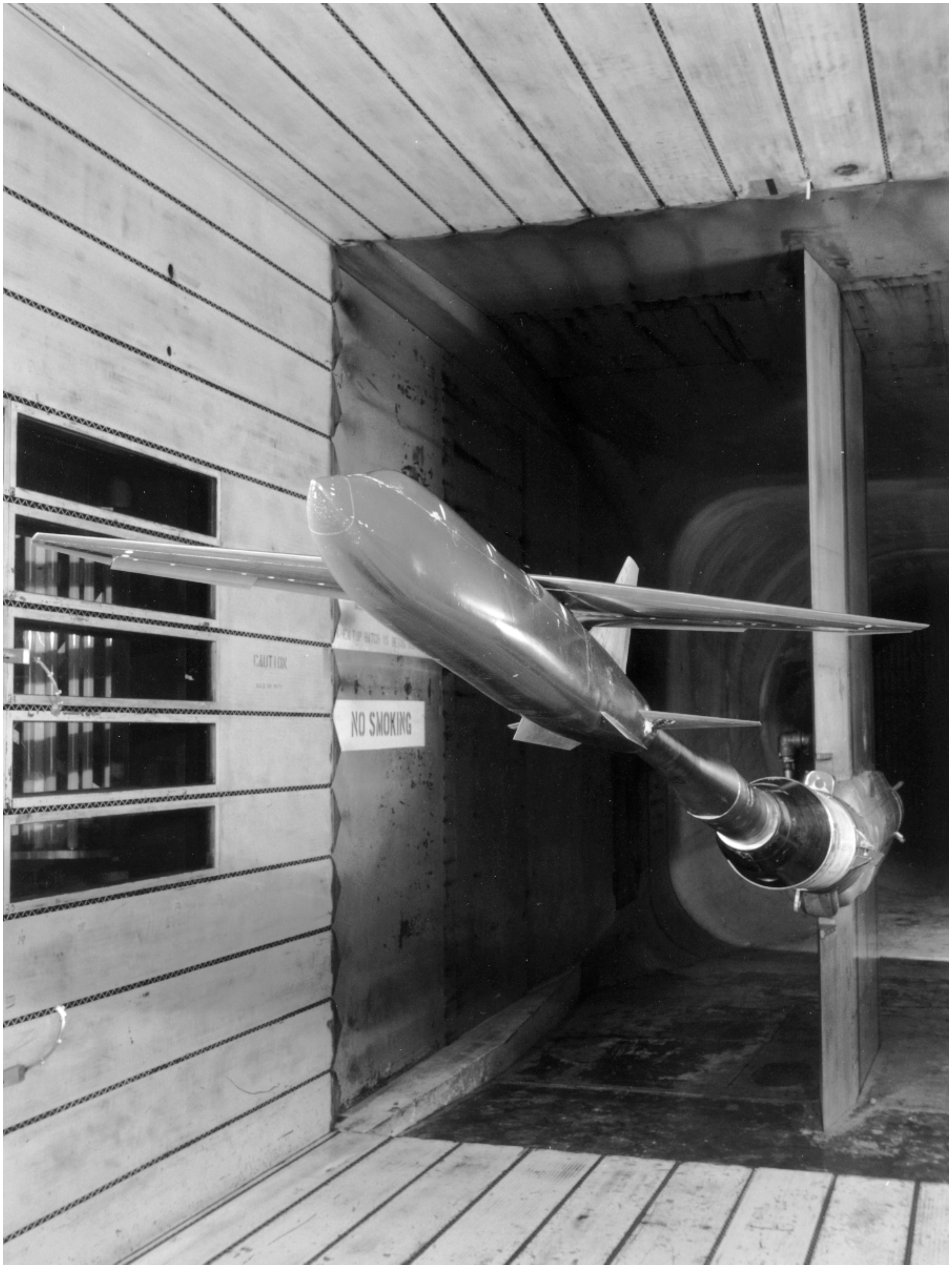

Figure 5(a). Installation photograph of the F-8 OWRA model with Ames 300 sq ft wing.

Figure 5(b). Installation photograph of the F-8 OWRA model with Ames 300 sq ft wing.

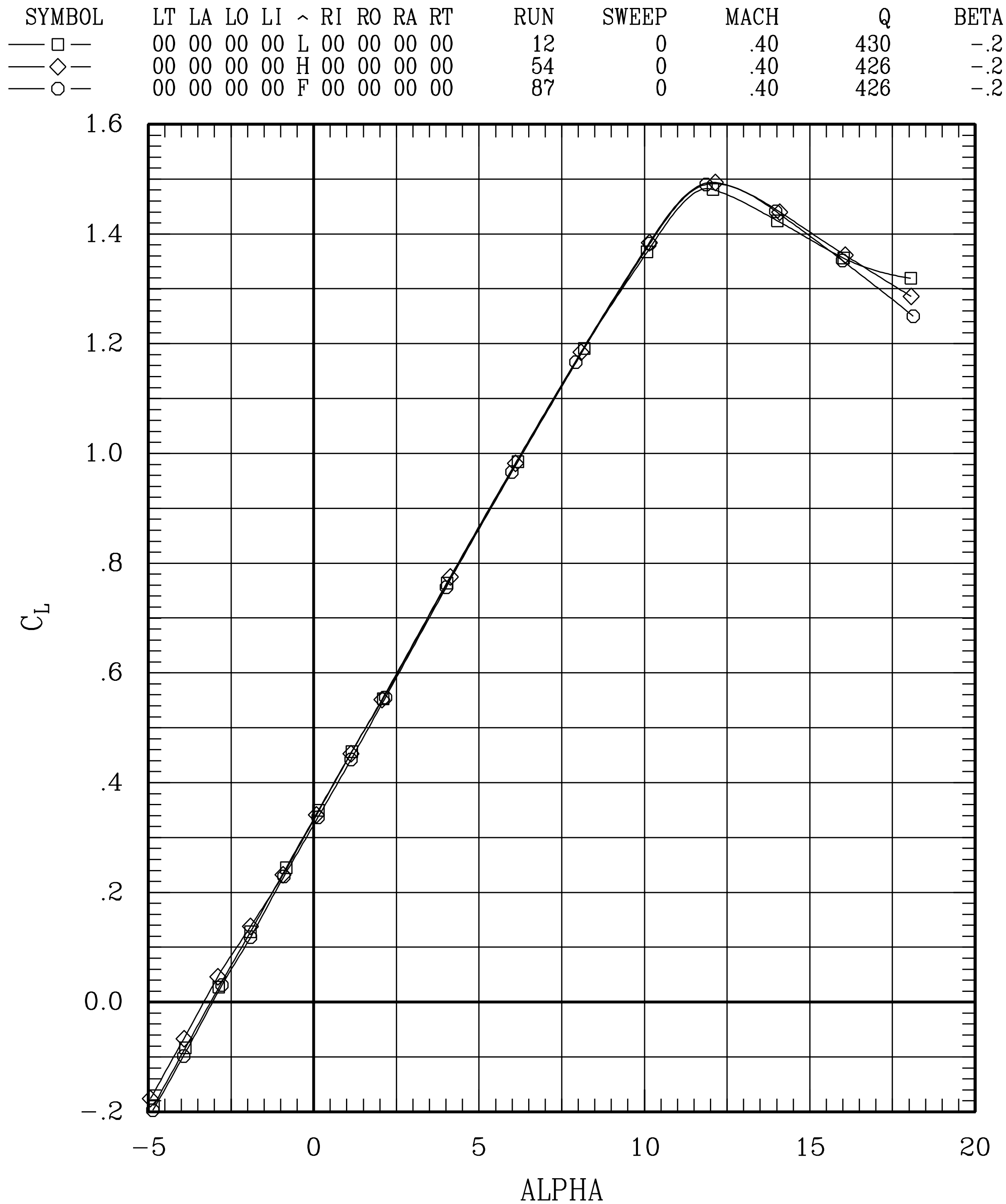

Figure 6(a). Effect of pivot height and fairing for sweep = 0 deg, Mach = 0.40.

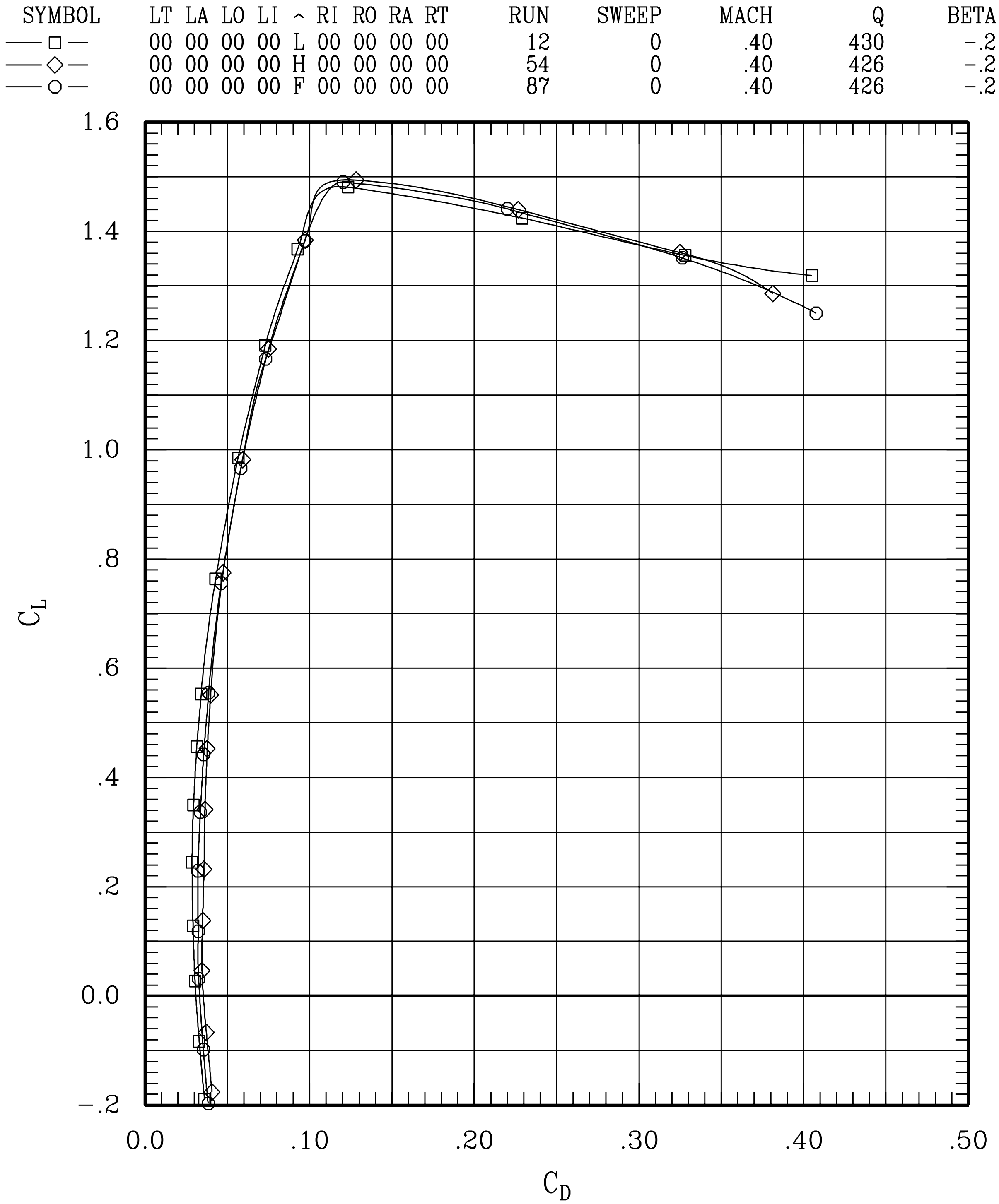

Figure 6(a). Effect of pivot height and fairing for sweep = 0 deg, Mach = 0.40.

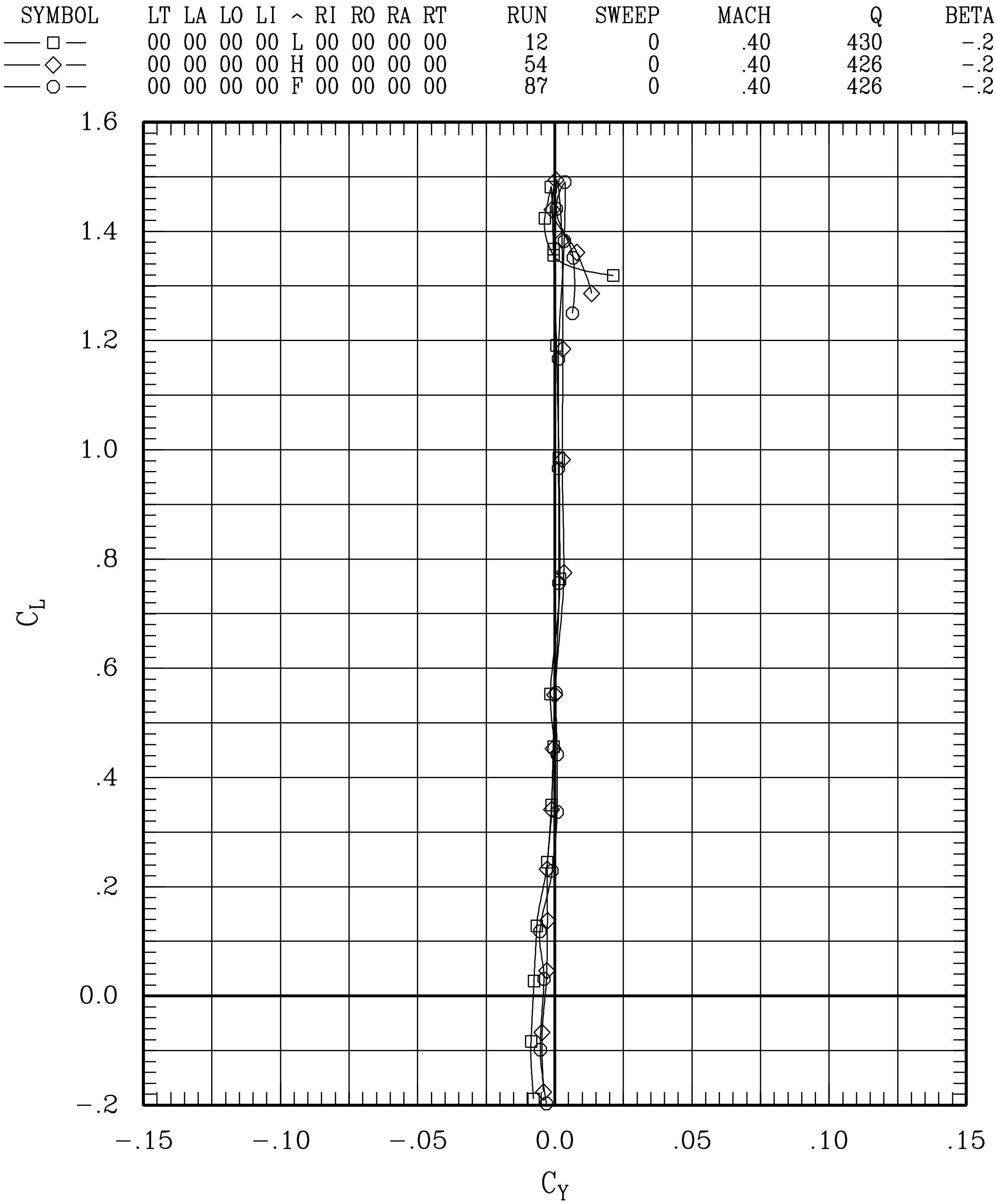

Figure 6(a). Effect of pivot height and fairing for sweep = 0 deg, Mach = 0.40.

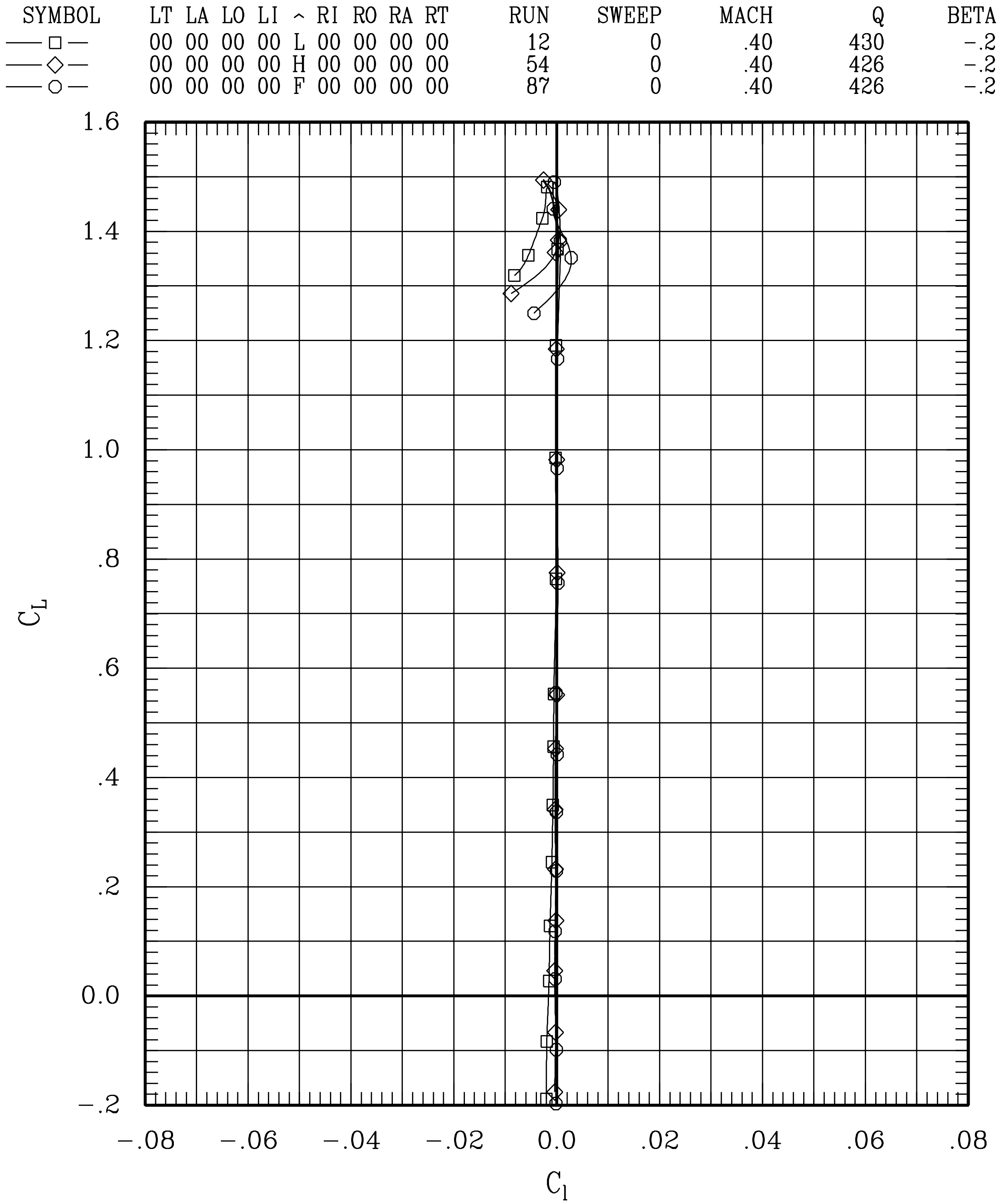

Figure 6(a). Effect of pivot height and fairing for sweep = 0 deg, Mach = 0.40.

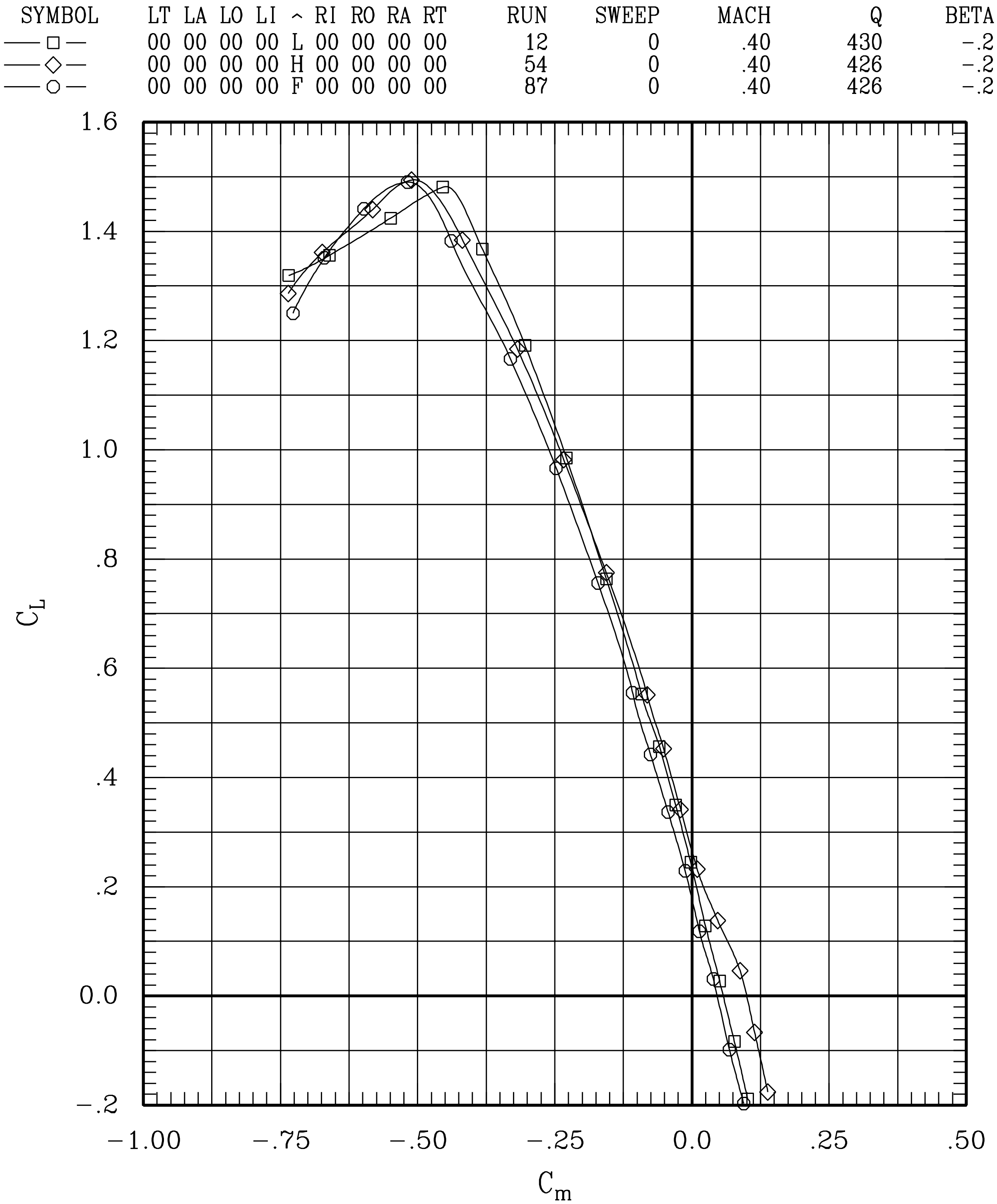

Figure 6(a). Effect of pivot height and fairing for sweep = 0 deg, Mach = 0.40.

SYMBOL	LT LA LO LI ^ RI RO RA RT	RUN	SWEEP	MACH	Q	BETA
—□—	00 00 00 00 L 00 00 00 00	12	0	.40	430	−.2
—◇—	00 00 00 00 H 00 00 00 00	54	0	.40	426	−.2
—○—	00 00 00 00 F 00 00 00 00	87	0	.40	426	−.2

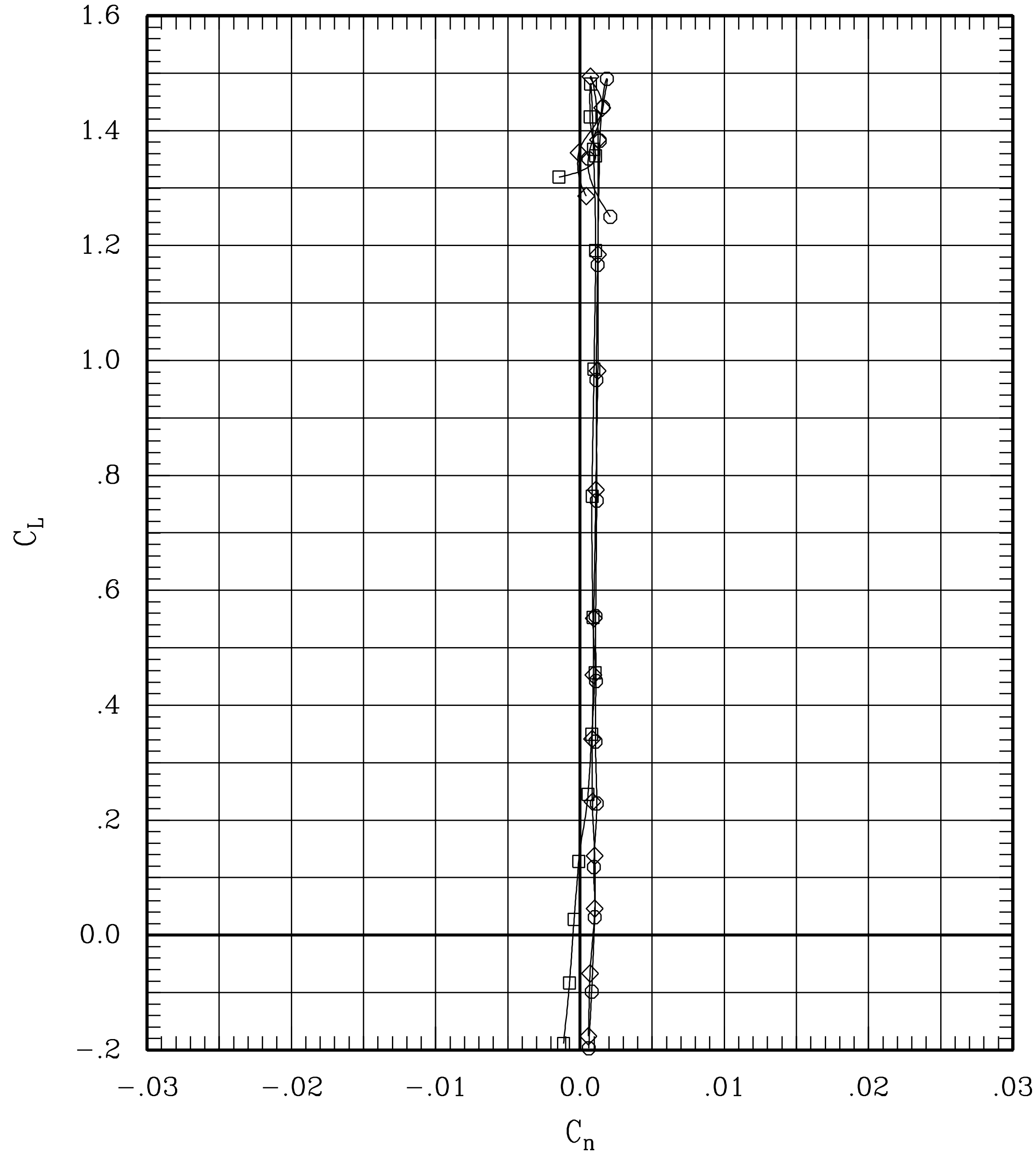

Figure 6(a). Effect of pivot height and fairing for sweep = 0 deg, Mach = 0.40.

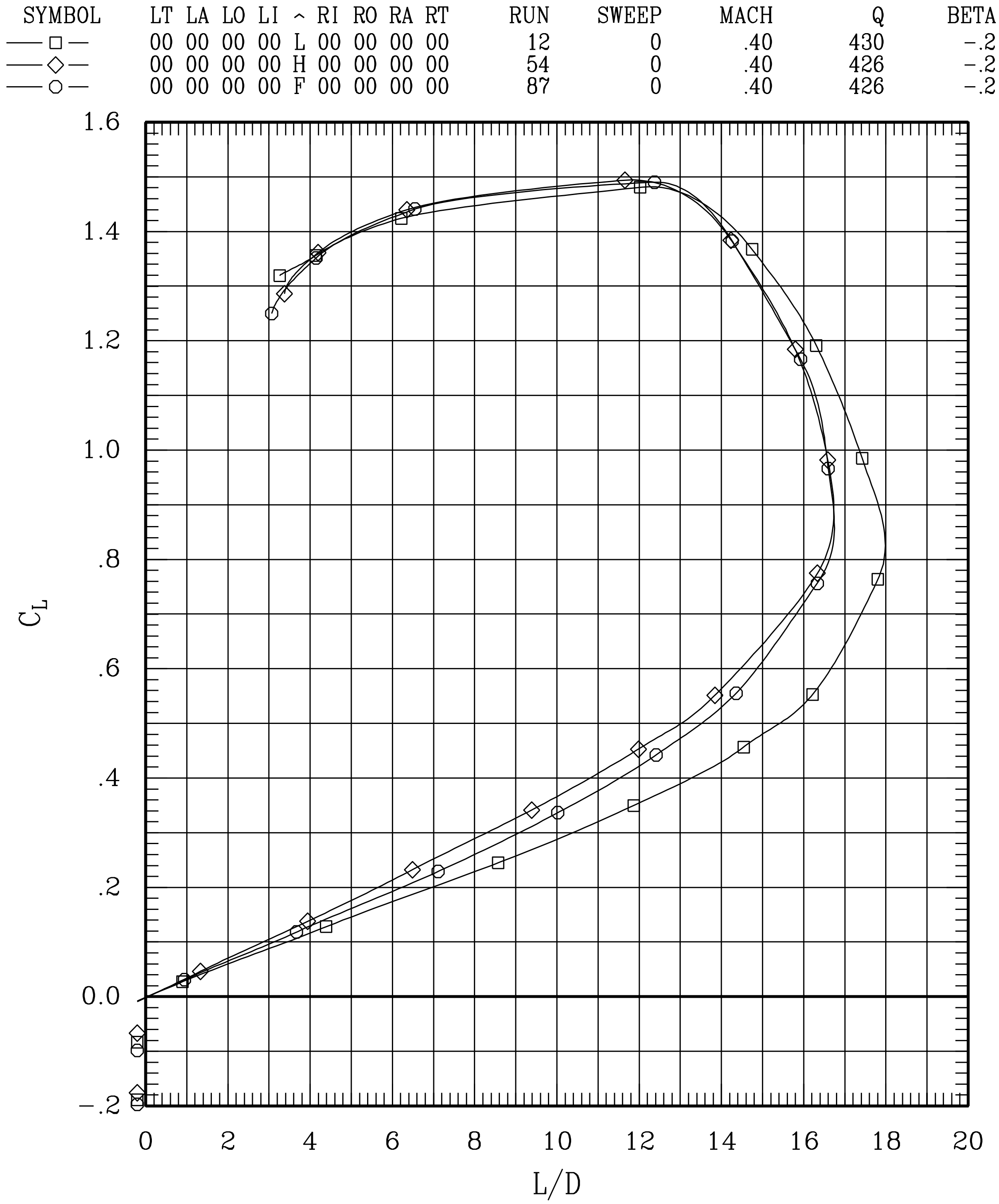

Figure 6(a). Effect of pivot height and fairing for sweep = 0 deg, Mach = 0.40.

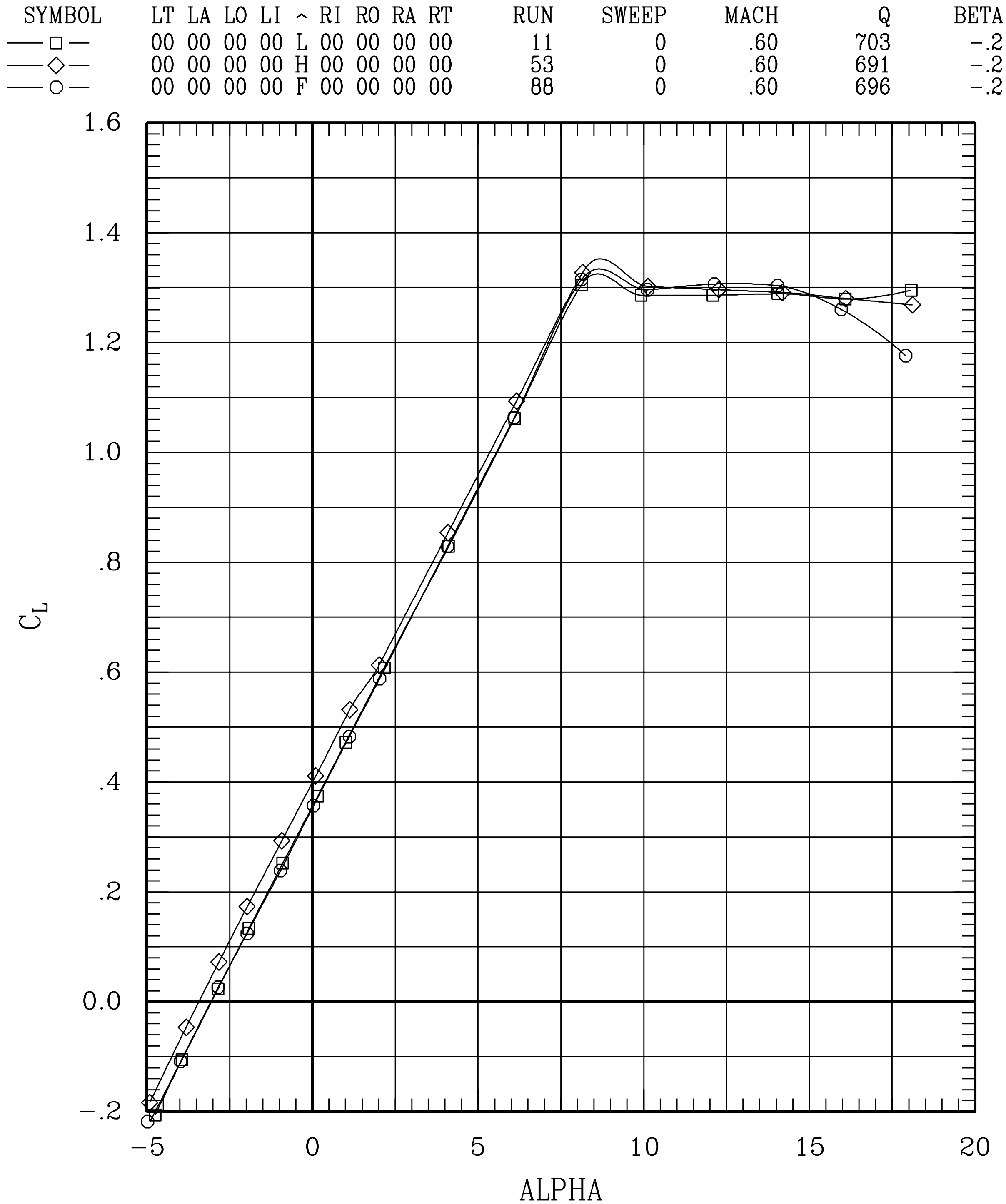

Figure 6(b). Effect of pivot height and fairing for sweep = 0 deg, Mach = 0.60.

SYMBOL	LT LA LO LI ^ RI RO RA RT	RUN	SWEEP	MACH	Q	BETA
—□—	00 00 00 00 L 00 00 00 00	11	0	.60	703	−.2
—◇—	00 00 00 00 H 00 00 00 00	53	0	.60	691	−.2
—○—	00 00 00 00 F 00 00 00 00	88	0	.60	696	−.2

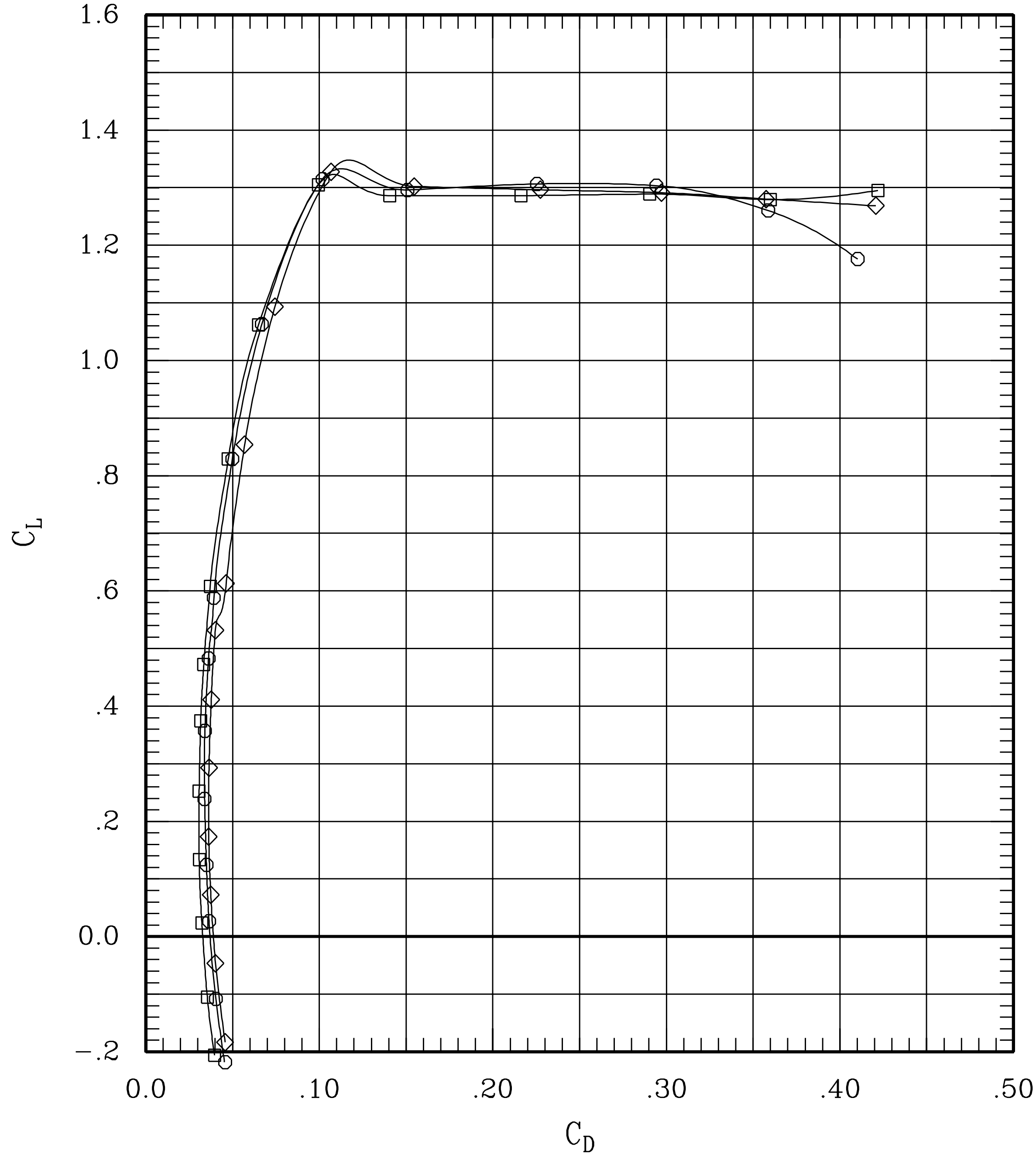

Figure 6(b). Effect of pivot height and fairing for sweep = 0 deg, Mach = 0.60.

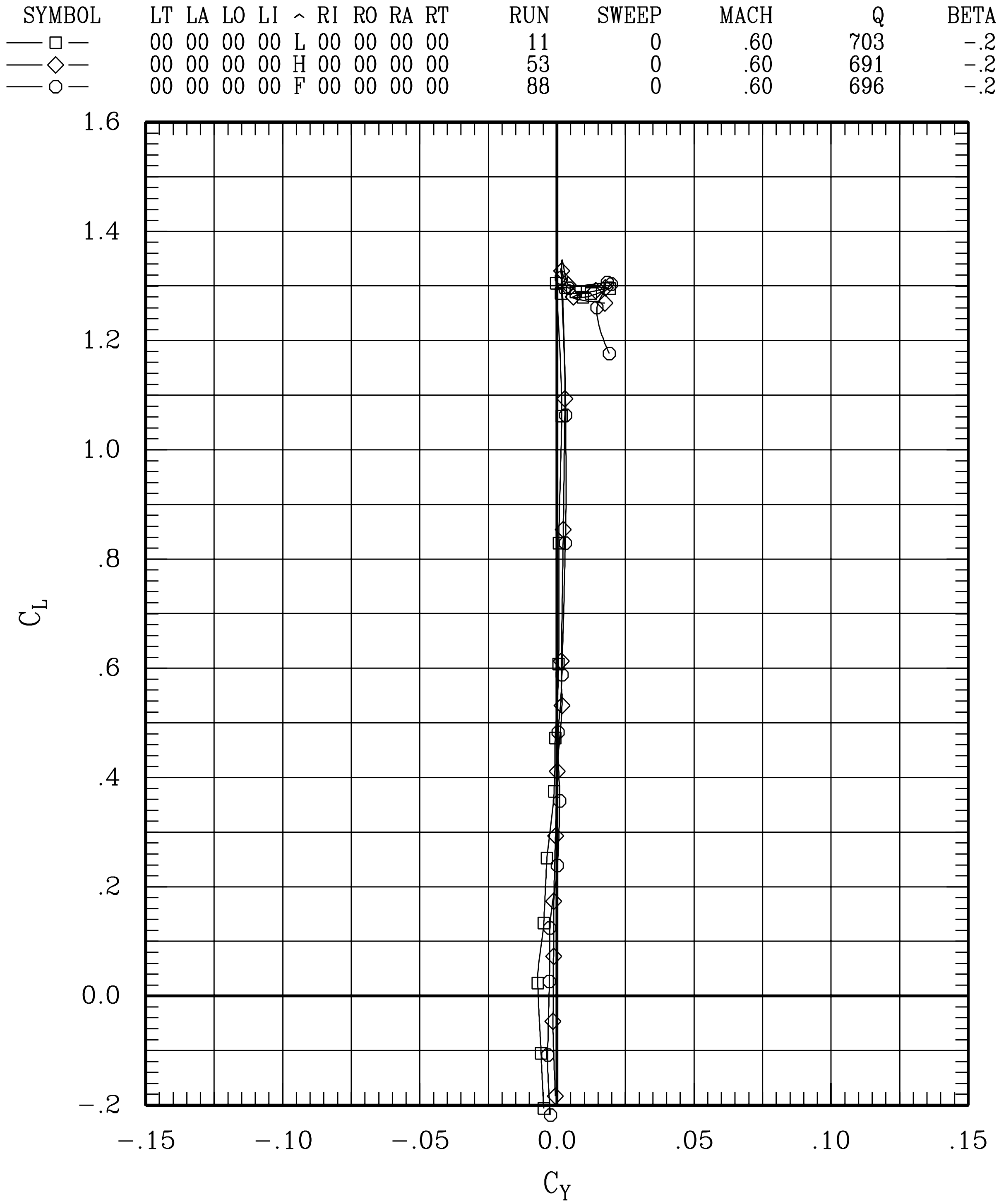

Figure 6(b). Effect of pivot height and fairing for sweep = 0 deg, Mach = 0.60.

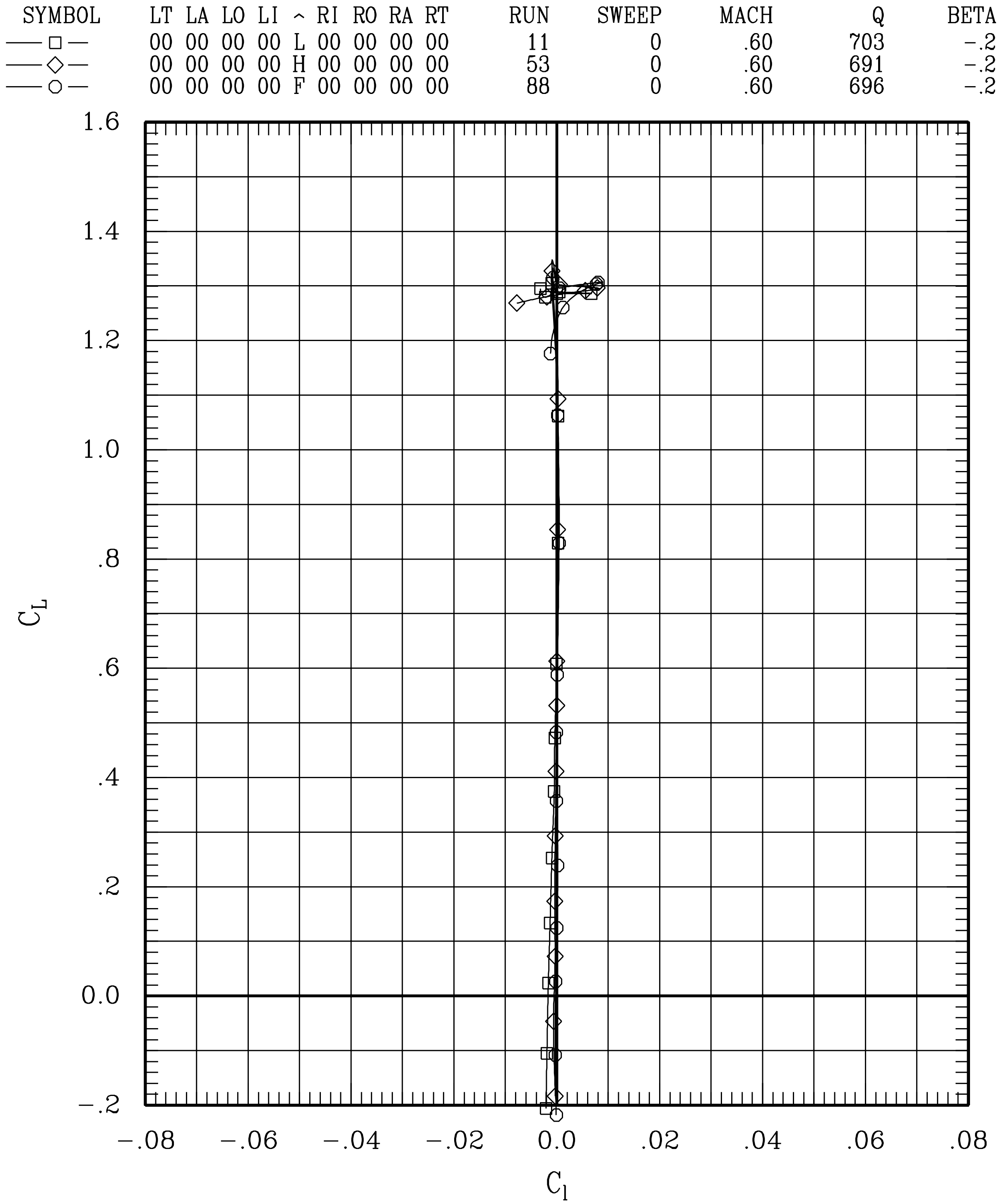

Figure 6(b). Effect of pivot height and fairing for sweep = 0 deg, Mach = 0.60.

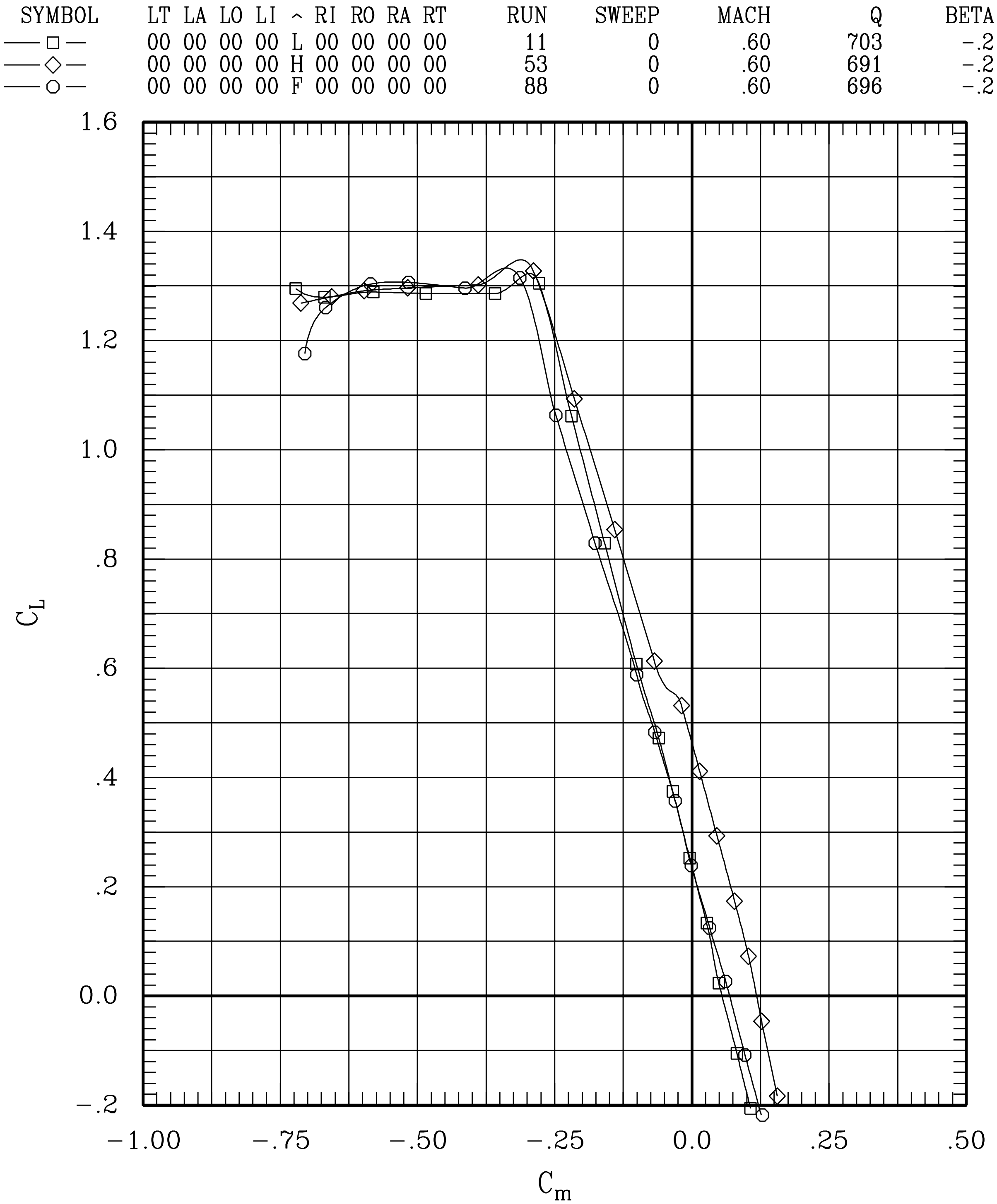

Figure 6(b). Effect of pivot height and fairing for sweep = 0 deg, Mach = 0.60.

SYMBOL	LT LA LO LI ^ RI RO RA RT	RUN	SWEEP	MACH	Q	BETA
—□—	00 00 00 00 L 00 00 00 00	11	0	.60	703	−.2
—◇—	00 00 00 00 H 00 00 00 00	53	0	.60	691	−.2
—○—	00 00 00 00 F 00 00 00 00	88	0	.60	696	−.2

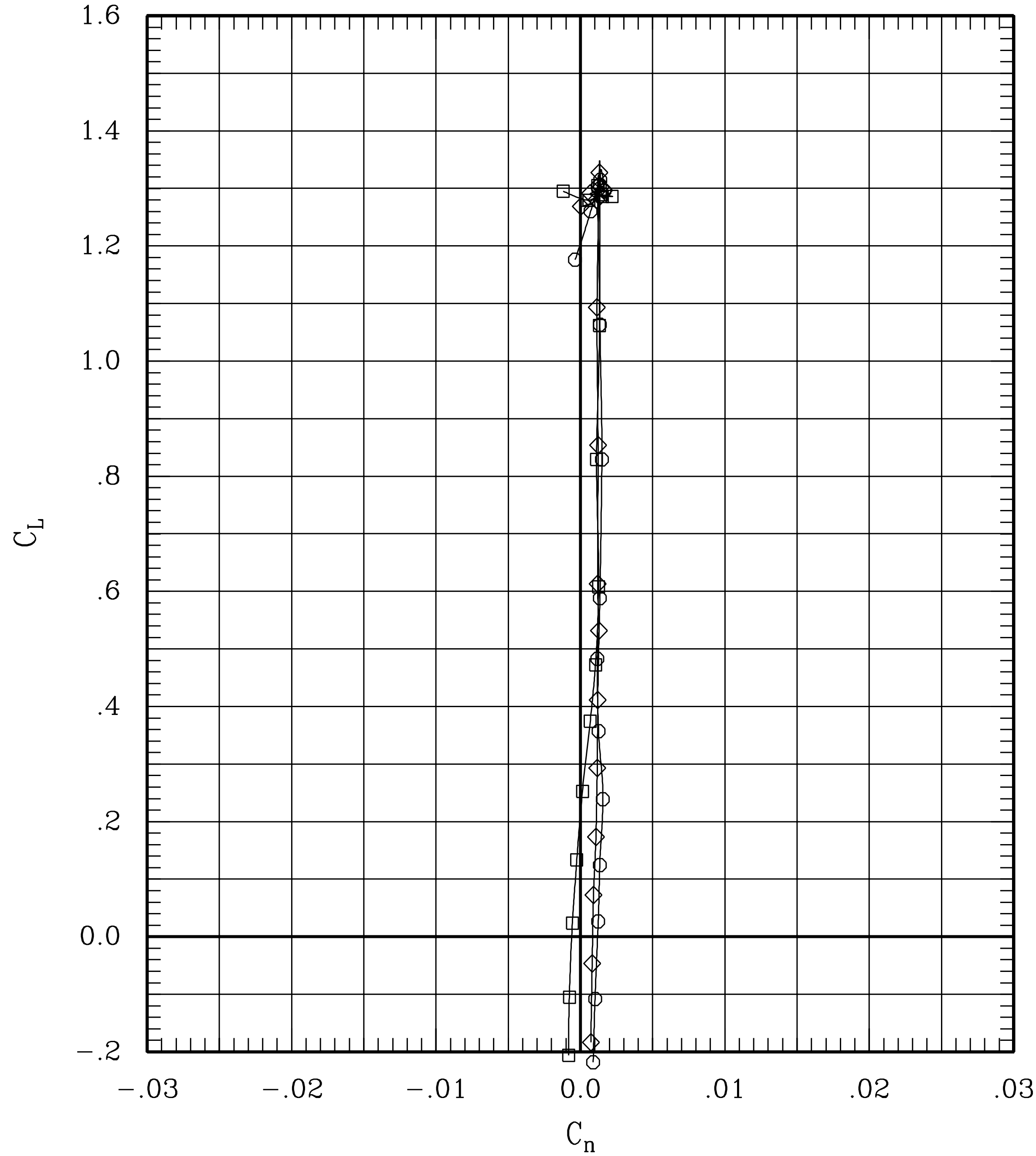

Figure 6(b). Effect of pivot height and fairing for sweep = 0 deg, Mach = 0.60.

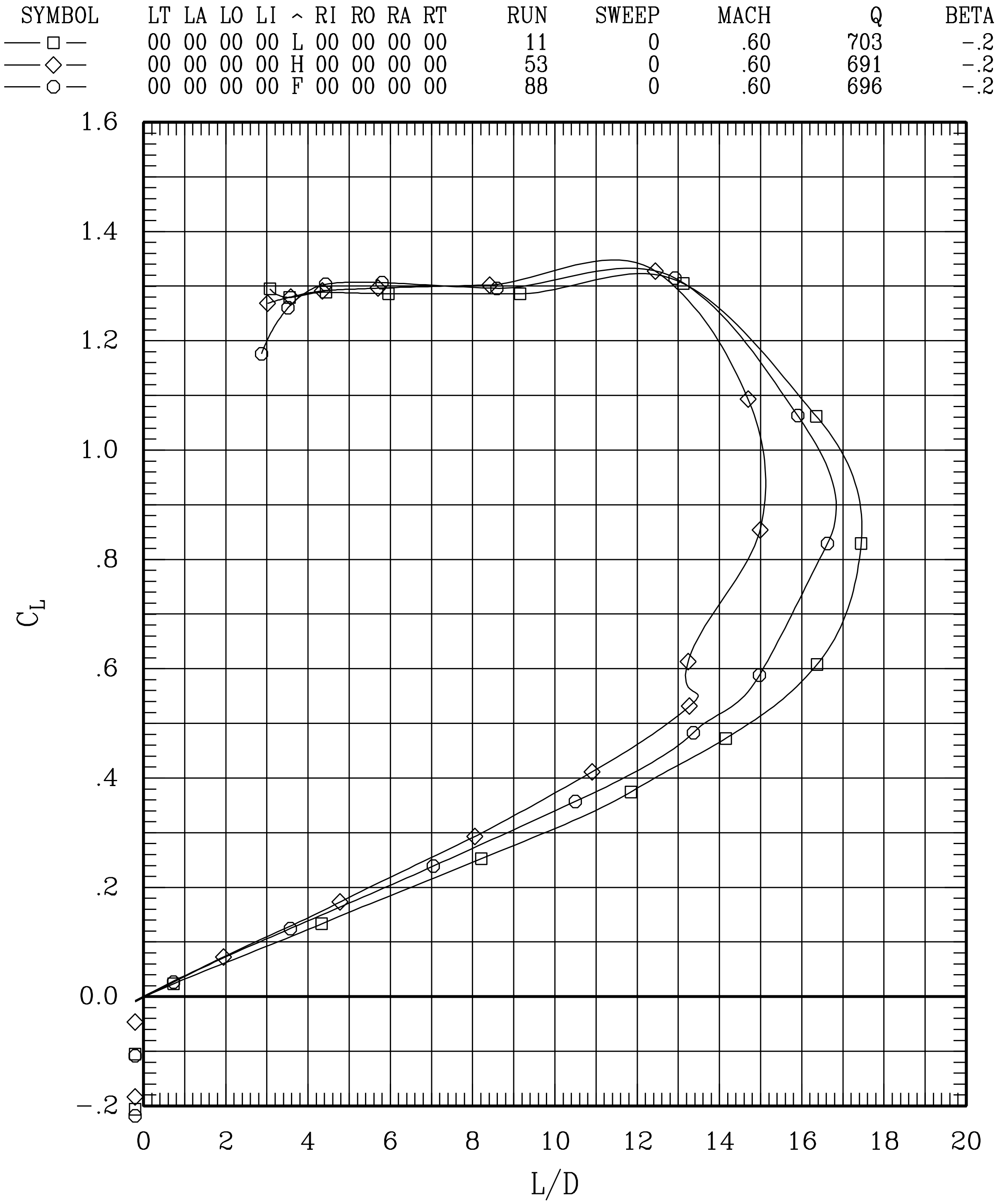

Figure 6(b). Effect of pivot height and fairing for sweep = 0 deg, Mach = 0.60.

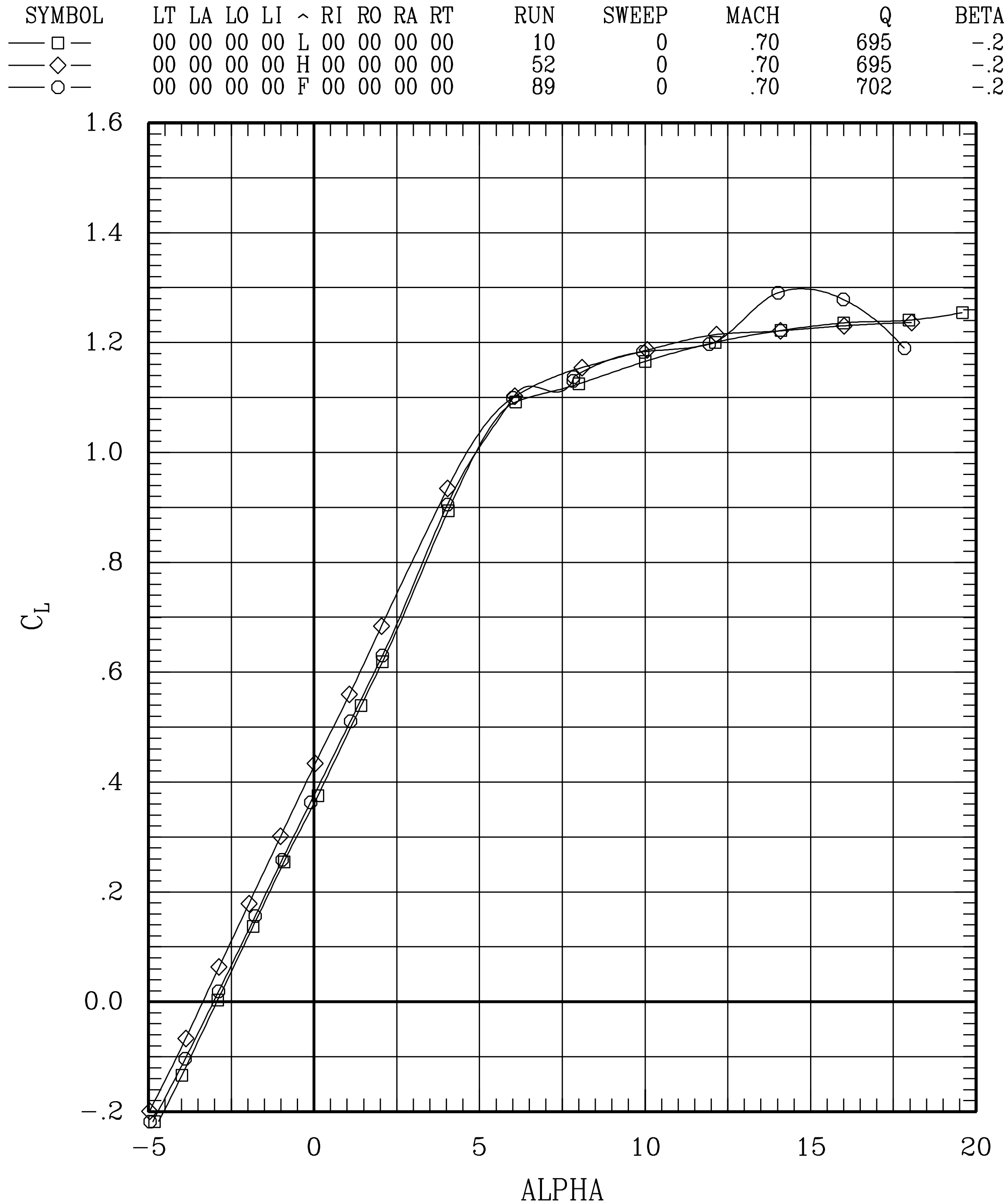

Figure 6(c). Effect of pivot height and fairing for sweep = 0 deg, Mach = 0.70.

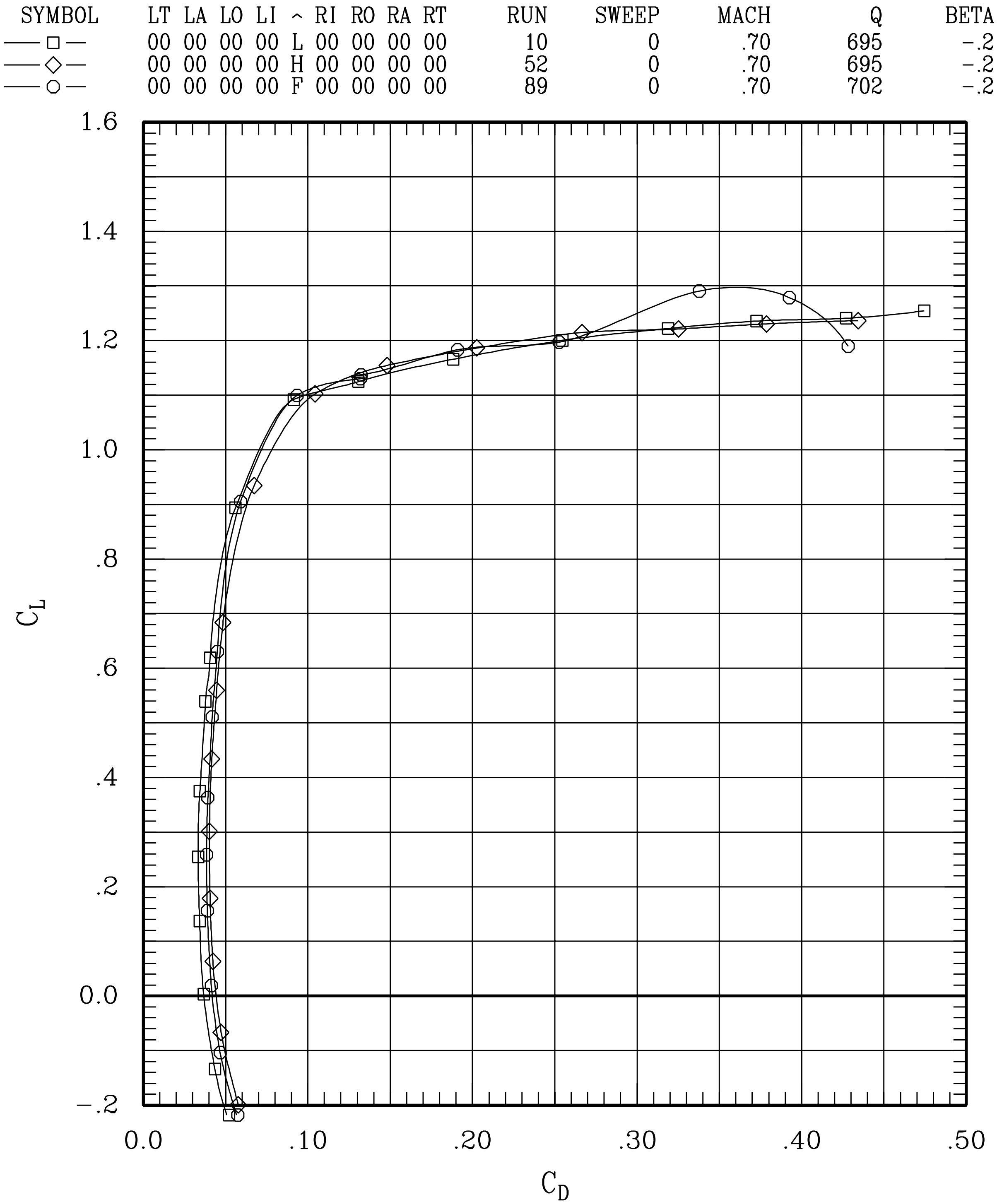

Figure 6(c). Effect of pivot height and fairing for sweep = 0 deg, Mach = 0.70.

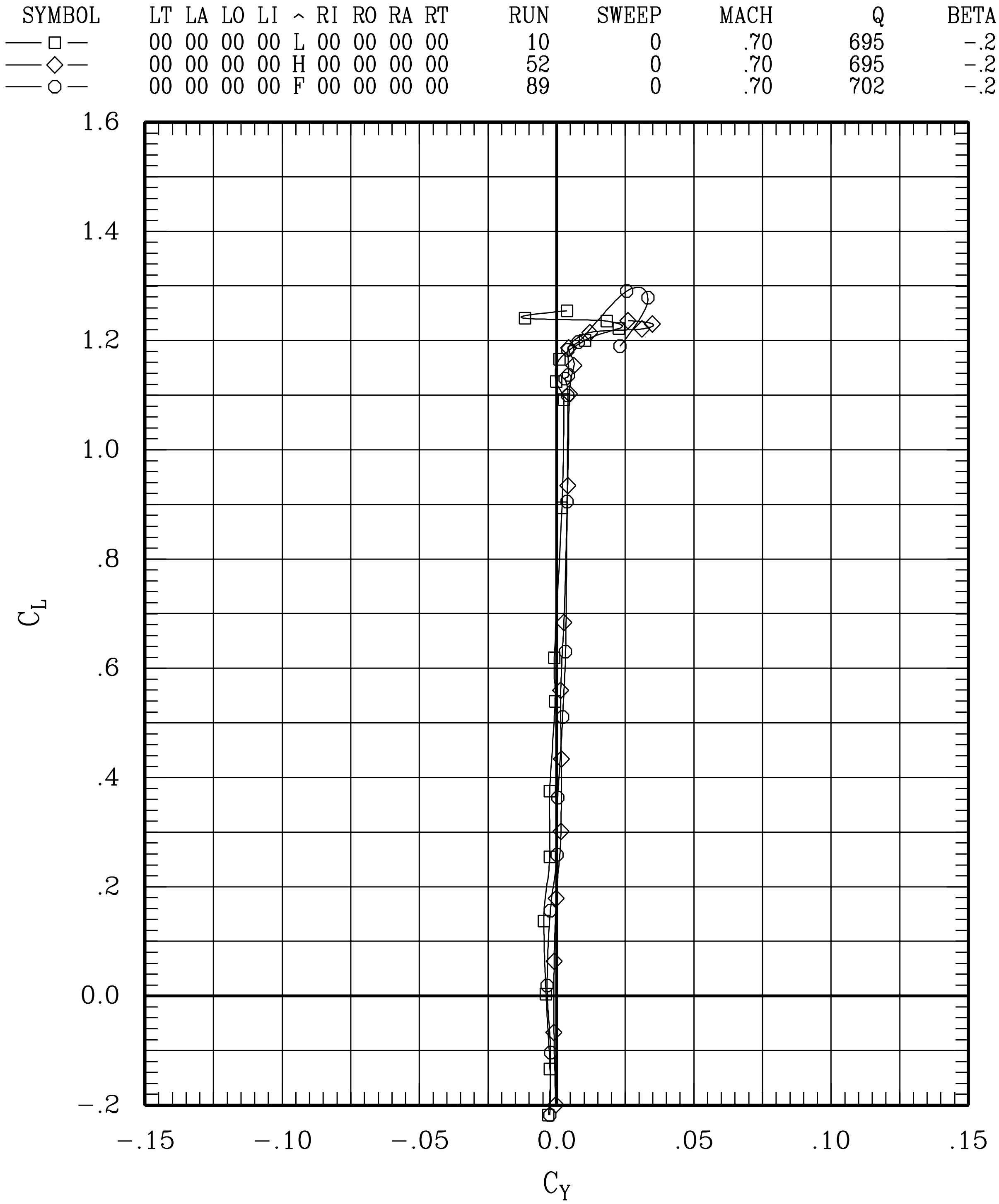

Figure 6(c). Effect of pivot height and fairing for sweep = 0 deg, Mach = 0.70.

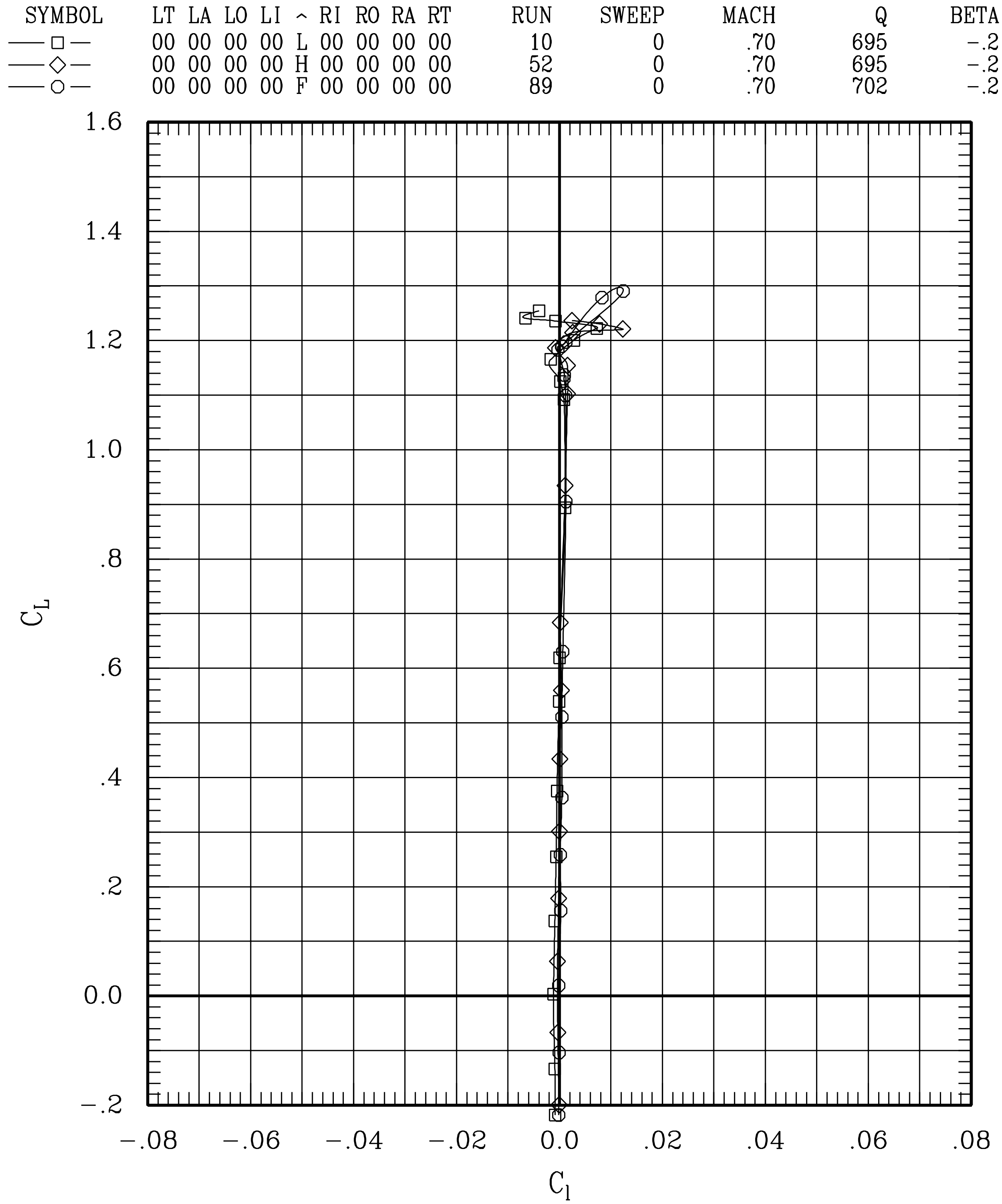

Figure 6(c). Effect of pivot height and fairing for sweep = 0 deg, Mach = 0.70.

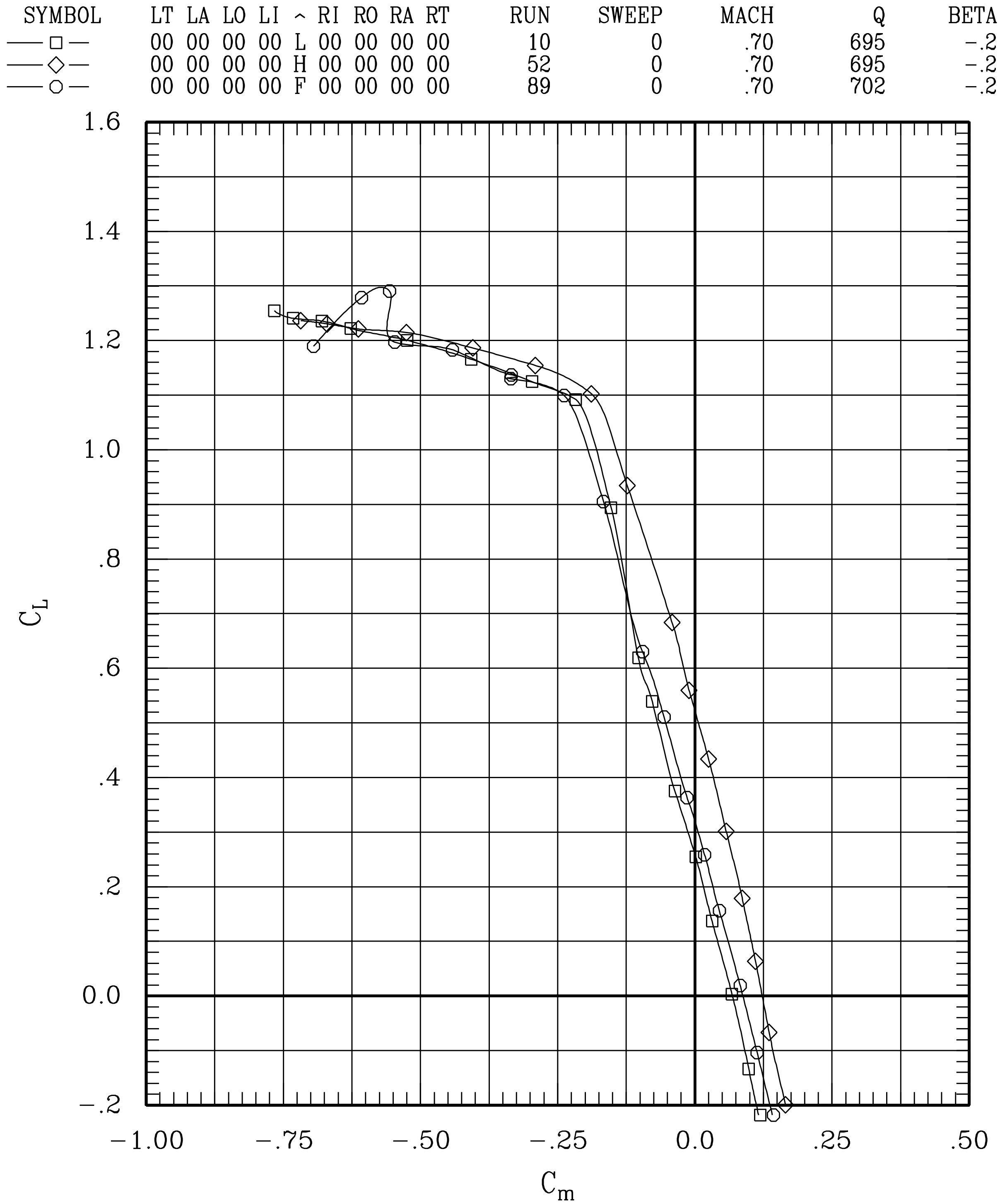

Figure 6(c). Effect of pivot height and fairing for sweep = 0 deg, Mach = 0.70.

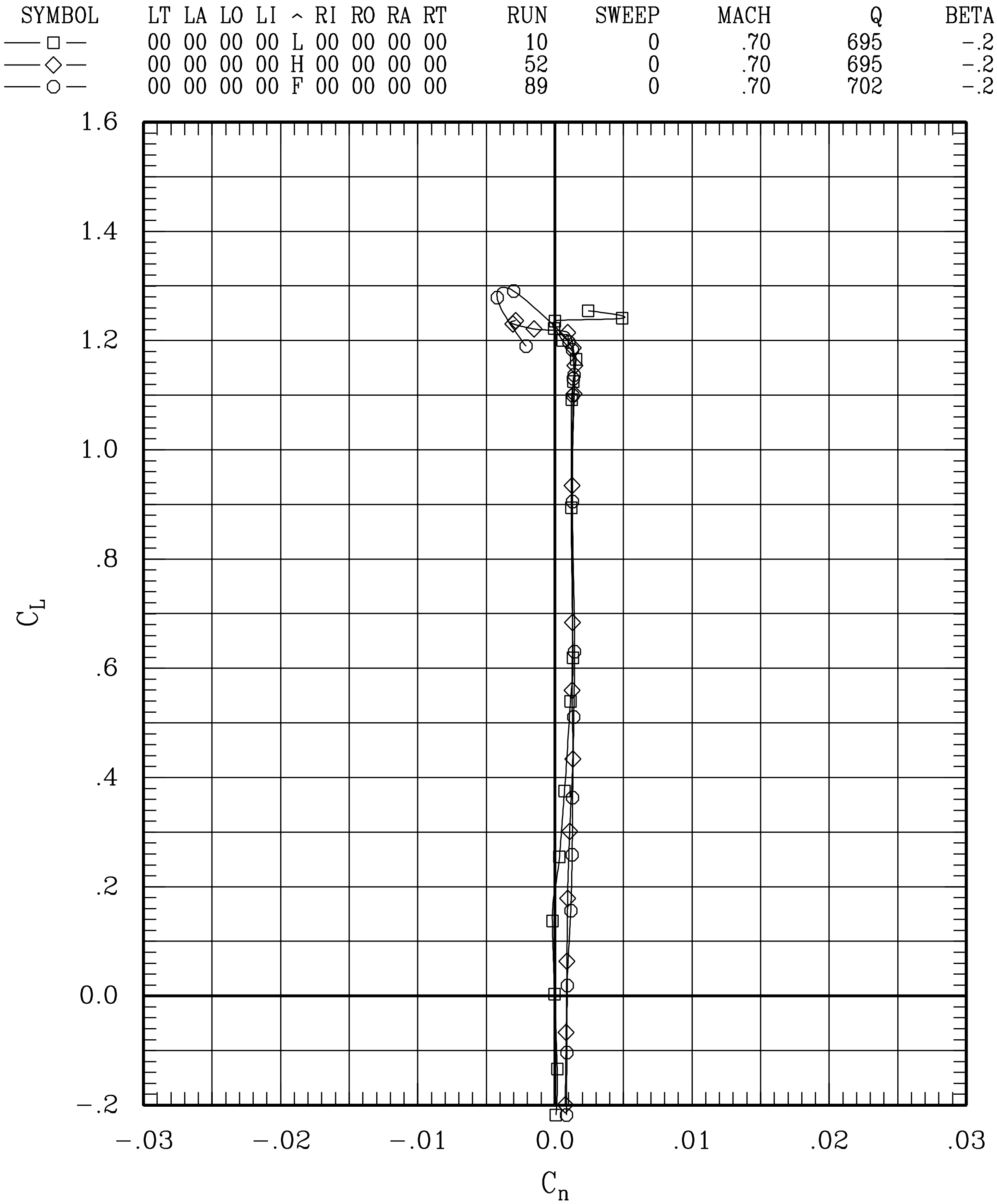

Figure 6(c). Effect of pivot height and fairing for sweep = 0 deg, Mach = 0.70.

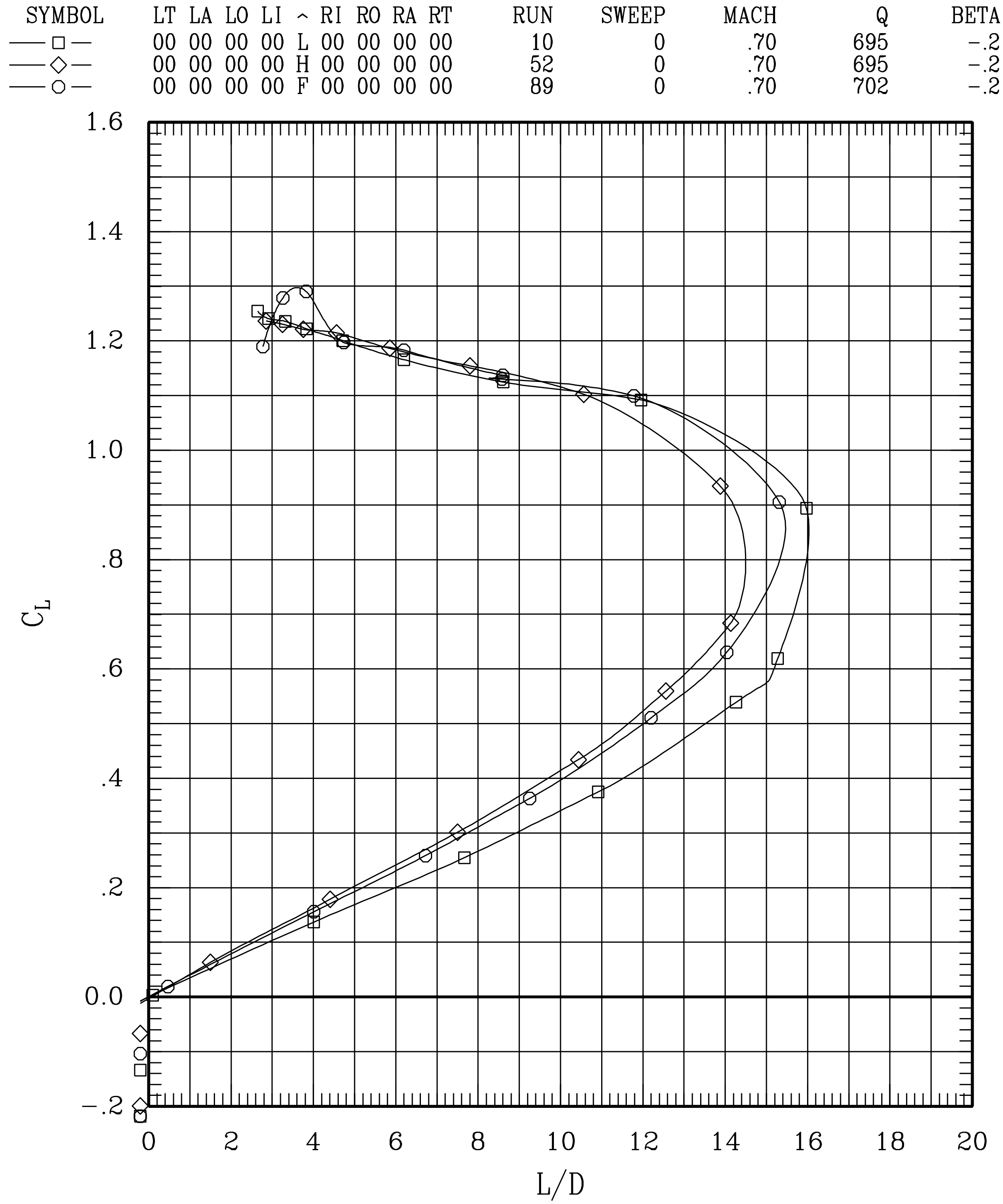

Figure 6(c). Effect of pivot height and fairing for sweep = 0 deg, Mach = 0.70.

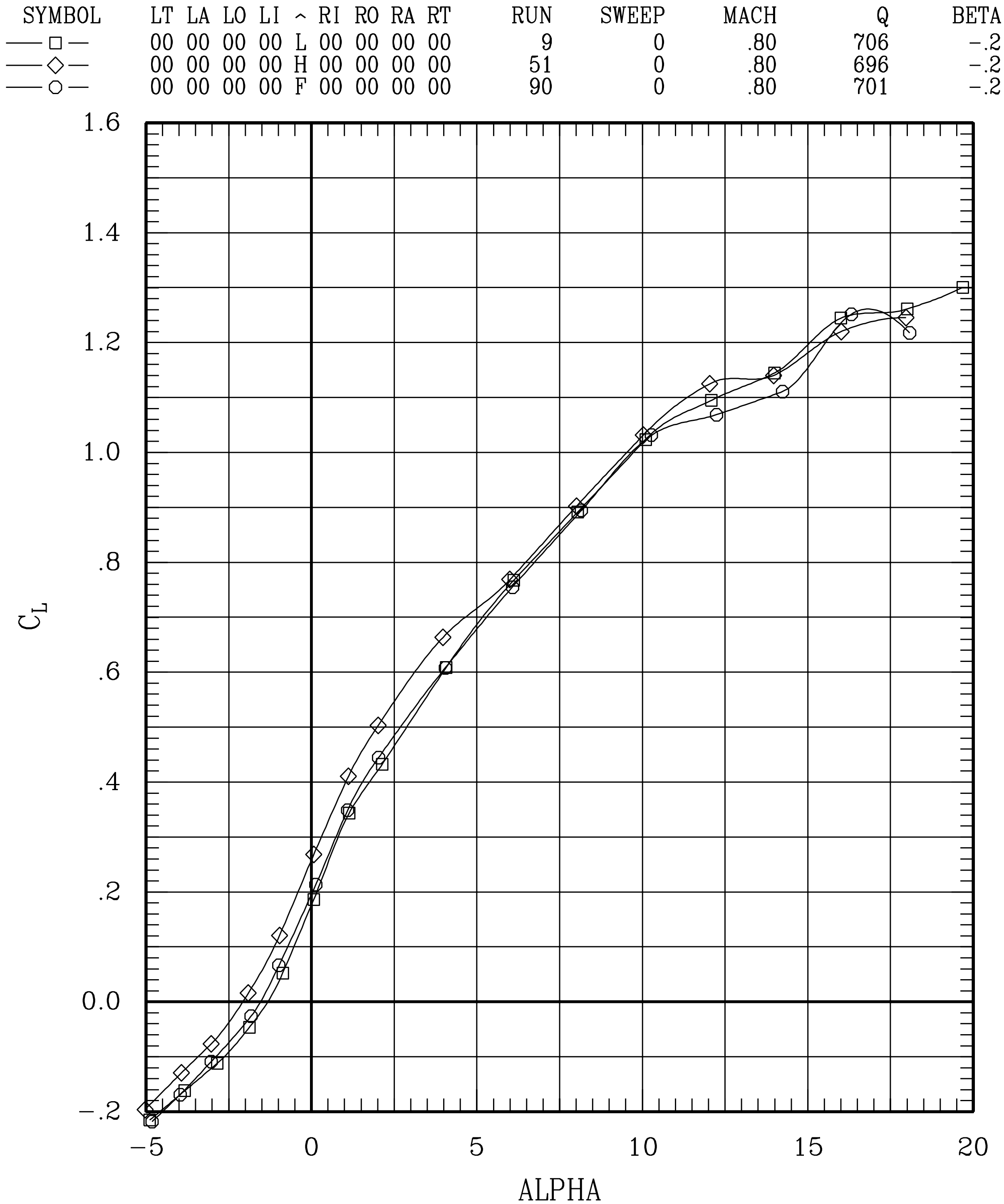

Figure 6(d). Effect of pivot height and fairing for sweep = 0 deg, Mach = 0.80.

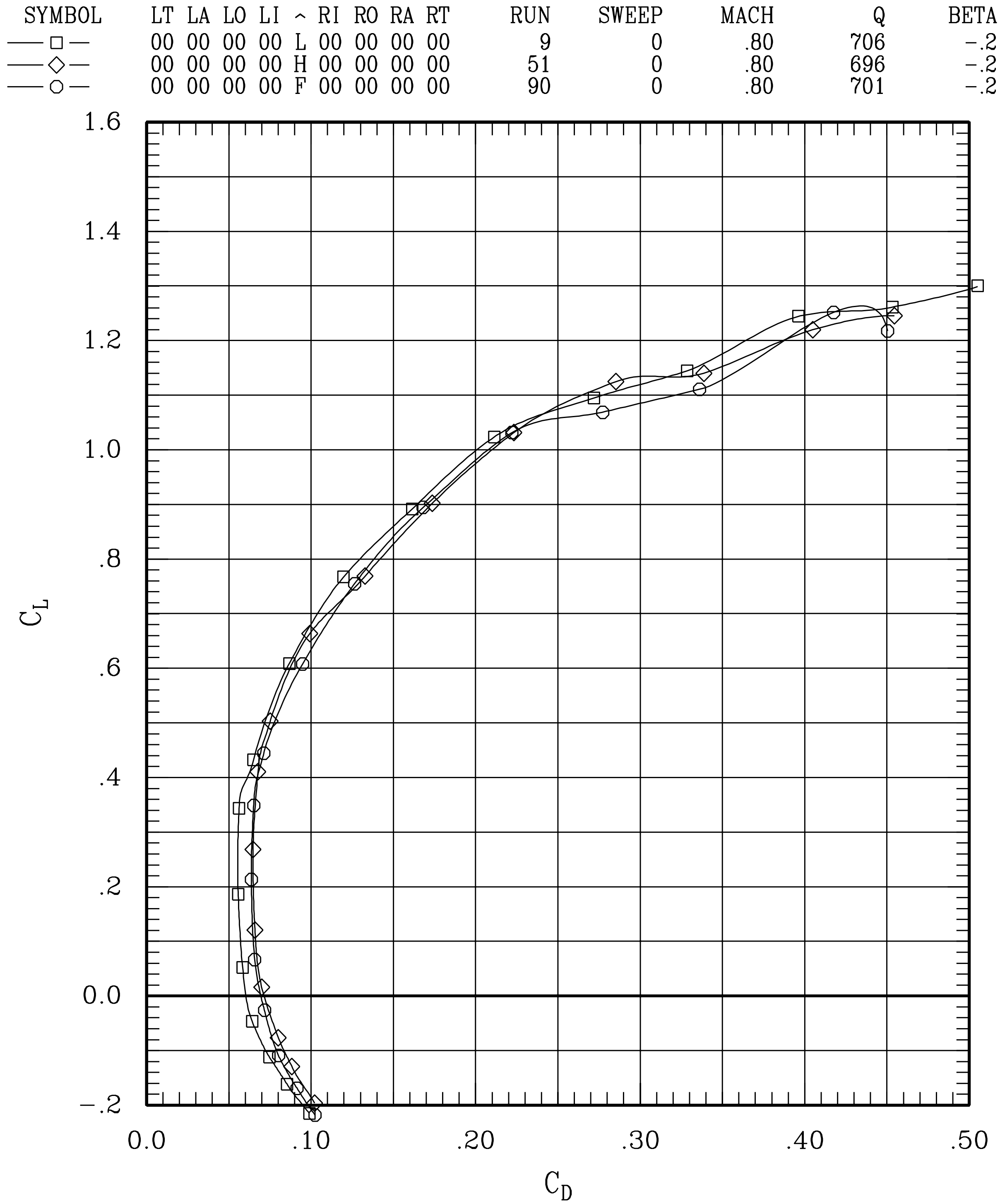

Figure 6(d). Effect of pivot height and fairing for sweep = 0 deg, Mach = 0.80.

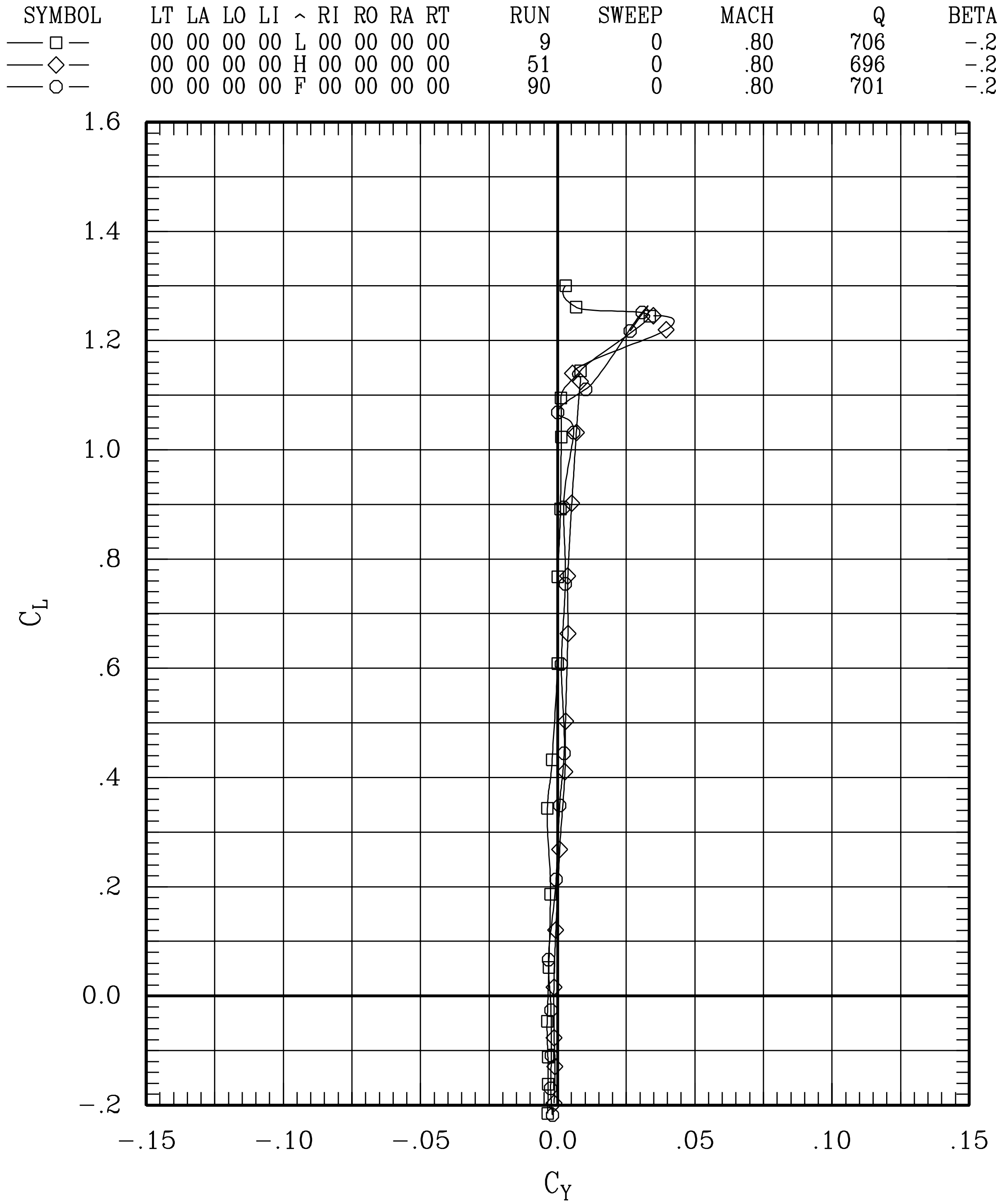

Figure 6(d). Effect of pivot height and fairing for sweep = 0 deg, Mach = 0.80.

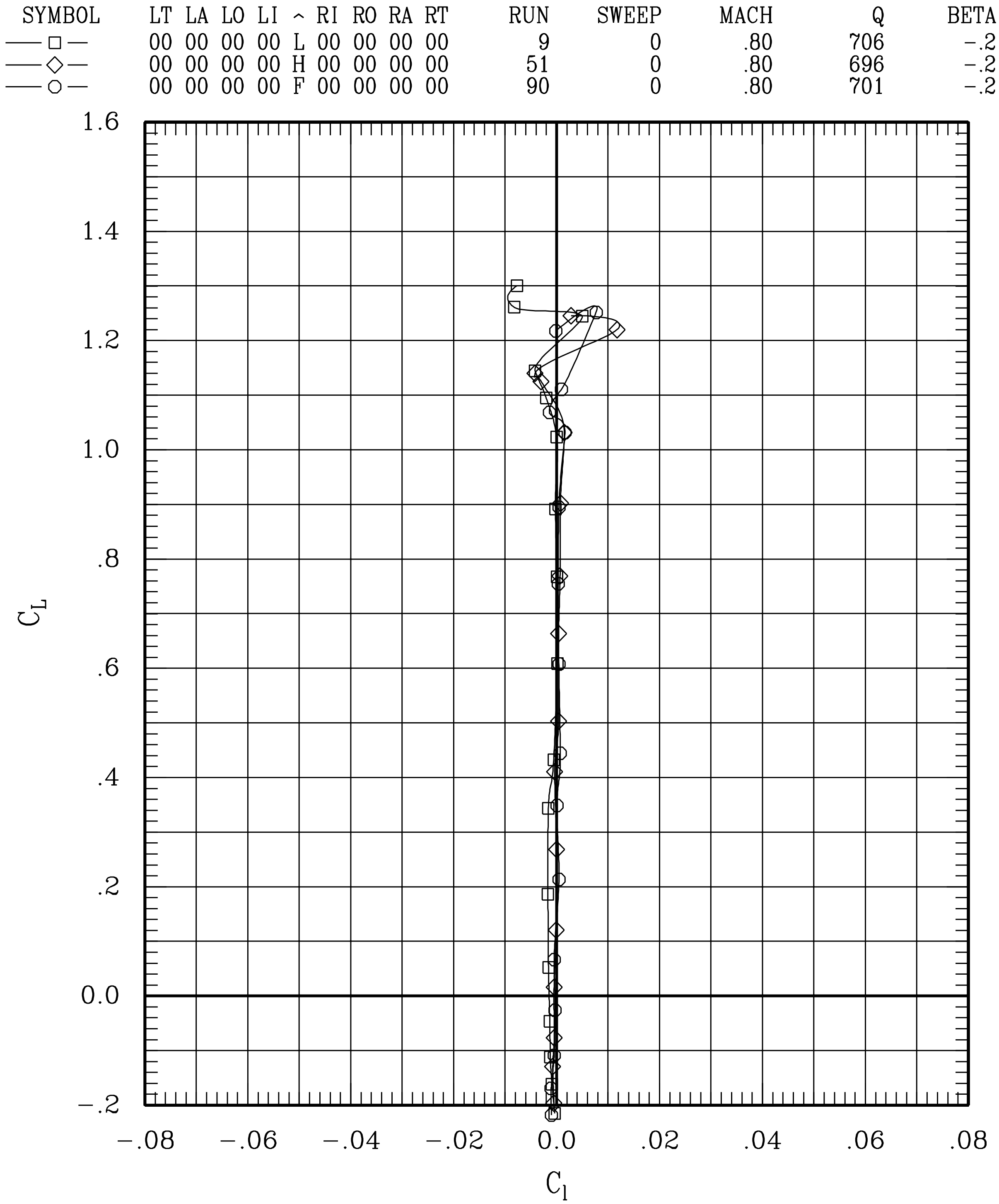

Figure 6(d). Effect of pivot height and fairing for sweep = 0 deg, Mach = 0.80.

SYMBOL	LT	LA	LO	LI	^	RI	RO	RA	RT	RUN	SWEEP	MACH	Q	BETA
—□—	00	00	00	00	L	00	00	00	00	9	0	.80	706	−.2
—◇—	00	00	00	00	H	00	00	00	00	51	0	.80	696	−.2
—○—	00	00	00	00	F	00	00	00	00	90	0	.80	701	−.2

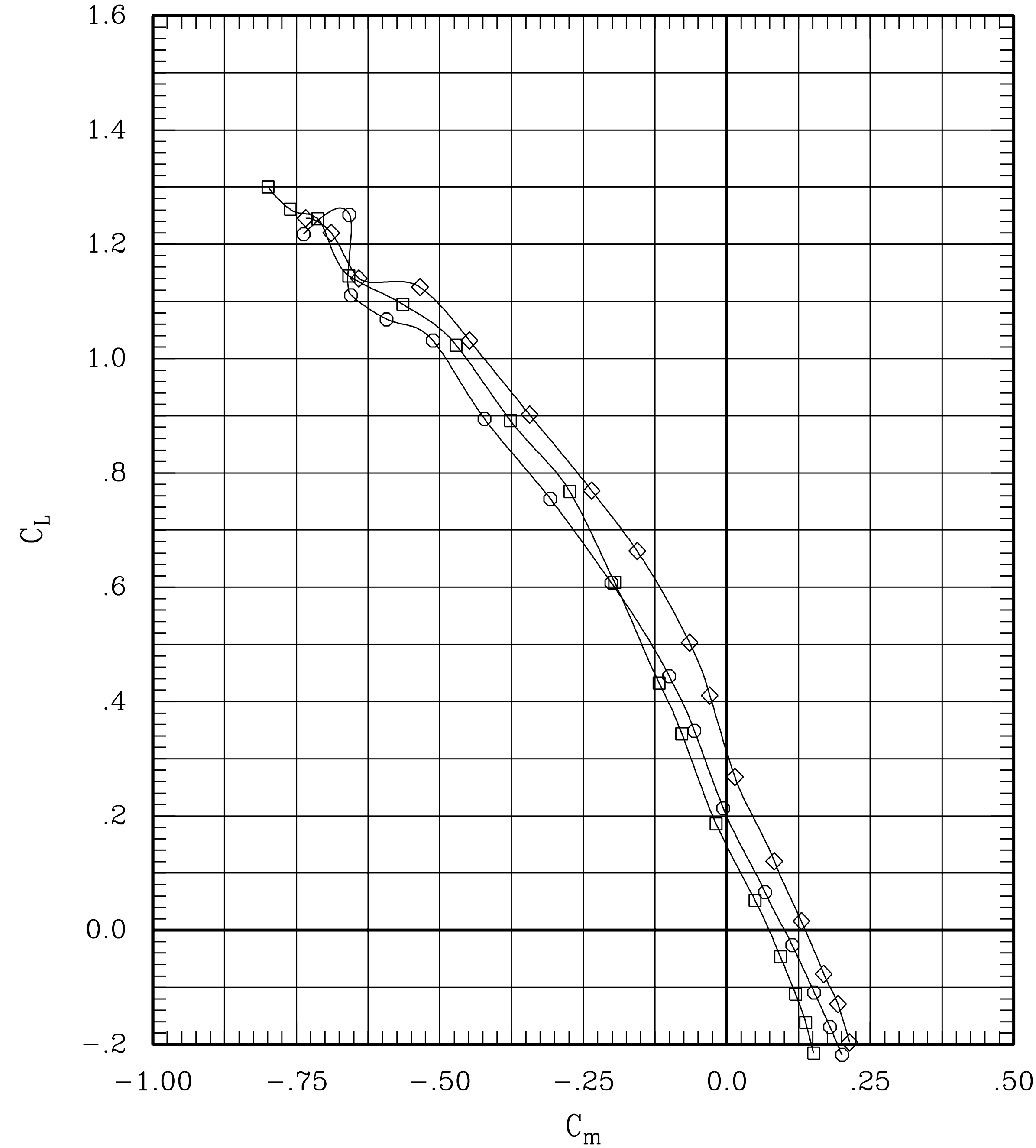

Figure 6(d). Effect of pivot height and fairing for sweep = 0 deg, Mach = 0.80.

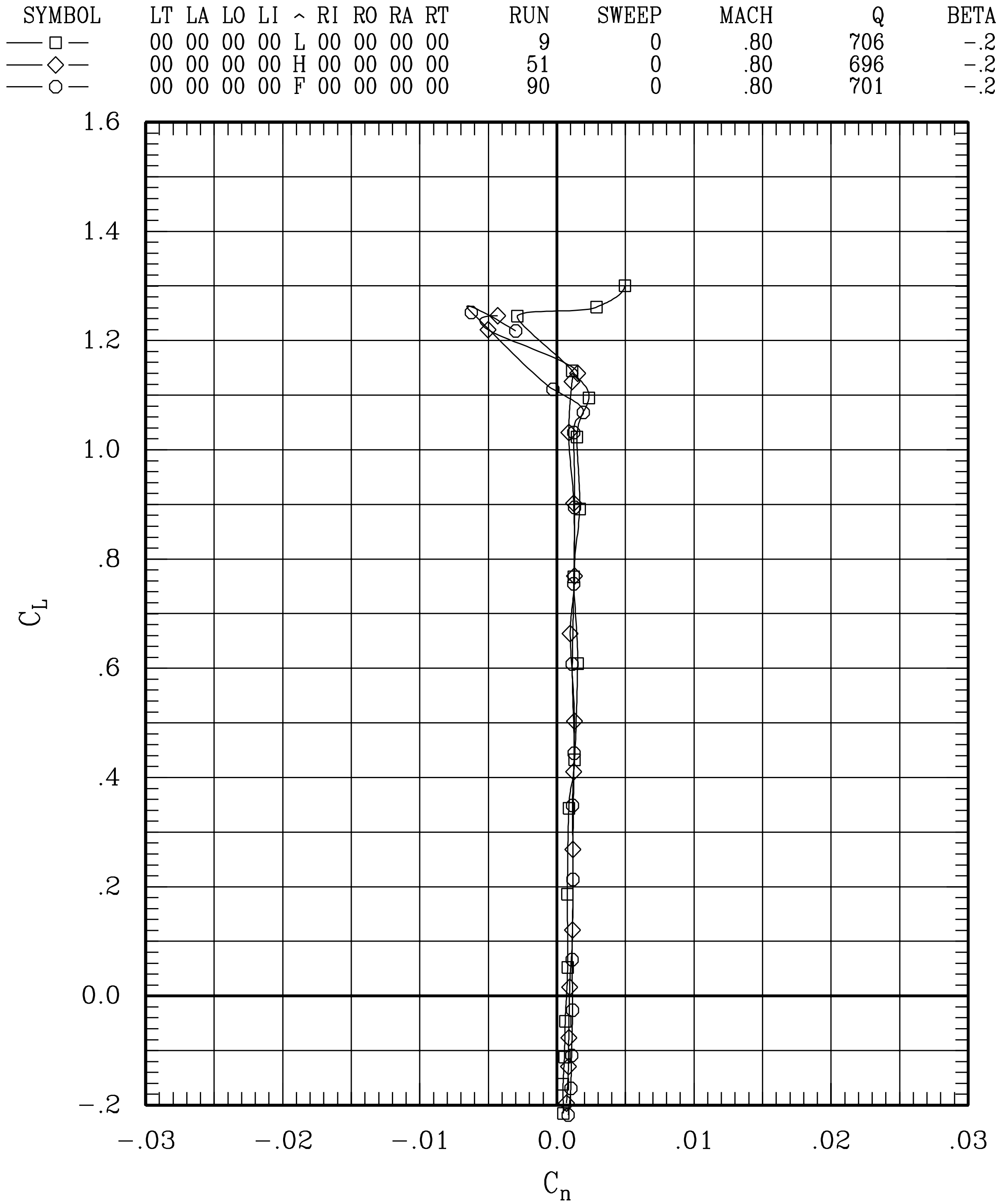

Figure 6(d). Effect of pivot height and fairing for sweep = 0 deg, Mach = 0.80.

SYMBOL	LT LA LO LI ^ RI RO RA RT	RUN	SWEEP	MACH	Q	BETA
—□—	00 00 00 00 L 00 00 00 00	9	0	.80	706	−.2
—◇—	00 00 00 00 H 00 00 00 00	51	0	.80	696	−.2
—○—	00 00 00 00 F 00 00 00 00	90	0	.80	701	−.2

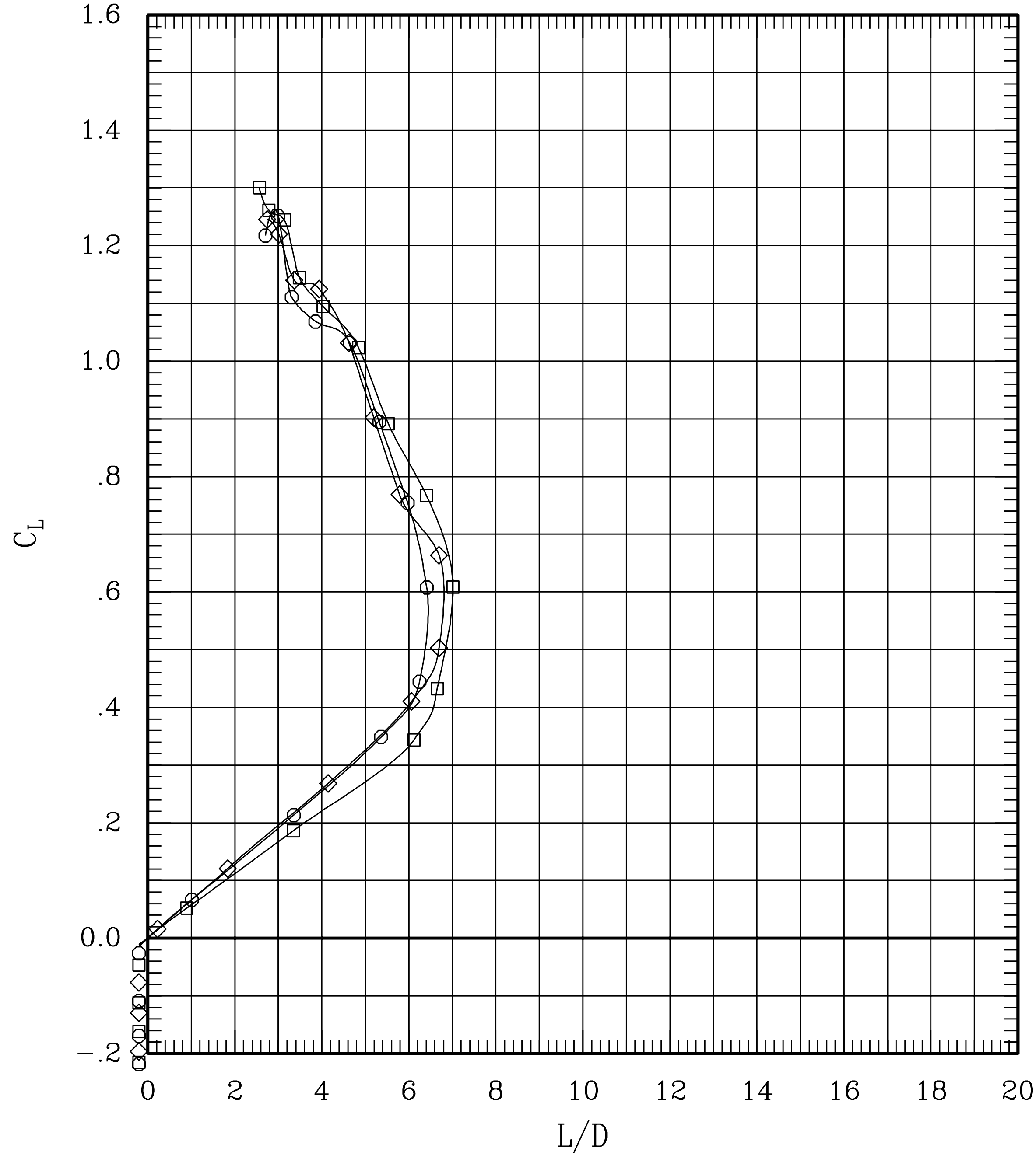

Figure 6(d). Effect of pivot height and fairing for sweep = 0 deg, Mach = 0.80.

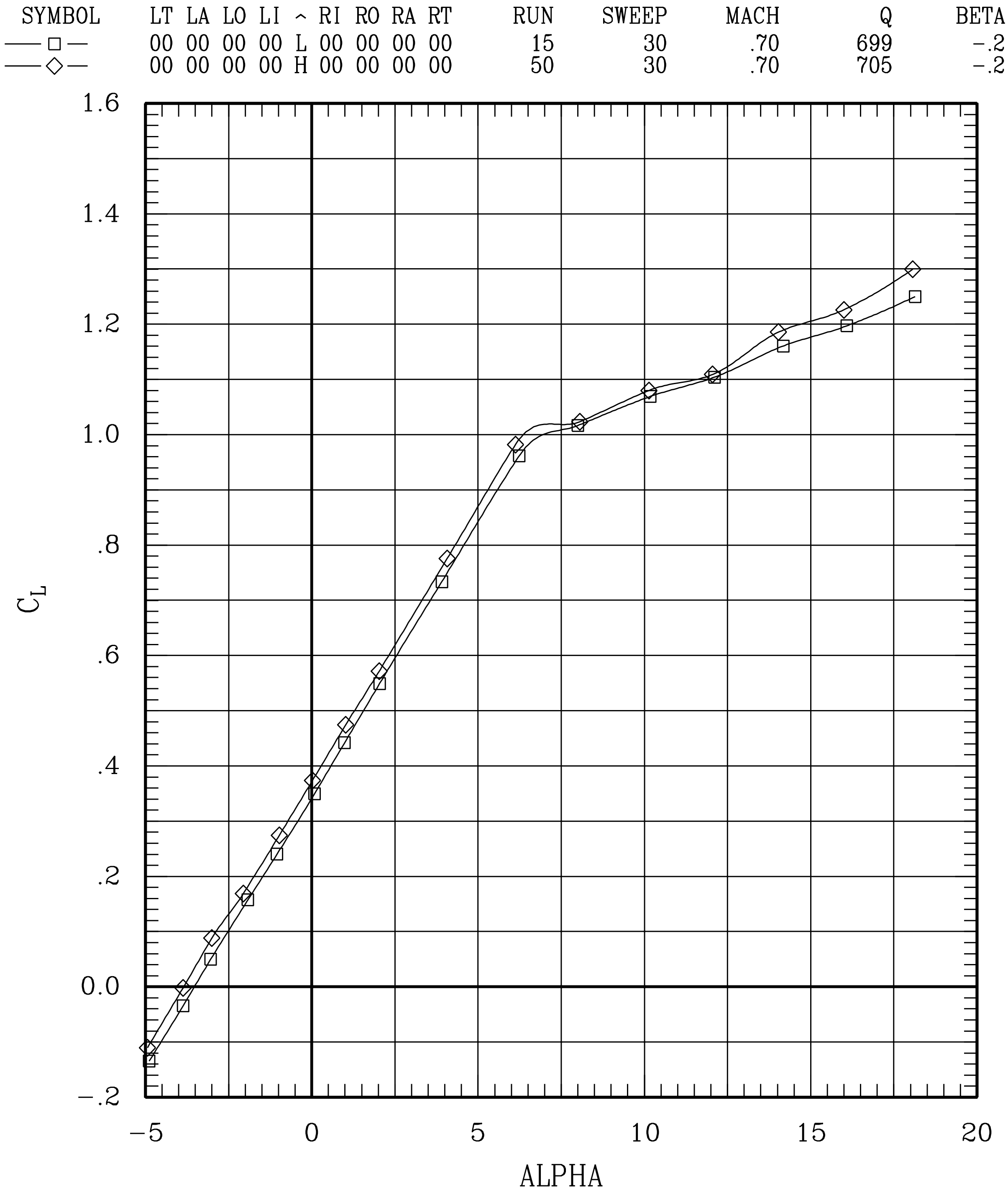

Figure 6(e). Effect of pivot height and fairing for sweep = 30 deg, Mach = 0.70.

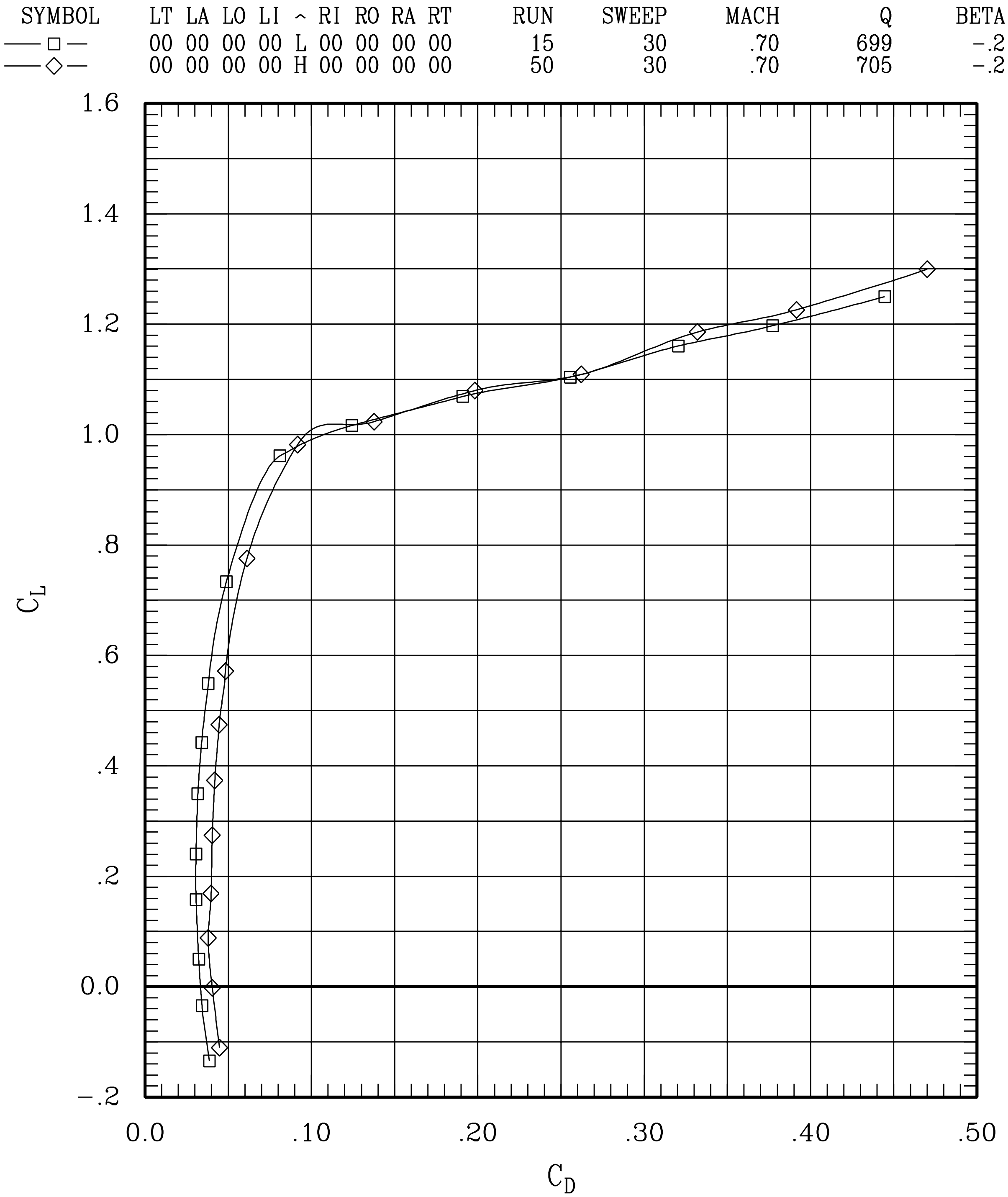

Figure 6(e). Effect of pivot height and fairing for sweep = 30 deg, Mach = 0.70.

SYMBOL	LT LA LO LI ^ RI RO RA RT	RUN	SWEEP	MACH	Q	BETA
—□—	00 00 00 00 L 00 00 00 00	15	30	.70	699	−.2
—◇—	00 00 00 00 H 00 00 00 00	50	30	.70	705	−.2

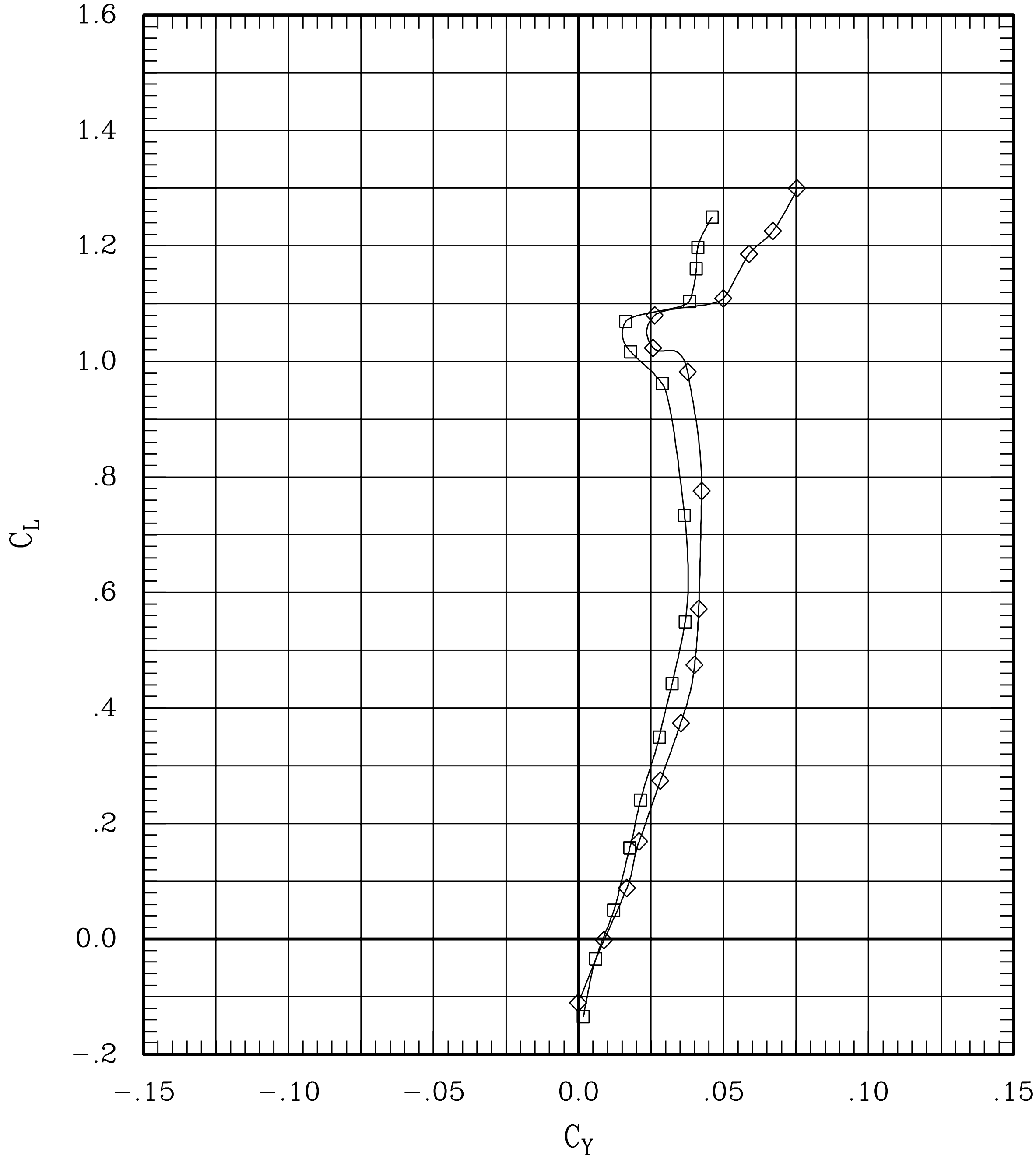

Figure 6(e). Effect of pivot height and fairing for sweep = 30 deg, Mach = 0.70.

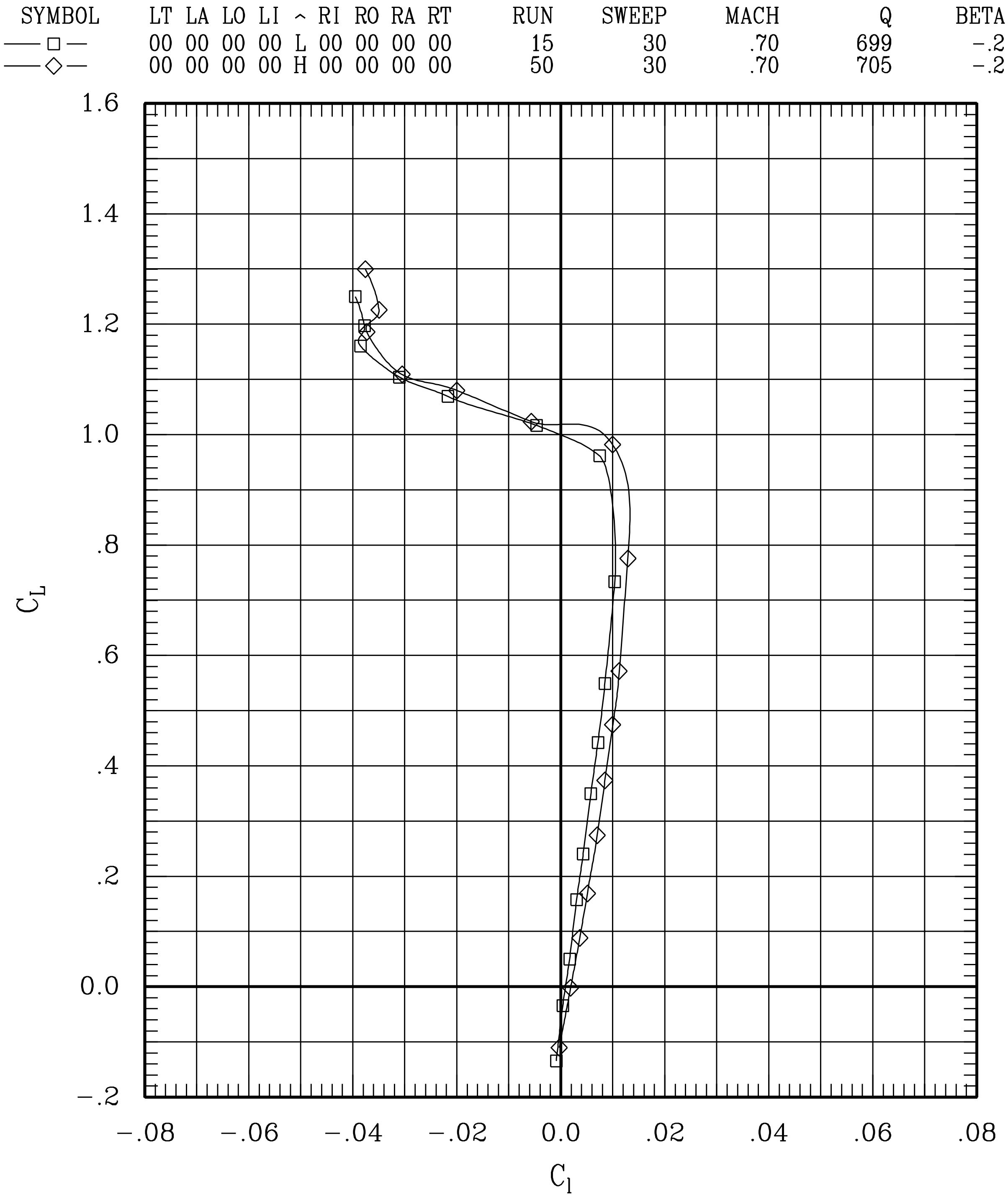

Figure 6(e). Effect of pivot height and fairing for sweep = 30 deg, Mach = 0.70.

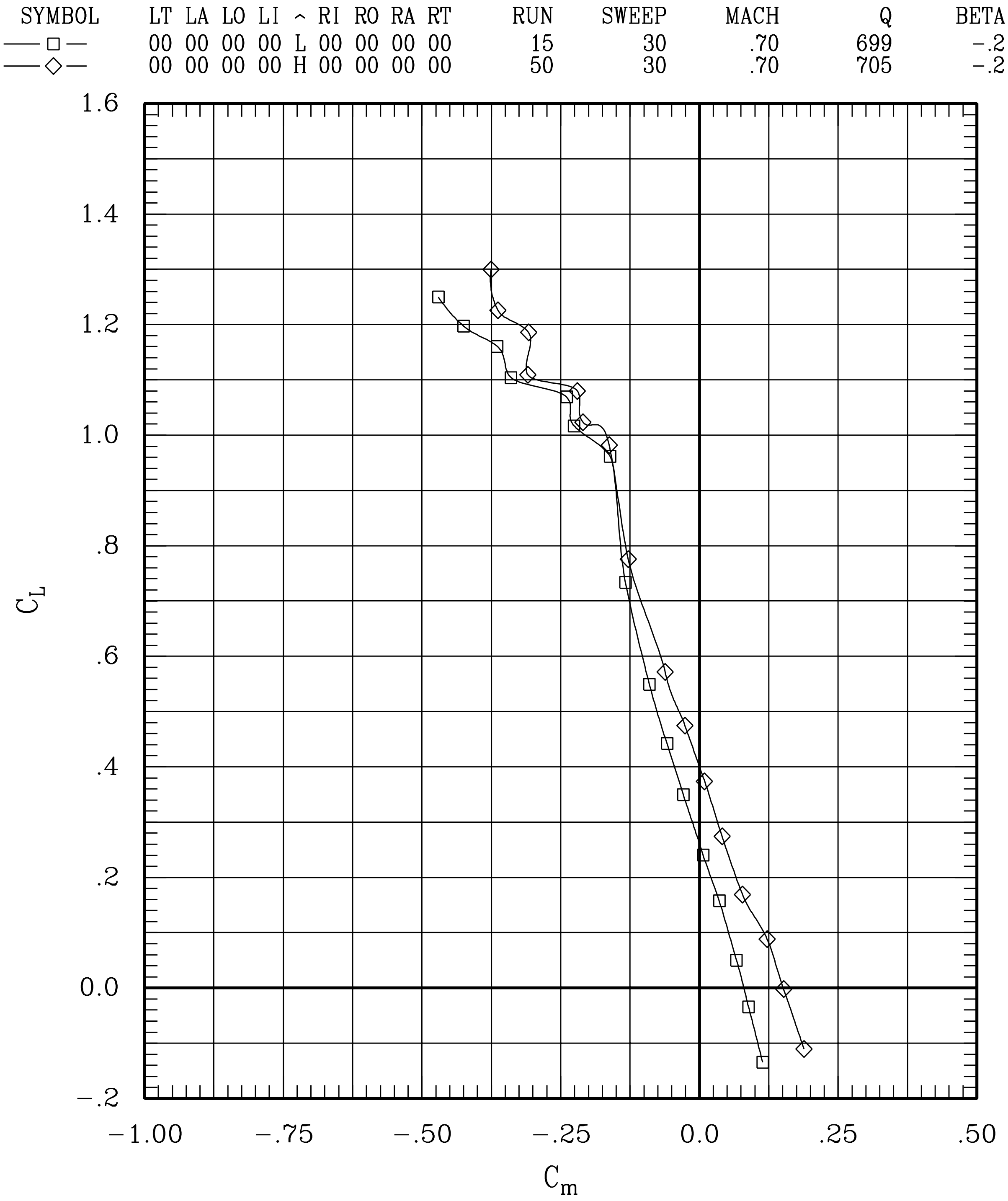

Figure 6(e). Effect of pivot height and fairing for sweep = 30 deg, Mach = 0.70.

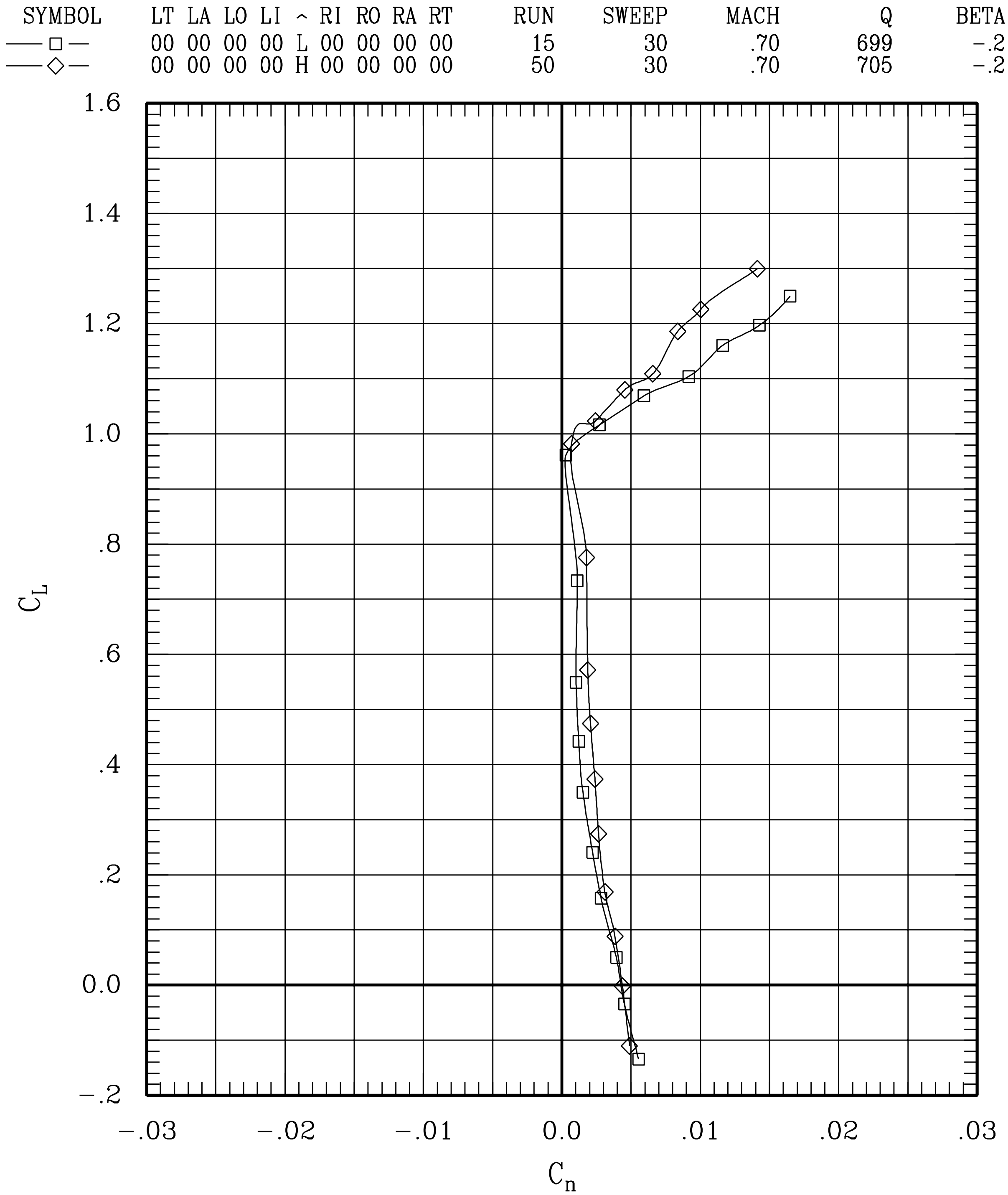

Figure 6(e). Effect of pivot height and fairing for sweep = 30 deg, Mach = 0.70.

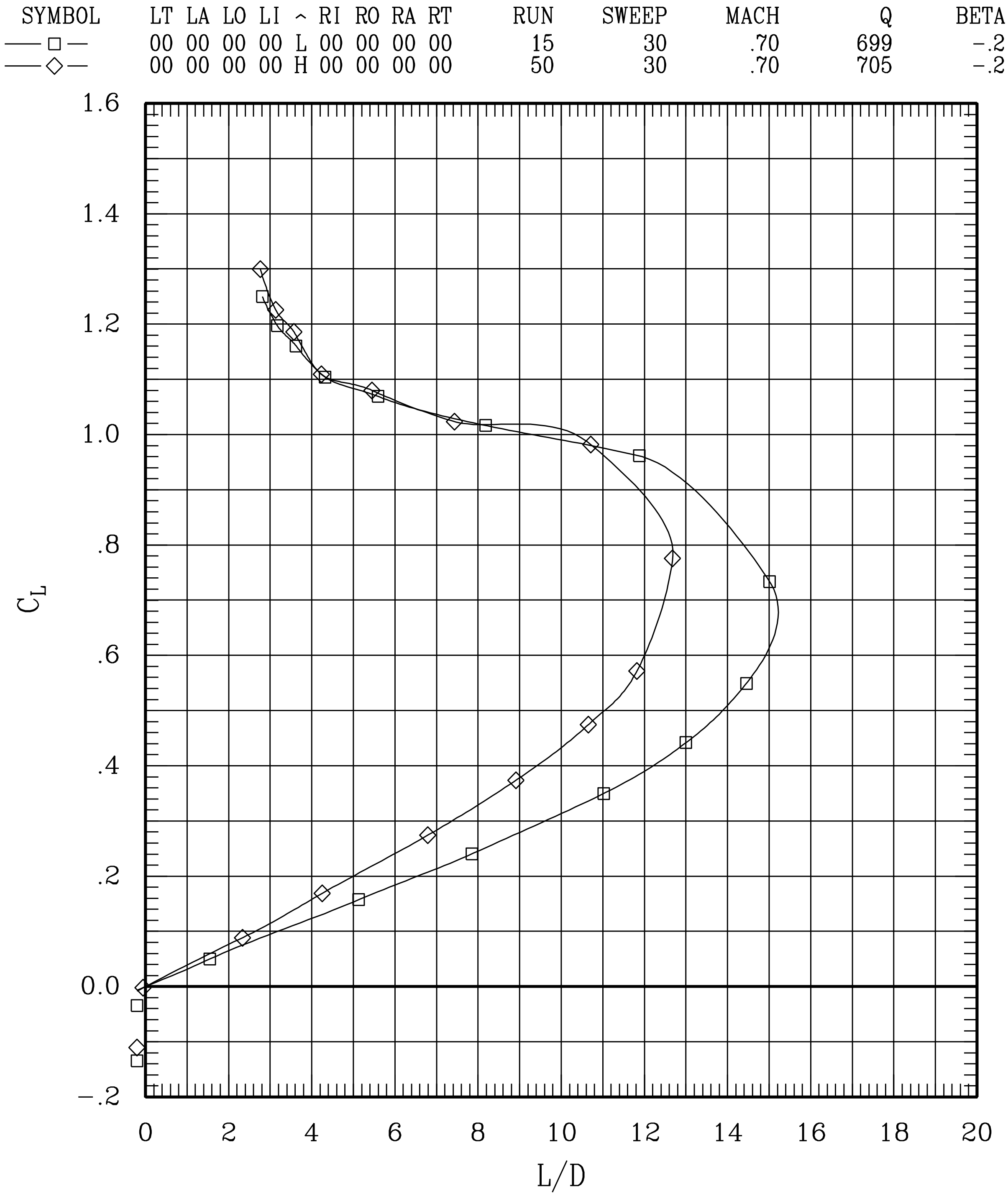

Figure 6(e). Effect of pivot height and fairing for sweep = 30 deg, Mach = 0.70.

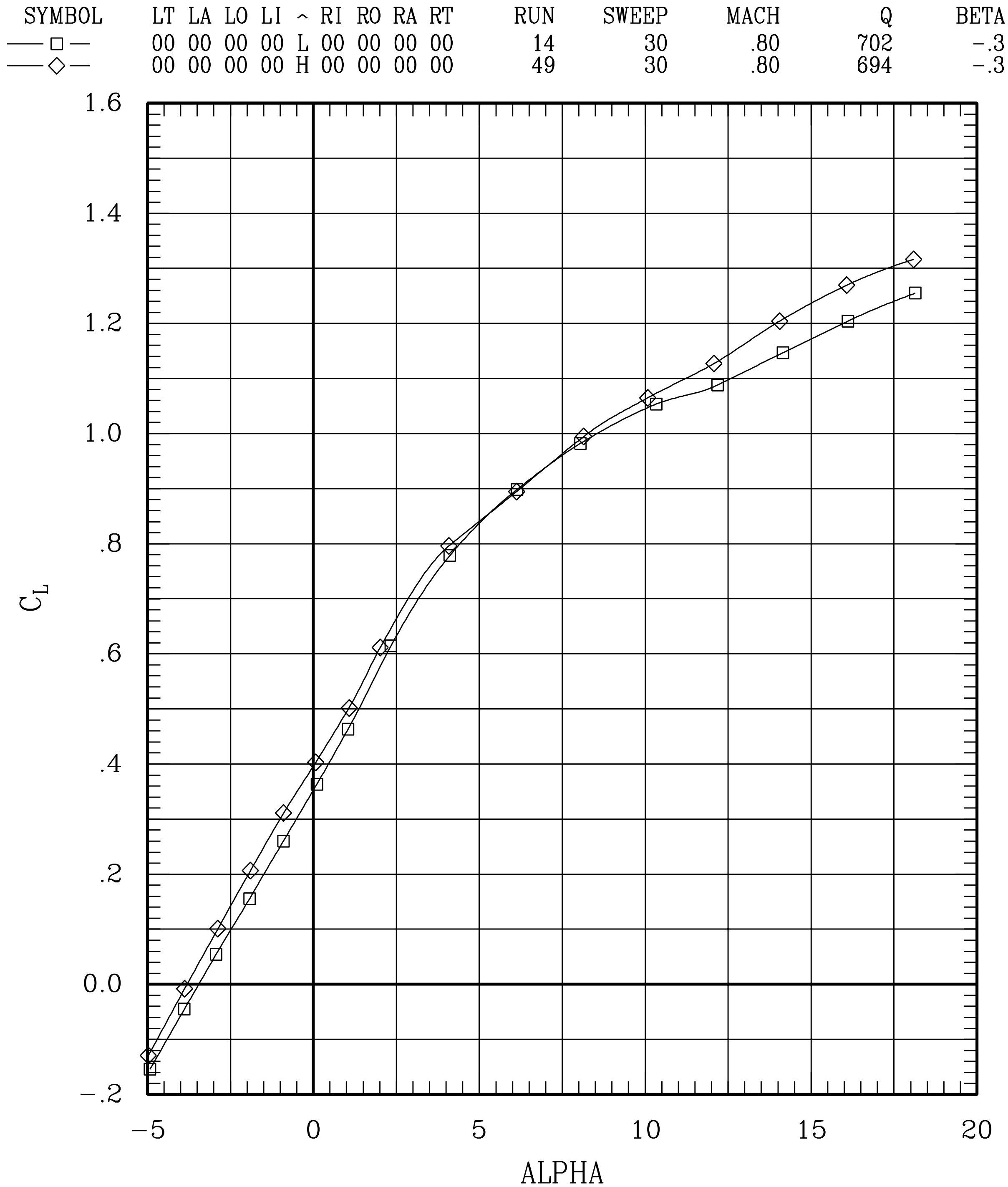

Figure 6(f). Effect of pivot height and fairing for sweep = 30 deg, Mach = 0.80.

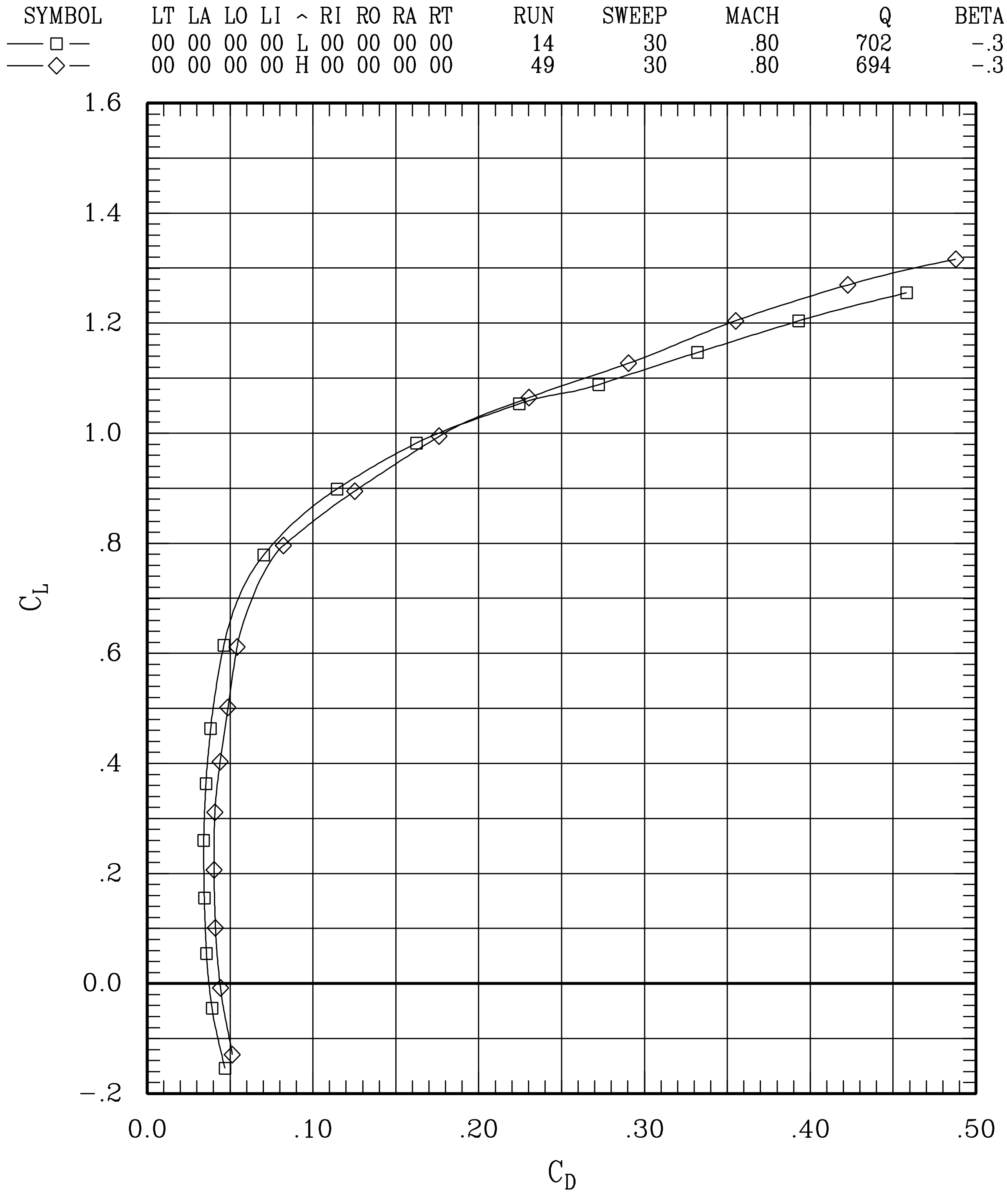

Figure 6(f). Effect of pivot height and fairing for sweep = 30 deg, Mach = 0.80.

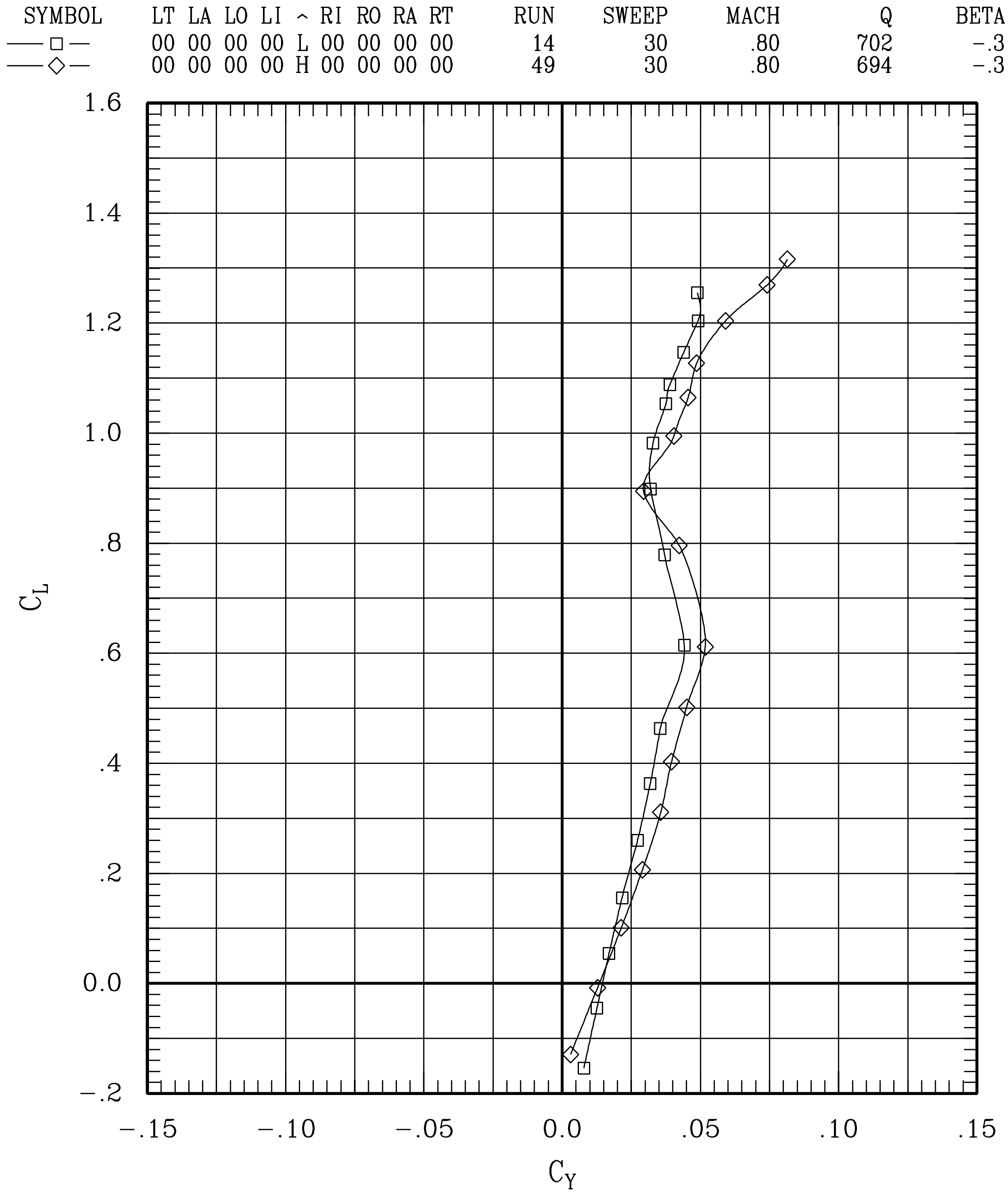

Figure 6(f). Effect of pivot height and fairing for sweep = 30 deg, Mach = 0.80.

SYMBOL	LT LA LO LI ^ RI RO RA RT	RUN	SWEEP	MACH	Q	BETA
—□—	00 00 00 00 L 00 00 00 00	14	30	.80	702	−.3
—◇—	00 00 00 00 H 00 00 00 00	49	30	.80	694	−.3

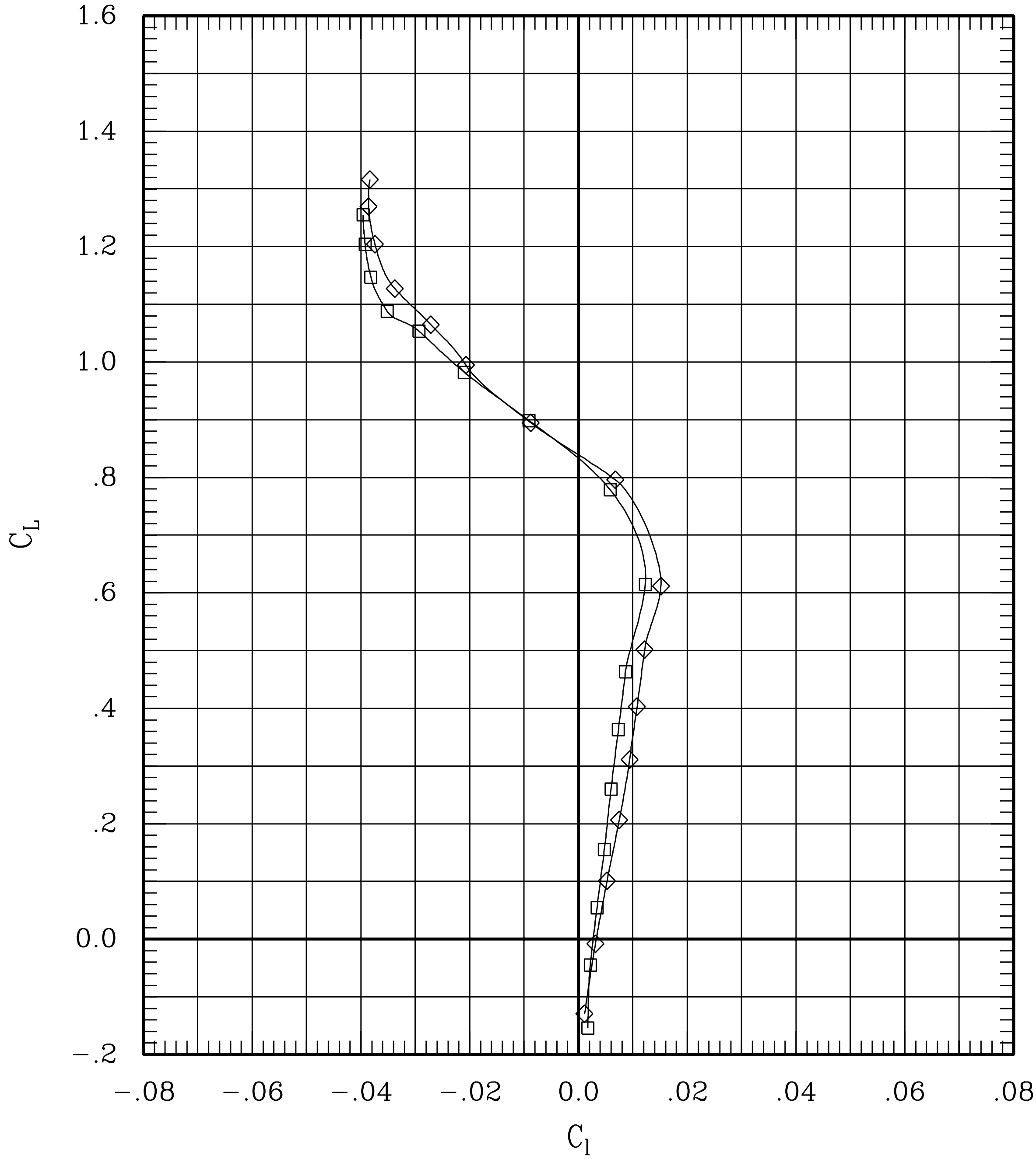

Figure 6(f). Effect of pivot height and fairing for sweep = 30 deg, Mach = 0.80.

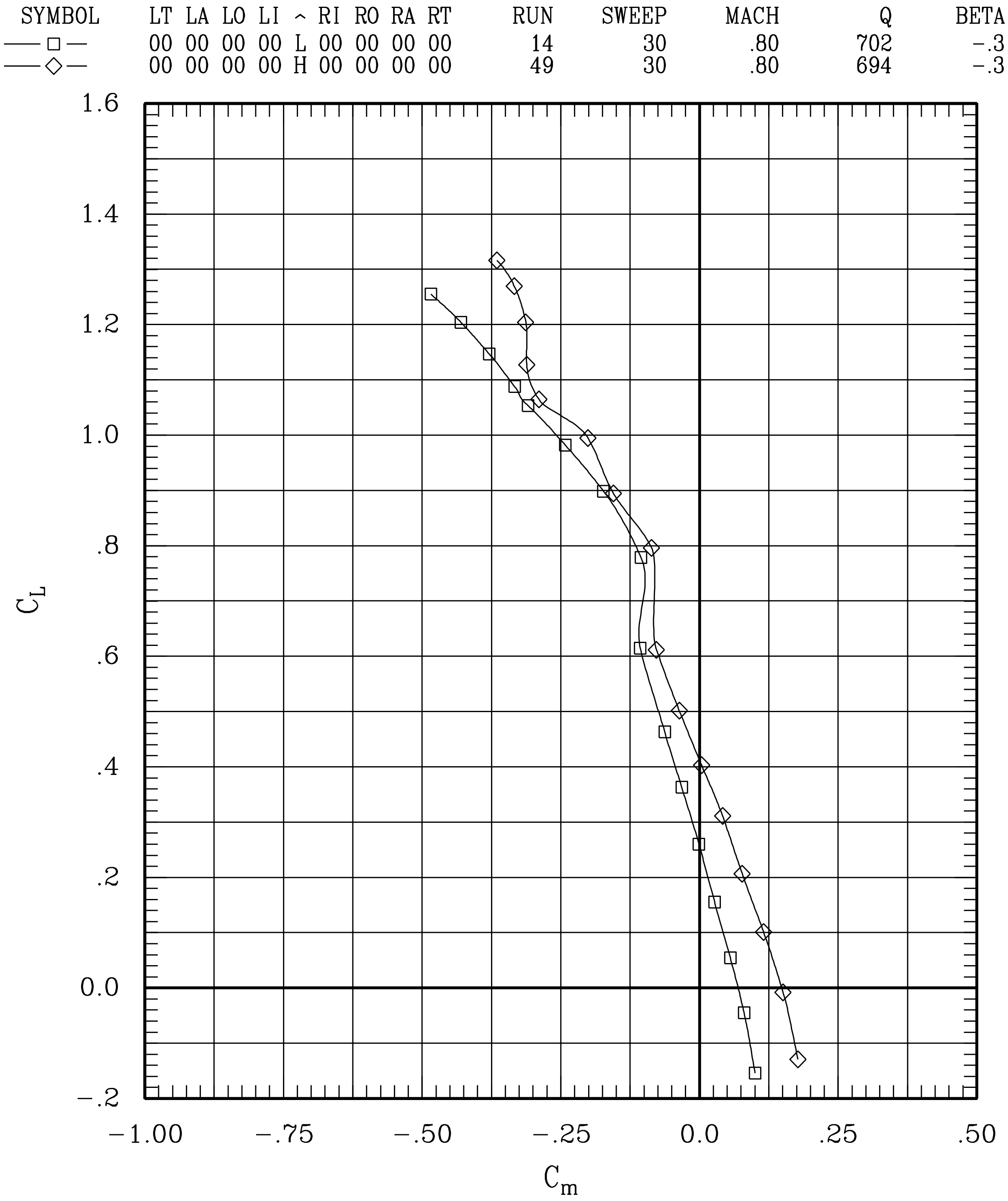

Figure 6(f). Effect of pivot height and fairing for sweep = 30 deg, Mach = 0.80.

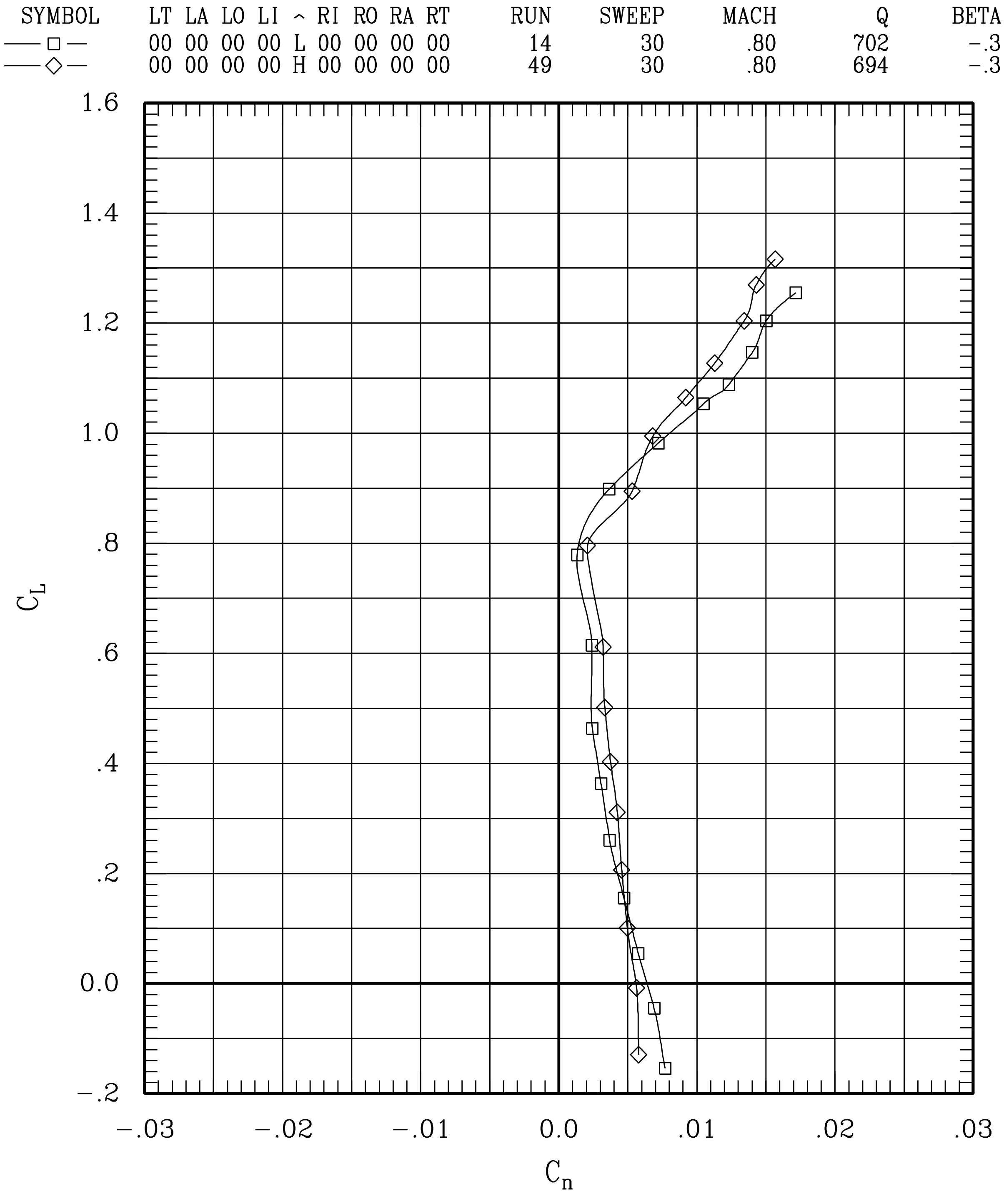

Figure 6(f). Effect of pivot height and fairing for sweep = 30 deg, Mach = 0.80.

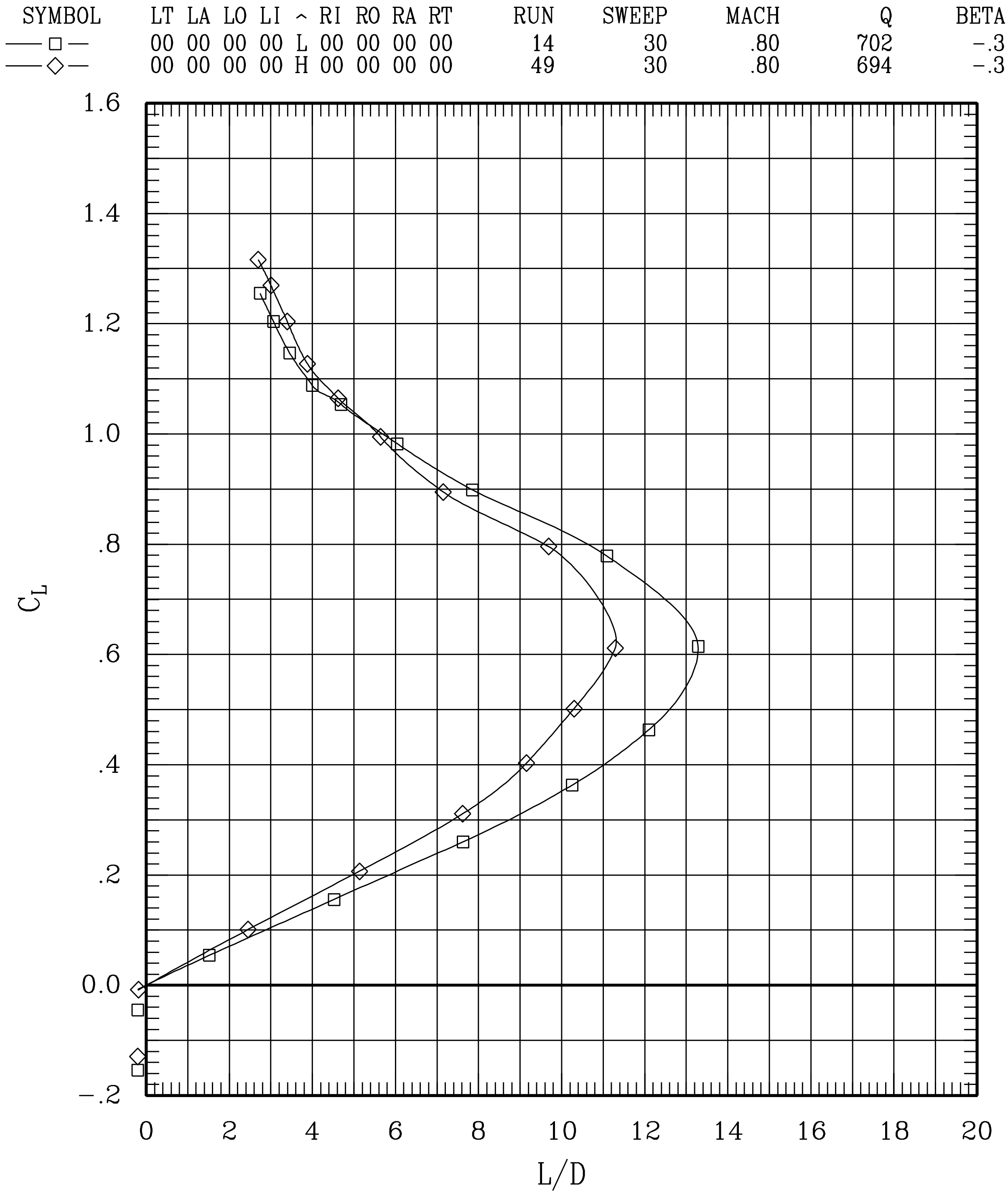

Figure 6(f). Effect of pivot height and fairing for sweep = 30 deg, Mach = 0.80.

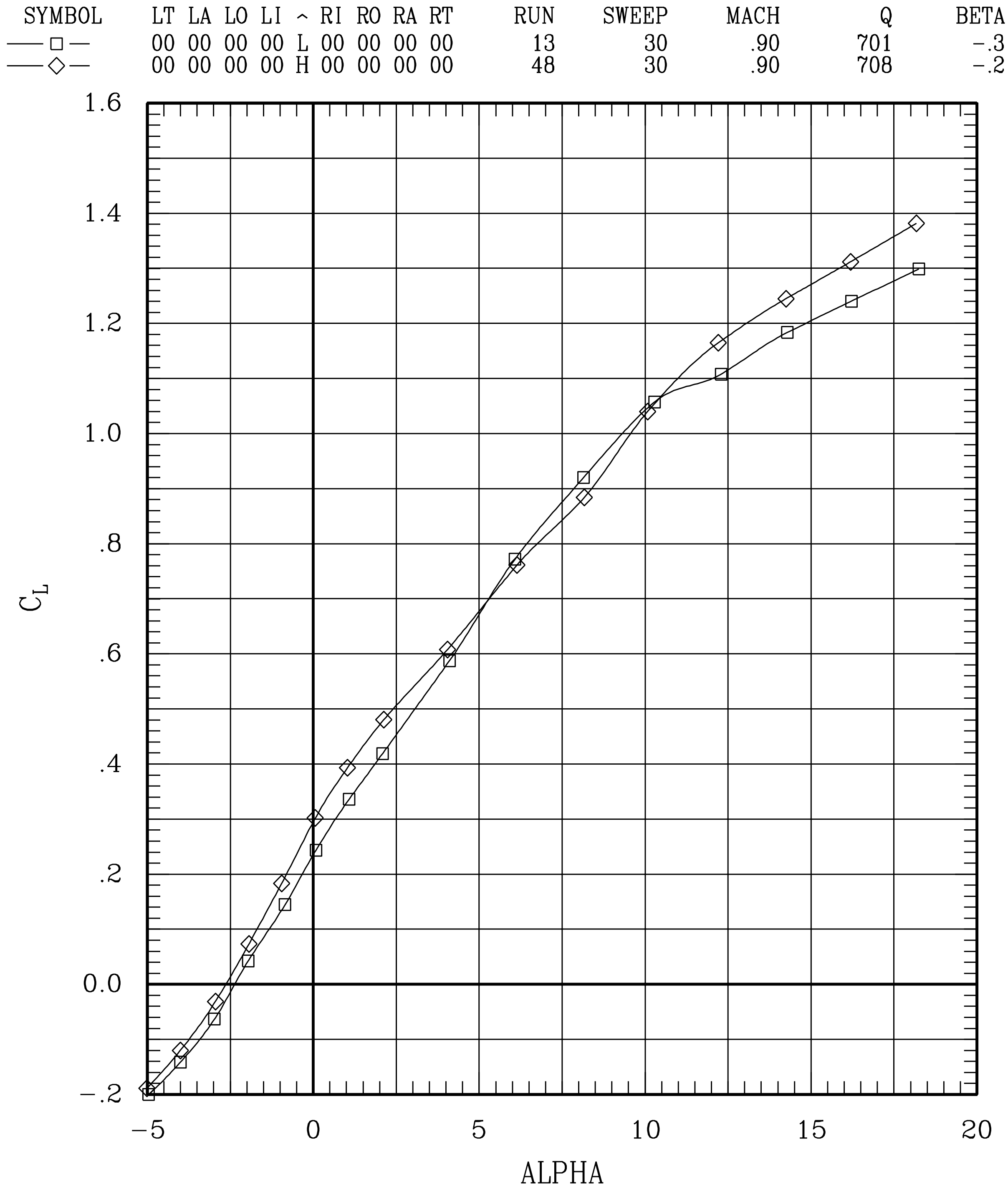

Figure 6(g). Effect of pivot height and fairing for sweep = 30 deg, Mach = 0.90.

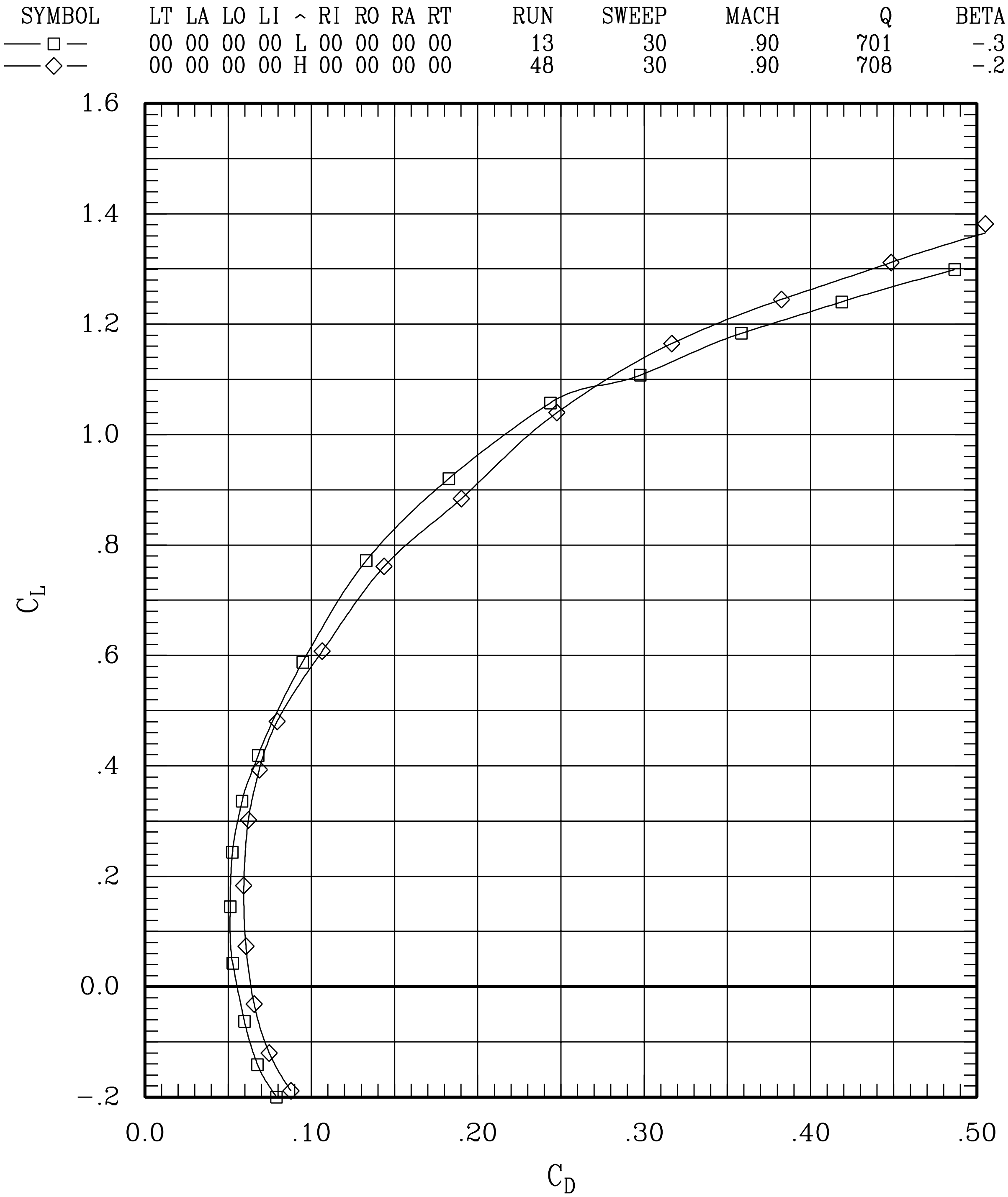

Figure 6(g). Effect of pivot height and fairing for sweep = 30 deg, Mach = 0.90.

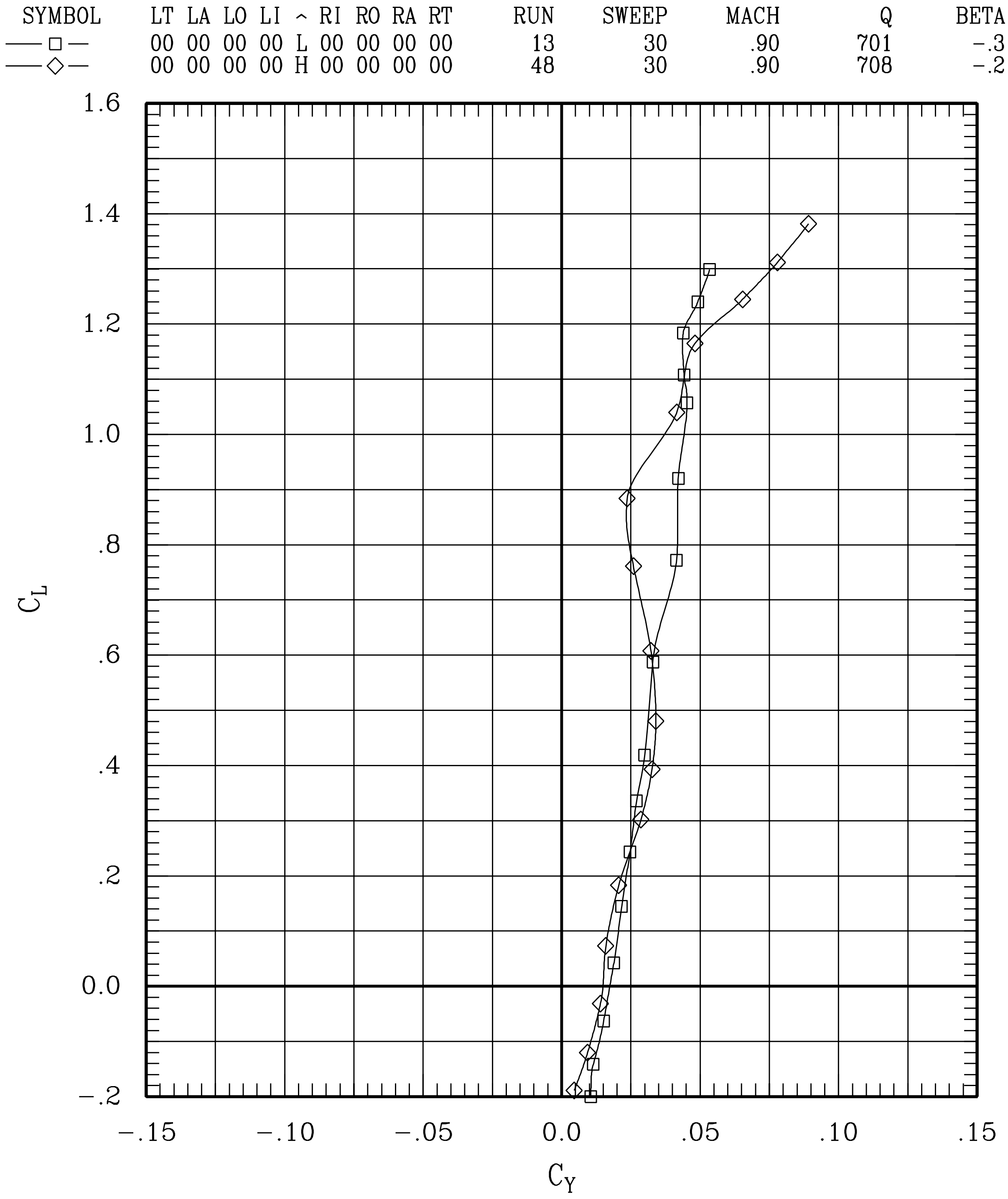

Figure 6(g). Effect of pivot height and fairing for sweep = 30 deg, Mach = 0.90.

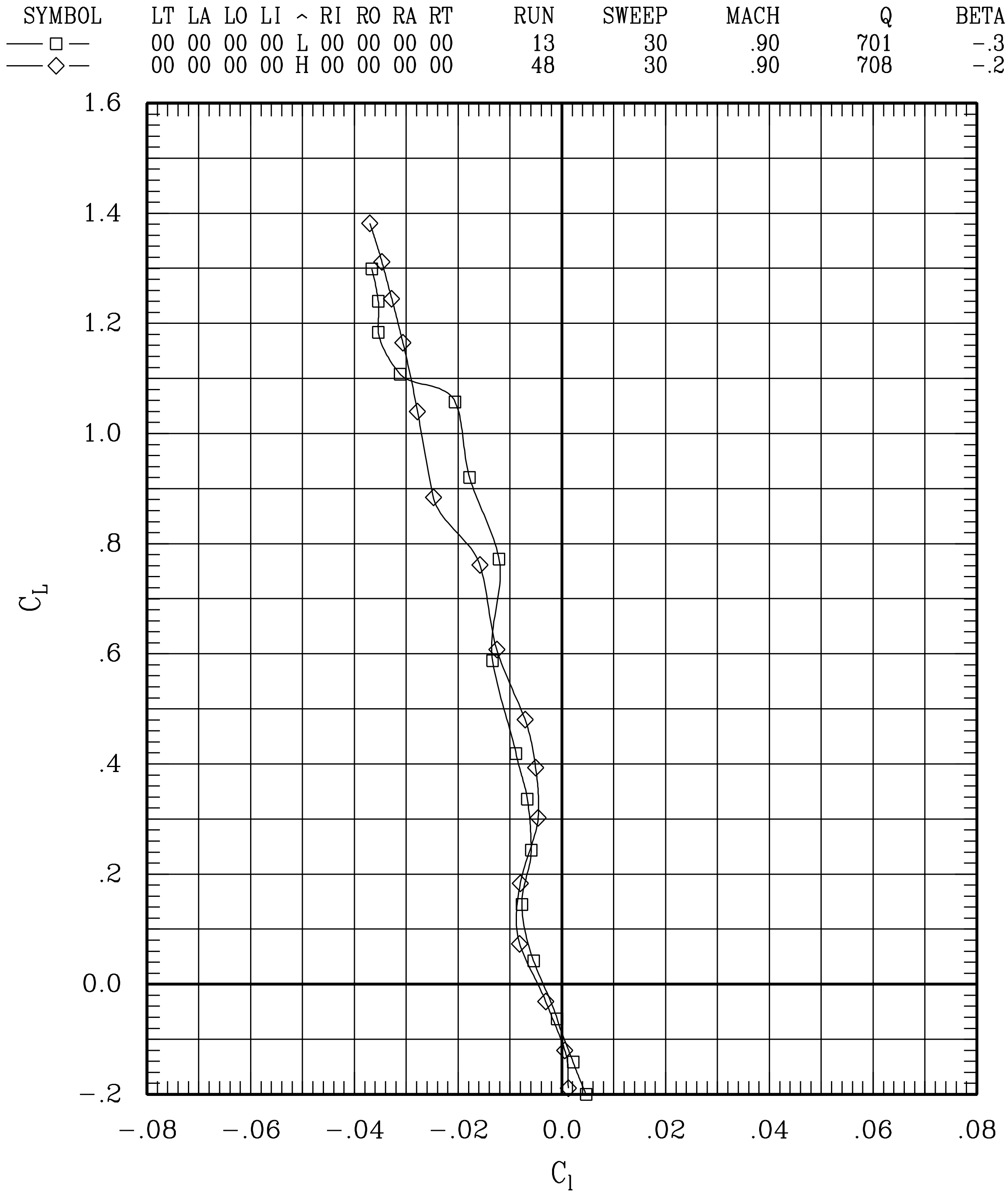

Figure 6(g). Effect of pivot height and fairing for sweep = 30 deg, Mach = 0.90.

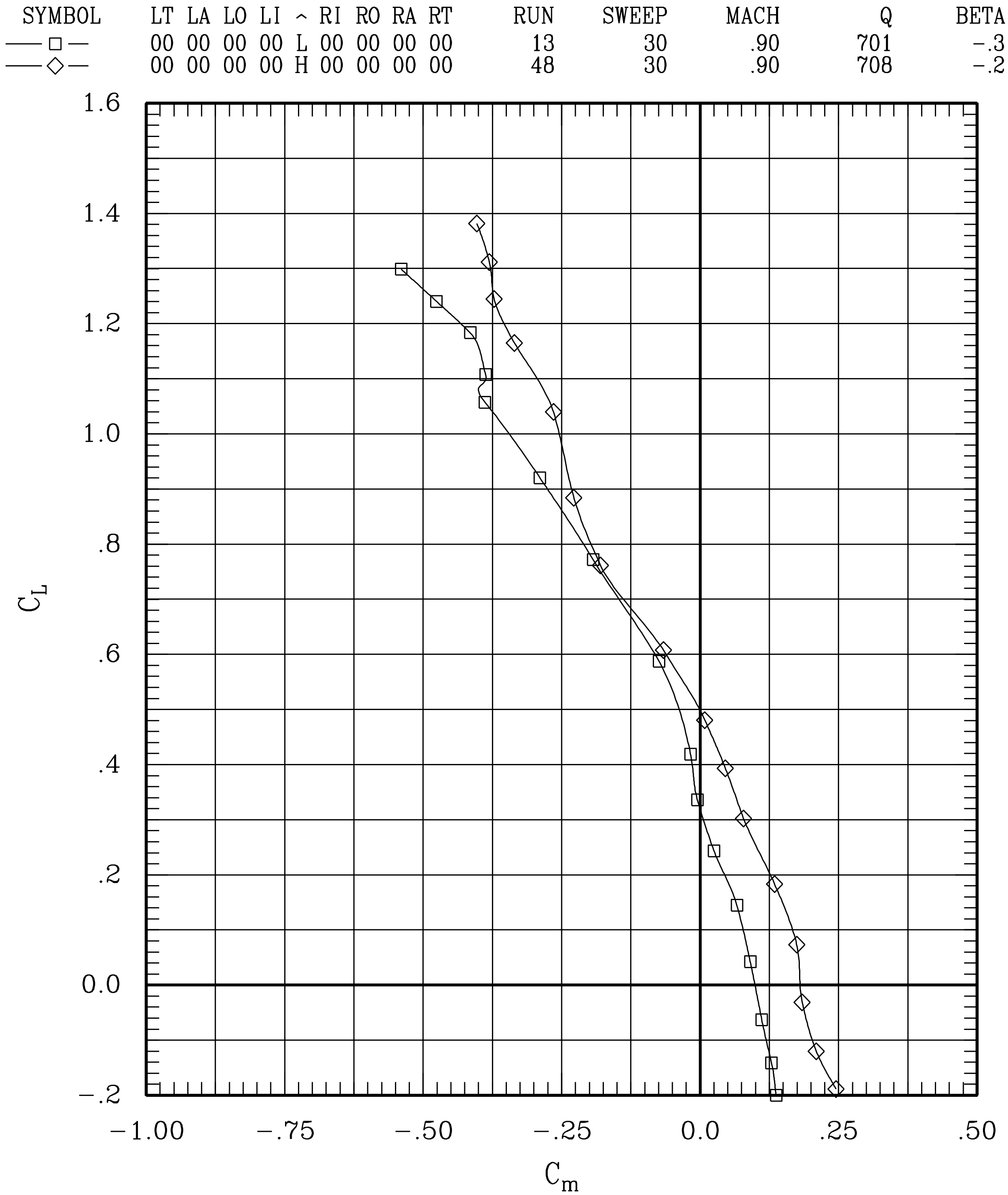

Figure 6(g). Effect of pivot height and fairing for sweep = 30 deg, Mach = 0.90.

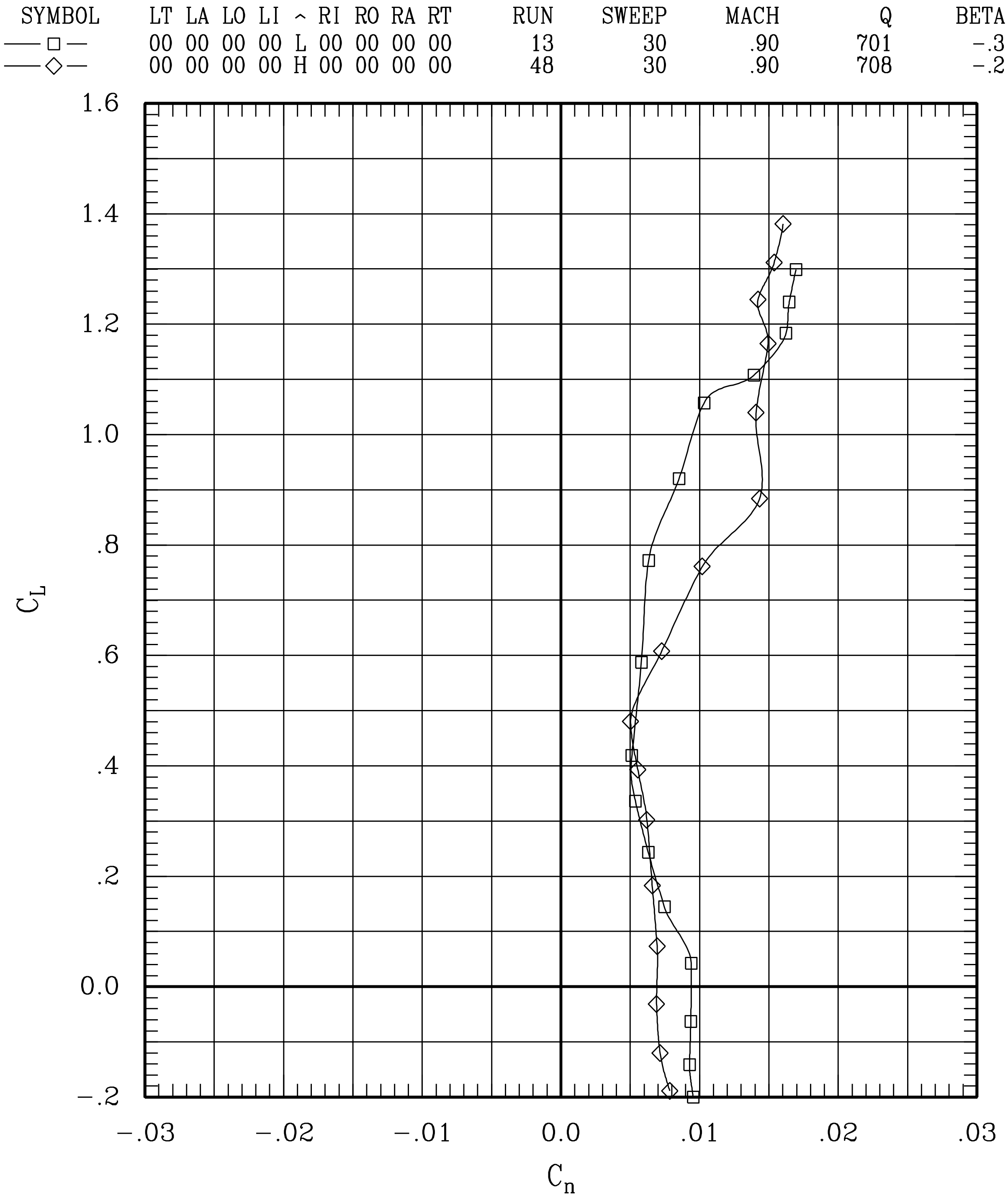

Figure 6(g). Effect of pivot height and fairing for sweep = 30 deg, Mach = 0.90.

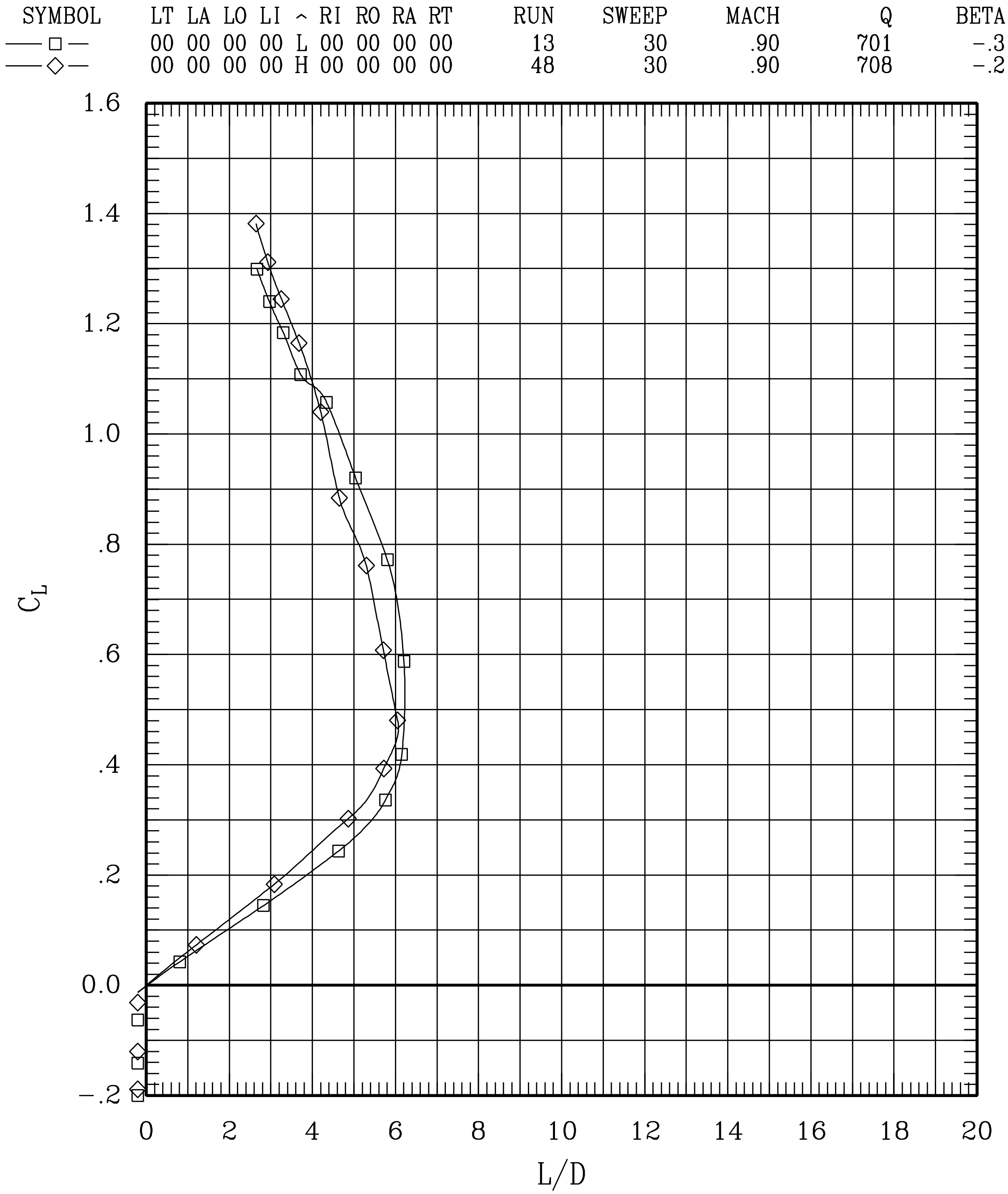

Figure 6(g). Effect of pivot height and fairing for sweep = 30 deg, Mach = 0.90.

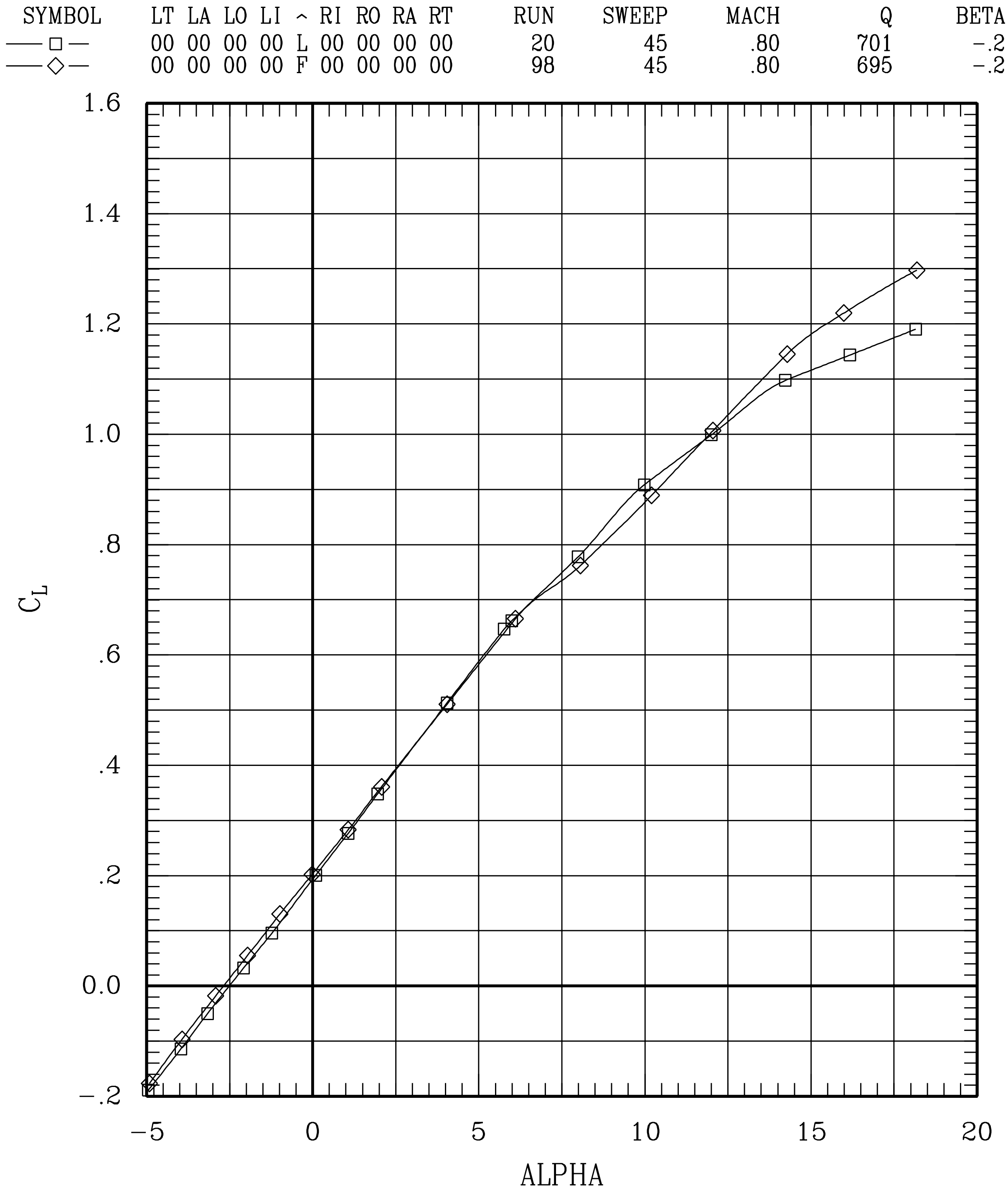

Figure 6(h). Effect of pivot height and fairing for sweep = 45 deg, Mach = 0.80.

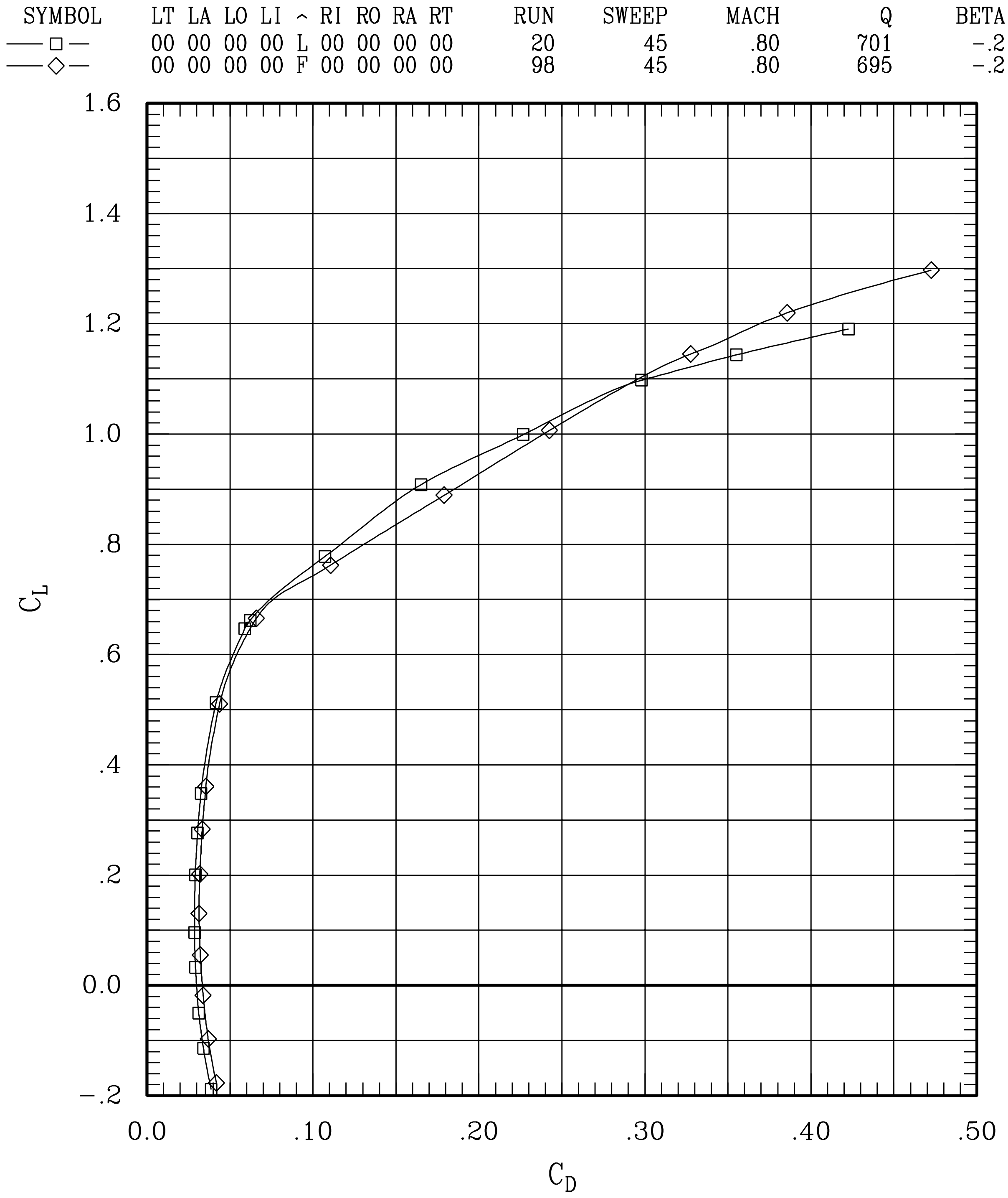

Figure 6(h). Effect of pivot height and fairing for sweep = 45 deg, Mach = 0.80.

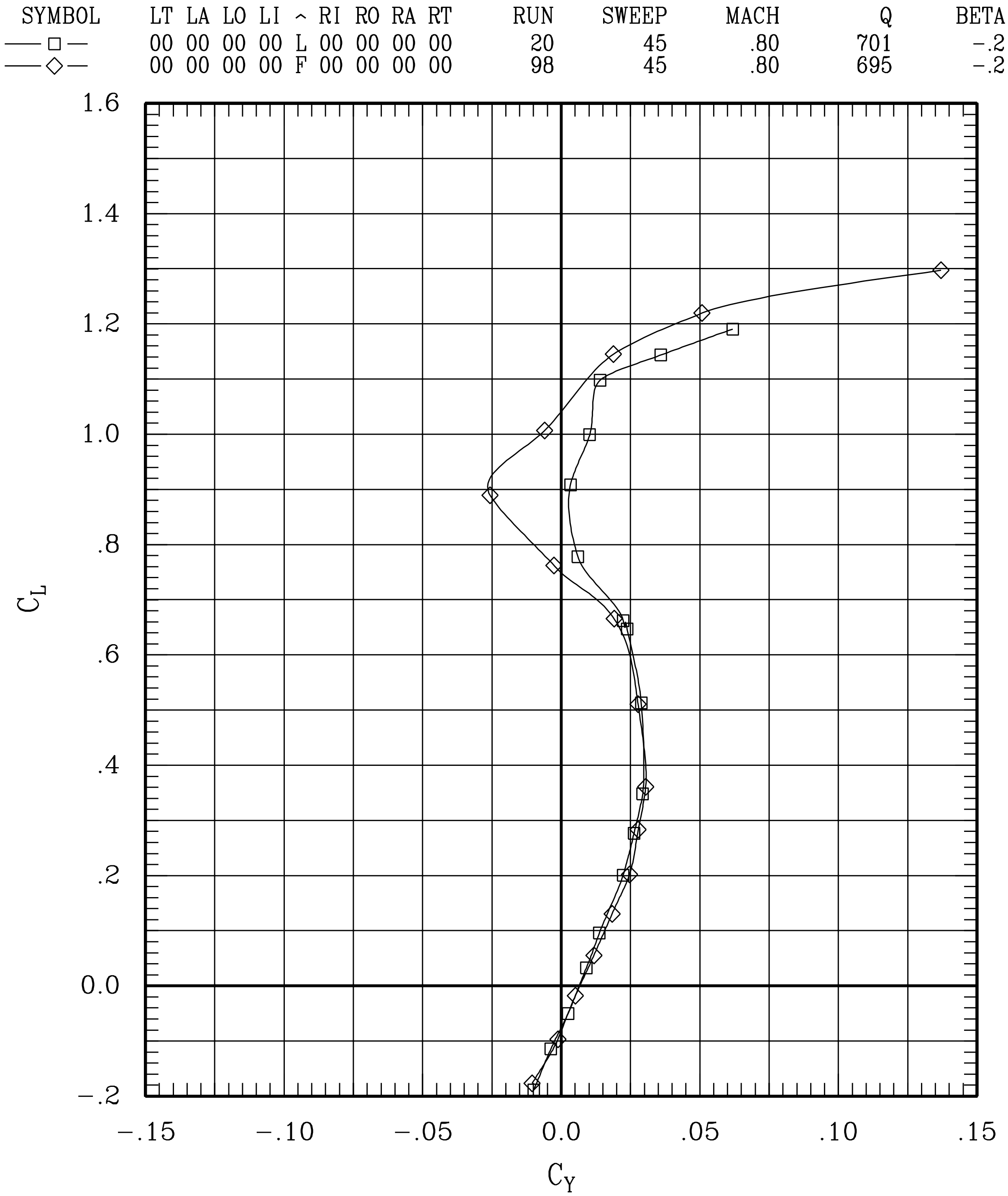

Figure 6(h). Effect of pivot height and fairing for sweep = 45 deg, Mach = 0.80.

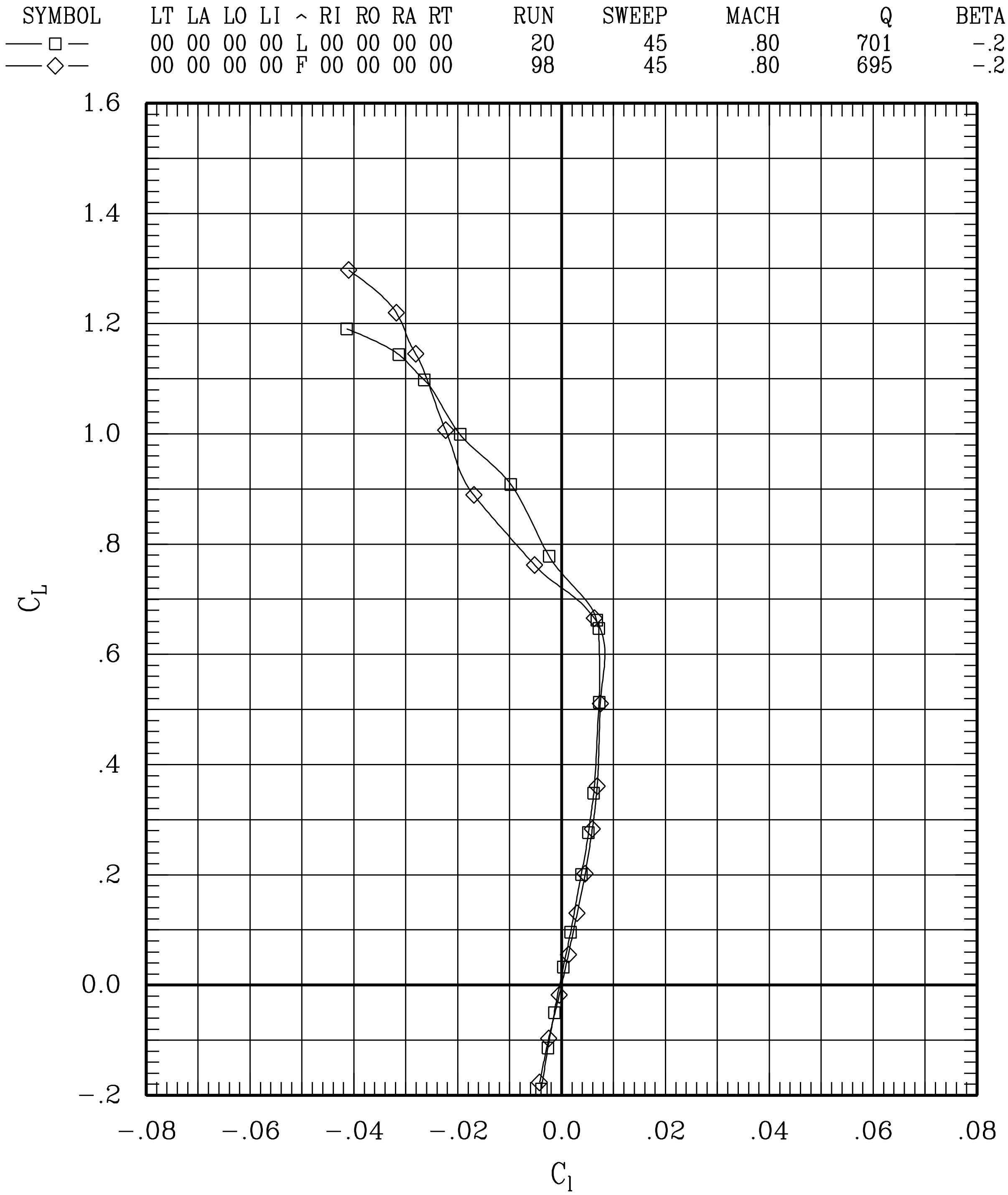

Figure 6(h). Effect of pivot height and fairing for sweep = 45 deg, Mach = 0.80.

SYMBOL	LT LA LO LI ^ RI RO RA RT	RUN	SWEEP	MACH	Q	BETA
—□—	00 00 00 00 L 00 00 00 00	20	45	.80	701	-.2
—◇—	00 00 00 00 F 00 00 00 00	98	45	.80	695	-.2

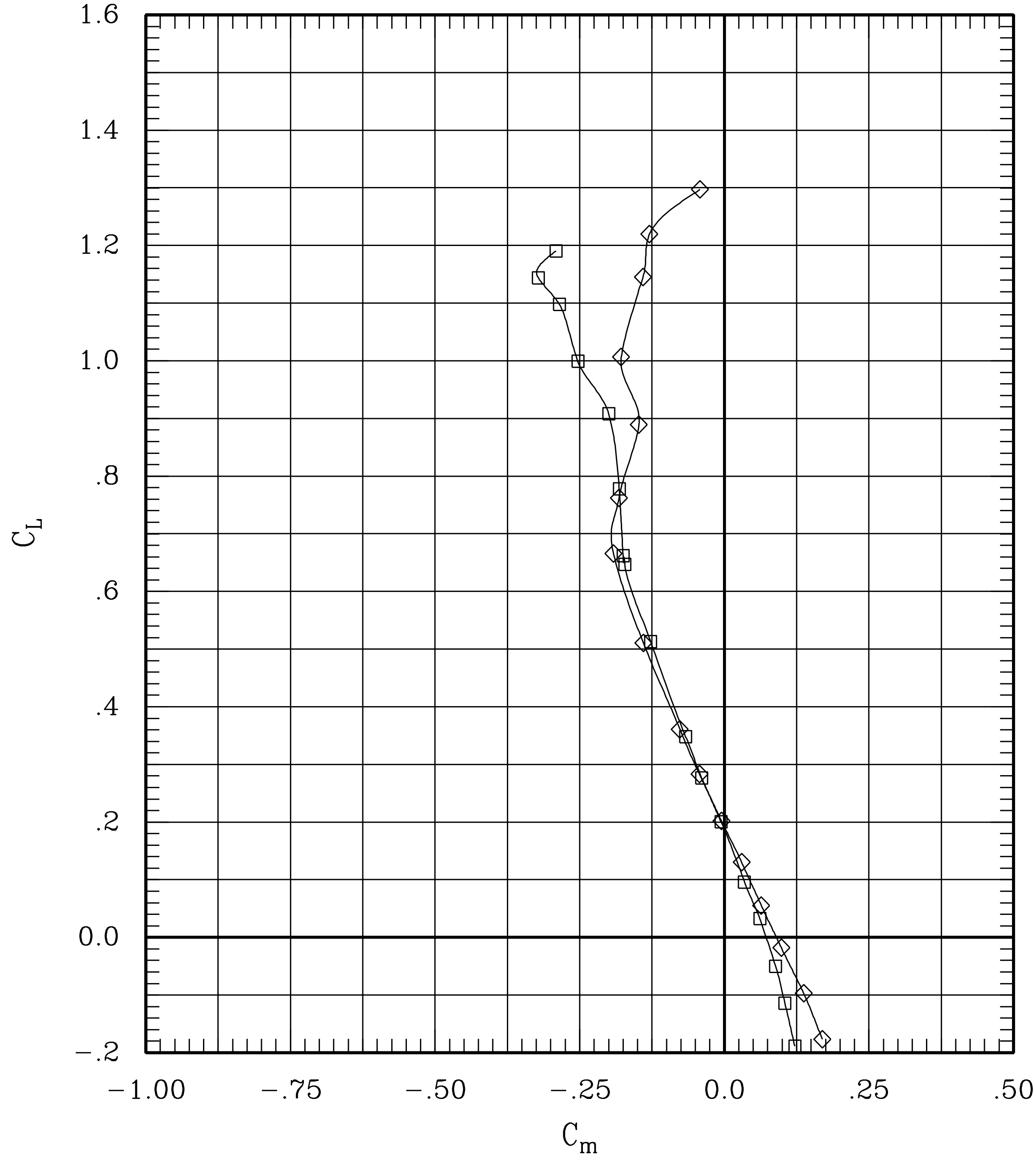

Figure 6(h). Effect of pivot height and fairing for sweep = 45 deg, Mach = 0.80.

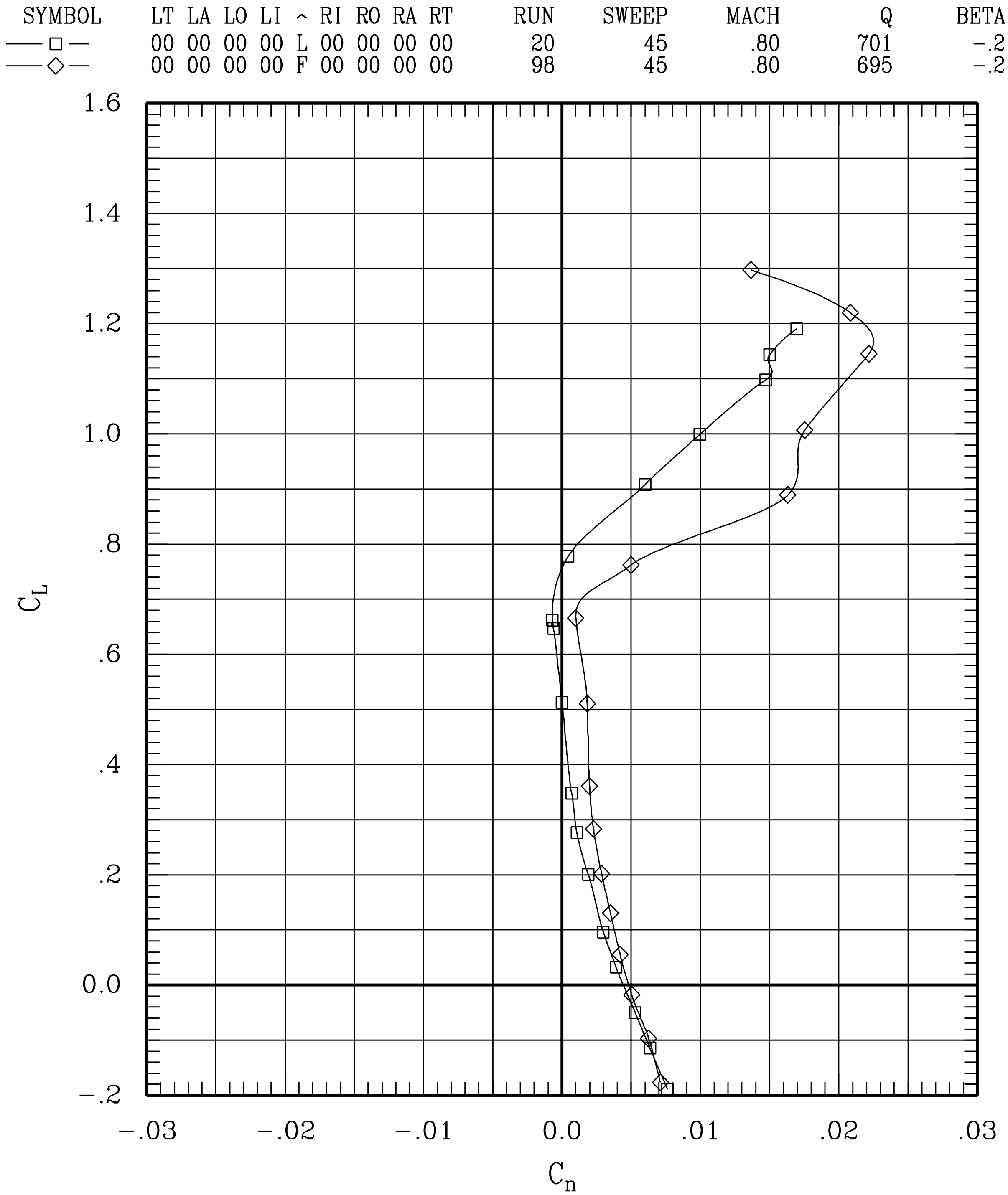

Figure 6(h). Effect of pivot height and fairing for sweep = 45 deg, Mach = 0.80.

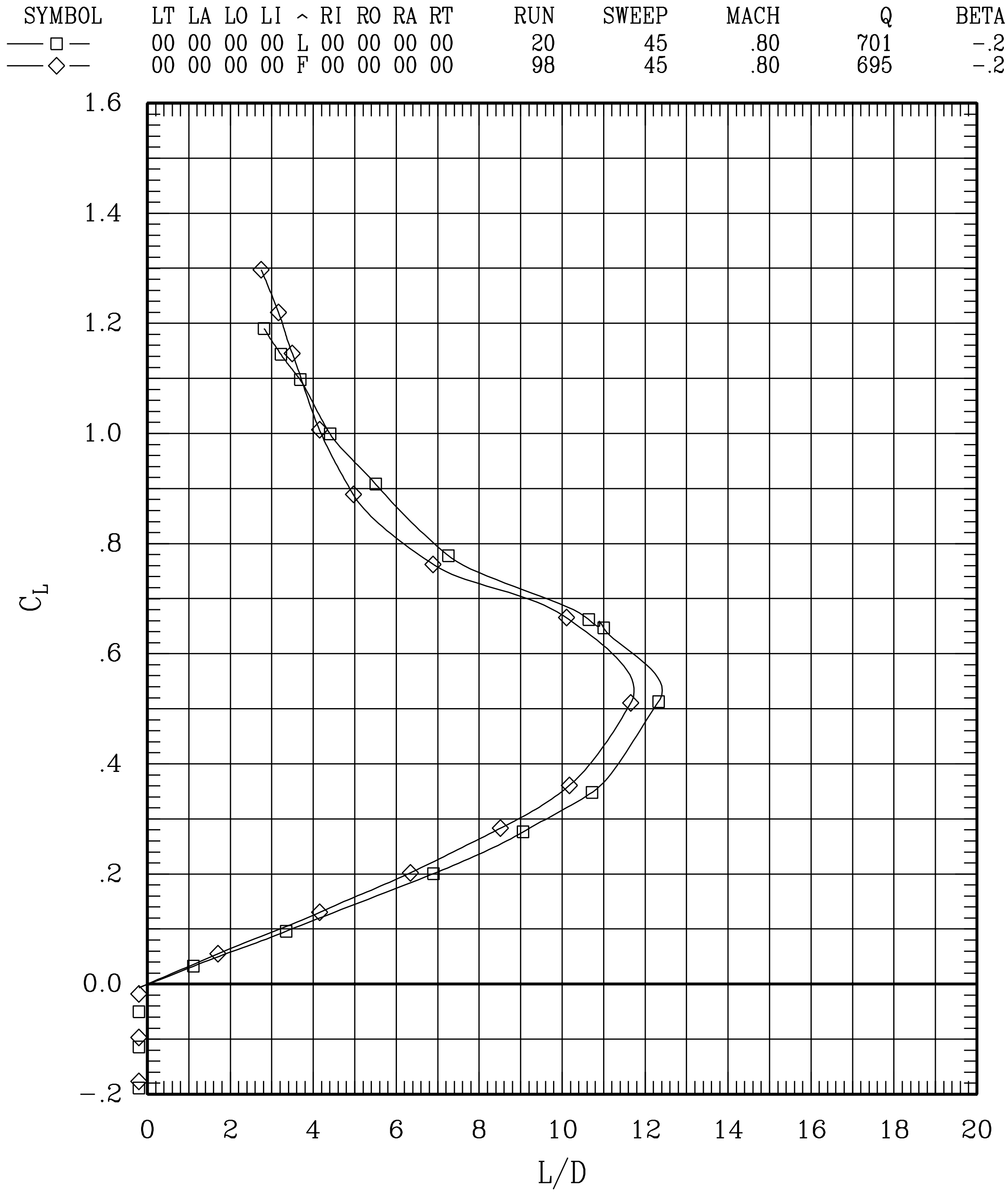

Figure 6(h). Effect of pivot height and fairing for sweep = 45 deg, Mach = 0.80.

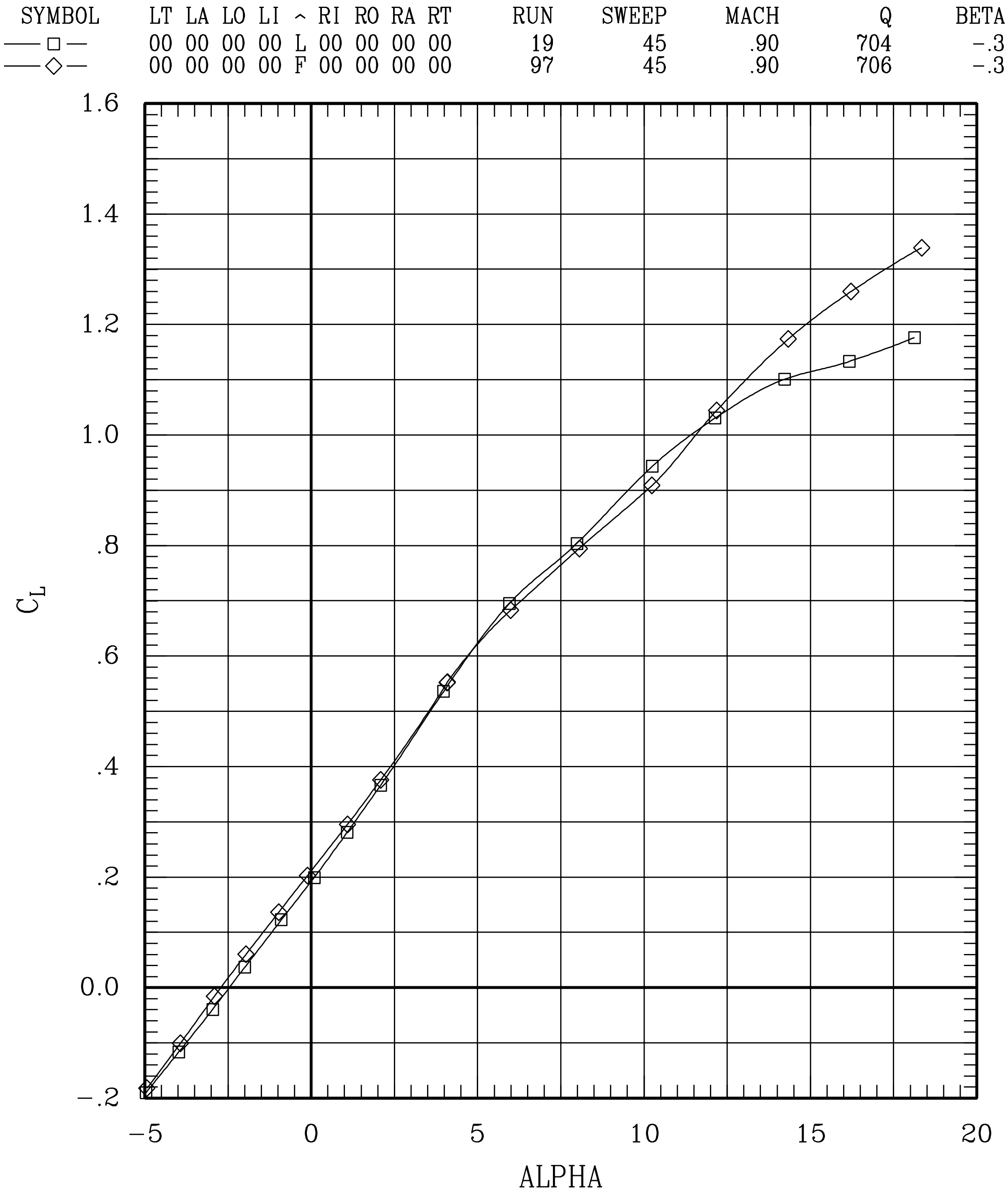

Figure 6(i). Effect of pivot height and fairing for sweep = 45 deg, Mach = 0.90.

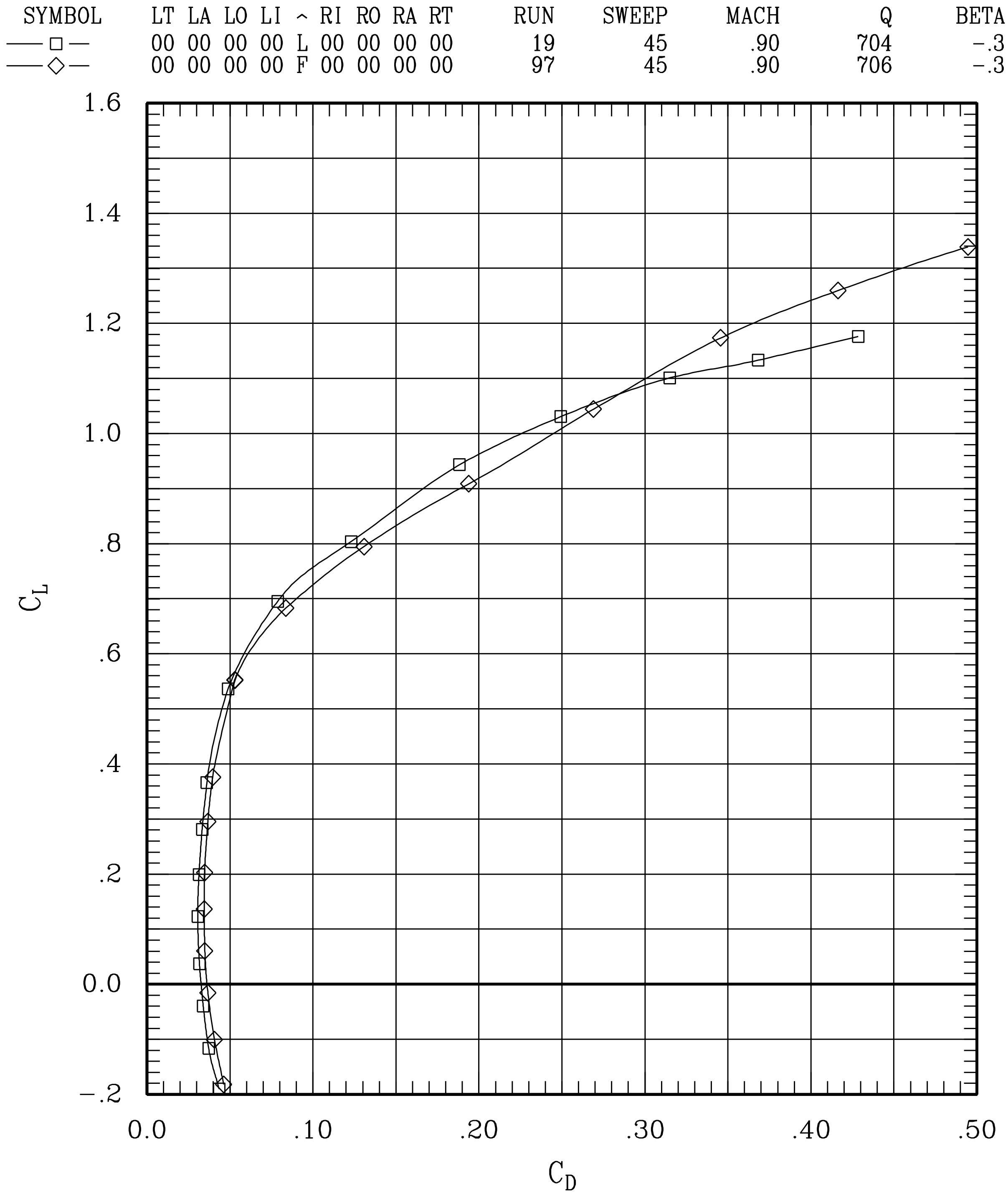

Figure 6(i). Effect of pivot height and fairing for sweep = 45 deg, Mach = 0.90.

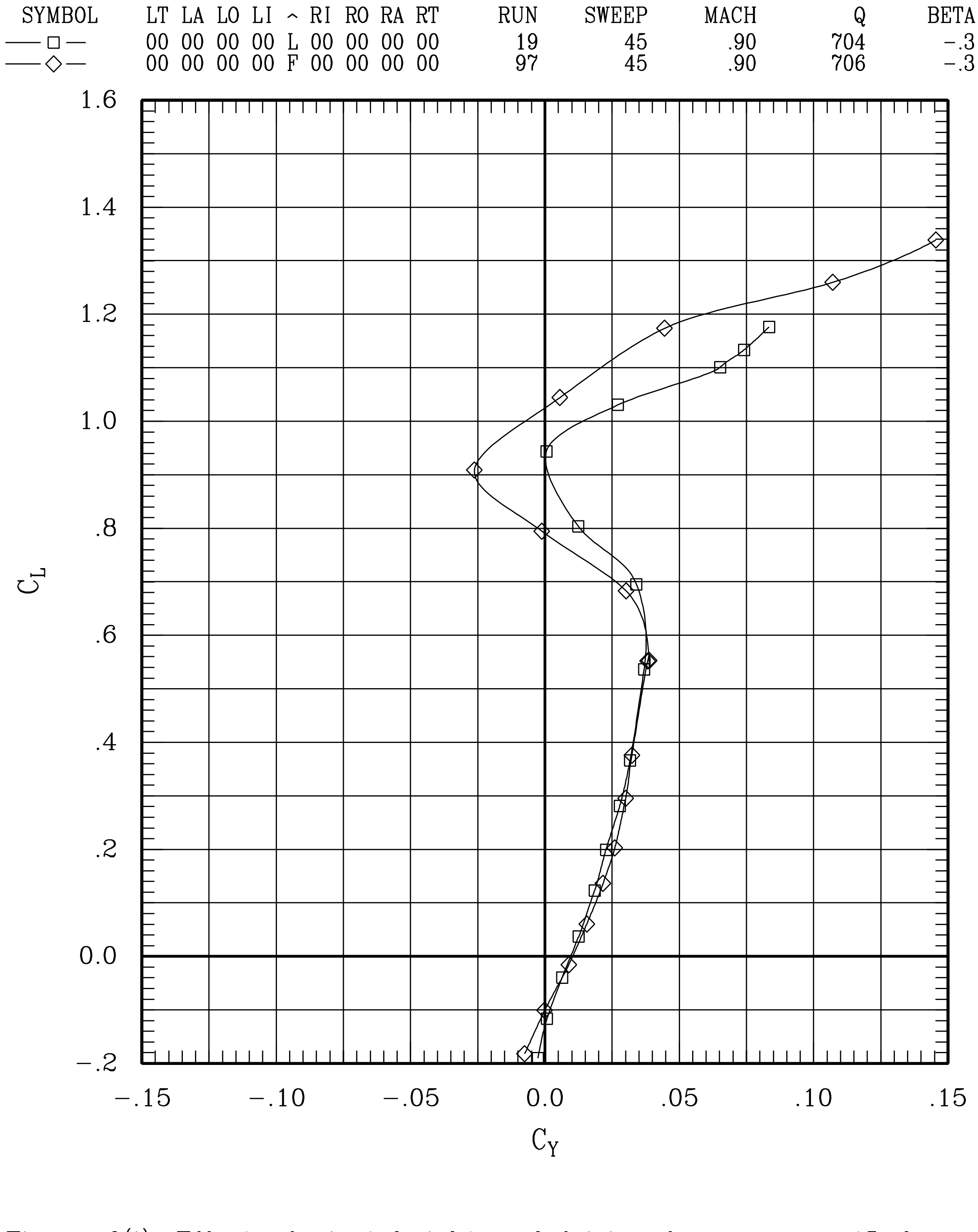

Figure 6(i). Effect of pivot height and fairing for sweep = 45 deg, Mach = 0.90.

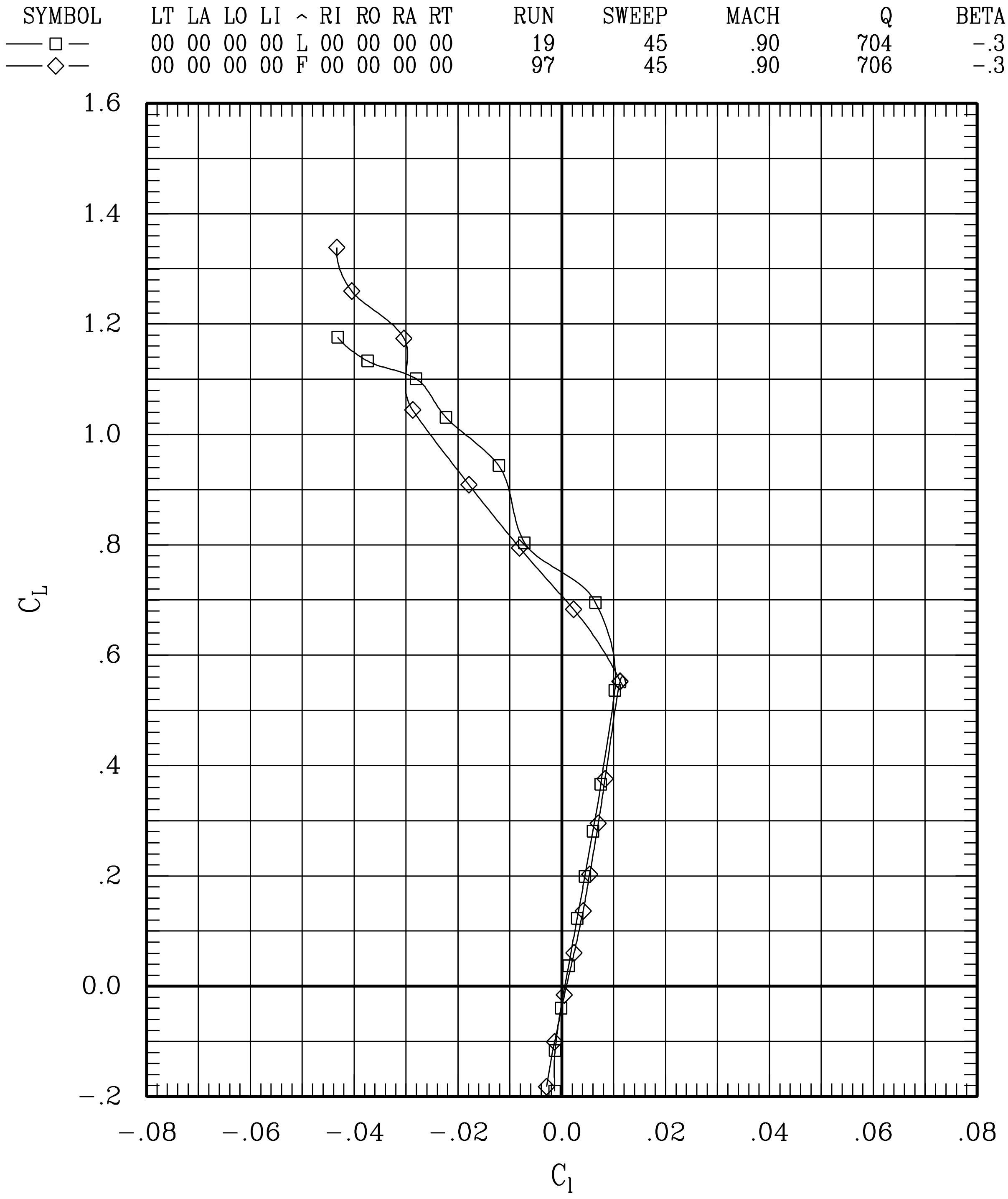

Figure 6(i). Effect of pivot height and fairing for sweep = 45 deg, Mach = 0.90.

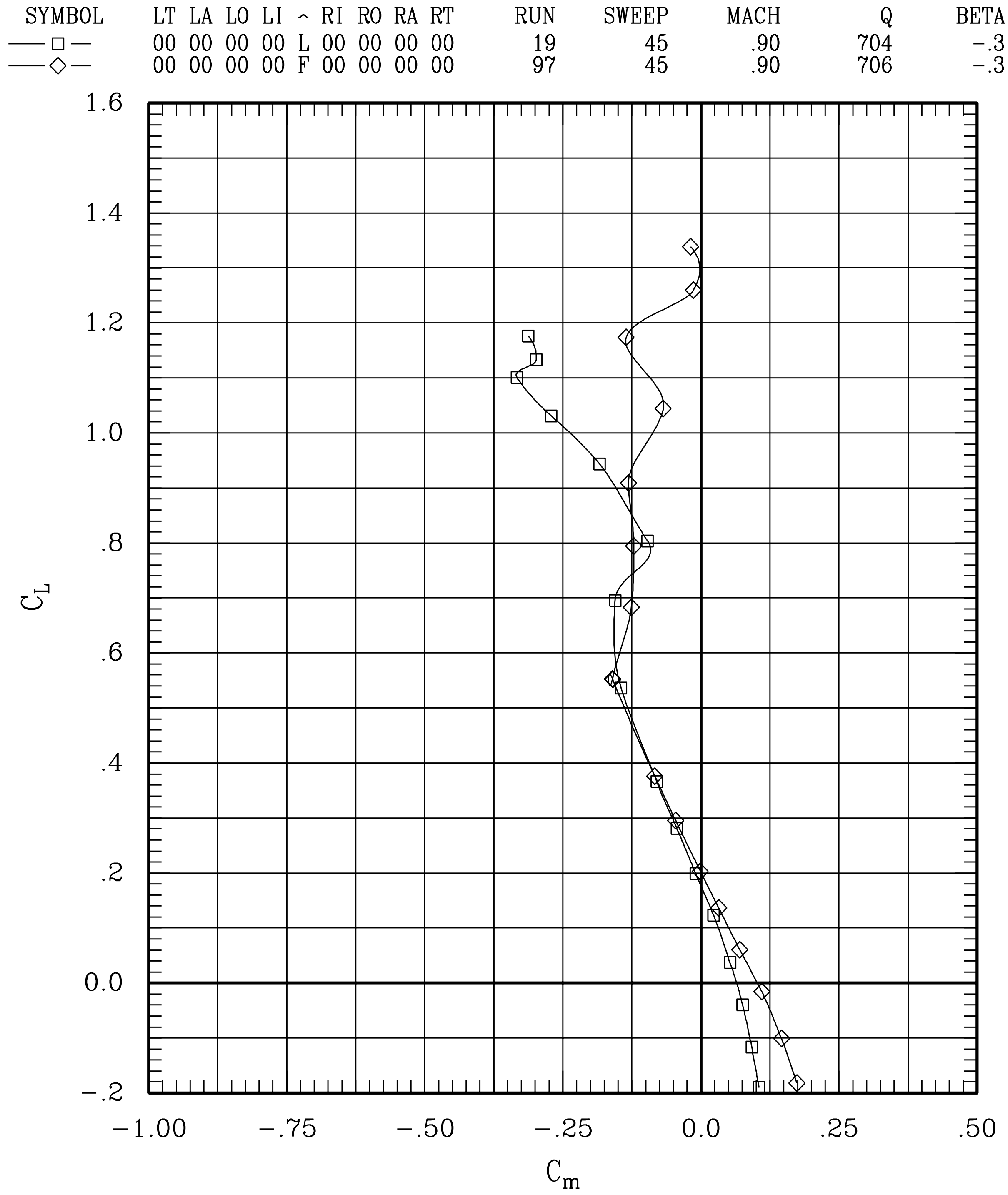

Figure 6(i). Effect of pivot height and fairing for sweep = 45 deg, Mach = 0.90.

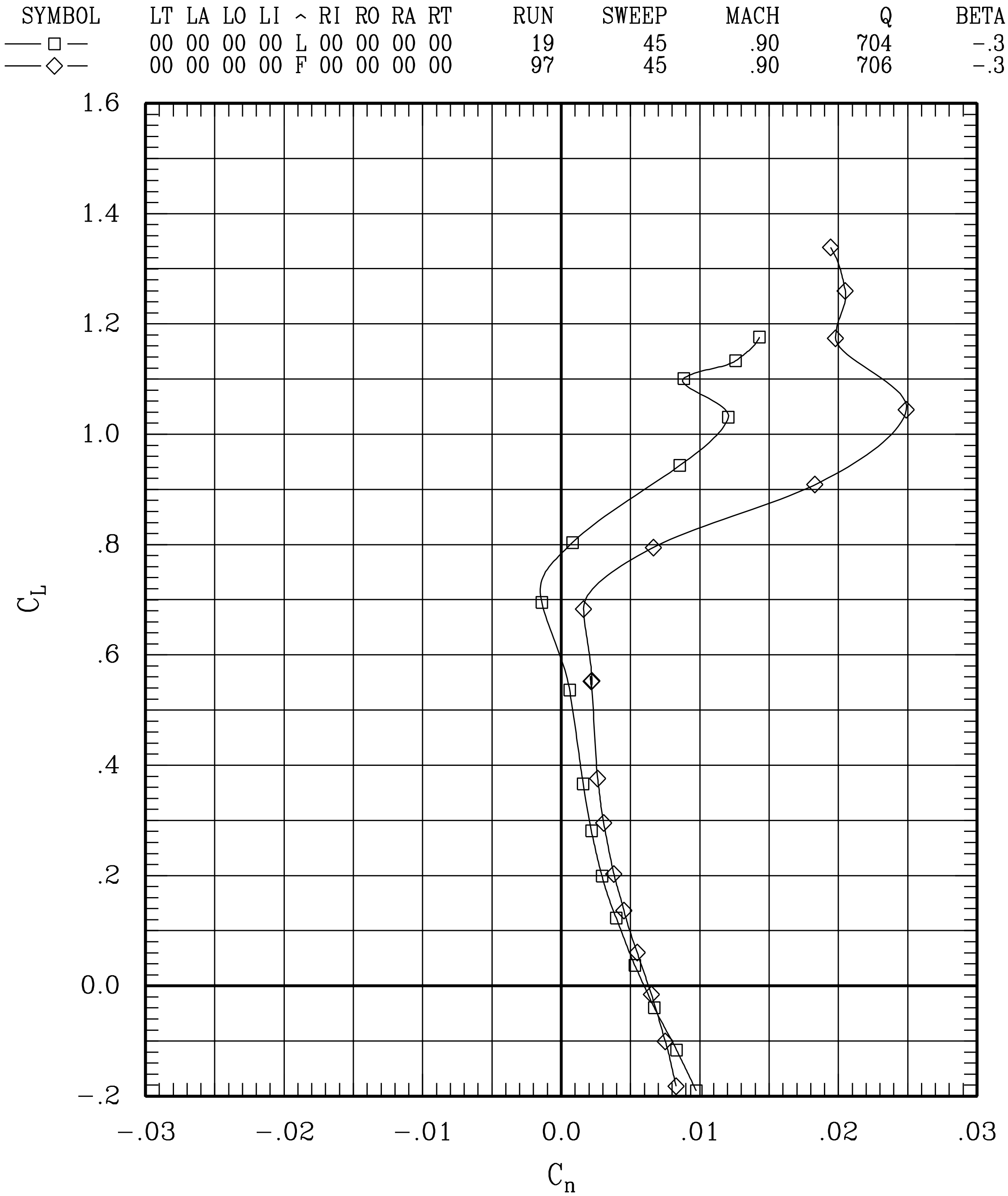

Figure 6(i). Effect of pivot height and fairing for sweep = 45 deg, Mach = 0.90.

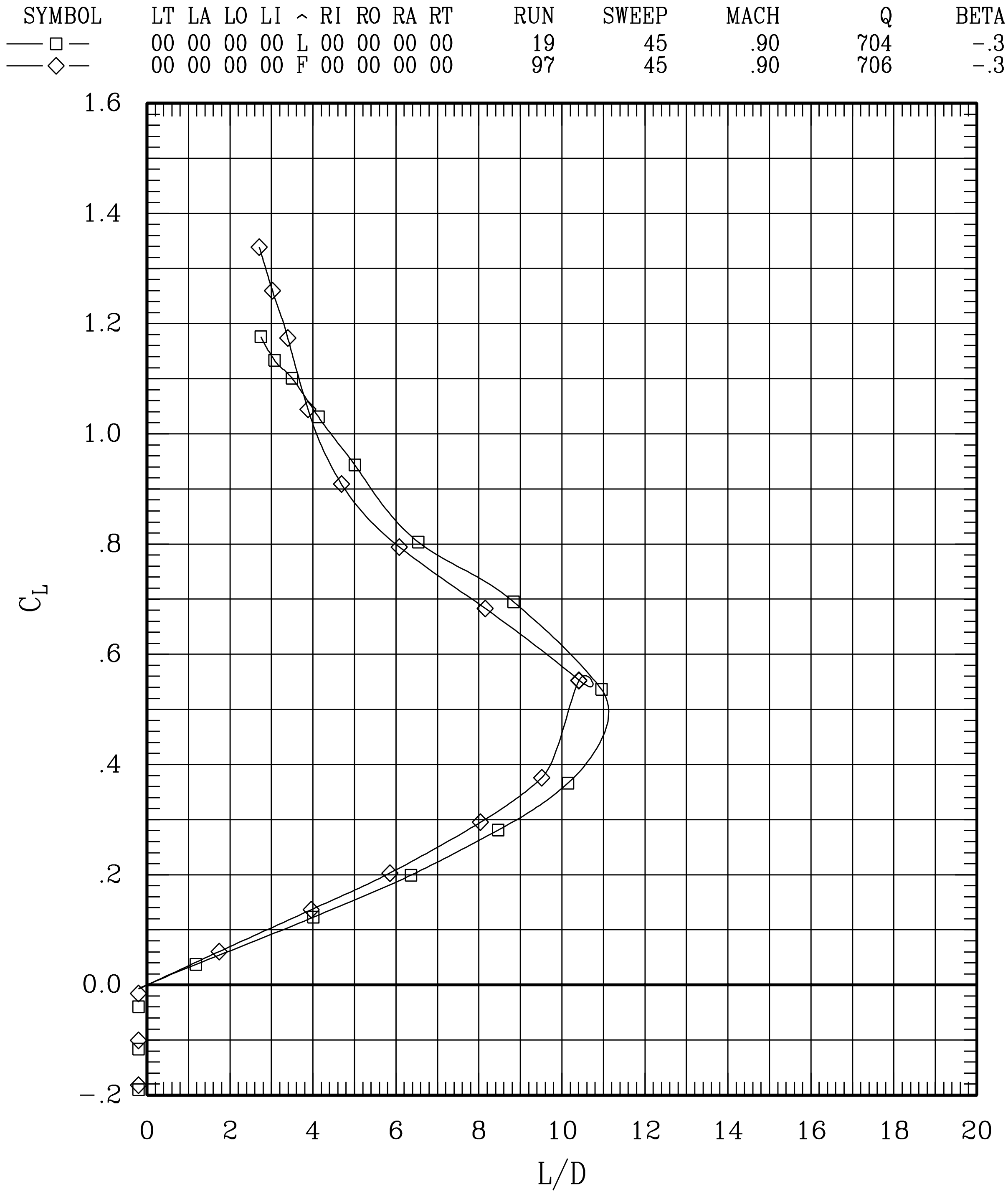

Figure 6(i). Effect of pivot height and fairing for sweep = 45 deg, Mach = 0.90.

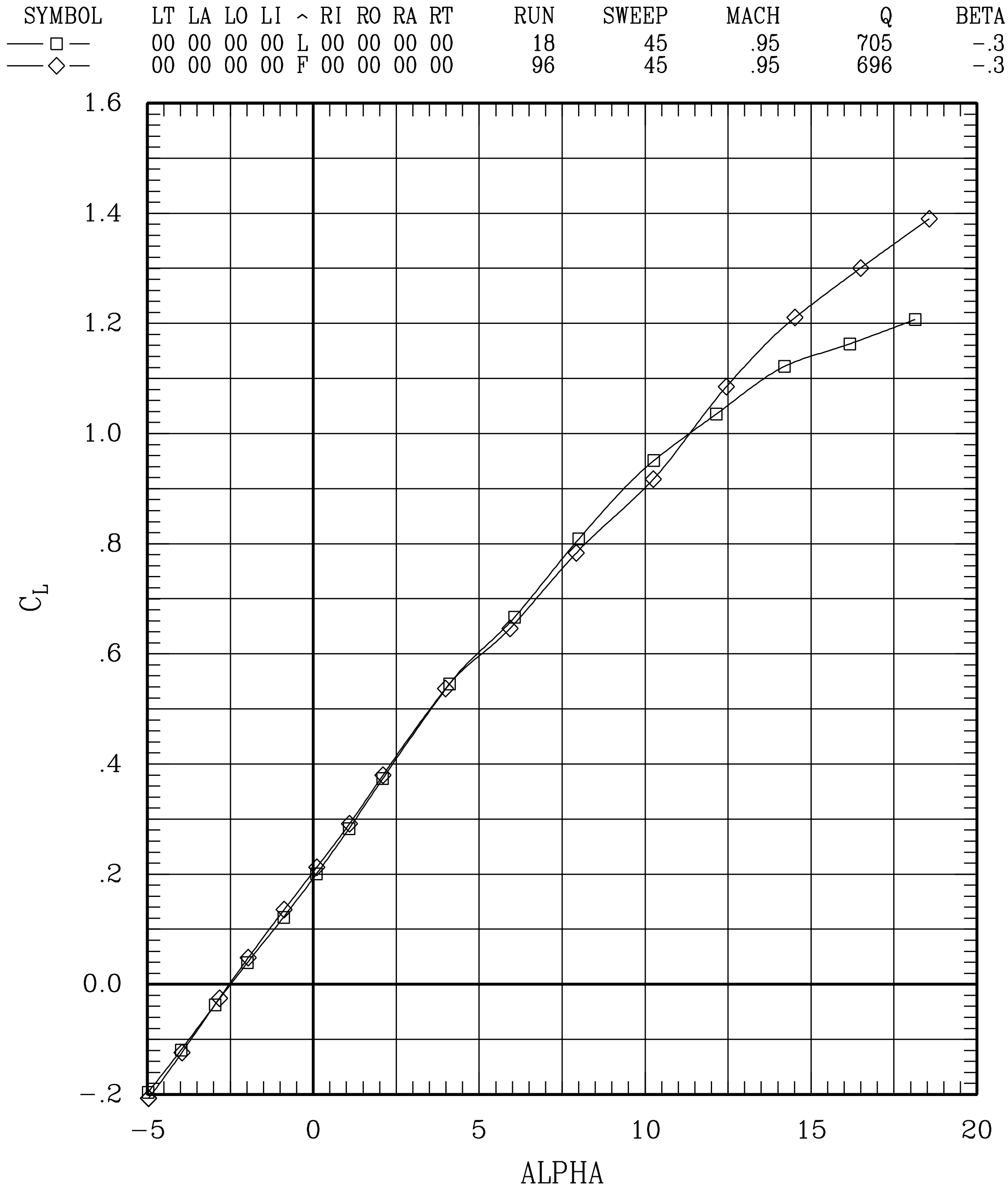

Figure 6(j). Effect of pivot height and fairing for sweep = 45 deg, Mach = 0.95.

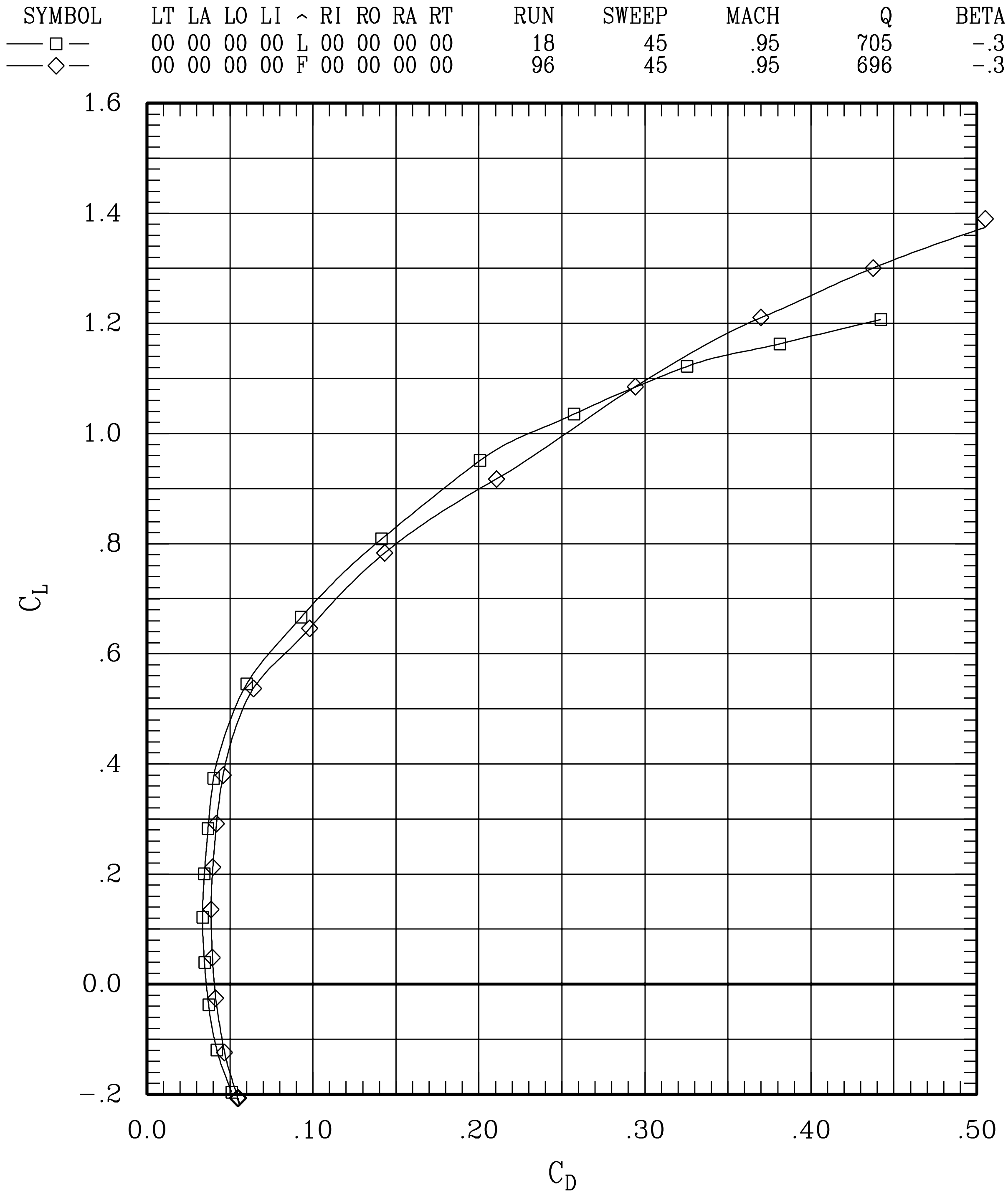

Figure 6(j). Effect of pivot height and fairing for sweep = 45 deg, Mach = 0.95.

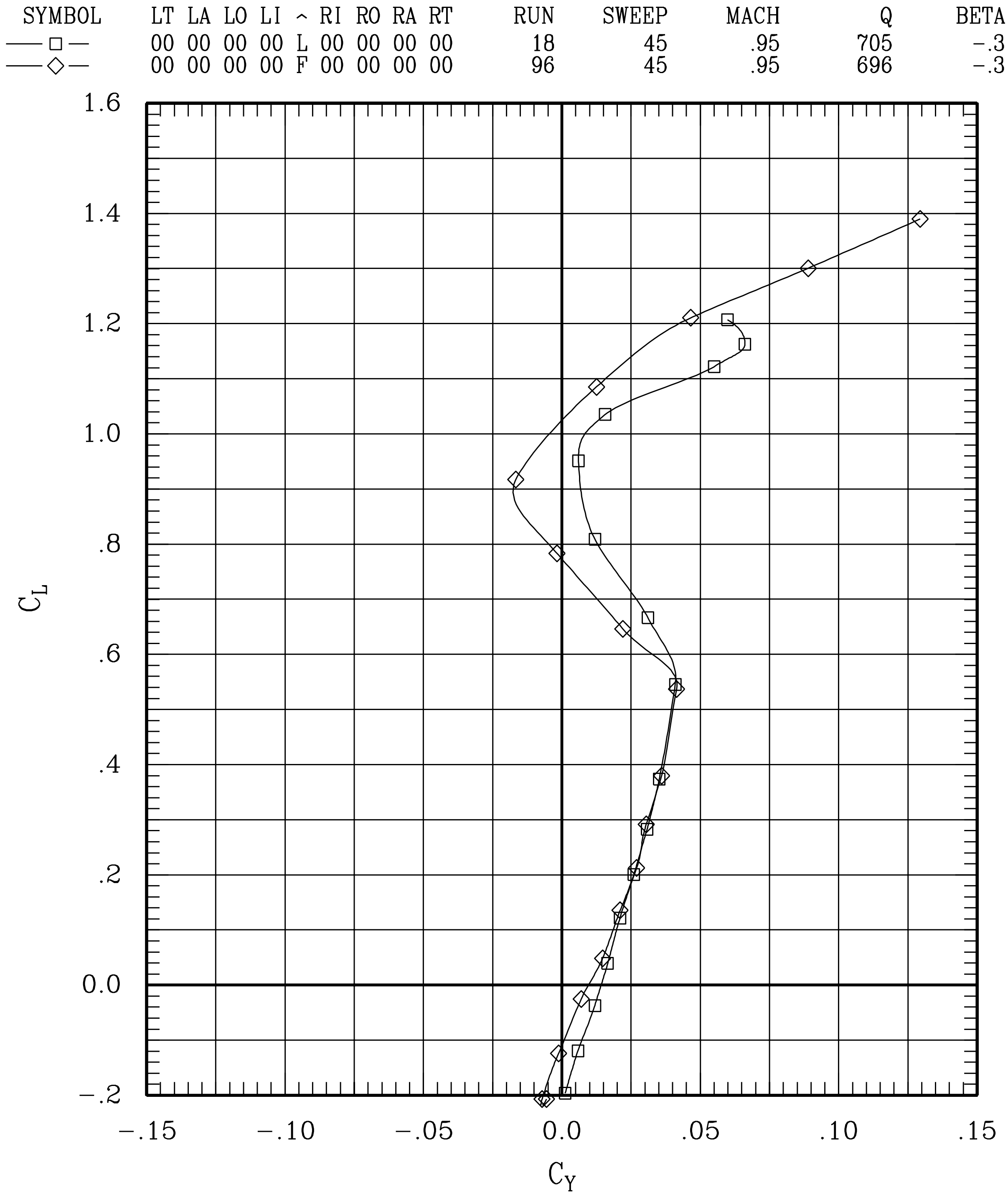

Figure 6(j). Effect of pivot height and fairing for sweep = 45 deg, Mach = 0.95.

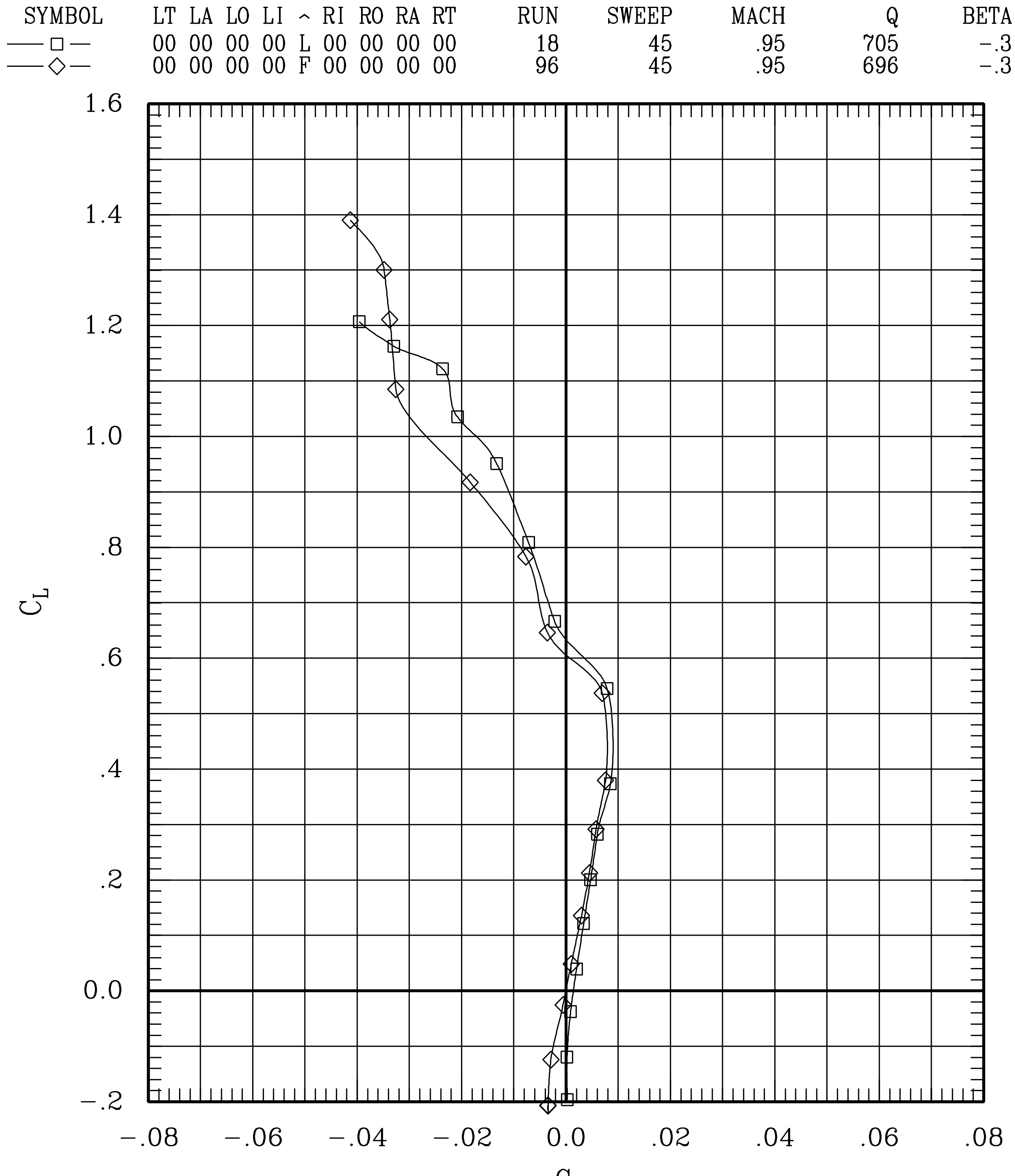

Figure 6(j). Effect of pivot height and fairing for sweep = 45 deg, Mach = 0.95.

SYMBOL	LT	LA	LO	LI	^	RI	RO	RA	RT	RUN	SWEEP	MACH	Q	BETA
—□—	00	00	00	00	L	00	00	00	00	18	45	.95	705	−.3
—◇—	00	00	00	00	F	00	00	00	00	96	45	.95	696	−.3

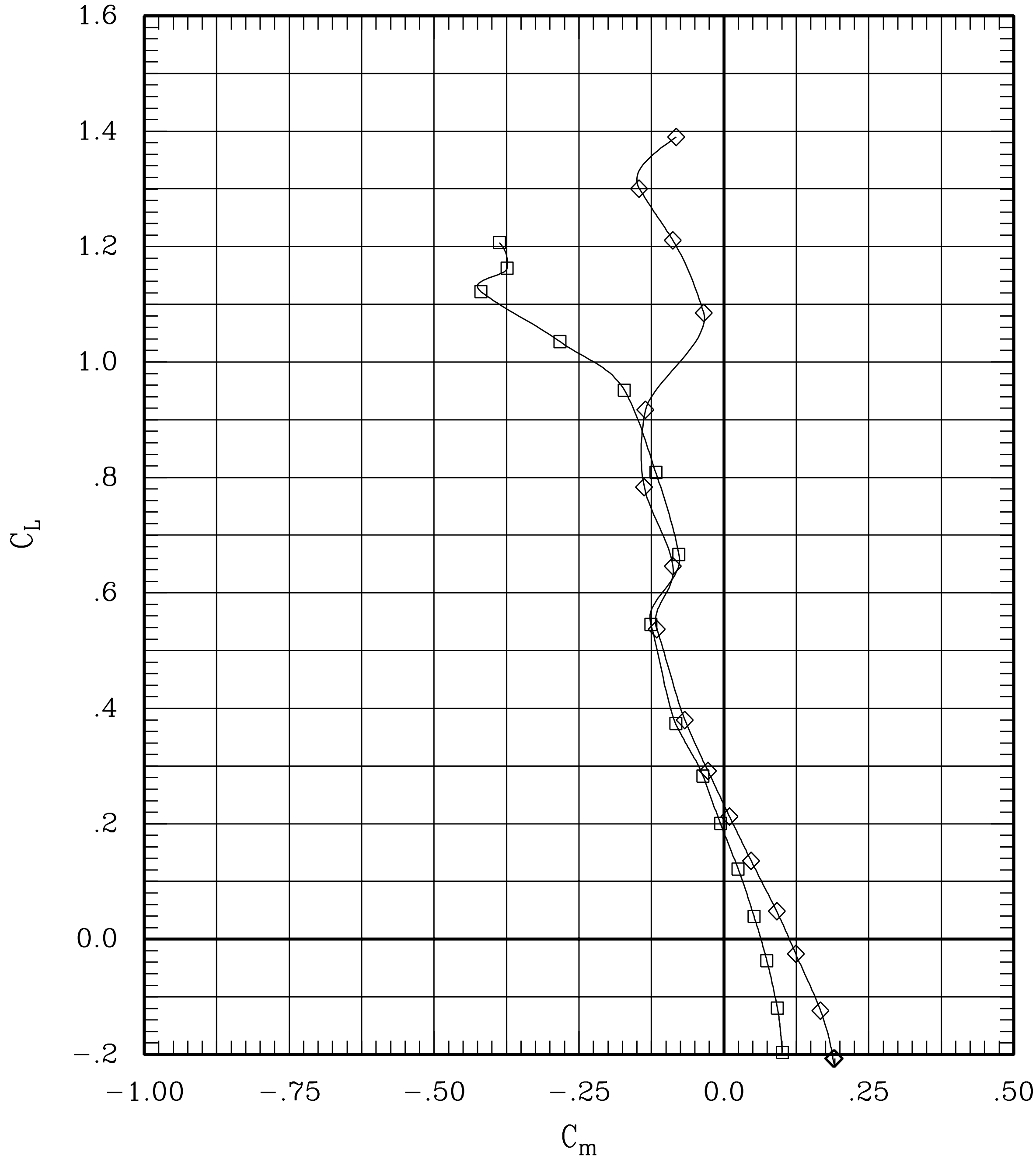

Figure 6(j). Effect of pivot height and fairing for sweep = 45 deg, Mach = 0.95.

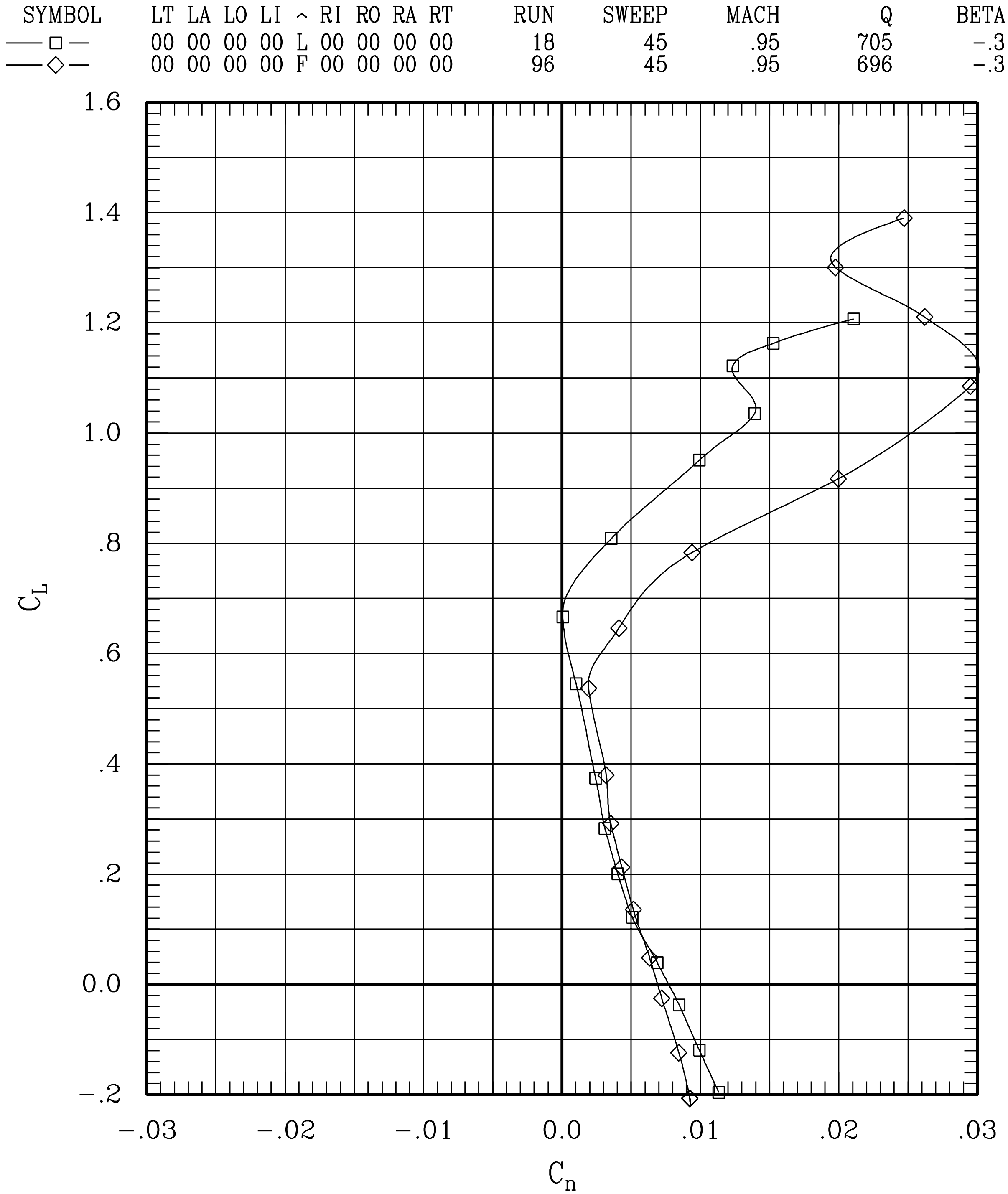

Figure 6(j). Effect of pivot height and fairing for sweep = 45 deg, Mach = 0.95.

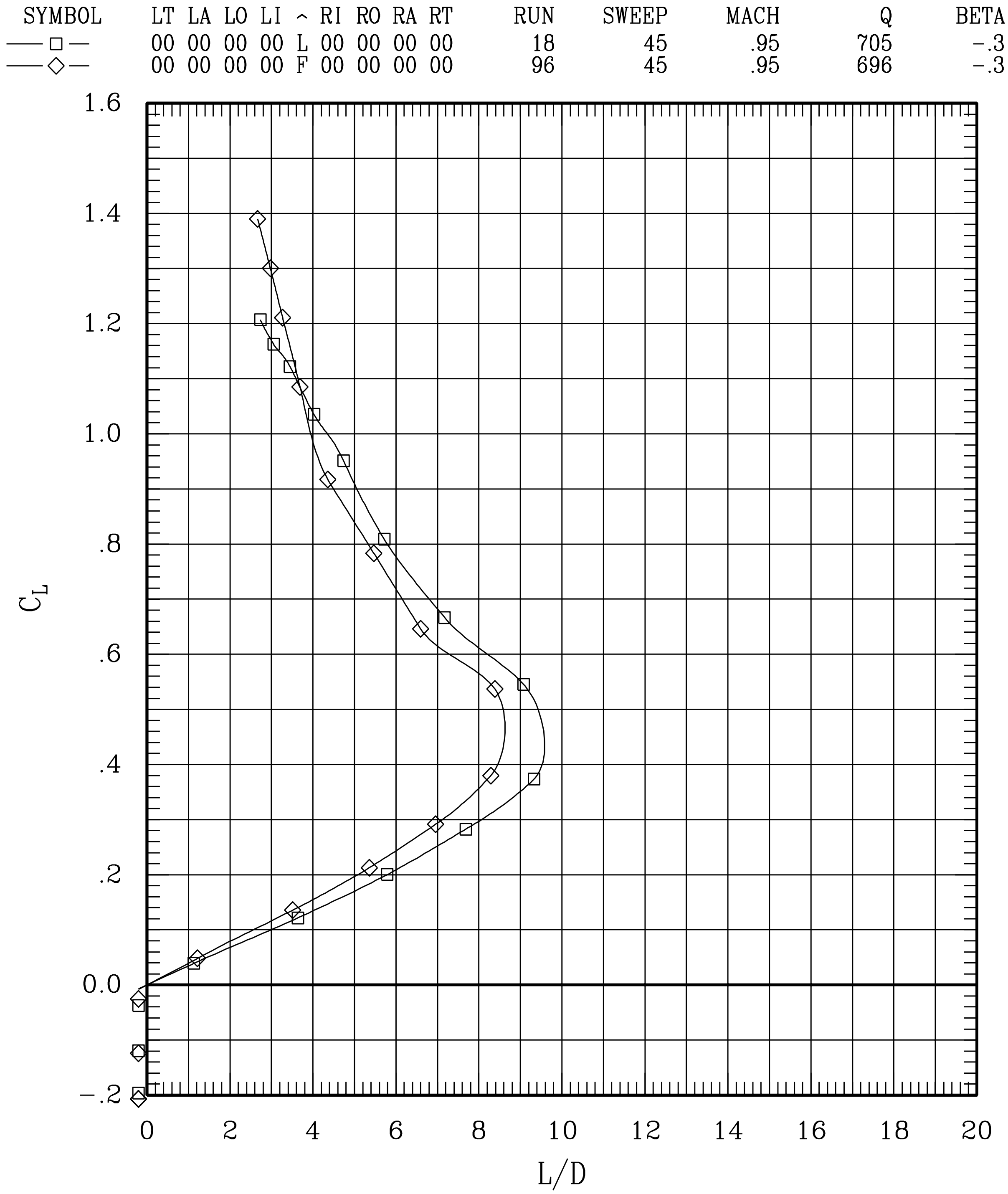

Figure 6(j). Effect of pivot height and fairing for sweep = 45 deg, Mach = 0.95.

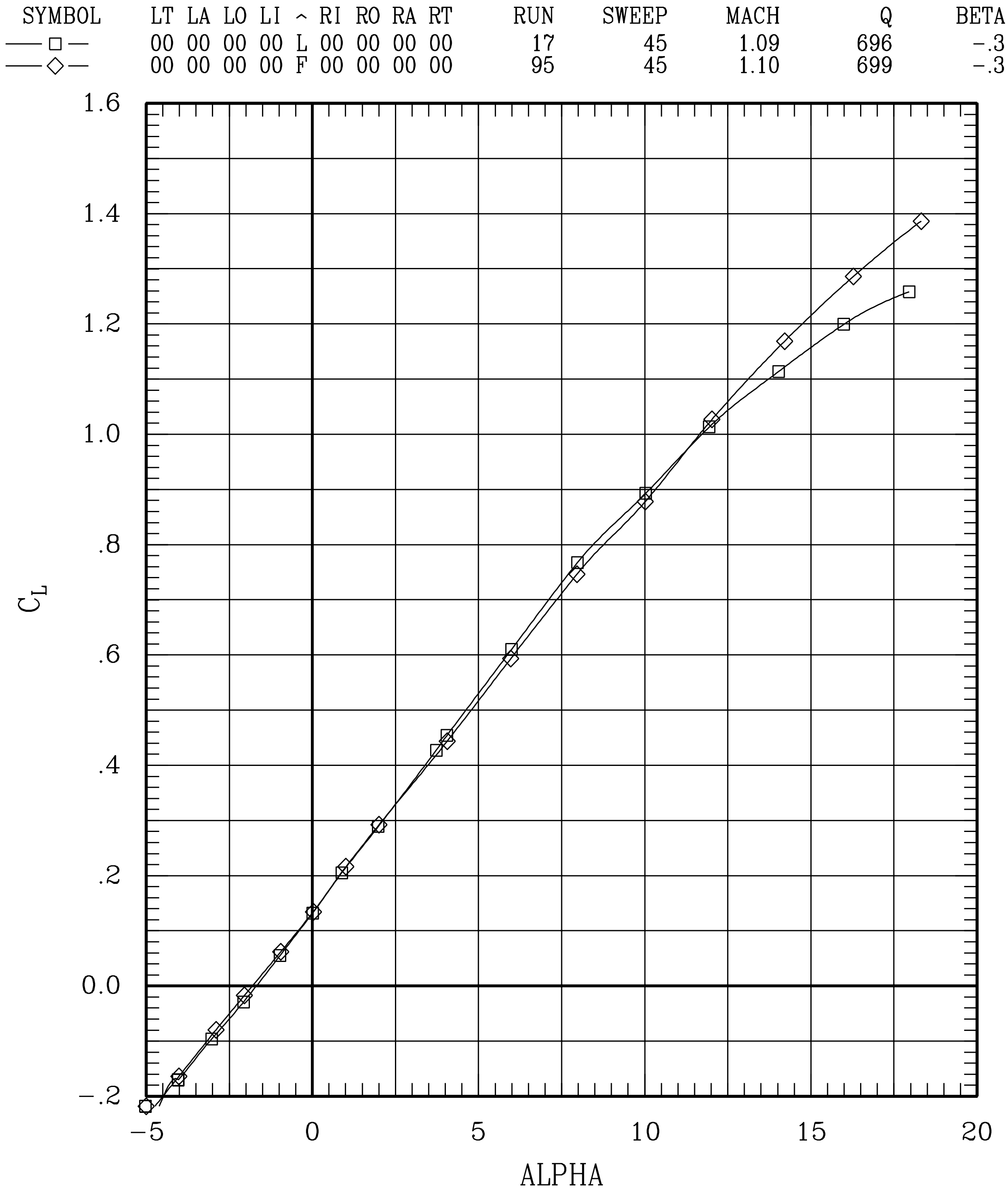

Figure 6(k). Effect of pivot height and fairing for sweep = 45 deg, Mach = 1.10.

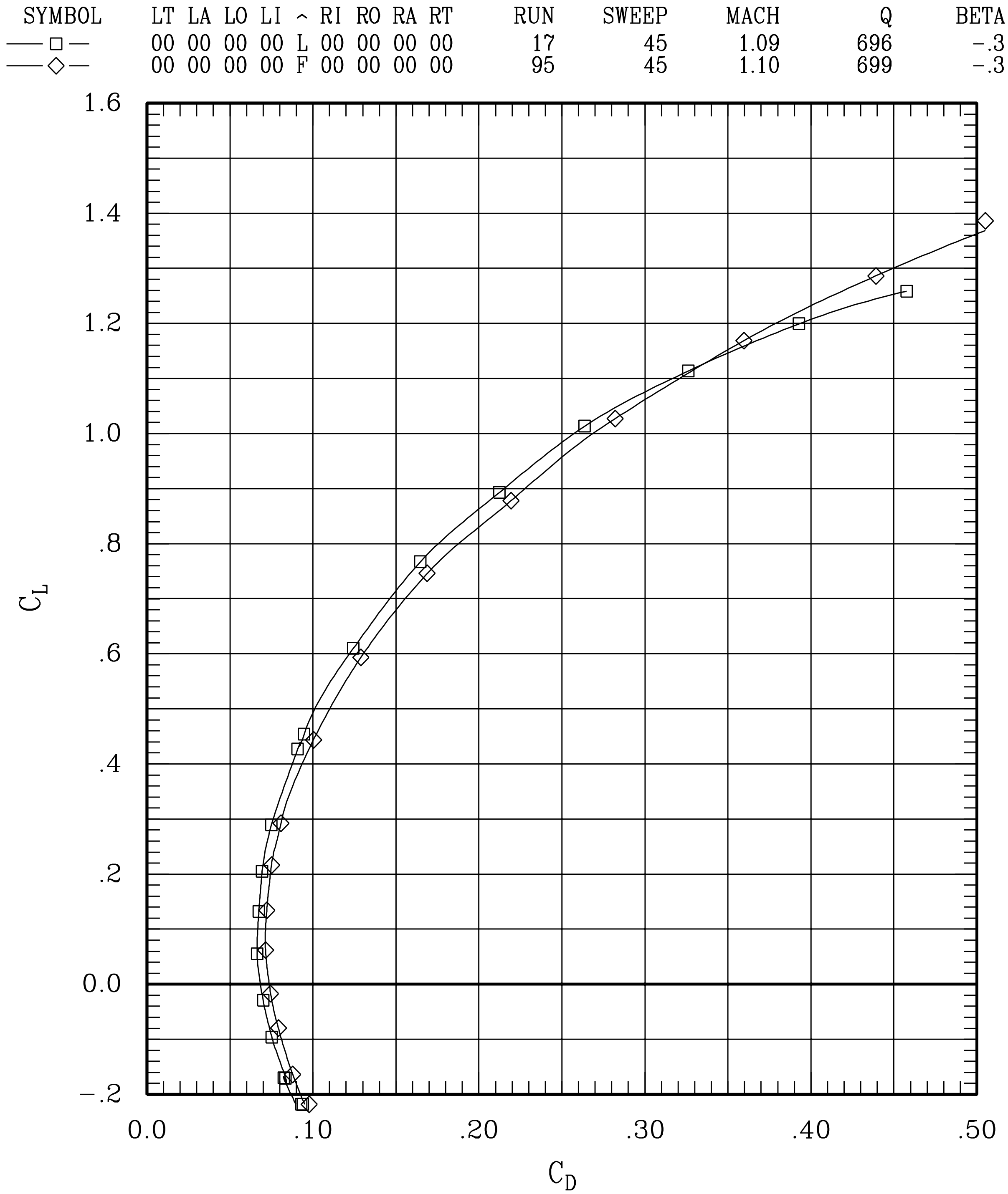

Figure 6(k). Effect of pivot height and fairing for sweep = 45 deg, Mach = 1.10.

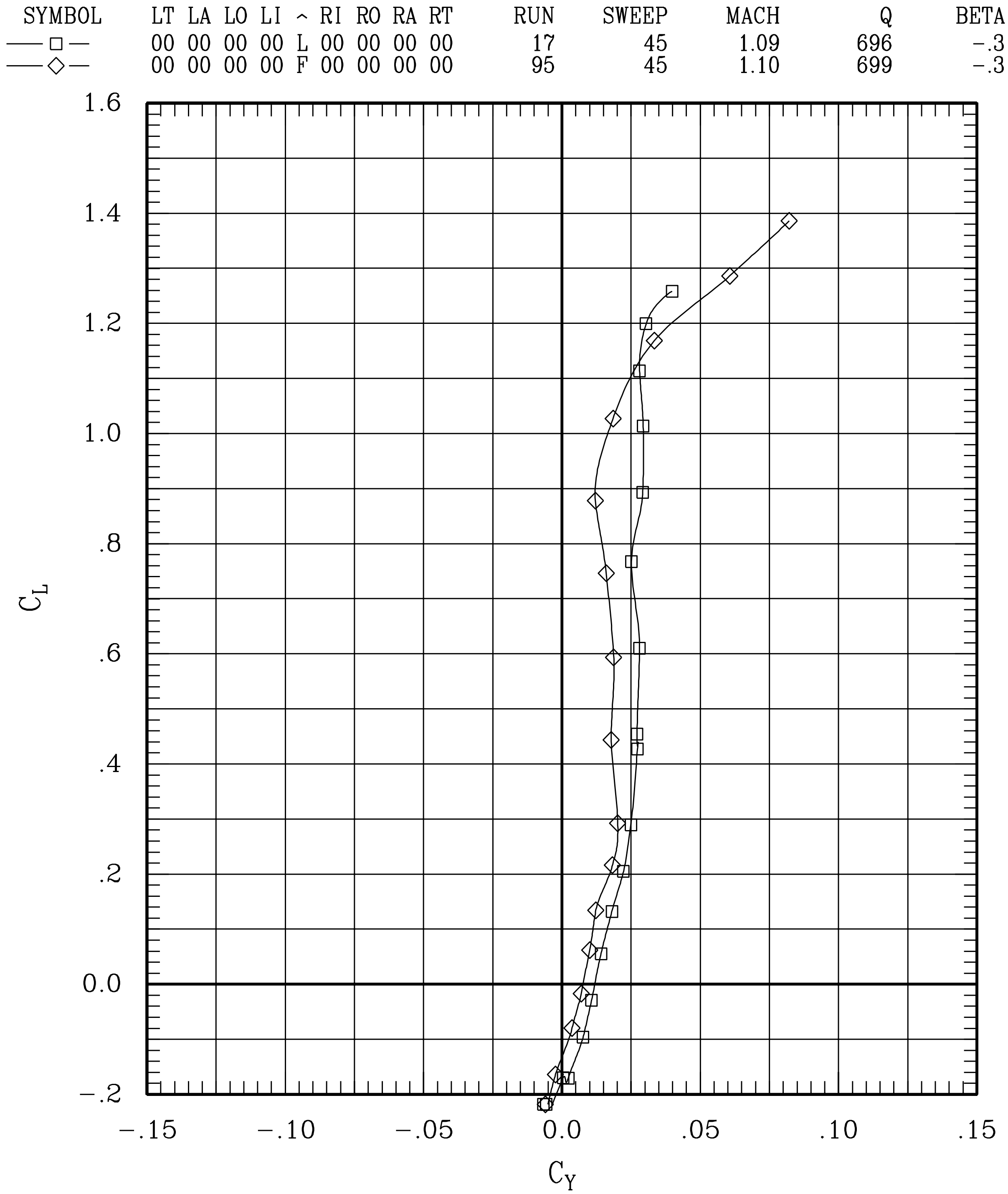

Figure 6(k). Effect of pivot height and fairing for sweep = 45 deg, Mach = 1.10.

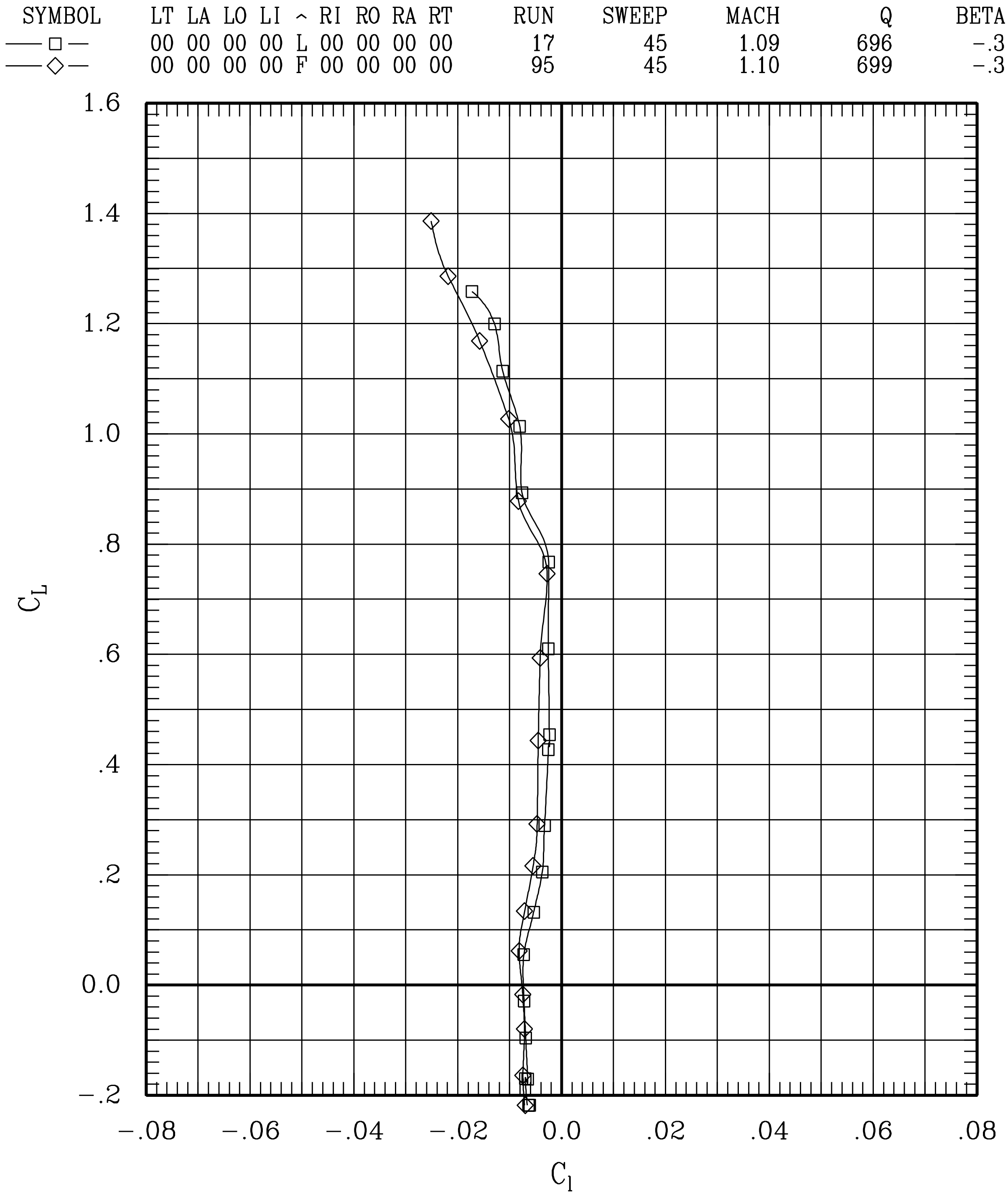

Figure 6(k). Effect of pivot height and fairing for sweep = 45 deg, Mach = 1.10.

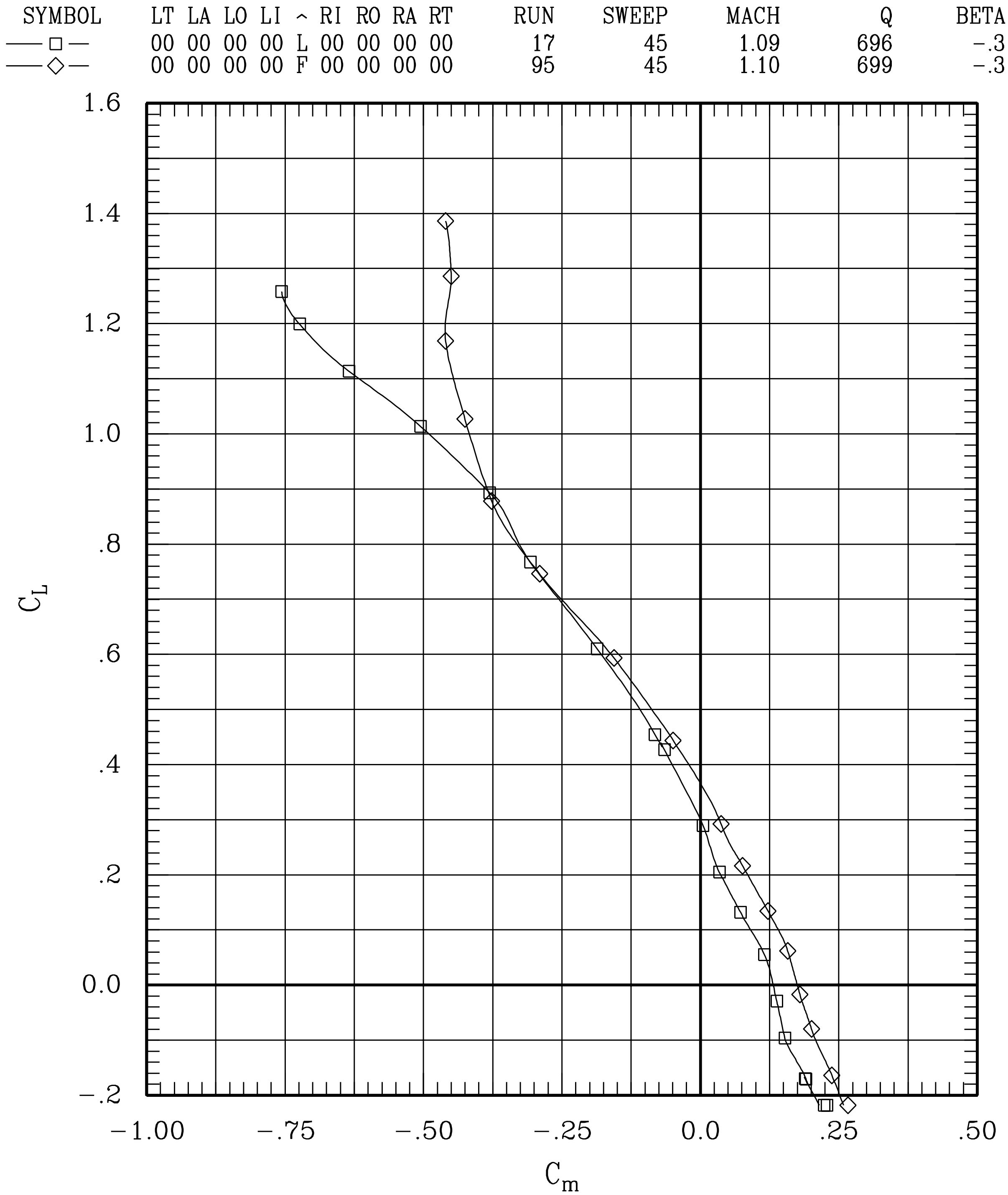

Figure 6(k). Effect of pivot height and fairing for sweep = 45 deg, Mach = 1.10.

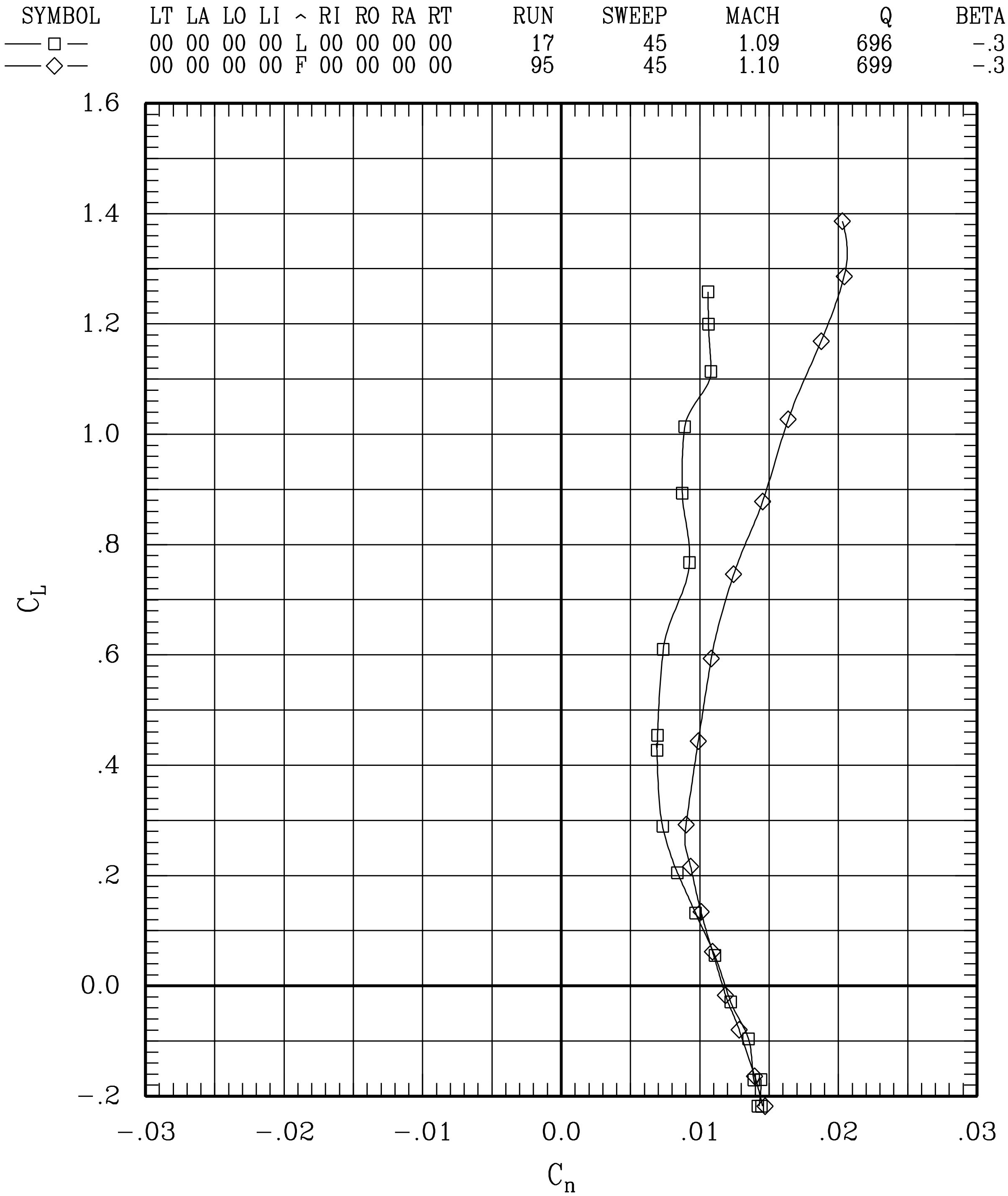

Figure 6(k). Effect of pivot height and fairing for sweep = 45 deg, Mach = 1.10.

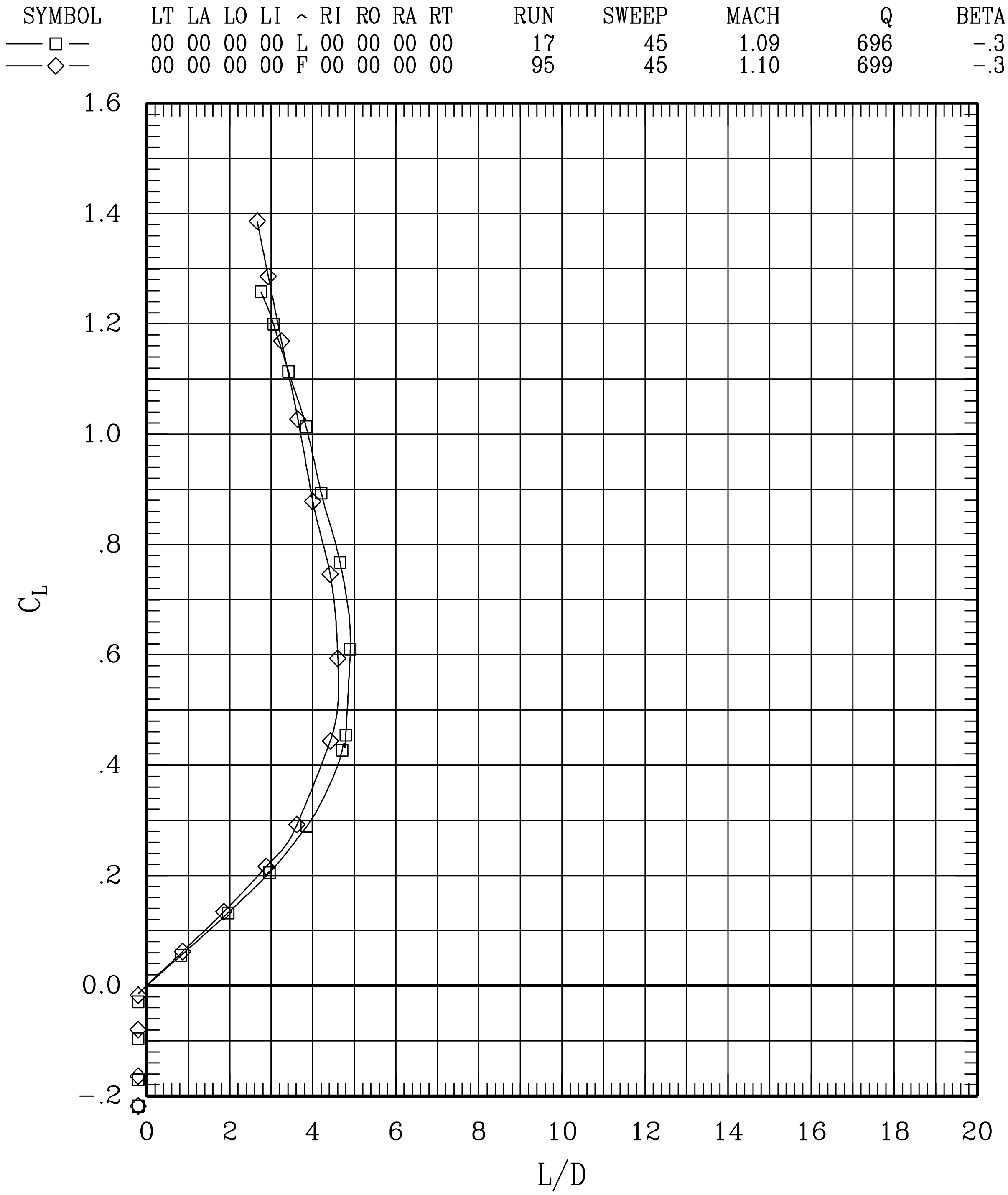

Figure 6(k). Effect of pivot height and fairing for sweep = 45 deg, Mach = 1.10.

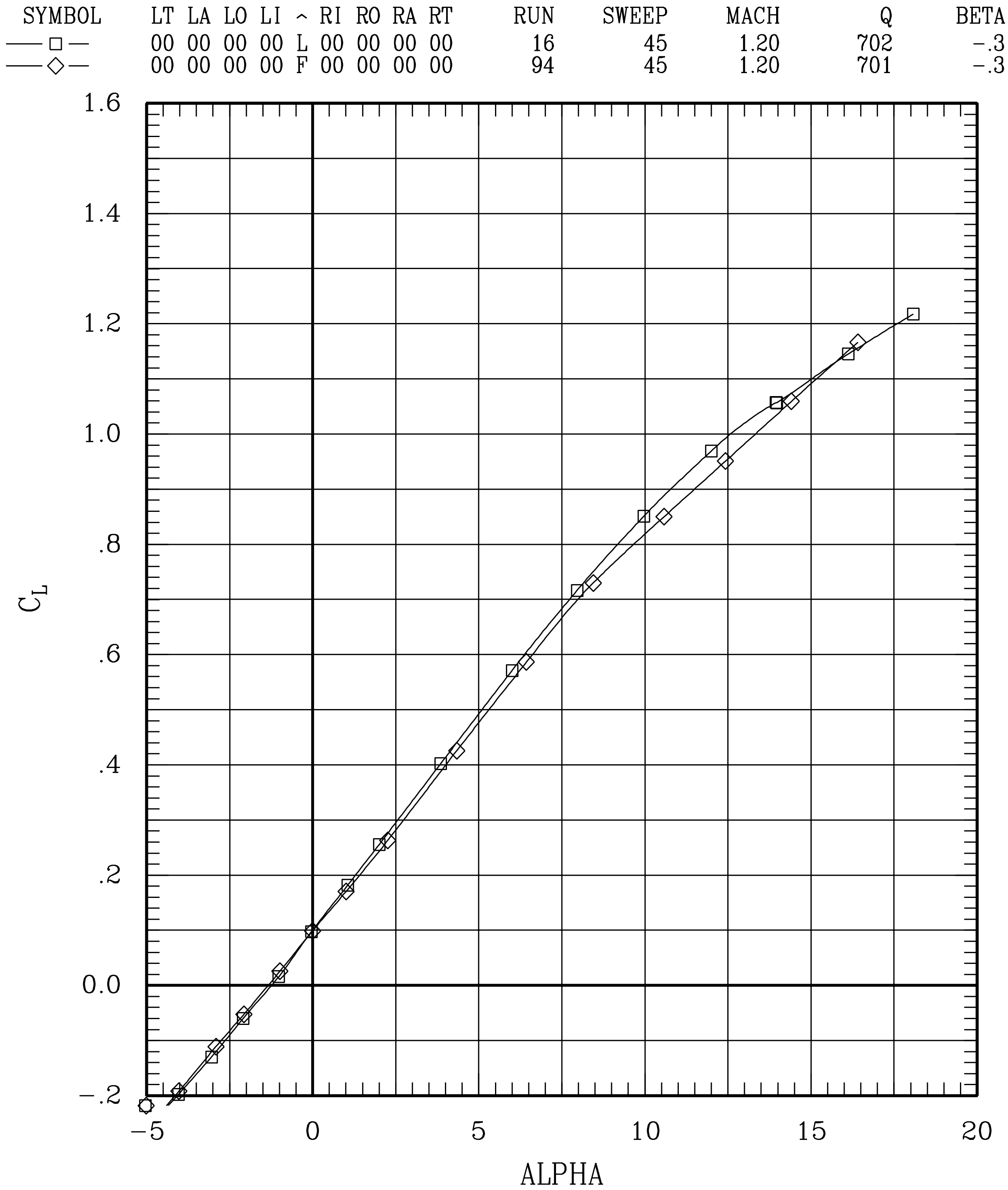

Figure 6(l). Effect of pivot height and fairing for sweep = 45 deg, Mach = 1.20.

SYMBOL	LT LA LO LI ^ RI RO RA RT	RUN	SWEEP	MACH	Q	BETA
—□—	00 00 00 00 L 00 00 00 00	16	45	1.20	702	−.3
—◇—	00 00 00 00 F 00 00 00 00	94	45	1.20	701	−.3

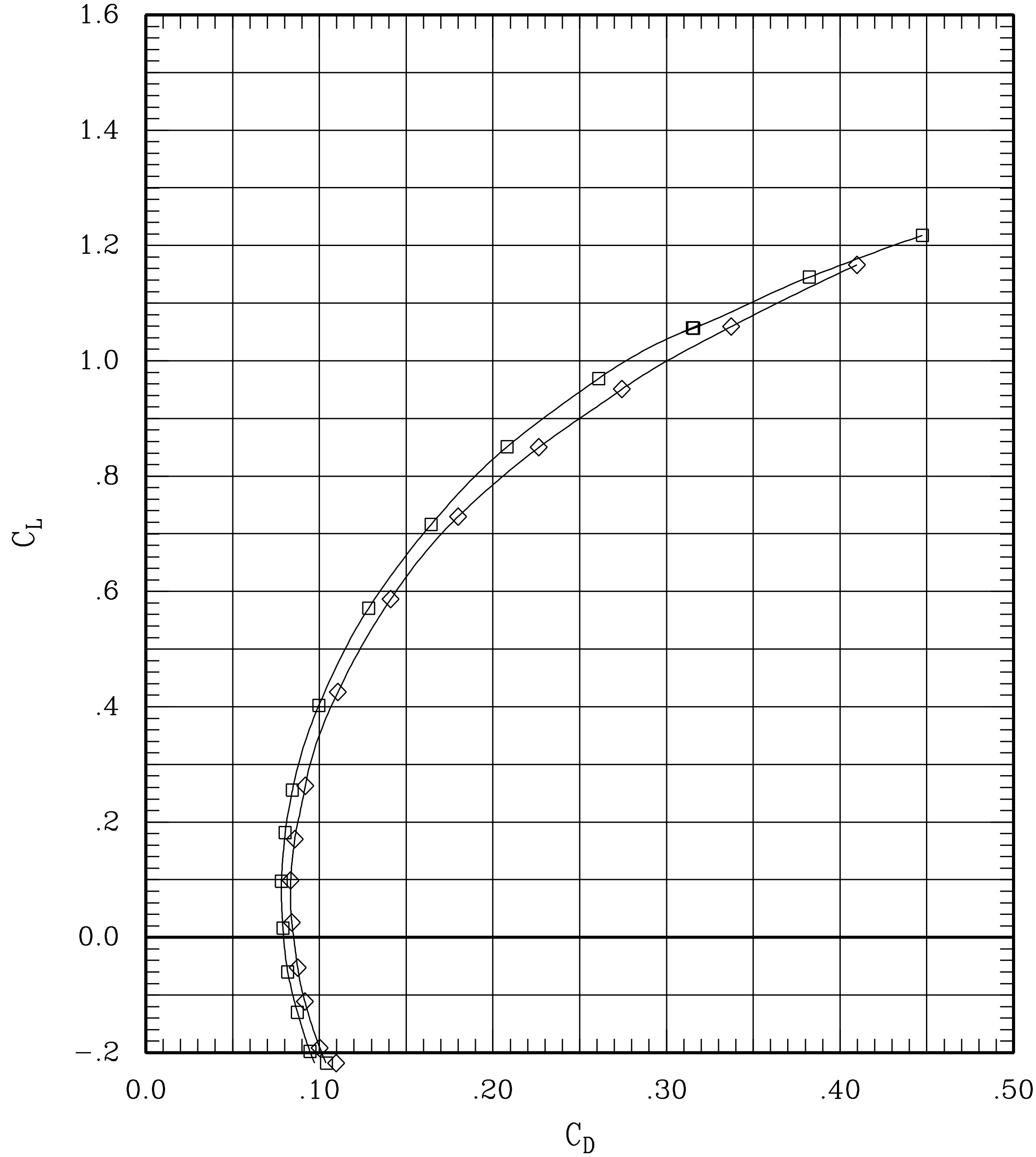

Figure 6(l). Effect of pivot height and fairing for sweep = 45 deg, Mach = 1.20.

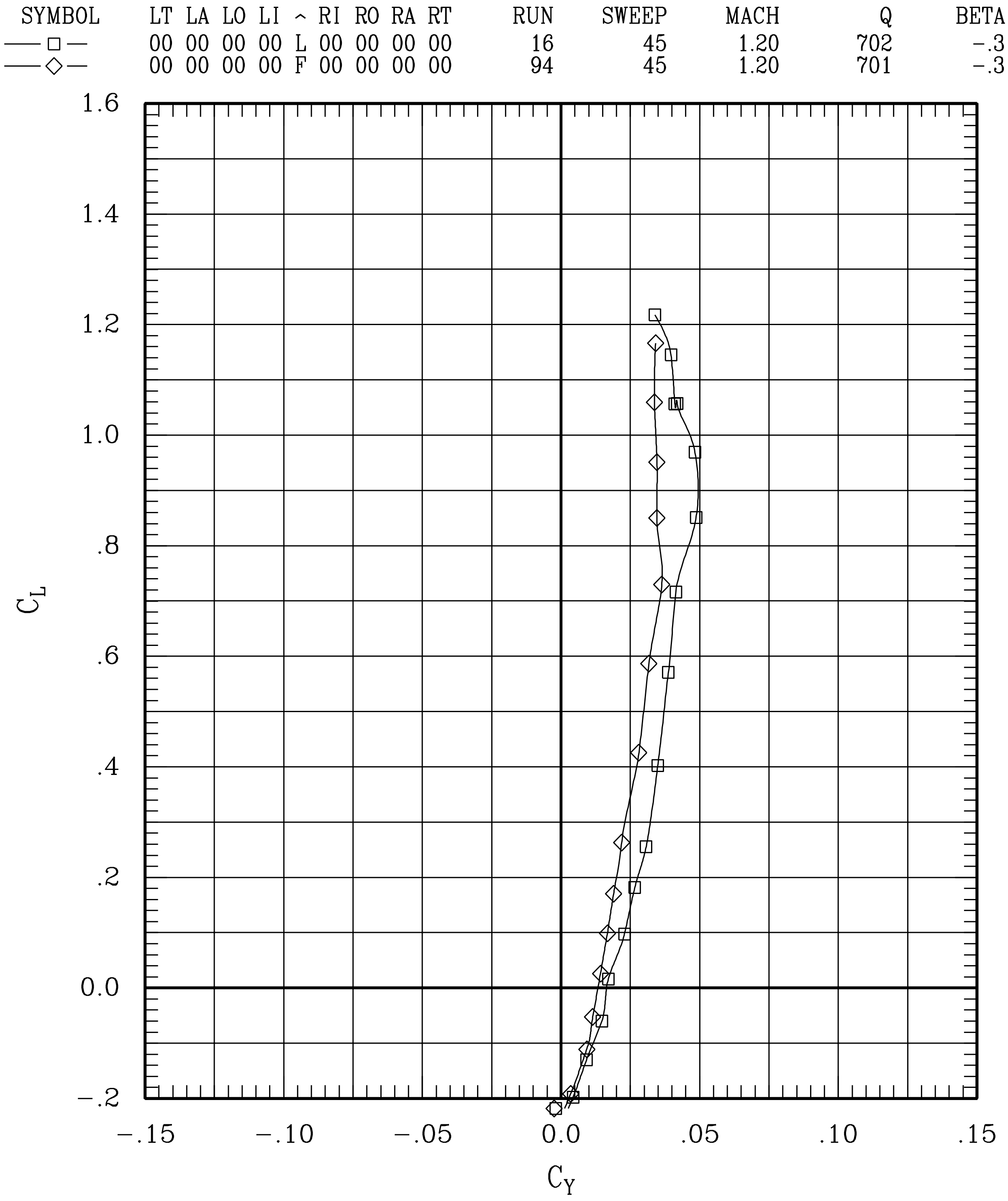

Figure 6(l). Effect of pivot height and fairing for sweep = 45 deg, Mach = 1.20.

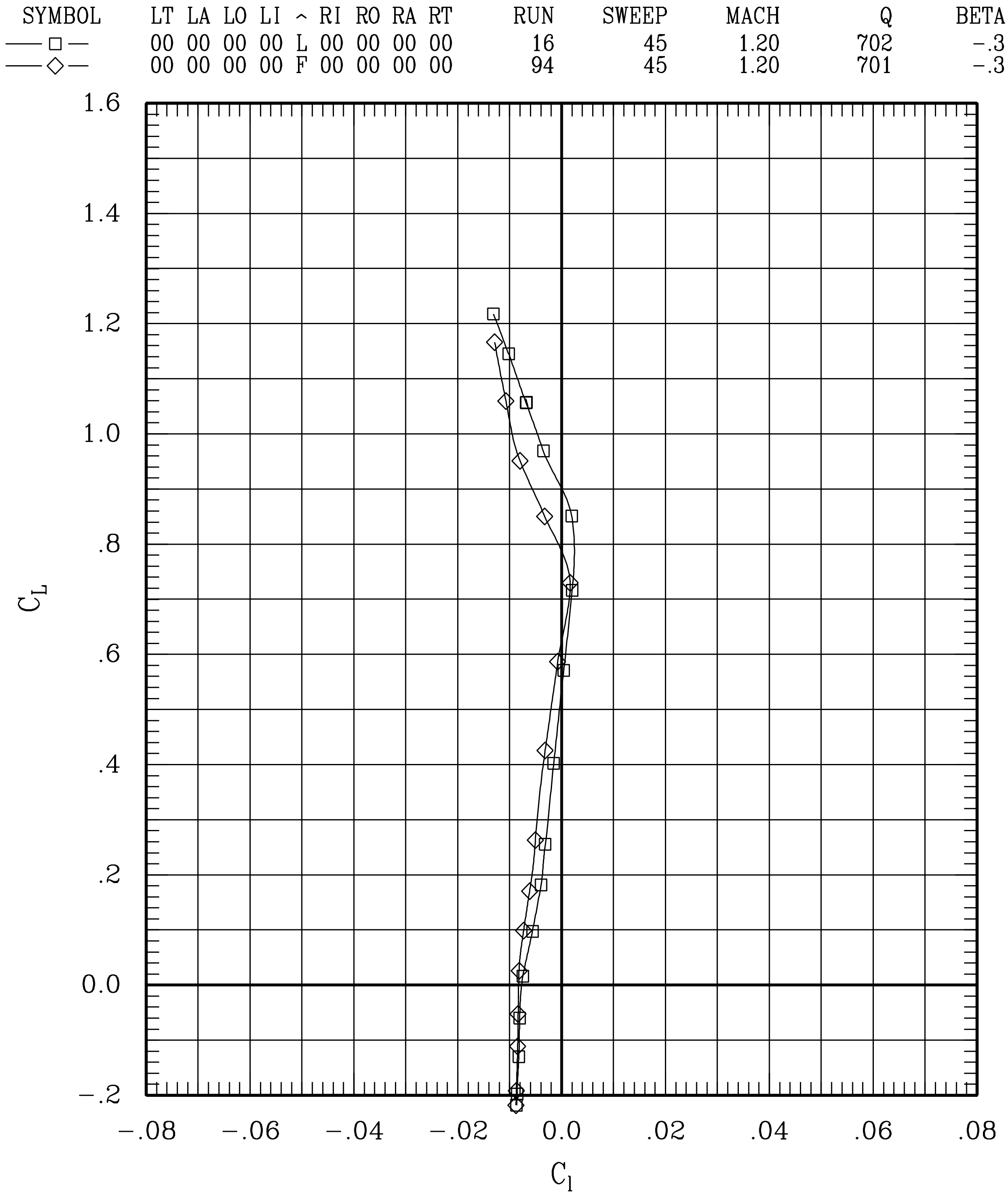

Figure 6(l). Effect of pivot height and fairing for sweep = 45 deg, Mach = 1.20.

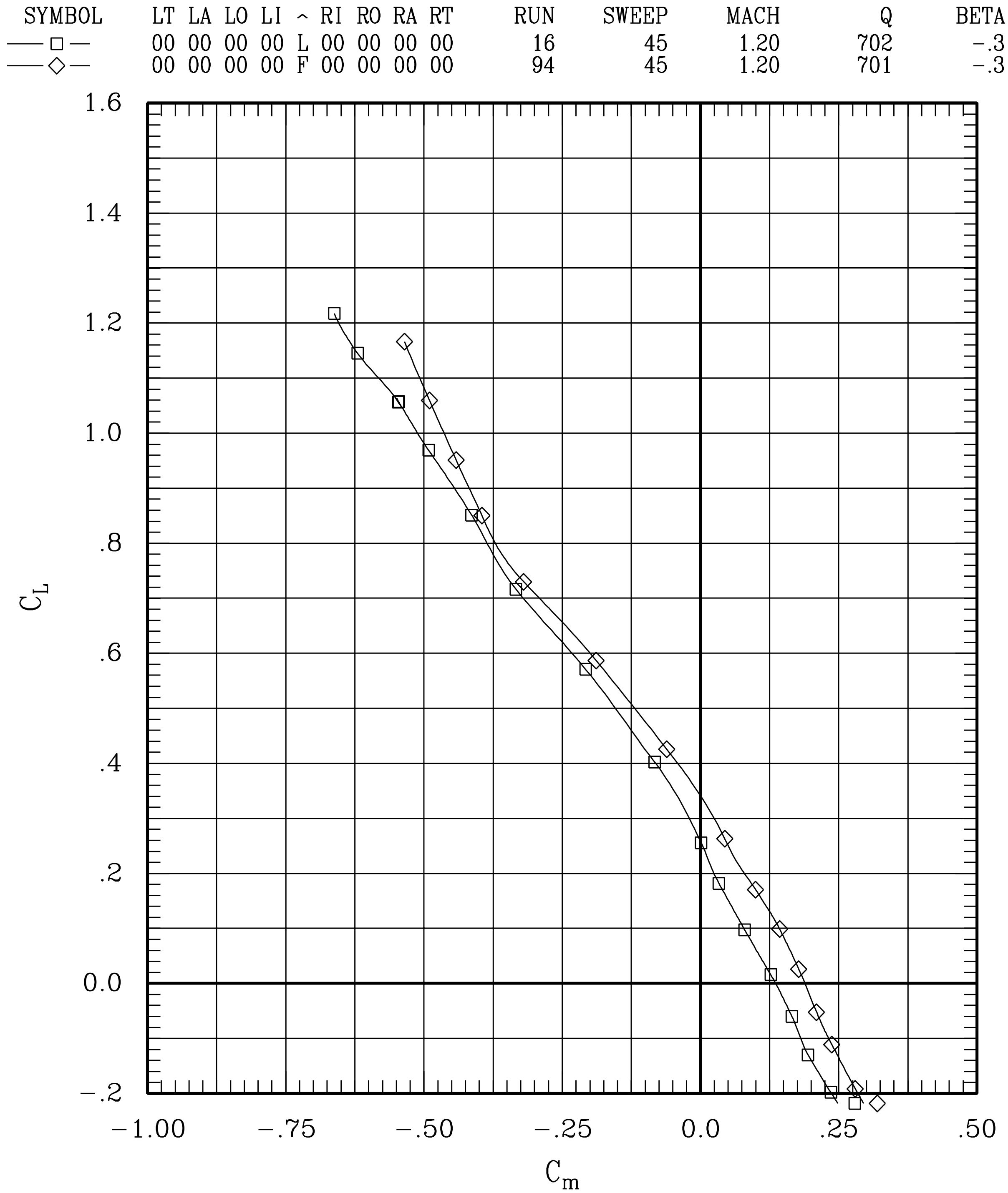

Figure 6(l). Effect of pivot height and fairing for sweep = 45 deg, Mach = 1.20.

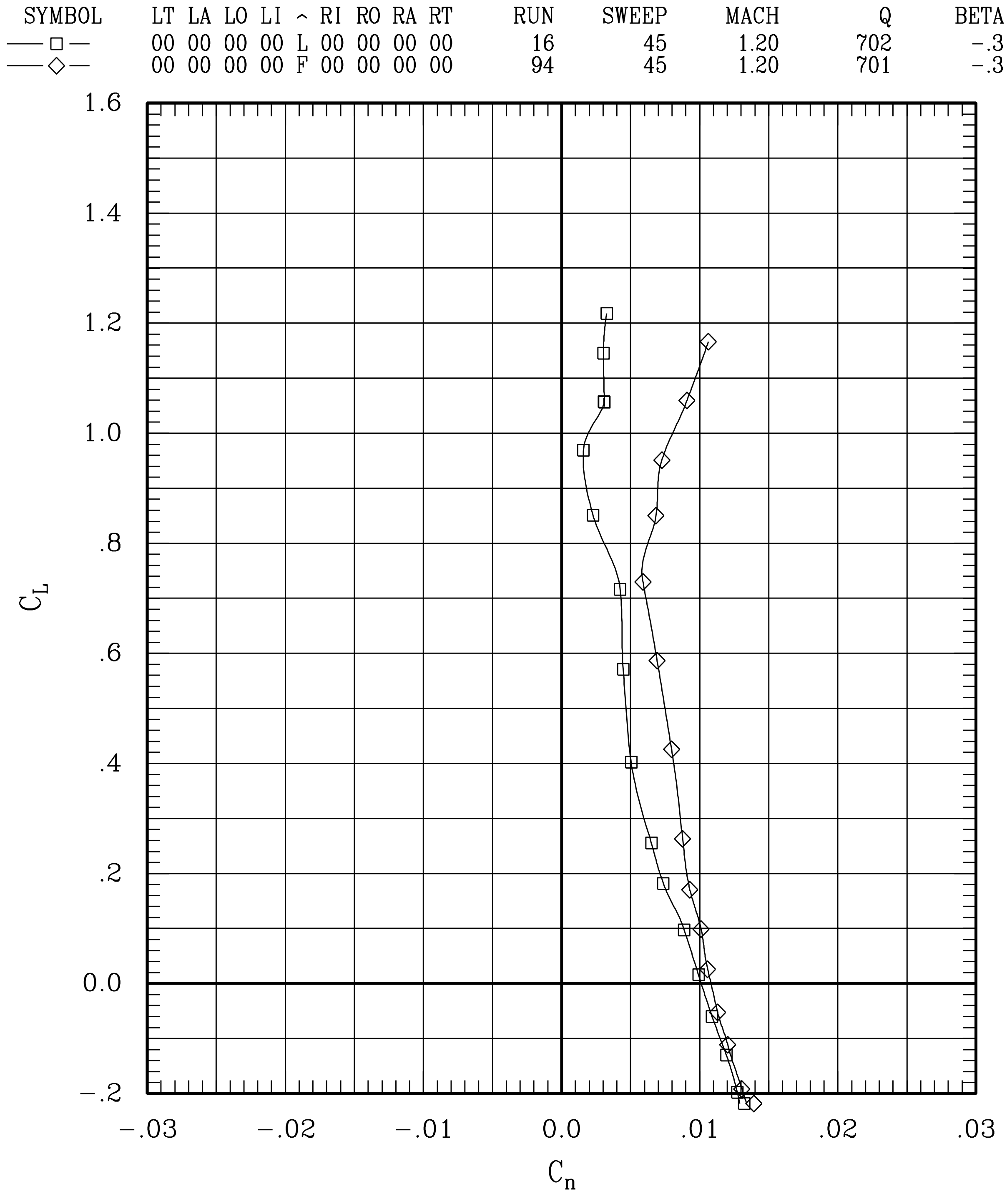

Figure 6(l). Effect of pivot height and fairing for sweep = 45 deg, Mach = 1.20.

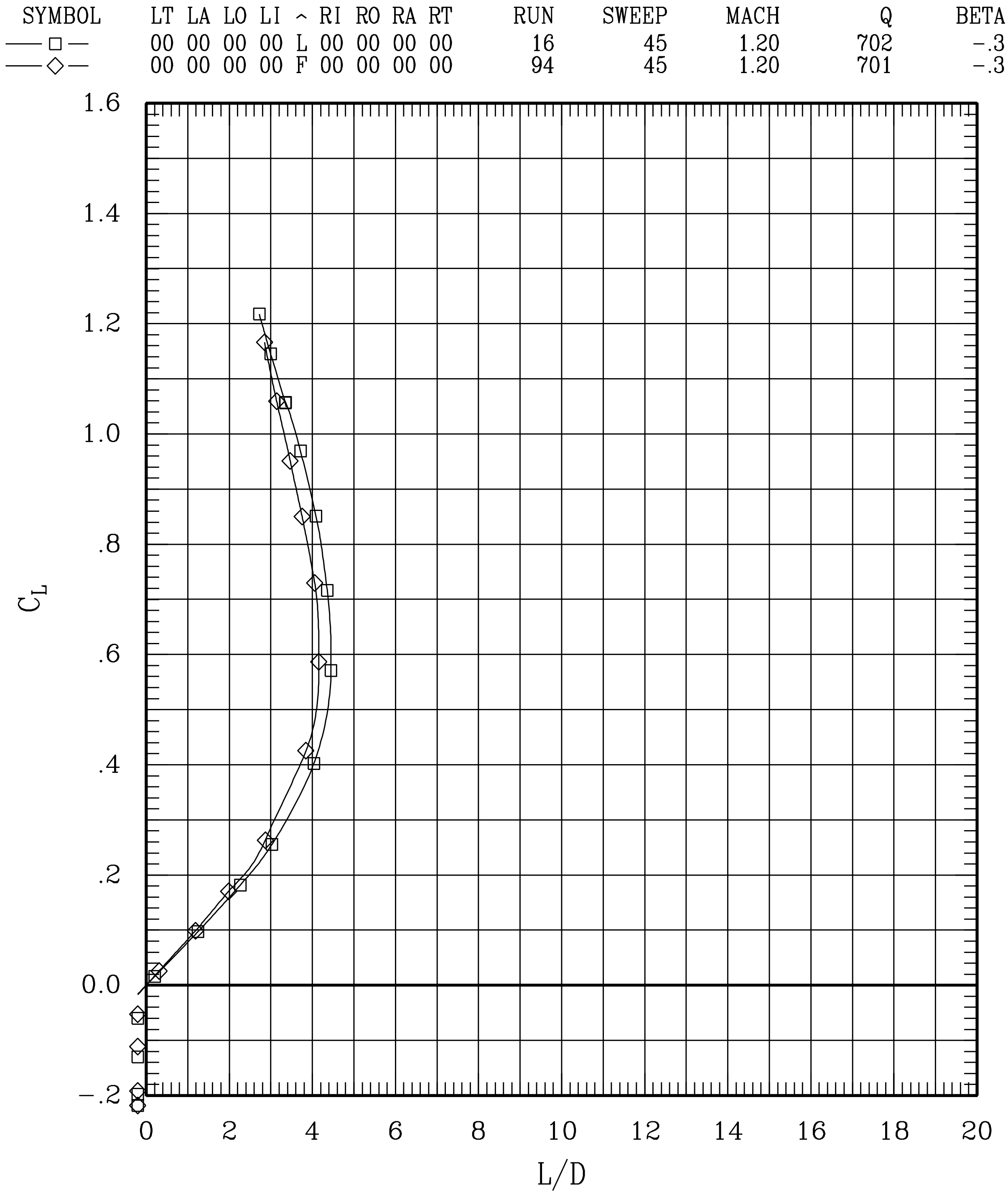

Figure 6(l). Effect of pivot height and fairing for sweep = 45 deg, Mach = 1.20.

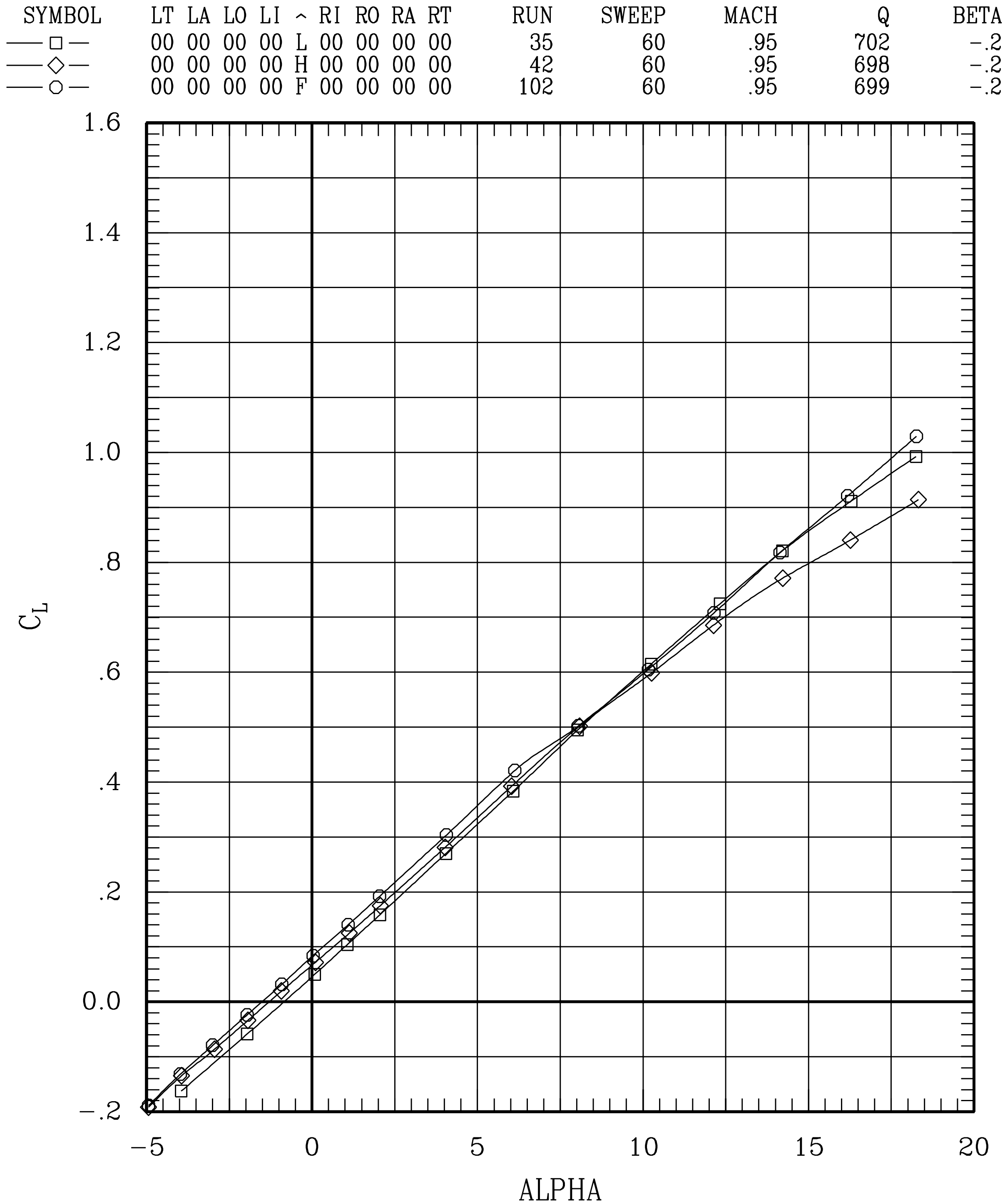

Figure 6(m). Effect of pivot height and fairing for sweep = 60 deg, Mach = 0.95.

SYMBOL	LT	LA	LO	LI	^	RI	RO	RA	RT	RUN	SWEEP	MACH	Q	BETA
—□—	00	00	00	00	L	00	00	00	00	35	60	.95	702	−.2
—◇—	00	00	00	00	H	00	00	00	00	42	60	.95	698	−.2
—○—	00	00	00	00	F	00	00	00	00	102	60	.95	699	−.2

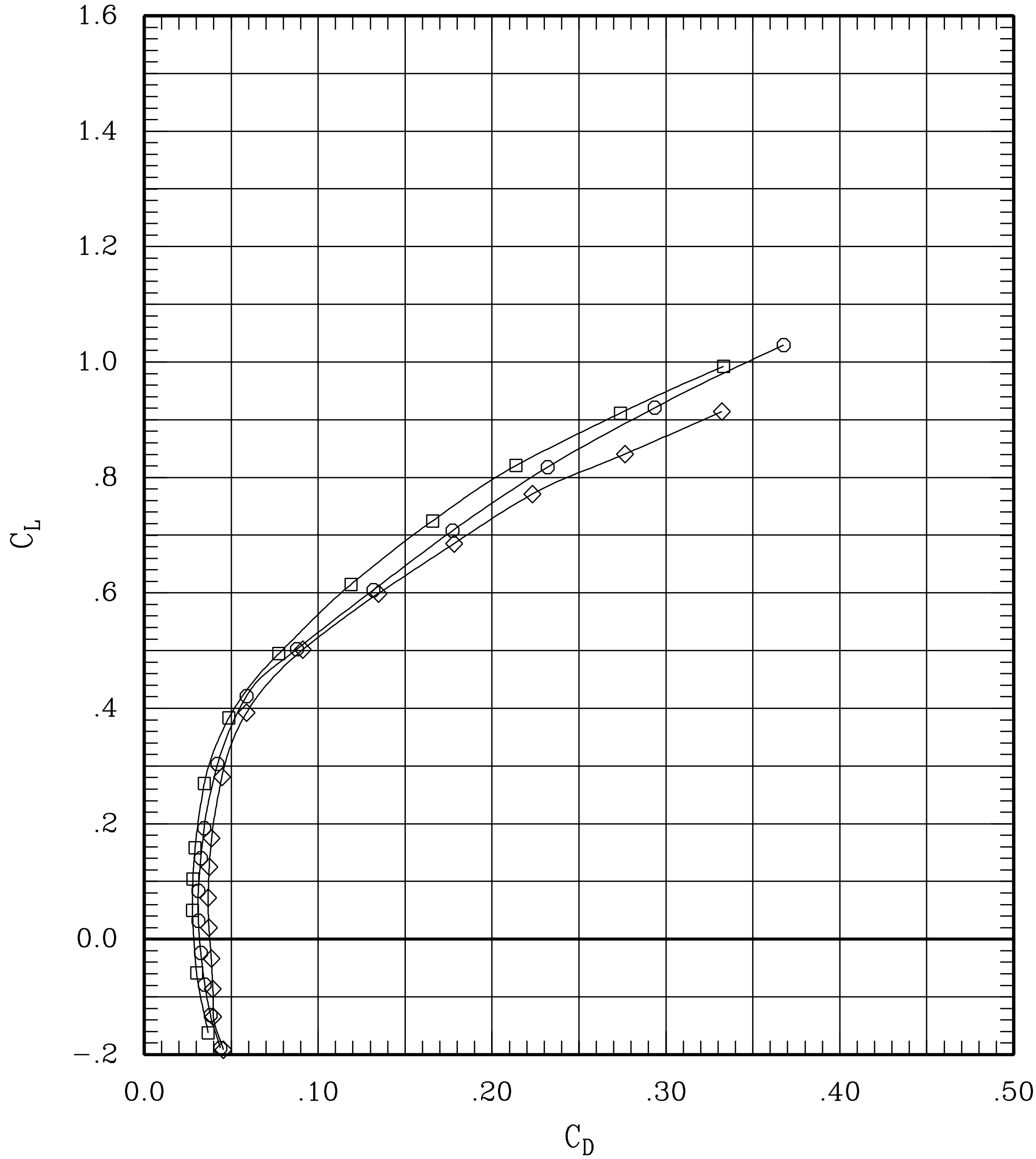

Figure 6(m). Effect of pivot height and fairing for sweep = 60 deg, Mach = 0.95.

SYMBOL	LT LA LO LI ^ RI RO RA RT	RUN	SWEEP	MACH	Q	BETA
—□—	00 00 00 00 L 00 00 00 00	35	60	.95	702	−.2
—◇—	00 00 00 00 H 00 00 00 00	42	60	.95	698	−.2
—○—	00 00 00 00 F 00 00 00 00	102	60	.95	699	−.2

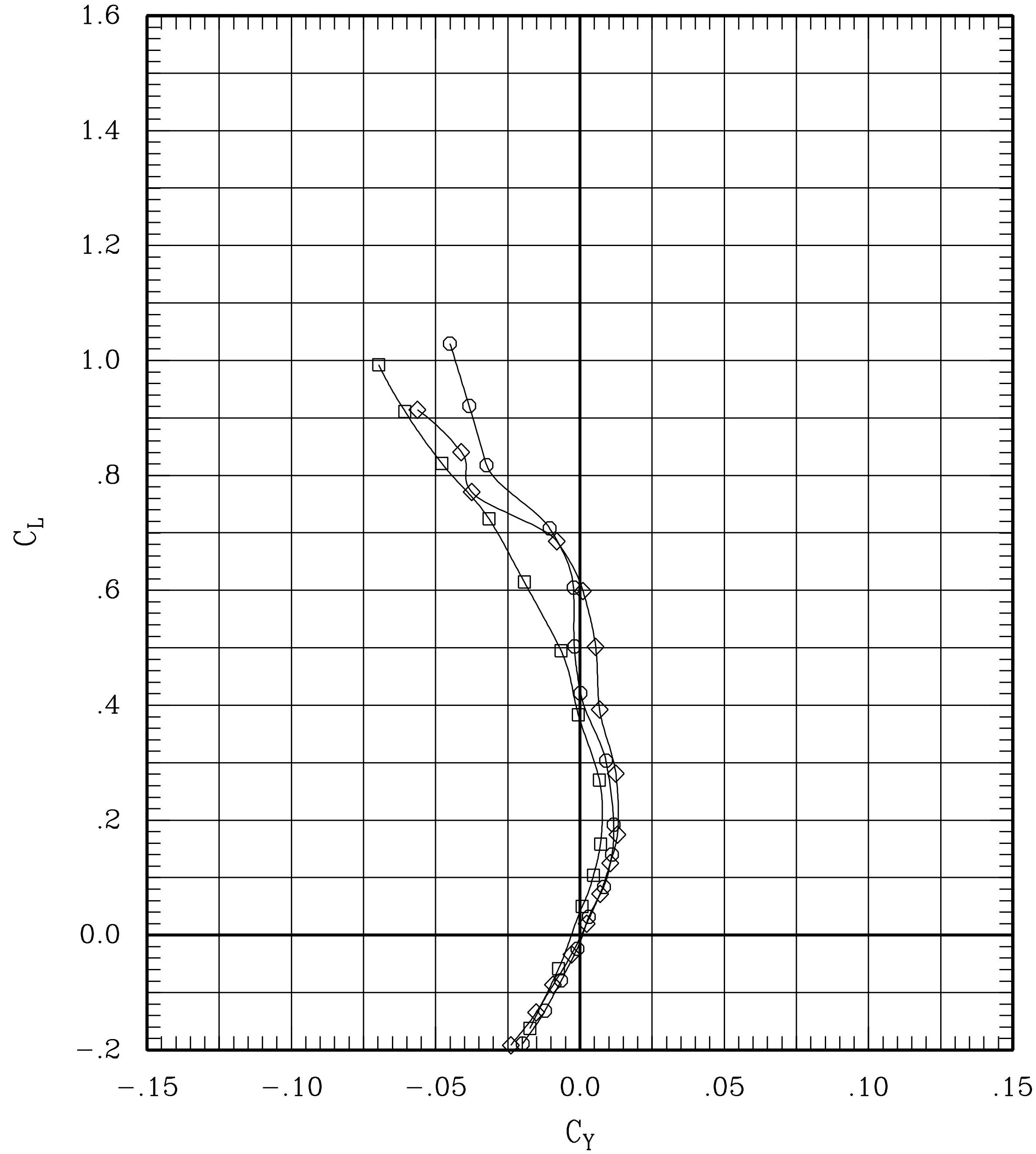

Figure 6(m). Effect of pivot height and fairing for sweep = 60 deg, Mach = 0.95.

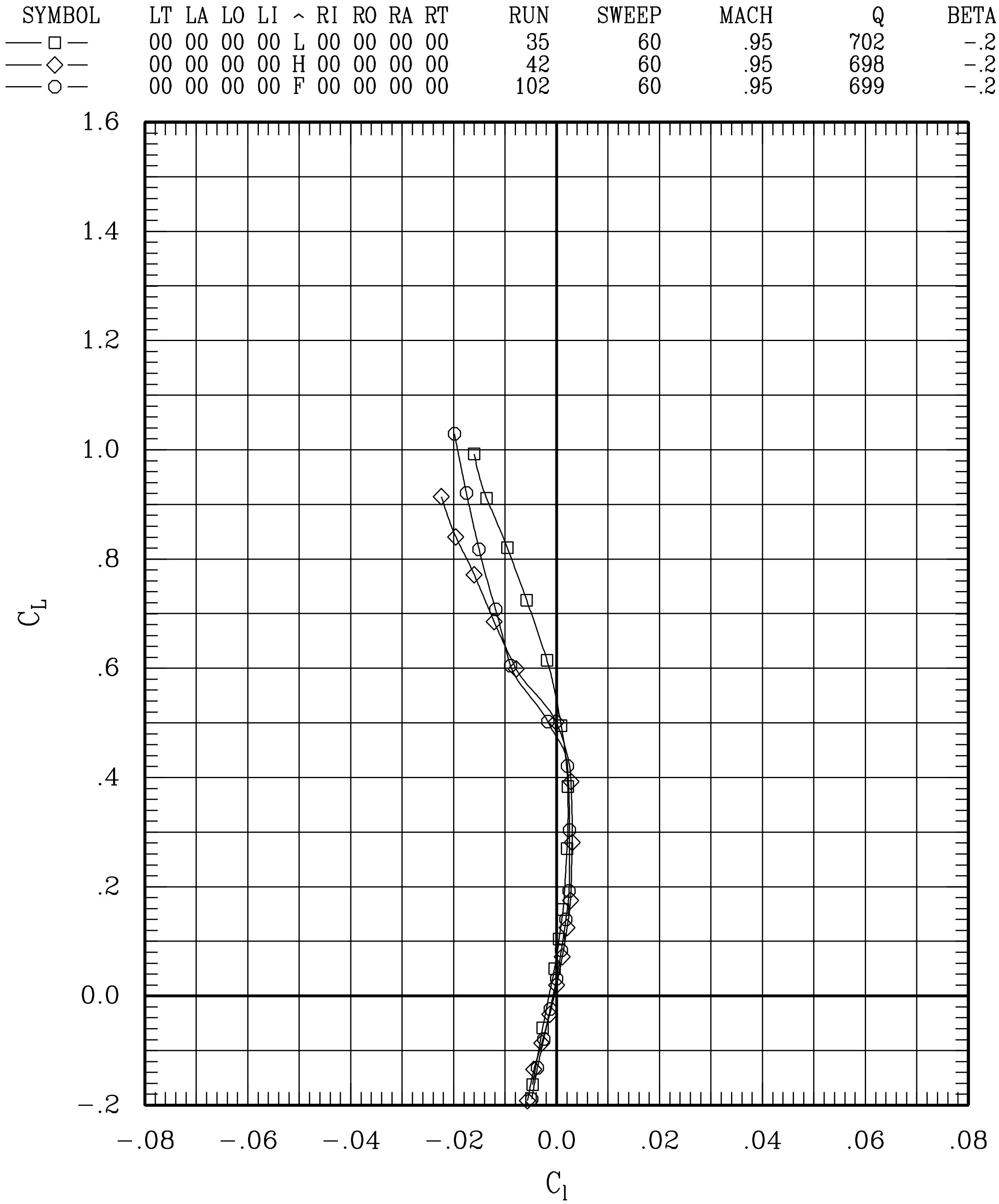

Figure 6(m). Effect of pivot height and fairing for sweep = 60 deg, Mach = 0.95.

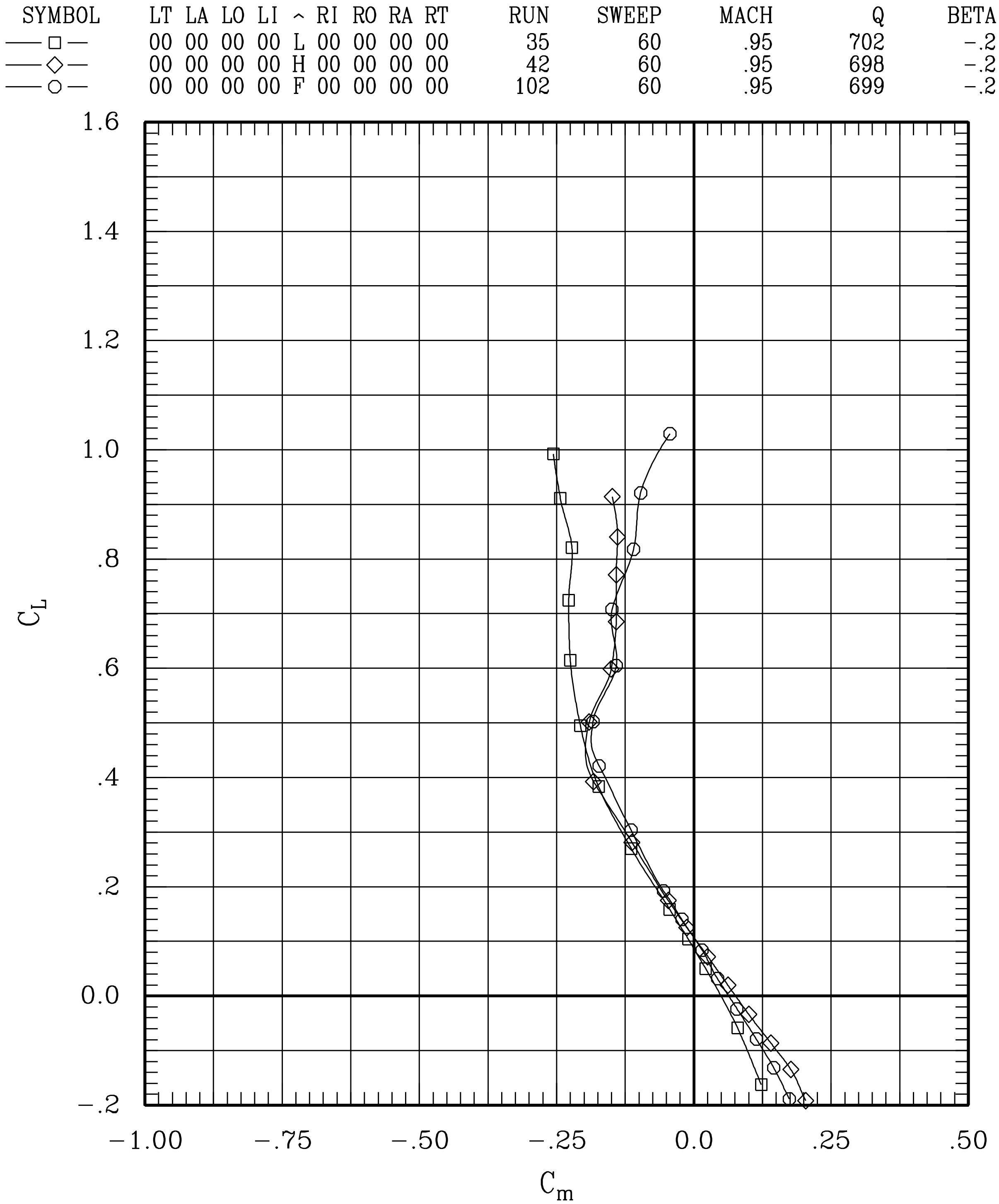

Figure 6(m). Effect of pivot height and fairing for sweep = 60 deg, Mach = 0.95.

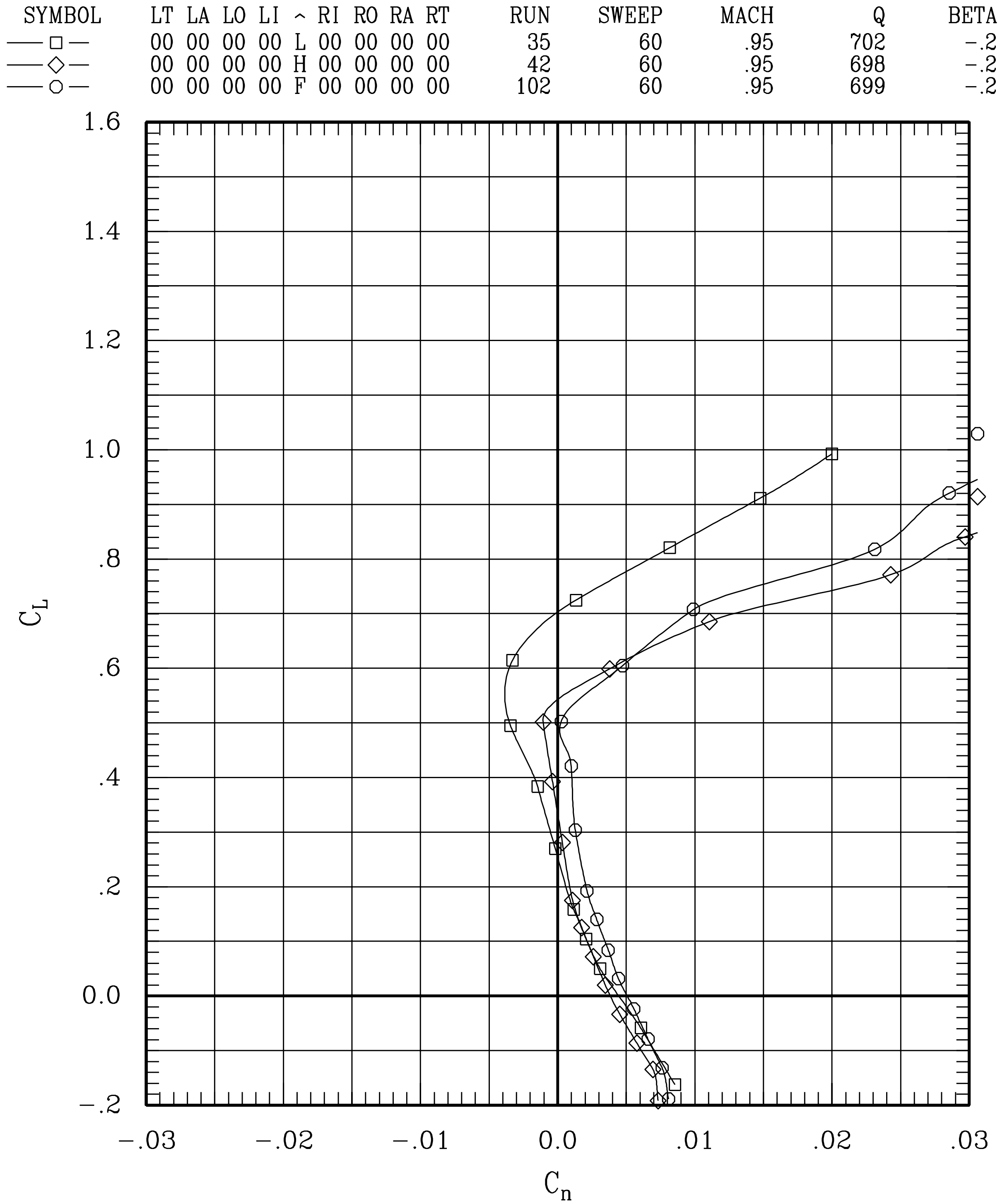

Figure 6(m). Effect of pivot height and fairing for sweep = 60 deg, Mach = 0.95.

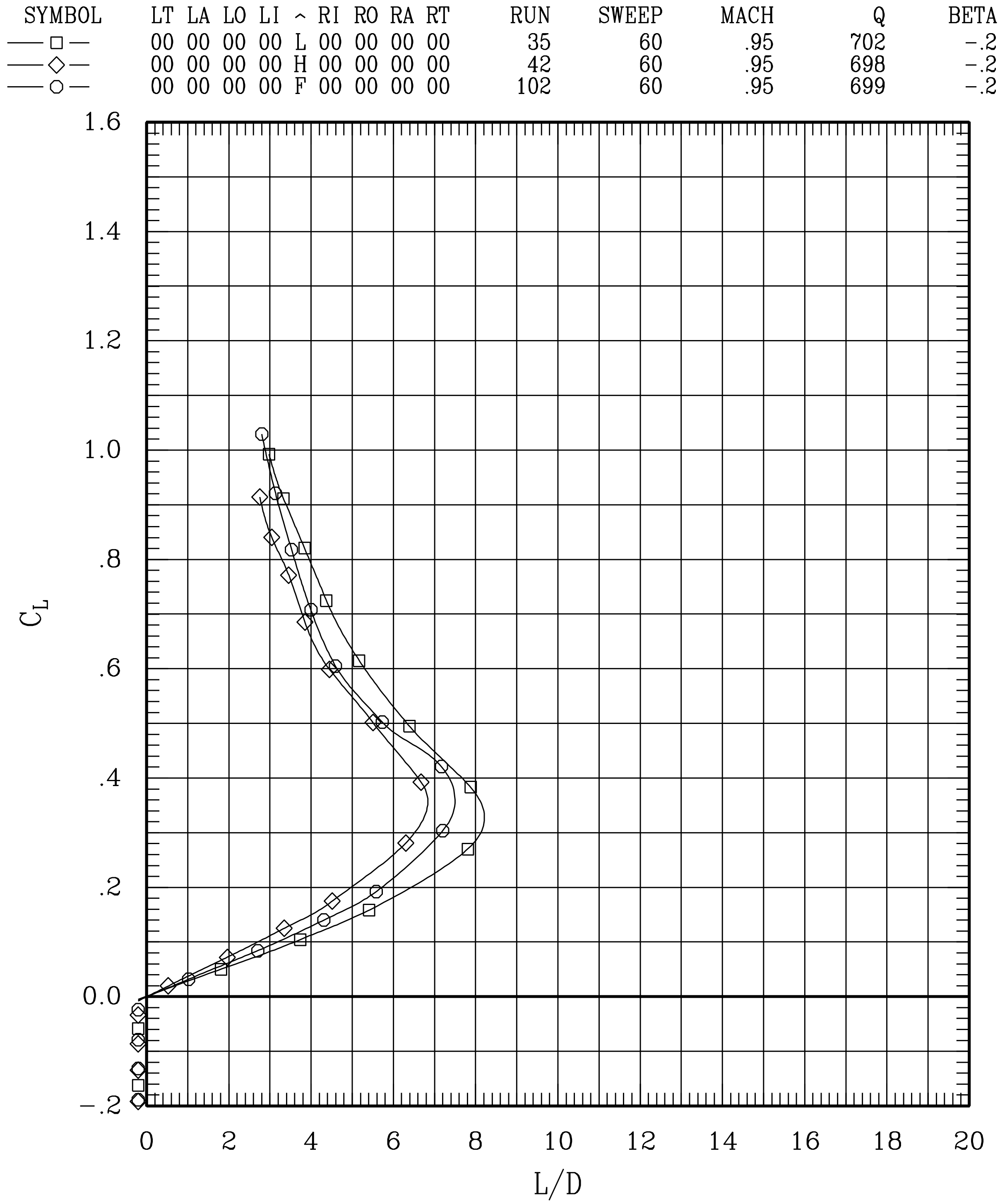

Figure 6(m). Effect of pivot height and fairing for sweep = 60 deg, Mach = 0.95.

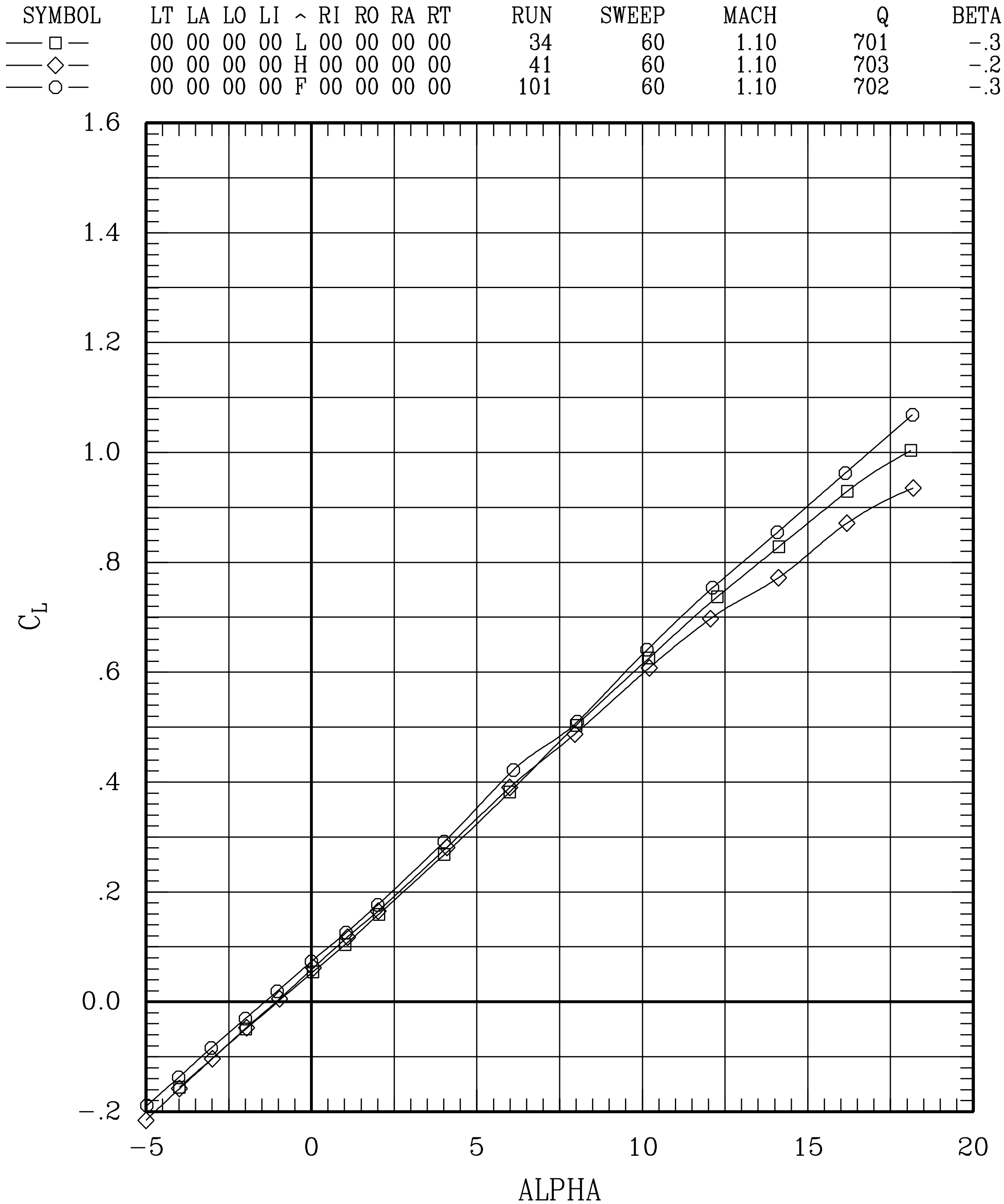

Figure 6(n). Effect of pivot height and fairing for sweep = 60 deg, Mach = 1.10.

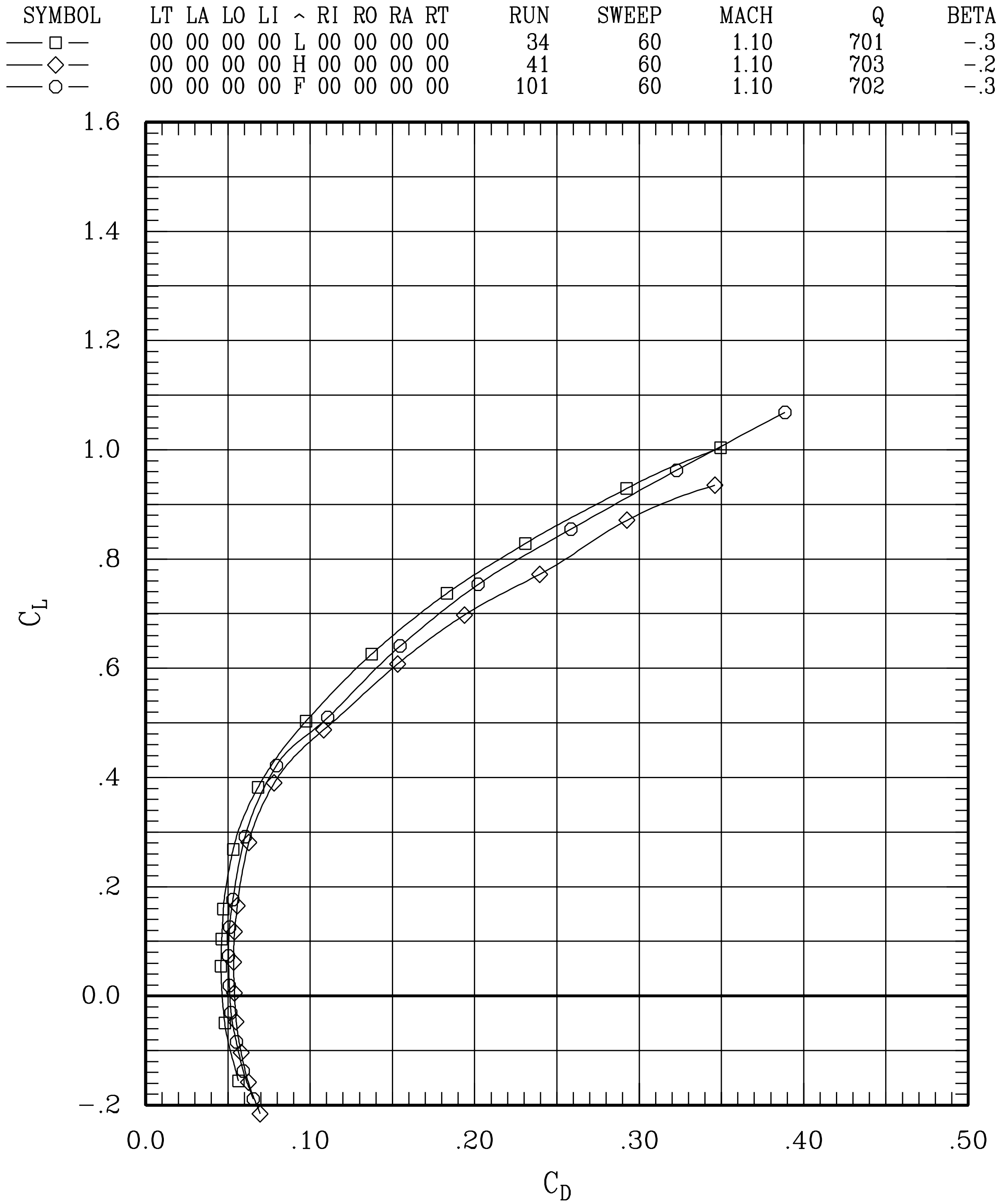

Figure 6(n). Effect of pivot height and fairing for sweep = 60 deg, Mach = 1.10.

SYMBOL	LT LA LO LI ^ RI RO RA RT	RUN	SWEEP	MACH	Q	BETA
—□—	00 00 00 00 L 00 00 00 00	34	60	1.10	701	−.3
—◇—	00 00 00 00 H 00 00 00 00	41	60	1.10	703	−.2
—○—	00 00 00 00 F 00 00 00 00	101	60	1.10	702	−.3

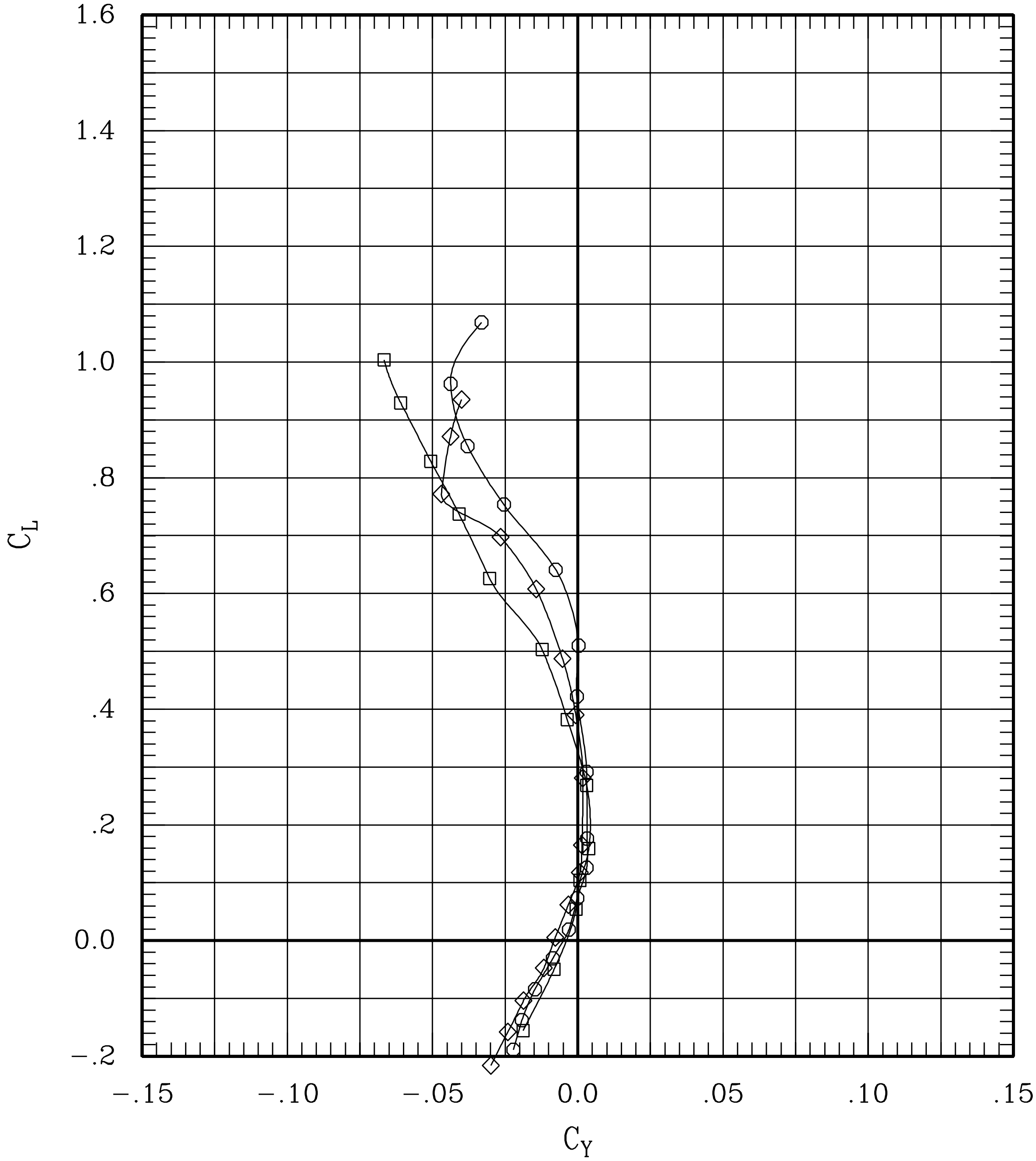

Figure 6(n). Effect of pivot height and fairing for sweep = 60 deg, Mach = 1.10.

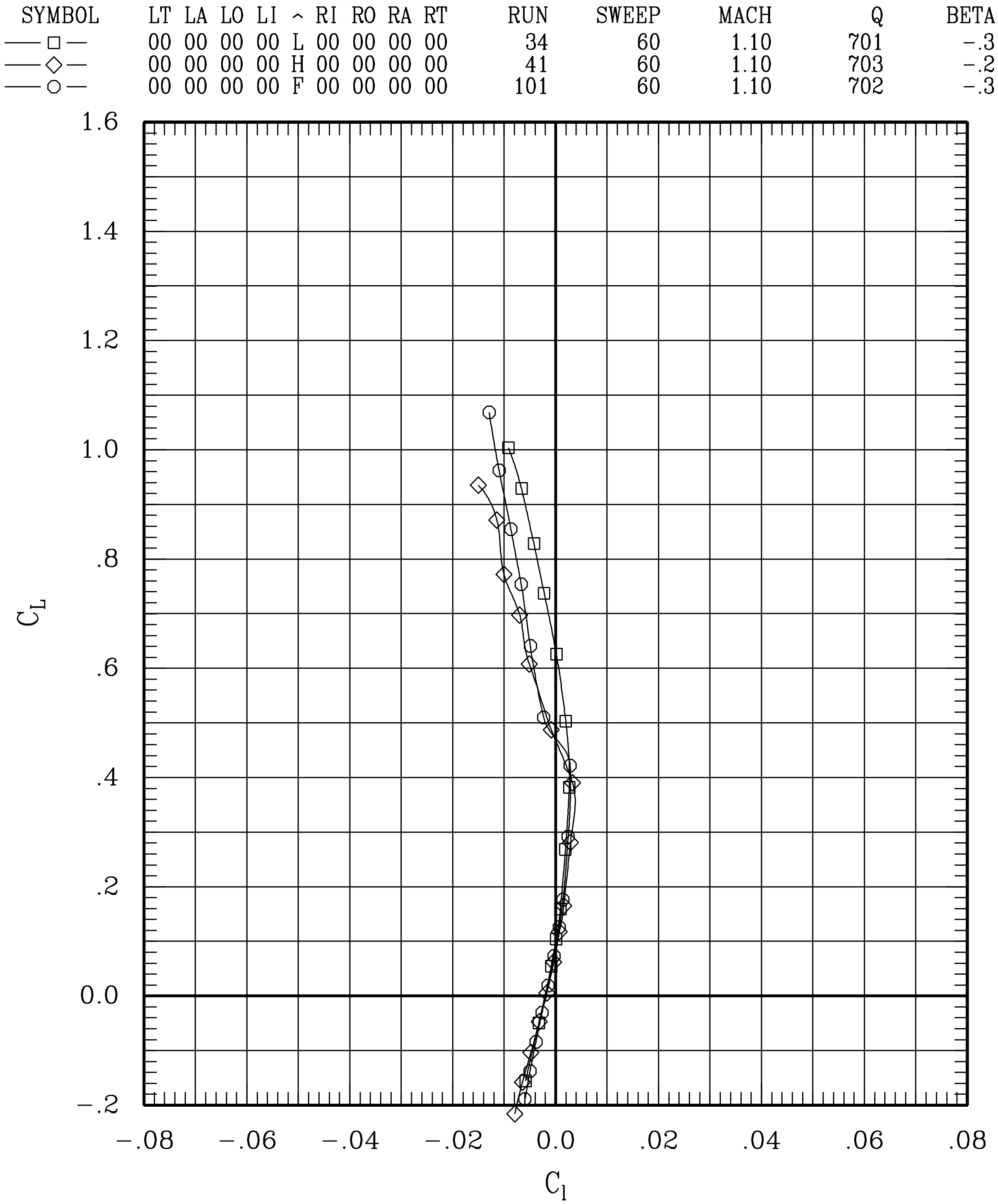

Figure 6(n). Effect of pivot height and fairing for sweep = 60 deg, Mach = 1.10.

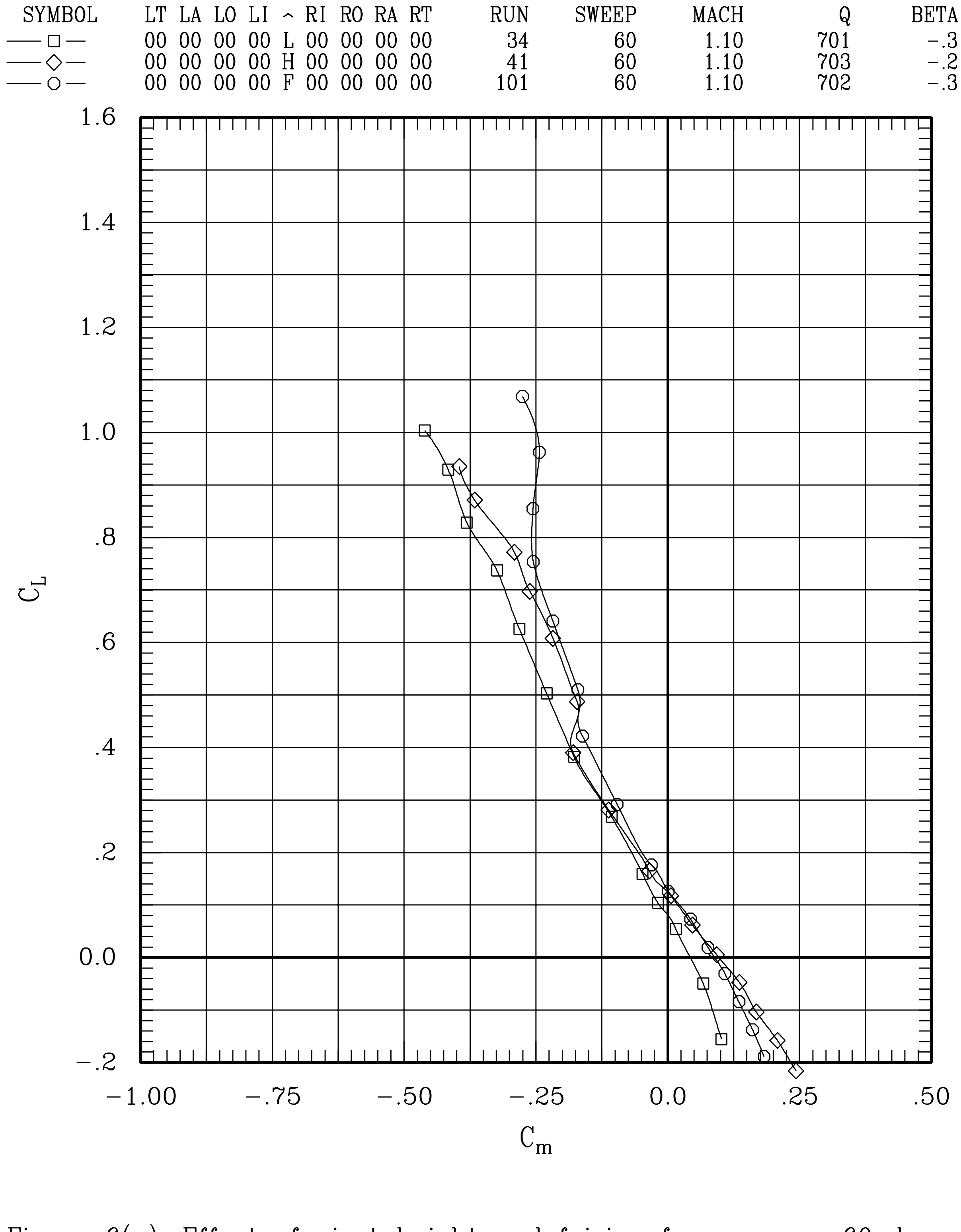

Figure 6(n). Effect of pivot height and fairing for sweep = 60 deg, Mach = 1.10.

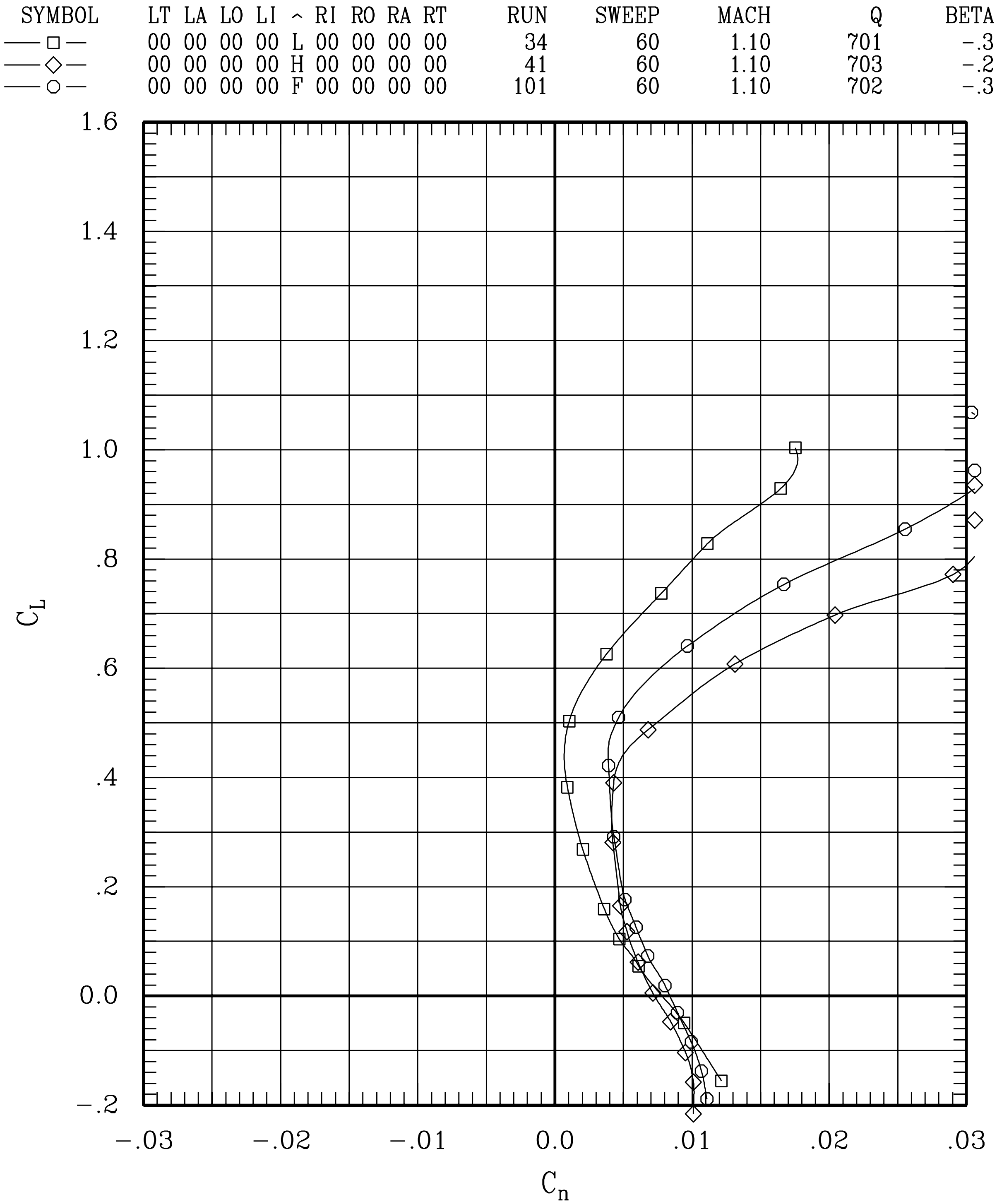

Figure 6(n). Effect of pivot height and fairing for sweep = 60 deg, Mach = 1.10.

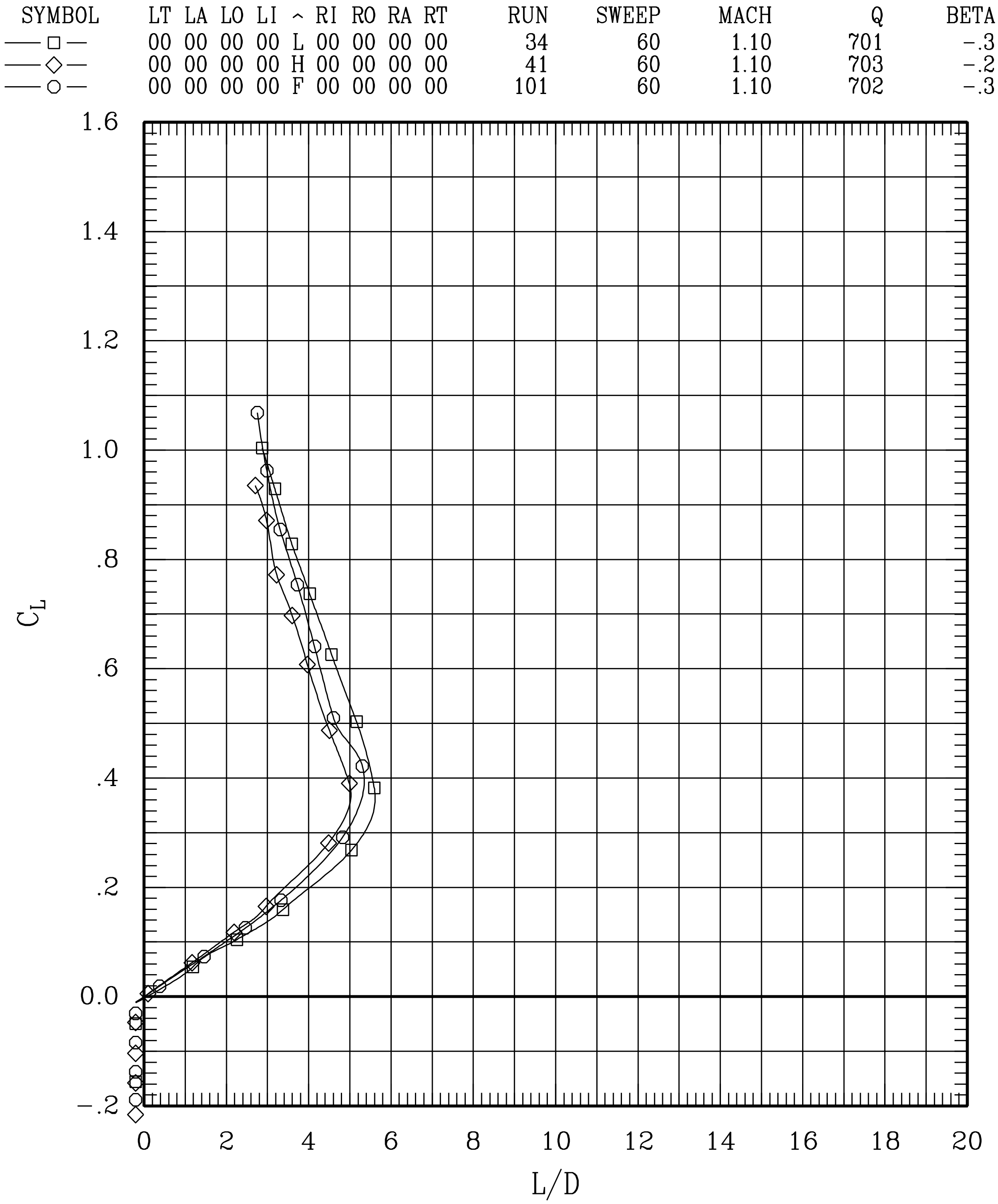

Figure 6(n). Effect of pivot height and fairing for sweep = 60 deg, Mach = 1.10.

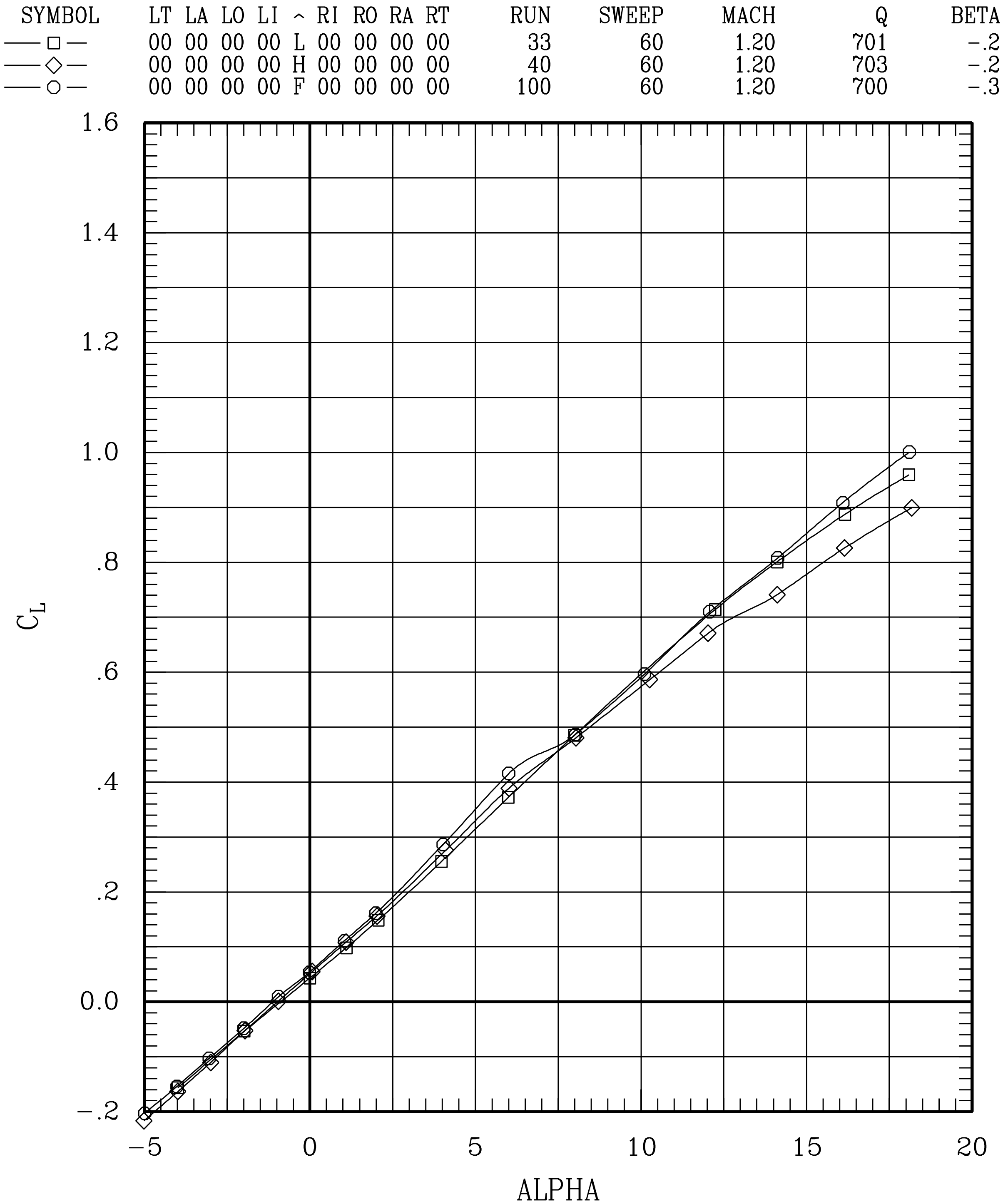

Figure 6(o). Effect of pivot height and fairing for sweep = 60 deg, Mach = 1.20.

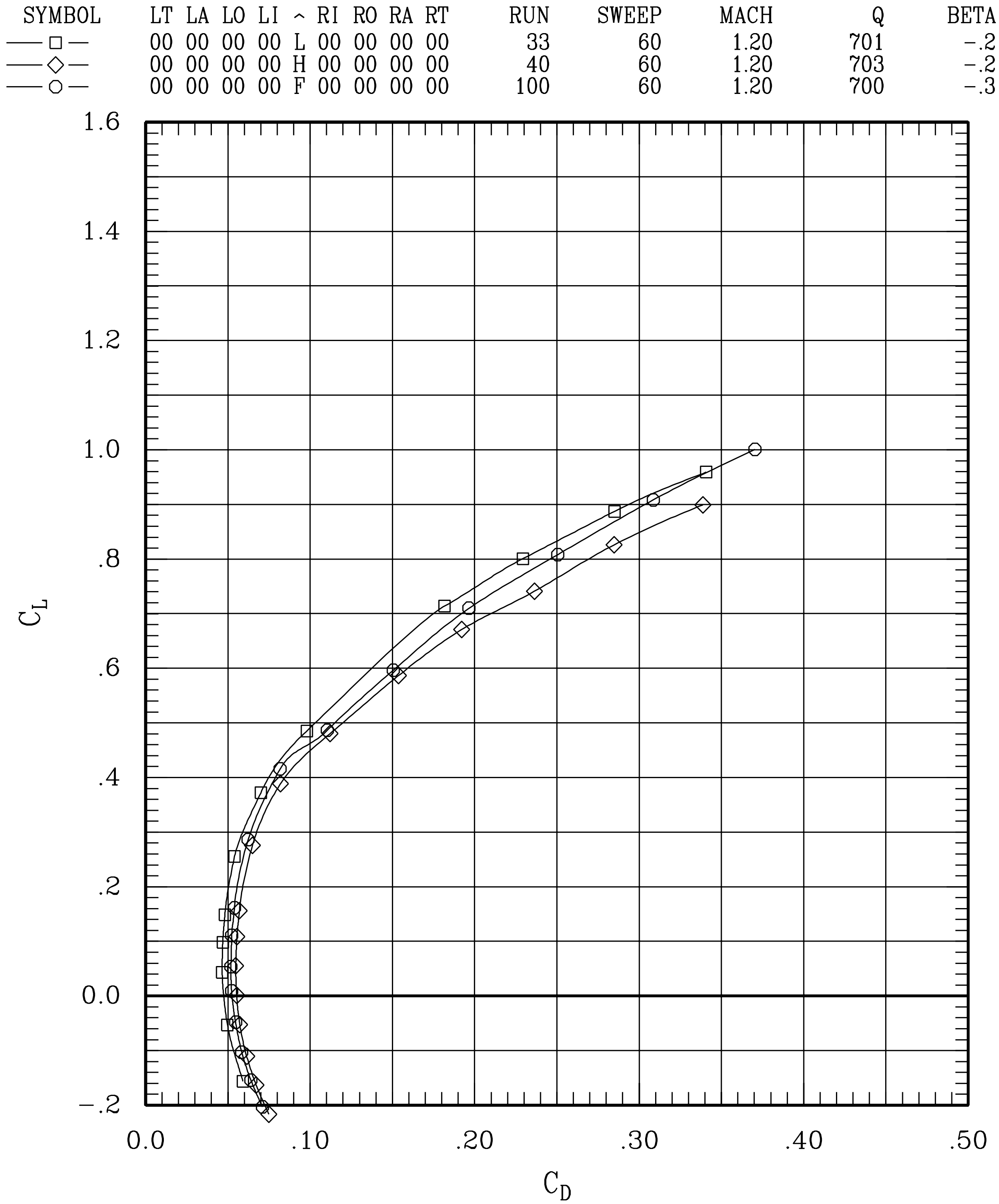

Figure 6(o). Effect of pivot height and fairing for sweep = 60 deg, Mach = 1.20.

SYMBOL	LT LA LO LI ^ RI RO RA RT	RUN	SWEEP	MACH	Q	BETA
—□—	00 00 00 00 L 00 00 00 00	33	60	1.20	701	−.2
—◇—	00 00 00 00 H 00 00 00 00	40	60	1.20	703	−.2
—○—	00 00 00 00 F 00 00 00 00	100	60	1.20	700	−.3

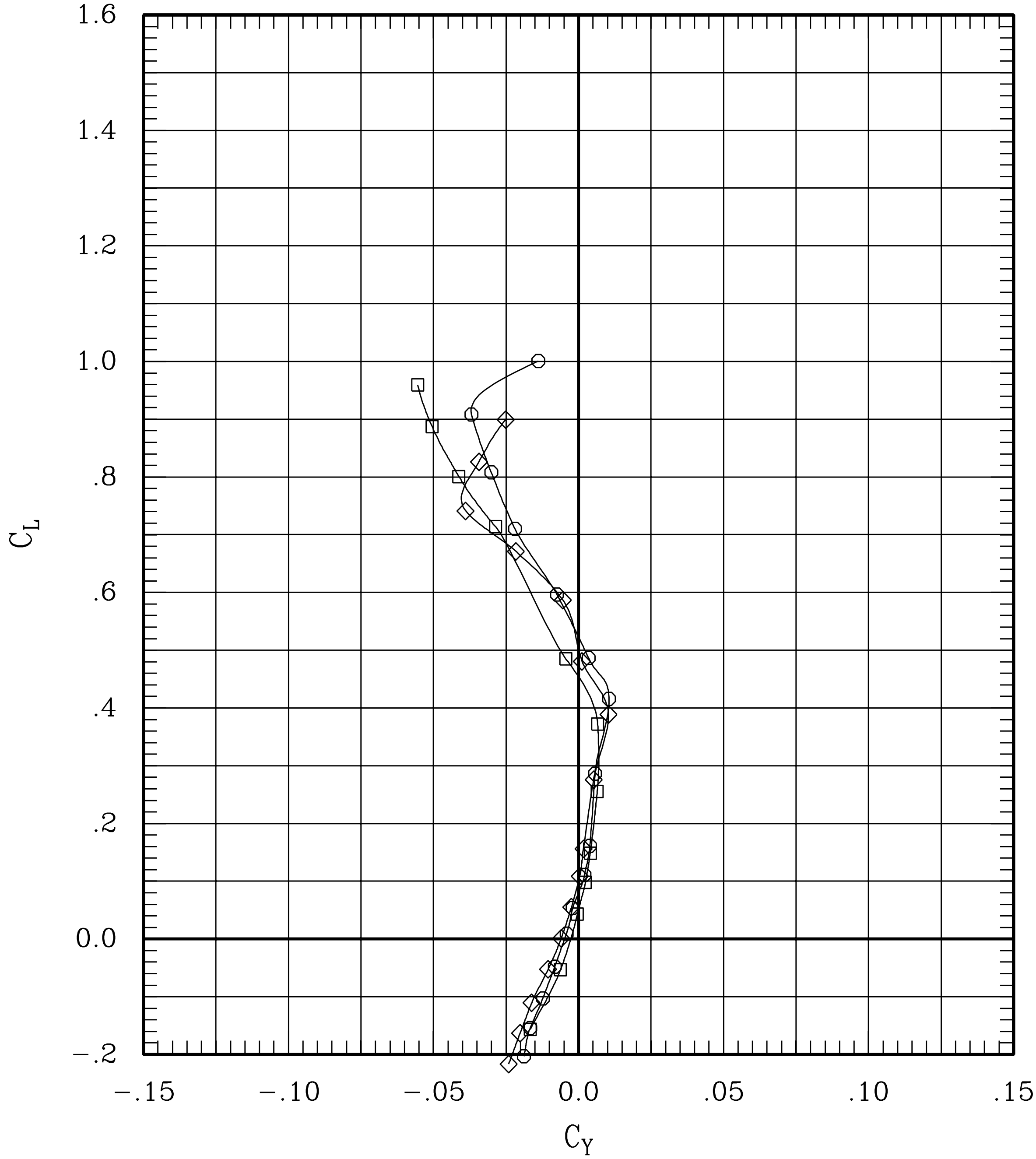

Figure 6(o). Effect of pivot height and fairing for sweep = 60 deg, Mach = 1.20.

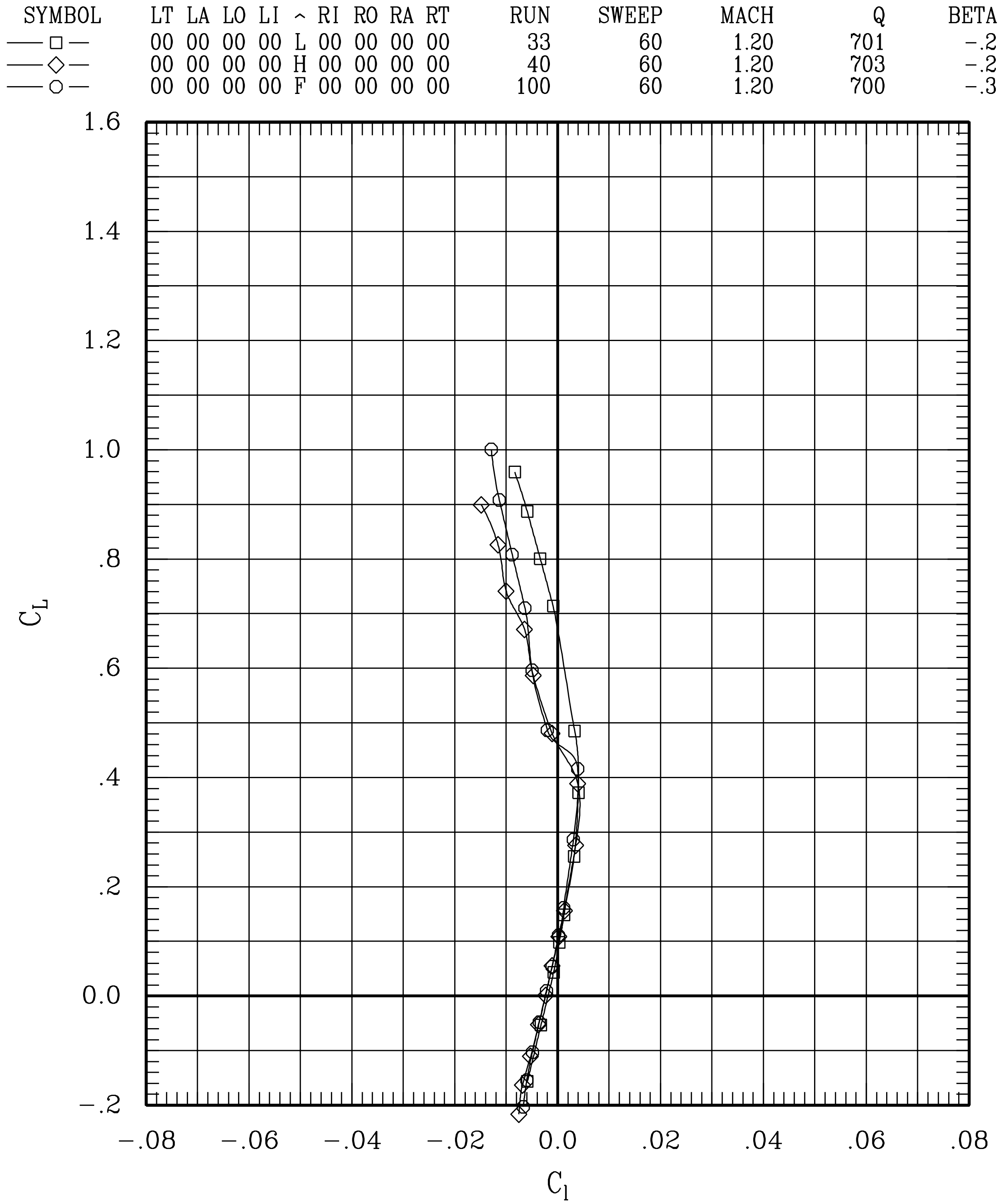

Figure 6(o). Effect of pivot height and fairing for sweep = 60 deg, Mach = 1.20.

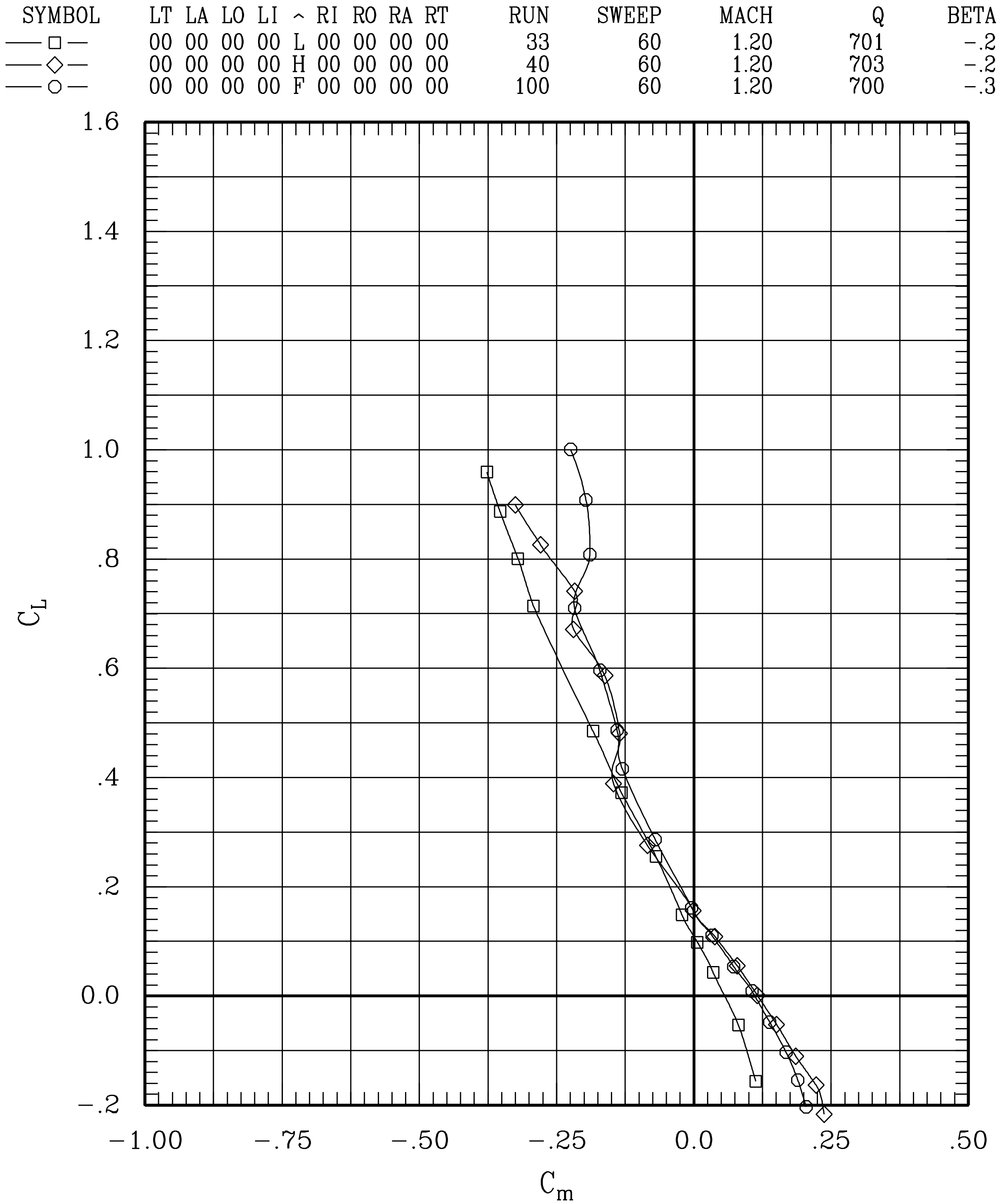

Figure 6(o). Effect of pivot height and fairing for sweep = 60 deg, Mach = 1.20.

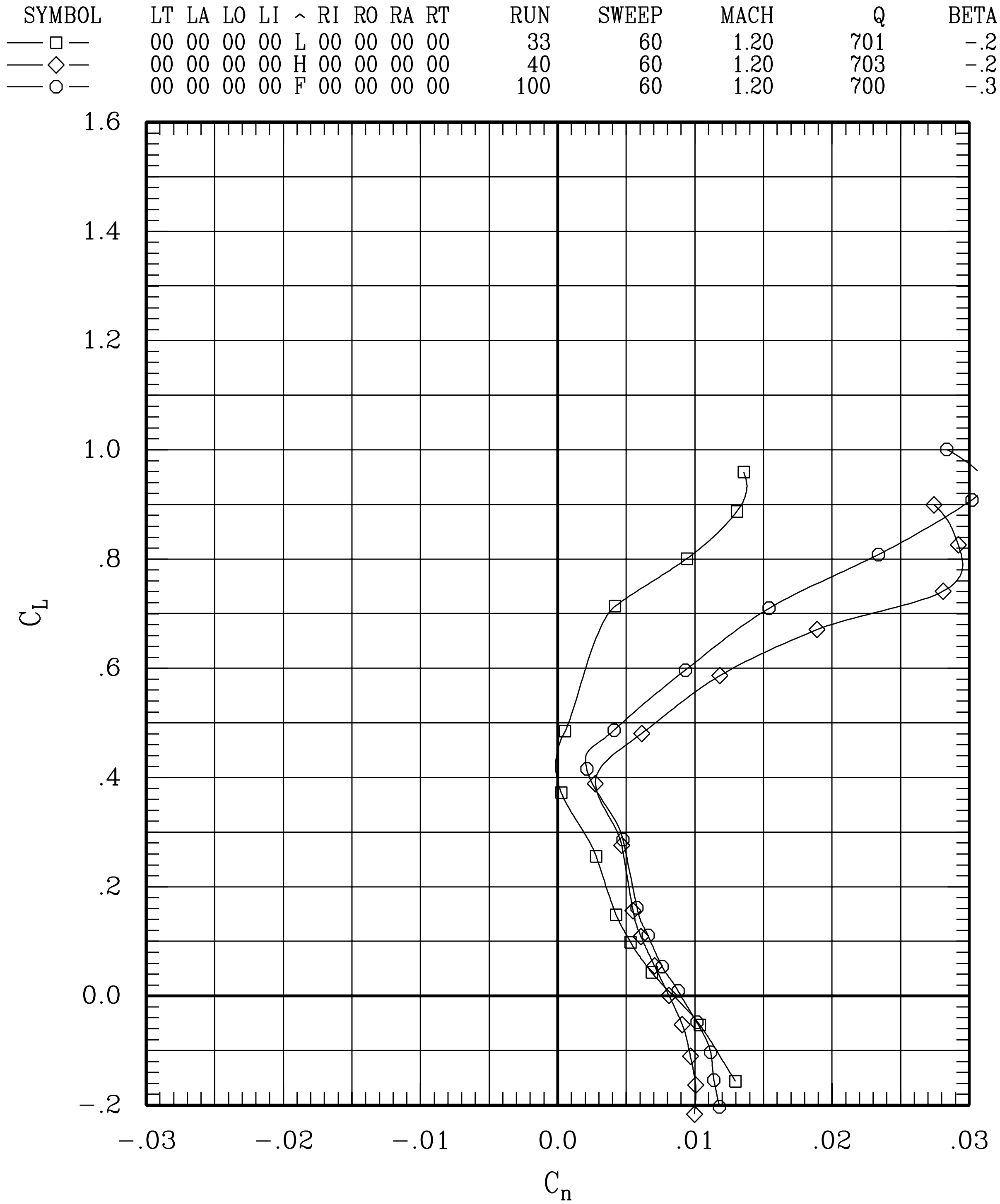

Figure 6(o). Effect of pivot height and fairing for sweep = 60 deg, Mach = 1.20.

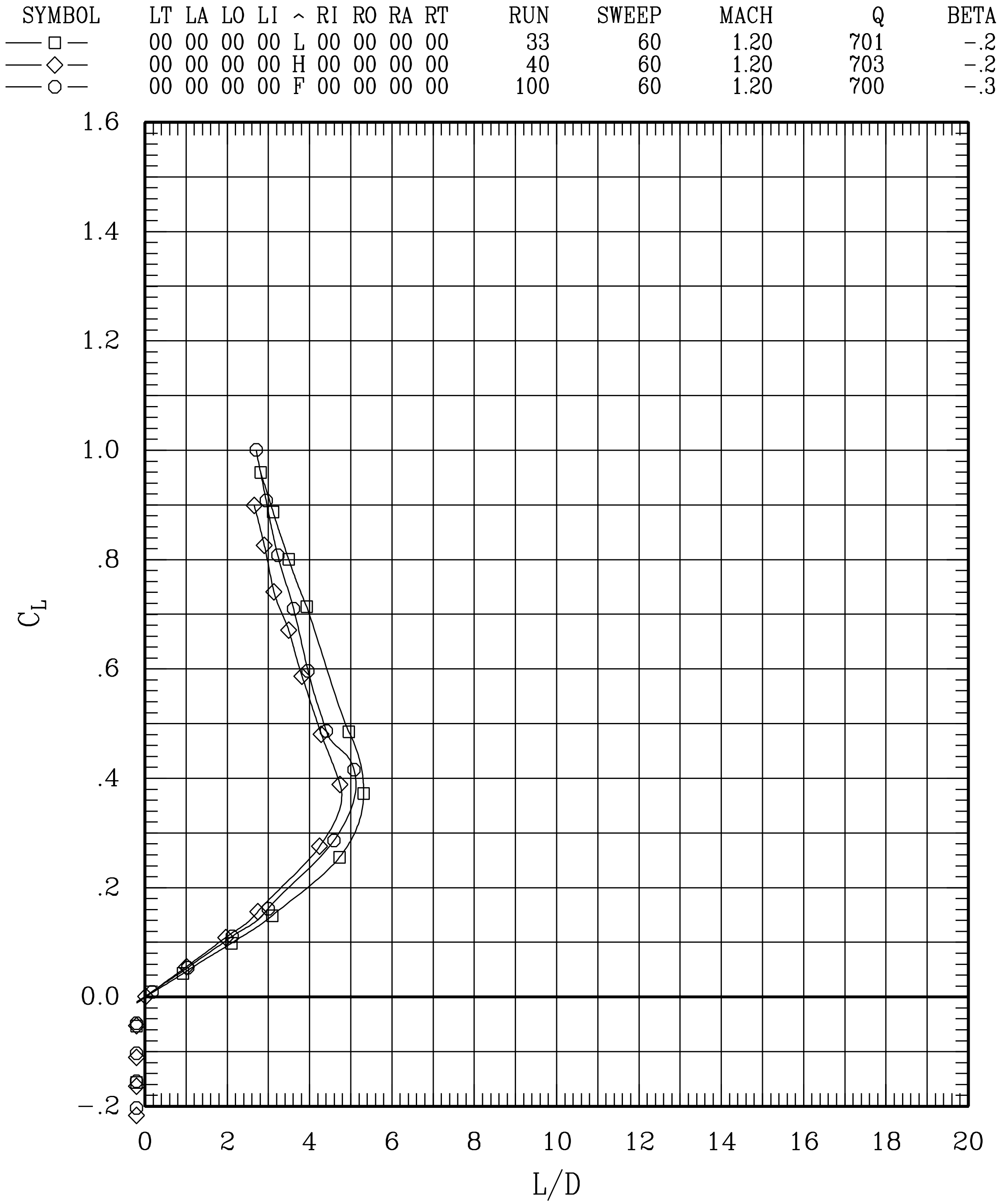

Figure 6(o). Effect of pivot height and fairing for sweep = 60 deg, Mach = 1.20.

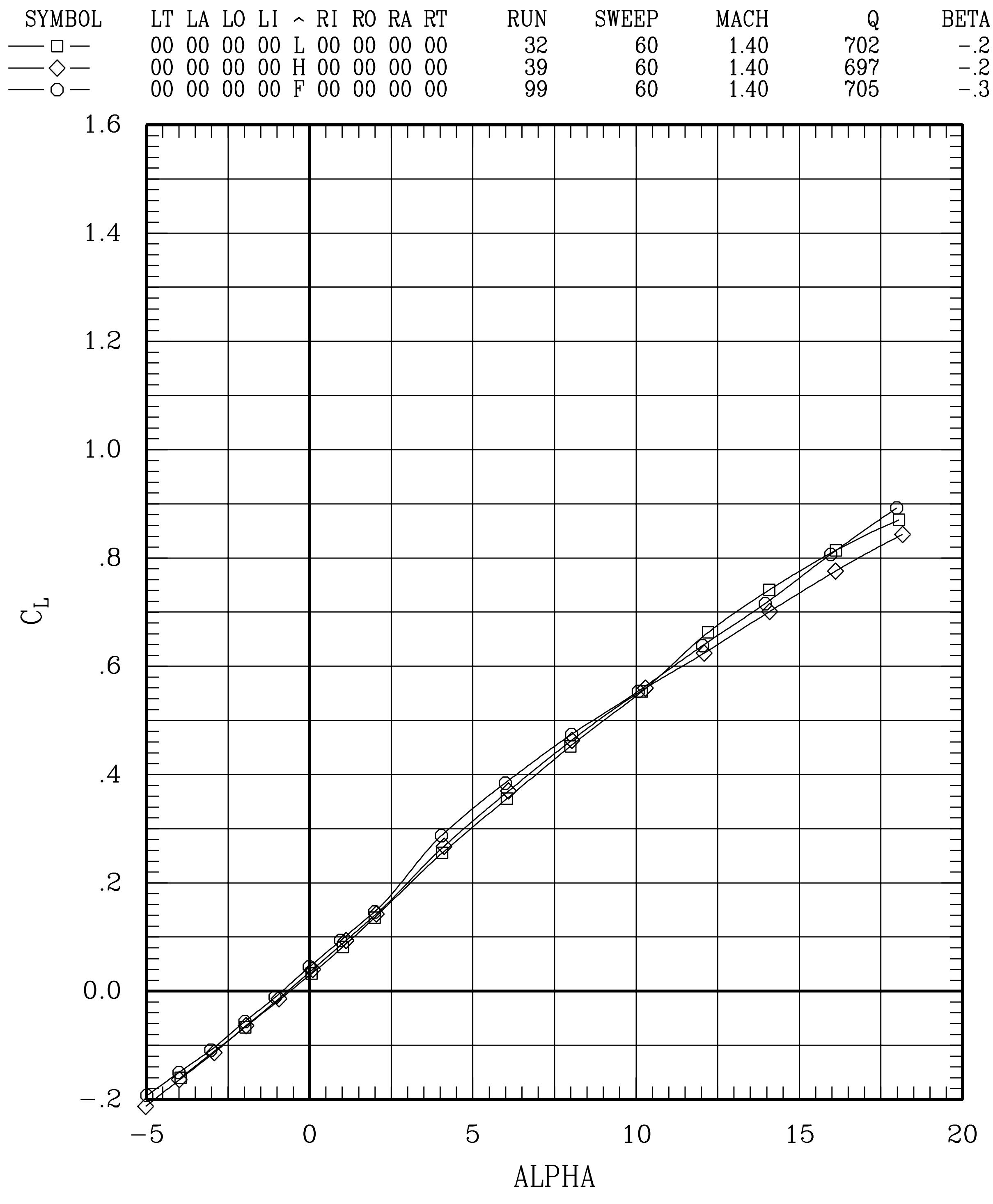

Figure 6(p). Effect of pivot height and fairing for sweep = 60 deg, Mach = 1.40.

SYMBOL	LT	LA	LO	LI	^	RI	RO	RA	RT	RUN	SWEEP	MACH	Q	BETA
—□—	00	00	00	00	L	00	00	00	00	32	60	1.40	702	−.2
—◇—	00	00	00	00	H	00	00	00	00	39	60	1.40	697	−.2
—○—	00	00	00	00	F	00	00	00	00	99	60	1.40	705	−.3

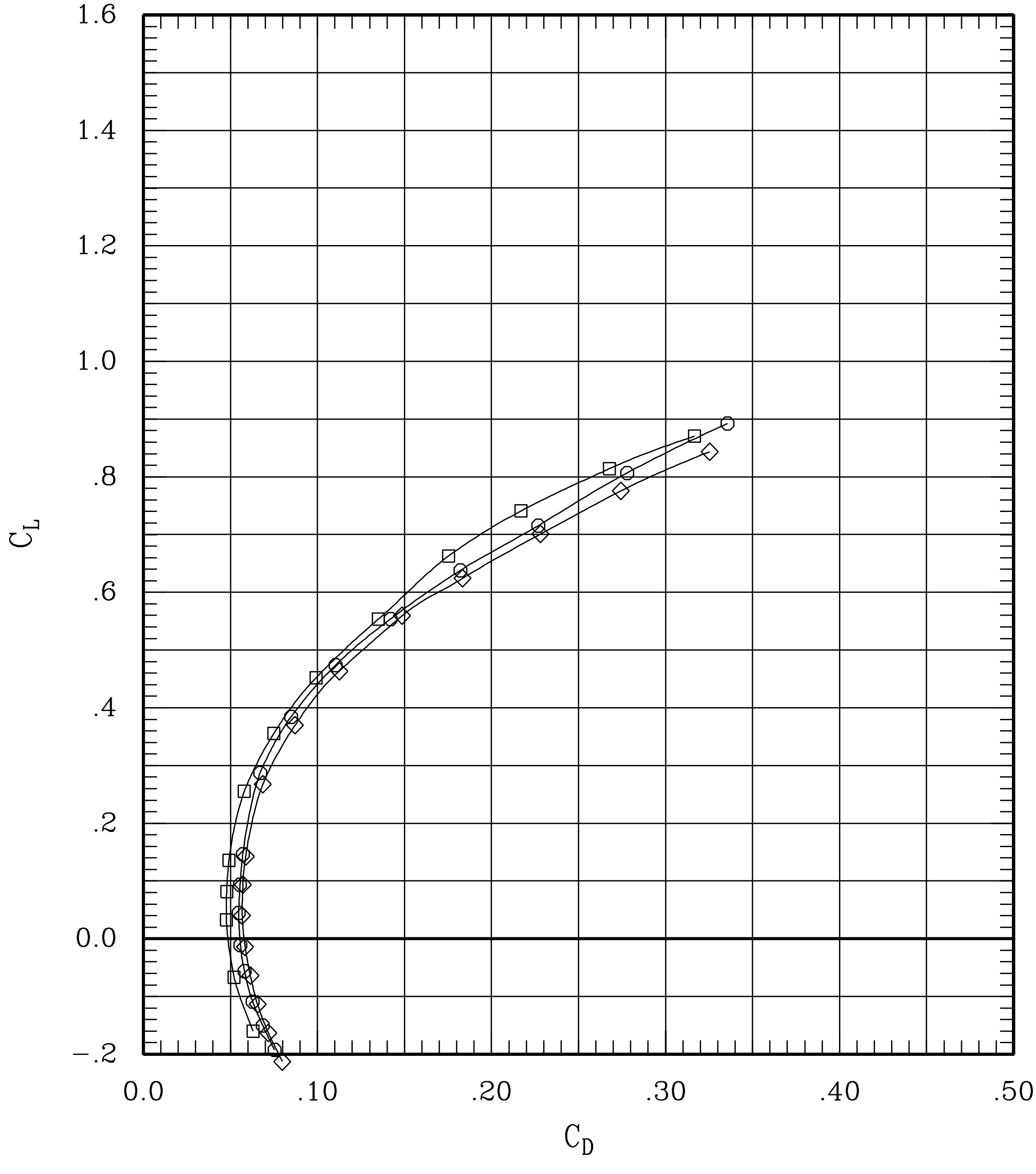

Figure 6(p). Effect of pivot height and fairing for sweep = 60 deg, Mach = 1.40.

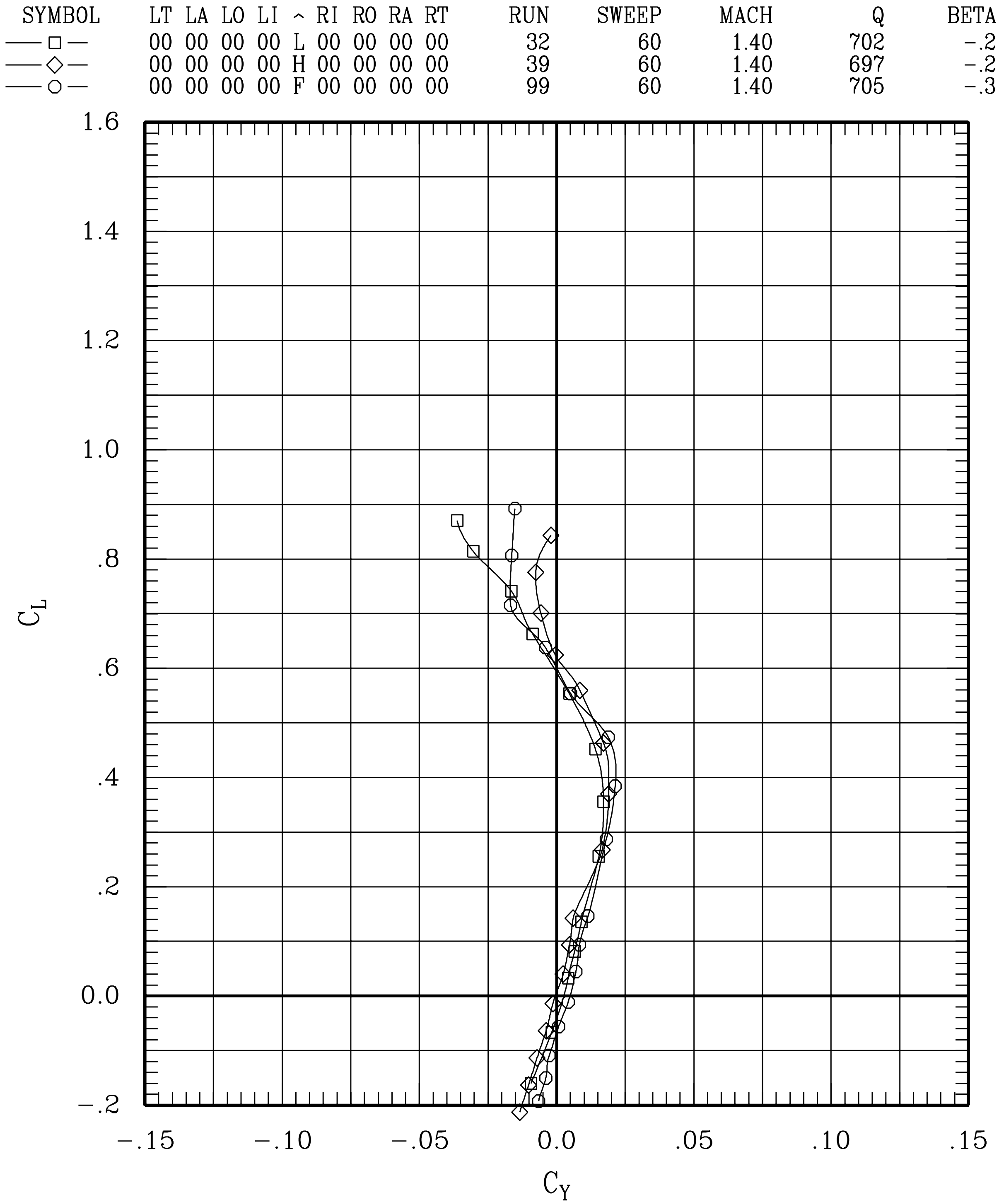

Figure 6(p). Effect of pivot height and fairing for sweep = 60 deg, Mach = 1.40.

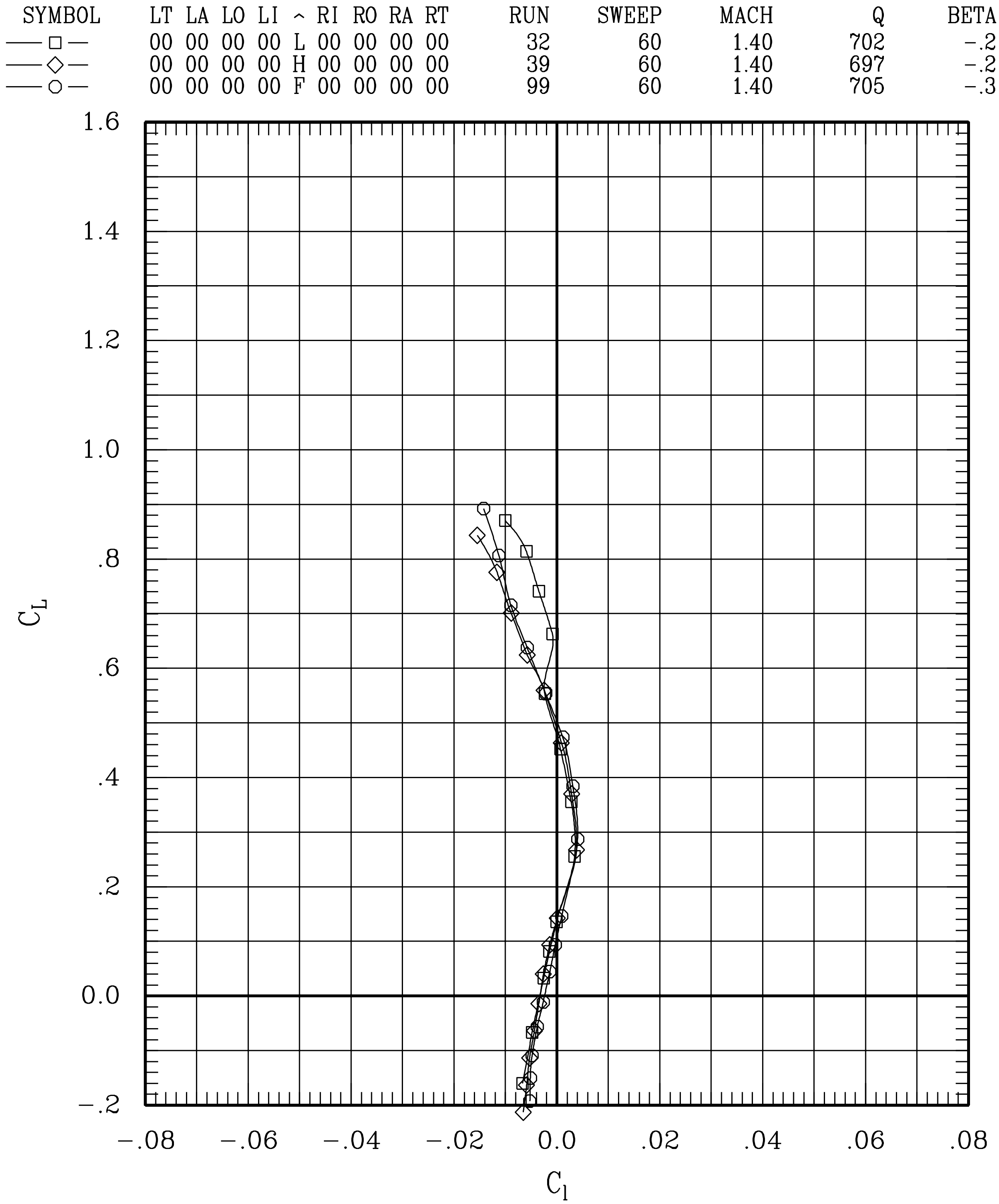

Figure 6(p). Effect of pivot height and fairing for sweep = 60 deg, Mach = 1.40.

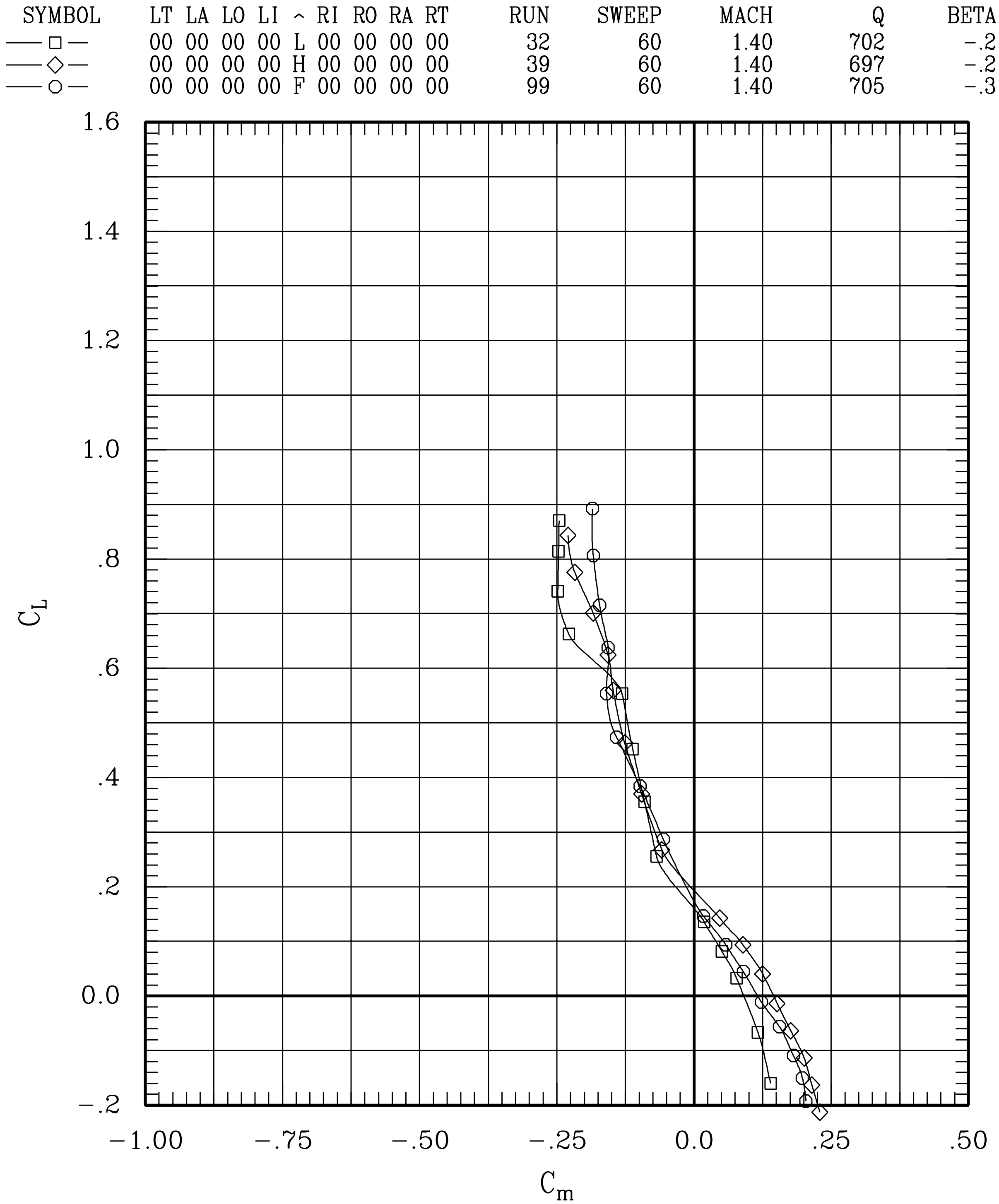

Figure 6(p). Effect of pivot height and fairing for sweep = 60 deg, Mach = 1.40.

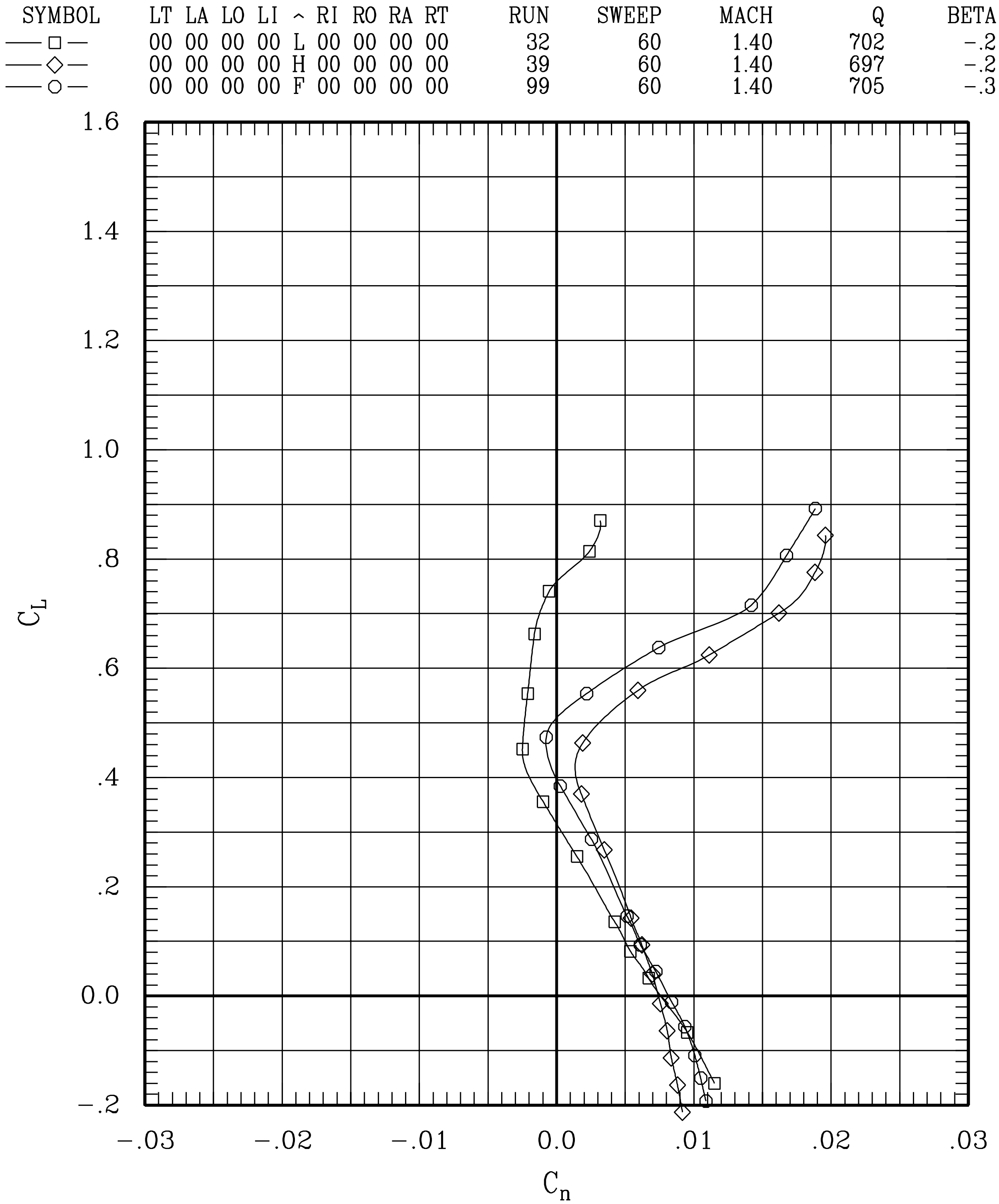

Figure 6(p). Effect of pivot height and fairing for sweep = 60 deg, Mach = 1.40.

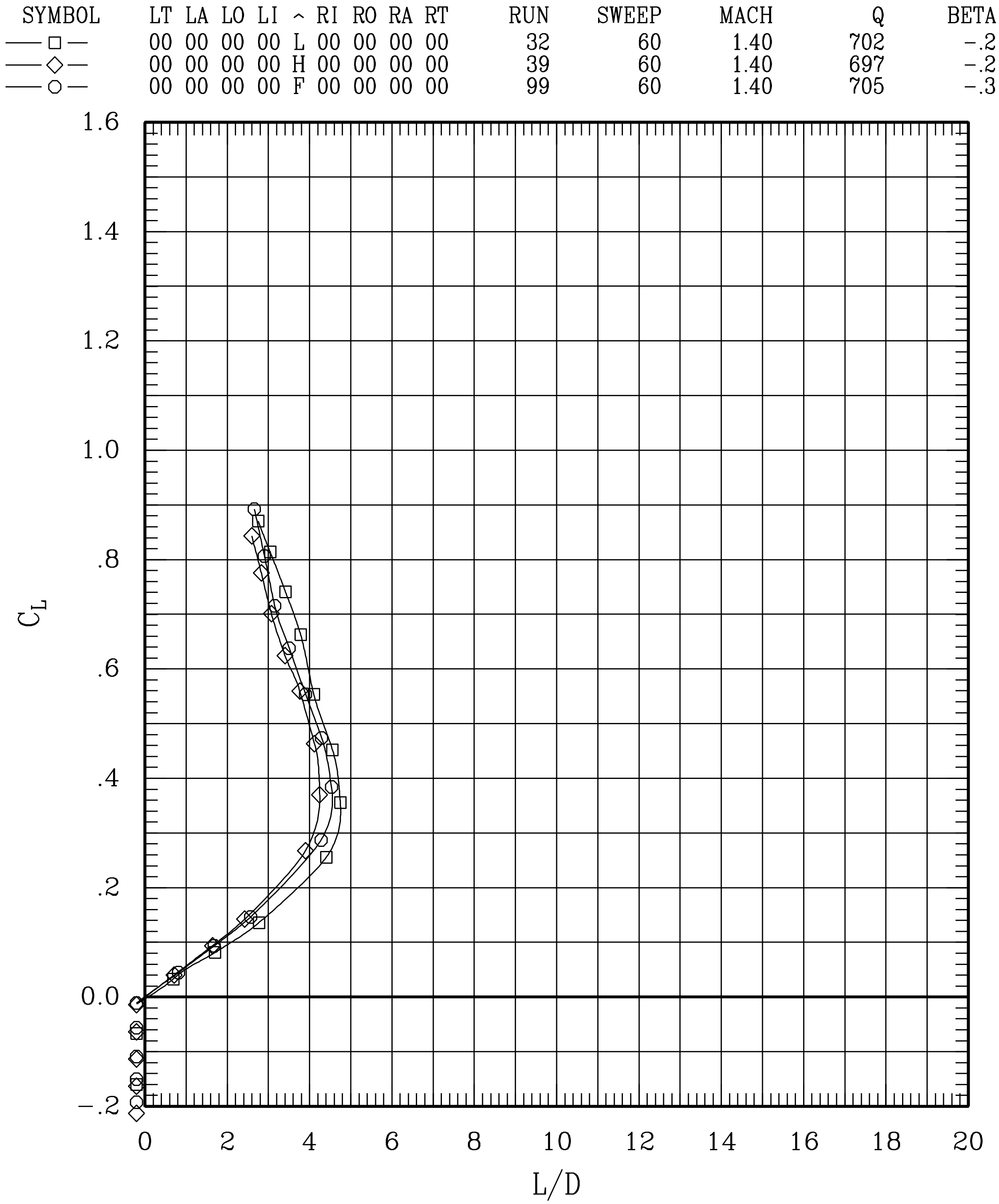

Figure 6(p). Effect of pivot height and fairing for sweep = 60 deg, Mach = 1.40.

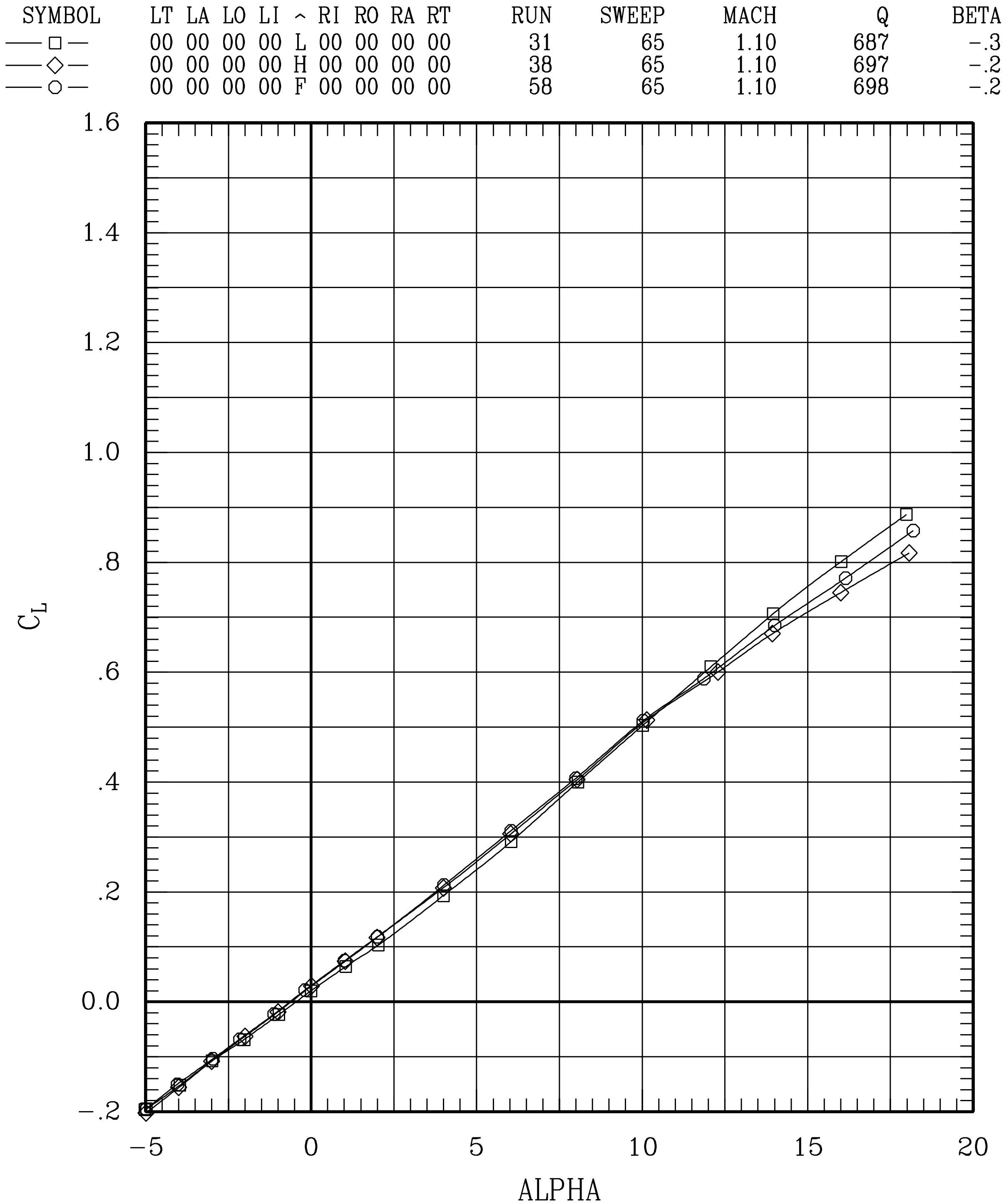

Figure 6(q). Effect of pivot height and fairing for sweep = 65 deg, Mach = 1.10.

SYMBOL	LT LA LO LI ^ RI RO RA RT	RUN	SWEEP	MACH	Q	BETA
—□—	00 00 00 00 L 00 00 00 00	31	65	1.10	687	-.3
—◇—	00 00 00 00 H 00 00 00 00	38	65	1.10	697	-.2
—○—	00 00 00 00 F 00 00 00 00	58	65	1.10	698	-.2

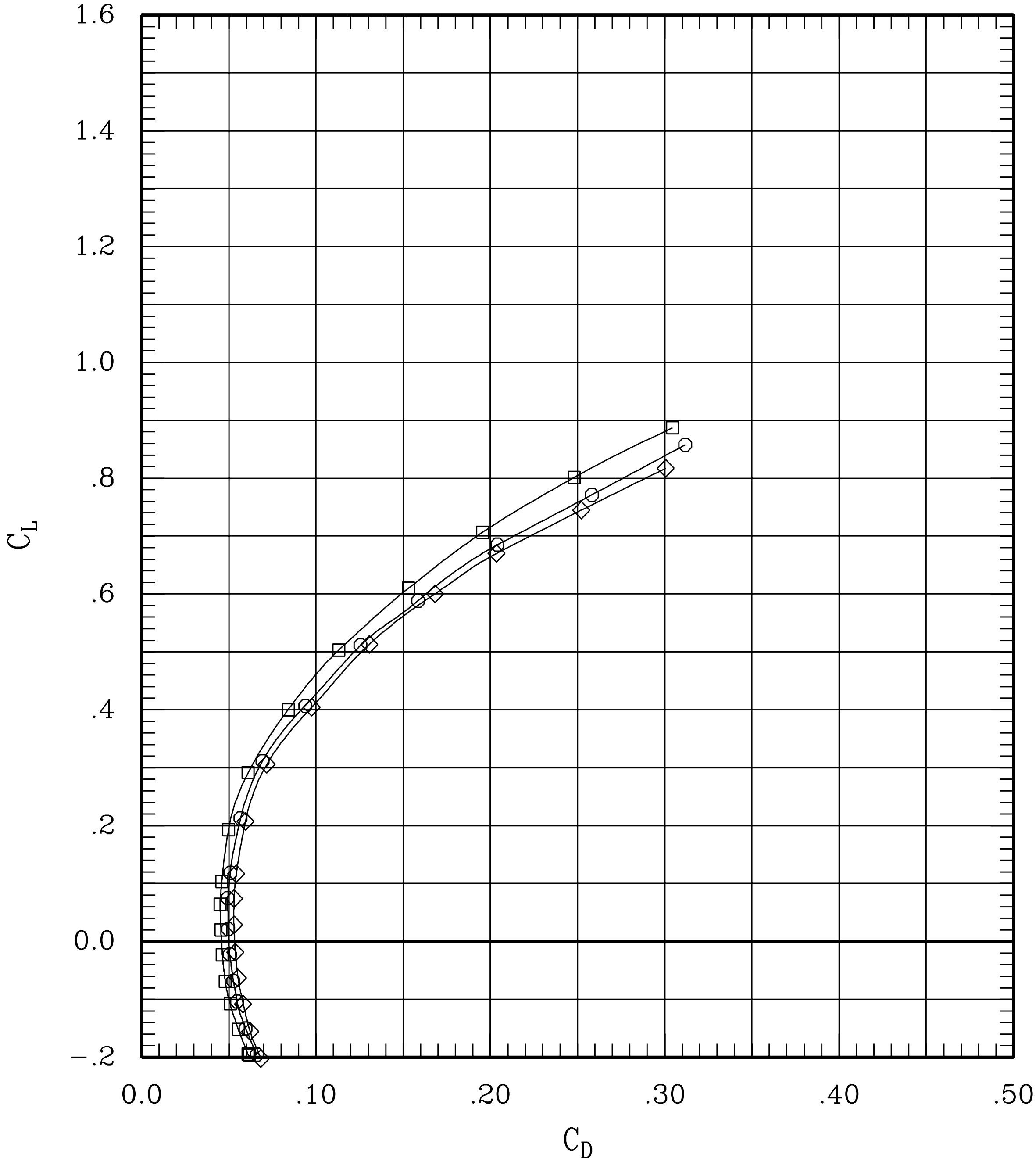

Figure 6(q). Effect of pivot height and fairing for sweep = 65 deg, Mach = 1.10.

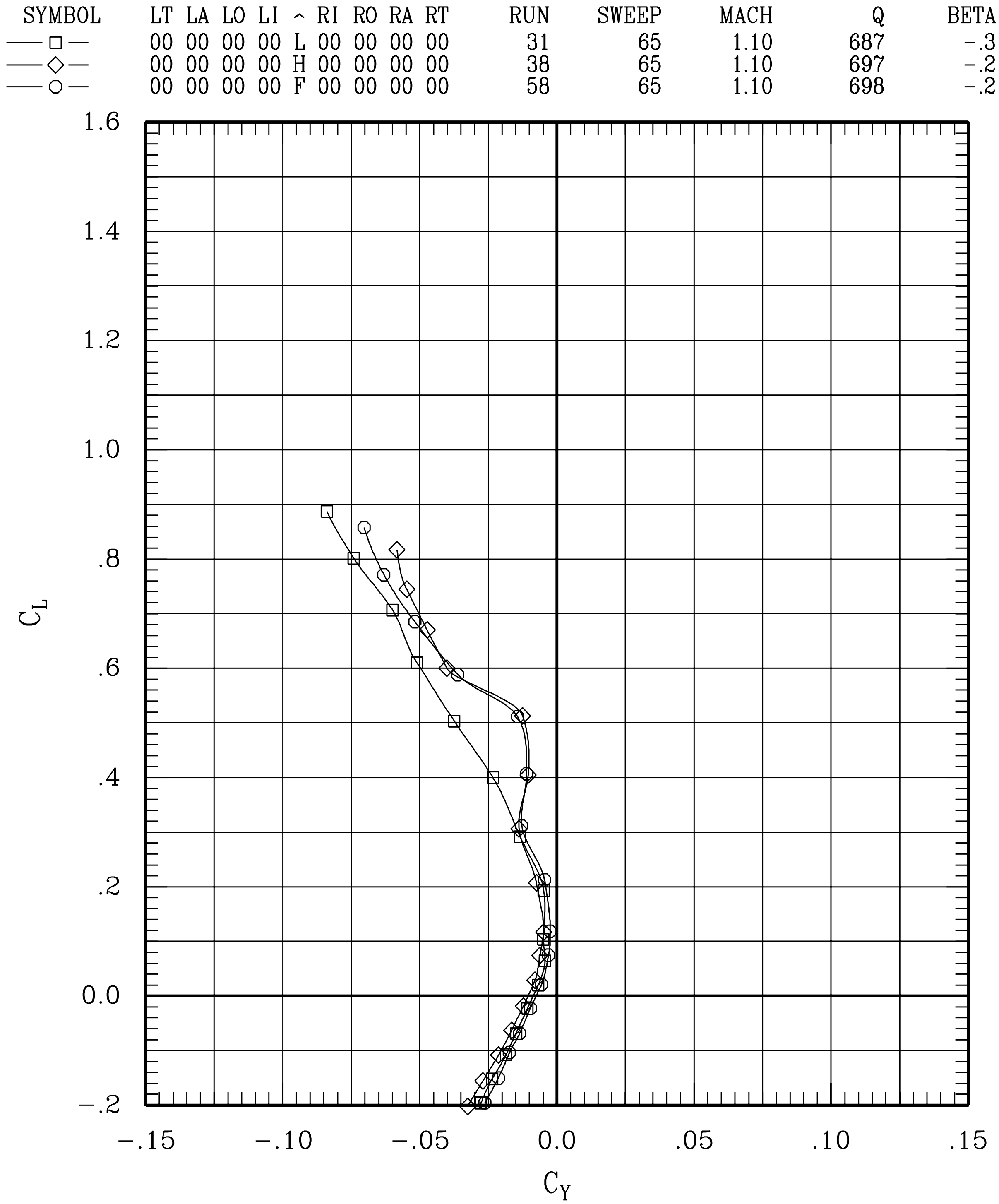

Figure 6(q). Effect of pivot height and fairing for sweep = 65 deg, Mach = 1.10.

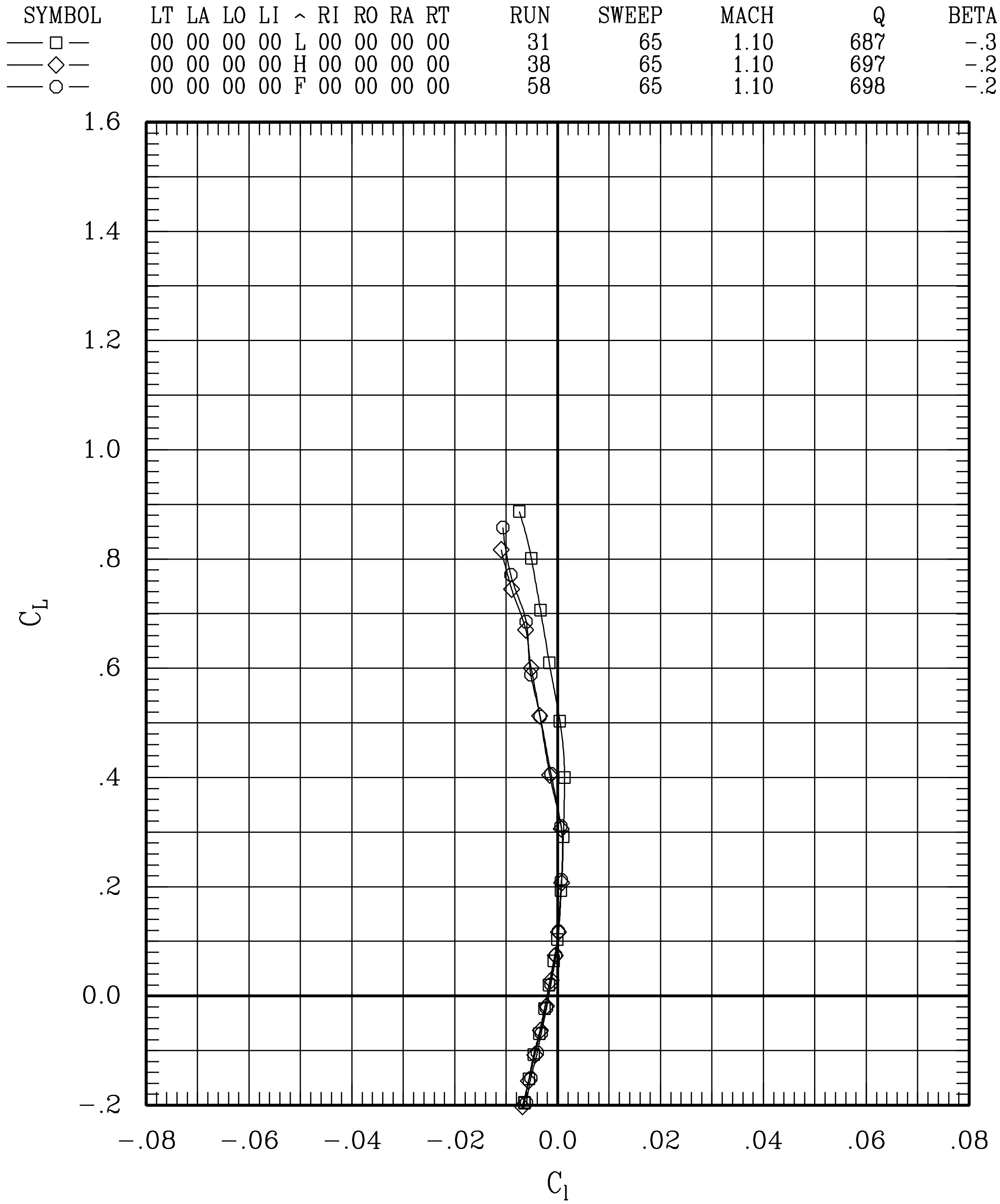

Figure 6(q). Effect of pivot height and fairing for sweep = 65 deg, Mach = 1.10.

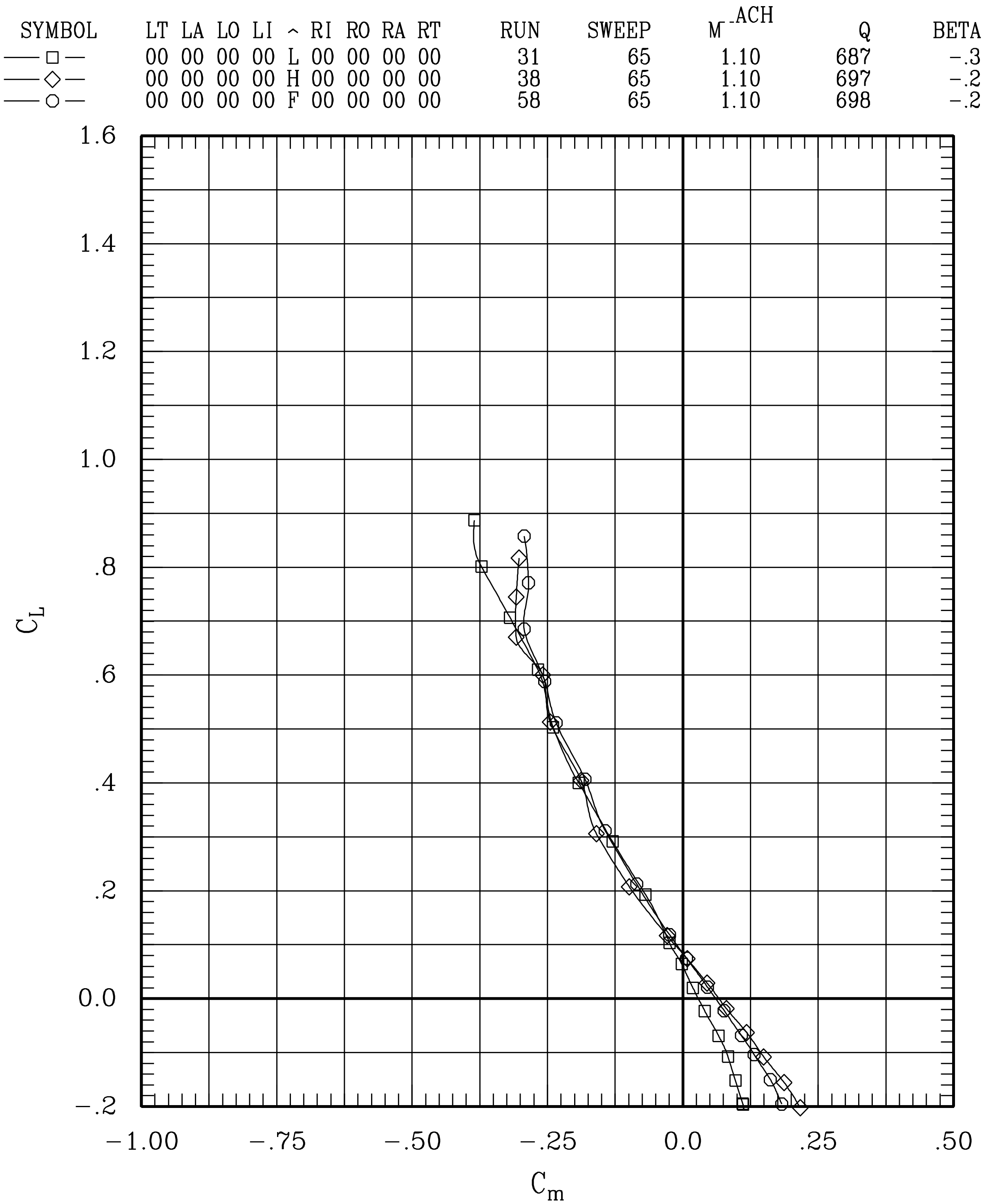

Figure 6(q). Effect of pivot height and fairing for sweep = 65 deg, Mach = 1.10.

SYMBOL	LT LA LO LI ^ RI RO RA RT	RUN	SWEEP	MACH	Q	BETA
—□—	00 00 00 00 L 00 00 00 00	31	65	1.10	687	−.3
—◇—	00 00 00 00 H 00 00 00 00	38	65	1.10	697	−.2
—○—	00 00 00 00 F 00 00 00 00	58	65	1.10	698	−.2

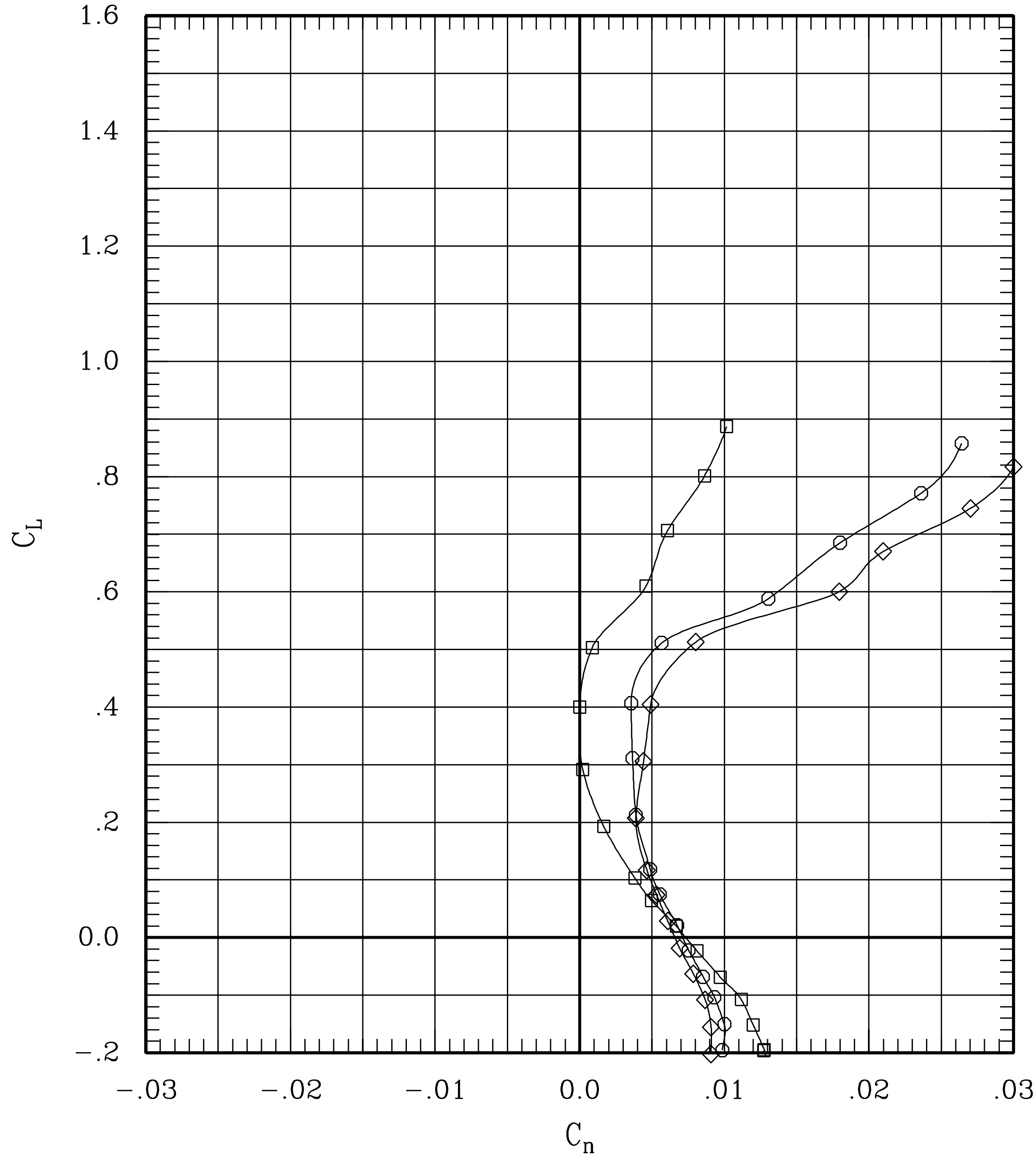

Figure 6(q). Effect of pivot height and fairing for sweep = 65 deg, Mach = 1.10.

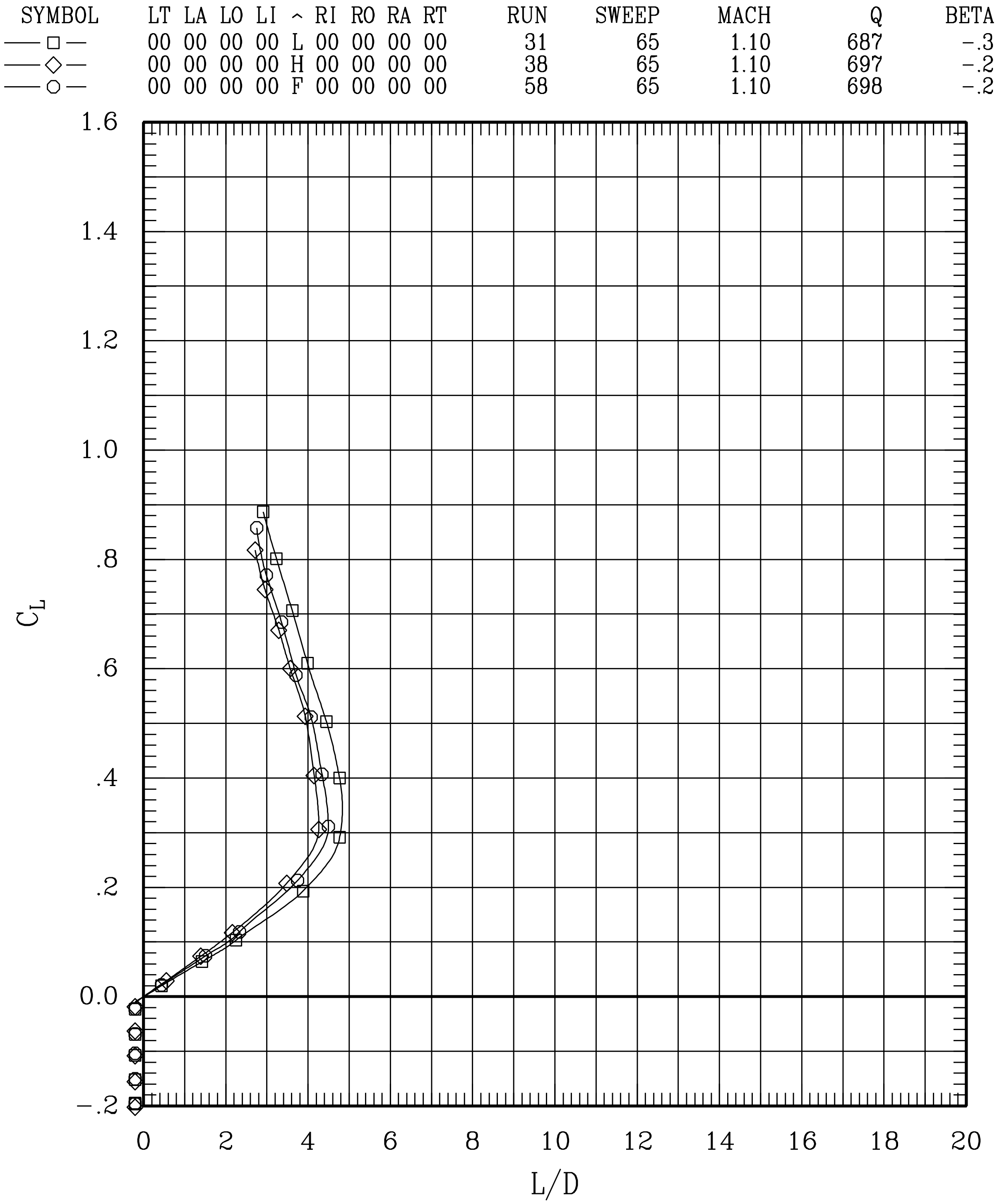

Figure 6(q). Effect of pivot height and fairing for sweep = 65 deg, Mach = 1.10.

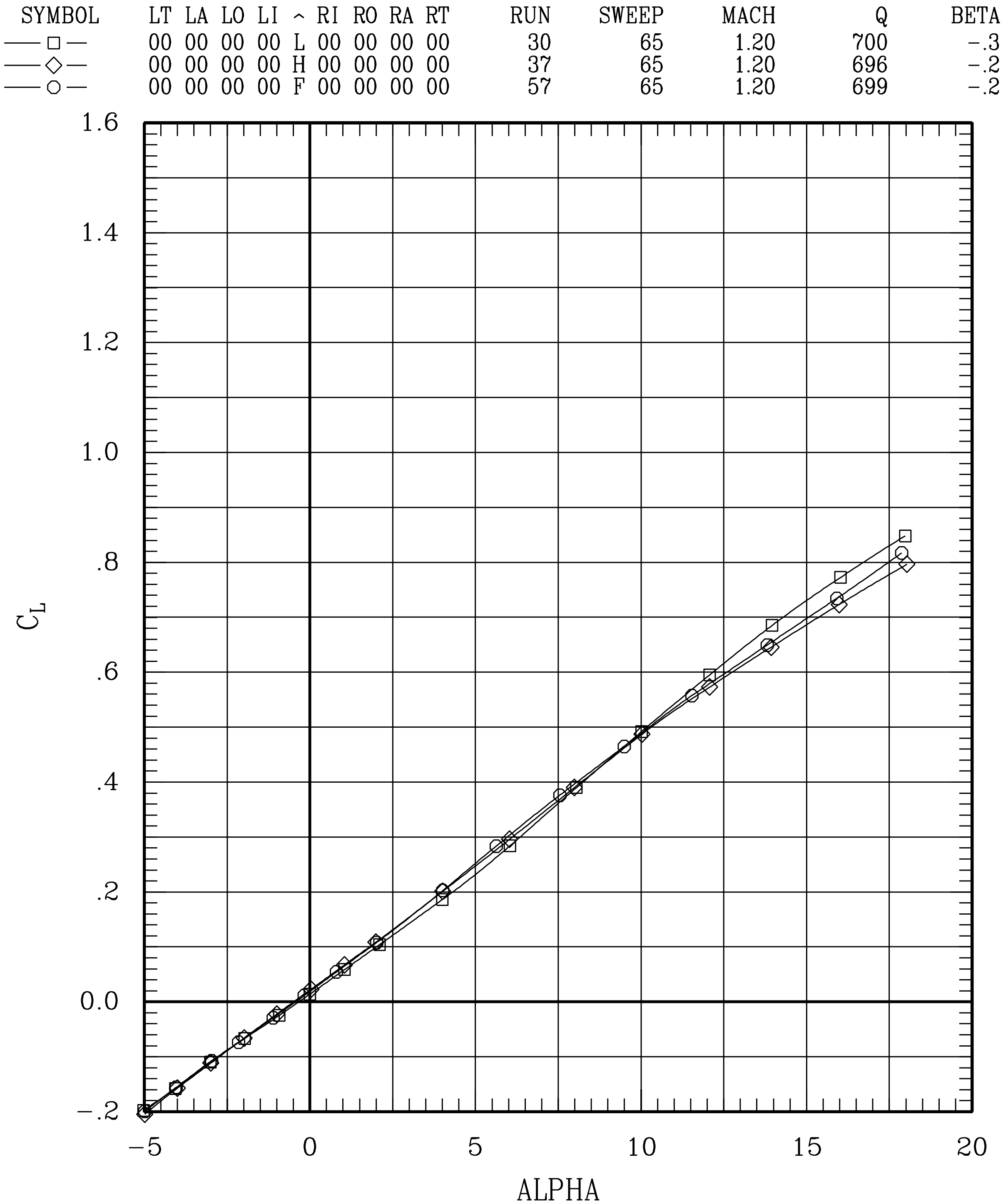

Figure 6(r). Effect of pivot height and fairing for sweep = 65 deg, Mach = 1.20.

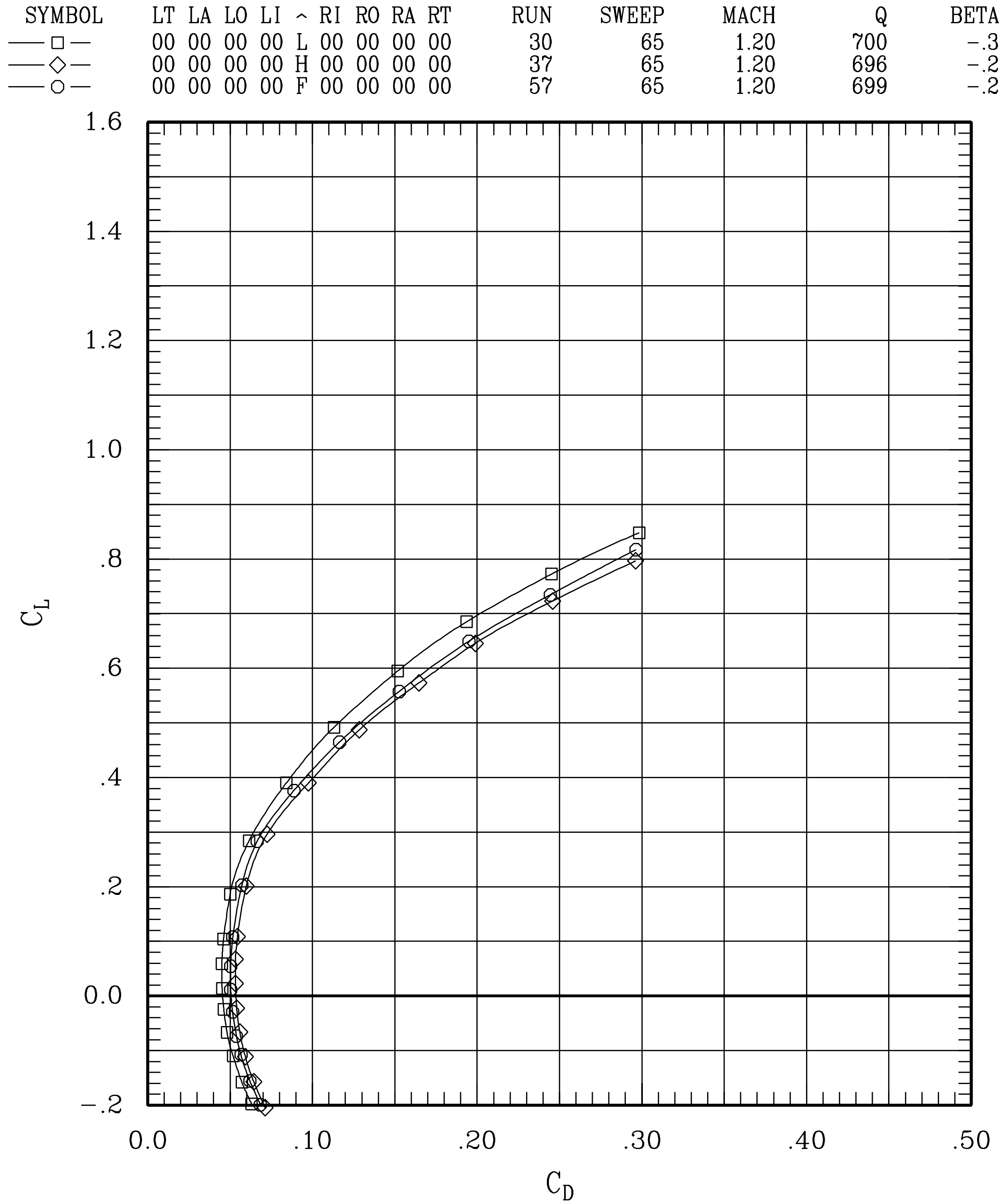

Figure 6(r). Effect of pivot height and fairing for sweep = 65 deg, Mach = 1.20.

SYMBOL	LT LA LO LI ^ RI RO RA RT	RUN	SWEEP	MACH	Q	BETA
—□—	00 00 00 00 L 00 00 00 00	30	65	1.20	700	−.3
—◇—	00 00 00 00 H 00 00 00 00	37	65	1.20	696	−.2
—○—	00 00 00 00 F 00 00 00 00	57	65	1.20	699	−.2

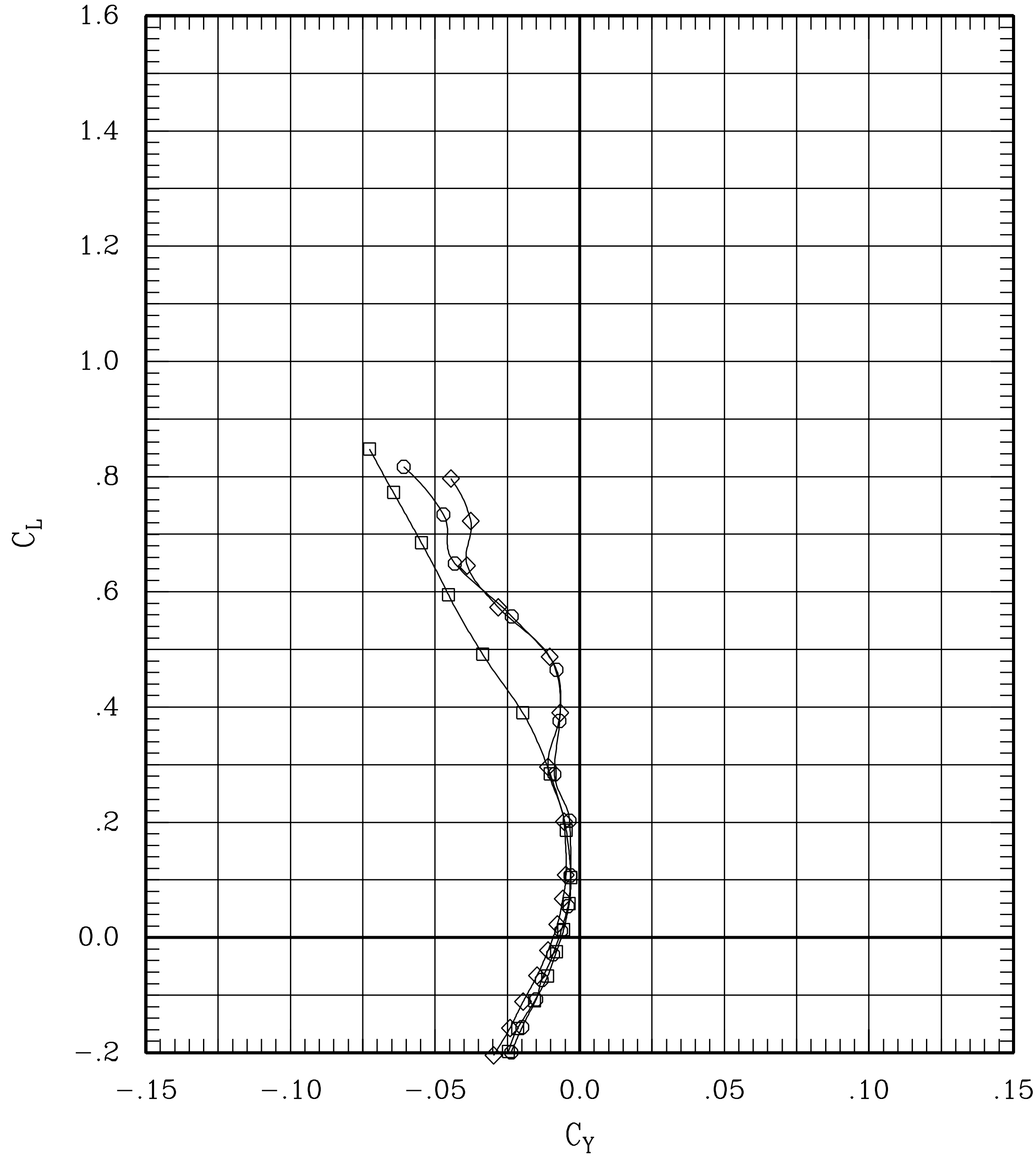

Figure 6(r). Effect of pivot height and fairing for sweep = 65 deg, Mach = 1.20.

SYMBOL	LT LA LO LI ^ RI RO RA RT	RUN	SWEEP	MACH	Q	BETA
—□—	00 00 00 00 L 00 00 00 00	30	65	1.20	700	−.3
—◇—	00 00 00 00 H 00 00 00 00	37	65	1.20	696	−.2
—○—	00 00 00 00 F 00 00 00 00	57	65	1.20	699	−.2

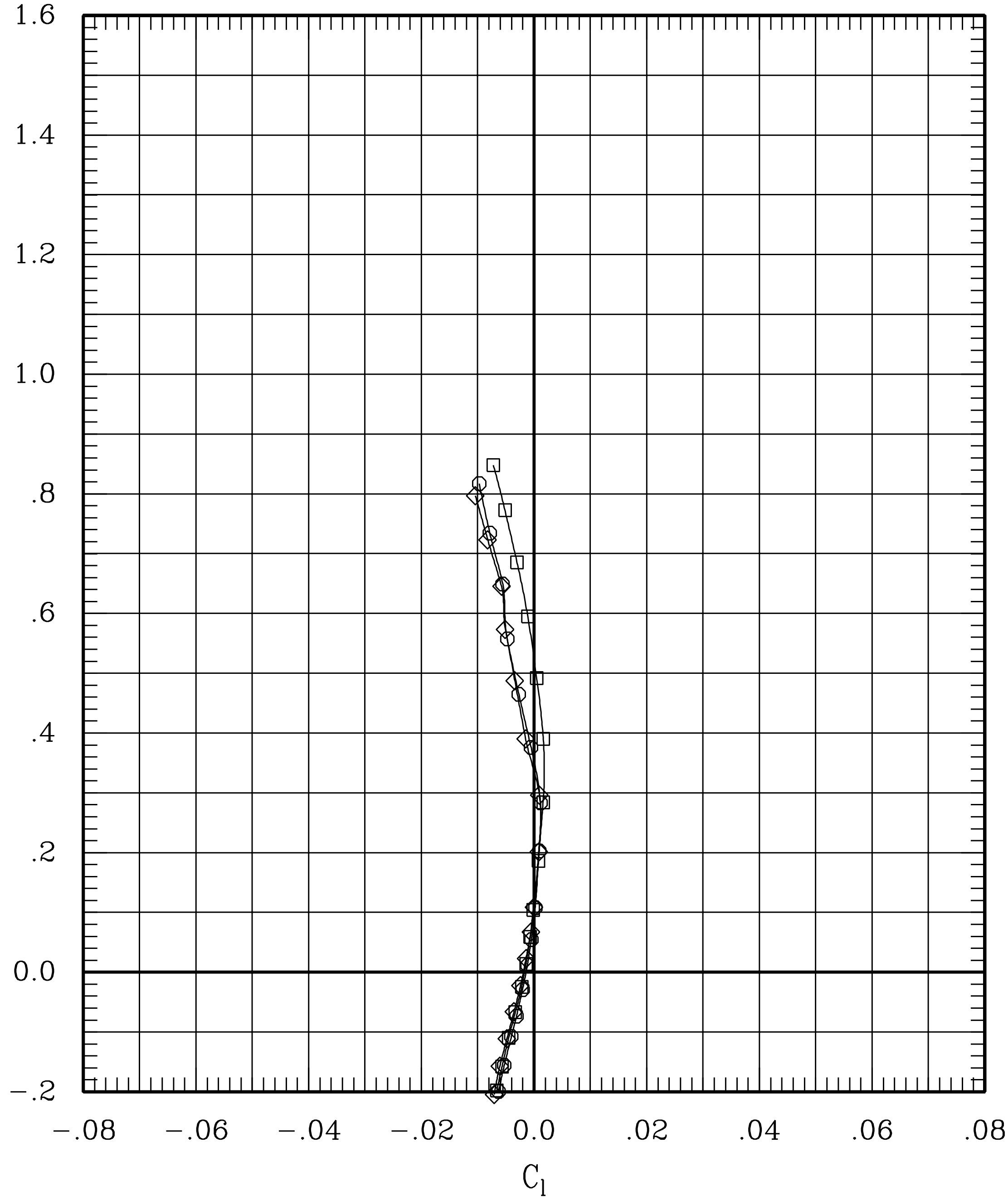

Figure 6(r). Effect of pivot height and fairing for sweep = 65 deg, Mach = 1.20.

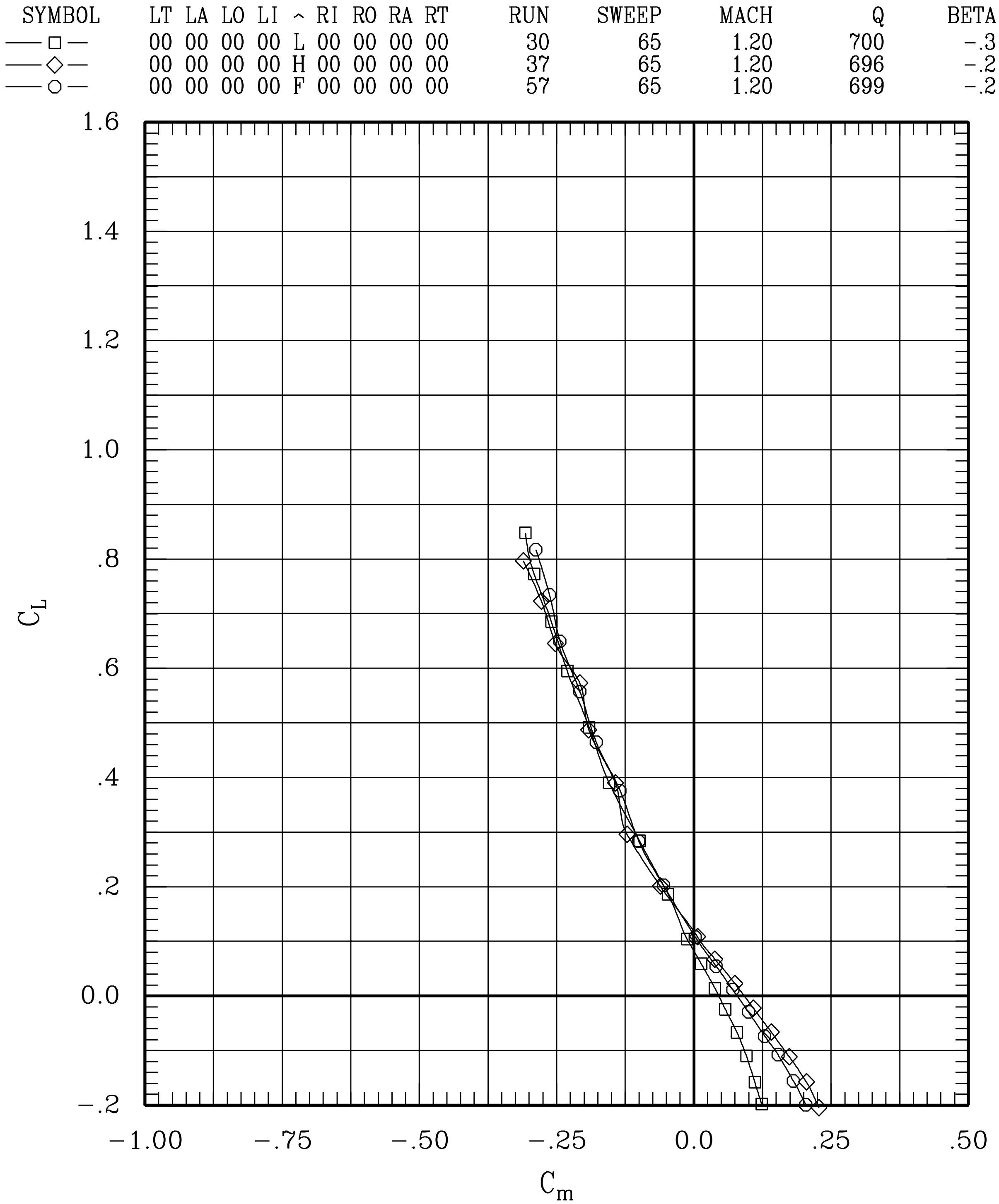

Figure 6(r). Effect of pivot height and fairing for sweep = 65 deg, Mach = 1.20.

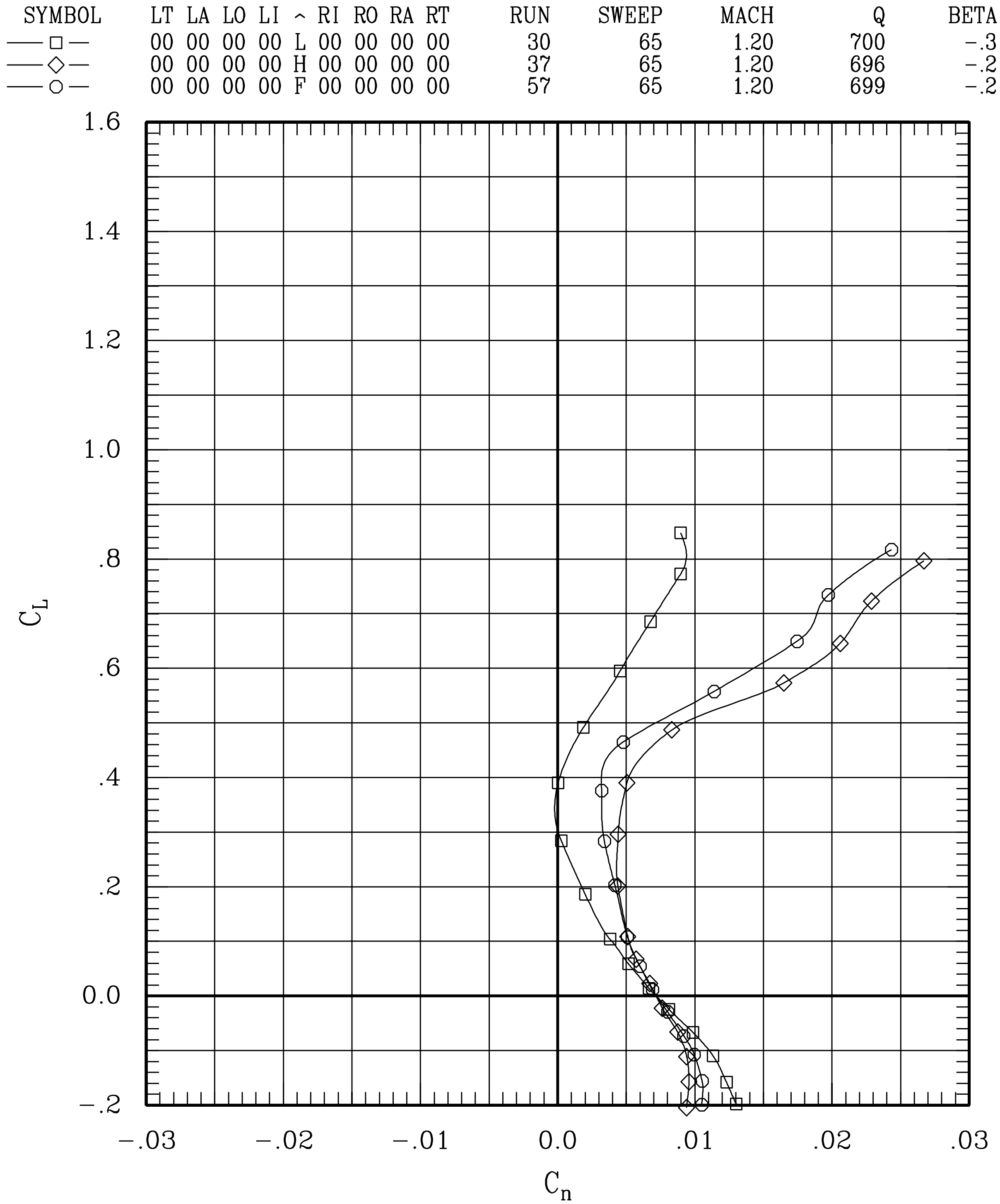

Figure 6(r). Effect of pivot height and fairing for sweep = 65 deg, Mach = 1.20.

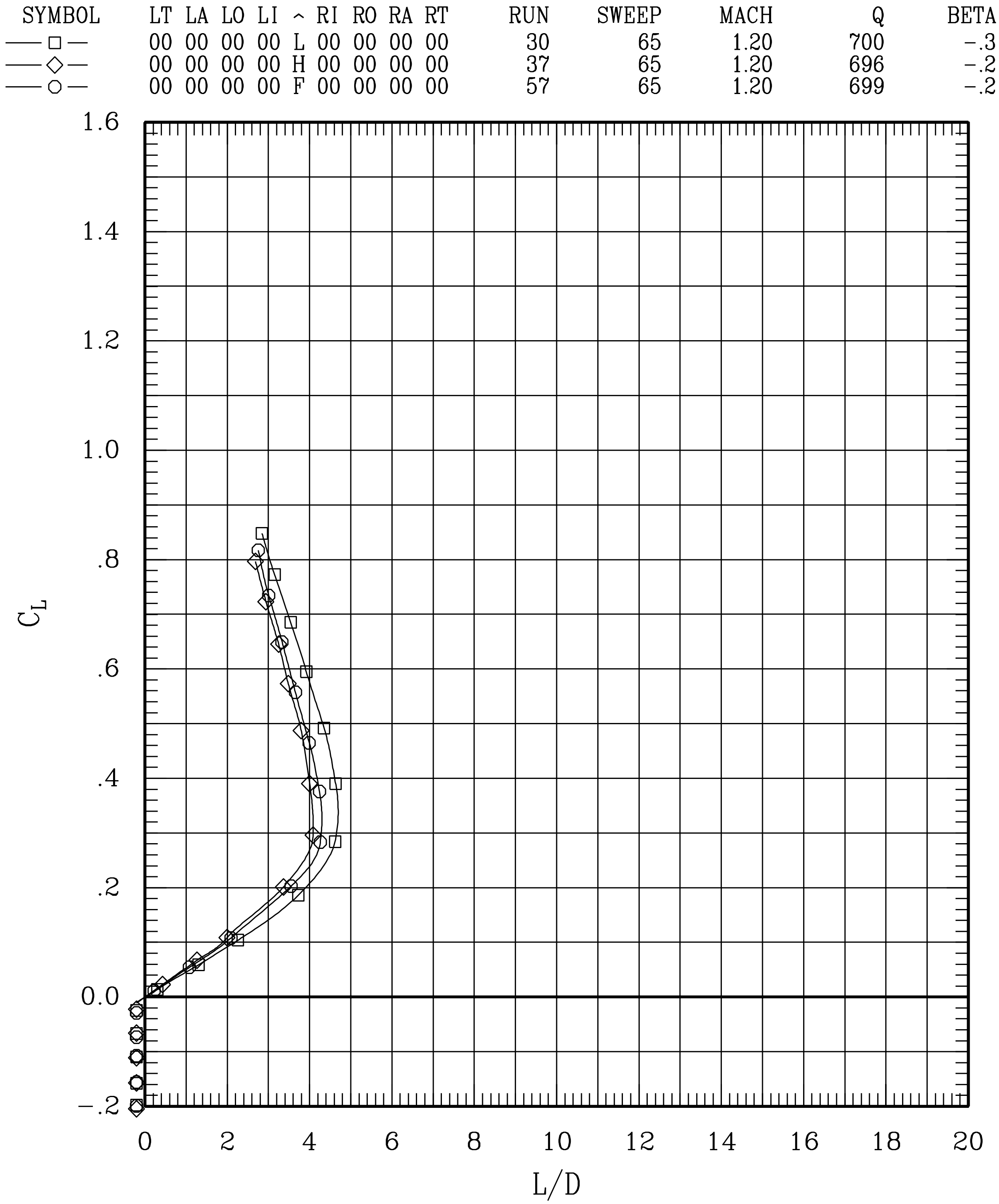

Figure 6(r). Effect of pivot height and fairing for sweep = 65 deg, Mach = 1.20.

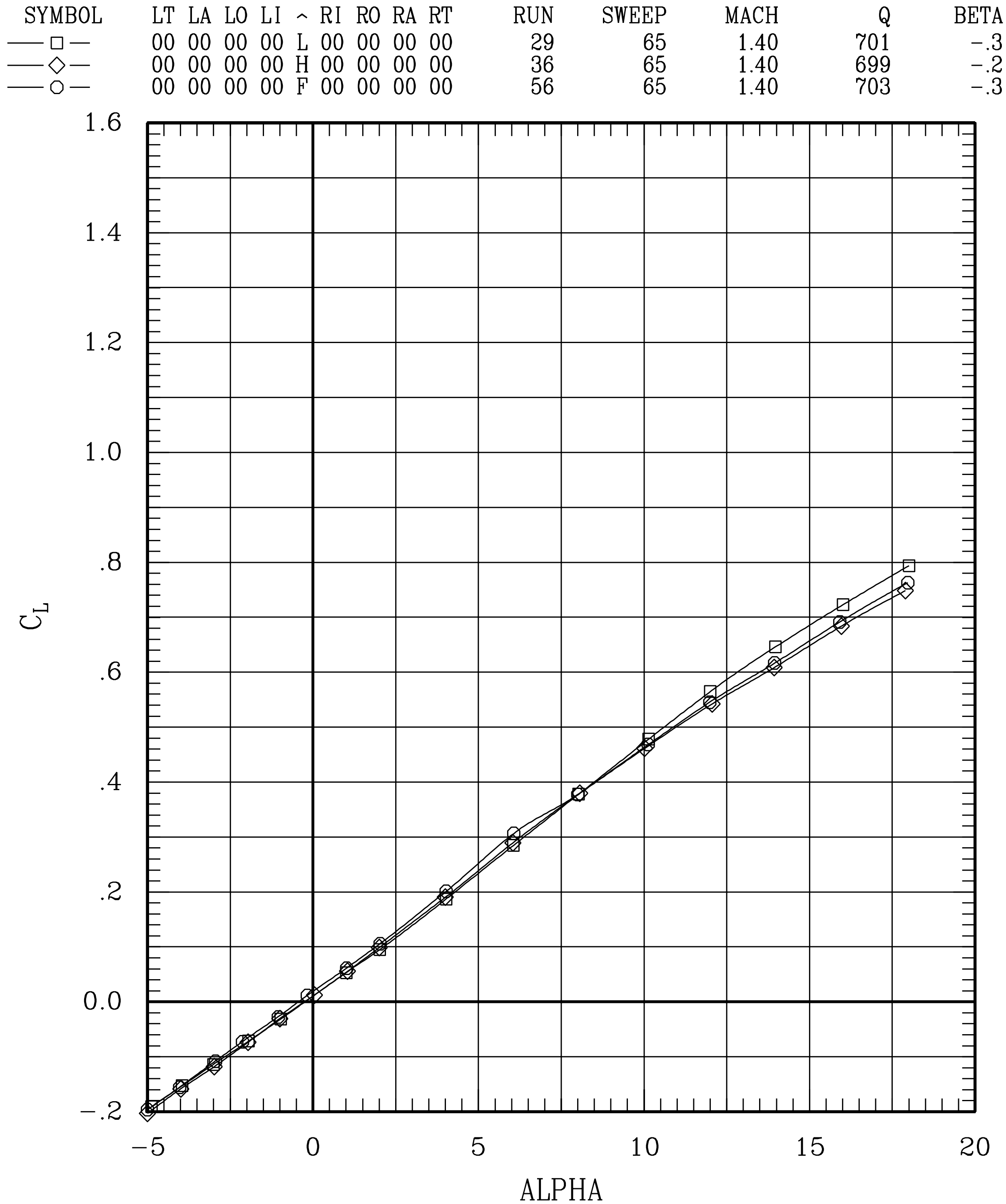

Figure 6(s). Effect of pivot height and fairing for sweep = 65 deg, Mach = 1.40.

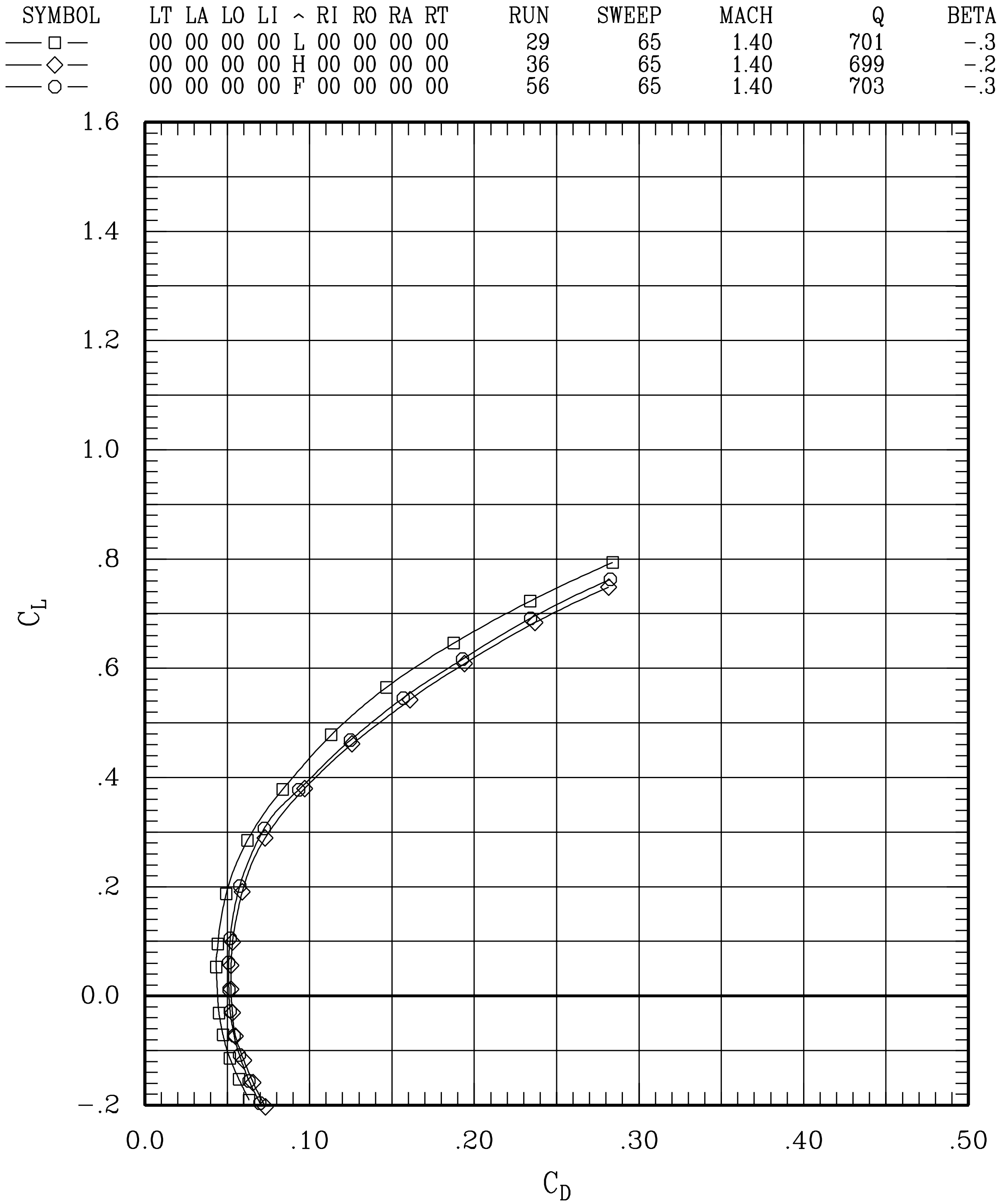

Figure 6(s). Effect of pivot height and fairing for sweep = 65 deg, Mach = 1.40.

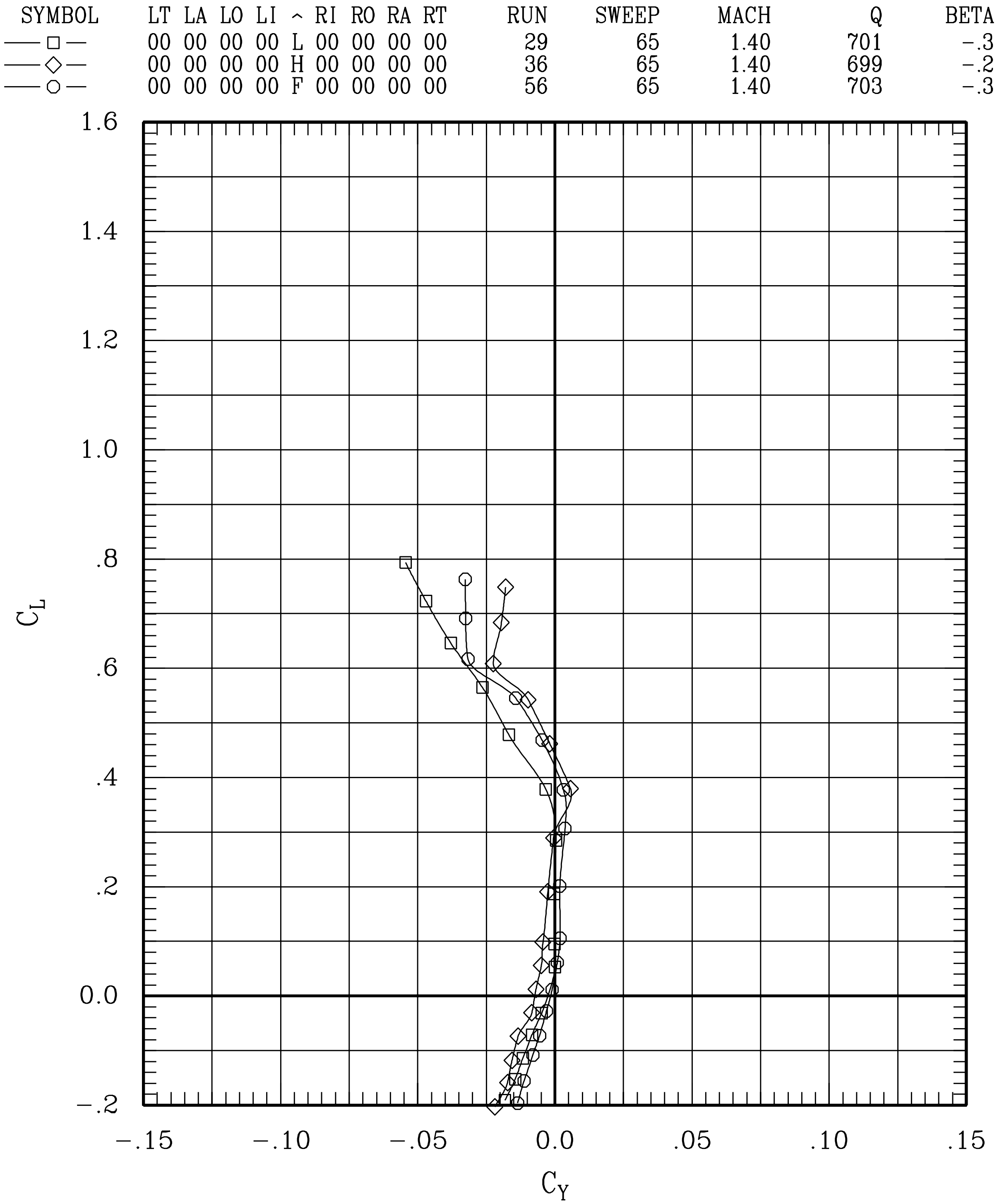

Figure 6(s). Effect of pivot height and fairing for sweep = 65 deg, Mach = 1.40.

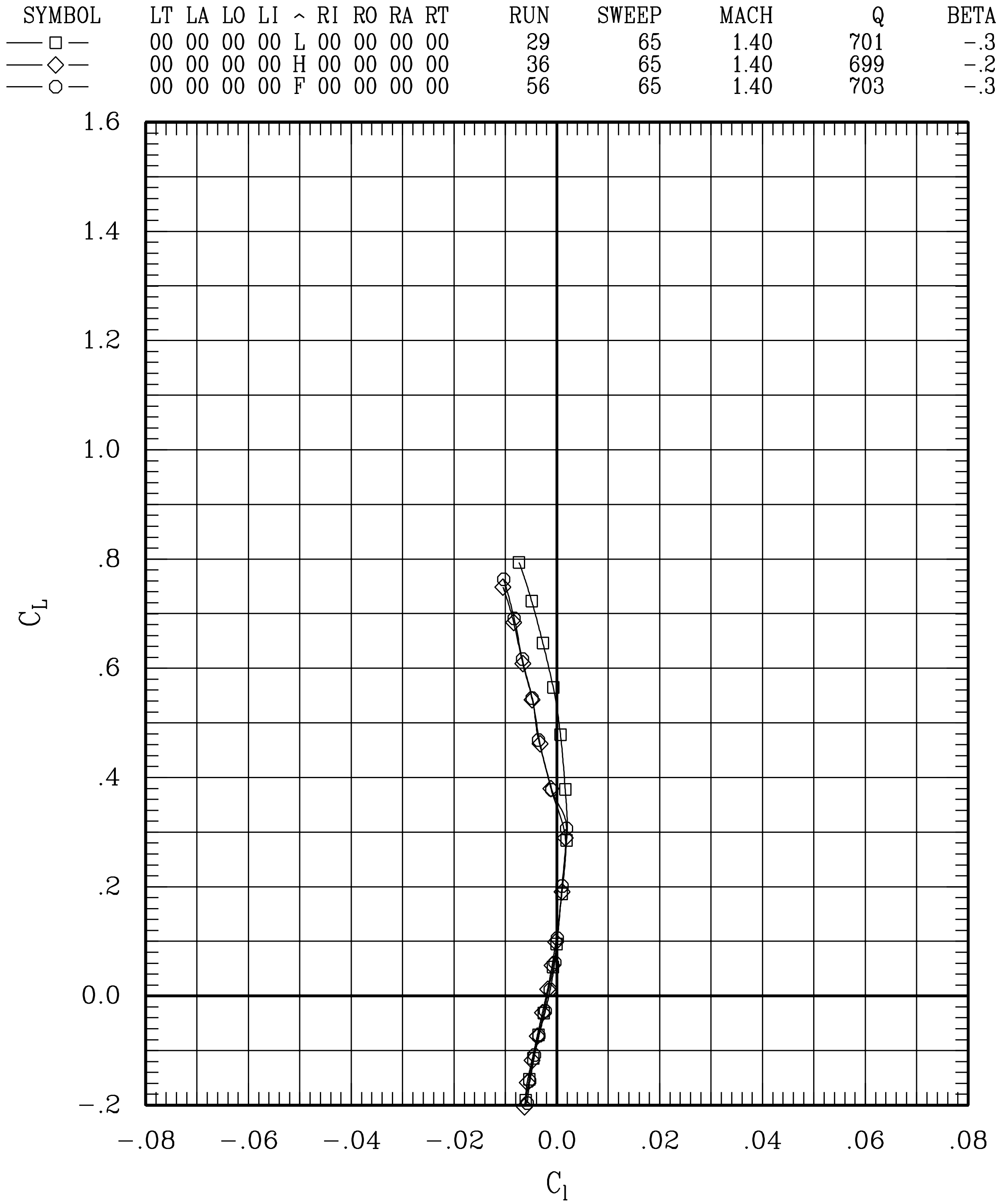

Figure 6(s). Effect of pivot height and fairing for sweep = 65 deg, Mach = 1.40.

SYMBOL	LT LA LO LI ^ RI RO RA RT	RUN	SWEEP	MACH	Q	BETA
—□—	00 00 00 00 L 00 00 00 00	29	65	1.40	701	−.3
—◇—	00 00 00 00 H 00 00 00 00	36	65	1.40	699	−.2
—○—	00 00 00 00 F 00 00 00 00	56	65	1.40	703	−.3

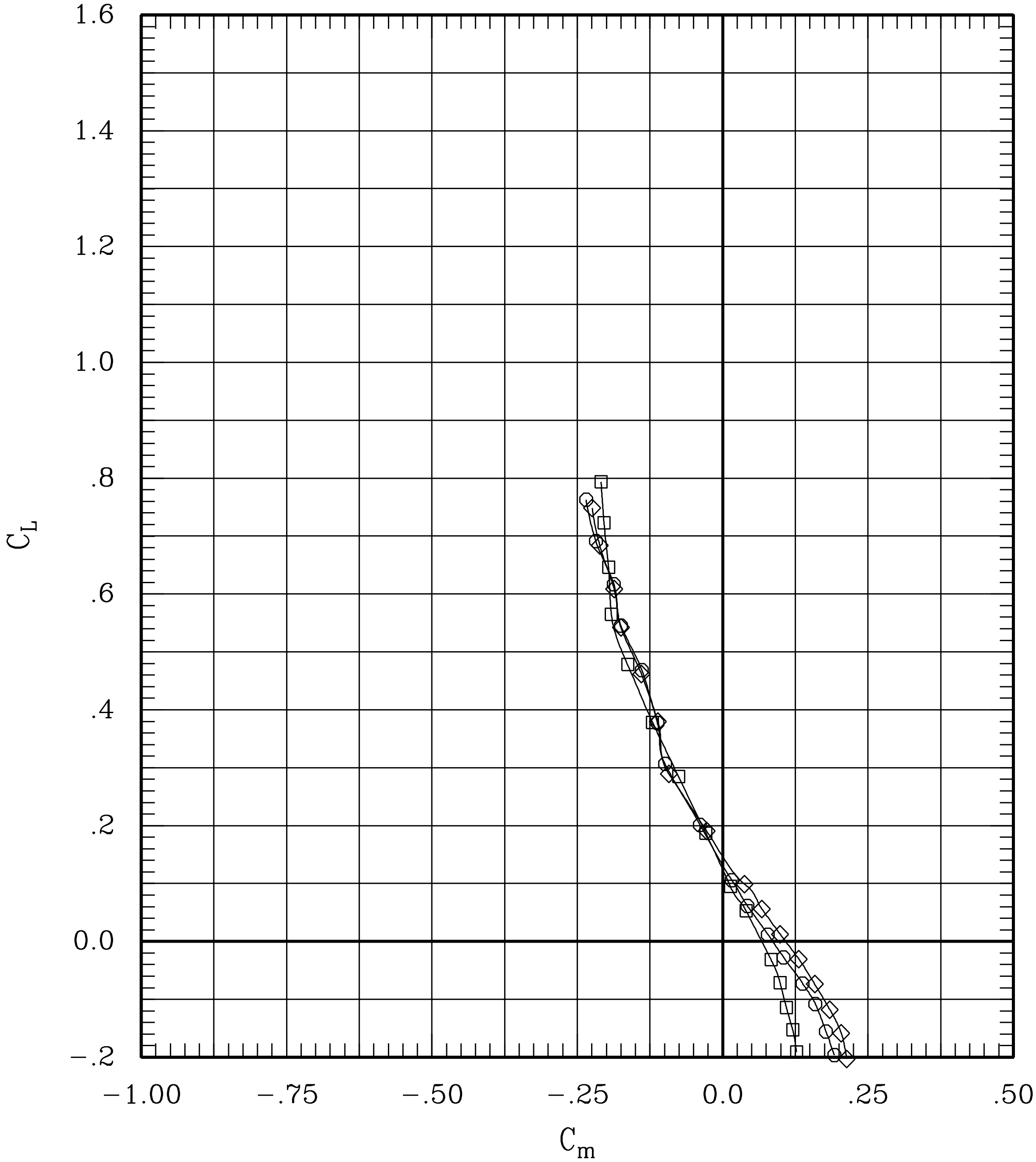

Figure 6(s). Effect of pivot height and fairing for sweep = 65 deg, Mach = 1.40.

SYMBOL	LT LA LO LI ^ RI RO RA RT	RUN	SWEEP	MACH	Q	BETA
—□—	00 00 00 00 L 00 00 00 00	29	65	1.40	701	−.3
—◇—	00 00 00 00 H 00 00 00 00	36	65	1.40	699	−.2
—○—	00 00 00 00 F 00 00 00 00	56	65	1.40	703	−.3

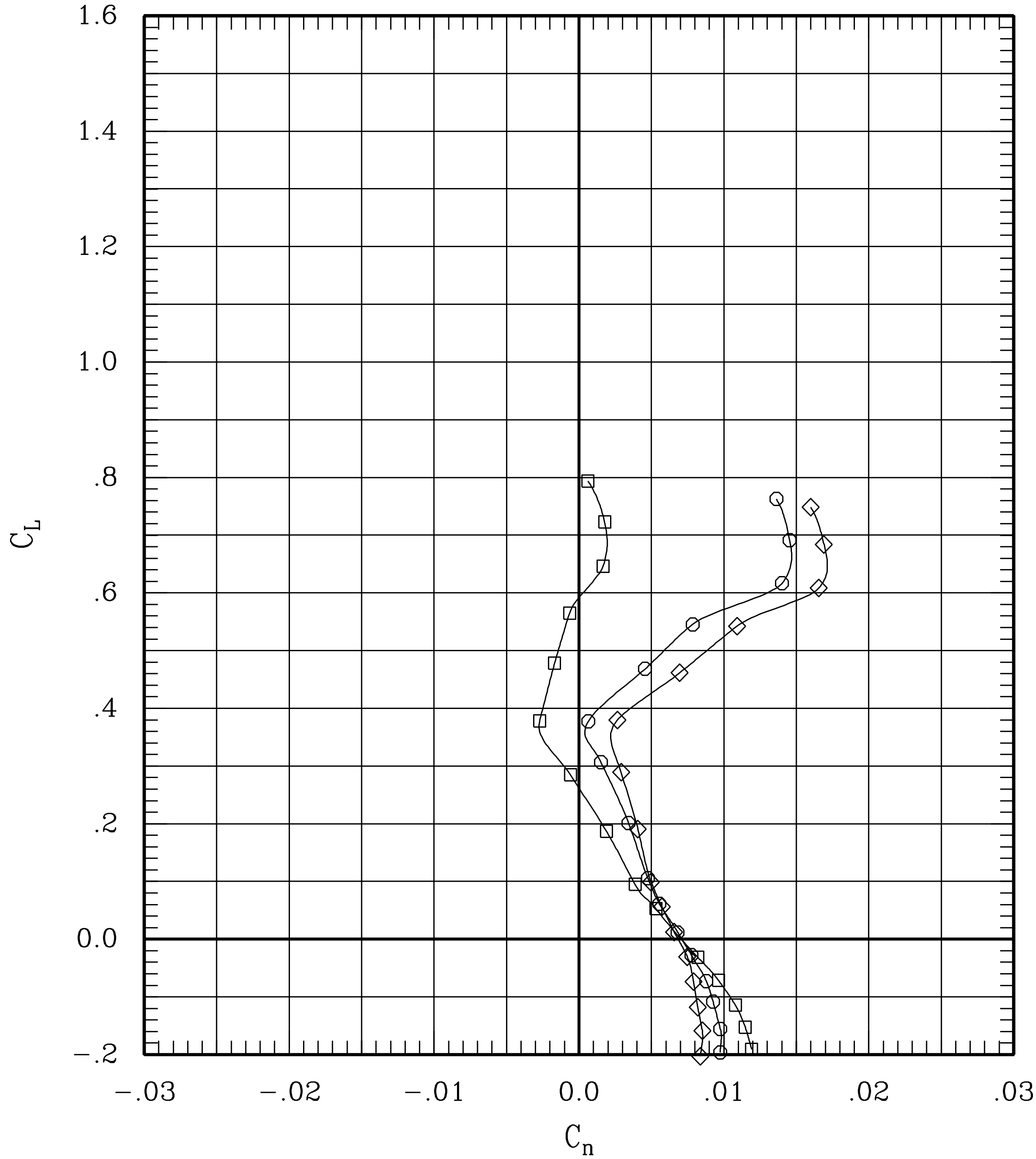

Figure 6(s). Effect of pivot height and fairing for sweep = 65 deg, Mach = 1.40.

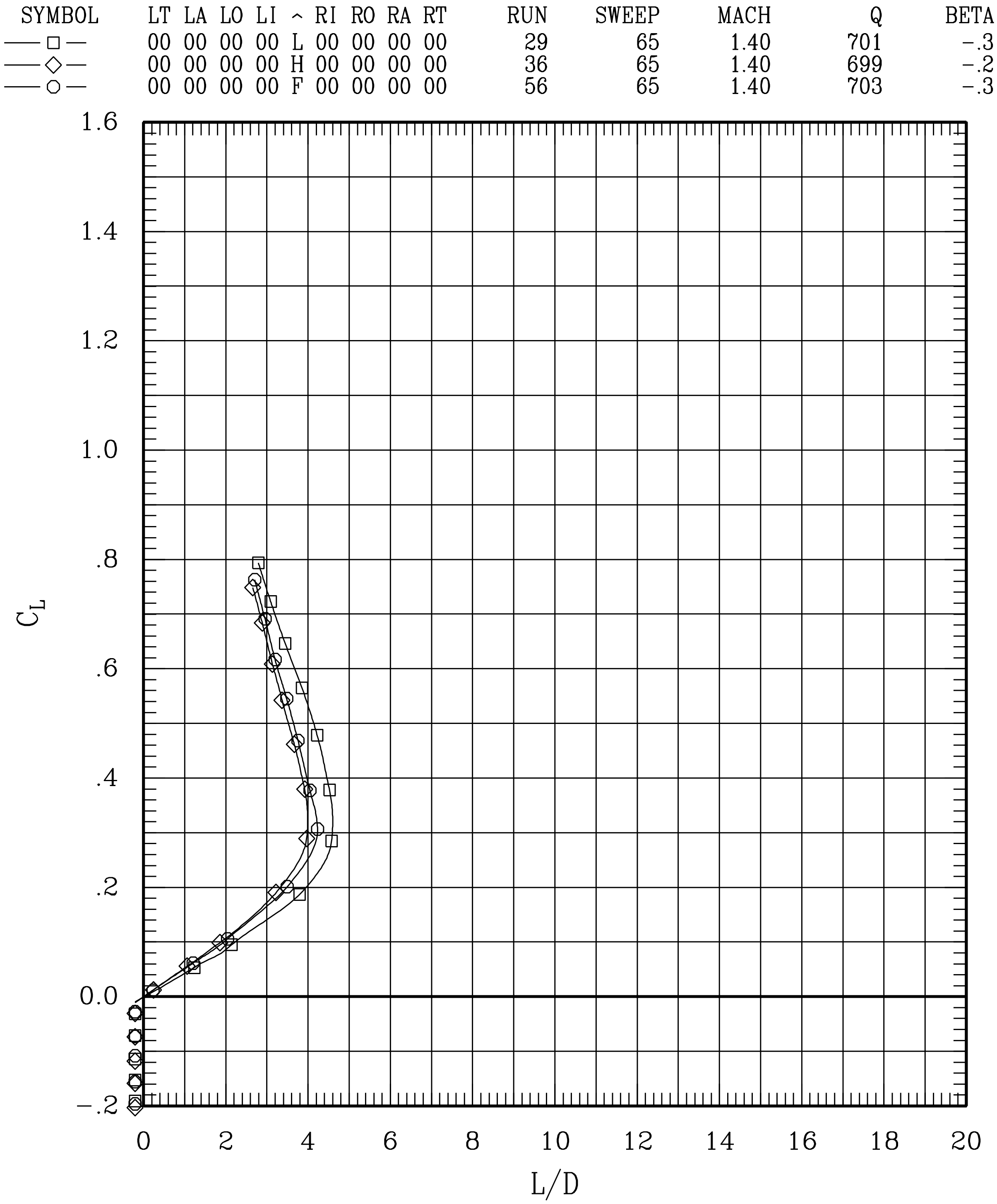

Figure 6(s). Effect of pivot height and fairing for sweep = 65 deg, Mach = 1.40.

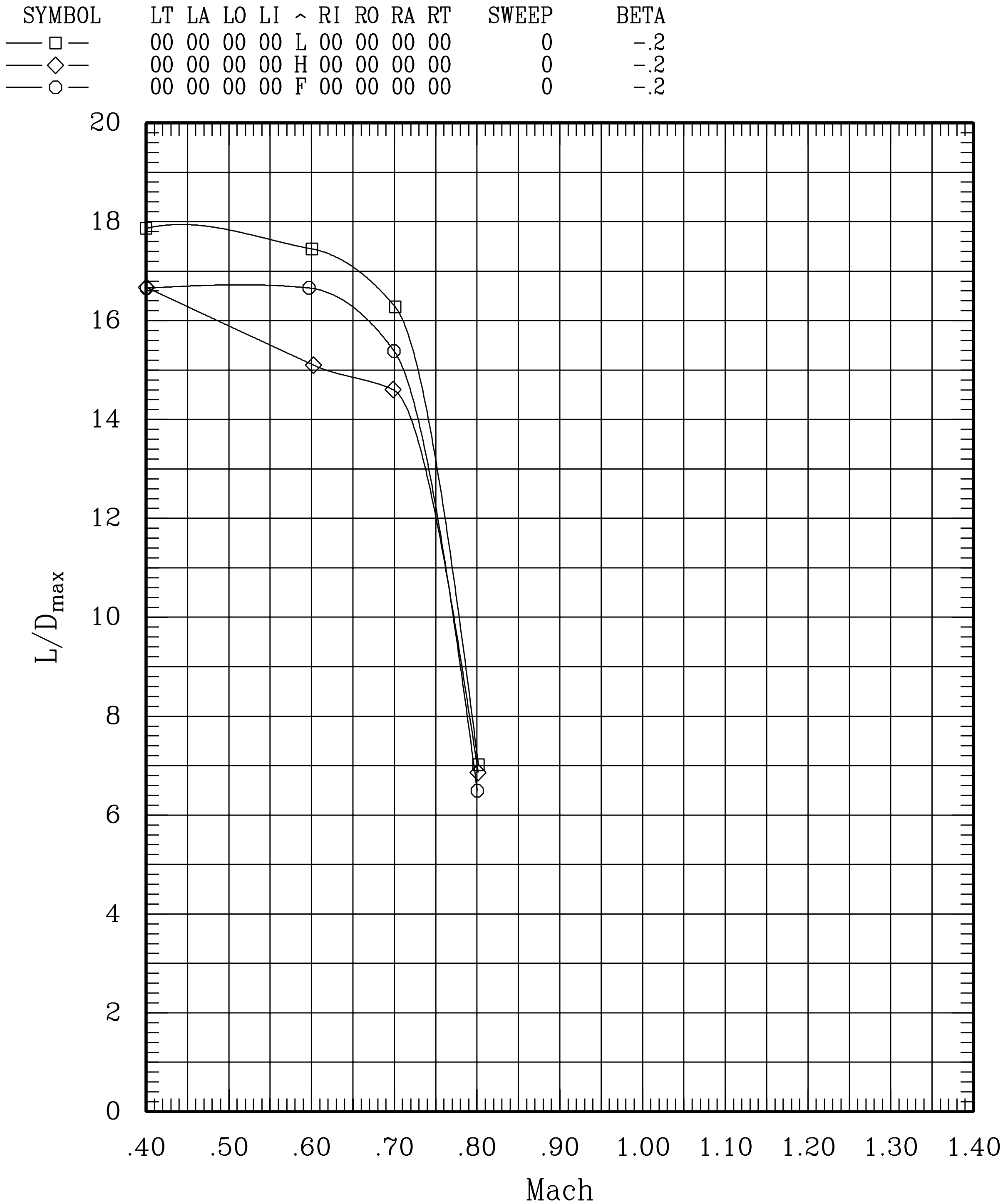

Figure 7(a). Summary quantities for the wing with different pivots; sweep = 0 deg.

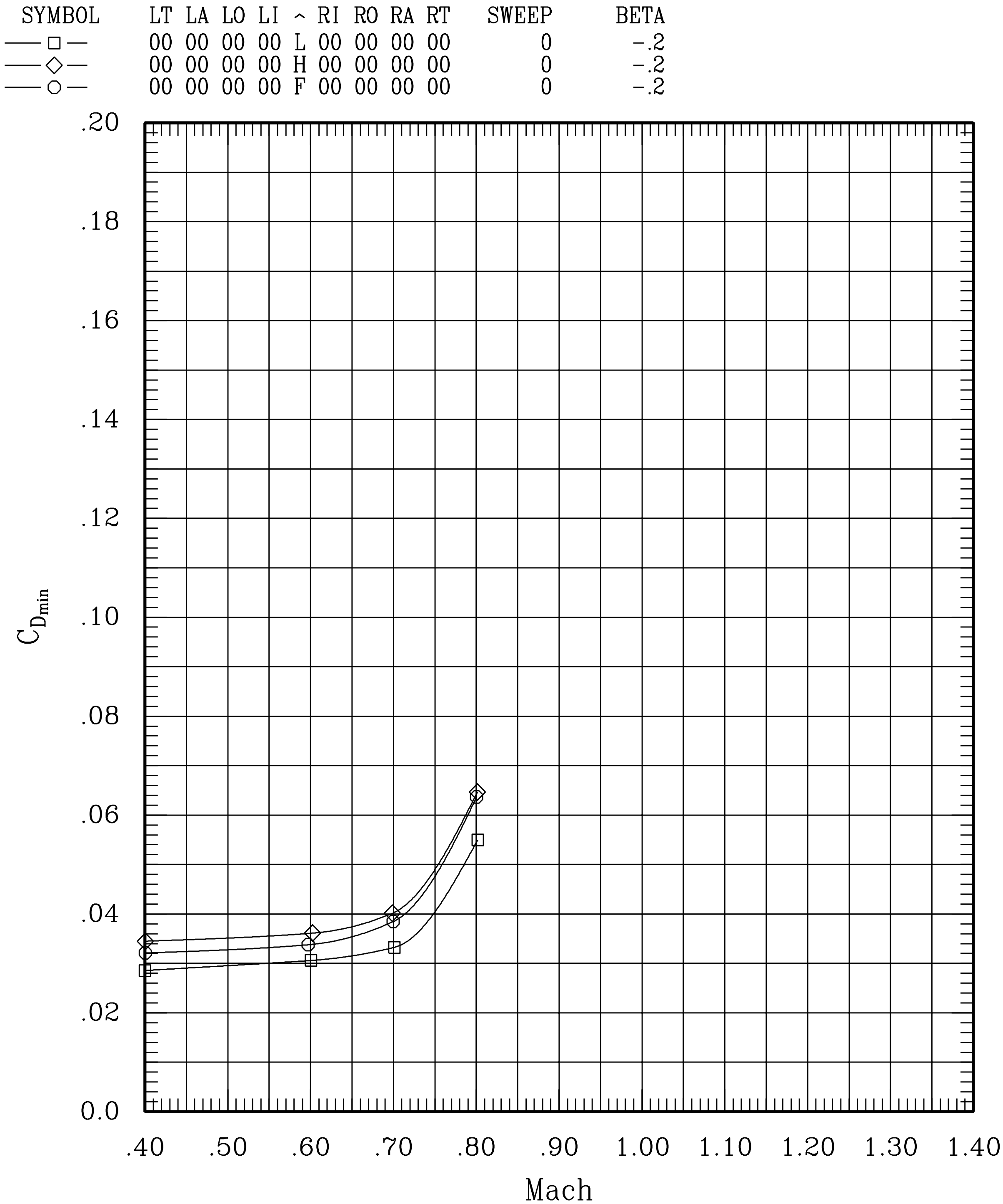

Figure 7(a). Summary quantities for the wing with different pivots; sweep = 0 deg.

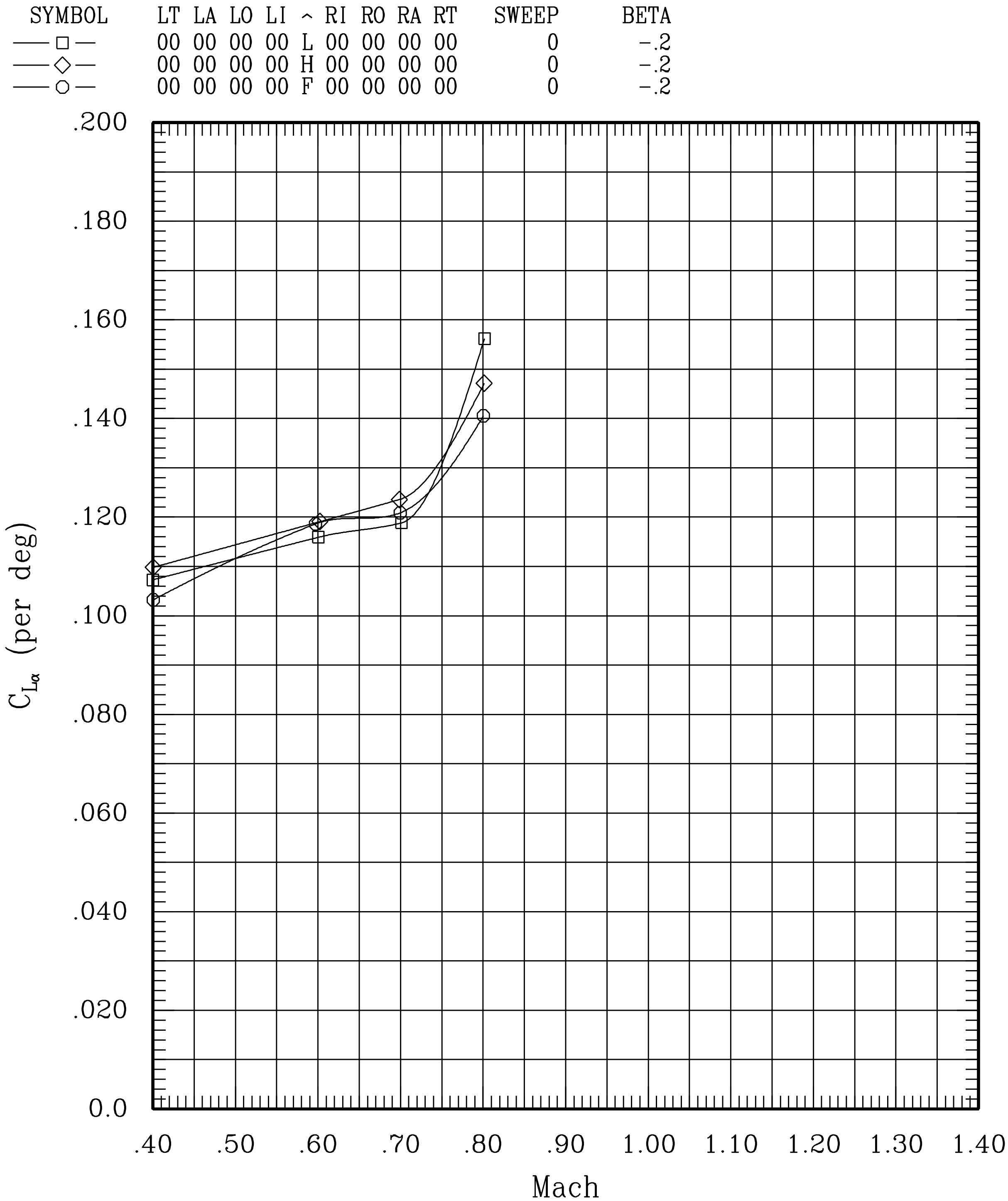

Figure 7(a). Summary quantities for the wing with different pivots; sweep = 0 deg.

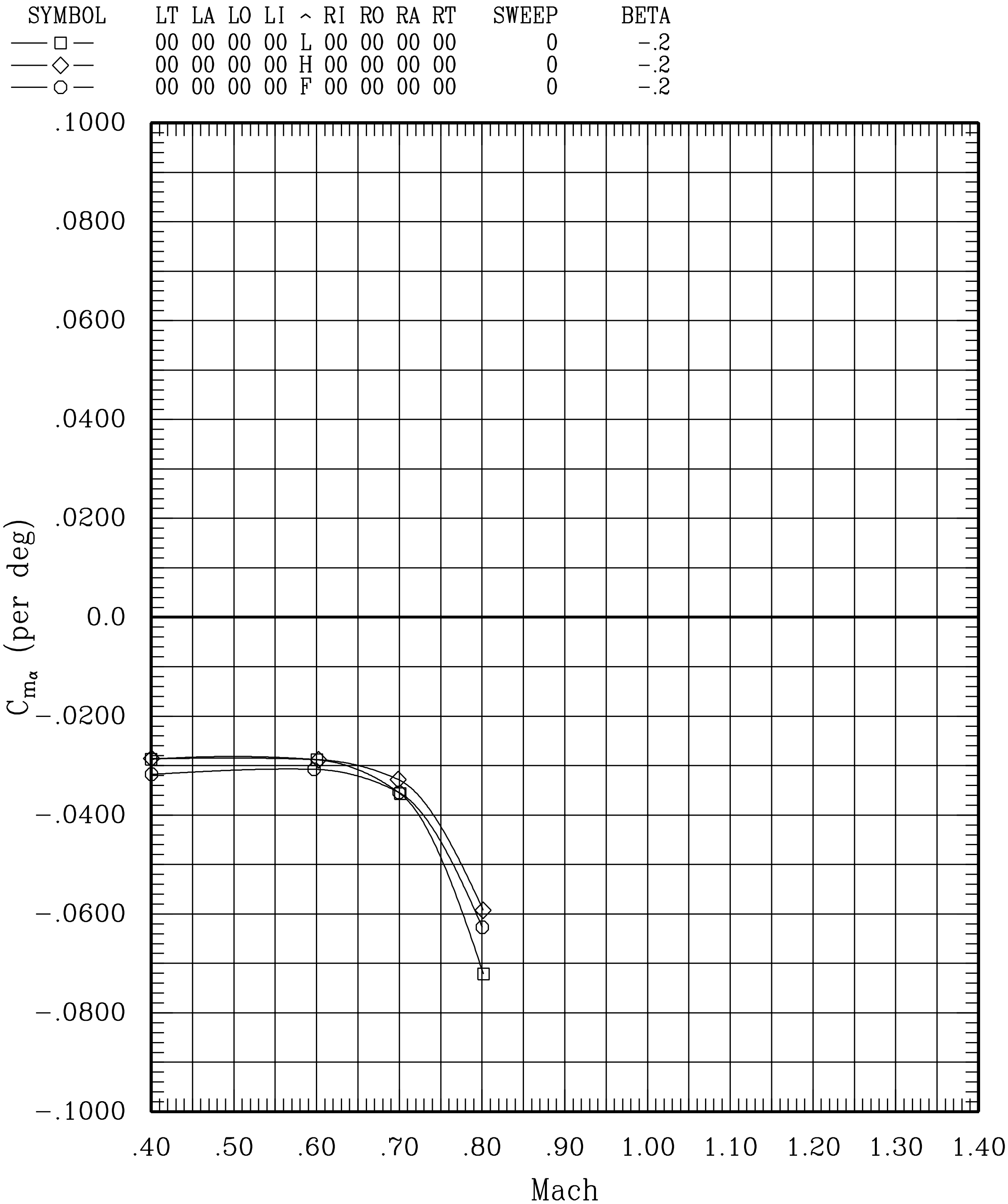

Figure 7(a). Summary quantities for the wing with different pivots; sweep = 0 deg.

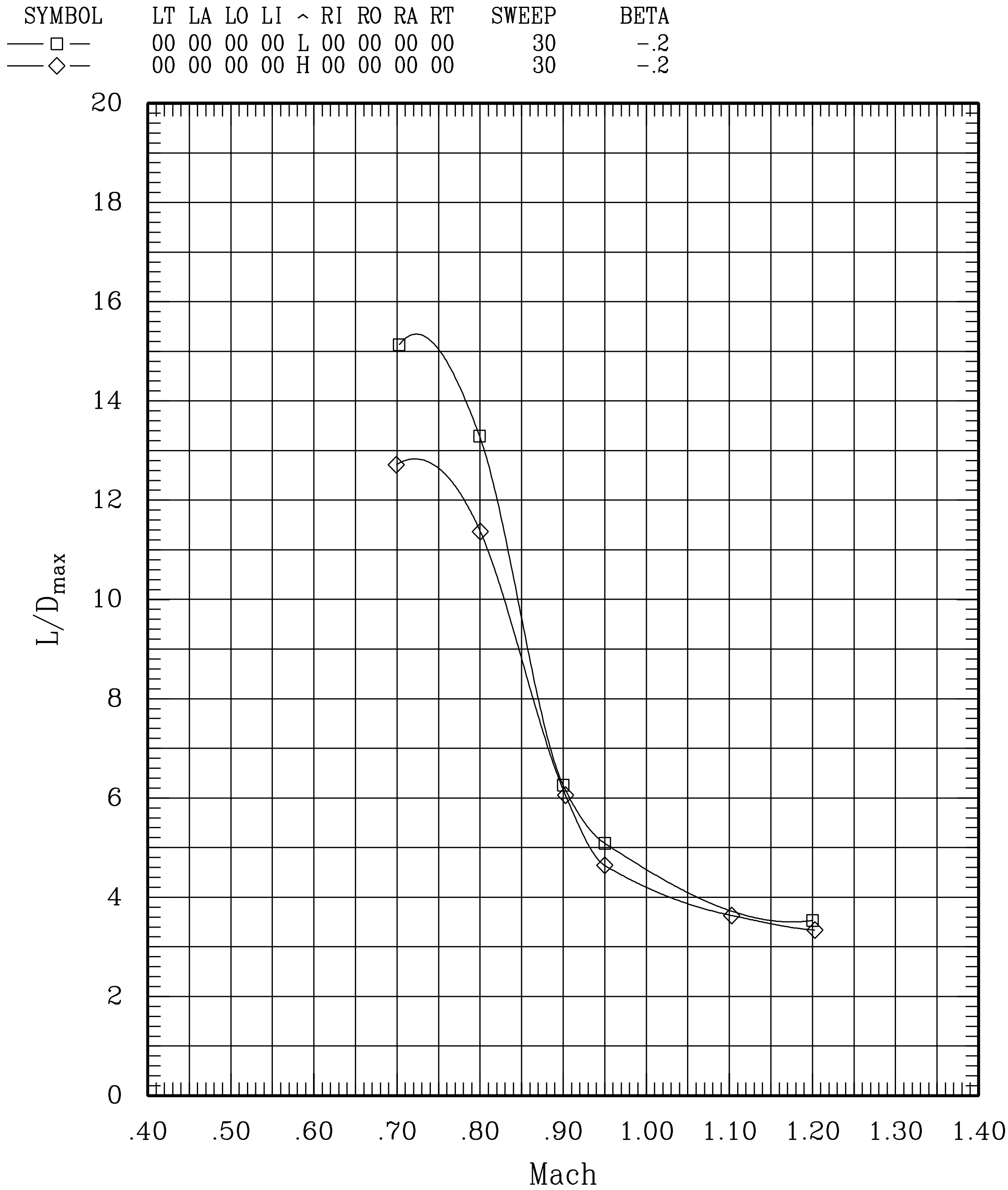

Figure 7(b). Summary quantities for the wing with different pivots; sweep = 30 deg.

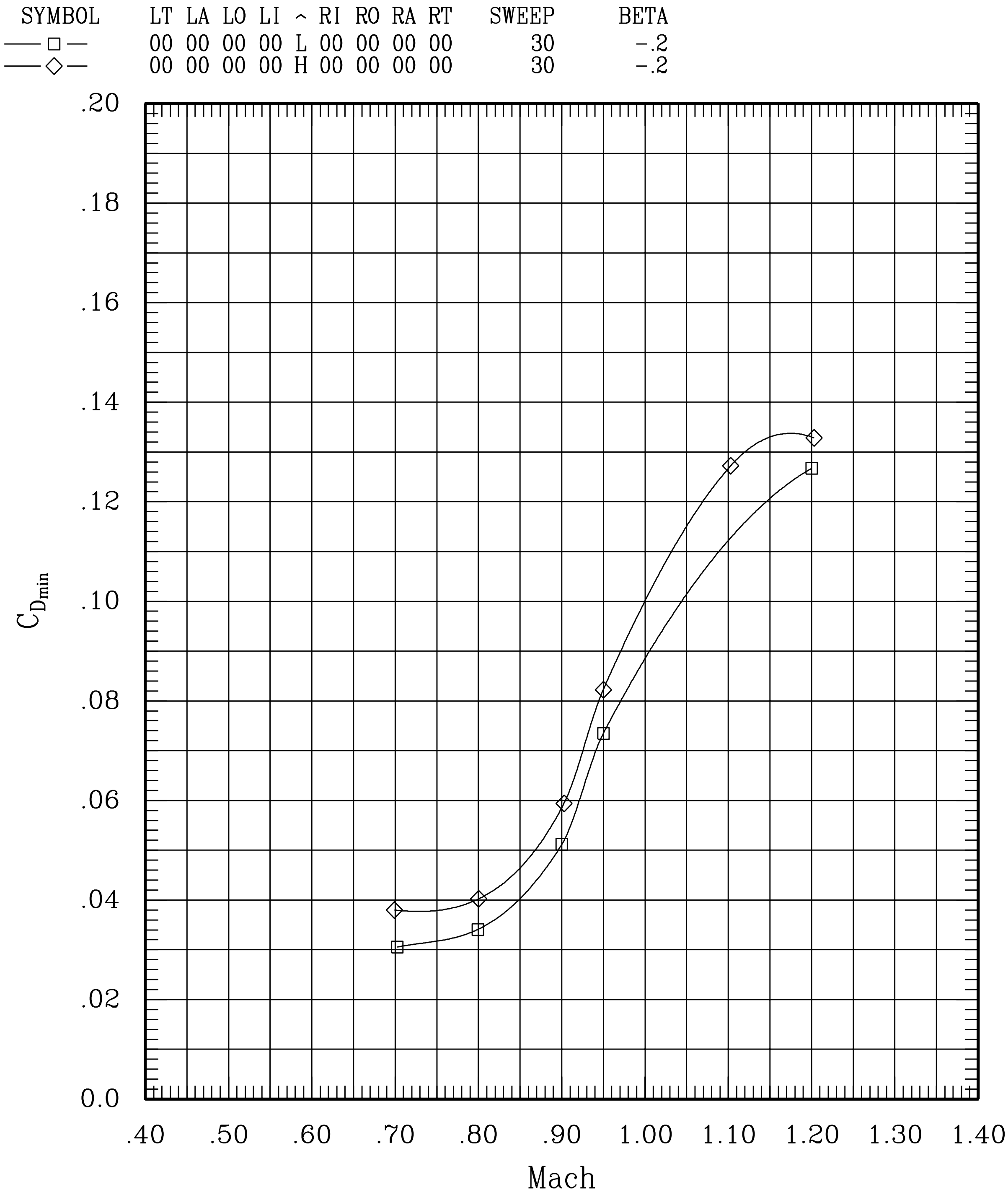

Figure 7(b). Summary quantities for the wing with different pivots; sweep = 30 deg.

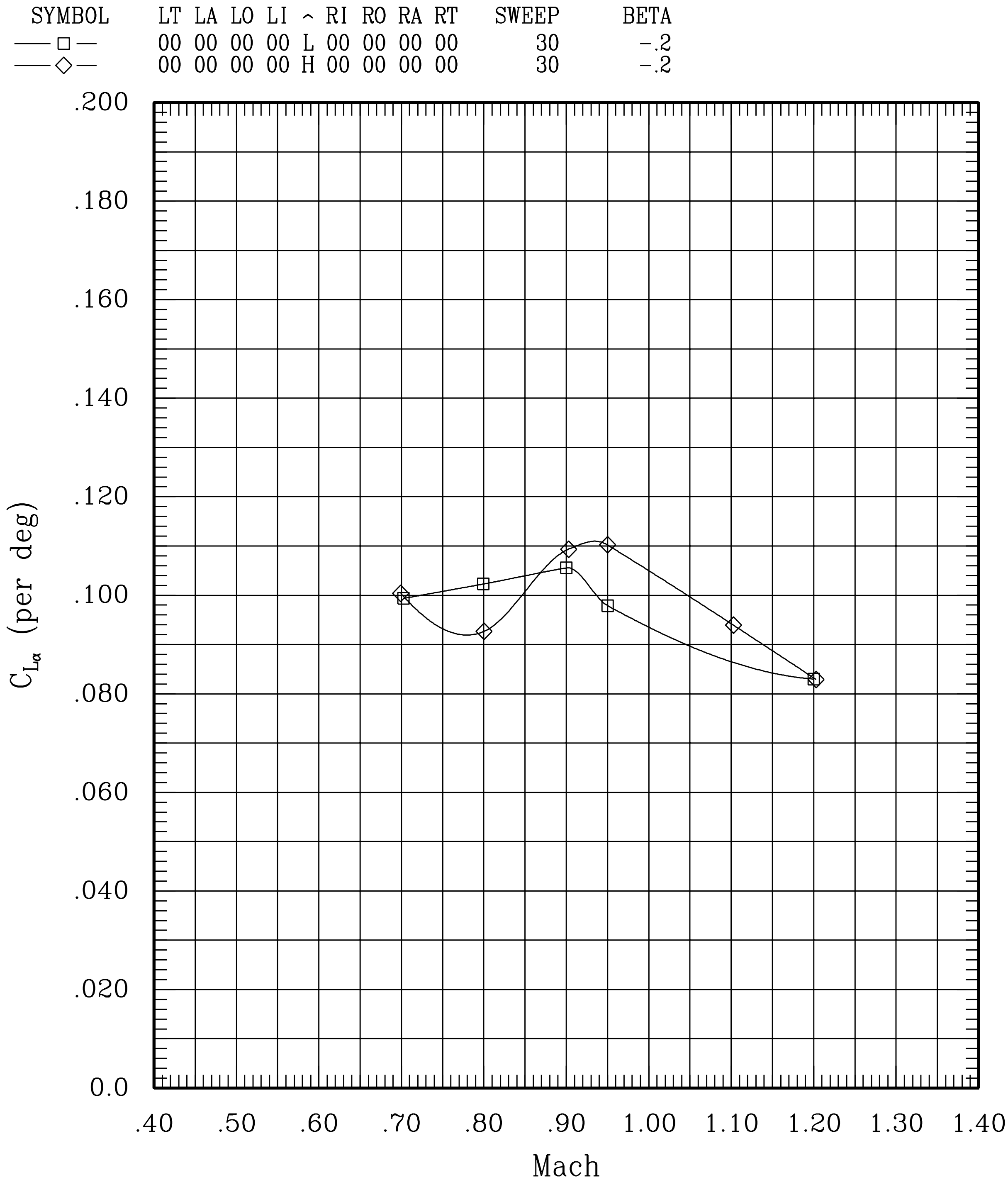

Figure 7(b). Summary quantities for the wing with different pivots; sweep = 30 deg.

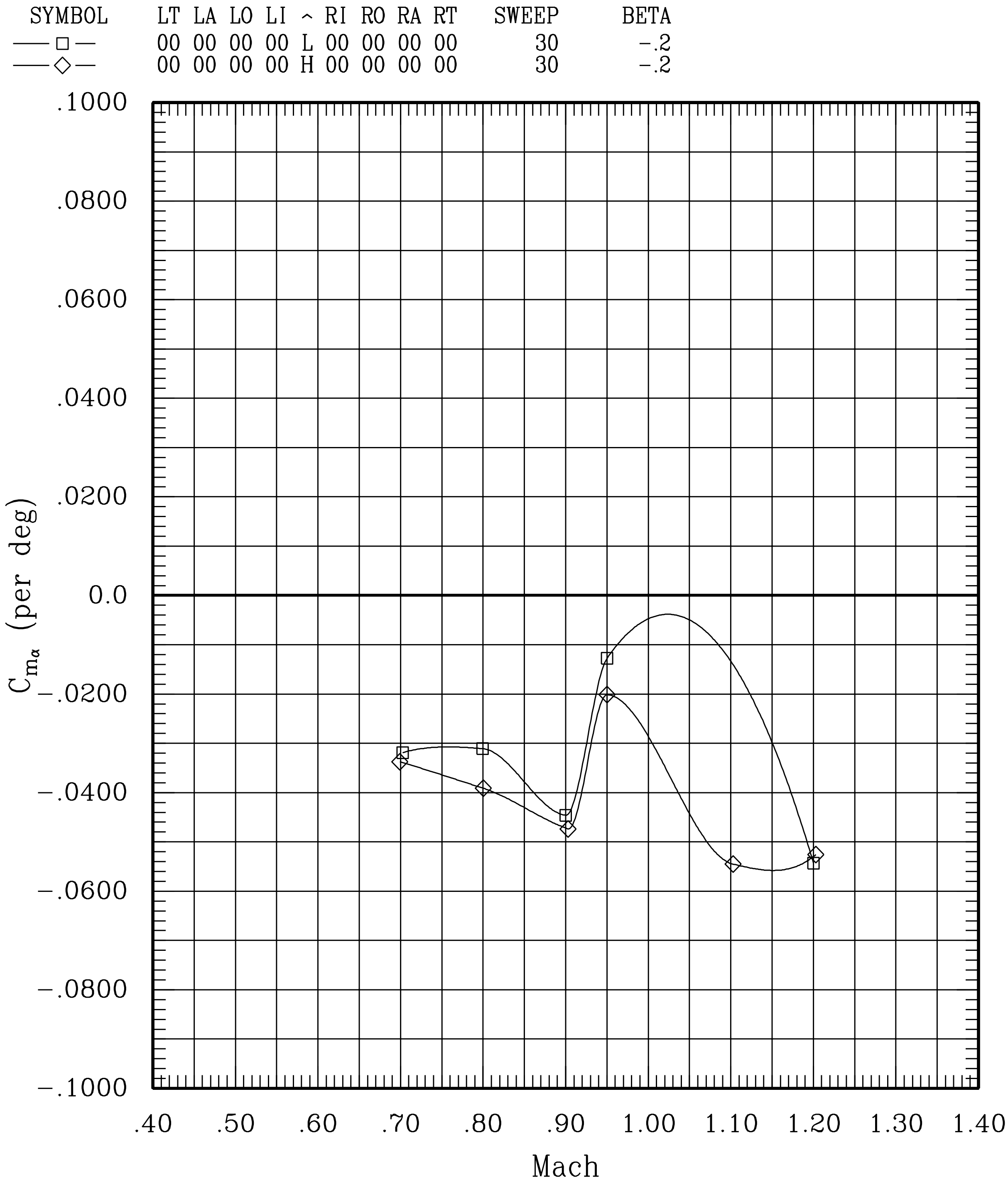

Figure 7(b). Summary quantities for the wing with different pivots; sweep = 30 deg.

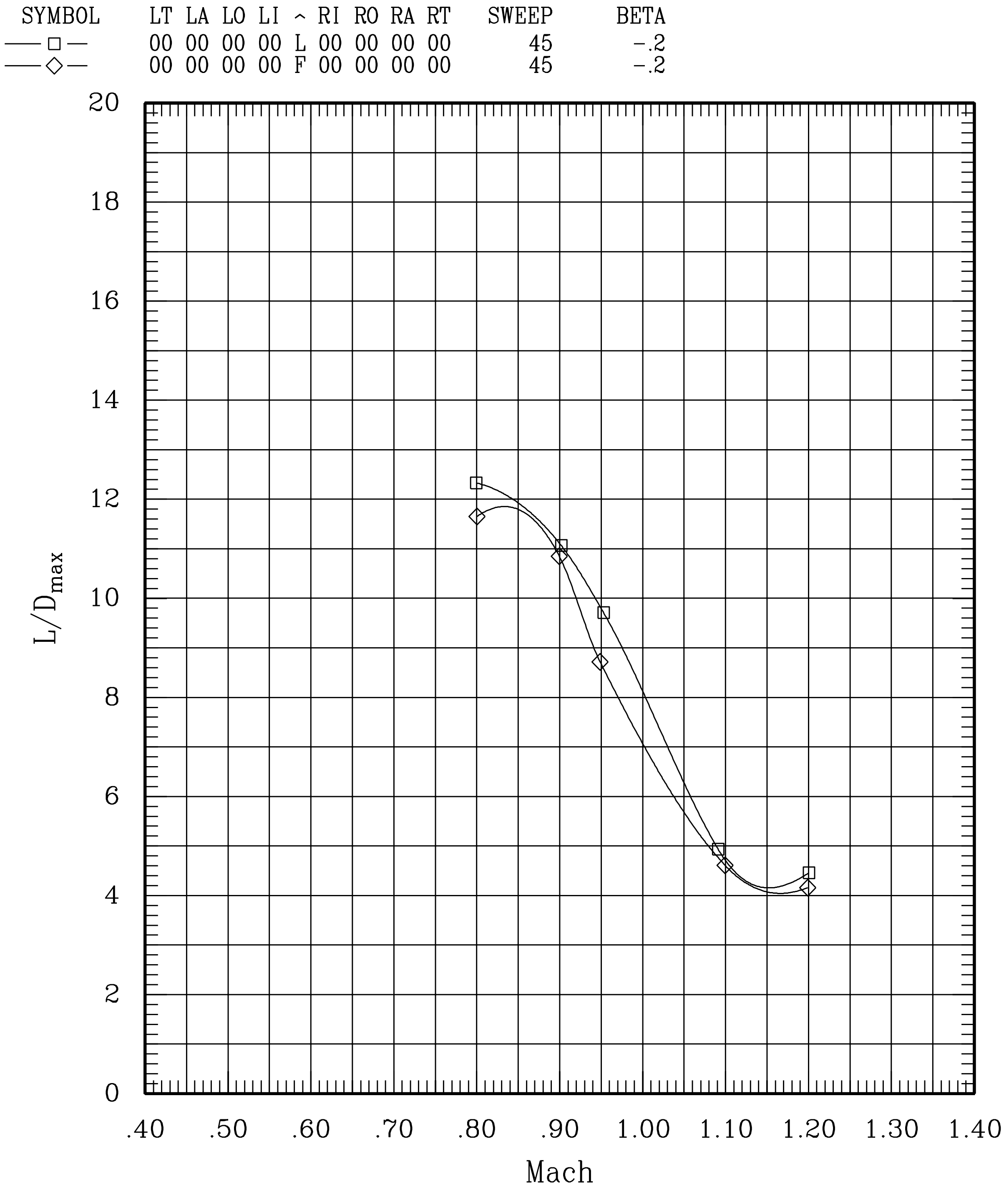

Figure 7(c). Summary quantities for the wing with different pivots; sweep = 45 deg.

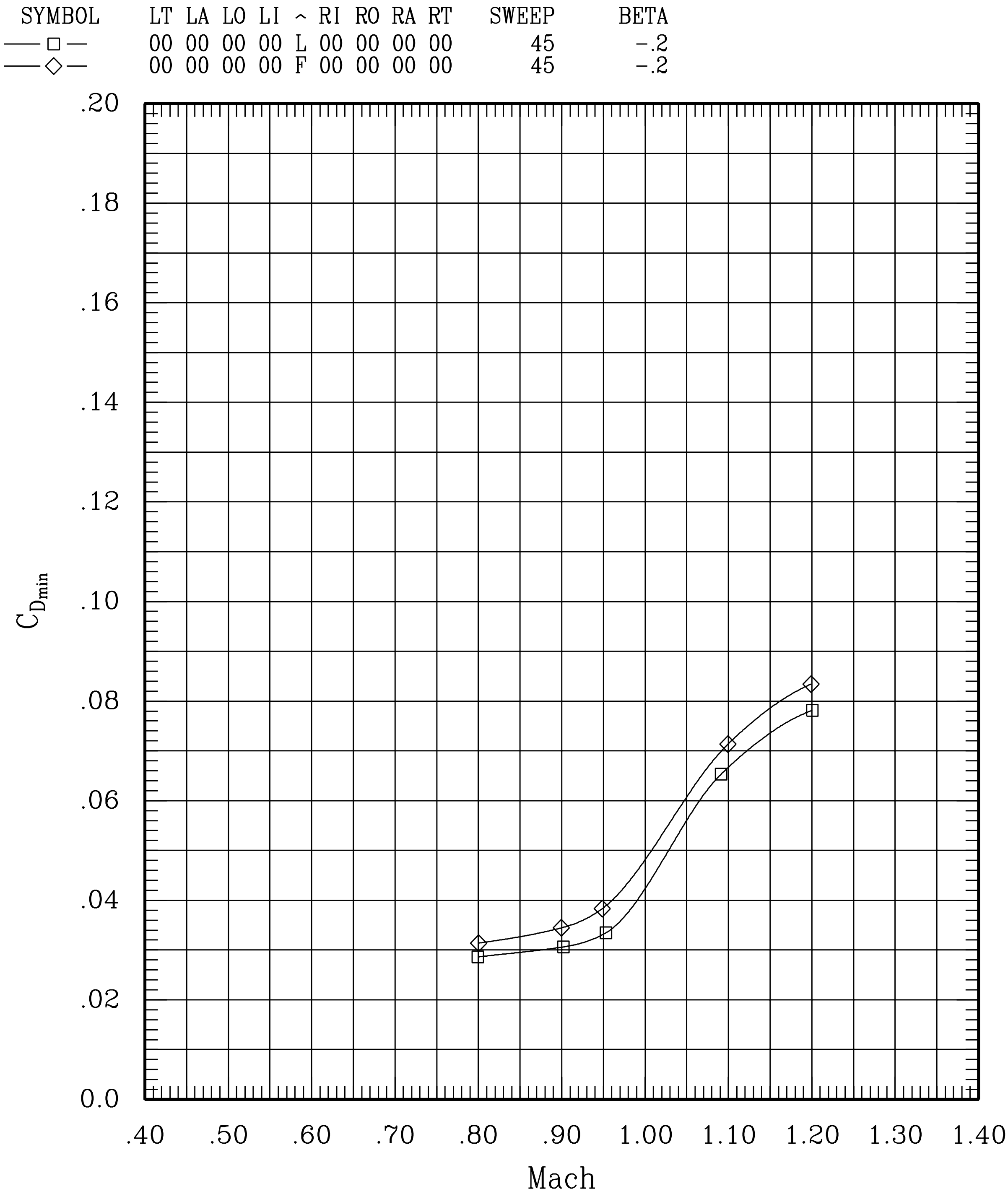

Figure 7(c). Summary quantities for the wing with different pivots; sweep = 45 deg.

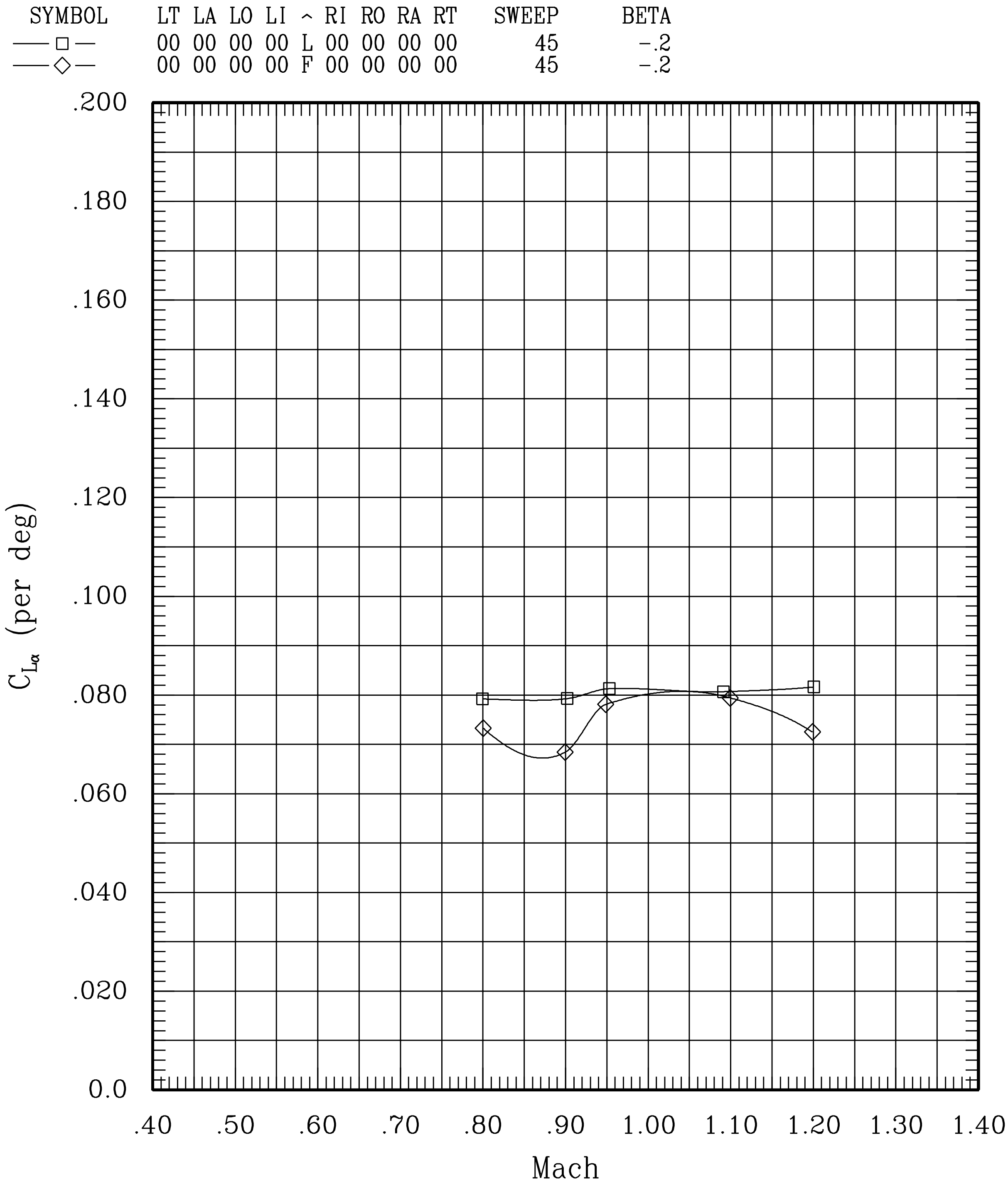

Figure 7(c). Summary quantities for the wing with different pivots; sweep = 45 deg.

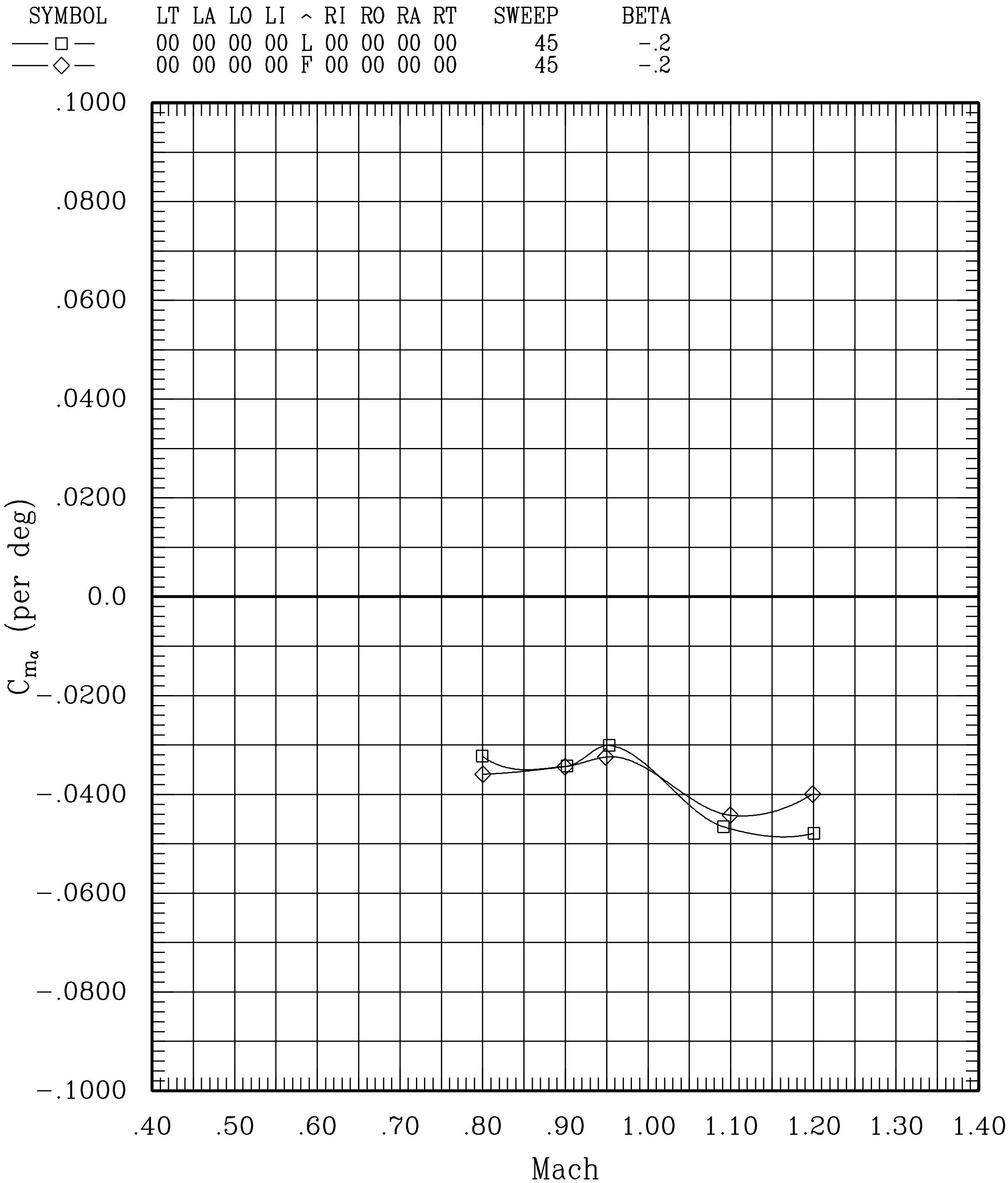

Figure 7(c). Summary quantities for the wing with different pivots; sweep = 45 deg.

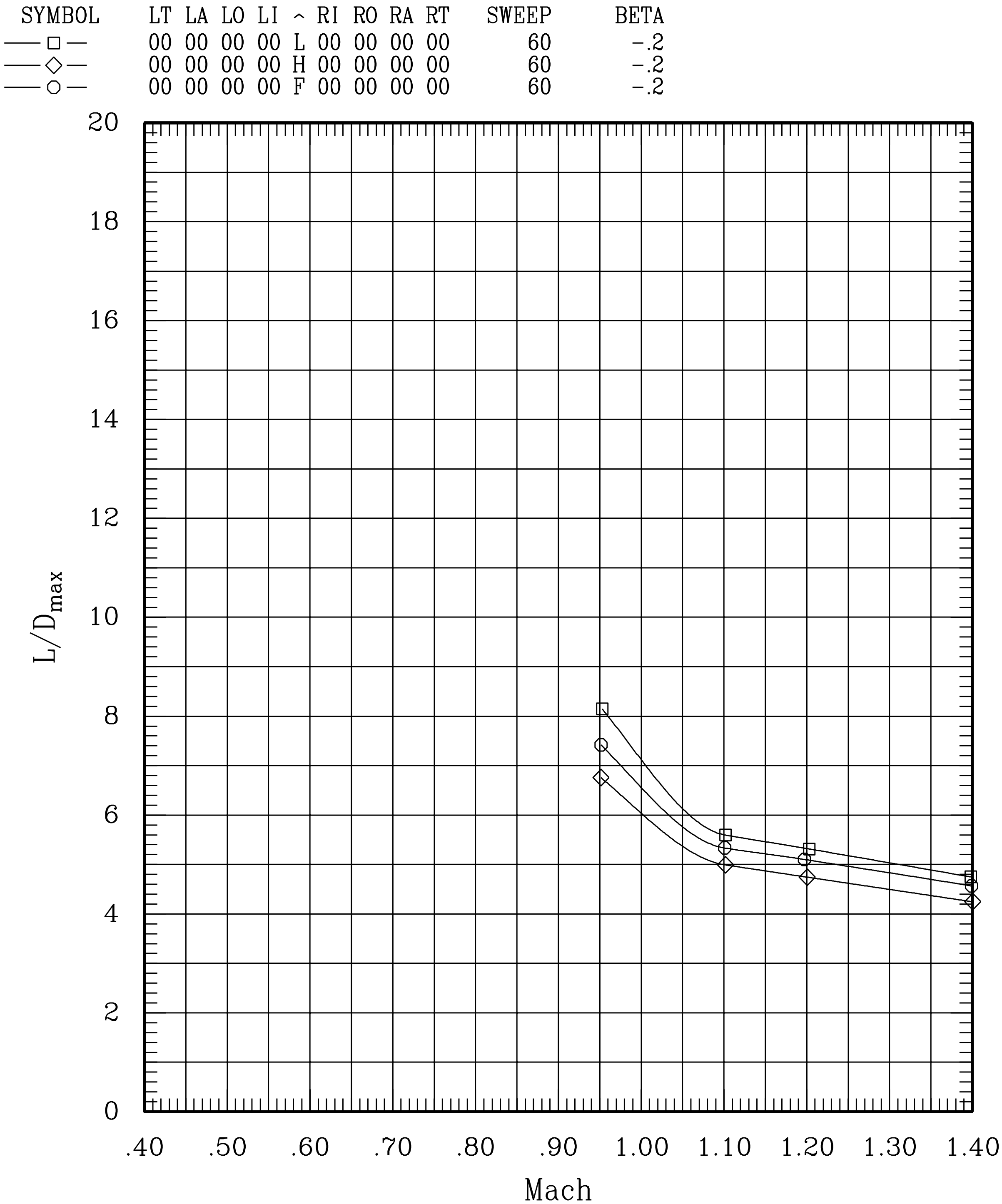

Figure 7(d). Summary quantities for the wing with different pivots; sweep = 60 deg.

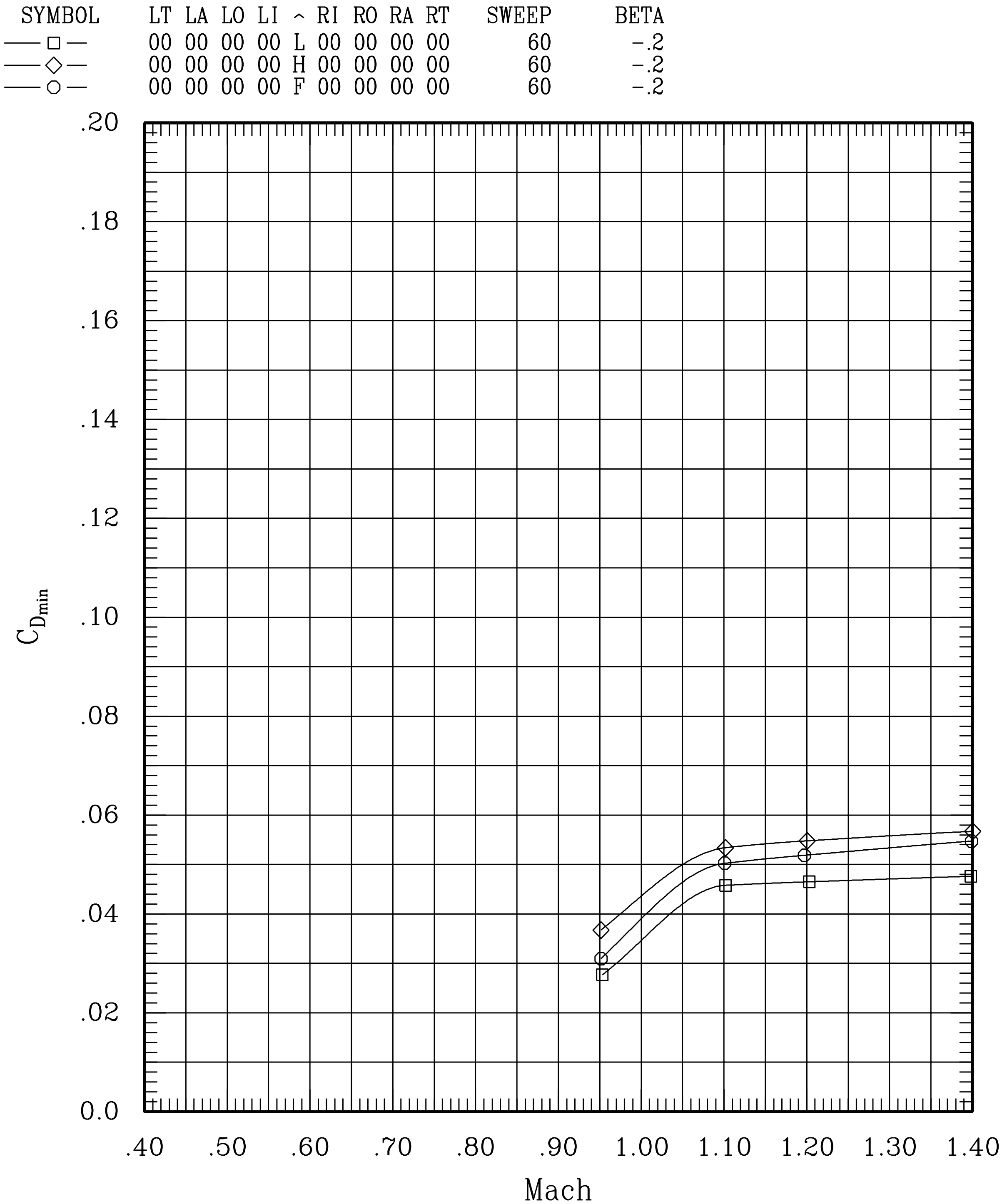

Figure 7(d). Summary quantities for the wing with different pivots; sweep = 60 deg.

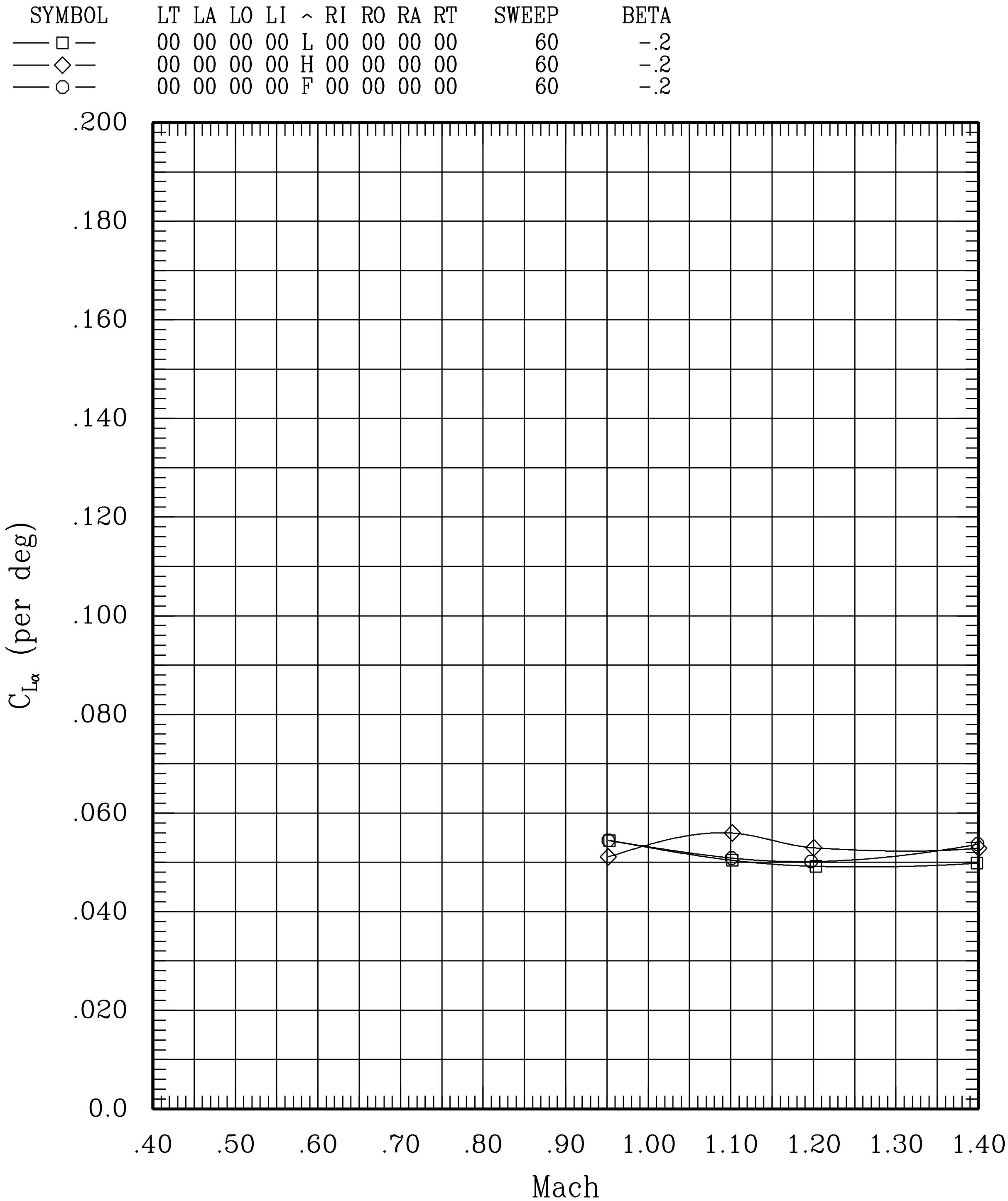

Figure 7(d). Summary quantities for the wing with different pivots; sweep = 60 deg.

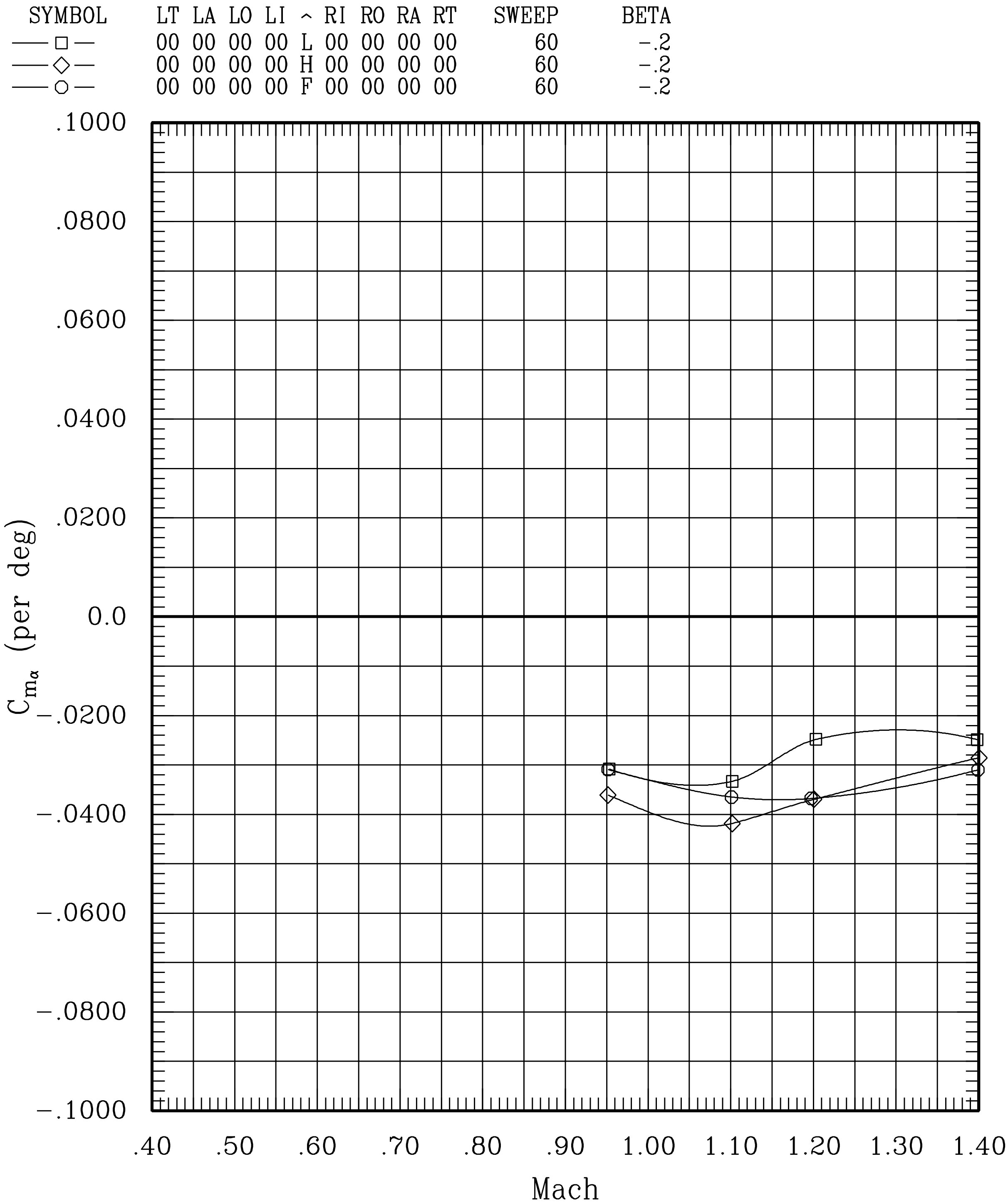

Figure 7(d). Summary quantities for the wing with different pivots; sweep = 60 deg.

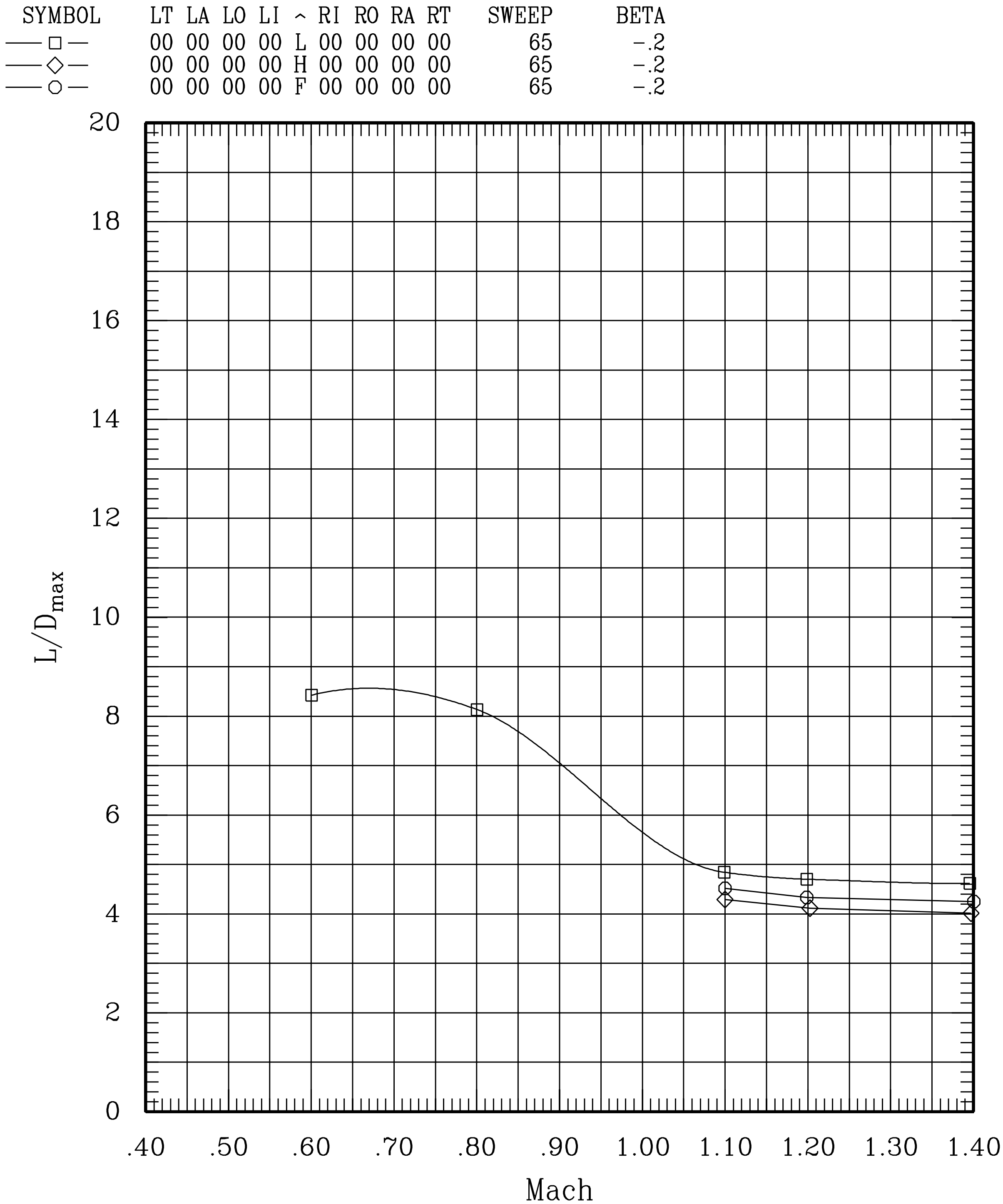

Figure 7(e). Summary quantities for the wing with different pivots; sweep = 65 deg.

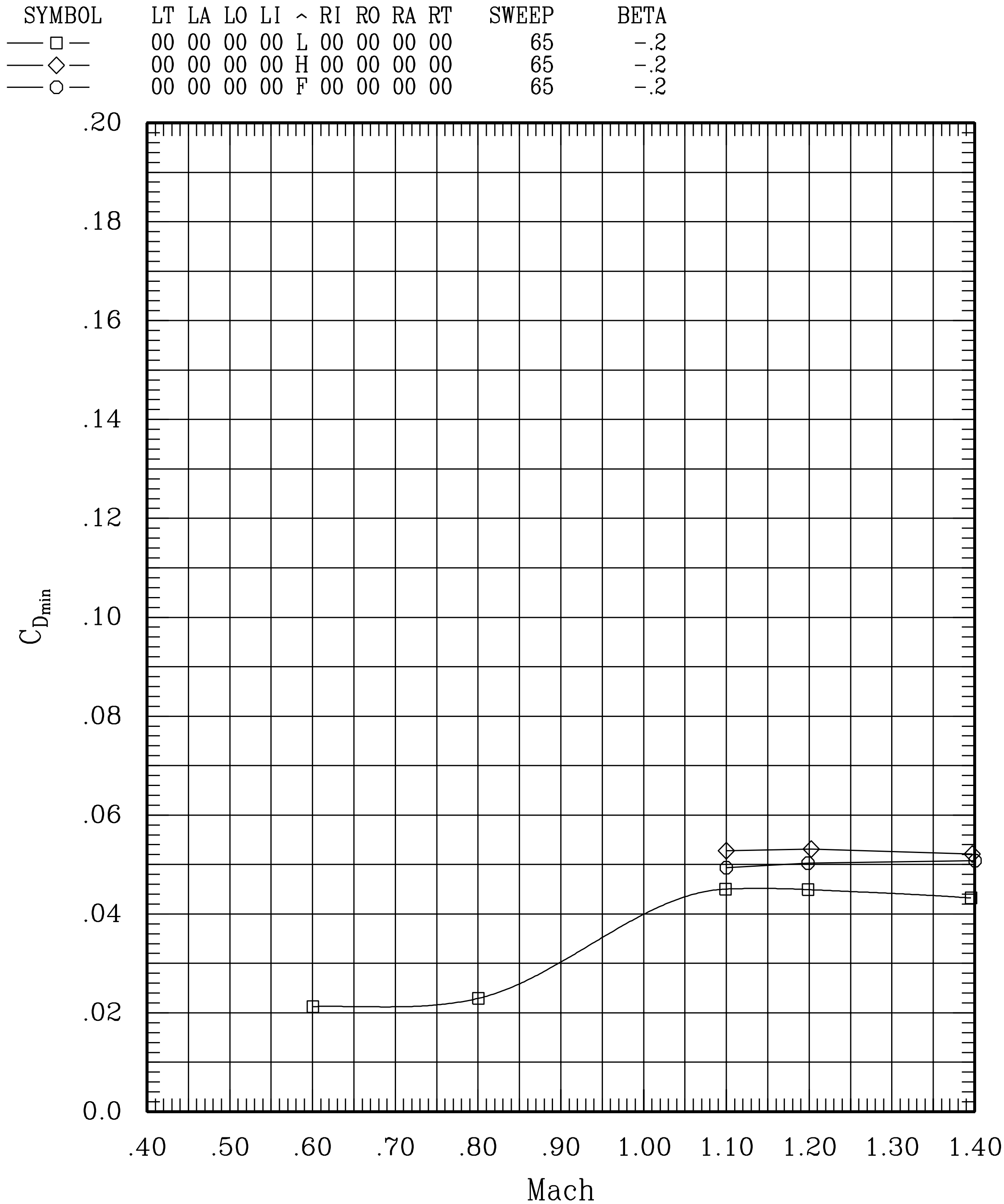

Figure 7(e). Summary quantities for the wing with different pivots; sweep = 65 deg.

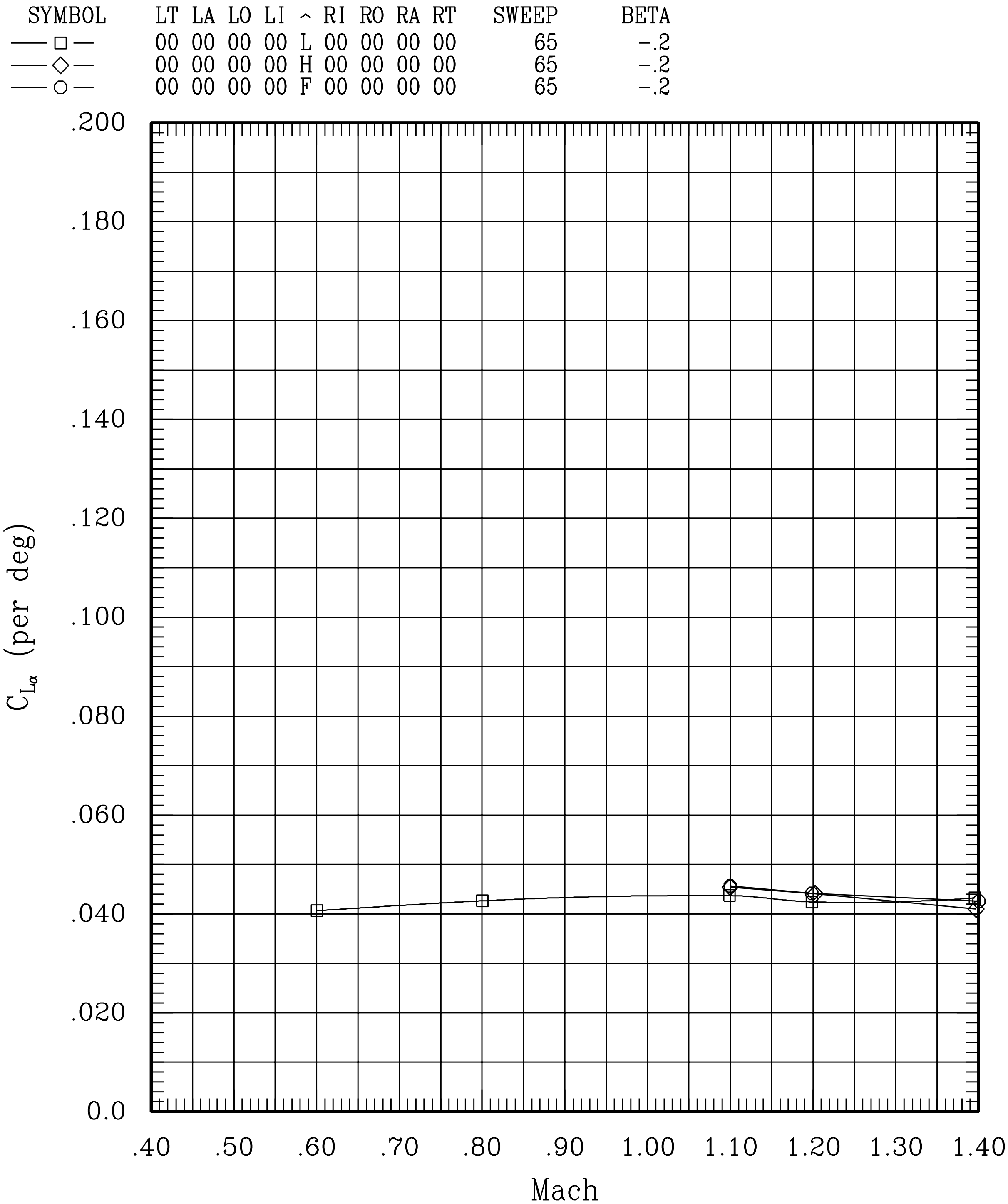

Figure 7(e). Summary quantities for the wing with different pivots; sweep = 65 deg.

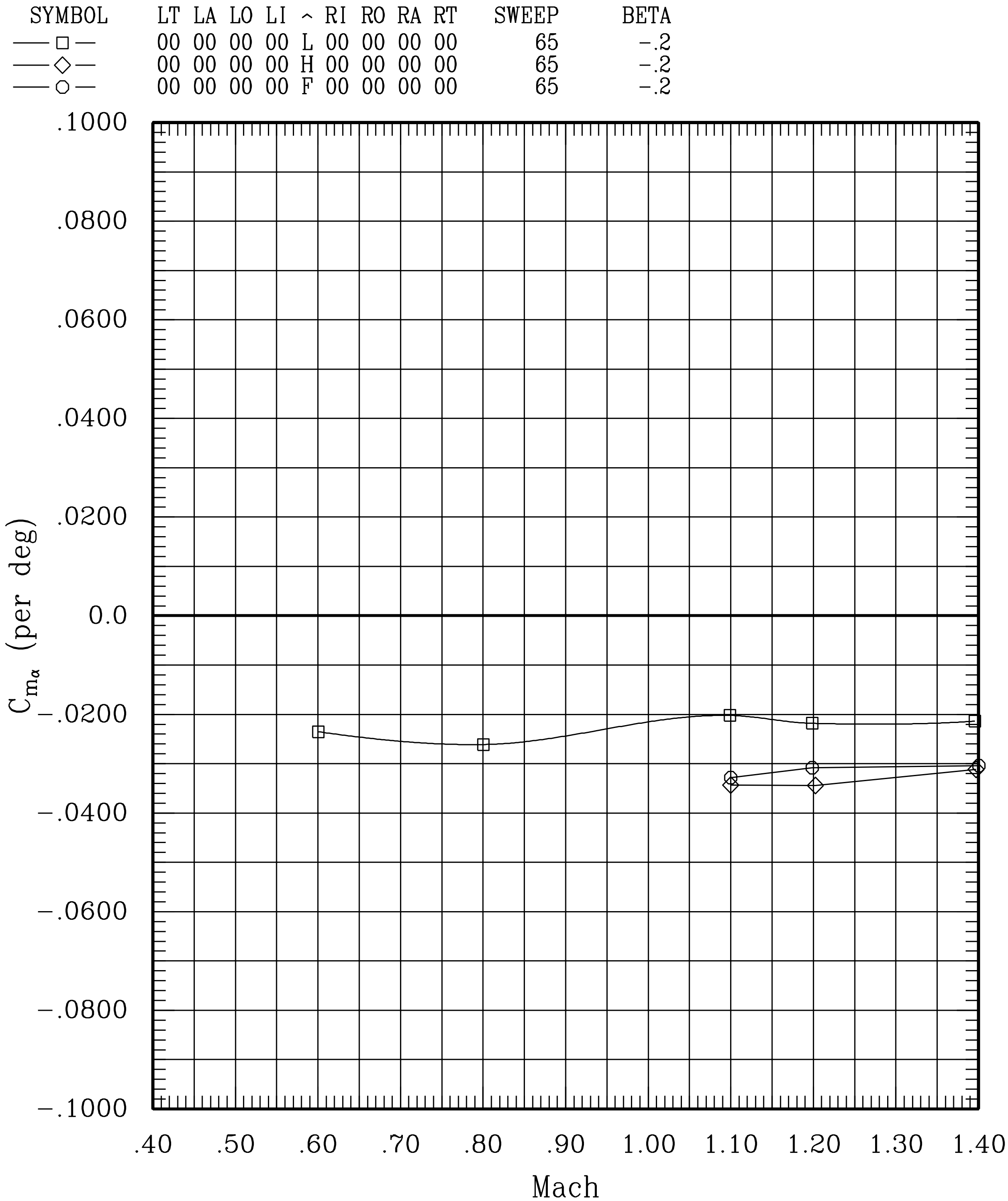

Figure 7(e). Summary quantities for the wing with different pivots; sweep = 65 deg.

SYMBOL	LT LA LO LI ^ RI RO RA RT	RUN	SWEEP	MACH	Q	BETA
—□—	00 00 00 00 L 00 00 00 00	11	0	.60	703	−.2
—◇—	00 00 00 00 L 00 00 00 00	105	65	.60	694	−.2

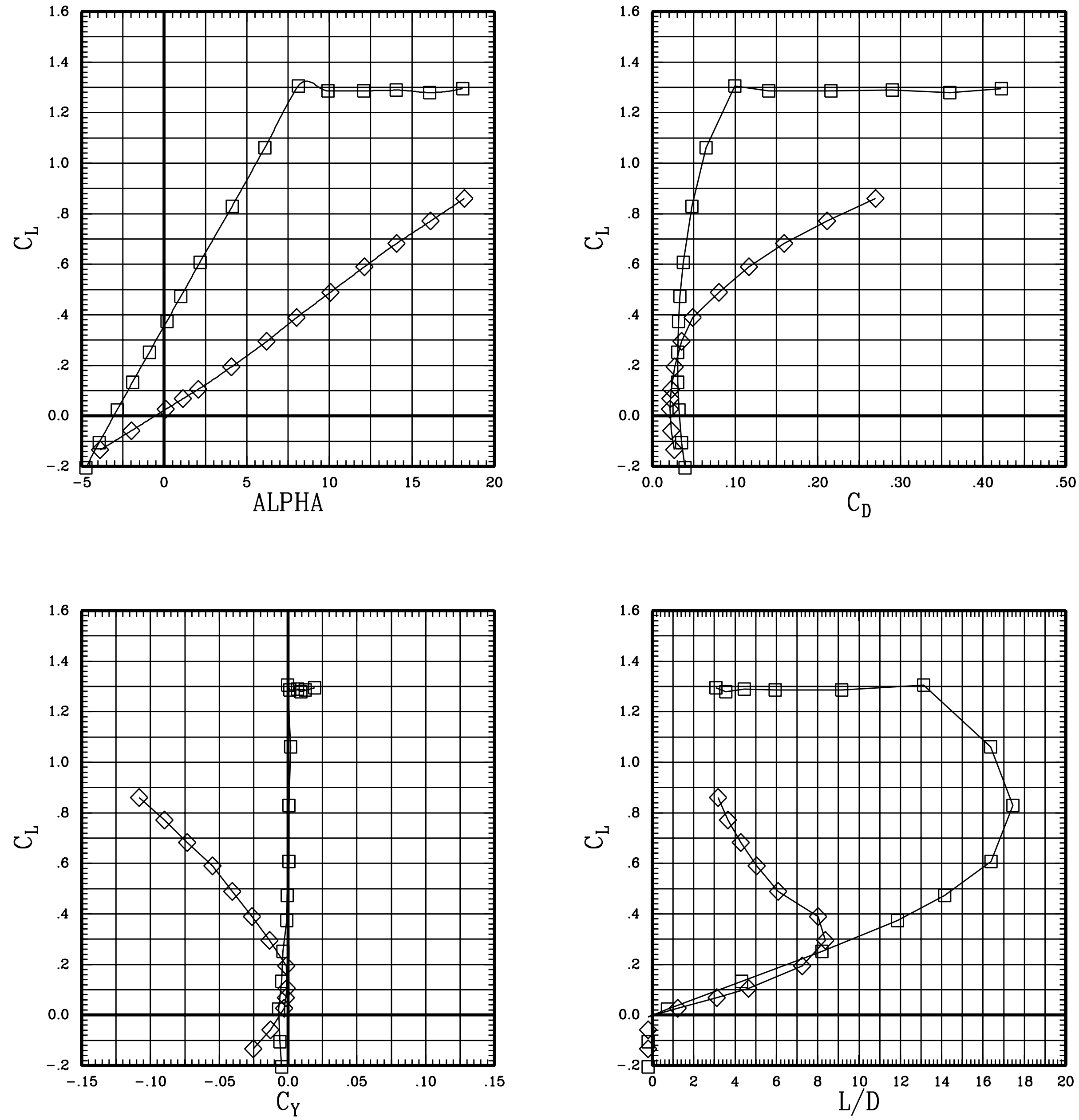

Figure 8(a). Effect of sweep for the wing with low pivot;
Mach = 0.60.

SYMBOL	LT LA LO LI ^ RI RO RA RT	RUN	SWEEP	MACH	Q	BETA
—□—	00 00 00 00 L 00 00 00 00	11	0	.60	703	−.2
—◇—	00 00 00 00 L 00 00 00 00	105	65	.60	694	−.2

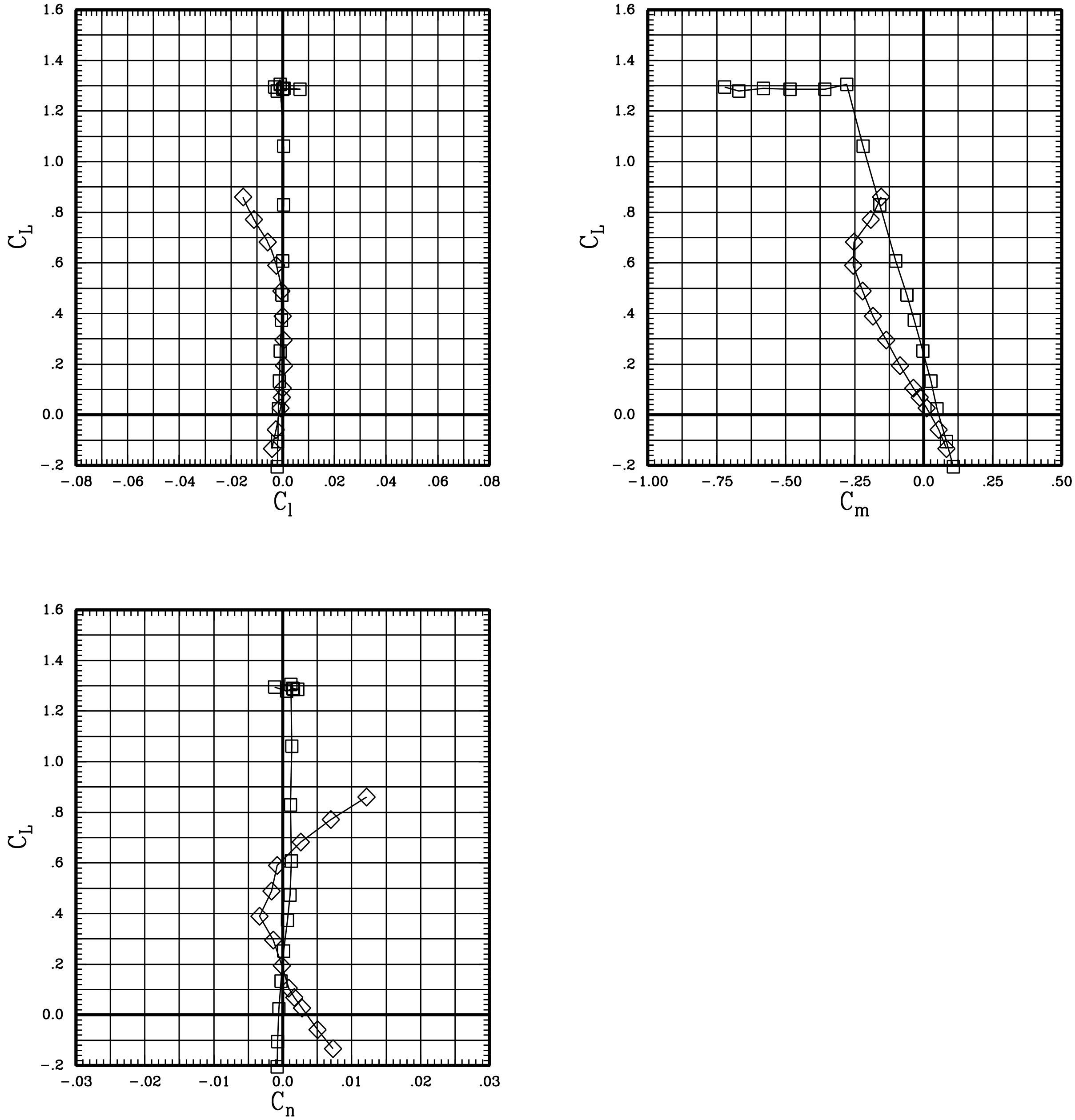

Figure 8(a). Effect of sweep for the wing with low pivot; Mach = 0.60.

SYMBOL	LT LA LO LI ^ RI RO RA RT	RUN	SWEEP	MACH	Q	BETA
—□—	00 00 00 00 L 00 00 00 00	10	0	.70	695	−.2
—◇—	00 00 00 00 L 00 00 00 00	15	30	.70	699	−.2

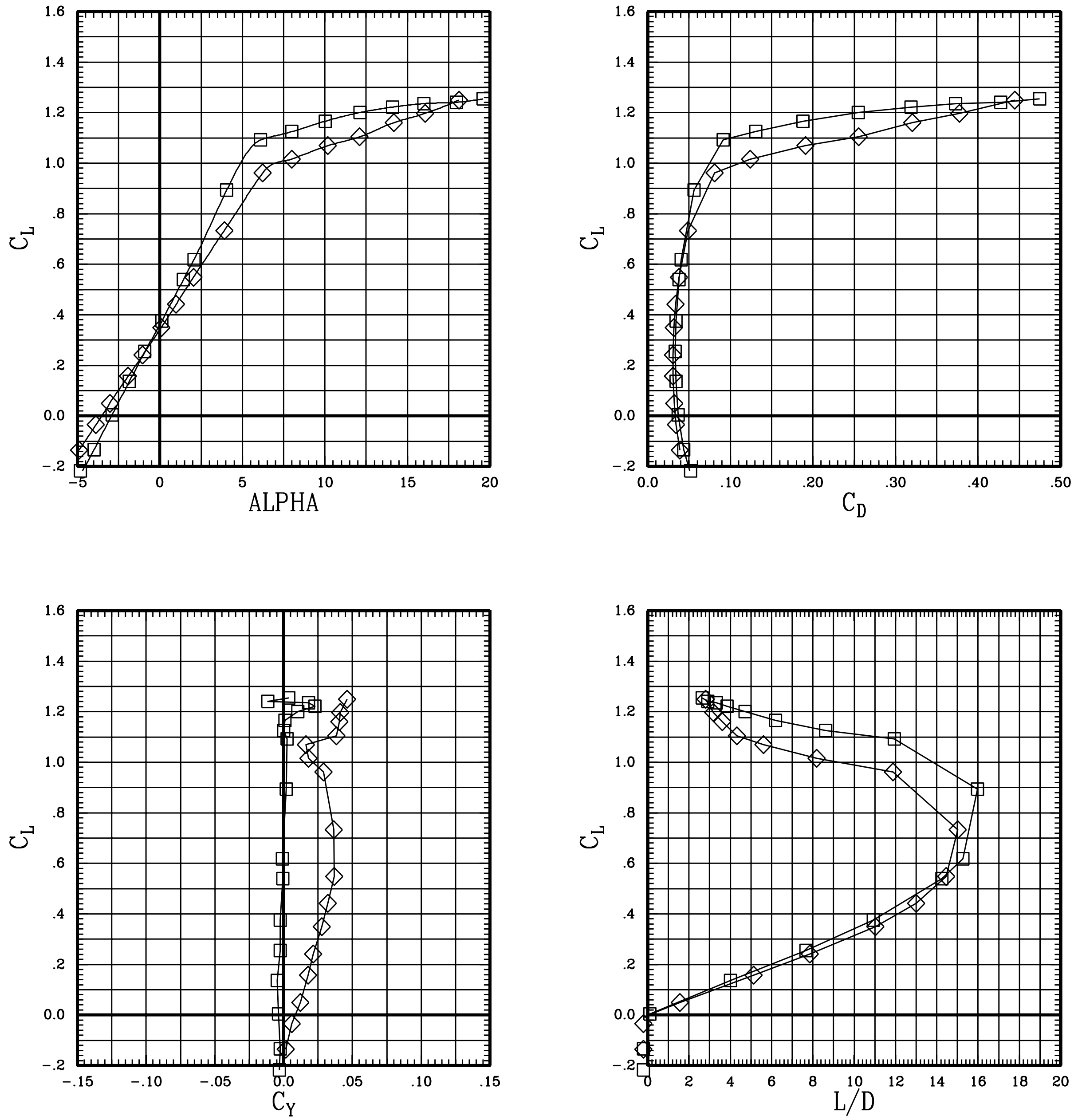

Figure 8(b). Effect of sweep for the wing with low pivot; Mach = 0.70.

SYMBOL	LT	LA	LO	LI	^	RI	RO	RA	RT	RUN	SWEEP	MACH	Q	BETA
—□—	00	00	00	00	L	00	00	00	00	10	0	.70	695	−.2
—◇—	00	00	00	00	L	00	00	00	00	15	30	.70	699	−.2

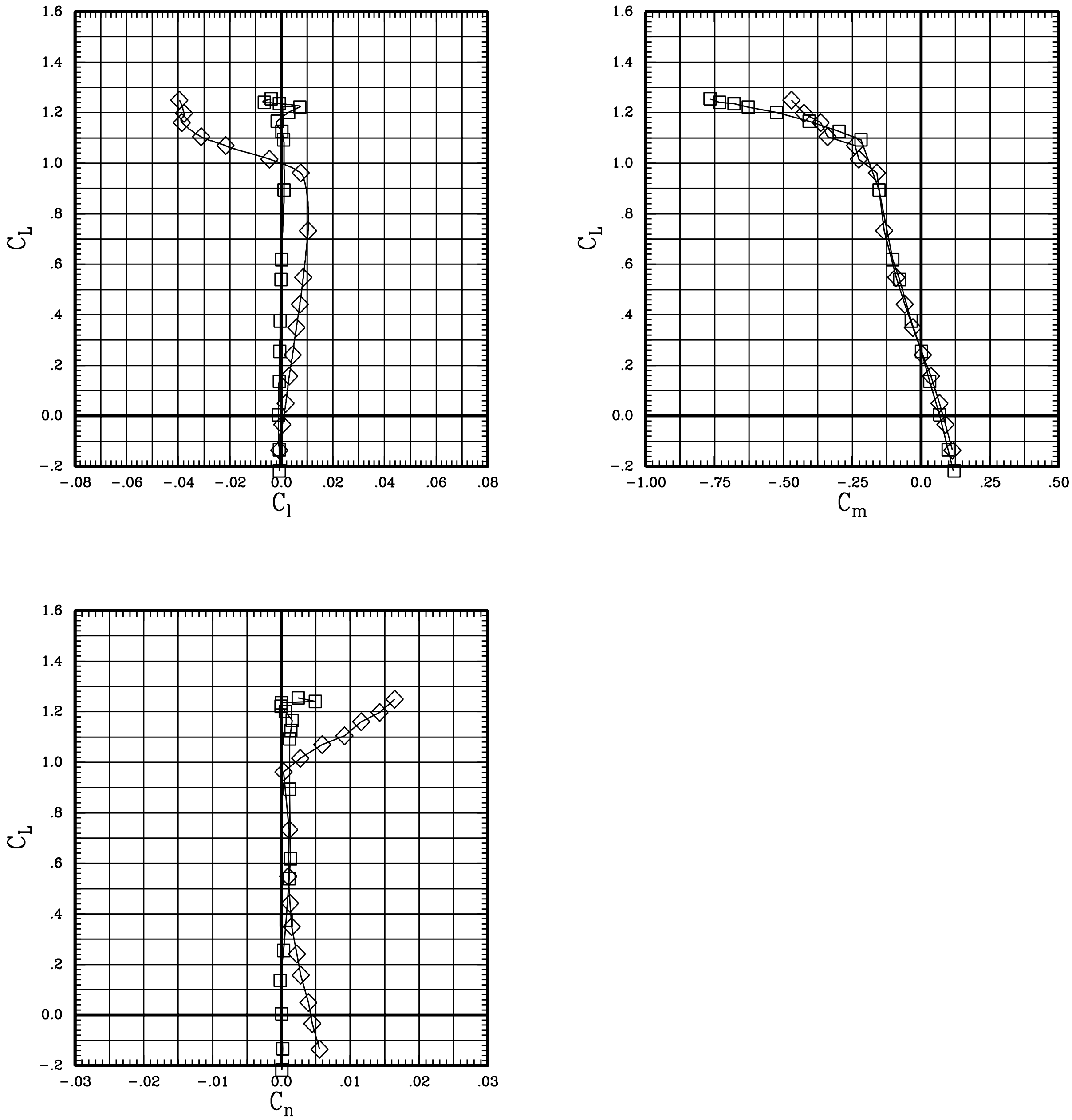

Figure 8(b). Effect of sweep for the wing with low pivot;
Mach = 0.70.

SYMBOL	LT LA LO LI ^ RI RO RA RT	RUN	SWEEP	MACH	Q	BETA
—□—	00 00 00 00 L 00 00 00 00	9	0	.80	706	−.2
—◇—	00 00 00 00 L 00 00 00 00	14	30	.80	702	−.3
—○—	00 00 00 00 L 00 00 00 00	20	45	.80	701	−.2
—△—	00 00 00 00 L 00 00 00 00	229	65	.80	704	−.2

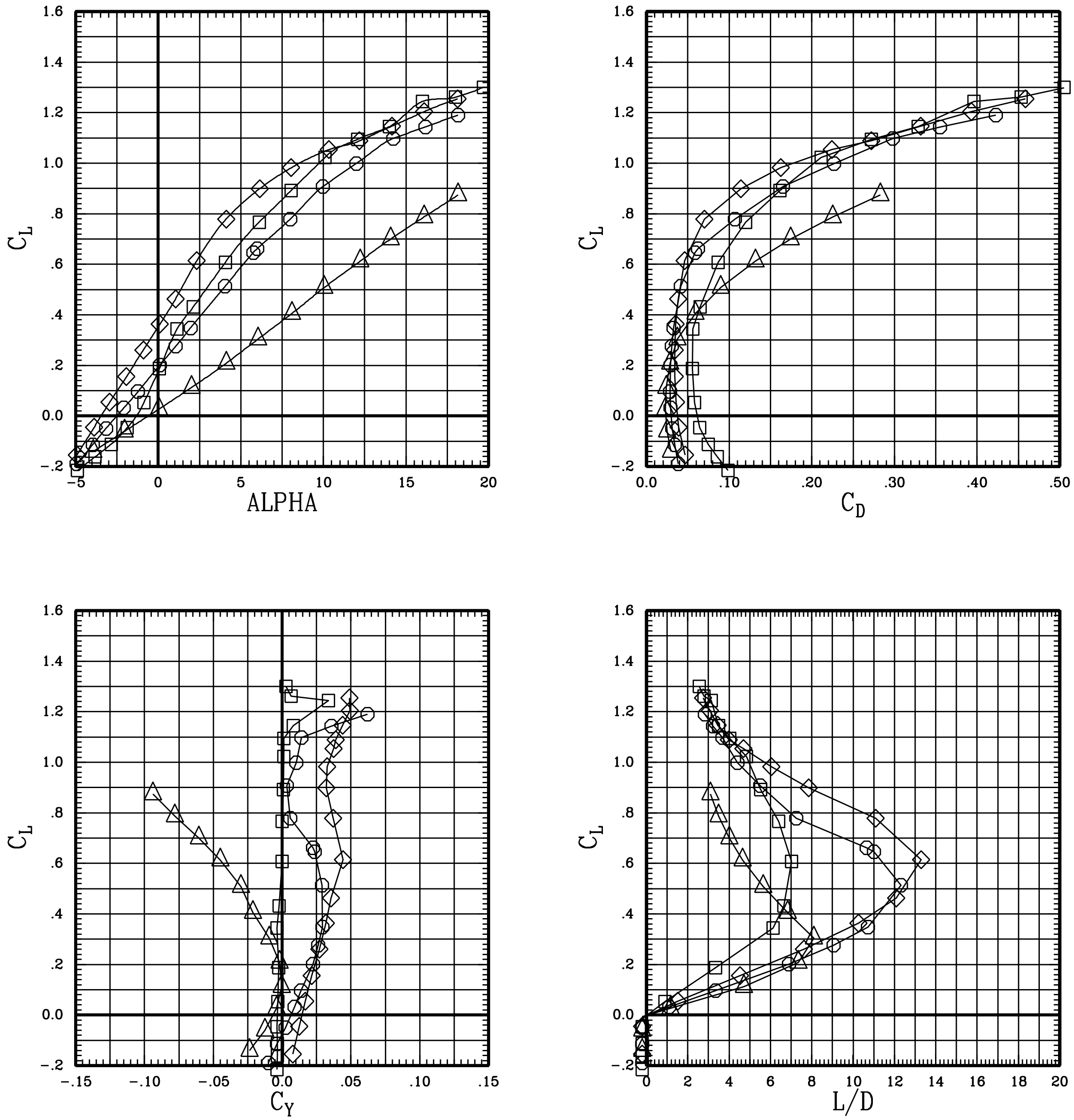

Figure 8(c). Effect of sweep for the wing with low pivot; Mach = 0.80.

SYMBOL	LT	LA	LO	LI	^	RI	RO	RA	RT	RUN	SWEEP	MACH	Q	BETA
—□—	00	00	00	00	L	00	00	00	00	9	0	.80	706	−.2
—◇—	00	00	00	00	L	00	00	00	00	14	30	.80	702	−.3
—○—	00	00	00	00	L	00	00	00	00	20	45	.80	701	−.2
—△—	00	00	00	00	L	00	00	00	00	229	65	.80	704	−.2

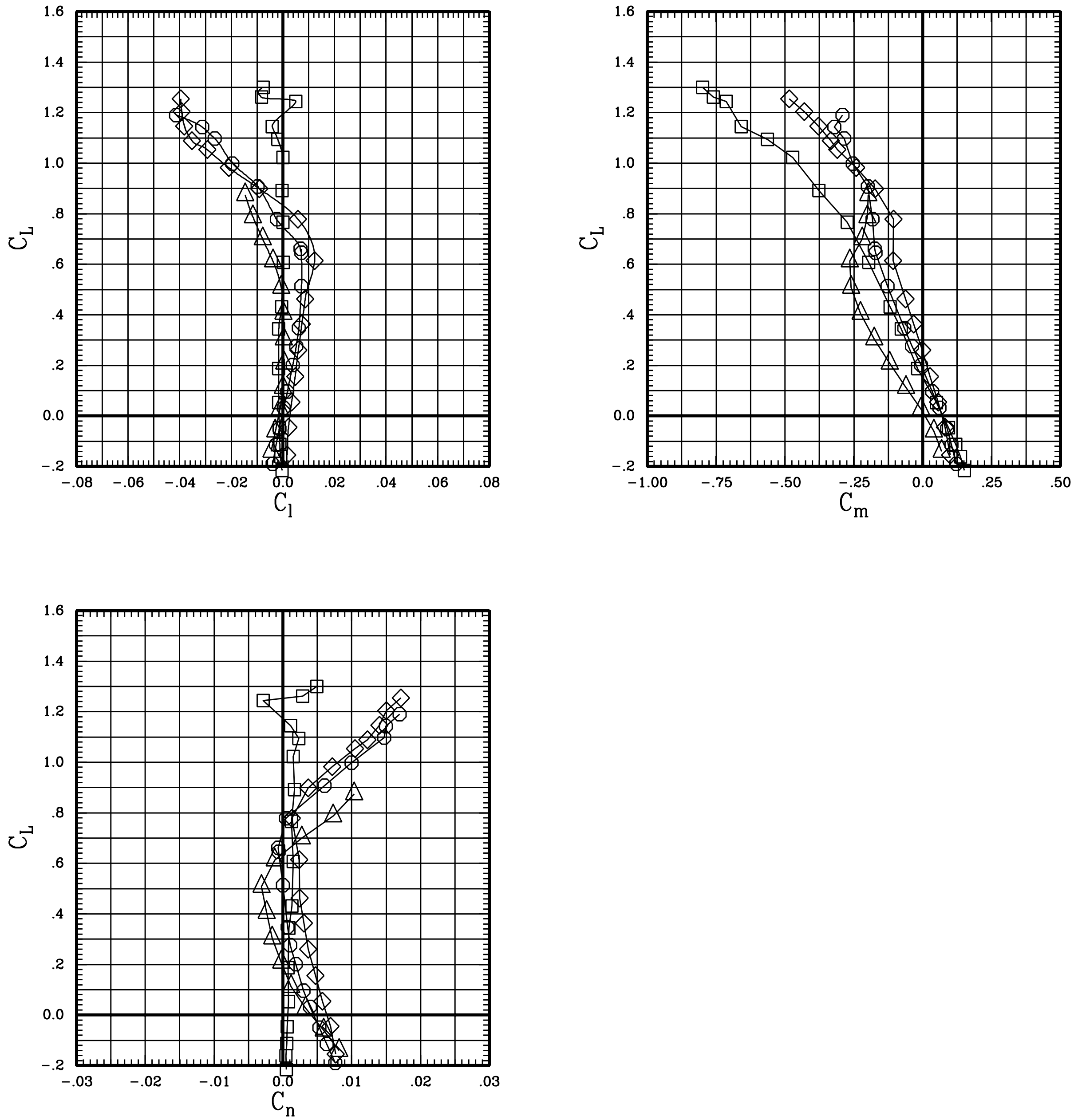

Figure 8(c). Effect of sweep for the wing with low pivot; Mach = 0.80.

SYMBOL	LT LA LO LI ^ RI RO RA RT	RUN	SWEEP	MACH	Q	BETA
—□—	00 00 00 00 L 00 00 00 00	13	30	.90	701	-.3
—◇—	00 00 00 00 L 00 00 00 00	19	45	.90	704	-.3

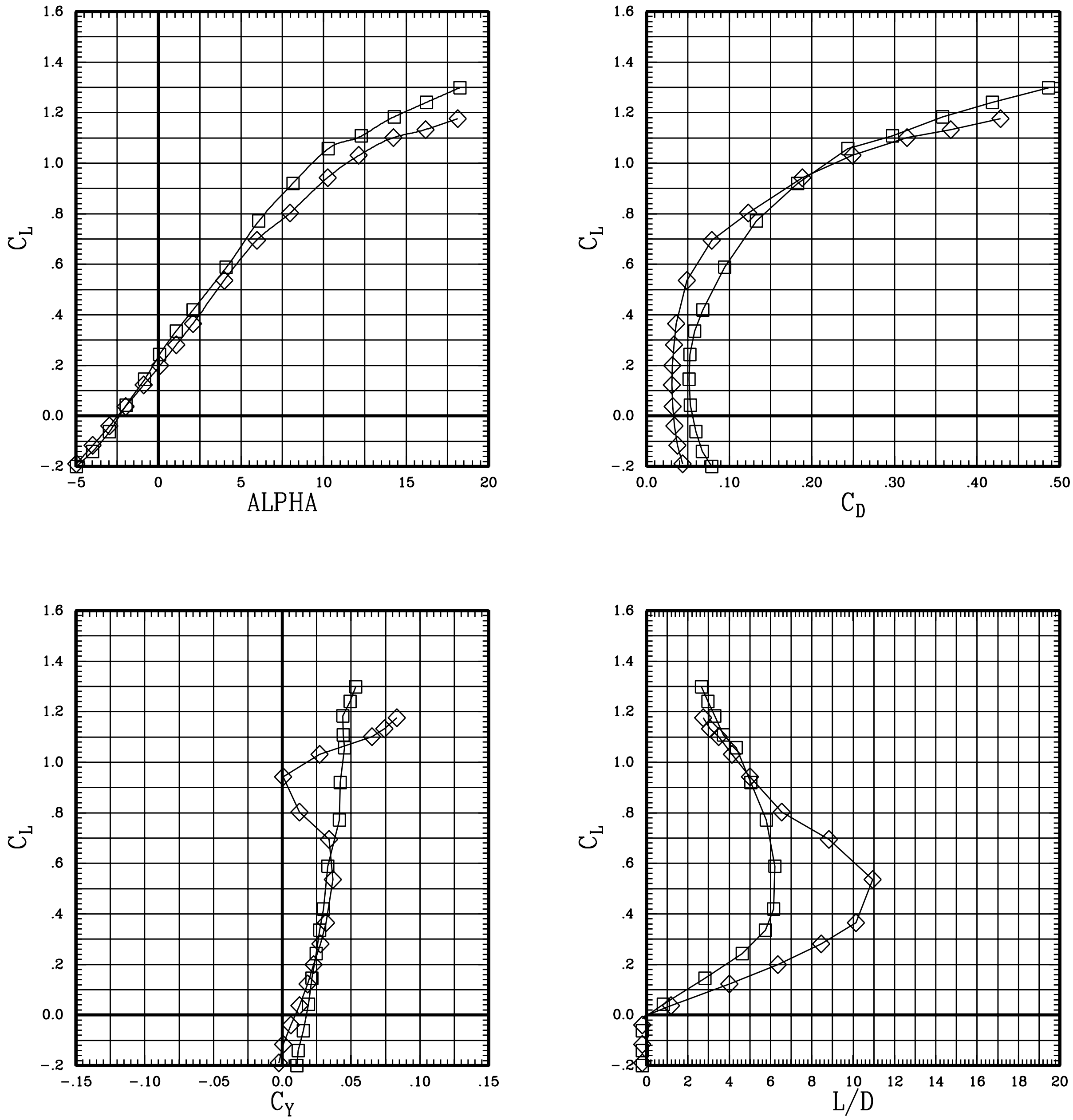

Figure 8(d). Effect of sweep for the wing with low pivot; Mach = 0.90.

SYMBOL	LT	LA	LO	LI	^	RI	RO	RA	RT	RUN	SWEEP	MACH	Q	BETA
—□—	00	00	00	00	L	00	00	00	00	13	30	.90	701	-.3
—◇—	00	00	00	00	L	00	00	00	00	19	45	.90	704	-.3

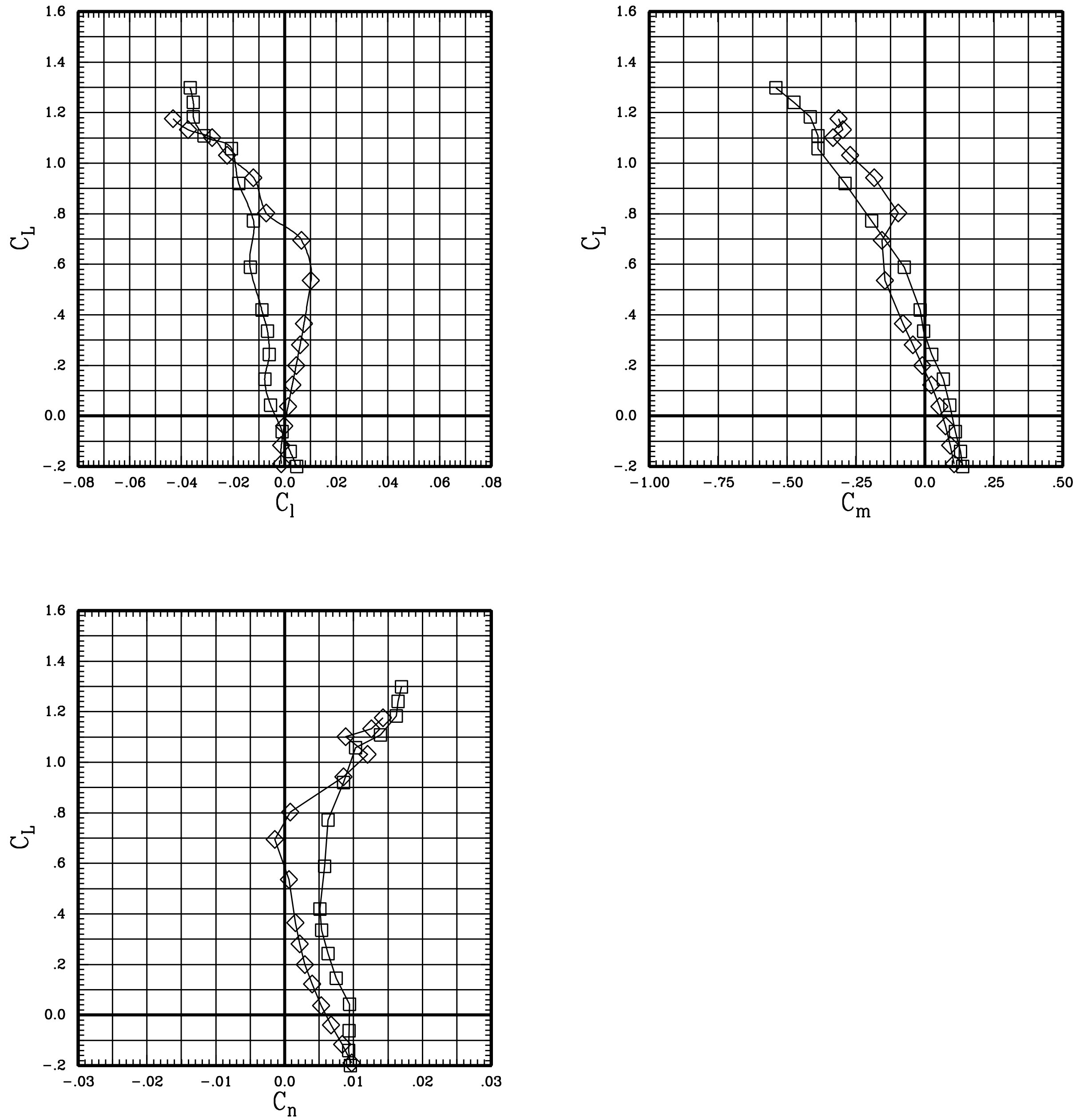

Figure 8(d). Effect of sweep for the wing with low pivot; Mach = 0.90.

SYMBOL	LT	LA	LO	LI	^	RI	RO	RA	RT	RUN	SWEEP	MACH	Q	BETA
—□—	00	00	00	00	L	00	00	00	00	17	45	1.09	696	−.3
—◇—	00	00	00	00	L	00	00	00	00	34	60	1.10	701	−.3
—○—	00	00	00	00	L	00	00	00	00	31	65	1.10	687	−.3

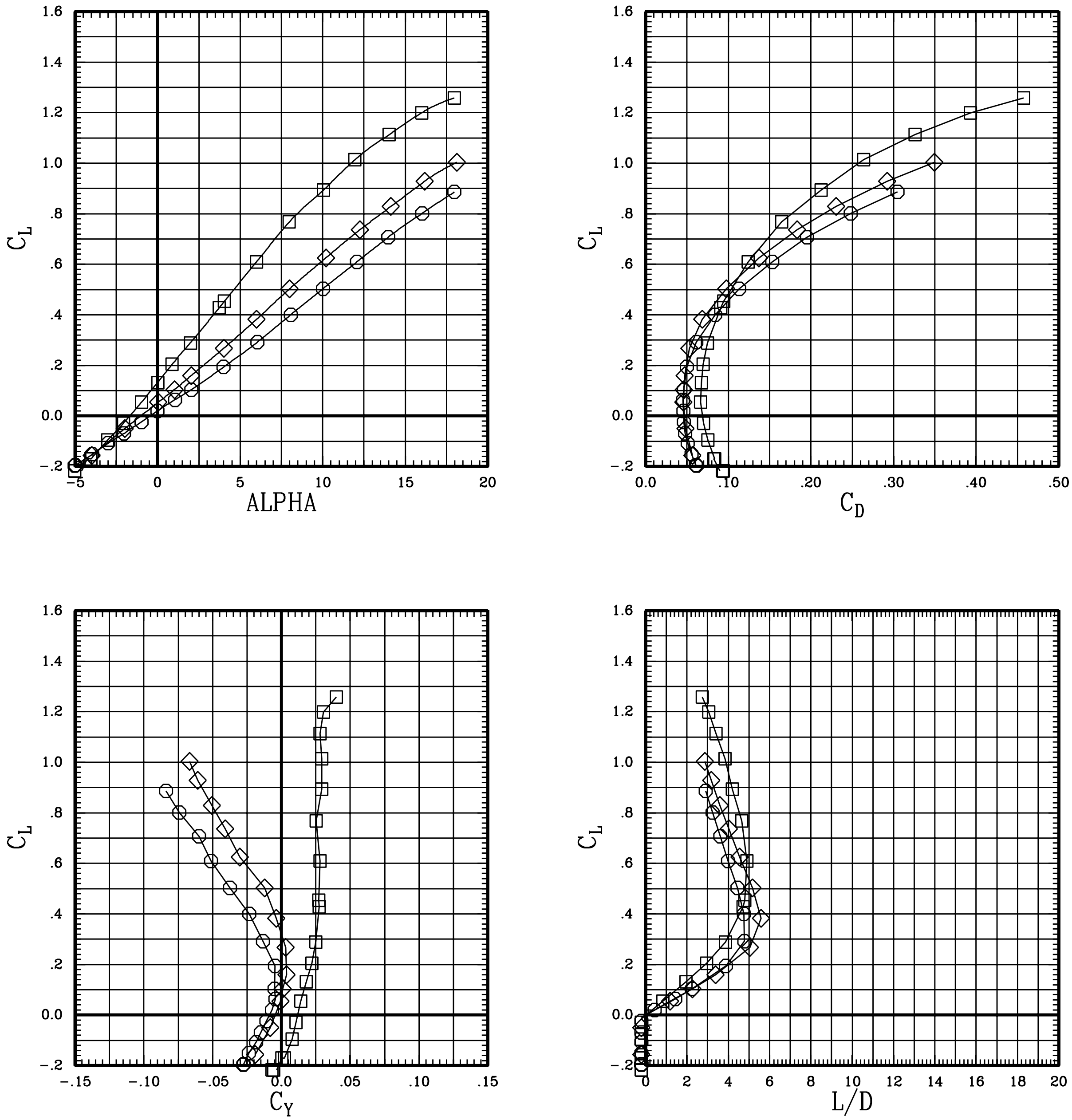

Figure 8(e). Effect of sweep for the wing with low pivot;
Mach = 1.10.

SYMBOL	LT LA LO LI ^ RI RO RA RT	RUN	SWEEP	MACH	Q	BETA
—□—	00 00 00 00 L 00 00 00 00	17	45	1.09	696	-.3
—◇—	00 00 00 00 L 00 00 00 00	34	60	1.10	701	-.3
—○—	00 00 00 00 L 00 00 00 00	31	65	1.10	687	-.3

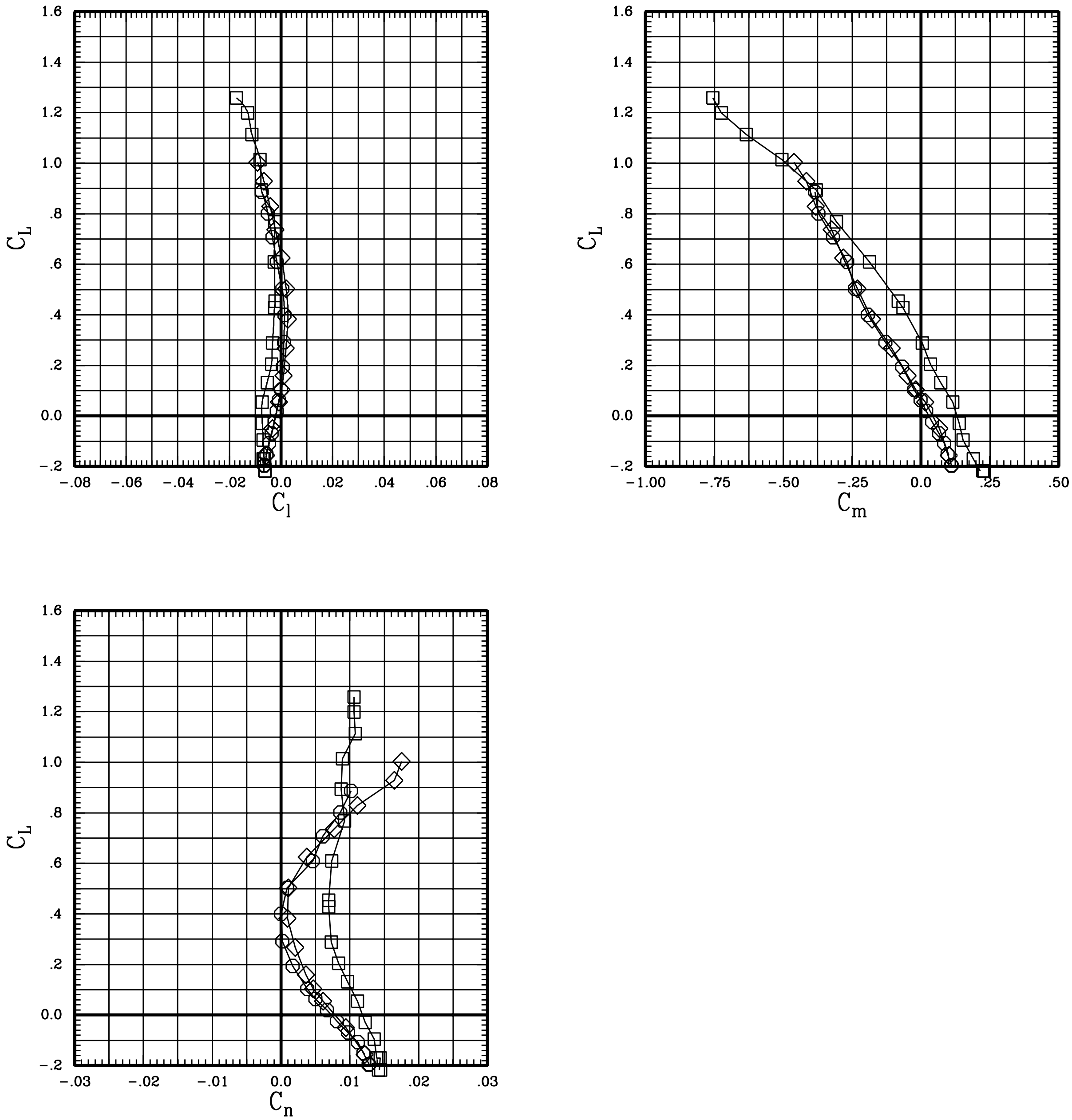

Figure 8(e). Effect of sweep for the wing with low pivot; Mach = 1.10.

SYMBOL	LT LA LO LI ^ RI RO RA RT	RUN	SWEEP	MACH	Q	BETA
—□—	00 00 00 00 L 00 00 00 00	16	45	1.20	702	−.3
—◇—	00 00 00 00 L 00 00 00 00	33	60	1.20	701	−.2
—○—	00 00 00 00 L 00 00 00 00	30	65	1.20	700	−.3

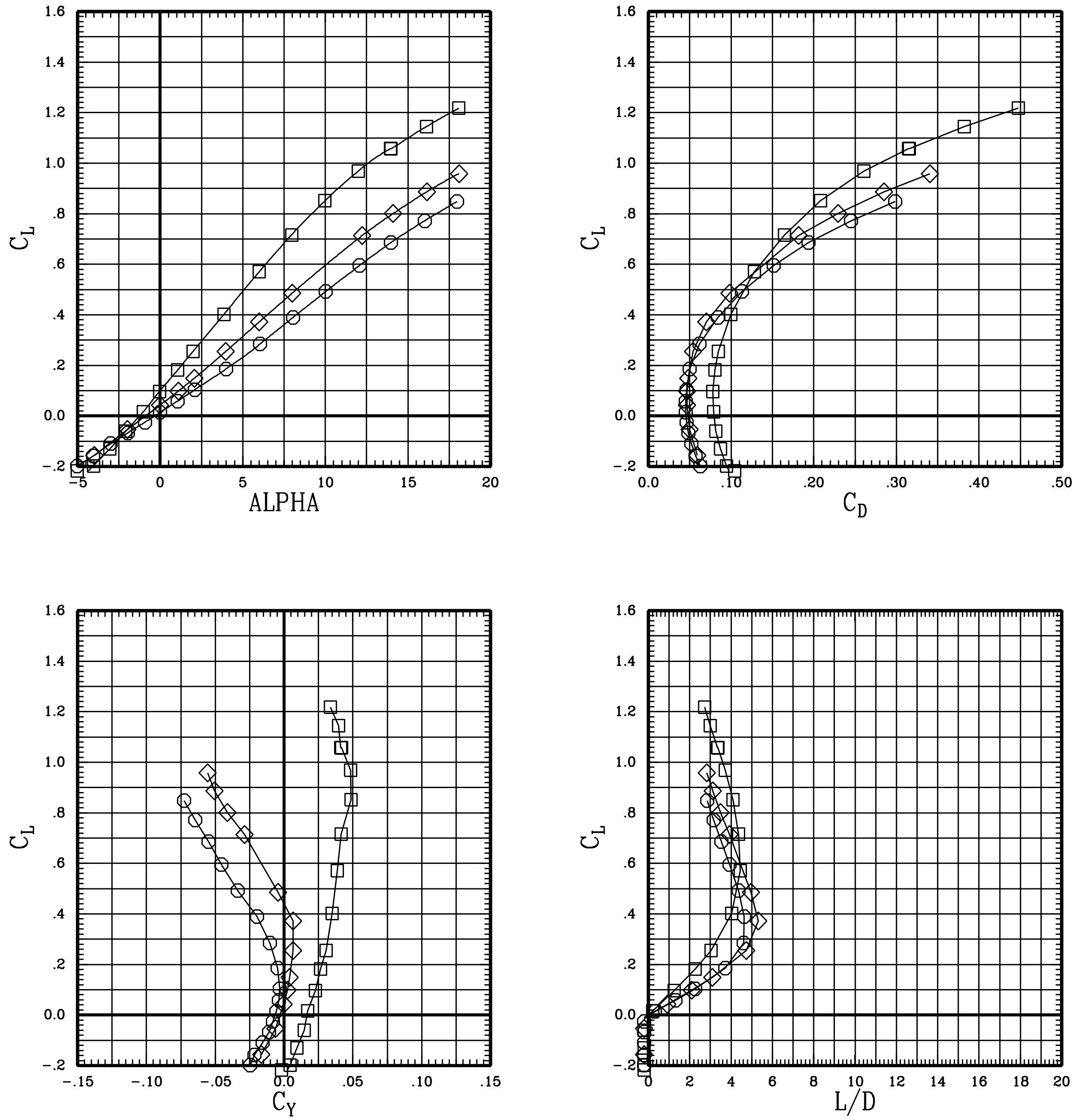

Figure 8(f). Effect of sweep for the wing with low pivot;
Mach = 1.20.

SYMBOL	LT LA LO LI ^ RI RO RA RT	RUN	SWEEP	MACH	Q	BETA
—□—	00 00 00 00 L 00 00 00 00	16	45	1.20	702	−.3
—◇—	00 00 00 00 L 00 00 00 00	33	60	1.20	701	−.2
—○—	00 00 00 00 L 00 00 00 00	30	65	1.20	700	−.3

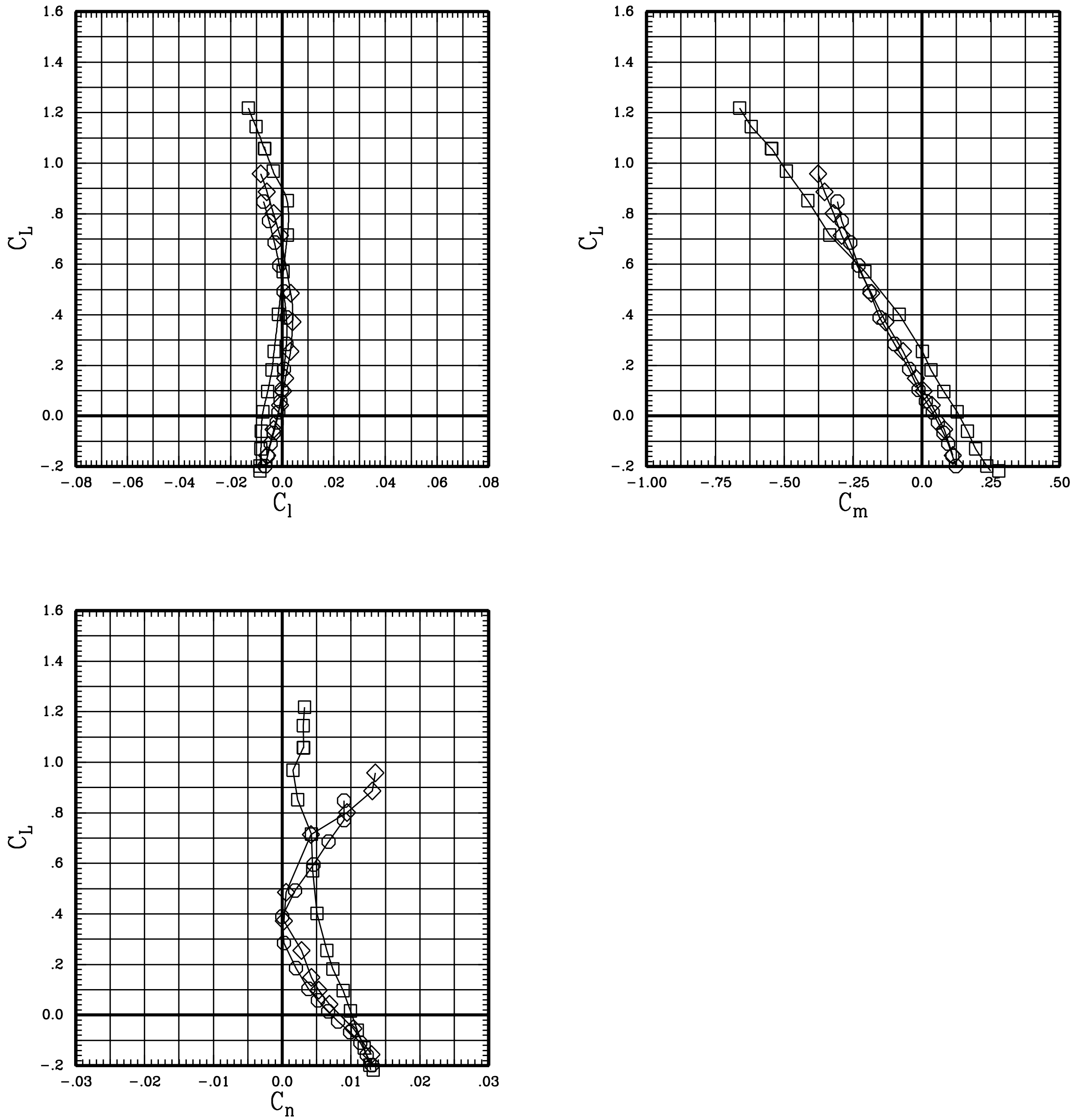

Figure 8(f). Effect of sweep for the wing with low pivot; Mach = 1.20.

SYMBOL	LT	LA	LO	LI	^	RI	RO	RA	RT	RUN	SWEEP	MACH	Q	BETA
—□—	00	00	00	00	L	00	00	00	00	32	60	1.40	702	−.2
—◇—	00	00	00	00	L	00	00	00	00	29	65	1.40	701	−.3

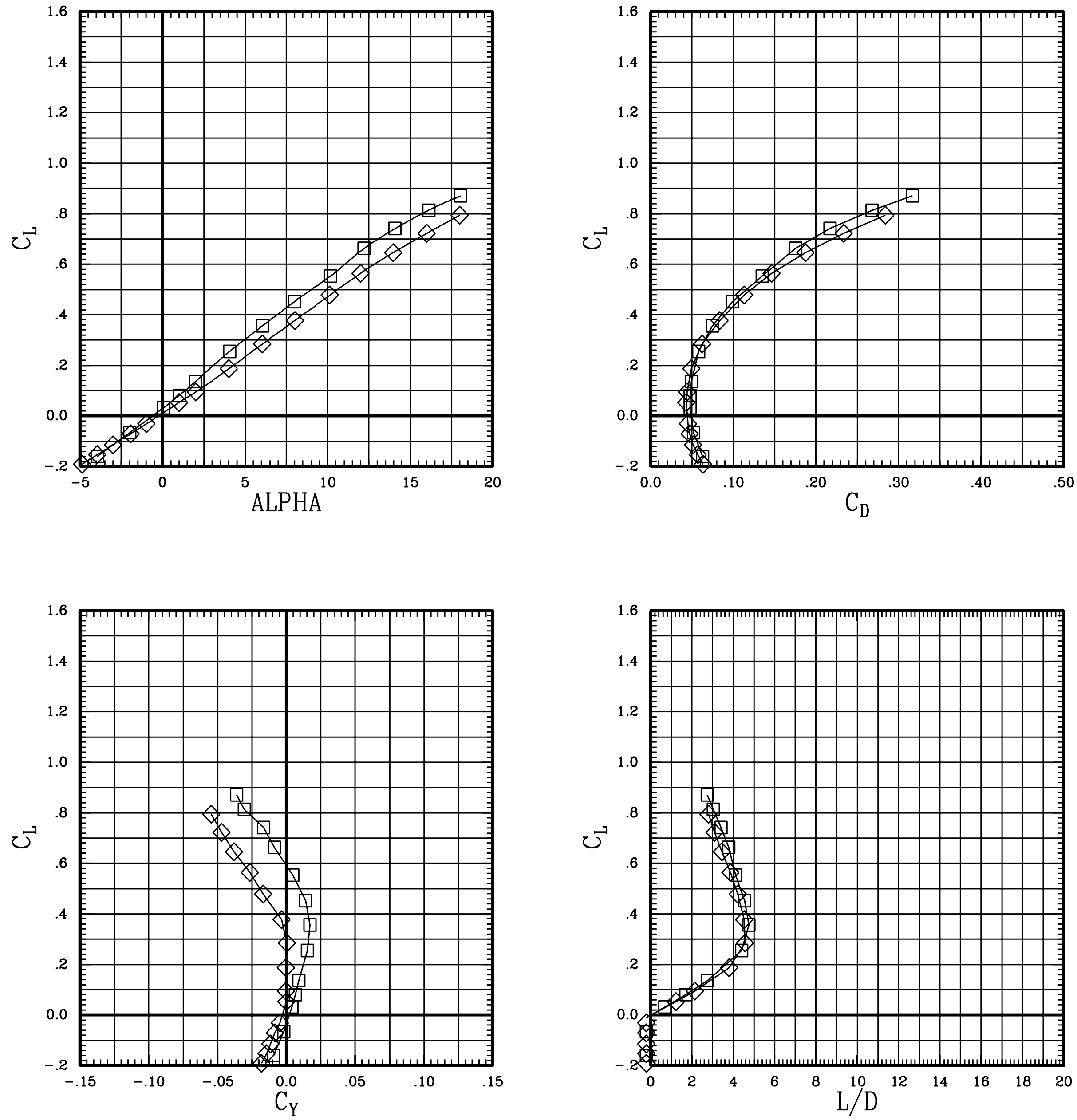

Figure 8(g). Effect of sweep for the wing with low pivot;
Mach = 1.40.

SYMBOL	LT LA LO LI ^ RI RO RA RT	RUN	SWEEP	MACH	Q	BETA
—□—	00 00 00 00 L 00 00 00 00	32	60	1.40	702	-.2
—◇—	00 00 00 00 L 00 00 00 00	29	65	1.40	701	-.3

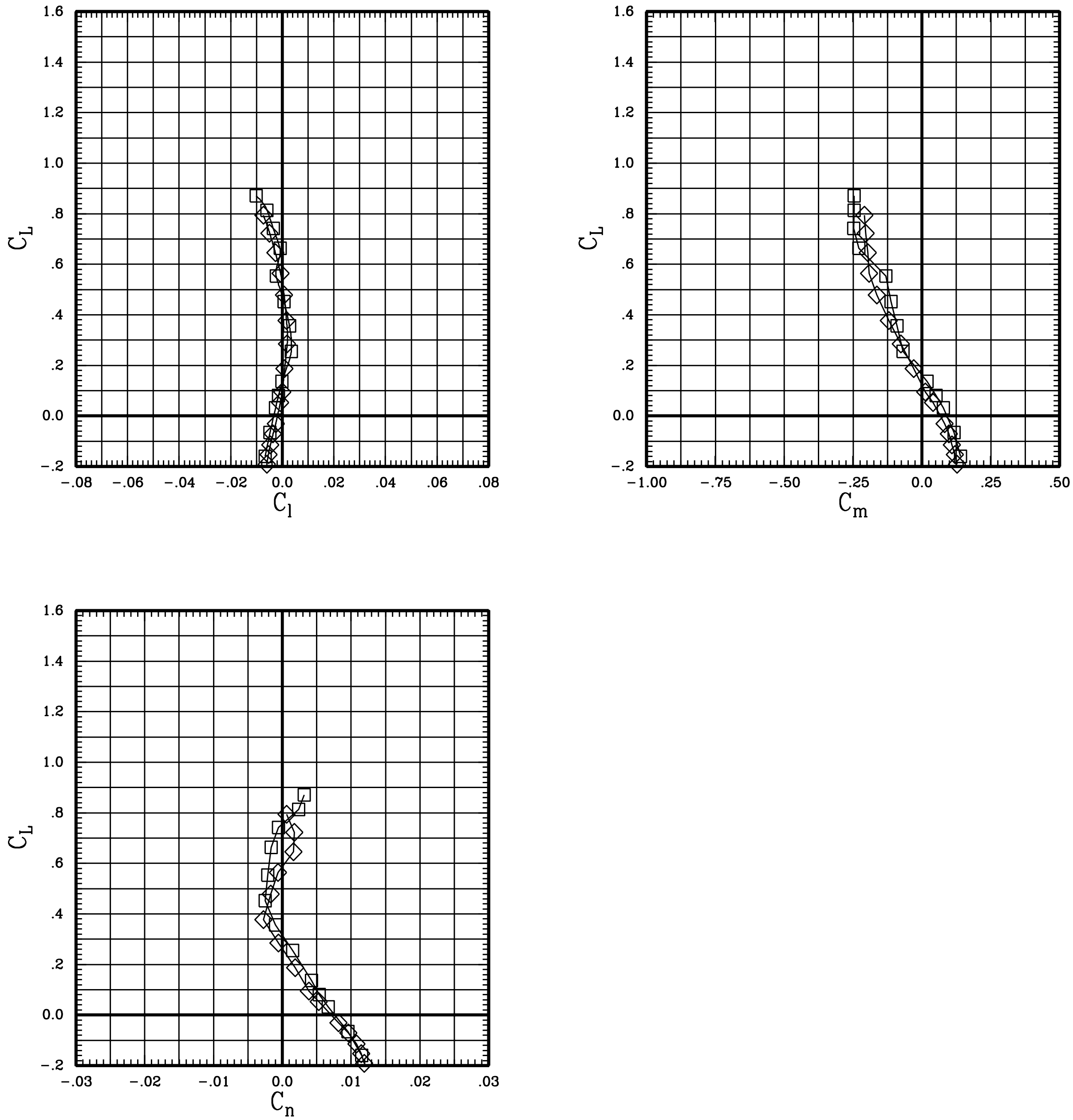

Figure 8(g). Effect of sweep for the wing with low pivot; Mach = 1.40.

SYMBOL	LT	LA	LO	LI	^	RI	RO	RA	RT	RUN	SWEEP	MACH	Q	BETA
—□—	00	00	00	00	L	00	00	00	00	12	0	.40	430	−.2
—◇—	00	00	00	00	L	00	00	00	00	11	0	.60	703	−.2
—○—	00	00	00	00	L	00	00	00	00	10	0	.70	695	−.2
—△—	00	00	00	00	L	00	00	00	00	9	0	.80	706	−.2

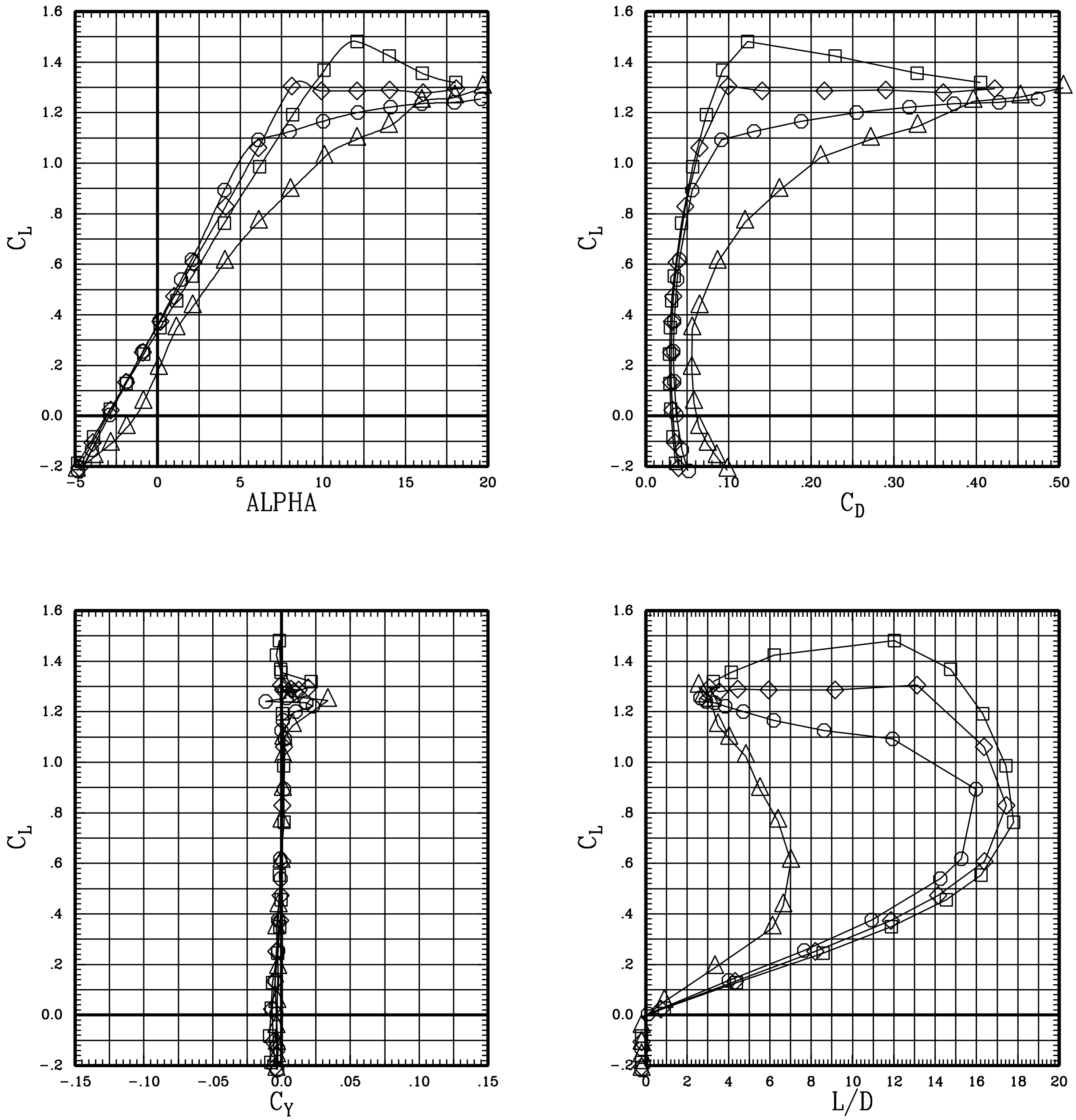

Figure 9(a). Effect of Mach number for the wing with low pivot; sweep = 0 deg.

SYMBOL	LT	LA	LO	LI	^	RI	RO	RA	RT	RUN	SWEEP	MACH	Q	BETA
—□—	00	00	00	00	L	00	00	00	00	12	0	.40	430	−.2
—◇—	00	00	00	00	L	00	00	00	00	11	0	.60	703	−.2
—○—	00	00	00	00	L	00	00	00	00	10	0	.70	695	−.2
—△—	00	00	00	00	L	00	00	00	00	9	0	.80	706	−.2

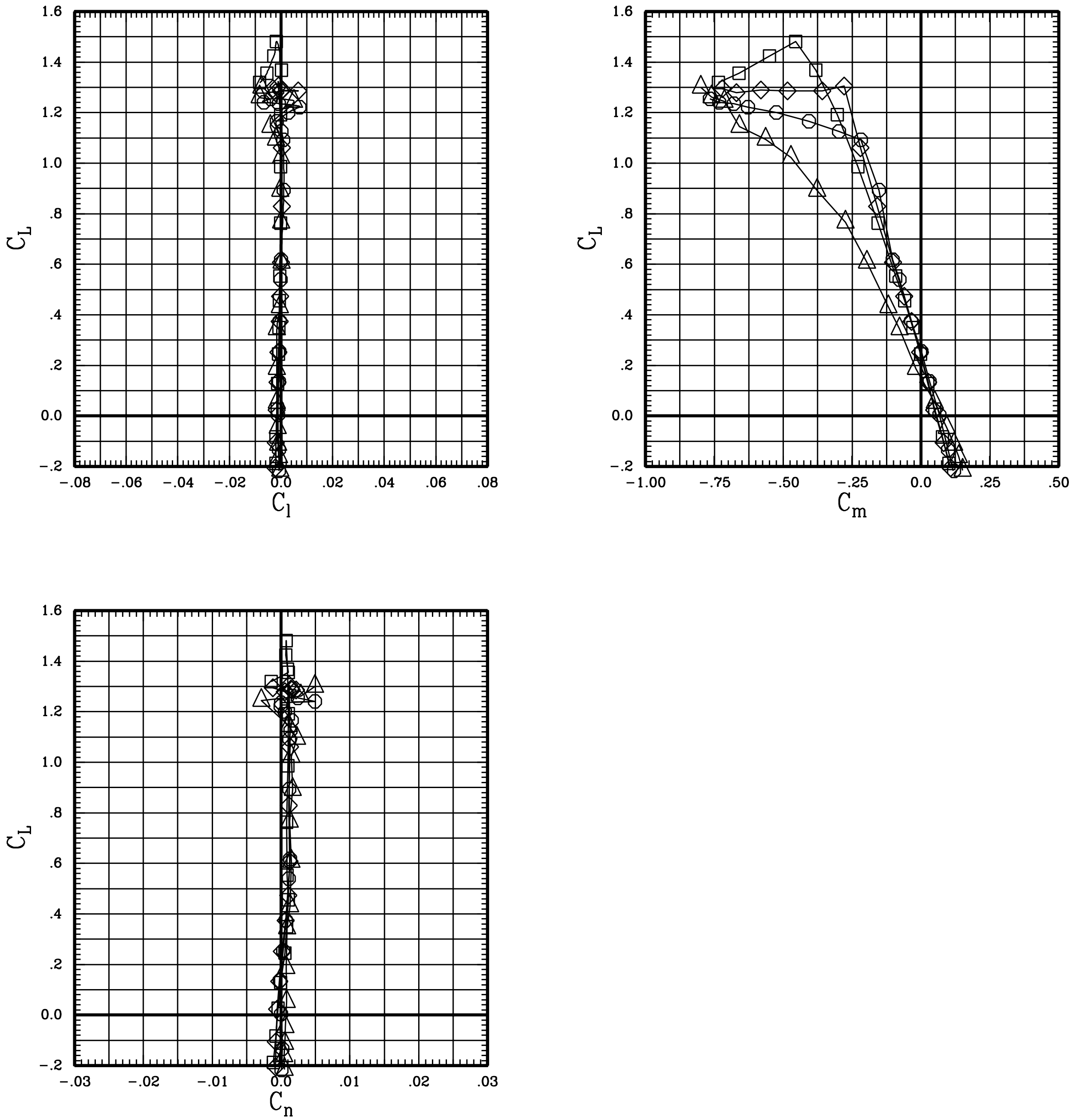

Figure 9(a). Effect of Mach number for the wing with low pivot; sweep = 0 deg.

SYMBOL	LT	LA	LO	LI	^	RI	RO	RA	RT	RUN	SWEEP	MACH	Q	BETA
—□—	00	00	00	00	L	00	00	00	00	15	30	.70	699	−.2
—◇—	00	00	00	00	L	00	00	00	00	14	30	.80	702	−.3
—○—	00	00	00	00	L	00	00	00	00	13	30	.90	701	−.3
—△—	00	00	00	00	L	00	00	00	00	238	30	.95	701	−.3
—⌂—	00	00	00	00	L	00	00	00	00	235	30	1.20	701	−.3

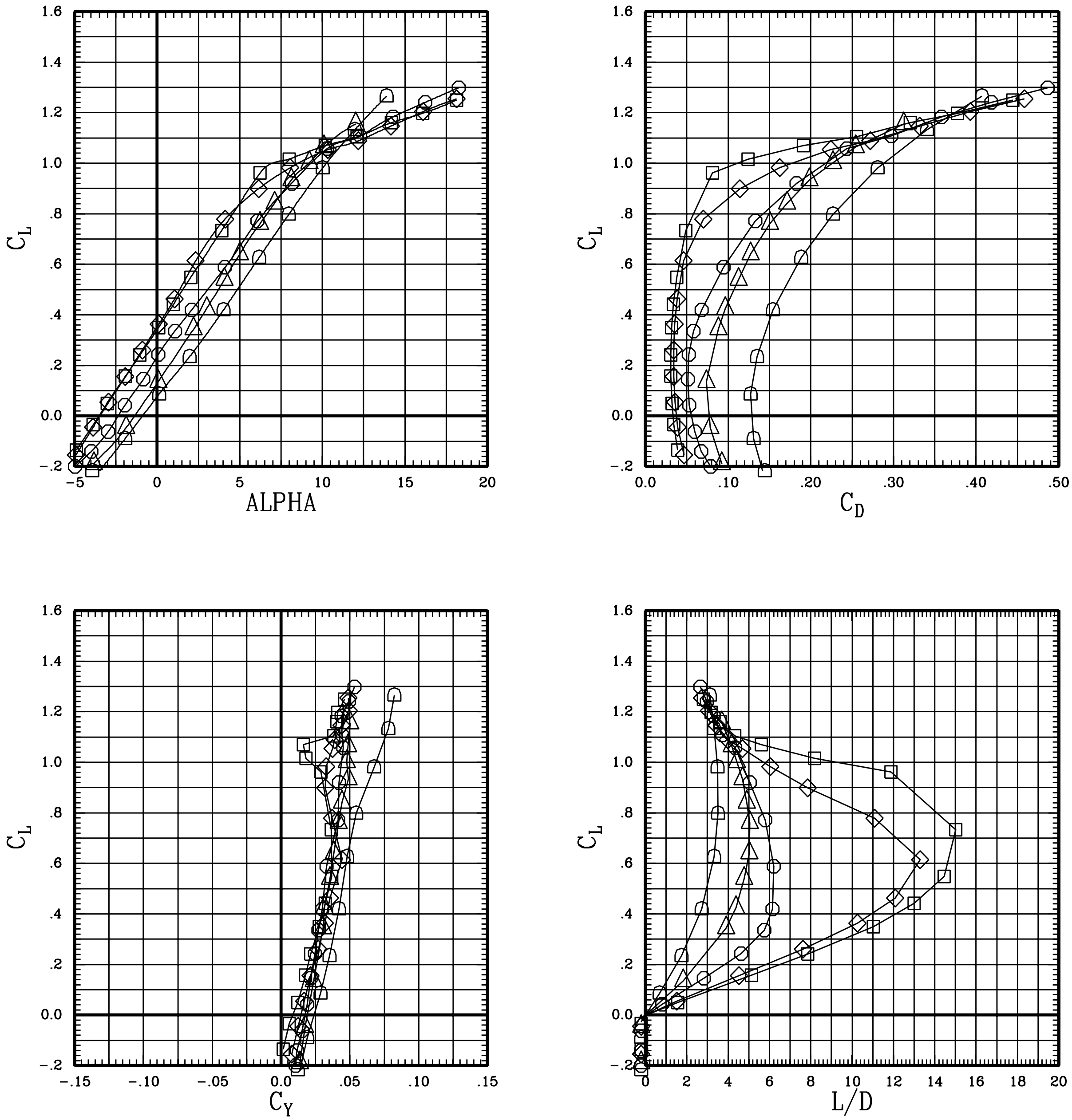

Figure 9(b). Effect of Mach number for the wing with low pivot; sweep = 30 deg.

SYMBOL	LT	LA	LO	LI	^	RI	RO	RA	RT	RUN	SWEEP	MACH	Q	BETA
—□—	00	00	00	00	L	00	00	00	00	15	30	.70	699	−.2
—◇—	00	00	00	00	L	00	00	00	00	14	30	.80	702	−.3
—○—	00	00	00	00	L	00	00	00	00	13	30	.90	701	−.3
—△—	00	00	00	00	L	00	00	00	00	238	30	.95	701	−.3
—⌂—	00	00	00	00	L	00	00	00	00	235	30	1.20	701	−.3

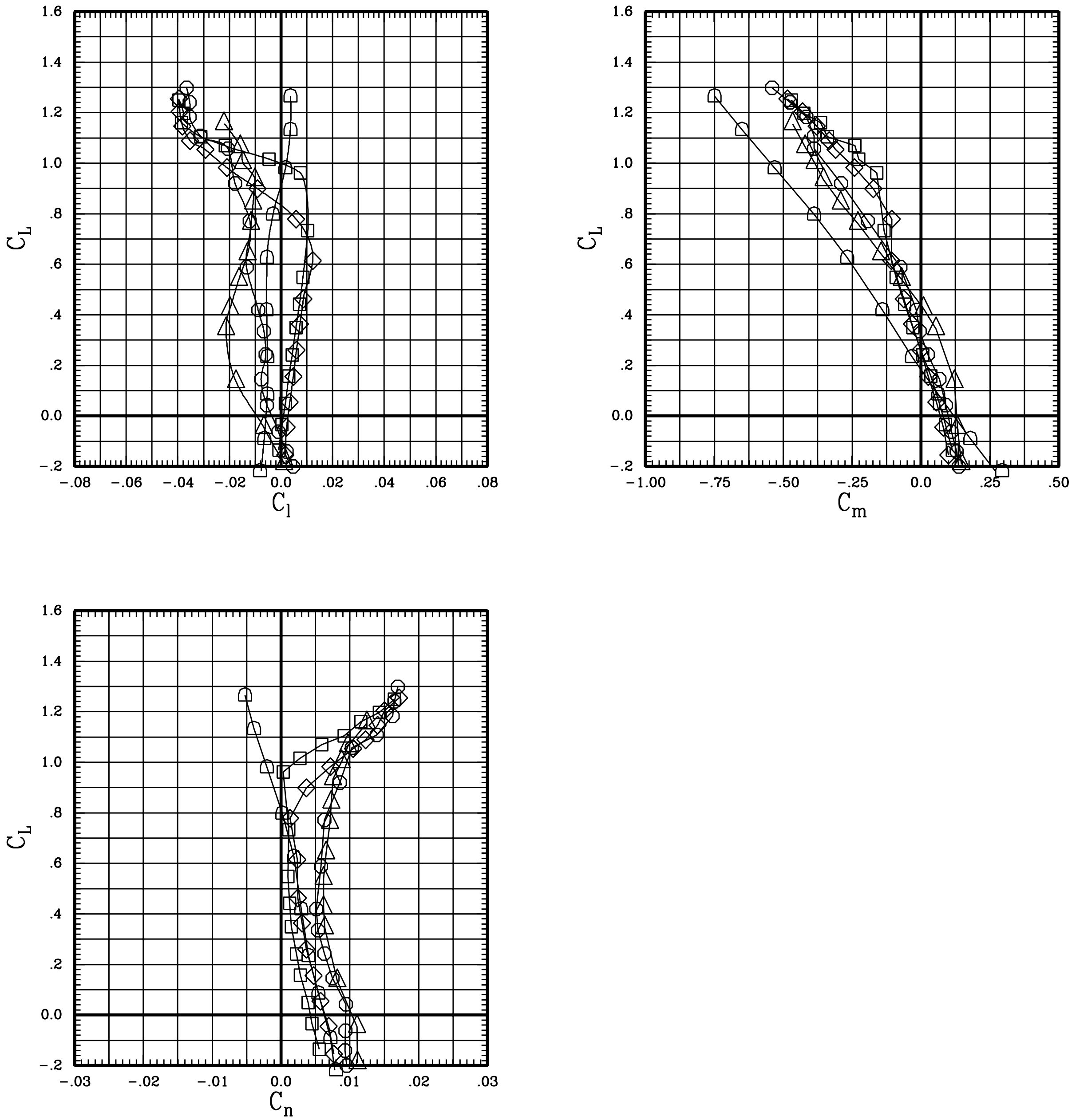

Figure 9(b). Effect of Mach number for the wing with low pivot; sweep = 30 deg.

SYMBOL	LT	LA	LO	LI	^	RI	RO	RA	RT	RUN	SWEEP	MACH	Q	BETA
—□—	00	00	00	00	L	00	00	00	00	20	45	.80	701	−.2
—◇—	00	00	00	00	L	00	00	00	00	19	45	.90	704	−.3
—○—	00	00	00	00	L	00	00	00	00	18	45	.95	705	−.3
—△—	00	00	00	00	L	00	00	00	00	17	45	1.09	696	−.3
—☖—	00	00	00	00	L	00	00	00	00	16	45	1.20	702	−.3

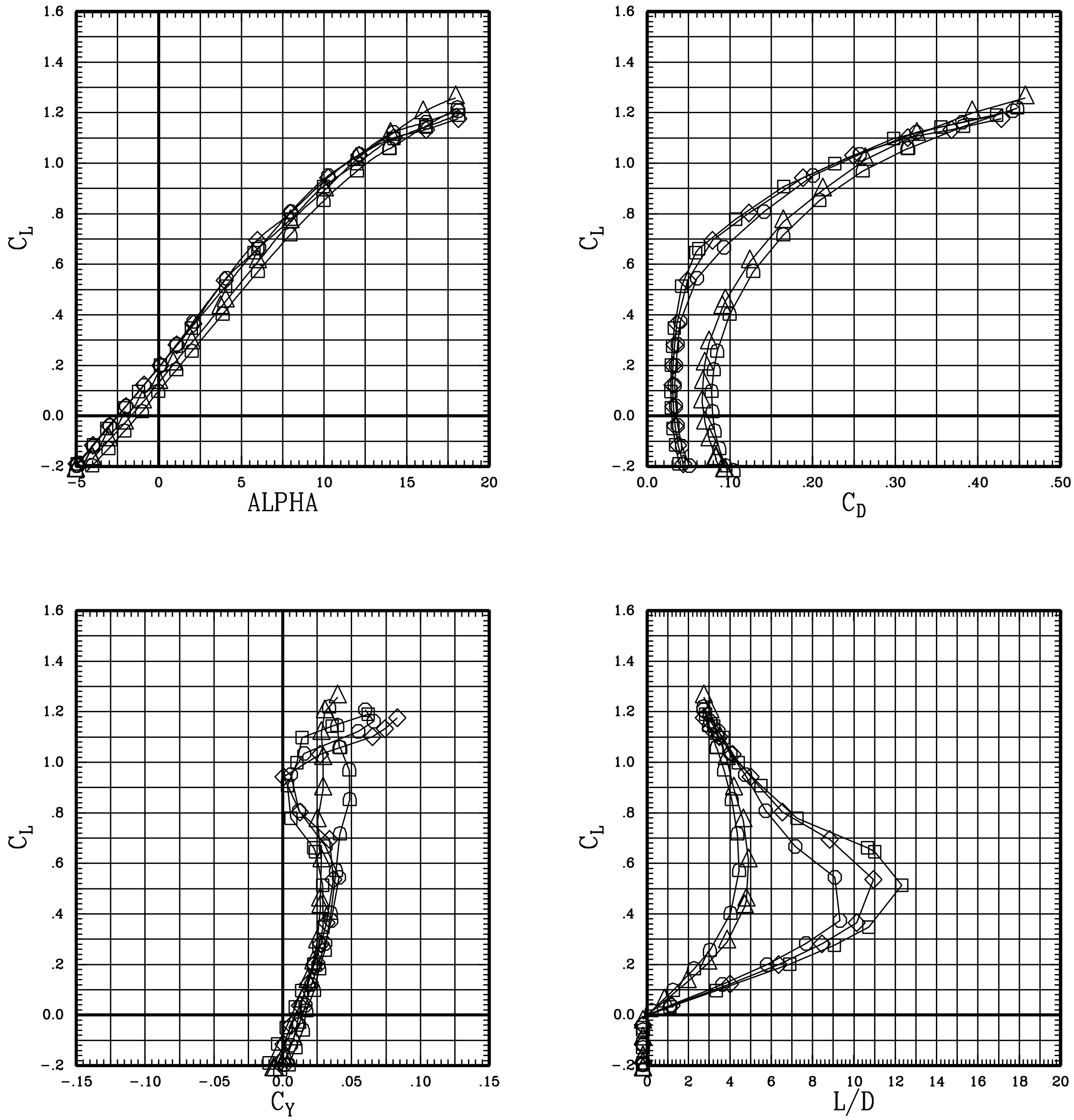

Figure 9(c). Effect of Mach number for the wing with low pivot; sweep = 45 deg.

SYMBOL	LT	LA	LO	LI	^	RI	RO	RA	RT	RUN	SWEEP	MACH	Q	BETA
—□—	00	00	00	00	L	00	00	00	00	20	45	.80	701	−.2
—◇—	00	00	00	00	L	00	00	00	00	19	45	.90	704	−.3
—○—	00	00	00	00	L	00	00	00	00	18	45	.95	705	−.3
—△—	00	00	00	00	L	00	00	00	00	17	45	1.09	696	−.3
—⌓—	00	00	00	00	L	00	00	00	00	16	45	1.20	702	−.3

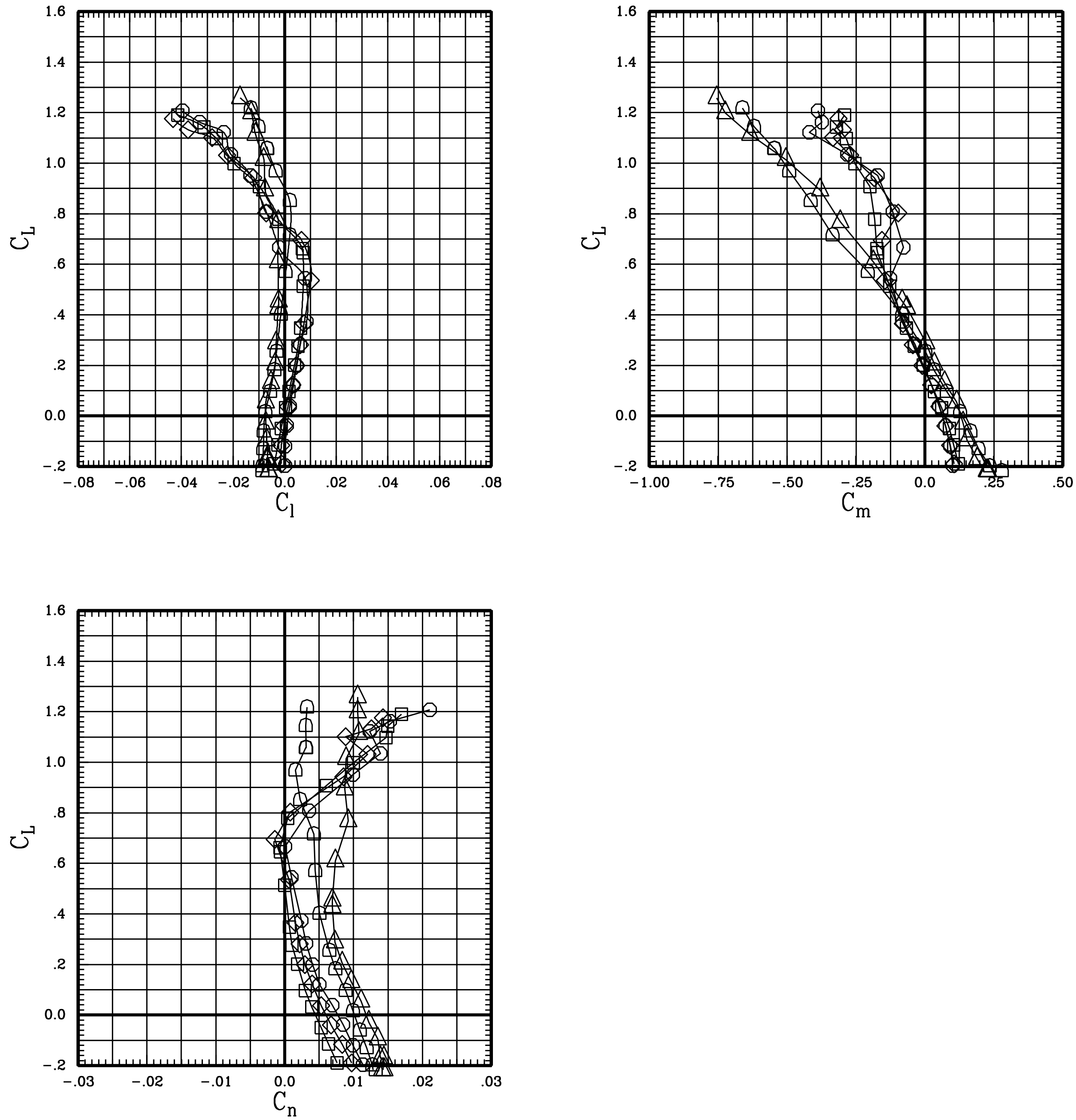

Figure 9(c). Effect of Mach number for the wing with low pivot; sweep = 45 deg.

SYMBOL	LT	LA	LO	LI	^	RI	RO	RA	RT	RUN	SWEEP	MACH	Q	BETA
—□—	00	00	00	00	L	00	00	00	00	35	60	.95	702	−.2
—◇—	00	00	00	00	L	00	00	00	00	34	60	1.10	701	−.3
—○—	00	00	00	00	L	00	00	00	00	33	60	1.20	701	−.2
—△—	00	00	00	00	L	00	00	00	00	32	60	1.40	702	−.2

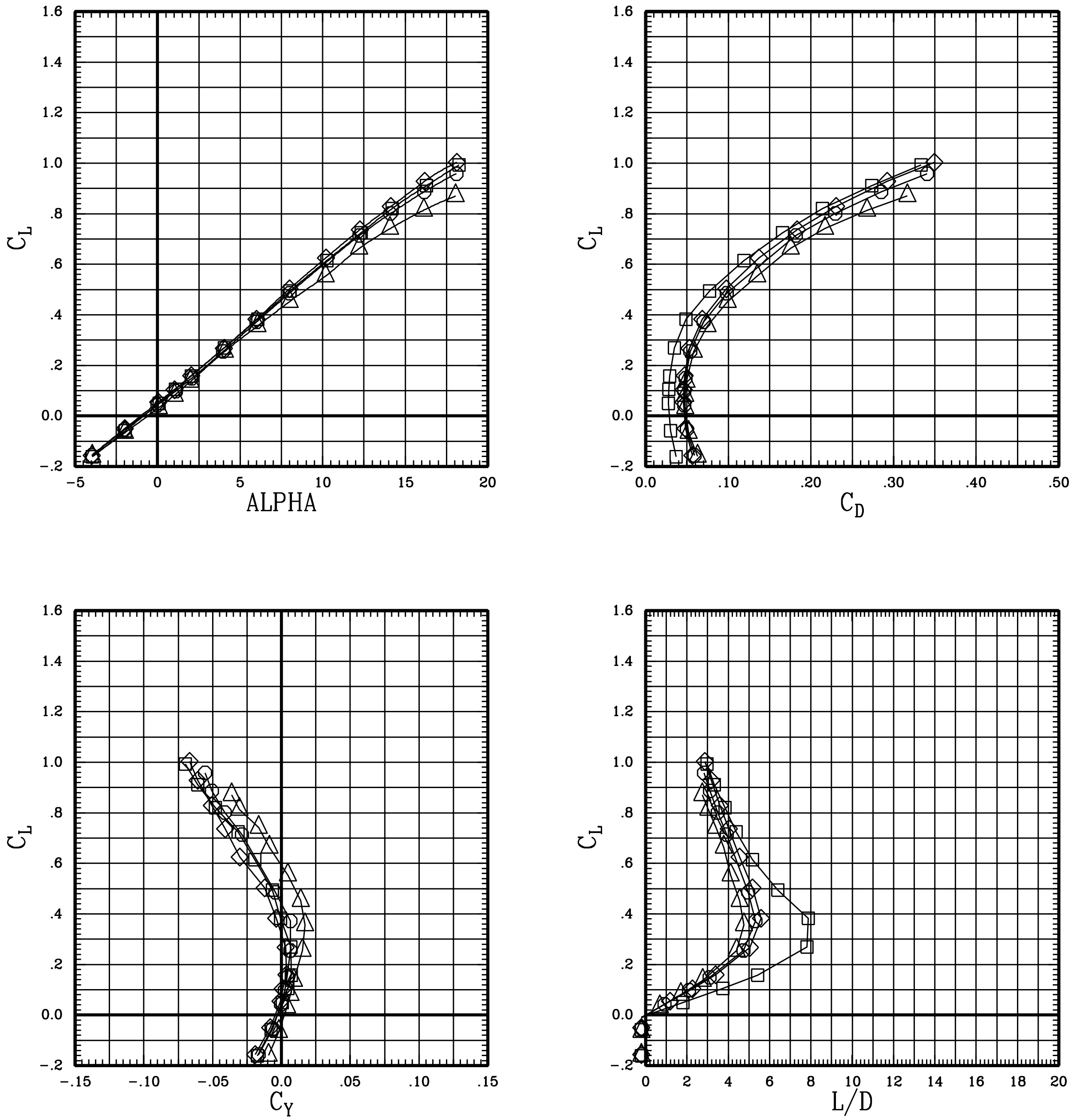

Figure 9(d). Effect of Mach number for the wing with low pivot; sweep = 60 deg.

SYMBOL	LT	LA	LO	LI	^	RI	RO	RA	RT	RUN	SWEEP	MACH	Q	BETA
—□—	00	00	00	00	L	00	00	00	00	35	60	.95	702	-.2
—◇—	00	00	00	00	L	00	00	00	00	34	60	1.10	701	-.3
—○—	00	00	00	00	L	00	00	00	00	33	60	1.20	701	-.2
—△—	00	00	00	00	L	00	00	00	00	32	60	1.40	702	-.2

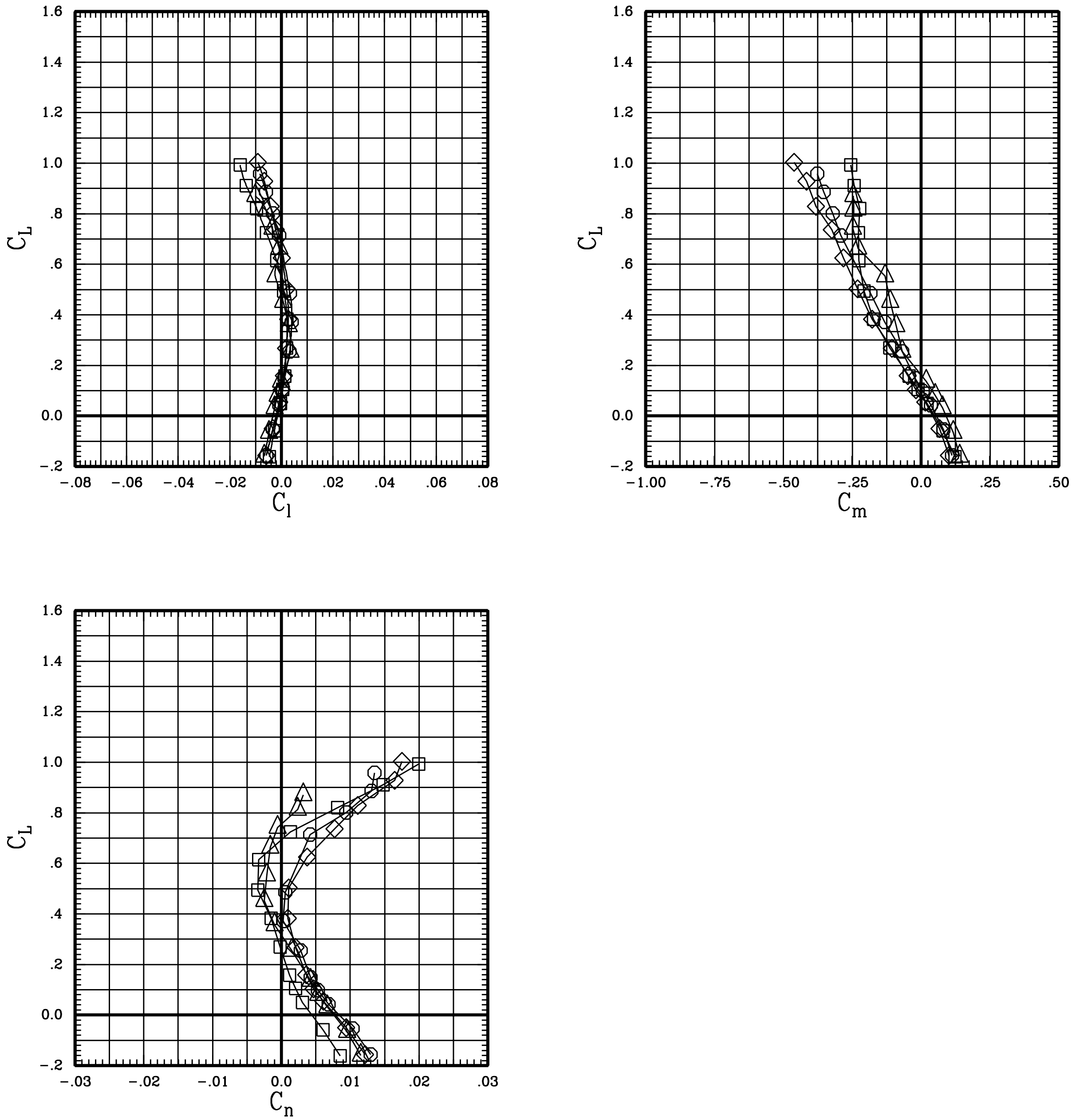

Figure 9(d). Effect of Mach number for the wing with low pivot; sweep = 60 deg.

SYMBOL	LT LA LO LI ^ RI RO RA RT	RUN	SWEEP	MACH	Q	BETA
—□—	00 00 00 00 L 00 00 00 00	31	65	1.10	687	-.3
—◇—	00 00 00 00 L 00 00 00 00	30	65	1.20	700	-.3
—○—	00 00 00 00 L 00 00 00 00	29	65	1.40	701	-.3

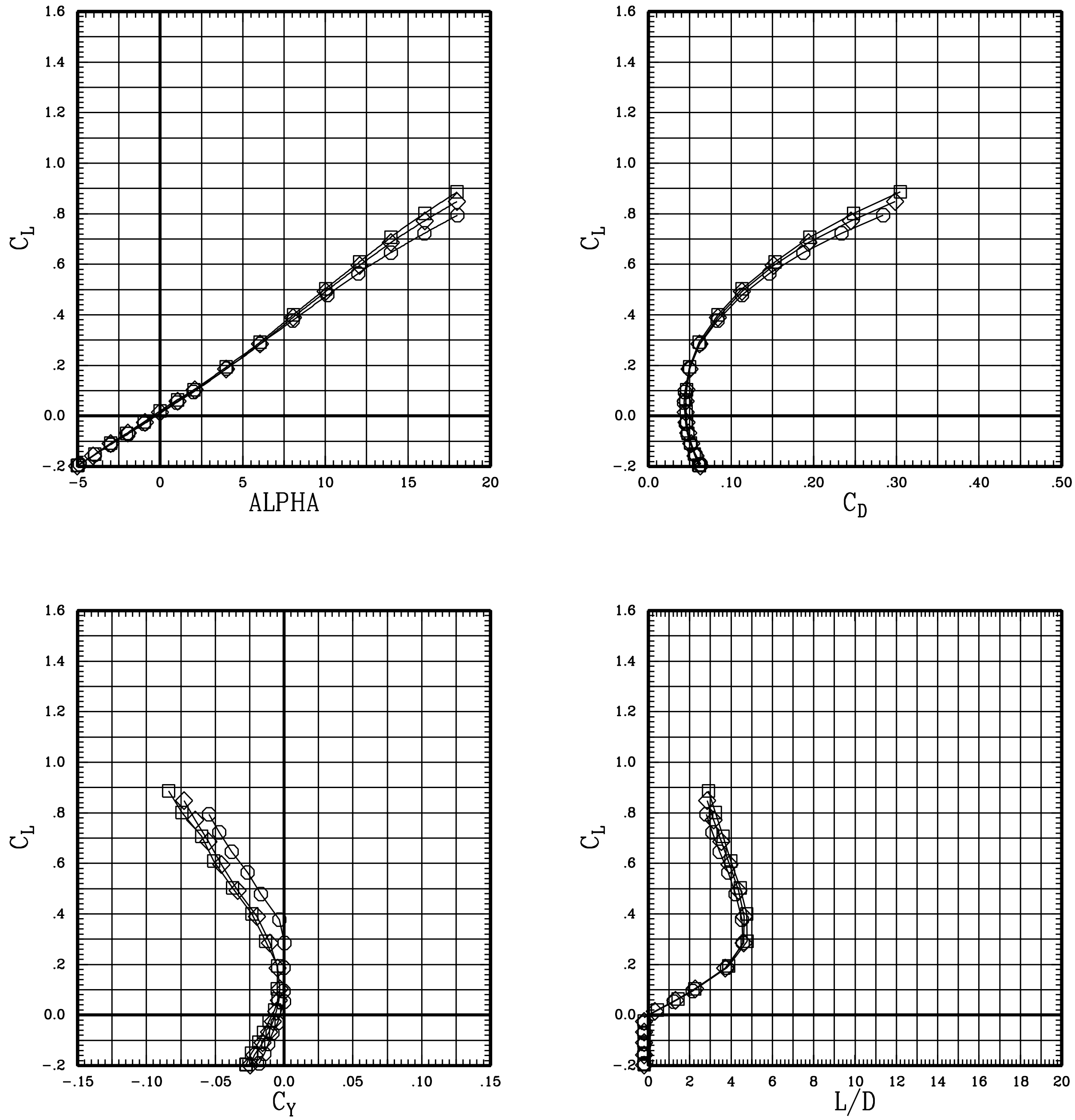

Figure 9(e). Effect of Mach number for the wing with low pivot;
sweep = 65 deg.

SYMBOL	LT	LA	LO	LI	^	RI	RO	RA	RT	RUN	SWEEP	MACH	Q	BETA
—□—	00	00	00	00	L	00	00	00	00	31	65	1.10	687	-.3
—◇—	00	00	00	00	L	00	00	00	00	30	65	1.20	700	-.3
—○—	00	00	00	00	L	00	00	00	00	29	65	1.40	701	-.3

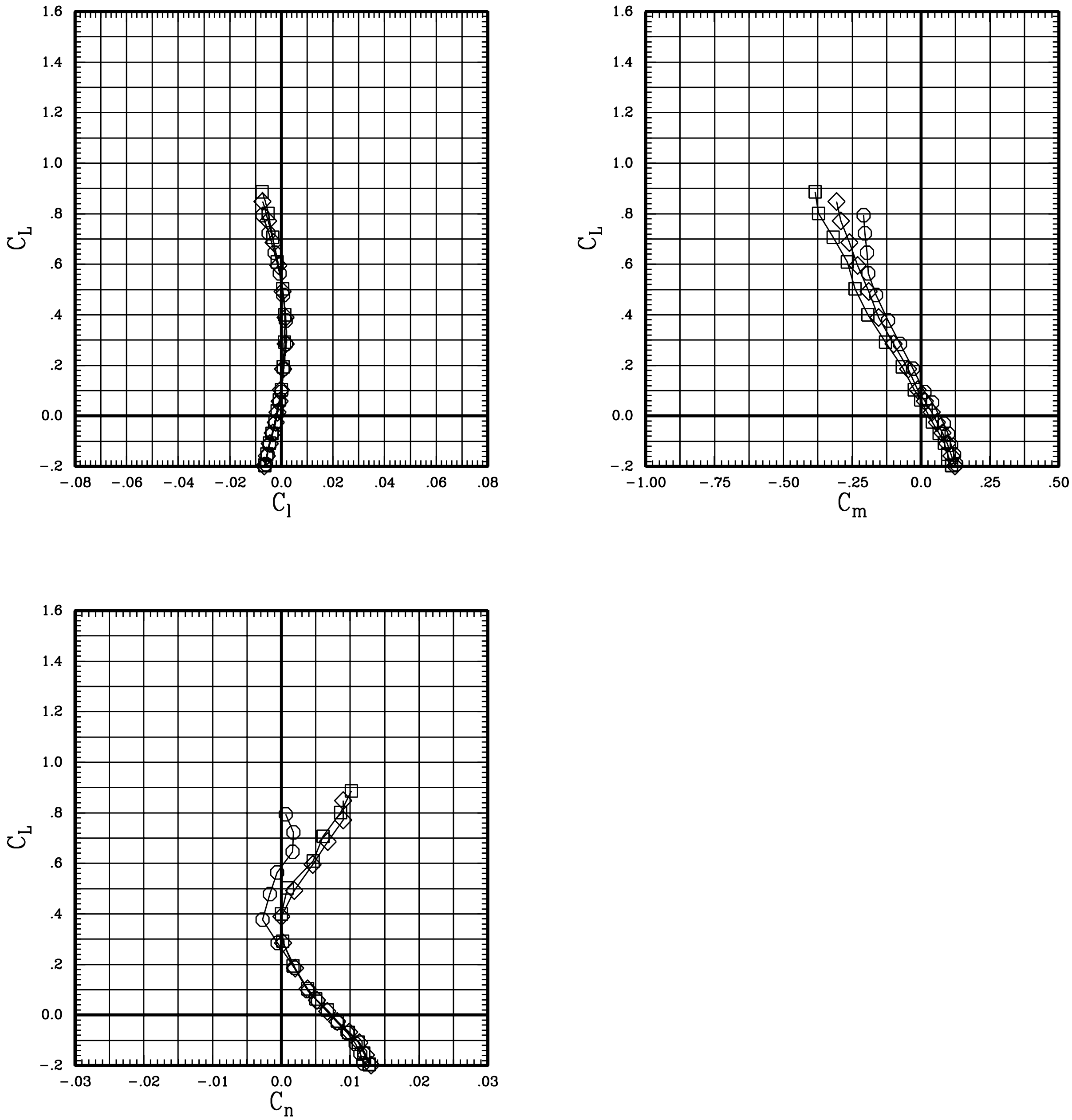

Figure 9(e). Effect of Mach number for the wing with low pivot; sweep = 65 deg.

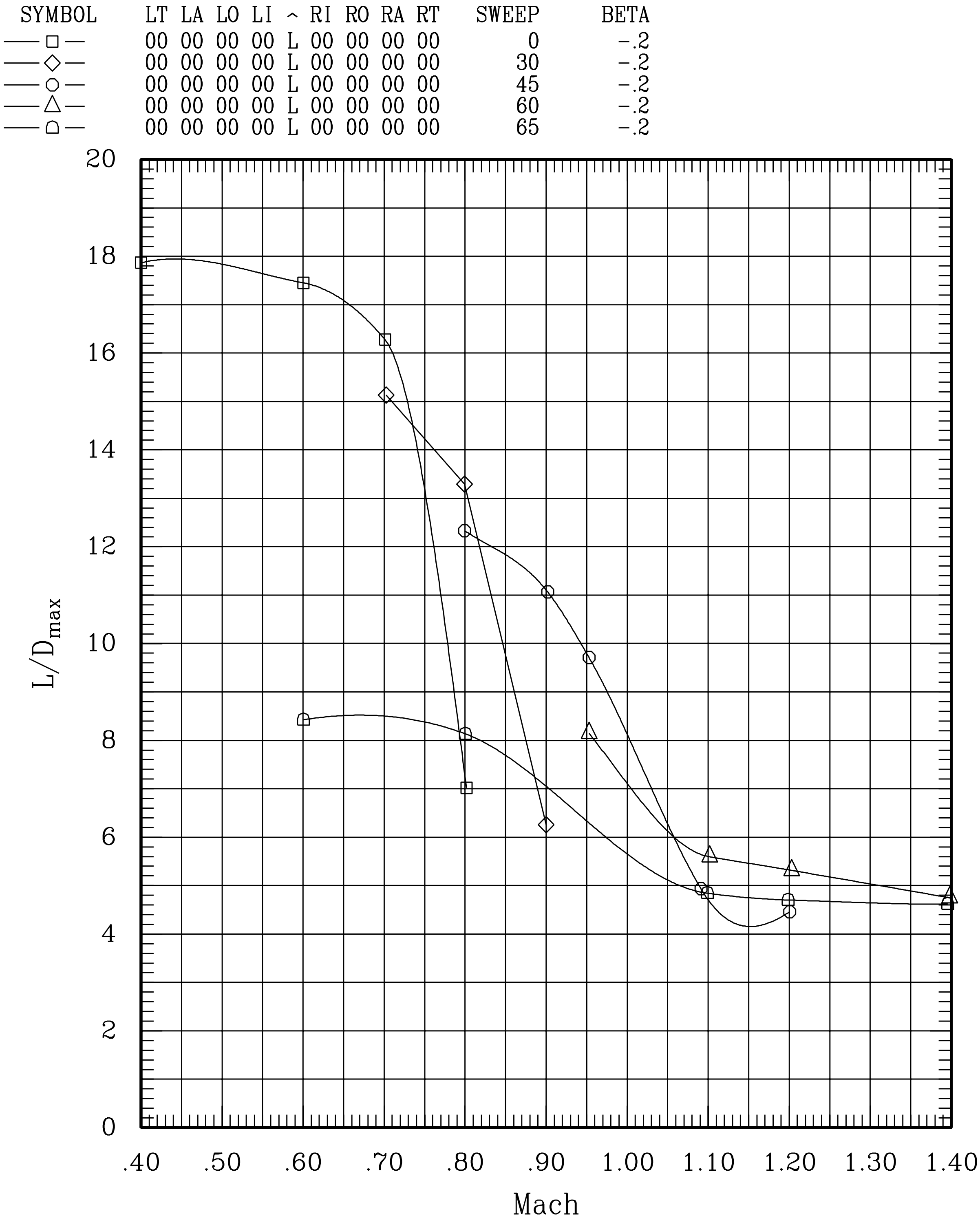

Figure 10. Summary of the effect of sweep for the low pivot.

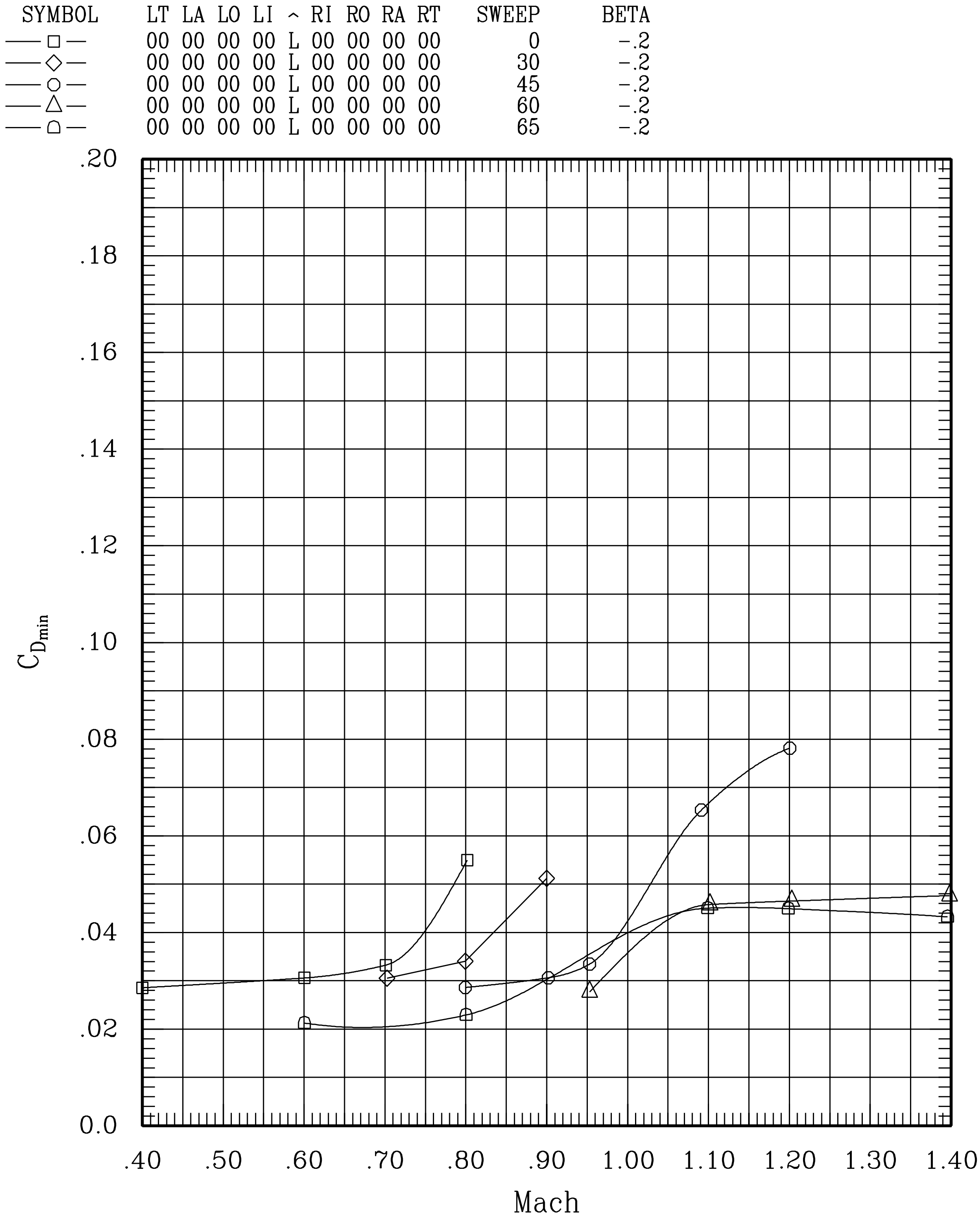

Figure 10. Summary of the effect of sweep for the low pivot.

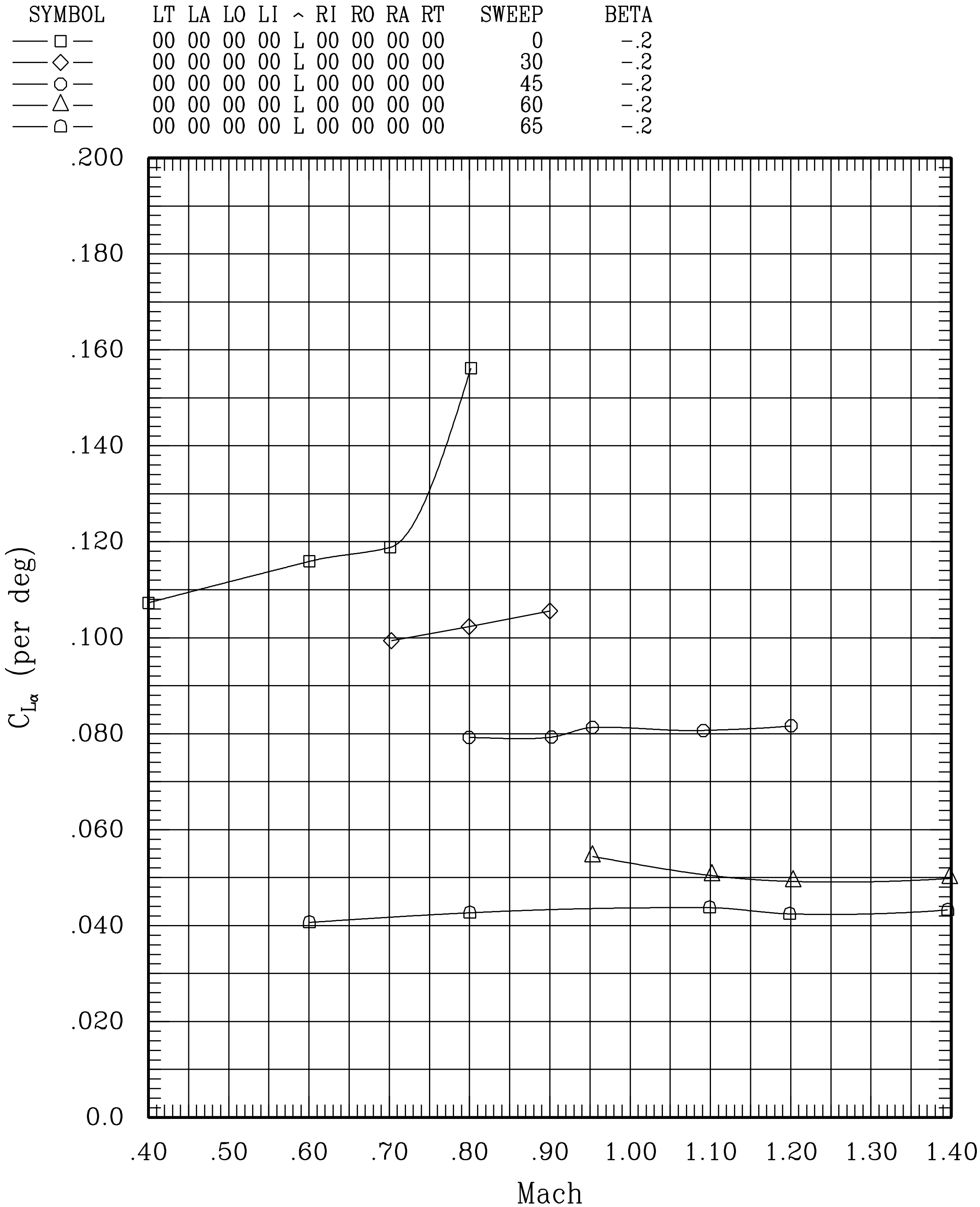

Figure 10. Summary of the effect of sweep for the low pivot.

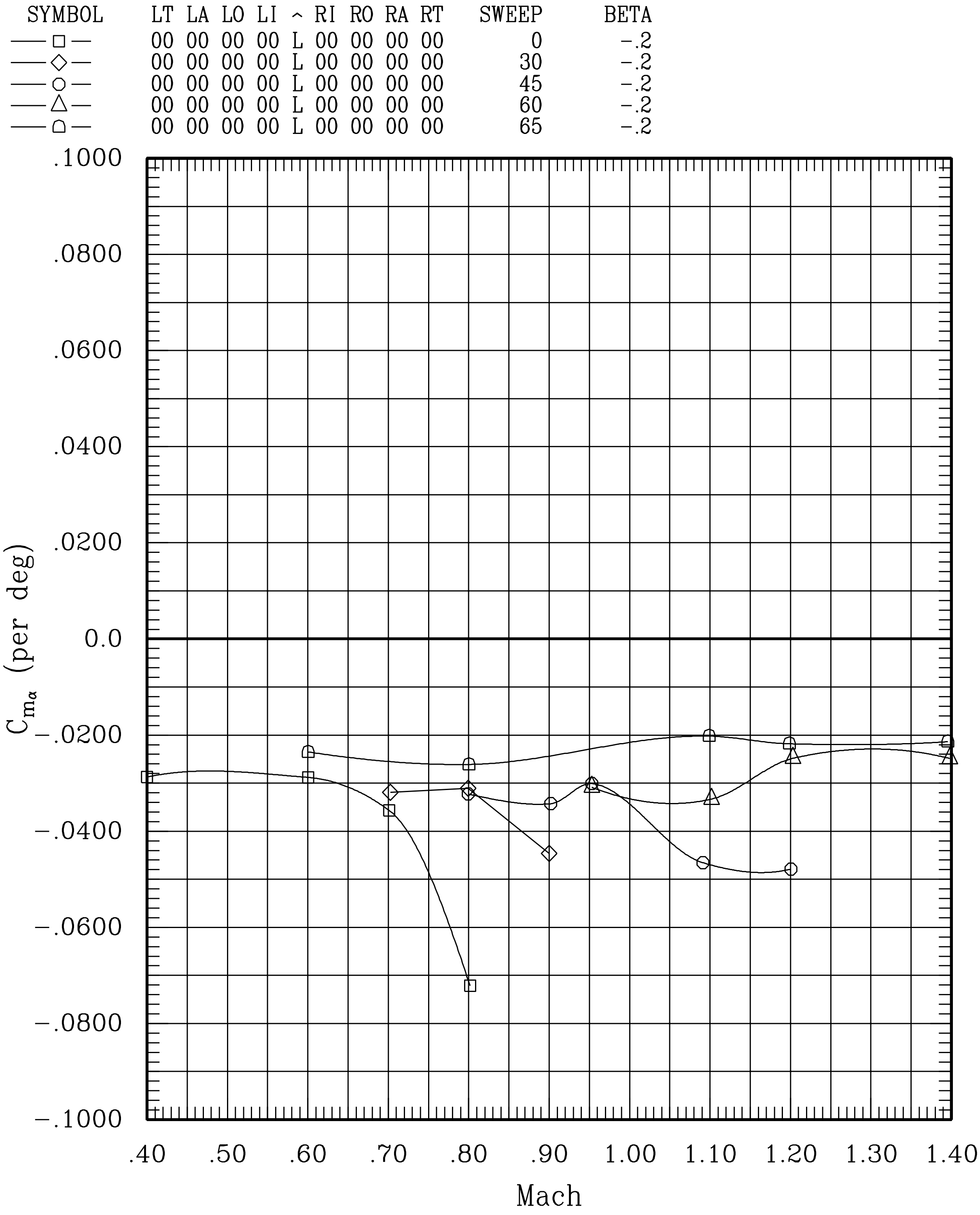

Figure 10. Summary of the effect of sweep for the low pivot.

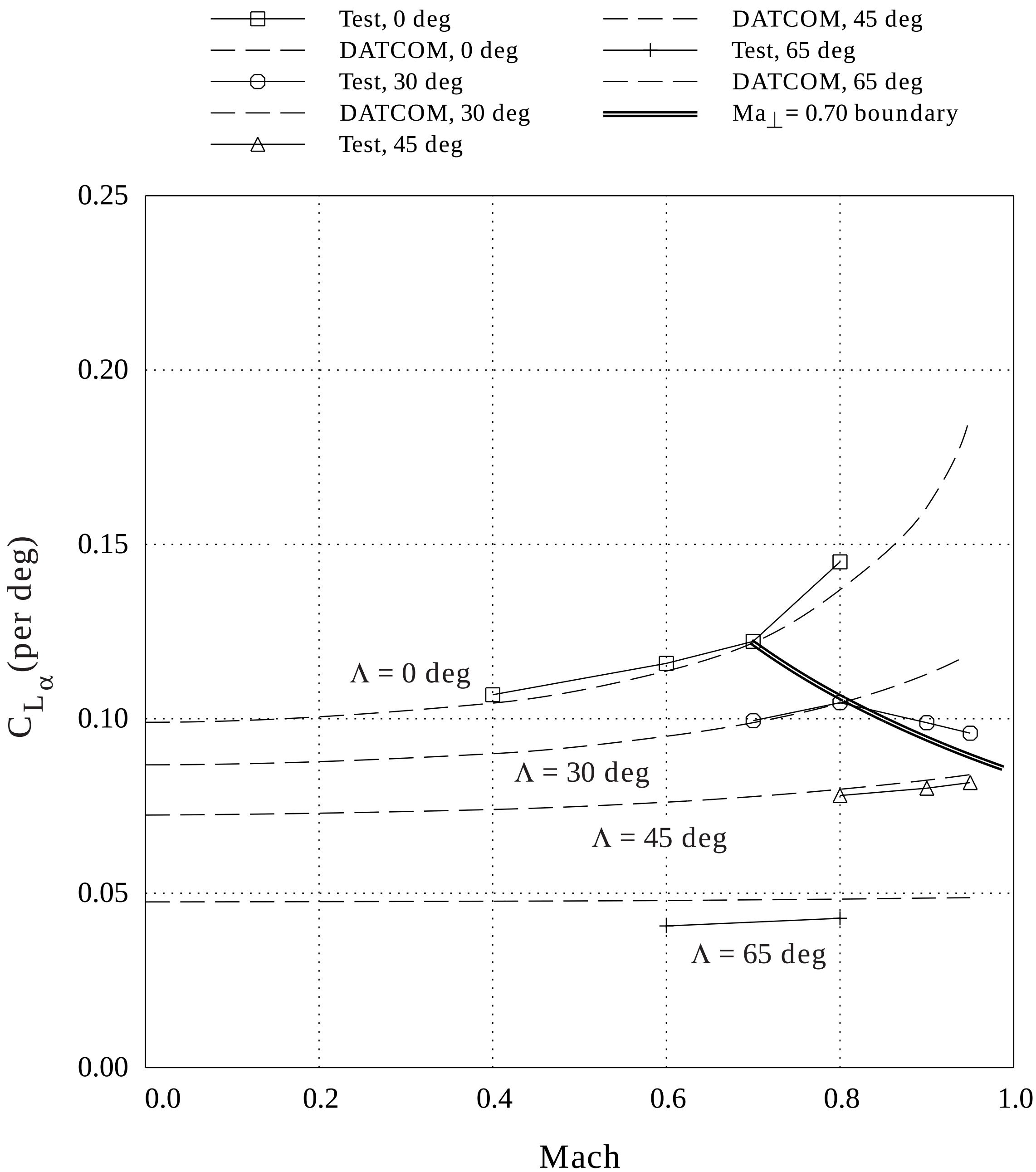

Figure 11. Effect of Mach number and sweep on lift-curve slope.

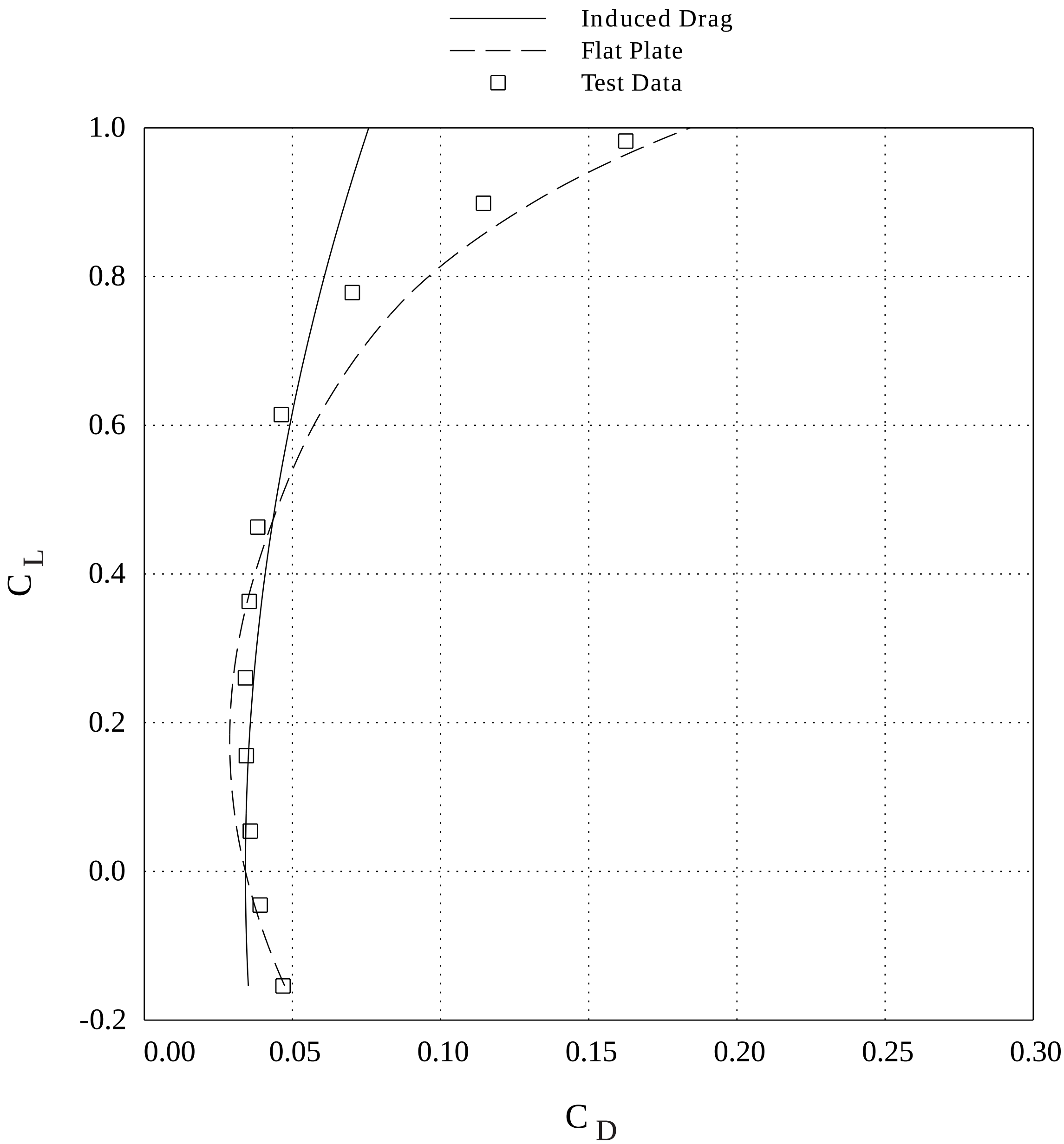

Figure 12(a). Evidence of flow separation at high sweep angles; sweep = 30 deg.

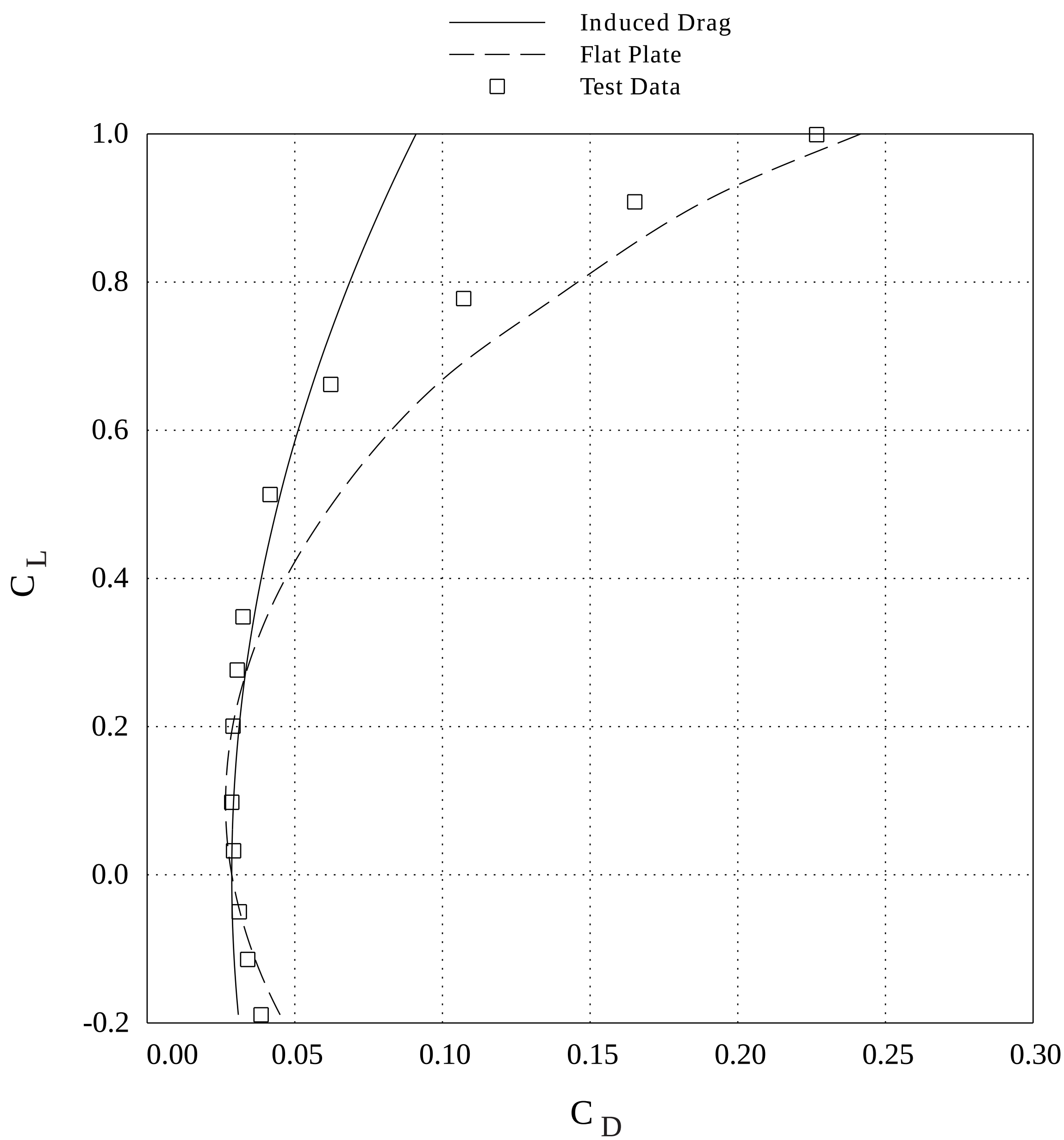

Figure 12(b). Evidence of flow separation at high sweep angles; sweep = 45 deg.

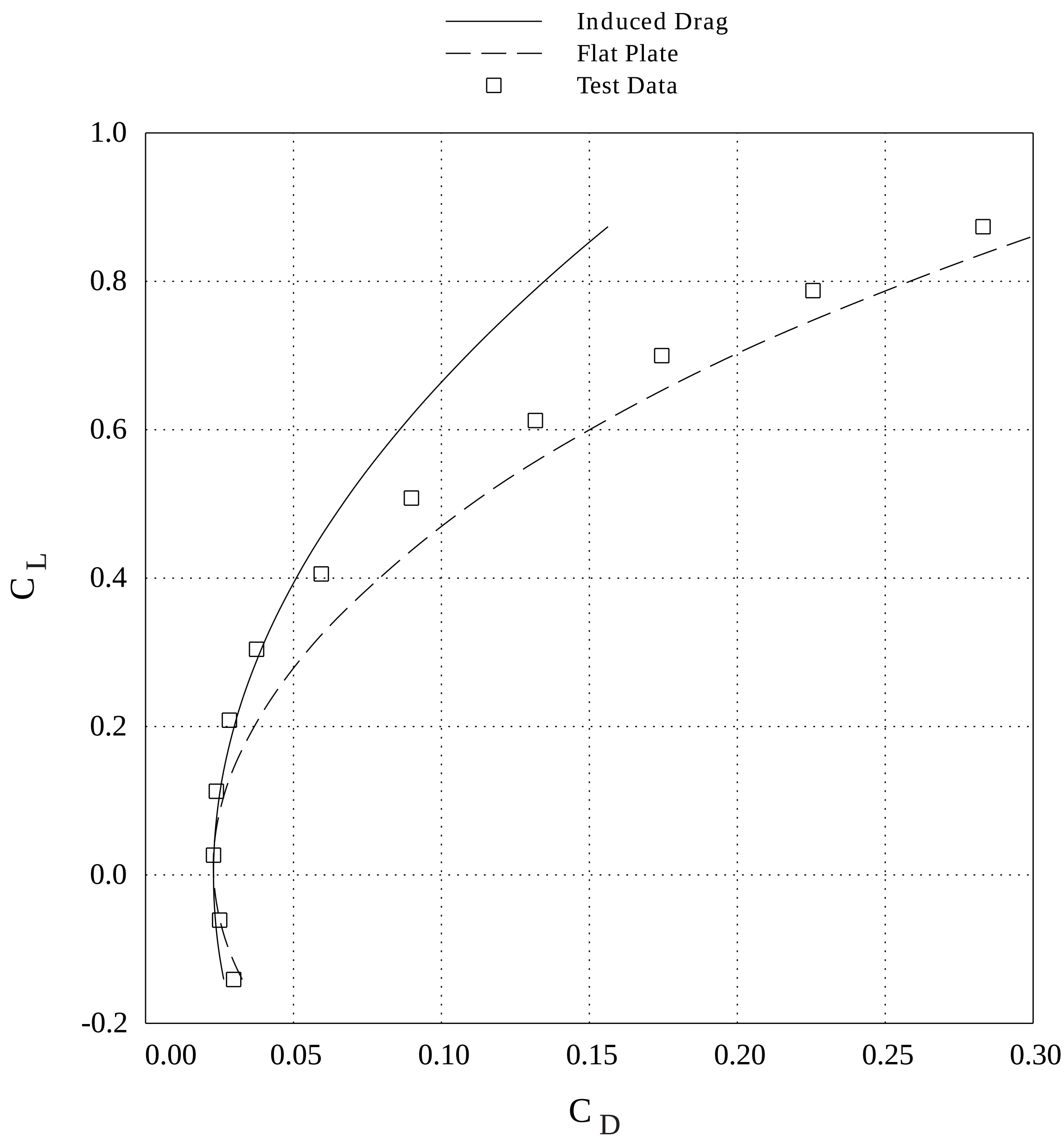

Figure 12(c). Evidence of flow separation at high sweep angles; sweep = 65 deg.

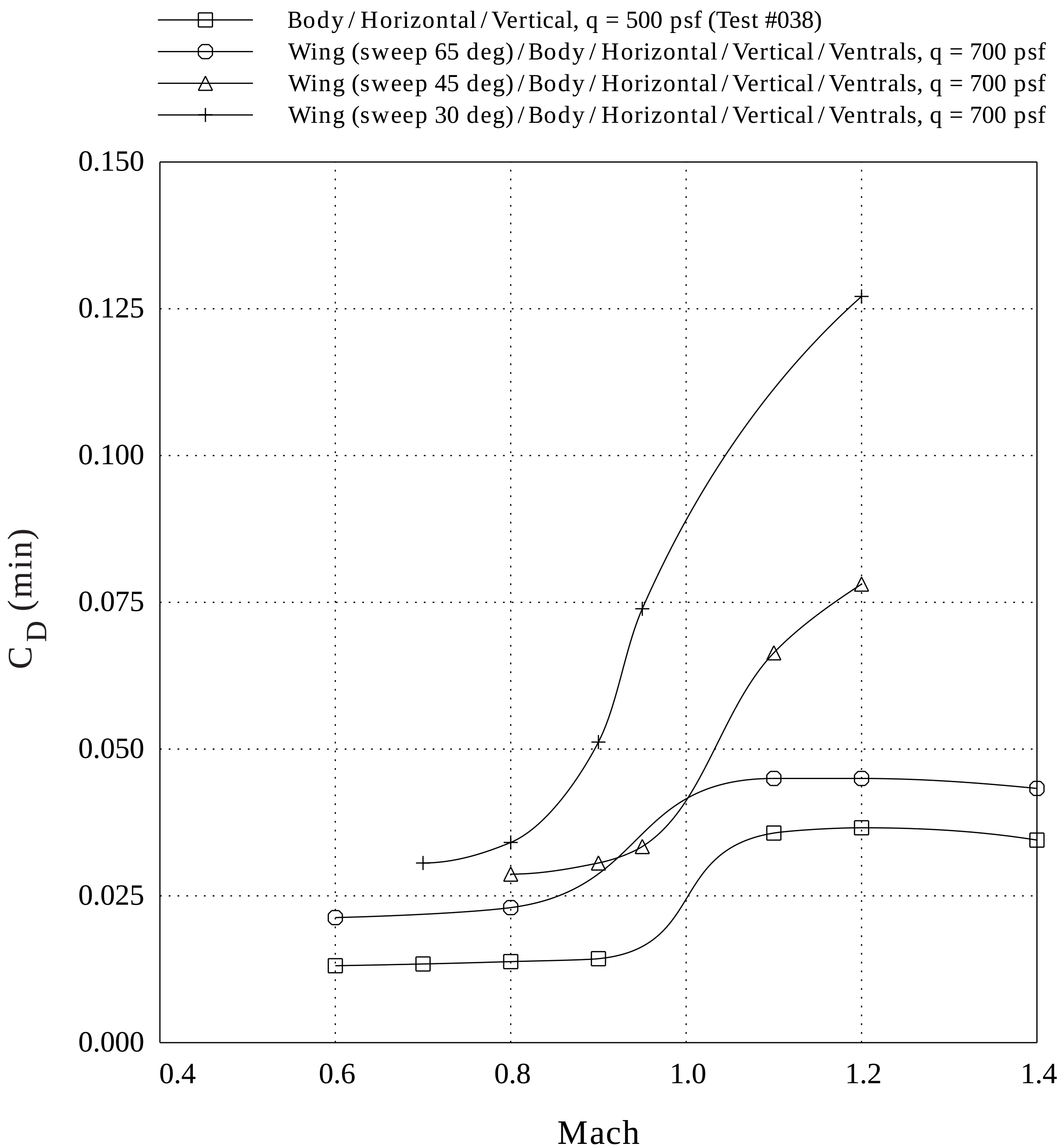

Figure 13. Effect of the wing on minimum drag coefficient.

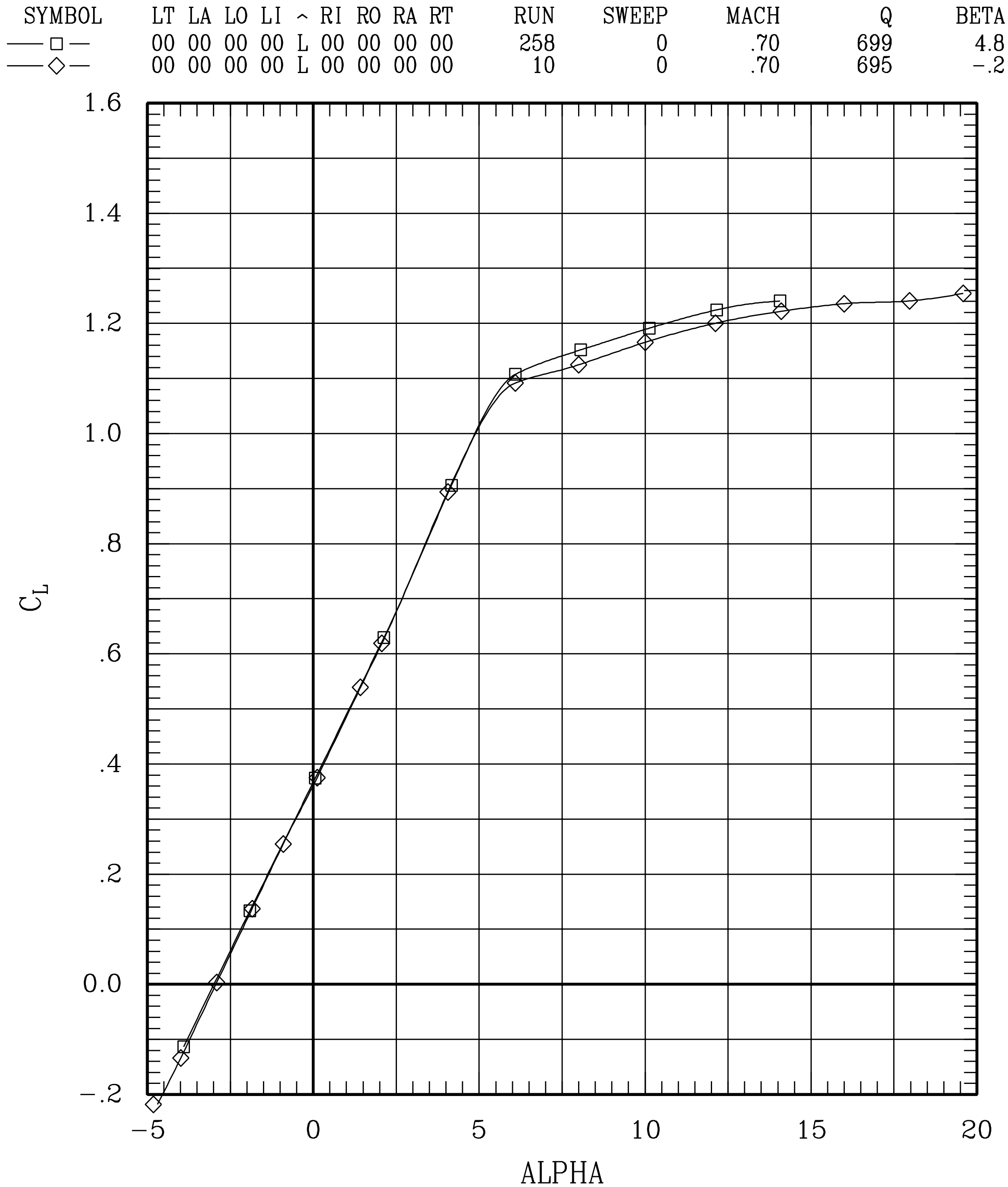

Figure 14(a). Aerodynamic characteristics in sideslip for sweep = 0 deg, Mach = 0.70.

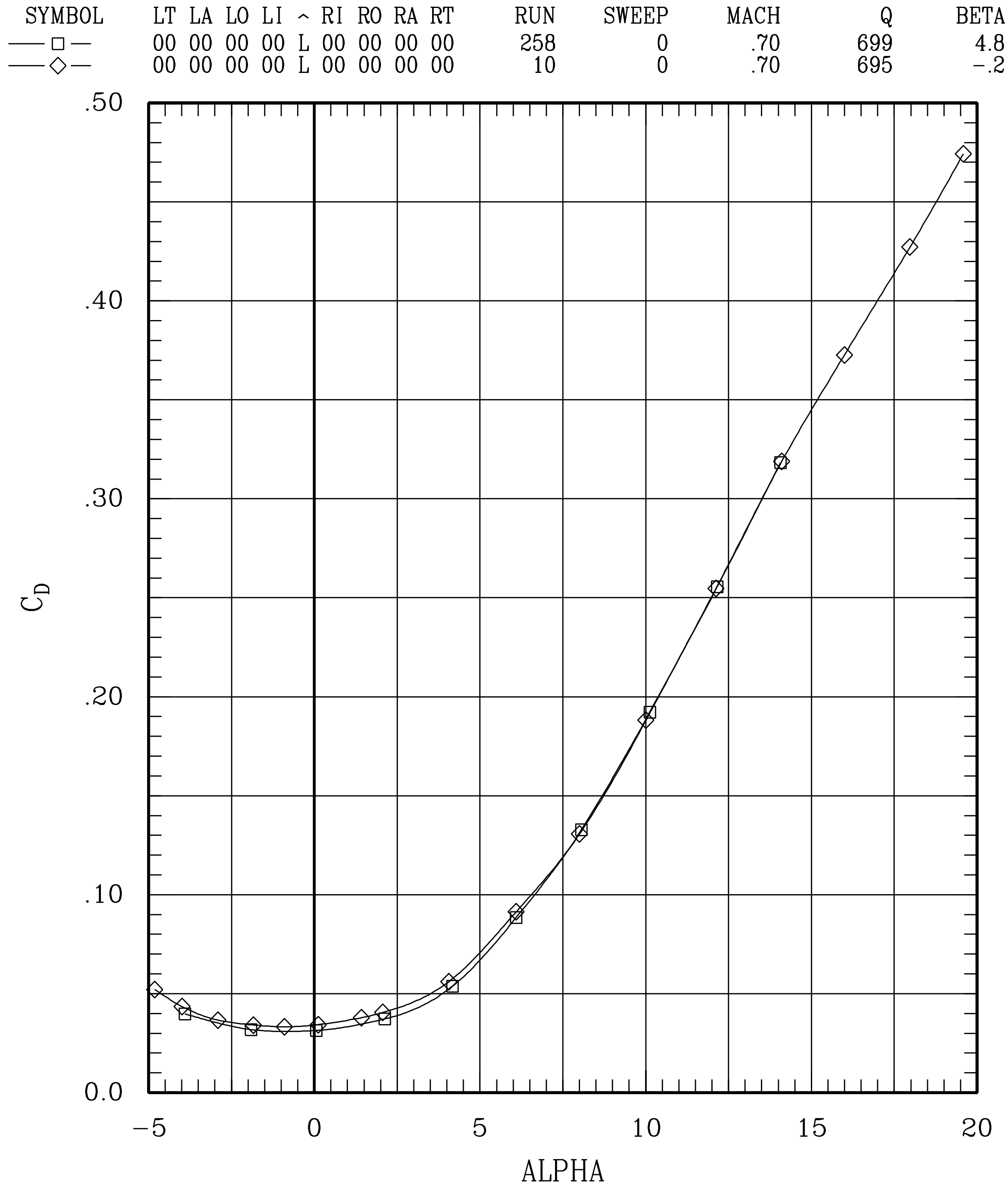

Figure 14(a). Aerodynamic characteristics in sideslip for sweep = 0 deg, Mach = 0.70.

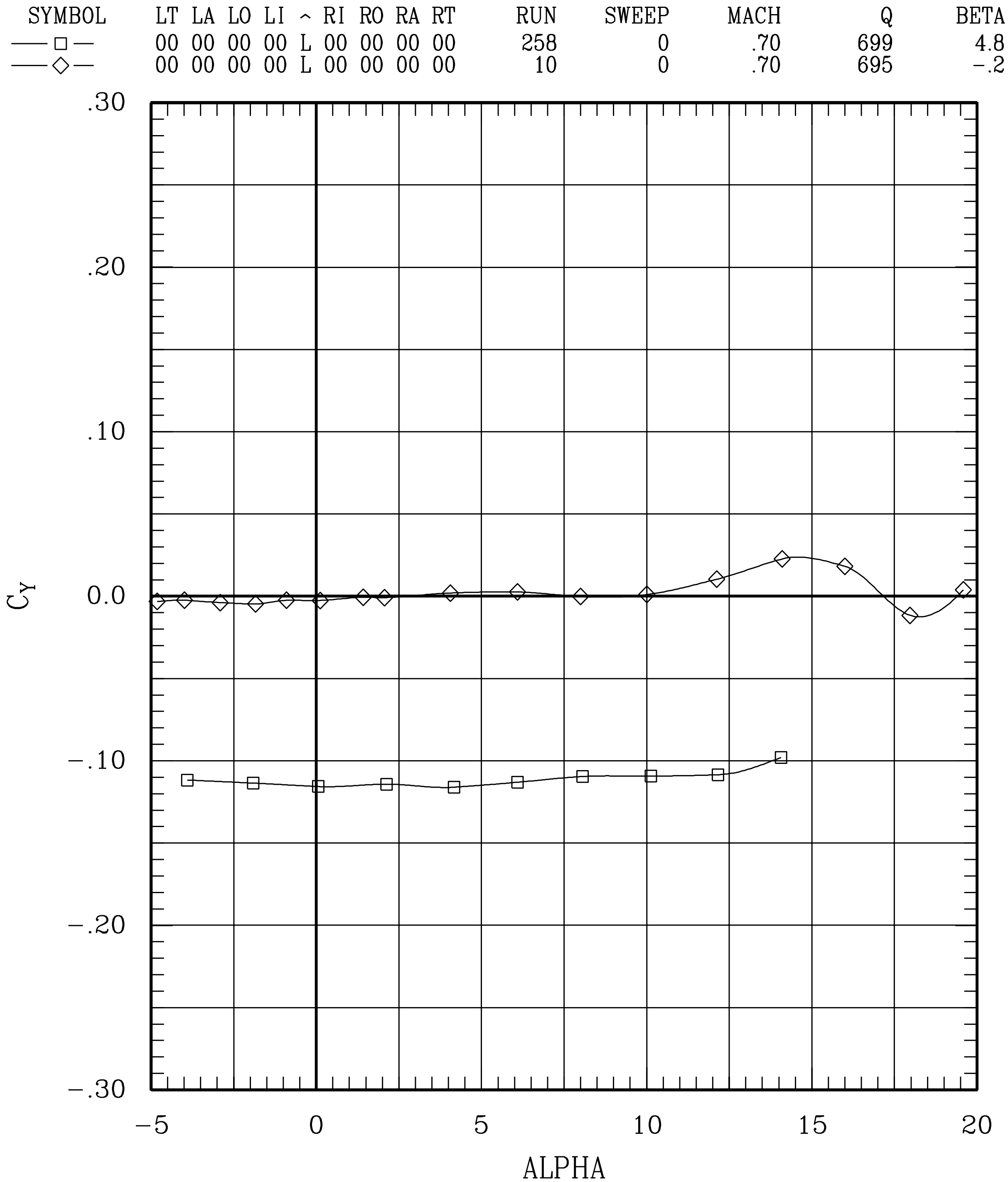

Figure 14(a). Aerodynamic characteristics in sideslip for sweep = 0 deg, Mach = 0.70.

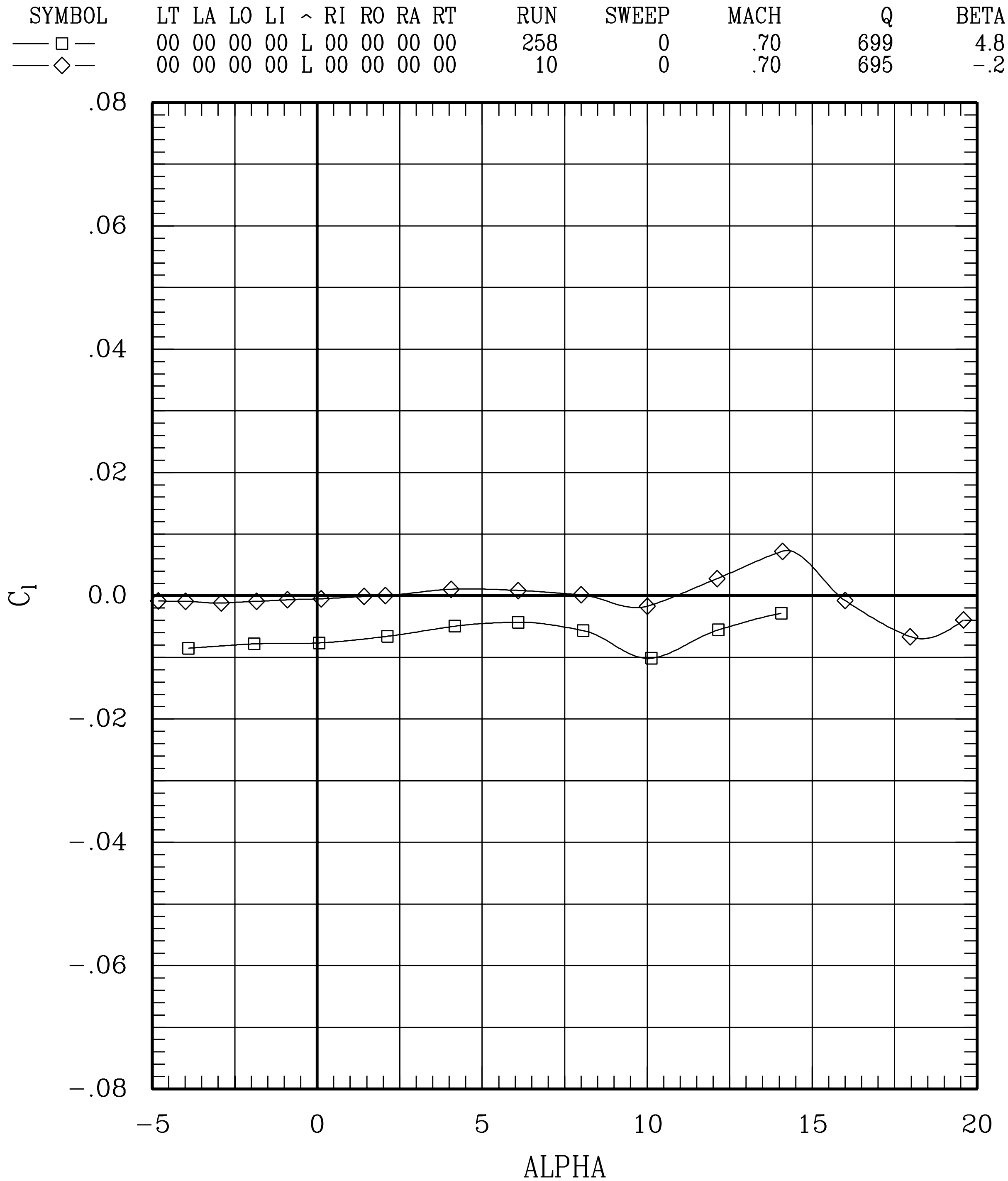

Figure 14(a). Aerodynamic characteristics in sideslip for sweep = 0 deg, Mach = 0.70.

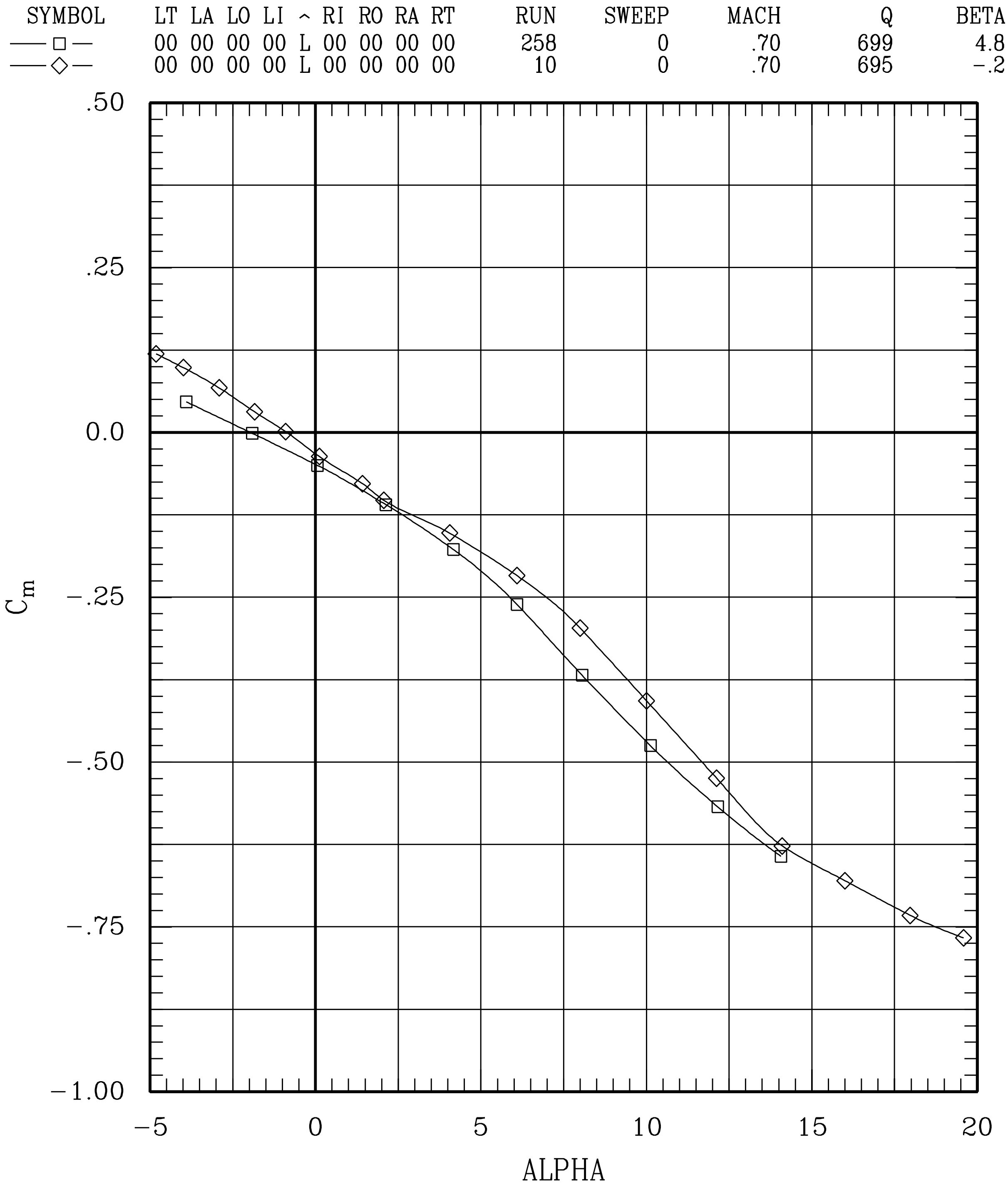

Figure 14(a). Aerodynamic characteristics in sideslip for sweep = 0 deg, Mach = 0.70.

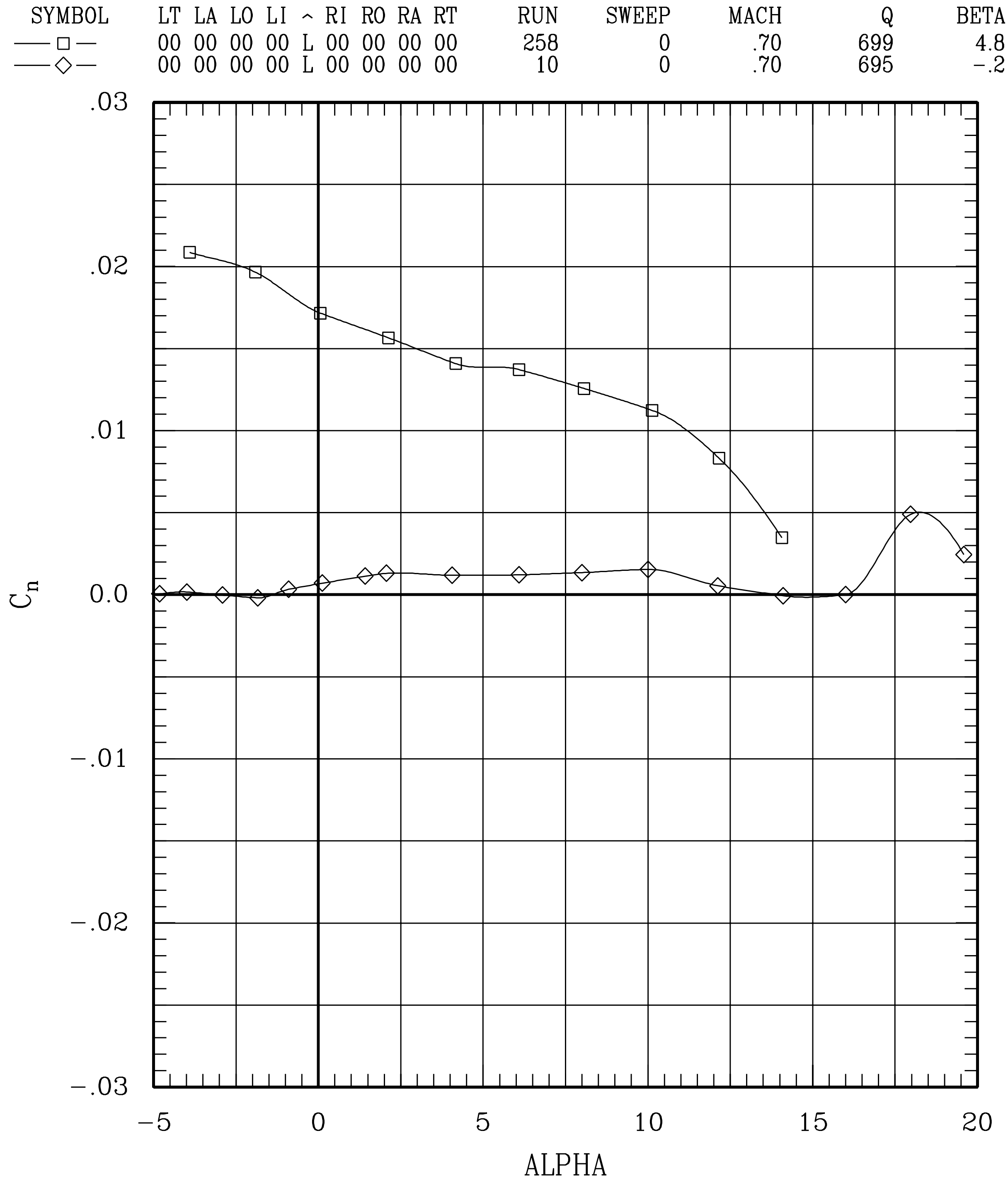

Figure 14(a). Aerodynamic characteristics in sideslip for sweep = 0 deg, Mach = 0.70.

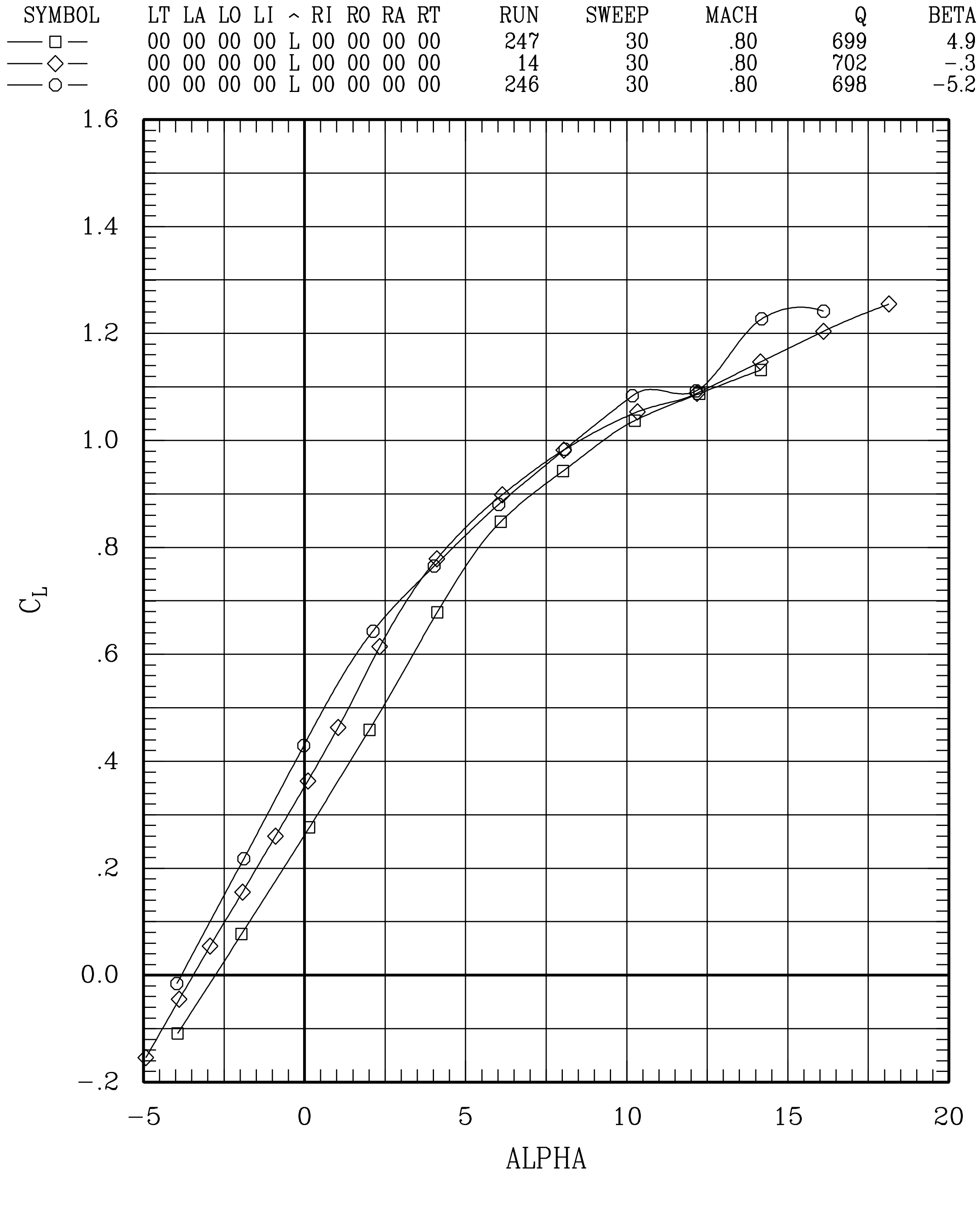

Figure 14(b). Aerodynamic characteristics in sideslip for sweep = 30 deg, Mach = 0.80.

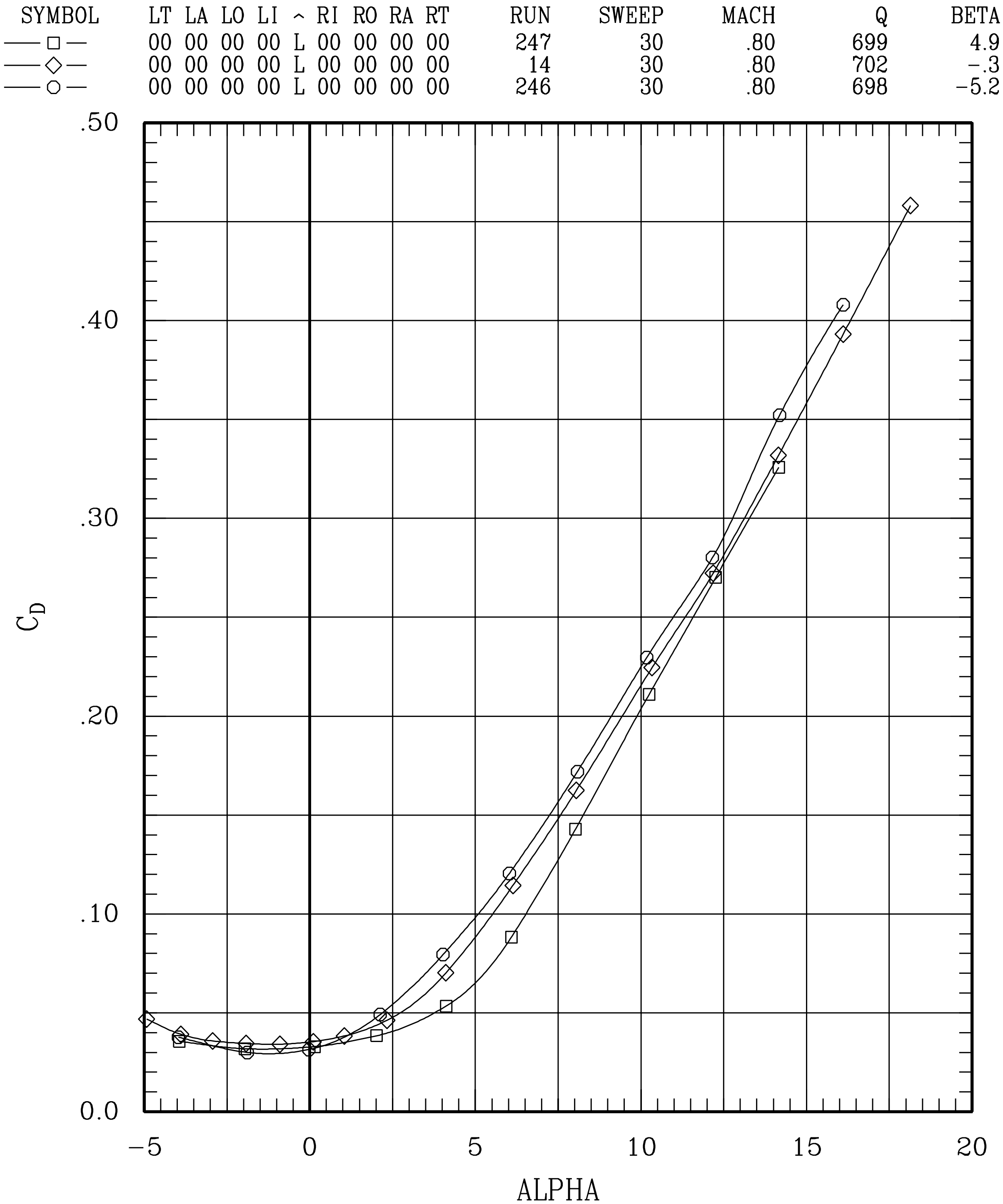

Figure 14(b). Aerodynamic characteristics in sideslip for sweep = 30 deg, Mach = 0.80.

SYMBOL	LT LA LO LI ^ RI RO RA RT	RUN	SWEEP	MACH	Q	BETA
—□—	00 00 00 00 L 00 00 00 00	247	30	.80	699	4.9
—◇—	00 00 00 00 L 00 00 00 00	14	30	.80	702	−.3
—○—	00 00 00 00 L 00 00 00 00	246	30	.80	698	−5.2

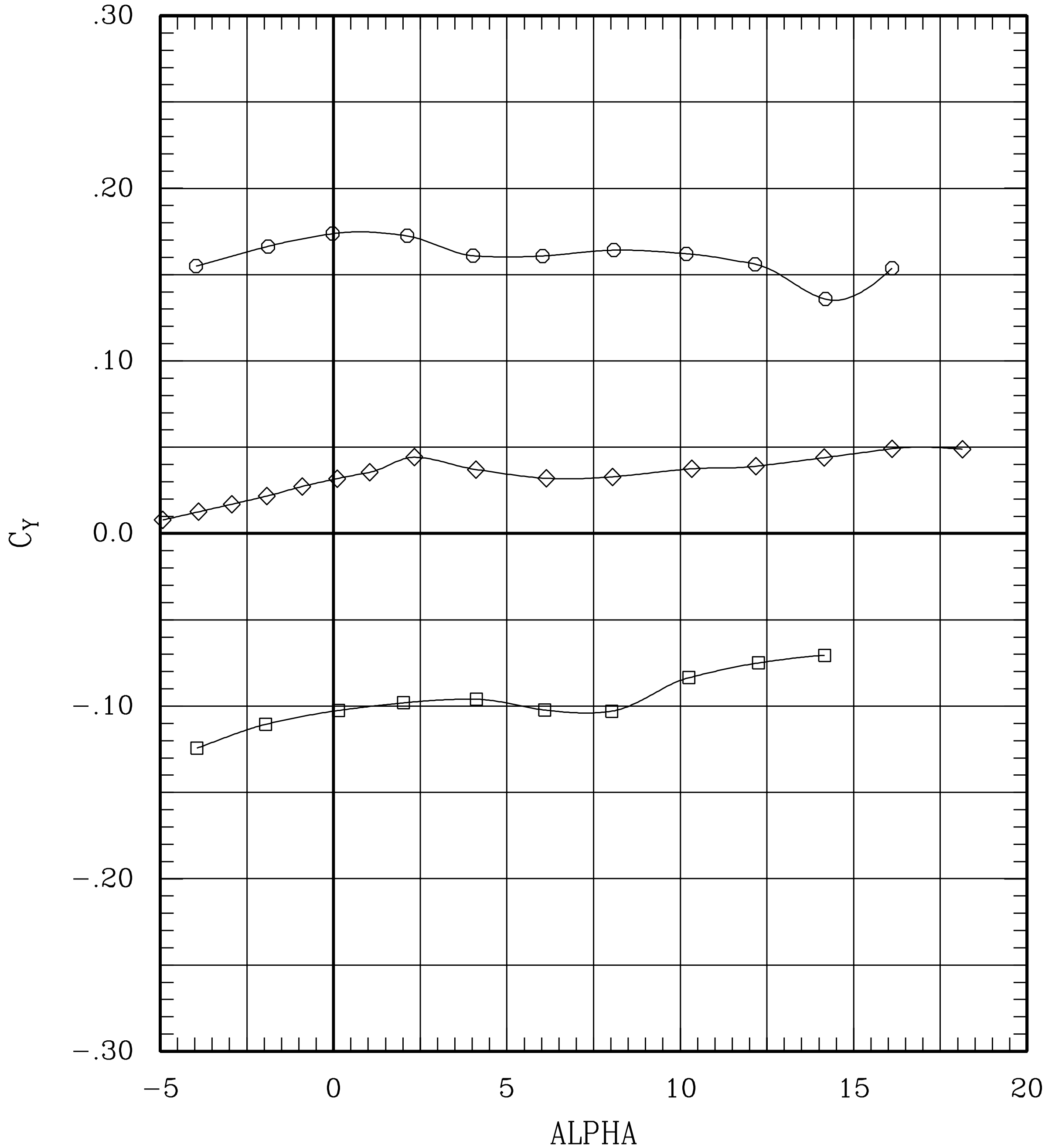

Figure 14(b). Aerodynamic characteristics in sideslip for sweep = 30 deg, Mach = 0.80.

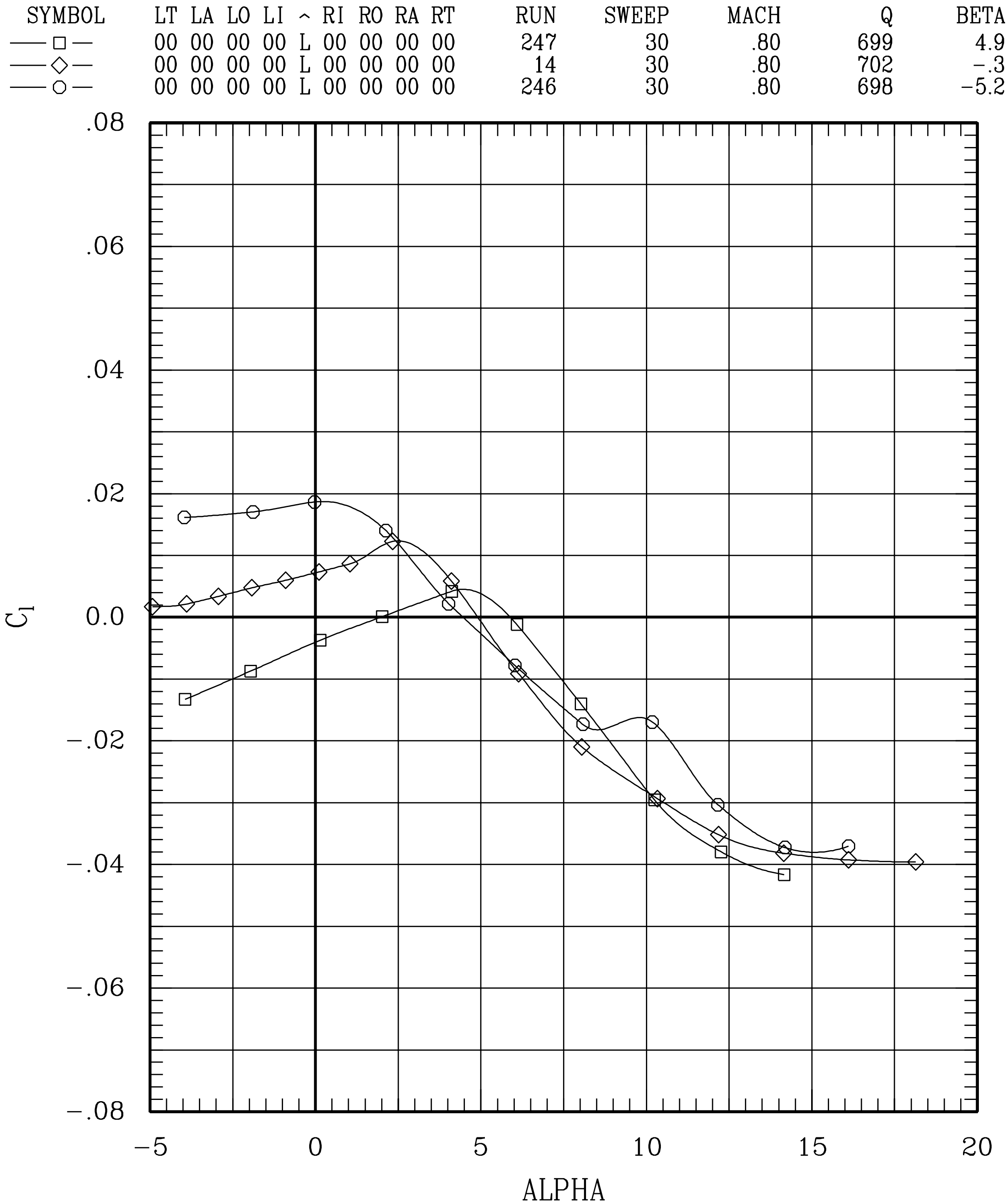

Figure 14(b). Aerodynamic characteristics in sideslip for sweep = 30 deg, Mach = 0.80.

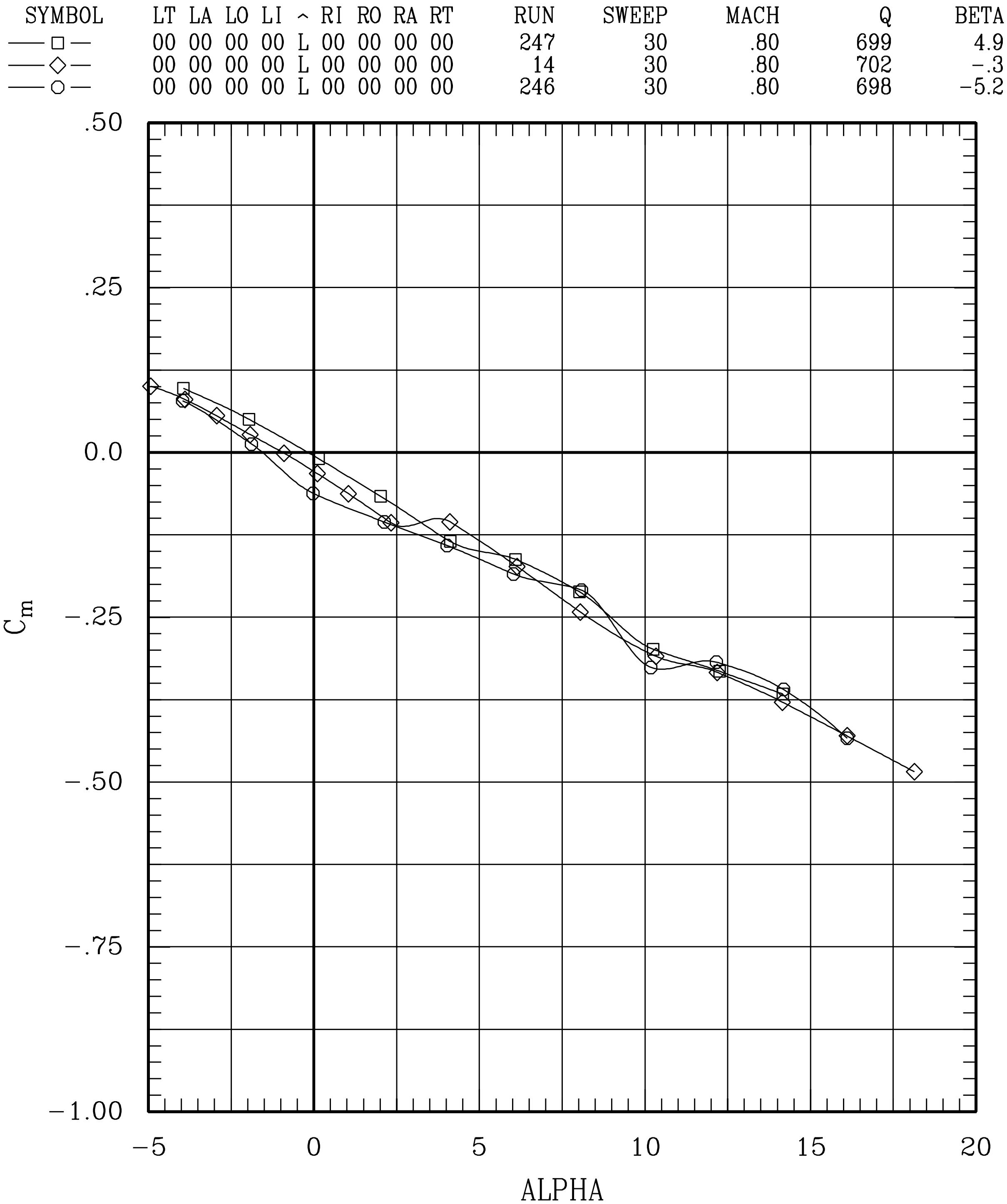

Figure 14(b). Aerodynamic characteristics in sideslip for sweep = 30 deg, Mach = 0.80.

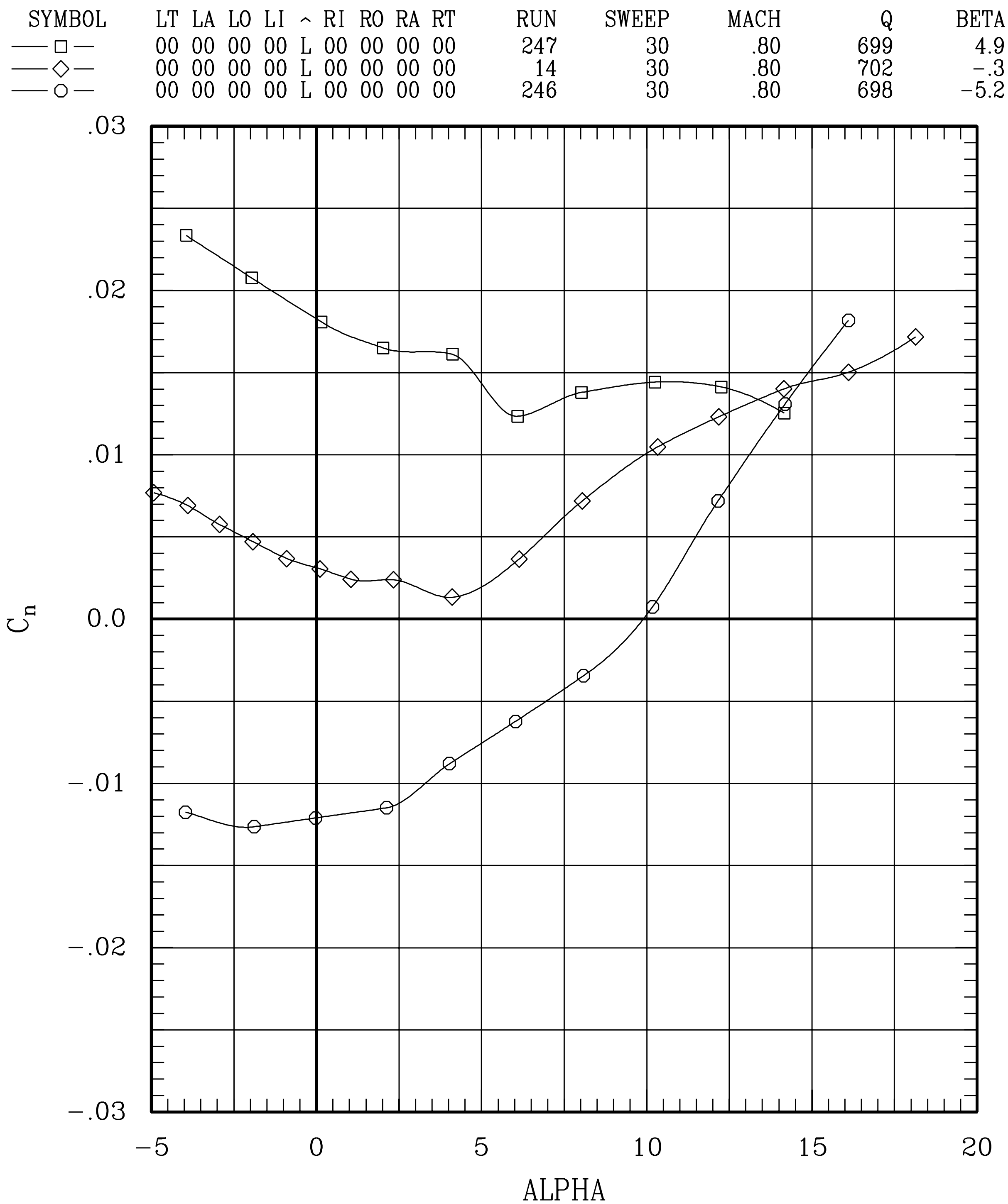

Figure 14(b). Aerodynamic characteristics in sideslip for sweep = 30 deg, Mach = 0.80.

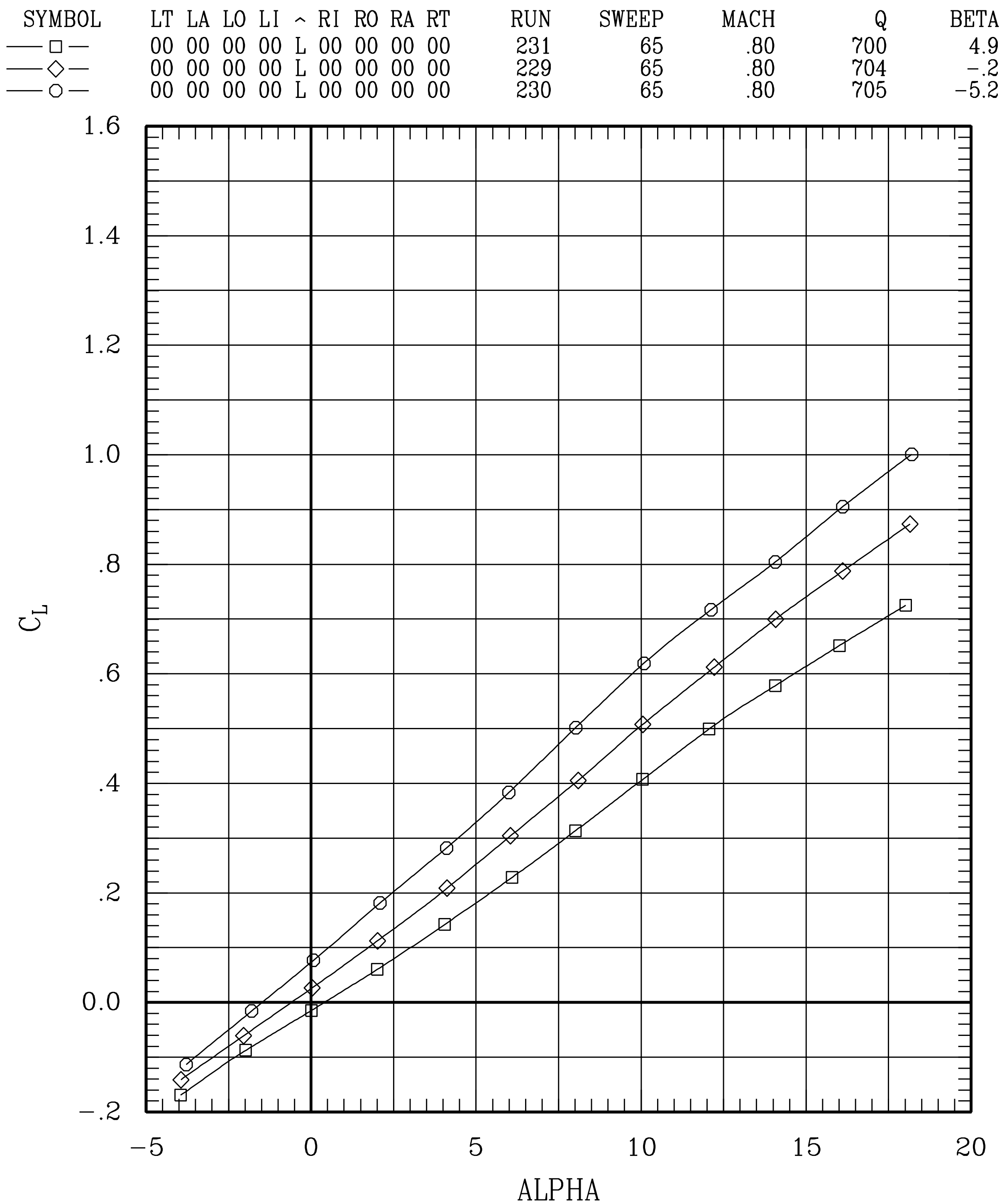

Figure 14(c). Aerodynamic characteristics in sideslip for sweep = 65 deg, Mach = 0.80.

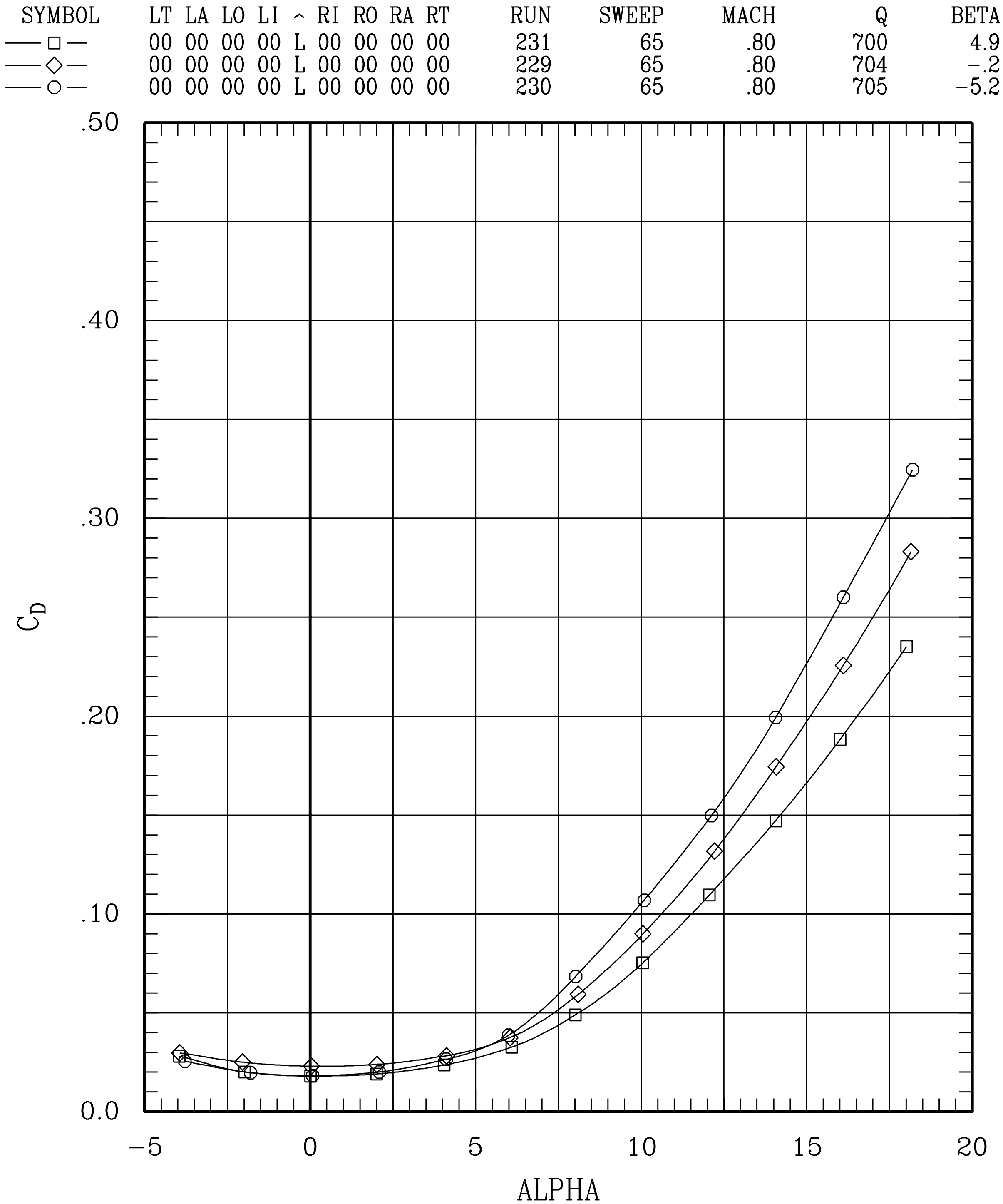

Figure 14(c). Aerodynamic characteristics in sideslip for sweep = 65 deg, Mach = 0.80.

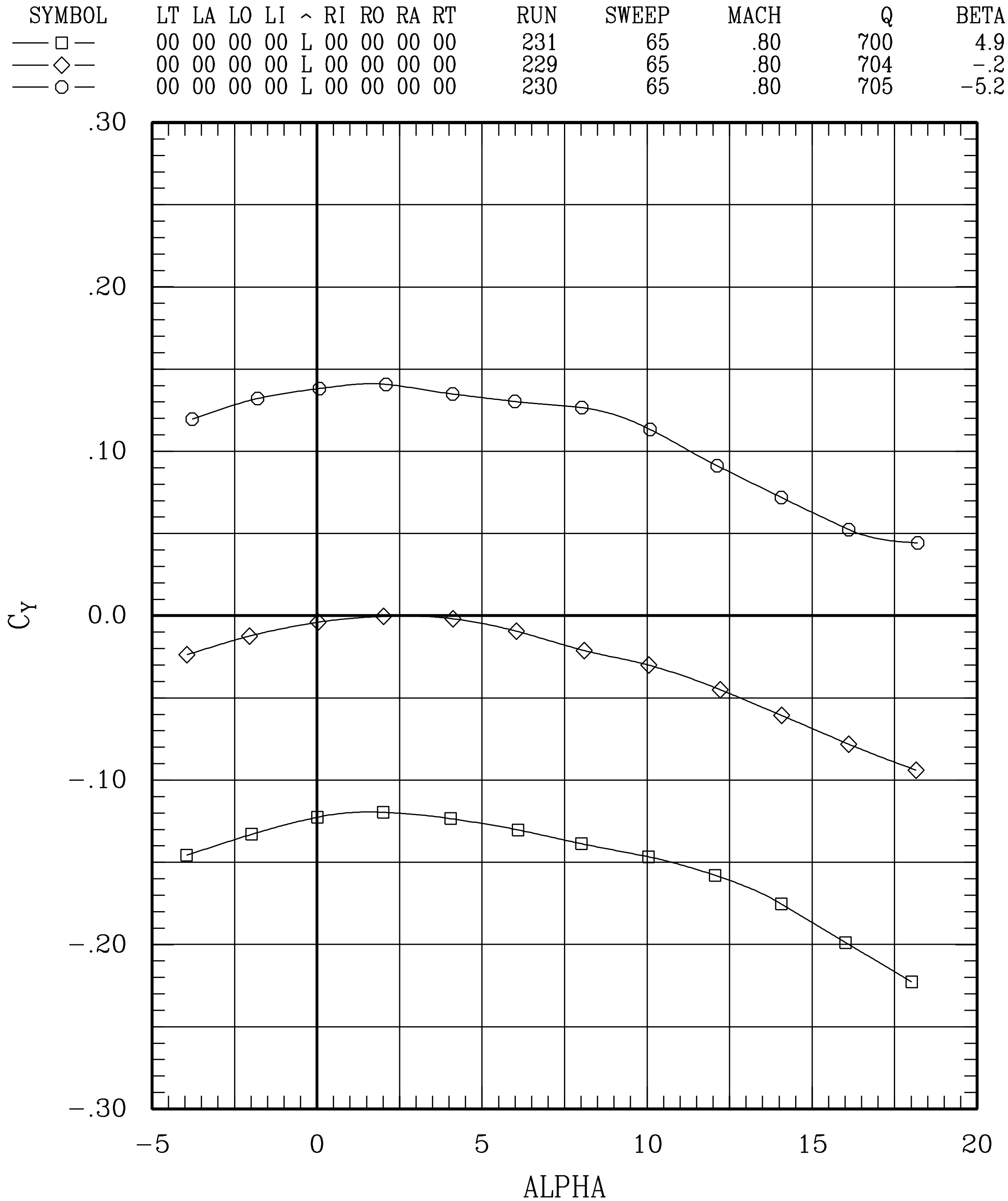

Figure 14(c). Aerodynamic characteristics in sideslip for sweep = 65 deg, Mach = 0.80.

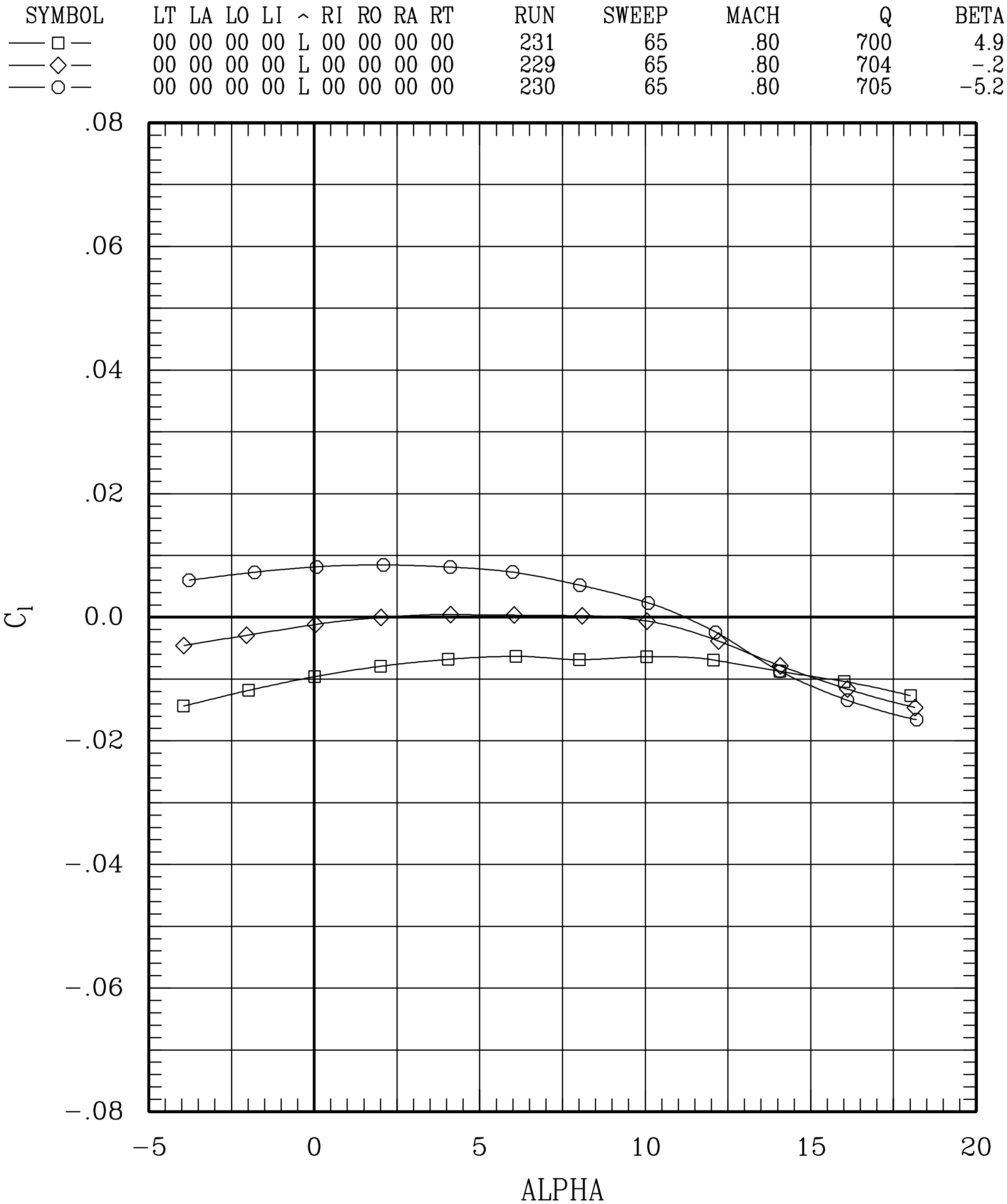

Figure 14(c). Aerodynamic characteristics in sideslip for sweep = 65 deg, Mach = 0.80.

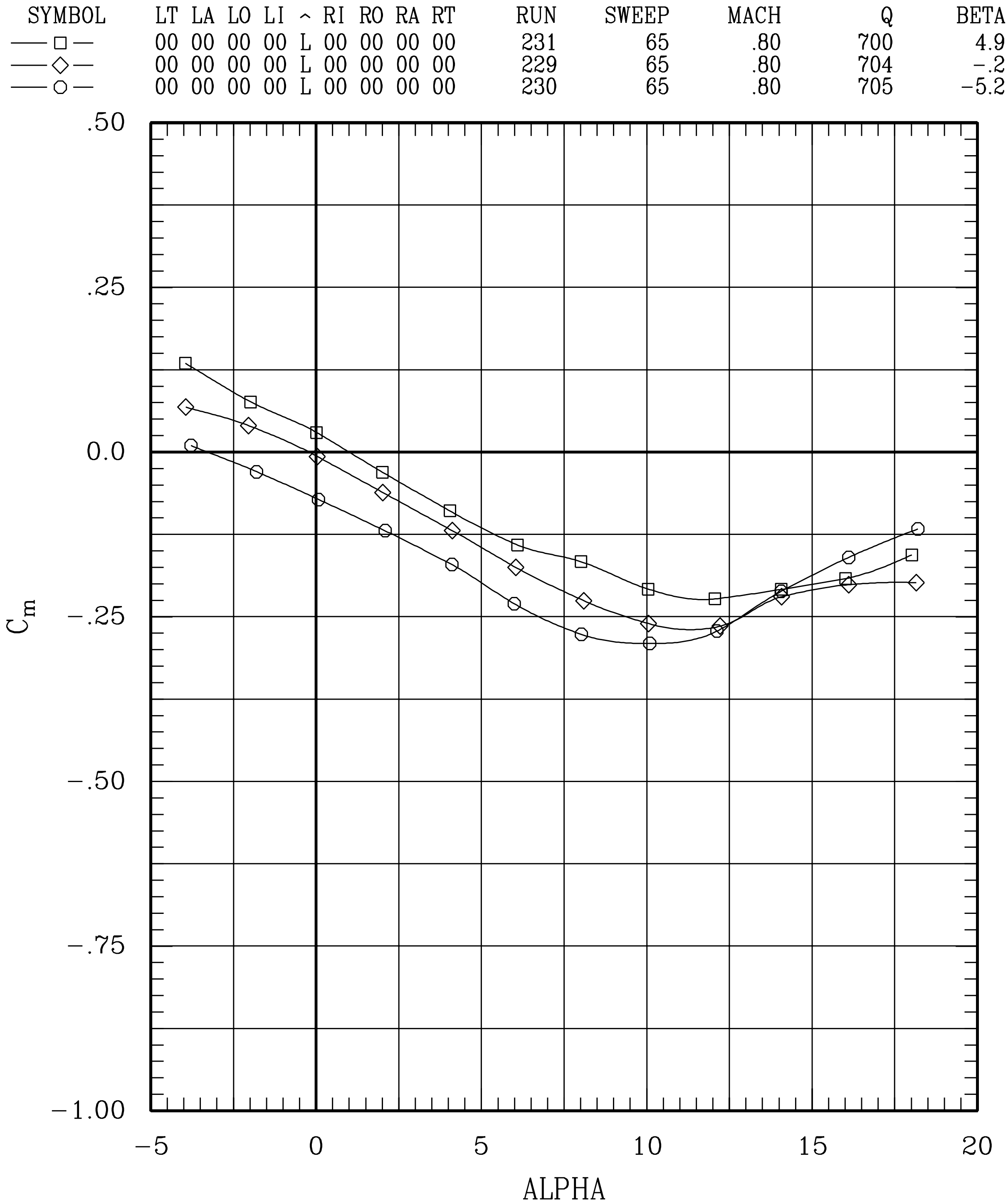

Figure 14(c). Aerodynamic characteristics in sideslip for sweep = 65 deg, Mach = 0.80.

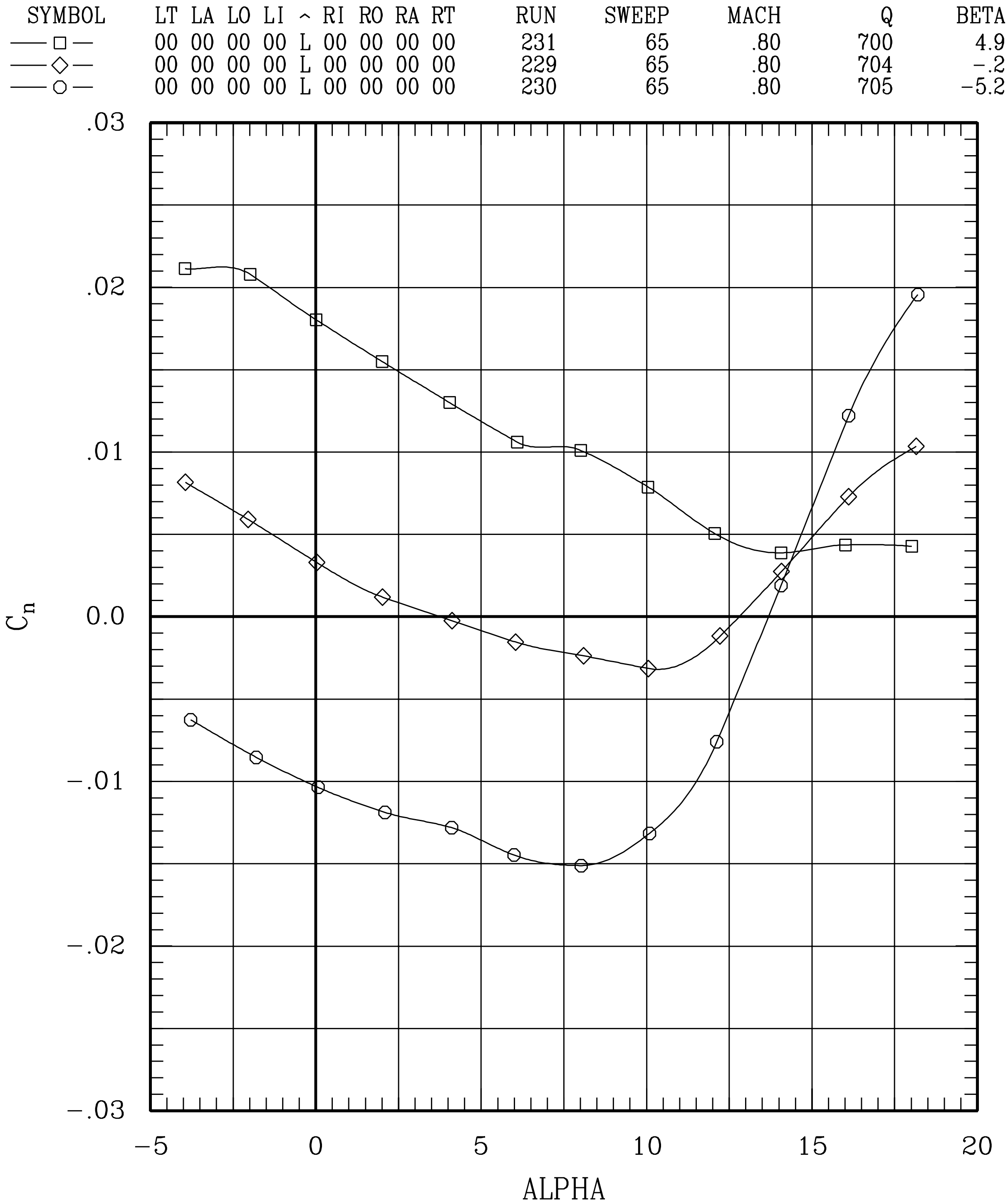

Figure 14(c). Aerodynamic characteristics in sideslip for sweep = 65 deg, Mach = 0.80.

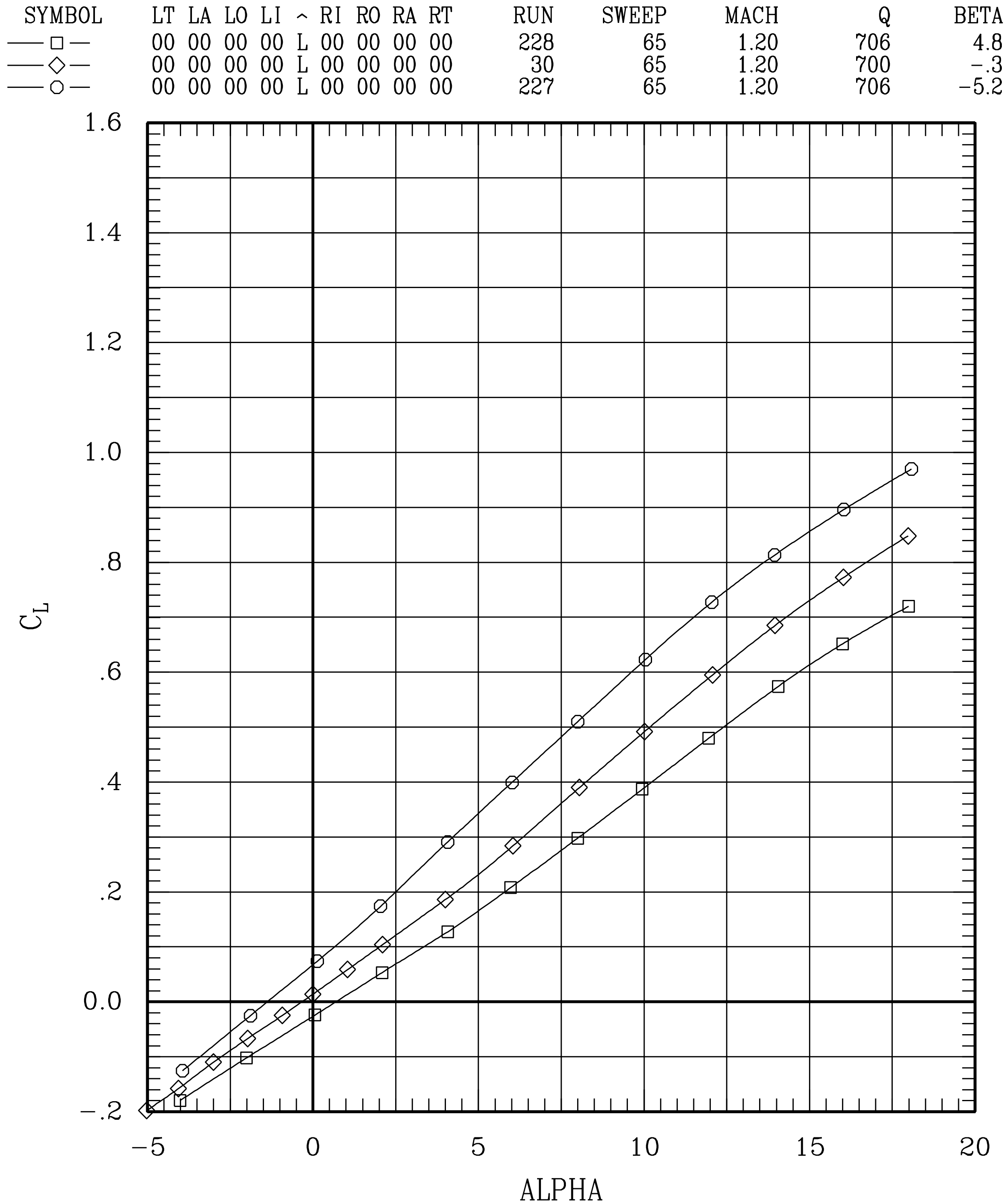

Figure 14(d). Aerodynamic characteristics in sideslip for sweep = 65 deg, Mach = 1.20.

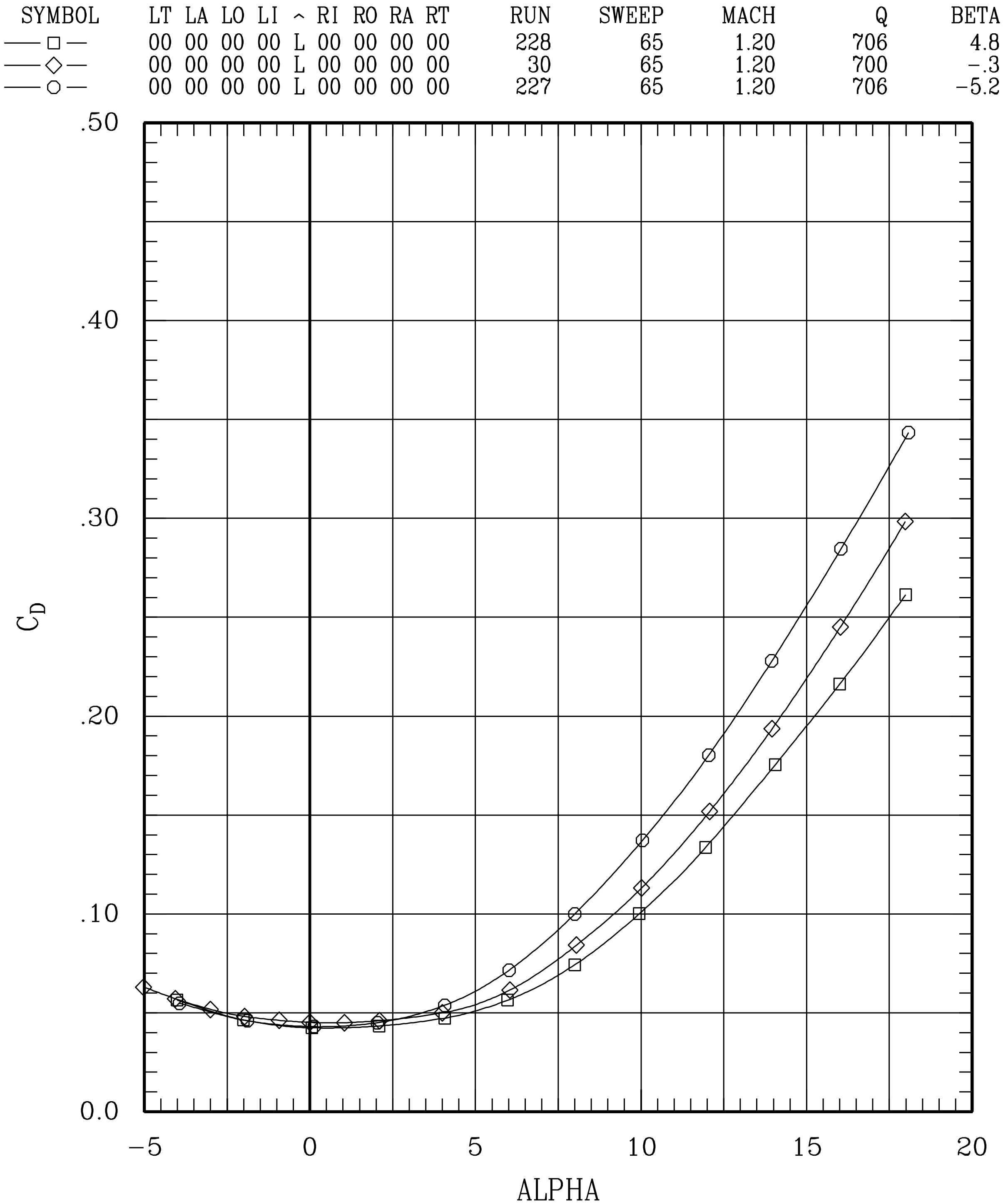

Figure 14(d). Aerodynamic characteristics in sideslip for sweep = 65 deg, Mach = 1.20.

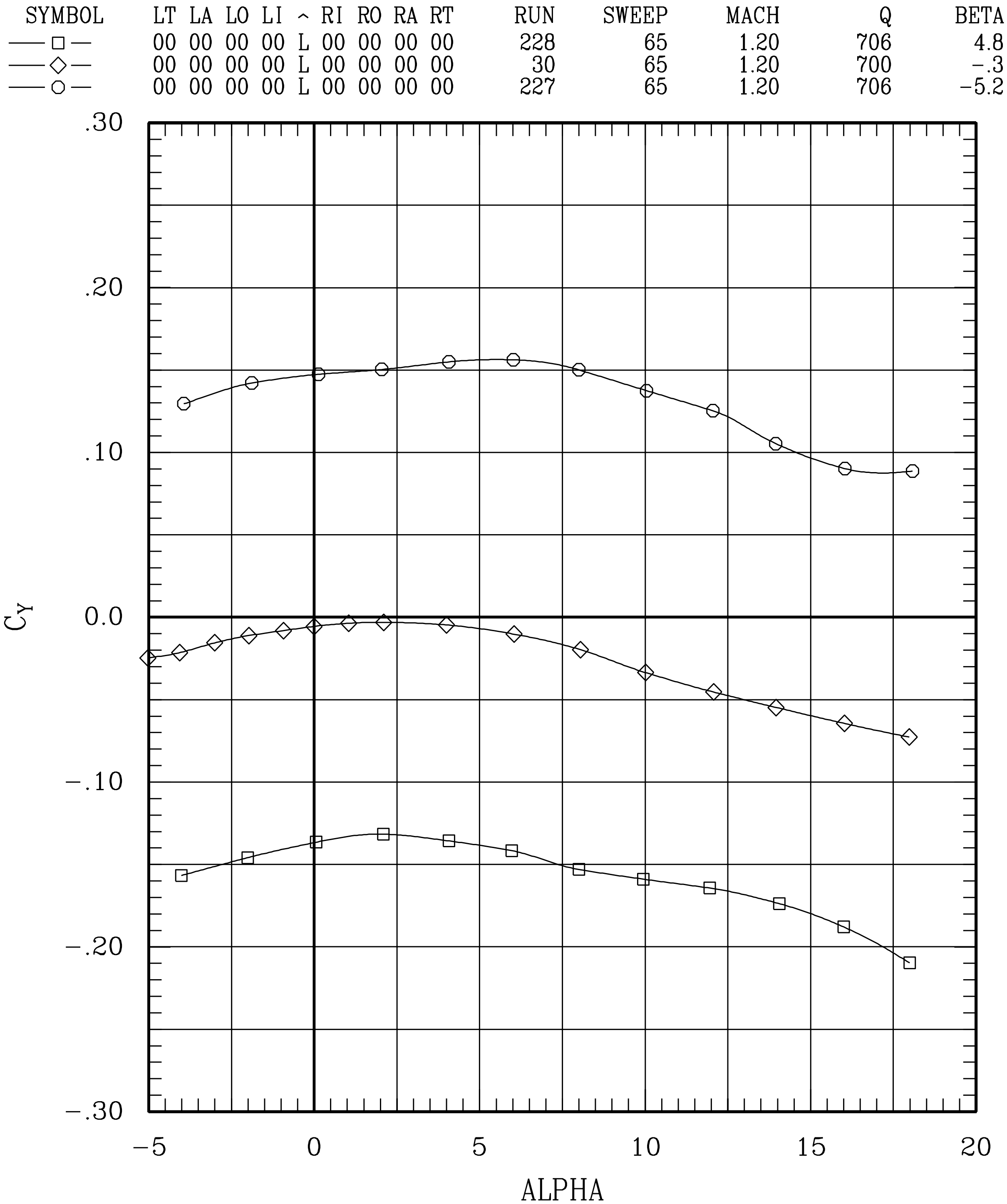

Figure 14(d). Aerodynamic characteristics in sideslip for
sweep = 65 deg, Mach = 1.20.

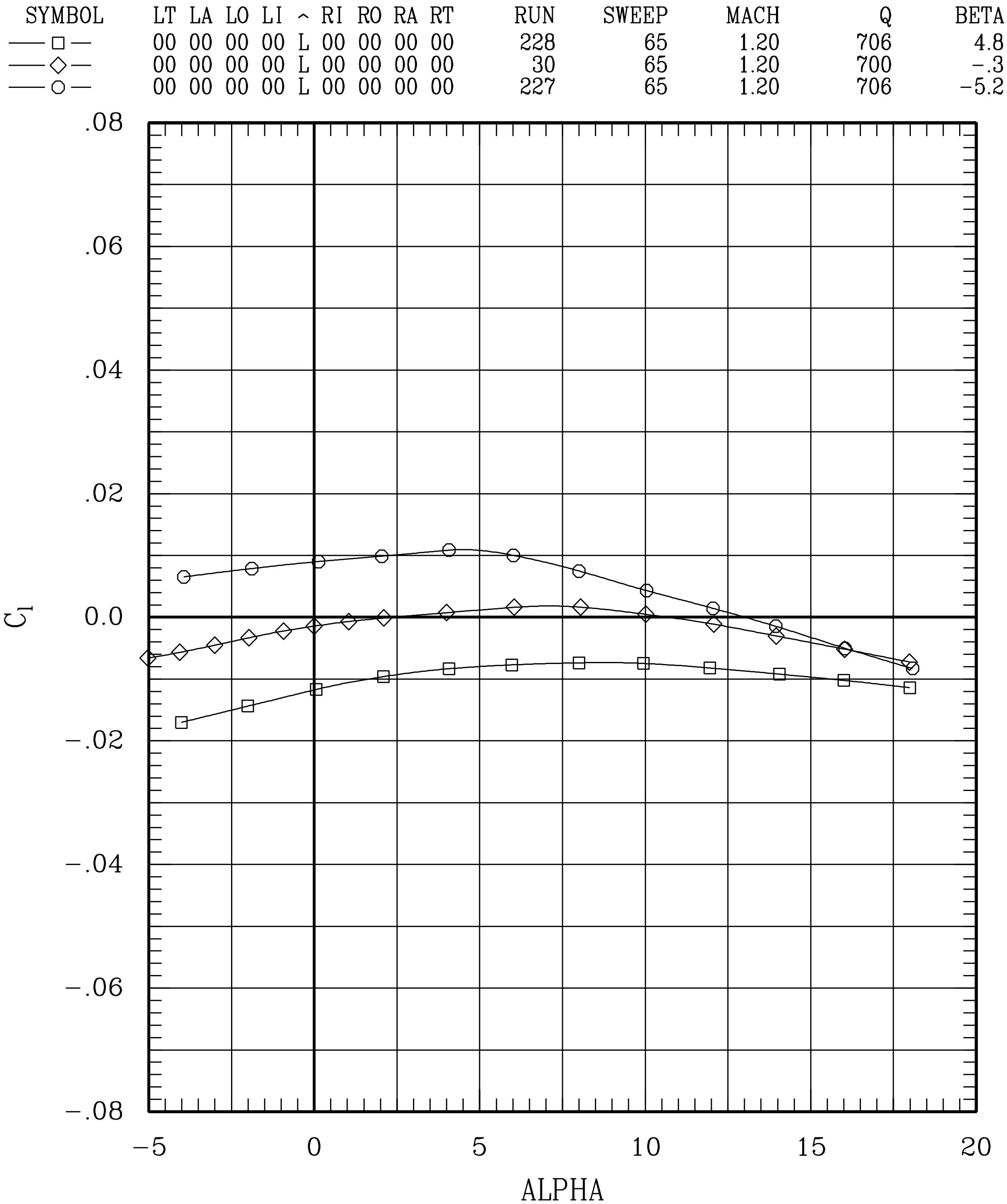

Figure 14(d). Aerodynamic characteristics in sideslip for sweep = 65 deg, Mach = 1.20.

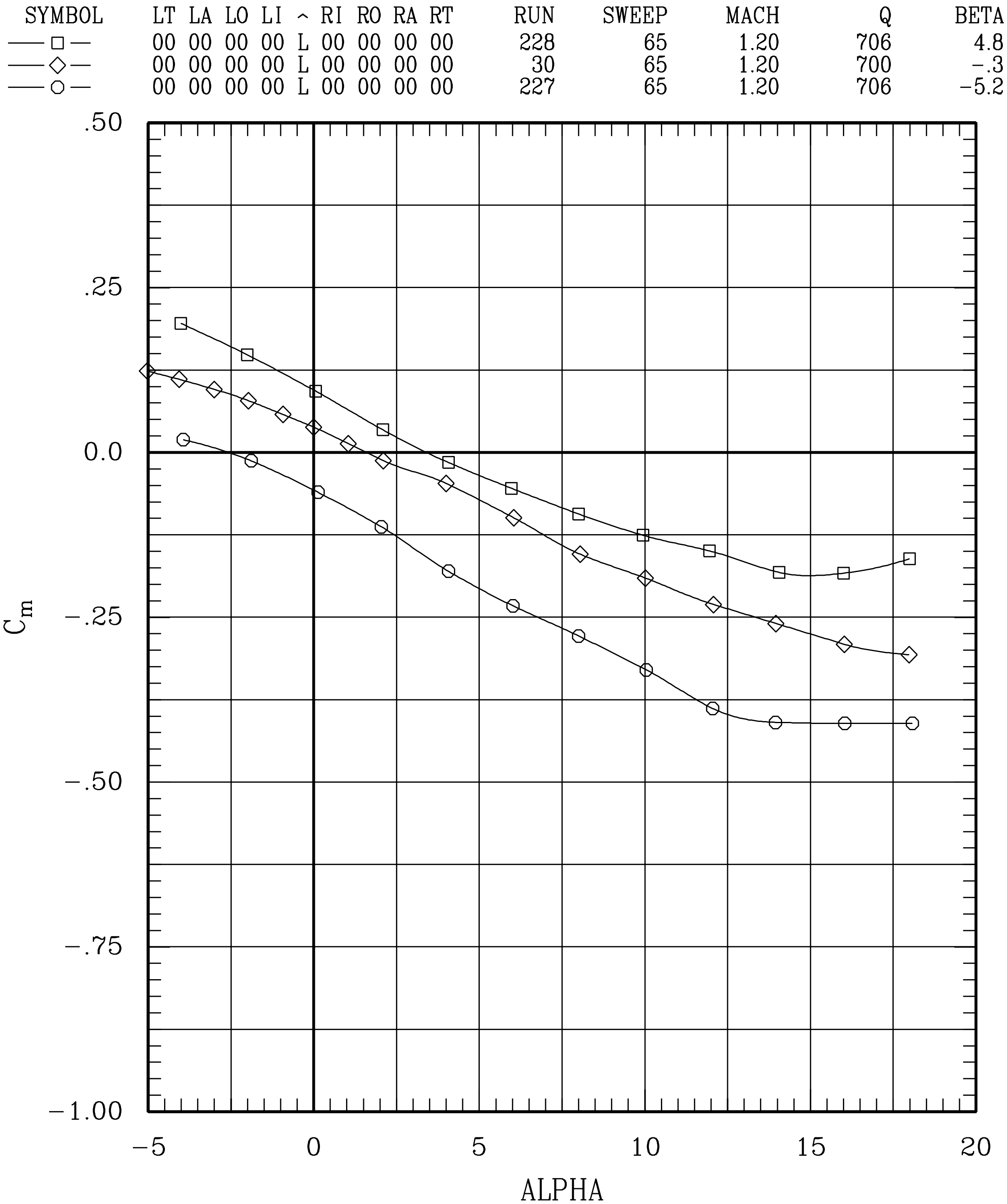

Figure 14(d). Aerodynamic characteristics in sideslip for sweep = 65 deg, Mach = 1.20.

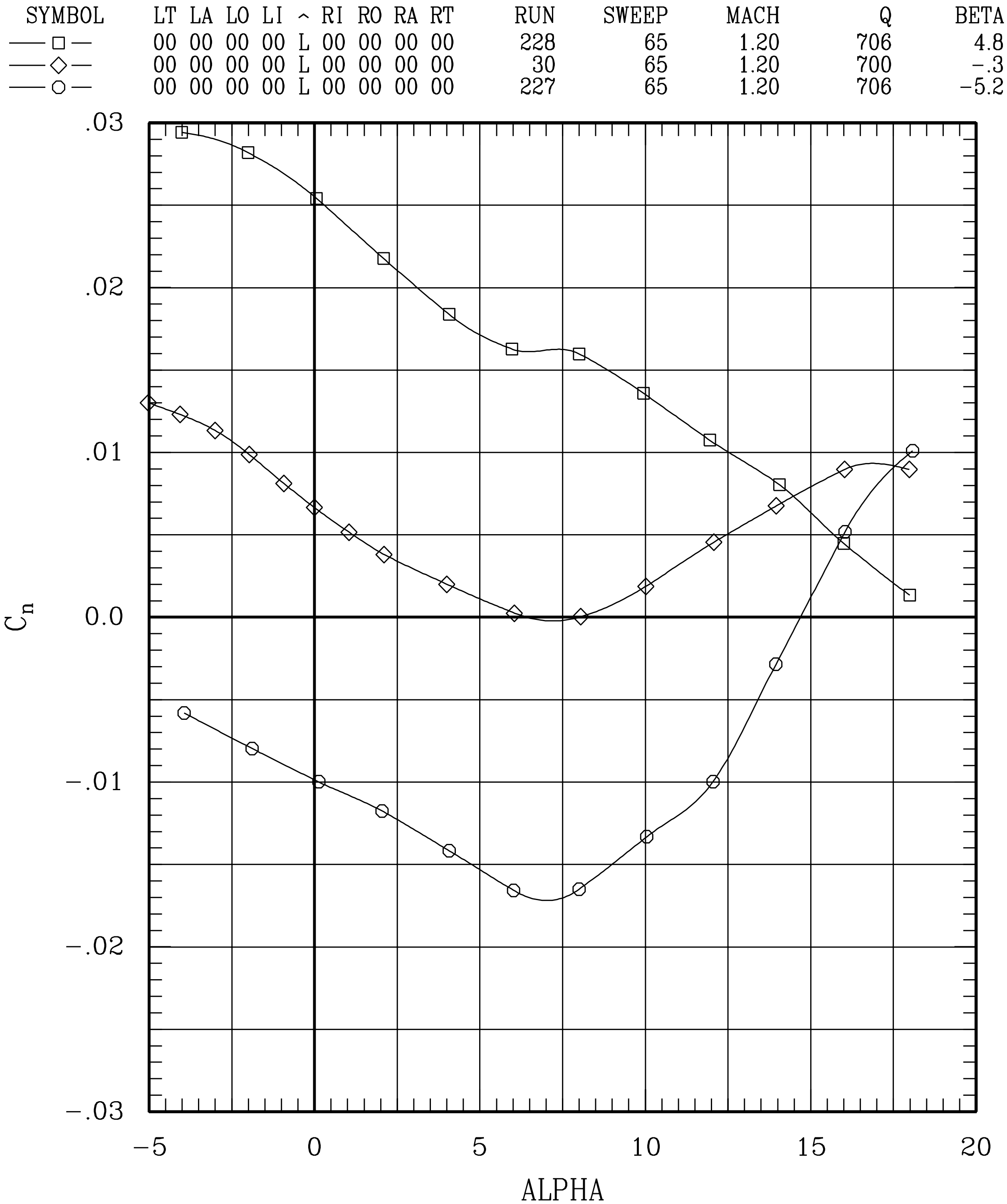

Figure 14(d). Aerodynamic characteristics in sideslip for sweep = 65 deg, Mach = 1.20.

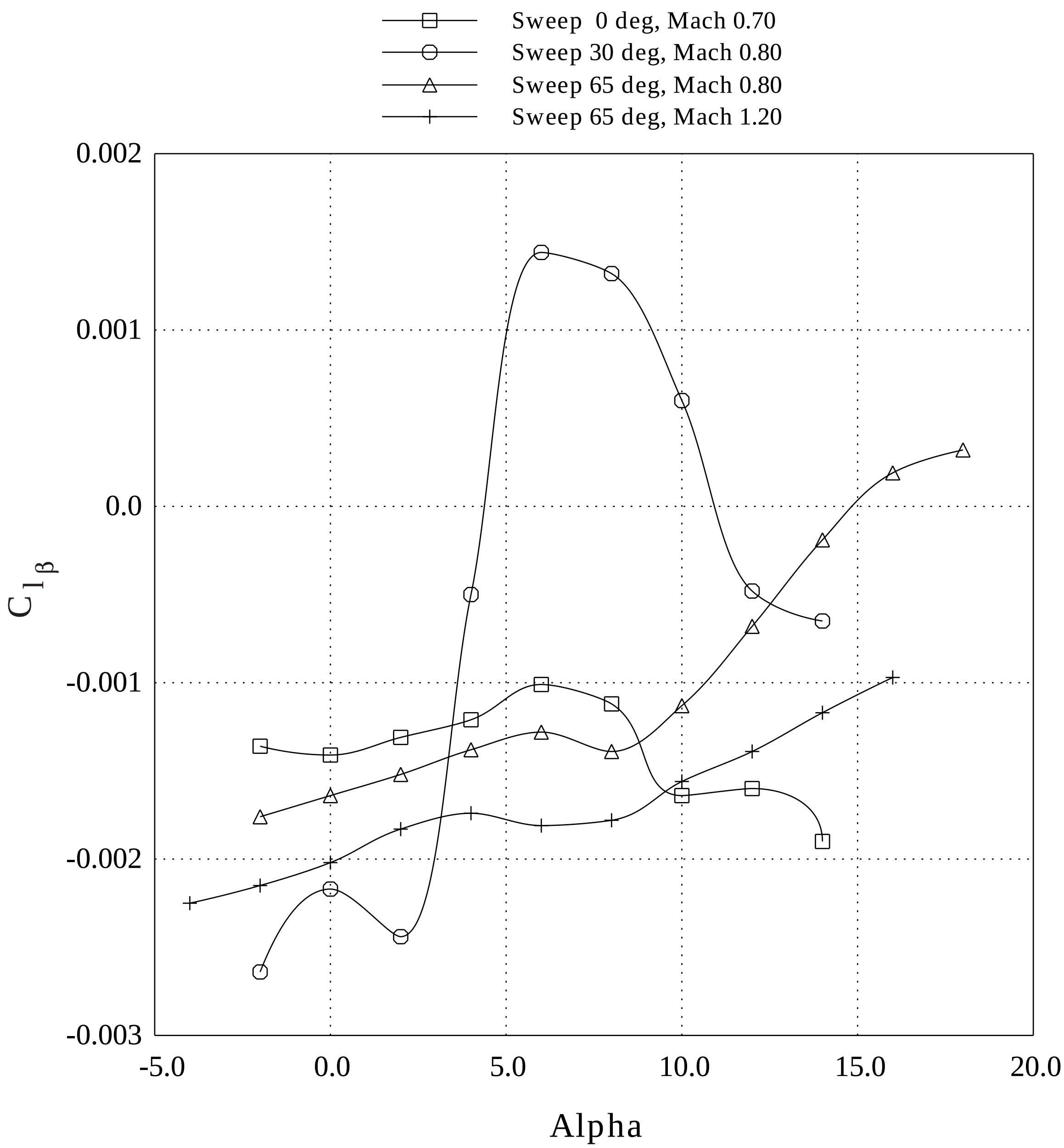

Figure 15(a). Dihedral effect stability parameter for positive sideslip angle.

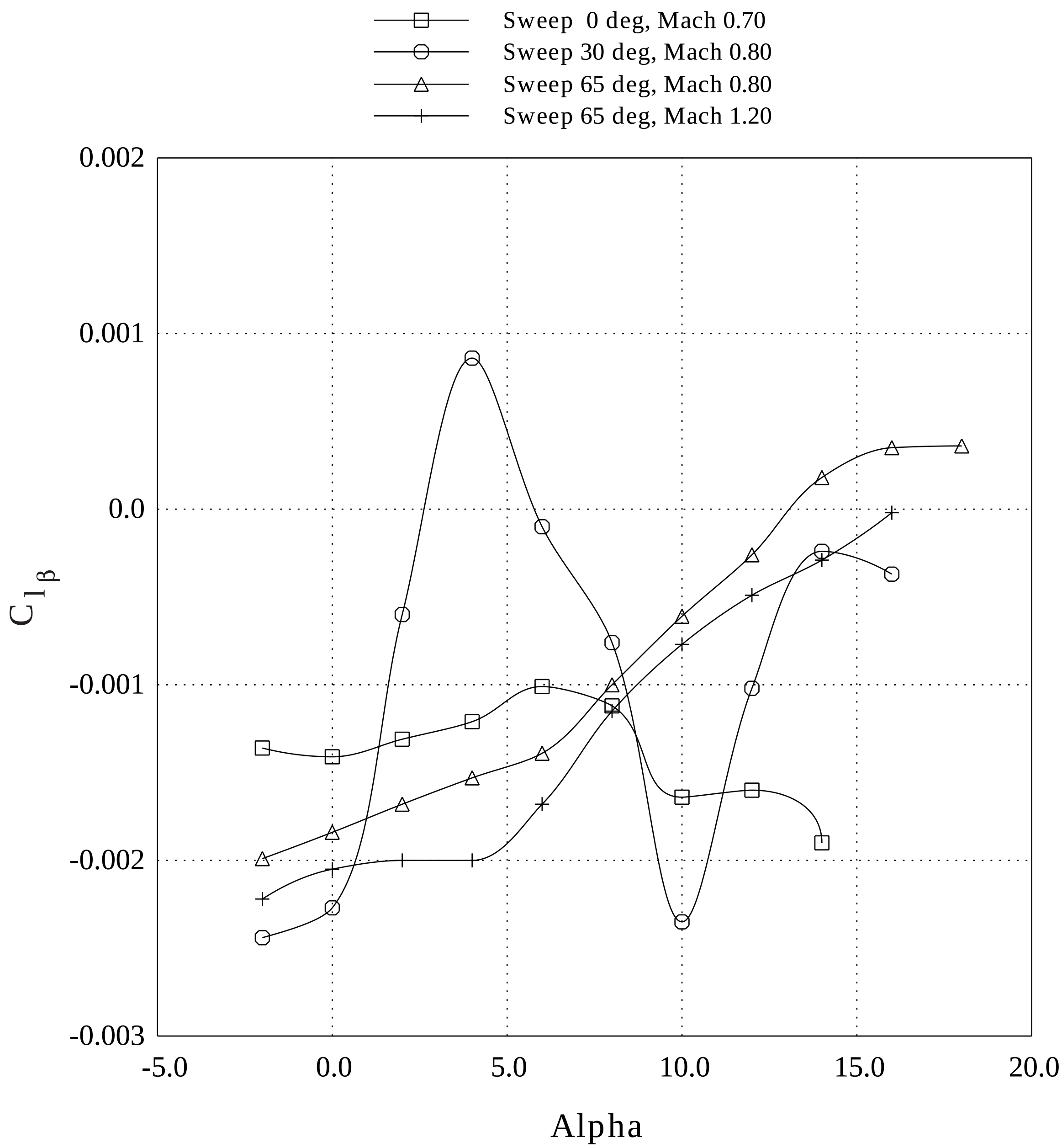

Figure 15(b). Dihedral effect stability parameter for negative sideslip angle.

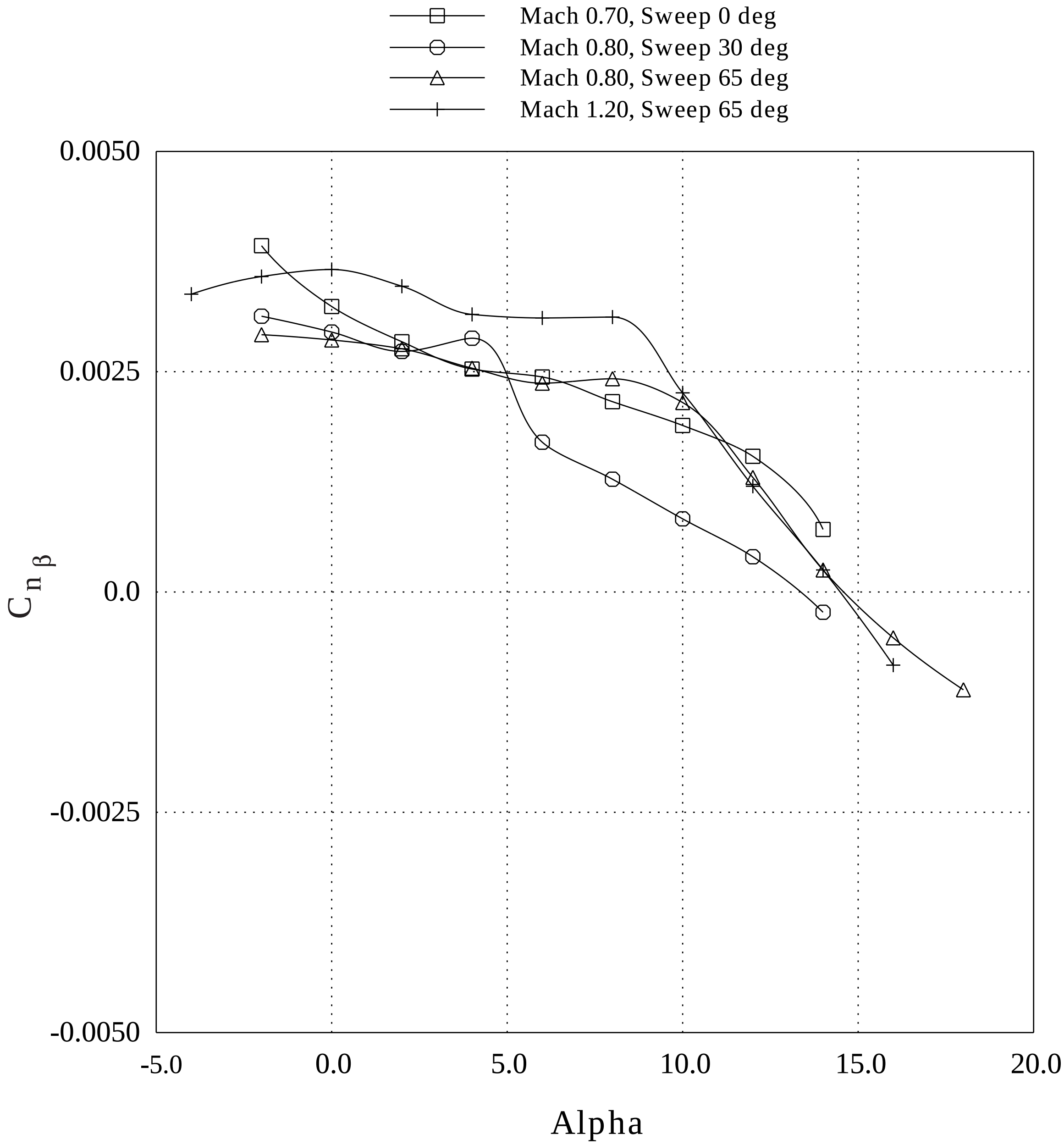

Figure 16(a). Directional stability parameter for positive sideslip angle.

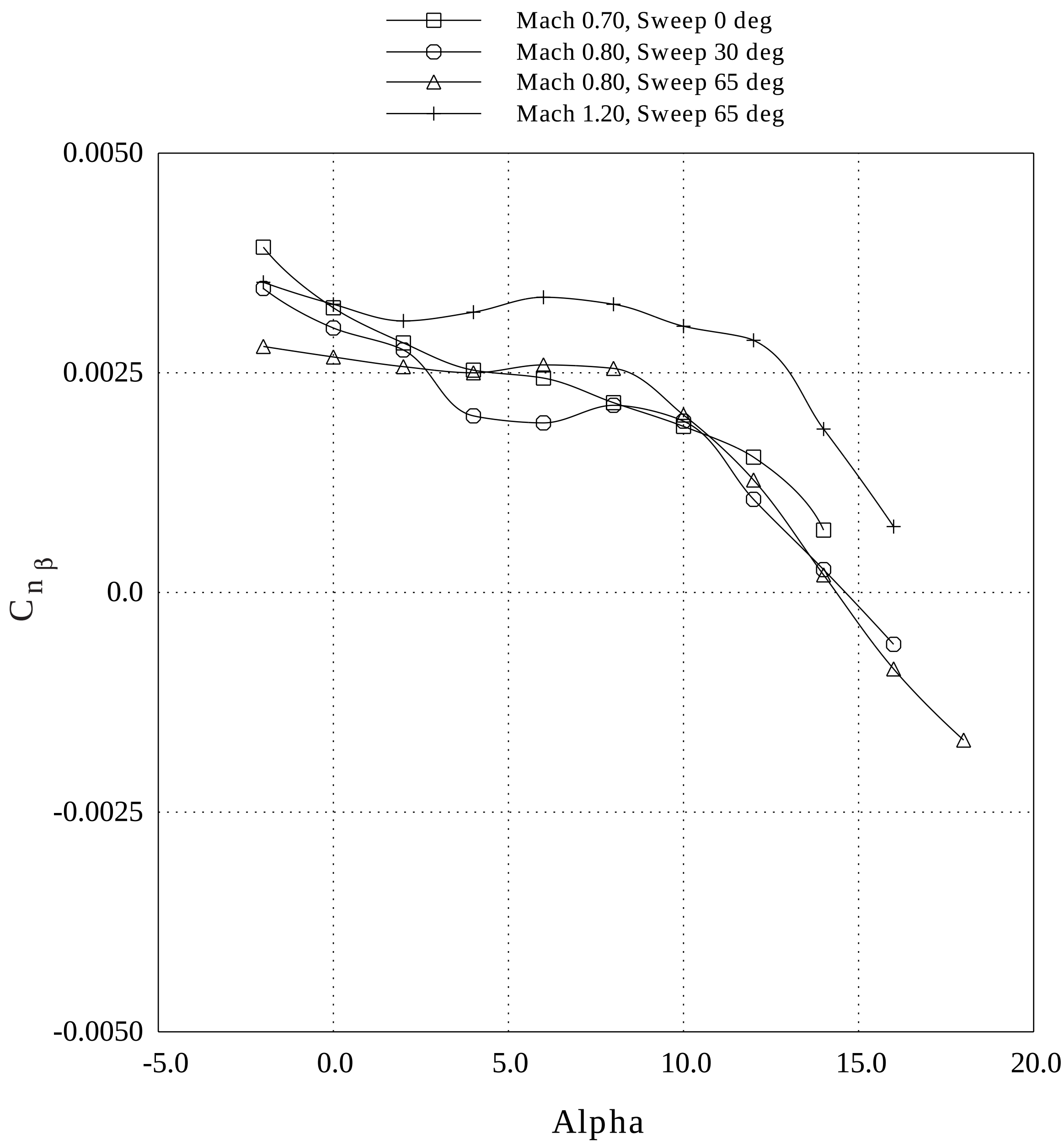

Figure 16(b). Directional stability parameter for negative sideslip angle.

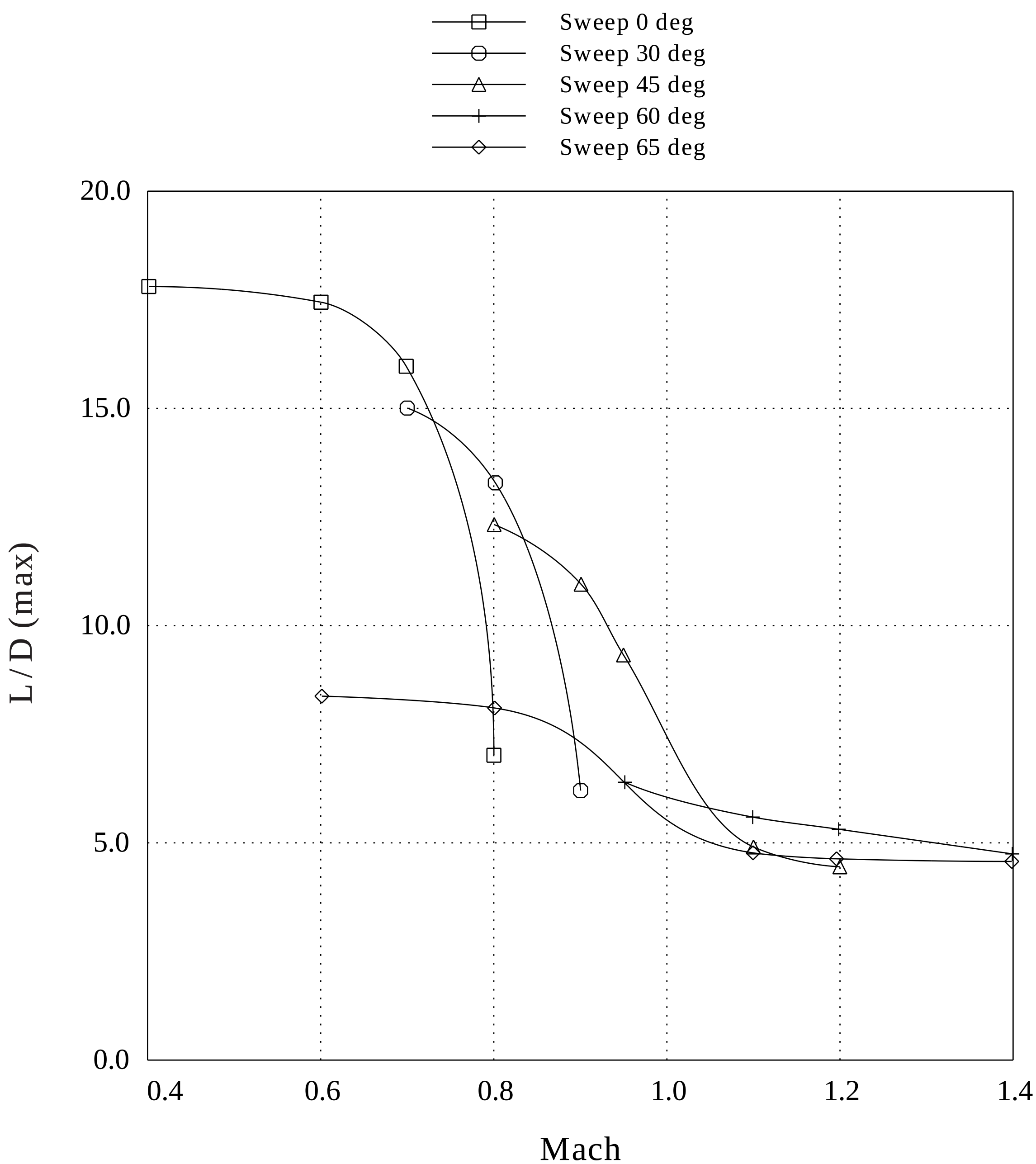

Figure 17. Effect of sweep on aerodynamic efficiency.

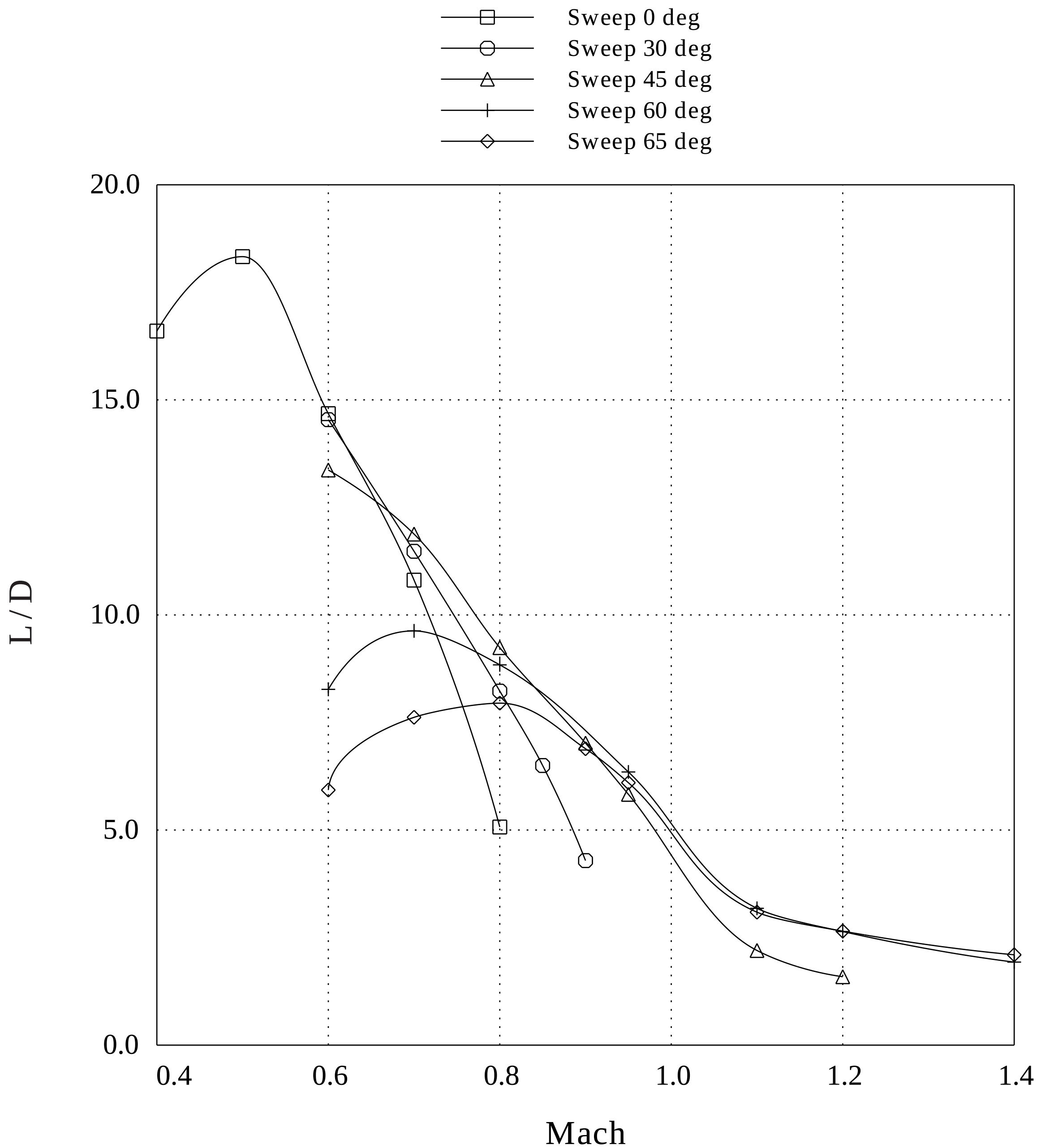

Figure 18. L / D for level flight.

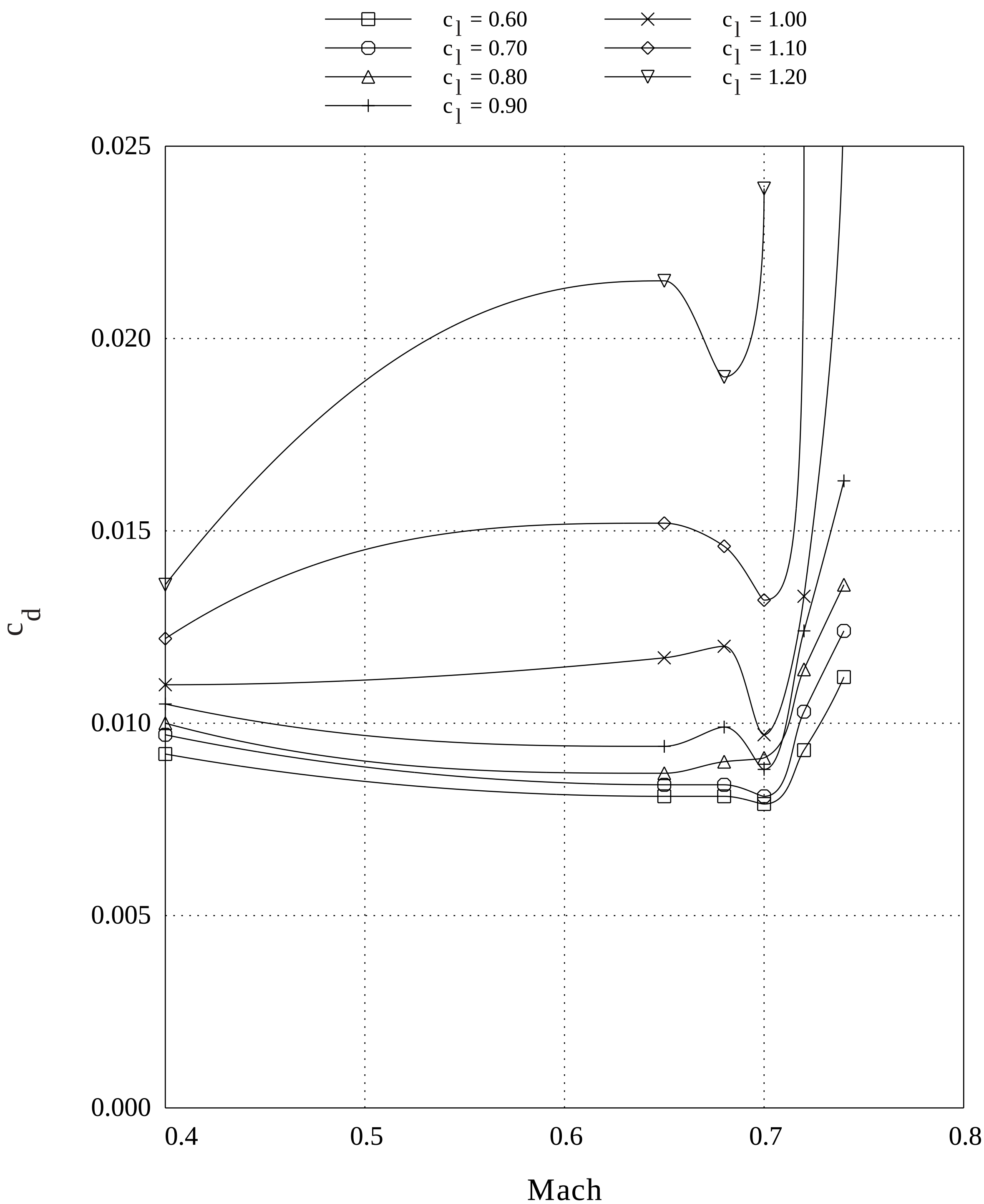

Figure 19. Experimental dragrise for airfoil OW 70-10-12.

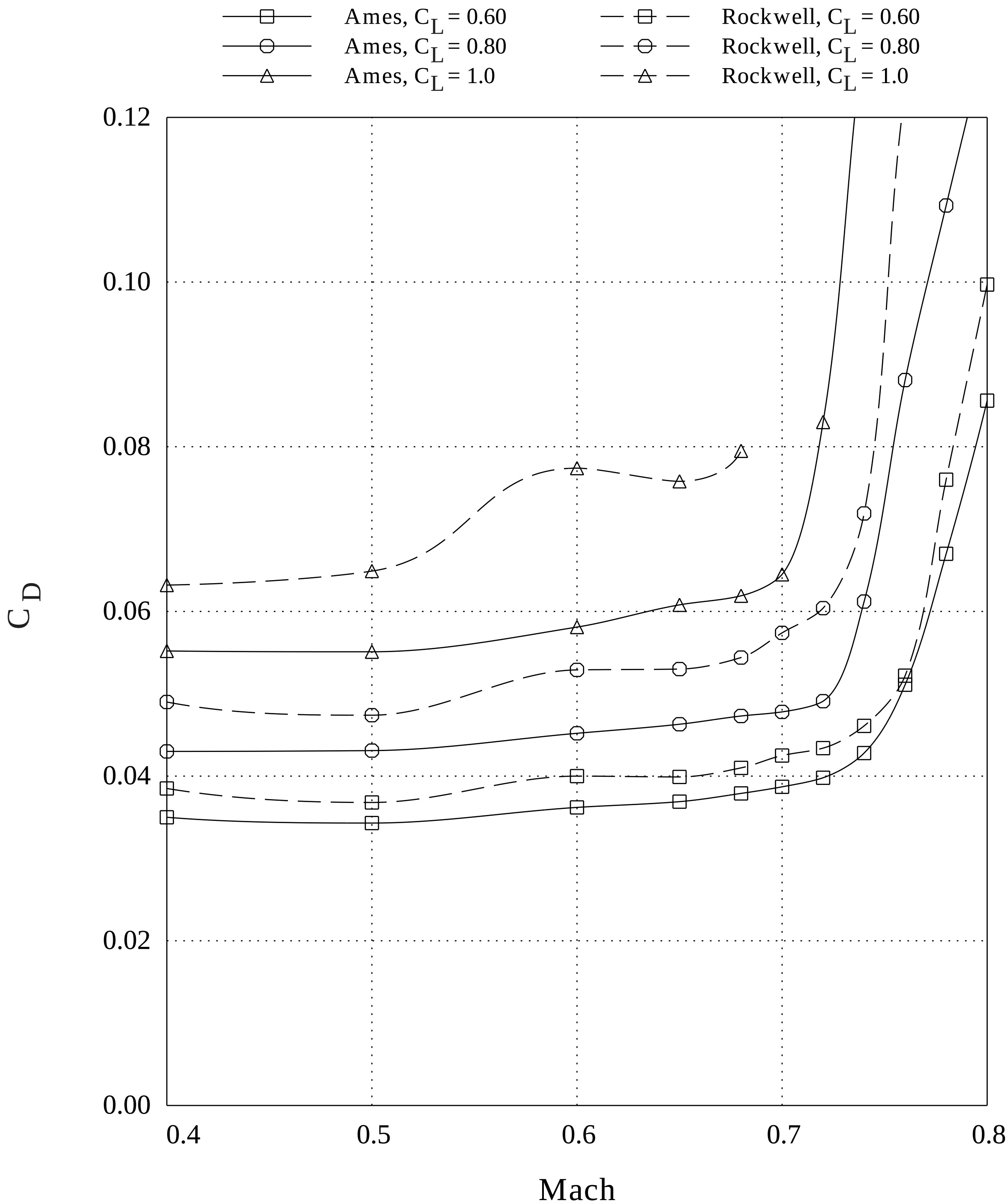

Figure 20. Zero-sweep dragrise for the Ames and Rockwell wings.

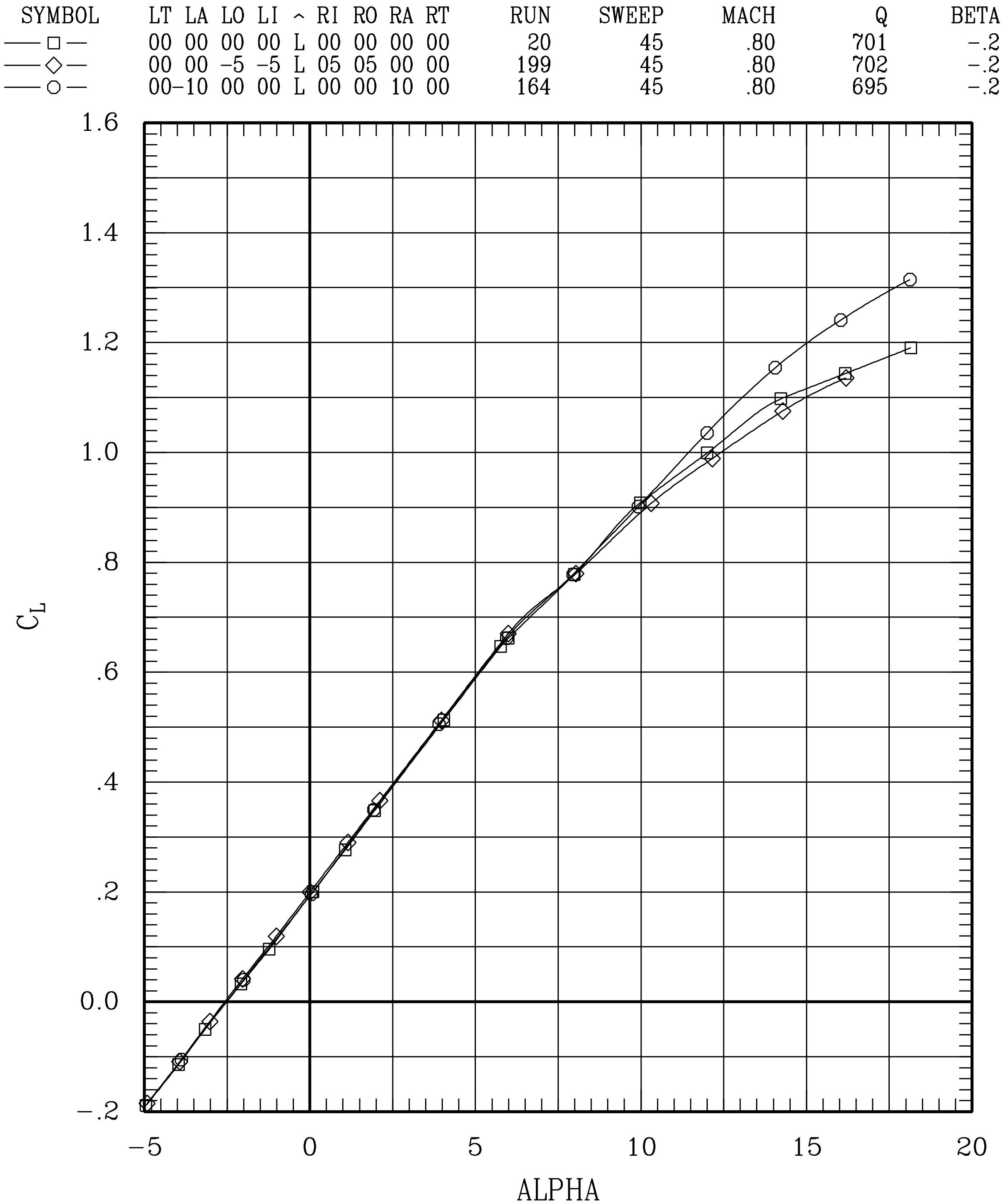

Figure 21(a). Effect of cruise flaps and ailerons for sweep = 45 deg, Mach = 0.80.

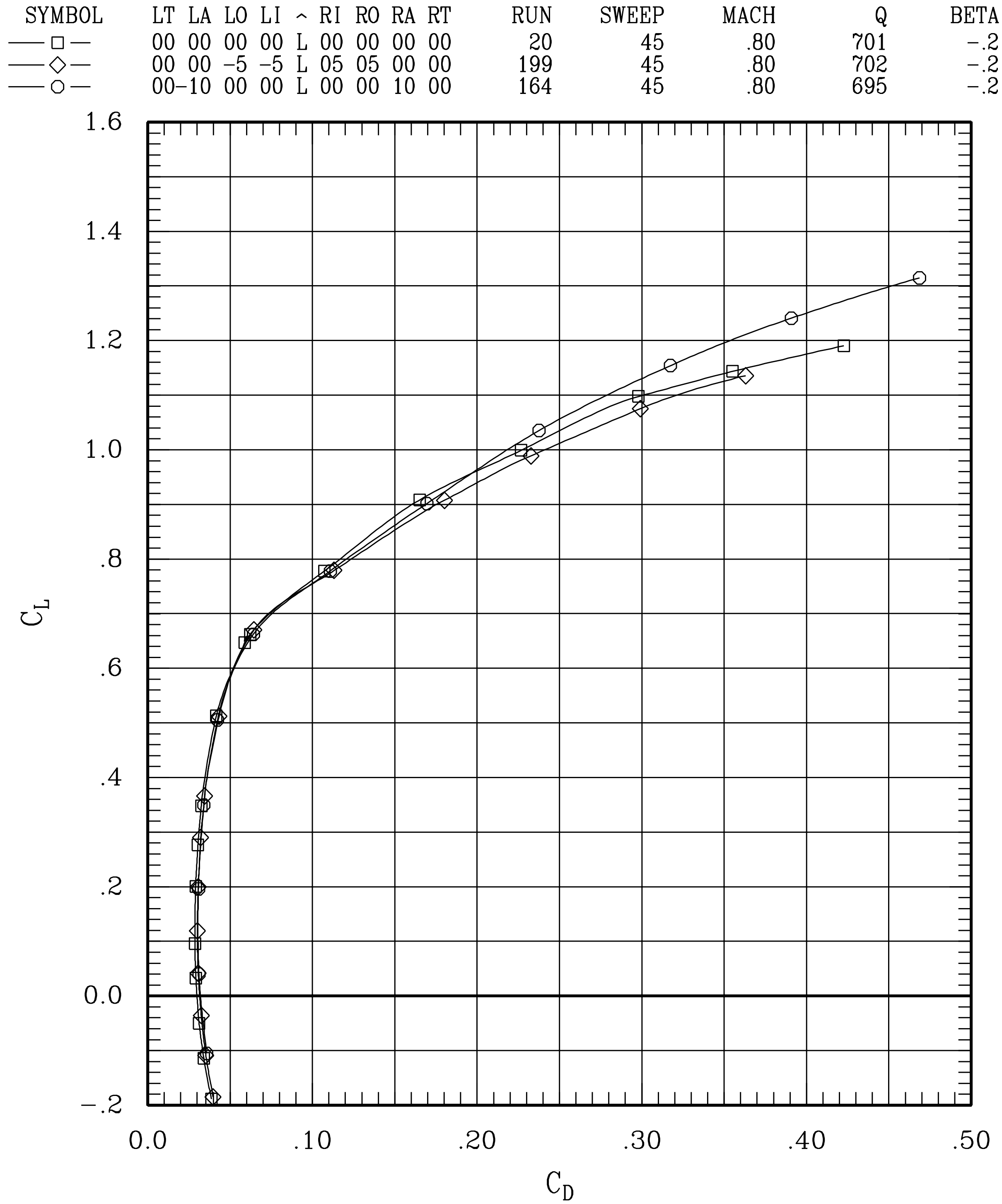

Figure 21(a). Effect of cruise flaps and ailerons for sweep = 45 deg, Mach = 0.80.

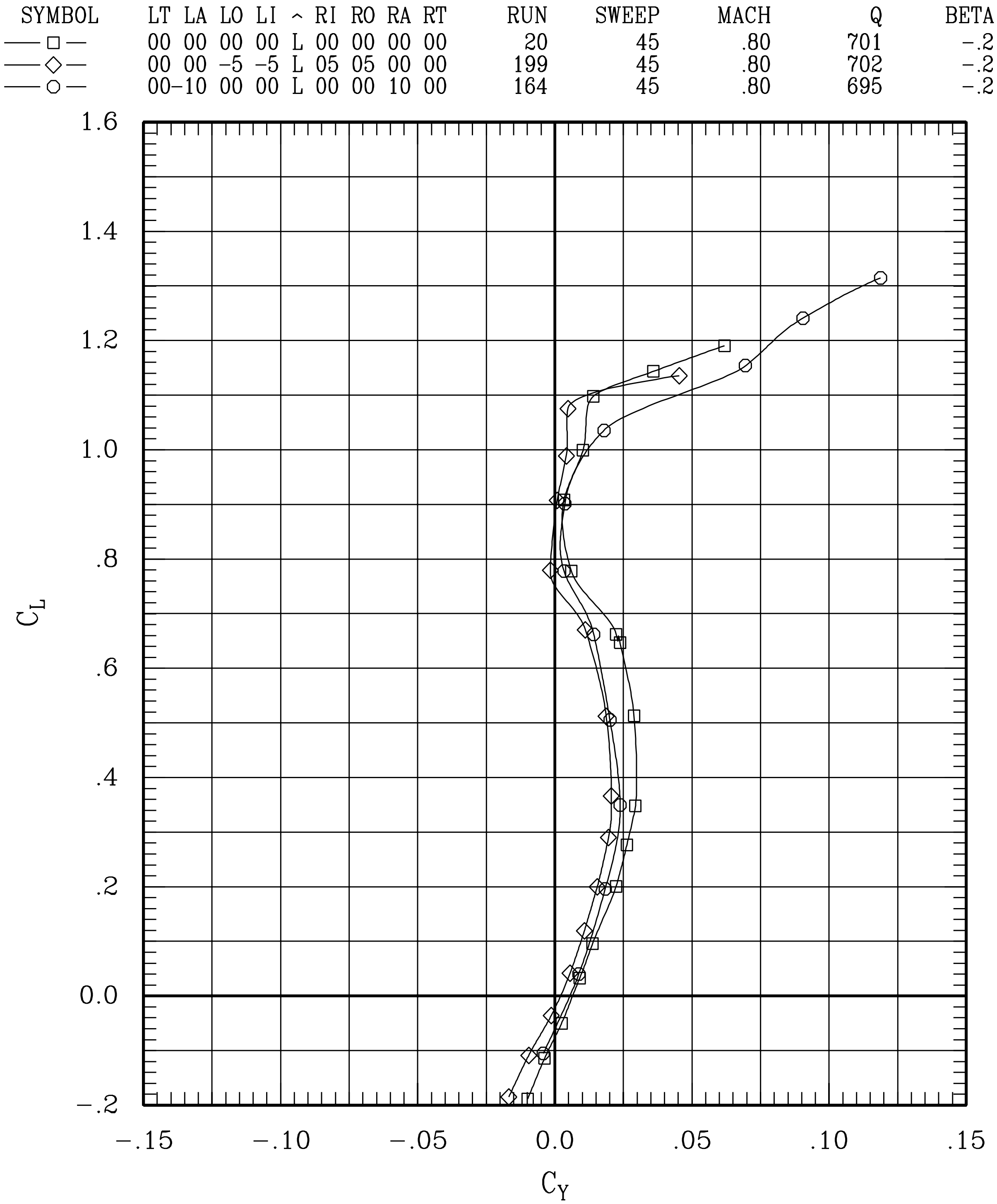

Figure 21(a). Effect of cruise flaps and ailerons for sweep = 45 deg, Mach = 0.80.

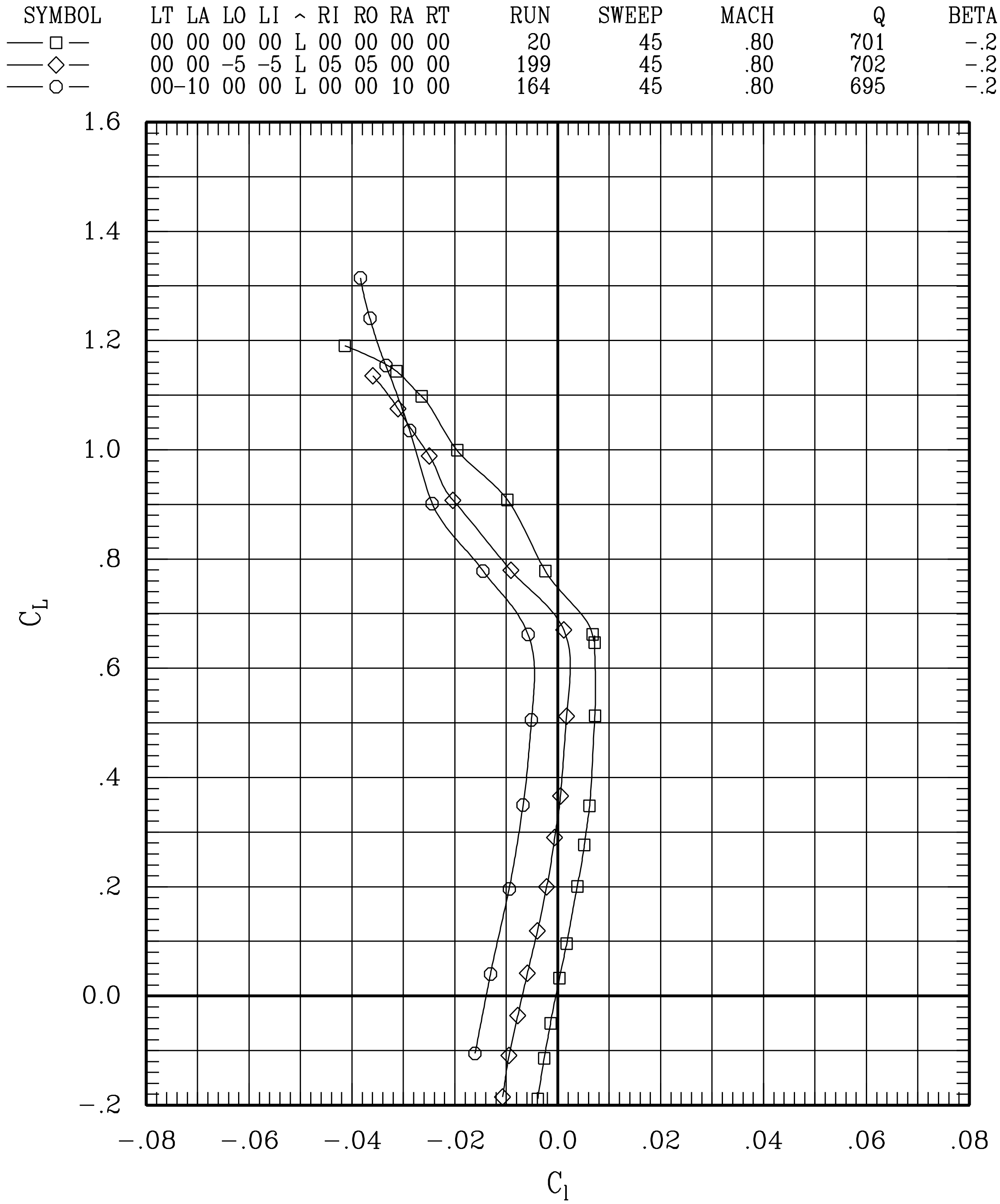

Figure 21(a). Effect of cruise flaps and ailerons for sweep = 45 deg, Mach = 0.80.

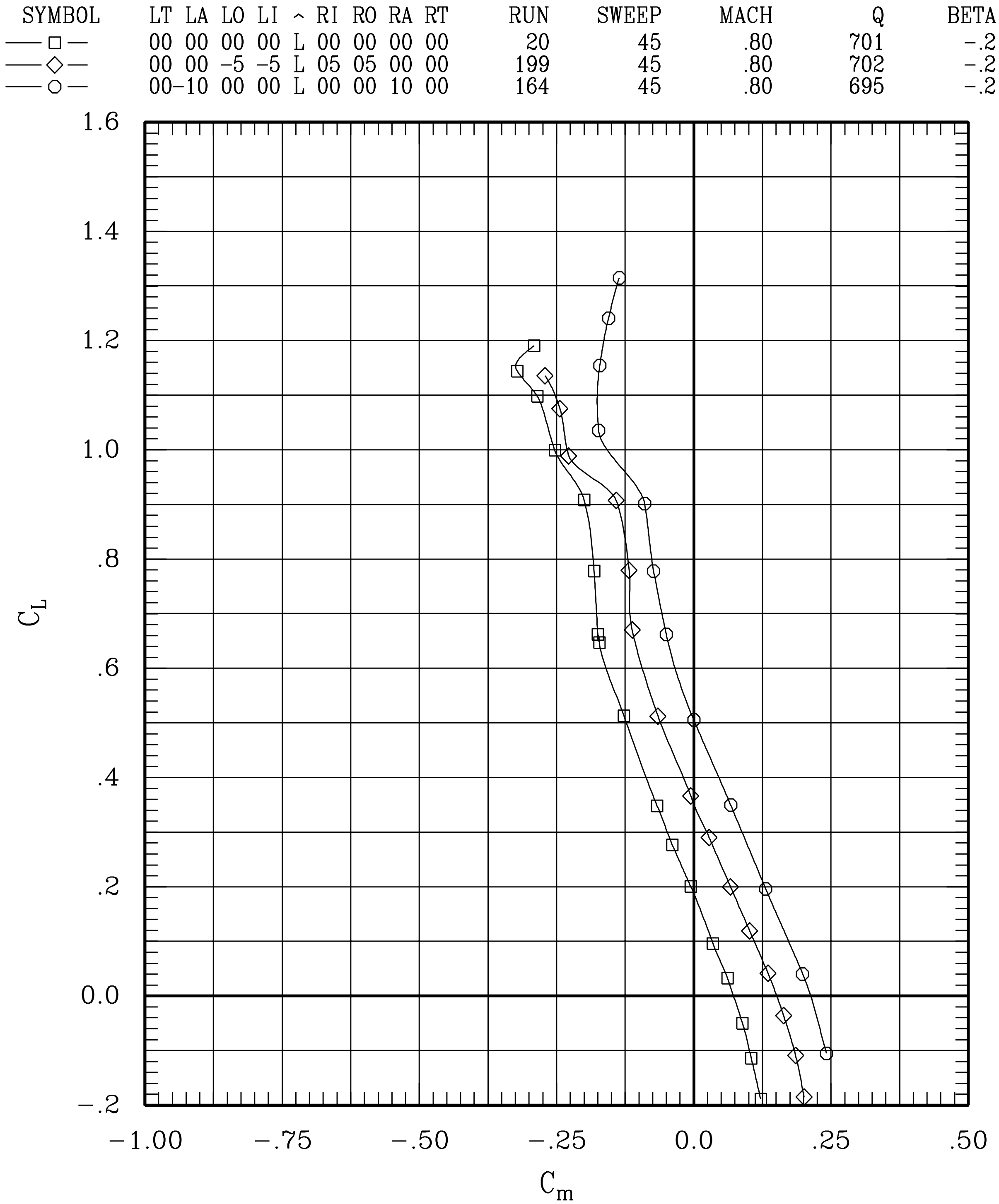

Figure 21(a). Effect of cruise flaps and ailerons for sweep = 45 deg, Mach = 0.80.

SYMBOL	LT LA LO LI ^ RI RO RA RT	RUN	SWEEP	MACH	Q	BETA
—□—	00 00 00 00 L 00 00 00 00	20	45	.80	701	−.2
—◇—	00 00 −5 −5 L 05 05 00 00	199	45	.80	702	−.2
—○—	00−10 00 00 L 00 00 10 00	164	45	.80	695	−.2

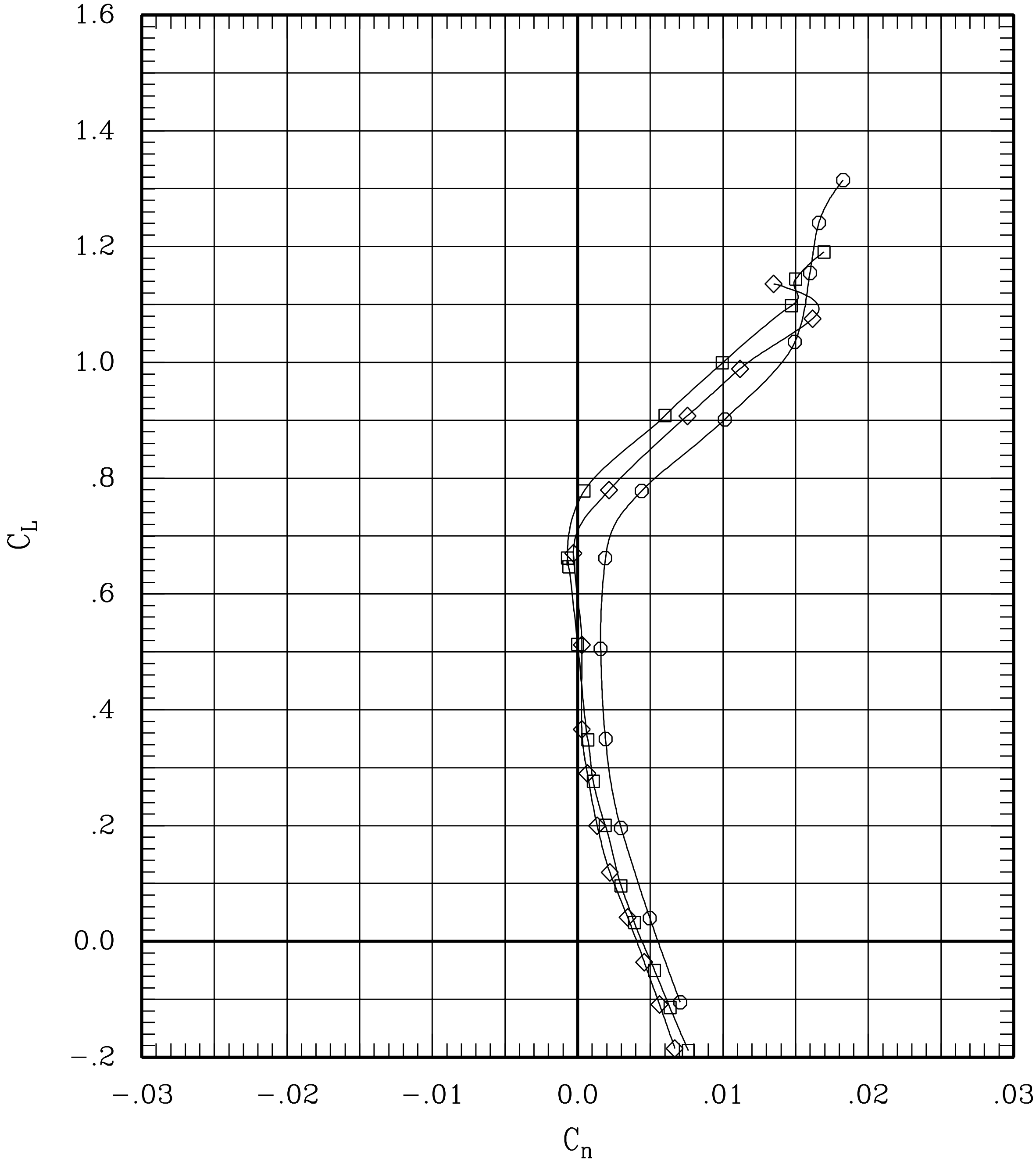

Figure 21(a). Effect of cruise flaps and ailerons for sweep = 45 deg, Mach = 0.80.

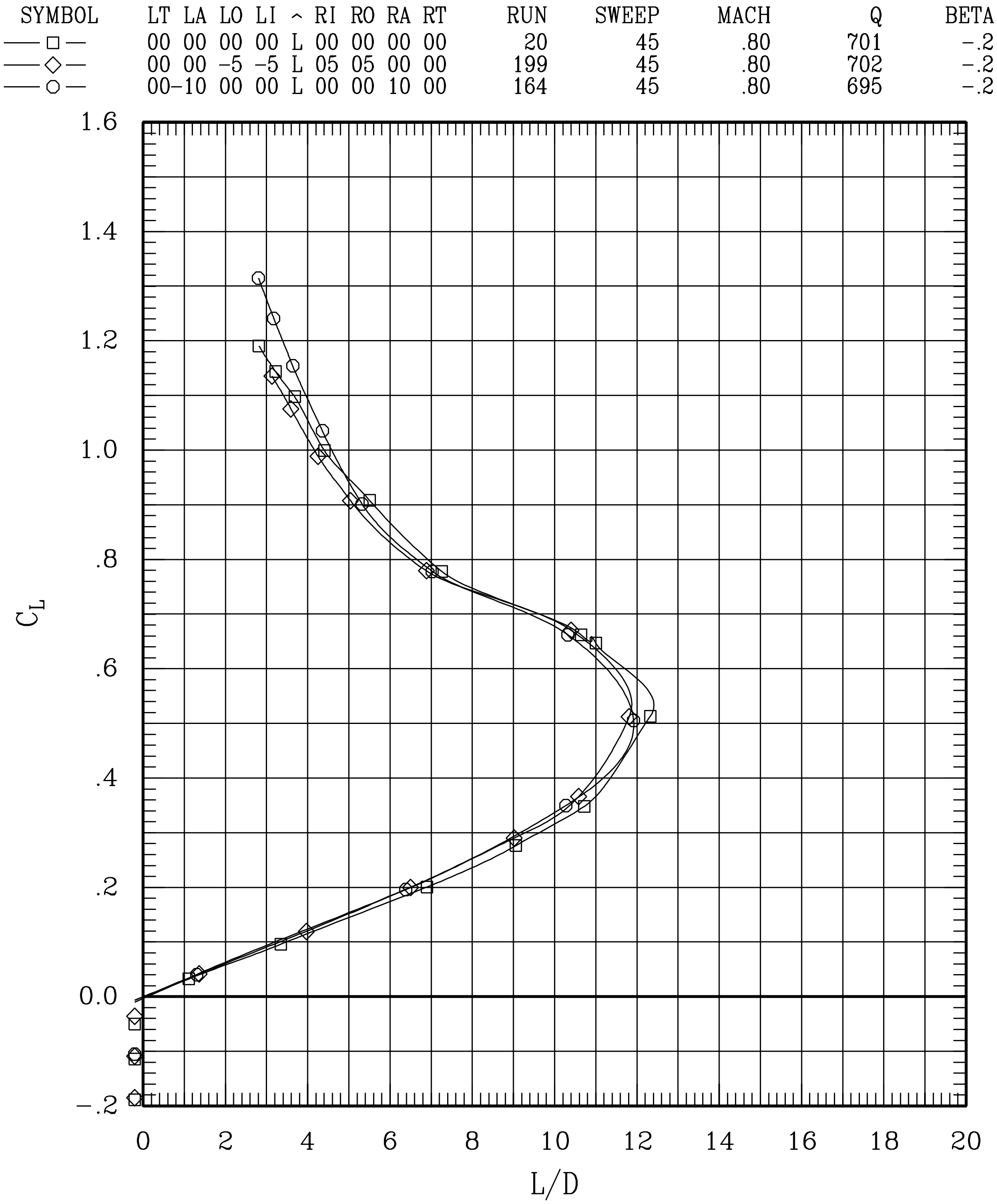

Figure 21(a). Effect of cruise flaps and ailerons for sweep = 45 deg, Mach = 0.80.

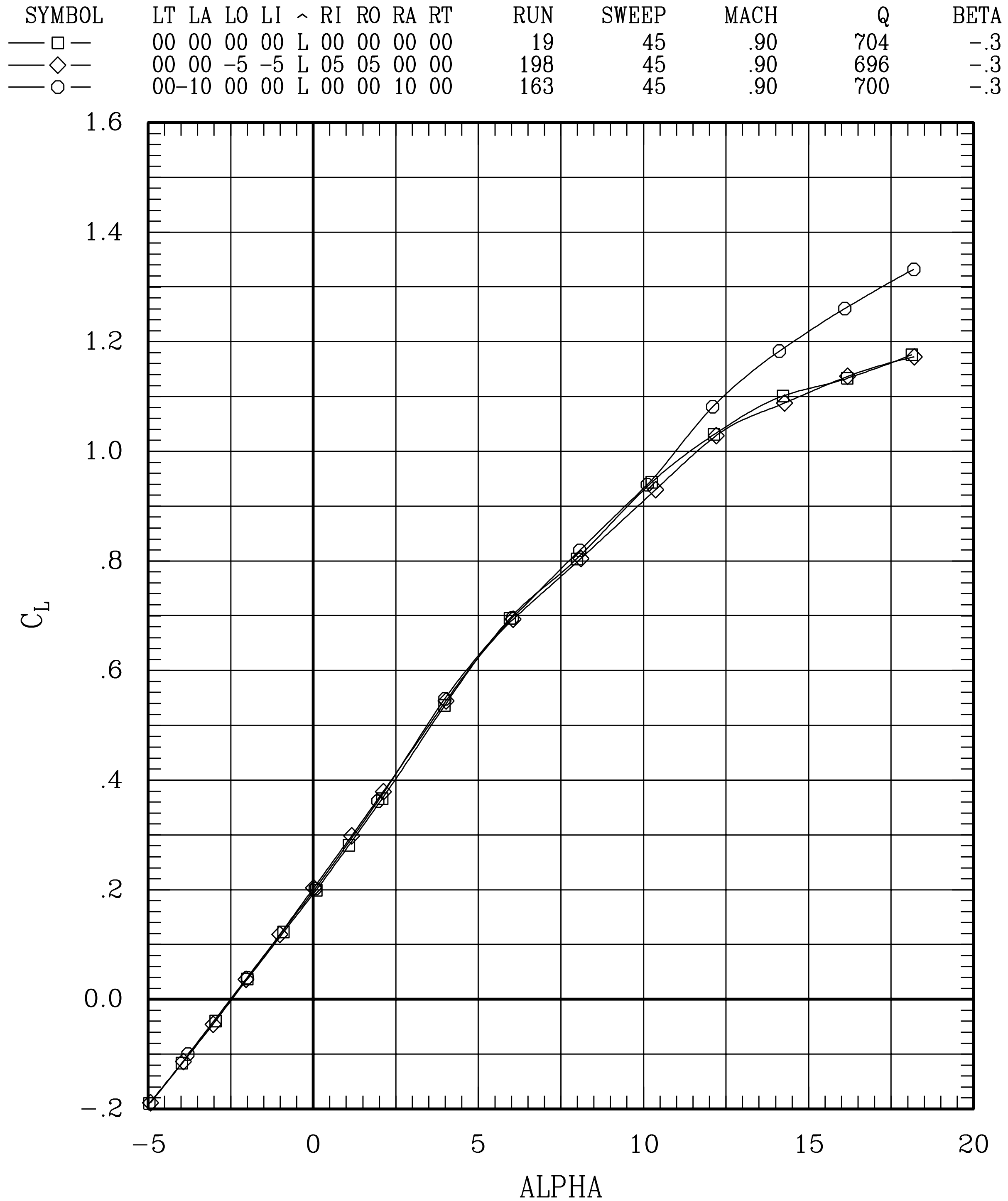

Figure 21(b). Effect of cruise flaps and ailerons for sweep = 45 deg, Mach = 0.90.

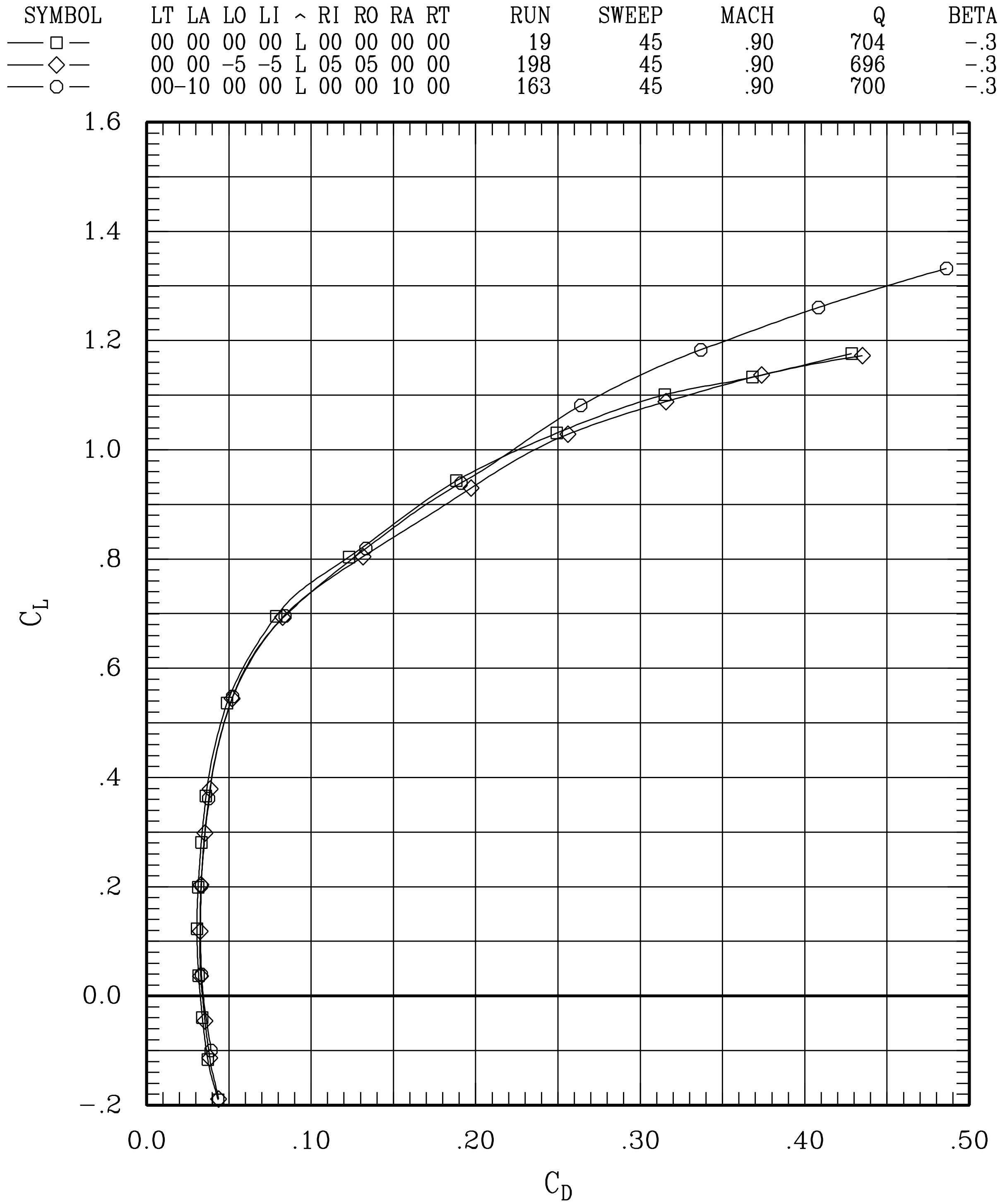

Figure 21(b). Effect of cruise flaps and ailerons for sweep = 45 deg, Mach = 0.90.

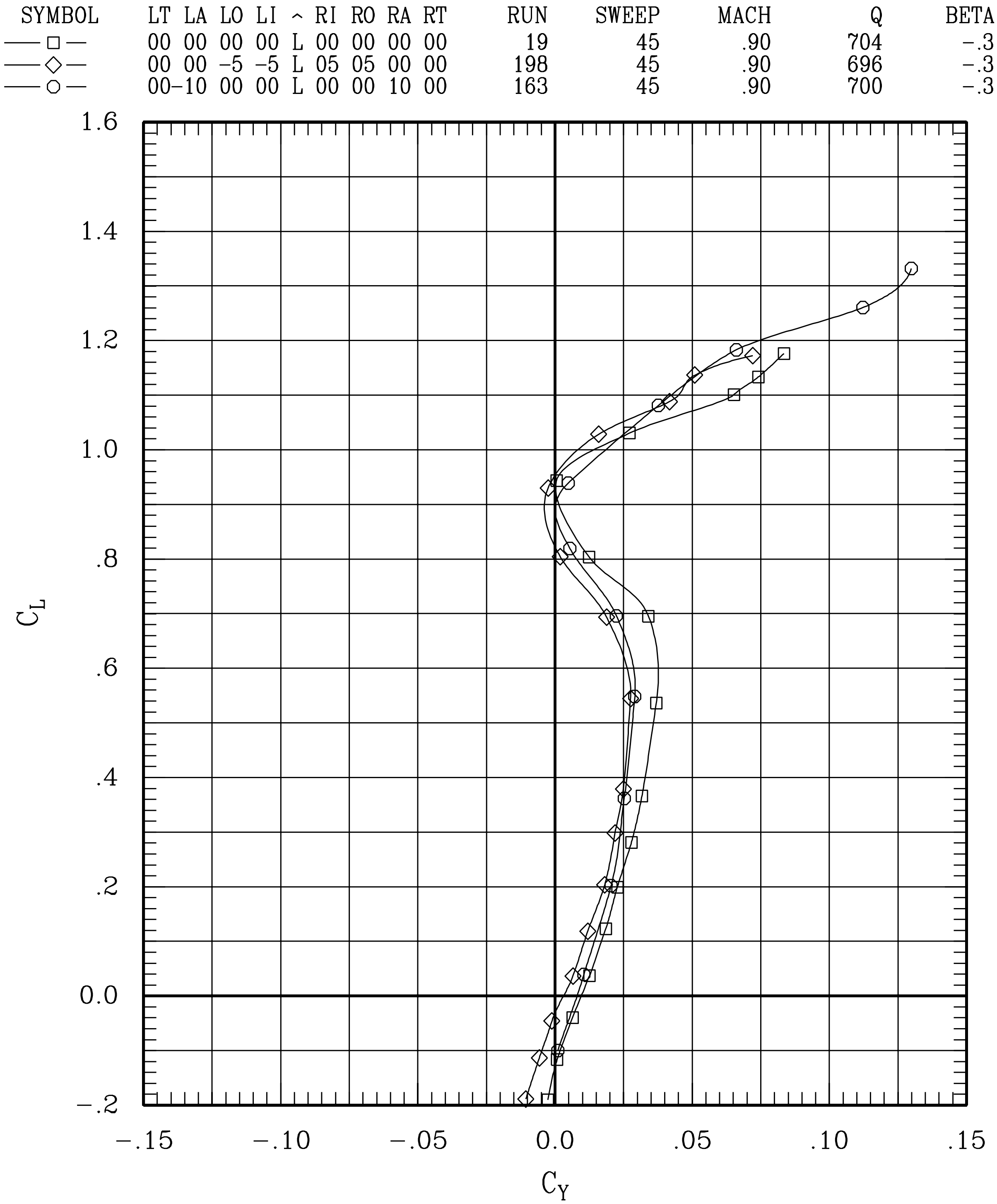

Figure 21(b). Effect of cruise flaps and ailerons for sweep = 45 deg, Mach = 0.90.

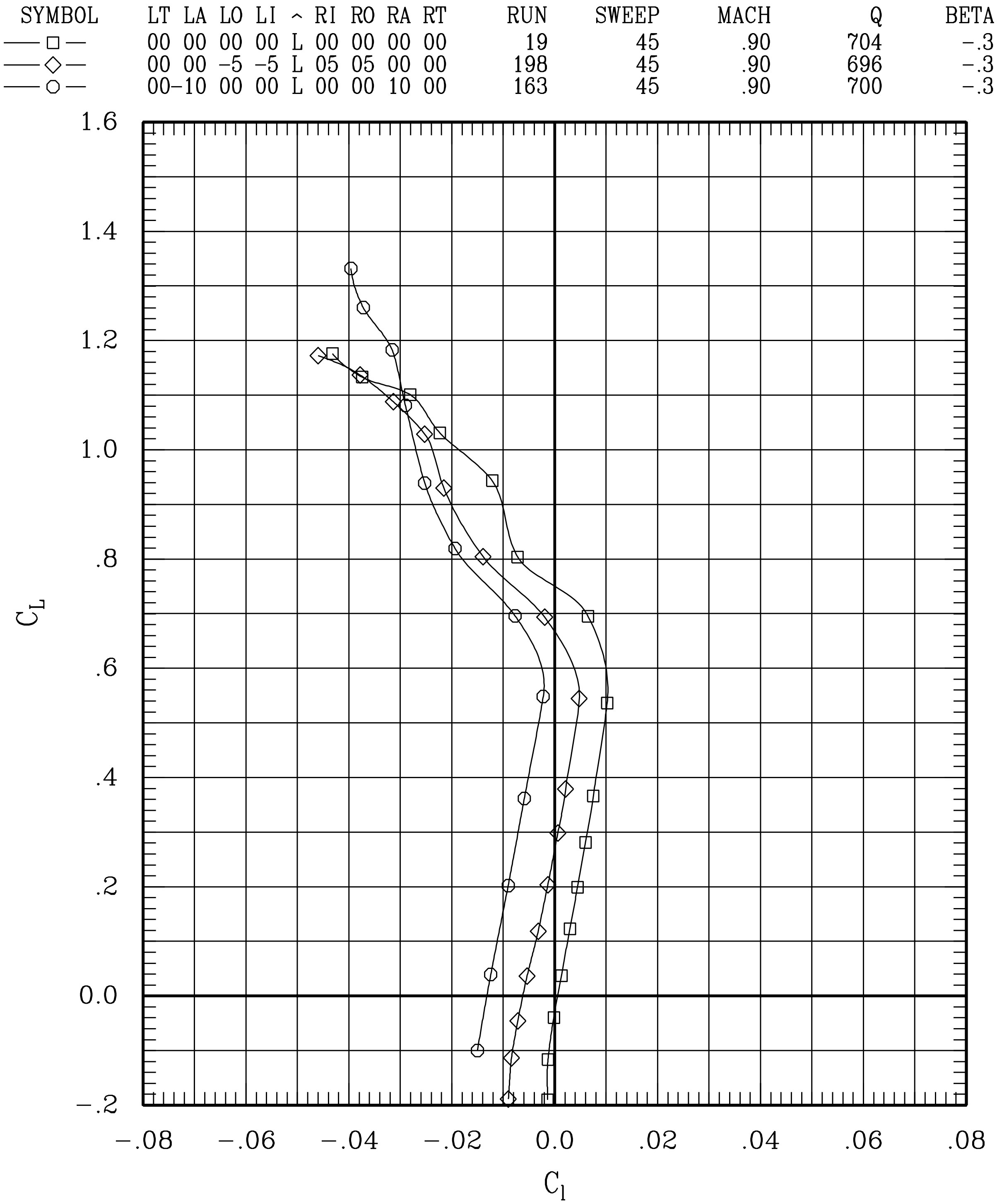

Figure 21(b). Effect of cruise flaps and ailerons for sweep = 45 deg, Mach = 0.90.

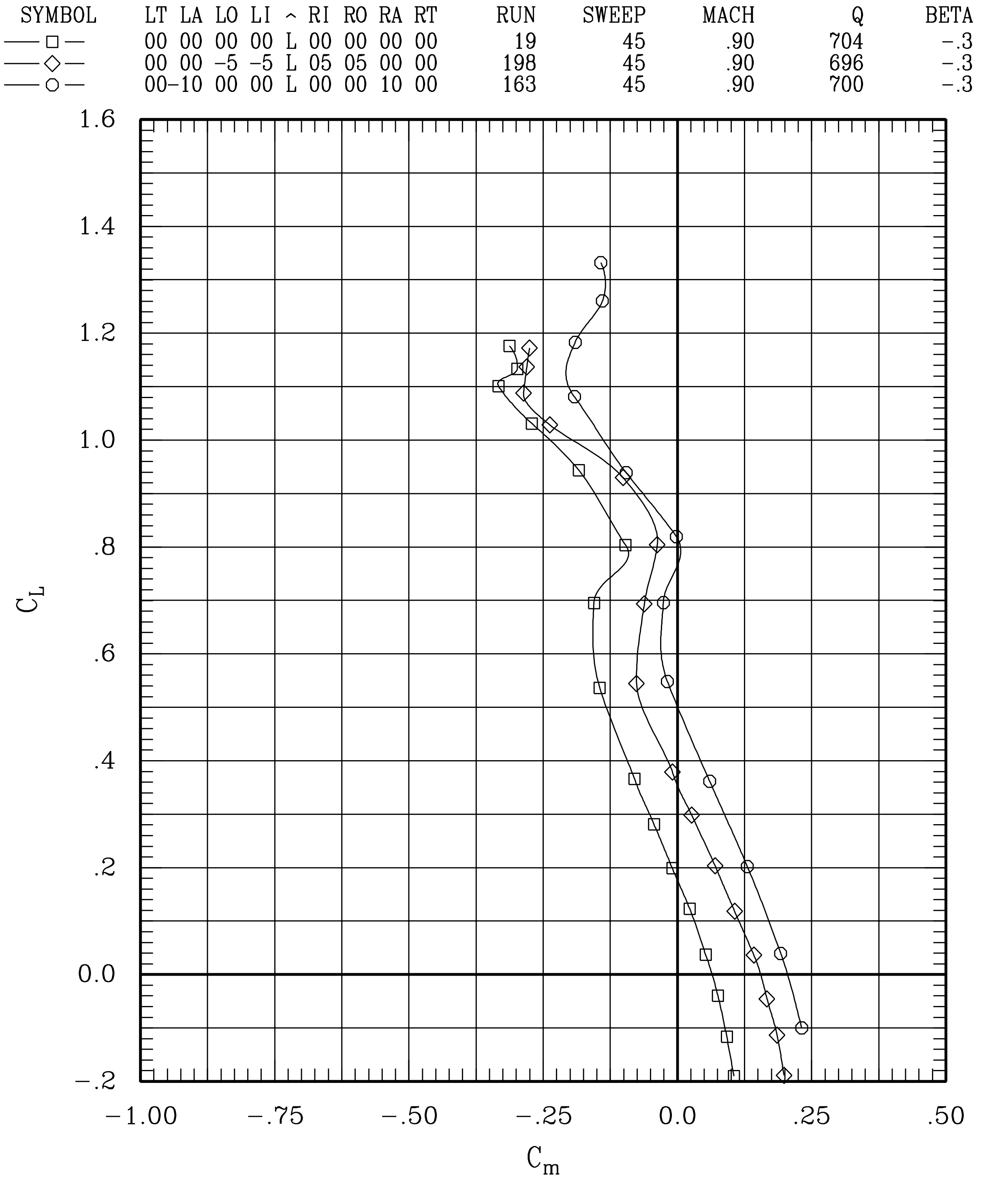

Figure 21(b). Effect of cruise flaps and ailerons for sweep = 45 deg, Mach = 0.90.

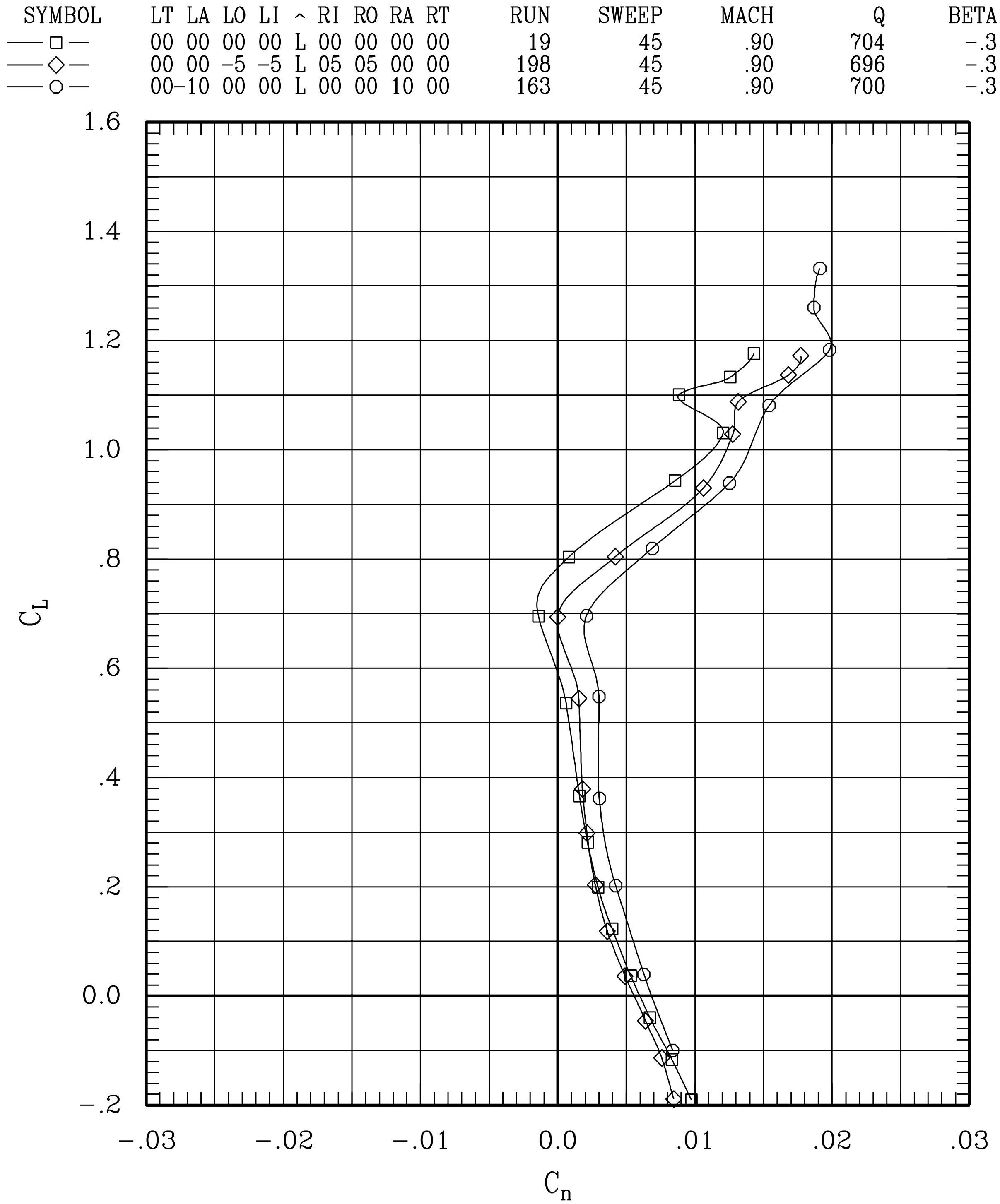

Figure 21(b). Effect of cruise flaps and ailerons for sweep = 45 deg, Mach = 0.90.

SYMBOL	LT LA LO LI ^ RI RO RA RT	RUN	SWEEP	MACH	Q	BETA
—□—	00 00 00 00 L 00 00 00 00	19	45	.90	704	−.3
—◇—	00 00 −5 −5 L 05 05 00 00	198	45	.90	696	−.3
—○—	00−10 00 00 L 00 00 10 00	163	45	.90	700	−.3

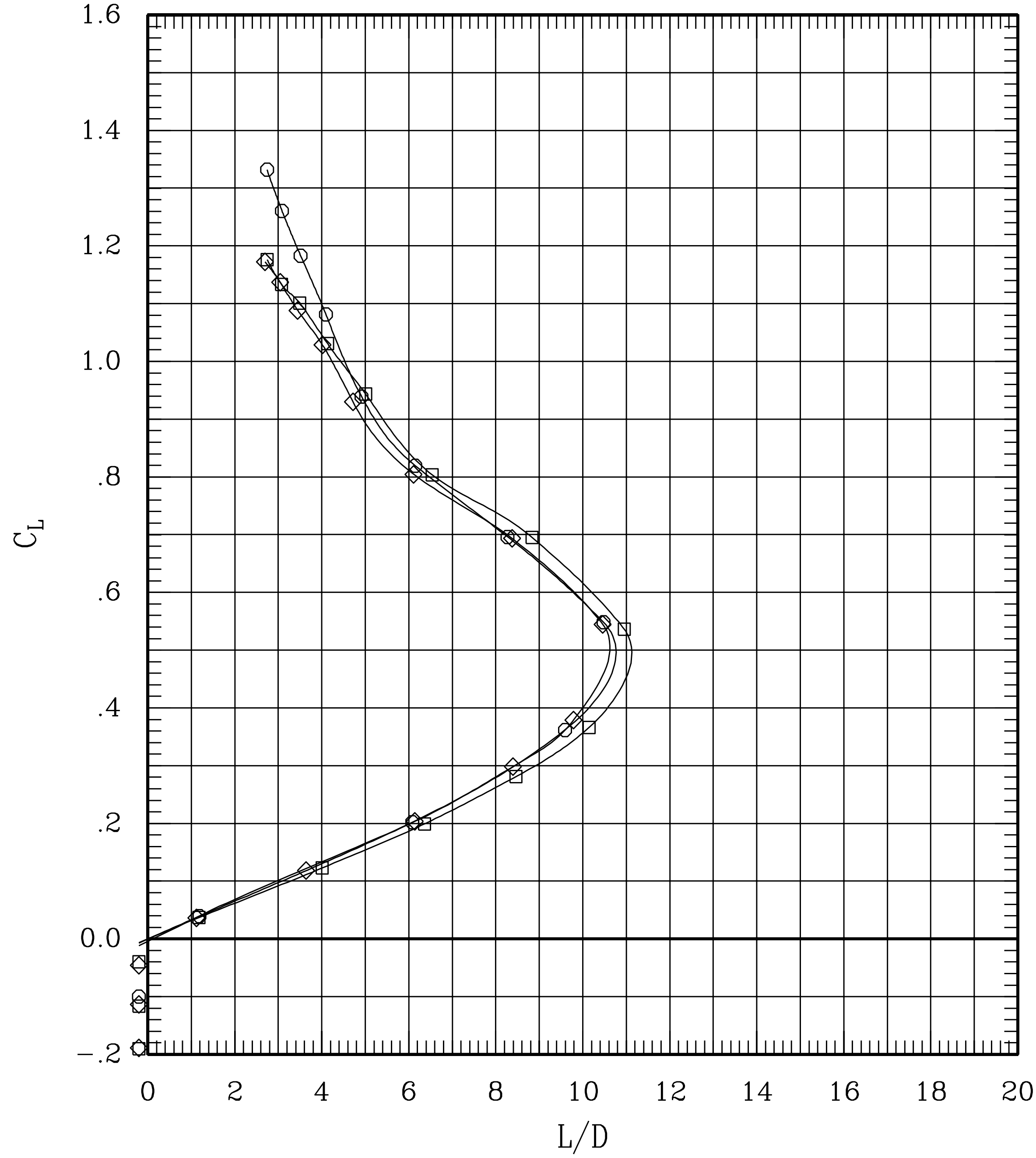

Figure 21(b). Effect of cruise flaps and ailerons for sweep = 45 deg, Mach = 0.90.

SYMBOL	LT LA LO LI ^ RI RO RA RT	RUN	SWEEP	MACH	Q	BETA
—□—	00 00 00 00 L 00 00 00 00	18	45	.95	705	−.3
—◇—	00 00 −5 −5 L 05 05 00 00	197	45	.95	700	−.3
—○—	00−10 00 00 L 00 00 10 00	162	45	.95	693	−.3

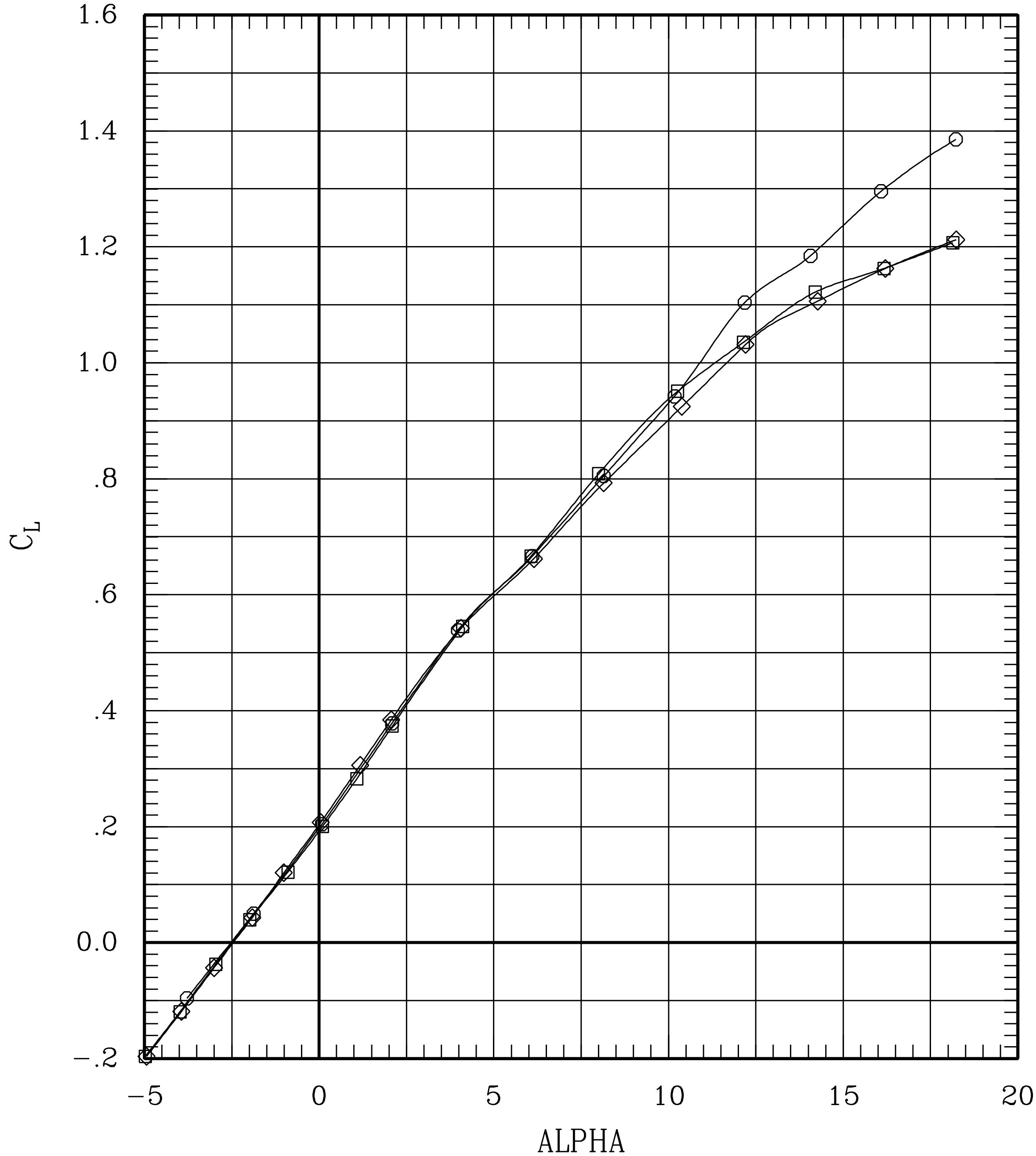

Figure 21(c). Effect of cruise flaps and ailerons for sweep = 45 deg, Mach = 0.95.

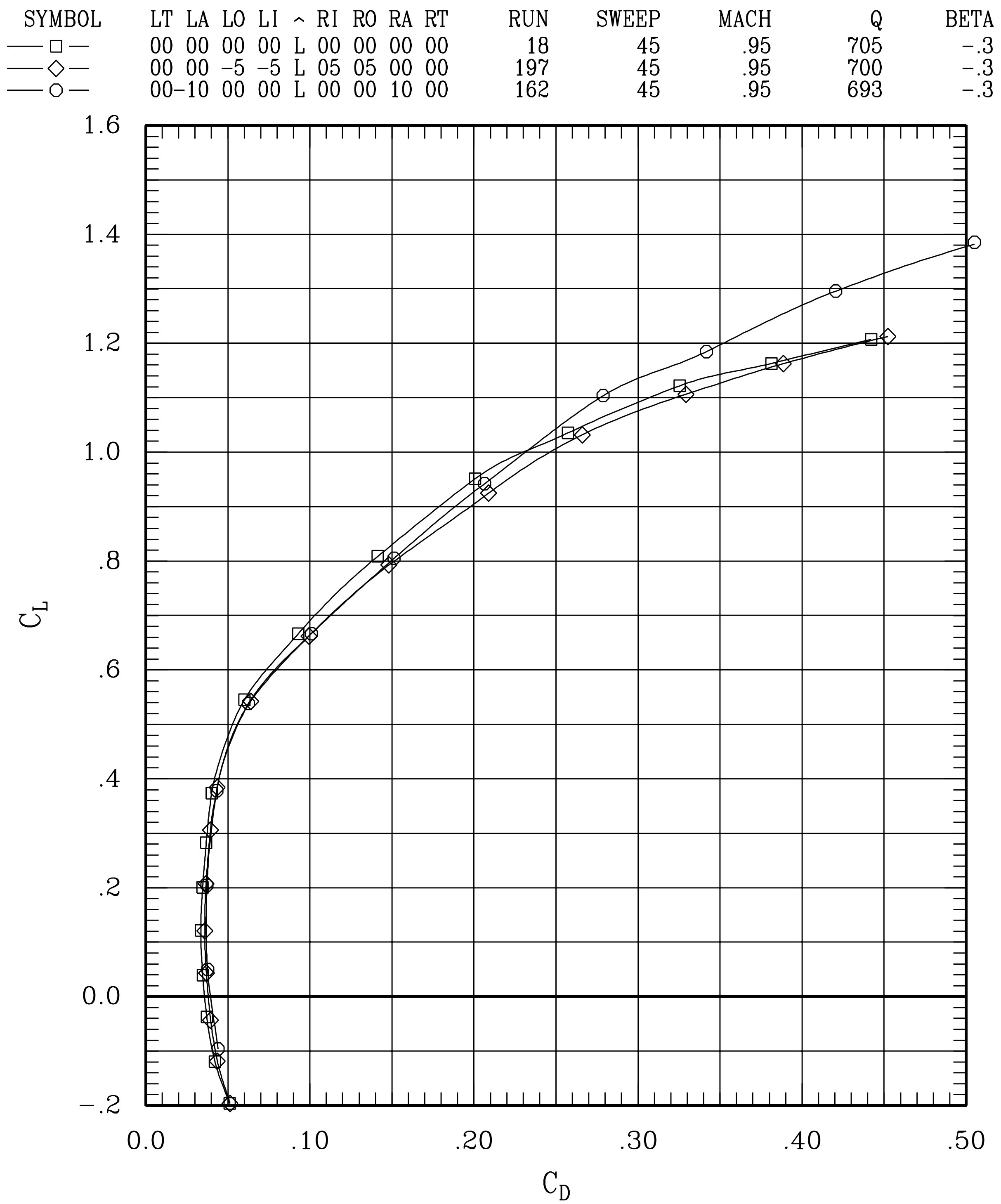

Figure 21(c). Effect of cruise flaps and ailerons for sweep = 45 deg, Mach = 0.95.

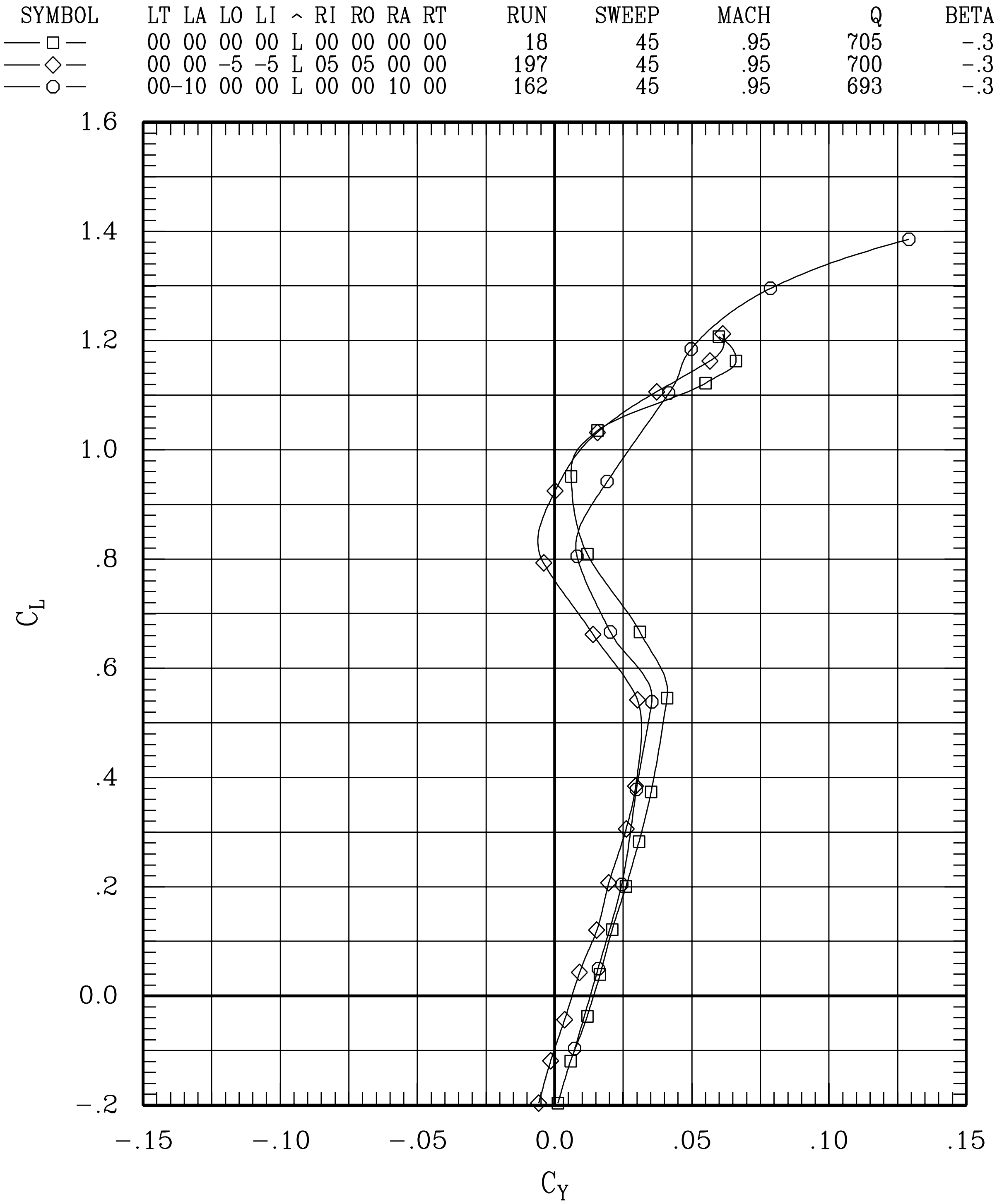

Figure 21(c). Effect of cruise flaps and ailerons for sweep = 45 deg, Mach = 0.95.

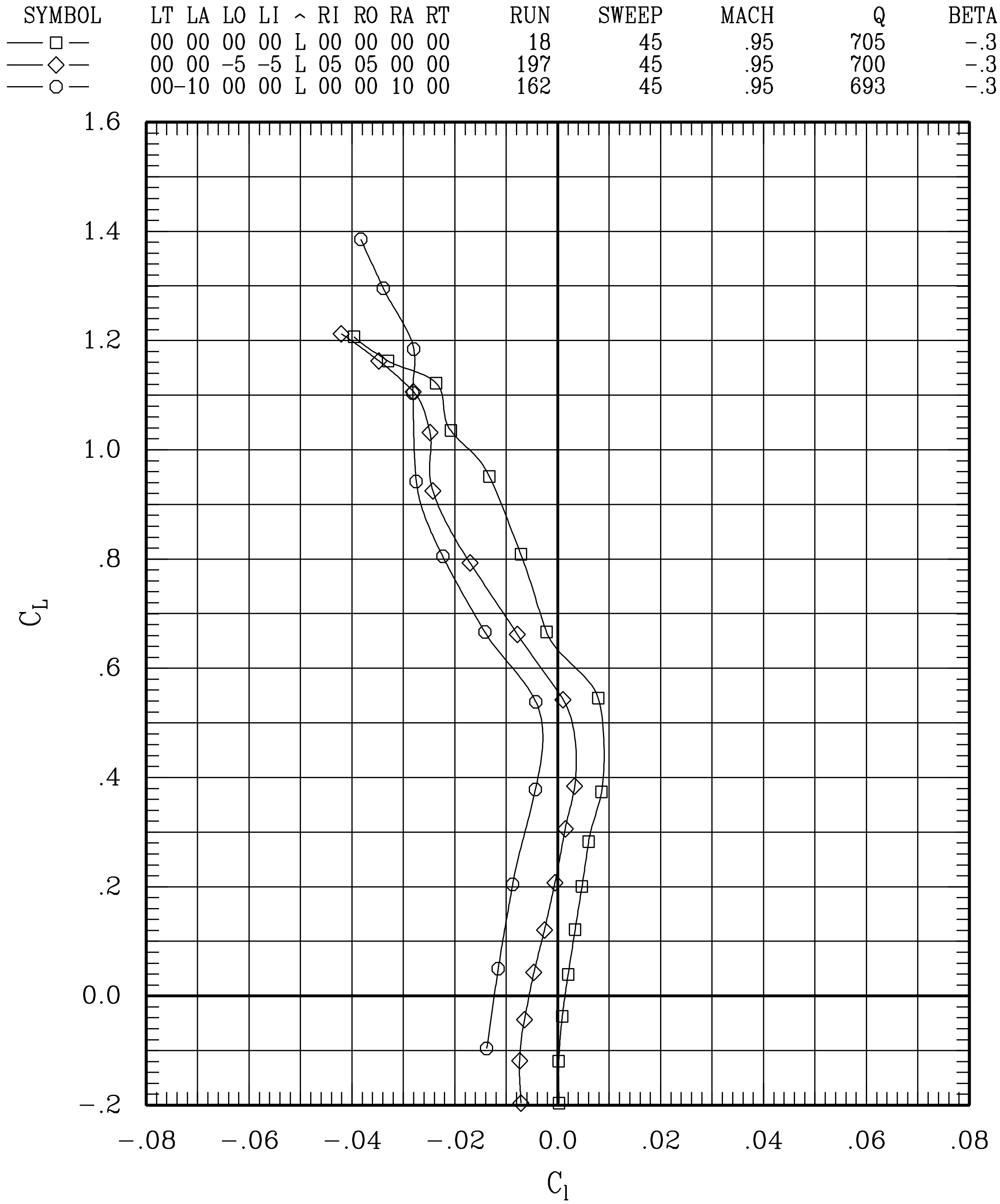

Figure 21(c). Effect of cruise flaps and ailerons for sweep = 45 deg, Mach = 0.95.

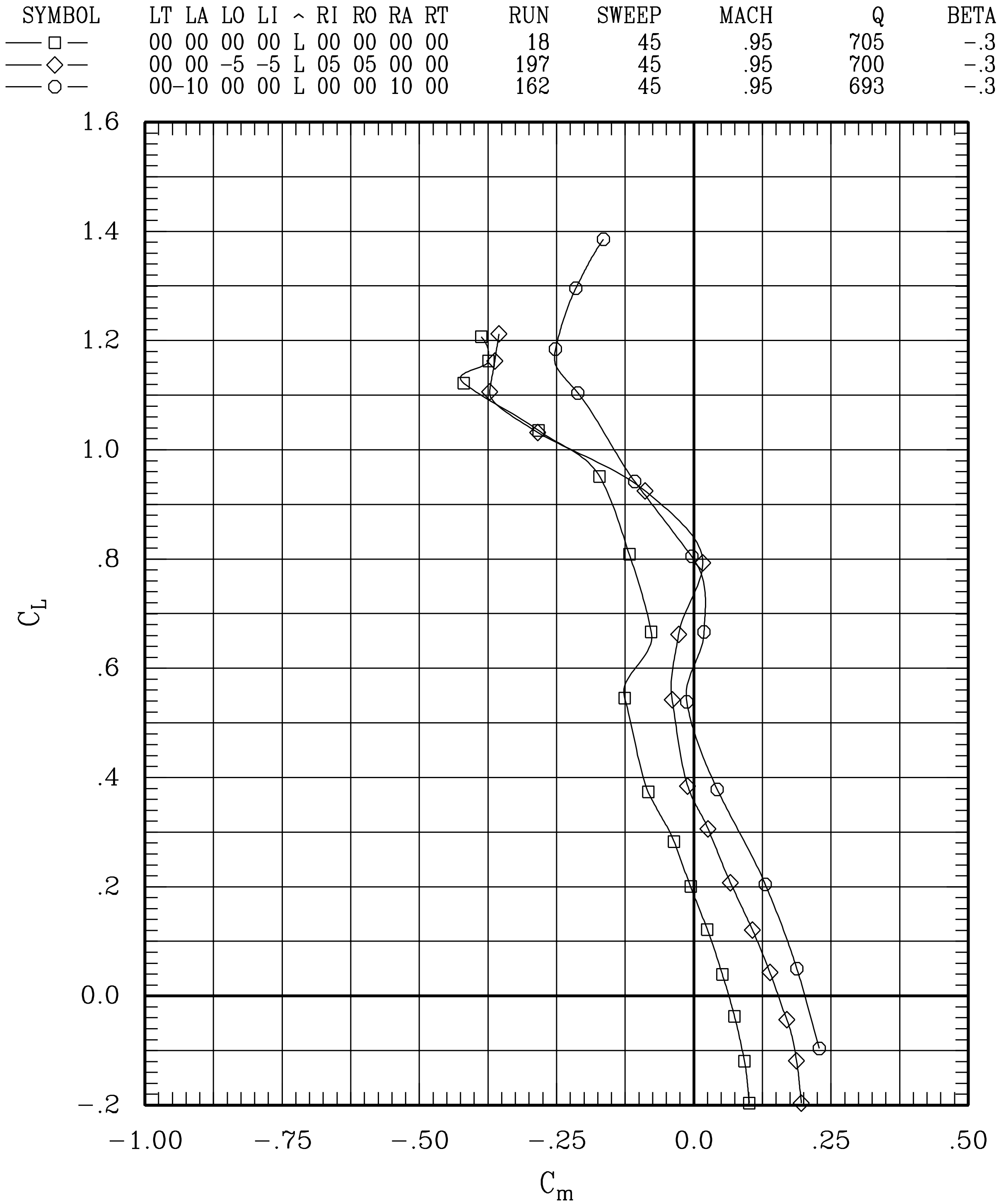

Figure 21(c). Effect of cruise flaps and ailerons for sweep = 45 deg, Mach = 0.95.

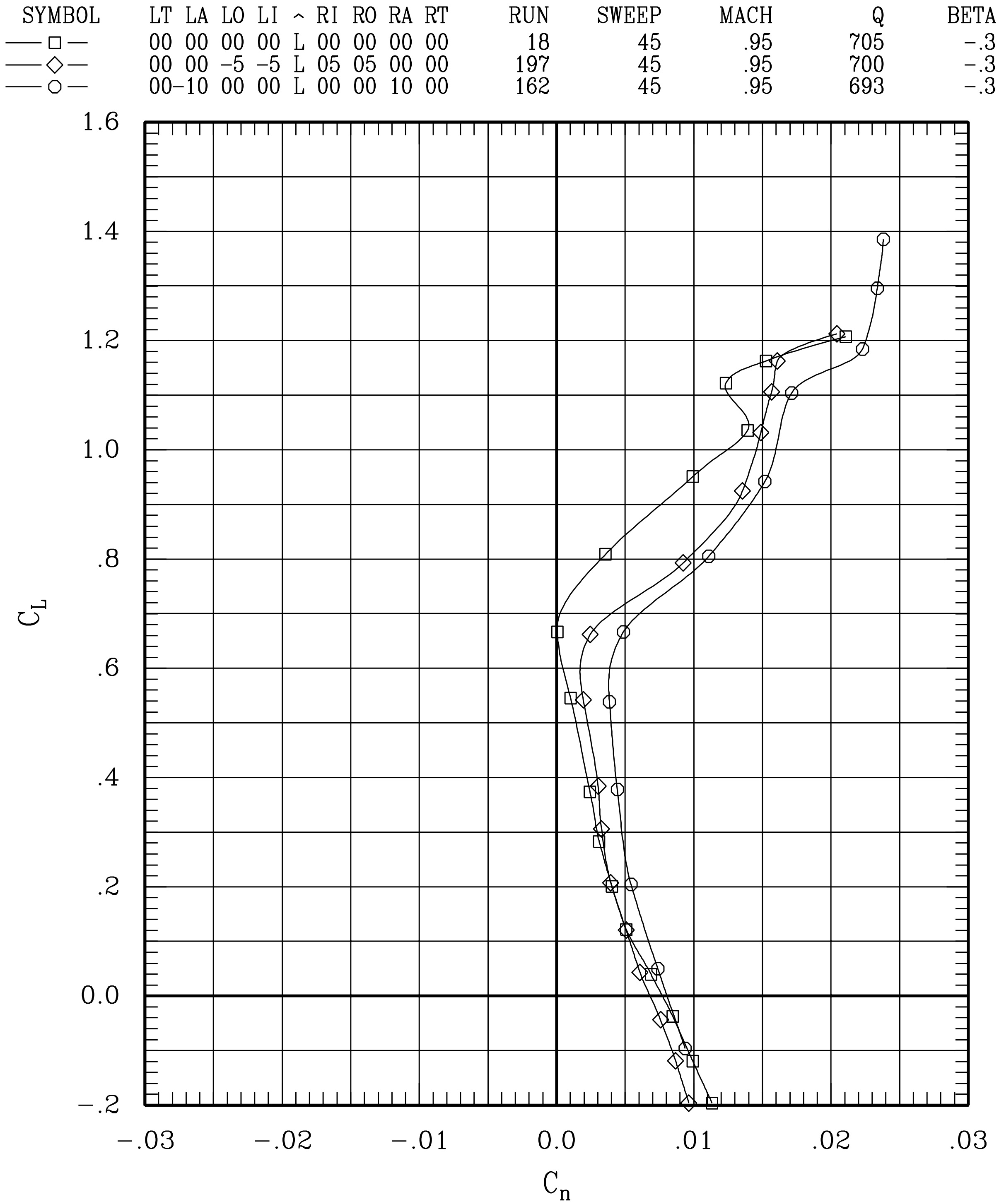

Figure 21(c). Effect of cruise flaps and ailerons for sweep = 45 deg, Mach = 0.95.

SYMBOL	LT LA LO LI ^ RI RO RA RT	RUN	SWEEP	MACH	Q	BETA
—□—	00 00 00 00 L 00 00 00 00	18	45	.95	705	-.3
—◇—	00 00 -5 -5 L 05 05 00 00	197	45	.95	700	-.3
—○—	00-10 00 00 L 00 00 10 00	162	45	.95	693	-.3

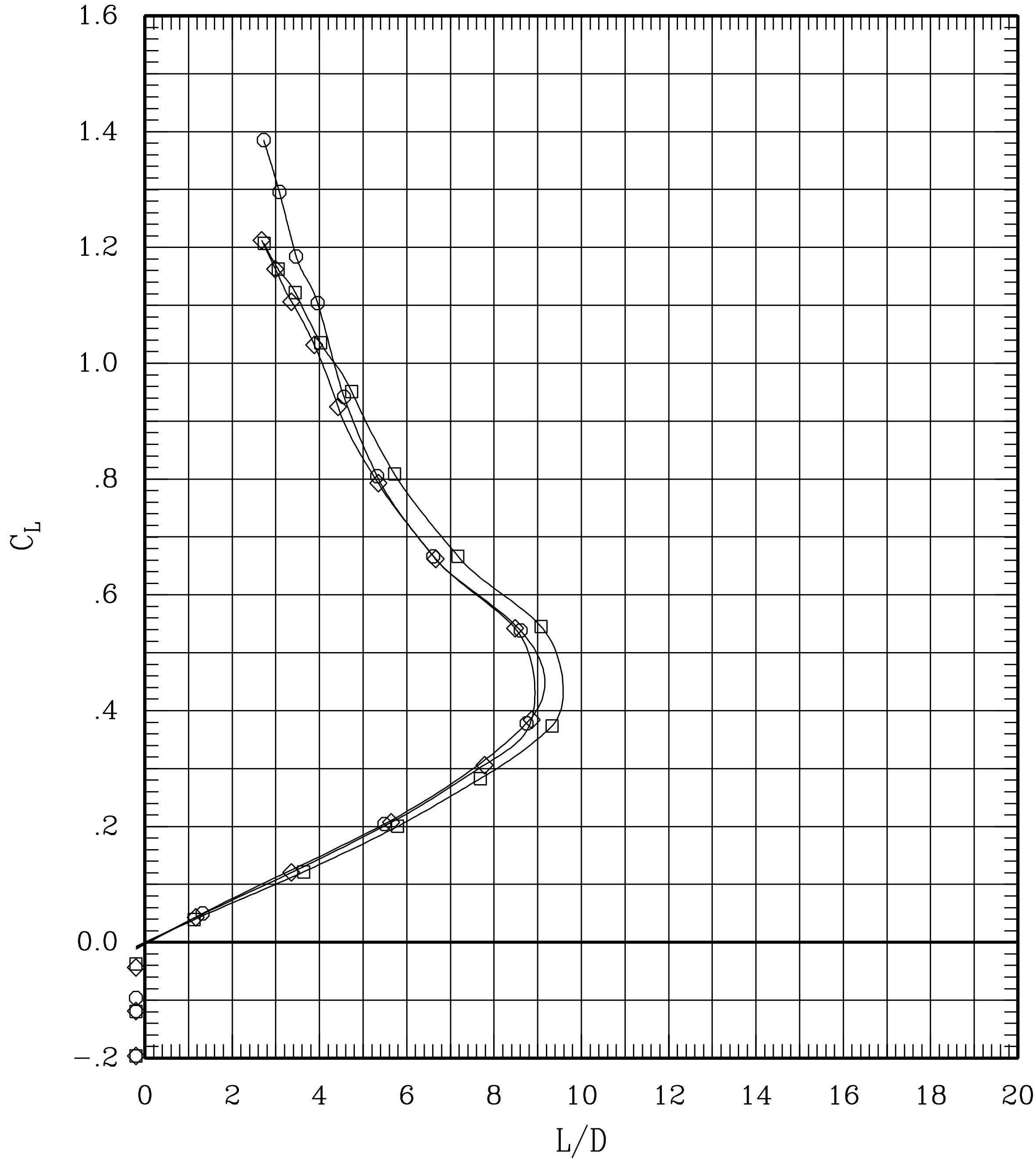

Figure 21(c). Effect of cruise flaps and ailerons for sweep = 45 deg, Mach = 0.95.

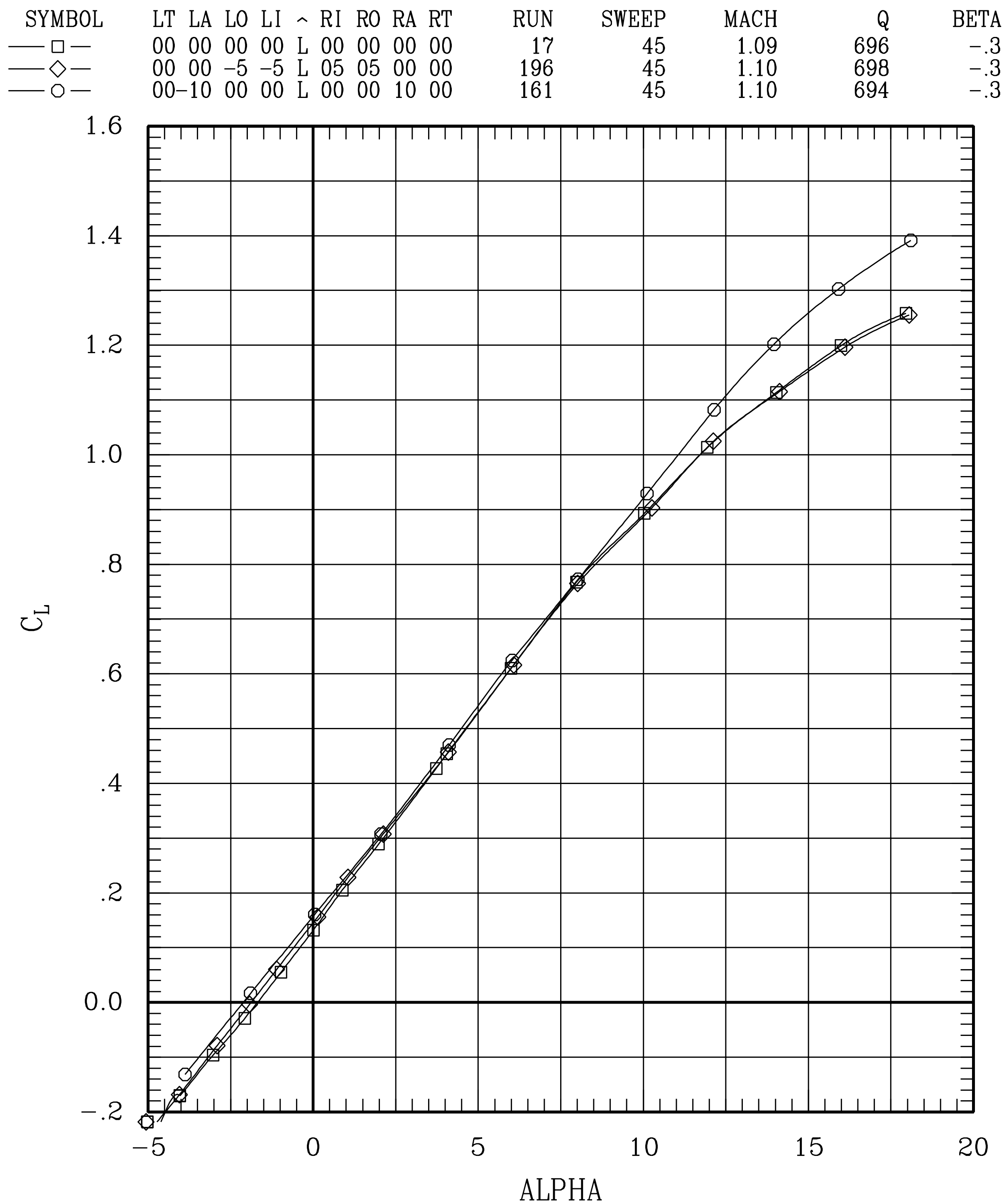

Figure 21(d). Effect of cruise flaps and ailerons for sweep = 45 deg, Mach = 1.10.

SYMBOL	LT LA LO LI ^ RI RO RA RT	RUN	SWEEP	MACH	Q	BETA
—□—	00 00 00 00 L 00 00 00 00	17	45	1.09	696	-.3
—◇—	00 00 -5 -5 L 05 05 00 00	196	45	1.10	698	-.3
—○—	00-10 00 00 L 00 00 10 00	161	45	1.10	694	-.3

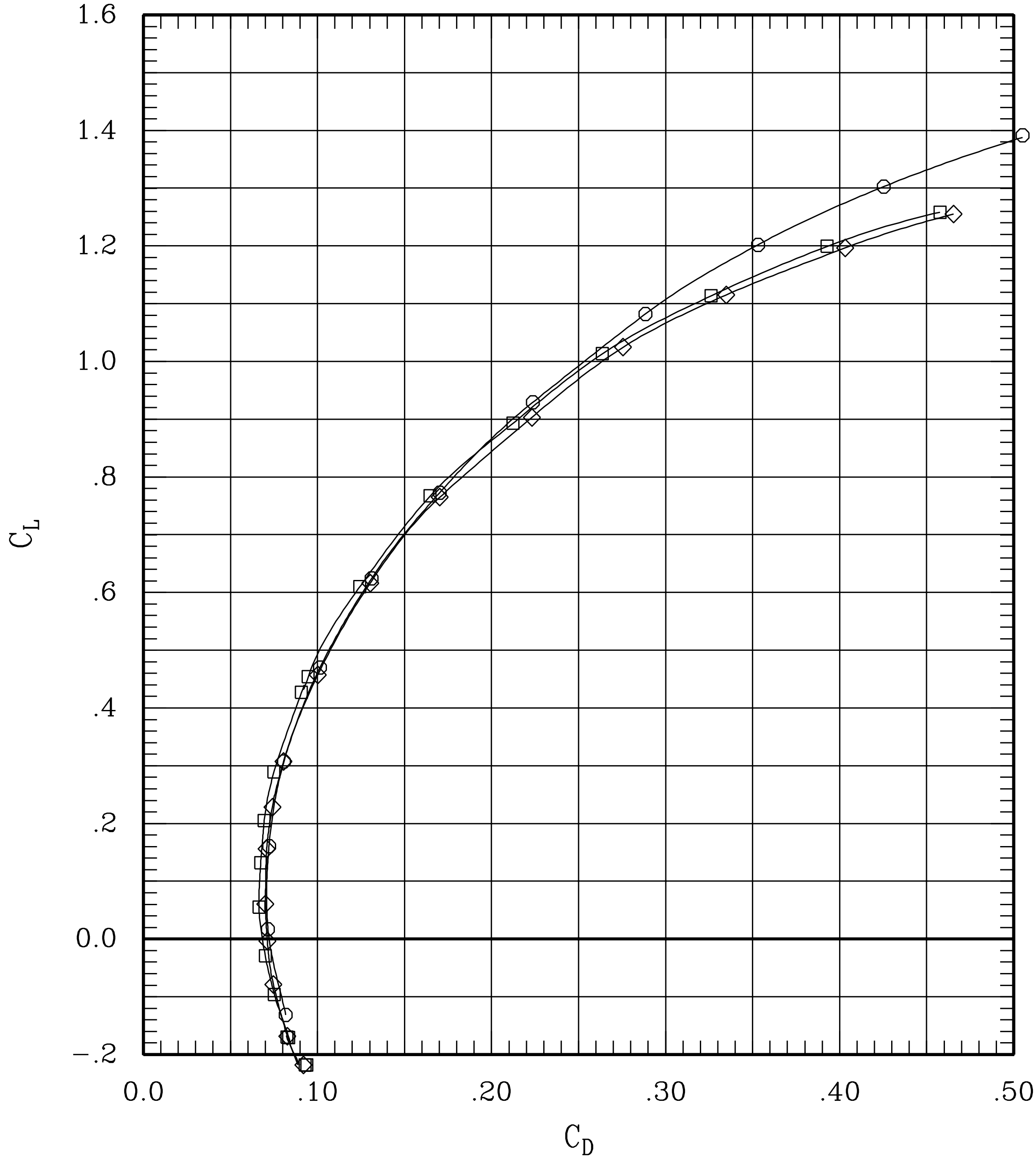

Figure 21(d). Effect of cruise flaps and ailerons for sweep = 45 deg, Mach = 1.10.

SYMBOL	LT LA LO LI ^ RI RO RA RT	RUN	SWEEP	MACH	Q	BETA
—□—	00 00 00 00 L 00 00 00 00	17	45	1.09	696	−.3
—◇—	00 00 −5 −5 L 05 05 00 00	196	45	1.10	698	−.3
—○—	00−10 00 00 L 00 00 10 00	161	45	1.10	694	−.3

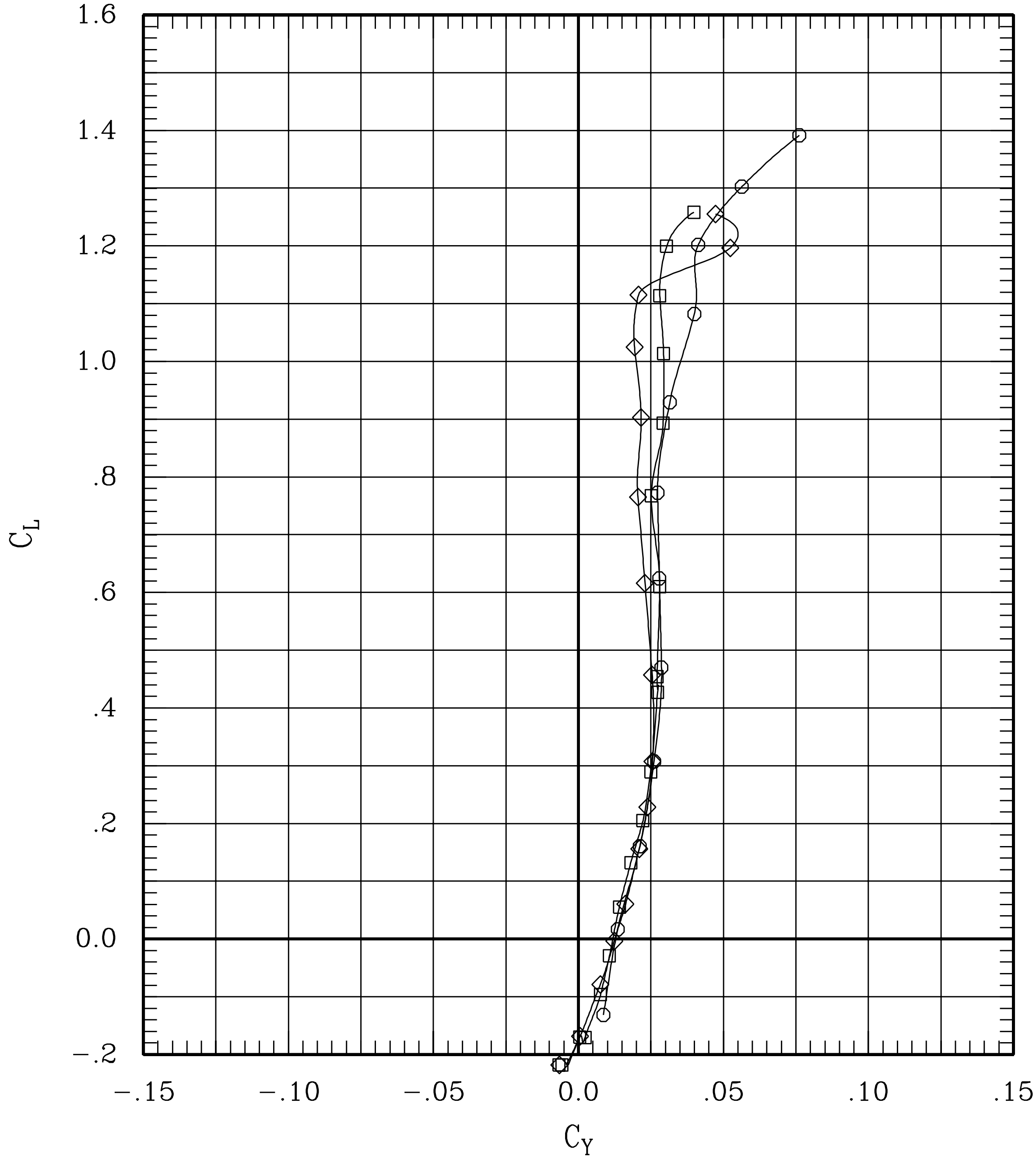

Figure 21(d). Effect of cruise flaps and ailerons for sweep = 45 deg, Mach = 1.10.

SYMBOL	LT LA LO LI ^ RI RO RA RT	RUN	SWEEP	MACH	Q	BETA
—□—	00 00 00 00 L 00 00 00 00	17	45	1.09	696	−.3
—◇—	00 00 −5 −5 L 05 05 00 00	196	45	1.10	698	−.3
—○—	00−10 00 00 L 00 00 10 00	161	45	1.10	694	−.3

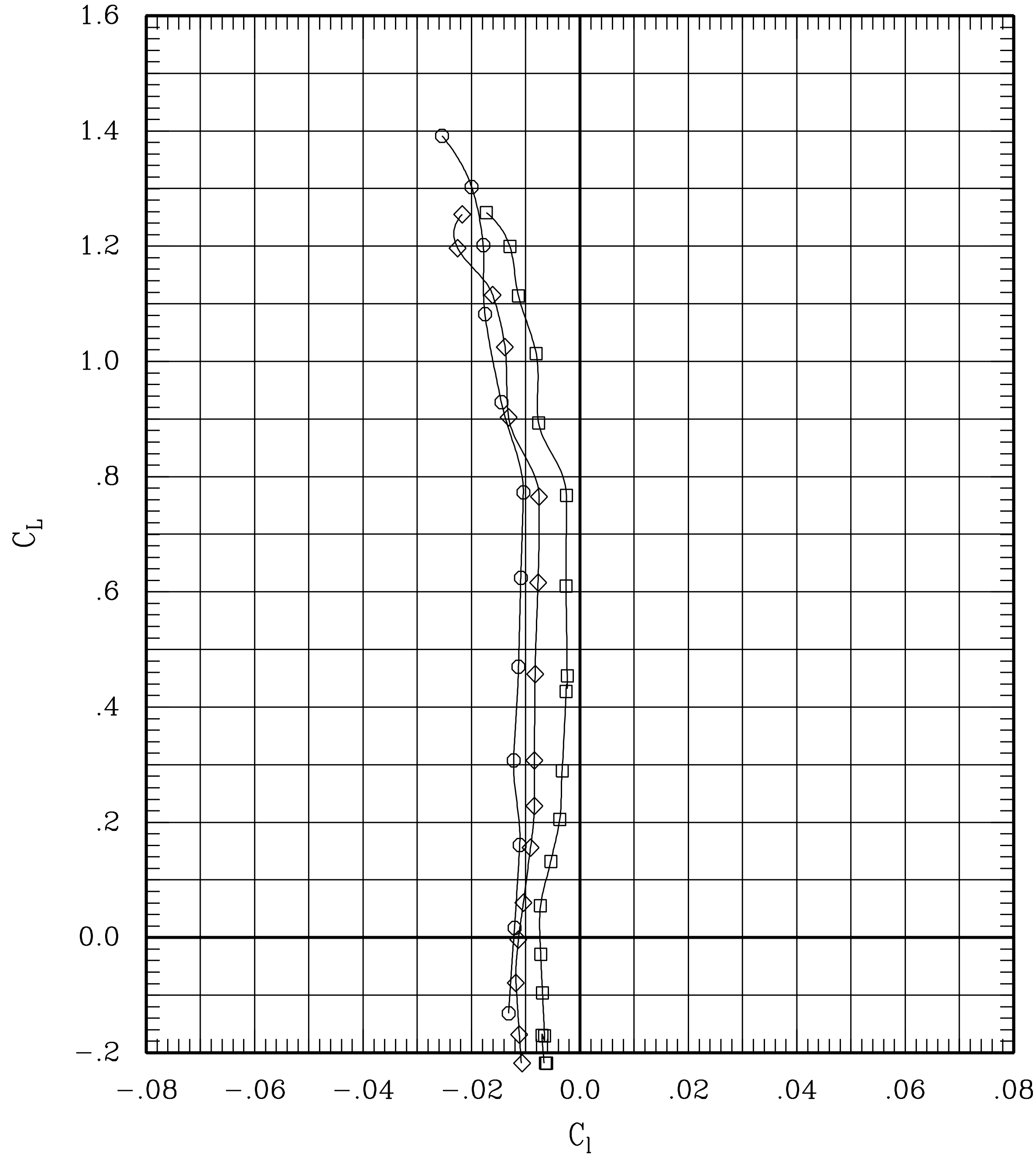

Figure 21(d). Effect of cruise flaps and ailerons for sweep = 45 deg, Mach = 1.10.

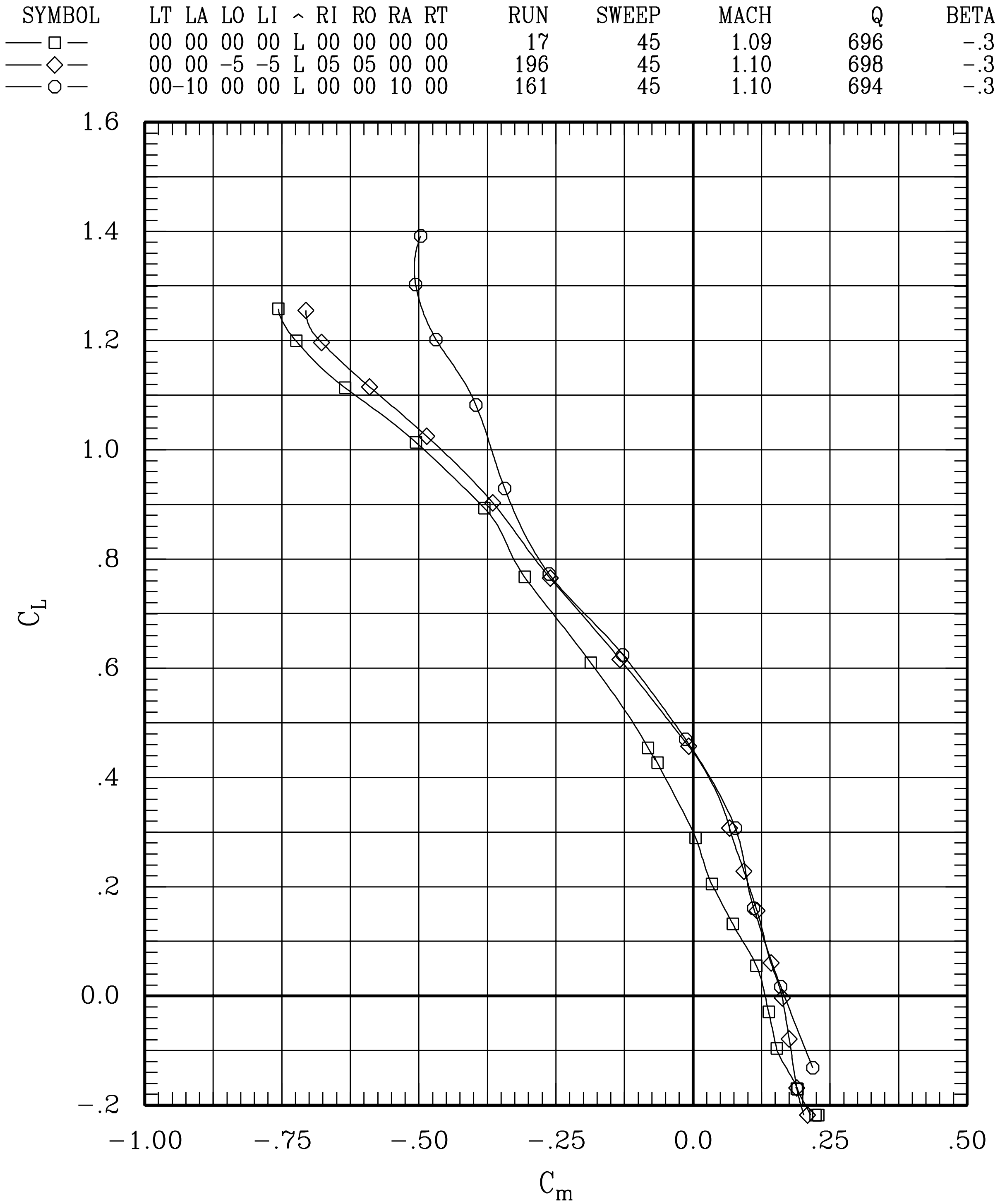

Figure 21(d). Effect of cruise flaps and ailerons for sweep = 45 deg, Mach = 1.10.

SYMBOL	LT LA LO LI ^ RI RO RA RT	RUN	SWEEP	MACH	Q	BETA
—□—	00 00 00 00 L 00 00 00 00	17	45	1.09	696	−.3
—◇—	00 00 −5 −5 L 05 05 00 00	196	45	1.10	698	−.3
—○—	00−10 00 00 L 00 00 10 00	161	45	1.10	694	−.3

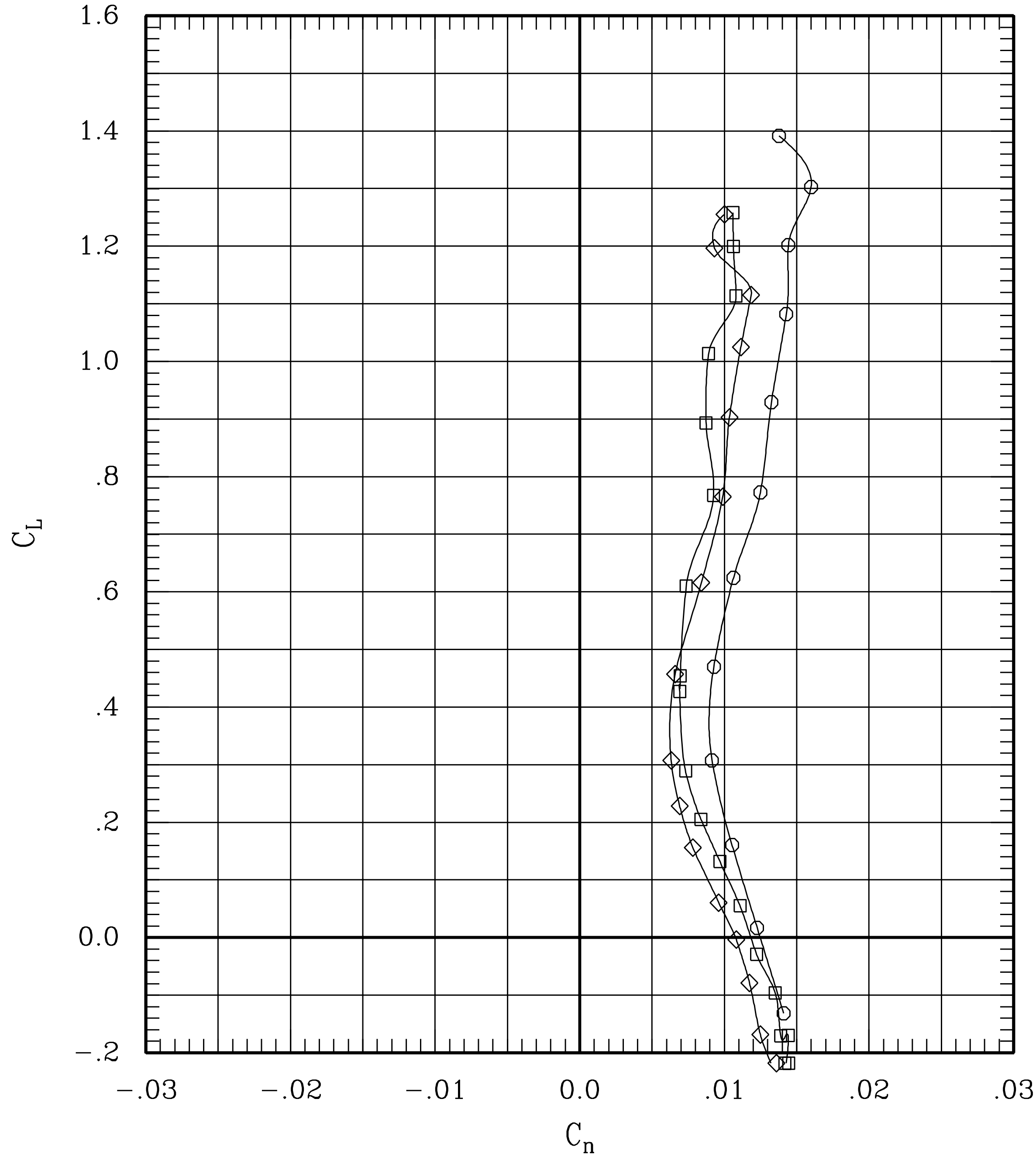

Figure 21(d). Effect of cruise flaps and ailerons for sweep = 45 deg, Mach = 1.10.

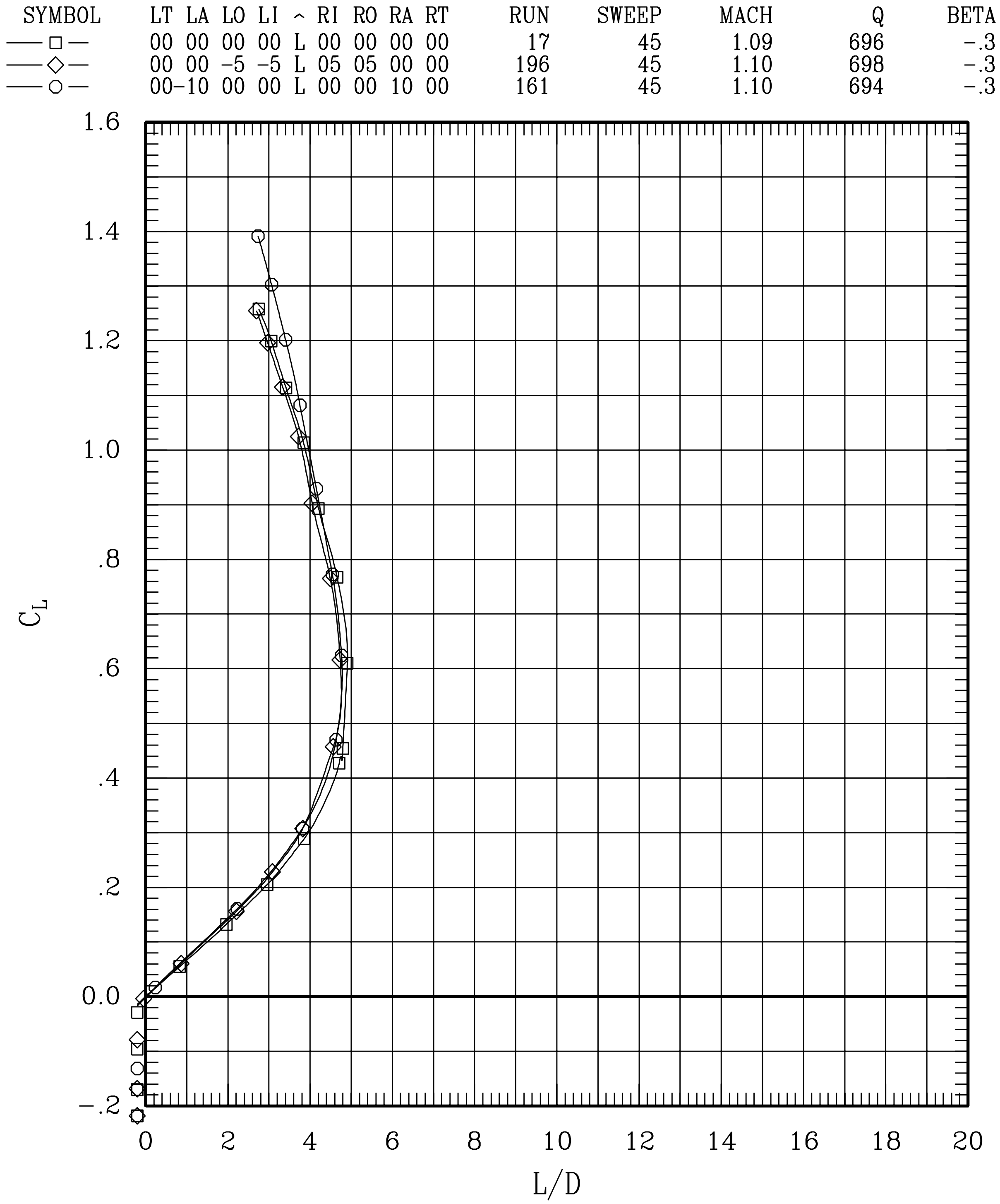

Figure 21(d). Effect of cruise flaps and ailerons for sweep = 45 deg, Mach = 1.10.

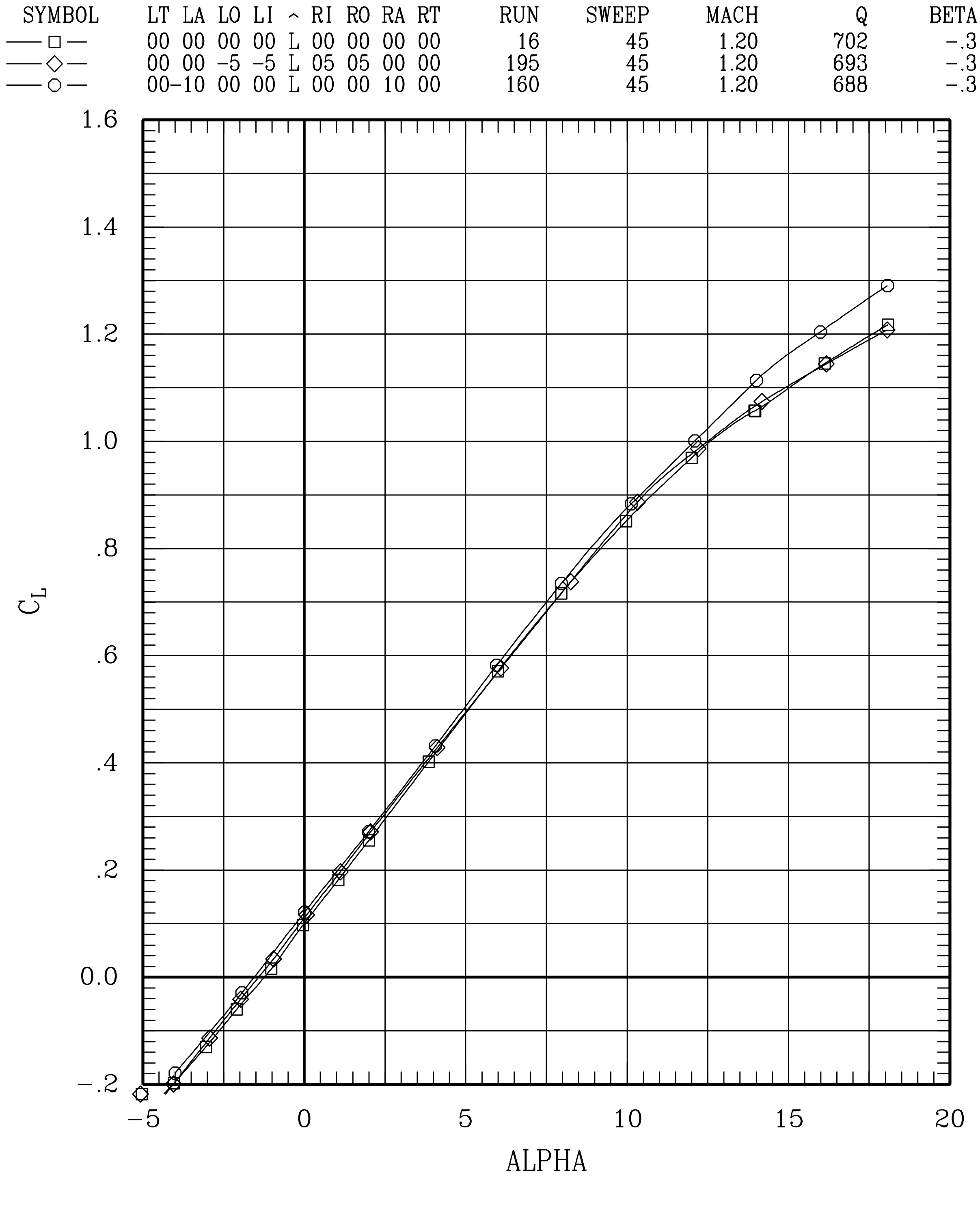

Figure 21(e). Effect of cruise flaps and ailerons for sweep = 45 deg, Mach = 1.20.

SYMBOL	LT LA LO LI ^ RI RO RA RT	RUN	SWEEP	MACH	Q	BETA
—□—	00 00 00 00 L 00 00 00 00	16	45	1.20	702	-.3
—◇—	00 00 -5 -5 L 05 05 00 00	195	45	1.20	693	-.3
—○—	00-10 00 00 L 00 00 10 00	160	45	1.20	688	-.3

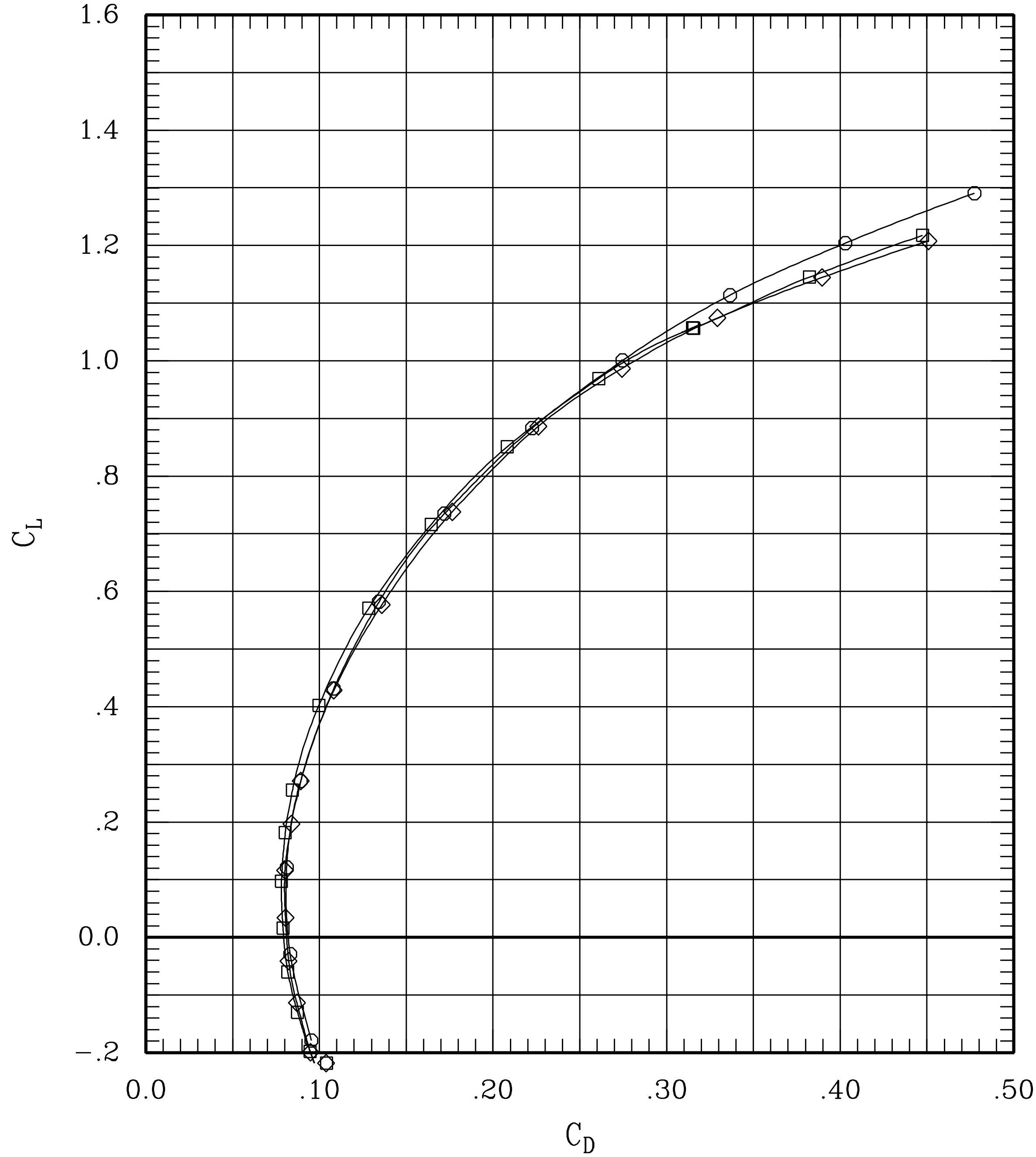

Figure 21(e). Effect of cruise flaps and ailerons for sweep = 45 deg, Mach = 1.20.

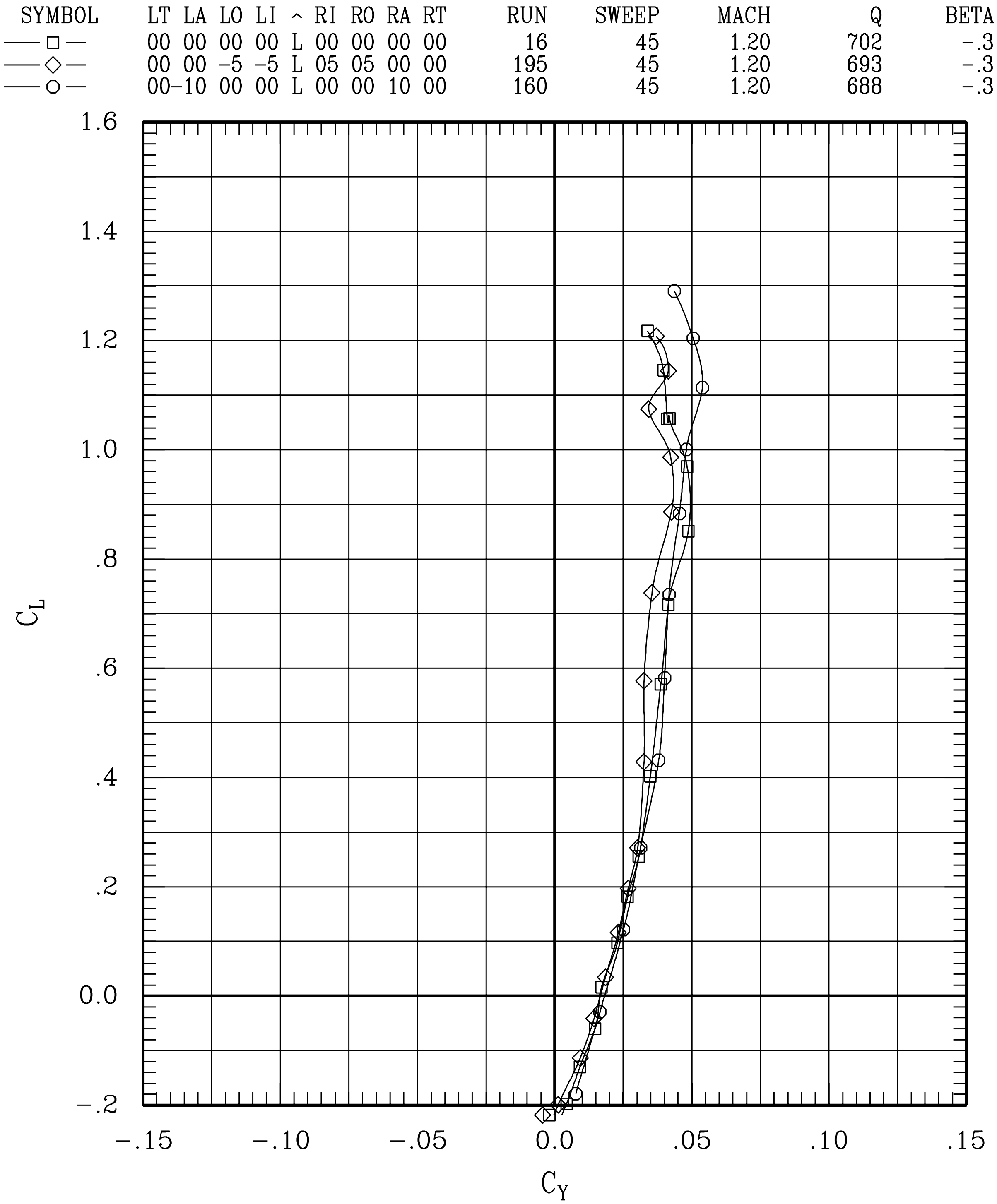

Figure 21(e). Effect of cruise flaps and ailerons for sweep = 45 deg, Mach = 1.20.

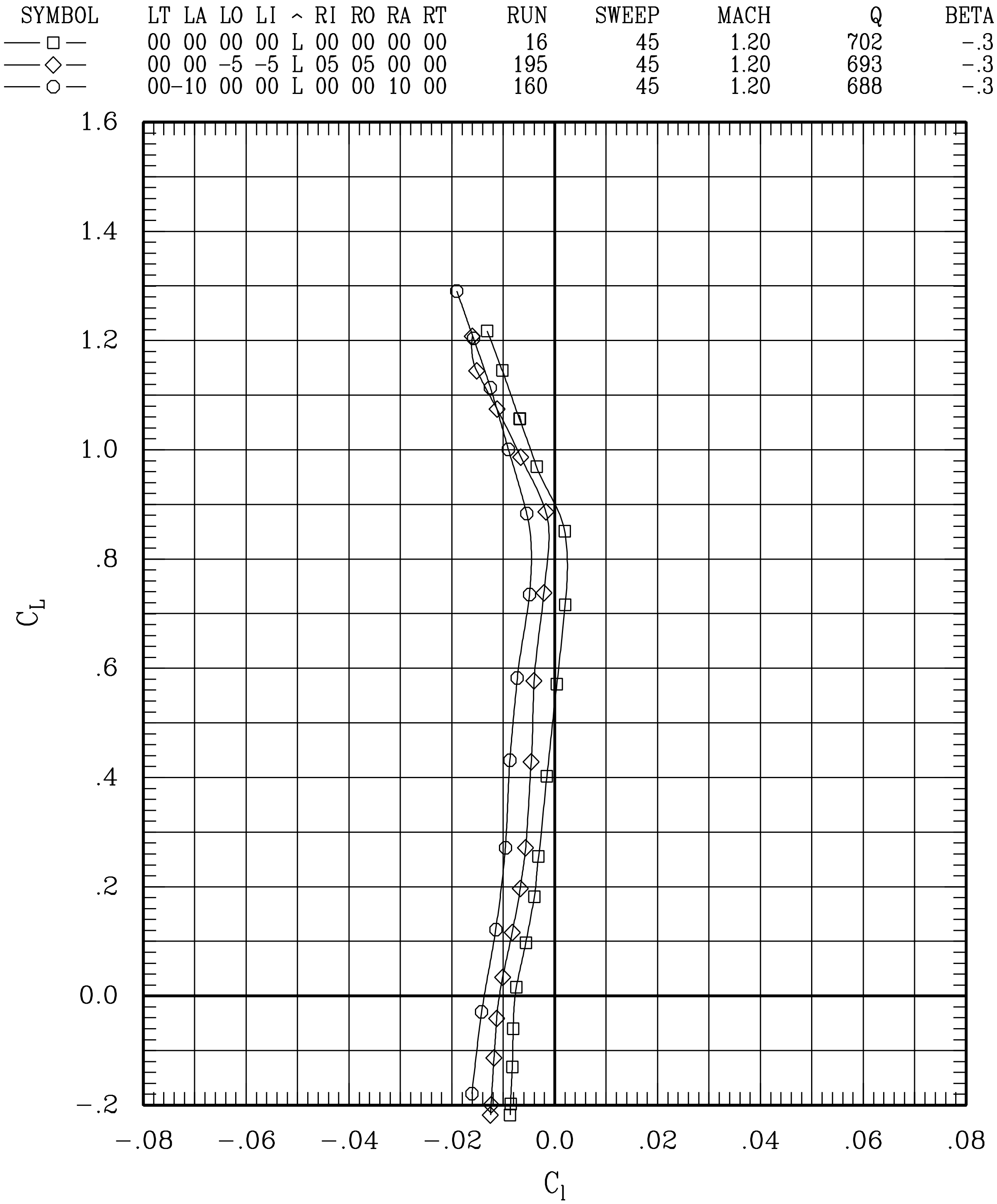

Figure 21(e). Effect of cruise flaps and ailerons for sweep = 45 deg, Mach = 1.20.

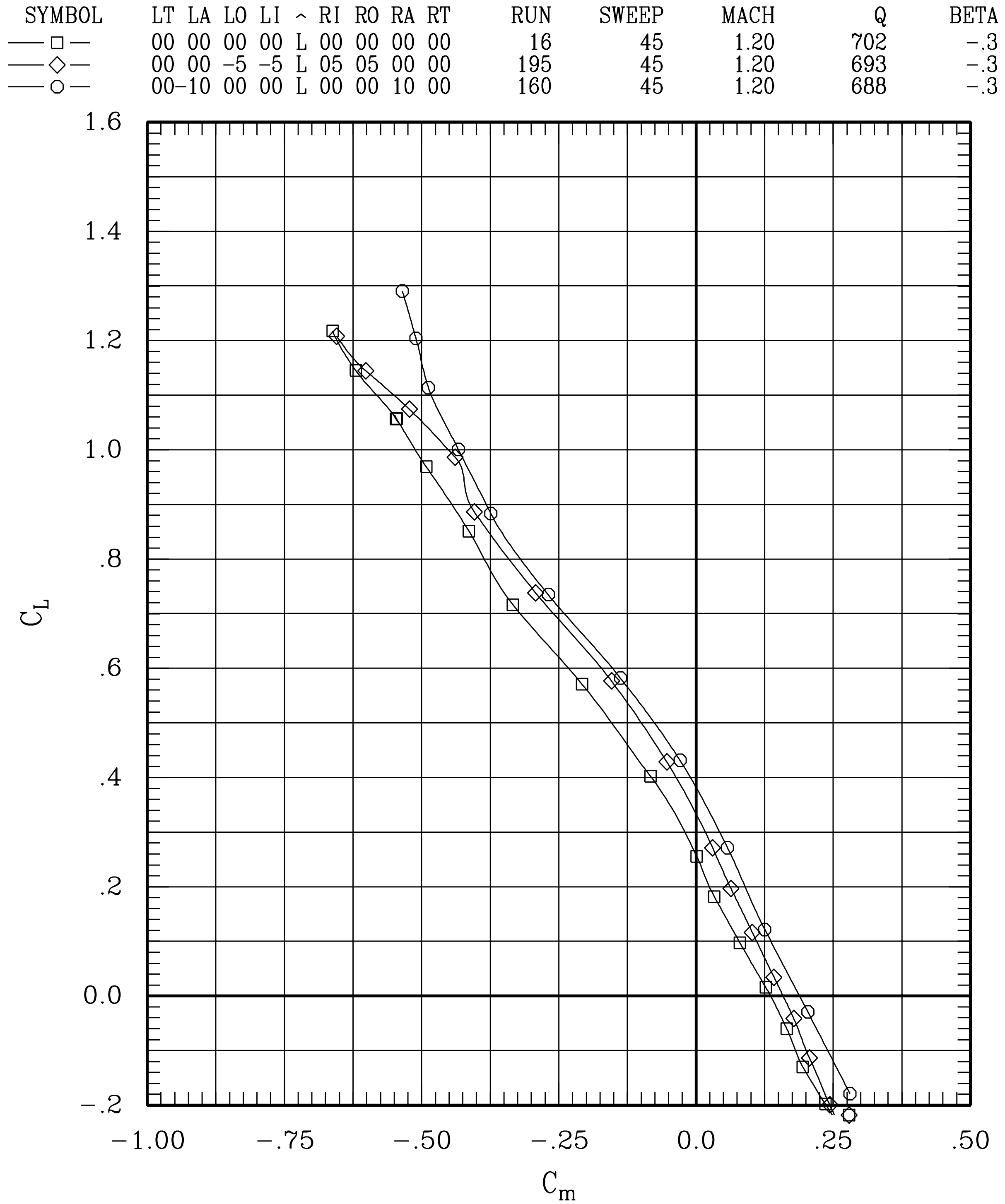

Figure 21(e). Effect of cruise flaps and ailerons for sweep = 45 deg, Mach = 1.20.

SYMBOL	LT LA LO LI ^ RI RO RA RT	RUN	SWEEP	MACH	Q	BETA
—□—	00 00 00 00 L 00 00 00 00	16	45	1.20	702	-.3
—◇—	00 00 -5 -5 L 05 05 00 00	195	45	1.20	693	-.3
—○—	00-10 00 00 L 00 00 10 00	160	45	1.20	688	-.3

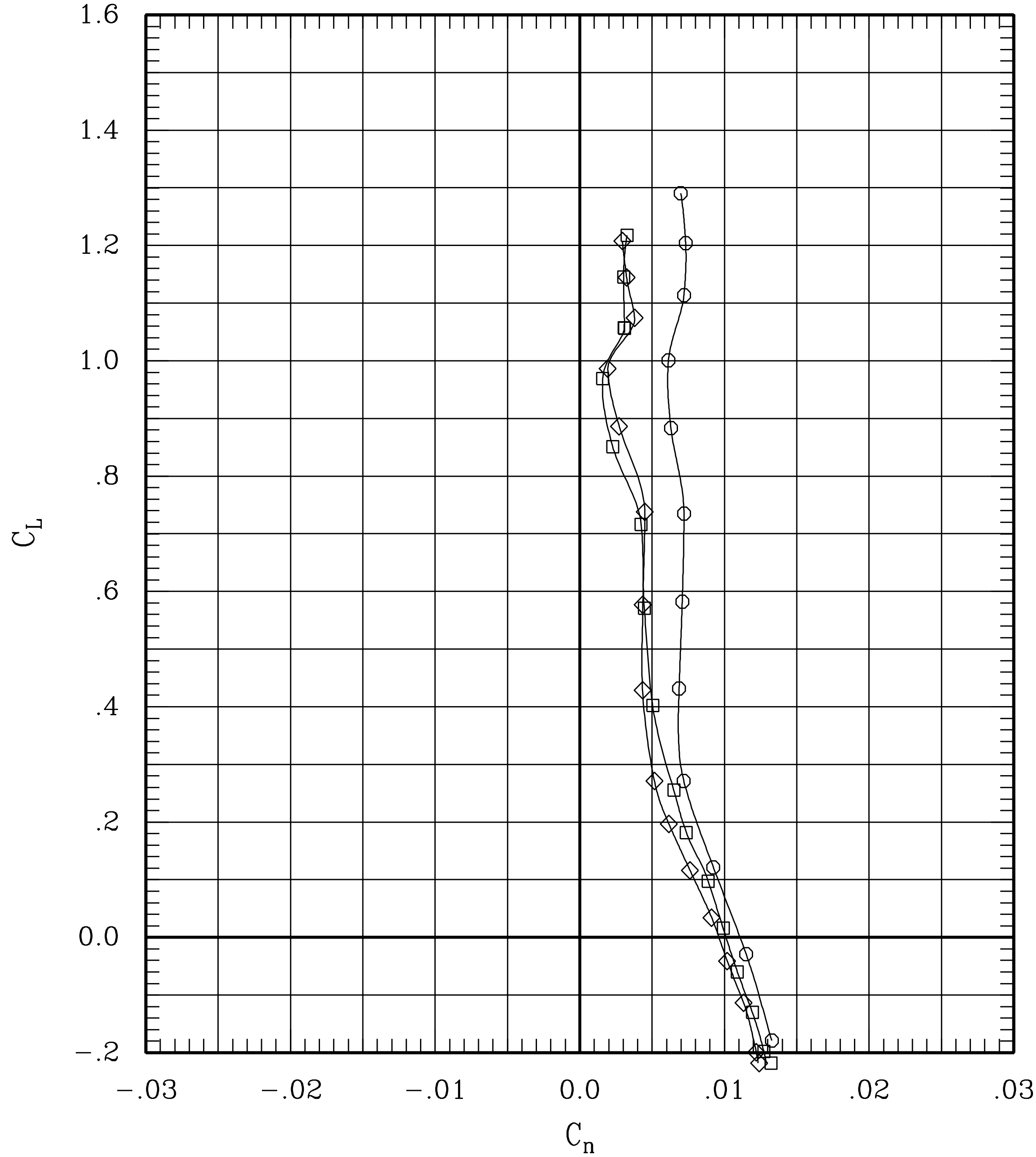

Figure 21(e). Effect of cruise flaps and ailerons for sweep = 45 deg, Mach = 1.20.

SYMBOL	LT LA LO LI ^ RI RO RA RT	RUN	SWEEP	MACH	Q	BETA
—□—	00 00 00 00 L 00 00 00 00	16	45	1.20	702	-.3
—◇—	00 00 -5 -5 L 05 05 00 00	195	45	1.20	693	-.3
—○—	00-10 00 00 L 00 00 10 00	160	45	1.20	688	-.3

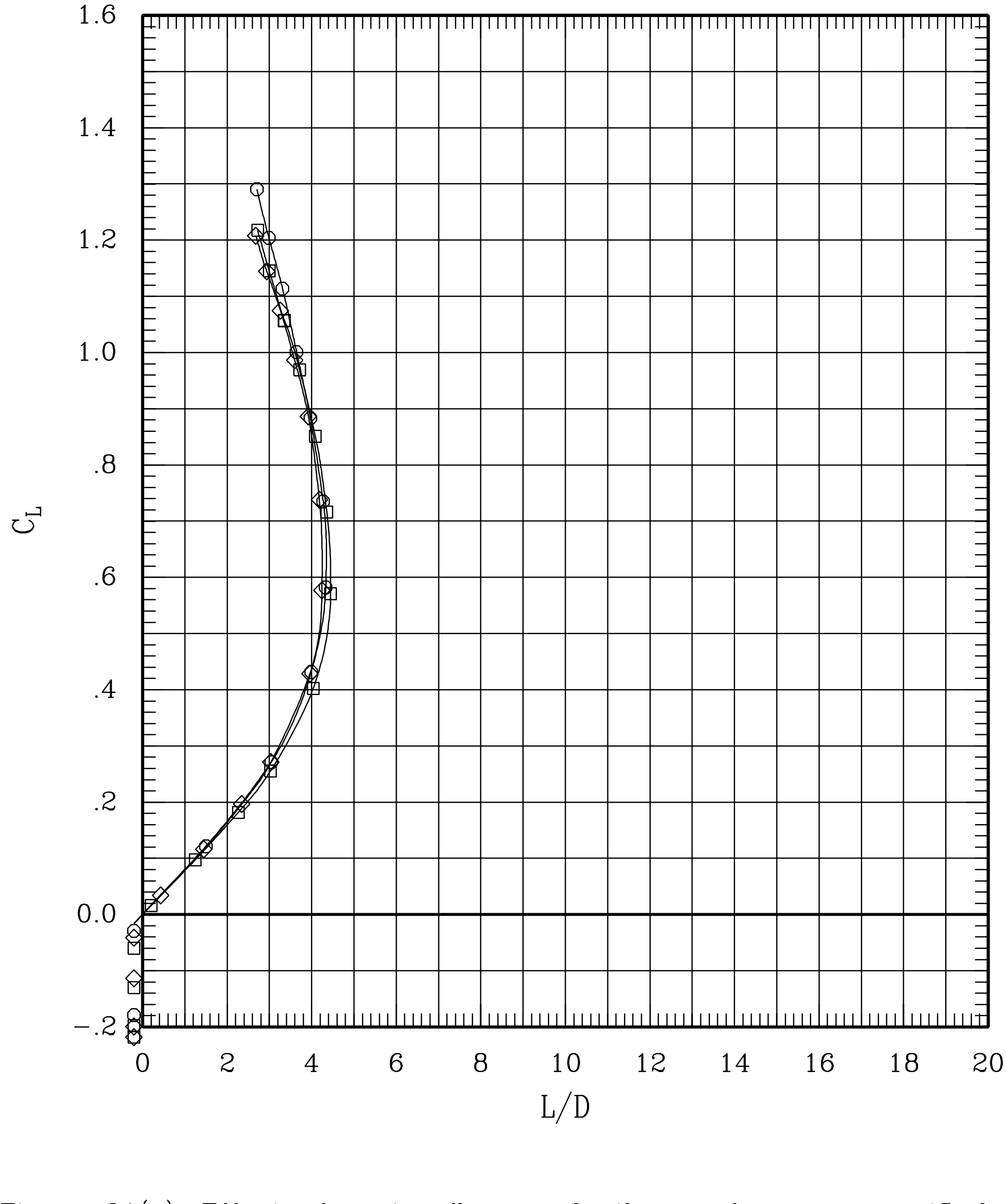

Figure 21(e). Effect of cruise flaps and ailerons for sweep = 45 deg, Mach = 1.20.

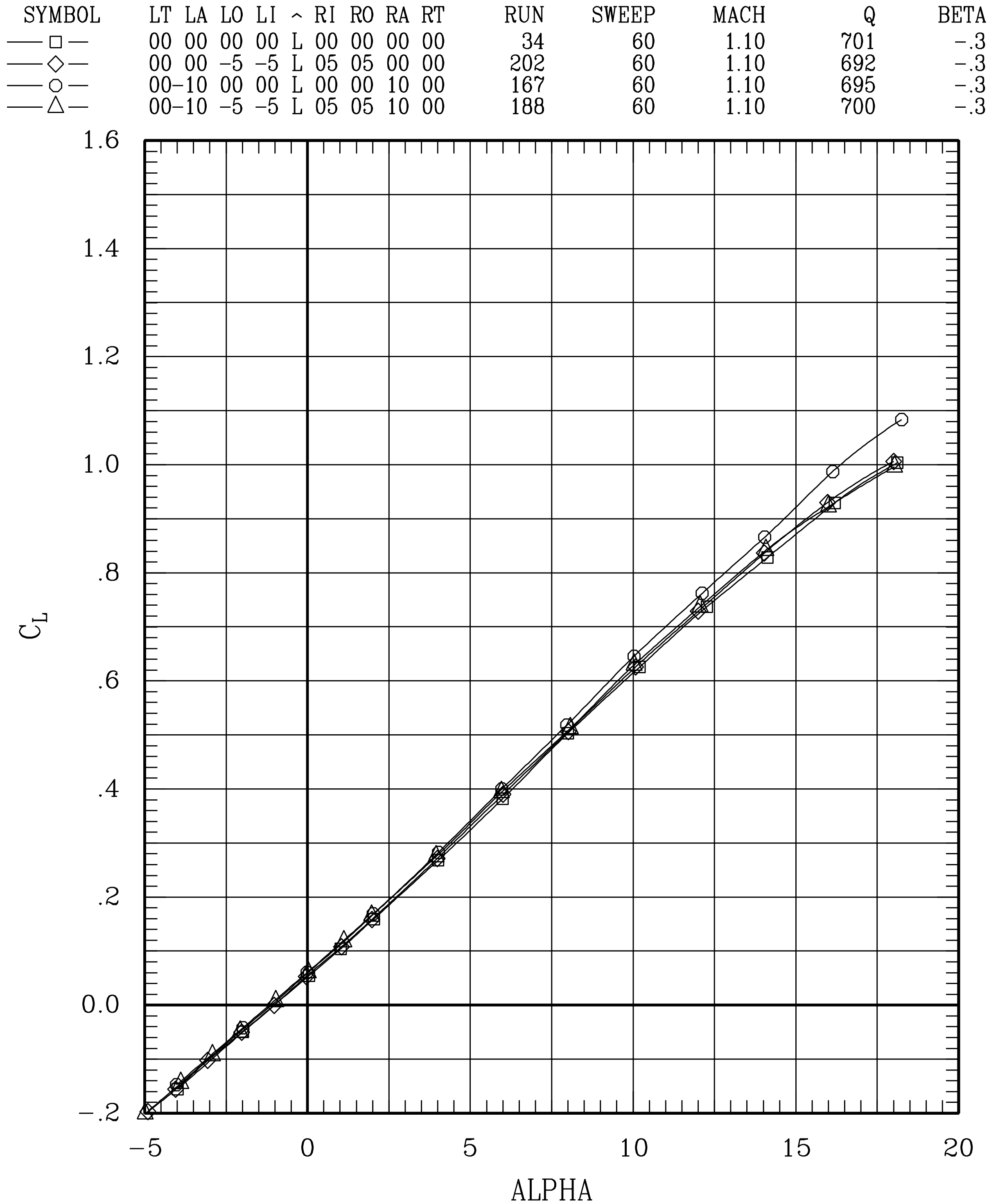

Figure 21(f). Effect of cruise flaps and ailerons for sweep = 60 deg, Mach = 1.10.

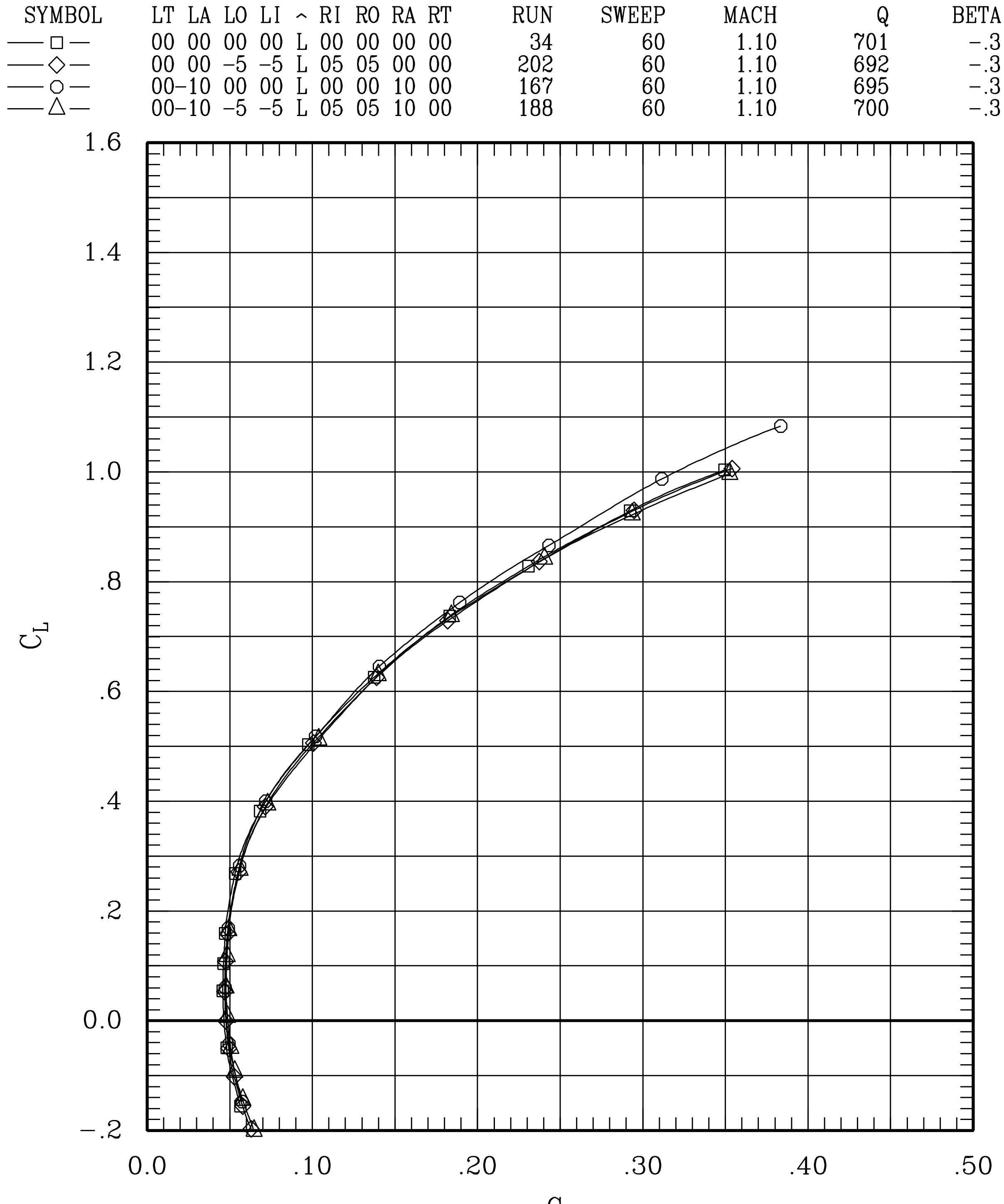

Figure 21(f). Effect of cruise flaps and ailerons for sweep = 60 deg, Mach = 1.10.

SYMBOL	LT LA LO LI ^ RI RO RA RT	RUN	SWEEP	MACH	Q	BETA
—□—	00 00 00 00 L 00 00 00 00	34	60	1.10	701	−.3
—◇—	00 00 −5 −5 L 05 05 00 00	202	60	1.10	692	−.3
—○—	00−10 00 00 L 00 00 10 00	167	60	1.10	695	−.3
—△—	00−10 −5 −5 L 05 05 10 00	188	60	1.10	700	−.3

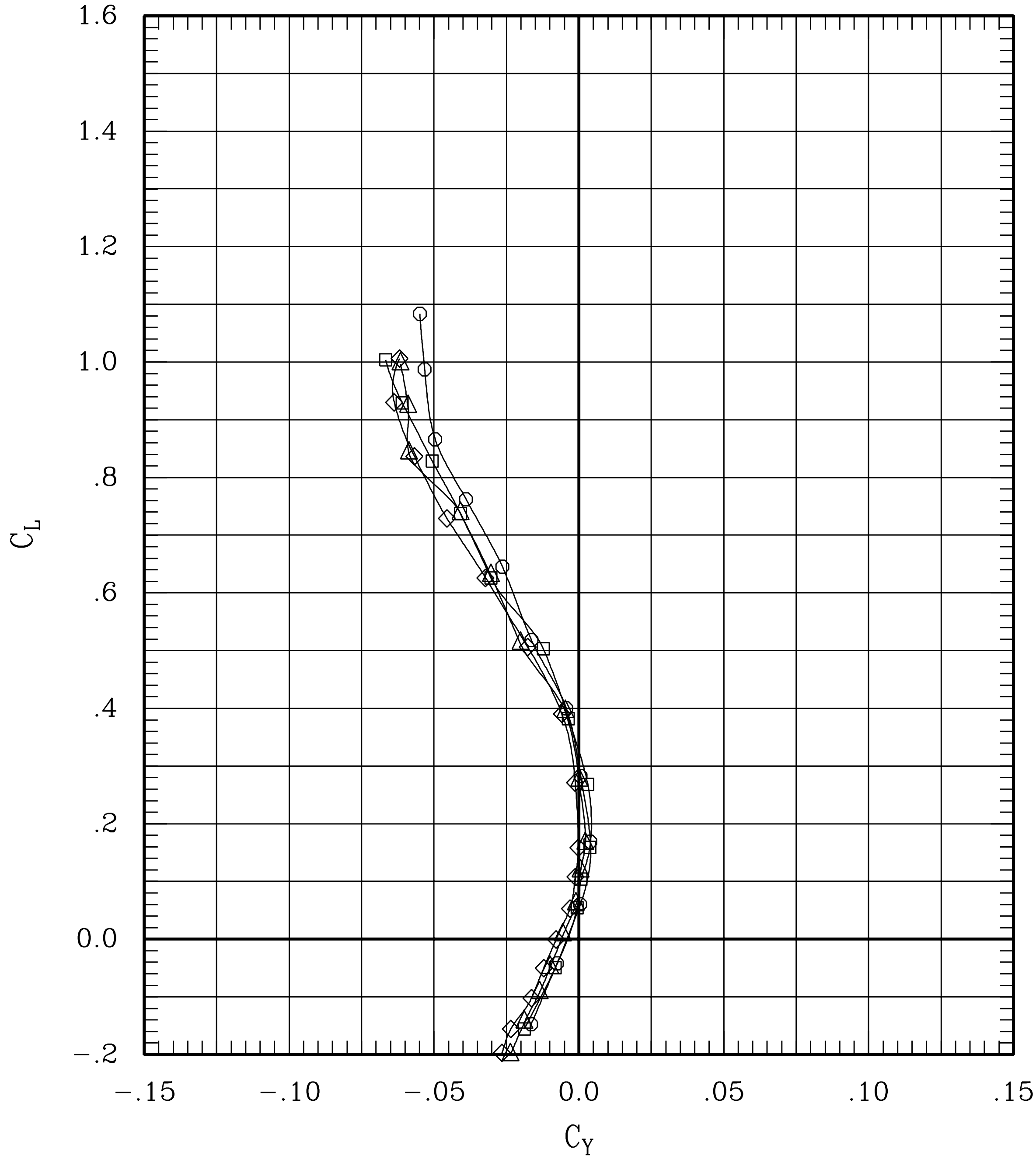

Figure 21(f). Effect of cruise flaps and ailerons for sweep = 60 deg, Mach = 1.10.

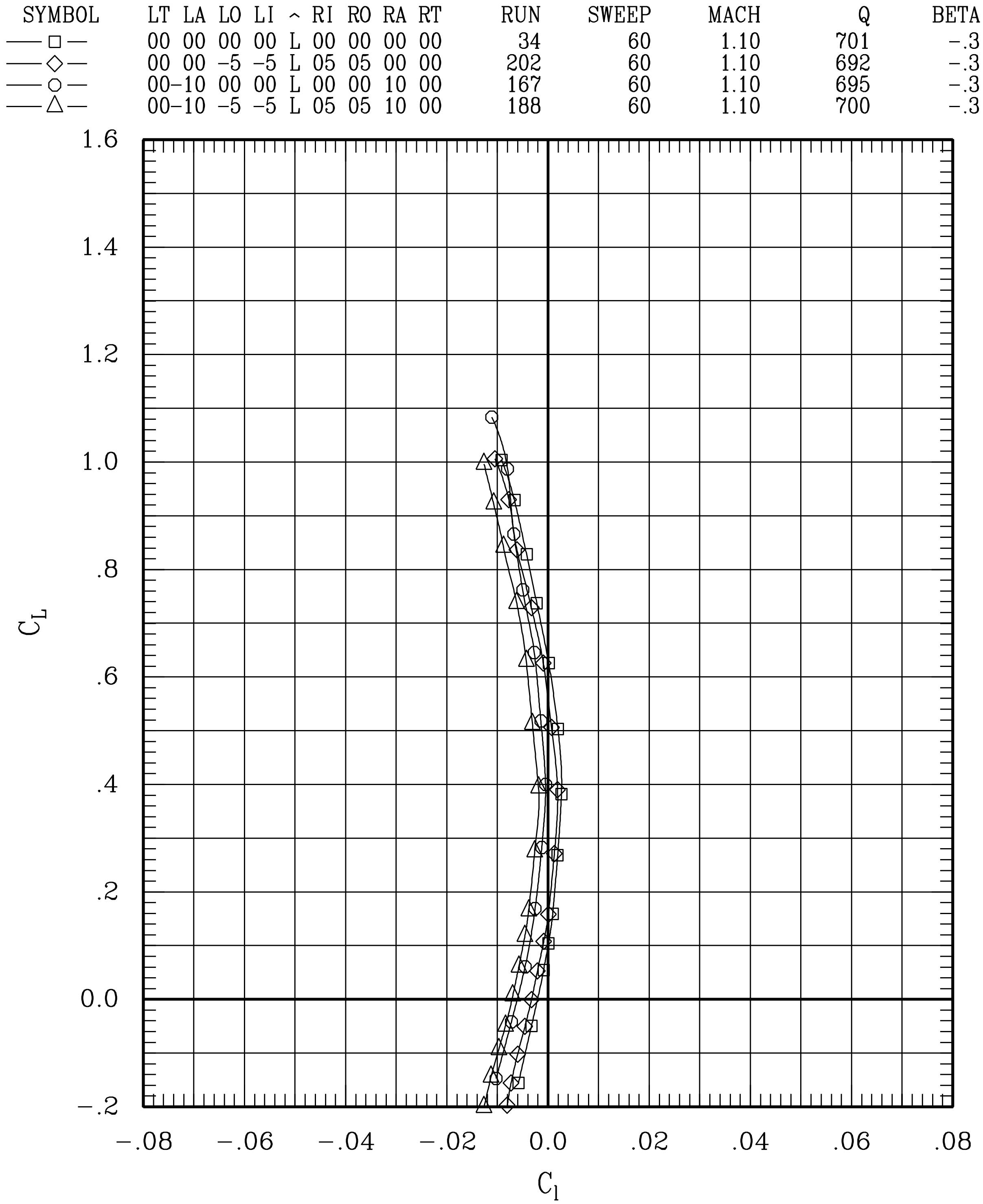

Figure 21(f). Effect of cruise flaps and ailerons for sweep = 60 deg, Mach = 1.10.

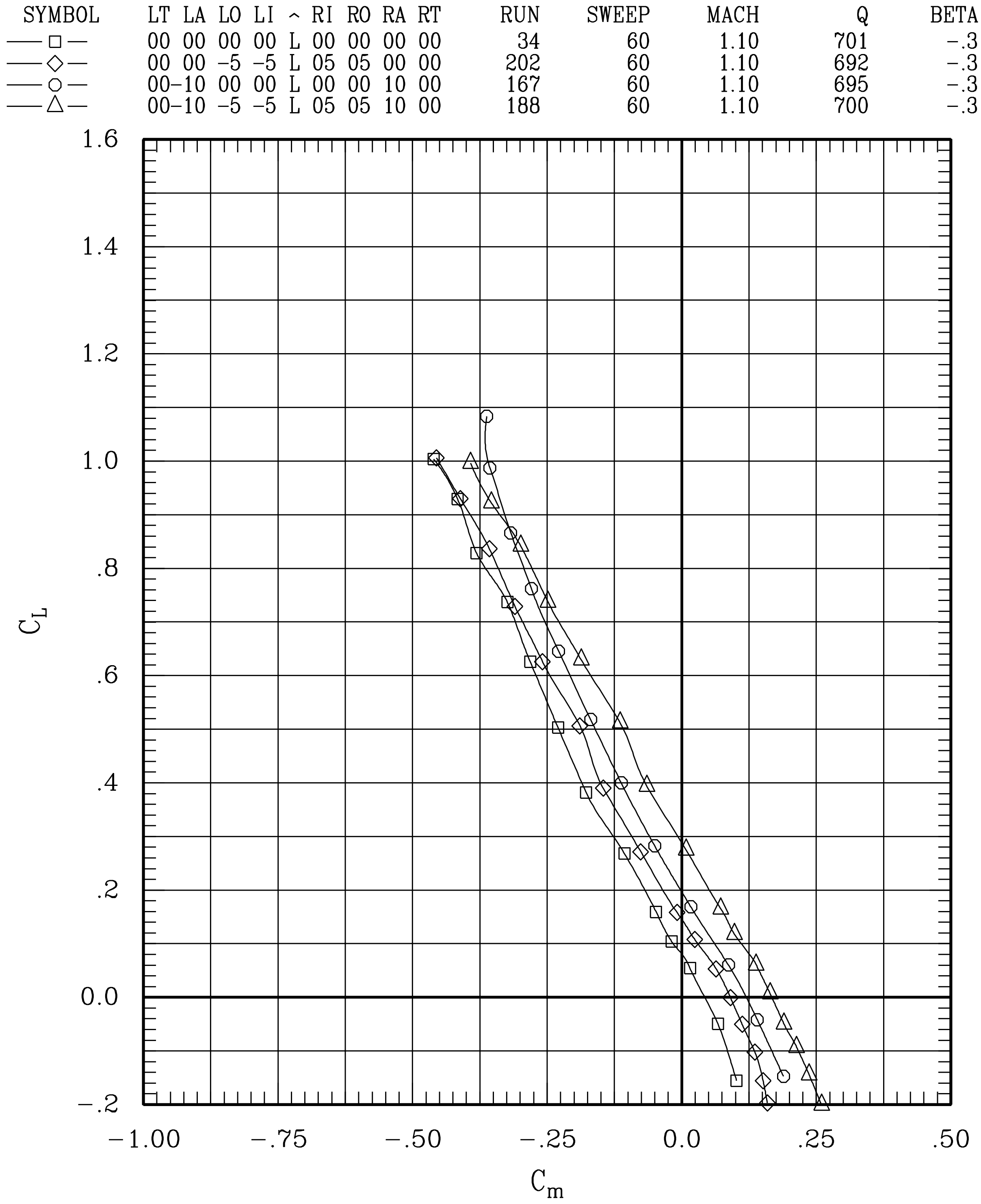

Figure 21(f). Effect of cruise flaps and ailerons for sweep = 60 deg, Mach = 1.10.

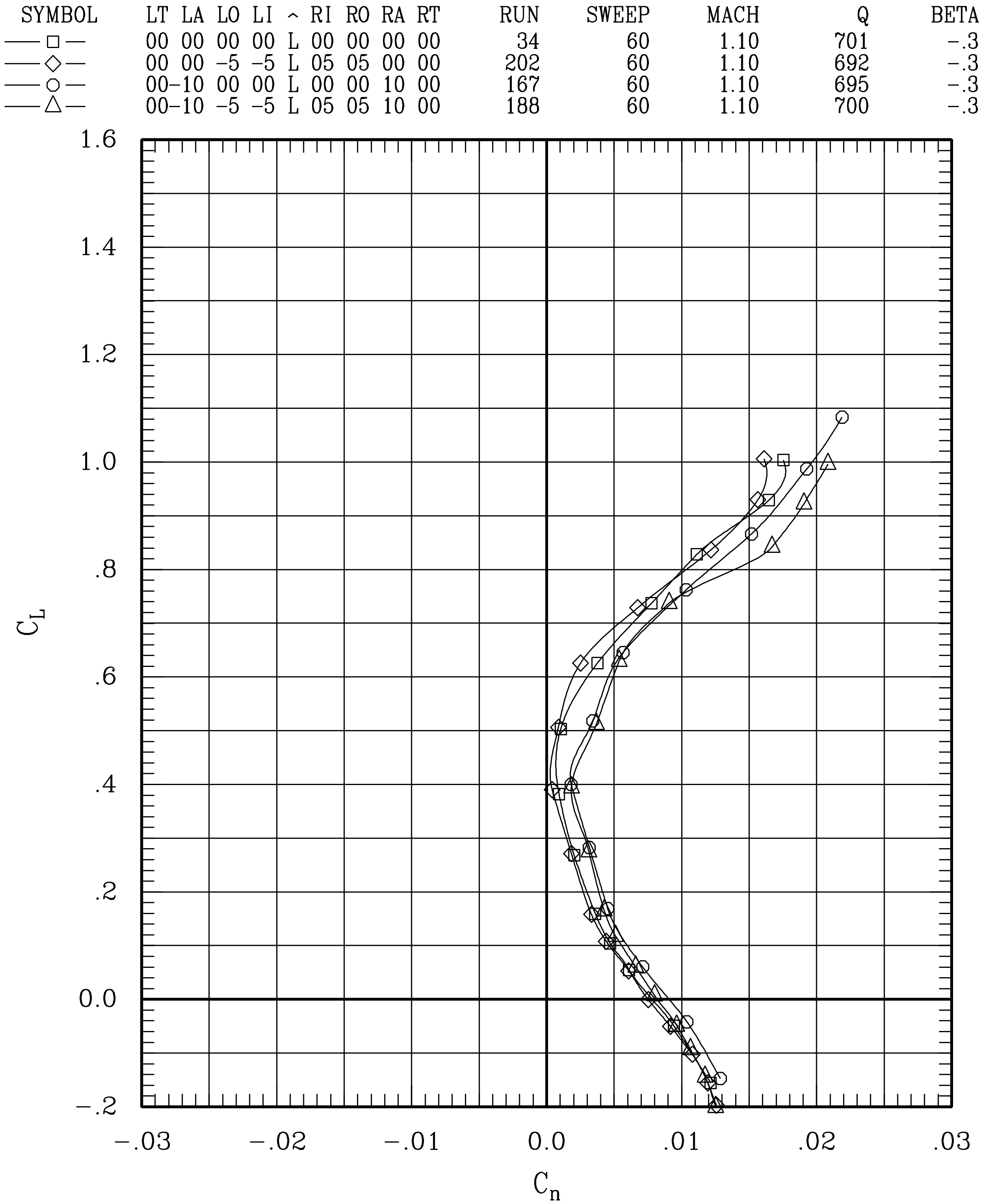

Figure 21(f). Effect of cruise flaps and ailerons for sweep = 60 deg, Mach = 1.10.

SYMBOL	LT LA LO LI ^ RI RO RA RT	RUN	SWEEP	MACH	Q	BETA
□	00 00 00 00 L 00 00 00 00	34	60	1.10	701	-.3
◇	00 00 -5 -5 L 05 05 00 00	202	60	1.10	692	-.3
○	00-10 00 00 L 00 00 10 00	167	60	1.10	695	-.3
△	00-10 -5 -5 L 05 05 10 00	188	60	1.10	700	-.3

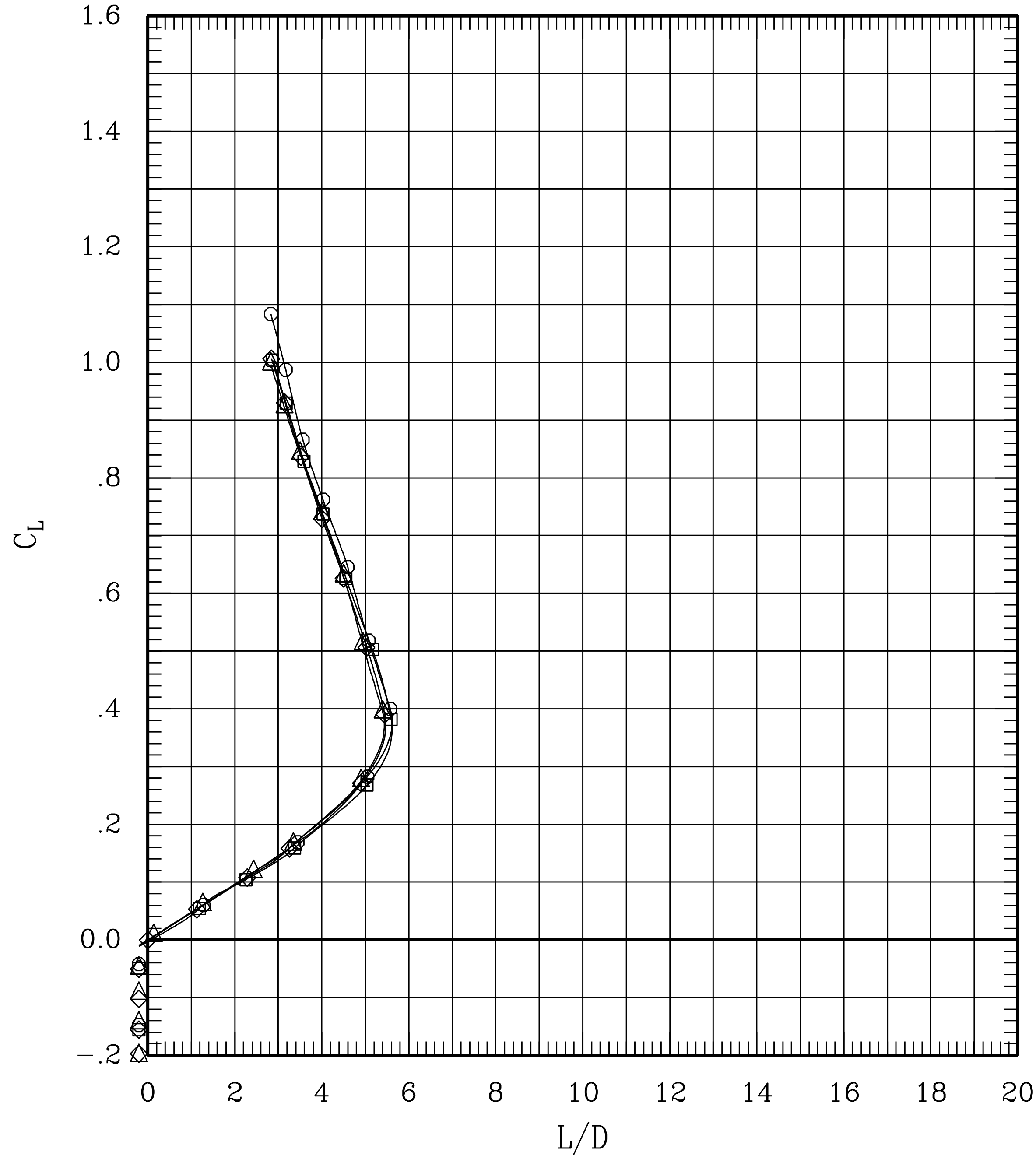

Figure 21(f). Effect of cruise flaps and ailerons for sweep = 60 deg, Mach = 1.10.

SYMBOL	LT LA LO LI ^ RI RO RA RT	RUN	SWEEP	MACH	Q	BETA
—□—	00 00 00 00 L 00 00 00 00	33	60	1.20	701	−.2
—◇—	00 00 −5 −5 L 05 05 00 00	201	60	1.20	690	−.3
—○—	00−10 00 00 L 00 00 10 00	166	60	1.20	694	−.3
—△—	00−10 −5 −5 L 05 05 10 00	187	60	1.20	703	−.3
—⌂—	00 00 −5 00 L 00 05 00 00	212	60	1.20	700	−.3

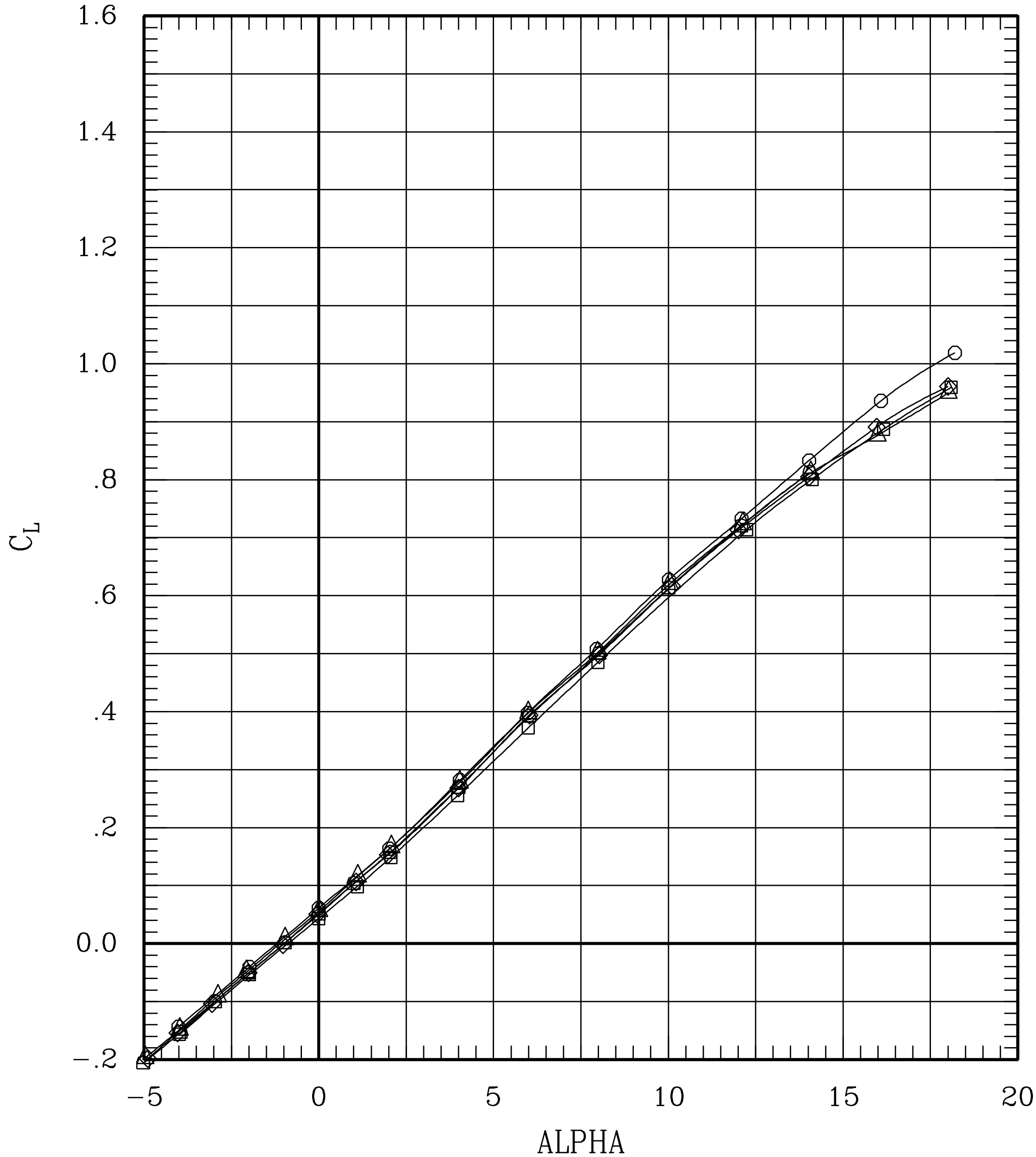

Figure 21(g). Effect of cruise flaps and ailerons for sweep = 60 deg, Mach = 1.20.

SYMBOL	LT LA LO LI ^ RI RO RA RT	RUN	SWEEP	MACH	Q	BETA
—□—	00 00 00 00 L 00 00 00 00	33	60	1.20	701	−.2
—◇—	00 00 −5 −5 L 05 05 00 00	201	60	1.20	690	−.3
—○—	00−10 00 00 L 00 00 10 00	166	60	1.20	694	−.3
—△—	00−10 −5 −5 L 05 05 10 00	187	60	1.20	703	−.3
—⌂—	00 00 −5 00 L 00 05 00 00	212	60	1.20	700	−.3

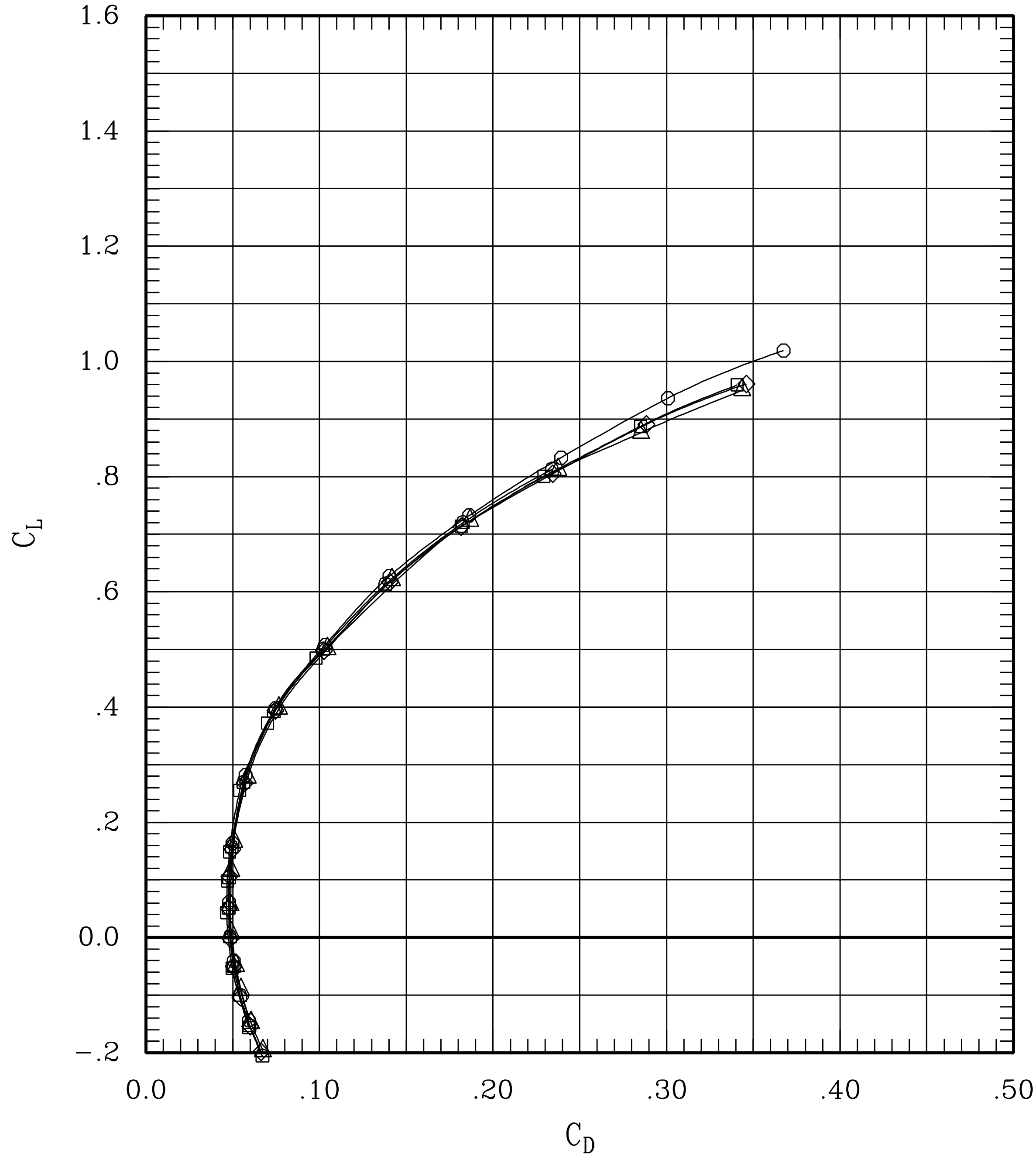

Figure 21(g). Effect of cruise flaps and ailerons for sweep = 60 deg, Mach = 1.20.

SYMBOL	LT LA LO LI ^ RI RO RA RT	RUN	SWEEP	MACH	Q	BETA
—□—	00 00 00 00 L 00 00 00 00	33	60	1.20	701	−.2
—◇—	00 00 −5 −5 L 05 05 00 00	201	60	1.20	690	−.3
—○—	00−10 00 00 L 00 00 10 00	166	60	1.20	694	−.3
—△—	00−10 −5 −5 L 05 05 10 00	187	60	1.20	703	−.3
—◠—	00 00 −5 00 L 00 05 00 00	212	60	1.20	700	−.3

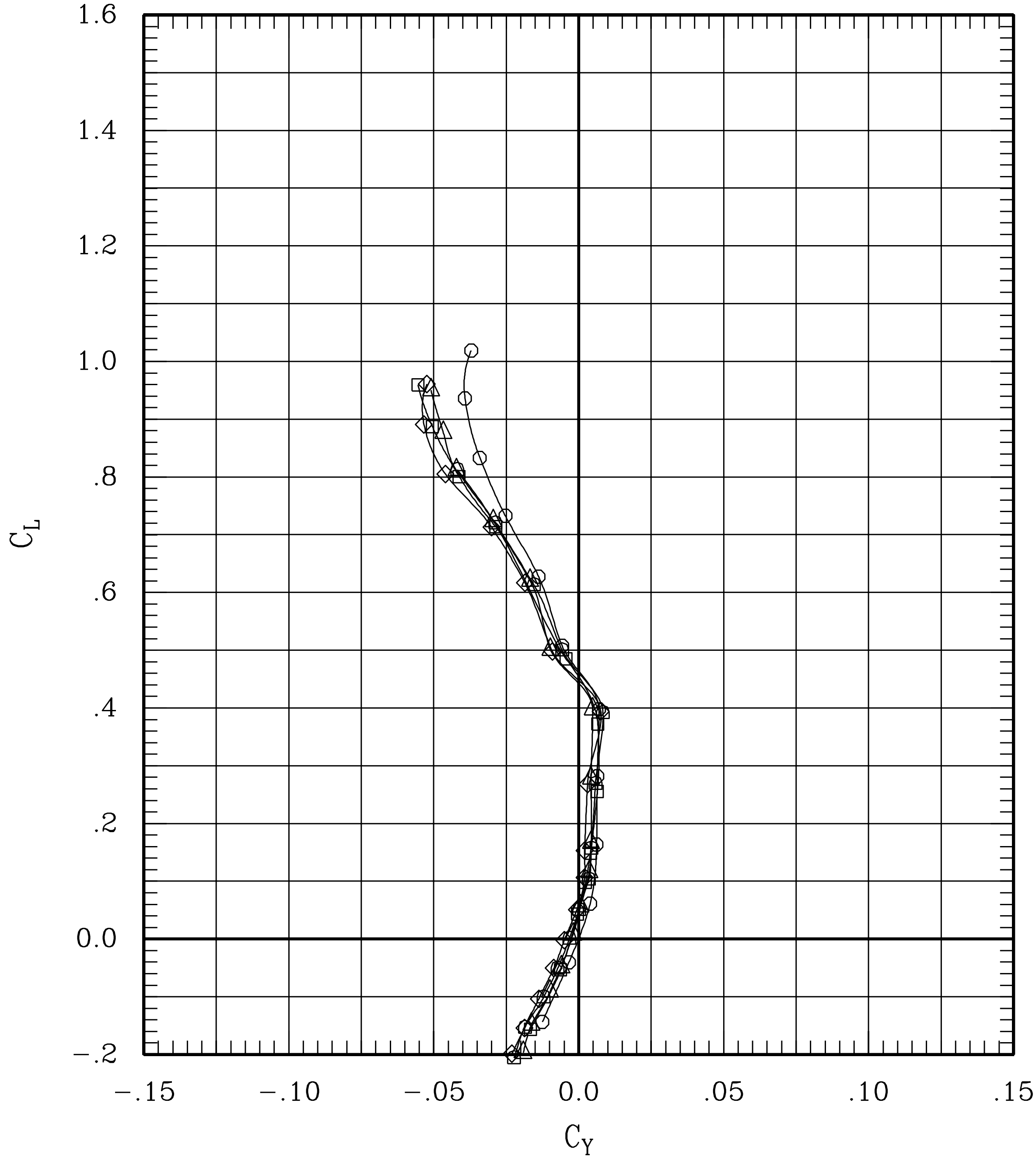

Figure 21(g). Effect of cruise flaps and ailerons for sweep = 60 deg, Mach = 1.20.

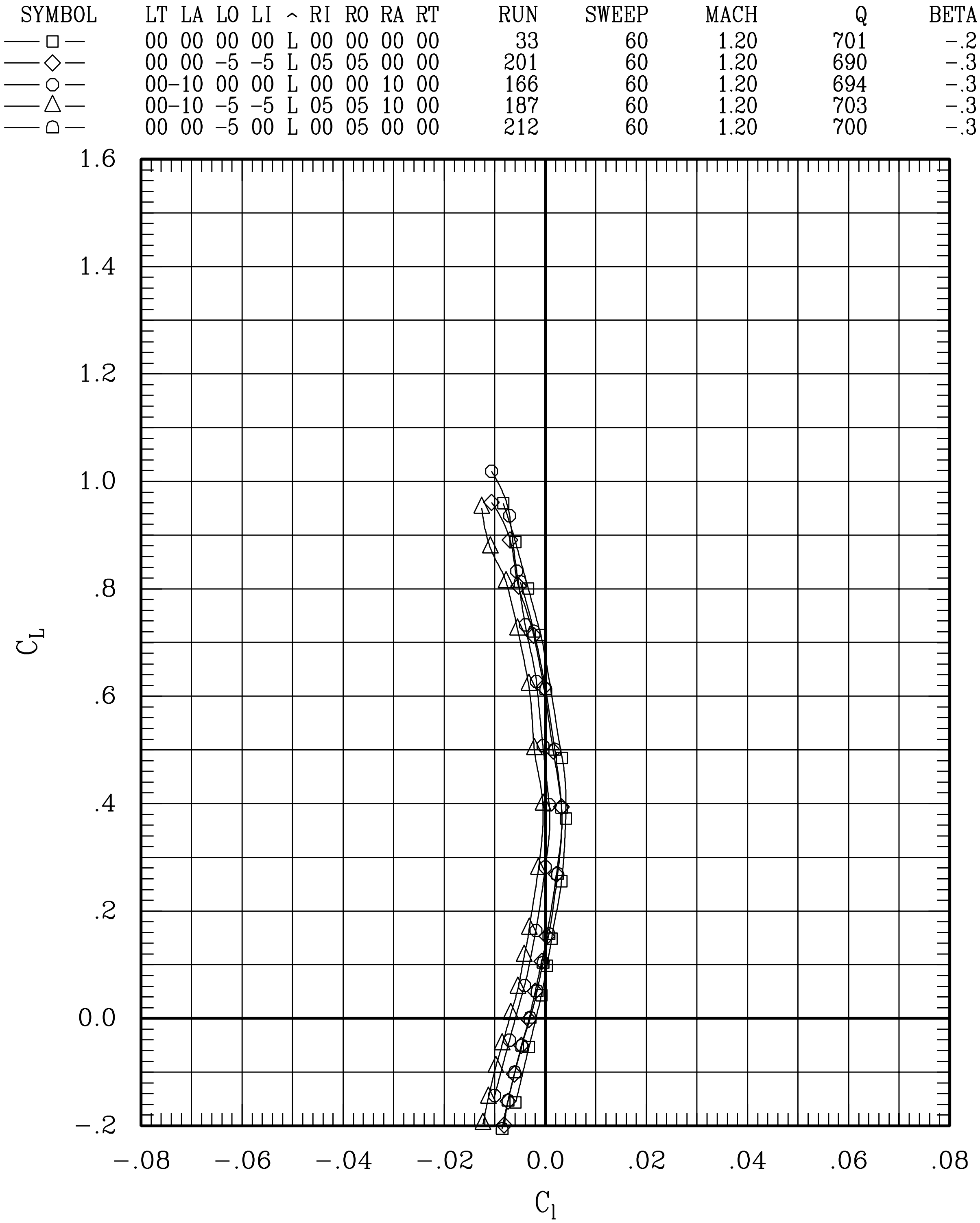

Figure 21(g). Effect of cruise flaps and ailerons for sweep = 60 deg, Mach = 1.20.

SYMBOL	LT LA LO LI ^ RI RO RA RT	RUN	SWEEP	MACH	Q	BETA
—□—	00 00 00 00 L 00 00 00 00	33	60	1.20	701	−.2
—◇—	00 00 −5 −5 L 05 05 00 00	201	60	1.20	690	−.3
—○—	00−10 00 00 L 00 00 10 00	166	60	1.20	694	−.3
—△—	00−10 −5 −5 L 05 05 10 00	187	60	1.20	703	−.3
—⌂—	00 00 −5 00 L 00 05 00 00	212	60	1.20	700	−.3

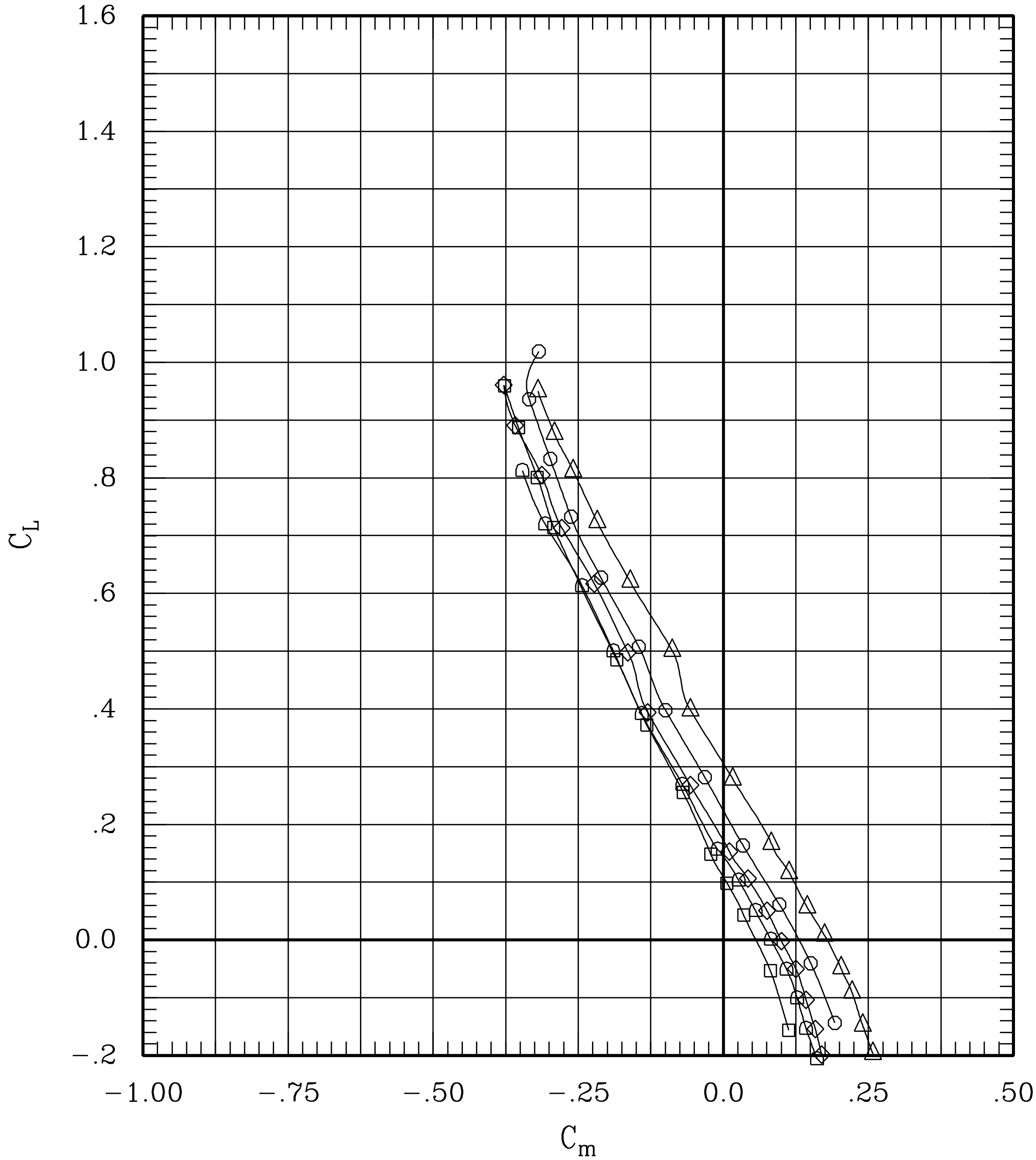

Figure 21(g). Effect of cruise flaps and ailerons for sweep = 60 deg, Mach = 1.20.

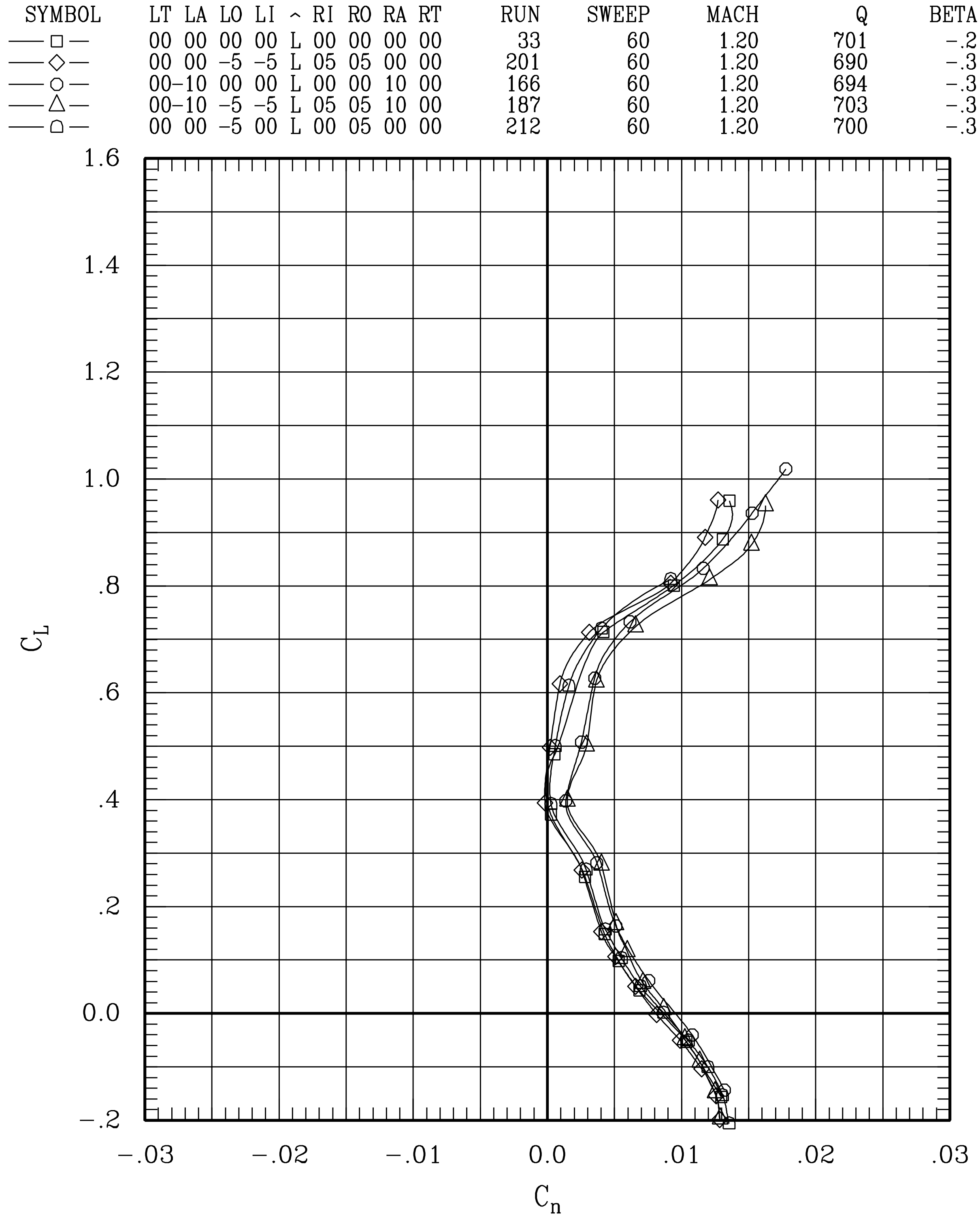

Figure 21(g). Effect of cruise flaps and ailerons for sweep = 60 deg, Mach = 1.20.

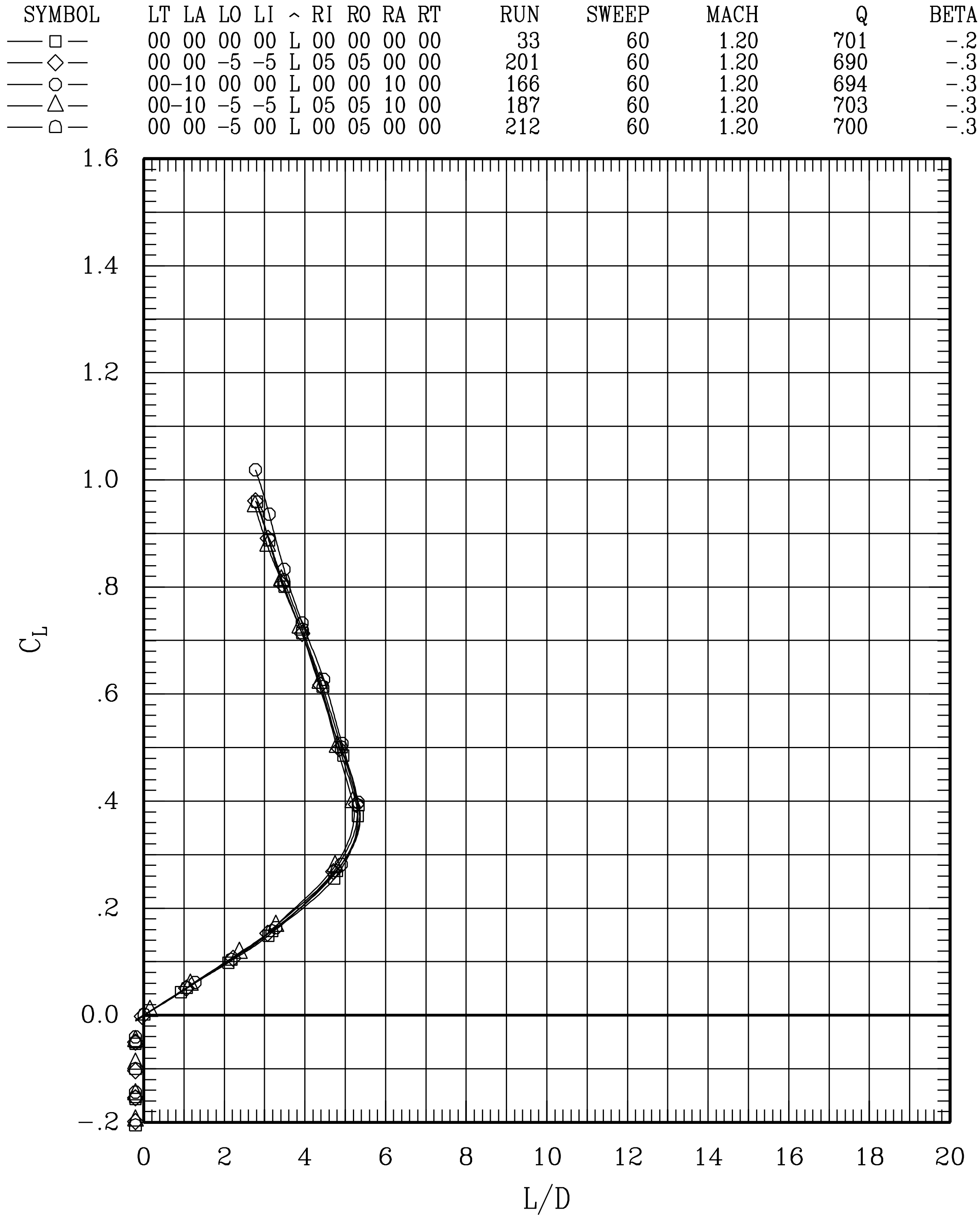

Figure 21(g). Effect of cruise flaps and ailerons for sweep = 60 deg, Mach = 1.20.

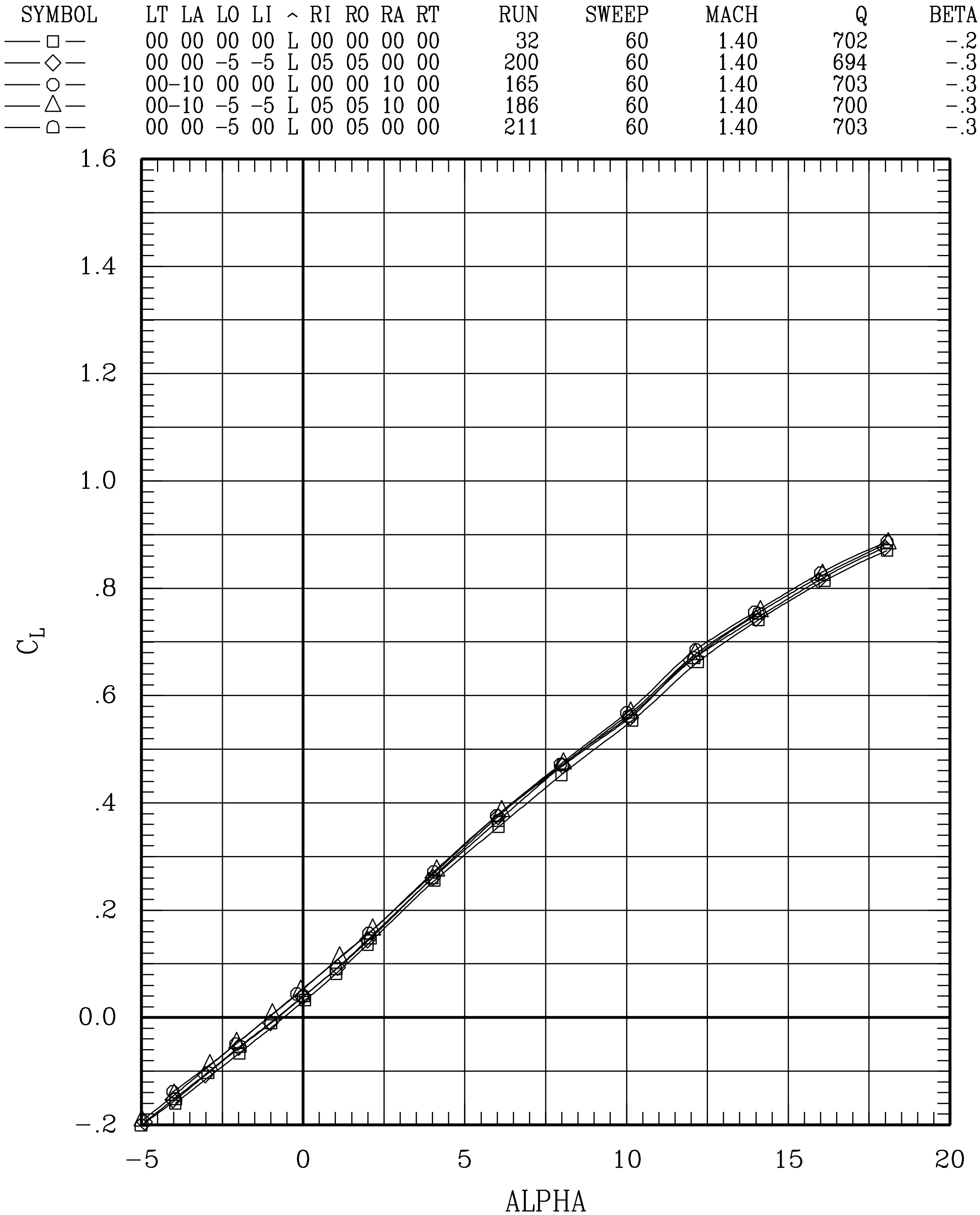

Figure 21(h). Effect of cruise flaps and ailerons for sweep = 60 deg, Mach = 1.40.

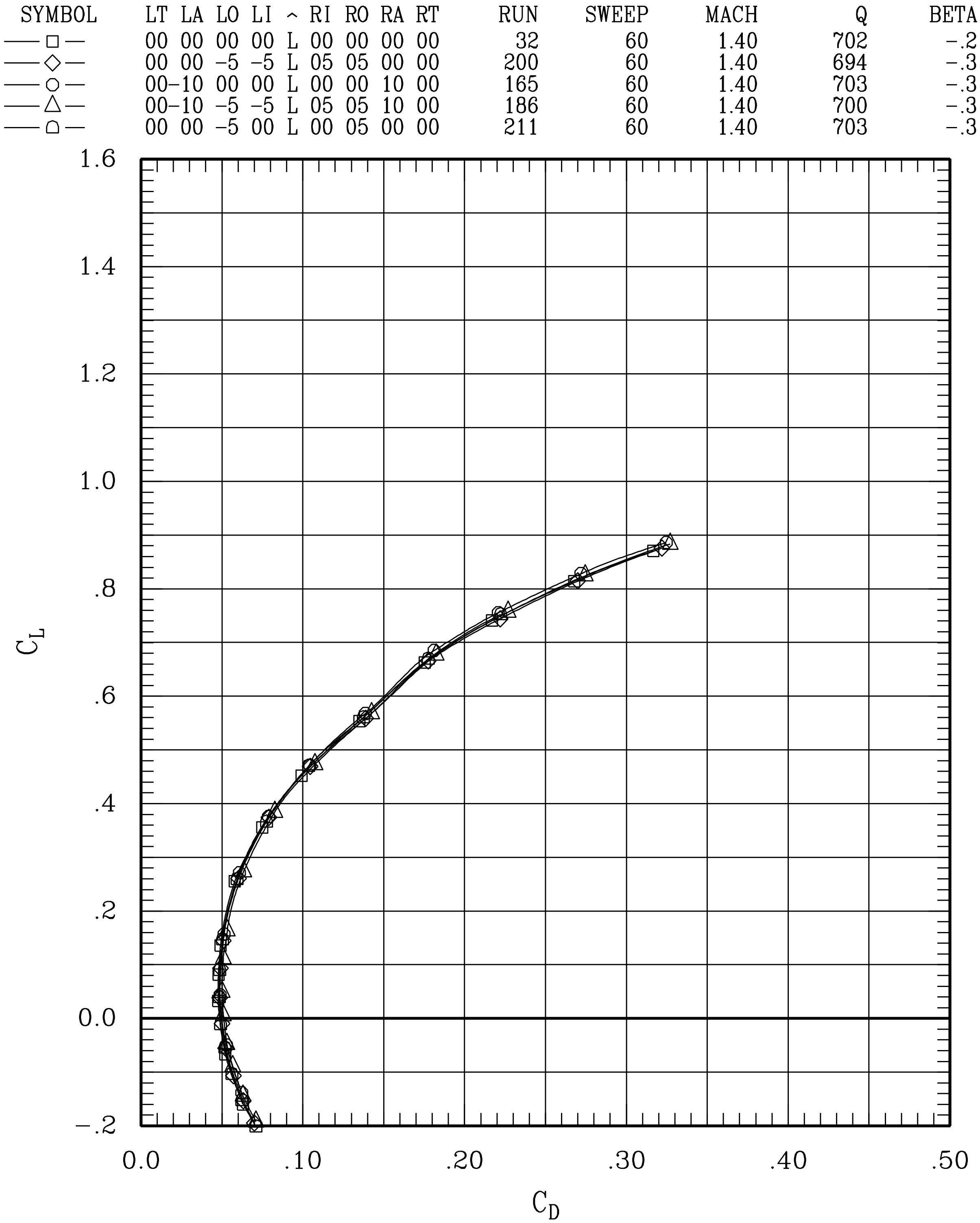

Figure 21(h). Effect of cruise flaps and ailerons for sweep = 60 deg, Mach = 1.40.

SYMBOL	LT LA LO LI ^ RI RO RA RT	RUN	SWEEP	MACH	Q	BETA
—□—	00 00 00 00 L 00 00 00 00	32	60	1.40	702	−.2
—◇—	00 00 −5 −5 L 05 05 00 00	200	60	1.40	694	−.3
—○—	00−10 00 00 L 00 00 10 00	165	60	1.40	703	−.3
—△—	00−10 −5 −5 L 05 05 10 00	186	60	1.40	700	−.3
—⌂—	00 00 −5 00 L 00 05 00 00	211	60	1.40	703	−.3

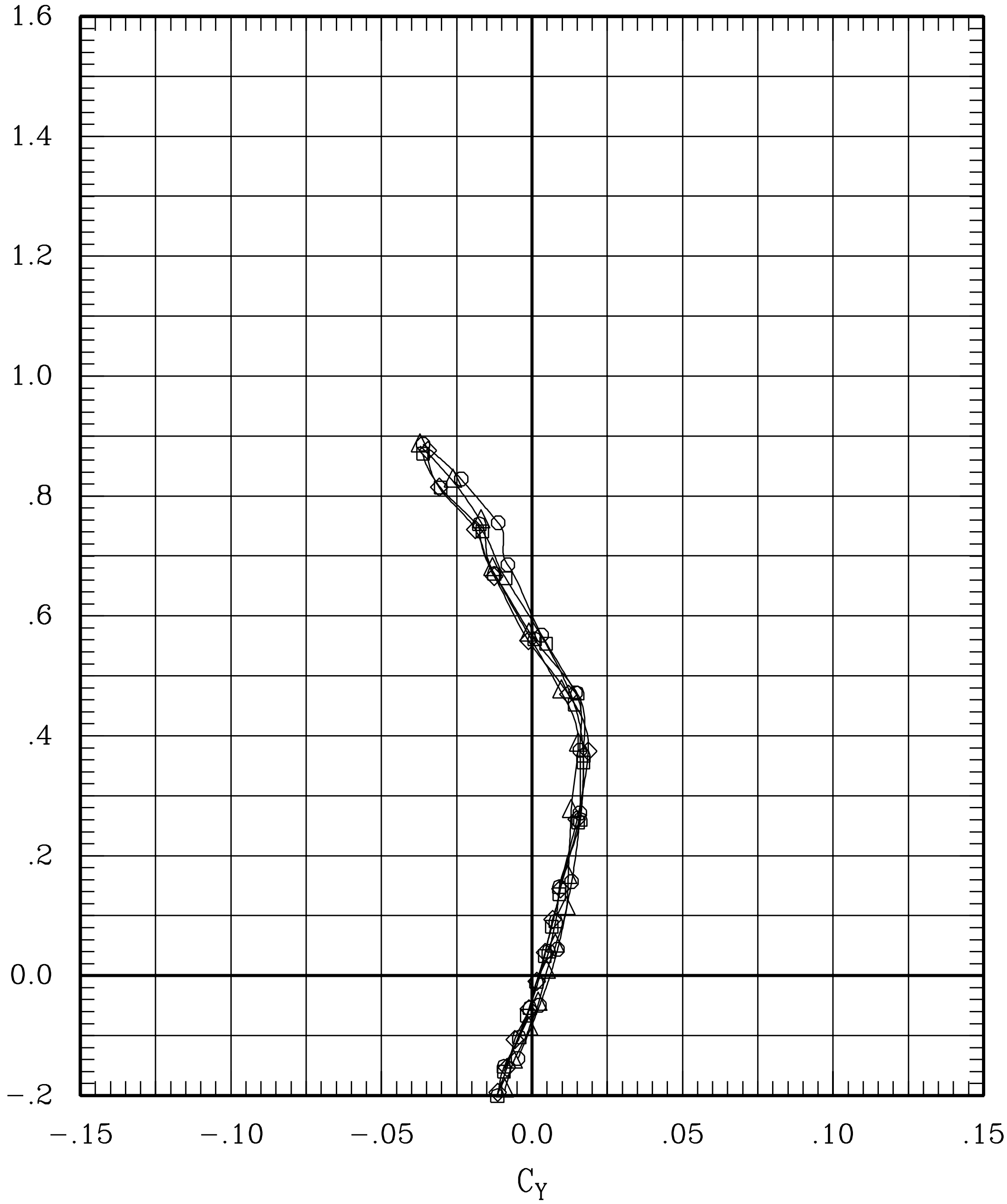

Figure 21(h). Effect of cruise flaps and ailerons for sweep = 60 deg, Mach = 1.40.

SYMBOL	LT LA LO LI ^ RI RO RA RT	RUN	SWEEP	MACH	Q	BETA
—□—	00 00 00 00 L 00 00 00 00	32	60	1.40	702	−.2
—◇—	00 00 −5 −5 L 05 05 00 00	200	60	1.40	694	−.3
—○—	00−10 00 00 L 00 00 10 00	165	60	1.40	703	−.3
—△—	00−10 −5 −5 L 05 05 10 00	186	60	1.40	700	−.3
—⌂—	00 00 −5 00 L 00 05 00 00	211	60	1.40	703	−.3

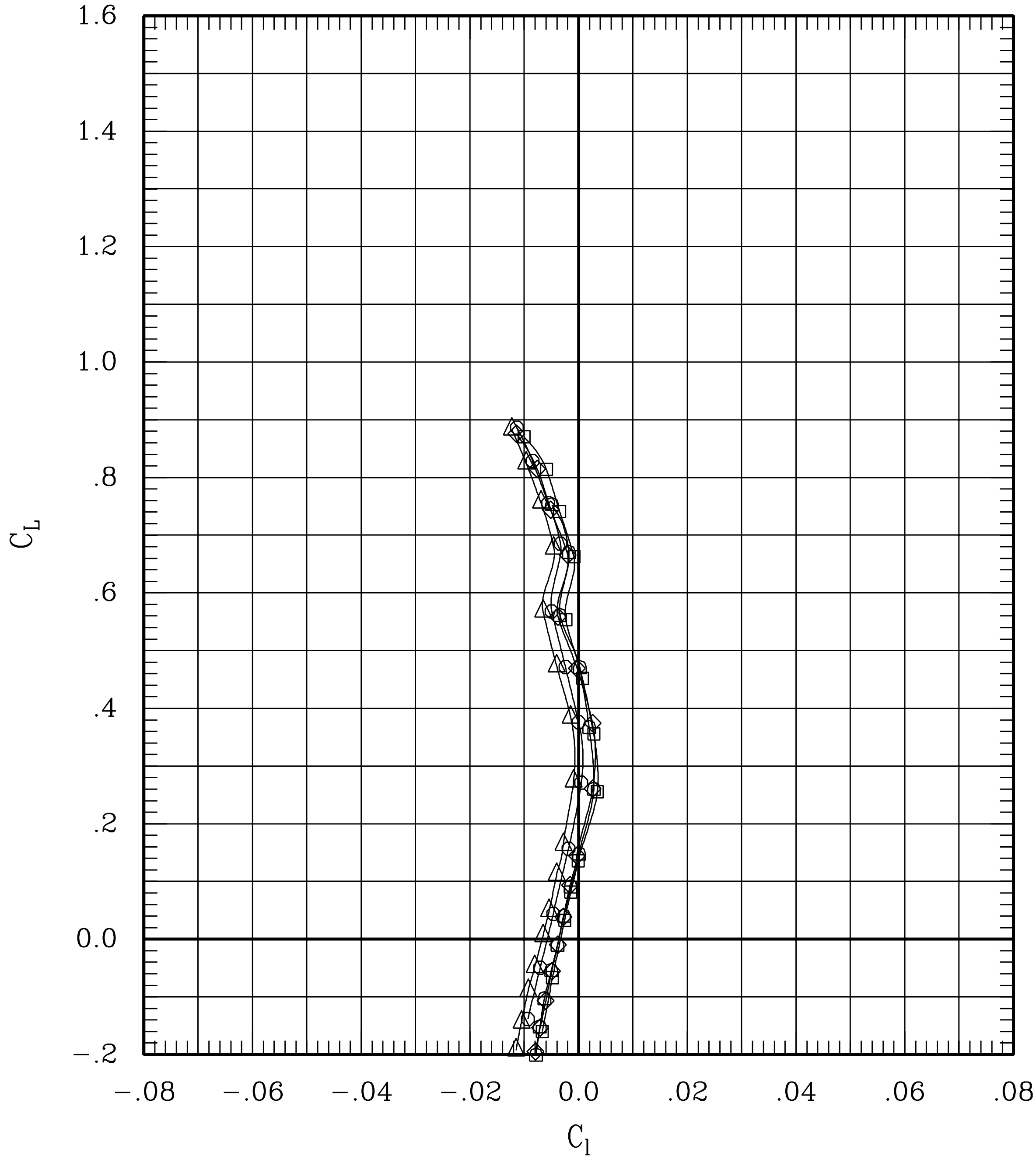

Figure 21(h). Effect of cruise flaps and ailerons for sweep = 60 deg, Mach = 1.40.

SYMBOL	LT LA LO LI ^ RI RO RA RT	RUN	SWEEP	MACH	Q	BETA
—□—	00 00 00 00 L 00 00 00 00	32	60	1.40	702	−.2
—◇—	00 00 −5 −5 L 05 05 00 00	200	60	1.40	694	−.3
—○—	00−10 00 00 L 00 00 10 00	165	60	1.40	703	−.3
—△—	00−10 −5 −5 L 05 05 10 00	186	60	1.40	700	−.3
—⌂—	00 00 −5 00 L 00 05 00 00	211	60	1.40	703	−.3

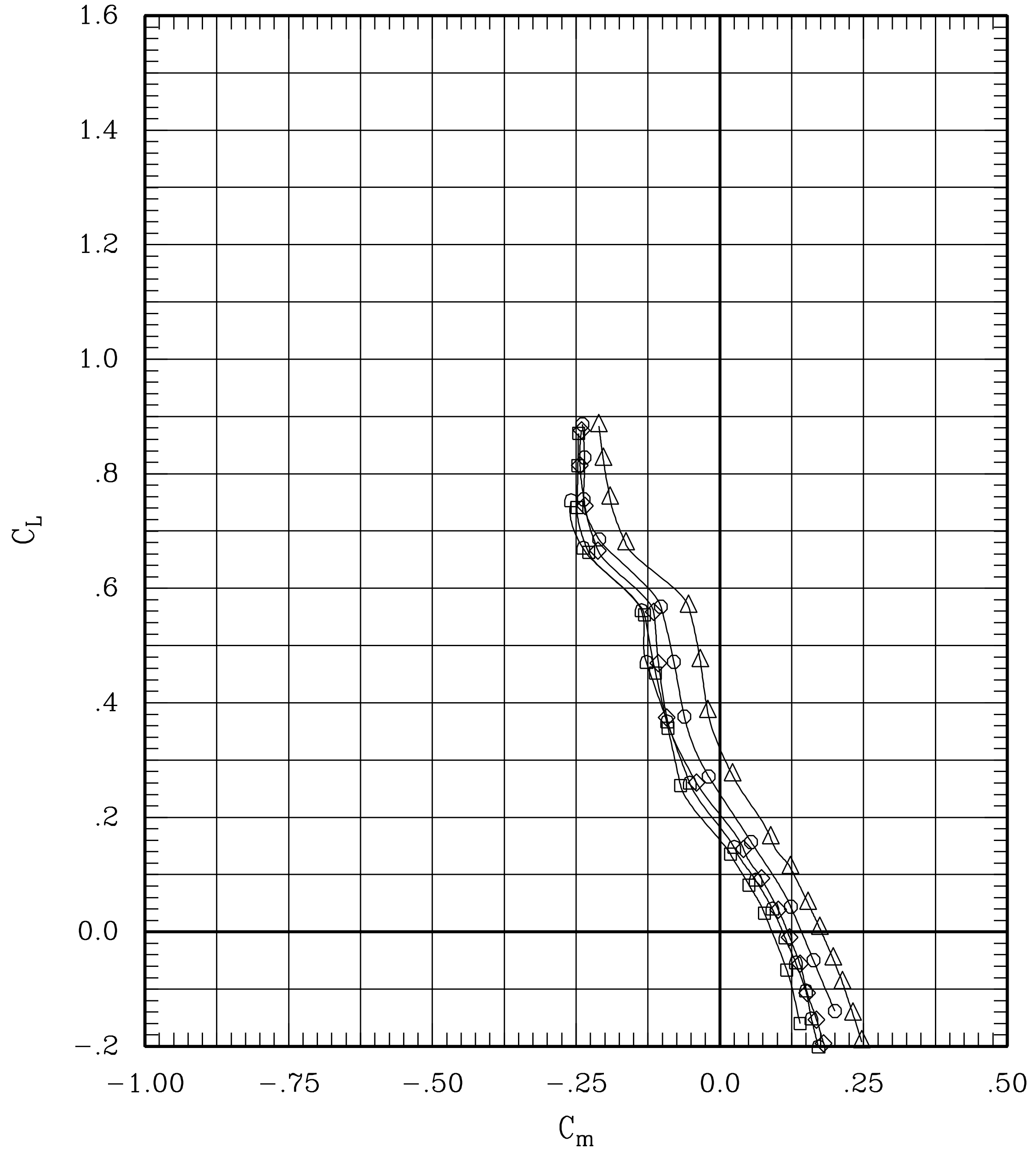

Figure 21(h). Effect of cruise flaps and ailerons for sweep = 60 deg, Mach = 1.40.

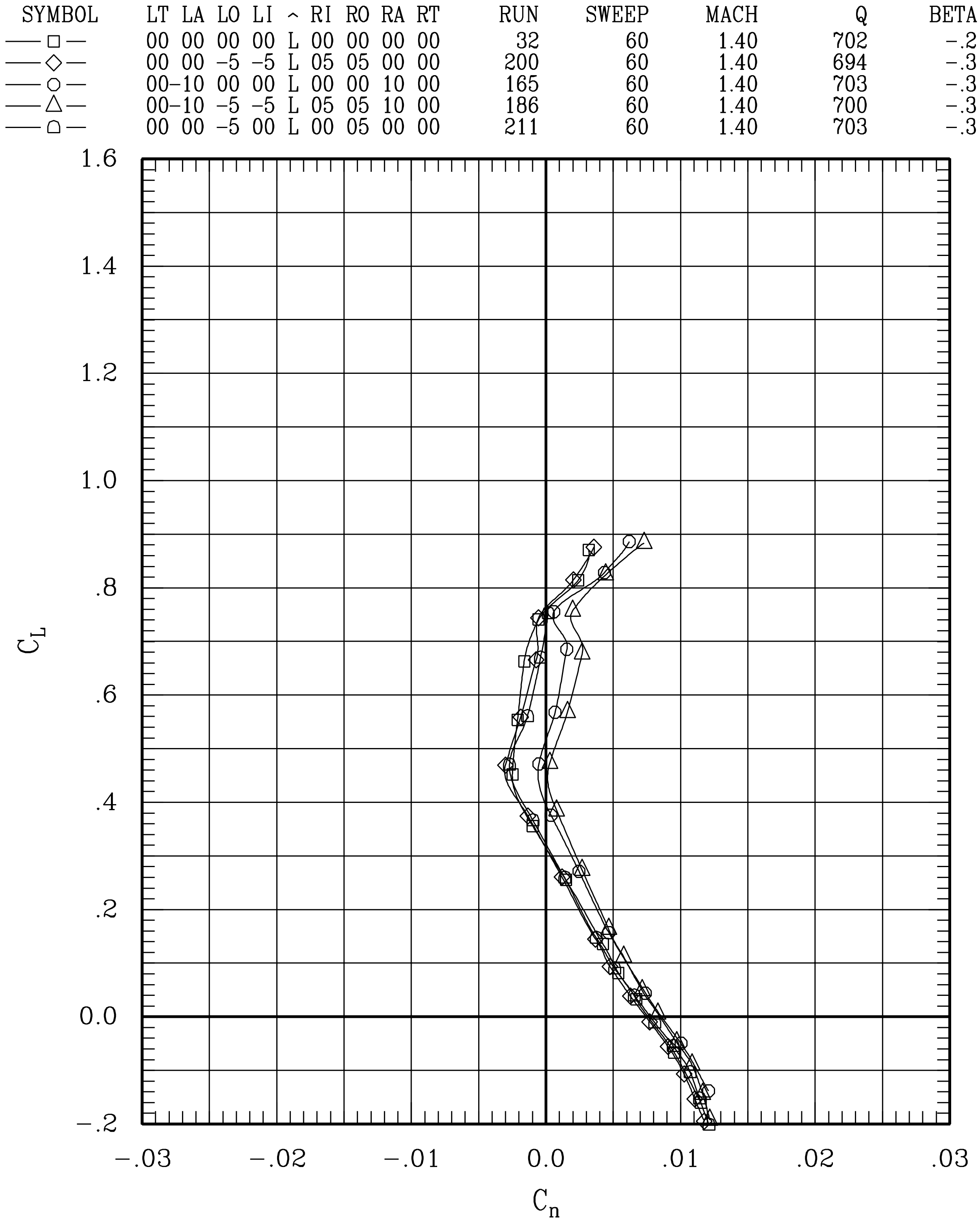

Figure 21(h). Effect of cruise flaps and ailerons for sweep = 60 deg, Mach = 1.40.

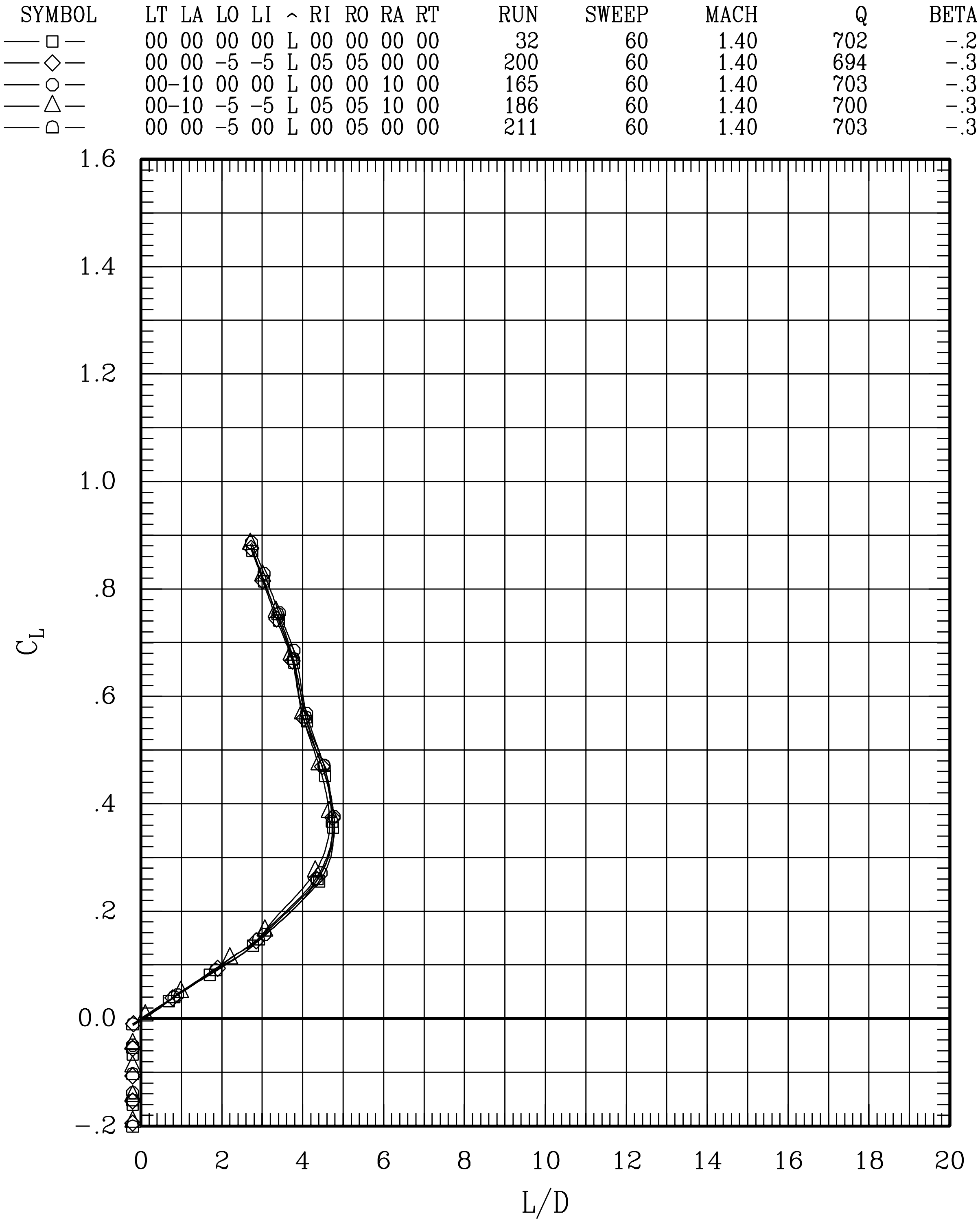

Figure 21(h). Effect of cruise flaps and ailerons for sweep = 60 deg, Mach = 1.40.

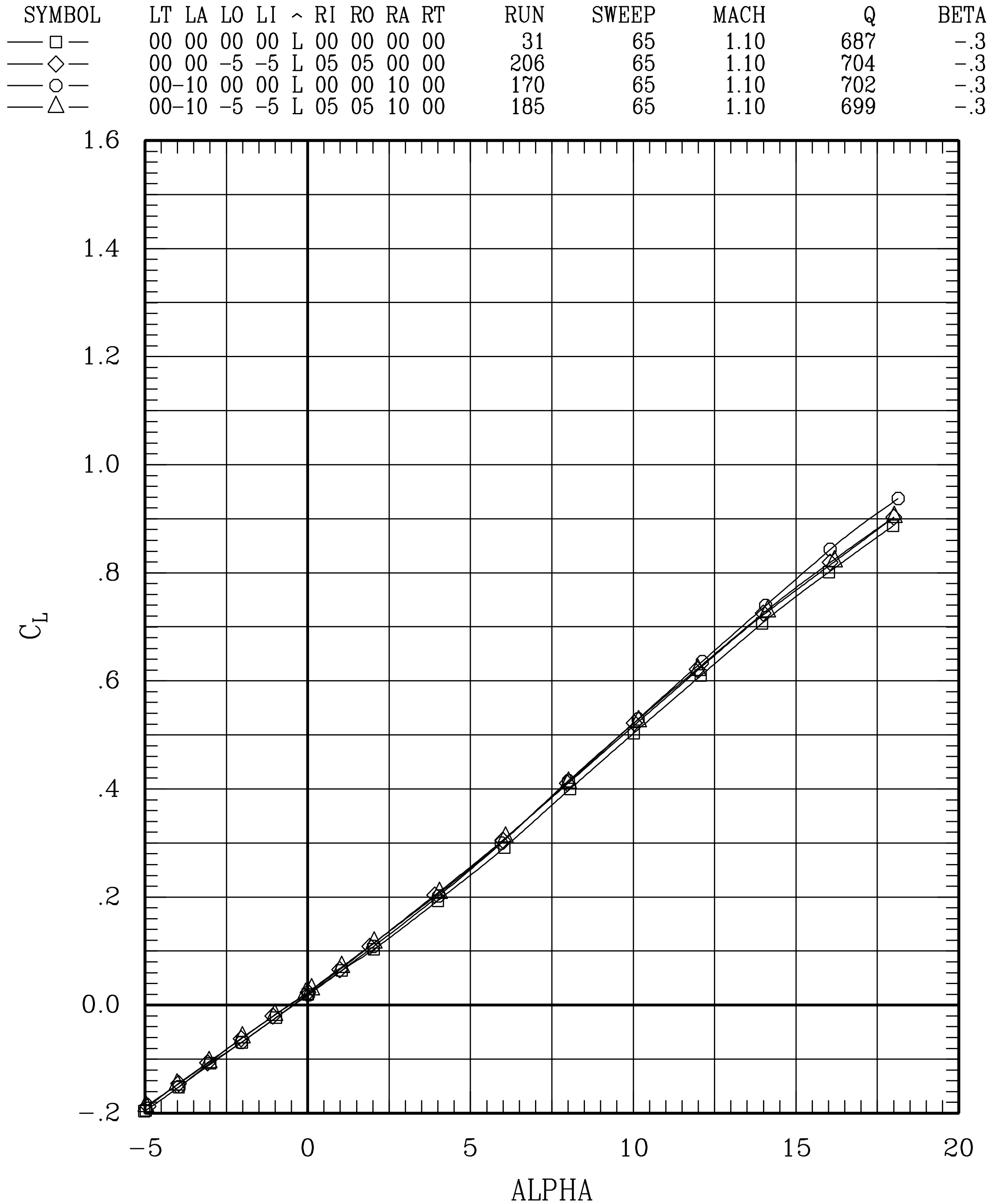

Figure 21(i). Effect of cruise flaps and ailerons for sweep = 65 deg, Mach = 1.10.

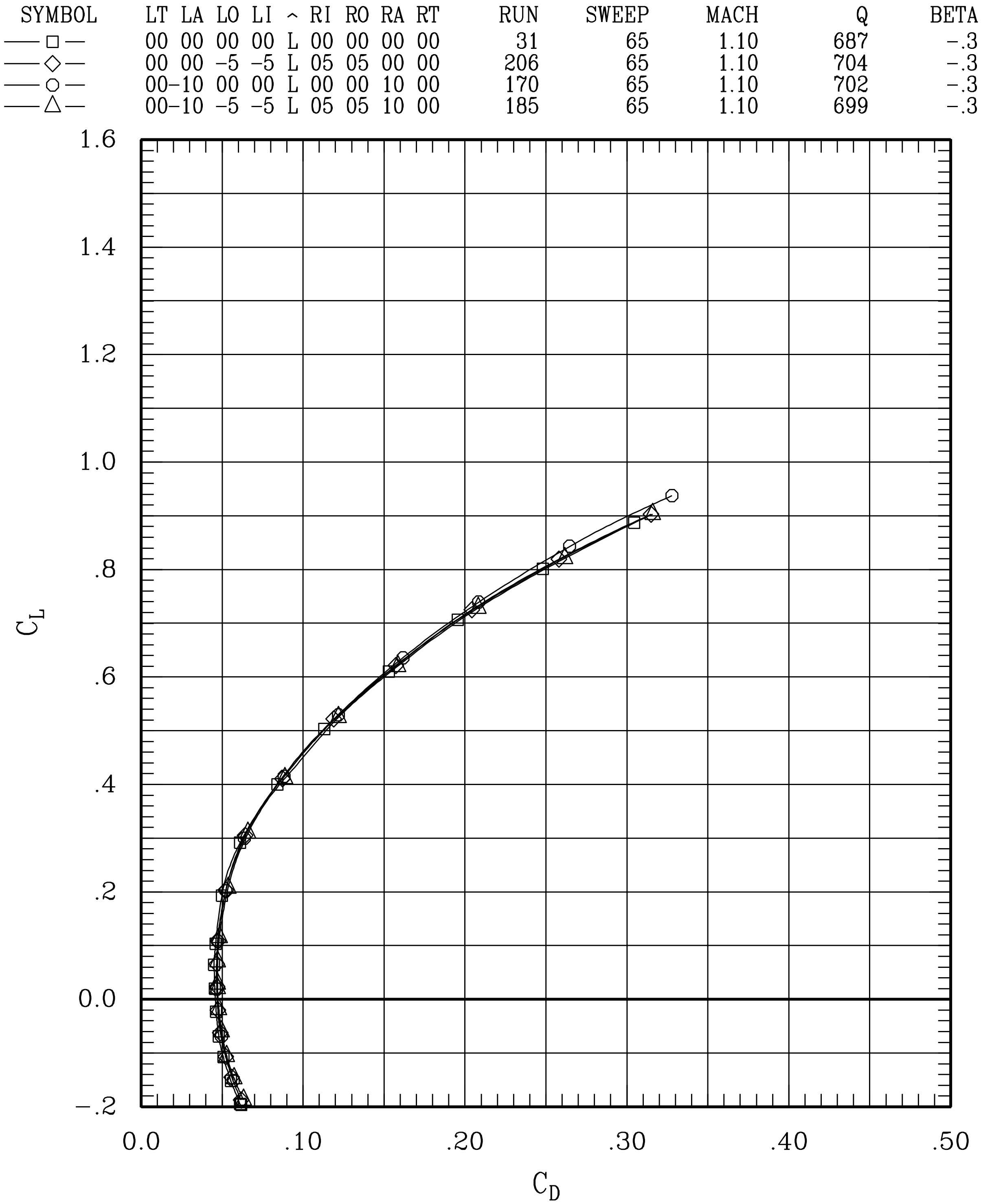

Figure 21(i). Effect of cruise flaps and ailerons for sweep = 65 deg, Mach = 1.10.

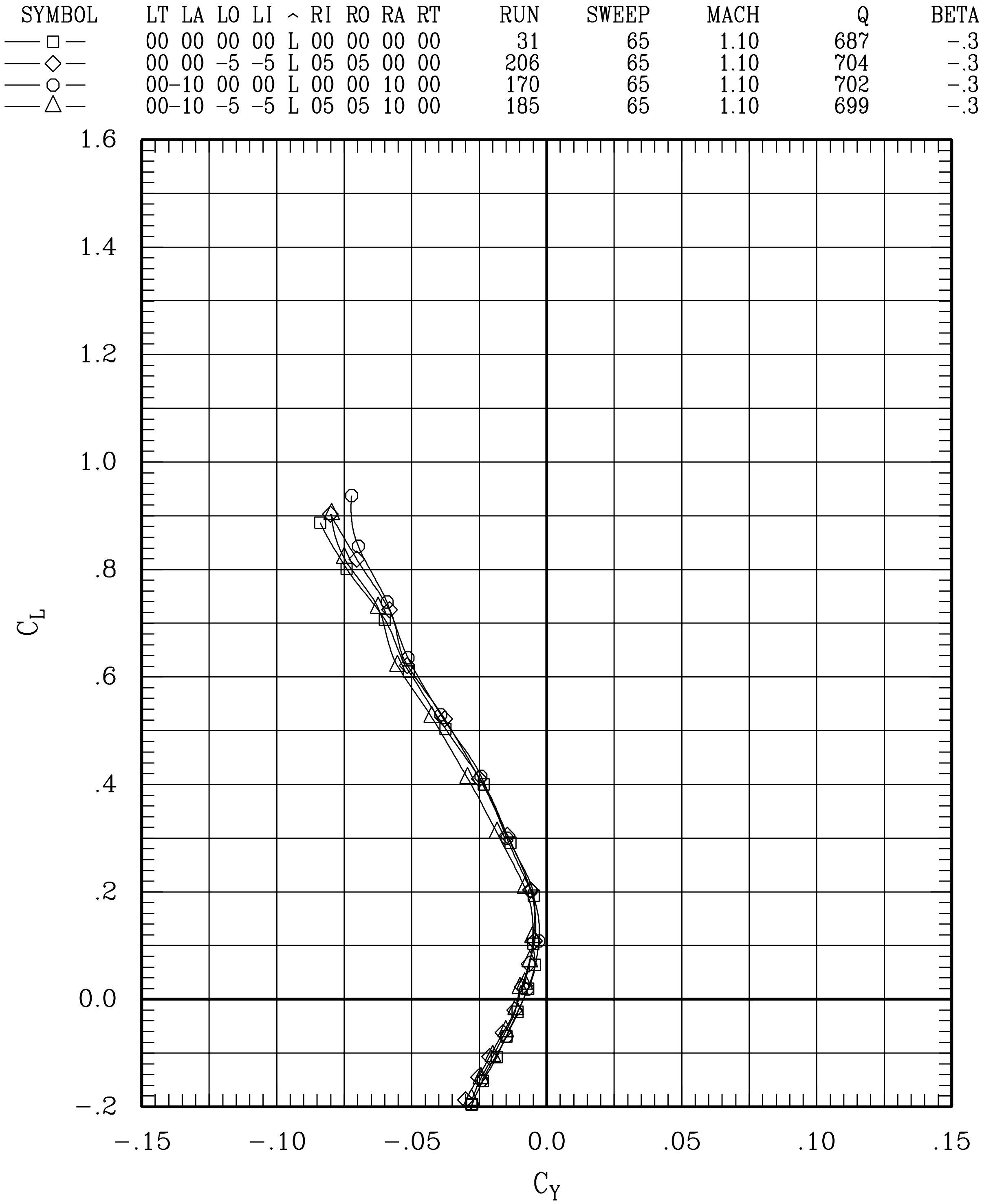

Figure 21(i). Effect of cruise flaps and ailerons for sweep = 65 deg, Mach = 1.10.

SYMBOL	LT LA LO LI ^ RI RO RA RT	RUN	SWEEP	MACH	Q	BETA
—□—	00 00 00 00 L 00 00 00 00	31	65	1.10	687	-.3
—◇—	00 00 -5 -5 L 05 05 00 00	206	65	1.10	704	-.3
—○—	00-10 00 00 L 00 00 10 00	170	65	1.10	702	-.3
—△—	00-10 -5 -5 L 05 05 10 00	185	65	1.10	699	-.3

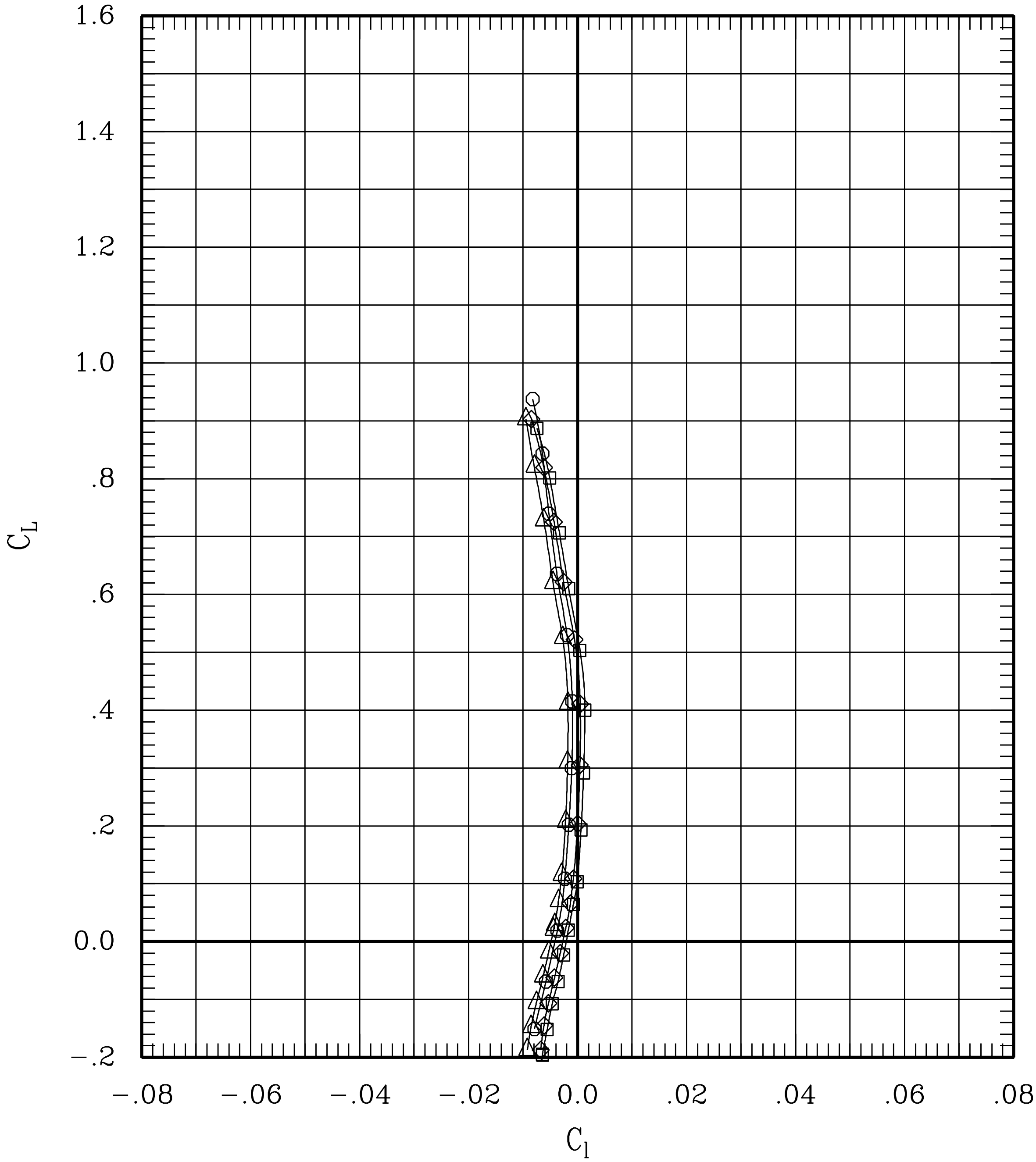

Figure 21(i). Effect of cruise flaps and ailerons for sweep = 65 deg, Mach = 1.10.

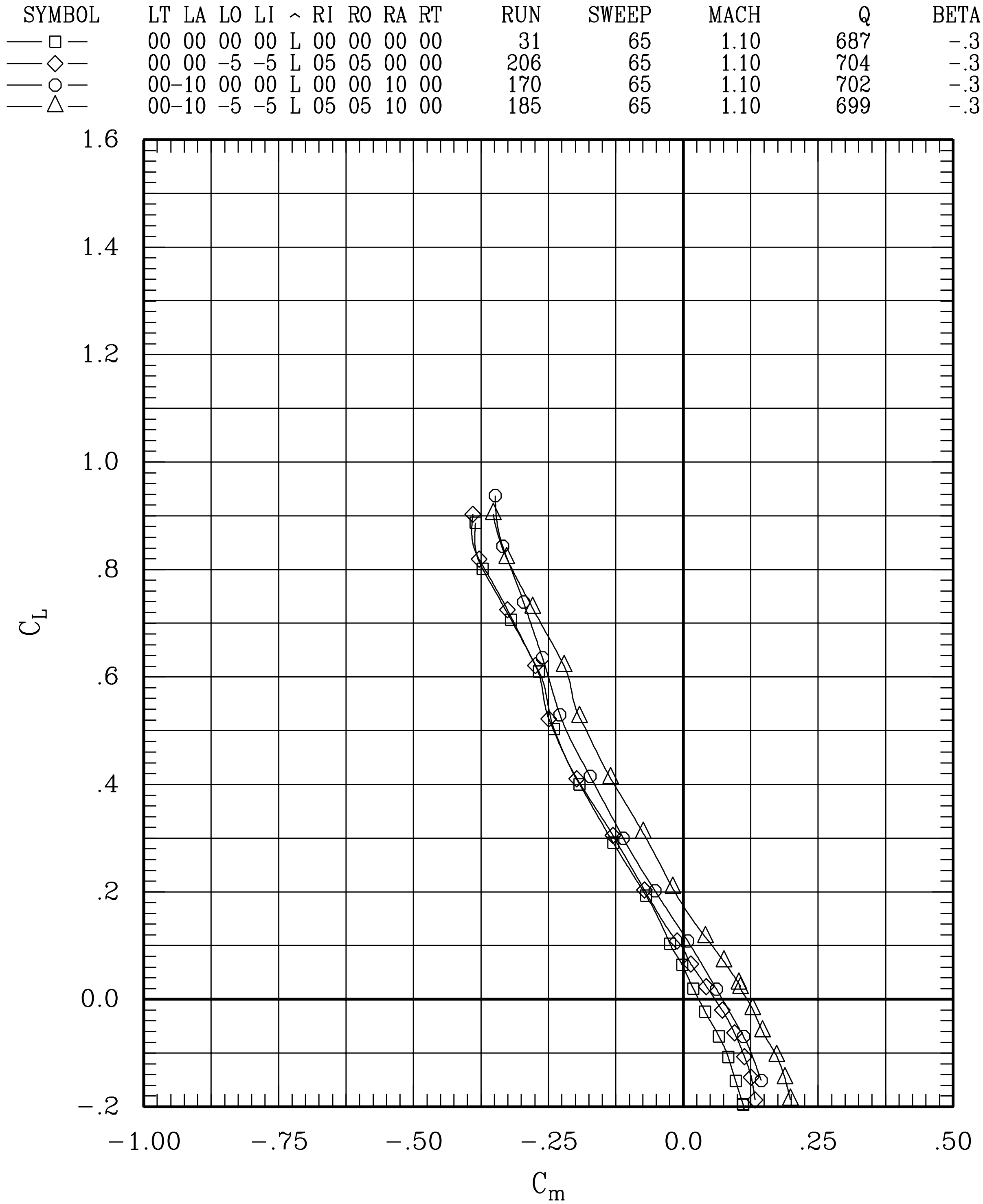

Figure 21(i). Effect of cruise flaps and ailerons for sweep = 65 deg, Mach = 1.10.

SYMBOL	LT LA LO LI ^ RI RO RA RT	RUN	SWEEP	MACH	Q	BETA
—□—	00 00 00 00 L 00 00 00 00	31	65	1.10	687	-.3
—◇—	00 00 -5 -5 L 05 05 00 00	206	65	1.10	704	-.3
—○—	00-10 00 00 L 00 00 10 00	170	65	1.10	702	-.3
—△—	00-10 -5 -5 L 05 05 10 00	185	65	1.10	699	-.3

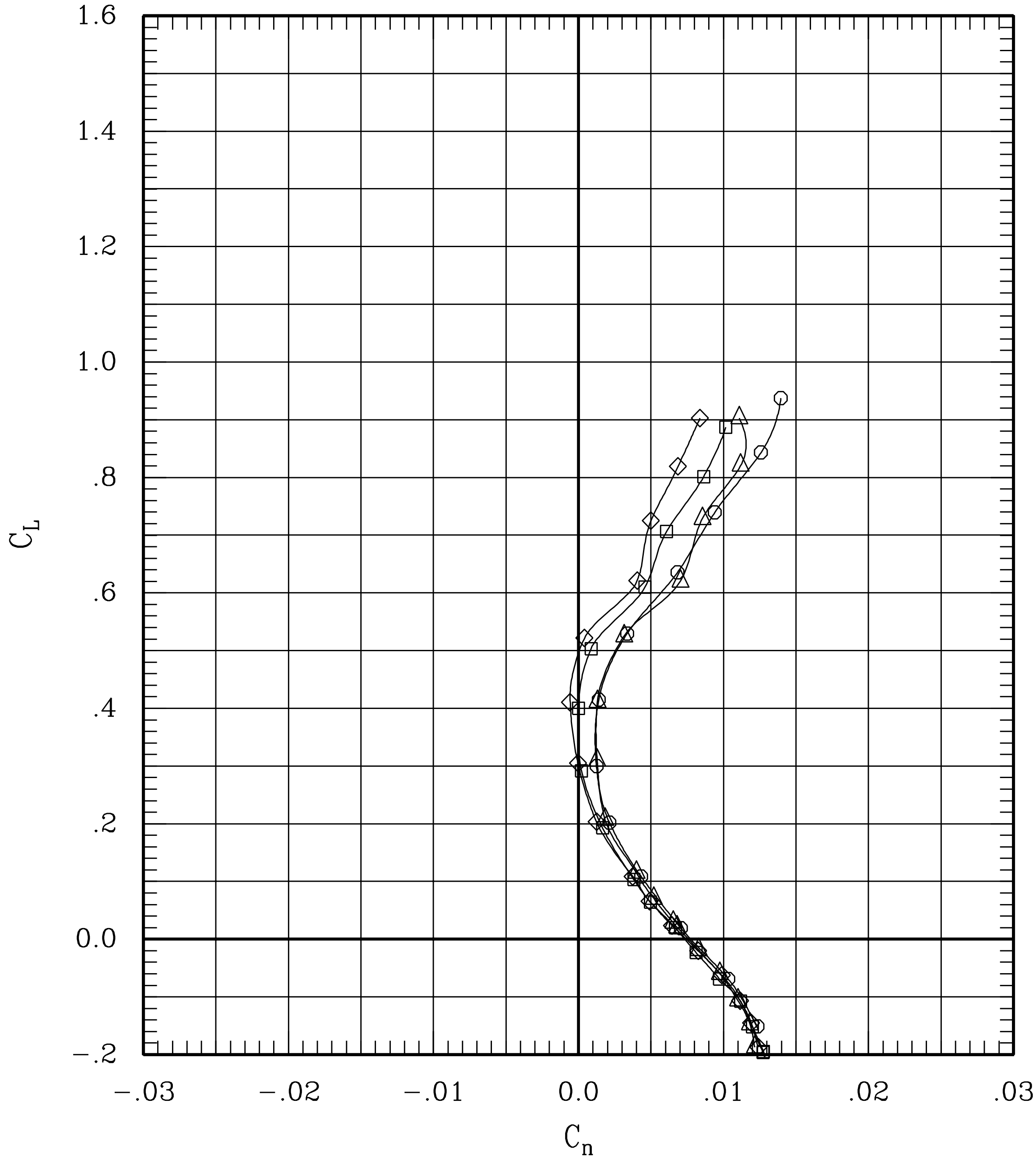

Figure 21(i). Effect of cruise flaps and ailerons for sweep = 65 deg, Mach = 1.10.

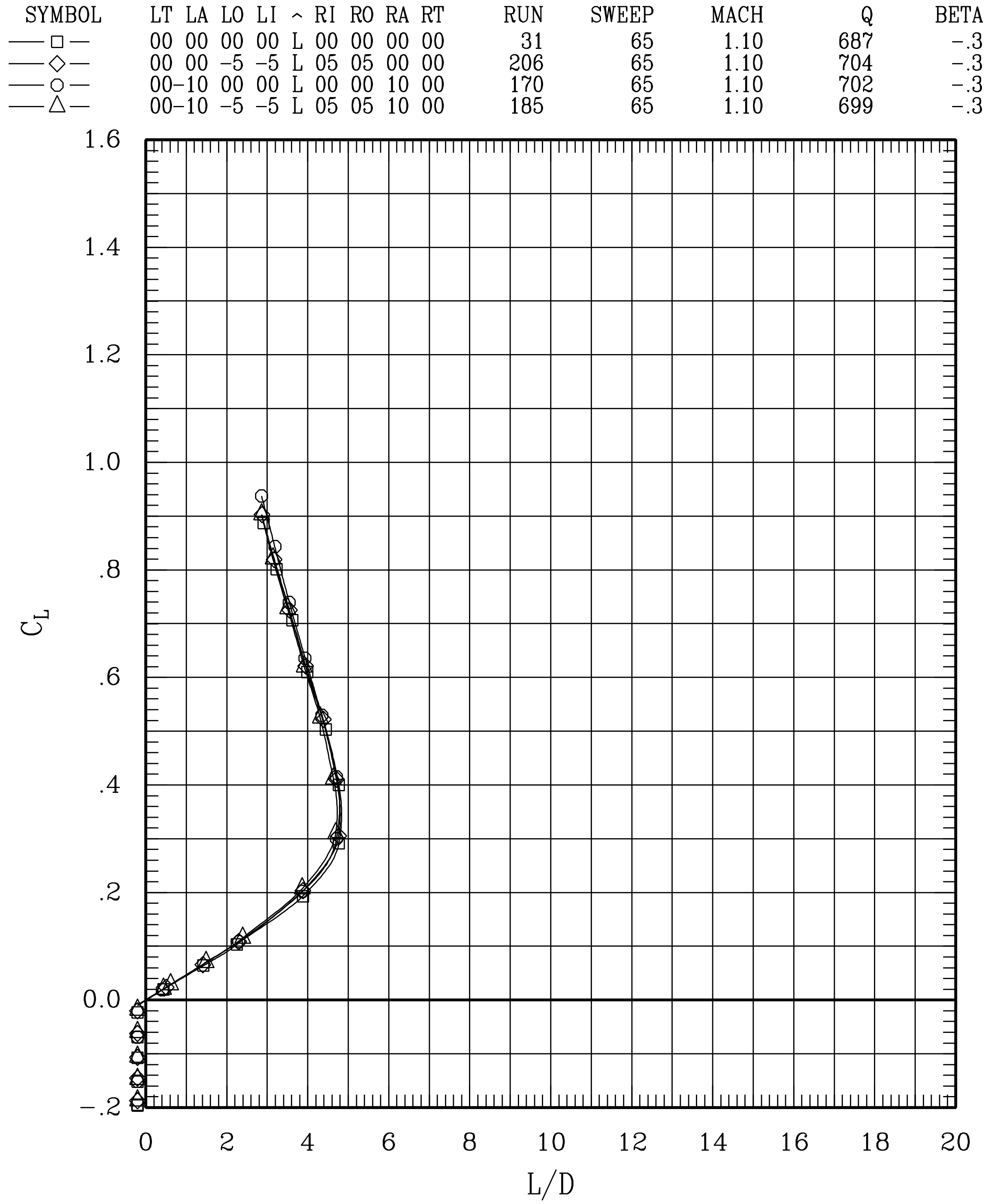

Figure 21(i). Effect of cruise flaps and ailerons for sweep = 65 deg, Mach = 1.10.

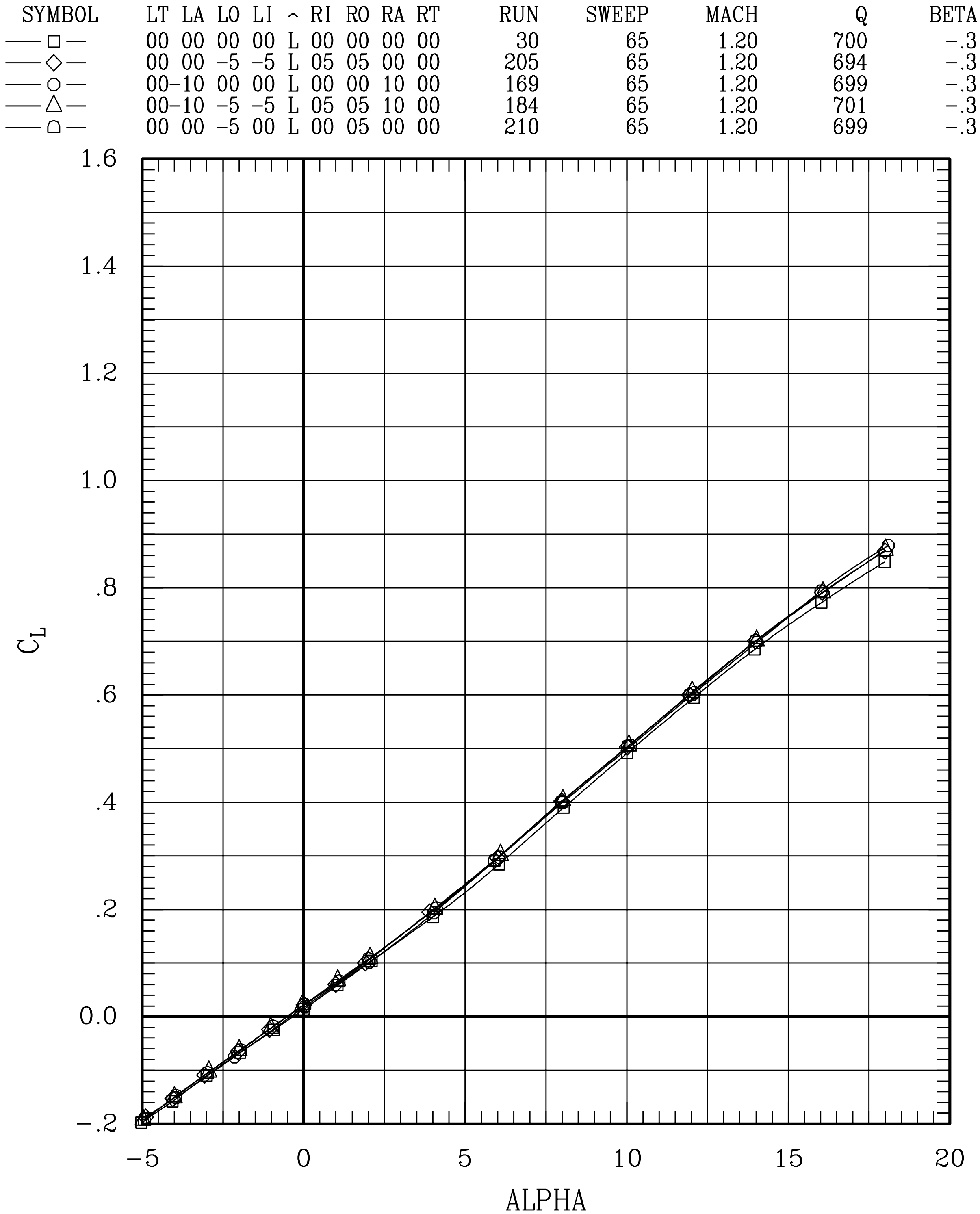

Figure 21(j). Effect of cruise flaps and ailerons for sweep = 65 deg, Mach = 1.20.

SYMBOL	LT LA LO LI ^ RI RO RA RT	RUN	SWEEP	MACH	Q	BETA
—□—	00 00 00 00 L 00 00 00 00	30	65	1.20	700	−.3
—◇—	00 00 −5 −5 L 05 05 00 00	205	65	1.20	694	−.3
—○—	00−10 00 00 L 00 00 10 00	169	65	1.20	699	−.3
—△—	00−10 −5 −5 L 05 05 10 00	184	65	1.20	701	−.3
—⌂—	00 00 −5 00 L 00 05 00 00	210	65	1.20	699	−.3

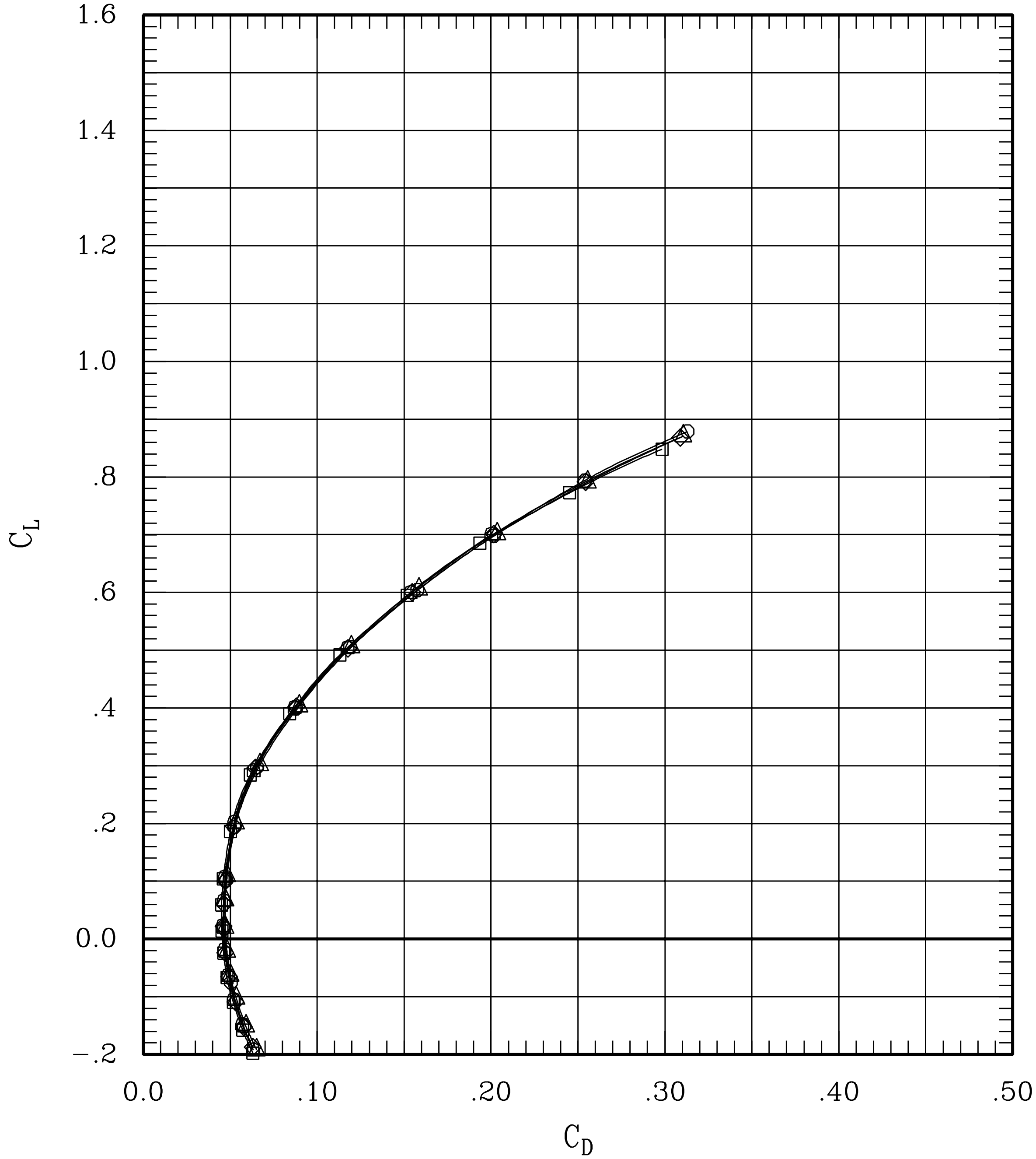

Figure 21(j). Effect of cruise flaps and ailerons for sweep = 65 deg, Mach = 1.20.

SYMBOL	LT	LA	LO	LI	^	RI	RO	RA	RT	RUN	SWEEP	MACH	Q	BETA
—□—	00	00	00	00	L	00	00	00	00	30	65	1.20	700	−.3
—◇—	00	00	−5	−5	L	05	05	00	00	205	65	1.20	694	−.3
—○—	00	−10	00	00	L	00	00	10	00	169	65	1.20	699	−.3
—△—	00	−10	−5	−5	L	05	05	10	00	184	65	1.20	701	−.3
—⌂—	00	00	−5	00	L	00	05	00	00	210	65	1.20	699	−.3

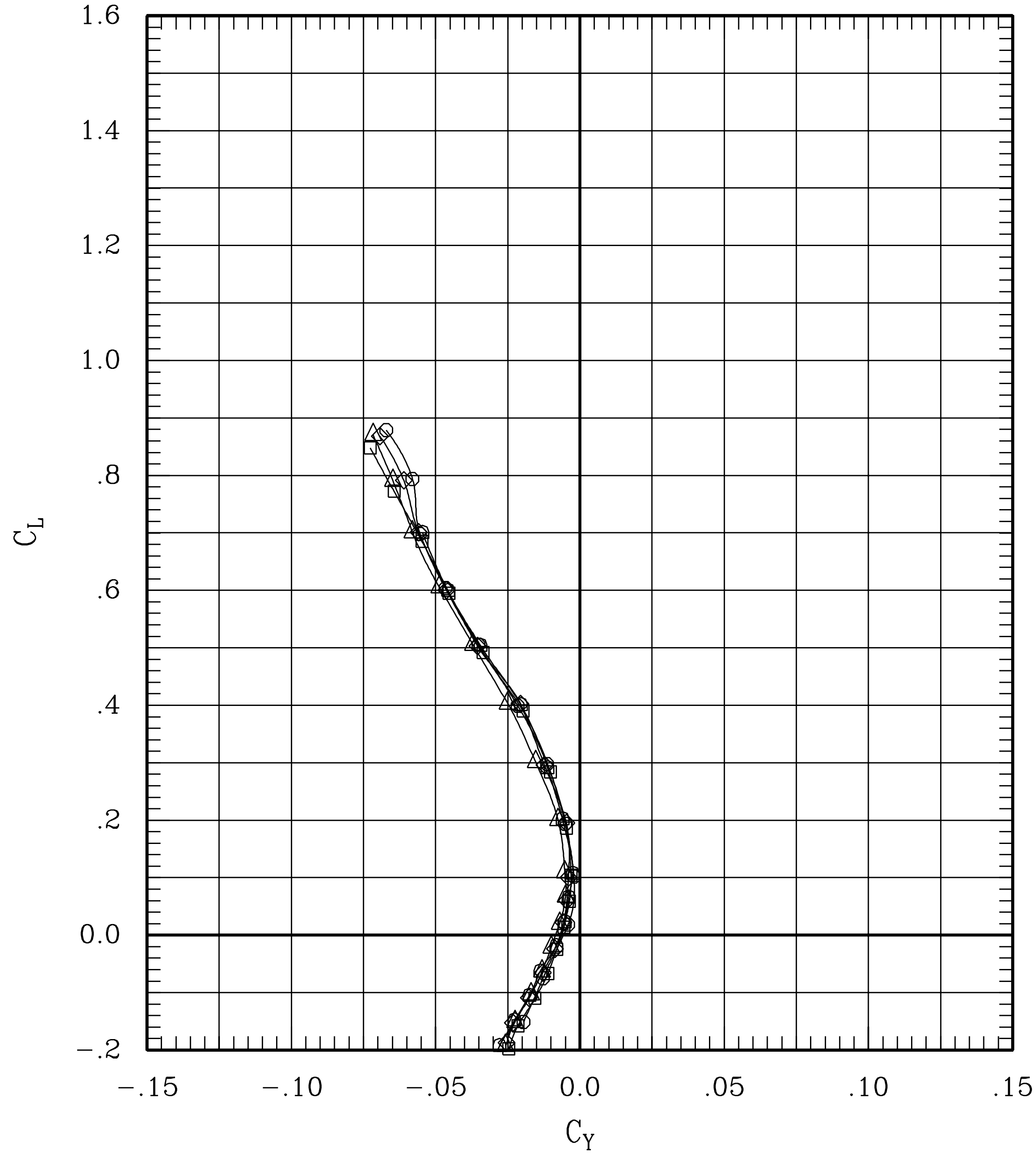

Figure 21(j). Effect of cruise flaps and ailerons for sweep = 65 deg, Mach = 1.20.

SYMBOL	LT LA LO LI ^ RI RO RA RT	RUN	SWEEP	MACH	Q	BETA
—□—	00 00 00 00 L 00 00 00 00	30	65	1.20	700	−.3
—◇—	00 00 −5 −5 L 05 05 00 00	205	65	1.20	694	−.3
—○—	00−10 00 00 L 00 00 10 00	169	65	1.20	699	−.3
—△—	00−10 −5 −5 L 05 05 10 00	184	65	1.20	701	−.3
—⌂—	00 00 −5 00 L 00 05 00 00	210	65	1.20	699	−.3

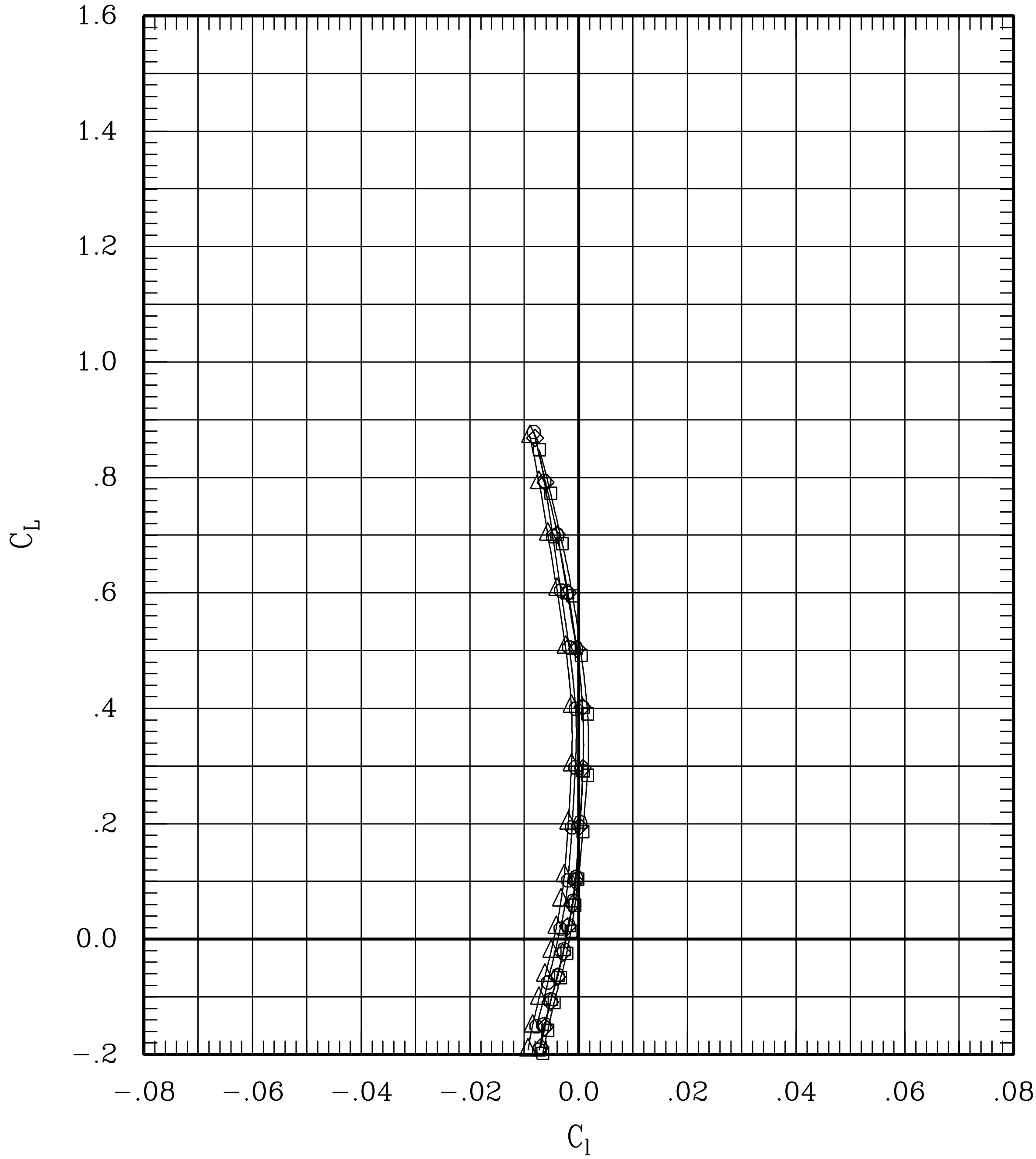

Figure 21(j). Effect of cruise flaps and ailerons for sweep = 65 deg, Mach = 1.20.

SYMBOL	LT LA LO LI ^ RI RO RA RT	RUN	SWEEP	MACH	Q	BETA
—□—	00 00 00 00 L 00 00 00 00	30	65	1.20	700	-.3
—◇—	00 00 -5 -5 L 05 05 00 00	205	65	1.20	694	-.3
—○—	00-10 00 00 L 00 00 10 00	169	65	1.20	699	-.3
—△—	00-10 -5 -5 L 05 05 10 00	184	65	1.20	701	-.3
—⌂—	00 00 -5 00 L 00 05 00 00	210	65	1.20	699	-.3

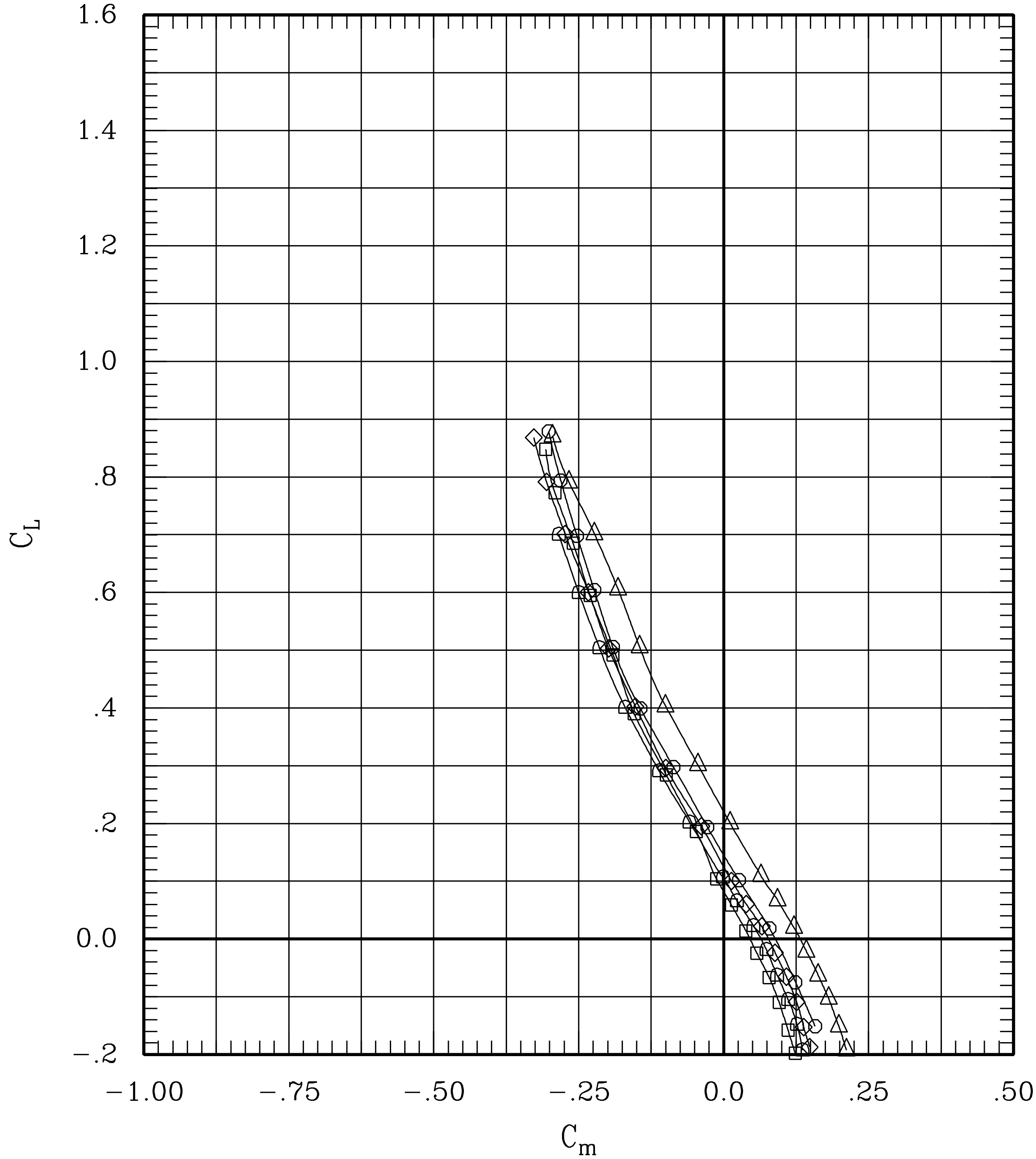

Figure 21(j). Effect of cruise flaps and ailerons for sweep = 65 deg, Mach = 1.20.

SYMBOL	LT LA LO LI ^ RI RO RA RT	RUN	SWEEP	MACH	Q	BETA
—□—	00 00 00 00 L 00 00 00 00	30	65	1.20	700	−.3
—◇—	00 00 −5 −5 L 05 05 00 00	205	65	1.20	694	−.3
—○—	00−10 00 00 L 00 00 10 00	169	65	1.20	699	−.3
—△—	00−10 −5 −5 L 05 05 10 00	184	65	1.20	701	−.3
—⌂—	00 00 −5 00 L 00 05 00 00	210	65	1.20	699	−.3

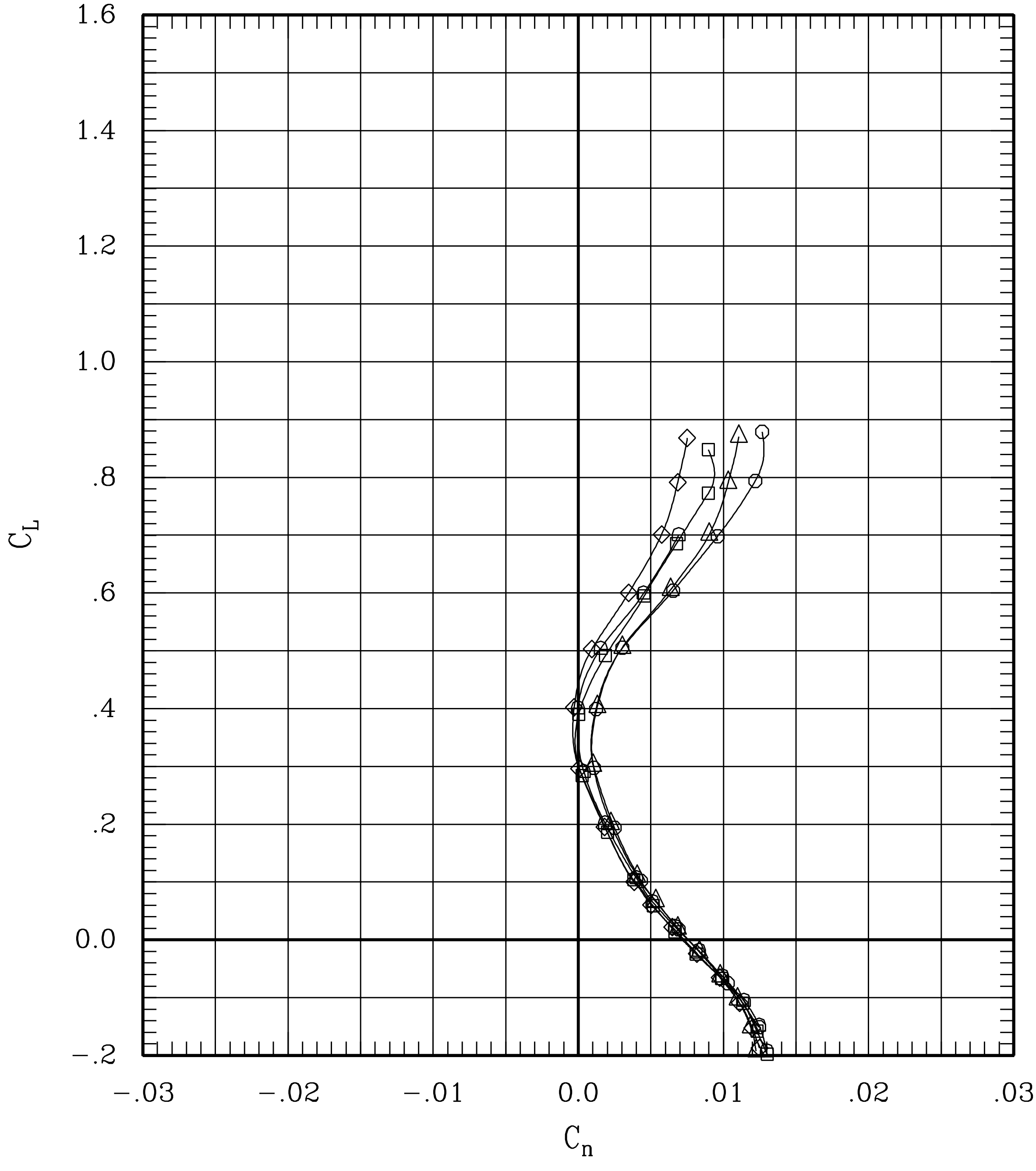

Figure 21(j). Effect of cruise flaps and ailerons for sweep = 65 deg, Mach = 1.20.

SYMBOL	LT LA LO LI ^ RI RO RA RT	RUN	SWEEP	MACH	Q	BETA
—□—	00 00 00 00 L 00 00 00 00	30	65	1.20	700	-.3
—◇—	00 00 -5 -5 L 05 05 00 00	205	65	1.20	694	-.3
—○—	00-10 00 00 L 00 00 10 00	169	65	1.20	699	-.3
—△—	00-10 -5 -5 L 05 05 10 00	184	65	1.20	701	-.3
—⌂—	00 00 -5 00 L 00 05 00 00	210	65	1.20	699	-.3

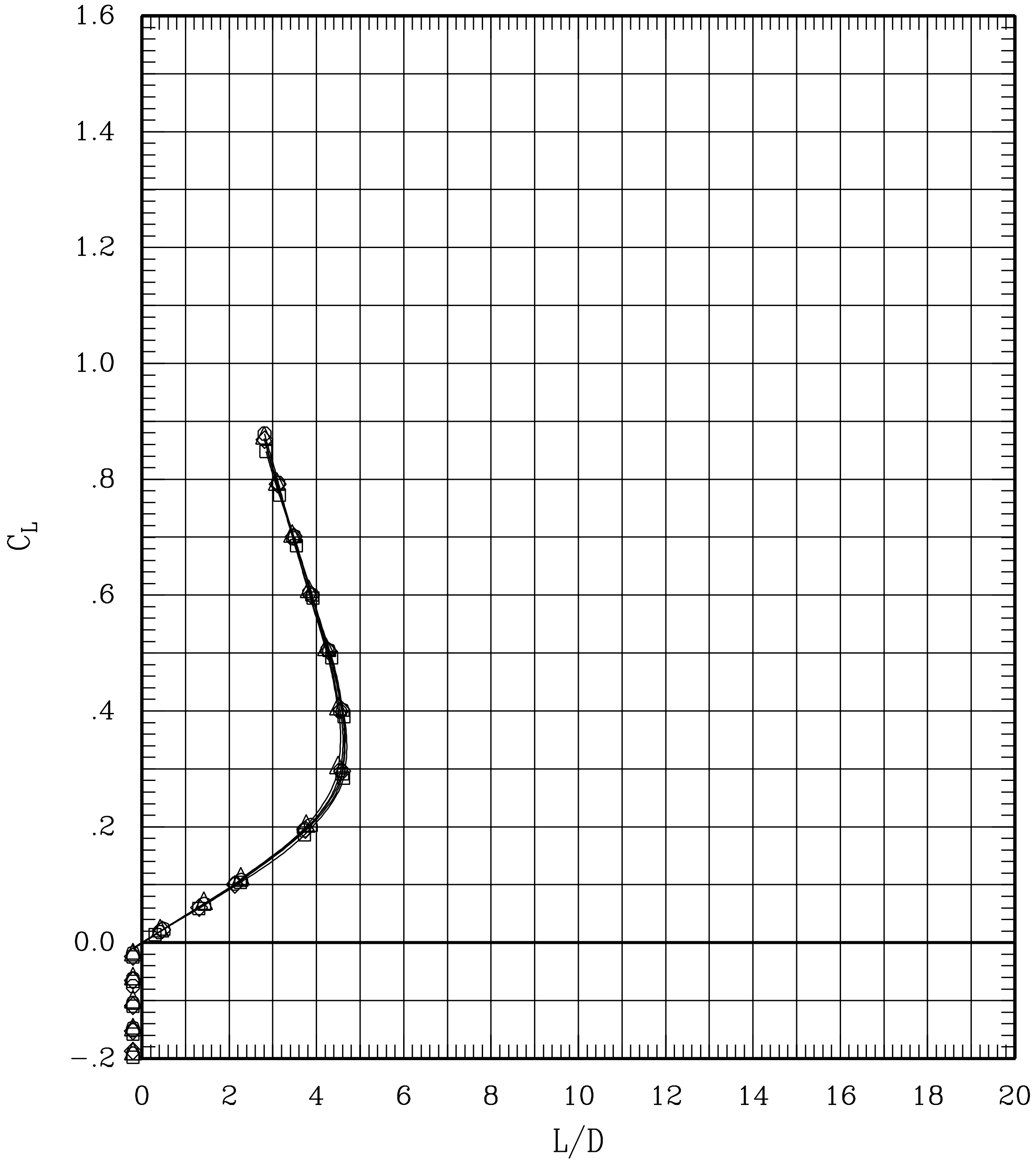

Figure 21(j). Effect of cruise flaps and ailerons for sweep = 65 deg, Mach = 1.20.

SYMBOL	LT LA LO LI ^ RI RO RA RT	RUN	SWEEP	MACH	Q	BETA
—□—	00 00 00 00 L 00 00 00 00	29	65	1.40	701	−.3
—◇—	00 00 −5 −5 L 05 05 00 00	204	65	1.40	696	−.3
—○—	00−10 00 00 L 00 00 10 00	168	65	1.40	703	−.3
—△—	00−10 −5 −5 L 05 05 10 00	182	65	1.40	699	−.3
—⌂—	00 00 −5 −5 L −5 −5 00 00	207	65	1.40	698	−.3
—◇—	00 00 −5 00 L 00 05 00 00	209	65	1.40	703	−.3

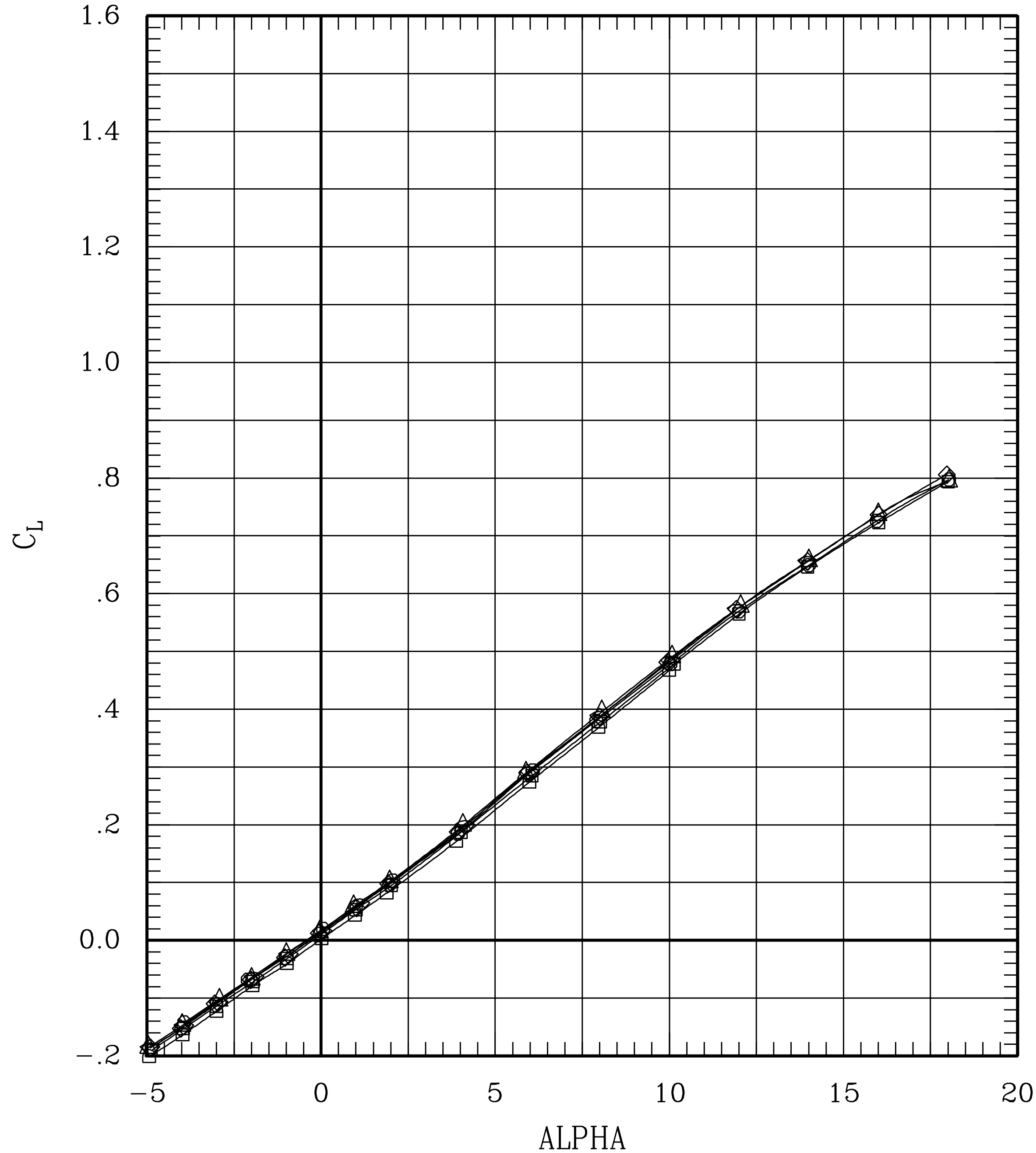

Figure 21(k). Effect of cruise flaps and ailerons for sweep = 65 deg, Mach = 1.40.

SYMBOL	LT LA LO LI ^ RI RO RA RT	RUN	SWEEP	MACH	Q	BETA
—□—	00 00 00 00 L 00 00 00 00	29	65	1.40	701	−.3
—◇—	00 00 −5 −5 L 05 05 00 00	204	65	1.40	696	−.3
—○—	00−10 00 00 L 00 00 10 00	168	65	1.40	703	−.3
—△—	00−10 −5 −5 L 05 05 10 00	182	65	1.40	699	−.3
—⌂—	00 00 −5 −5 L −5 −5 00 00	207	65	1.40	698	−.3
—◇—	00 00 −5 00 L 00 05 00 00	209	65	1.40	703	−.3

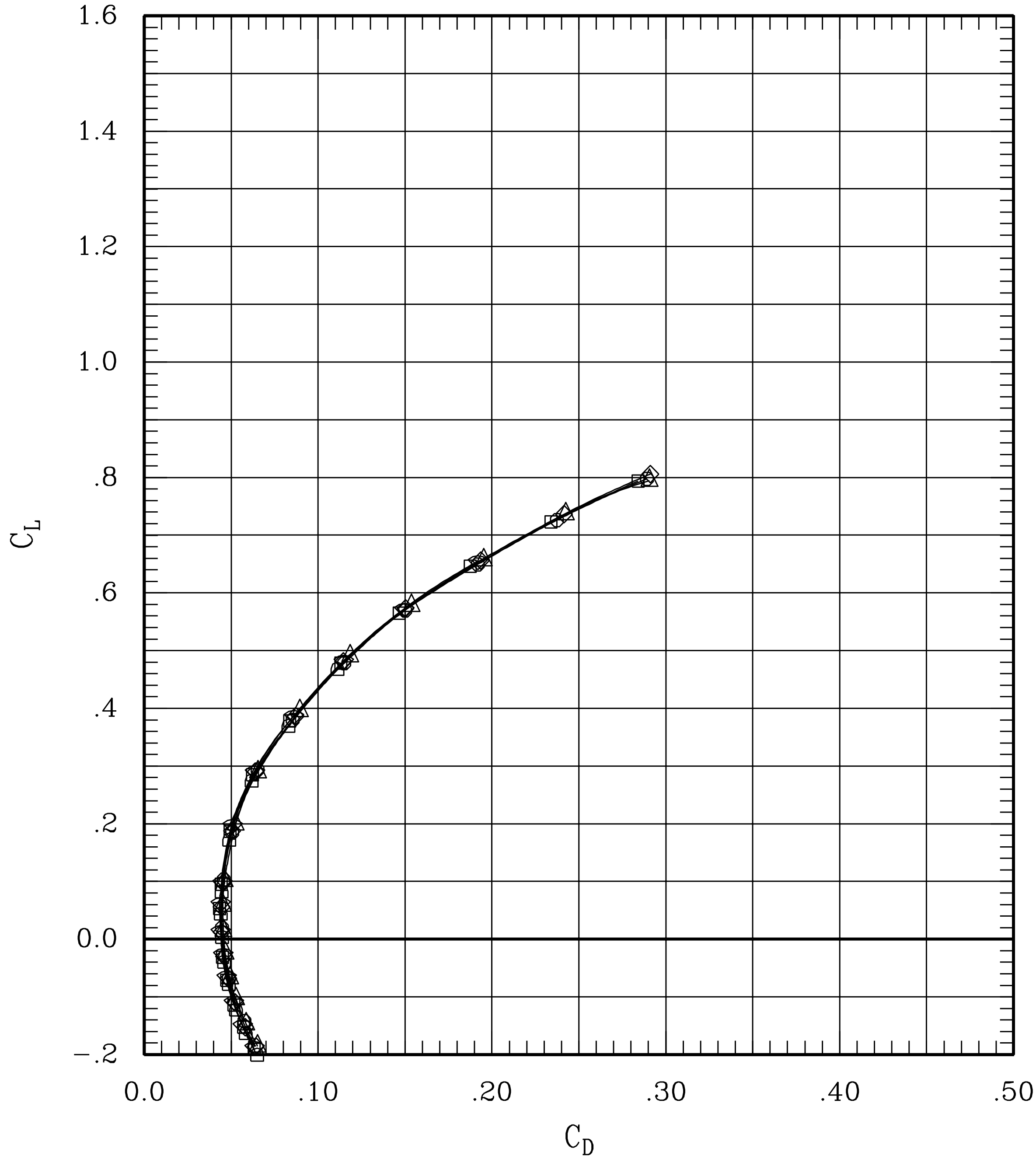

Figure 21(k). Effect of cruise flaps and ailerons for sweep = 65 deg, Mach = 1.40.

SYMBOL	LT	LA	LO	LI	^	RI	RO	RA	RT	RUN	SWEEP	MACH	Q	BETA
—□—	00	00	00	00	L	00	00	00	00	29	65	1.40	701	−.3
—◇—	00	00	−5	−5	L	05	05	00	00	204	65	1.40	696	−.3
—○—	00	−10	00	00	L	00	00	10	00	168	65	1.40	703	−.3
—△—	00	−10	−5	−5	L	05	05	10	00	182	65	1.40	699	−.3
—⌂—	00	00	−5	−5	L	−5	−5	00	00	207	65	1.40	698	−.3
—♢—	00	00	−5	00	L	00	05	00	00	209	65	1.40	703	−.3

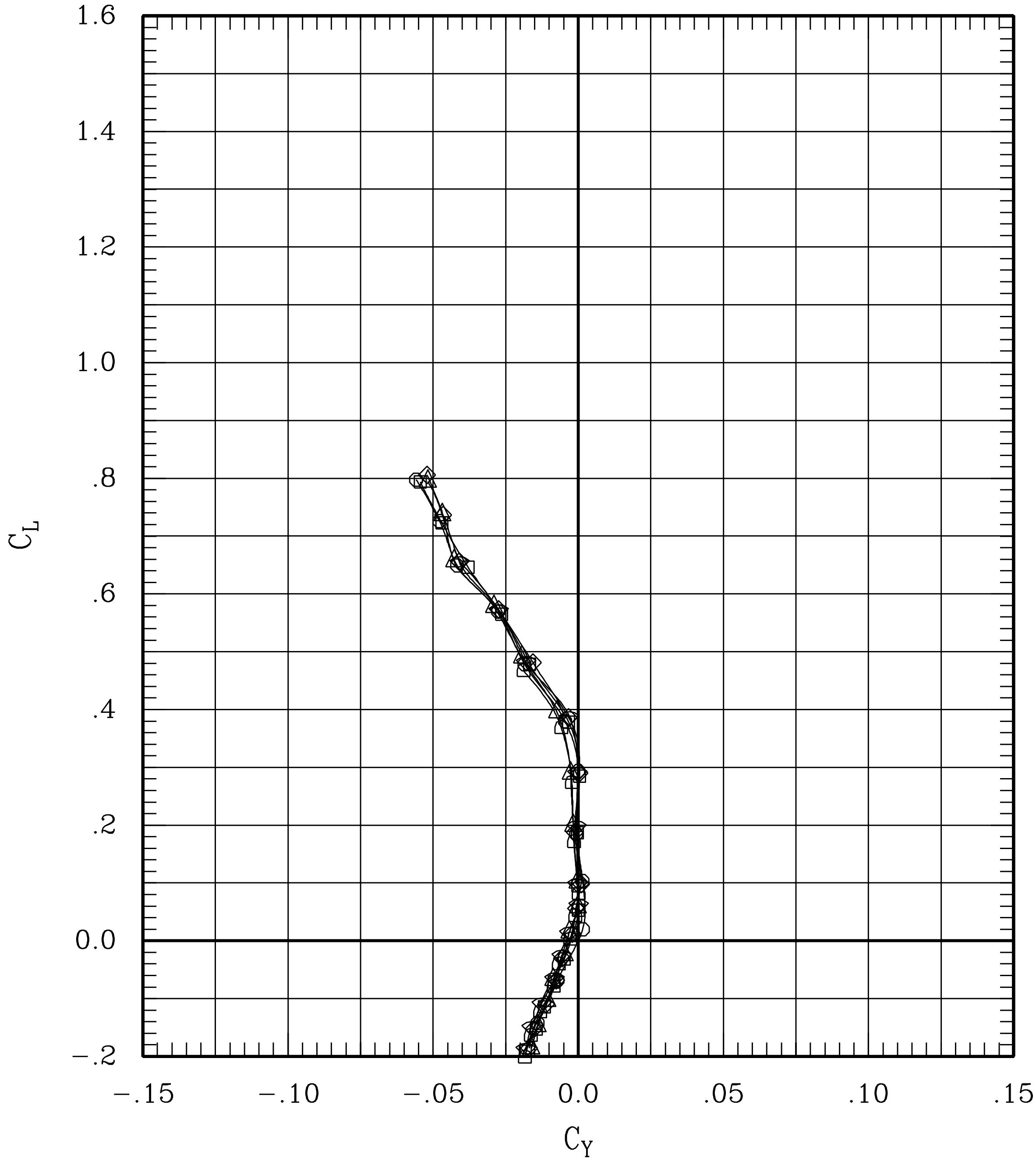

Figure 21(k). Effect of cruise flaps and ailerons for sweep = 65 deg, Mach = 1.40.

SYMBOL	LT LA LO LI ^ RI RO RA RT	RUN	SWEEP	MACH	Q	BETA
—□—	00 00 00 00 L 00 00 00 00	29	65	1.40	701	-.3
—◇—	00 00 -5 -5 L 05 05 00 00	204	65	1.40	696	-.3
—○—	00-10 00 00 L 00 00 10 00	168	65	1.40	703	-.3
—△—	00-10 -5 -5 L 05 05 10 00	182	65	1.40	699	-.3
—⌂—	00 00 -5 -5 L -5 -5 00 00	207	65	1.40	698	-.3
—⬠—	00 00 -5 00 L 00 05 00 00	209	65	1.40	703	-.3

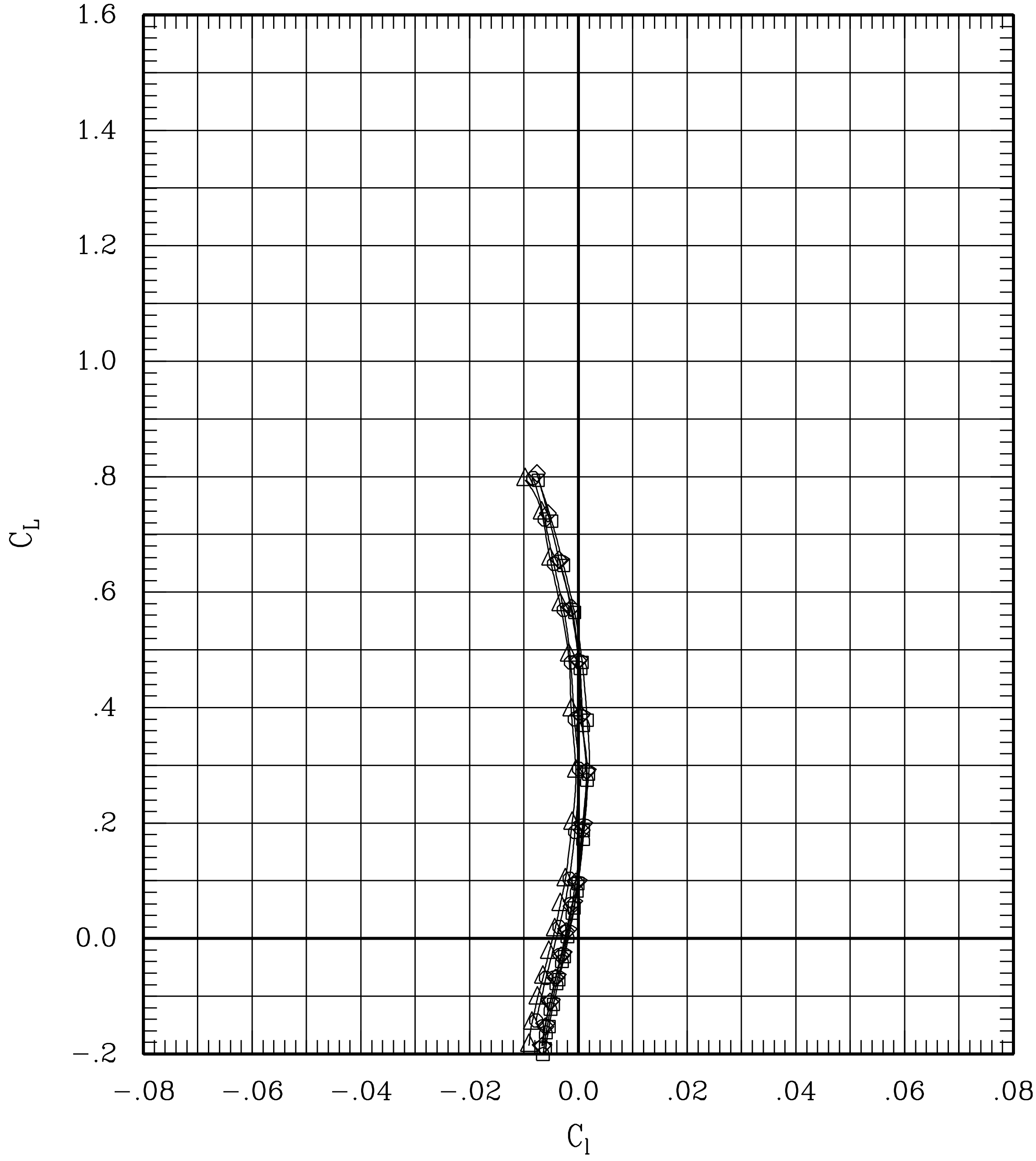

Figure 21(k). Effect of cruise flaps and ailerons for sweep = 65 deg, Mach = 1.40.

SYMBOL	LT LA LO LI ^ RI RO RA RT	RUN	SWEEP	MACH	Q	BETA
—□—	00 00 00 00 L 00 00 00 00	29	65	1.40	701	−.3
—◇—	00 00 −5 −5 L 05 05 00 00	204	65	1.40	696	−.3
—○—	00−10 00 00 L 00 00 10 00	168	65	1.40	703	−.3
—△—	00−10 −5 −5 L 05 05 10 00	182	65	1.40	699	−.3
—◠—	00 00 −5 −5 L −5 −5 00 00	207	65	1.40	698	−.3
—▽—	00 00 −5 00 L 00 05 00 00	209	65	1.40	703	−.3

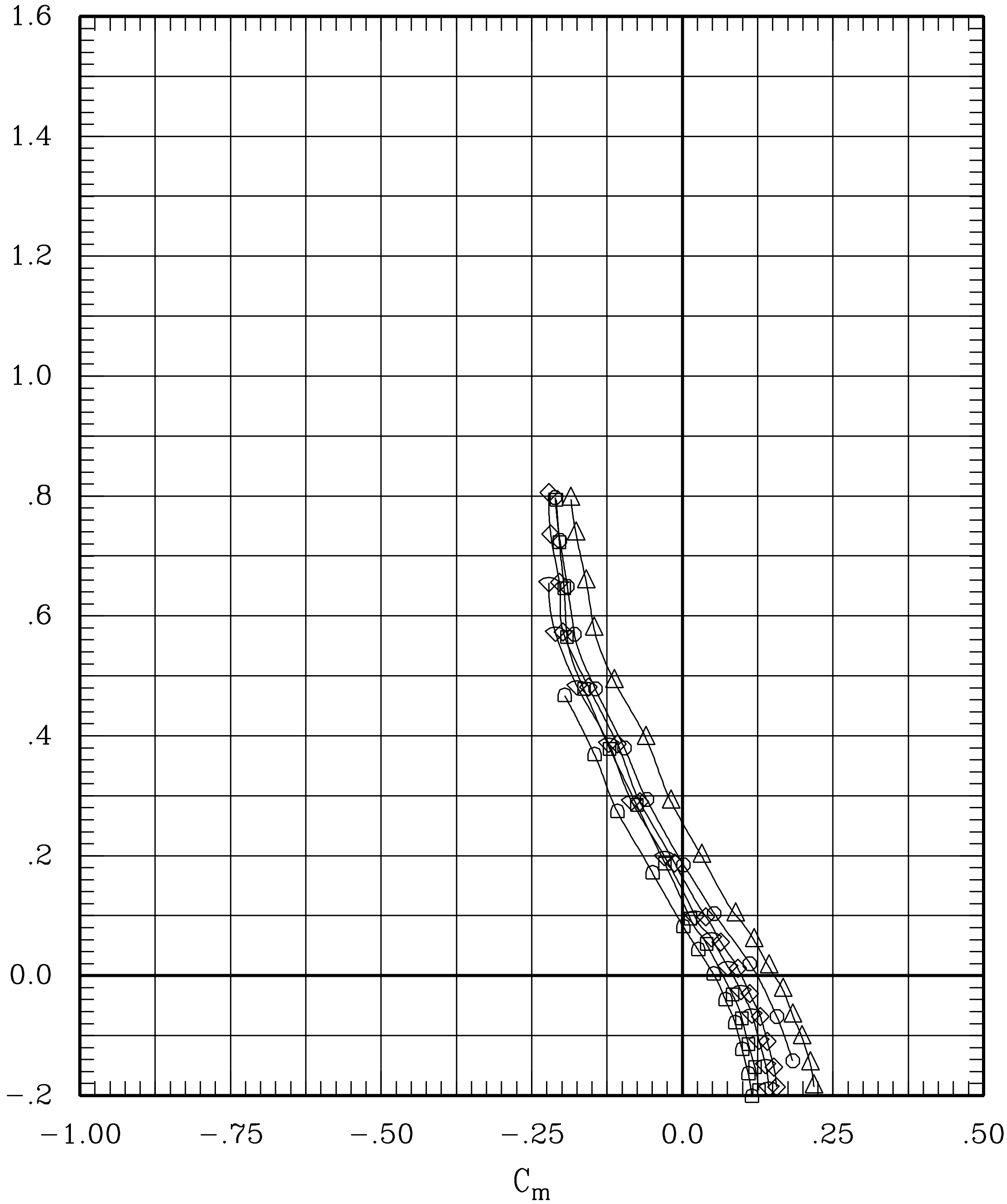

Figure 21(k). Effect of cruise flaps and ailerons for sweep = 65 deg, Mach = 1.40.

SYMBOL	LT	LA	LO	LI	^	RI	RO	RA	RT	RUN	SWEEP	MACH	Q	BETA
—□—	00	00	00	00	L	00	00	00	00	29	65	1.40	701	−.3
—◇—	00	00	−5	−5	L	05	05	00	00	204	65	1.40	696	−.3
—○—	00	−10	00	00	L	00	00	10	00	168	65	1.40	703	−.3
—△—	00	−10	−5	−5	L	05	05	10	00	182	65	1.40	699	−.3
—⌂—	00	00	−5	−5	L	−5	−5	00	00	207	65	1.40	698	−.3
—♢—	00	00	−5	00	L	00	05	00	00	209	65	1.40	703	−.3

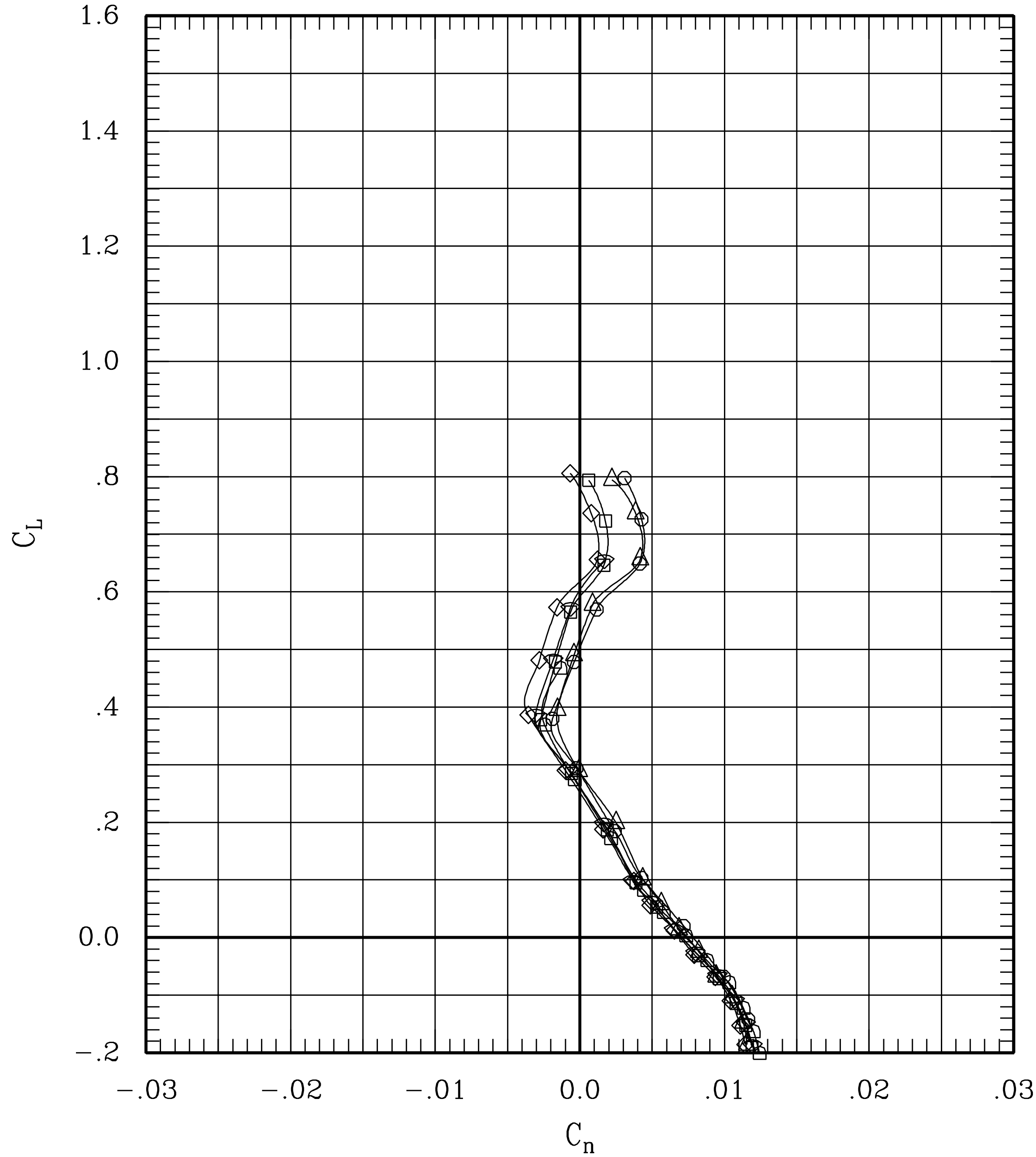

Figure 21(k). Effect of cruise flaps and ailerons for sweep = 65 deg, Mach = 1.40.

SYMBOL	LT	LA	LO	LI	^	RI	RO	RA	RT	RUN	SWEEP	MACH	Q	BETA
—□—	00	00	00	00	L	00	00	00	00	29	65	1.40	701	−.3
—◇—	00	00	−5	−5	L	05	05	00	00	204	65	1.40	696	−.3
—○—	00	−10	00	00	L	00	00	10	00	168	65	1.40	703	−.3
—△—	00	−10	−5	−5	L	05	05	10	00	182	65	1.40	699	−.3
—⌂—	00	00	−5	−5	L	−5	−5	00	00	207	65	1.40	698	−.3
—▽—	00	00	−5	00	L	00	05	00	00	209	65	1.40	703	−.3

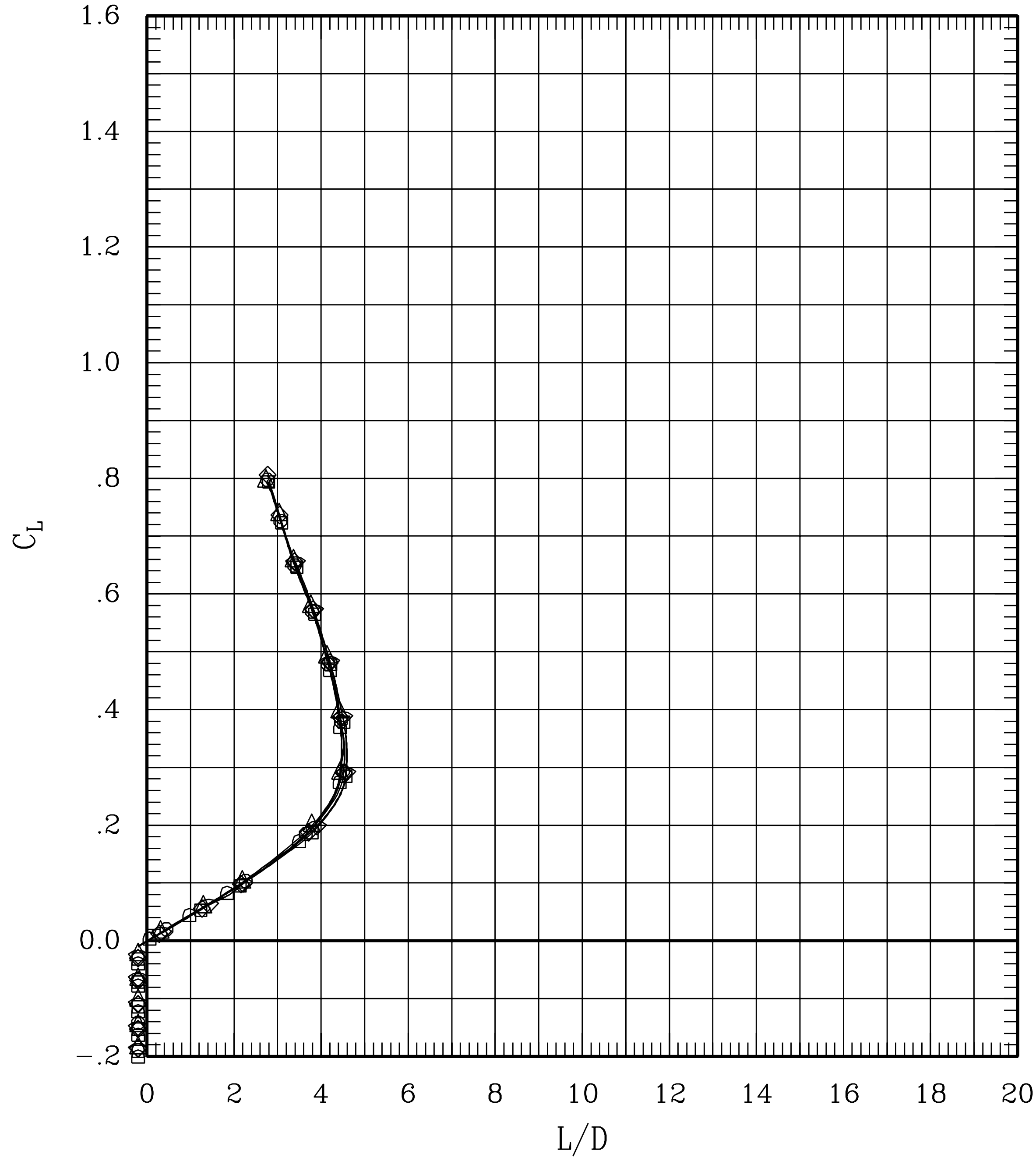

Figure 21(k). Effect of cruise flaps and ailerons for sweep = 65 deg, Mach = 1.40.

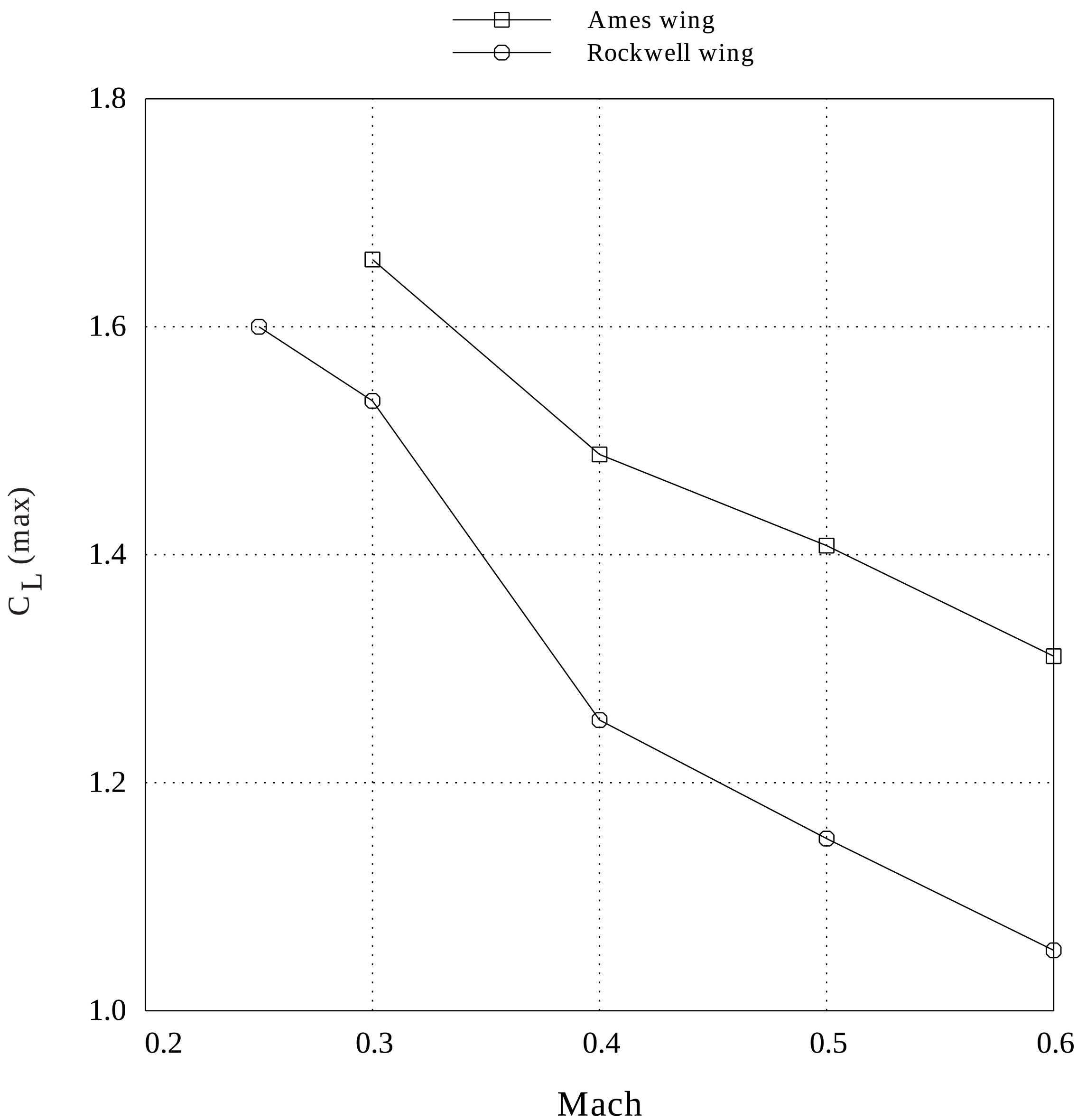

Figure 22. Low-speed, clean wing performance of Ames and Rockwell wings.

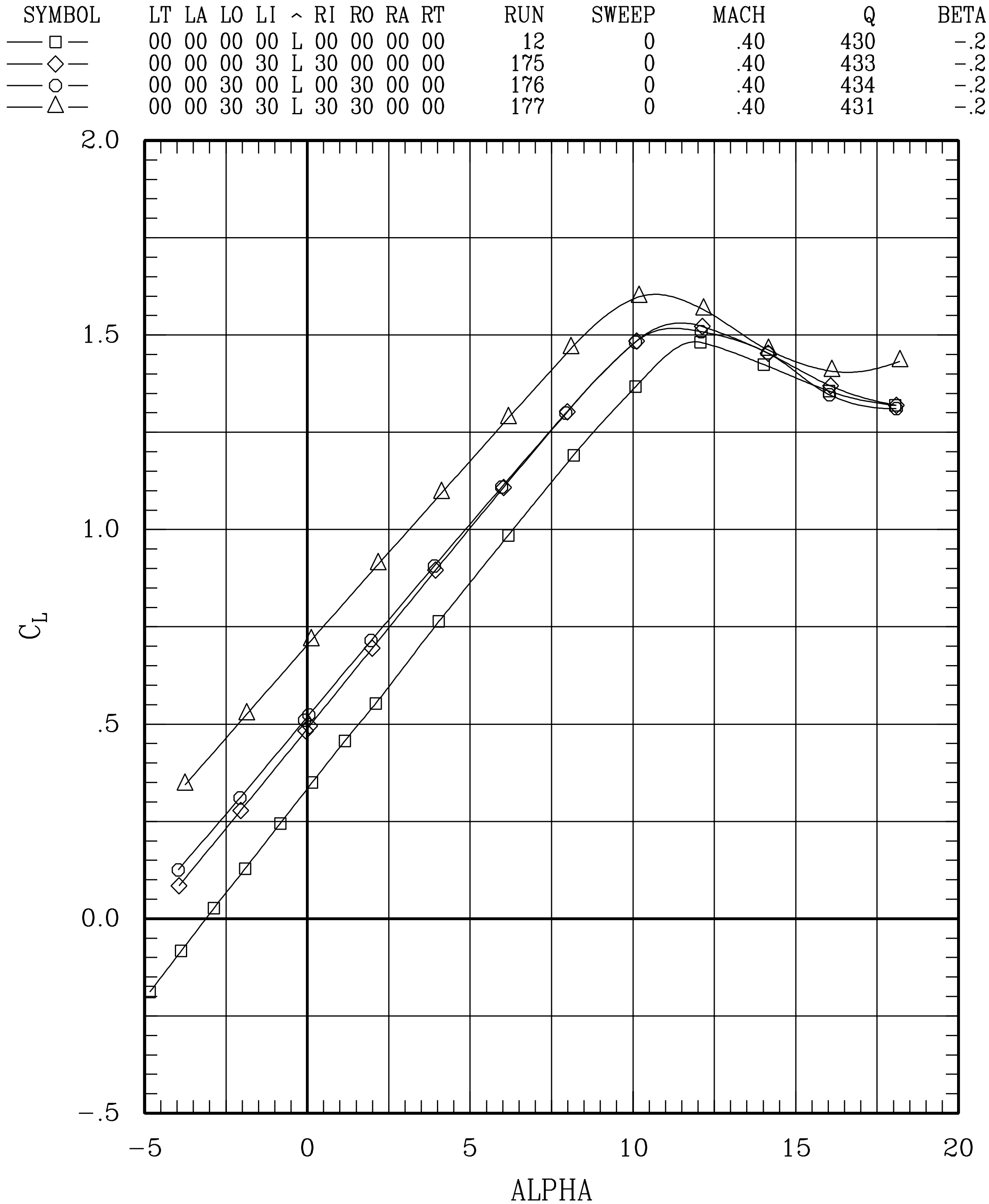

Figure 23(a). Low speed performance with 30 deg deflected flaps.

SYMBOL	LT	LA	LO	LI	^	RI	RO	RA	RT	RUN	SWEEP	MACH	Q	BETA
—□—	00	00	00	00	L	00	00	00	00	12	0	.40	430	−.2
—◇—	00	00	00	30	L	30	00	00	00	175	0	.40	433	−.2
—○—	00	00	30	00	L	00	30	00	00	176	0	.40	434	−.2
—△—	00	00	30	30	L	30	30	00	00	177	0	.40	431	−.2

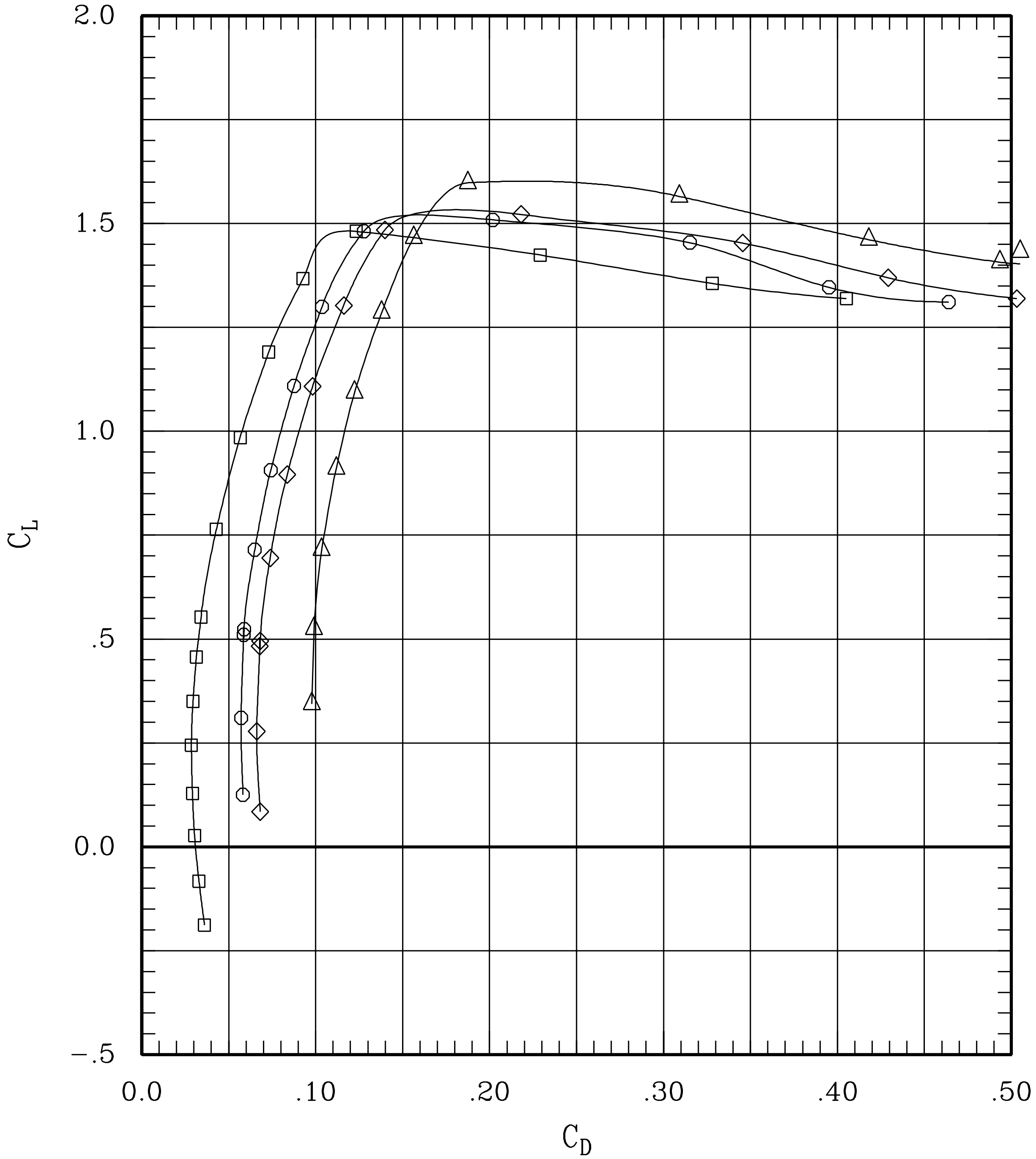

Figure 23(a). Low speed performance with 30 deg deflected flaps.

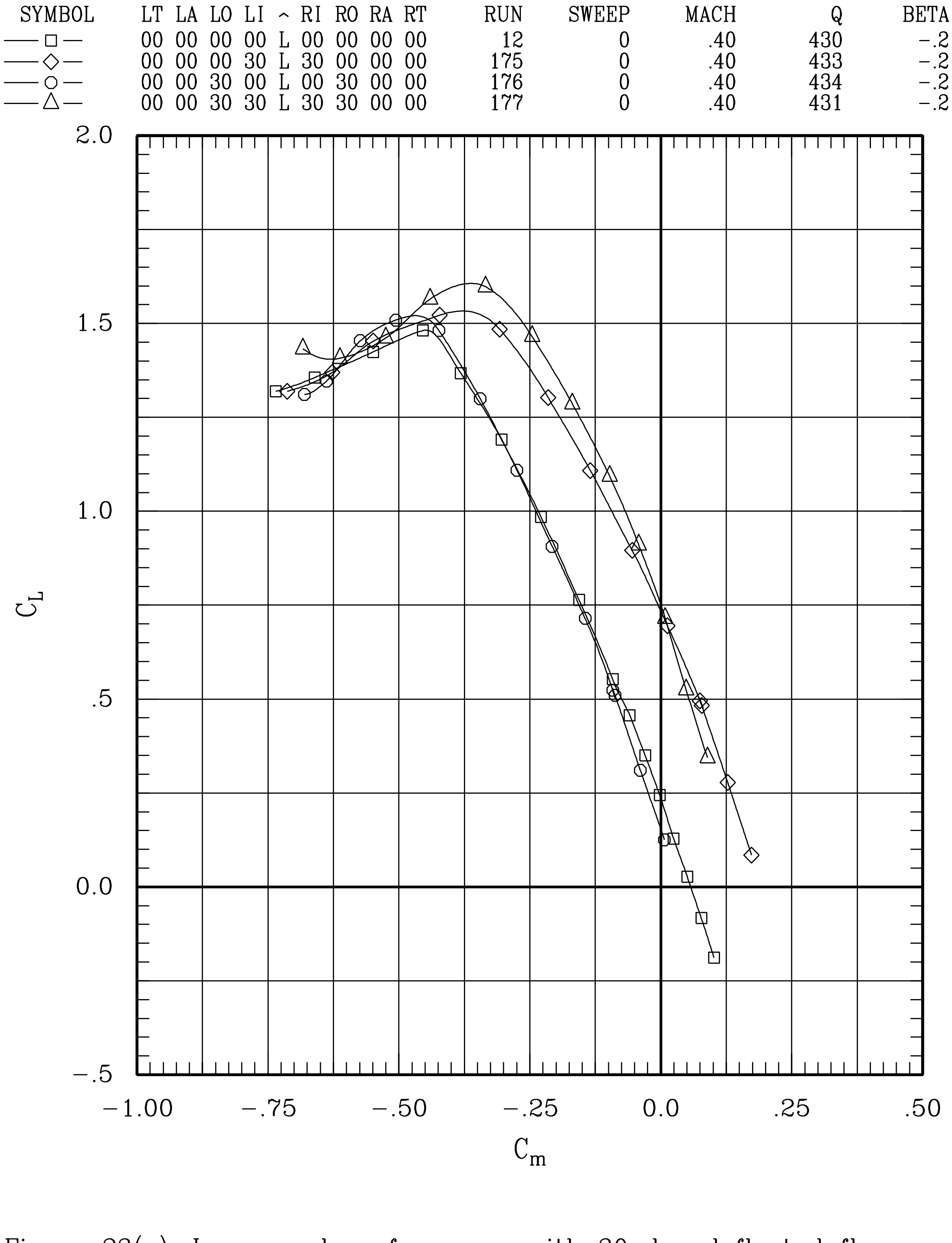

Figure 23(a). Low speed performance with 30 deg deflected flaps.

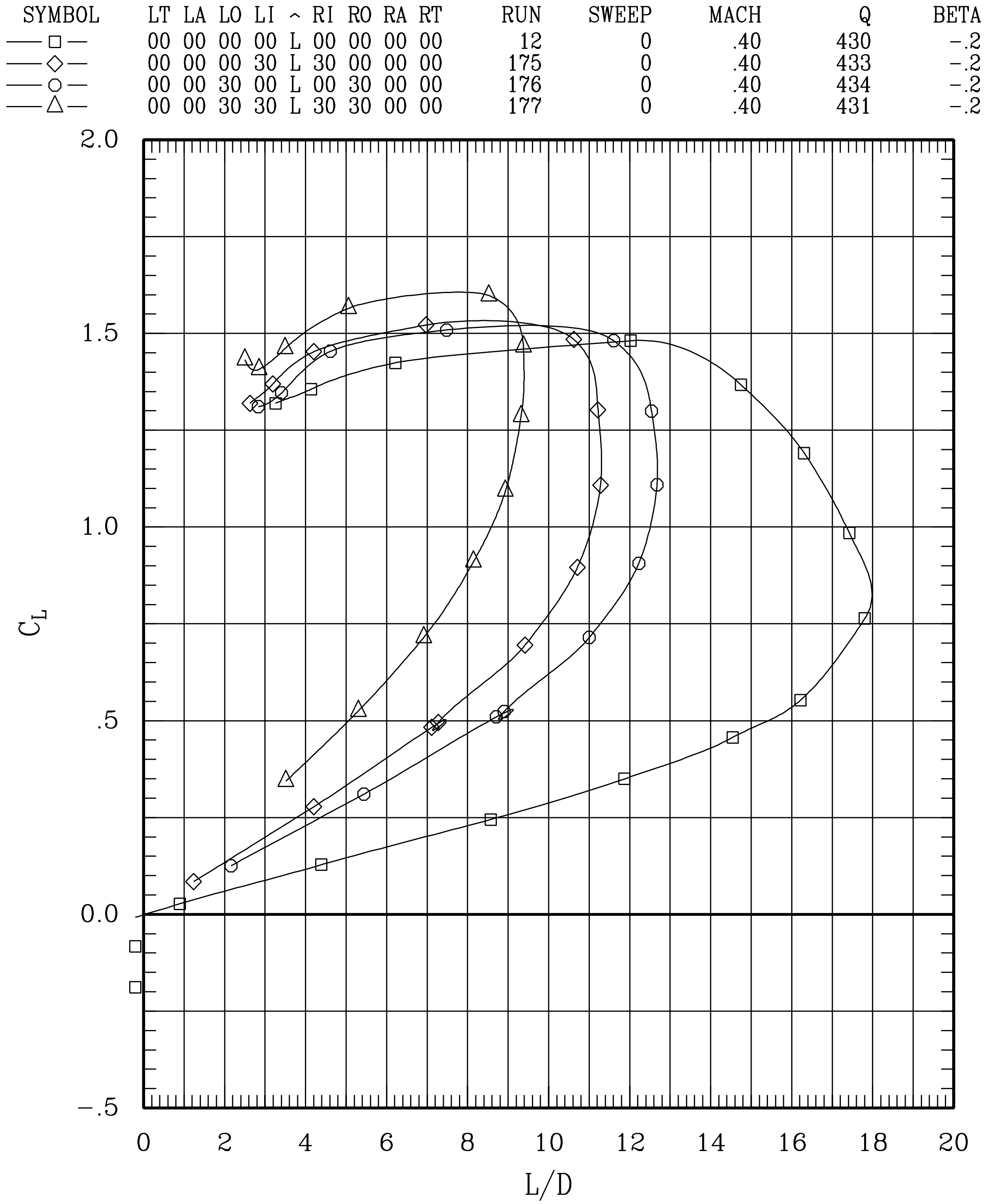

Figure 23(a). Low speed performance with 30 deg deflected flaps.

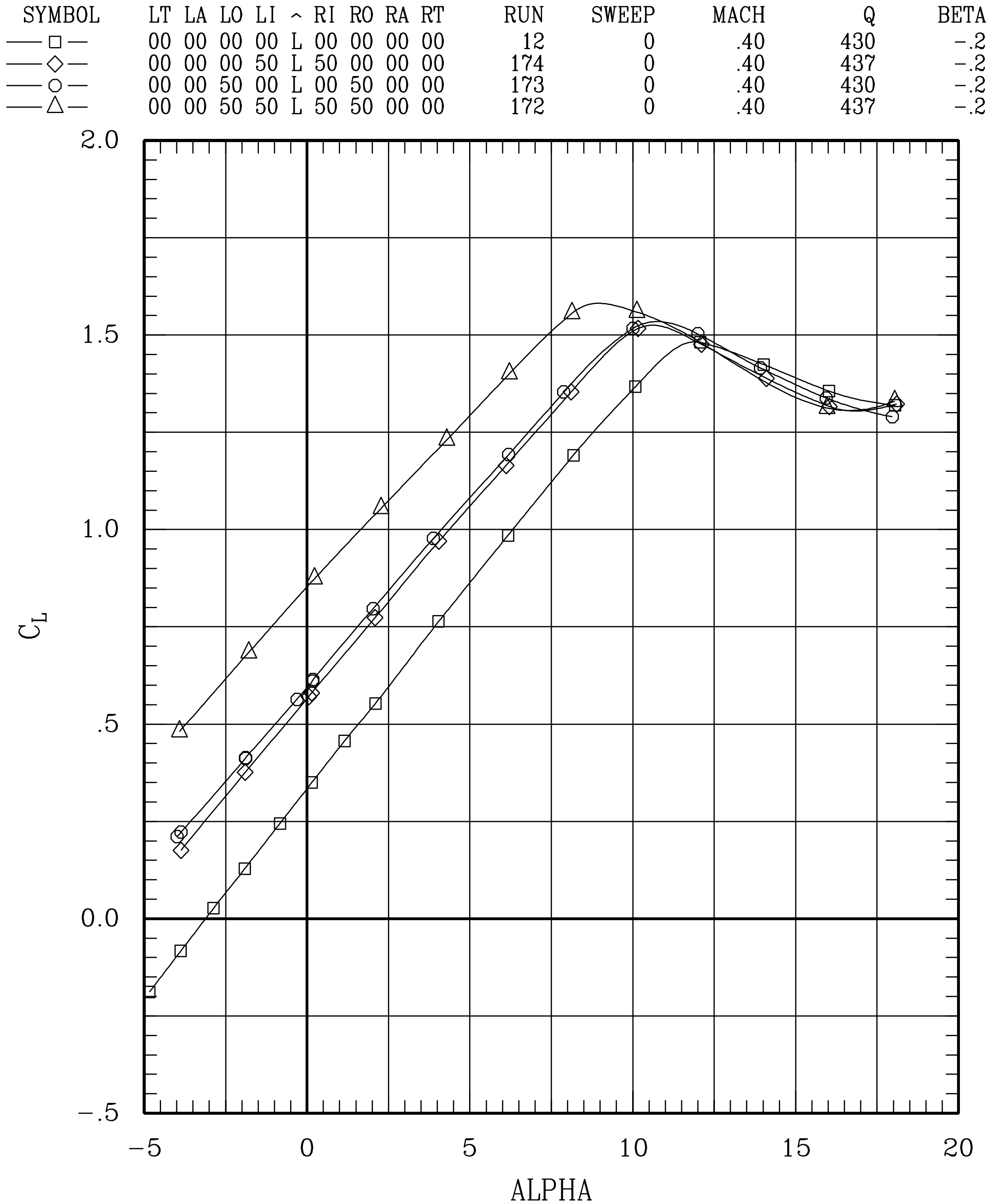

Figure 23(b). Low speed performance with 50 deg deflected flaps.

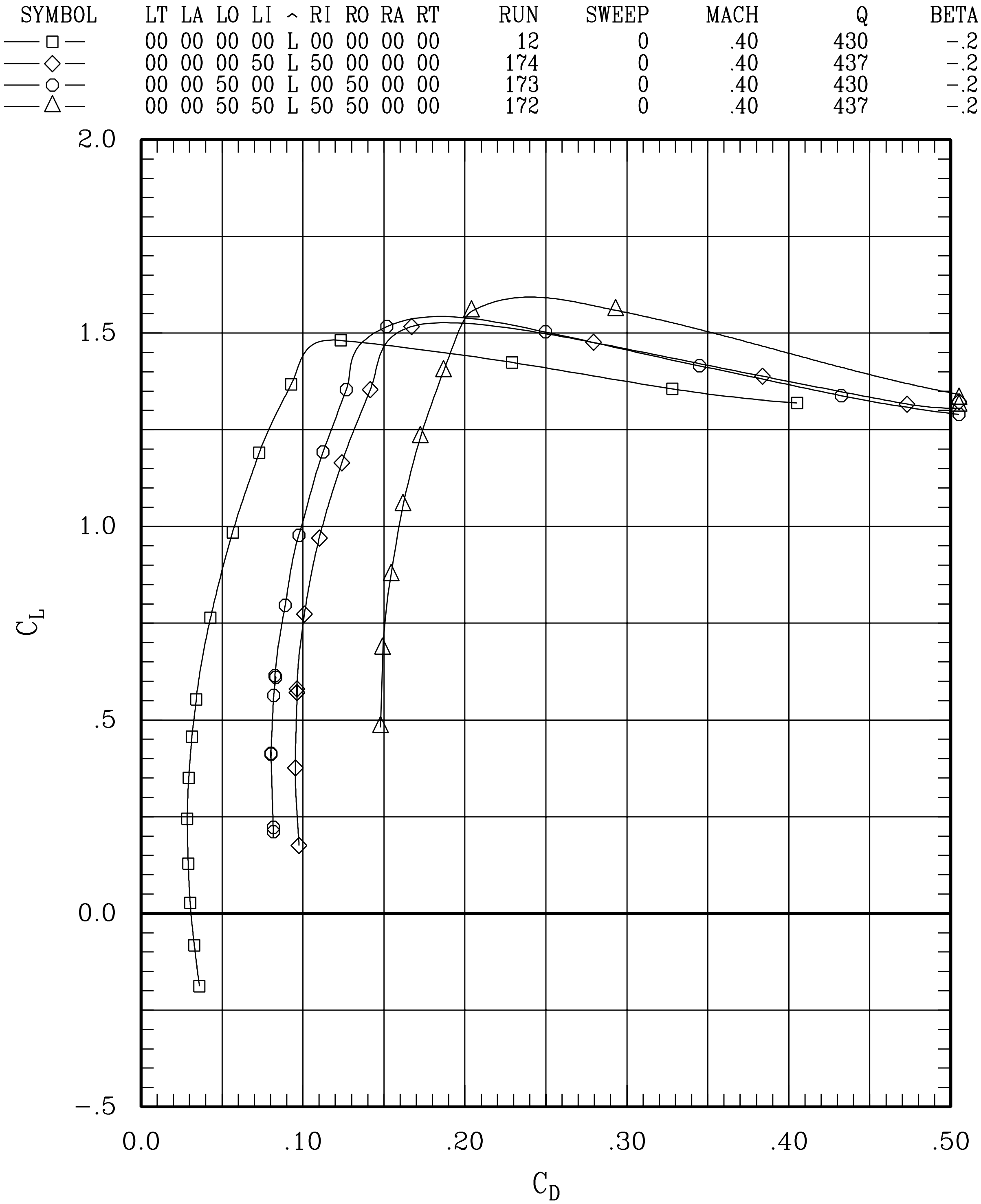

Figure 23(b). Low speed performance with 50 deg deflected flaps.

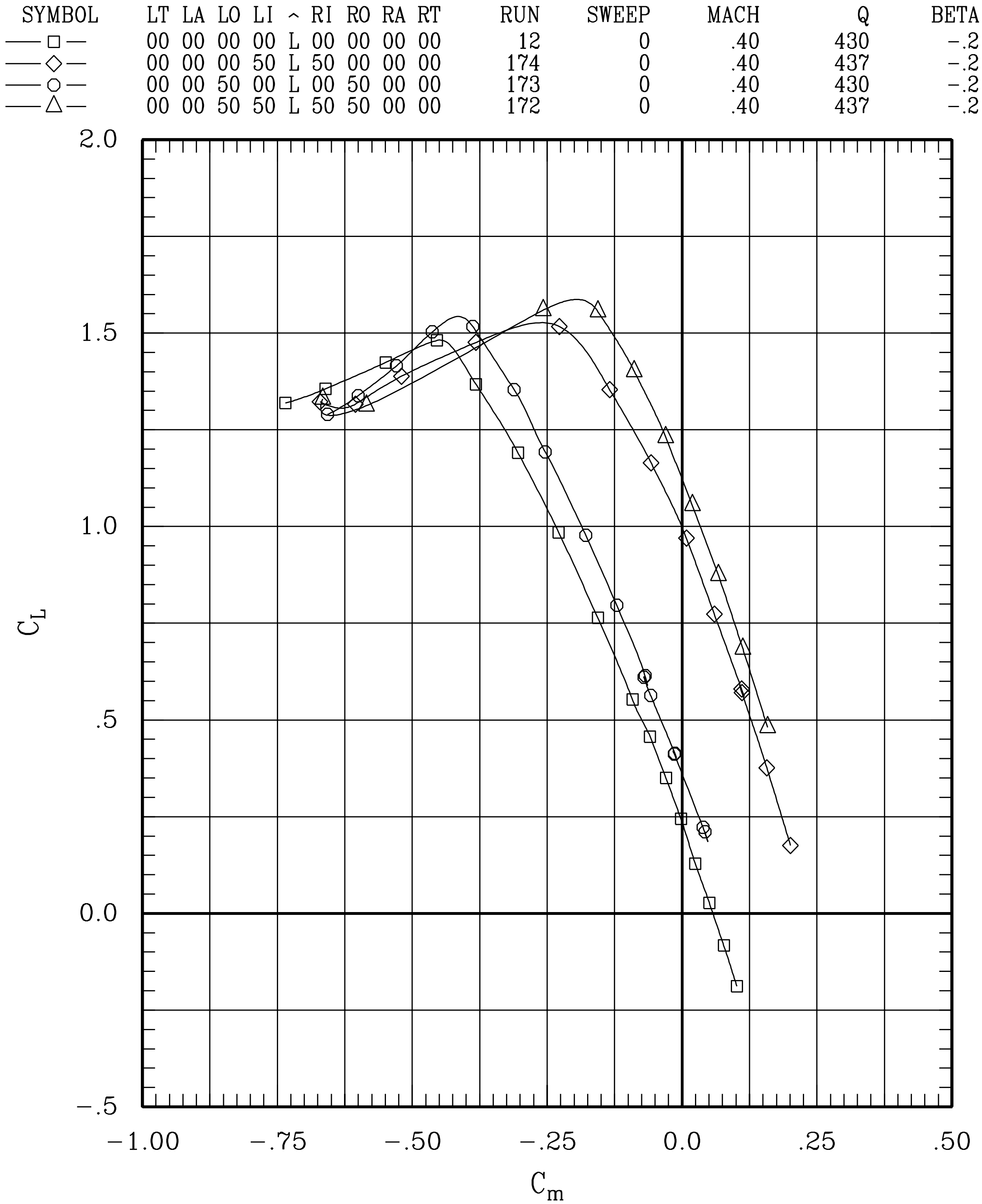

Figure 23(b). Low speed performance with 50 deg deflected flaps.

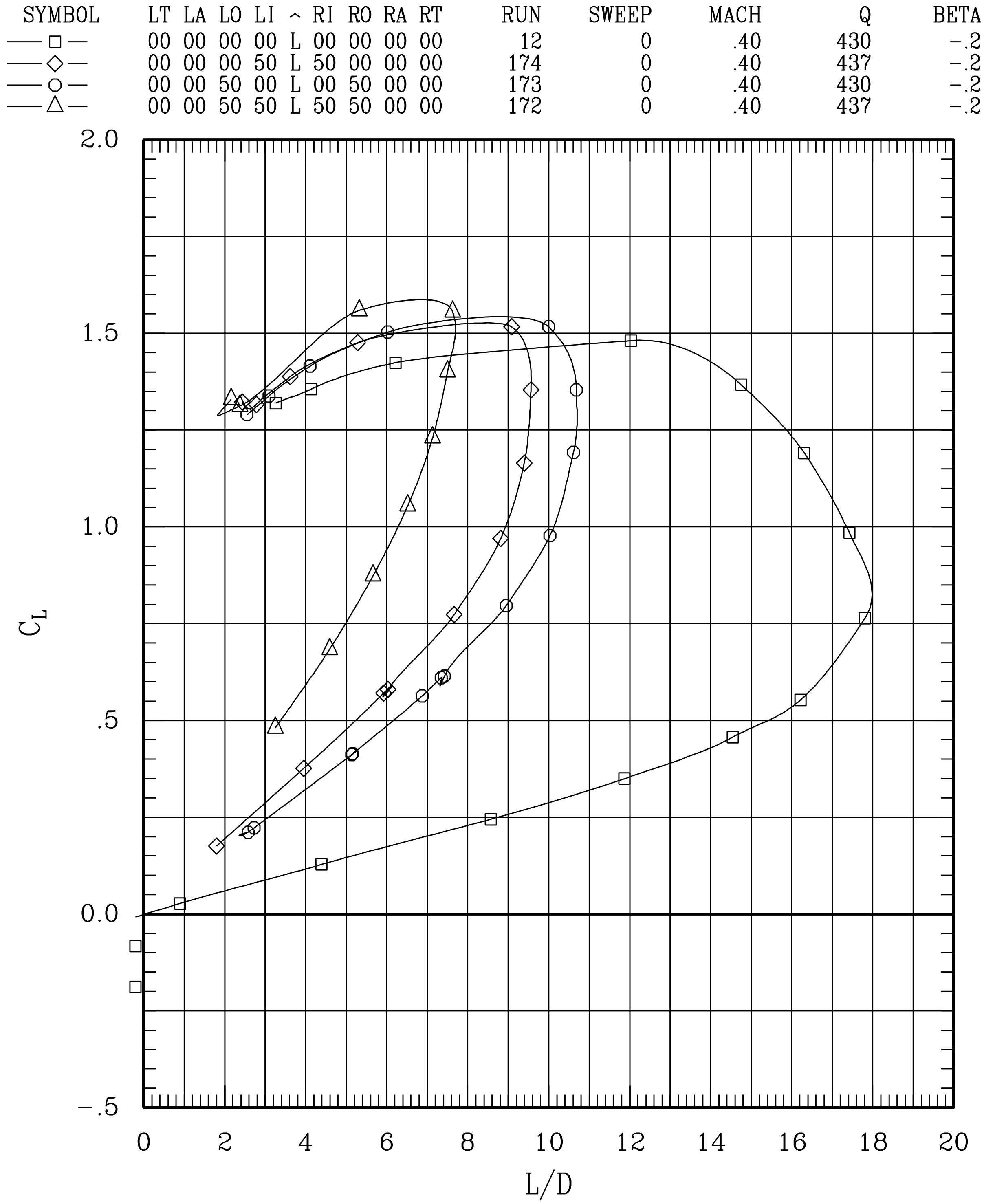

Figure 23(b). Low speed performance with 50 deg deflected flaps.

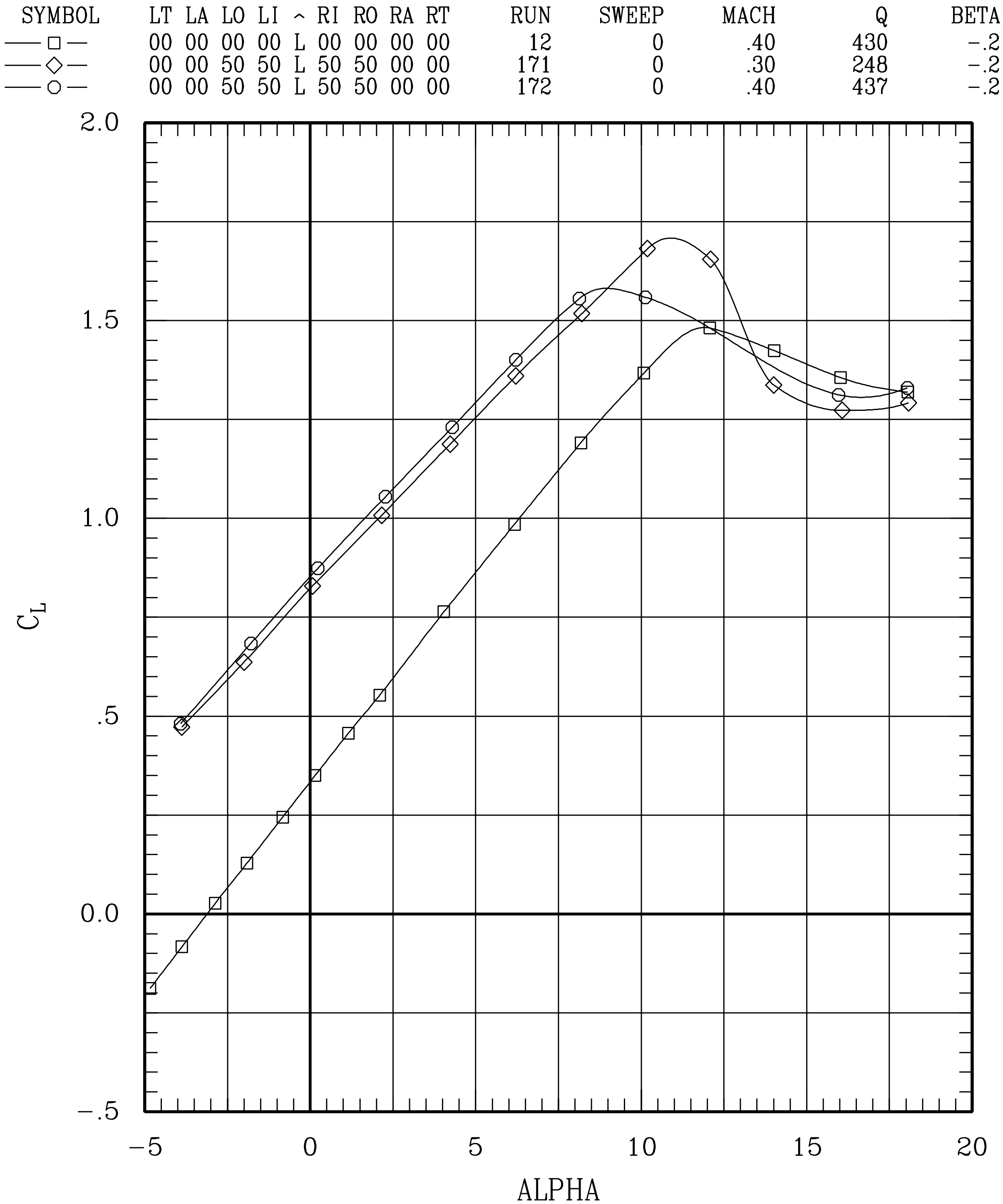

Figure 24. Effect of Mach on combined, 50 deg deflected flaps.

SYMBOL	LT LA LO LI ^ RI RO RA RT	RUN	SWEEP	MACH	Q	BETA
—□—	00 00 00 00 L 00 00 00 00	12	0	.40	430	−.2
—◇—	00 00 50 50 L 50 50 00 00	171	0	.30	248	−.2
—○—	00 00 50 50 L 50 50 00 00	172	0	.40	437	−.2

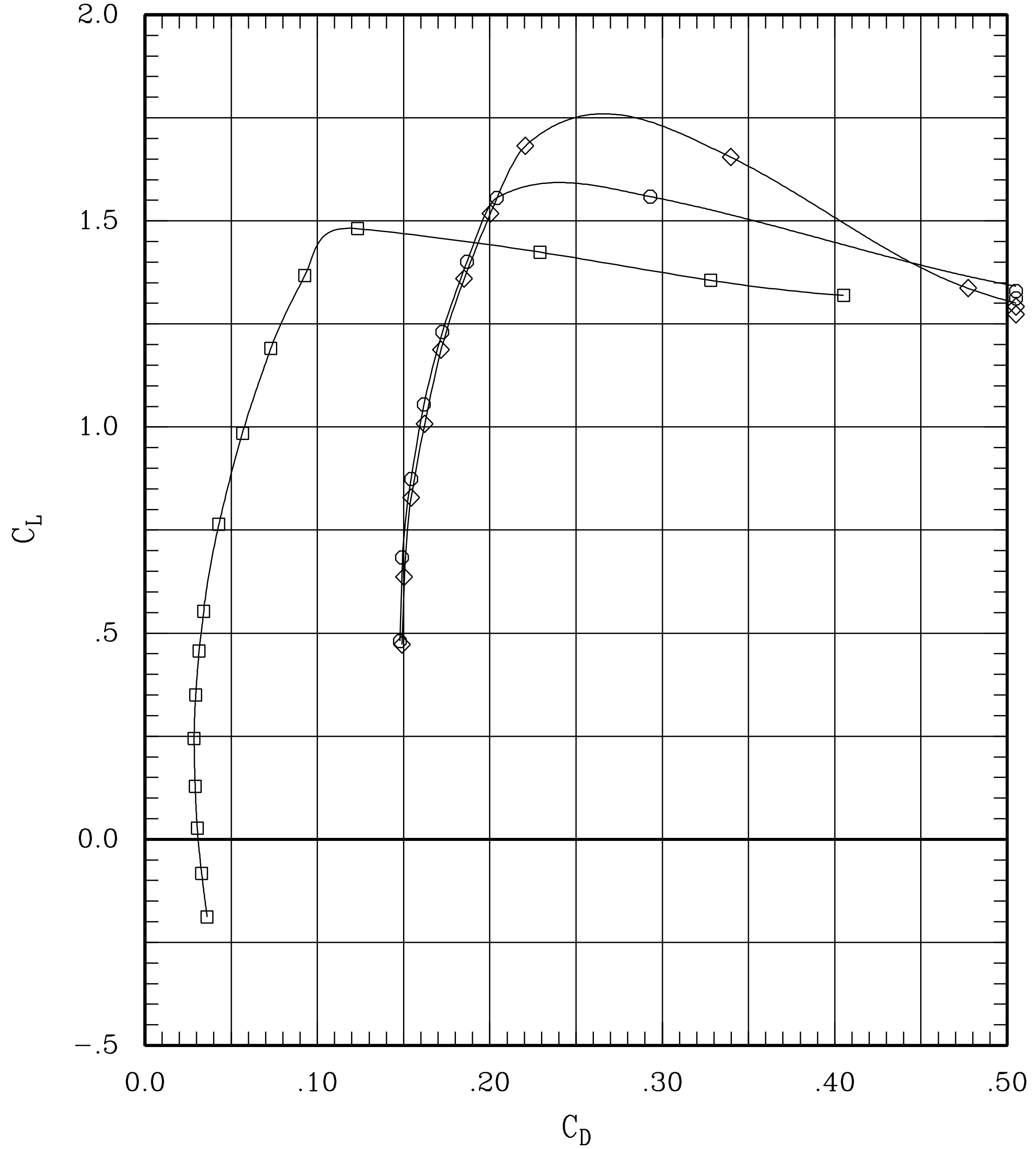

Figure 24. Effect of Mach on combined, 50 deg deflected flaps.

SYMBOL	LT	LA	LO	LI	^	RI	RO	RA	RT	RUN	SWEEP	MACH	Q	BETA
—□—	00	00	00	00	L	00	00	00	00	12	0	.40	430	−.2
—◇—	00	00	50	50	L	50	50	00	00	171	0	.30	248	−.2
—○—	00	00	50	50	L	50	50	00	00	172	0	.40	437	−.2

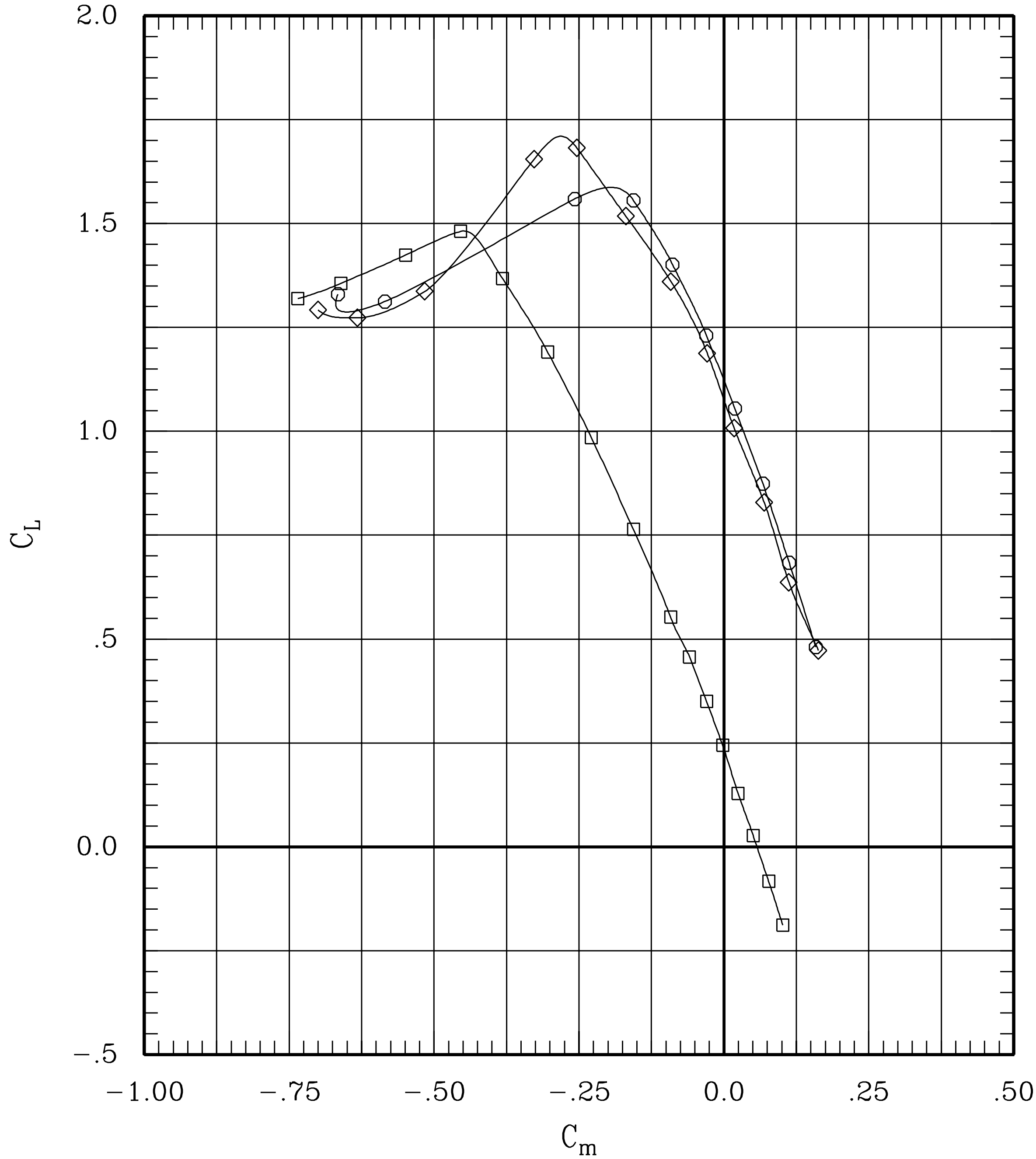

Figure 24. Effect of Mach on combined, 50 deg deflected flaps.

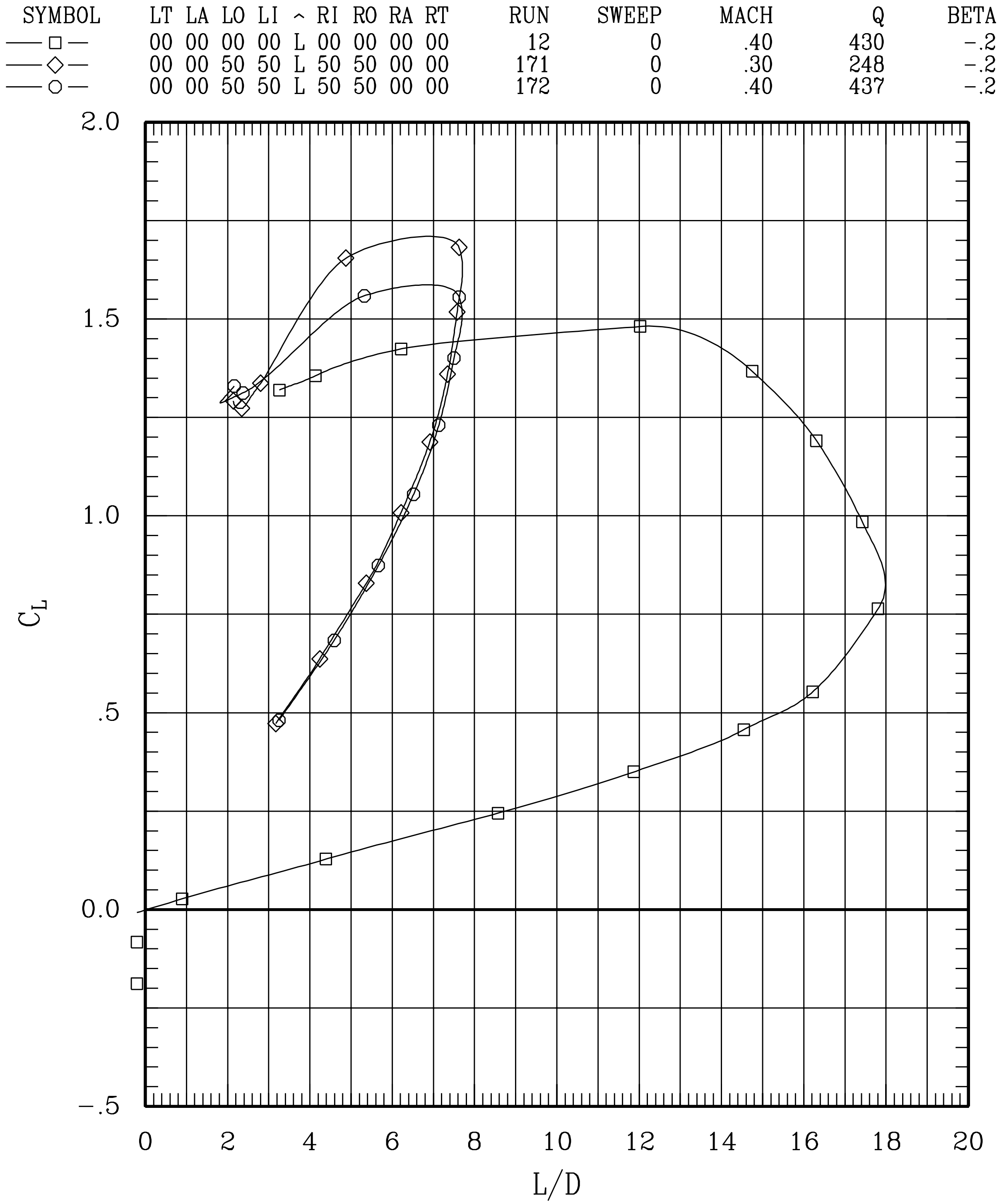

Figure 24. Effect of Mach on combined, 50 deg deflected flaps.

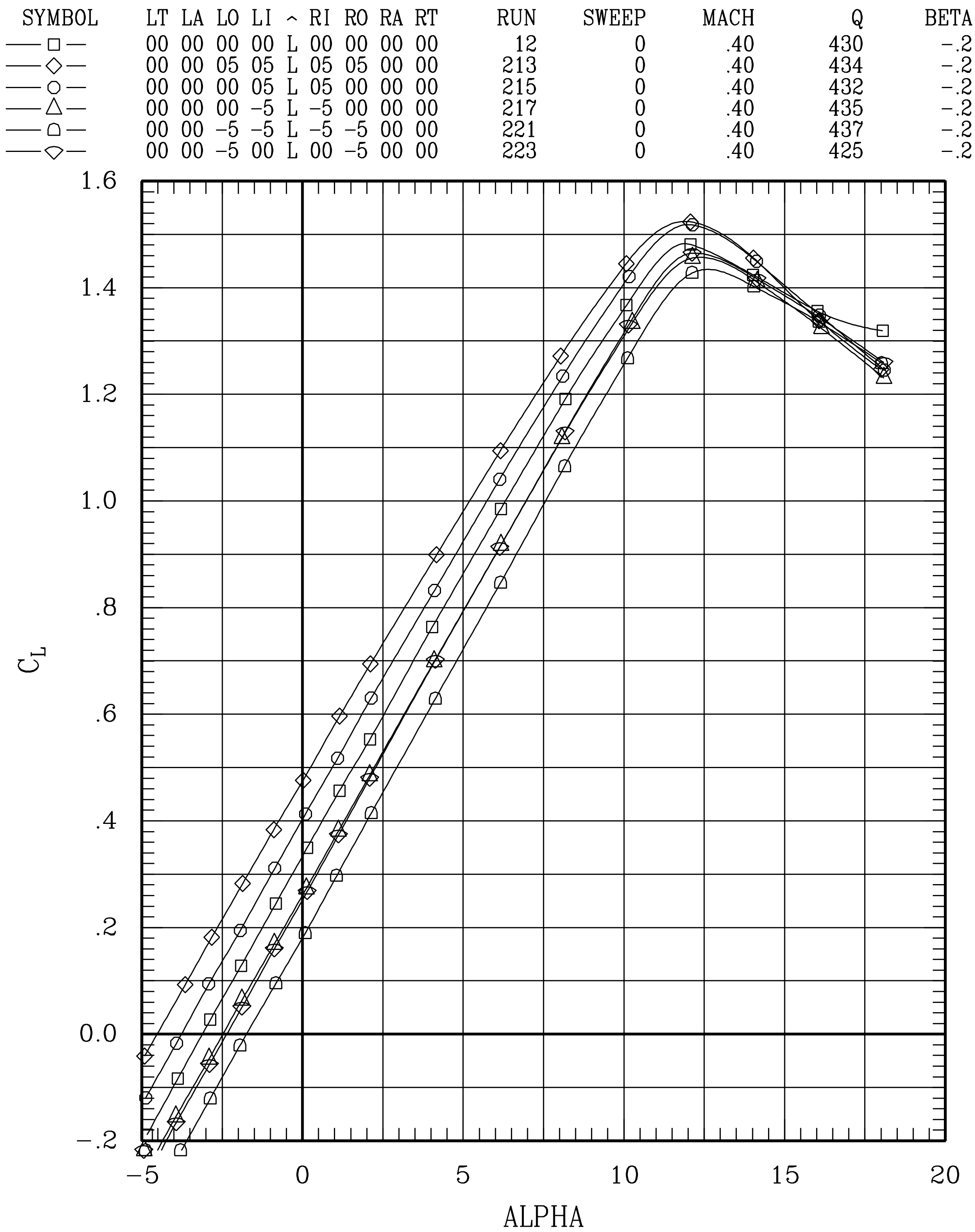

Figure 25(a). Effect of flap deflection on loiter performance for Mach = 0.40.

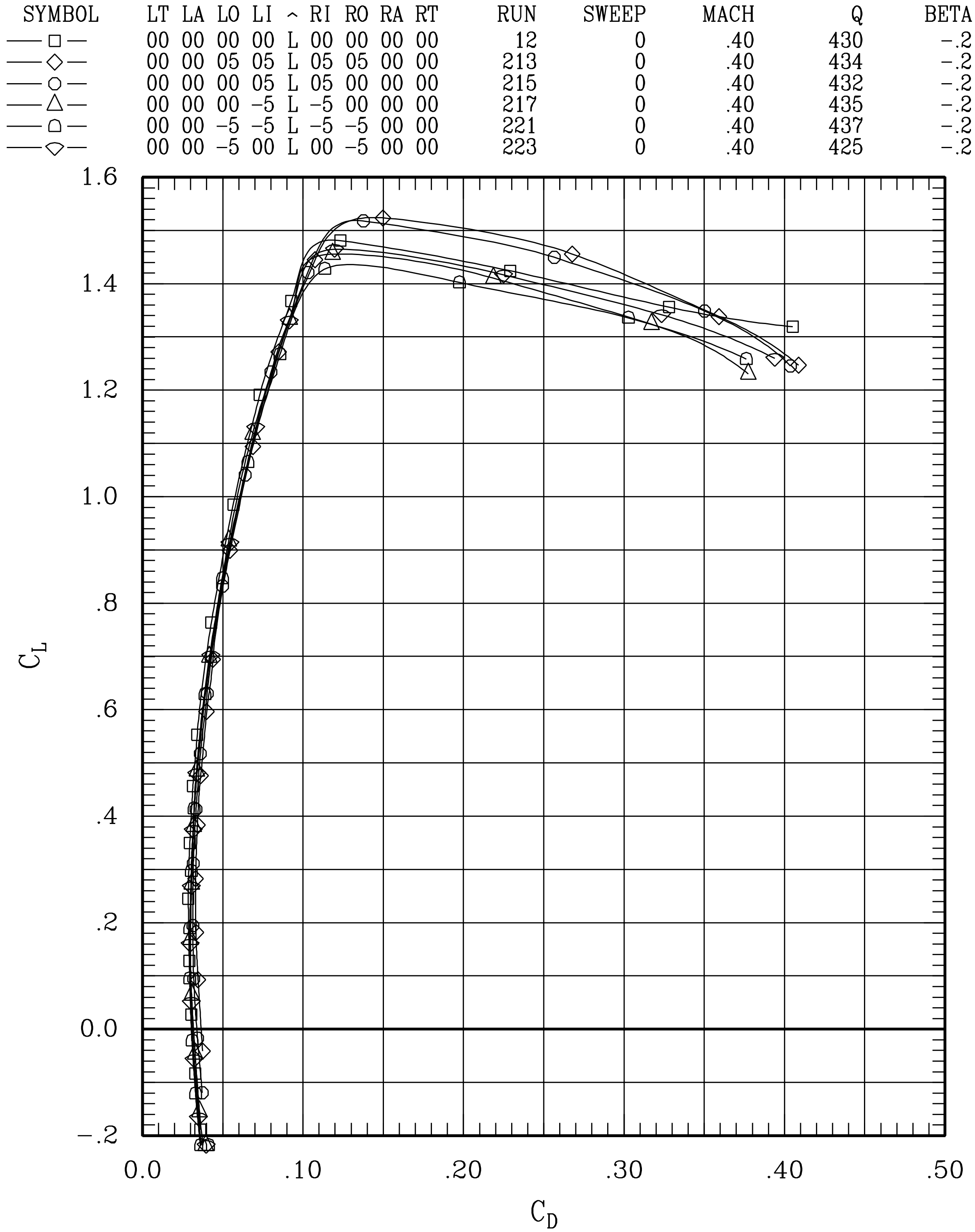

Figure 25(a). Effect of flap deflection on loiter performance for Mach = 0.40.

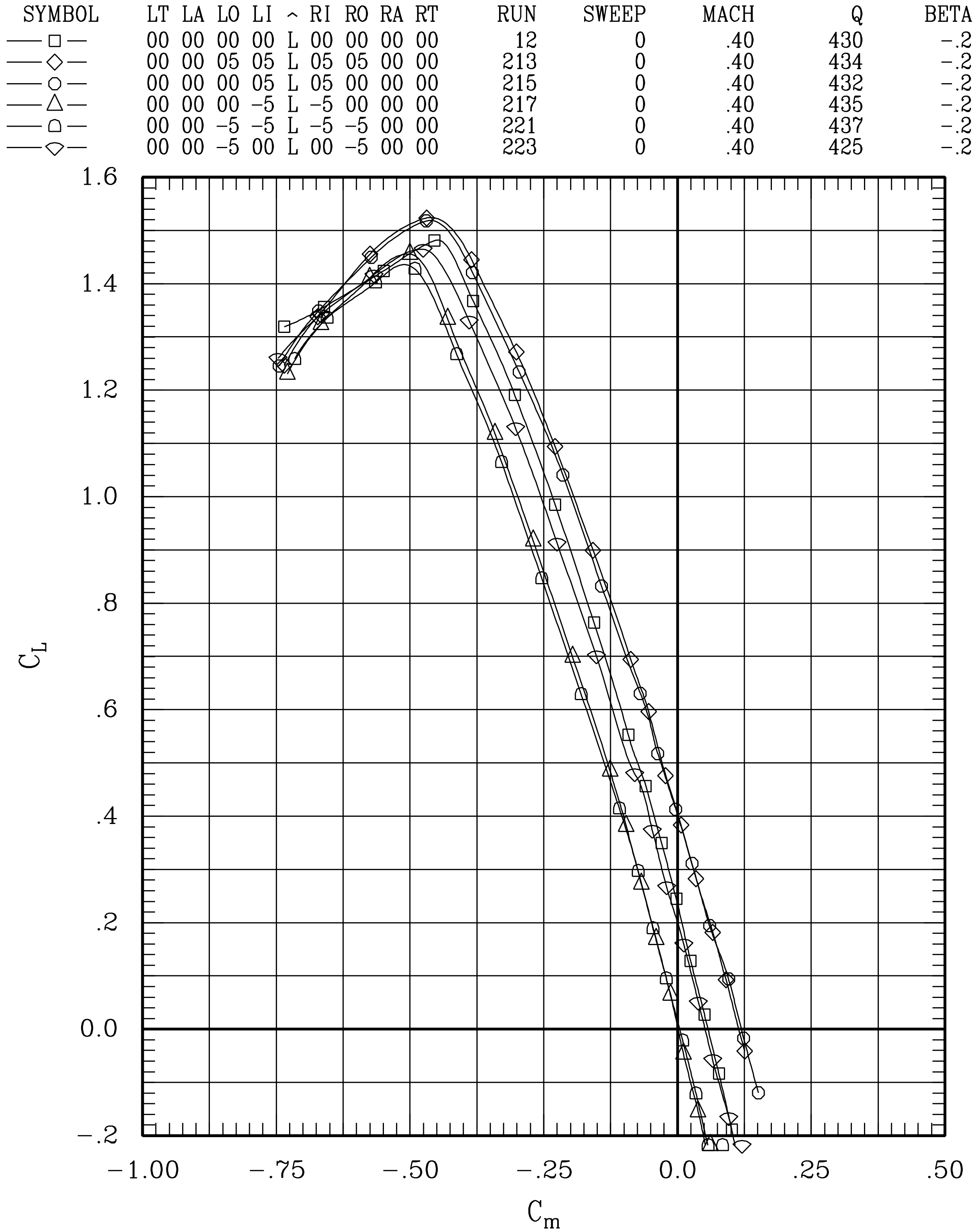

Figure 25(a). Effect of flap deflection on loiter performance for Mach = 0.40.

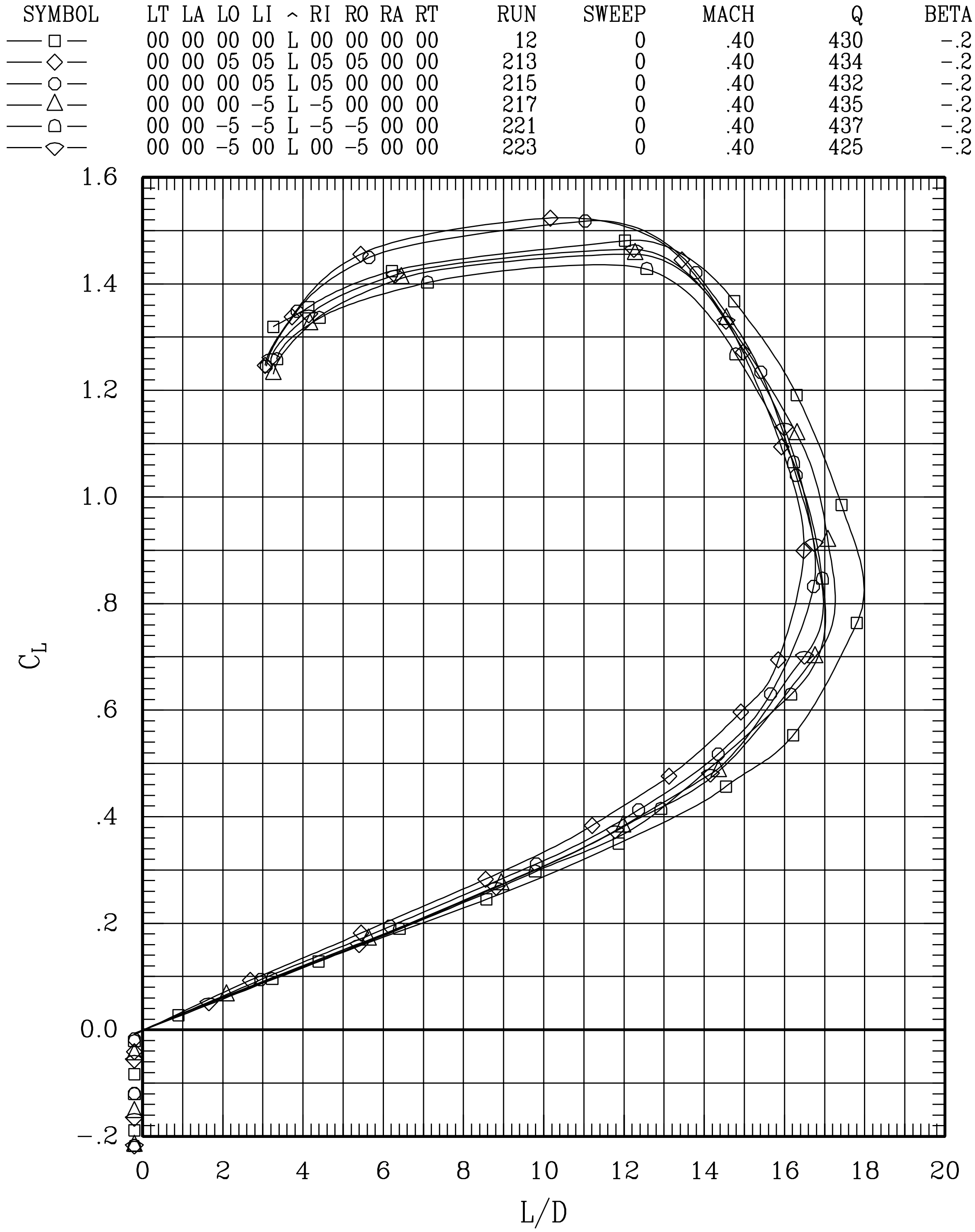

Figure 25(a). Effect of flap deflection on loiter performance for Mach = 0.40.

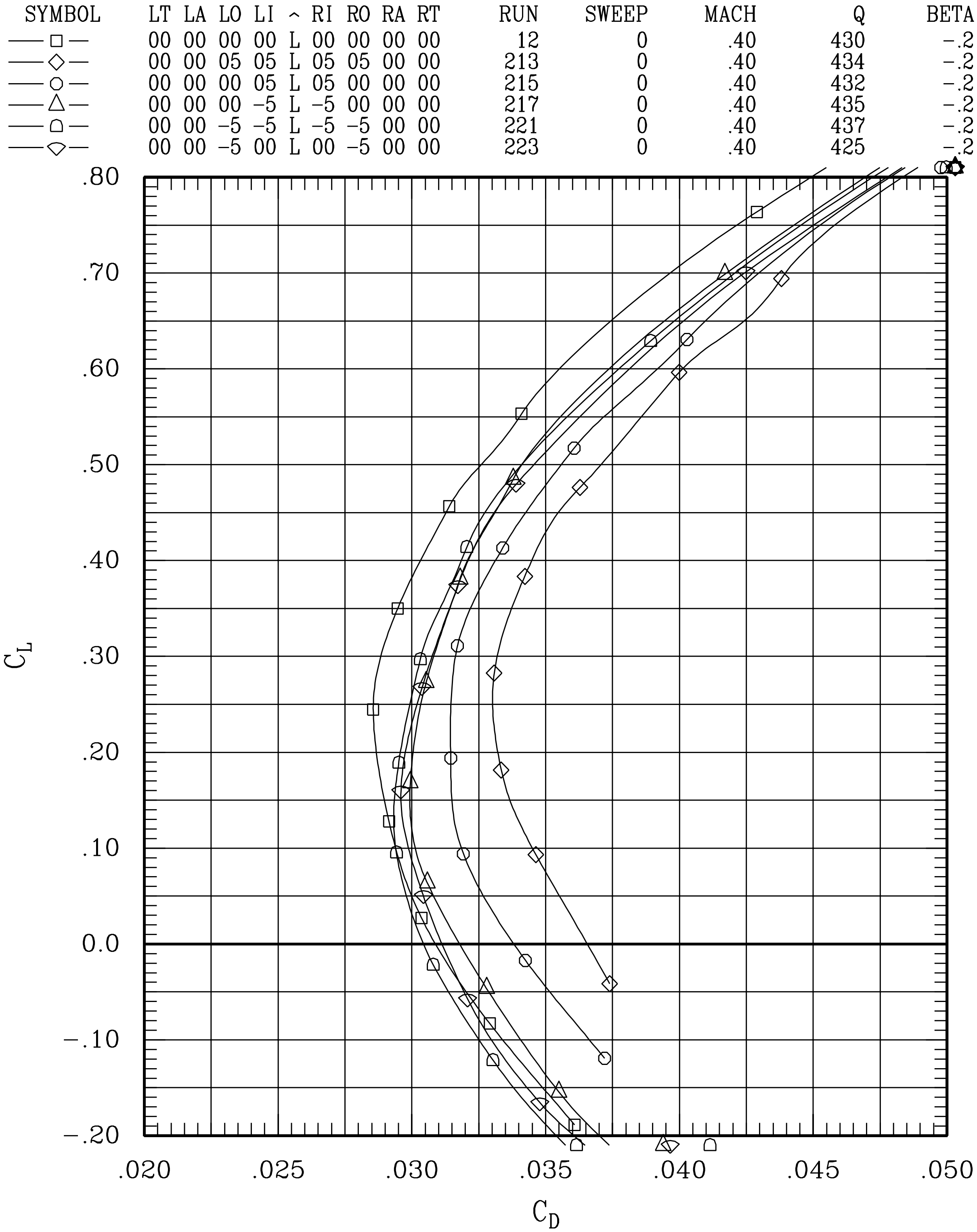

Figure 25(a). Effect of flap deflection on loiter performance for Mach = 0.40.

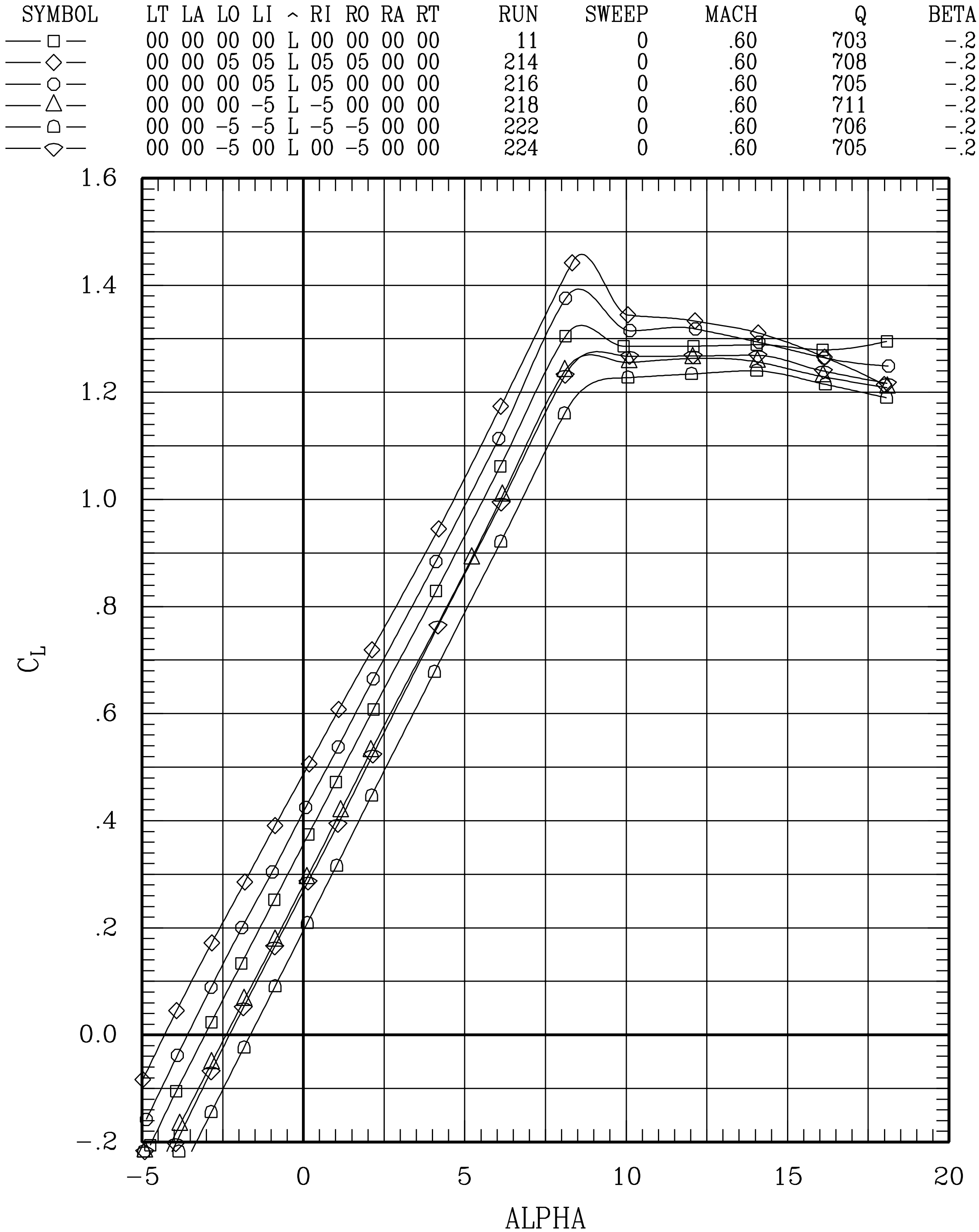

Figure 25(b). Effect of flap deflection on loiter performance for Mach = 0.60.

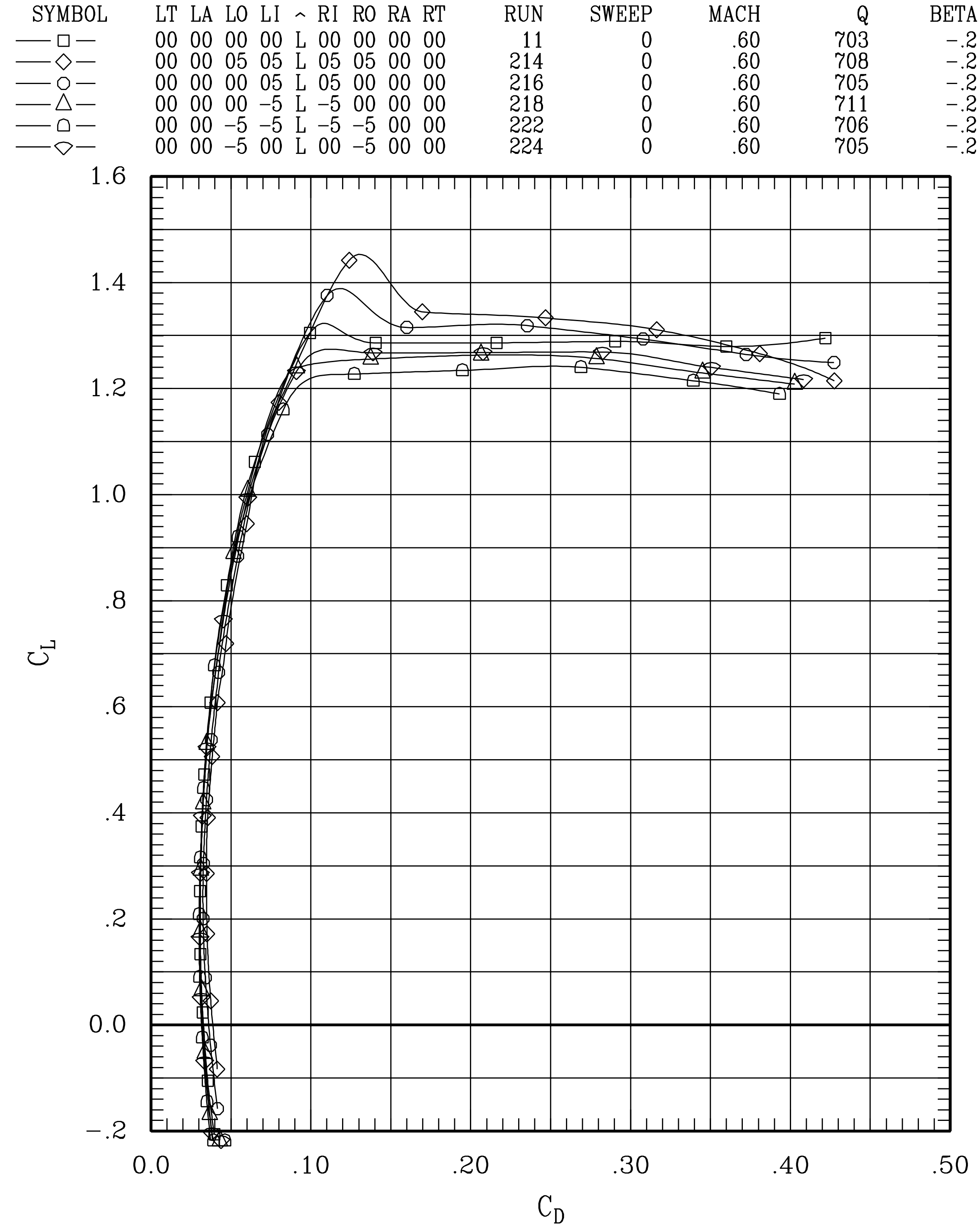

Figure 25(b). Effect of flap deflection on loiter performance for Mach = 0.60.

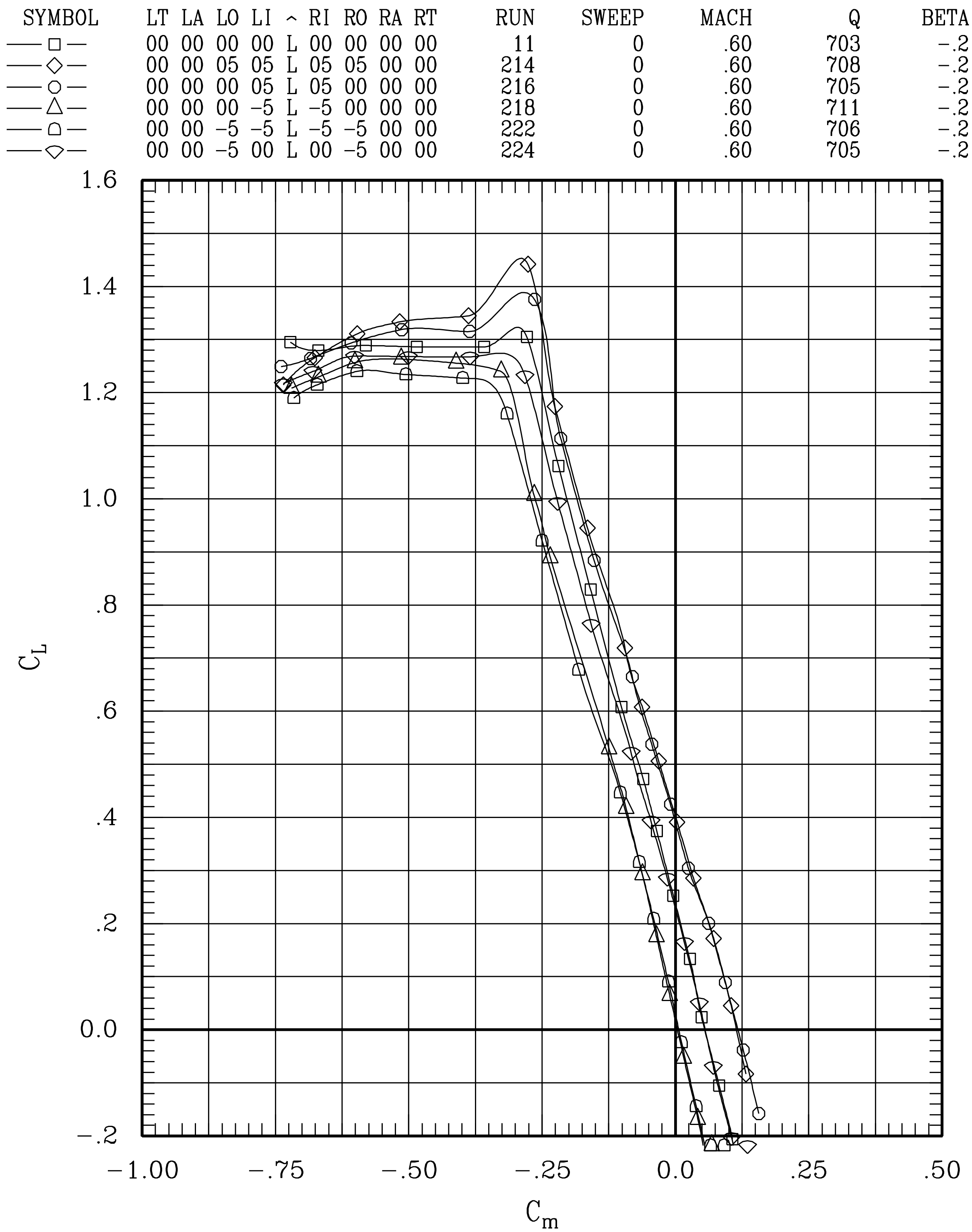

Figure 25(b). Effect of flap deflection on loiter performance for Mach = 0.60.

SYMBOL	LT	LA	LO	LI	^	RI	RO	RA	RT	RUN	SWEEP	MACH	Q	BETA
—□—	00	00	00	00	L	00	00	00	00	11	0	.60	703	−.2
—◇—	00	00	05	05	L	05	05	00	00	214	0	.60	708	−.2
—○—	00	00	00	05	L	05	00	00	00	216	0	.60	705	−.2
—△—	00	00	00	−5	L	−5	00	00	00	218	0	.60	711	−.2
—⌂—	00	00	−5	−5	L	−5	−5	00	00	222	0	.60	706	−.2
—▽—	00	00	−5	00	L	00	−5	00	00	224	0	.60	705	−.2

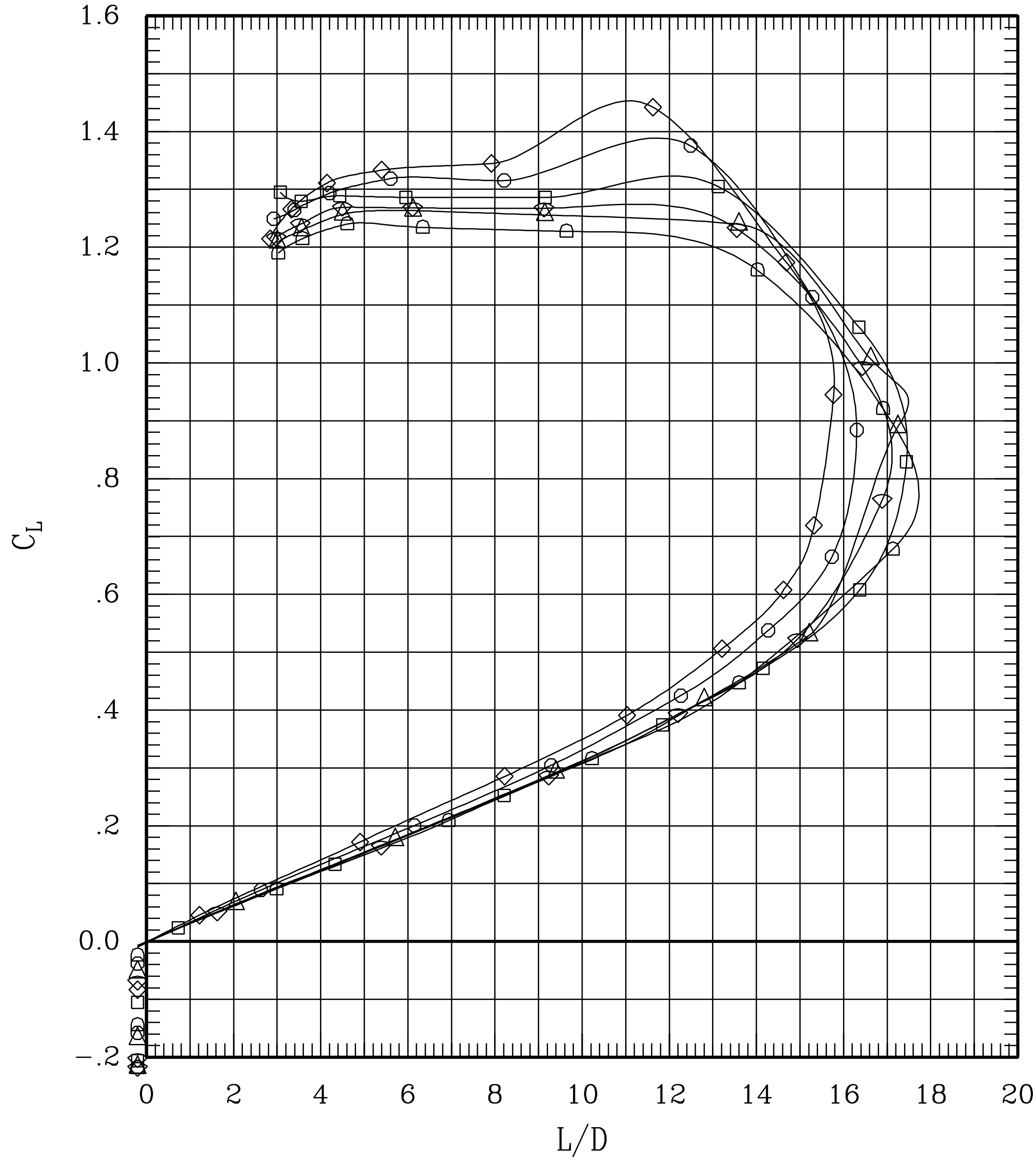

Figure 25(b). Effect of flap deflection on loiter performance for Mach = 0.60.

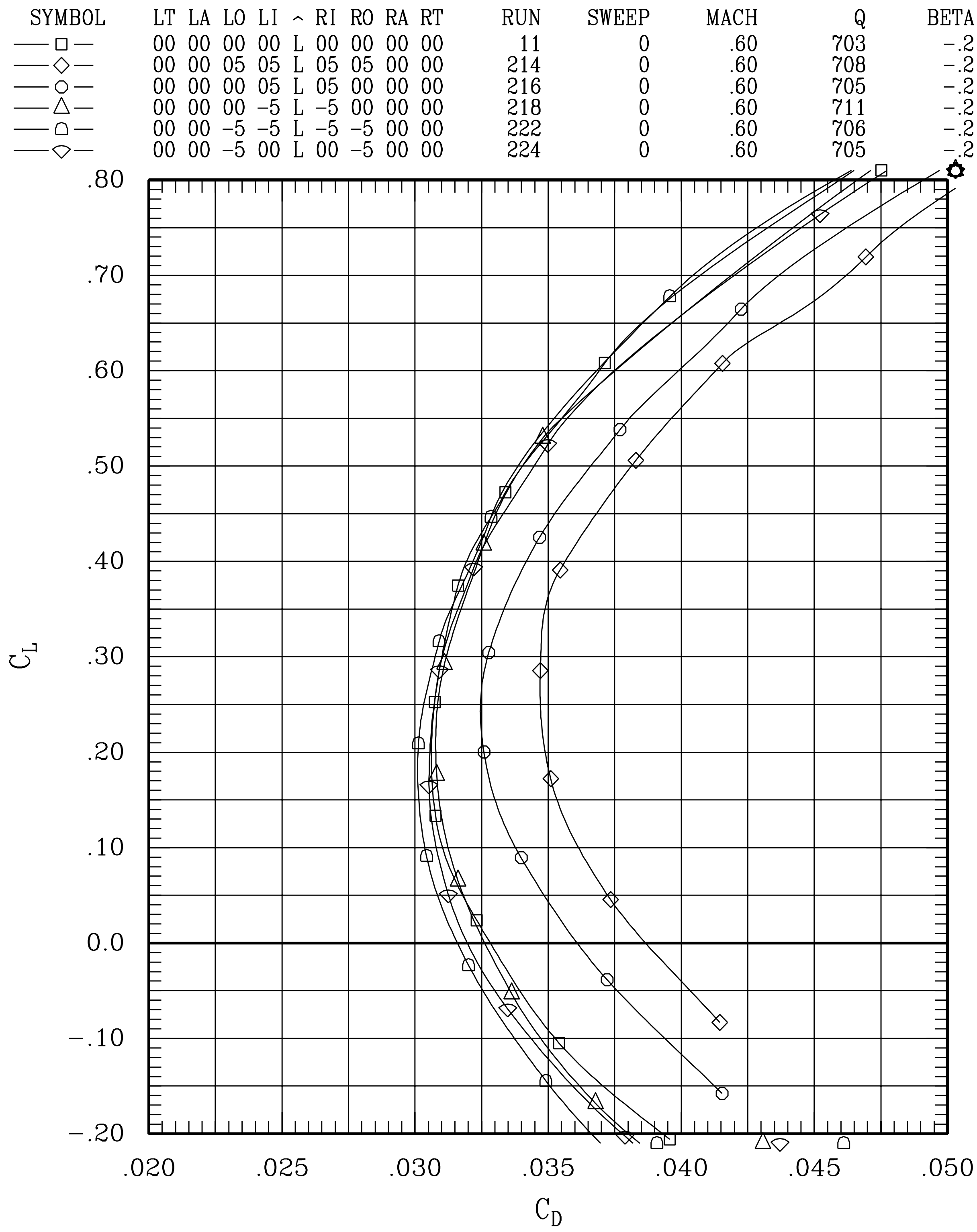

Figure 25(b). Effect of flap deflection on loiter performance for Mach = 0.60.

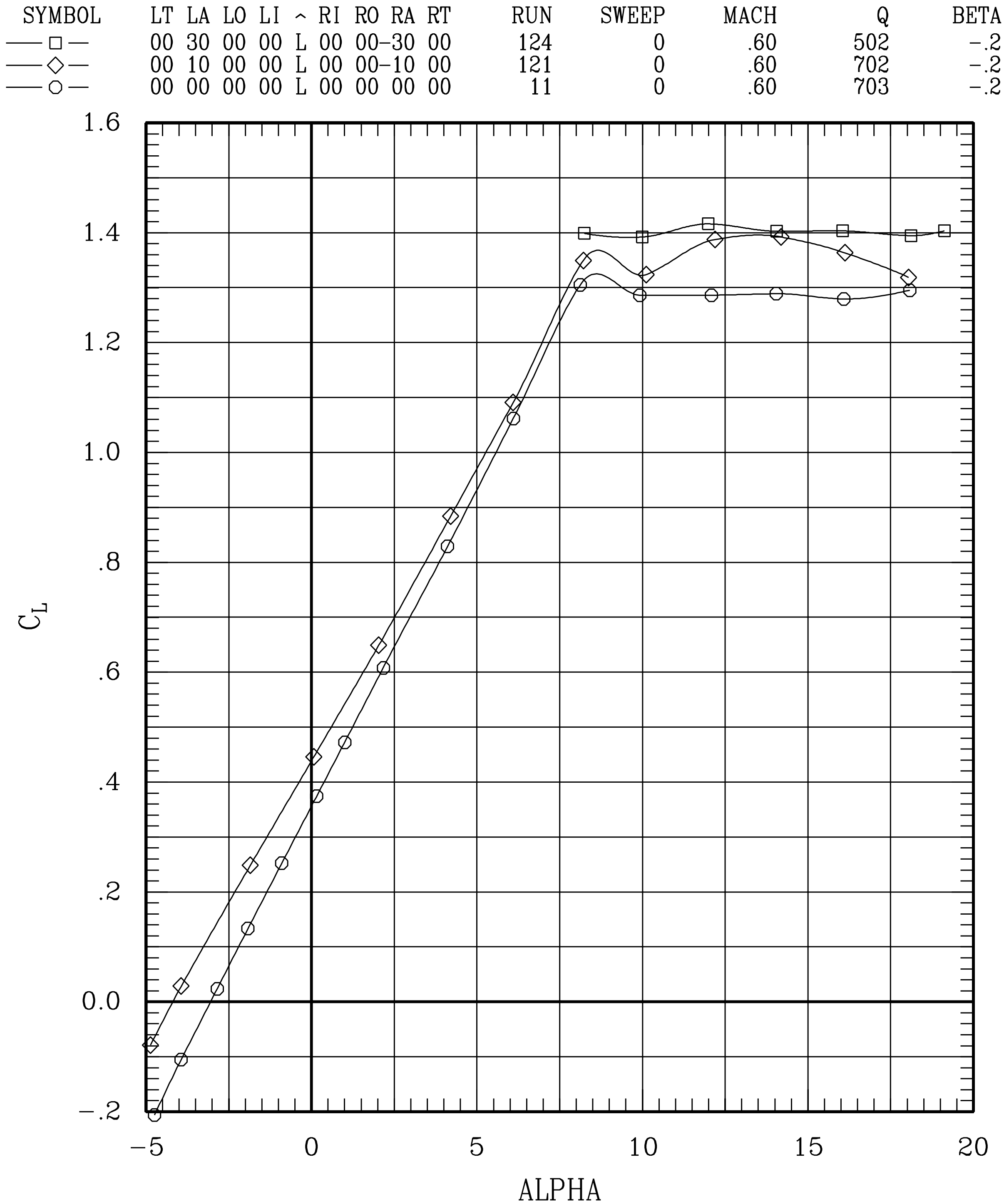

Figure 26(a). Effect of aileron deflection for sweep = 0 deg, Mach = 0.60 (Test #079).

SYMBOL	LT LA LO LI ^ RI RO RA RT	RUN	SWEEP	MACH	Q	BETA
—□—	00 30 00 00 L 00 00-30 00	124	0	.60	502	-.2
—◇—	00 10 00 00 L 00 00-10 00	121	0	.60	702	-.2
—○—	00 00 00 00 L 00 00 00 00	11	0	.60	703	-.2

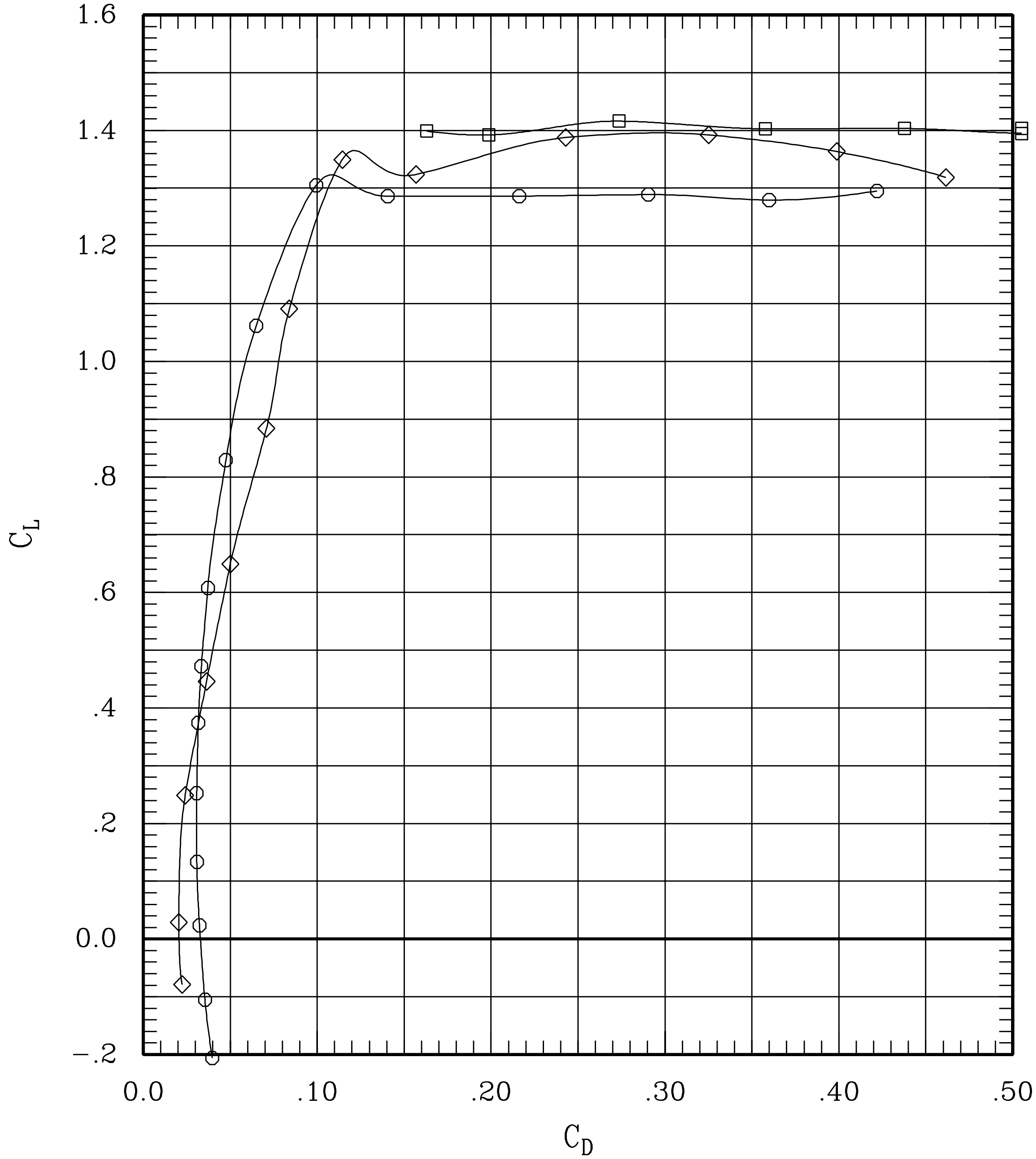

Figure 26(a). Effect of aileron deflection for sweep = 0 deg, Mach = 0.60 (Test #079).

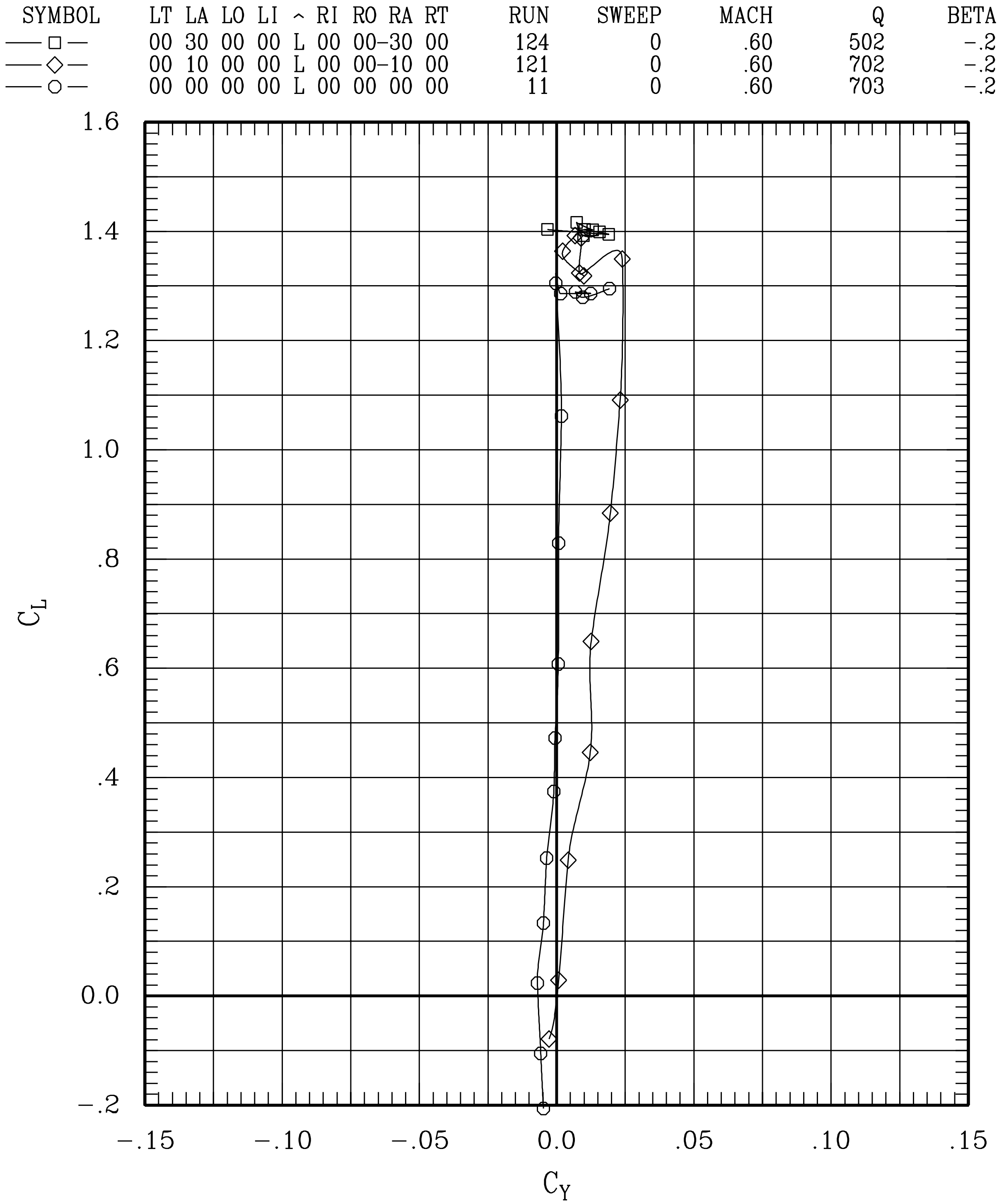

Figure 26(a). Effect of aileron deflection for sweep = 0 deg, Mach = 0.60 (Test #079).

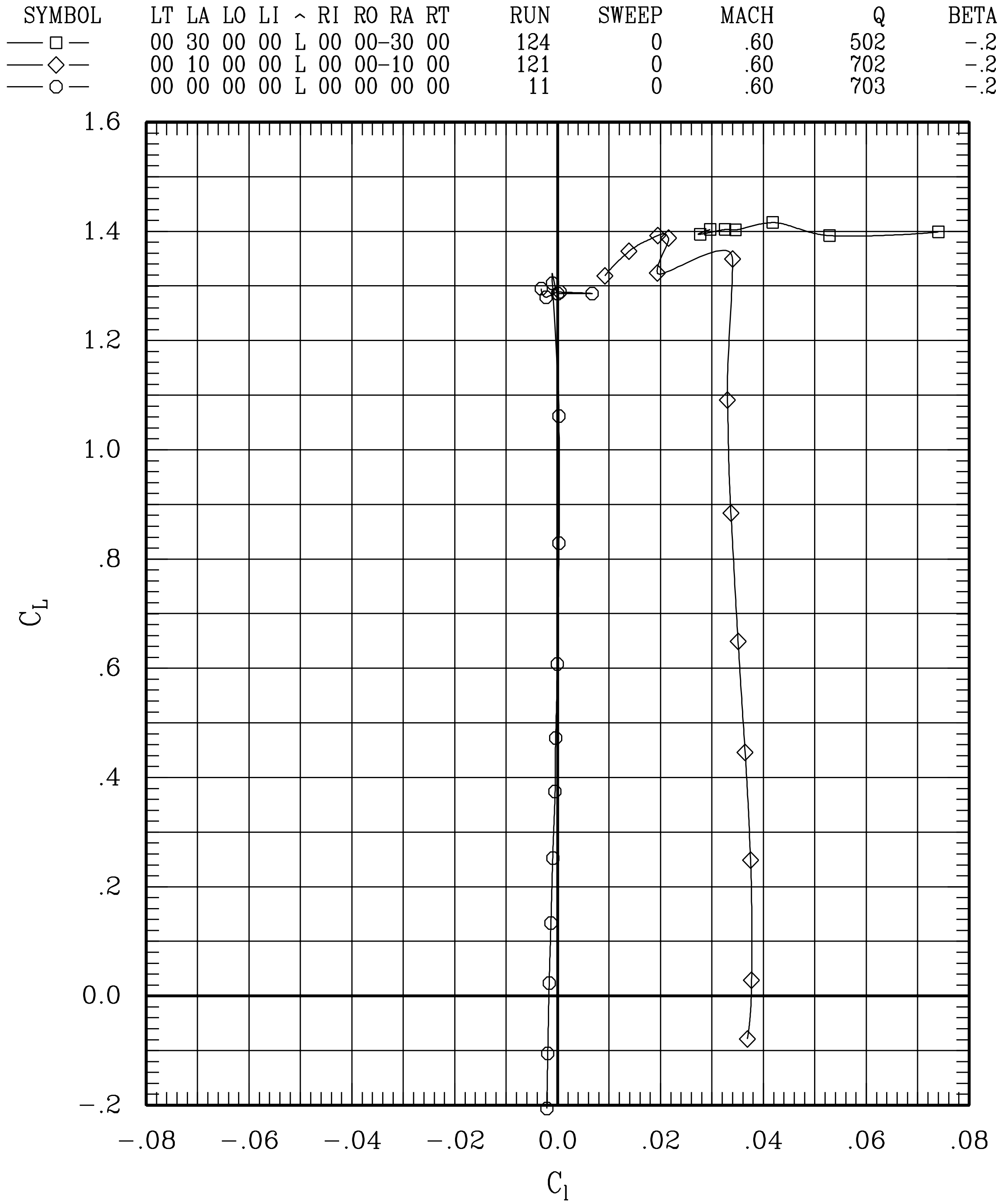

Figure 26(a). Effect of aileron deflection for sweep = 0 deg, Mach = 0.60 (Test #079).

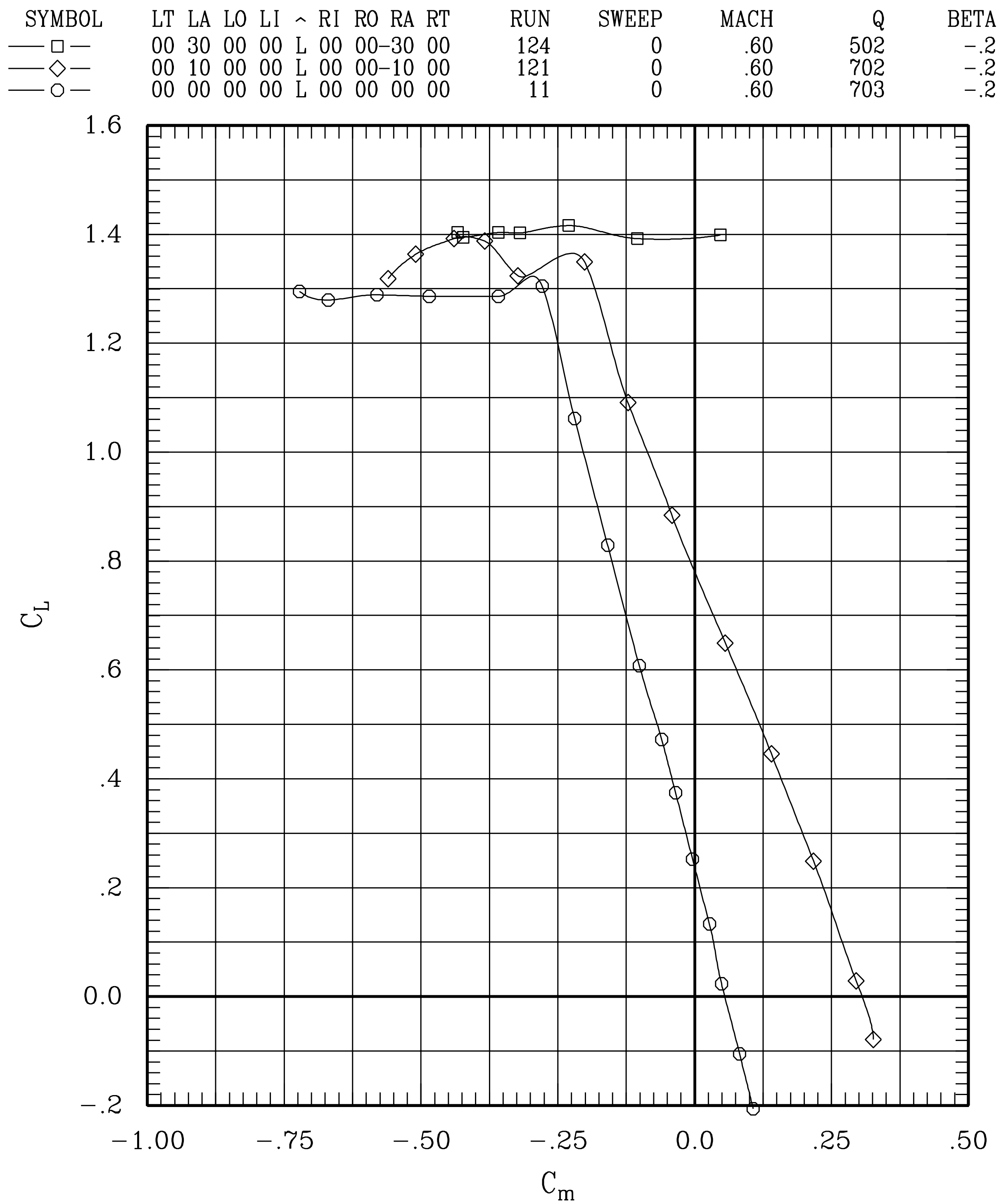

Figure 26(a). Effect of aileron deflection for sweep = 0 deg, Mach = 0.60 (Test #079).

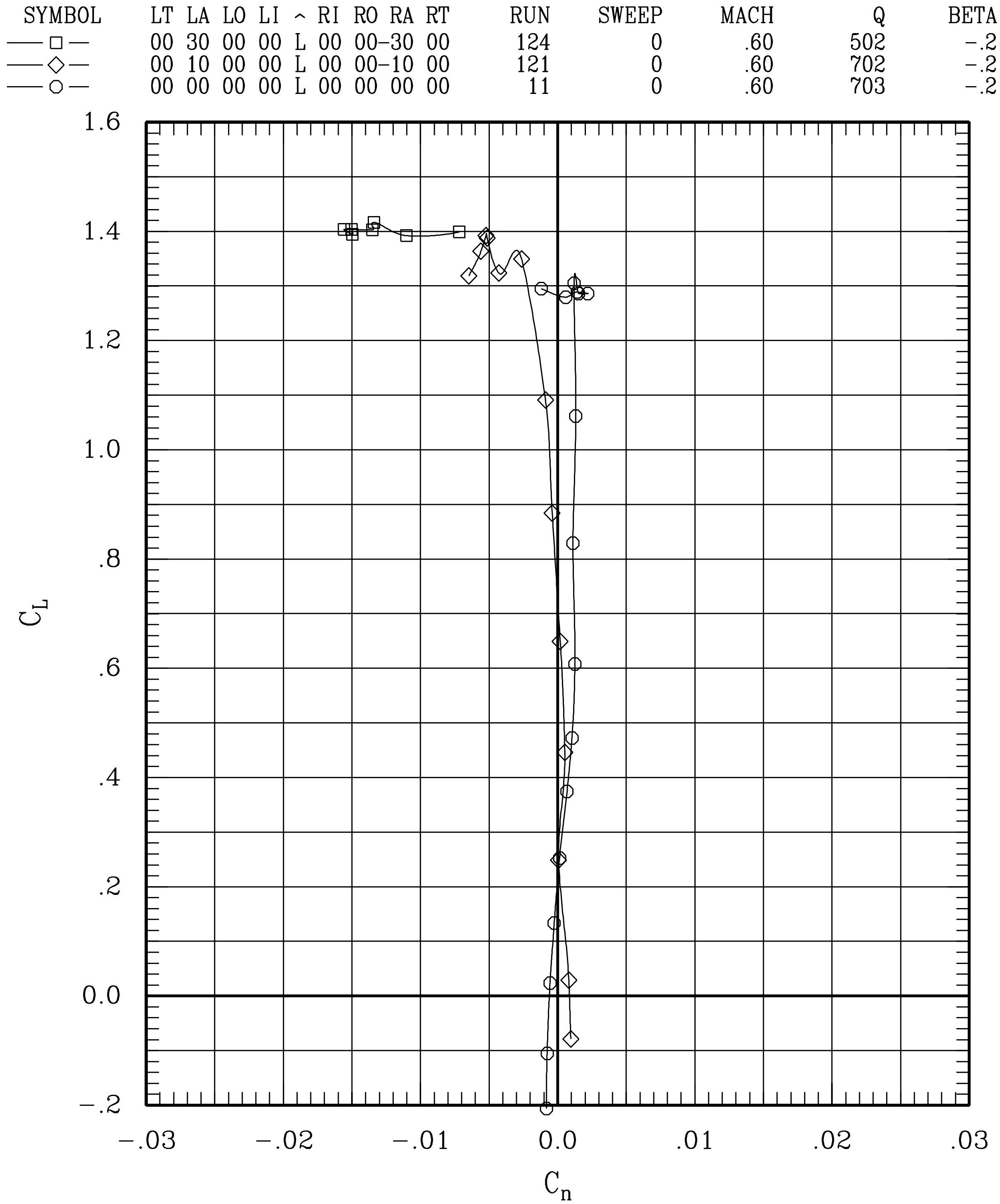

Figure 26(a). Effect of aileron deflection for sweep = 0 deg, Mach = 0.60 (Test #079).

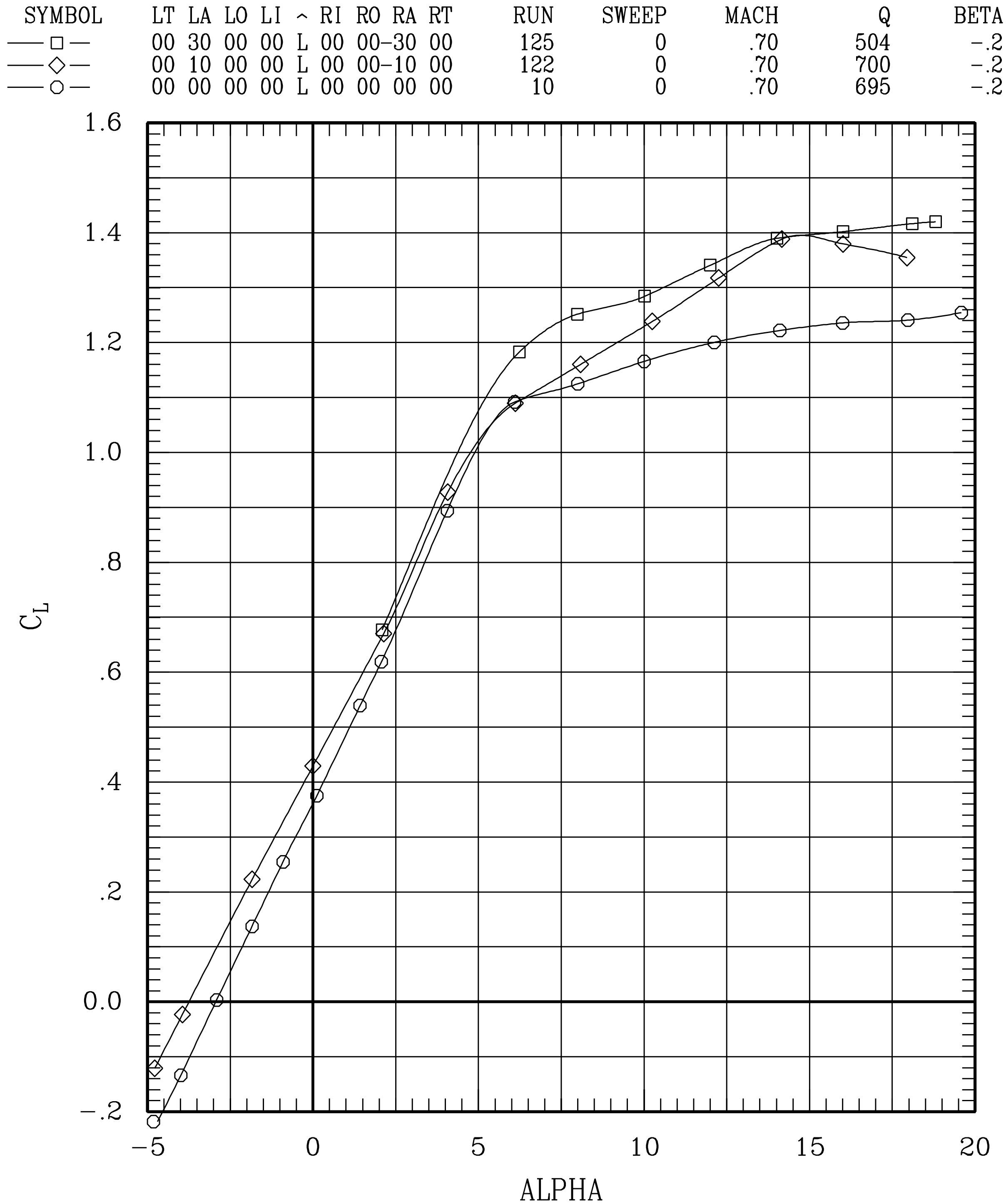

Figure 26(b). Effect of aileron deflection for sweep = 0 deg, Mach = 0.70 (Test #079).

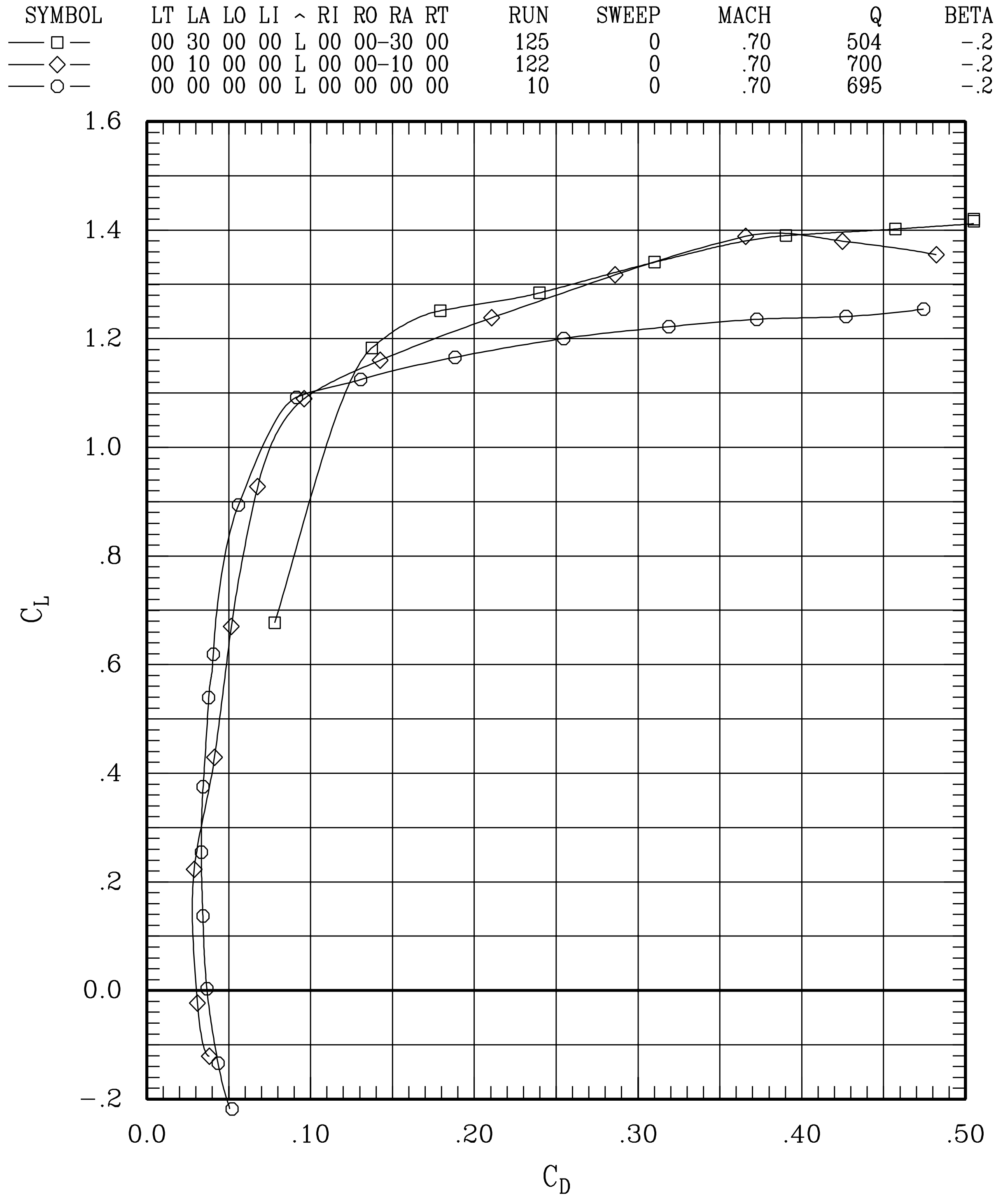

Figure 26(b). Effect of aileron deflection for sweep = 0 deg, Mach = 0.70 (Test #079).

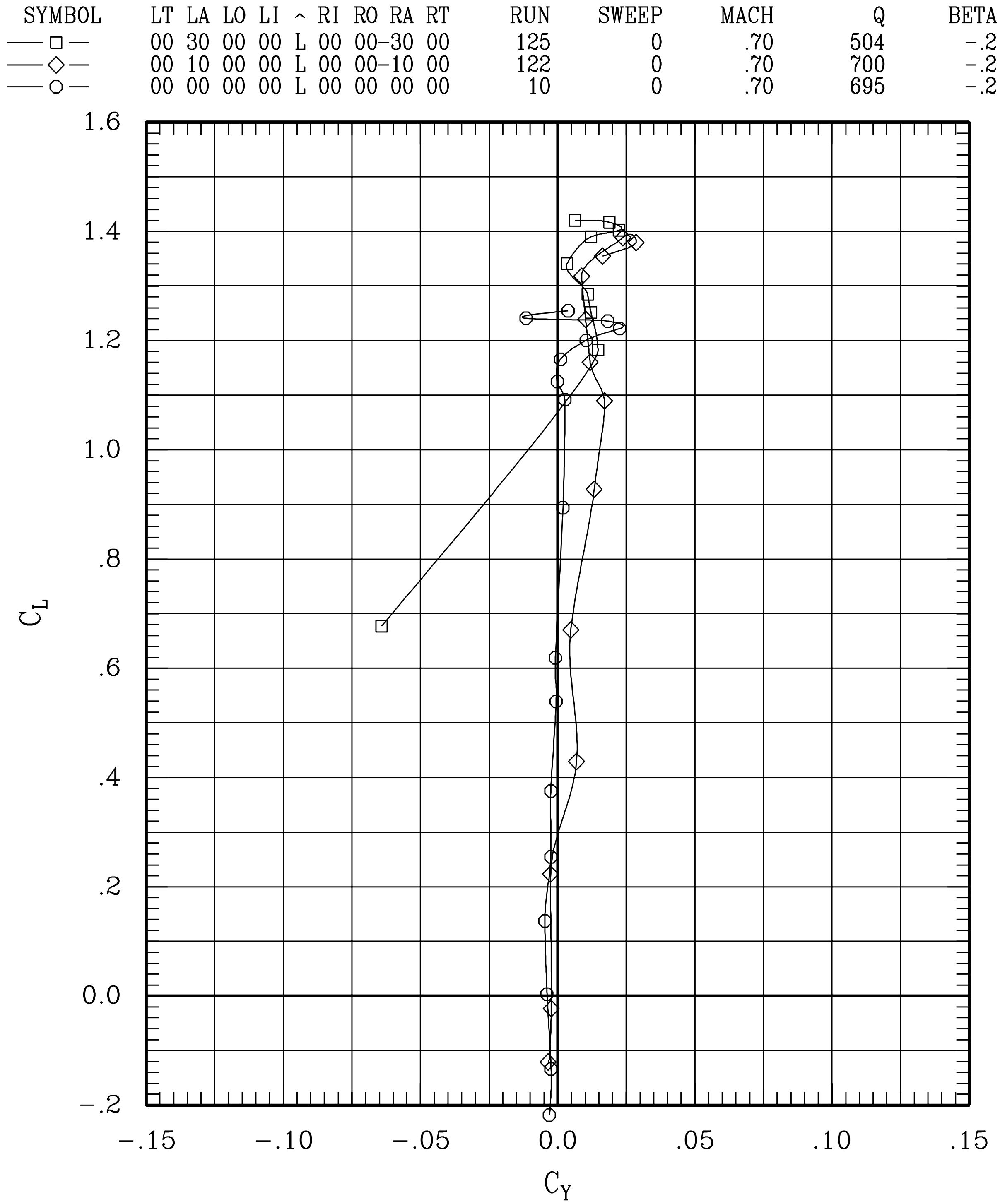

Figure 26(b). Effect of aileron deflection for sweep = 0 deg, Mach = 0.70 (Test #079).

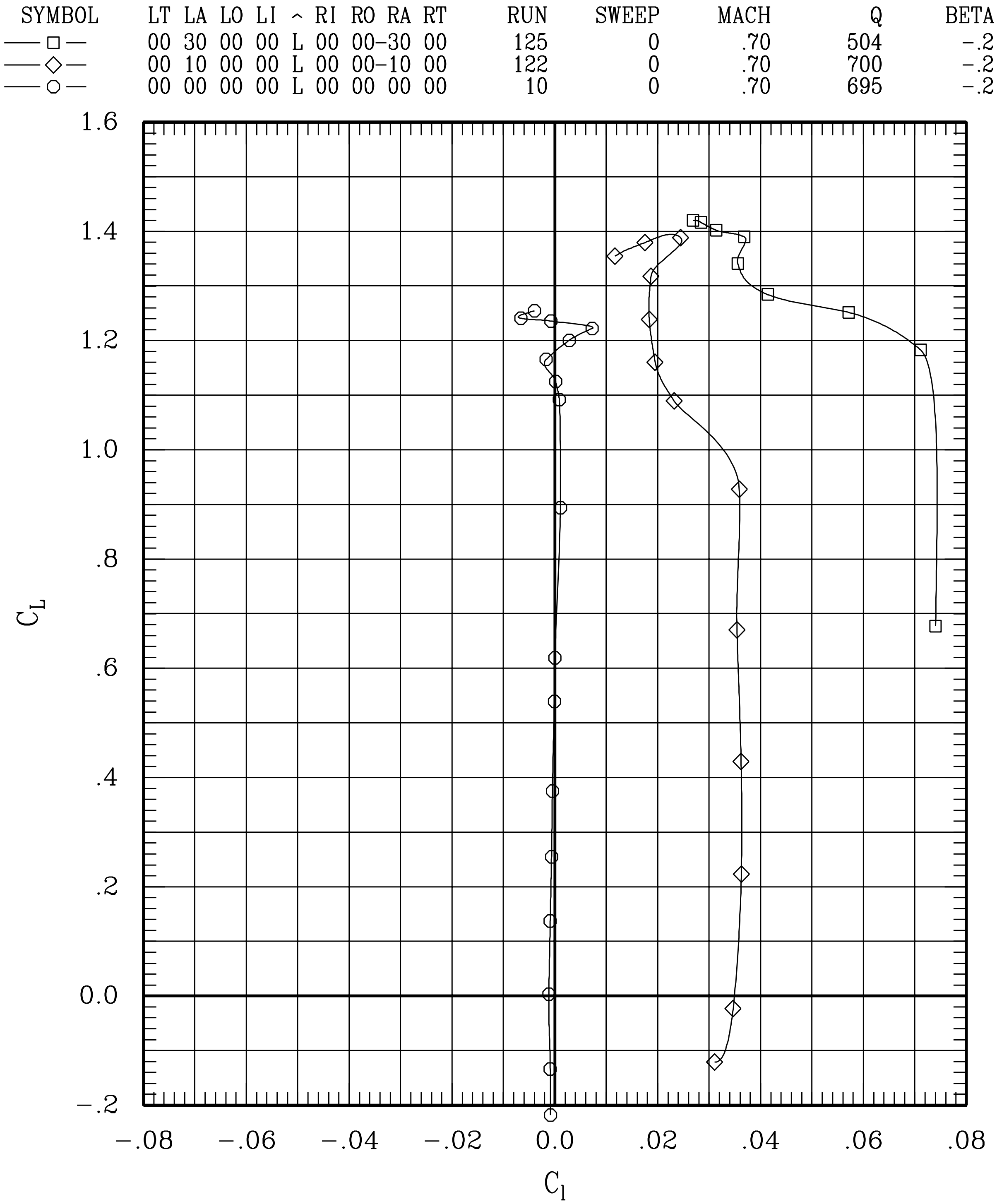

Figure 26(b). Effect of aileron deflection for sweep = 0 deg, Mach = 0.70 (Test #079).

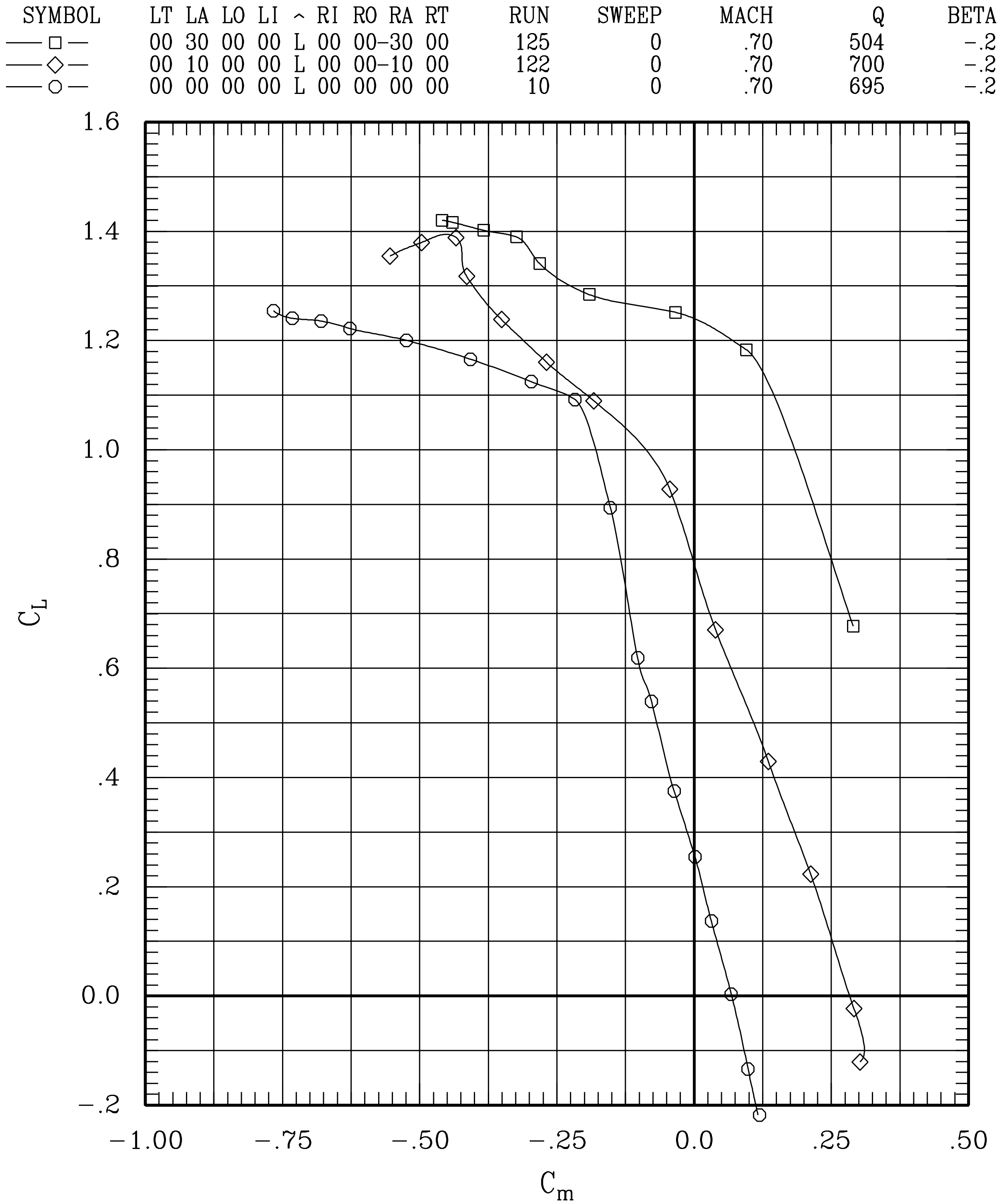

Figure 26(b). Effect of aileron deflection for sweep = 0 deg, Mach = 0.70 (Test #079).

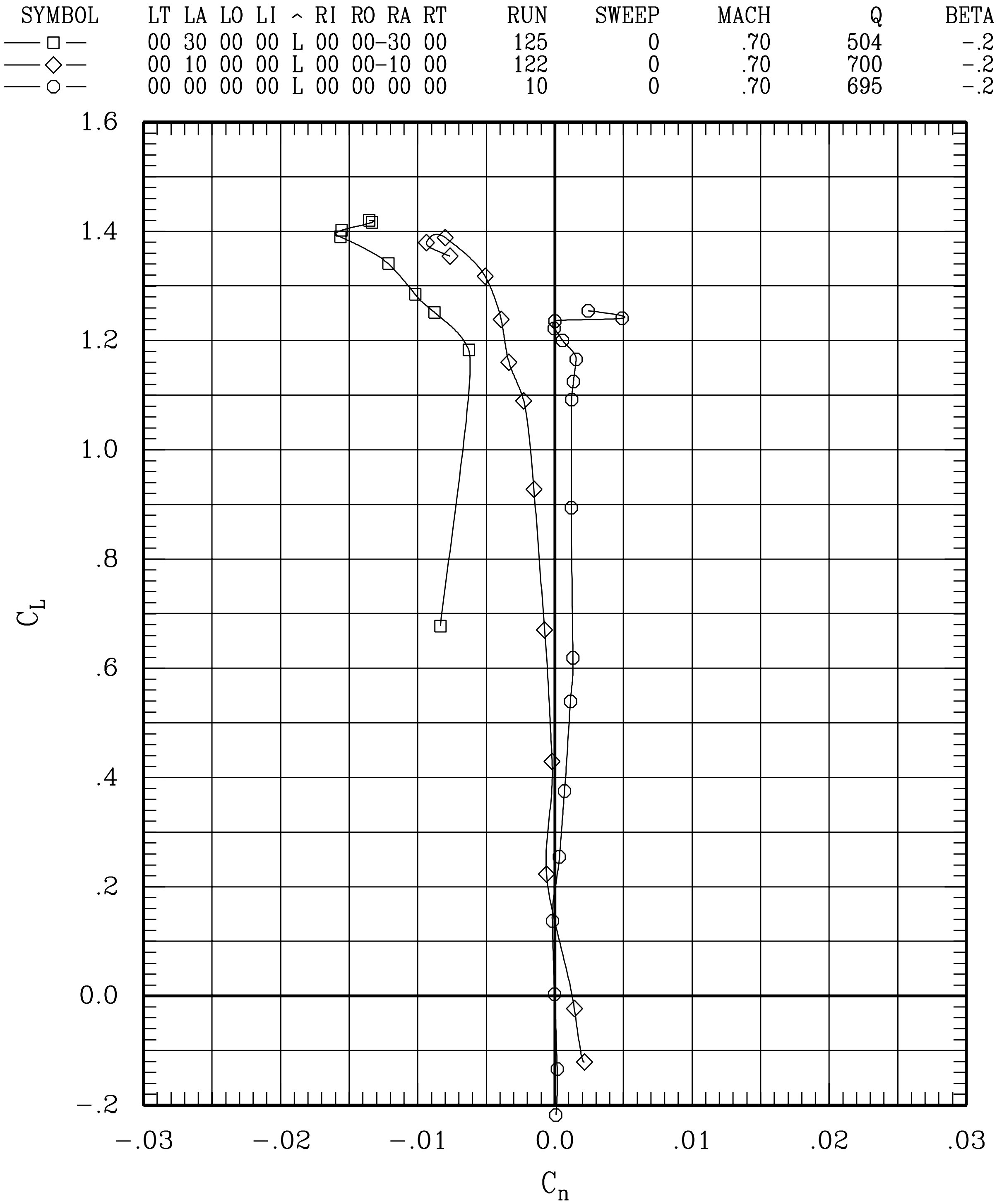

Figure 26(b). Effect of aileron deflection for sweep = 0 deg, Mach = 0.70 (Test #079).

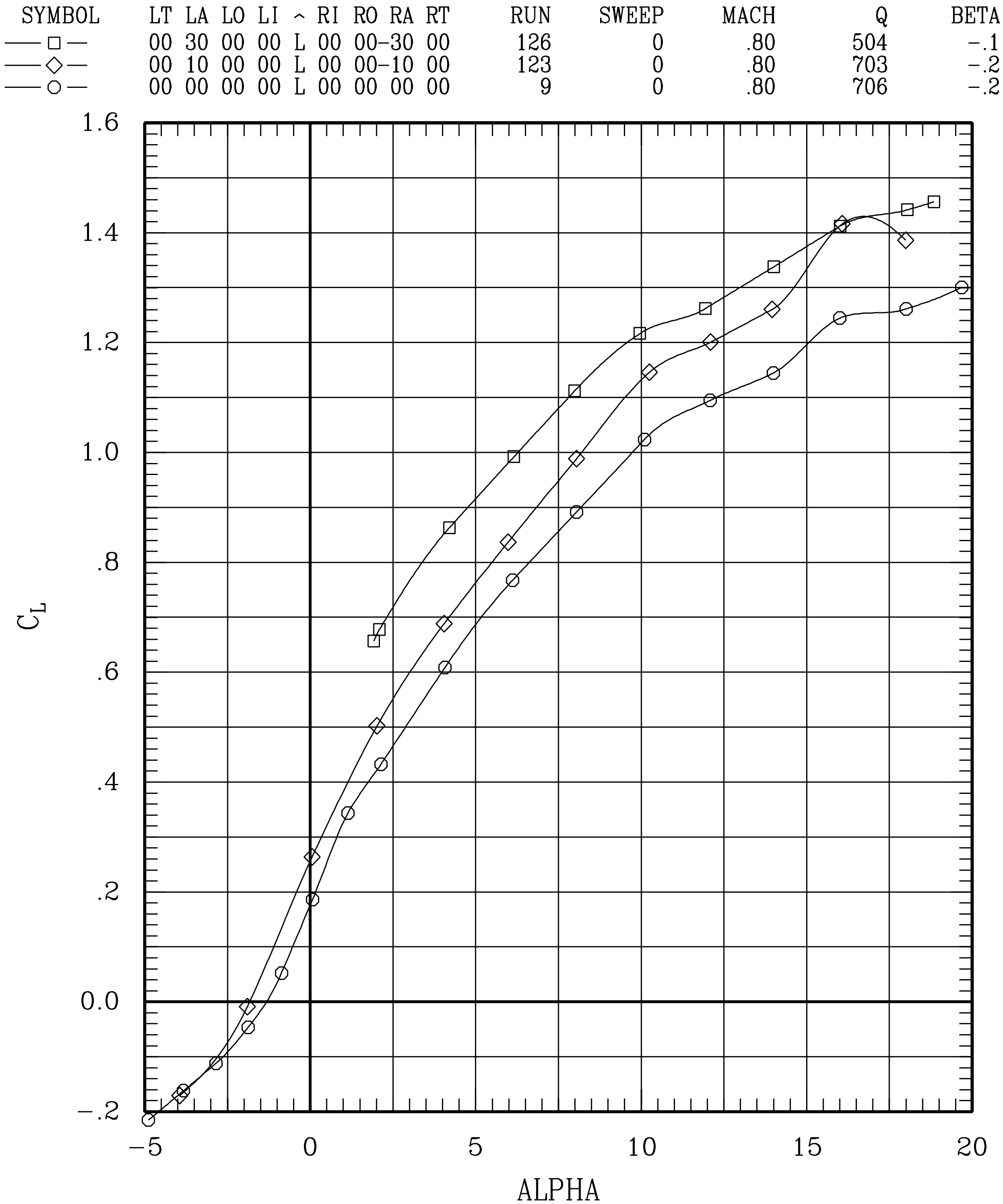

Figure 26(c). Effect of aileron deflection for sweep = 0 deg, Mach = 0.80 (Test #079).

SYMBOL	LT LA LO LI ^ RI RO RA RT	RUN	SWEEP	MACH	Q	BETA
—□—	00 30 00 00 L 00 00-30 00	126	0	.80	504	-.1
—◇—	00 10 00 00 L 00 00-10 00	123	0	.80	703	-.2
—○—	00 00 00 00 L 00 00 00 00	9	0	.80	706	-.2

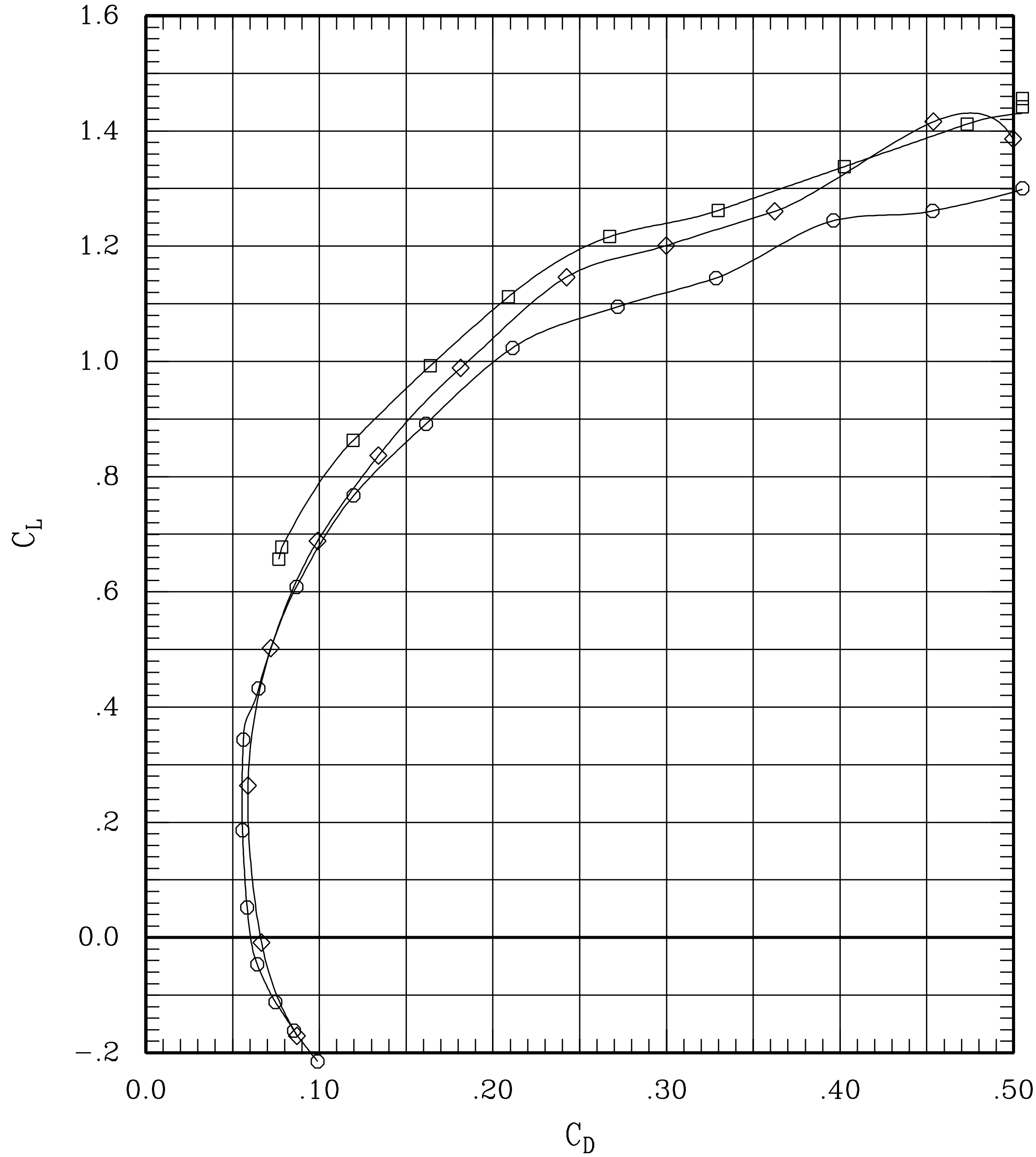

Figure 26(c). Effect of aileron deflection for sweep = 0 deg, Mach = 0.80 (Test #079).

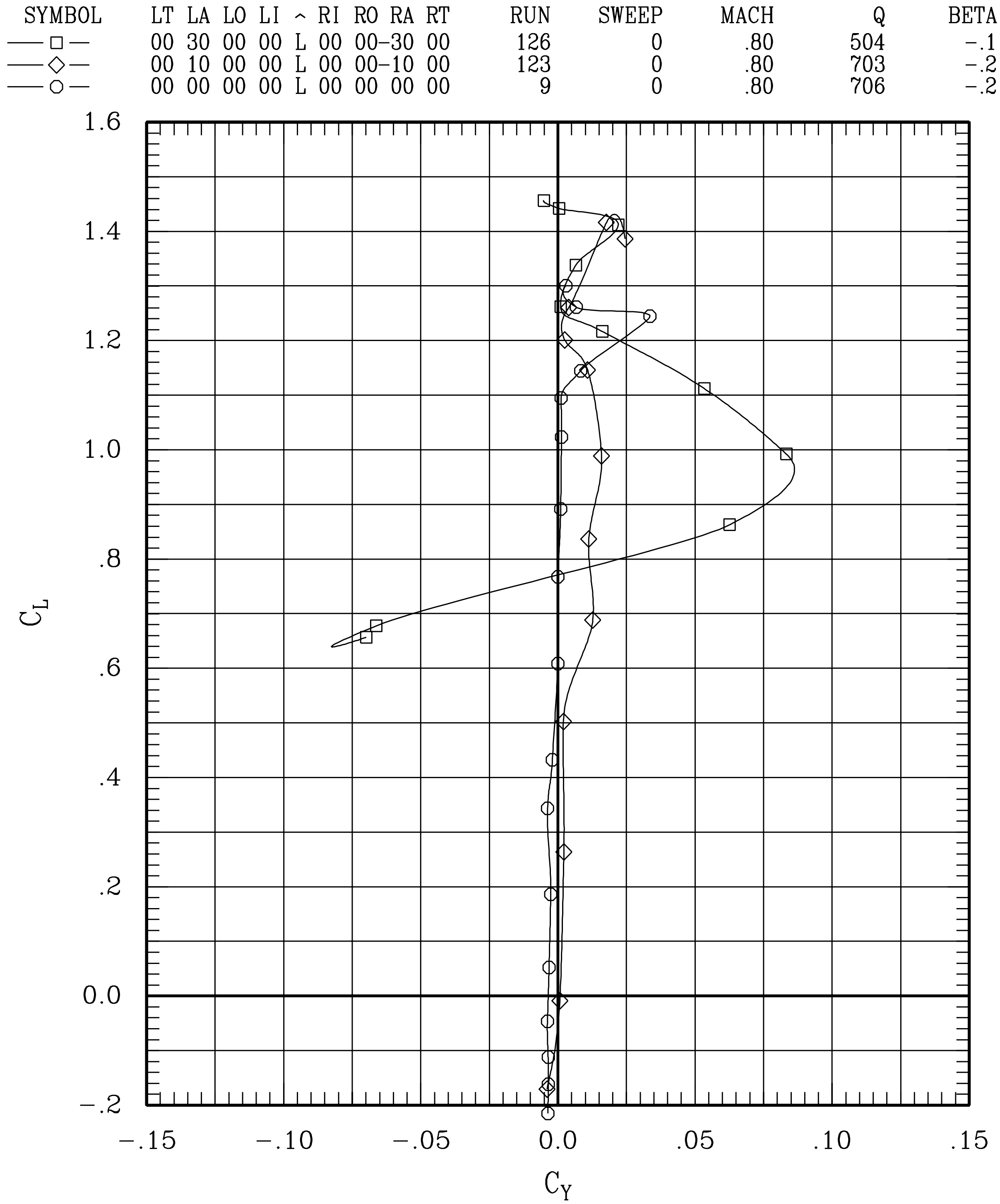

Figure 26(c). Effect of aileron deflection for sweep = 0 deg, Mach = 0.80 (Test #079).

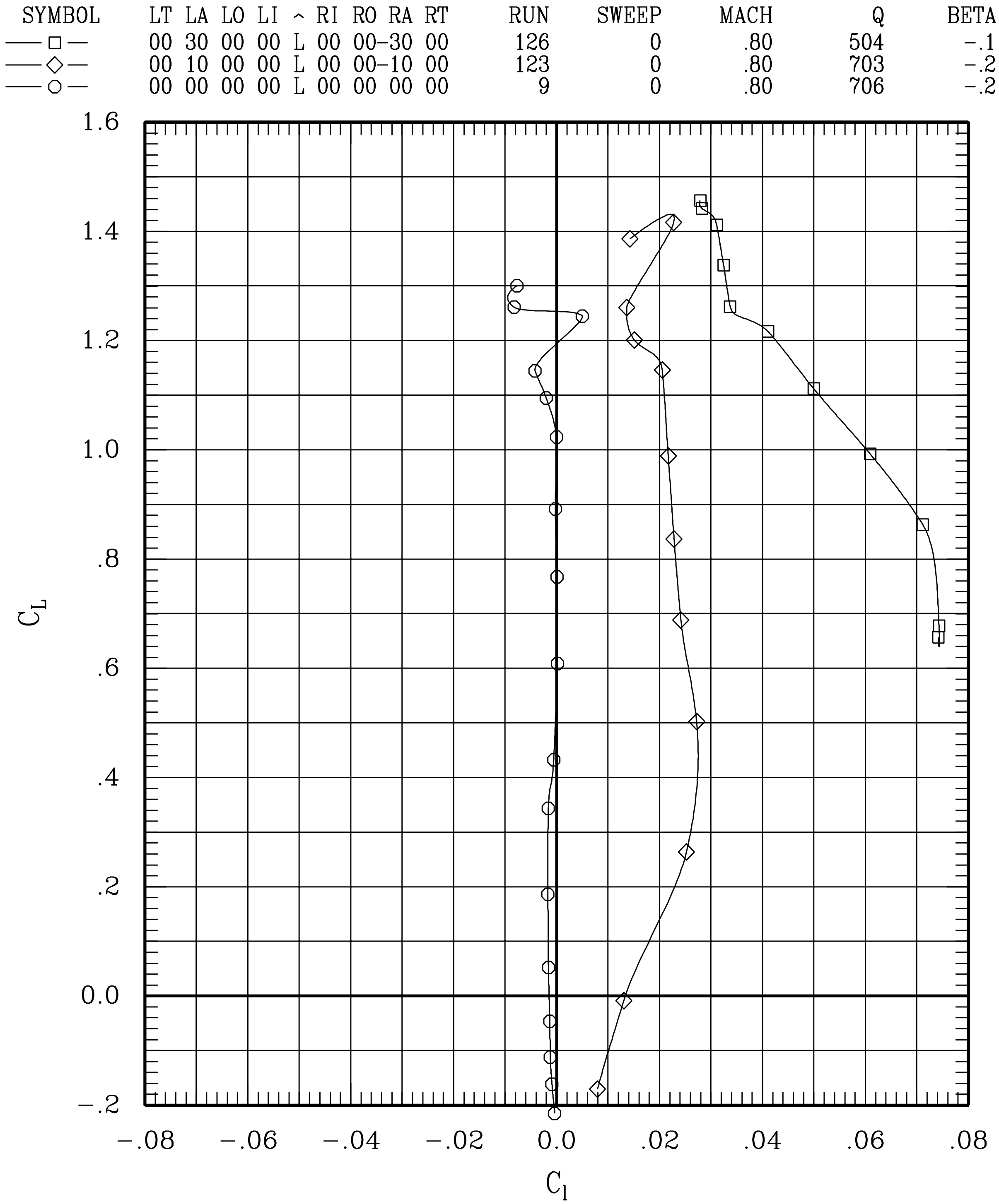

Figure 26(c). Effect of aileron deflection for sweep = 0 deg, Mach = 0.80 (Test #079).

SYMBOL	LT LA LO LI ^ RI RO RA RT	RUN	SWEEP	MACH	Q	BETA
—□—	00 30 00 00 L 00 00-30 00	126	0	.80	504	-.1
—◇—	00 10 00 00 L 00 00-10 00	123	0	.80	703	-.2
—○—	00 00 00 00 L 00 00 00 00	9	0	.80	706	-.2

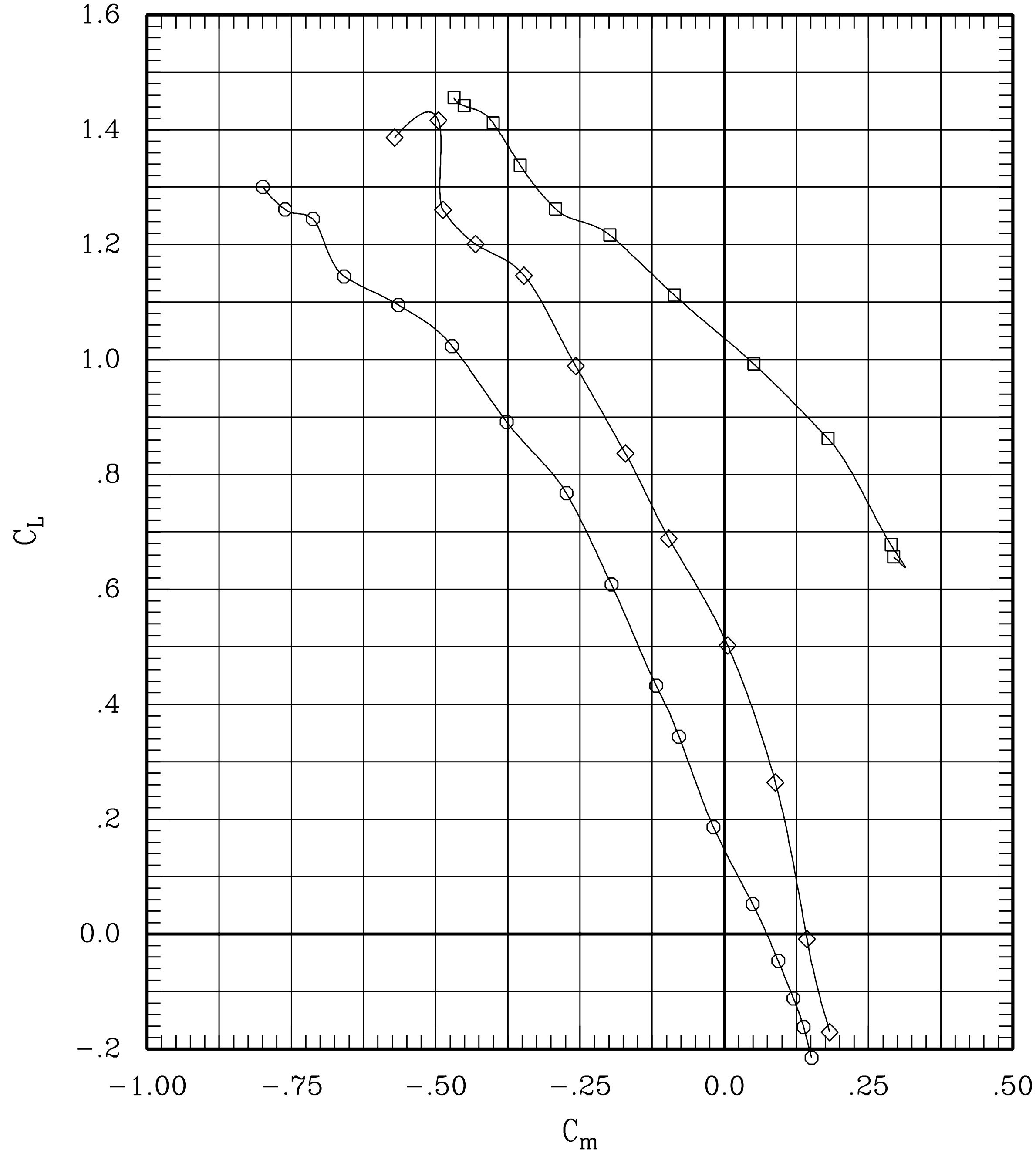

Figure 26(c). Effect of aileron deflection for sweep = 0 deg, Mach = 0.80 (Test #079).

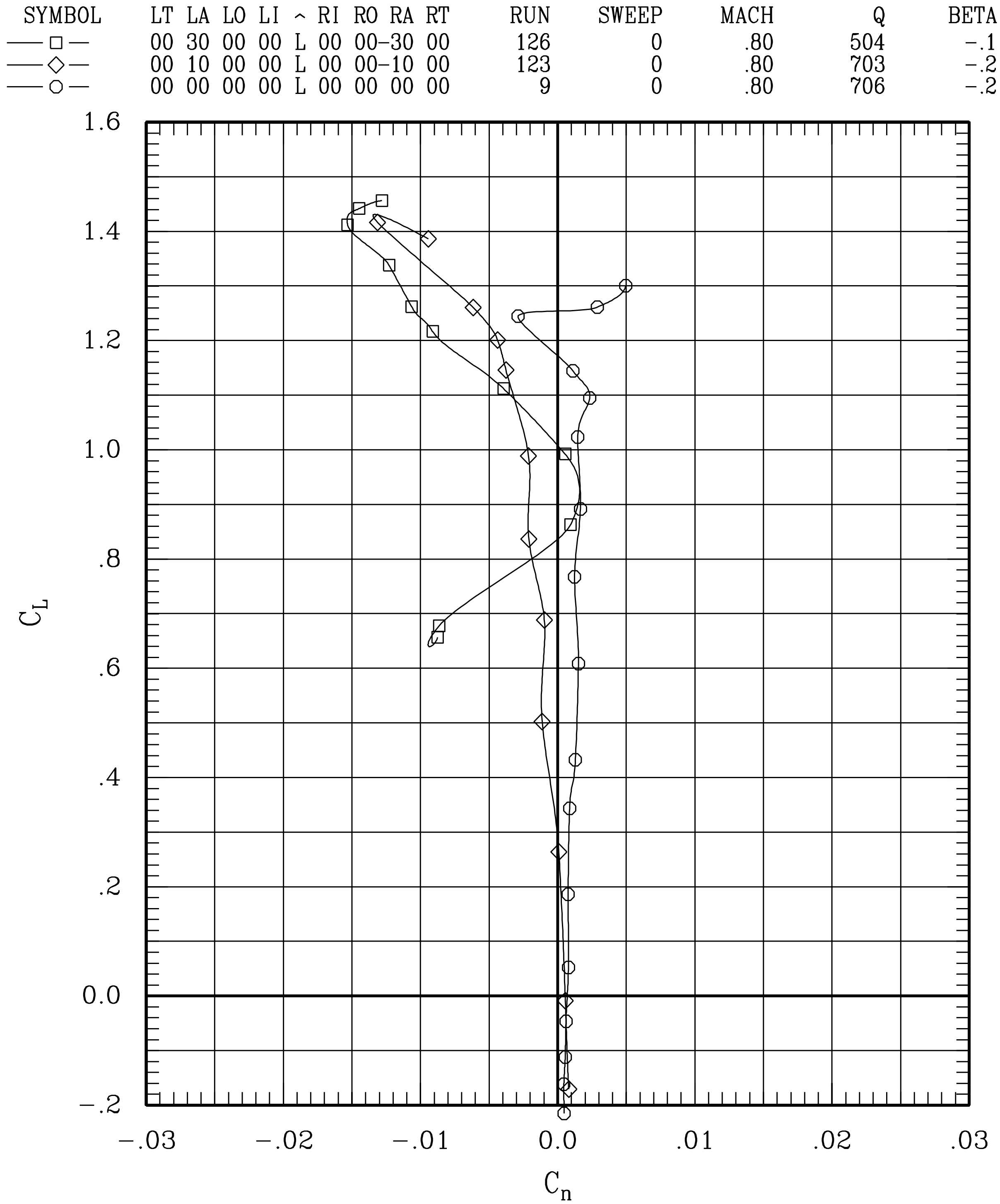

Figure 26(c). Effect of aileron deflection for sweep = 0 deg, Mach = 0.80 (Test #079).

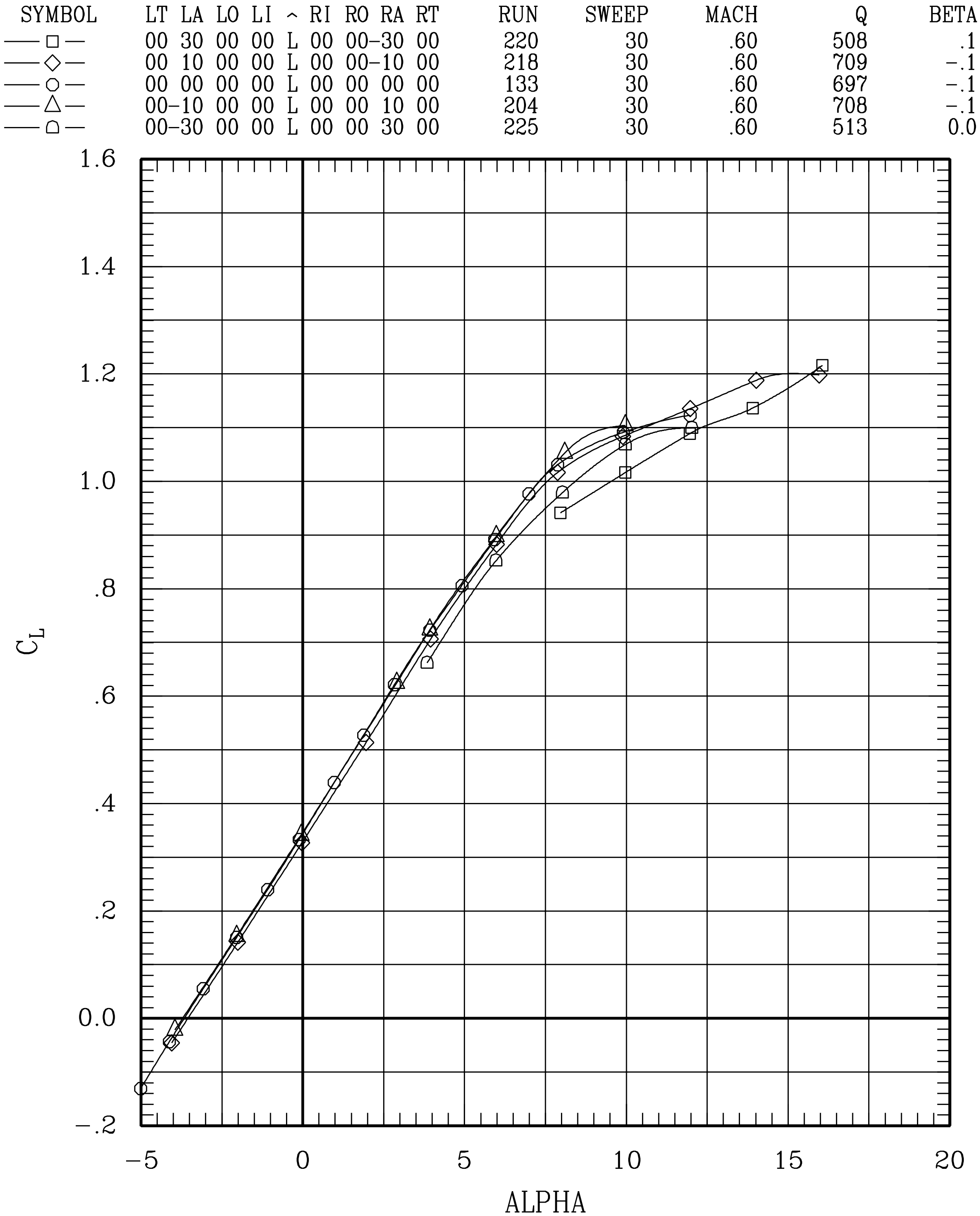

Figure 26(d). Effect of aileron deflection for sweep = 30 deg, Mach = 0.60 (Test #100).

SYMBOL	LT LA LO LI ^ RI RO RA RT	RUN	SWEEP	MACH	Q	BETA
—□—	00 30 00 00 L 00 00-30 00	220	30	.60	508	.1
—◇—	00 10 00 00 L 00 00-10 00	218	30	.60	709	-.1
—○—	00 00 00 00 L 00 00 00 00	133	30	.60	697	-.1
—△—	00-10 00 00 L 00 00 10 00	204	30	.60	708	-.1
—⌂—	00-30 00 00 L 00 00 30 00	225	30	.60	513	0.0

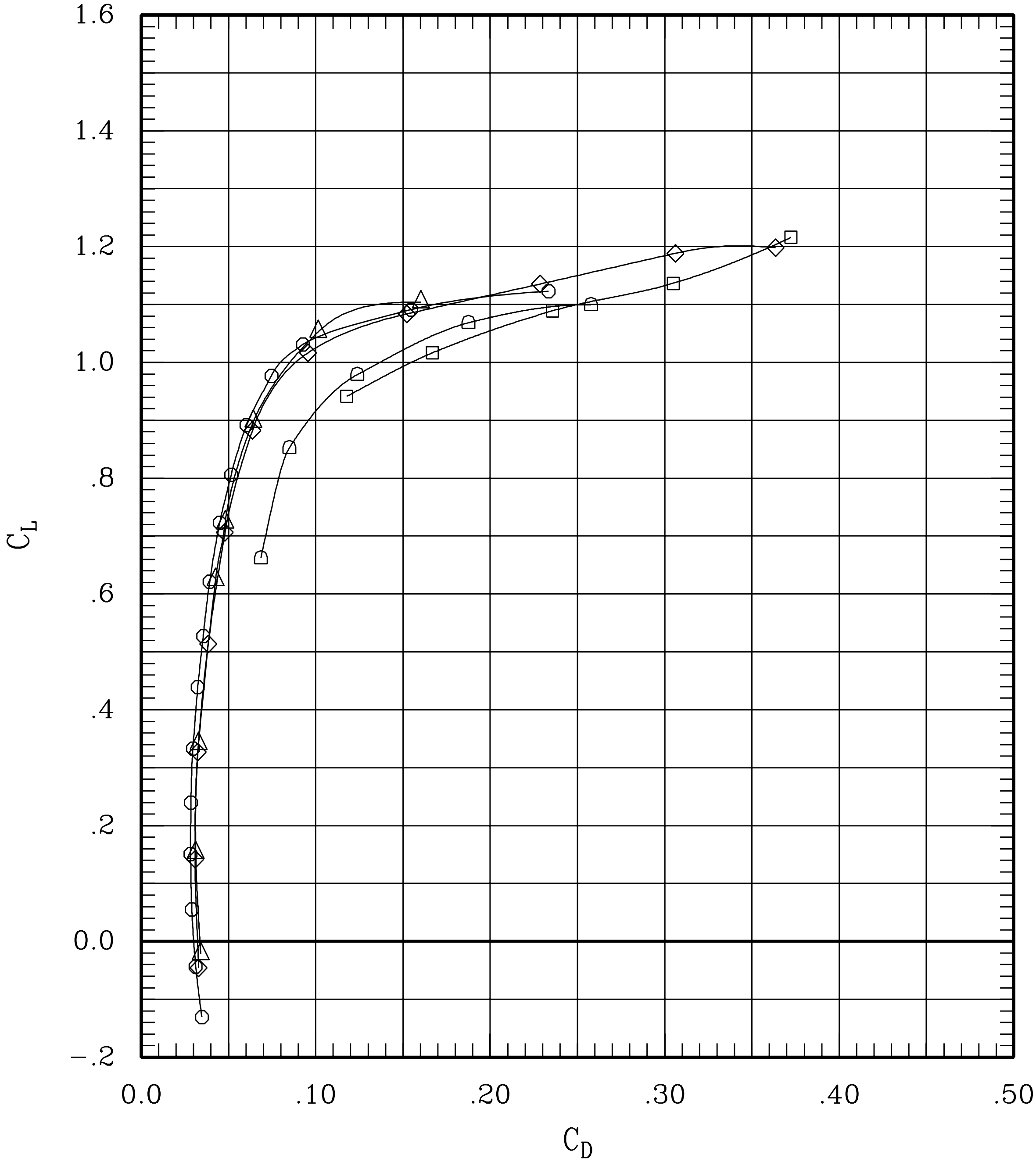

Figure 26(d). Effect of aileron deflection for sweep = 30 deg, Mach = 0.60 (Test #100).

SYMBOL	LT LA LO LI ^ RI RO RA RT	RUN	SWEEP	MACH	Q	BETA
—□—	00 30 00 00 L 00 00−30 00	220	30	.60	508	.1
—◇—	00 10 00 00 L 00 00−10 00	218	30	.60	709	−.1
—○—	00 00 00 00 L 00 00 00 00	133	30	.60	697	−.1
—△—	00−10 00 00 L 00 00 10 00	204	30	.60	708	−.1
—⌂—	00−30 00 00 L 00 00 30 00	225	30	.60	513	0.0

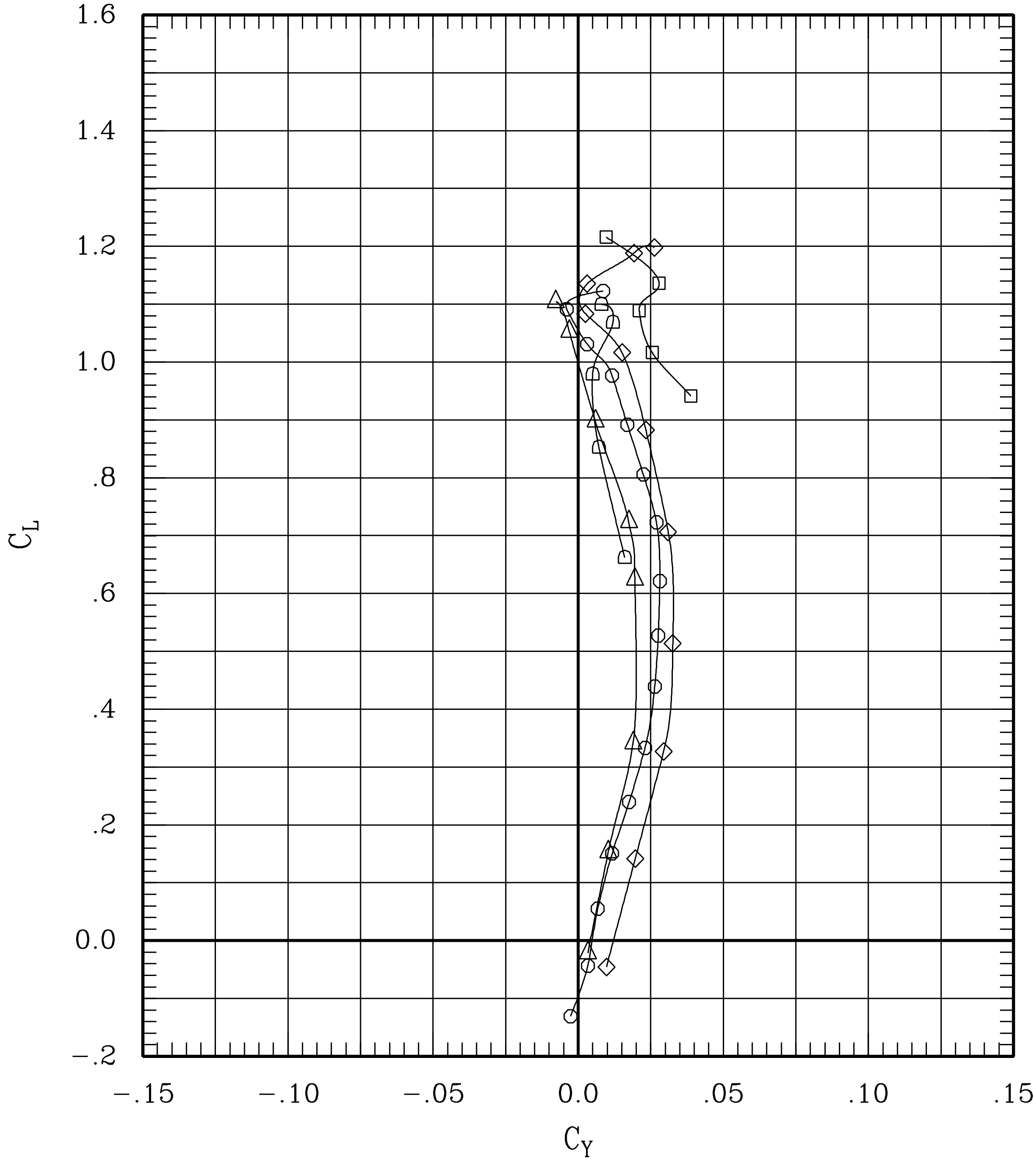

Figure 26(d). Effect of aileron deflection for sweep = 30 deg, Mach = 0.60 (Test #100).

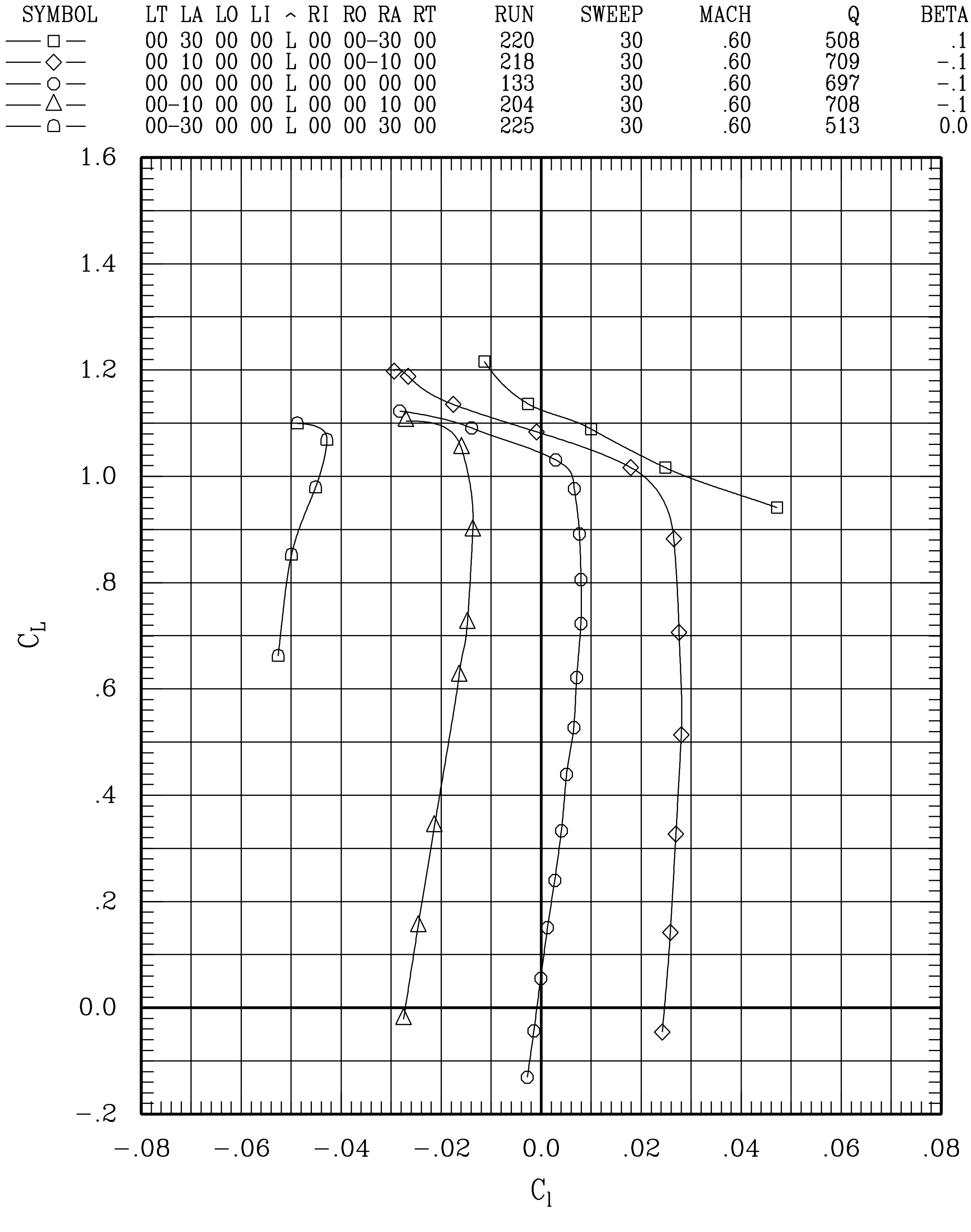

Figure 26(d). Effect of aileron deflection for sweep = 30 deg, Mach = 0.60 (Test #100).

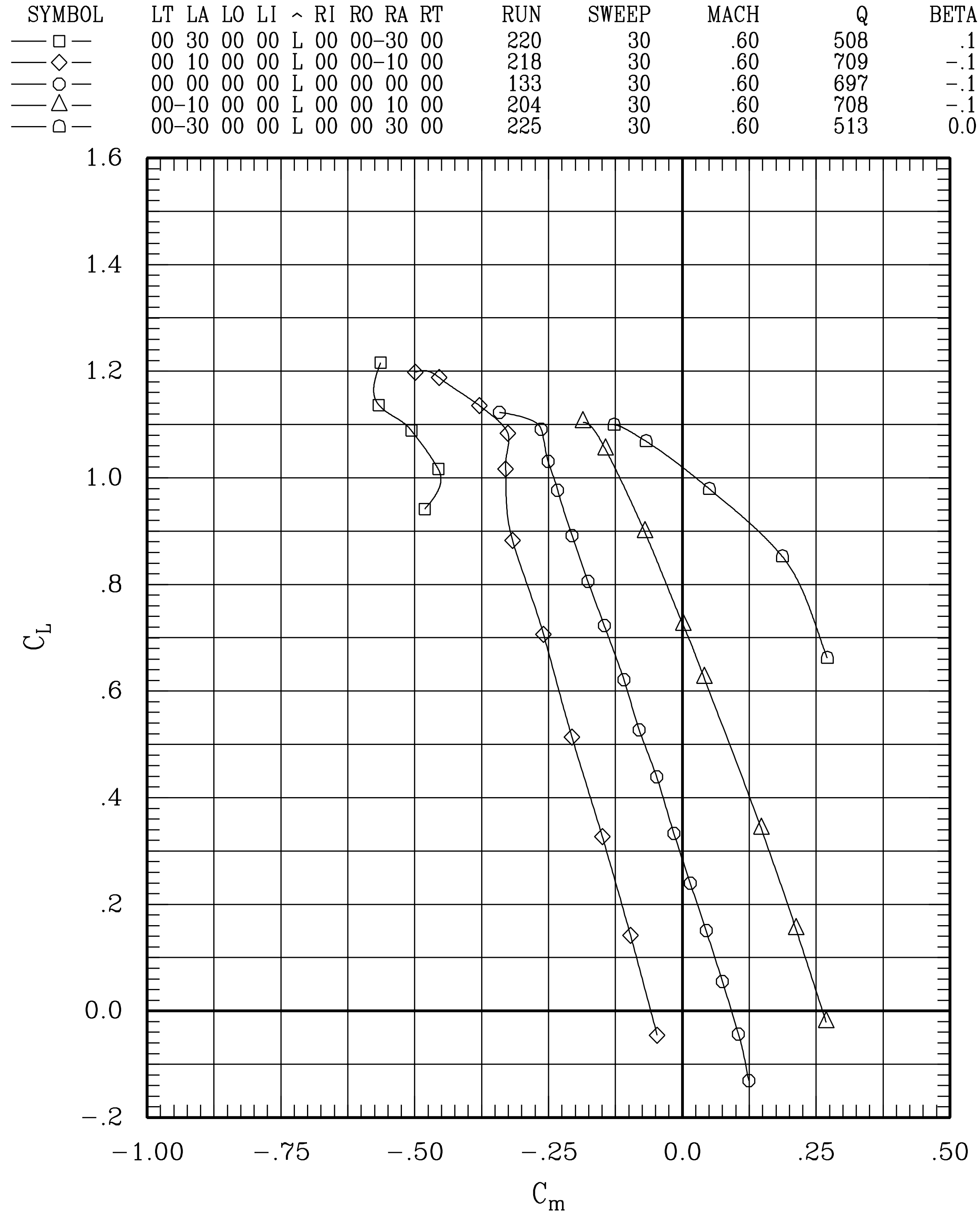

Figure 26(d). Effect of aileron deflection for sweep = 30 deg, Mach = 0.60 (Test #100).

SYMBOL	LT LA LO LI ^ RI RO RA RT	RUN	SWEEP	MACH	Q	BETA
□	00 30 00 00 L 00 00-30 00	220	30	.60	508	.1
◇	00 10 00 00 L 00 00-10 00	218	30	.60	709	-.1
○	00 00 00 00 L 00 00 00 00	133	30	.60	697	-.1
△	00-10 00 00 L 00 00 10 00	204	30	.60	708	-.1
⌂	00-30 00 00 L 00 00 30 00	225	30	.60	513	0.0

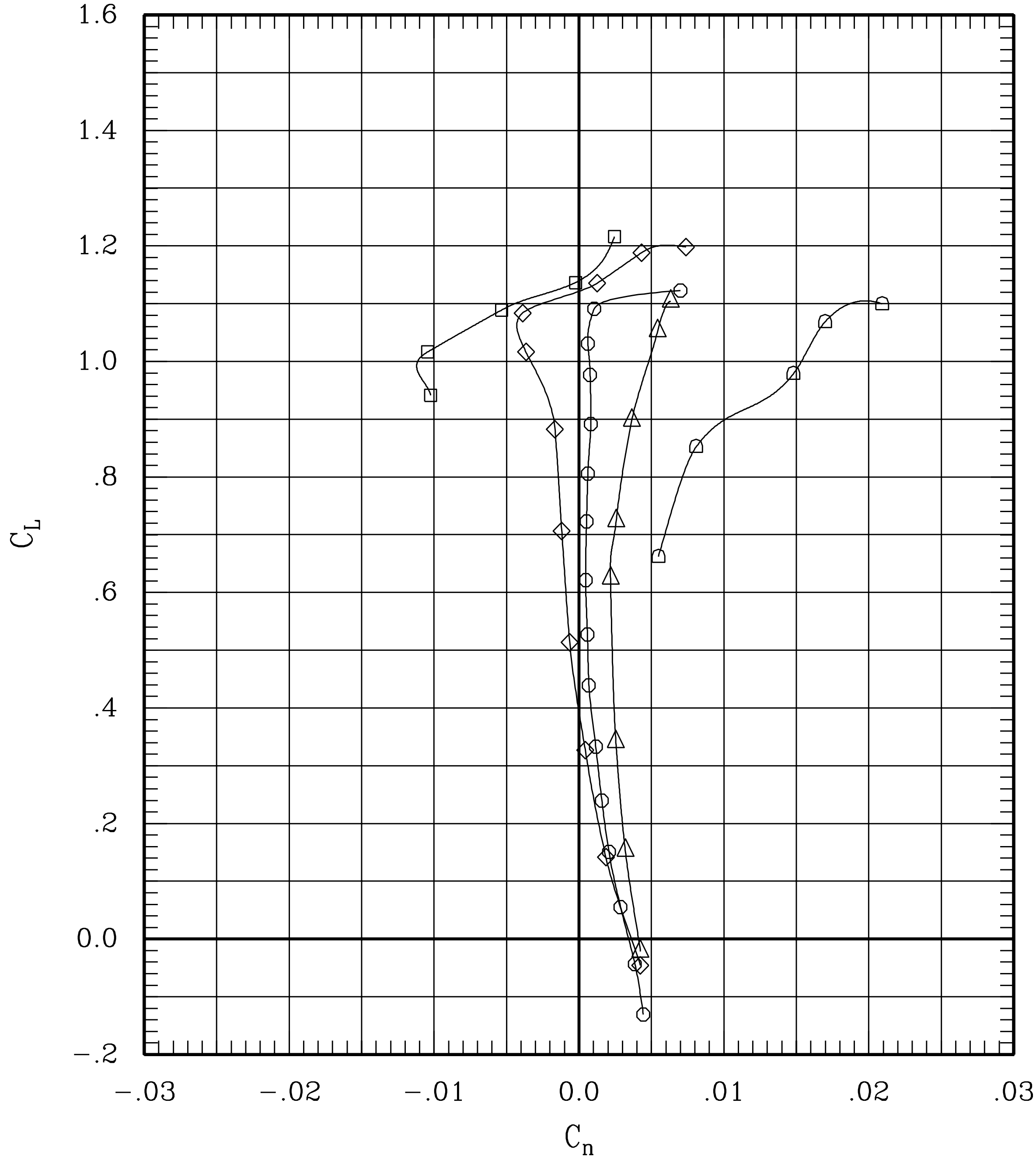

Figure 26(d). Effect of aileron deflection for sweep = 30 deg, Mach = 0.60 (Test #100).

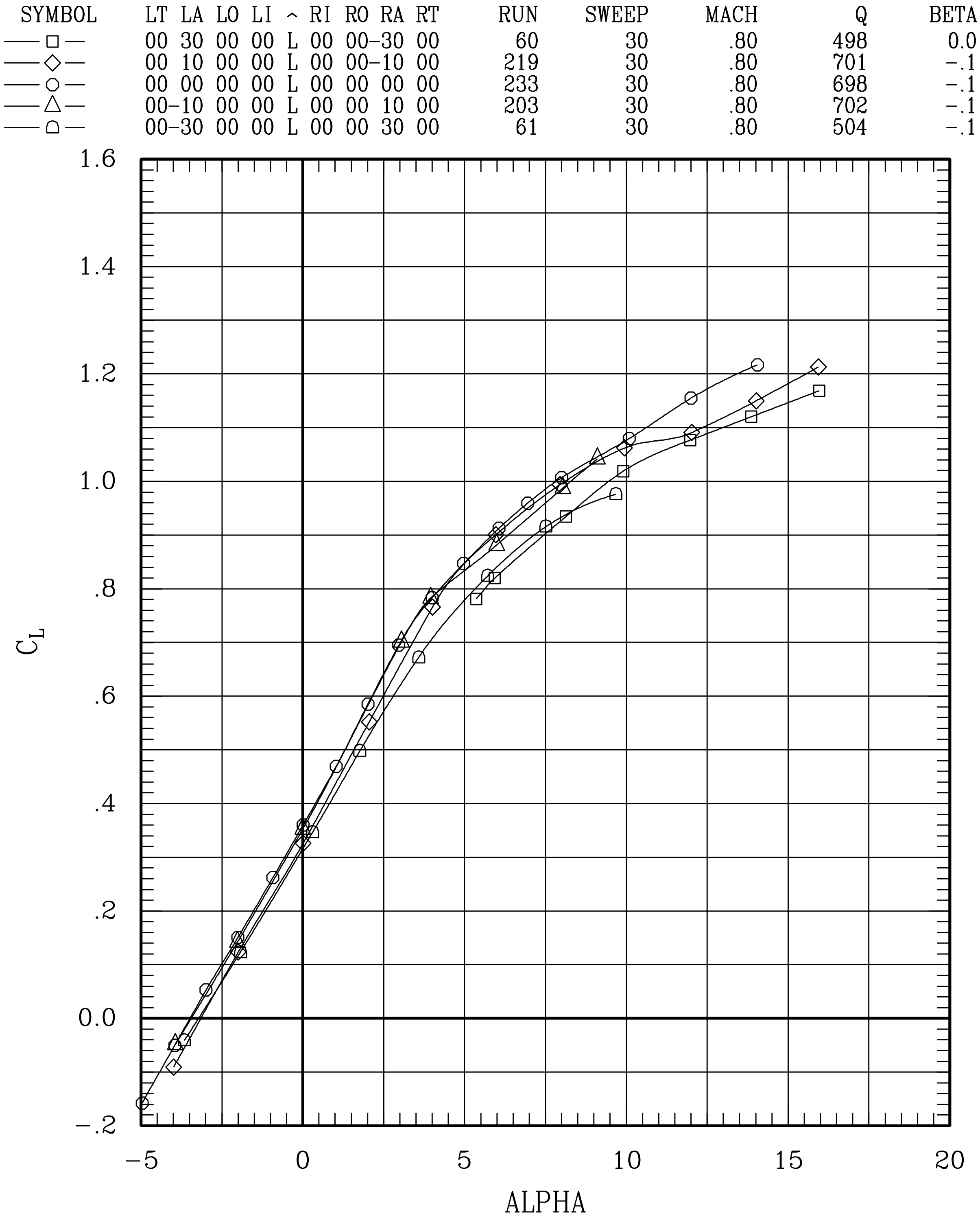

Figure 26(e). Effect of aileron deflection for sweep = 30 deg, Mach = 0.80 (Test #100).

SYMBOL	LT LA LO LI ^ RI RO RA RT	RUN	SWEEP	MACH	Q	BETA
—□—	00 30 00 00 L 00 00-30 00	60	30	.80	498	0.0
—◇—	00 10 00 00 L 00 00-10 00	219	30	.80	701	-.1
—○—	00 00 00 00 L 00 00 00 00	233	30	.80	698	-.1
—△—	00-10 00 00 L 00 00 10 00	203	30	.80	702	-.1
—⌂—	00-30 00 00 L 00 00 30 00	61	30	.80	504	-.1

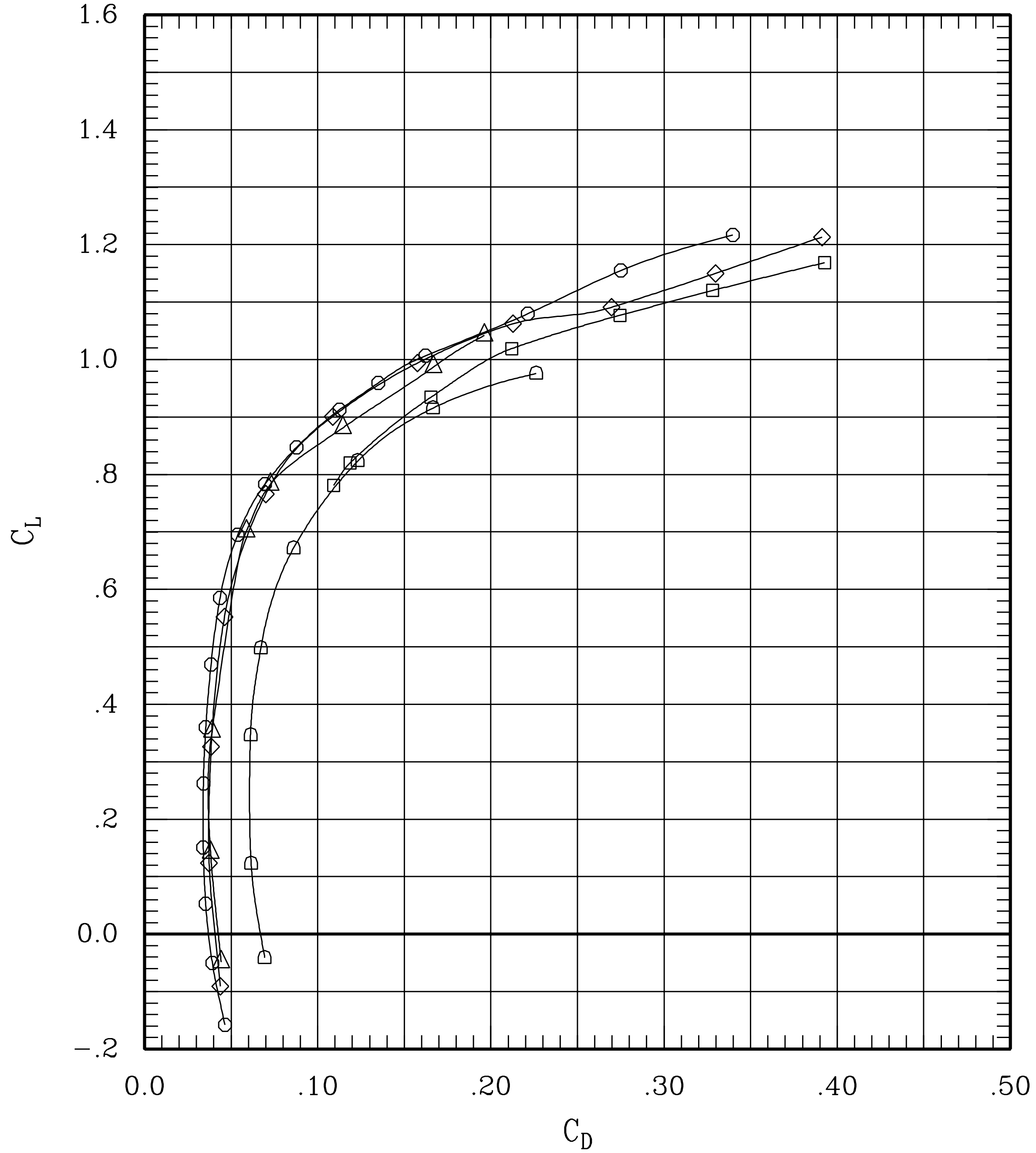

Figure 26(e). Effect of aileron deflection for sweep = 30 deg, Mach = 0.80 (Test #100).

SYMBOL	LT LA LO LI ^ RI RO RA RT	RUN	SWEEP	MACH	Q	BETA
—□—	00 30 00 00 L 00 00-30 00	60	30	.80	498	0.0
—◇—	00 10 00 00 L 00 00-10 00	219	30	.80	701	-.1
—○—	00 00 00 00 L 00 00 00 00	233	30	.80	698	-.1
—△—	00-10 00 00 L 00 00 10 00	203	30	.80	702	-.1
—⌂—	00-30 00 00 L 00 00 30 00	61	30	.80	504	-.1

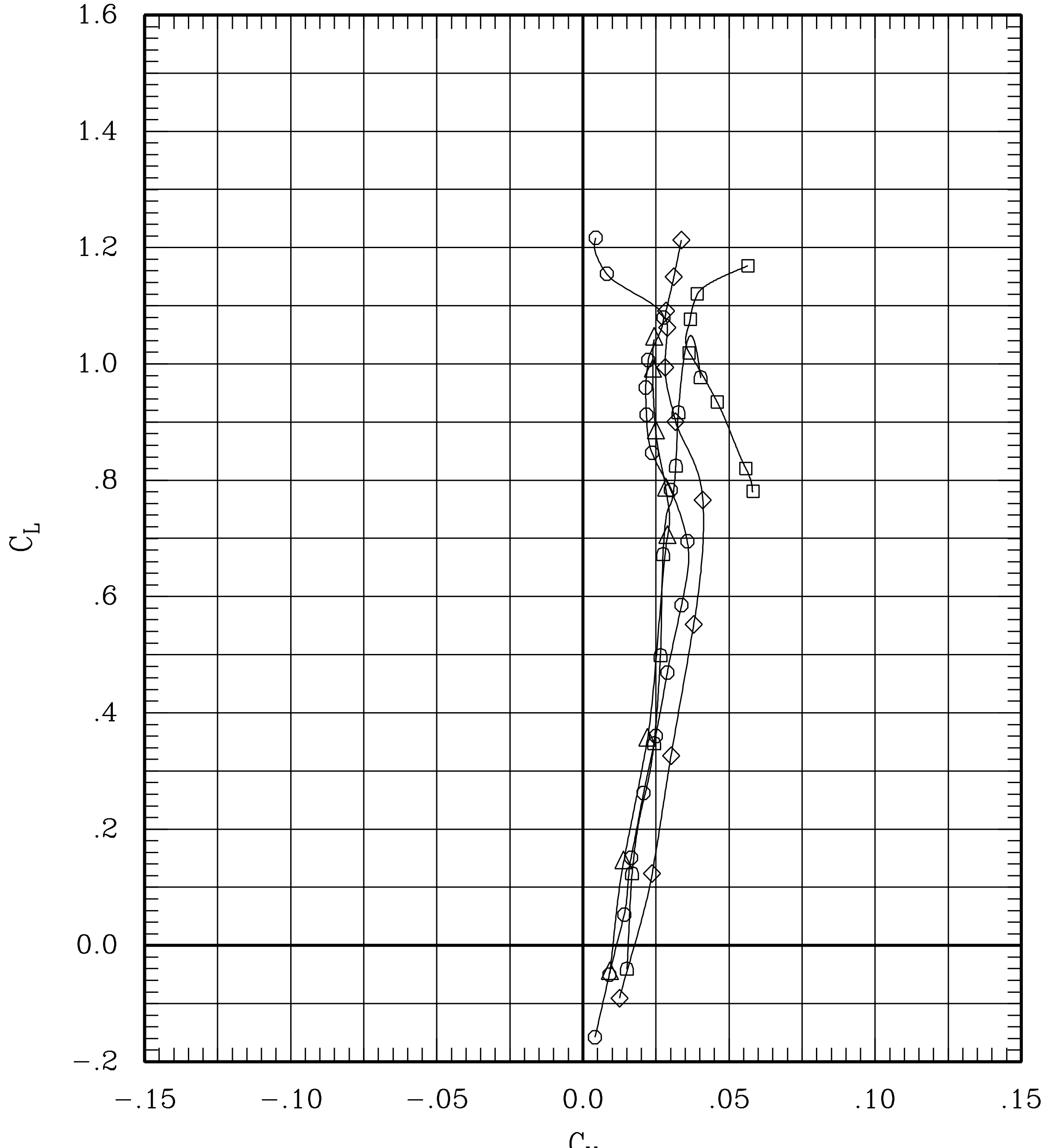

Figure 26(e). Effect of aileron deflection for sweep = 30 deg, Mach = 0.80 (Test #100).

SYMBOL	LT LA LO LI ^ RI RO RA RT	RUN	SWEEP	MACH	Q	BETA
—□—	00 30 00 00 L 00 00-30 00	60	30	.80	498	0.0
—◇—	00 10 00 00 L 00 00-10 00	219	30	.80	701	-.1
—○—	00 00 00 00 L 00 00 00 00	233	30	.80	698	-.1
—△—	00-10 00 00 L 00 00 10 00	203	30	.80	702	-.1
—⌂—	00-30 00 00 L 00 00 30 00	61	30	.80	504	-.1

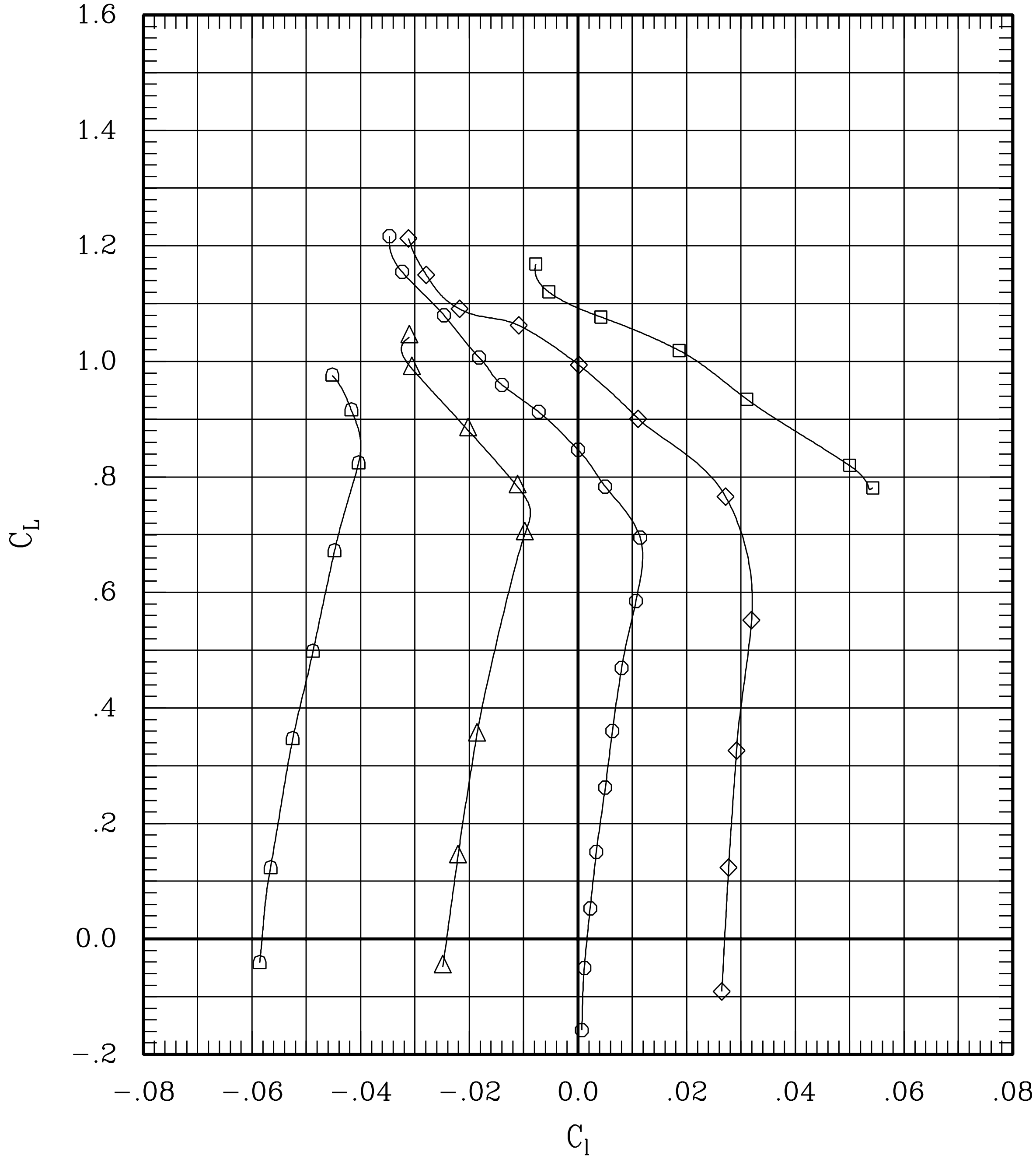

Figure 26(e). Effect of aileron deflection for sweep = 30 deg, Mach = 0.80 (Test #100).

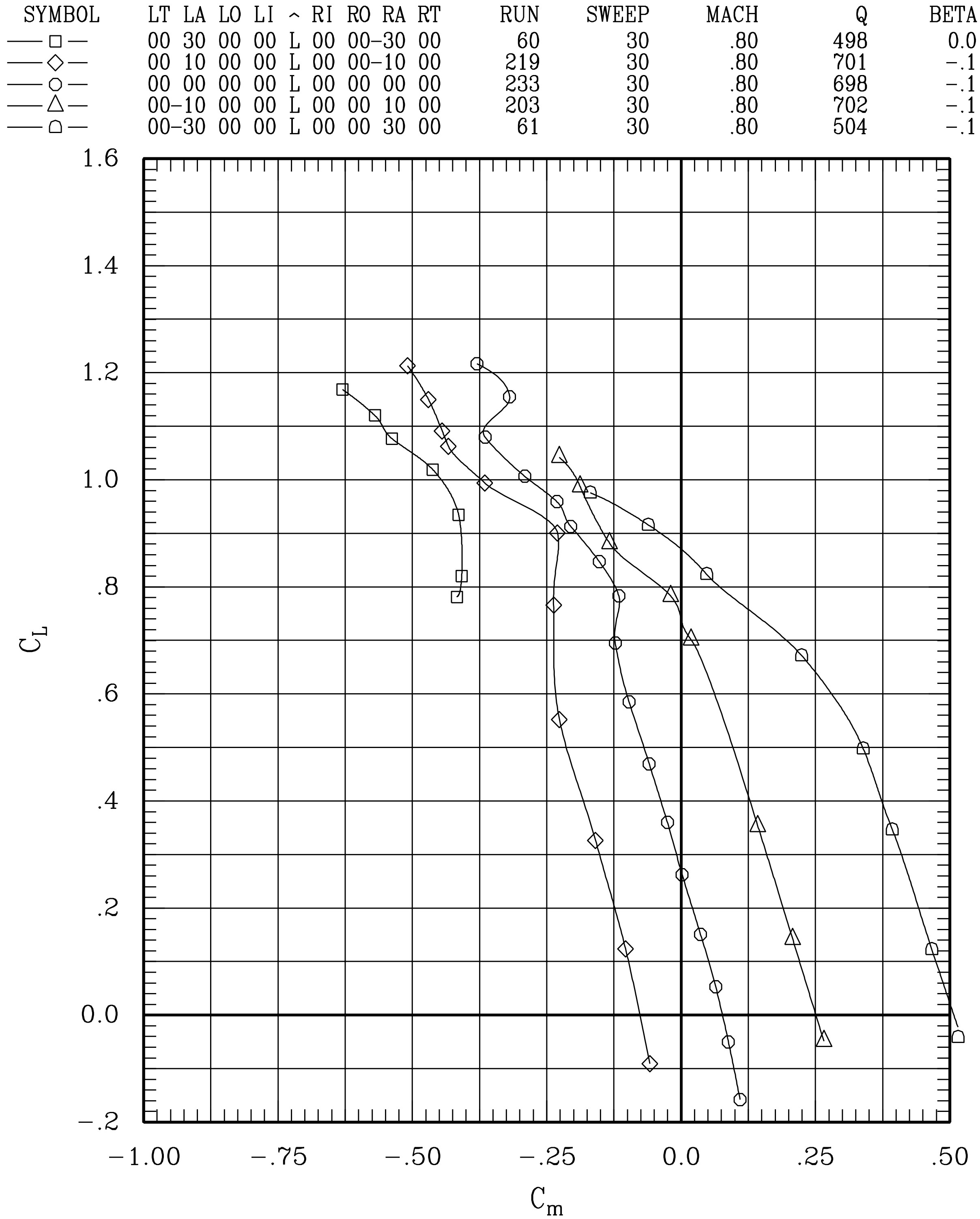

Figure 26(e). Effect of aileron deflection for sweep = 30 deg, Mach = 0.80 (Test #100).

SYMBOL	LT LA LO LI ^ RI RO RA RT	RUN	SWEEP	MACH	Q	BETA
—□—	00 30 00 00 L 00 00-30 00	60	30	.80	498	0.0
—◇—	00 10 00 00 L 00 00-10 00	219	30	.80	701	-.1
—○—	00 00 00 00 L 00 00 00 00	233	30	.80	698	-.1
—△—	00-10 00 00 L 00 00 10 00	203	30	.80	702	-.1
—⌂—	00-30 00 00 L 00 00 30 00	61	30	.80	504	-.1

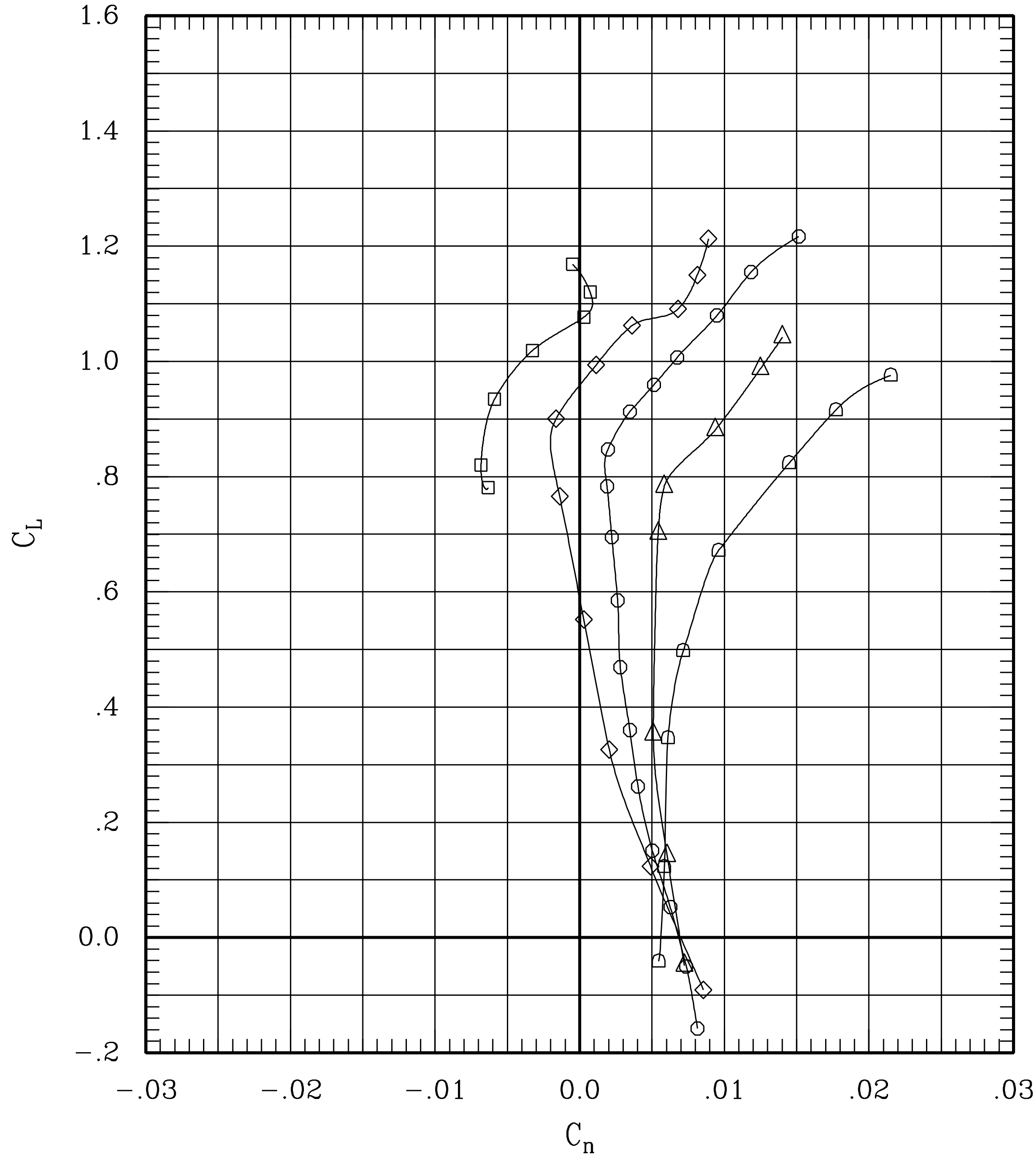

Figure 26(e). Effect of aileron deflection for sweep = 30 deg, Mach = 0.80 (Test #100).

SYMBOL	LT LA LO LI ^ RI RO RA RT	RUN	SWEEP	MACH	Q	BETA
—□—	00 30 00 00 L 00 00-30 00	221	45	.60	697	.1
—◇—	00 10 00 00 L 00 00-10 00	215	45	.60	696	-.1
—○—	00 00 00 00 L 00 00 00 00	21	45	.60	700	-.1
—△—	00-10 00 00 L 00 00 10 00	207	45	.60	691	-.1
—⌂—	00-30 00 00 L 00 00 30 00	224	45	.60	694	-.1

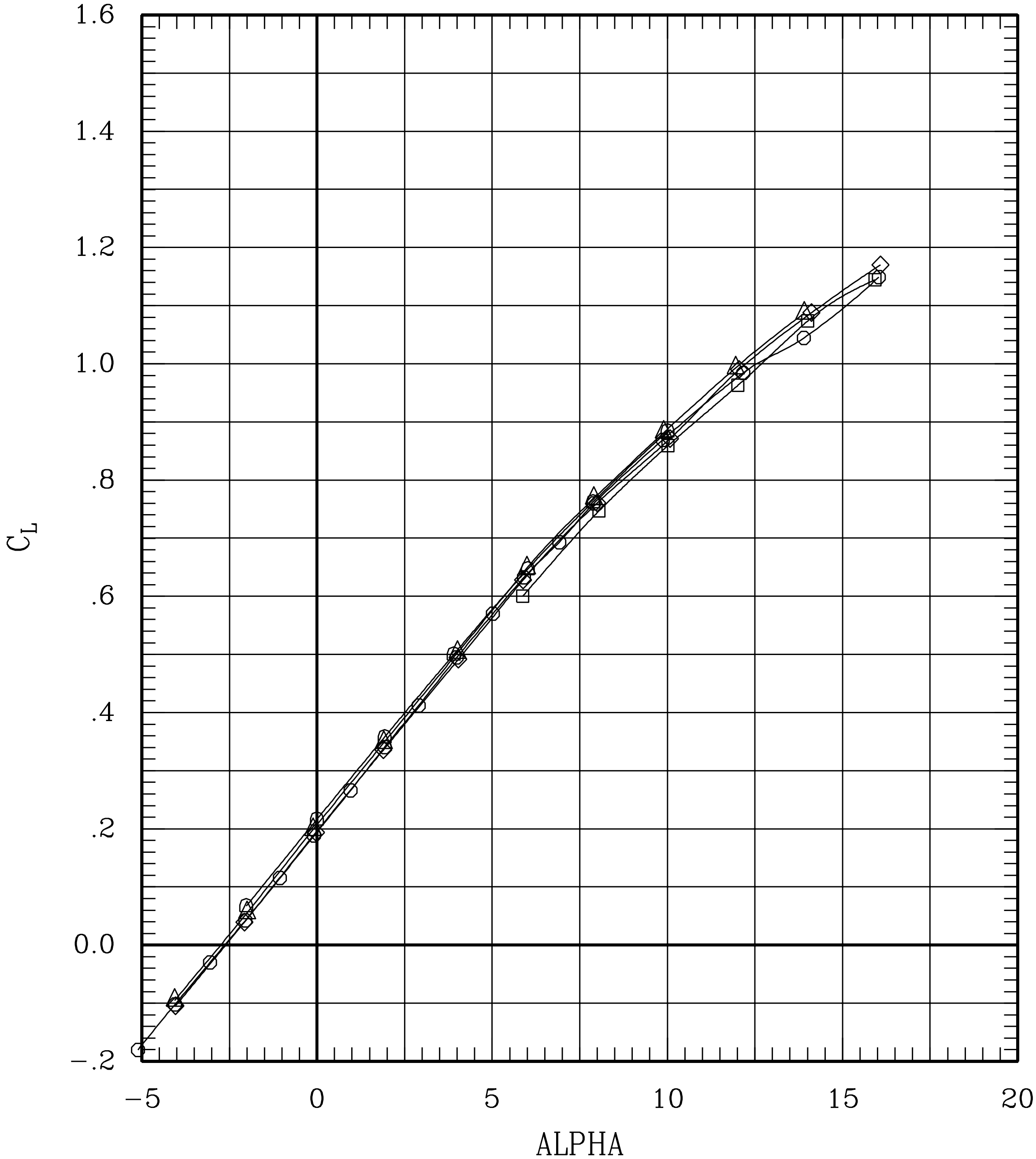

Figure 26(f). Effect of aileron deflection for sweep = 45 deg, Mach = 0.60 (Test #100).

SYMBOL	LT LA LO LI ^ RI RO RA RT	RUN	SWEEP	MACH	Q	BETA
—□—	00 30 00 00 L 00 00–30 00	221	45	.60	697	.1
—◇—	00 10 00 00 L 00 00–10 00	215	45	.60	696	–.1
—○—	00 00 00 00 L 00 00 00 00	21	45	.60	700	–.1
—△—	00–10 00 00 L 00 00 10 00	207	45	.60	691	–.1
—⌂—	00–30 00 00 L 00 00 30 00	224	45	.60	694	–.1

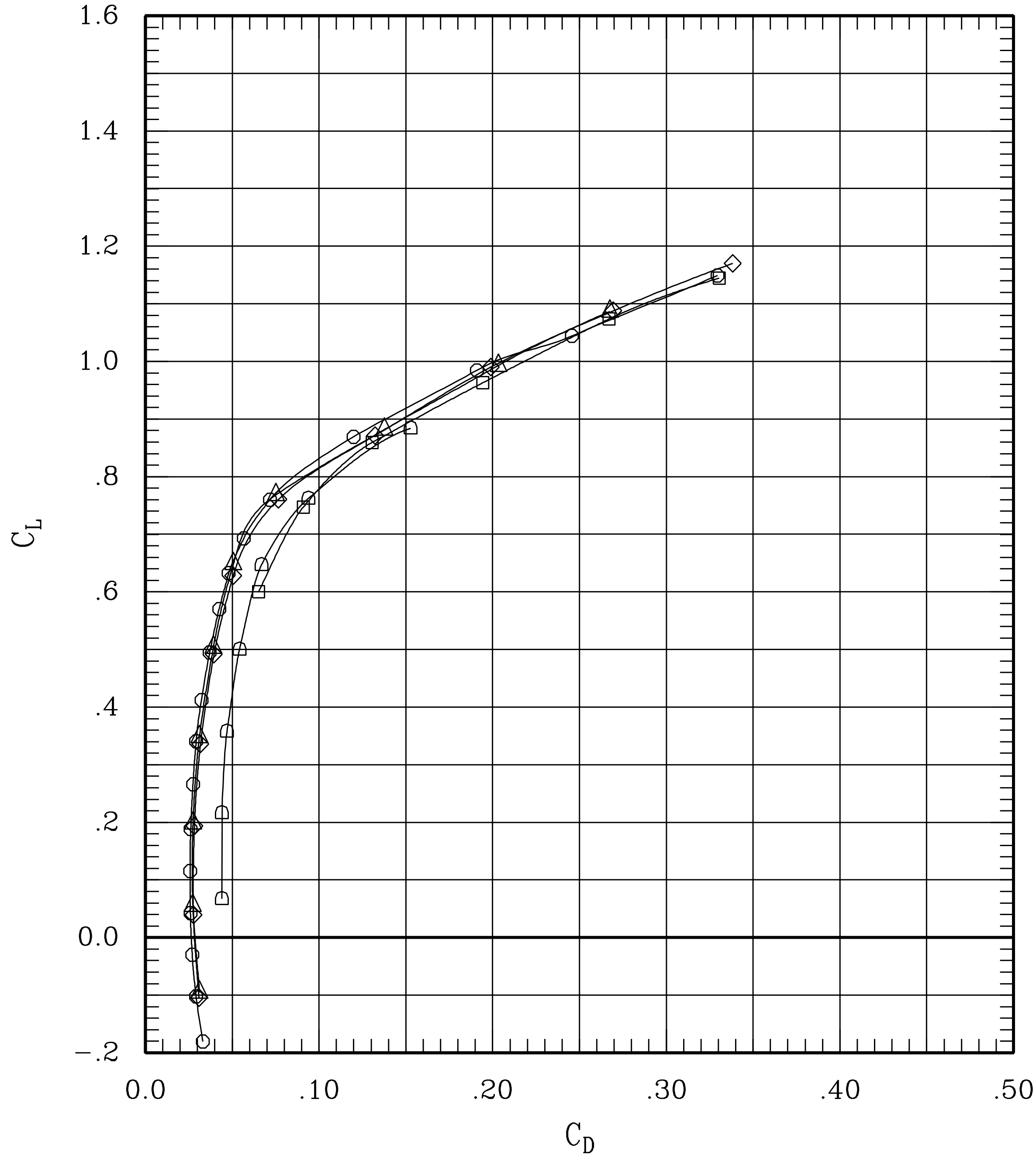

Figure 26(f). Effect of aileron deflection for sweep = 45 deg, Mach = 0.60 (Test #100).

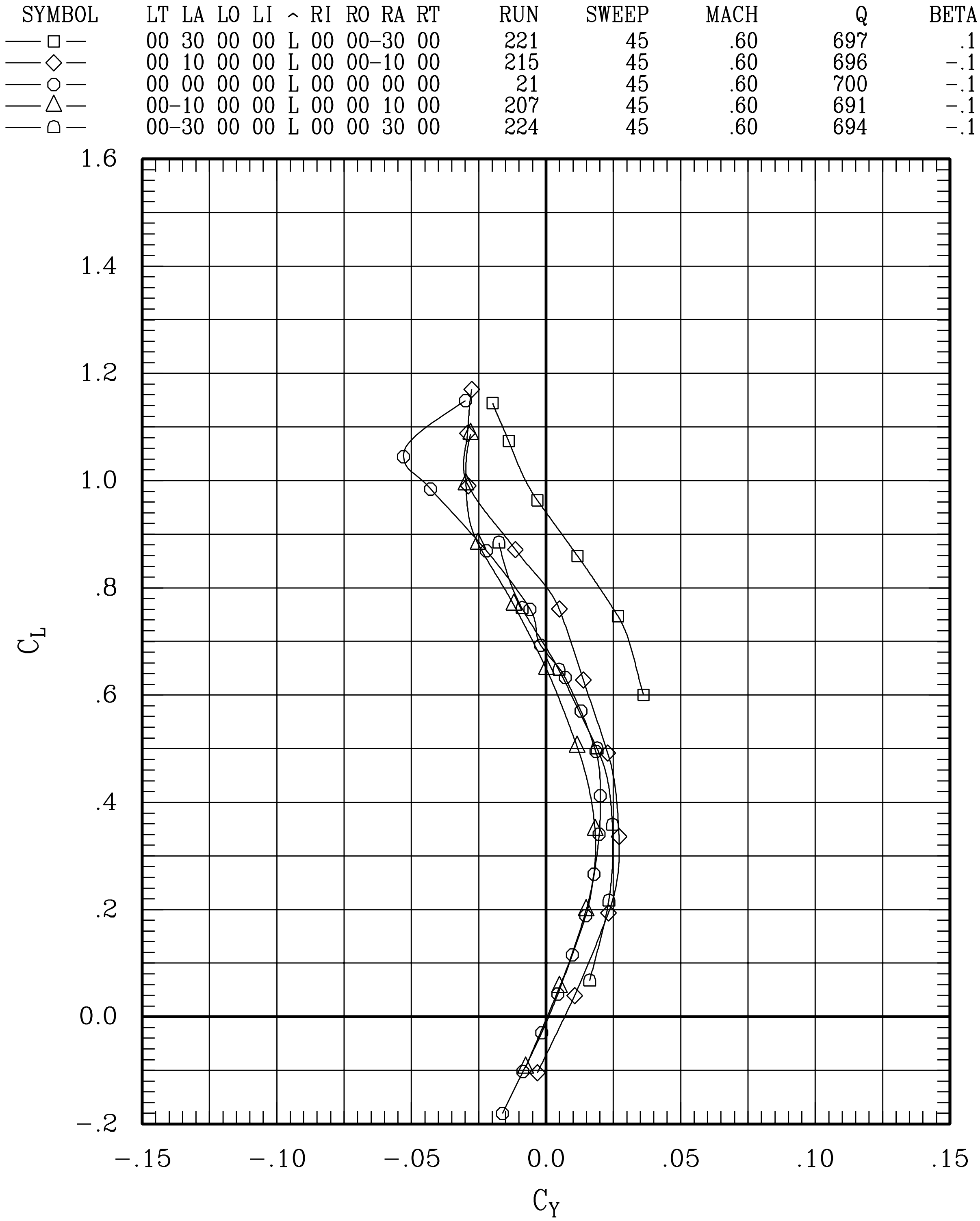

Figure 26(f). Effect of aileron deflection for sweep = 45 deg, Mach = 0.60 (Test #100).

SYMBOL	LT LA LO LI ^ RI RO RA RT	RUN	SWEEP	MACH	Q	BETA
—□—	00 30 00 00 L 00 00−30 00	221	45	.60	697	.1
—◇—	00 10 00 00 L 00 00−10 00	215	45	.60	696	−.1
—○—	00 00 00 00 L 00 00 00 00	21	45	.60	700	−.1
—△—	00−10 00 00 L 00 00 10 00	207	45	.60	691	−.1
—⌂—	00−30 00 00 L 00 00 30 00	224	45	.60	694	−.1

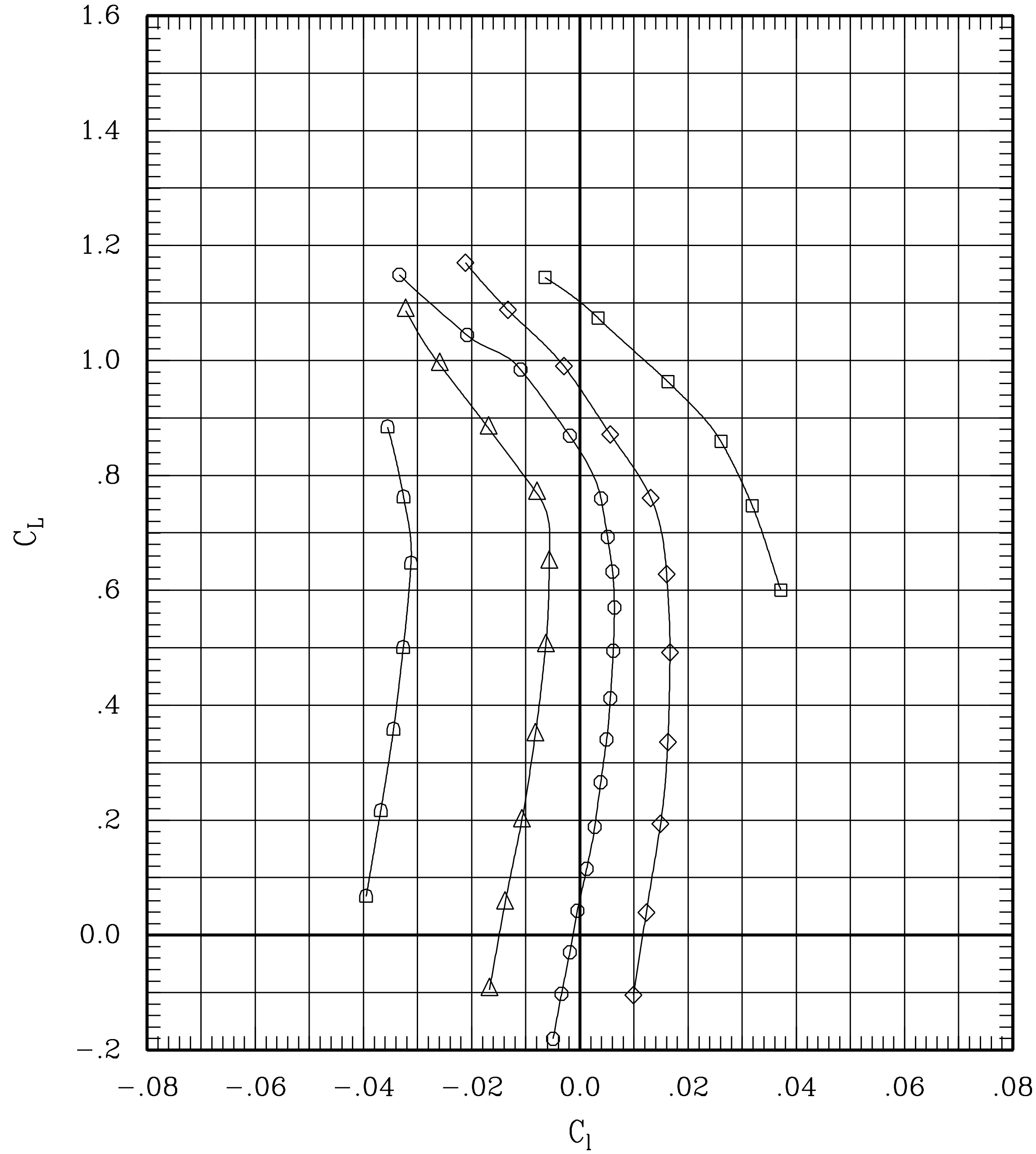

Figure 26(f). Effect of aileron deflection for sweep = 45 deg, Mach = 0.60 (Test #100).

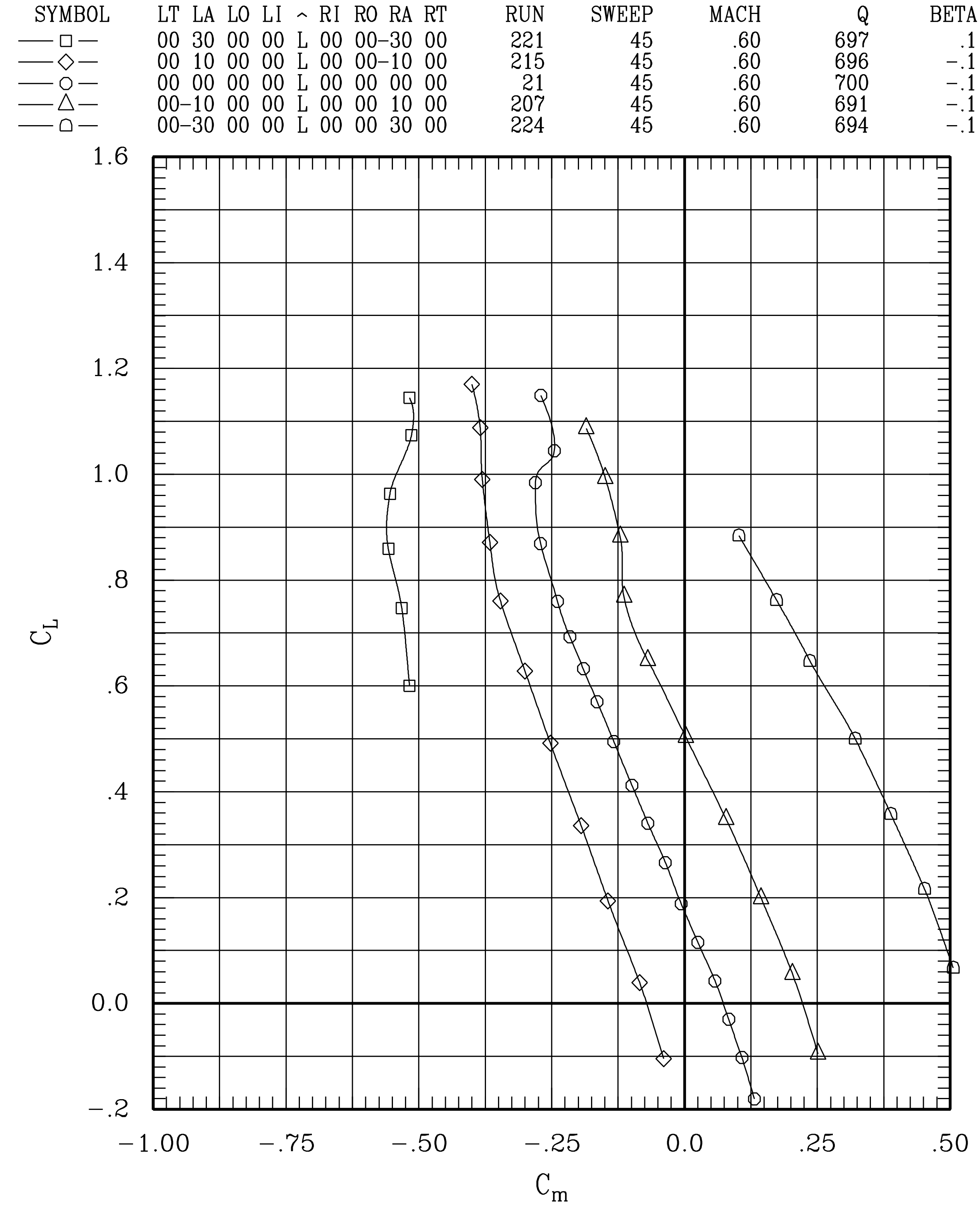

Figure 26(f). Effect of aileron deflection for sweep = 45 deg, Mach = 0.60 (Test #100).

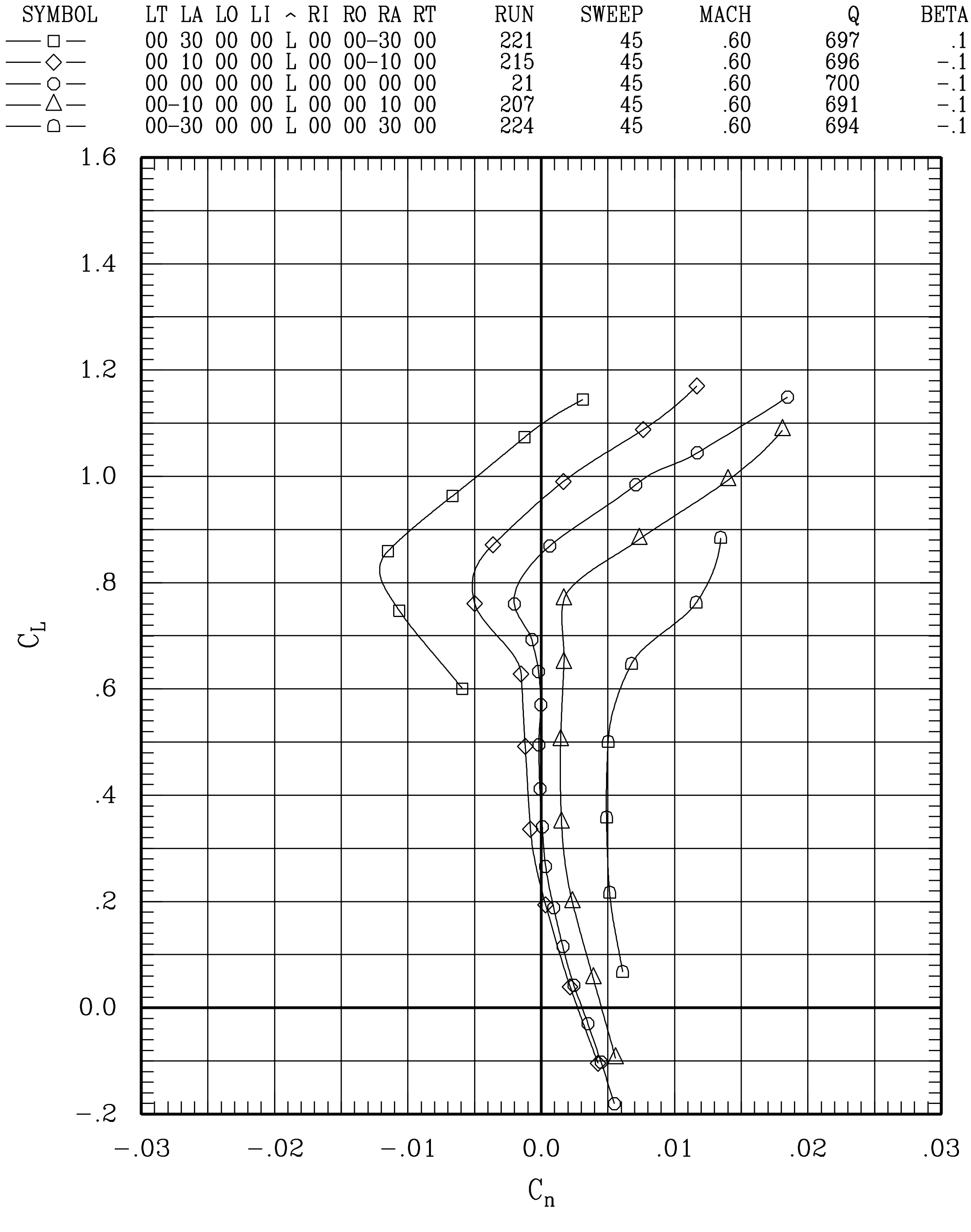

Figure 26(f). Effect of aileron deflection for sweep = 45 deg, Mach = 0.60 (Test #100).

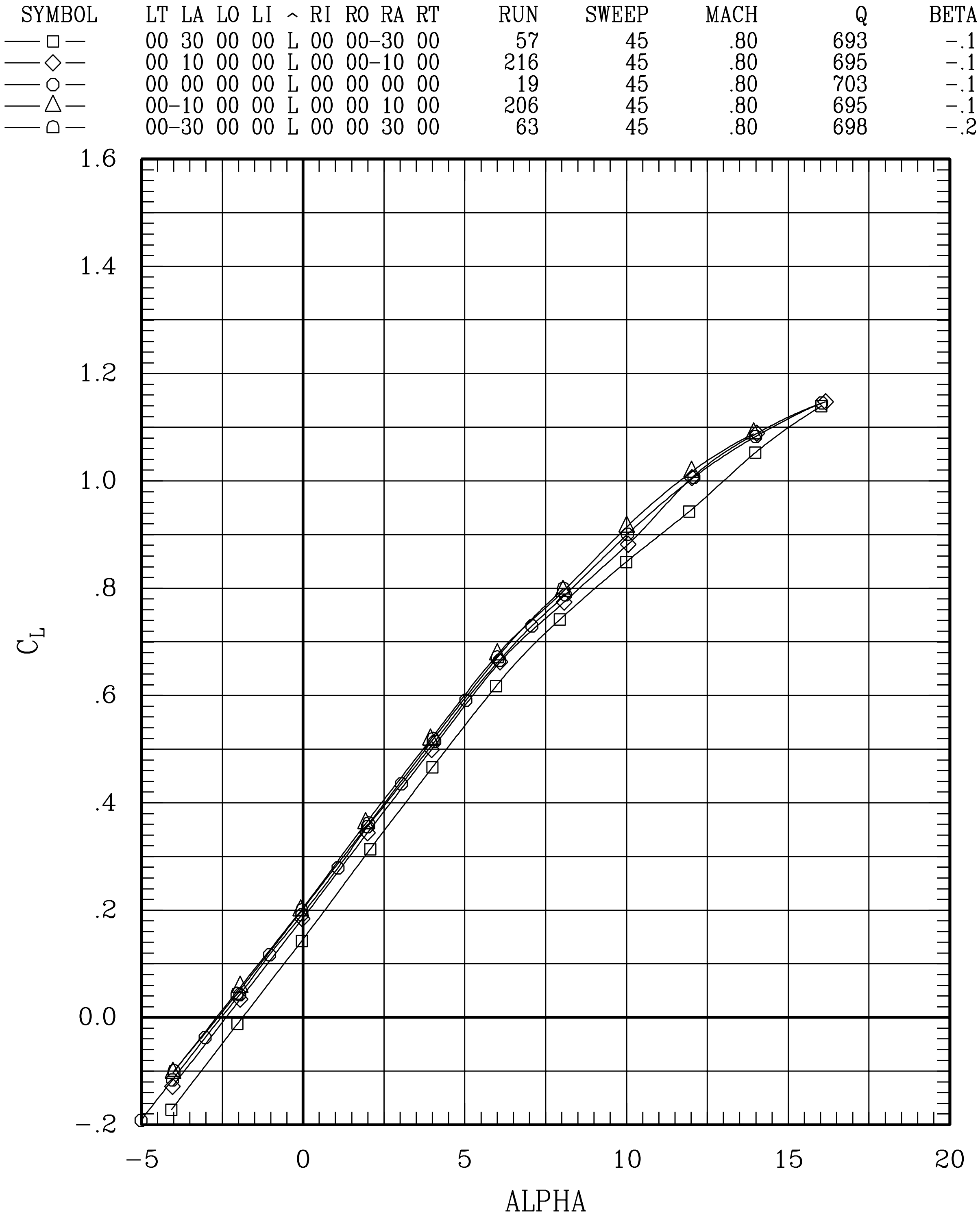

Figure 26(g). Effect of aileron deflection for sweep = 45 deg, Mach = 0.80 (Test #100).

SYMBOL	LT LA LO LI ^ RI RO RA RT	RUN	SWEEP	MACH	Q	BETA
—□—	00 30 00 00 L 00 00-30 00	57	45	.80	693	-.1
—◇—	00 10 00 00 L 00 00-10 00	216	45	.80	695	-.1
—○—	00 00 00 00 L 00 00 00 00	19	45	.80	703	-.1
—△—	00-10 00 00 L 00 00 10 00	206	45	.80	695	-.1
—⌂—	00-30 00 00 L 00 00 30 00	63	45	.80	698	-.2

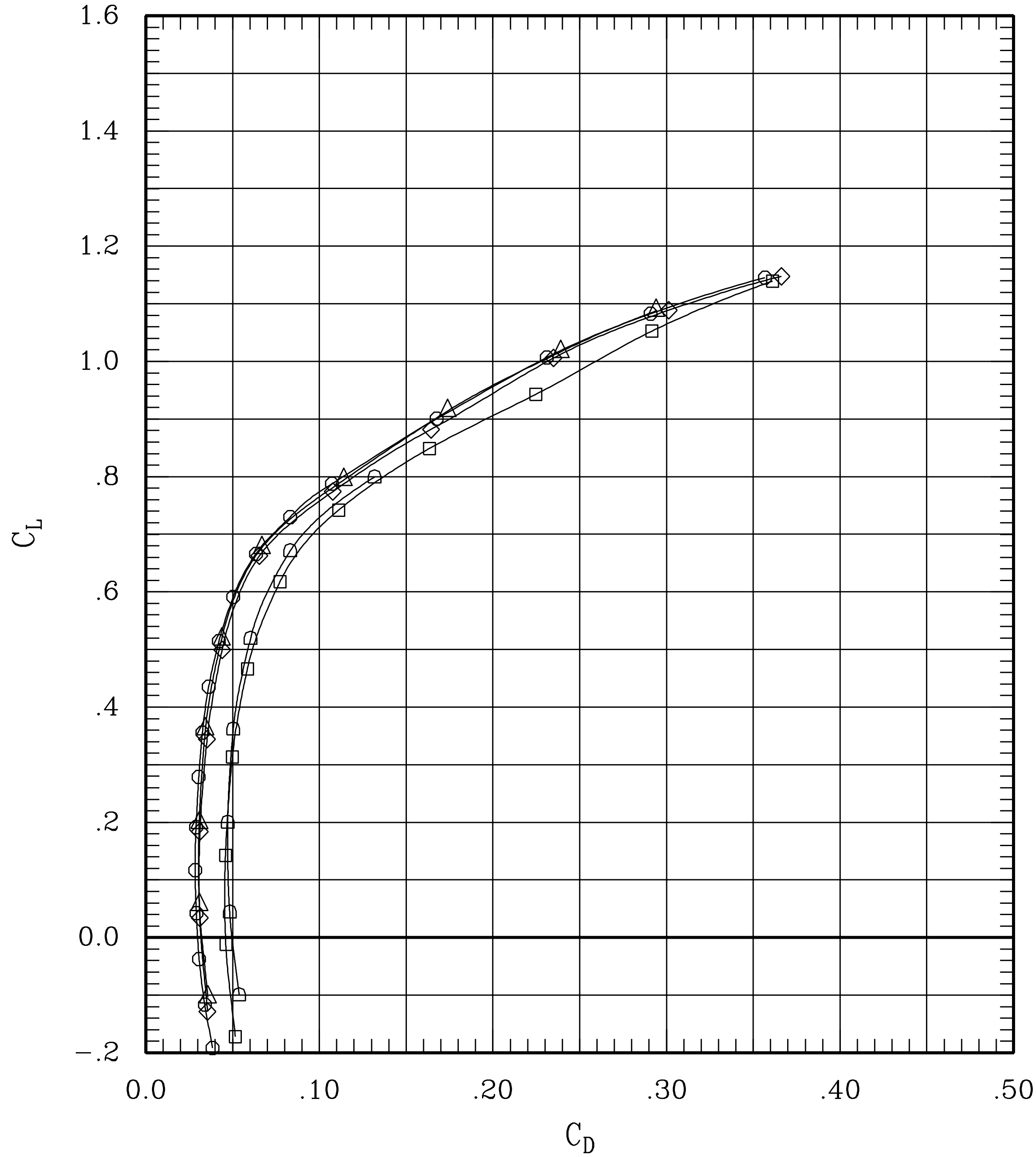

Figure 26(g). Effect of aileron deflection for sweep = 45 deg, Mach = 0.80 (Test #100).

SYMBOL	LT LA LO LI ^ RI RO RA RT	RUN	SWEEP	MACH	Q	BETA
—□—	00 30 00 00 L 00 00−30 00	57	45	.80	693	−.1
—◇—	00 10 00 00 L 00 00−10 00	216	45	.80	695	−.1
—○—	00 00 00 00 L 00 00 00 00	19	45	.80	703	−.1
—△—	00−10 00 00 L 00 00 10 00	206	45	.80	695	−.1
—⌓—	00−30 00 00 L 00 00 30 00	63	45	.80	698	−.2

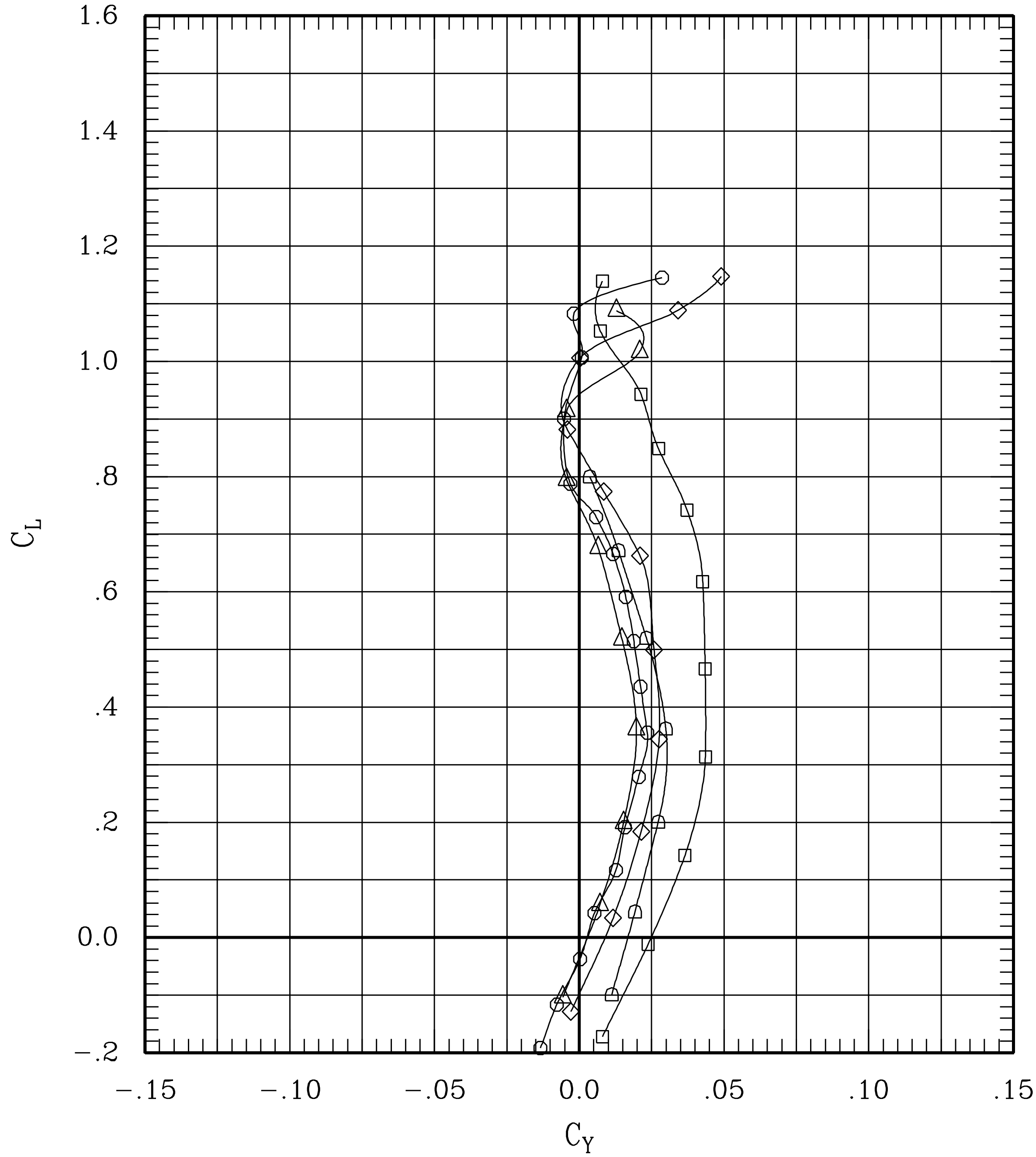

Figure 26(g). Effect of aileron deflection for sweep = 45 deg, Mach = 0.80 (Test #100).

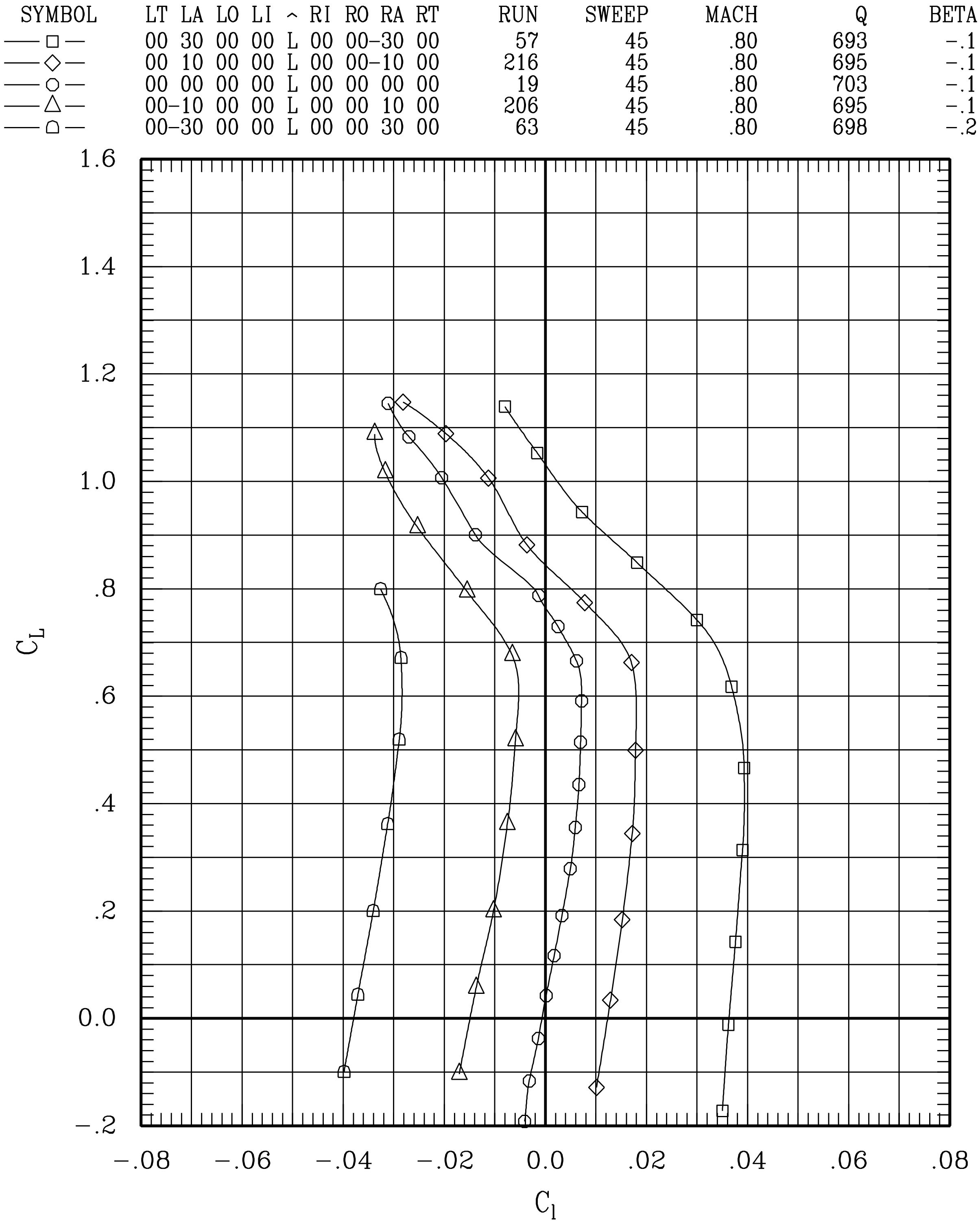

Figure 26(g). Effect of aileron deflection for sweep = 45 deg, Mach = 0.80 (Test #100).

SYMBOL	LT LA LO LI ^ RI RO RA RT	RUN	SWEEP	MACH	Q	BETA
—□—	00 30 00 00 L 00 00−30 00	57	45	.80	693	−.1
—◇—	00 10 00 00 L 00 00−10 00	216	45	.80	695	−.1
—○—	00 00 00 00 L 00 00 00 00	19	45	.80	703	−.1
—△—	00−10 00 00 L 00 00 10 00	206	45	.80	695	−.1
—⌂—	00−30 00 00 L 00 00 30 00	63	45	.80	698	−.2

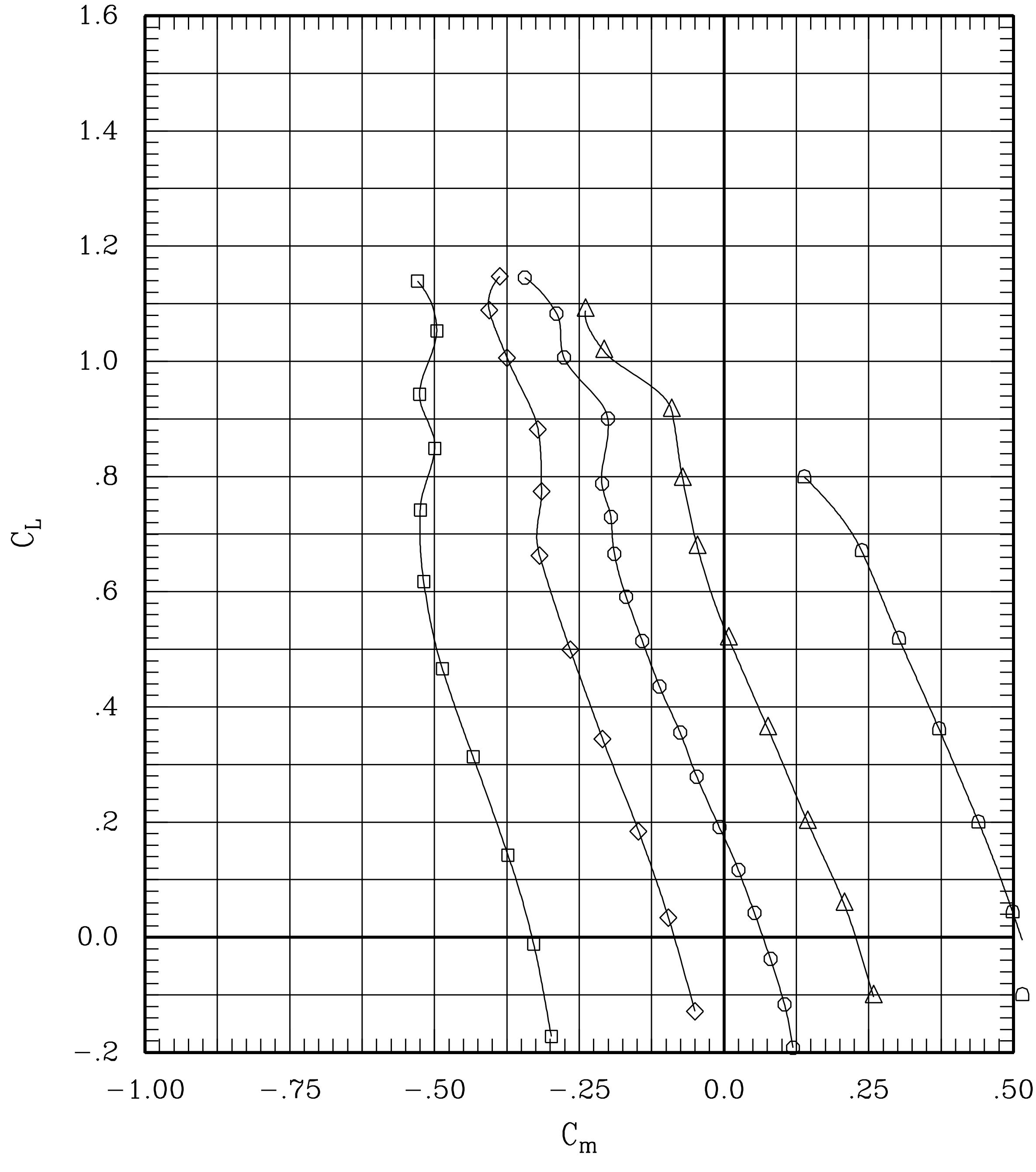

Figure 26(g). Effect of aileron deflection for sweep = 45 deg, Mach = 0.80 (Test #100).

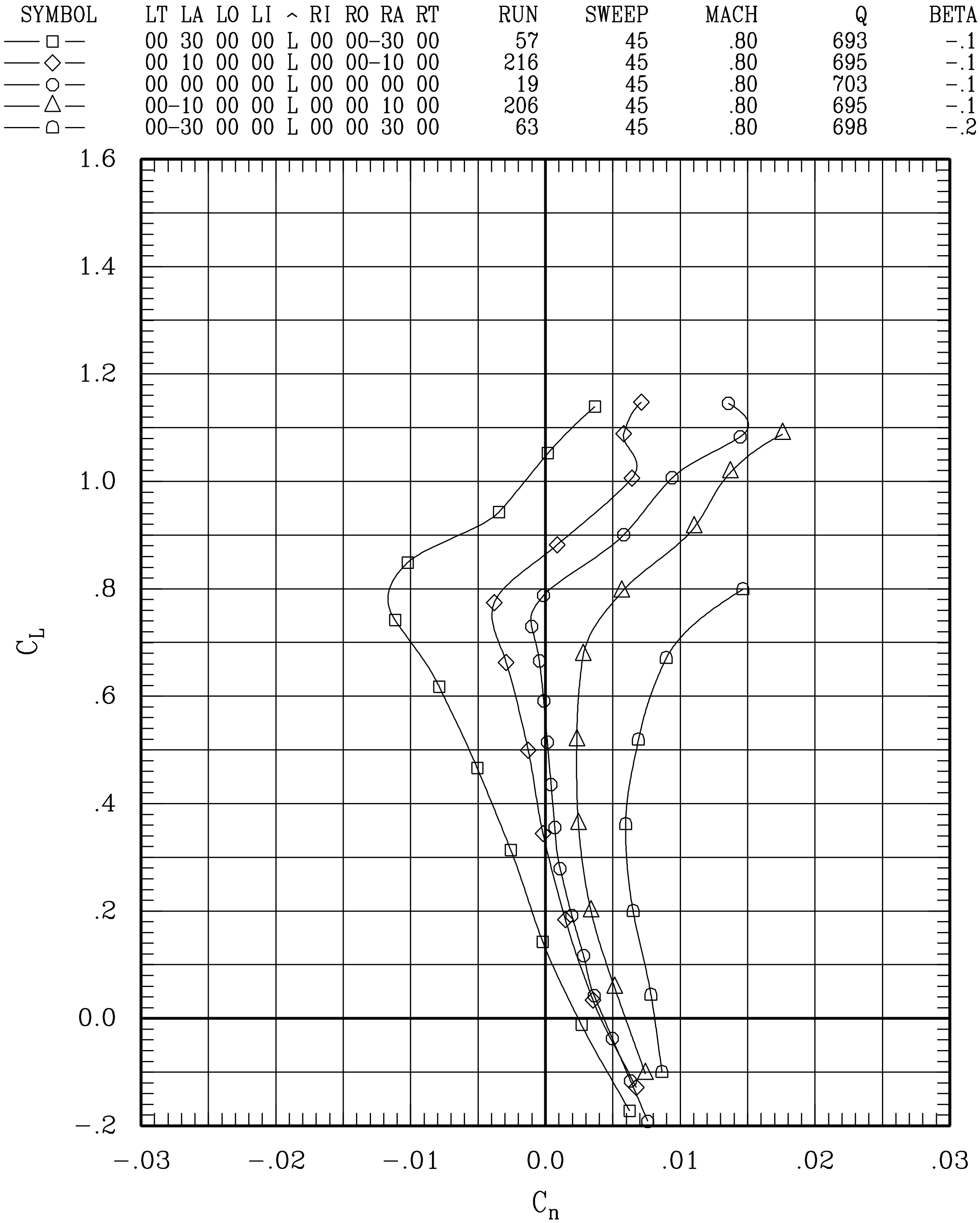

Figure 26(g). Effect of aileron deflection for sweep = 45 deg, Mach = 0.80 (Test #100).

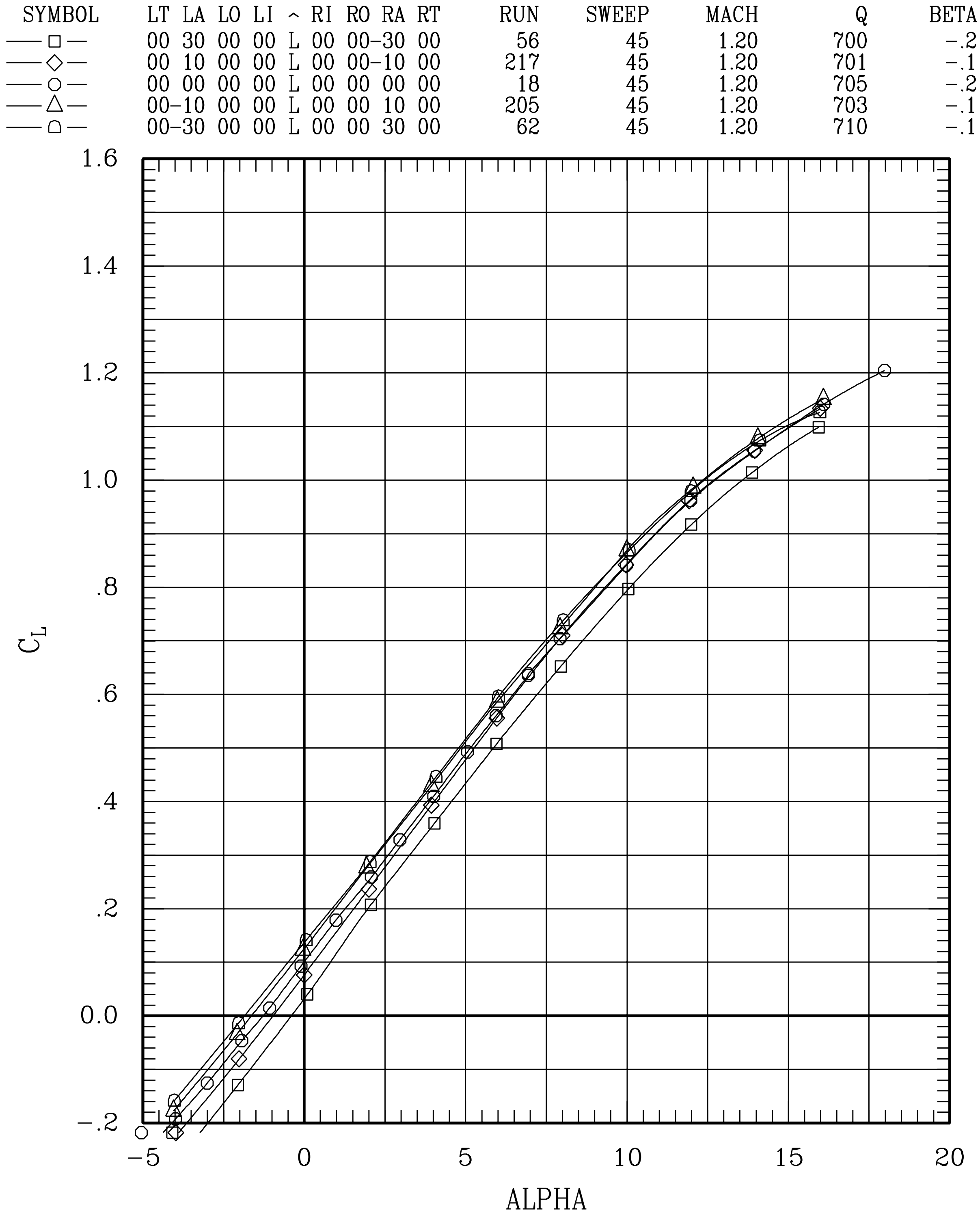

Figure 26(h). Effect of aileron deflection for sweep = 45 deg, Mach = 1.20 (Test #100).

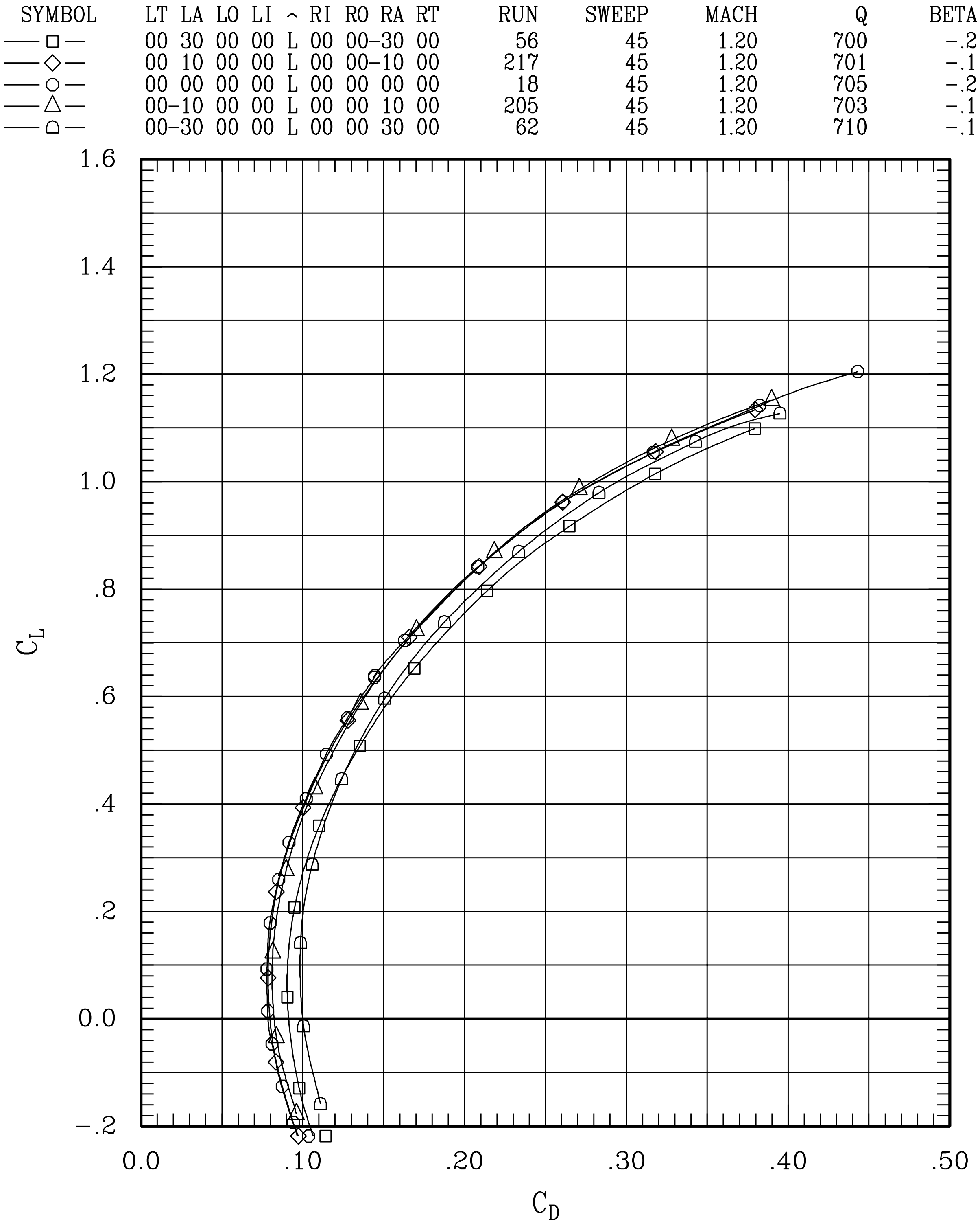

Figure 26(h). Effect of aileron deflection for sweep = 45 deg, Mach = 1.20 (Test #100).

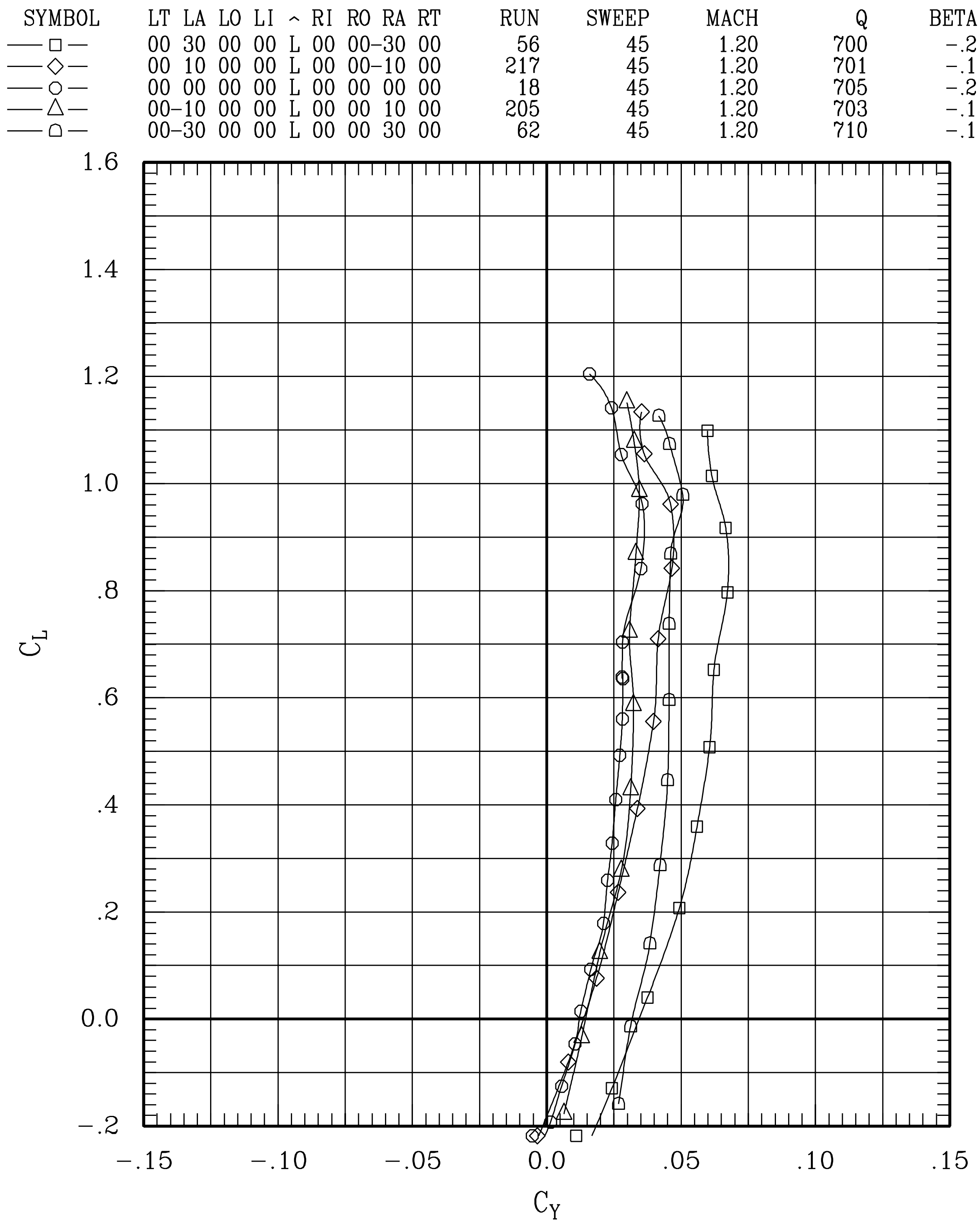

Figure 26(h). Effect of aileron deflection for sweep = 45 deg, Mach = 1.20 (Test #100).

SYMBOL	LT LA LO LI ^ RI RO RA RT	RUN	SWEEP	MACH	Q	BETA
—□—	00 30 00 00 L 00 00–30 00	56	45	1.20	700	−.2
—◇—	00 10 00 00 L 00 00–10 00	217	45	1.20	701	−.1
—○—	00 00 00 00 L 00 00 00 00	18	45	1.20	705	−.2
—△—	00–10 00 00 L 00 00 10 00	205	45	1.20	703	−.1
—⌂—	00–30 00 00 L 00 00 30 00	62	45	1.20	710	−.1

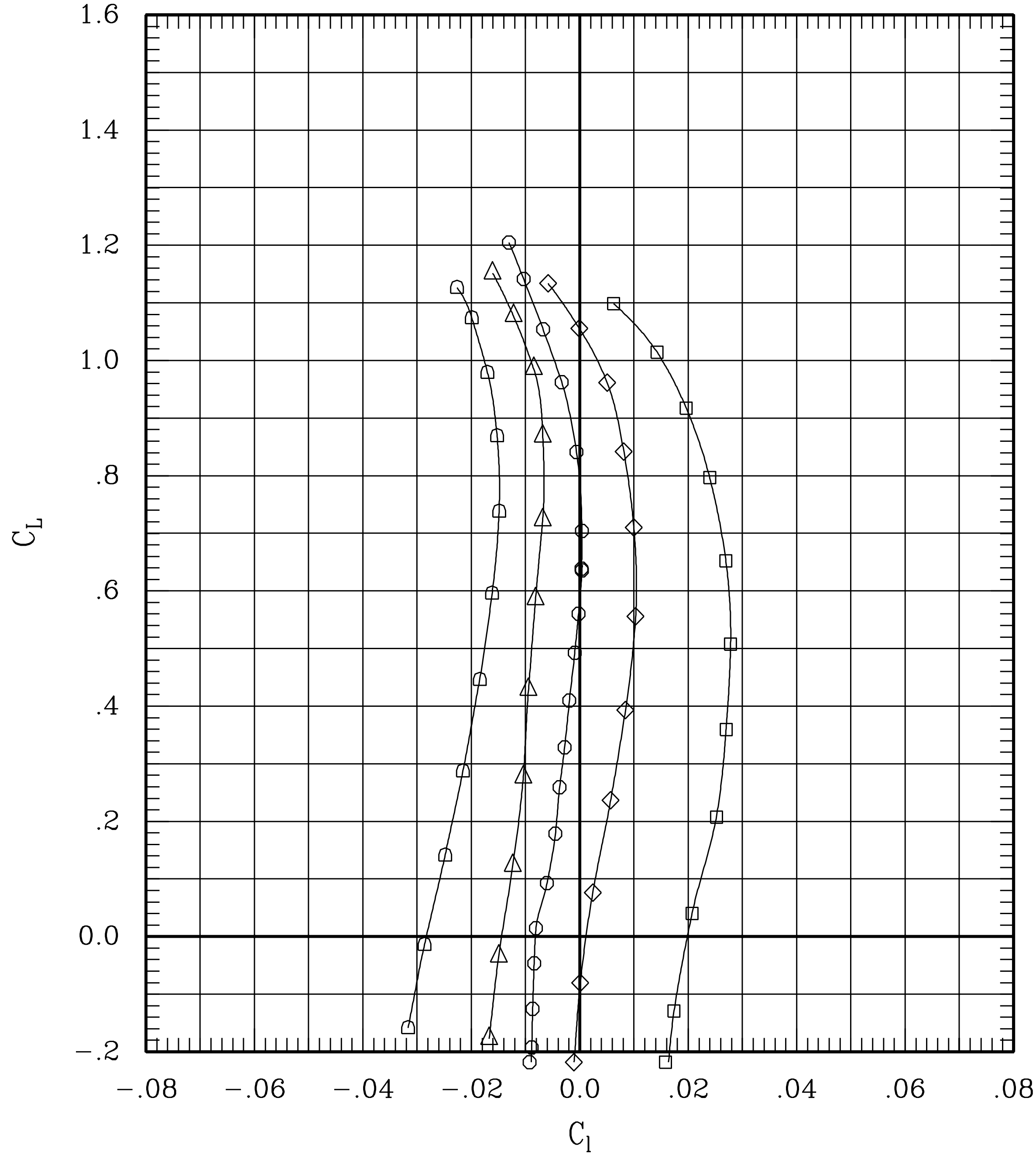

Figure 26(h). Effect of aileron deflection for sweep = 45 deg, Mach = 1.20 (Test #100).

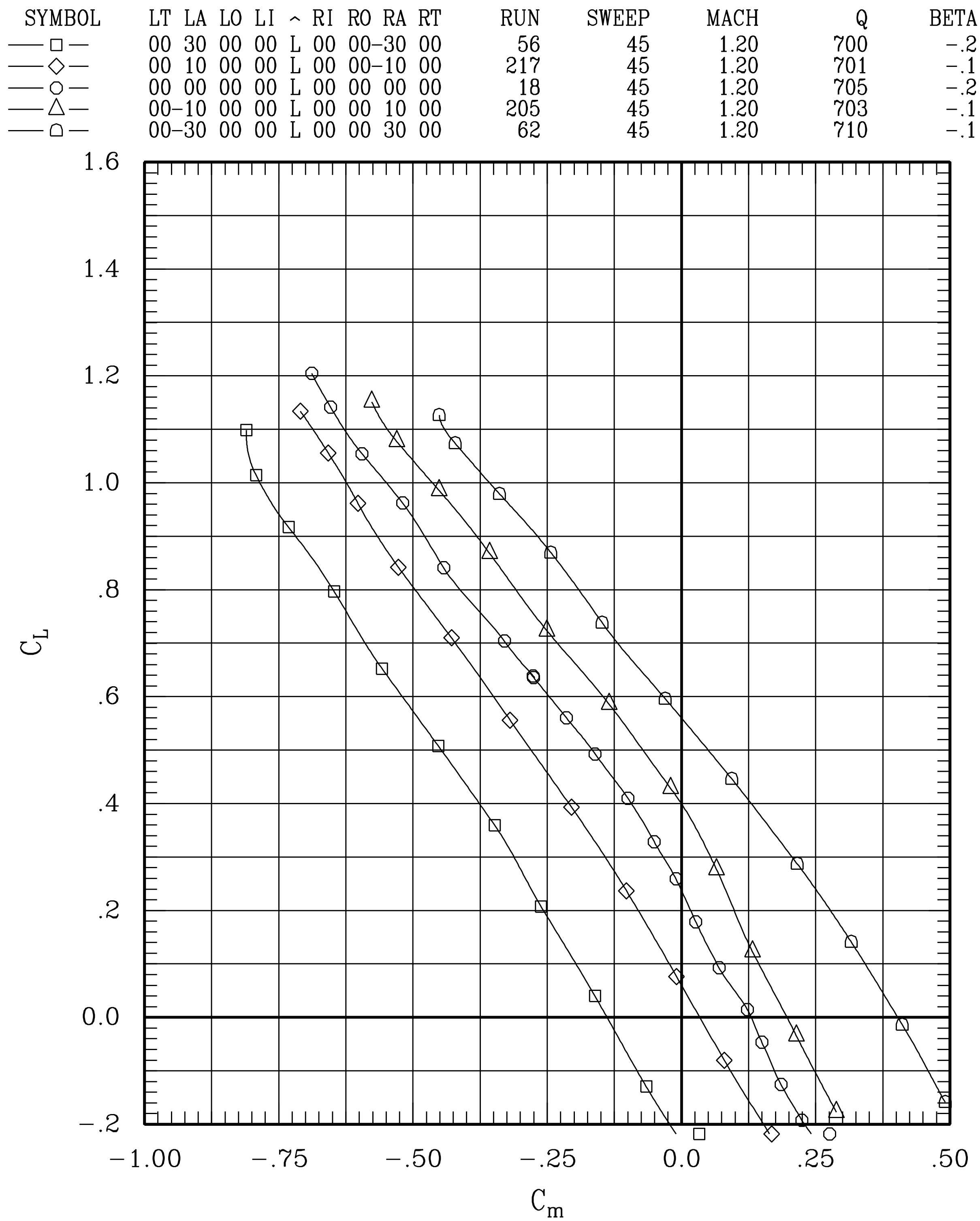

Figure 26(h). Effect of aileron deflection for sweep = 45 deg, Mach = 1.20 (Test #100).

SYMBOL	LT LA LO LI ^ RI RO RA RT	RUN	SWEEP	MACH	Q	BETA
—□—	00 30 00 00 L 00 00-30 00	56	45	1.20	700	-.2
—◇—	00 10 00 00 L 00 00-10 00	217	45	1.20	701	-.1
—○—	00 00 00 00 L 00 00 00 00	18	45	1.20	705	-.2
—△—	00-10 00 00 L 00 00 10 00	205	45	1.20	703	-.1
—⌂—	00-30 00 00 L 00 00 30 00	62	45	1.20	710	-.1

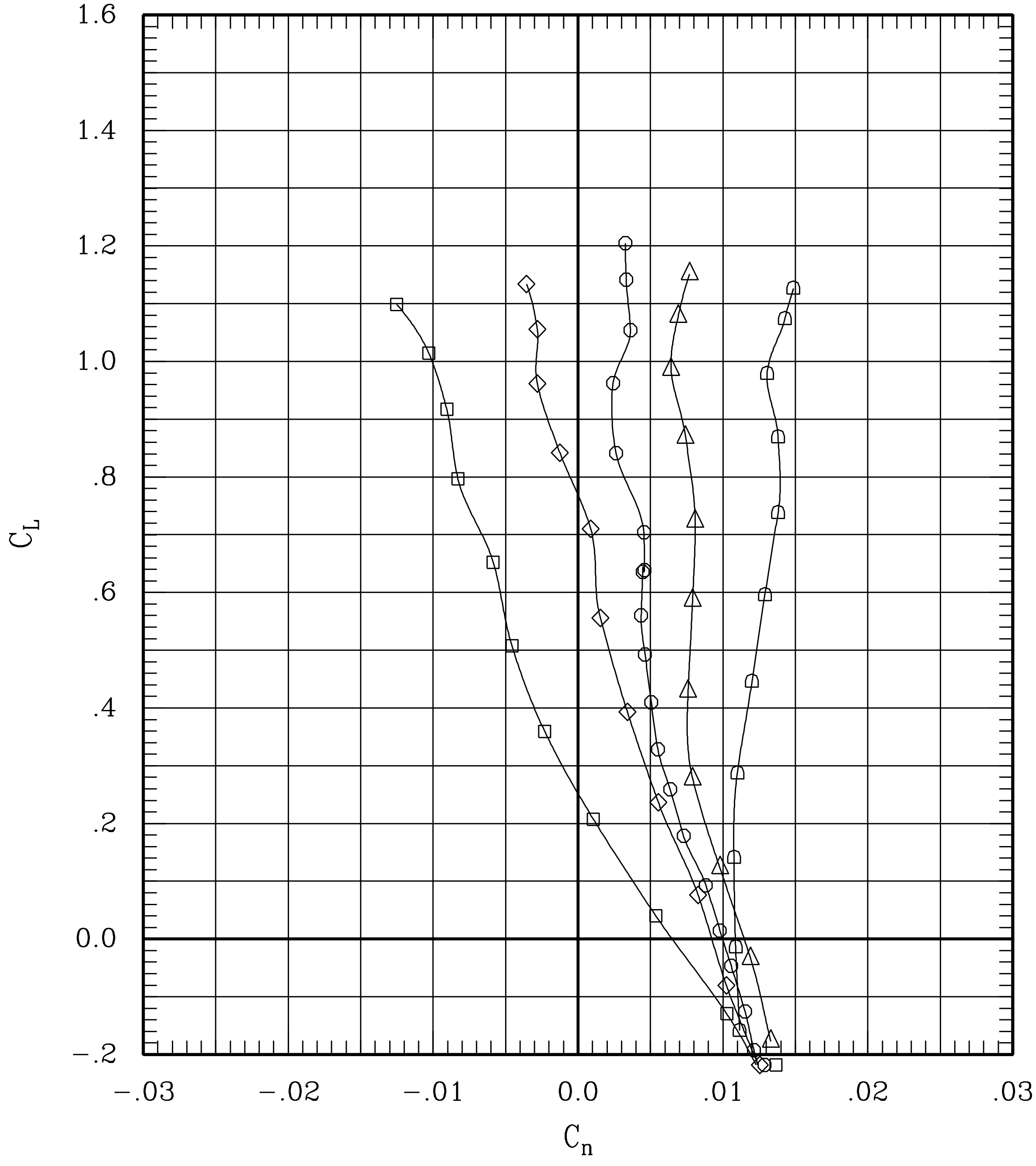

Figure 26(h). Effect of aileron deflection for sweep = 45 deg, Mach = 1.20 (Test #100).

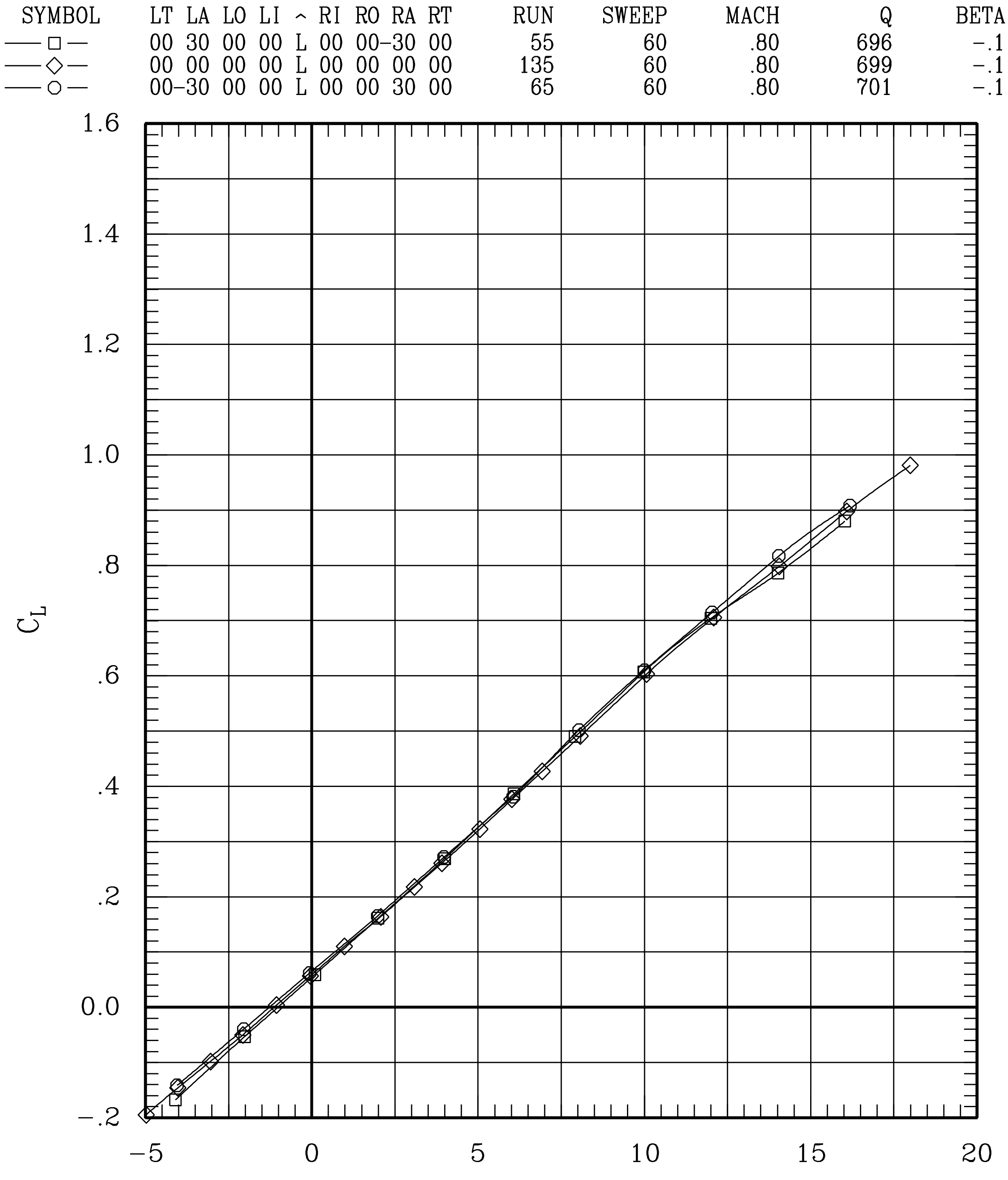

Figure 26(i). Effect of aileron deflection for sweep = 60 deg, Mach = 0.80 (Test #100).

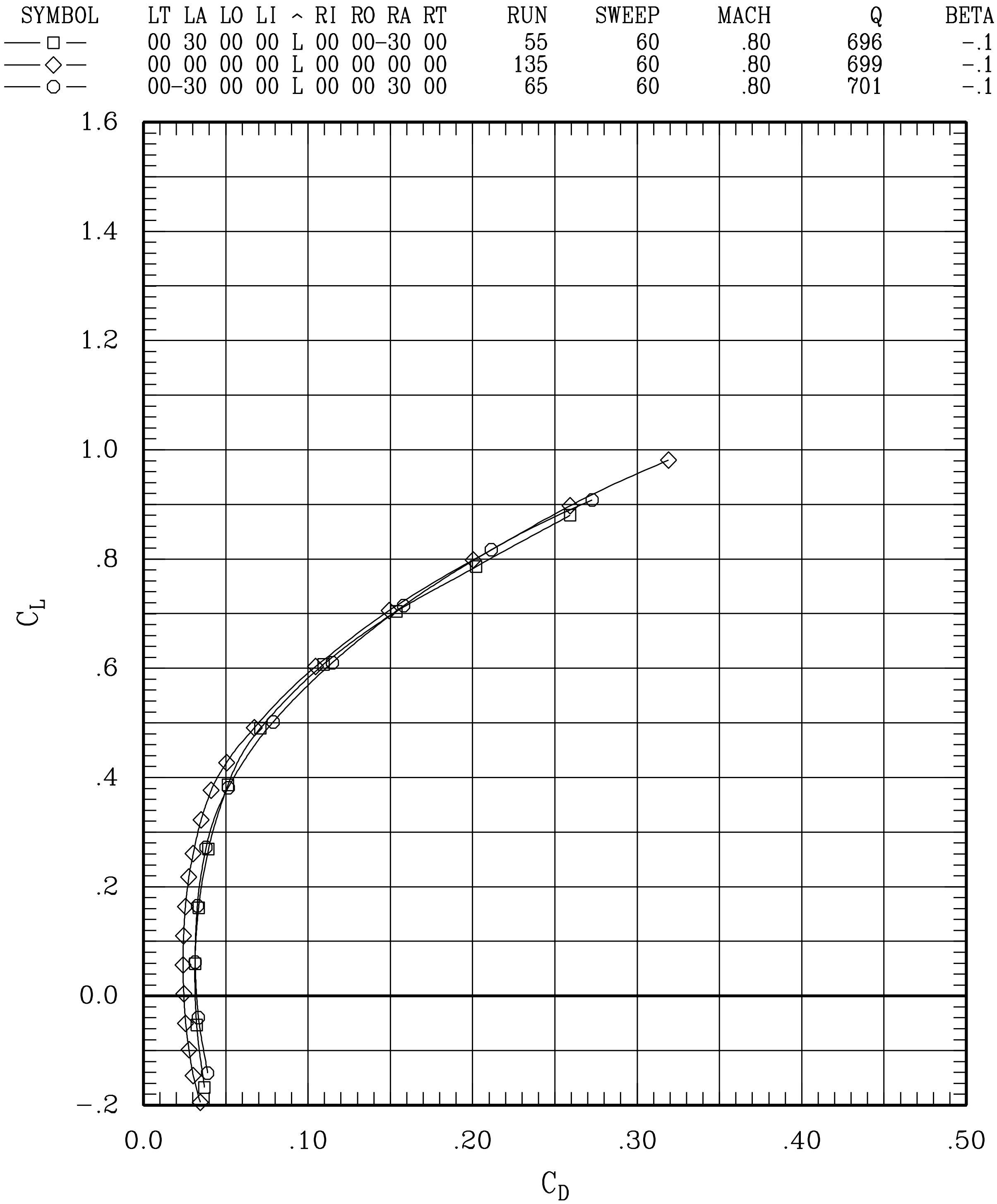

Figure 26(i). Effect of aileron deflection for sweep = 60 deg, Mach = 0.80 (Test #100).

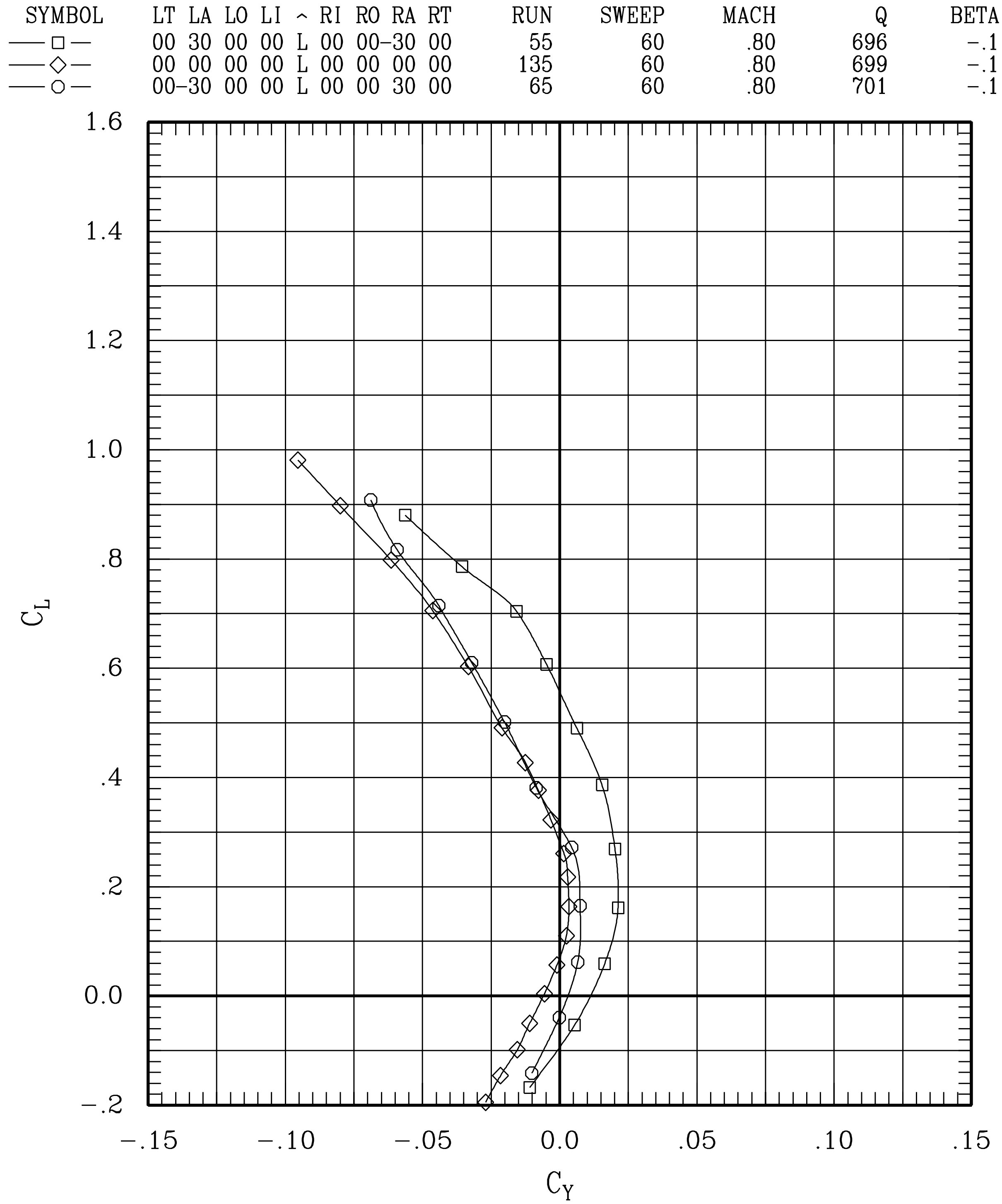

Figure 26(i). Effect of aileron deflection for sweep = 60 deg, Mach = 0.80 (Test #100).

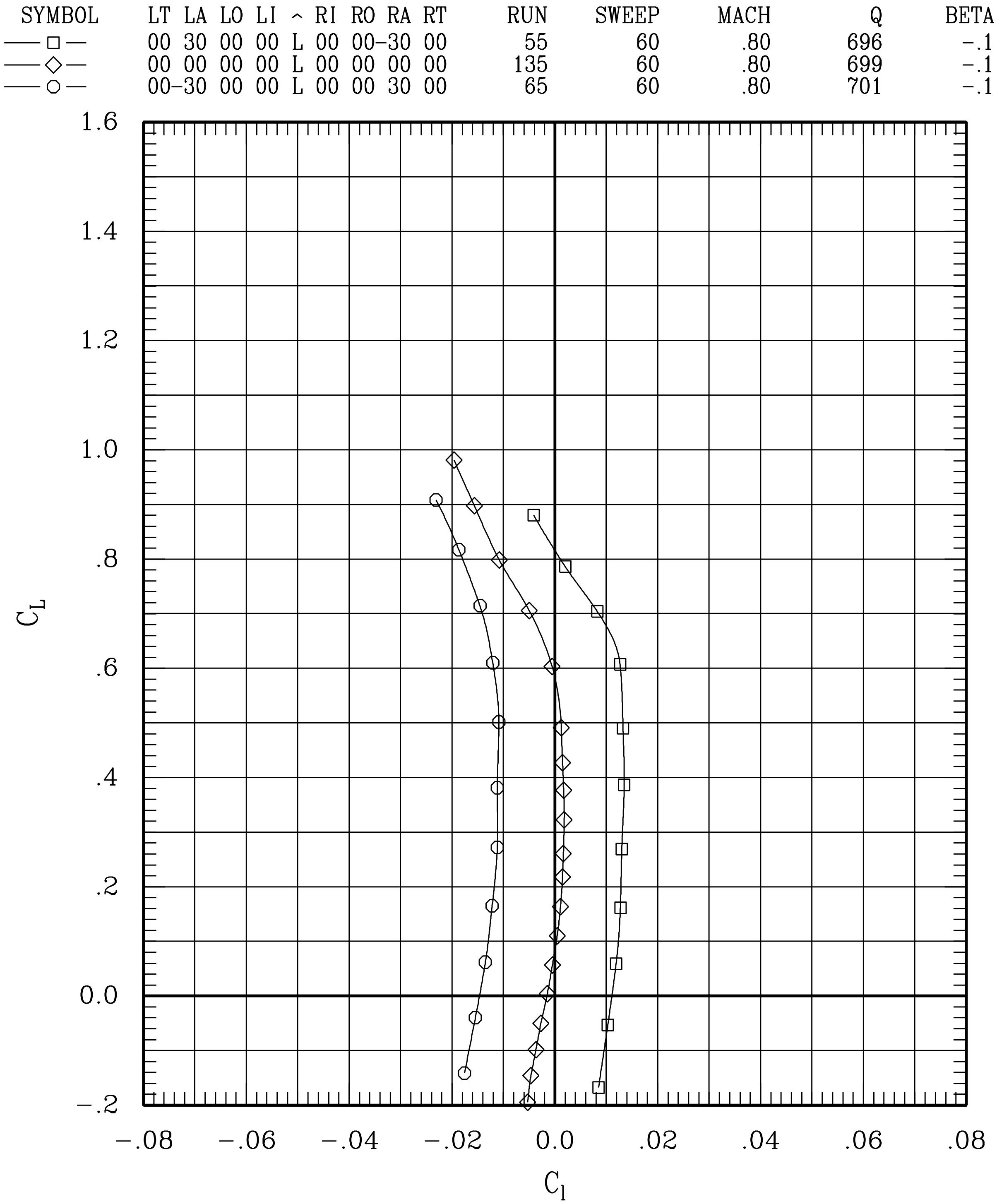

Figure 26(i). Effect of aileron deflection for sweep = 60 deg, Mach = 0.80 (Test #100).

SYMBOL	LT LA LO LI ^ RI RO RA RT	RUN	SWEEP	MACH	Q	BETA
—□—	00 30 00 00 L 00 00-30 00	55	60	.80	696	-.1
—◇—	00 00 00 00 L 00 00 00 00	135	60	.80	699	-.1
—○—	00-30 00 00 L 00 00 30 00	65	60	.80	701	-.1

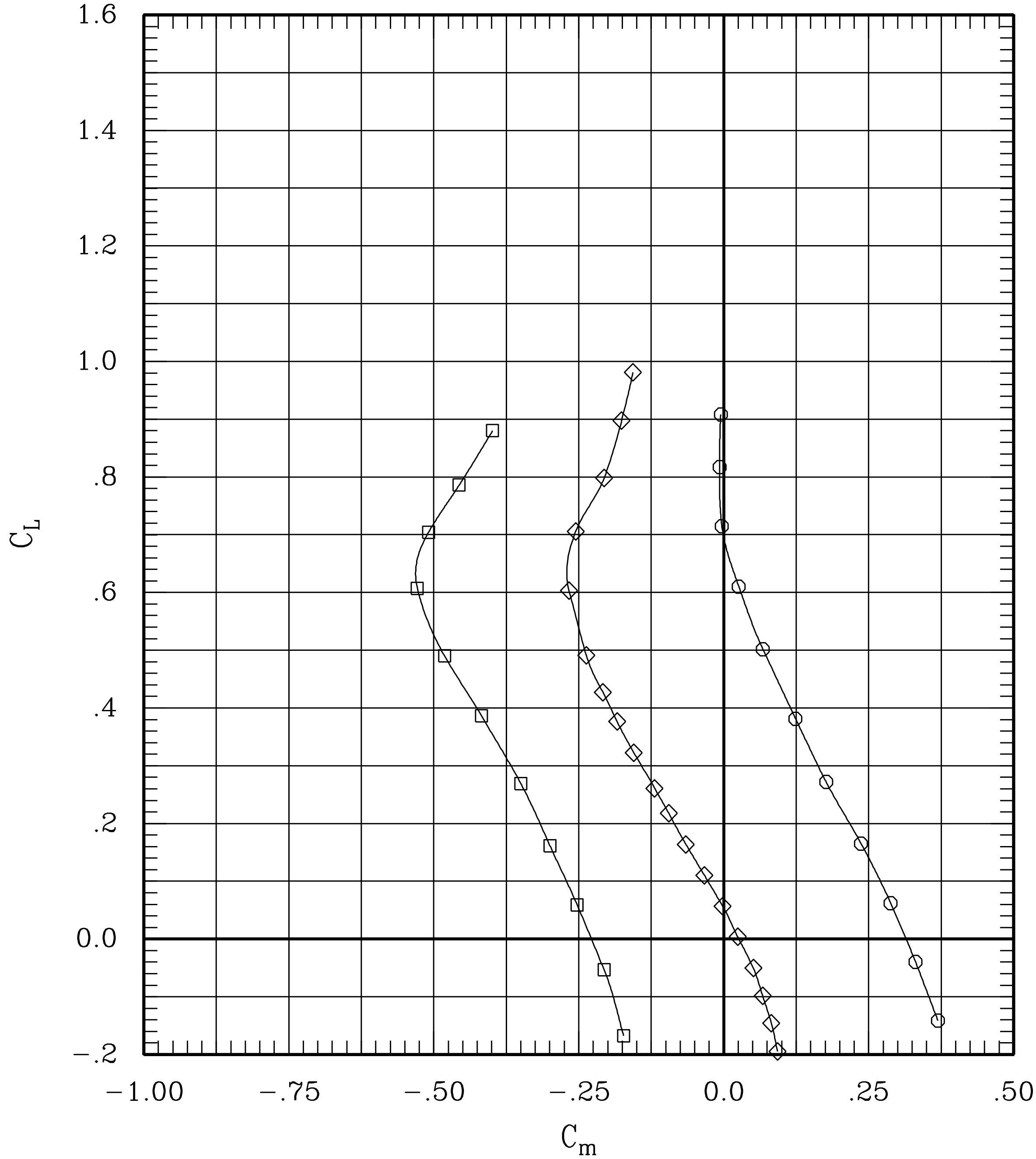

Figure 26(i). Effect of aileron deflection for sweep = 60 deg, Mach = 0.80 (Test #100).

SYMBOL	LT LA LO LI ^ RI RO RA RT	RUN	SWEEP	MACH	Q	BETA
—□—	00 30 00 00 L 00 00−30 00	55	60	.80	696	−.1
—◇—	00 00 00 00 L 00 00 00 00	135	60	.80	699	−.1
—○—	00−30 00 00 L 00 00 30 00	65	60	.80	701	−.1

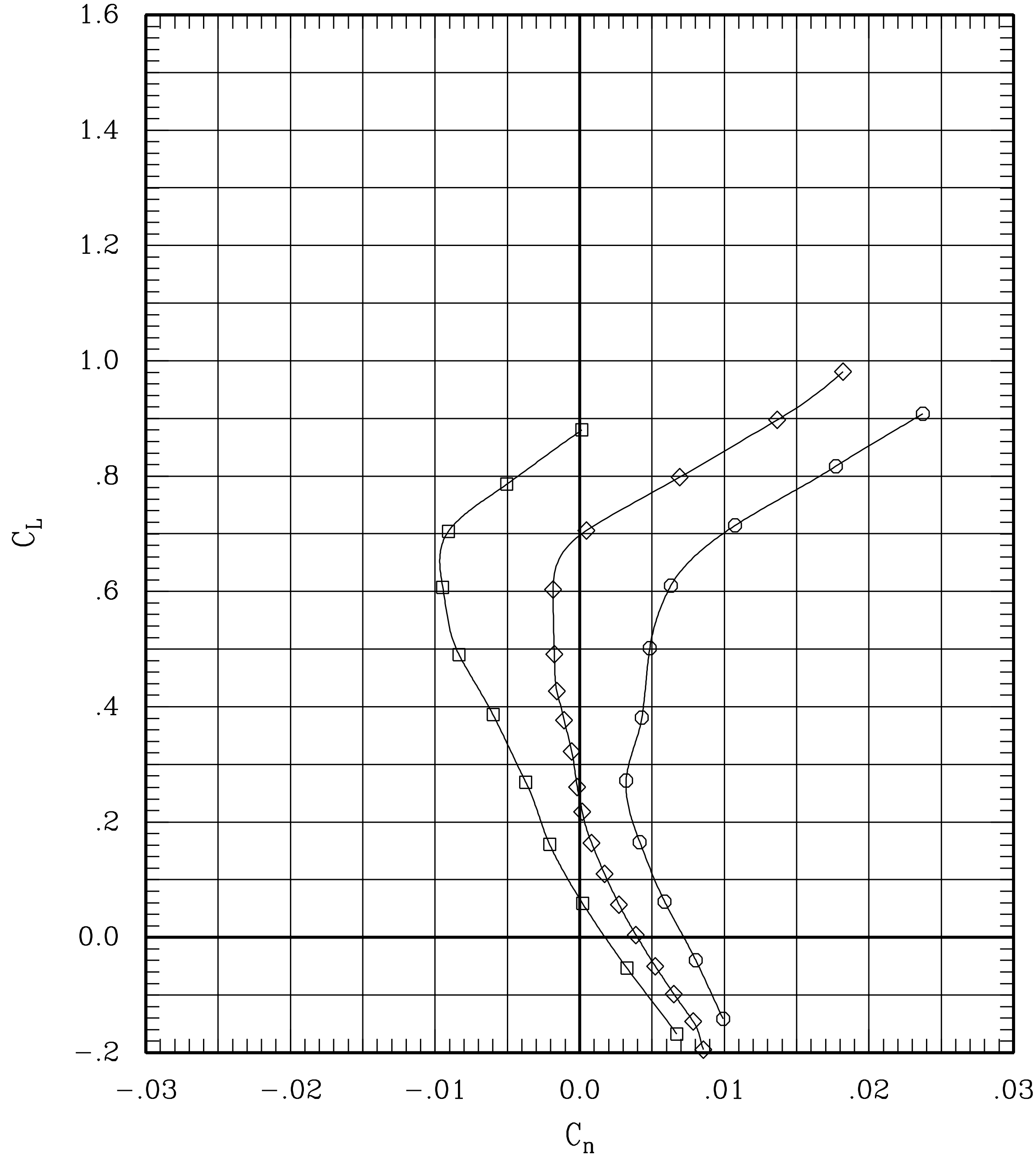

Figure 26(i). Effect of aileron deflection for sweep = 60 deg, Mach = 0.80 (Test #100).

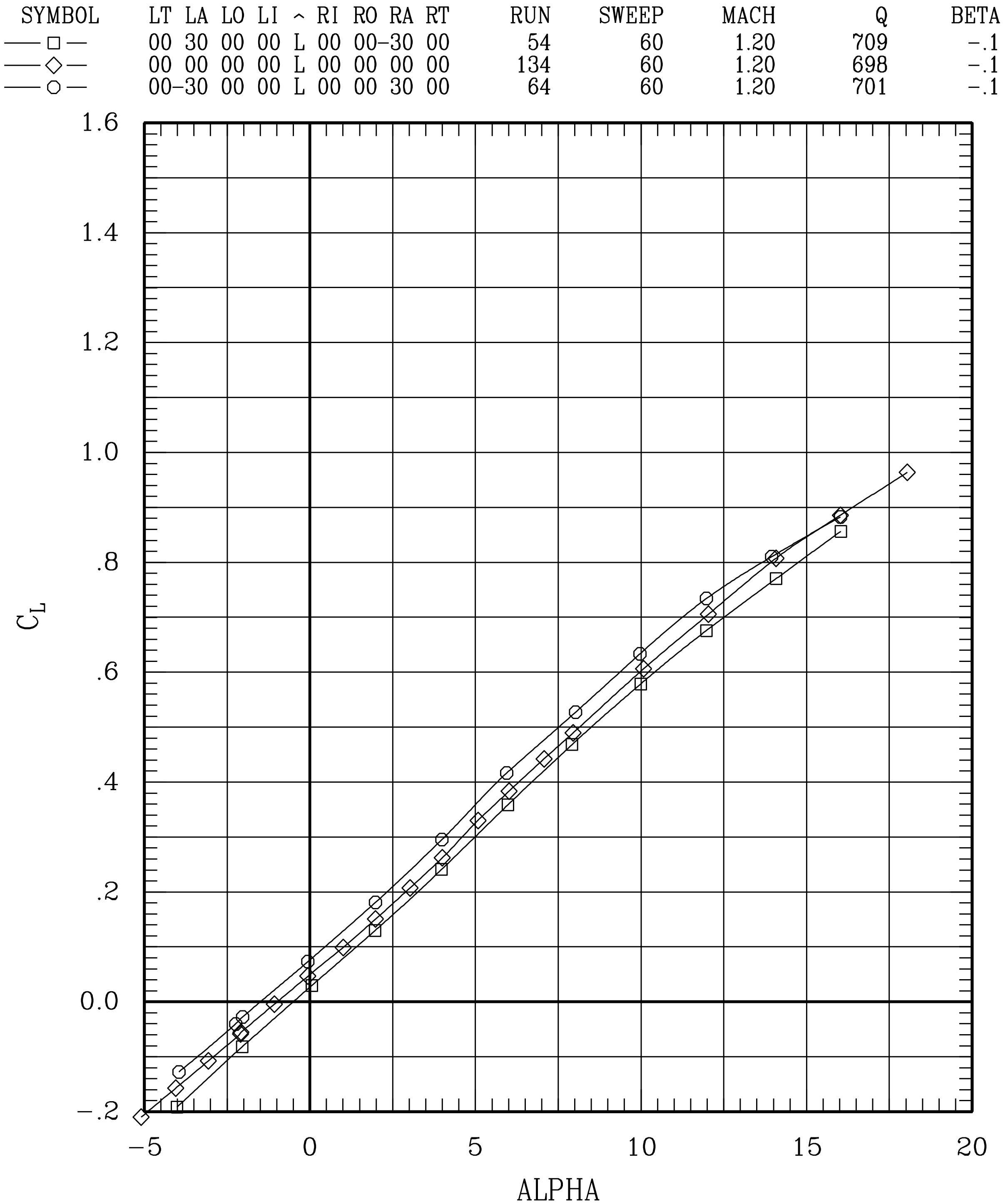

Figure 26(j). Effect of aileron deflection for sweep = 60 deg, Mach = 1.20 (Test #100).

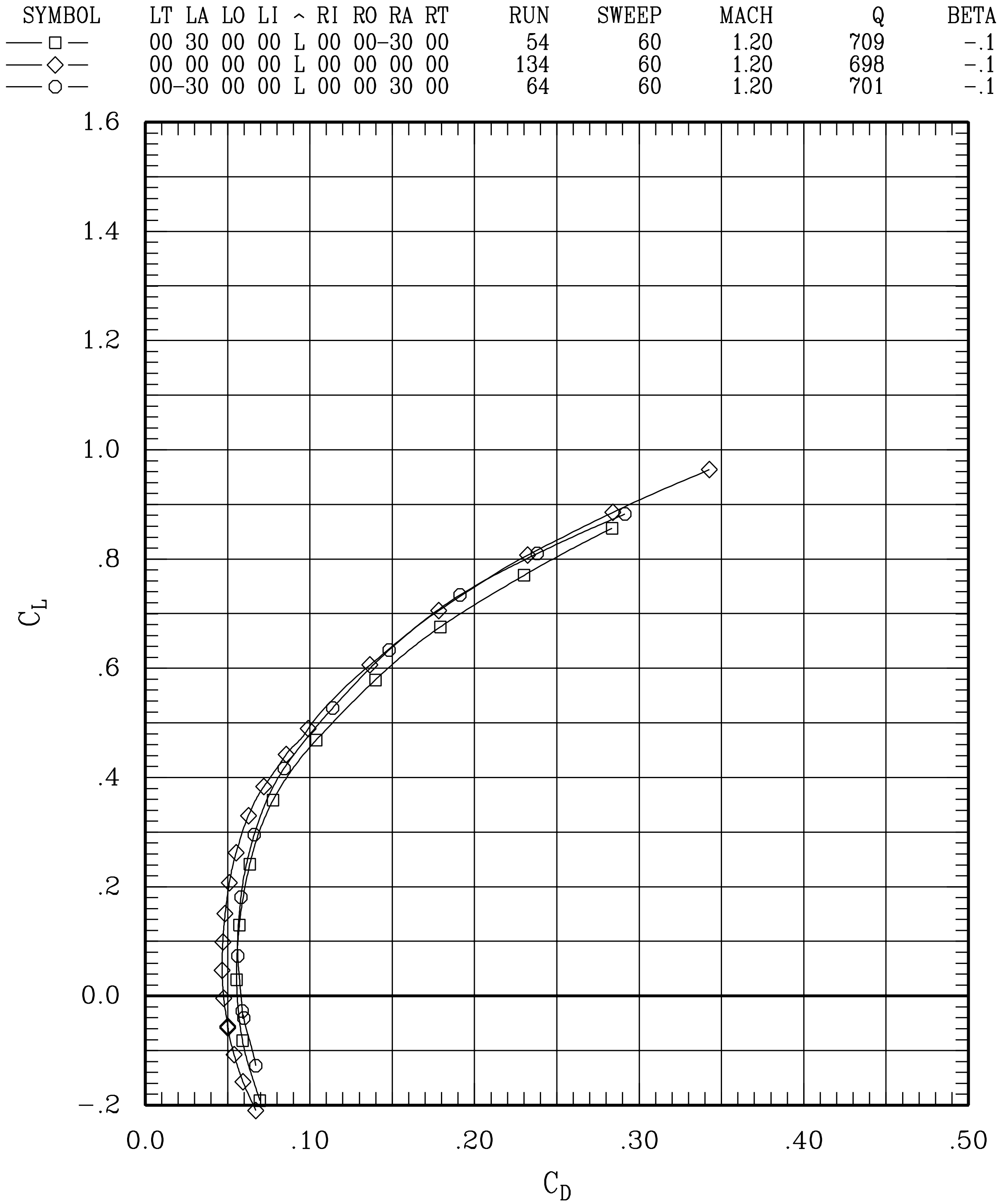

Figure 26(j). Effect of aileron deflection for sweep = 60 deg, Mach = 1.20 (Test #100).

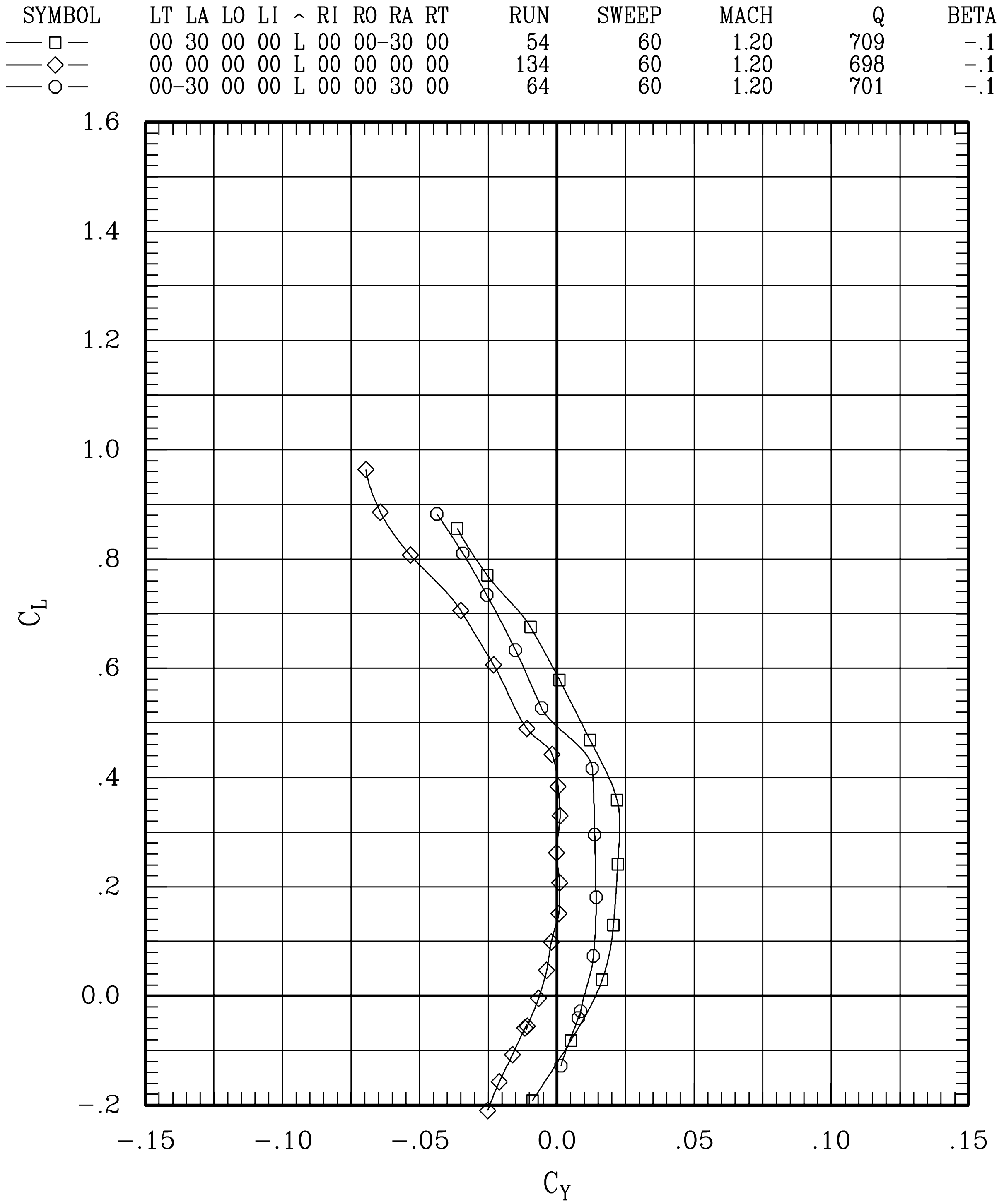

Figure 26(j). Effect of aileron deflection for sweep = 60 deg, Mach = 1.20 (Test #100).

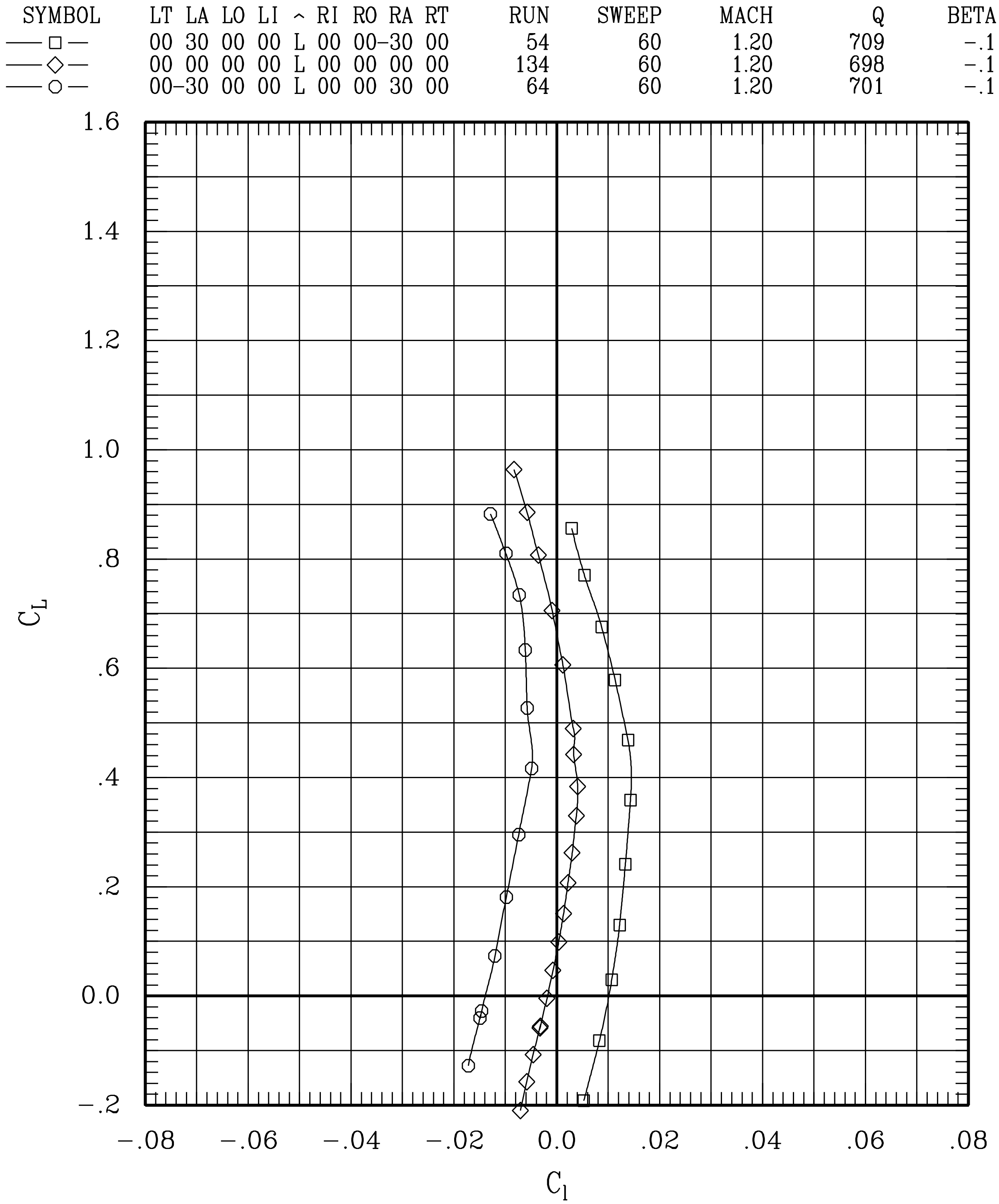

Figure 26(j). Effect of aileron deflection for sweep = 60 deg, Mach = 1.20 (Test #100).

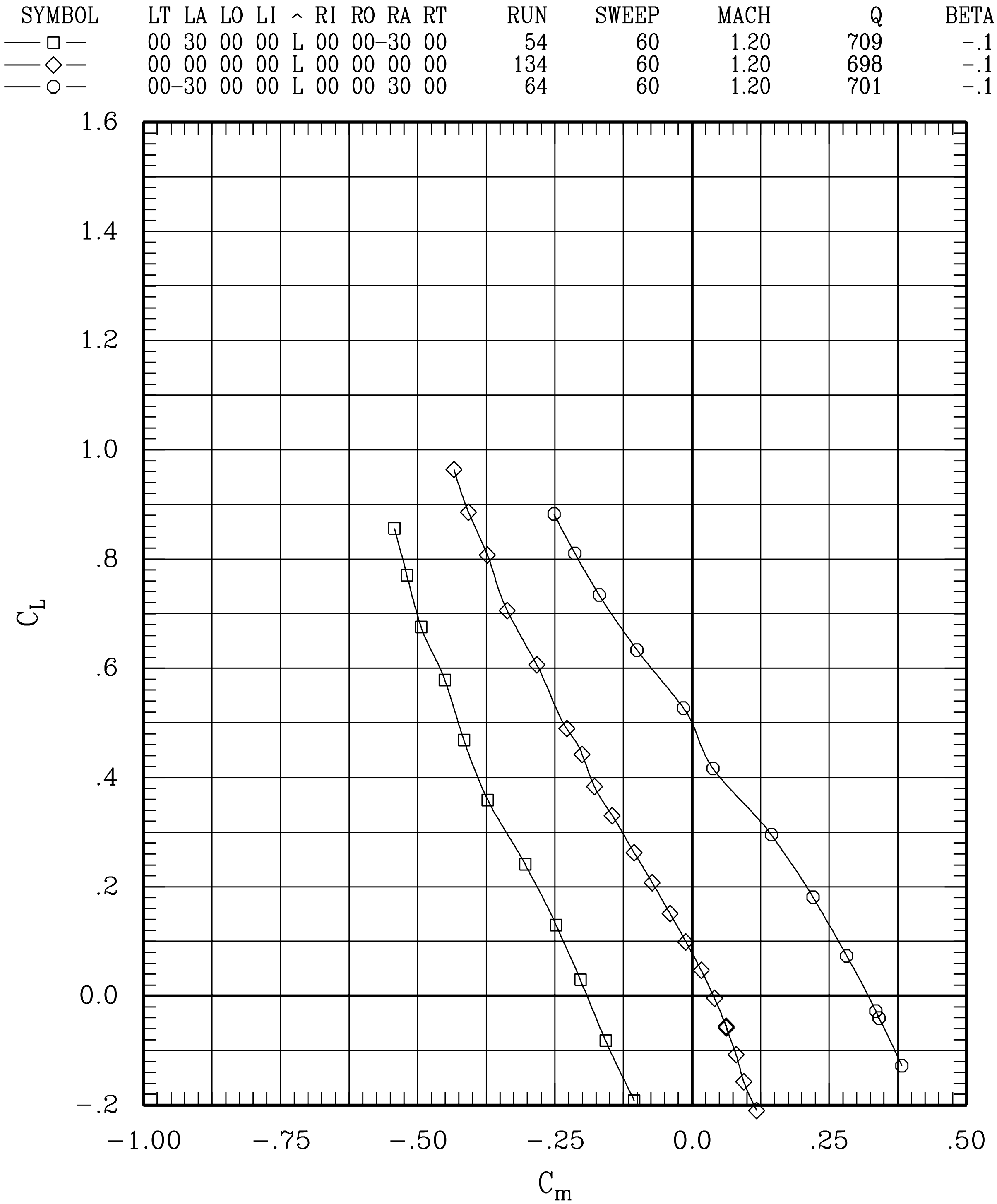

Figure 26(j). Effect of aileron deflection for sweep = 60 deg, Mach = 1.20 (Test #100).

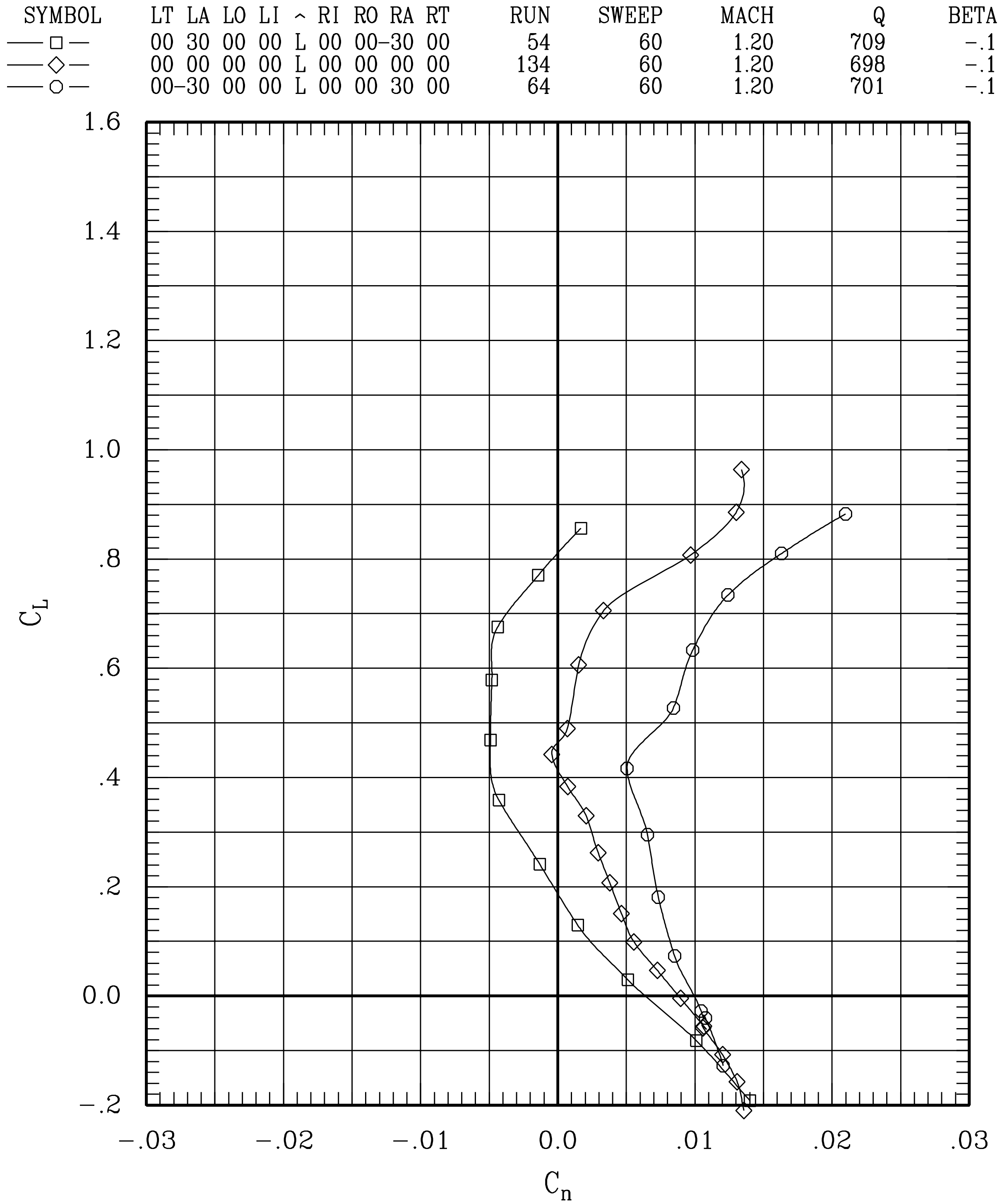

Figure 26(j). Effect of aileron deflection for sweep = 60 deg, Mach = 1.20 (Test #100).

SYMBOL	LT LA LO LI ^ RI RO RA RT	RUN	SWEEP	MACH	Q	BETA
—□—	00 30 00 00 L 00 00-30 00	222	65	.60	696	-.1
—◇—	00 10 00 00 L 00 00-10 00	213	65	.60	709	-.1
—○—	00 00 00 00 L 00 00 00 00	29	65	.60	704	-.1
—△—	00-10 00 00 L 00 00 10 00	211	65	.60	696	-.1
—⌂—	00-30 00 00 L 00 00 30 00	223	65	.60	694	-.1

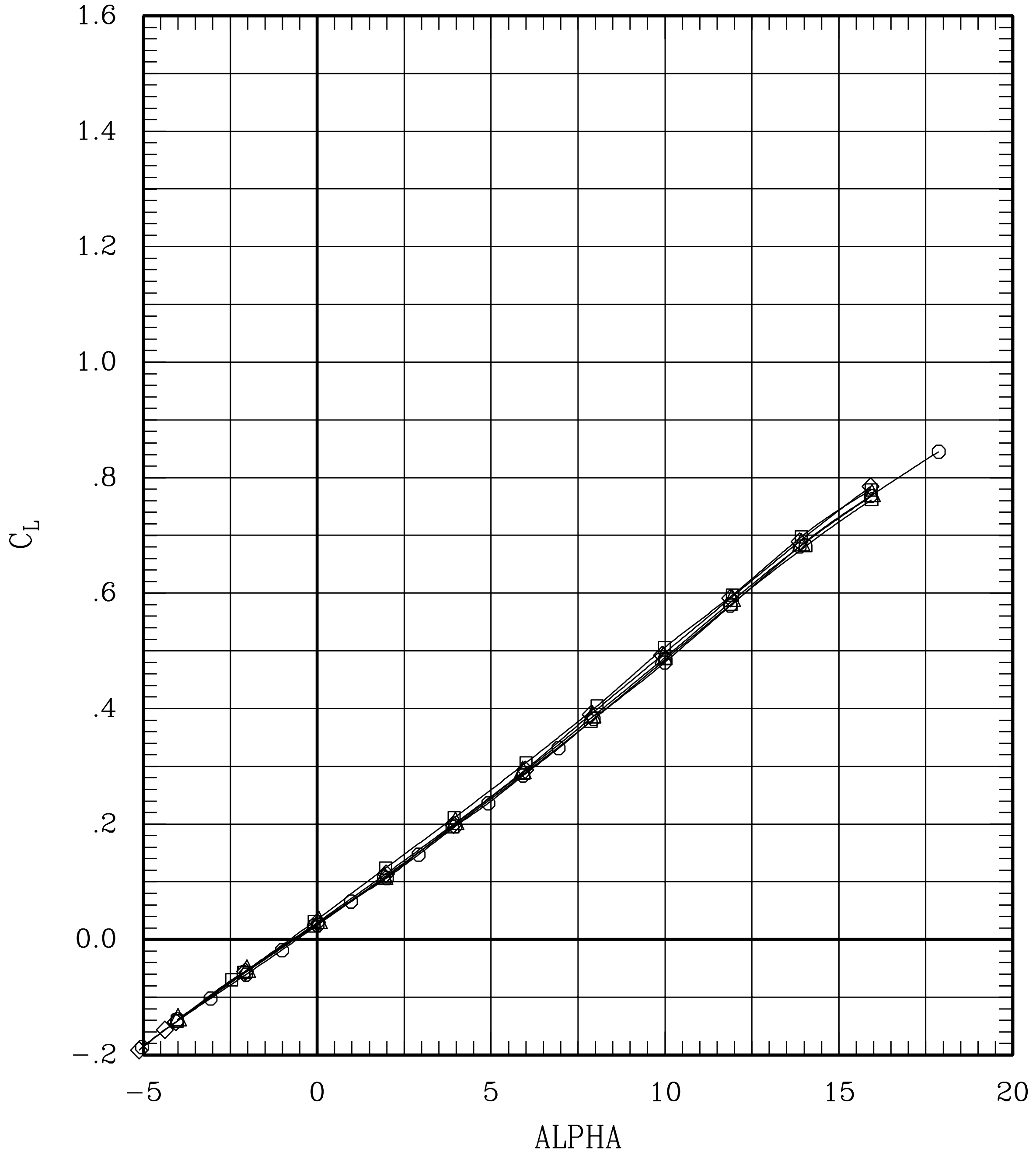

Figure 26(k). Effect of aileron deflection for sweep = 65 deg, Mach = 0.60 (Test #100).

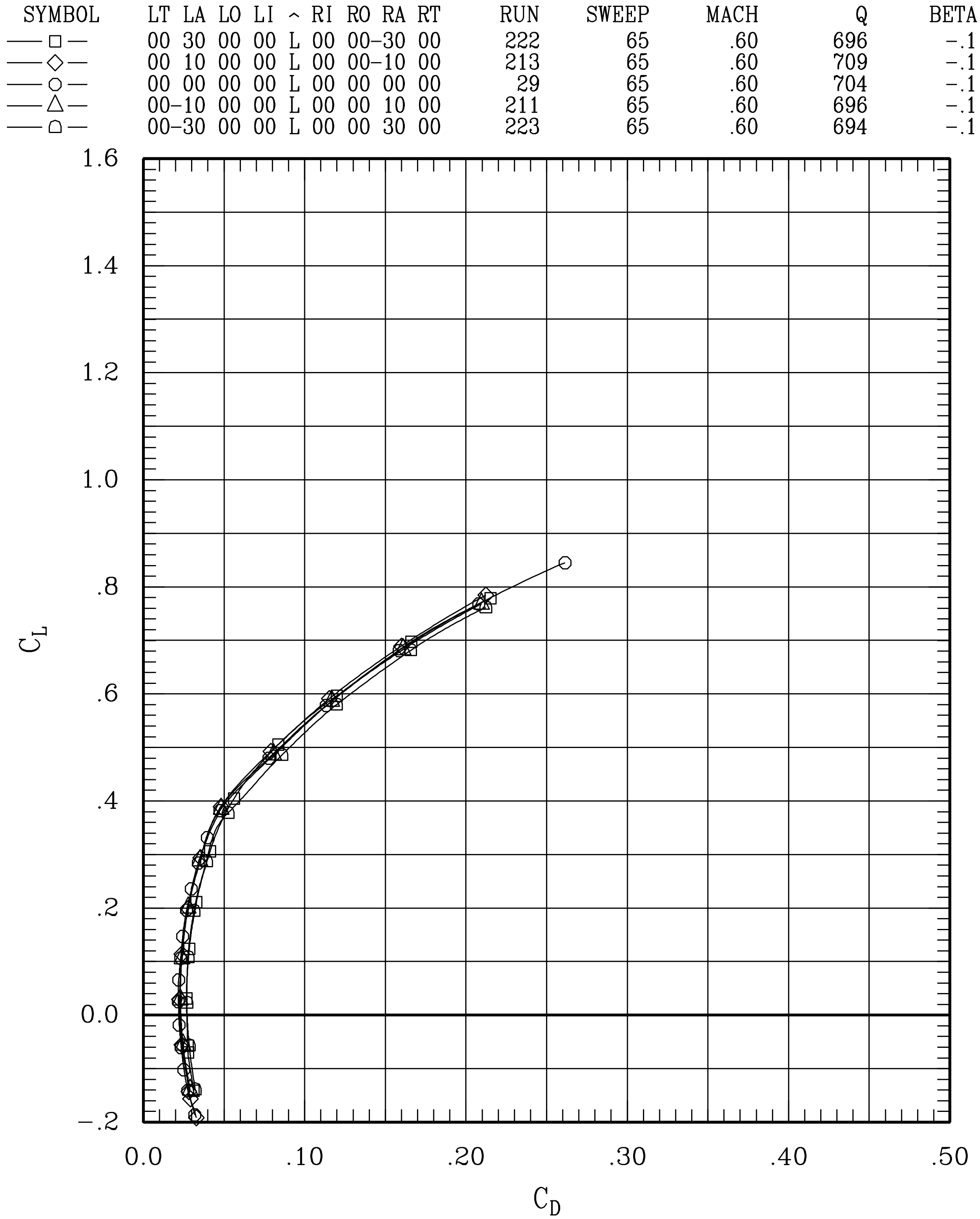

Figure 26(k). Effect of aileron deflection for sweep = 65 deg, Mach = 0.60 (Test #100).

SYMBOL	LT LA LO LI ^ RI RO RA RT	RUN	SWEEP	MACH	Q	BETA
—□—	00 30 00 00 L 00 00-30 00	222	65	.60	696	-.1
—◇—	00 10 00 00 L 00 00-10 00	213	65	.60	709	-.1
—○—	00 00 00 00 L 00 00 00 00	29	65	.60	704	-.1
—△—	00-10 00 00 L 00 00 10 00	211	65	.60	696	-.1
—⌂—	00-30 00 00 L 00 00 30 00	223	65	.60	694	-.1

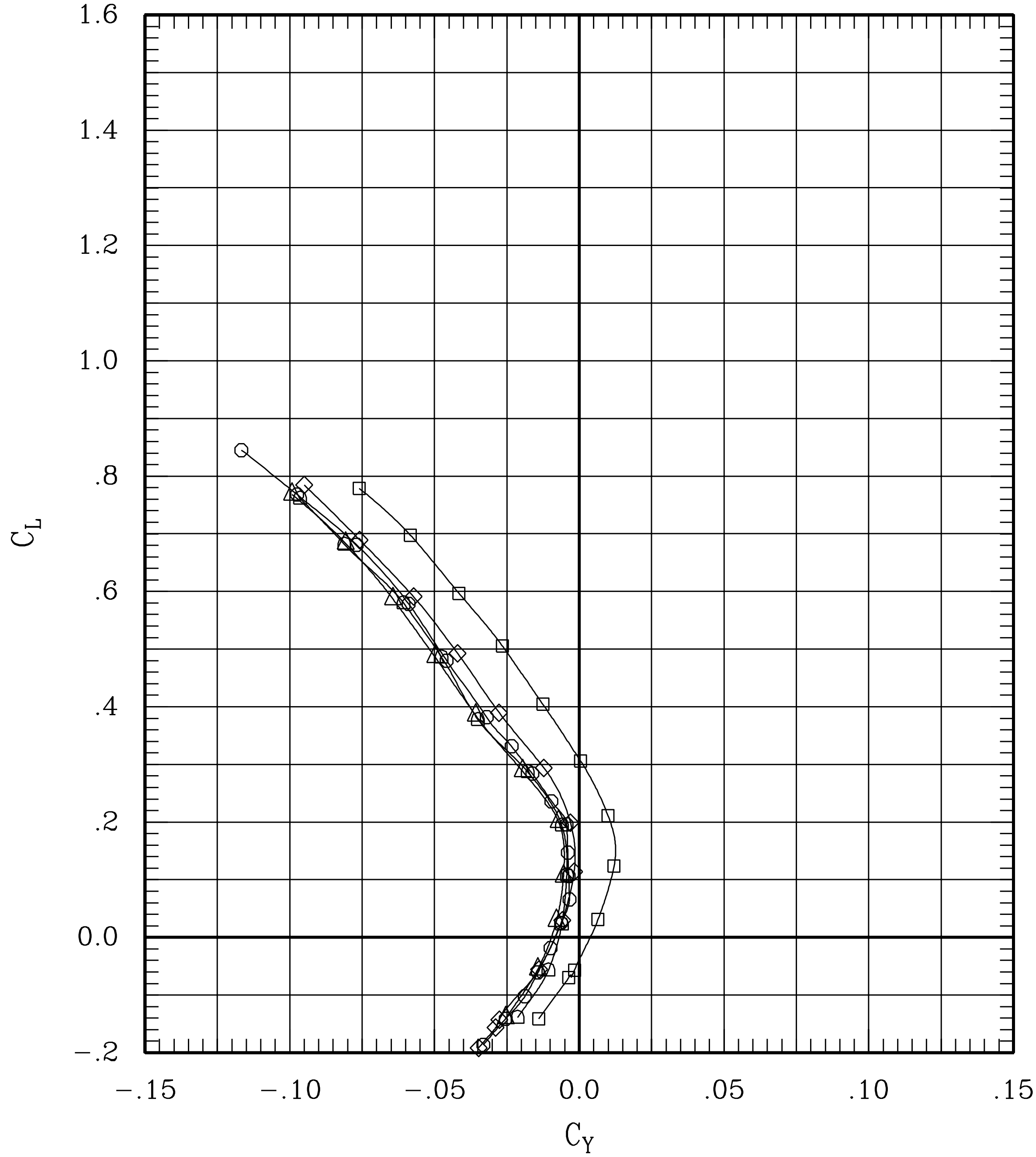

Figure 26(k). Effect of aileron deflection for sweep = 65 deg, Mach = 0.60 (Test #100).

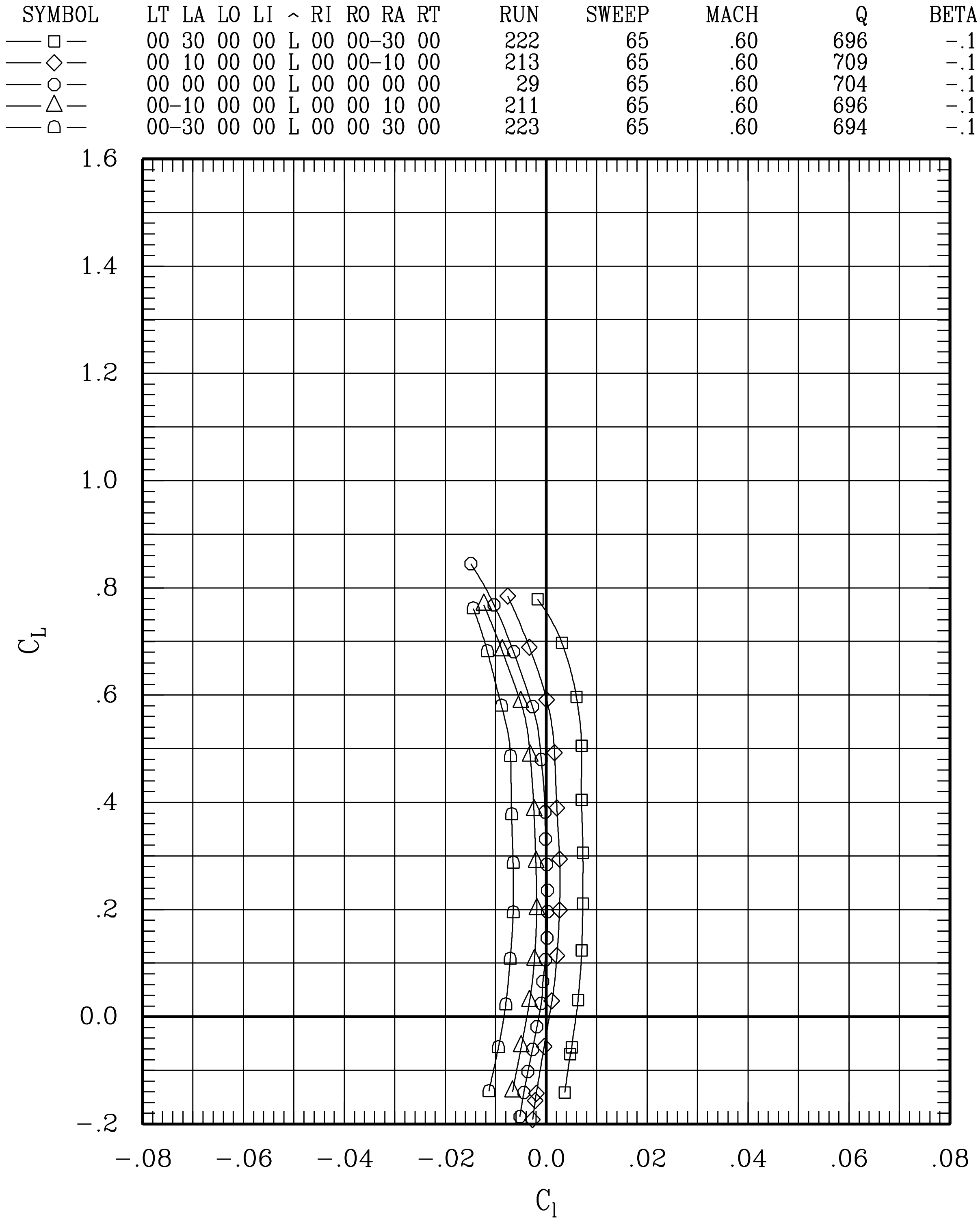

Figure 26(k). Effect of aileron deflection for sweep = 65 deg, Mach = 0.60 (Test #100).

SYMBOL	LT LA LO LI ^ RI RO RA RT	RUN	SWEEP	MACH	Q	BETA
—□—	00 30 00 00 L 00 00−30 00	222	65	.60	696	−.1
—◇—	00 10 00 00 L 00 00−10 00	213	65	.60	709	−.1
—○—	00 00 00 00 L 00 00 00 00	29	65	.60	704	−.1
—△—	00−10 00 00 L 00 00 10 00	211	65	.60	696	−.1
—⌂—	00−30 00 00 L 00 00 30 00	223	65	.60	694	−.1

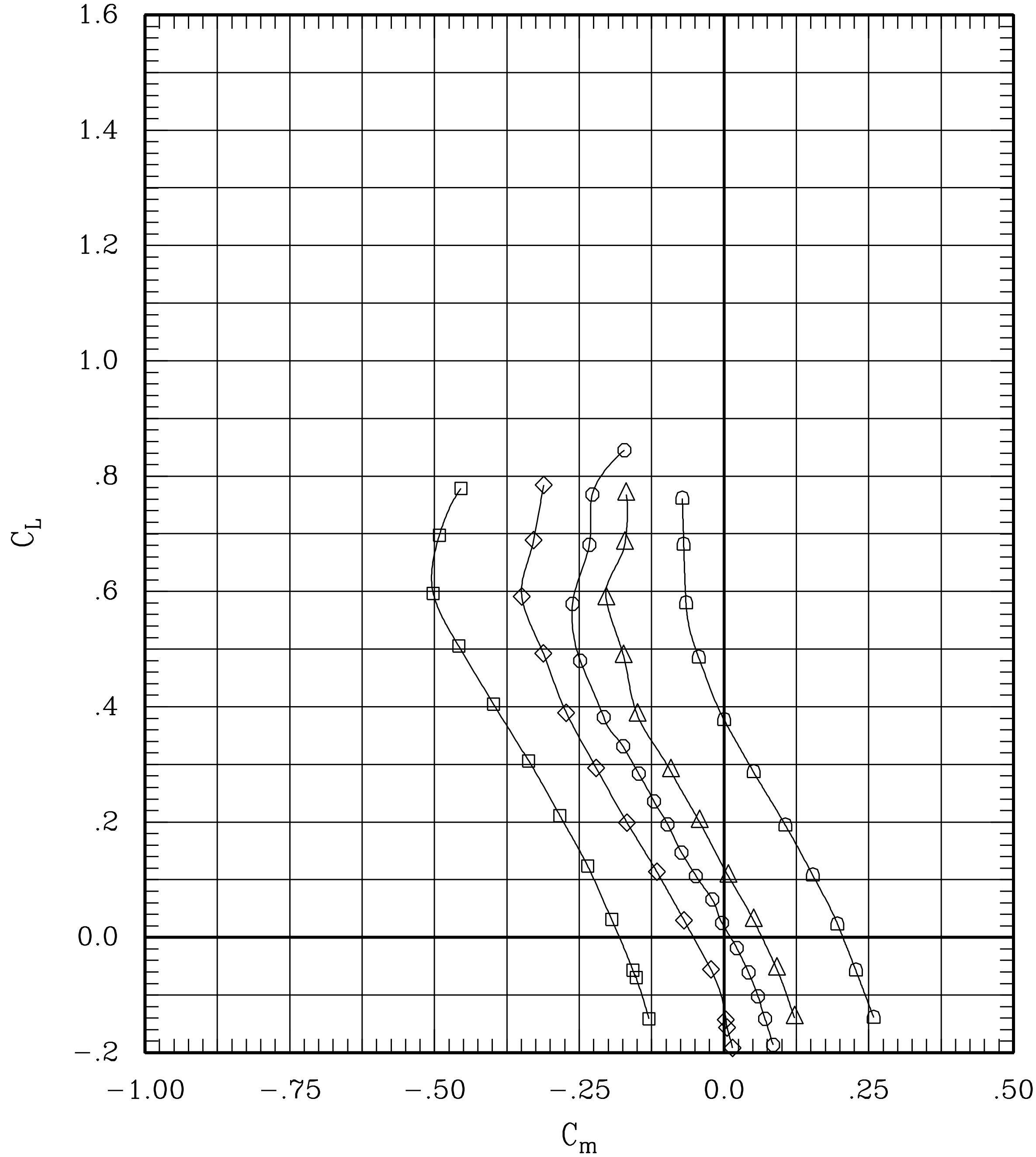

Figure 26(k). Effect of aileron deflection for sweep = 65 deg, Mach = 0.60 (Test #100).

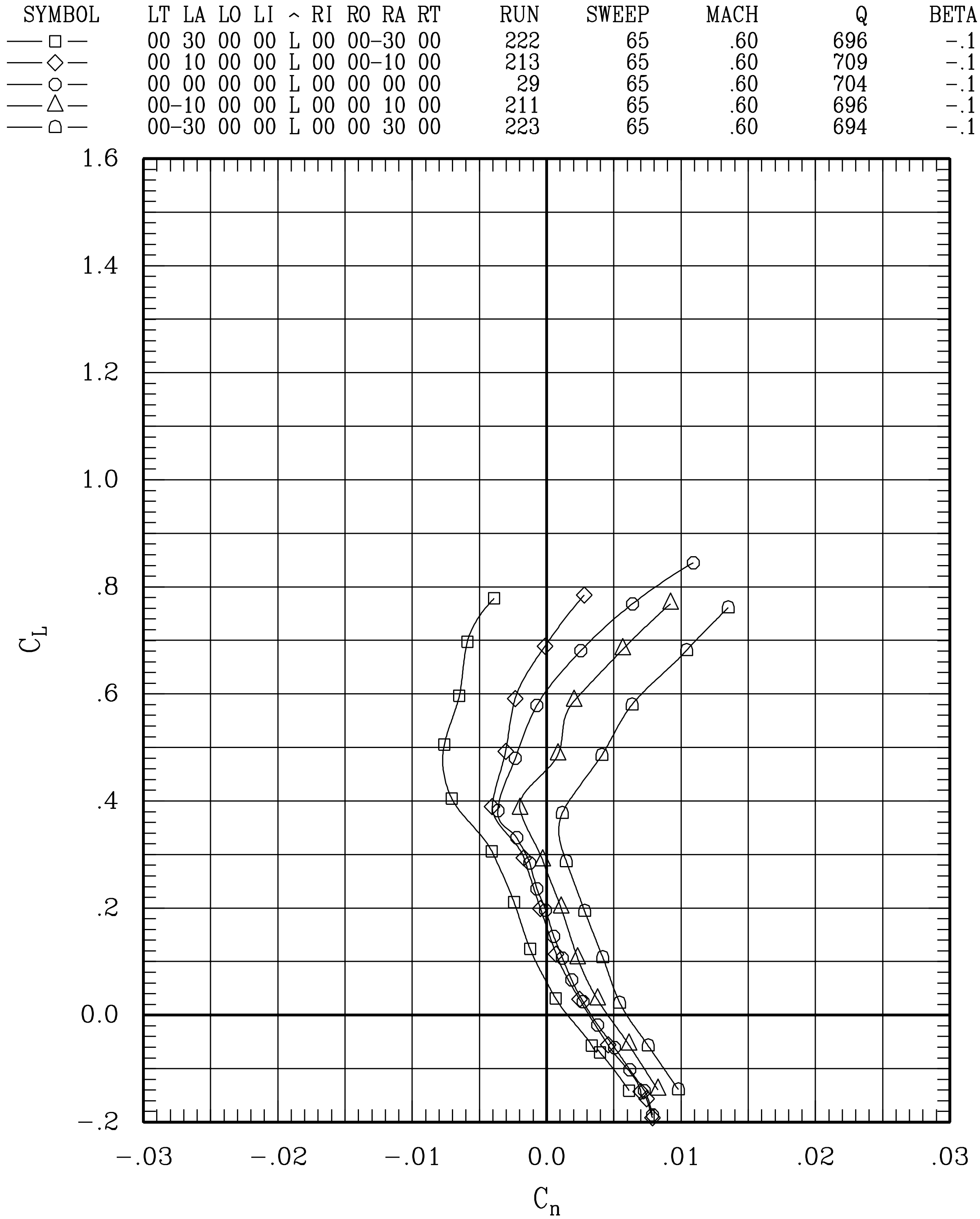

Figure 26(k). Effect of aileron deflection for sweep = 65 deg, Mach = 0.60 (Test #100).

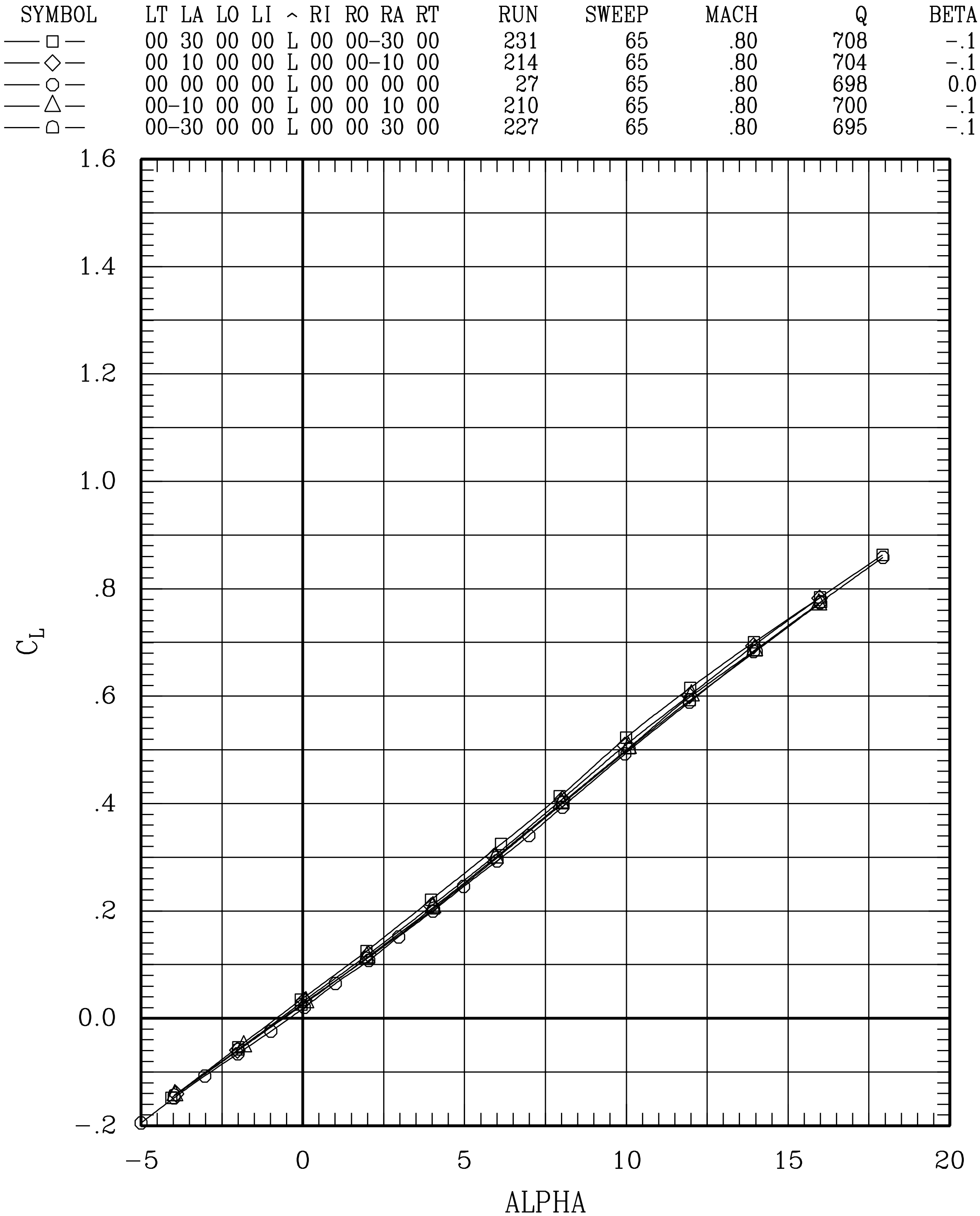

Figure 26(l). Effect of aileron deflection for sweep = 65 deg, Mach = 0.80 (Test #100).

SYMBOL	LT LA LO LI ^ RI RO RA RT	RUN	SWEEP	MACH	Q	BETA
□	00 30 00 00 L 00 00-30 00	231	65	.80	708	-.1
◇	00 10 00 00 L 00 00-10 00	214	65	.80	704	-.1
○	00 00 00 00 L 00 00 00 00	27	65	.80	698	0.0
△	00-10 00 00 L 00 00 10 00	210	65	.80	700	-.1
⌂	00-30 00 00 L 00 00 30 00	227	65	.80	695	-.1

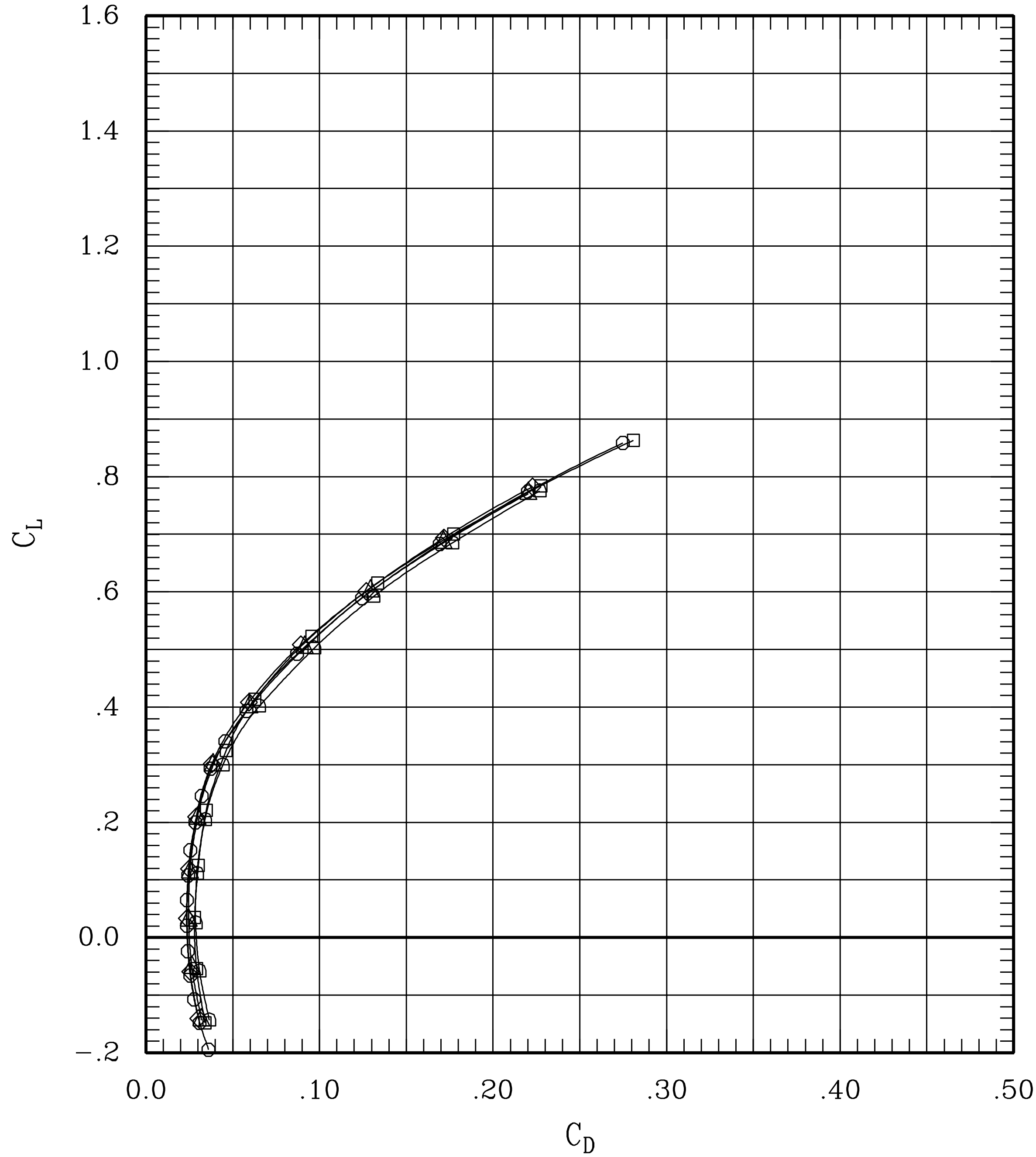

Figure 26(l). Effect of aileron deflection for sweep = 65 deg, Mach = 0.80 (Test #100).

SYMBOL	LT LA LO LI ^ RI RO RA RT	RUN	SWEEP	MACH	Q	BETA
—□—	00 30 00 00 L 00 00-30 00	231	65	.80	708	-.1
—◇—	00 10 00 00 L 00 00-10 00	214	65	.80	704	-.1
—○—	00 00 00 00 L 00 00 00 00	27	65	.80	698	0.0
—△—	00-10 00 00 L 00 00 10 00	210	65	.80	700	-.1
—⌂—	00-30 00 00 L 00 00 30 00	227	65	.80	695	-.1

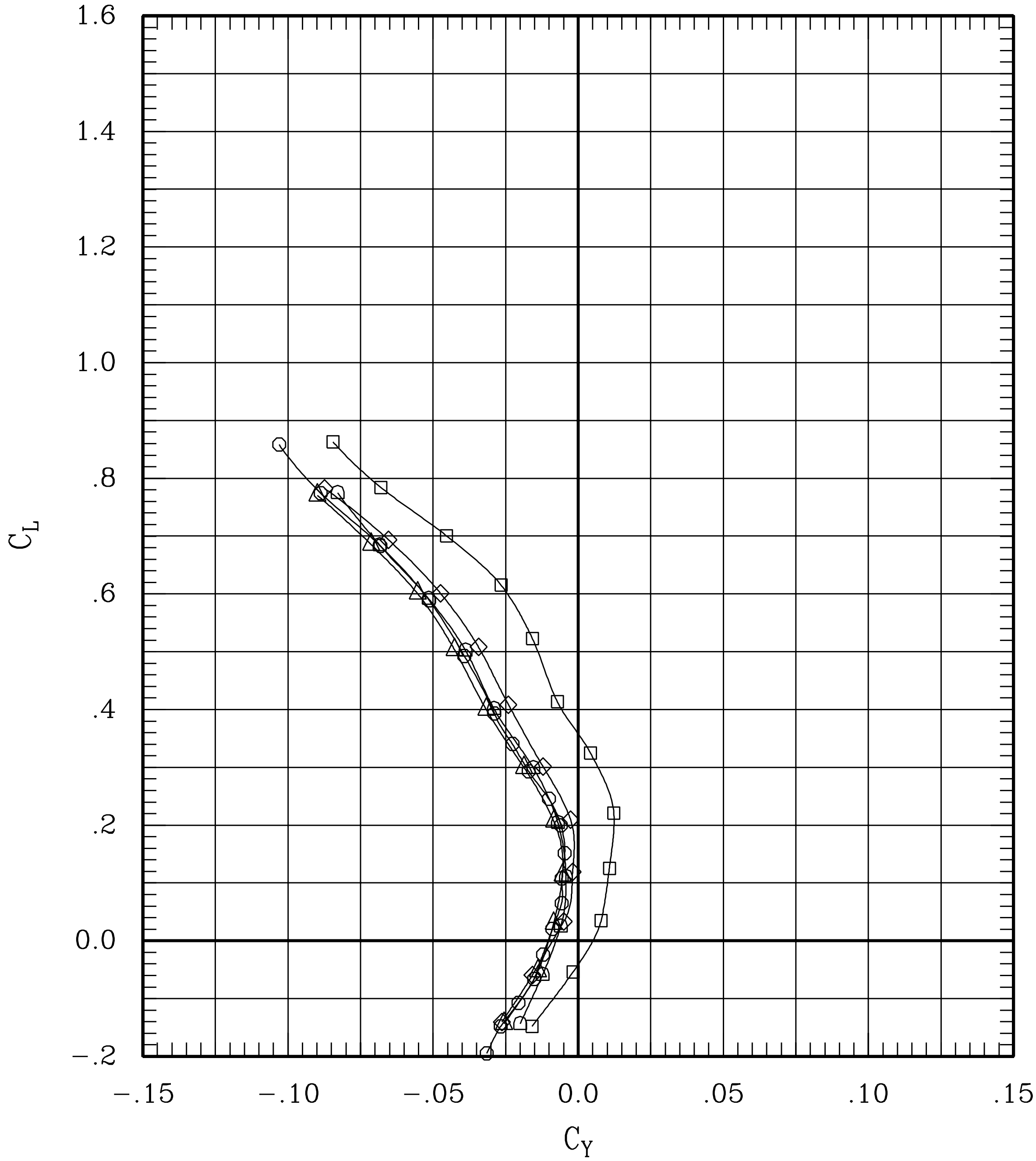

Figure 26(l). Effect of aileron deflection for sweep = 65 deg, Mach = 0.80 (Test #100).

SYMBOL	LT LA LO LI ^ RI RO RA RT	RUN	SWEEP	MACH	Q	BETA
□	00 30 00 00 L 00 00-30 00	231	65	.80	708	-.1
◇	00 10 00 00 L 00 00-10 00	214	65	.80	704	-.1
○	00 00 00 00 L 00 00 00 00	27	65	.80	698	0.0
△	00-10 00 00 L 00 00 10 00	210	65	.80	700	-.1
⌂	00-30 00 00 L 00 00 30 00	227	65	.80	695	-.1

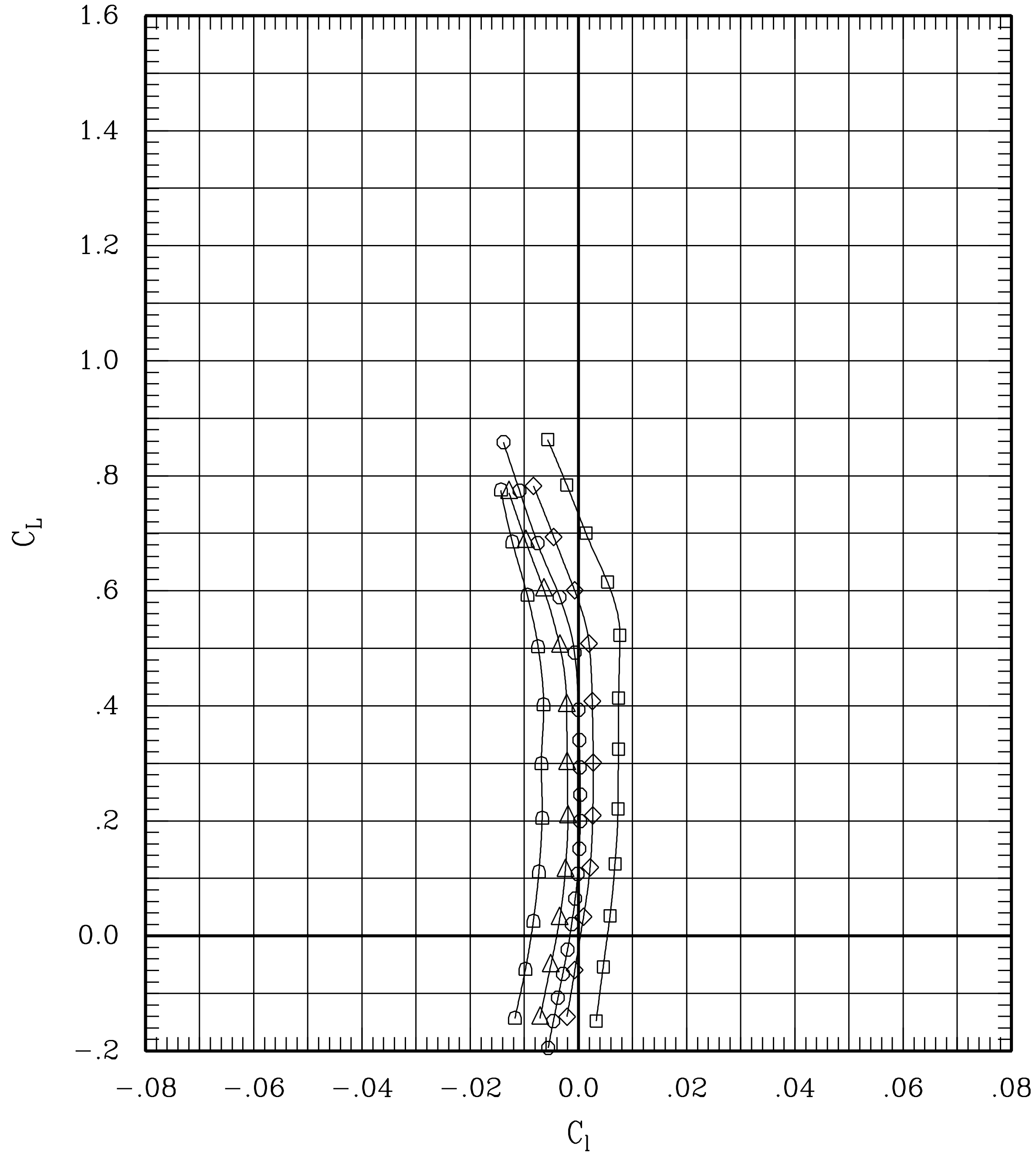

Figure 26(l). Effect of aileron deflection for sweep = 65 deg, Mach = 0.80 (Test #100).

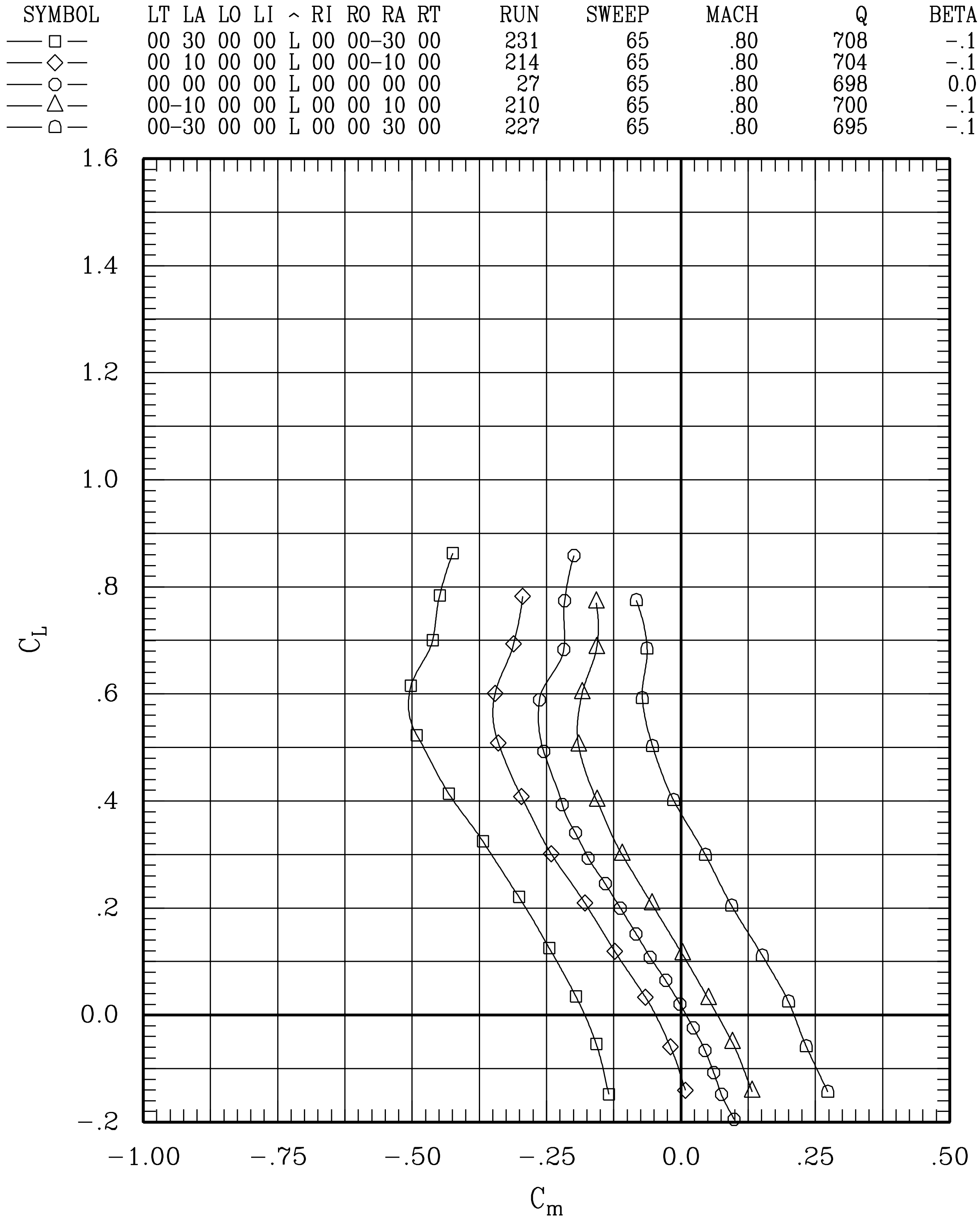

Figure 26(l). Effect of aileron deflection for sweep = 65 deg, Mach = 0.80 (Test #100).

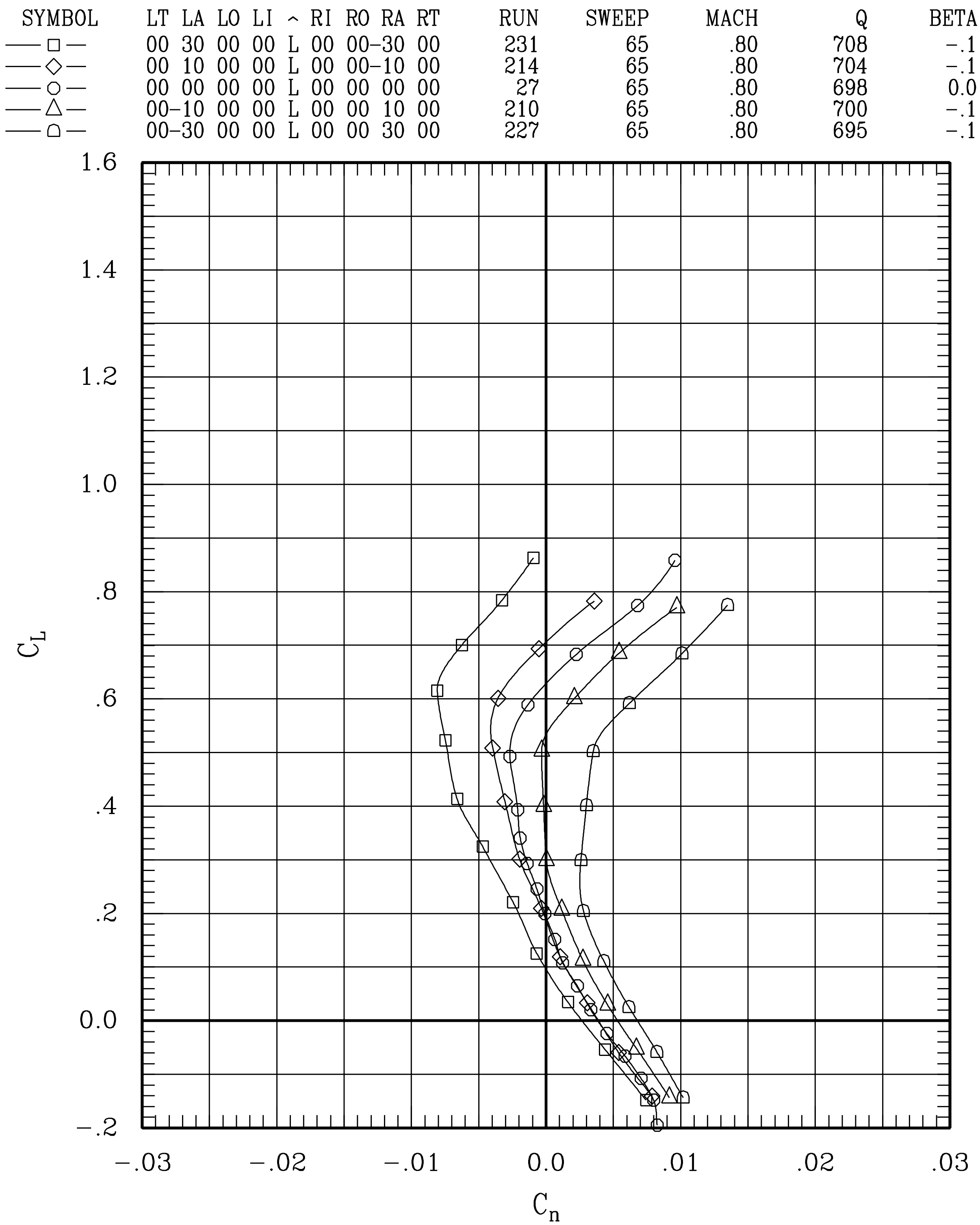

Figure 26(l). Effect of aileron deflection for sweep = 65 deg, Mach = 0.80 (Test #100).

SYMBOL	LT LA LO LI ^ RI RO RA RT	RUN	SWEEP	MACH	Q	BETA
□	00 30 00 00 L 00 00-30 00	230	65	1.20	696	-.1
◇	00 10 00 00 L 00 00-10 00	212	65	1.20	694	-.1
○	00 00 00 00 L 00 00 00 00	23	65	1.20	695	-.1
△	00-10 00 00 L 00 00 10 00	209	65	1.20	702	-.1
⌂	00-30 00 00 L 00 00 30 00	226	65	1.20	702	-.1

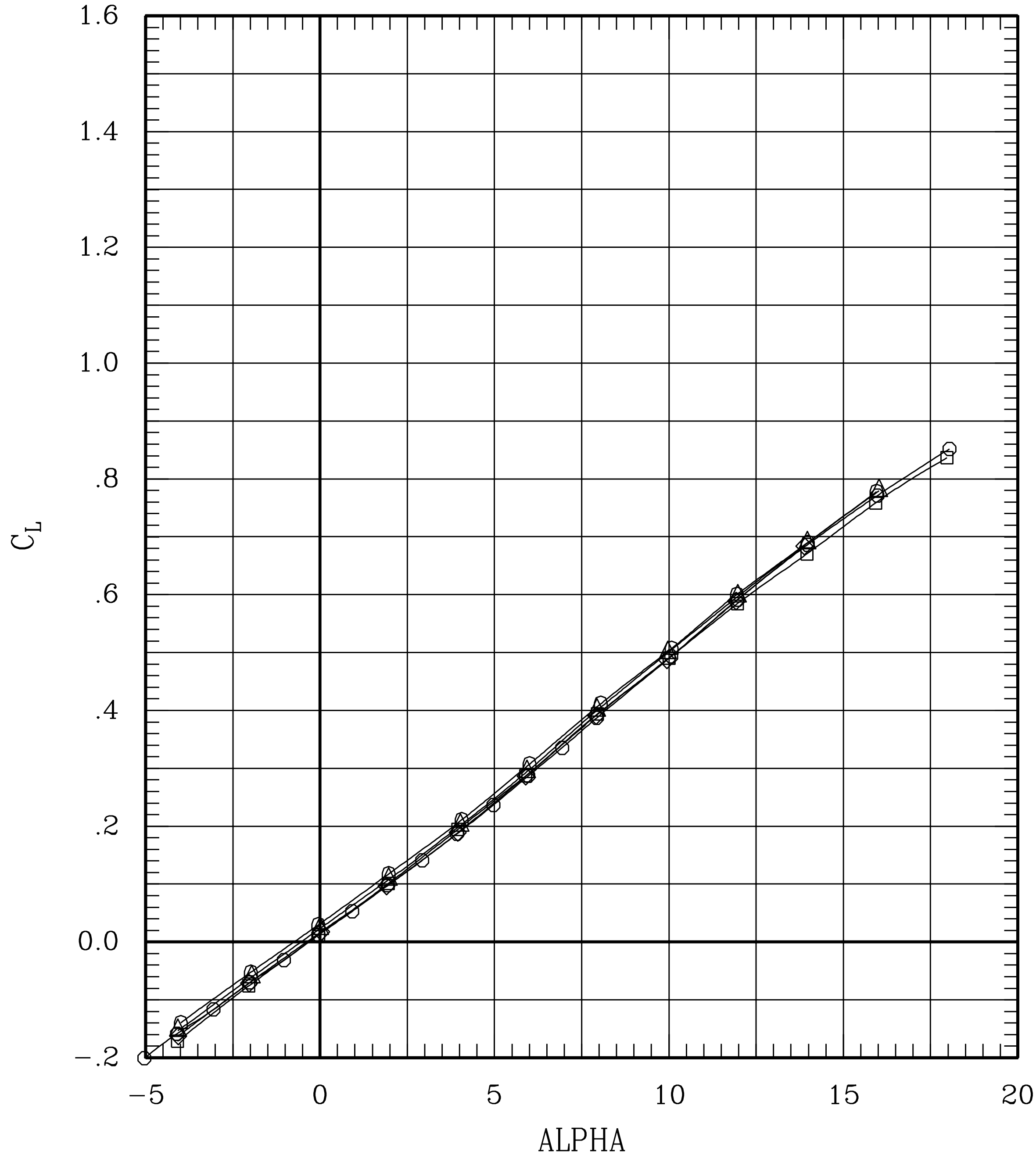

Figure 26(m). Effect of aileron deflection for sweep = 65 deg, Mach = 1.20 (Test #100).

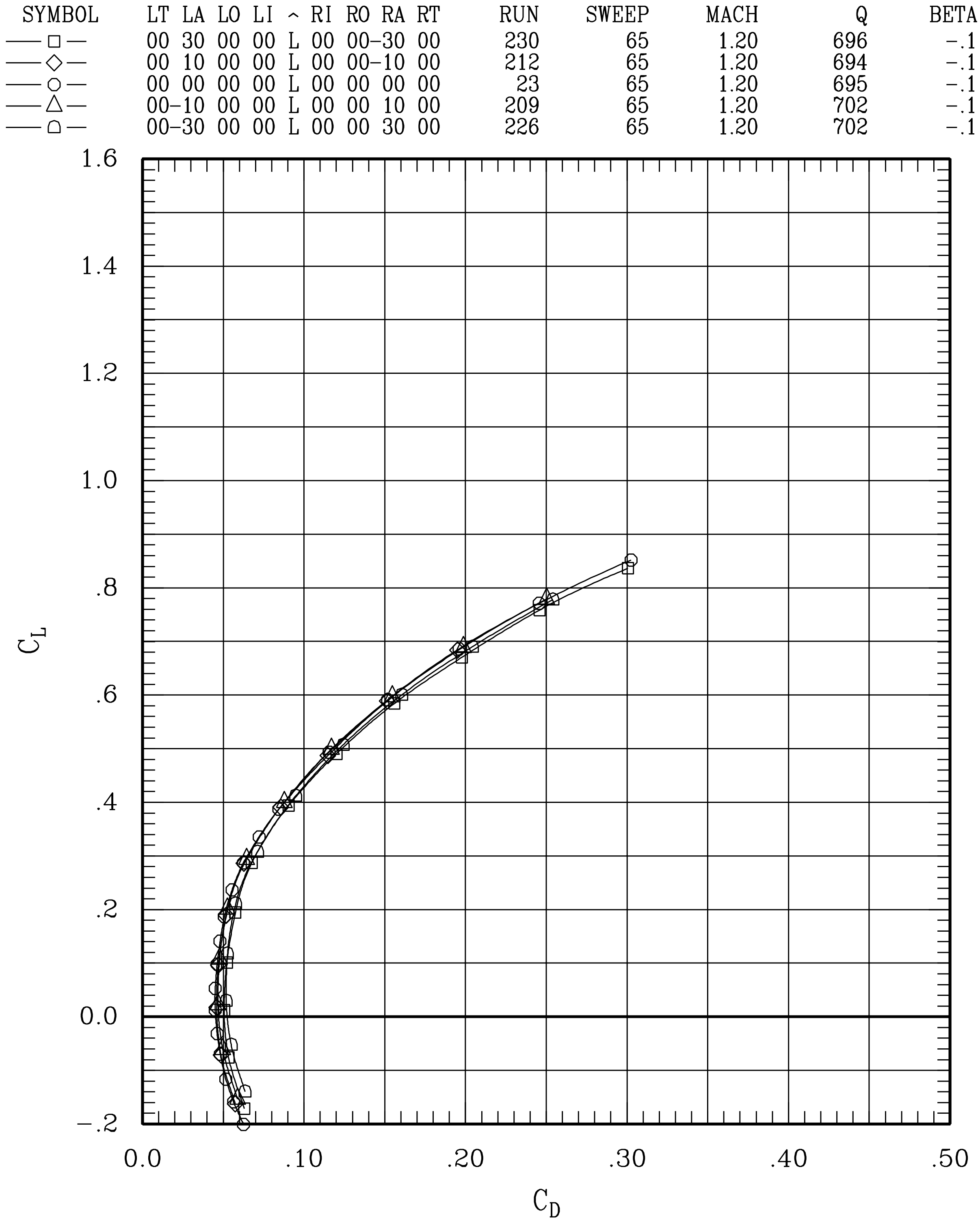

Figure 26(m). Effect of aileron deflection for sweep = 65 deg, Mach = 1.20 (Test #100).

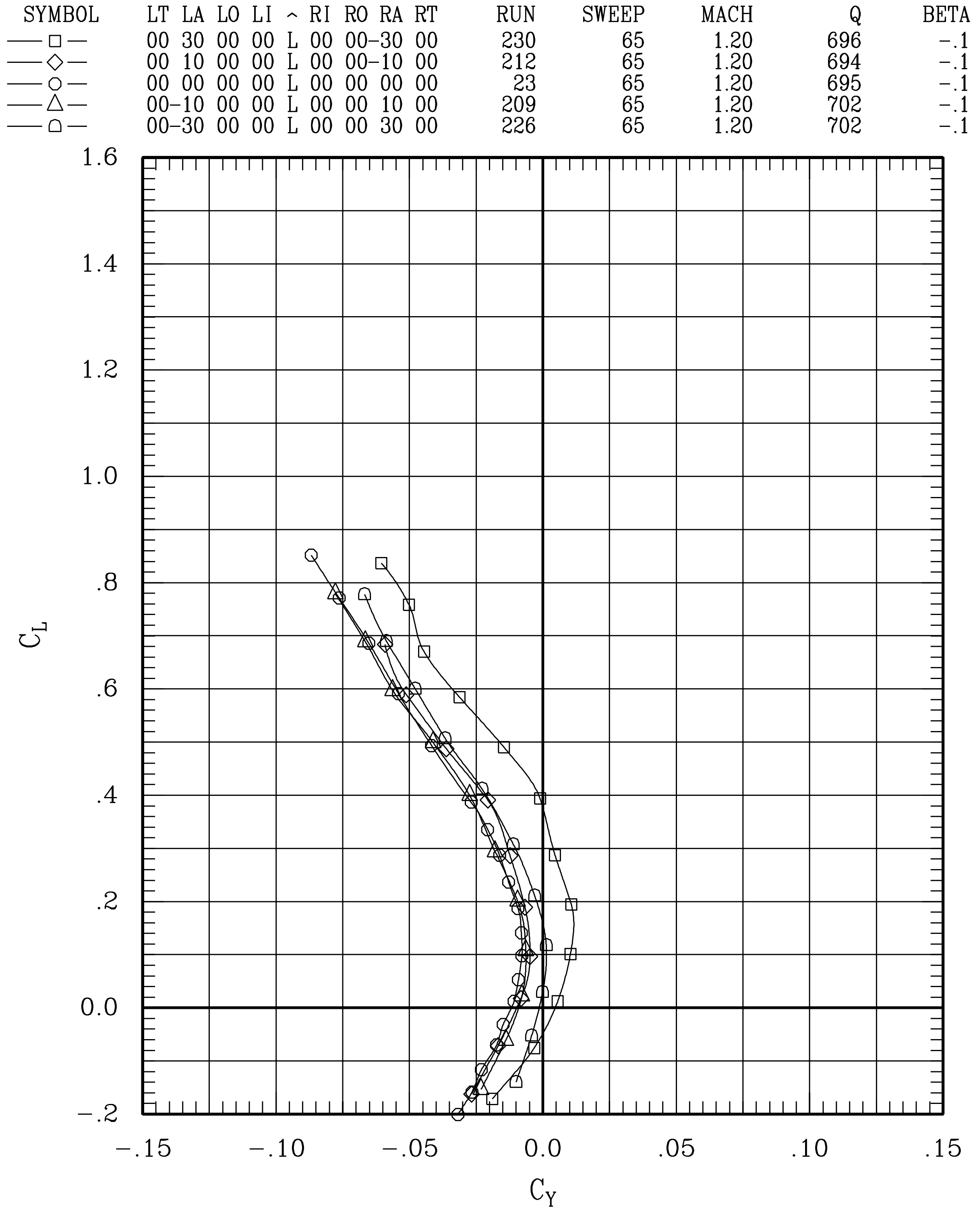

Figure 26(m). Effect of aileron deflection for sweep = 65 deg, Mach = 1.20 (Test #100).

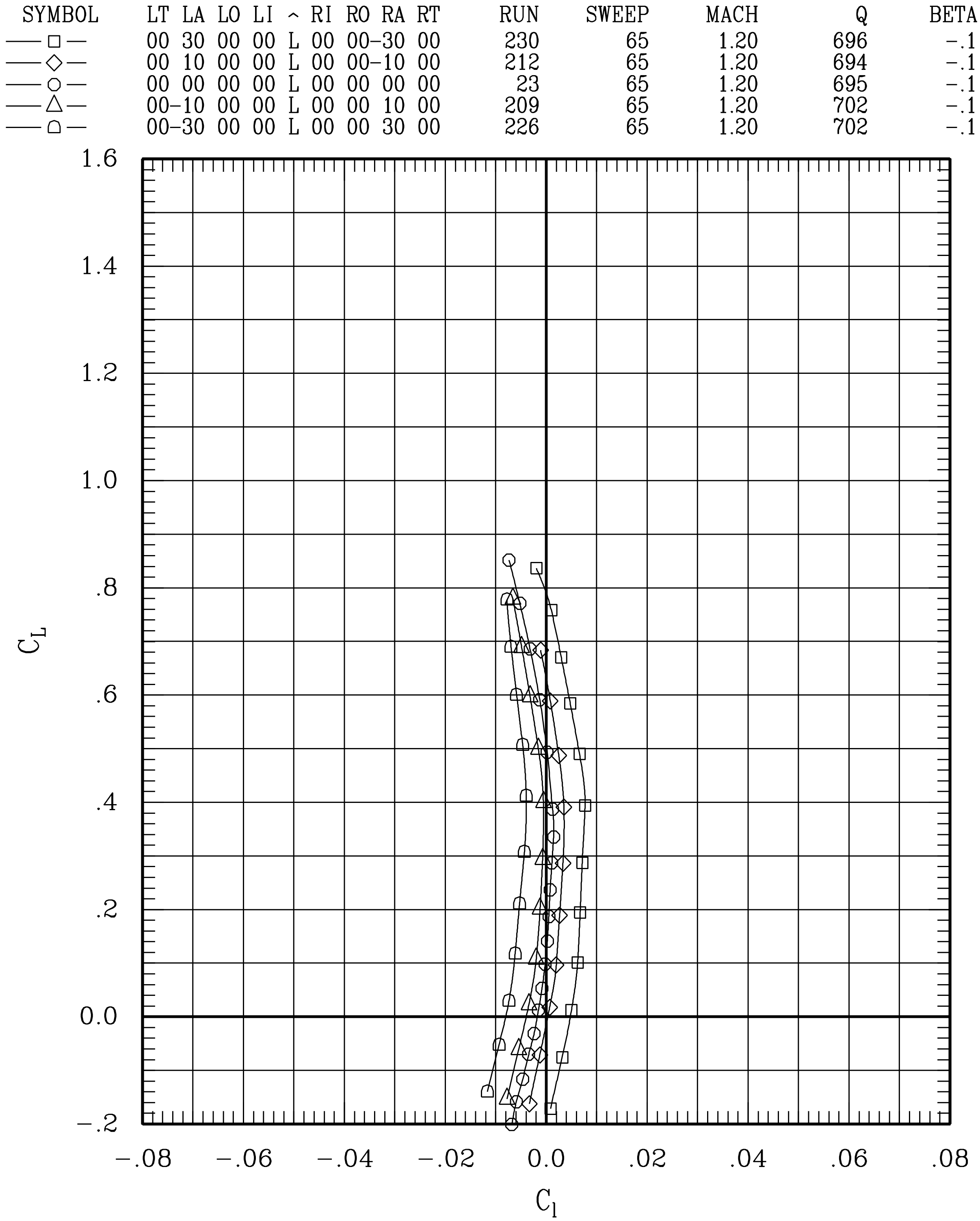

Figure 26(m). Effect of aileron deflection for sweep = 65 deg, Mach = 1.20 (Test #100).

SYMBOL	LT LA LO LI ^ RI RO RA RT	RUN	SWEEP	MACH	Q	BETA
—□—	00 30 00 00 L 00 00-30 00	230	65	1.20	696	-.1
—◇—	00 10 00 00 L 00 00-10 00	212	65	1.20	694	-.1
—○—	00 00 00 00 L 00 00 00 00	23	65	1.20	695	-.1
—△—	00-10 00 00 L 00 00 10 00	209	65	1.20	702	-.1
—⌂—	00-30 00 00 L 00 00 30 00	226	65	1.20	702	-.1

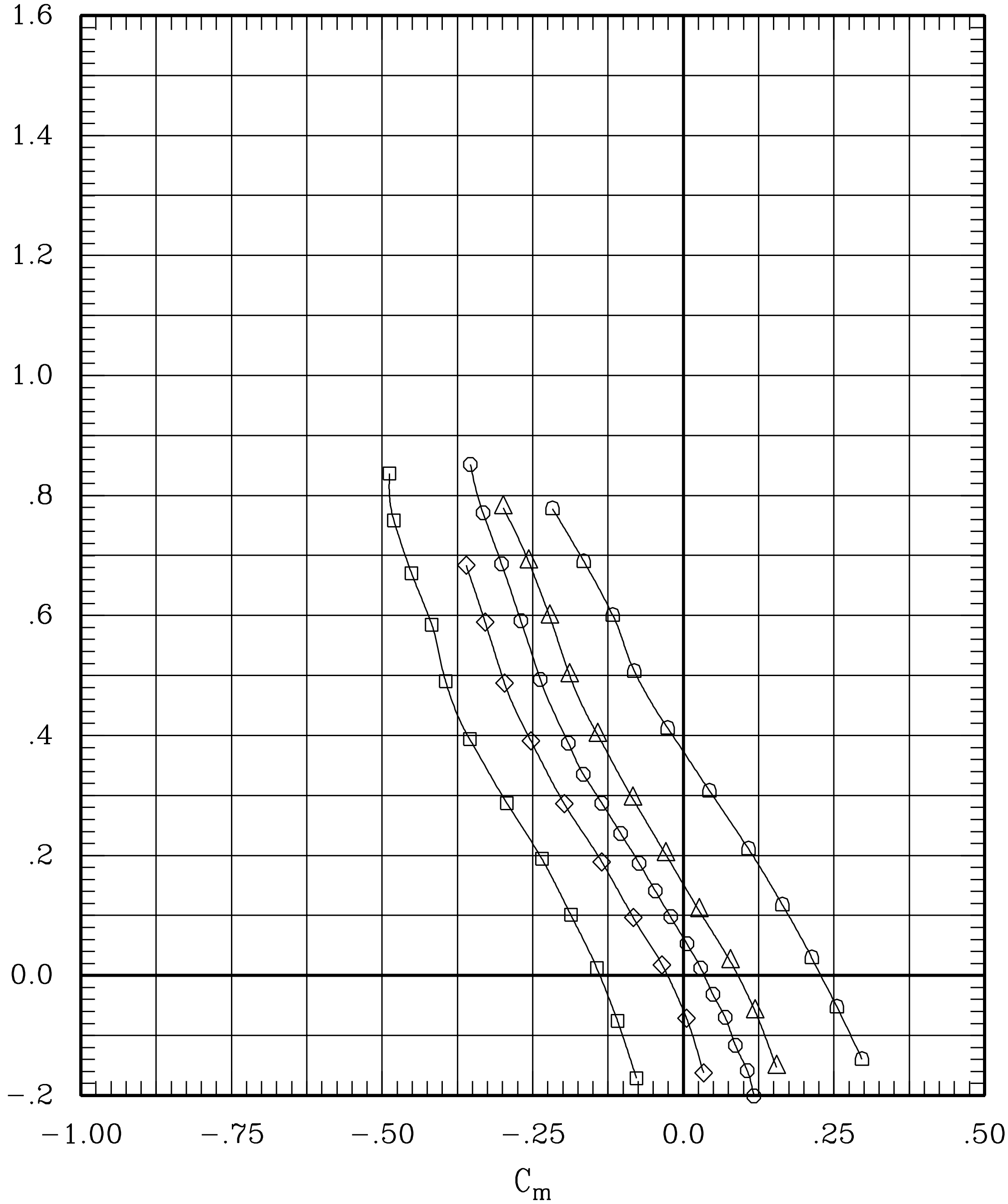

Figure 26(m). Effect of aileron deflection for sweep = 65 deg, Mach = 1.20 (Test #100).

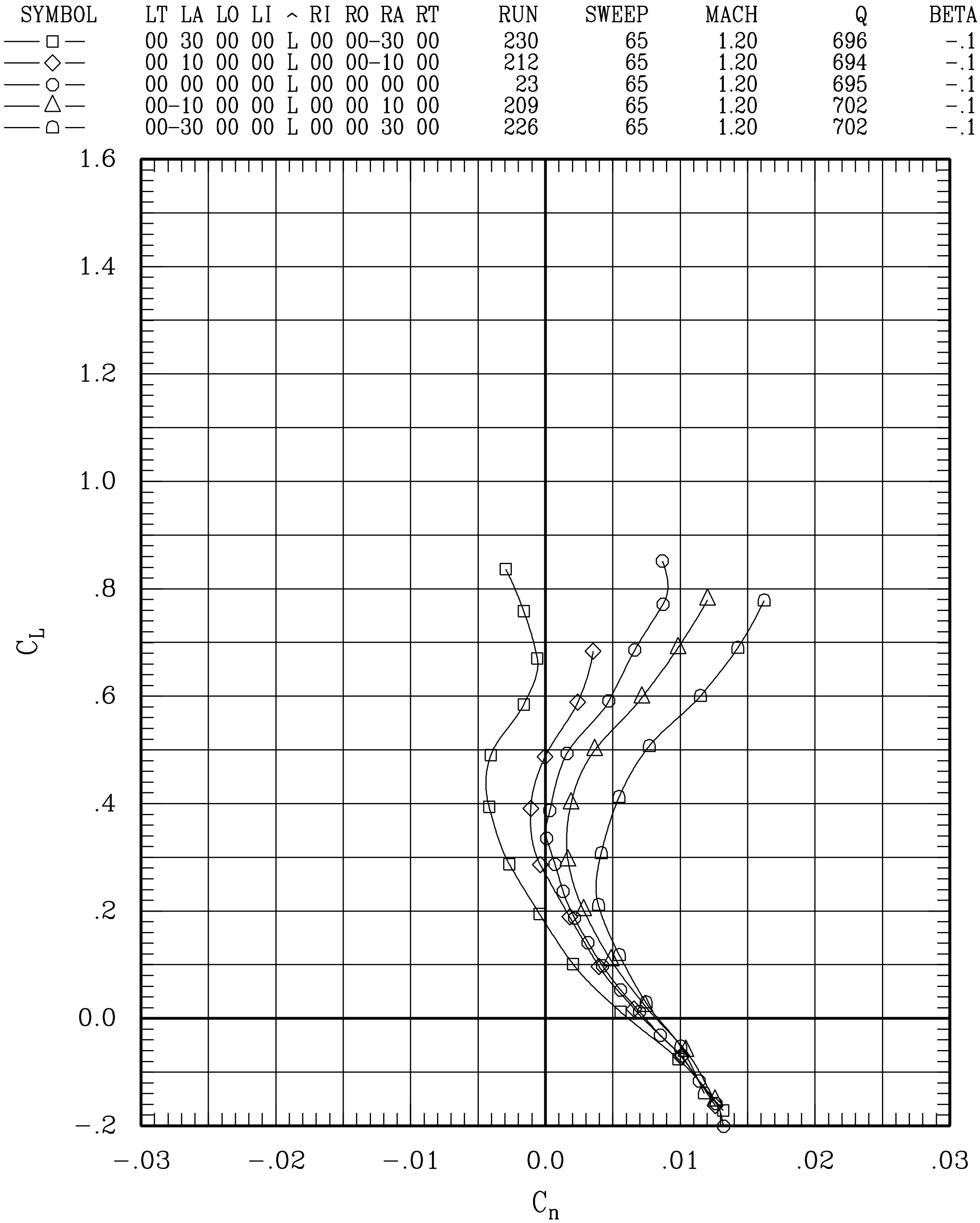

Figure 26(m). Effect of aileron deflection for sweep = 65 deg, Mach = 1.20 (Test #100).

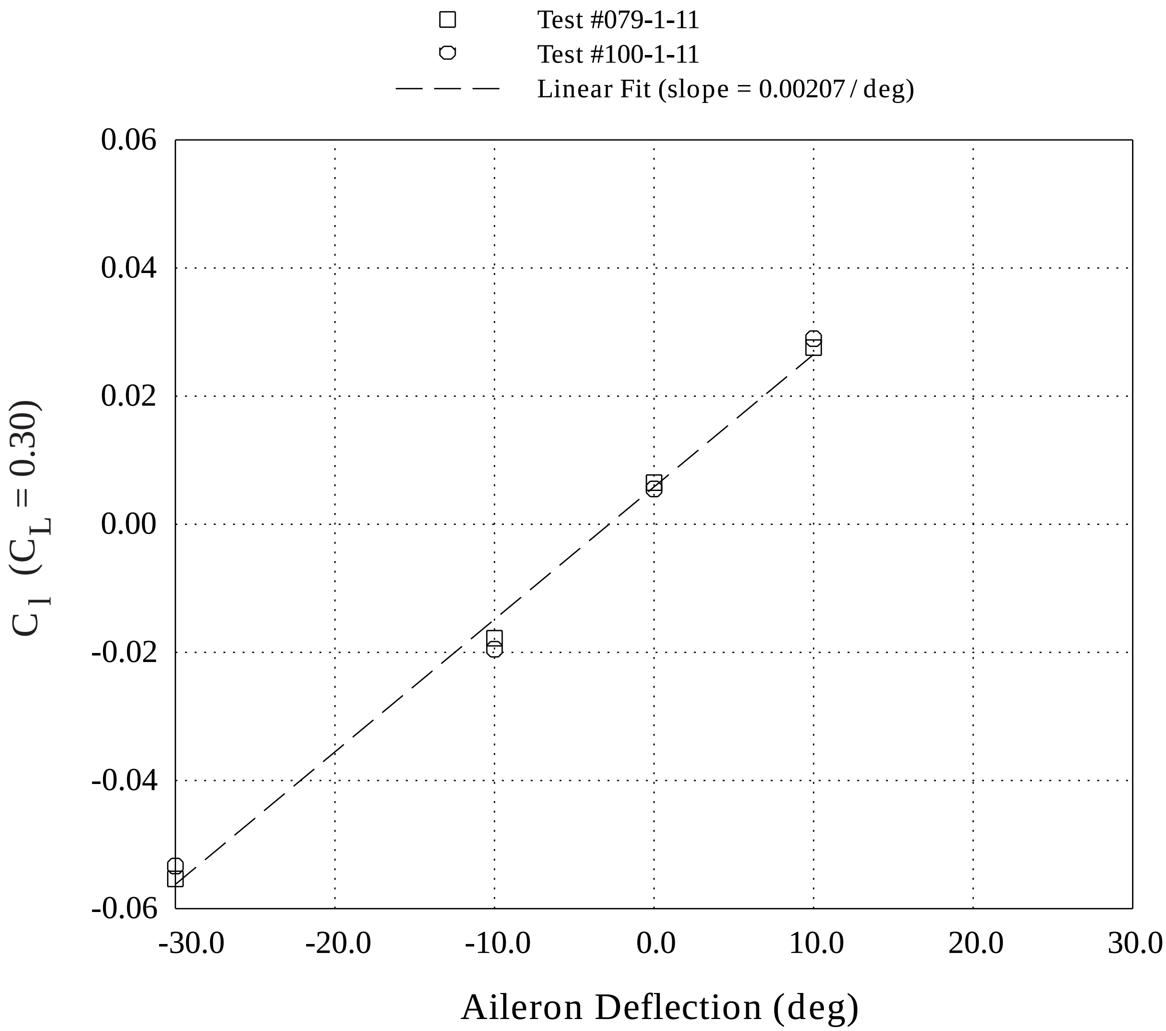

Figure 27(a). Aileron roll effectiveness for sweep = 30 deg, Mach = 0.80.

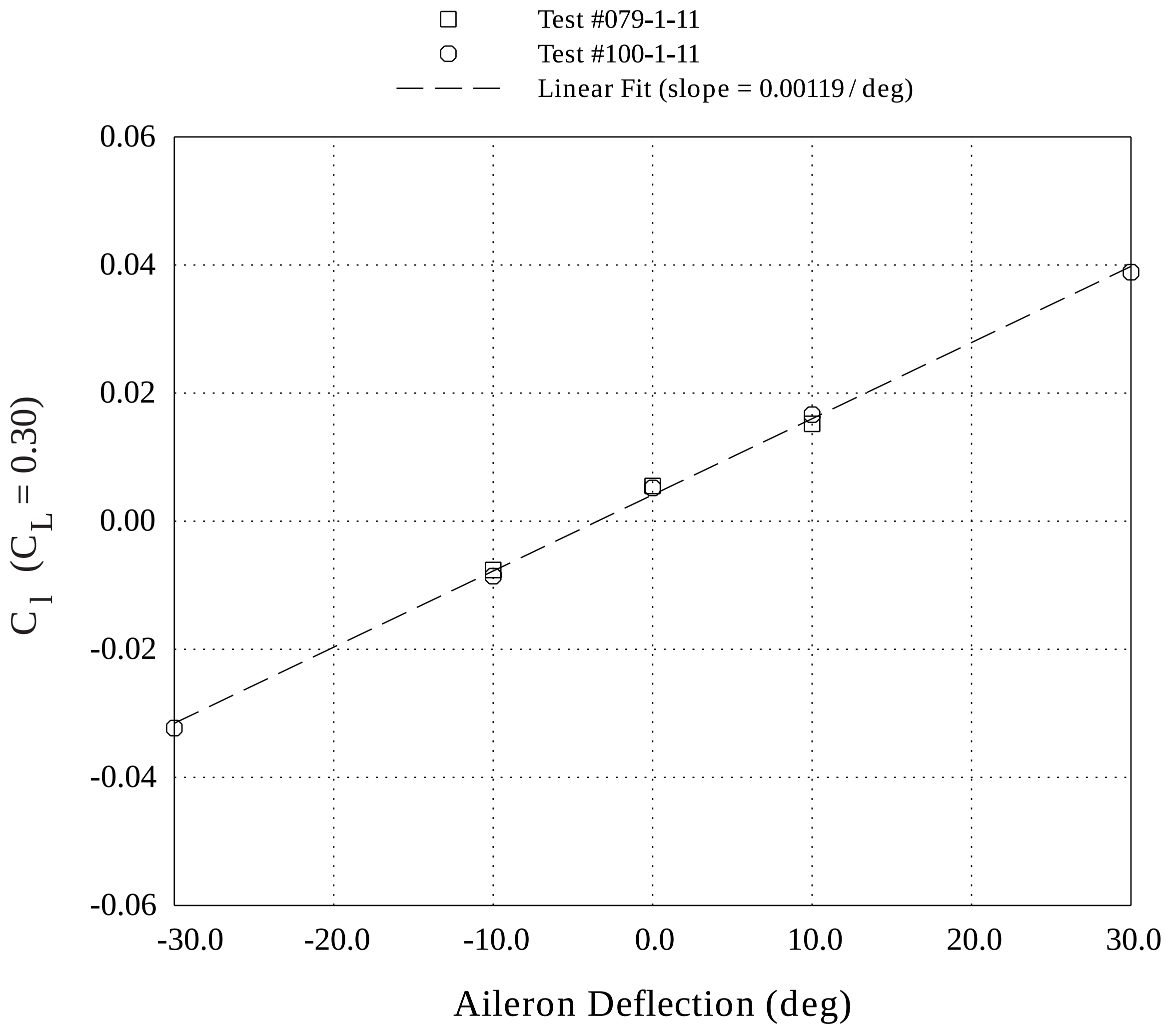

Figure 27(b). Aileron roll effectiveness for sweep = 45 deg, Mach = 0.80.

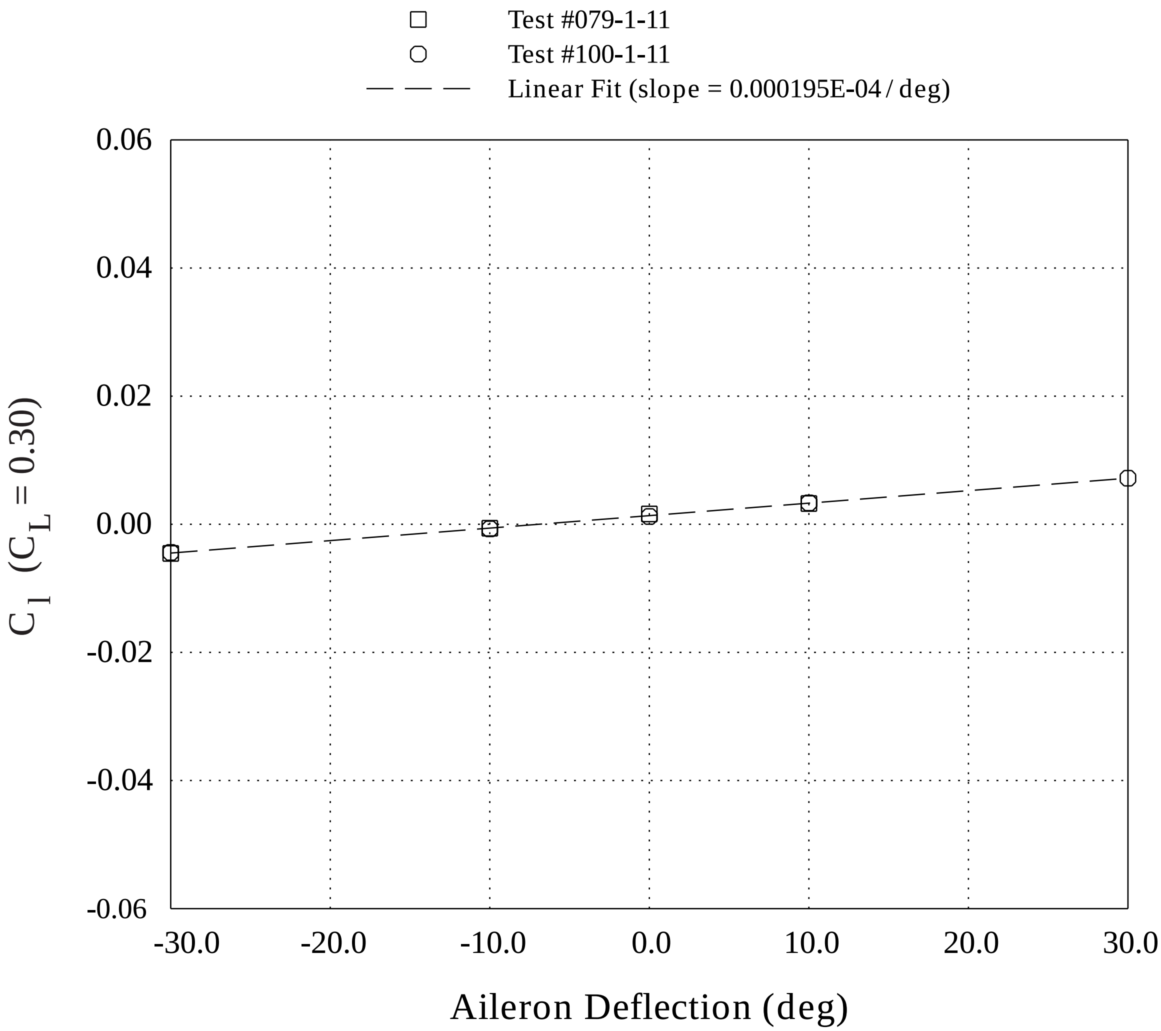

Figure 27(c). Aileron roll effectiveness for sweep = 65 deg, Mach = 1.20.

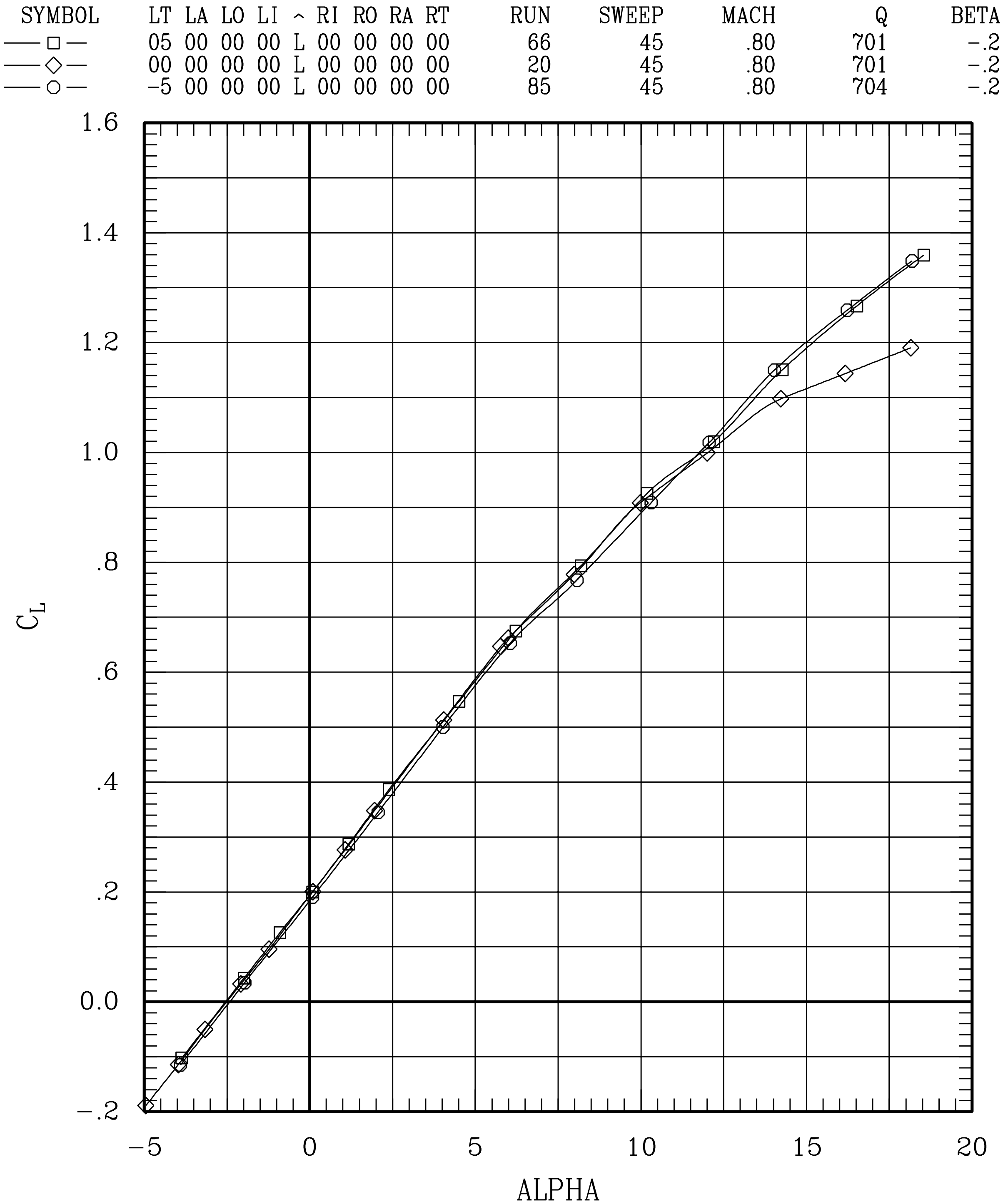

Figure 28(a). Left tip deflection for sweep = 45 deg, Mach = 0.80.

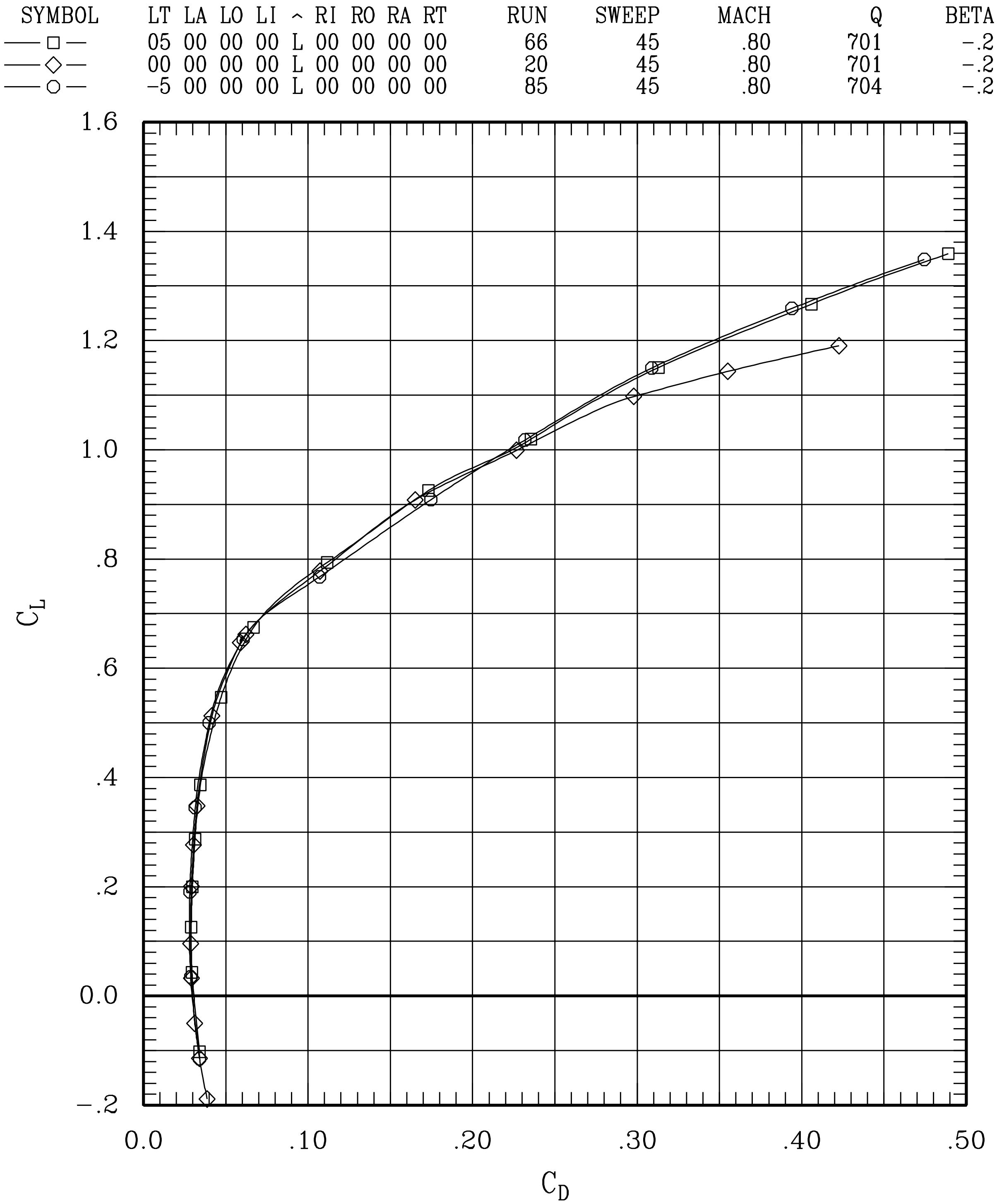

Figure 28(a). Left tip deflection for sweep = 45 deg, Mach = 0.80.

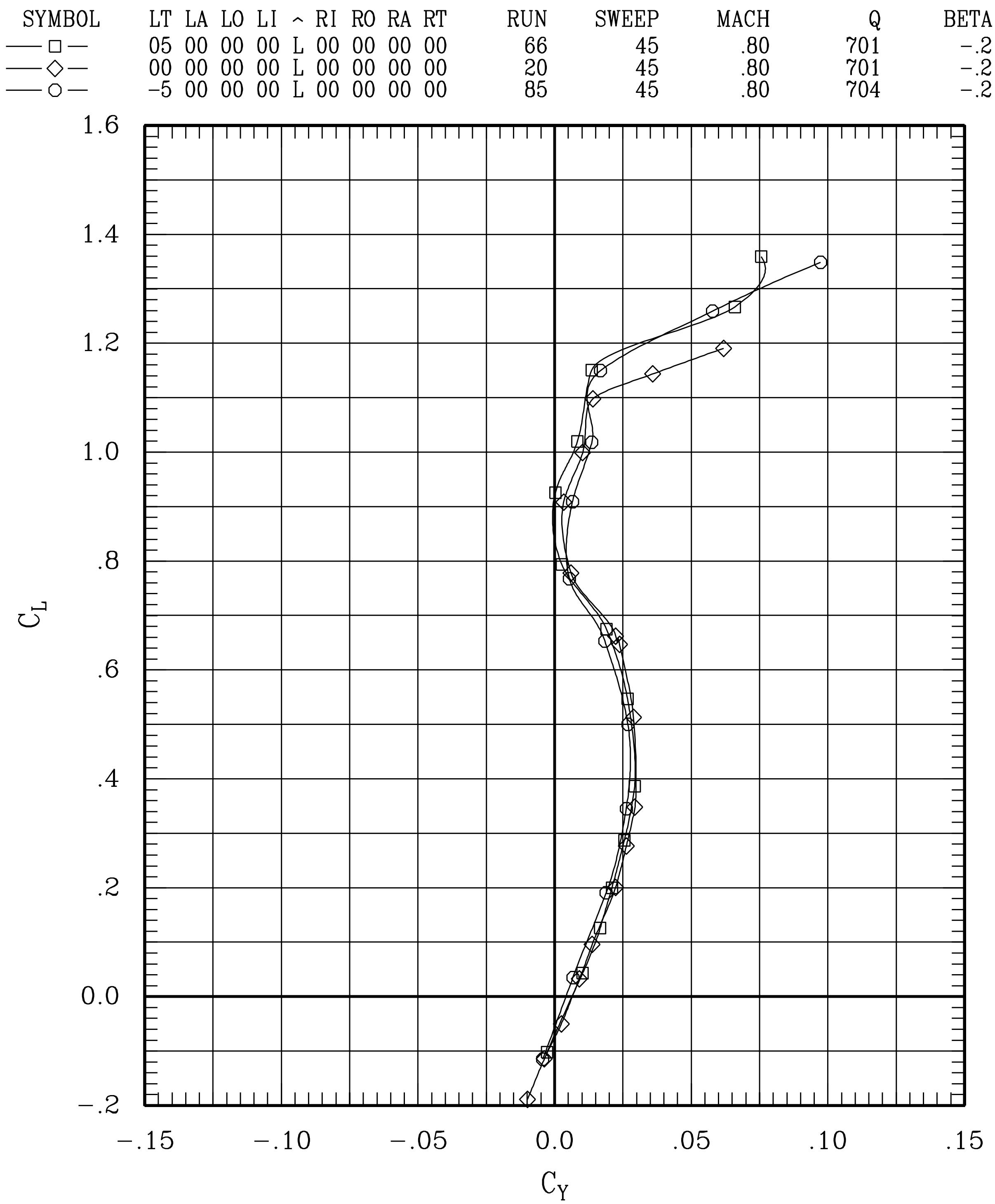

Figure 28(a). Left tip deflection for sweep = 45 deg, Mach = 0.80.

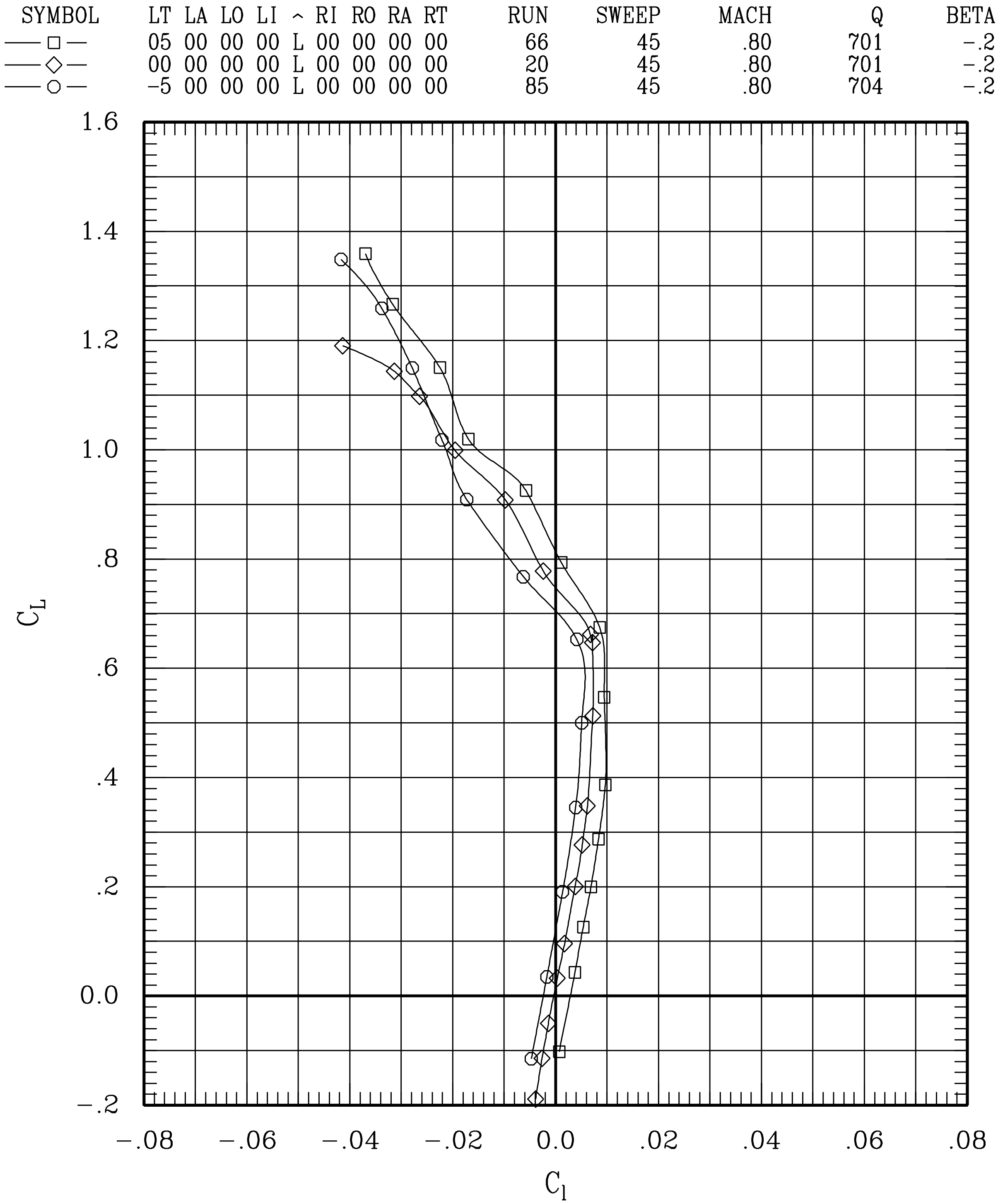

Figure 28(a). Left tip deflection for sweep = 45 deg, Mach = 0.80.

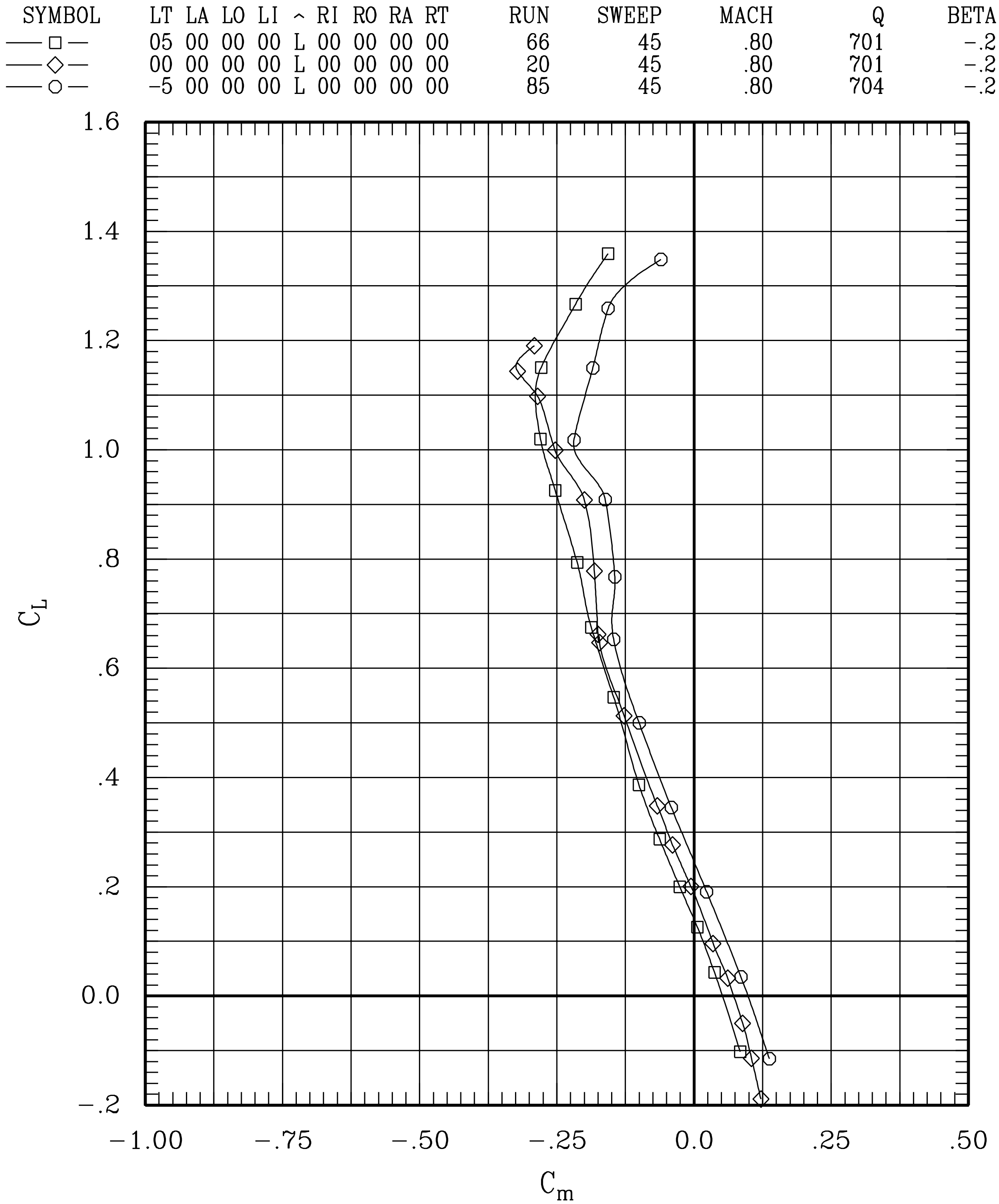

Figure 28(a). Left tip deflection for sweep = 45 deg, Mach = 0.80.

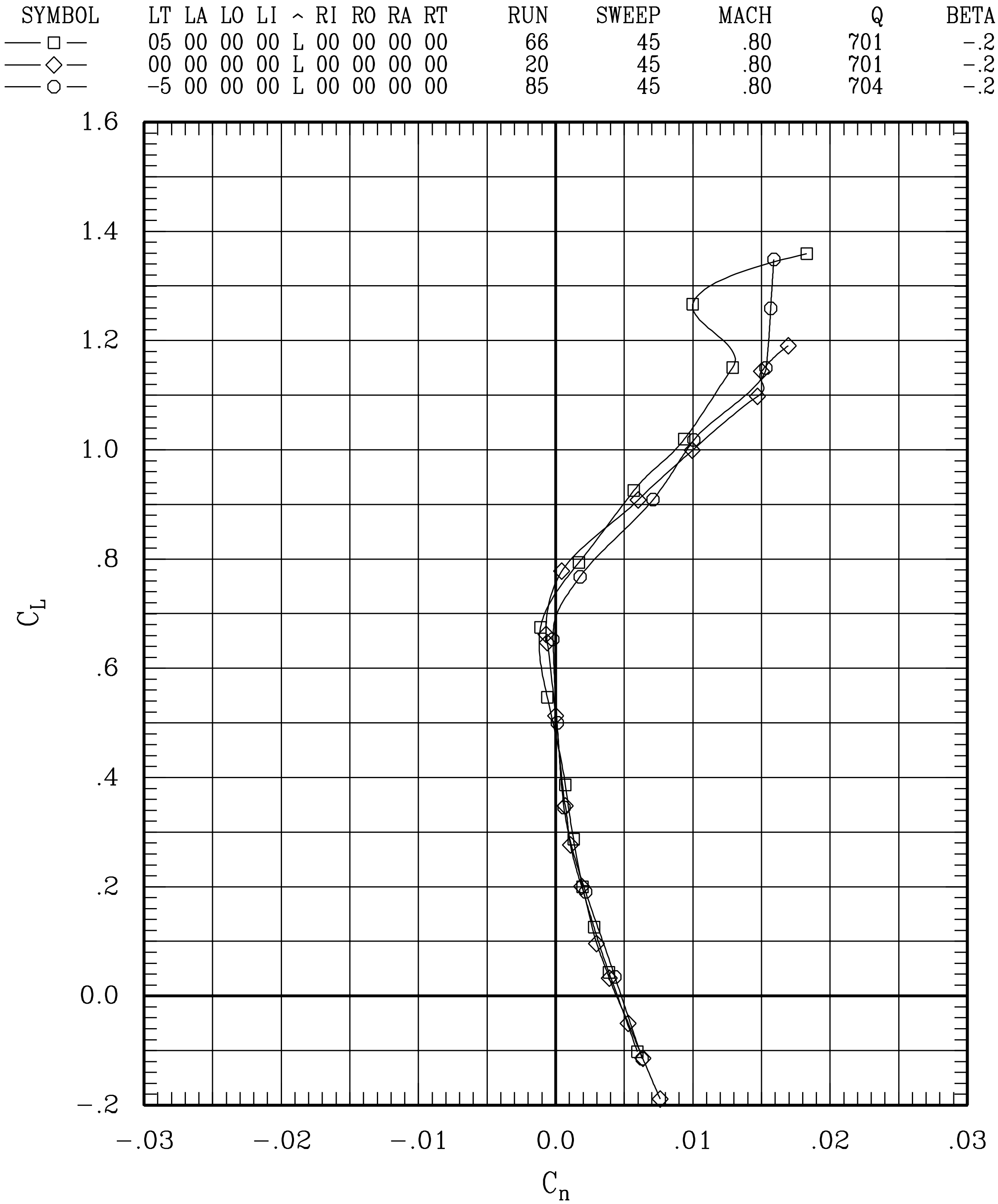

Figure 28(a). Left tip deflection for sweep = 45 deg, Mach = 0.80.

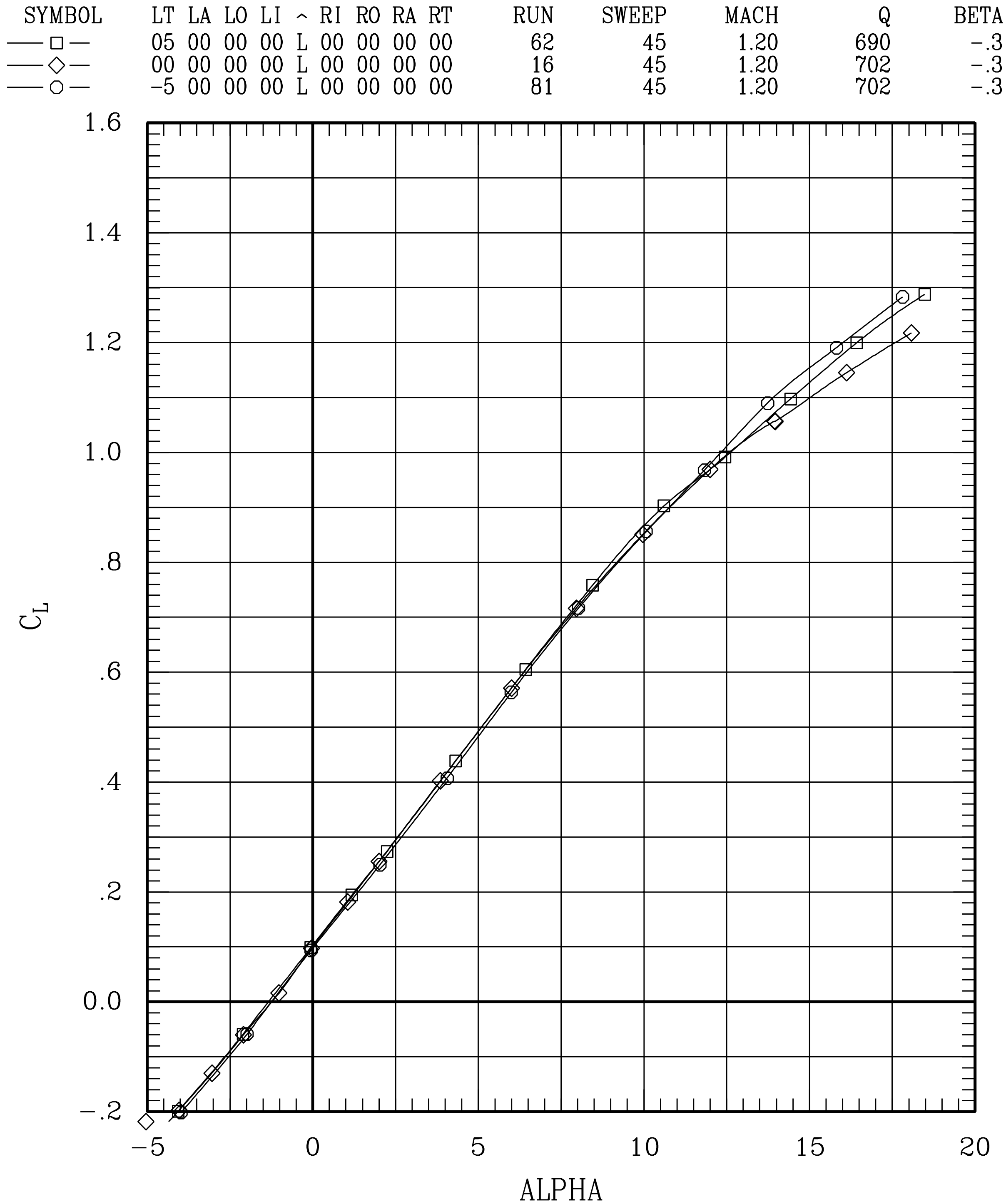

Figure 28(b). Left tip deflection for sweep = 45 deg, Mach = 1.20.

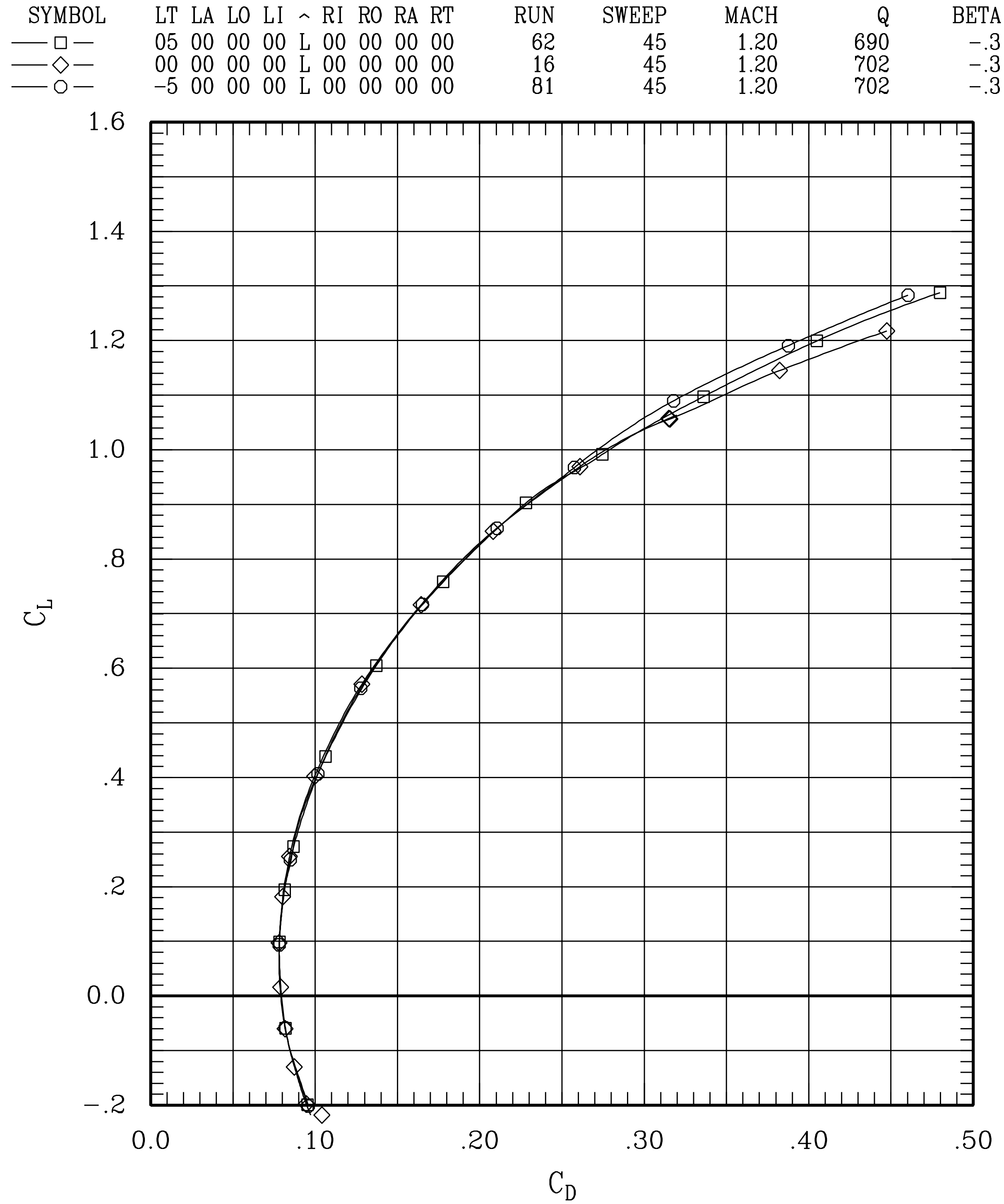

Figure 28(b). Left tip deflection for sweep = 45 deg, Mach = 1.20.

SYMBOL	LT LA LO LI ^ RI RO RA RT	RUN	SWEEP	MACH	Q	BETA
—□—	05 00 00 00 L 00 00 00 00	62	45	1.20	690	-.3
—◇—	00 00 00 00 L 00 00 00 00	16	45	1.20	702	-.3
—○—	-5 00 00 00 L 00 00 00 00	81	45	1.20	702	-.3

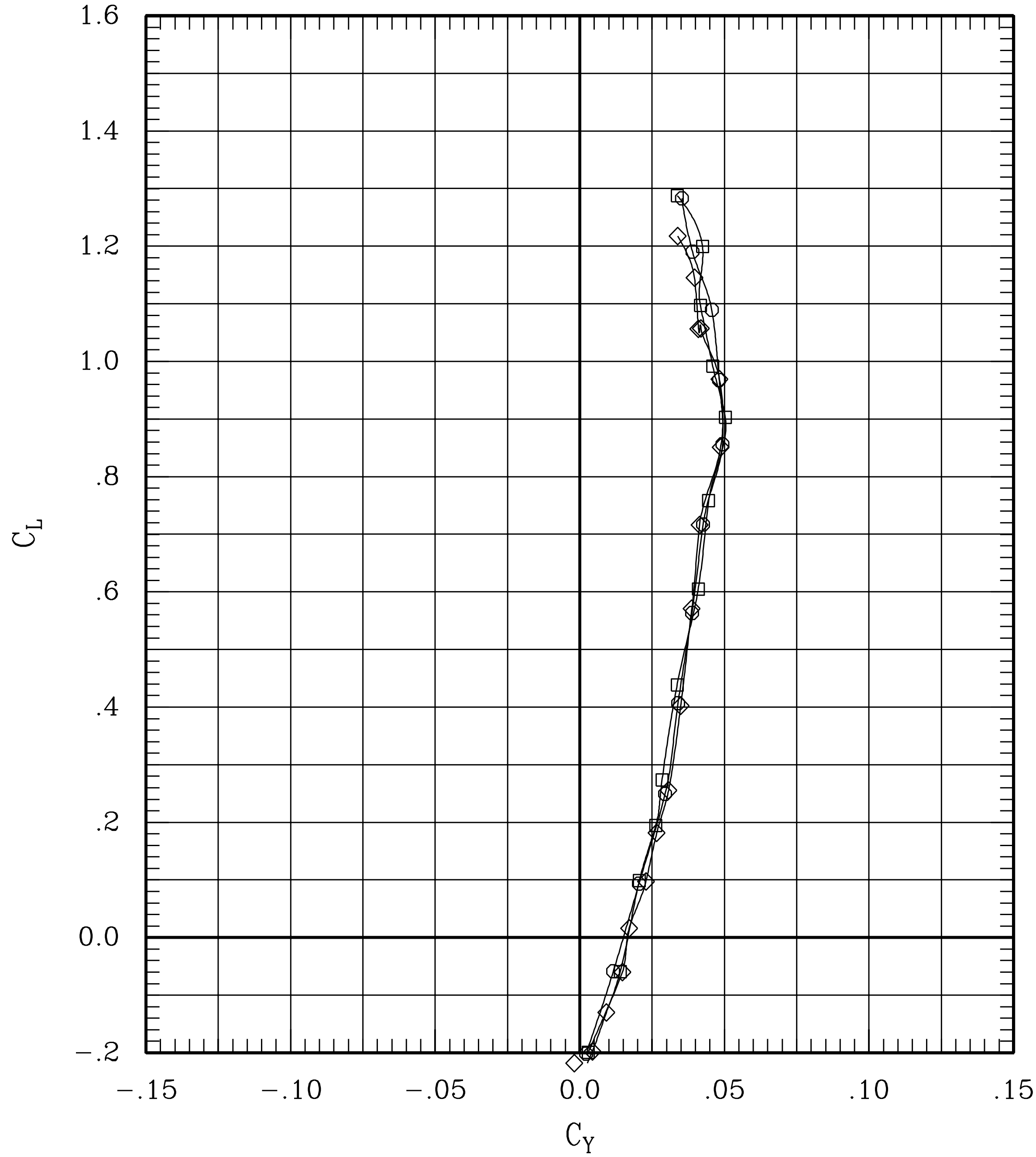

Figure 28(b). Left tip deflection for sweep = 45 deg, Mach = 1.20.

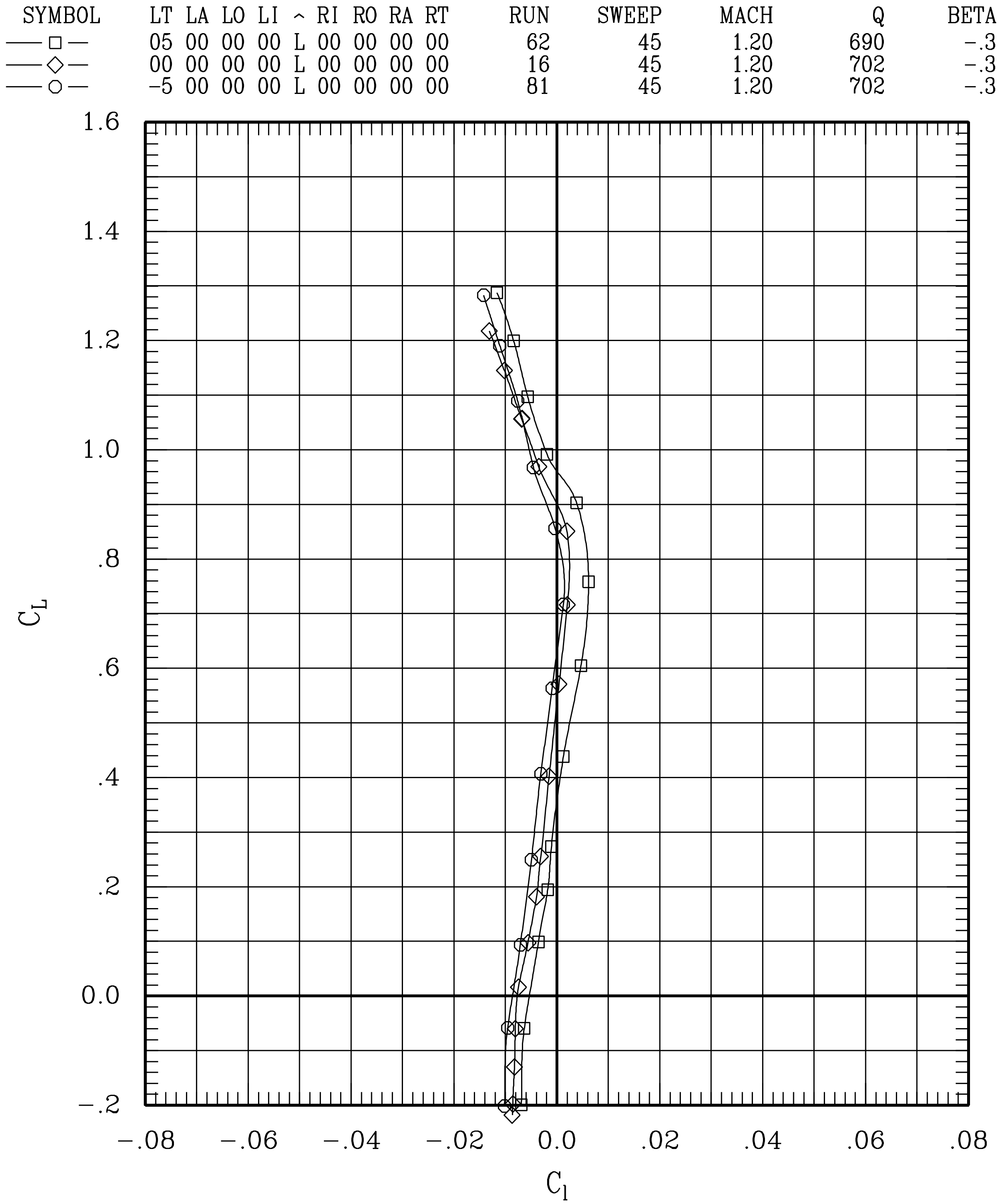

Figure 28(b). Left tip deflection for sweep = 45 deg, Mach = 1.20.

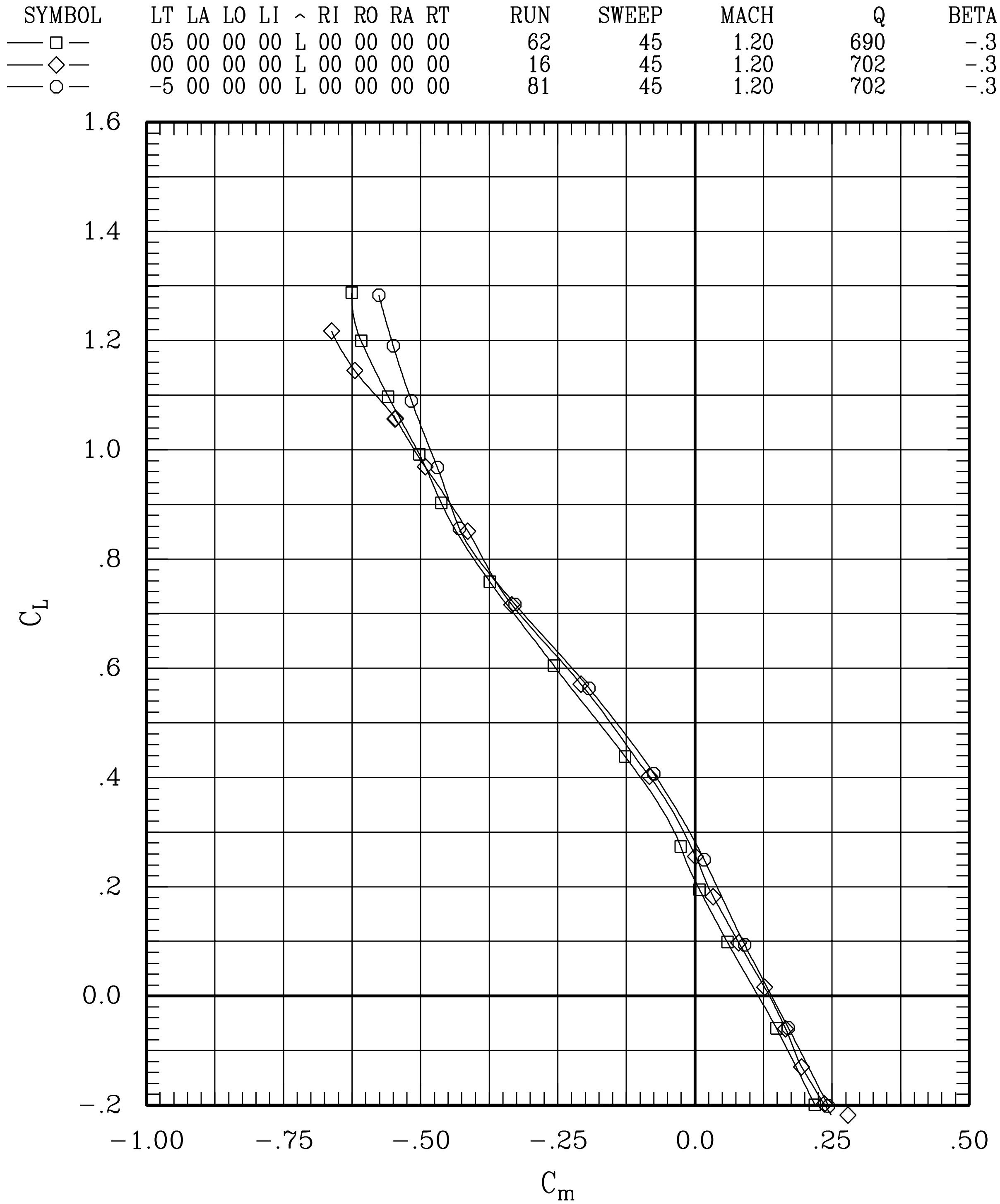

Figure 28(b). Left tip deflection for sweep = 45 deg, Mach = 1.20.

SYMBOL	LT	LA	LO	LI	^	RI	RO	RA	RT	RUN	SWEEP	MACH	Q	BETA
—□—	05	00	00	00	L	00	00	00	00	62	45	1.20	690	−.3
—◇—	00	00	00	00	L	00	00	00	00	16	45	1.20	702	−.3
—○—	−5	00	00	00	L	00	00	00	00	81	45	1.20	702	−.3

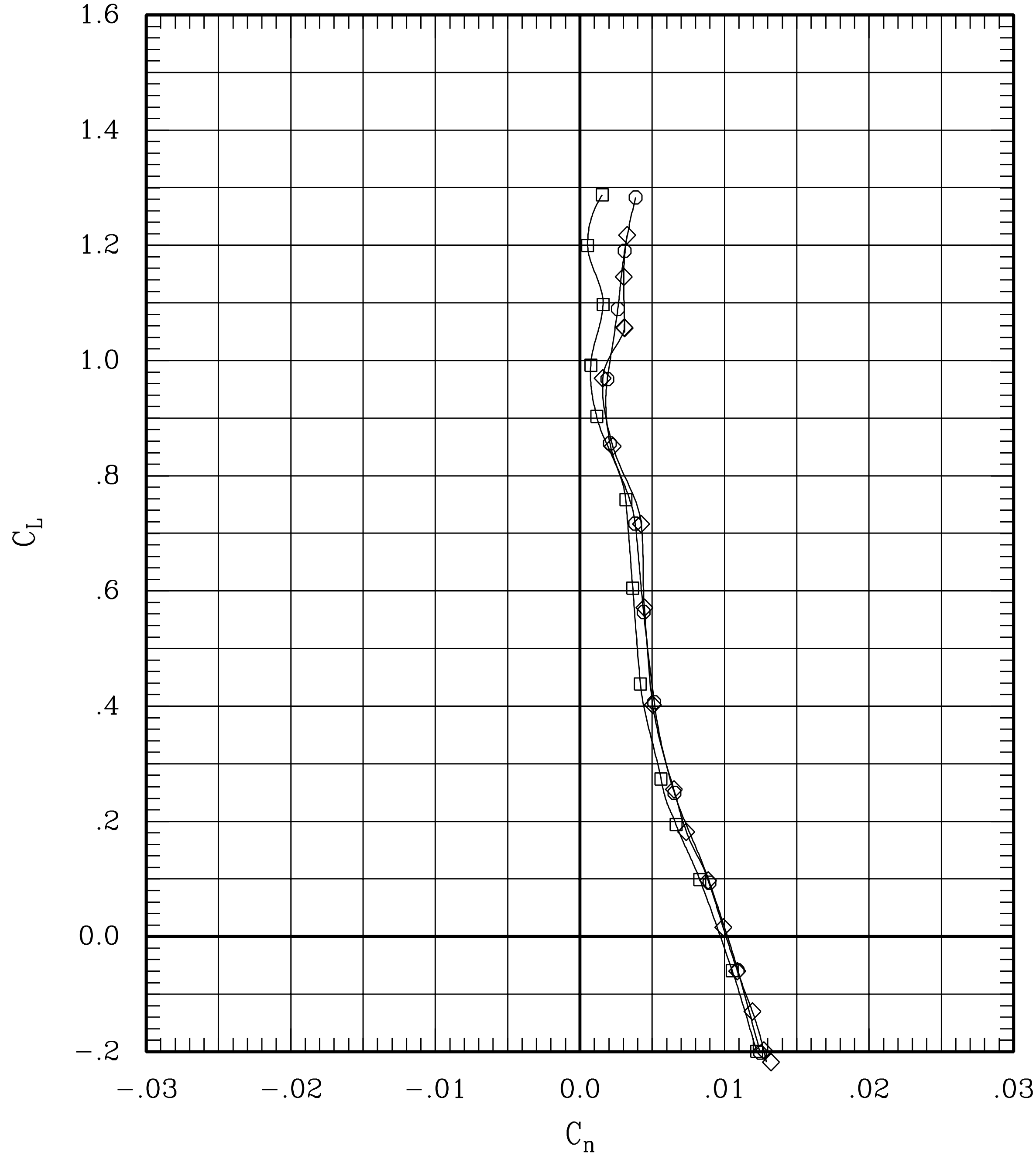

Figure 28(b). Left tip deflection for sweep = 45 deg, Mach = 1.20.

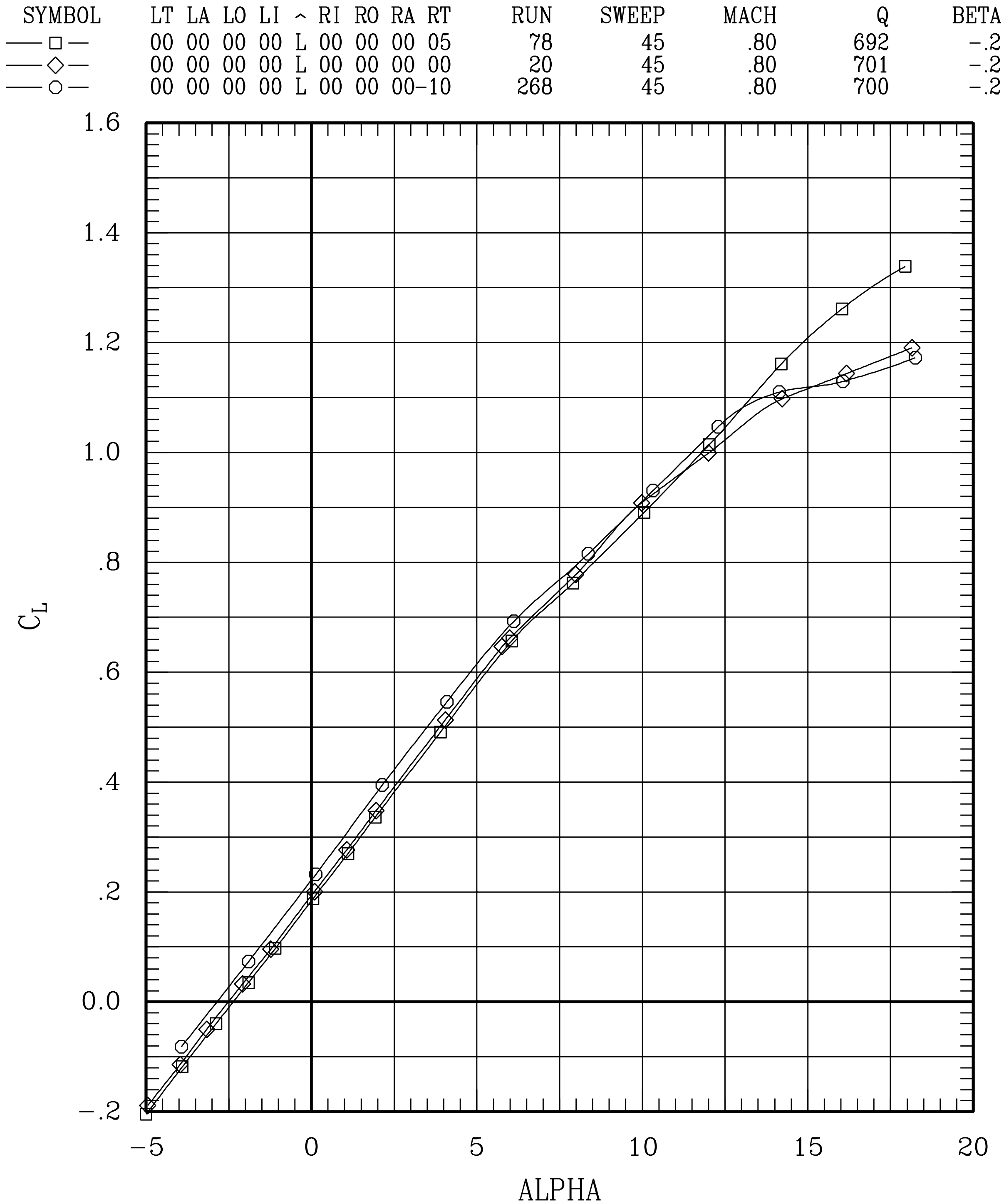

Figure 28(c). Right tip deflection for sweep = 45 deg, Mach = 0.80.

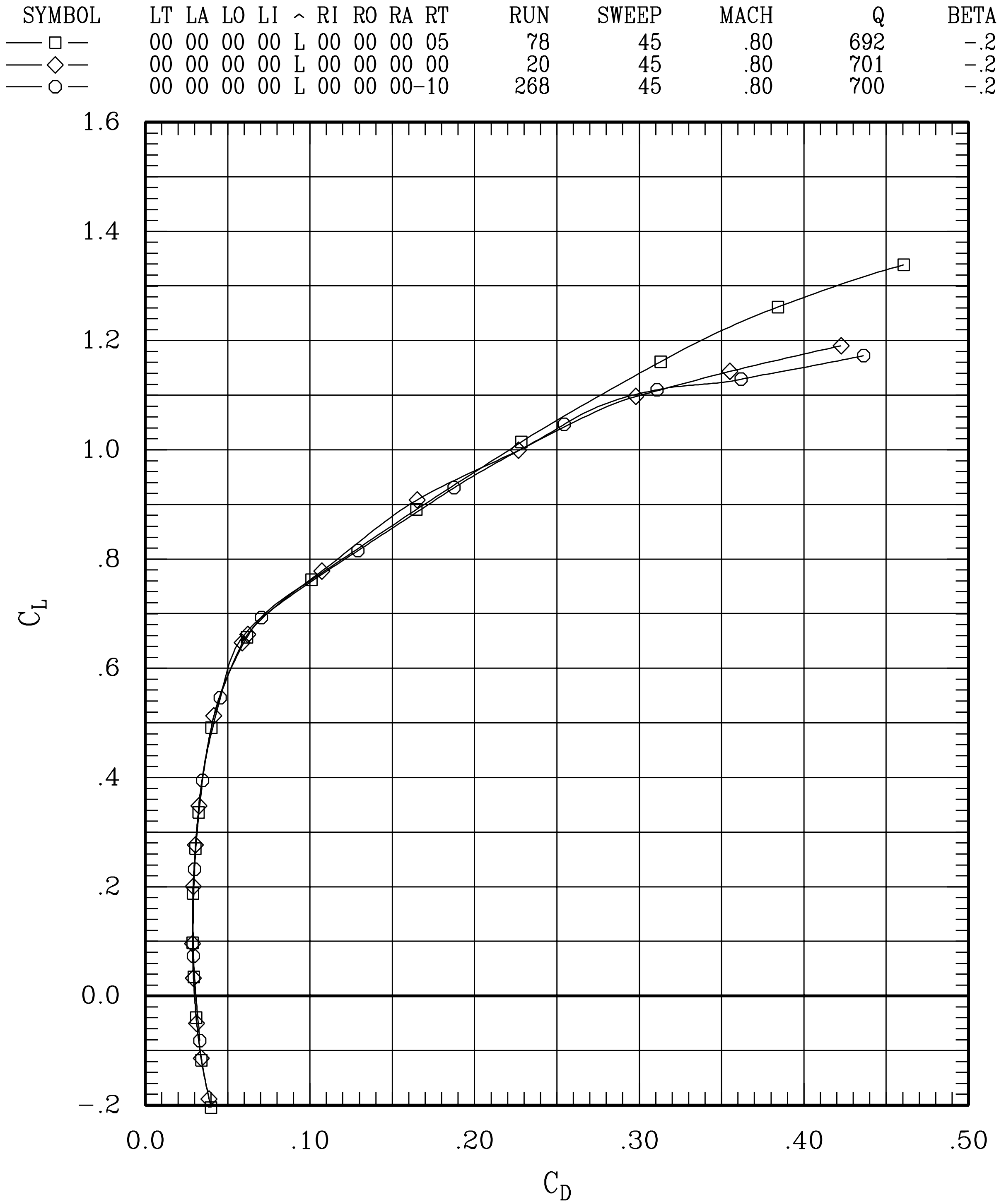

Figure 28(c). Right tip deflection for sweep = 45 deg, Mach = 0.80.

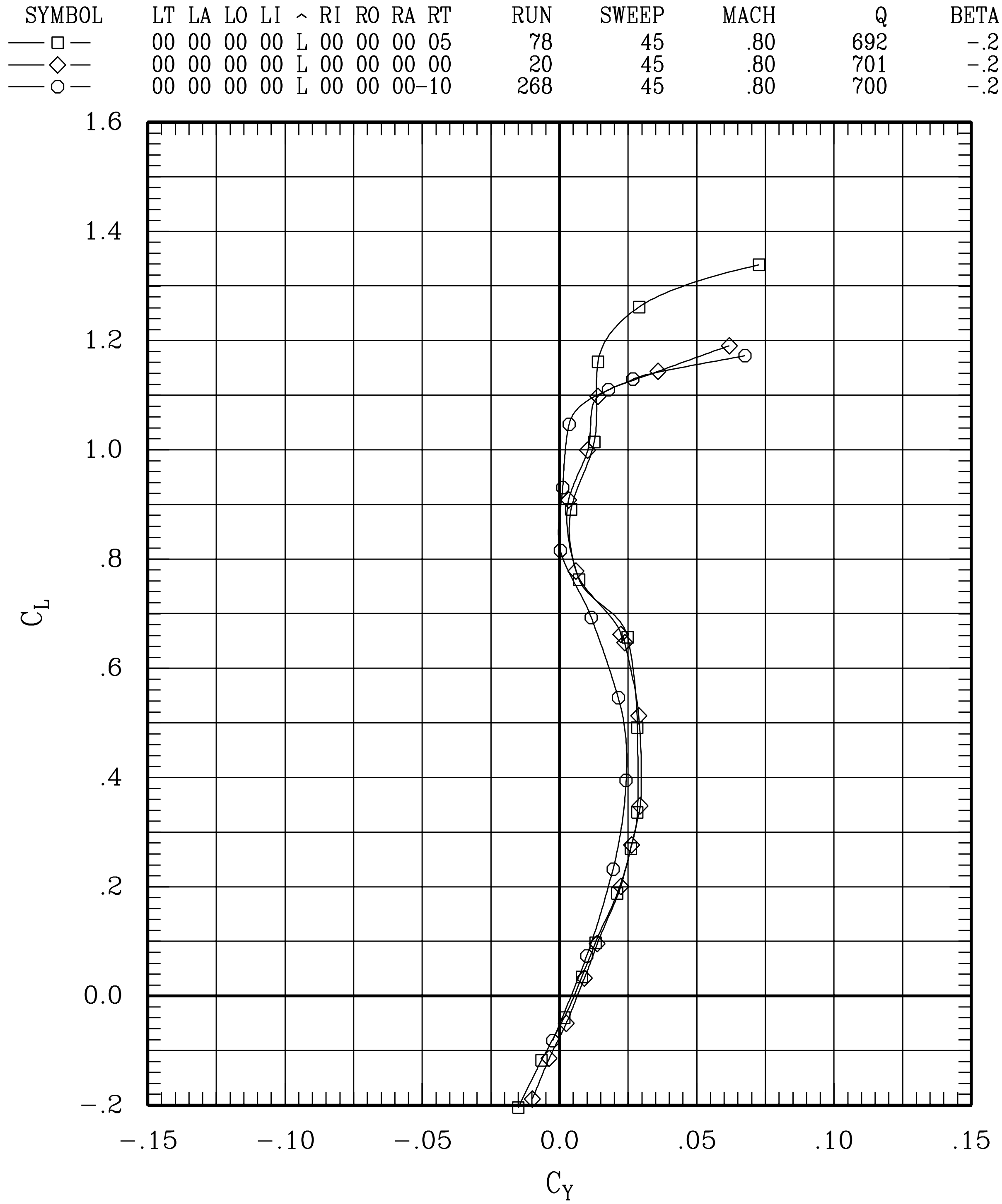

Figure 28(c). Right tip deflection for sweep = 45 deg, Mach = 0.80.

SYMBOL	LT LA LO LI ^ RI RO RA RT	RUN	SWEEP	MACH	Q	BETA
—□—	00 00 00 00 L 00 00 00 05	78	45	.80	692	−.2
—◇—	00 00 00 00 L 00 00 00 00	20	45	.80	701	−.2
—○—	00 00 00 00 L 00 00 00−10	268	45	.80	700	−.2

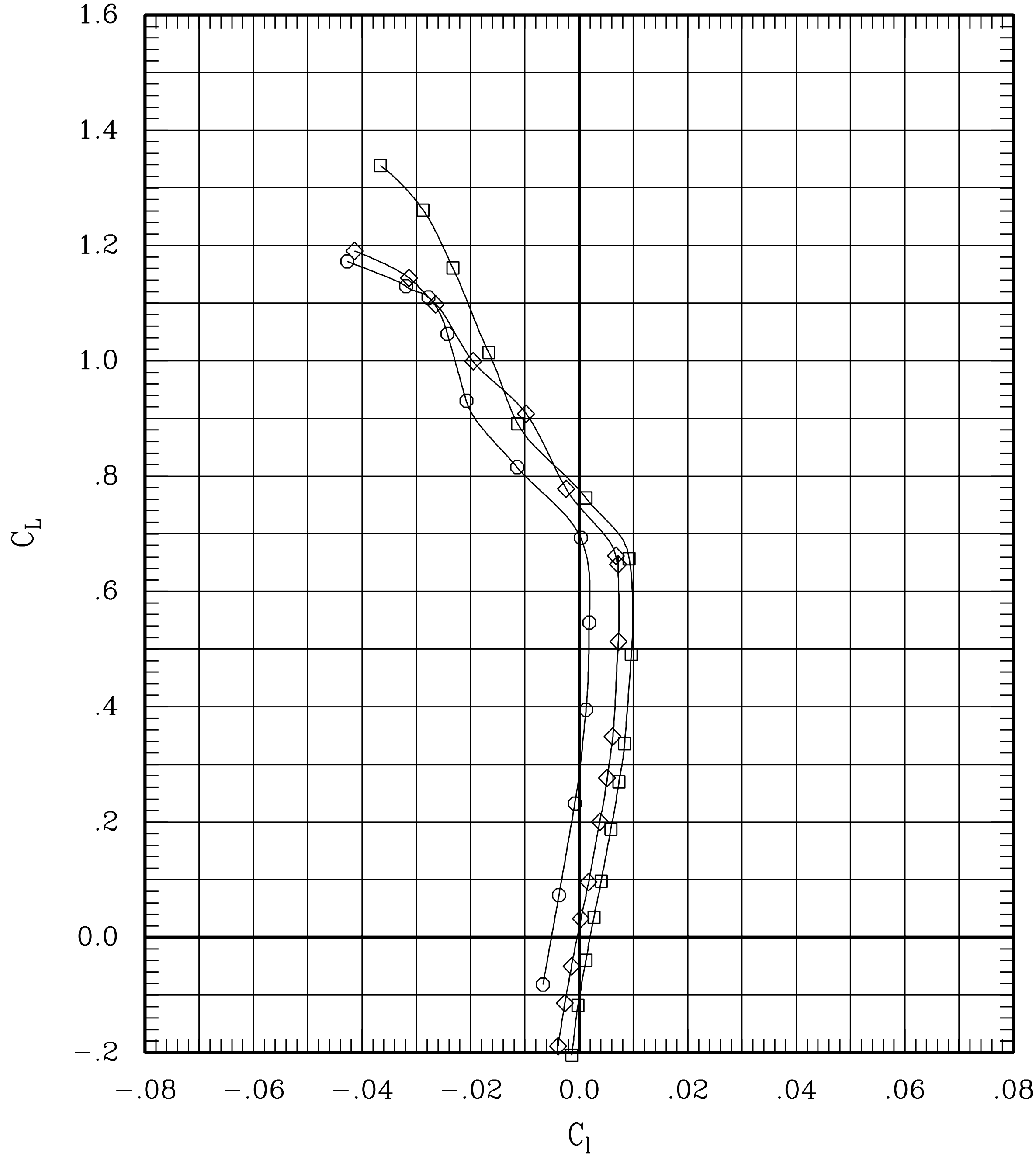

Figure 28(c). Right tip deflection for sweep = 45 deg, Mach = 0.80.

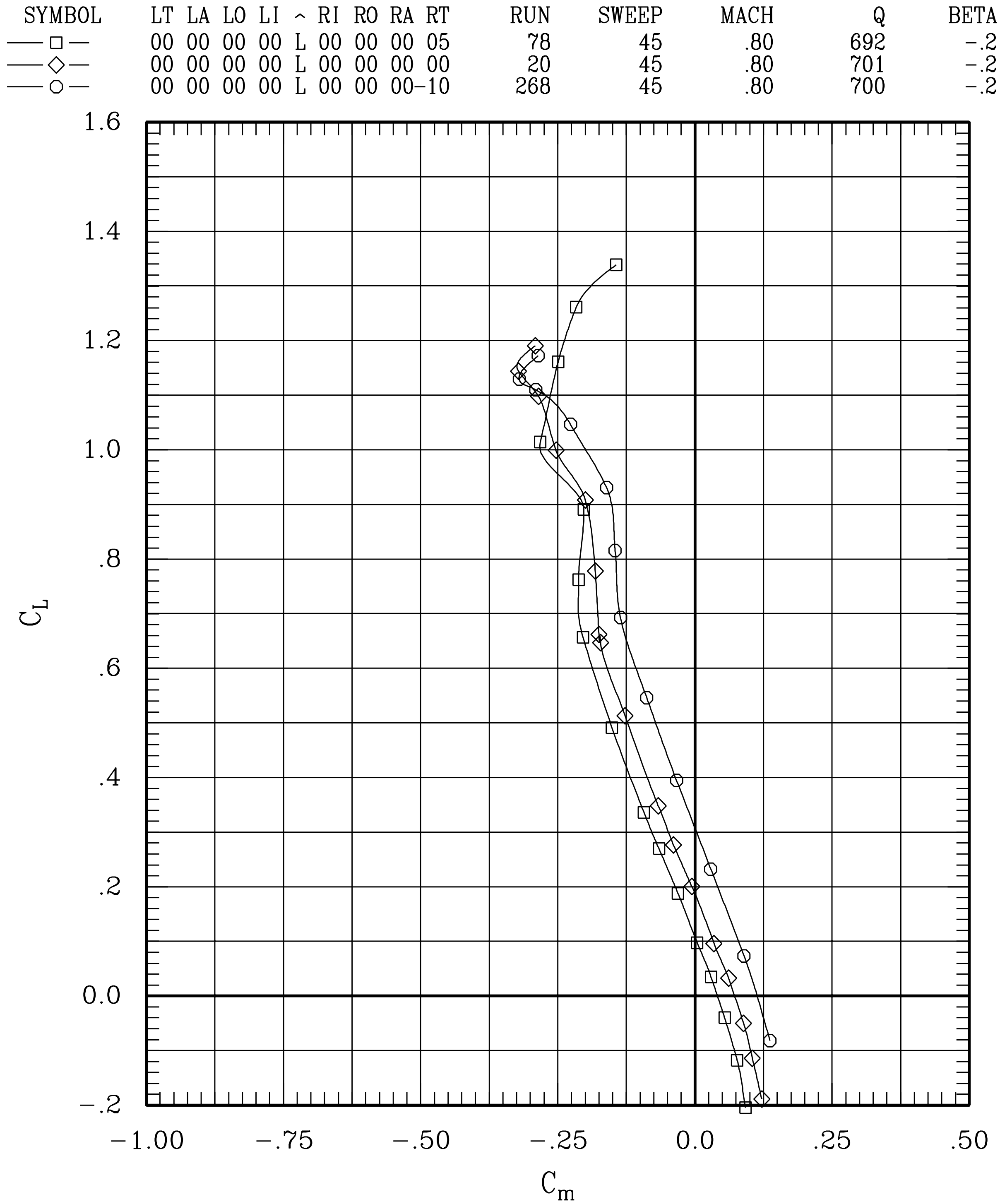

Figure 28(c). Right tip deflection for sweep = 45 deg, Mach = 0.80.

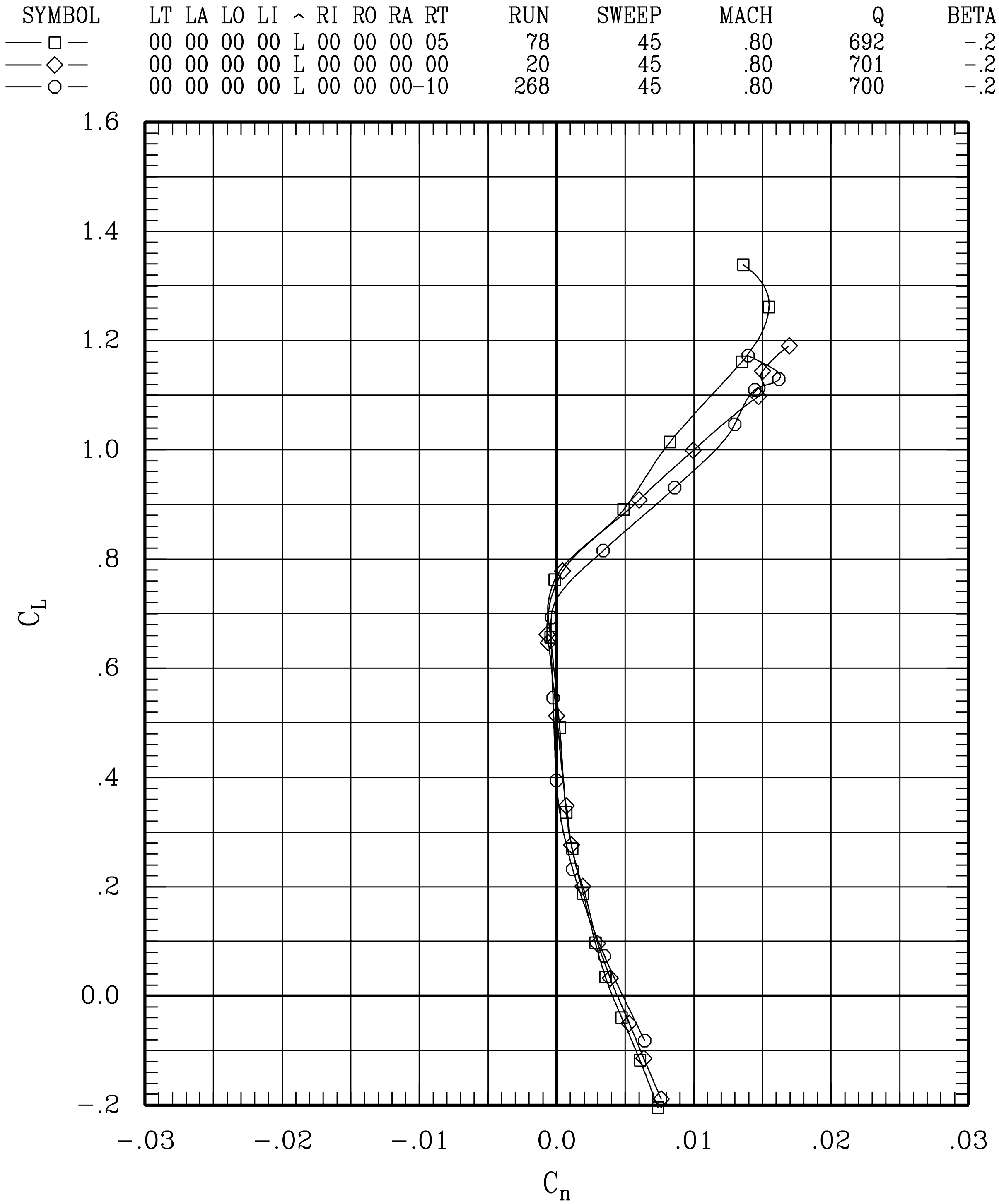

Figure 28(c). Right tip deflection for sweep = 45 deg, Mach = 0.80.

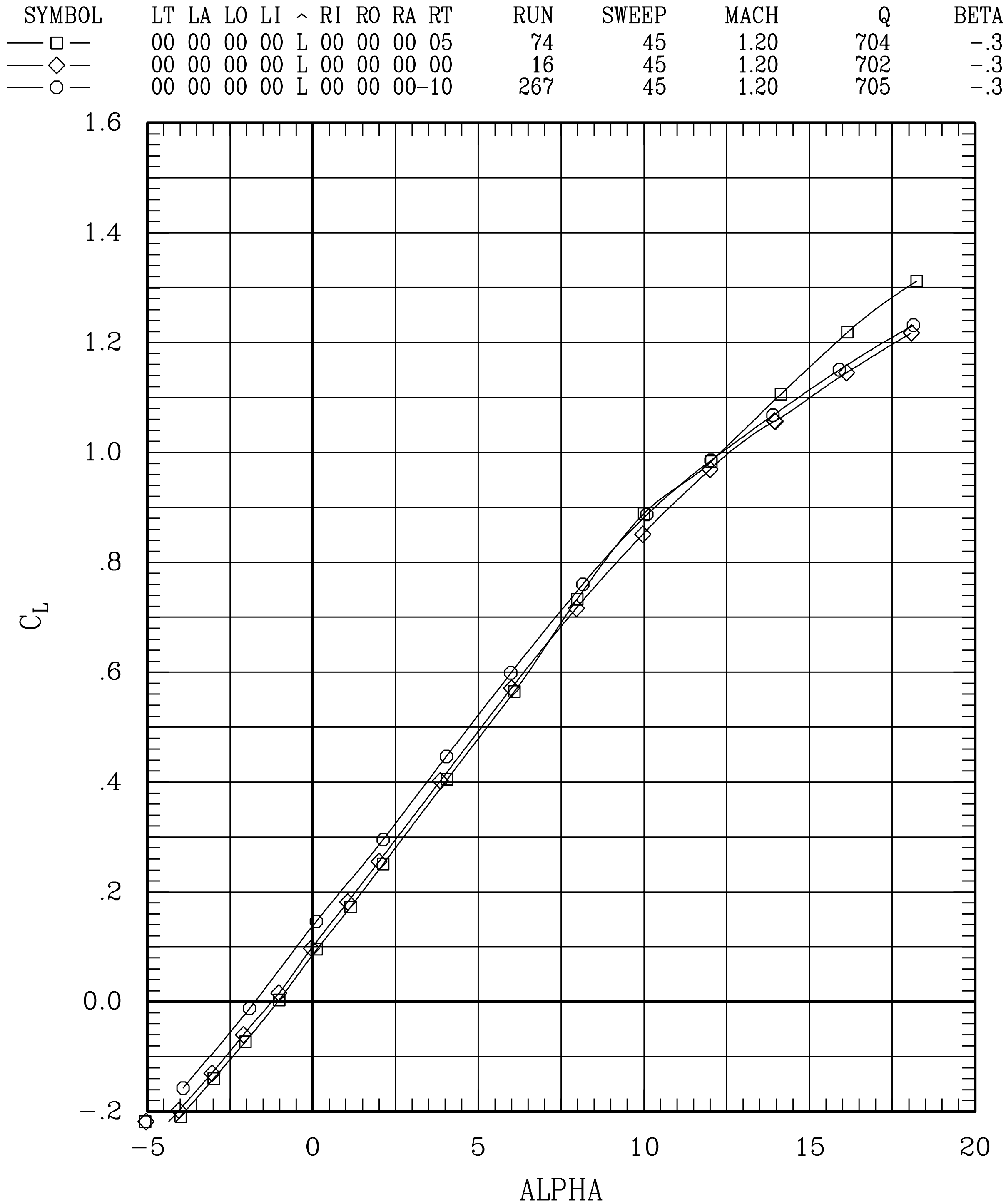

Figure 28(d). Right tip deflection for sweep = 45 deg, Mach = 1.20.

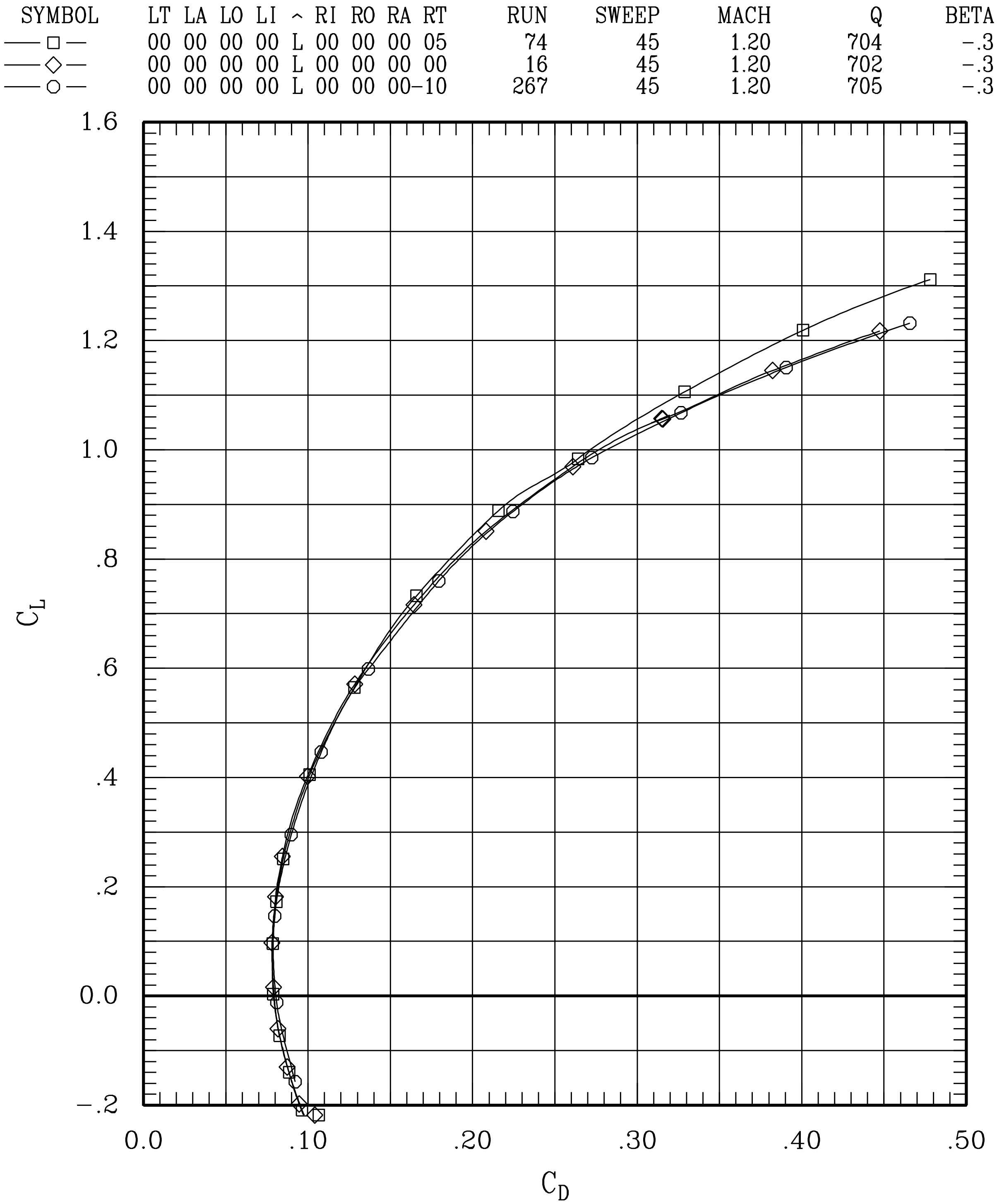

Figure 28(d). Right tip deflection for sweep = 45 deg, Mach = 1.20.

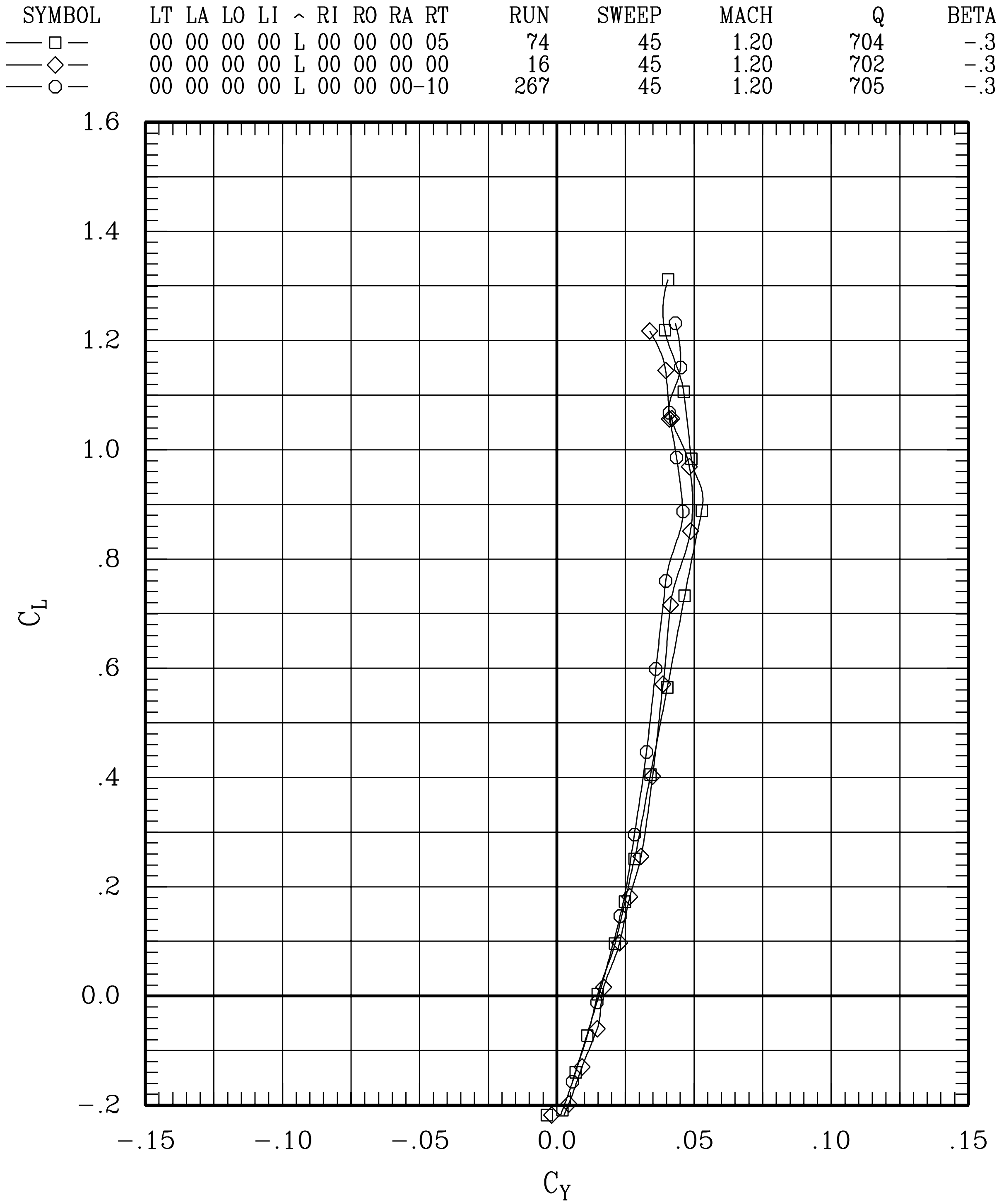

Figure 28(d). Right tip deflection for sweep = 45 deg, Mach = 1.20.

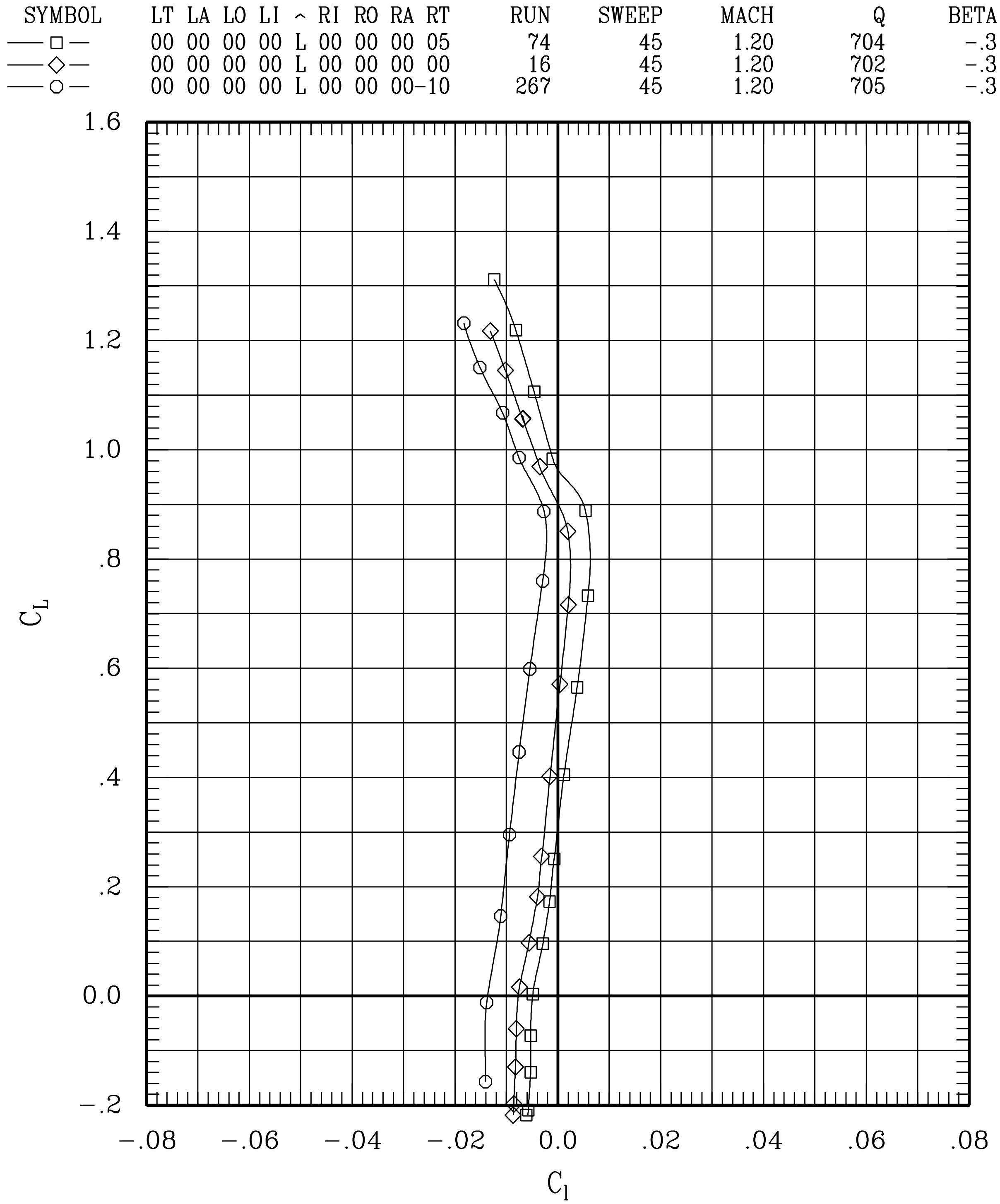

Figure 28(d). Right tip deflection for sweep = 45 deg, Mach = 1.20.

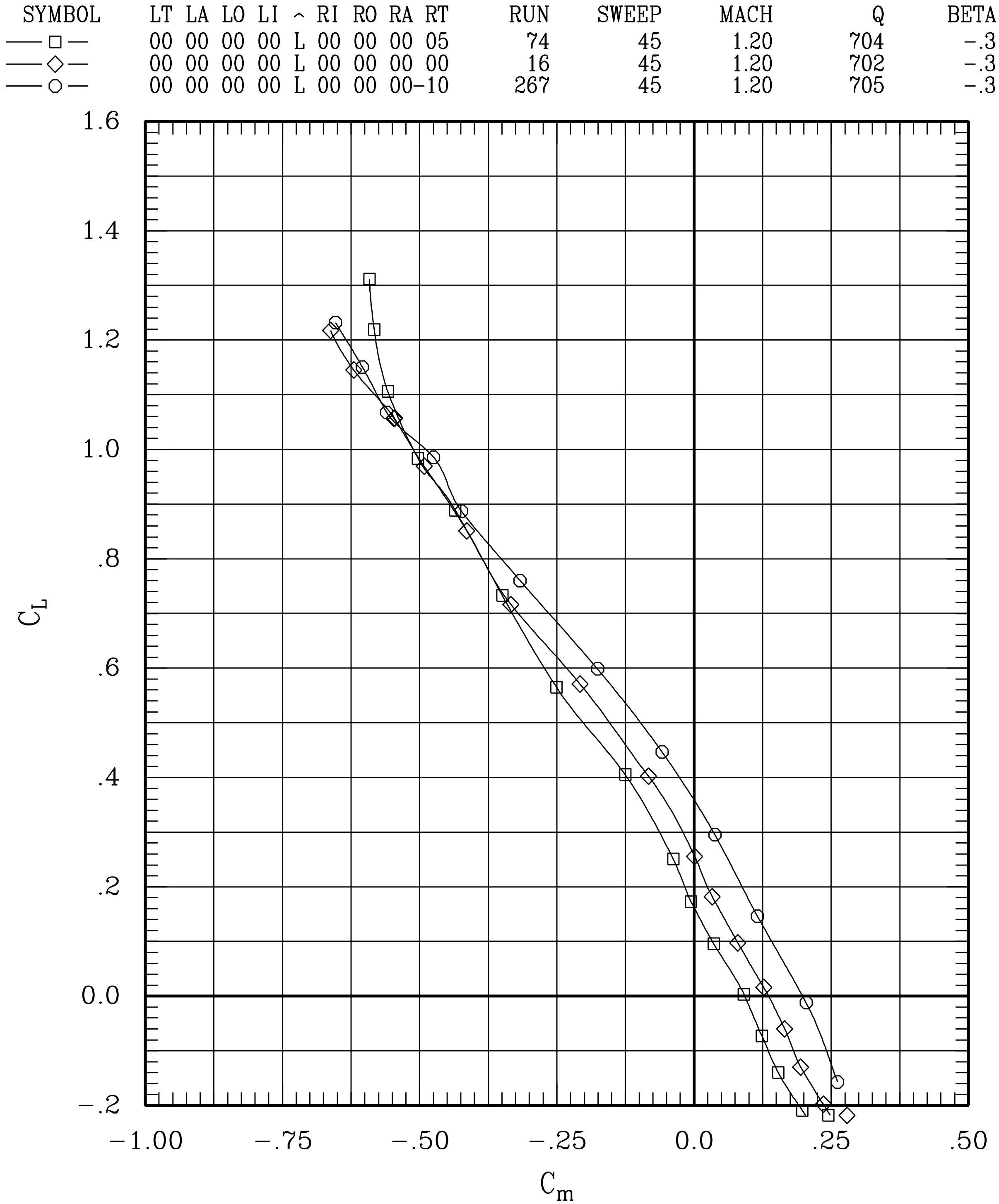

Figure 28(d). Right tip deflection for sweep = 45 deg, Mach = 1.20.

SYMBOL	LT LA LO LI ^ RI RO RA RT	RUN	SWEEP	MACH	Q	BETA
—□—	00 00 00 00 L 00 00 00 05	74	45	1.20	704	-.3
—◇—	00 00 00 00 L 00 00 00 00	16	45	1.20	702	-.3
—○—	00 00 00 00 L 00 00 00-10	267	45	1.20	705	-.3

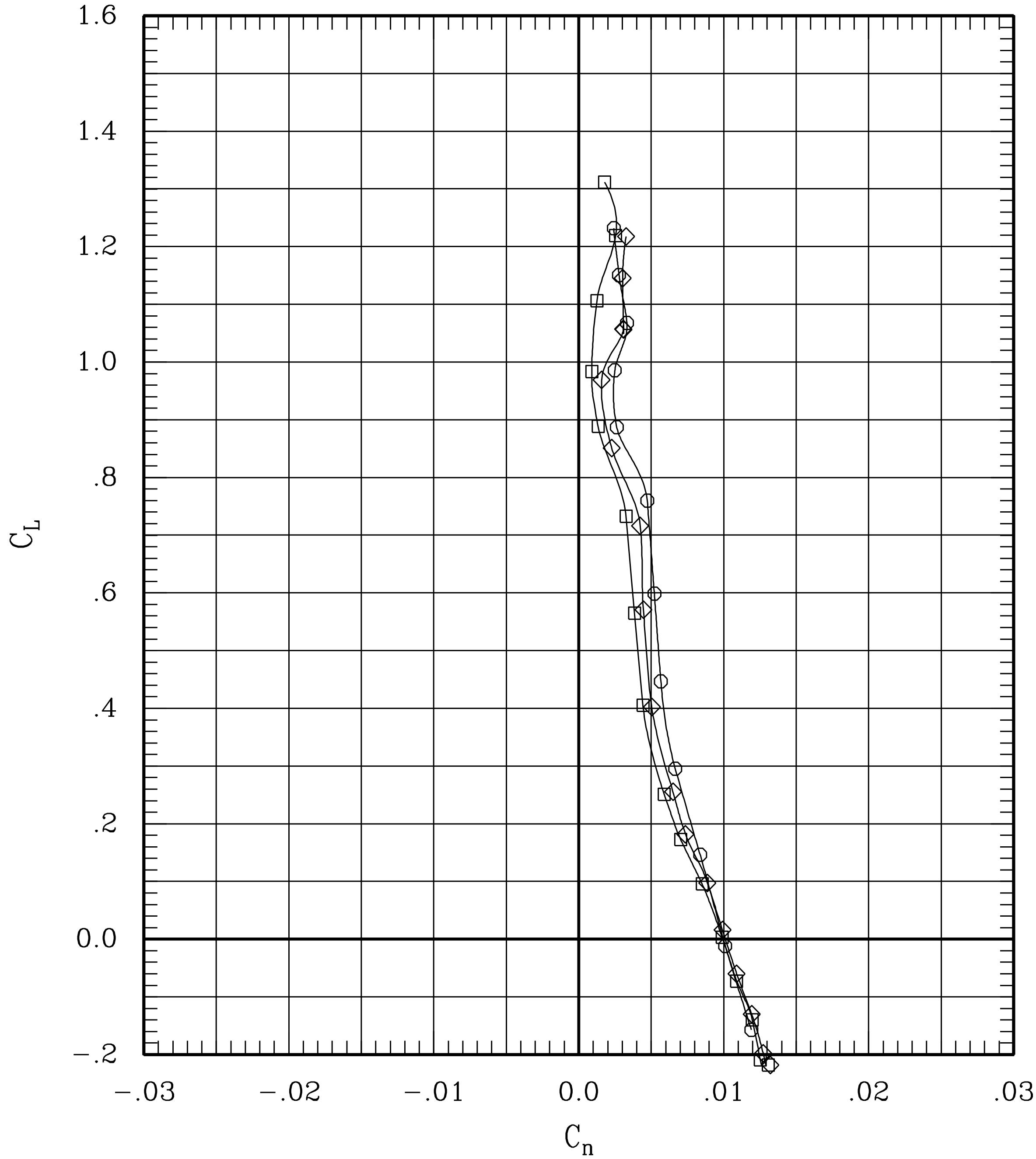

Figure 28(d). Right tip deflection for sweep = 45 deg, Mach = 1.20.

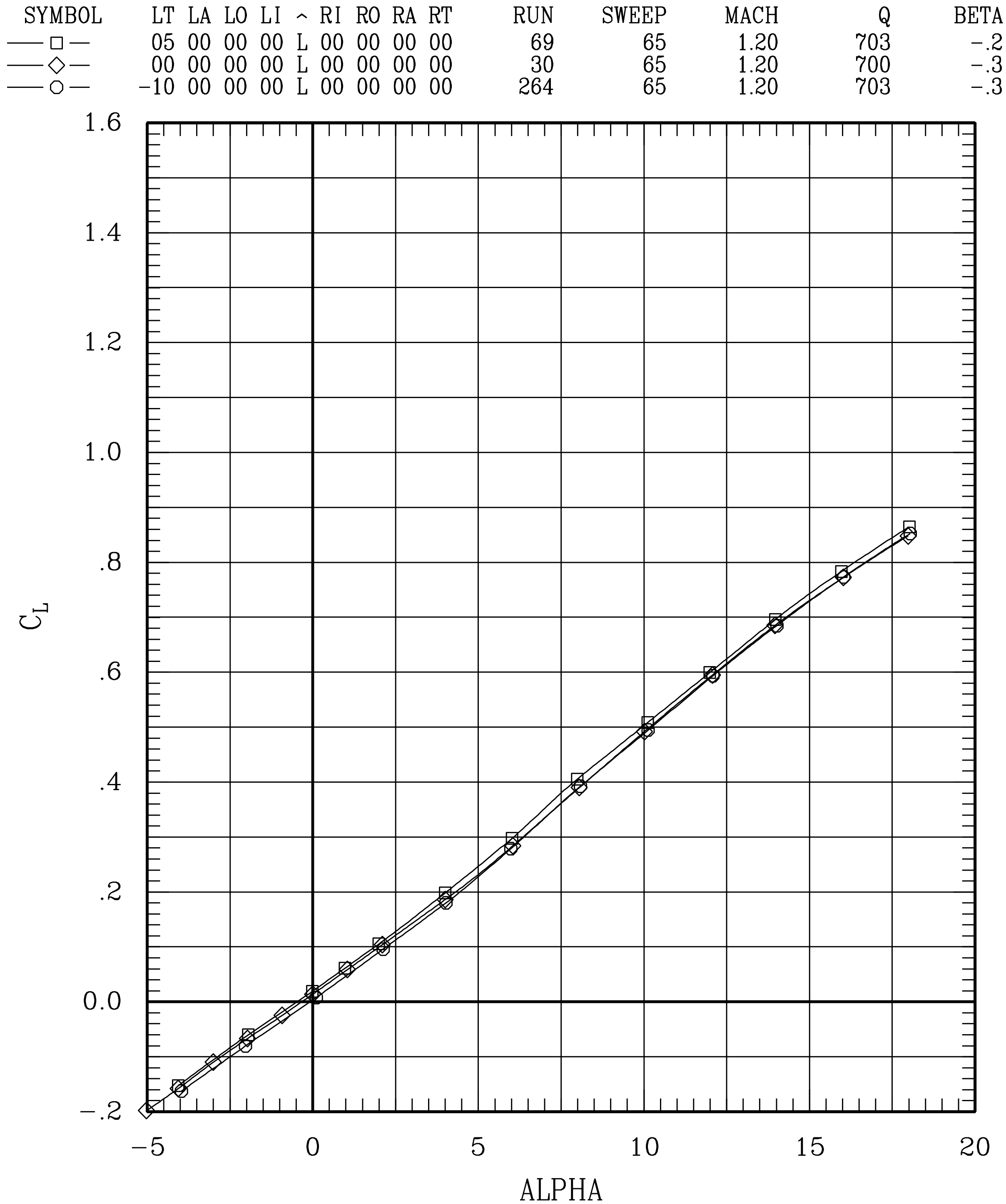

Figure 28(e). Left tip deflection for sweep = 65 deg, Mach = 1.20.

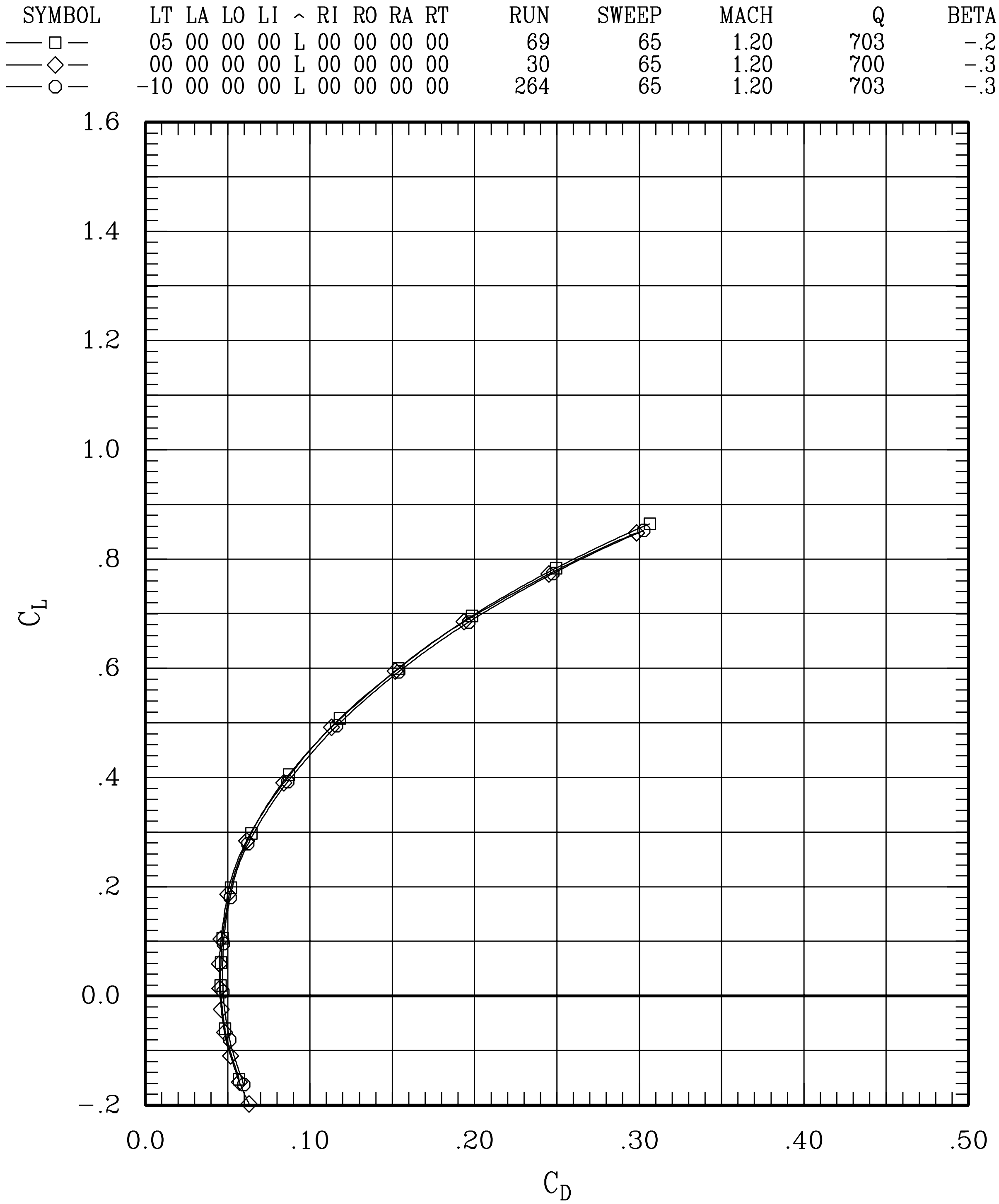

Figure 28(e). Left tip deflection for sweep = 65 deg, Mach = 1.20.

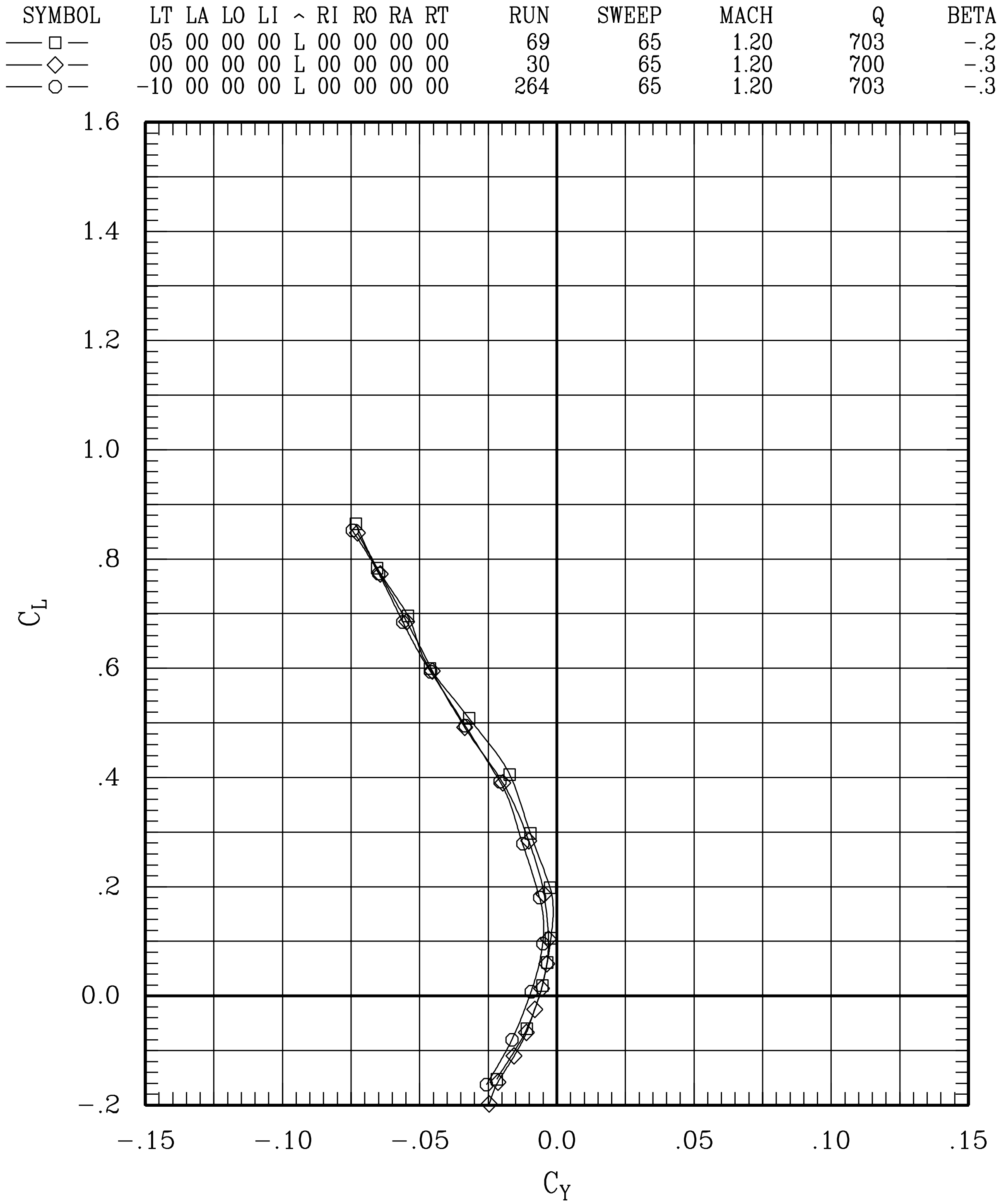

Figure 28(e). Left tip deflection for sweep = 65 deg, Mach = 1.20.

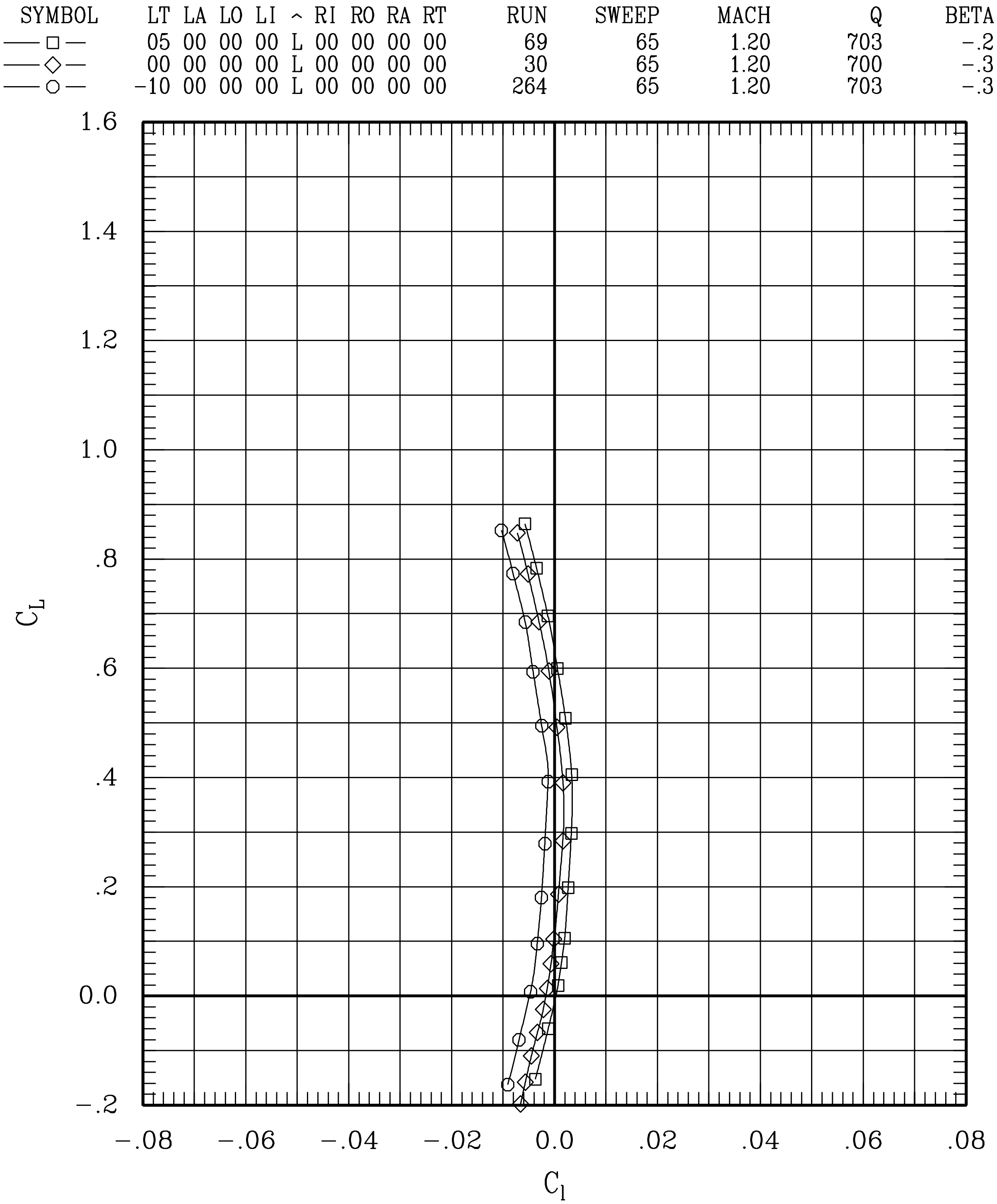

Figure 28(e). Left tip deflection for sweep = 65 deg, Mach = 1.20.

SYMBOL	LT LA LO LI ^ RI RO RA RT	RUN	SWEEP	MACH	Q	BETA
—□—	05 00 00 00 L 00 00 00 00	69	65	1.20	703	−.2
—◇—	00 00 00 00 L 00 00 00 00	30	65	1.20	700	−.3
—○—	−10 00 00 00 L 00 00 00 00	264	65	1.20	703	−.3

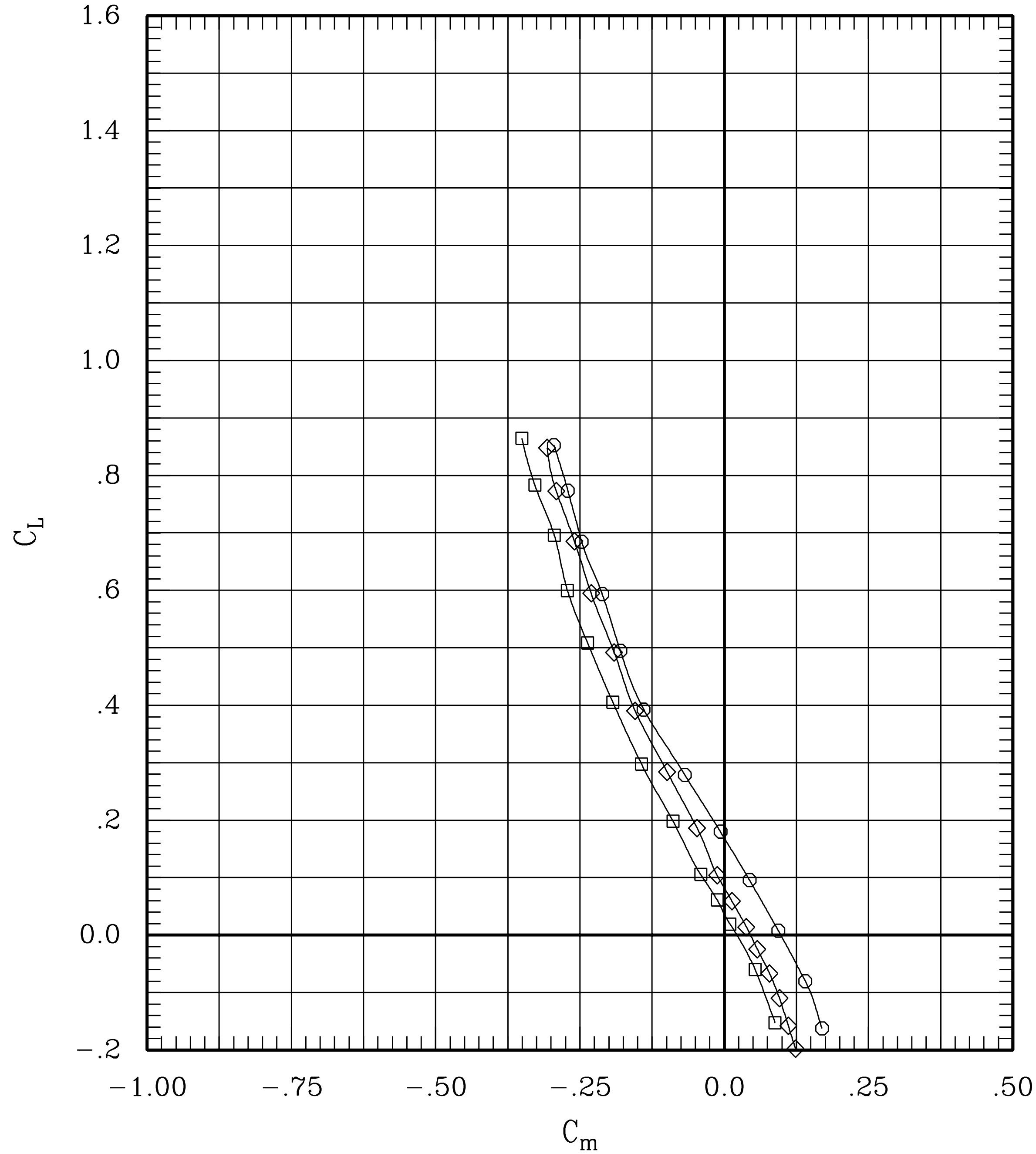

Figure 28(e). Left tip deflection for sweep = 65 deg, Mach = 1.20.

SYMBOL	LT LA LO LI ^ RI RO RA RT	RUN	SWEEP	MACH	Q	BETA
—□—	05 00 00 00 L 00 00 00 00	69	65	1.20	703	−.2
—◇—	00 00 00 00 L 00 00 00 00	30	65	1.20	700	−.3
—○—	−10 00 00 00 L 00 00 00 00	264	65	1.20	703	−.3

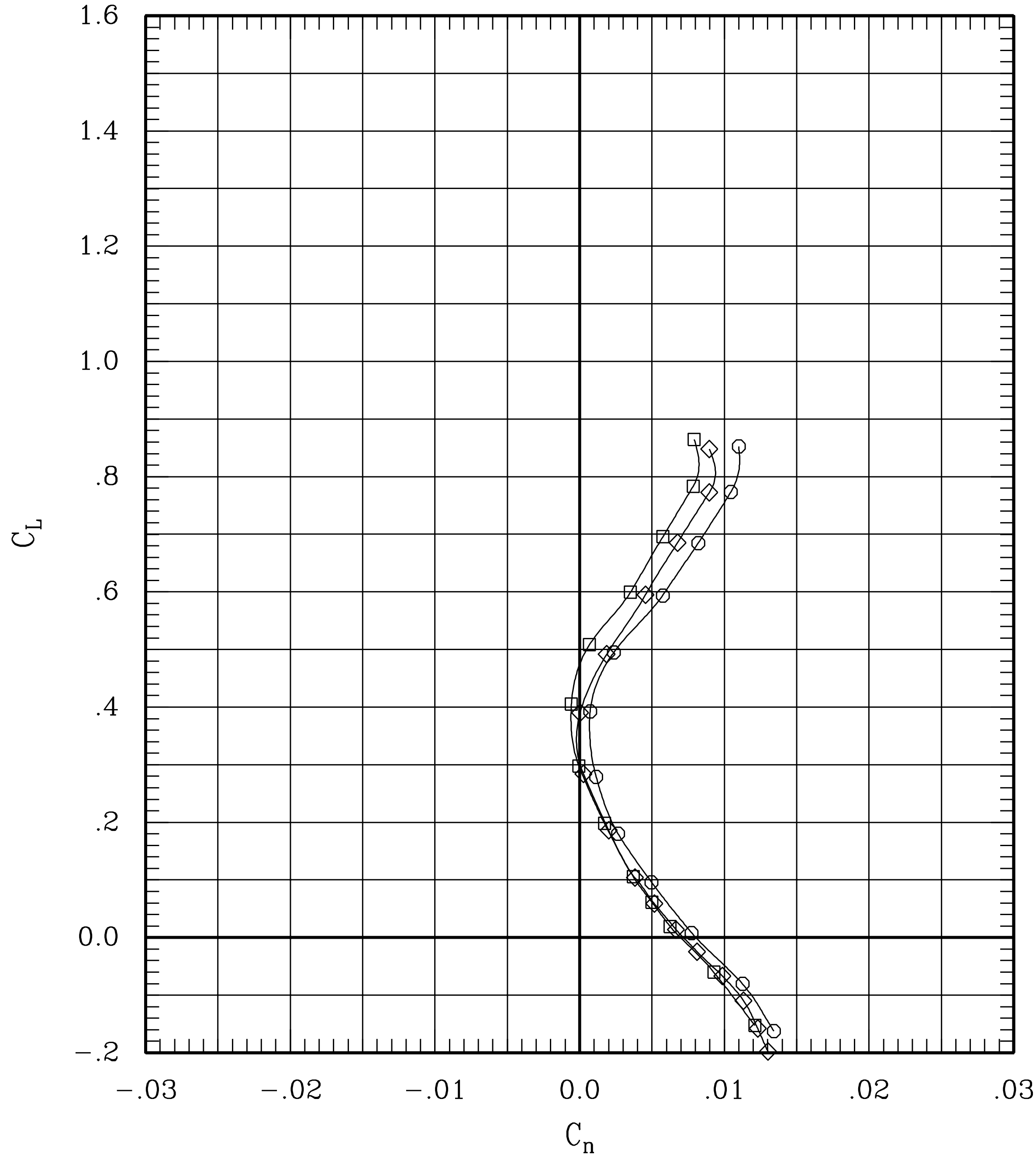

Figure 28(e). Left tip deflection for sweep = 65 deg, Mach = 1.20.

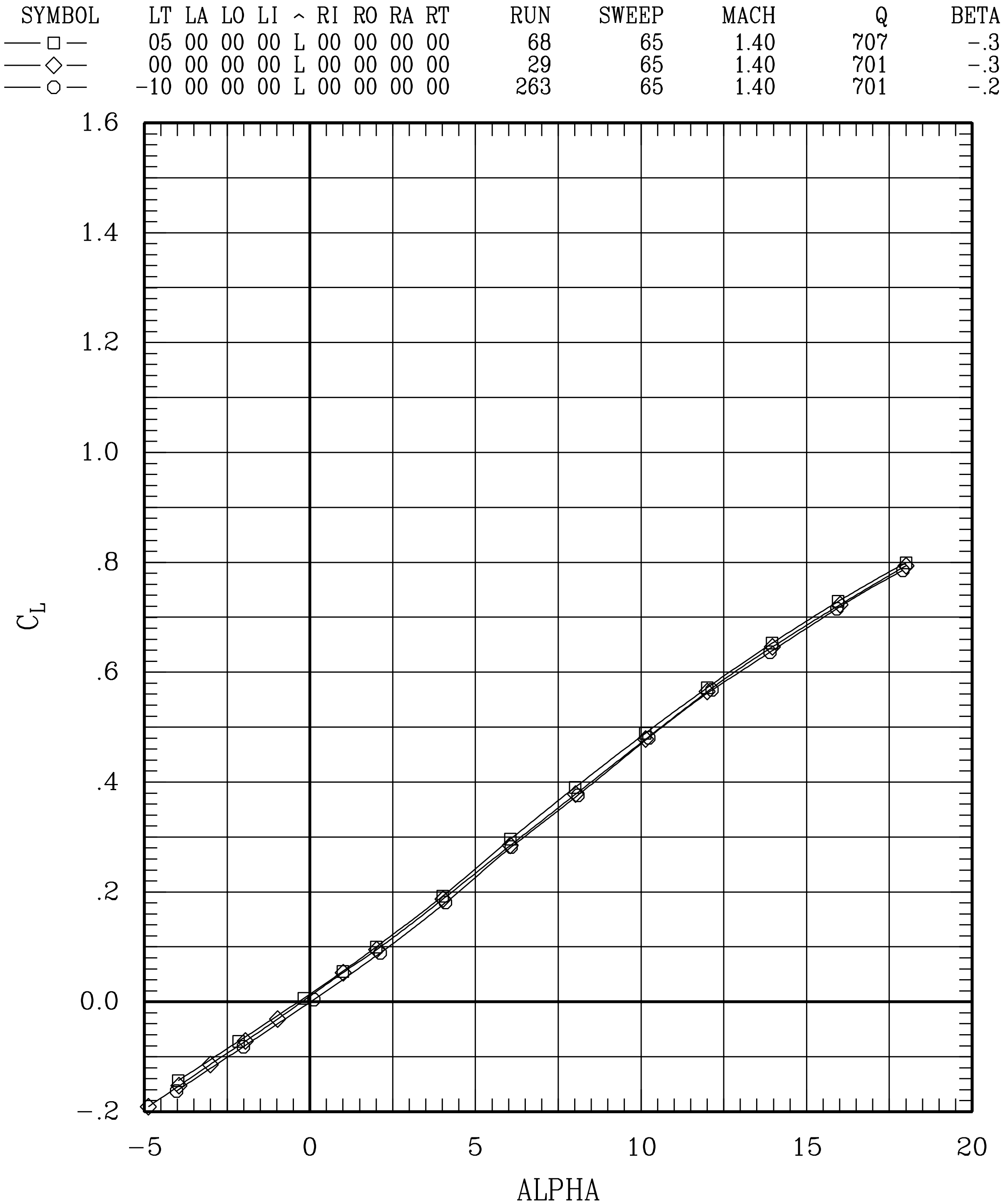

Figure 28(f). Left tip deflection for sweep = 65 deg, Mach = 1.40.

SYMBOL	LT	LA	LO	LI	^	RI	RO	RA	RT	RUN	SWEEP	MACH	Q	BETA
—□—	05	00	00	00	L	00	00	00	00	68	65	1.40	707	−.3
—◇—	00	00	00	00	L	00	00	00	00	29	65	1.40	701	−.3
—○—	−10	00	00	00	L	00	00	00	00	263	65	1.40	701	−.2

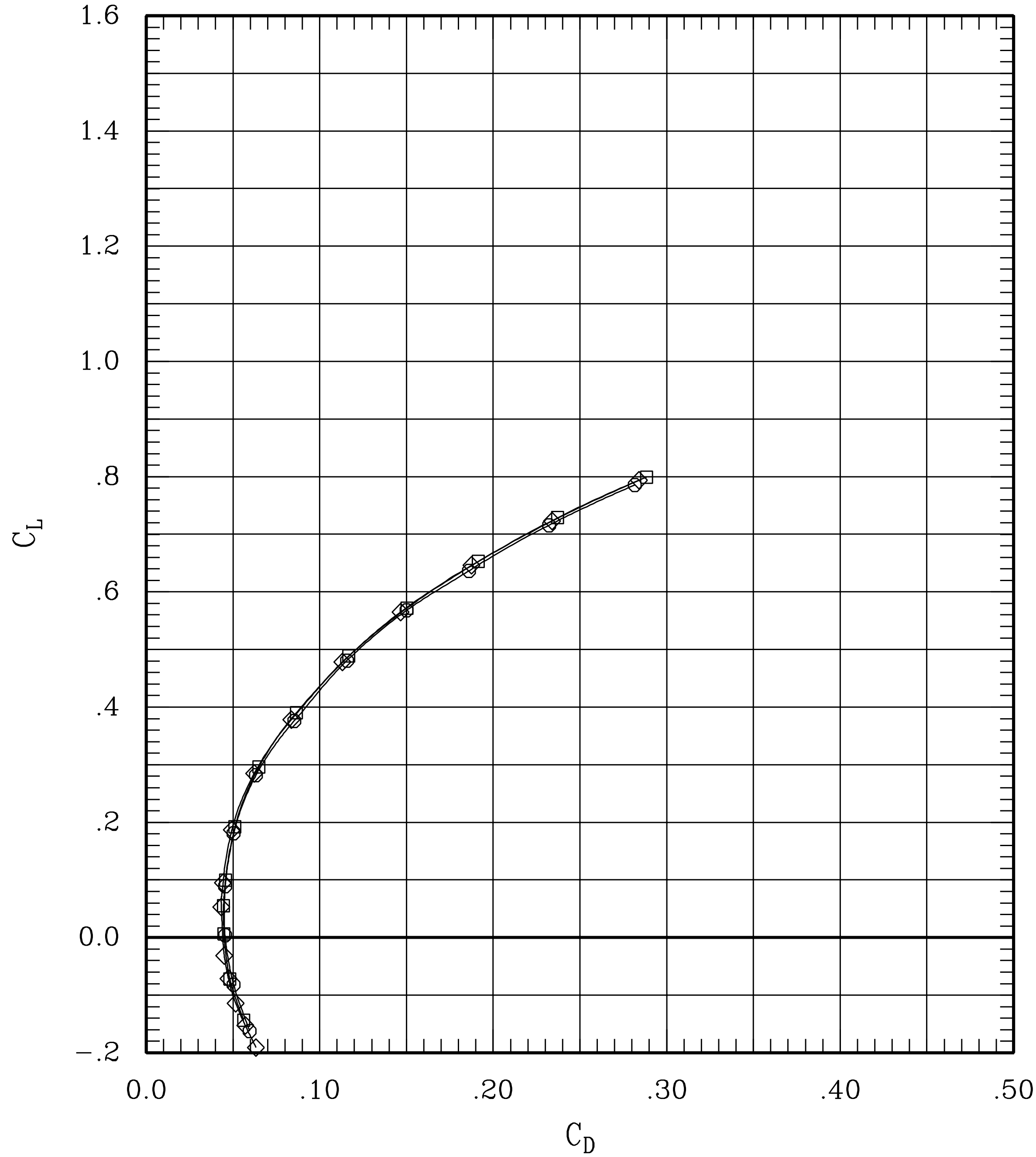

Figure 28(f). Left tip deflection for sweep = 65 deg, Mach = 1.40.

SYMBOL	LT LA LO LI ^ RI RO RA RT	RUN	SWEEP	MACH	Q	BETA
—□—	05 00 00 00 L 00 00 00 00	68	65	1.40	707	−.3
—◇—	00 00 00 00 L 00 00 00 00	29	65	1.40	701	−.3
—○—	−10 00 00 00 L 00 00 00 00	263	65	1.40	701	−.2

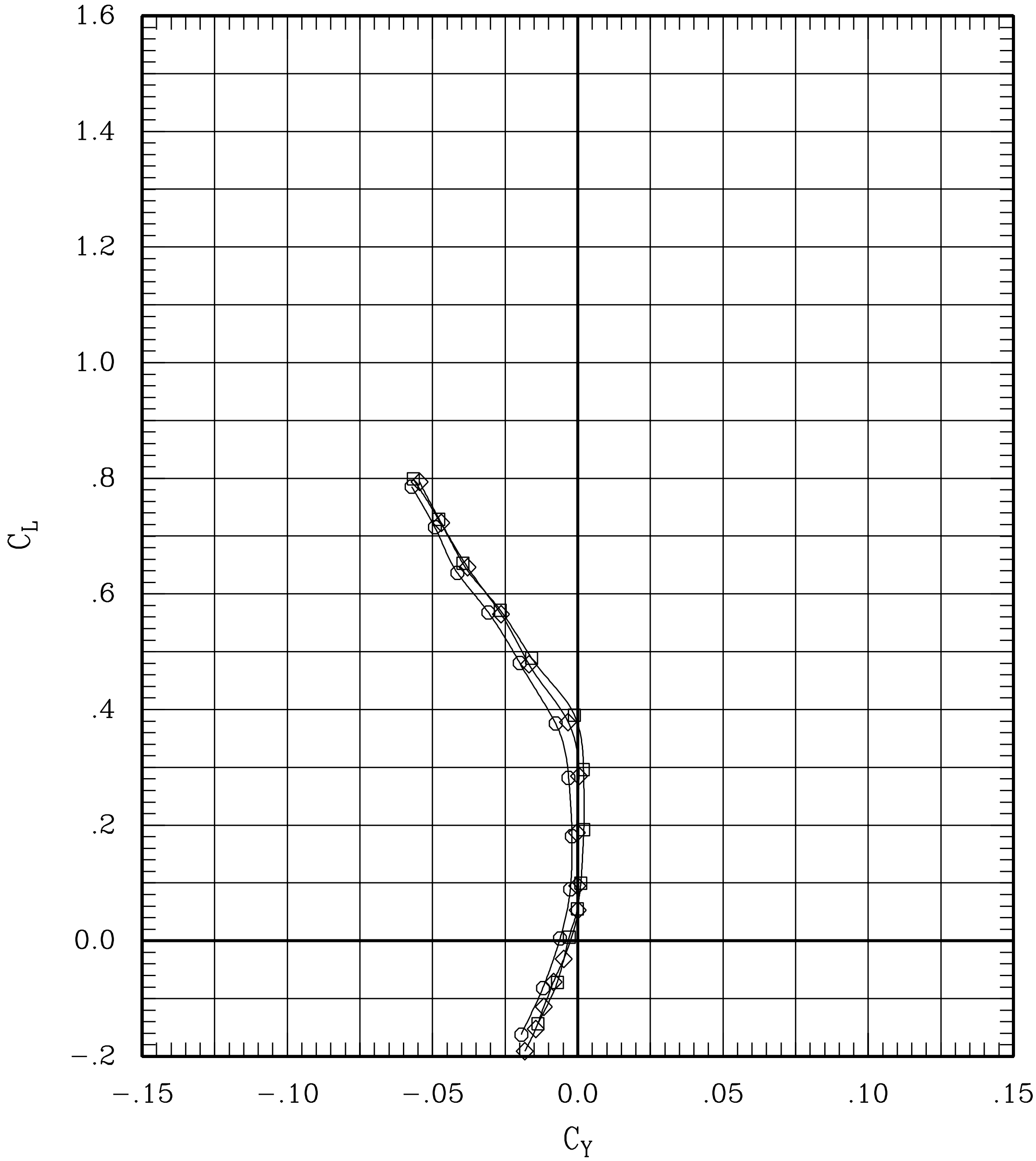

Figure 28(f). Left tip deflection for sweep = 65 deg, Mach = 1.40.

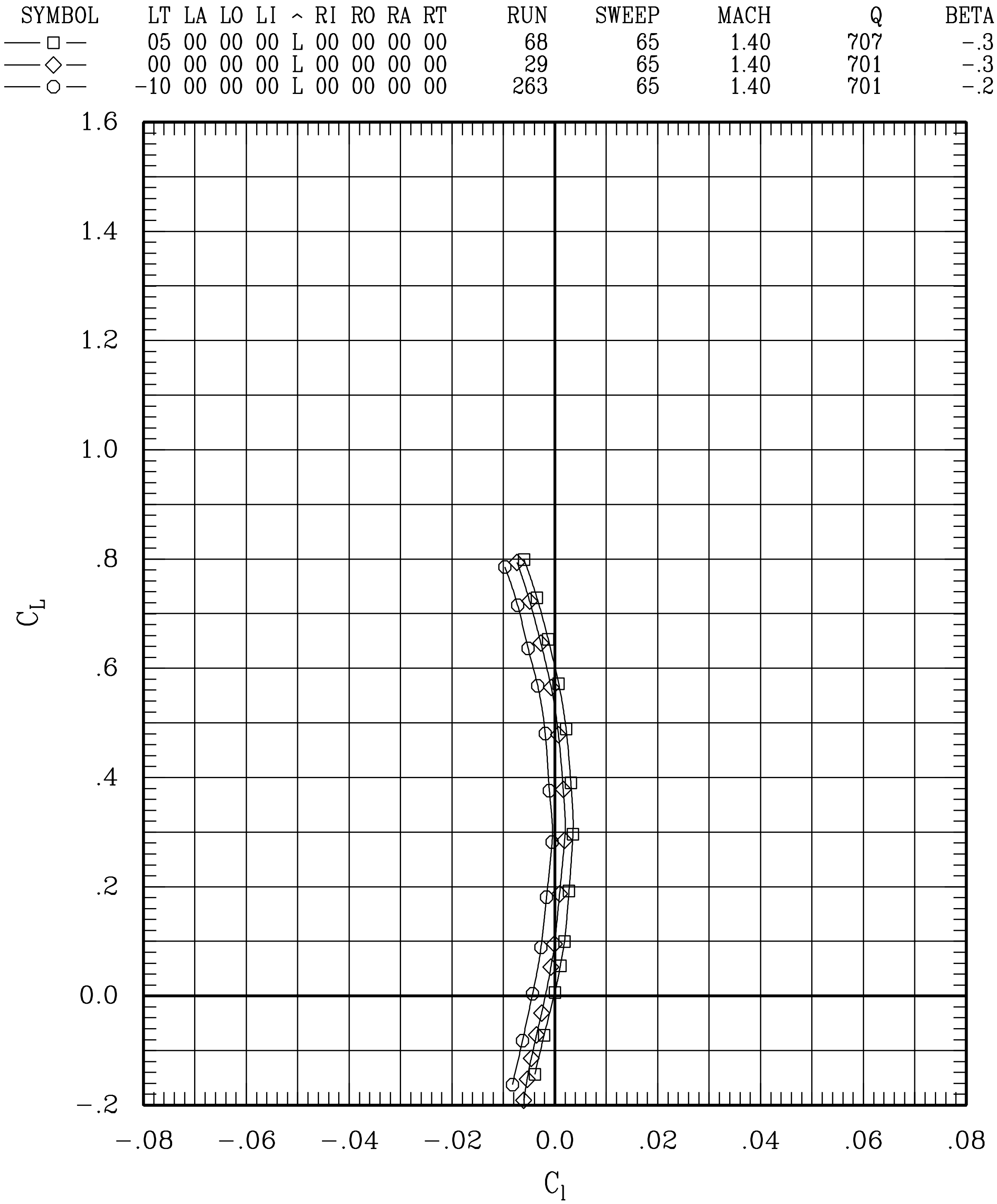

Figure 28(f). Left tip deflection for sweep = 65 deg, Mach = 1.40.

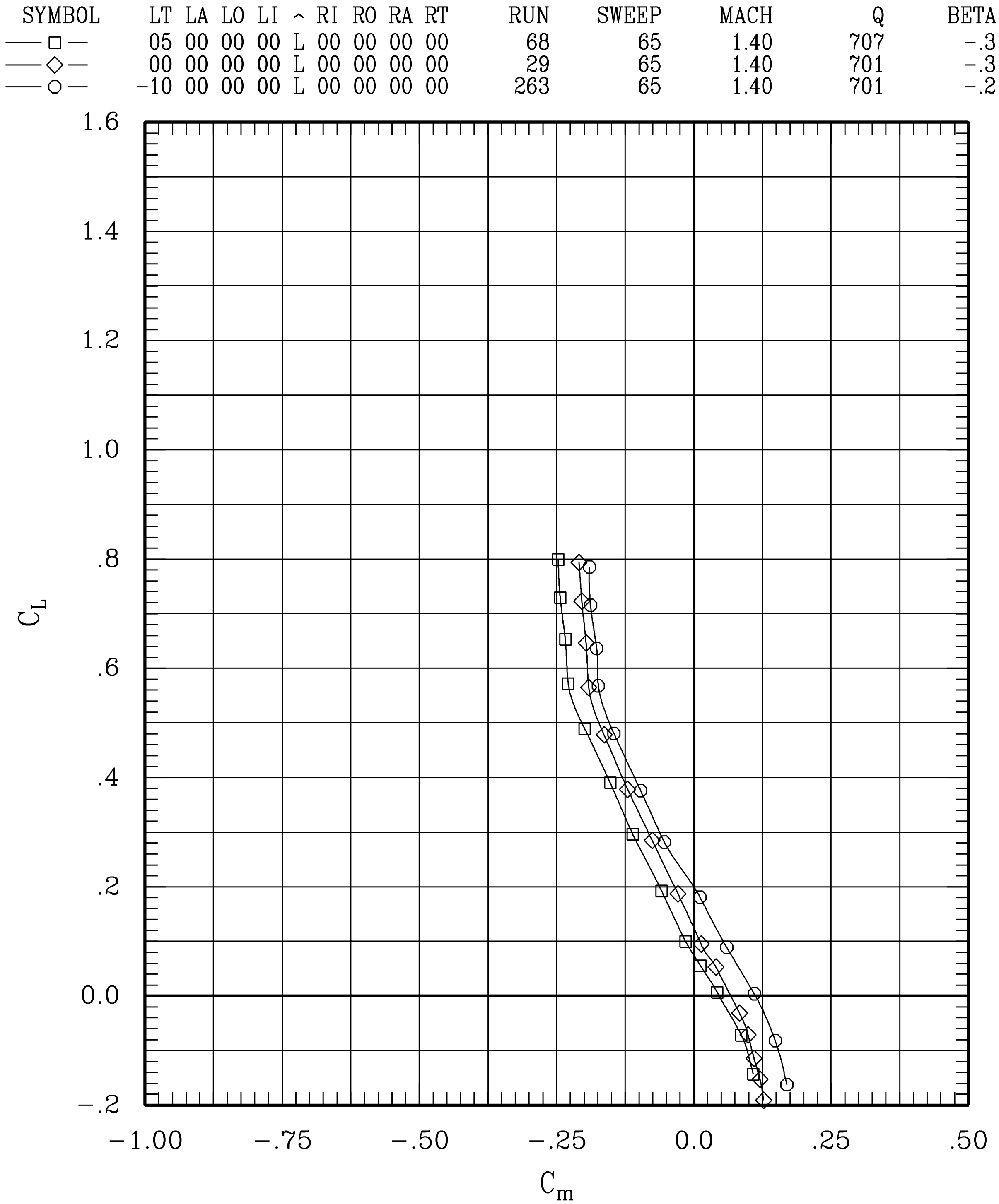

Figure 28(f). Left tip deflection for sweep = 65 deg, Mach = 1.40.

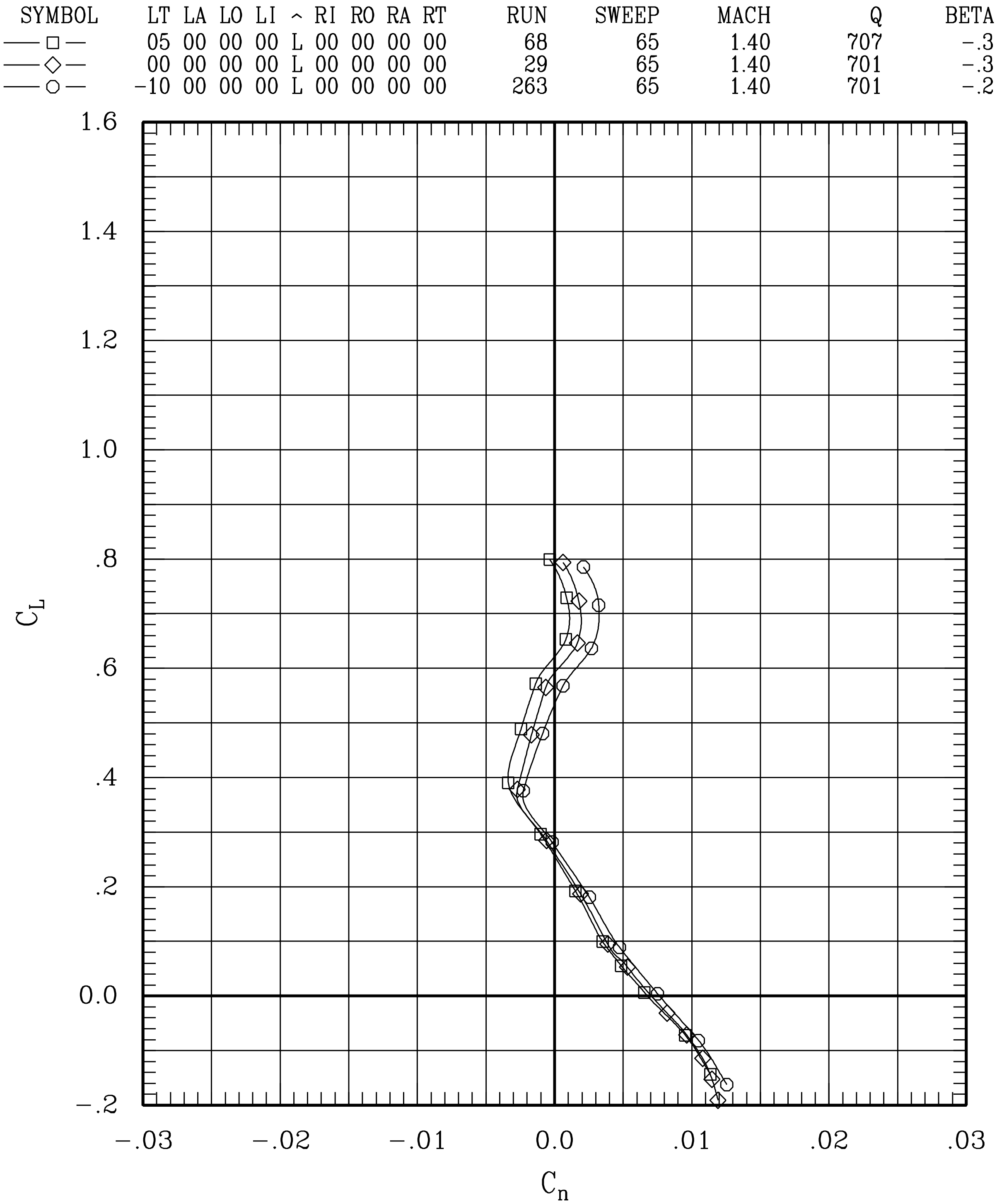

Figure 28(f). Left tip deflection for sweep = 65 deg, Mach = 1.40.

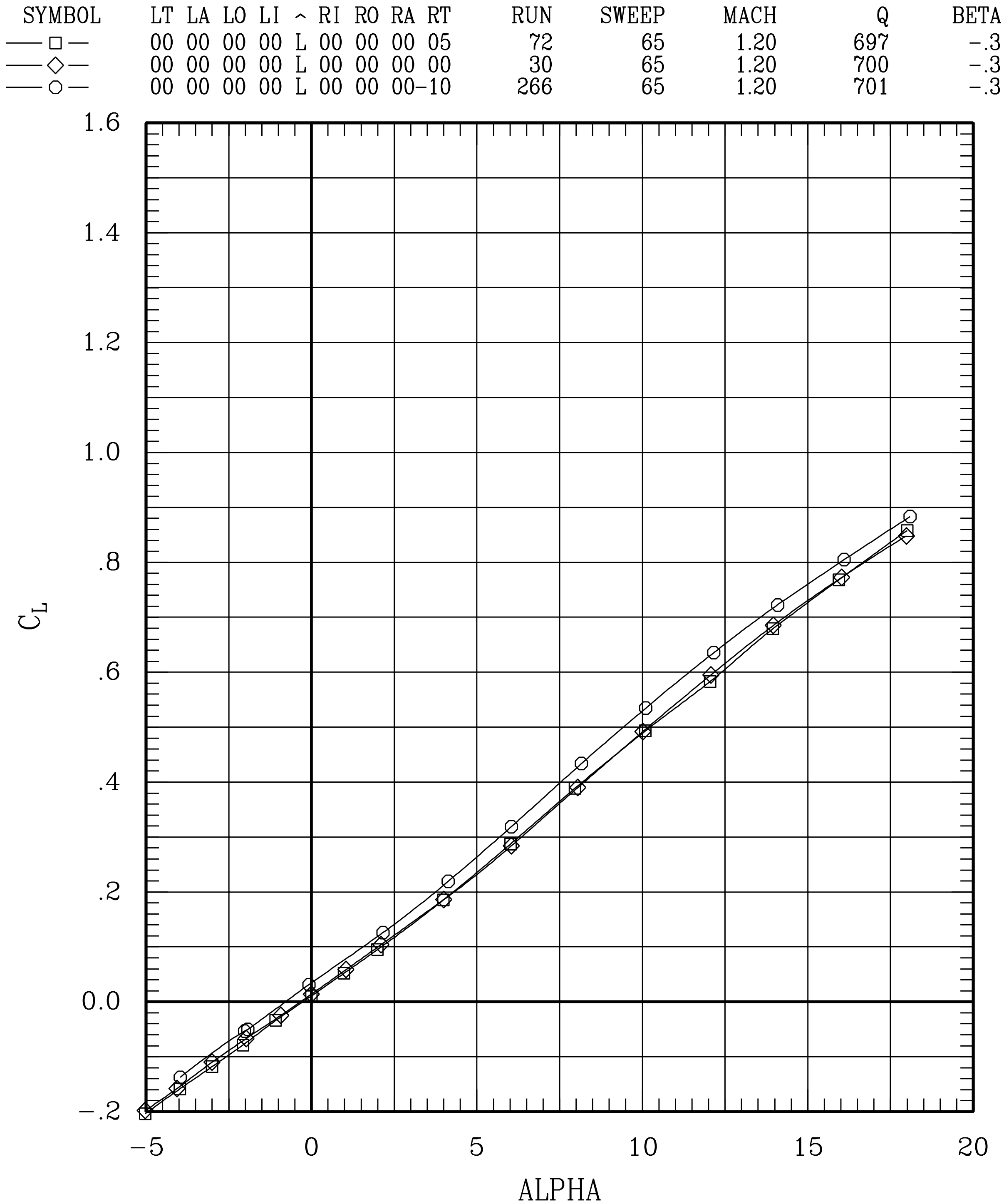

Figure 28(g). Right tip deflection for sweep = 65 deg, Mach = 1.20.

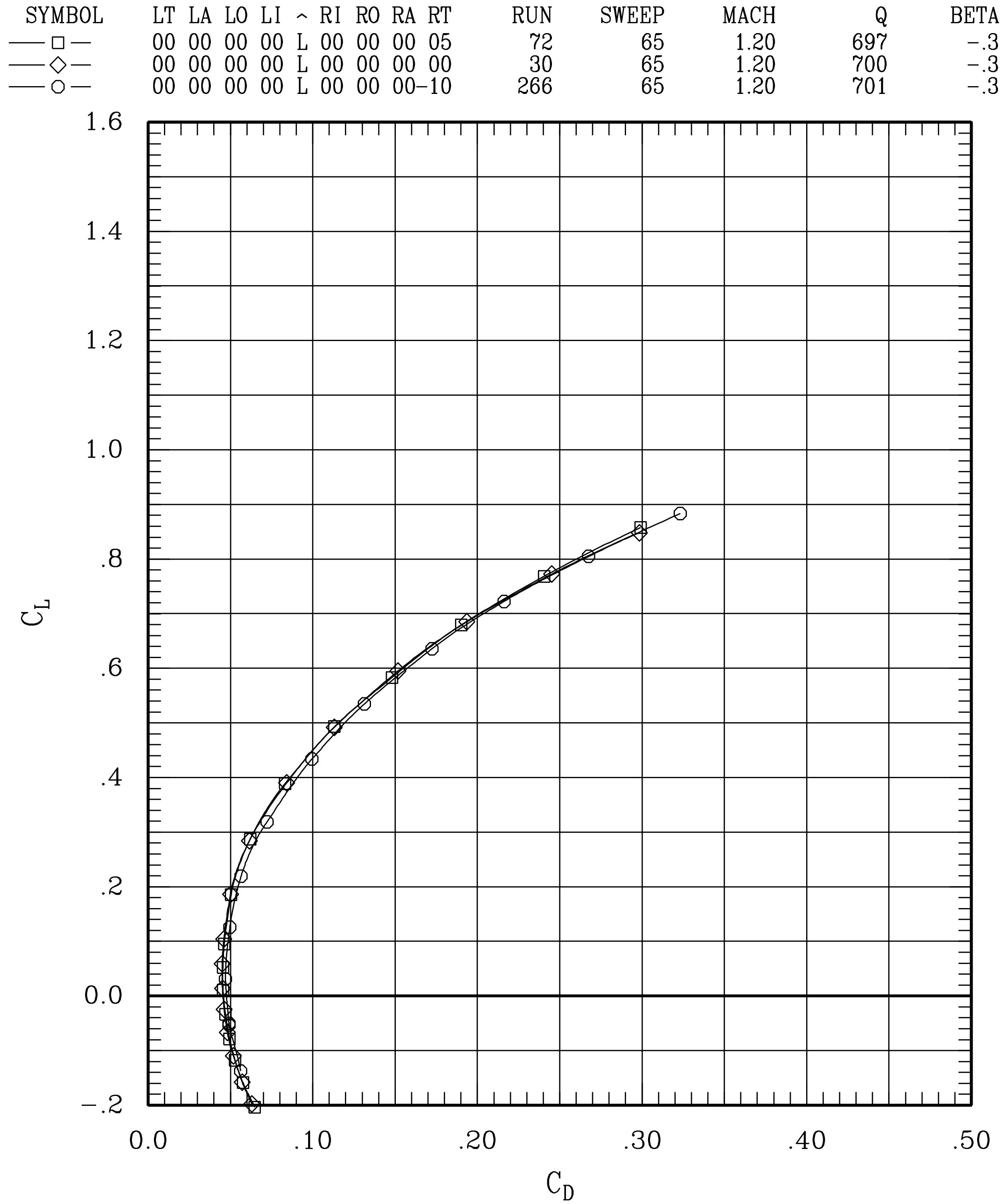

Figure 28(g). Right tip deflection for sweep = 65 deg, Mach = 1.20.

SYMBOL	LT LA LO LI ^ RI RO RA RT	RUN	SWEEP	MACH	Q	BETA
—□—	00 00 00 00 L 00 00 00 05	72	65	1.20	697	-.3
—◇—	00 00 00 00 L 00 00 00 00	30	65	1.20	700	-.3
—○—	00 00 00 00 L 00 00 00-10	266	65	1.20	701	-.3

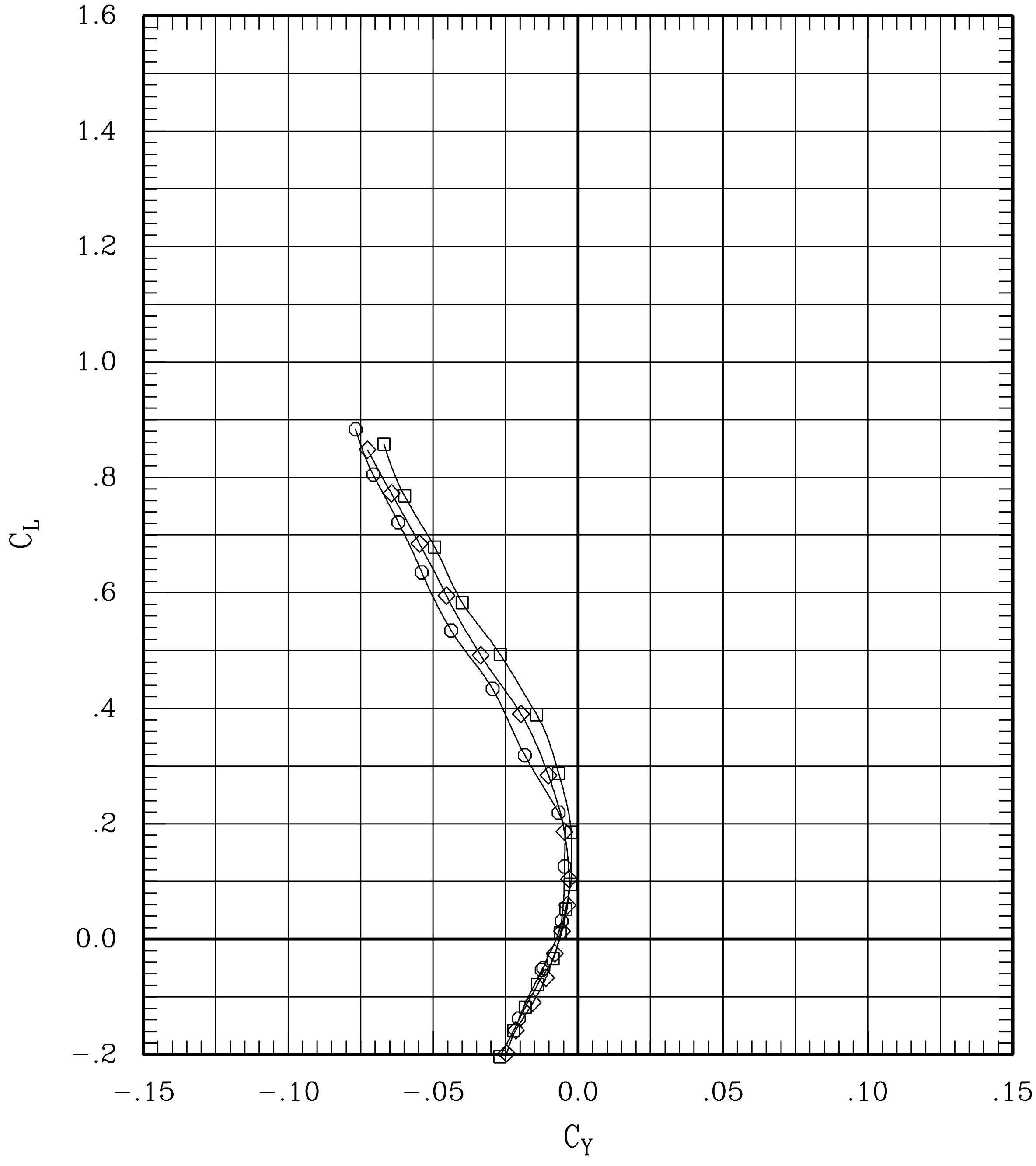

Figure 28(g). Right tip deflection for sweep = 65 deg, Mach = 1.20.

SYMBOL	LT LA LO LI ^ RI RO RA RT	RUN	SWEEP	MACH	Q	BETA
—□—	00 00 00 00 L 00 00 00 05	72	65	1.20	697	−.3
—◇—	00 00 00 00 L 00 00 00 00	30	65	1.20	700	−.3
—○—	00 00 00 00 L 00 00 00−10	266	65	1.20	701	−.3

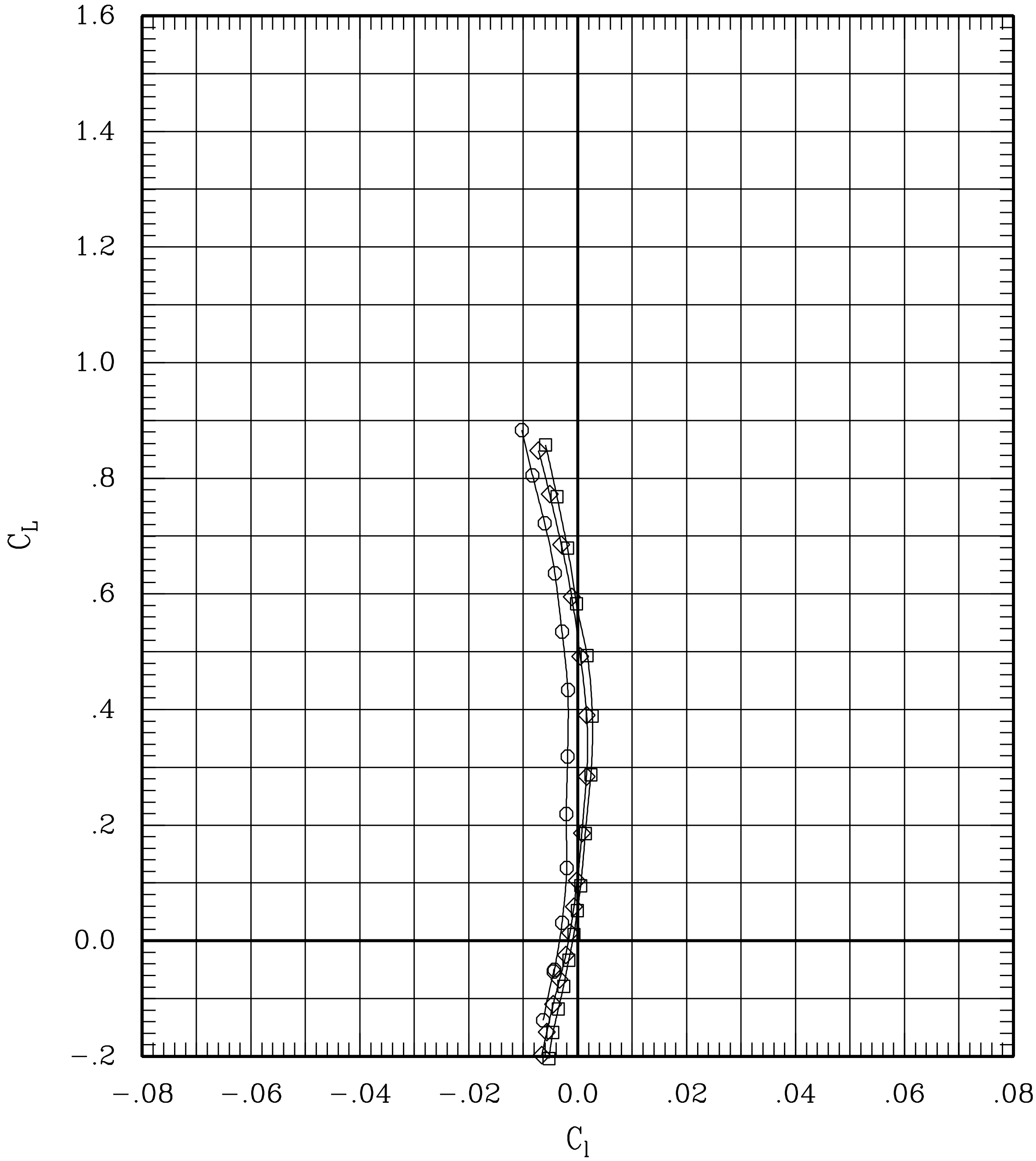

Figure 28(g). Right tip deflection for sweep = 65 deg, Mach = 1.20.

SYMBOL	LT LA LO LI ^ RI RO RA RT	RUN	SWEEP	MACH	Q	BETA
—□—	00 00 00 00 L 00 00 00 05	72	65	1.20	697	−.3
—◇—	00 00 00 00 L 00 00 00 00	30	65	1.20	700	−.3
—○—	00 00 00 00 L 00 00 00−10	266	65	1.20	701	−.3

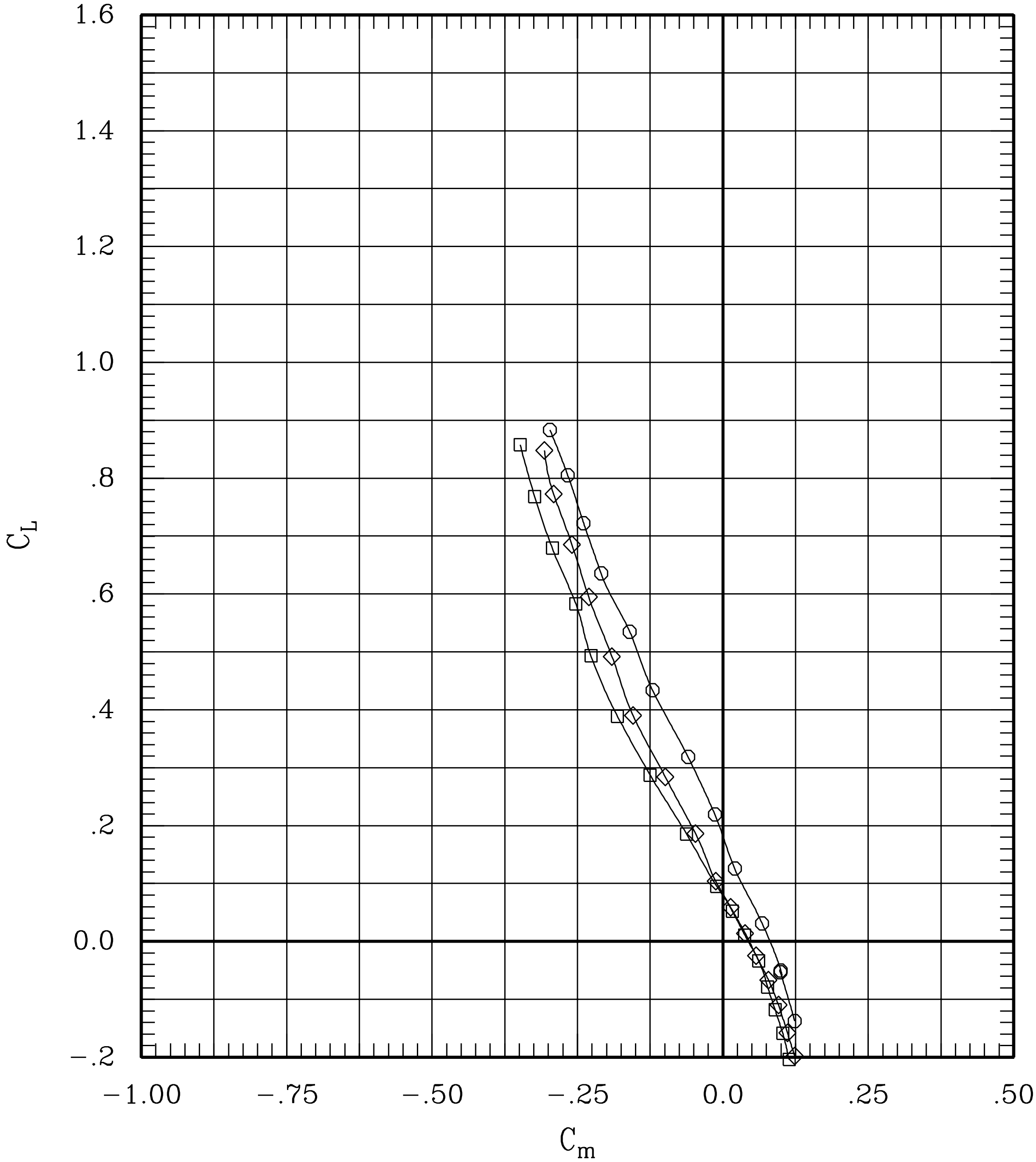

Figure 28(g). Right tip deflection for sweep = 65 deg, Mach = 1.20.

SYMBOL	LT LA LO LI ^ RI RO RA RT	RUN	SWEEP	MACH	Q	BETA
—□—	00 00 00 00 L 00 00 00 05	72	65	1.20	697	-.3
—◇—	00 00 00 00 L 00 00 00 00	30	65	1.20	700	-.3
—○—	00 00 00 00 L 00 00 00-10	266	65	1.20	701	-.3

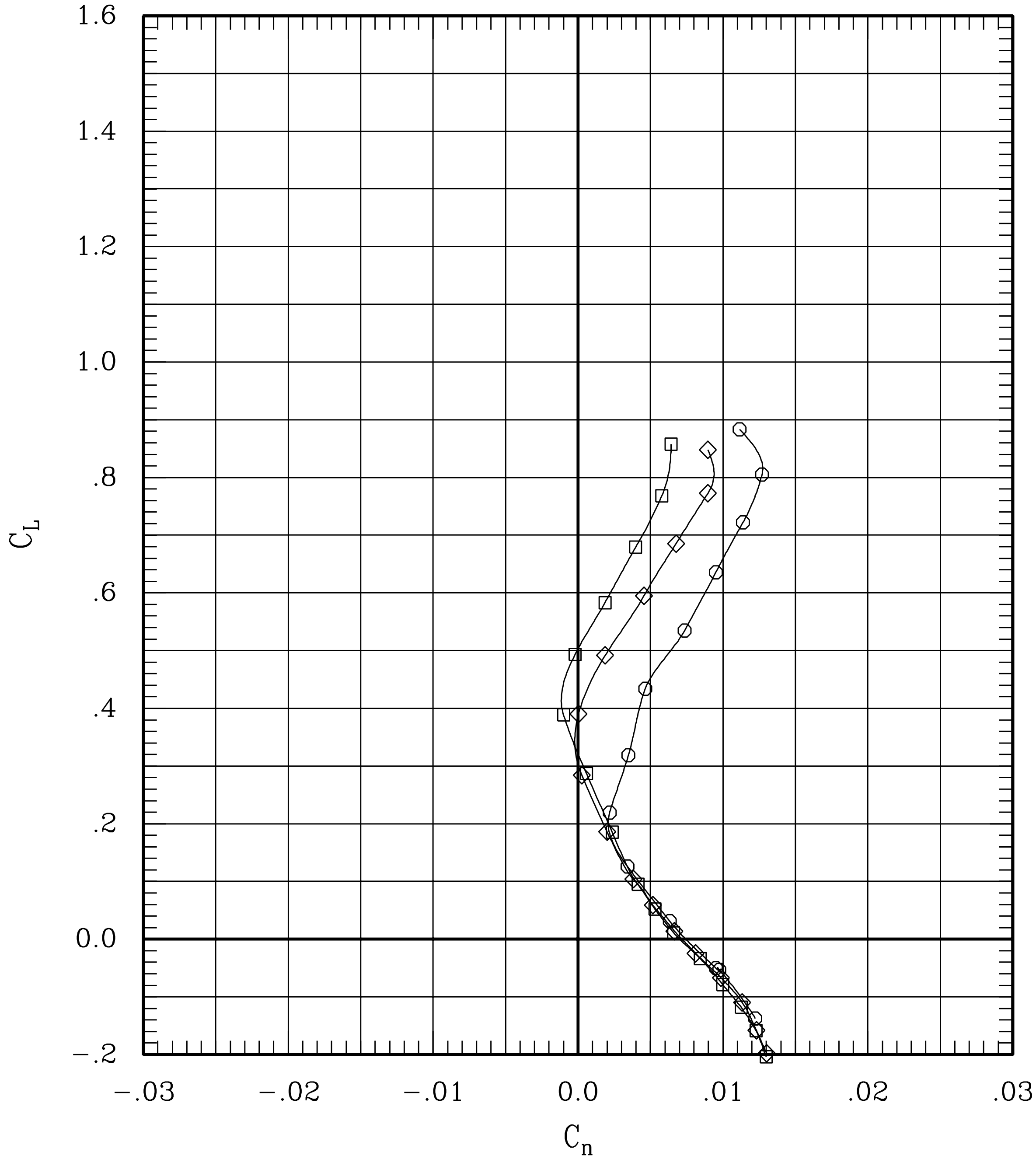

Figure 28(g). Right tip deflection for sweep = 65 deg, Mach = 1.20.

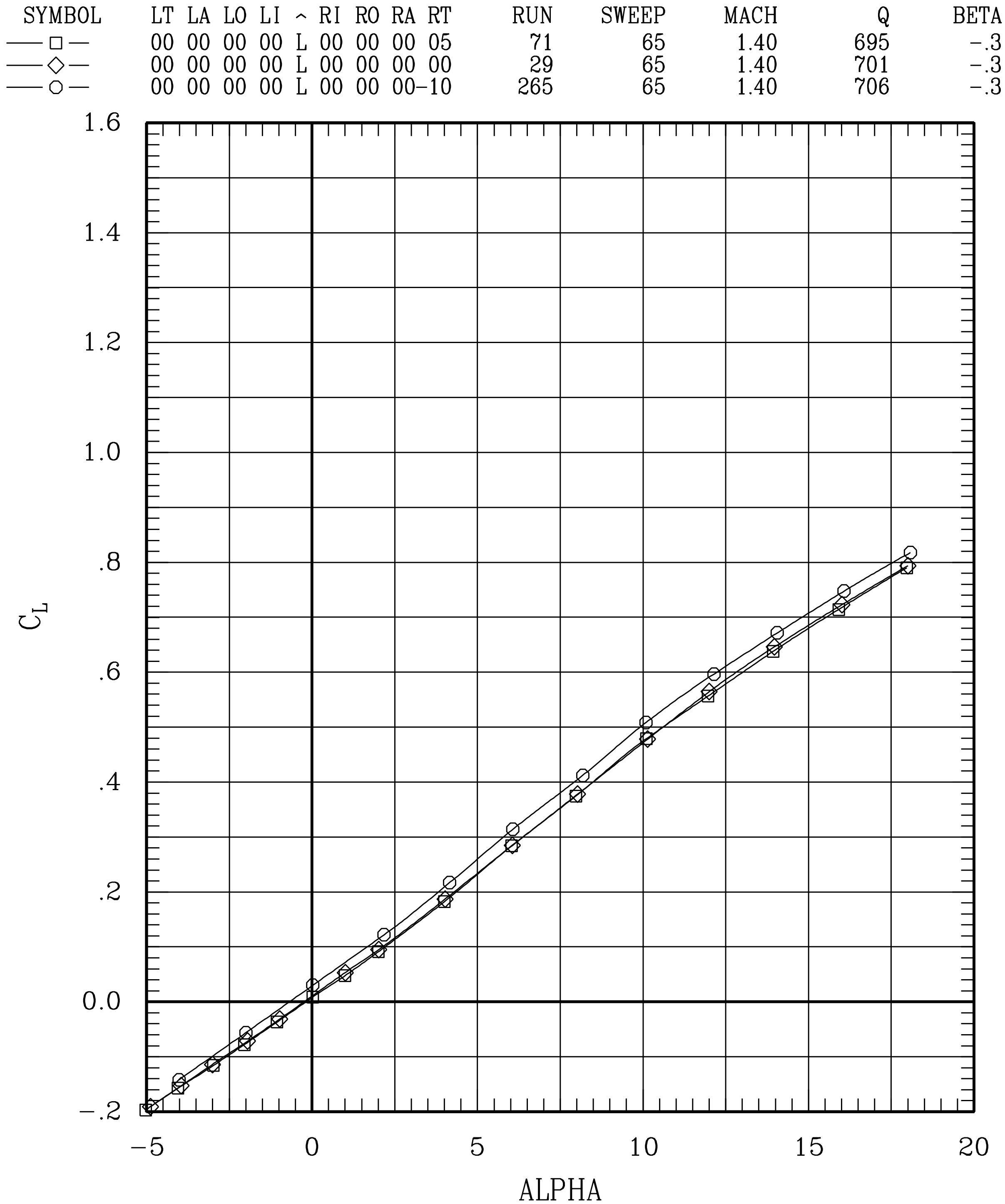

Figure 28(h). Right tip deflection for sweep = 65 deg, Mach = 1.40.

SYMBOL	LT LA LO LI ^ RI RO RA RT	RUN	SWEEP	MACH	Q	BETA
—□—	00 00 00 00 L 00 00 00 05	71	65	1.40	695	-.3
—◇—	00 00 00 00 L 00 00 00 00	29	65	1.40	701	-.3
—○—	00 00 00 00 L 00 00 00-10	265	65	1.40	706	-.3

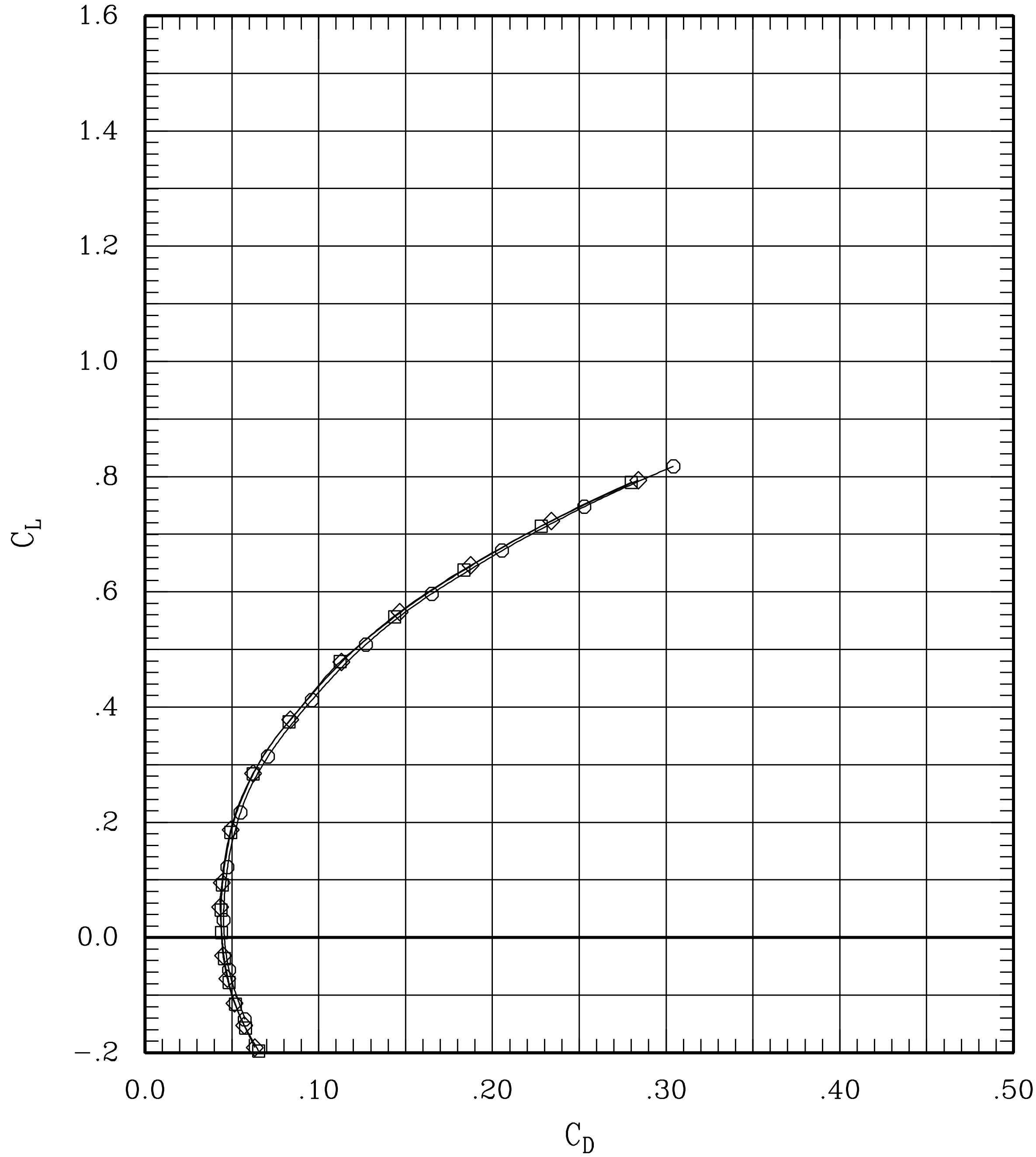

Figure 28(h). Right tip deflection for sweep = 65 deg, Mach = 1.40.

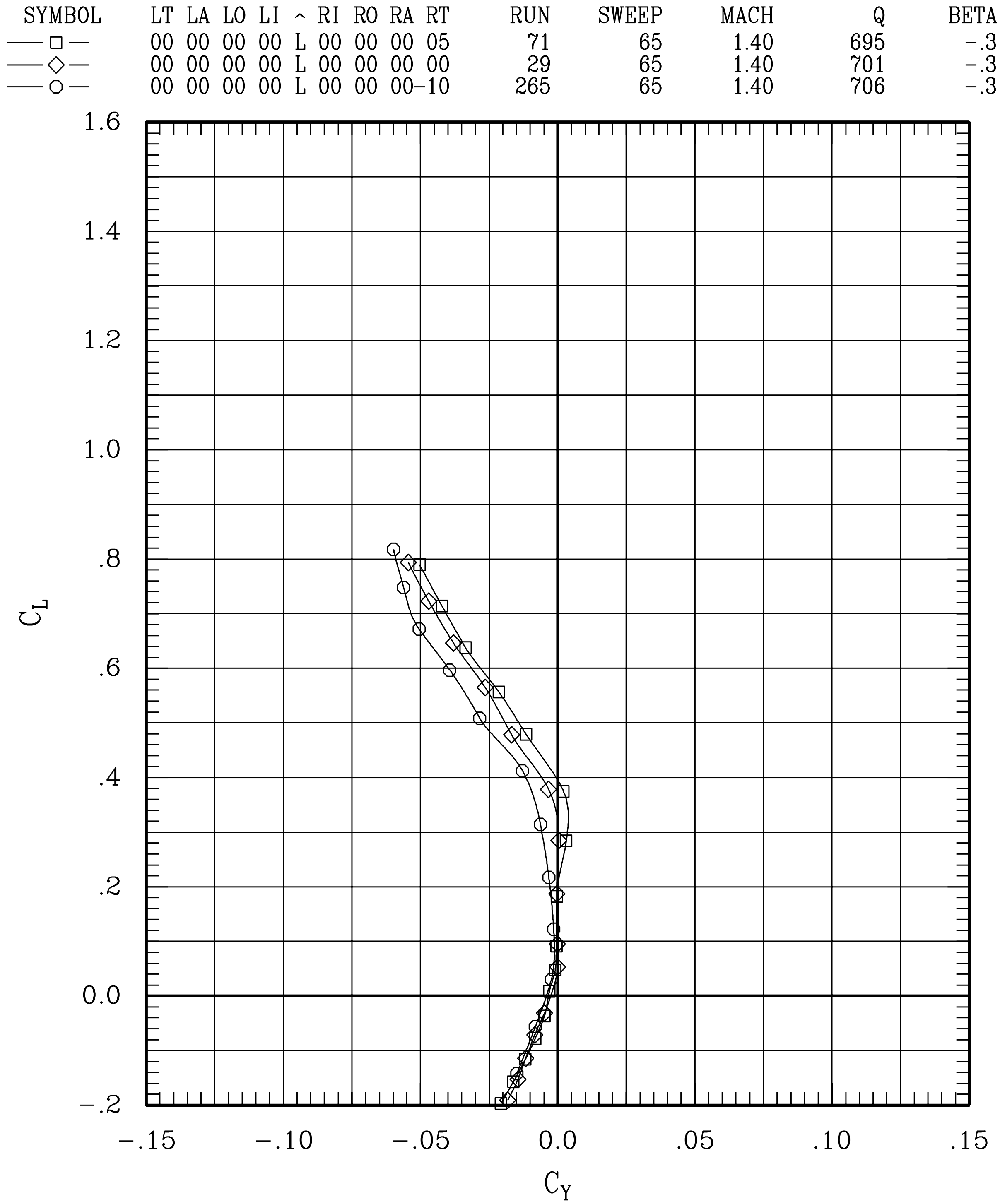

Figure 28(h). Right tip deflection for sweep = 65 deg, Mach = 1.40.

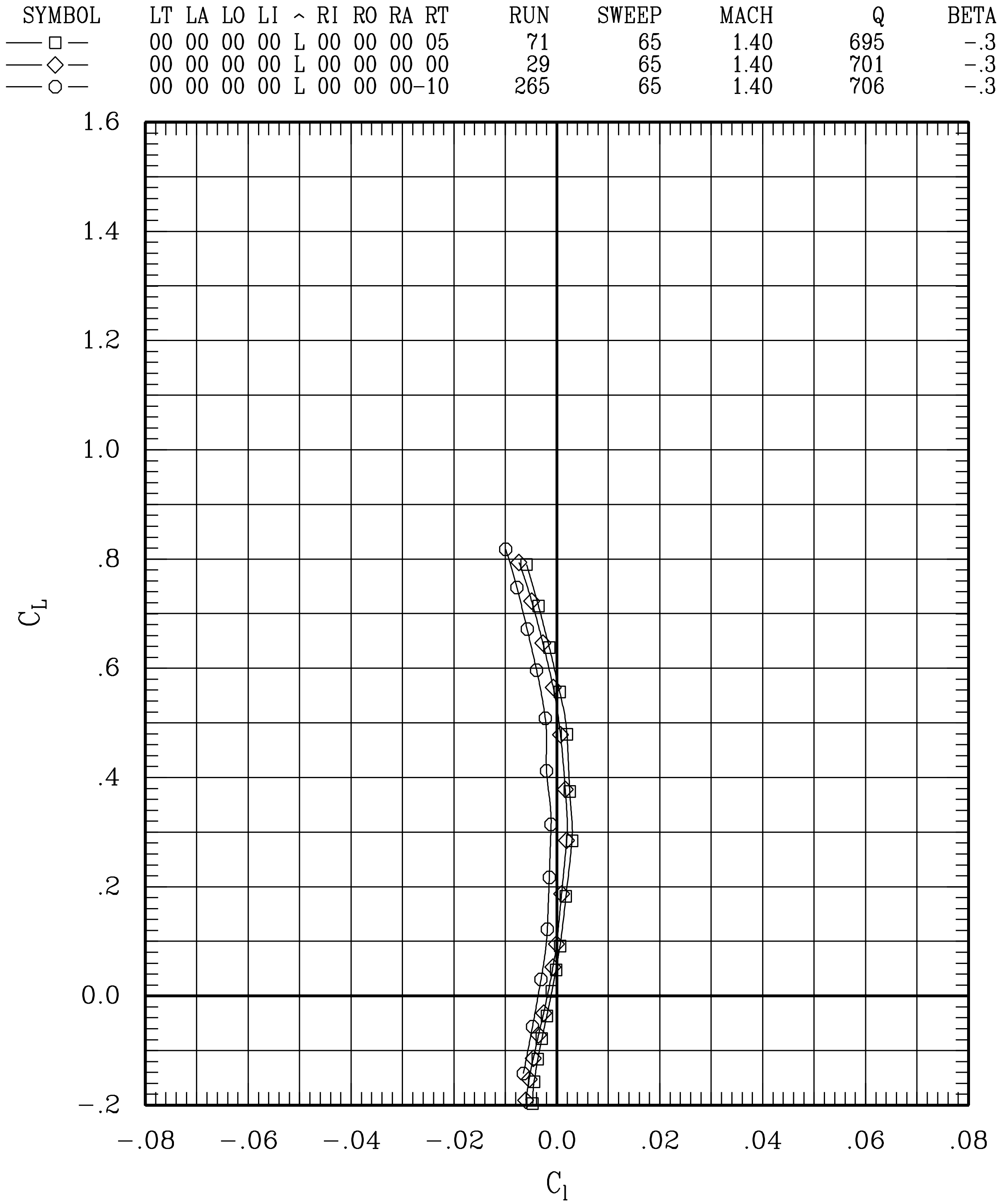

Figure 28(h). Right tip deflection for sweep = 65 deg, Mach = 1.40.

SYMBOL	LT LA LO LI ^ RI RO RA RT	RUN	SWEEP	MACH	Q	BETA
—□—	00 00 00 00 L 00 00 00 05	71	65	1.40	695	-.3
—◇—	00 00 00 00 L 00 00 00 00	29	65	1.40	701	-.3
—○—	00 00 00 00 L 00 00 00-10	265	65	1.40	706	-.3

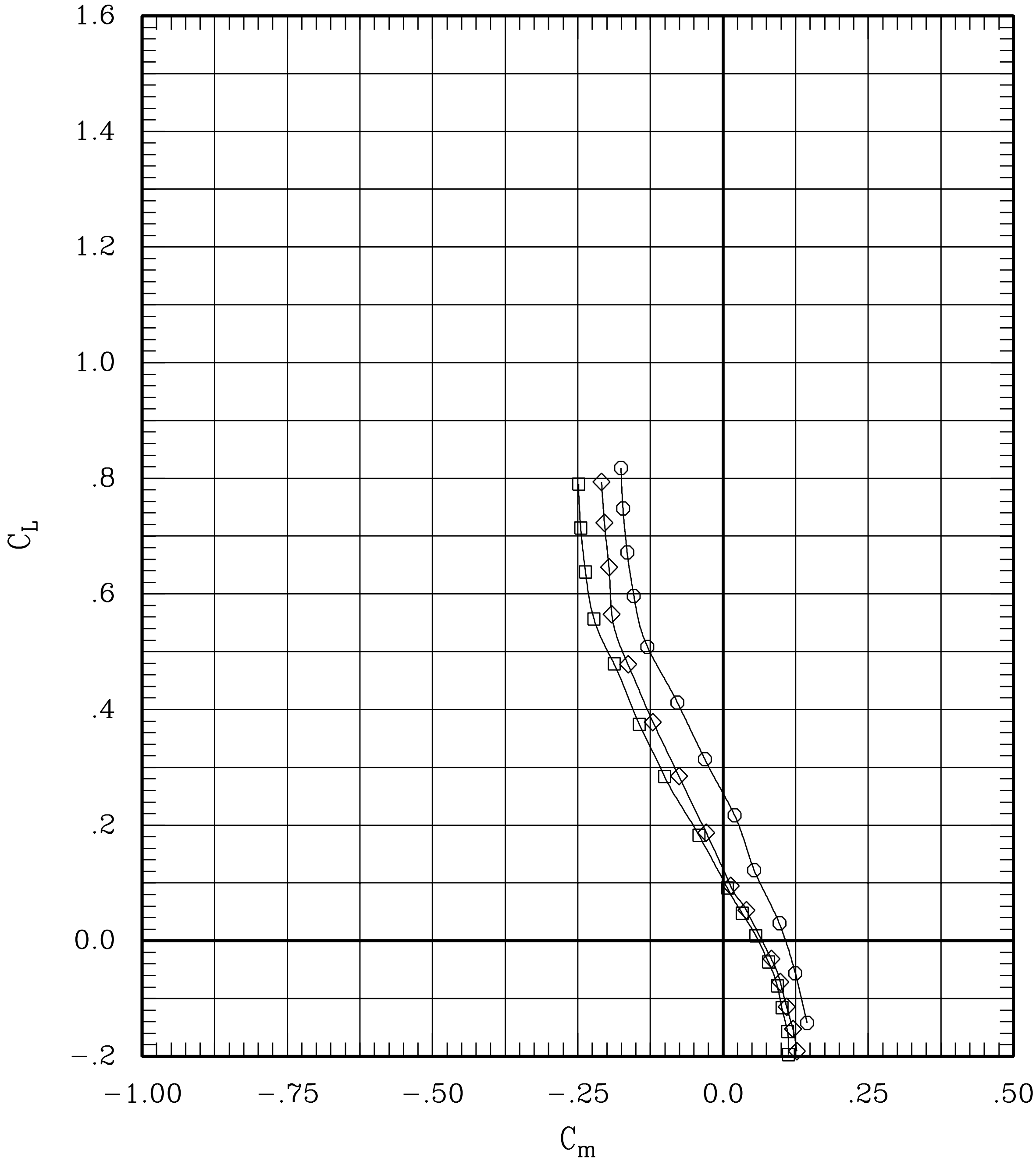

Figure 28(h). Right tip deflection for sweep = 65 deg, Mach = 1.40.

SYMBOL	LT LA LO LI ^ RI RO RA RT	RUN	SWEEP	MACH	Q	BETA
—□—	00 00 00 00 L 00 00 00 05	71	65	1.40	695	−.3
—◇—	00 00 00 00 L 00 00 00 00	29	65	1.40	701	−.3
—○—	00 00 00 00 L 00 00 00−10	265	65	1.40	706	−.3

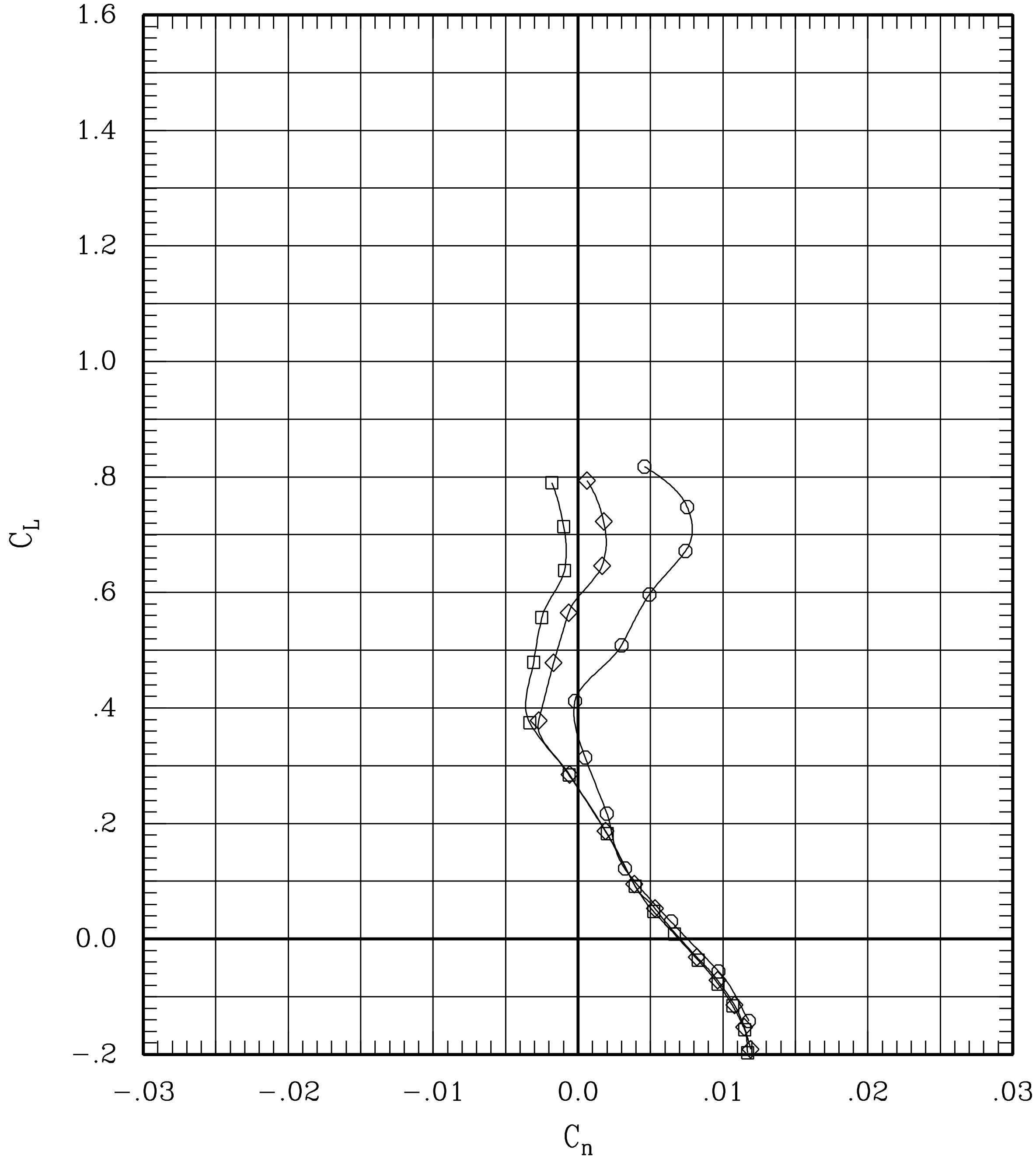

Figure 28(h). Right tip deflection for sweep = 65 deg, Mach = 1.40.

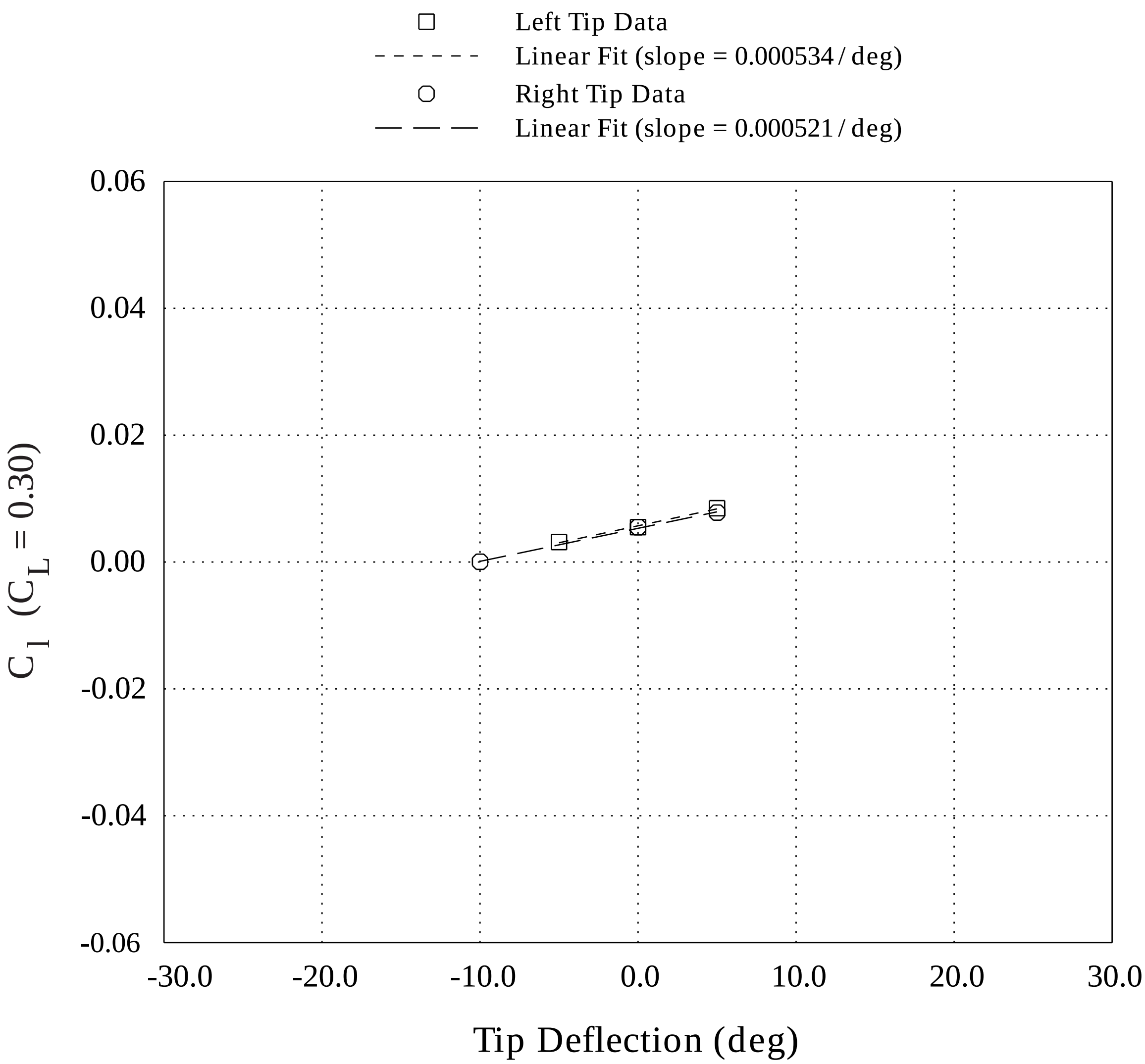

Figure 29(a). Tip deflection effectiveness for sweep = 45 deg, Mach = 0.80.

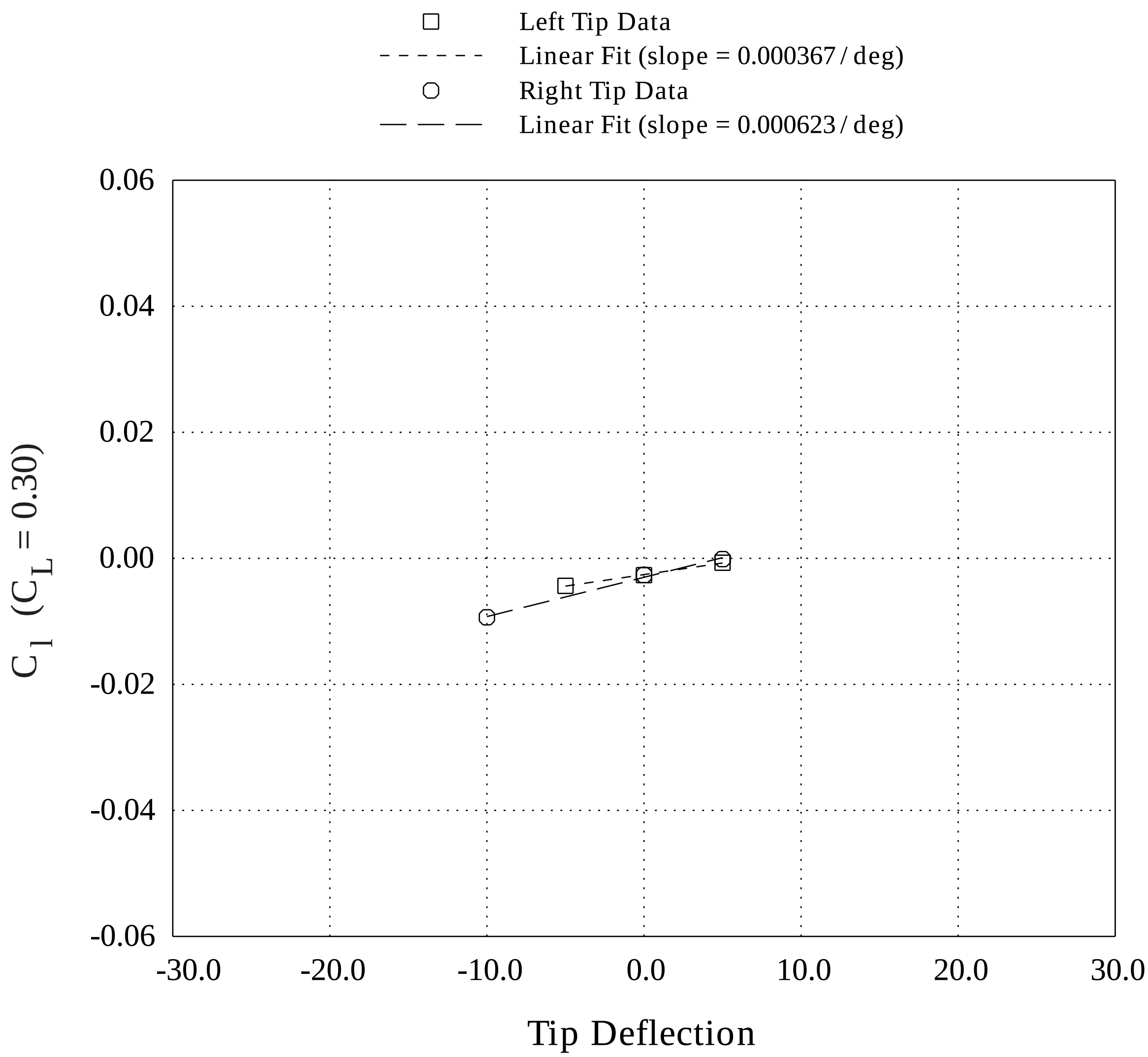

Figure 29(b). Tip deflection effectiveness for sweep = 45 deg, Mach = 1.20.

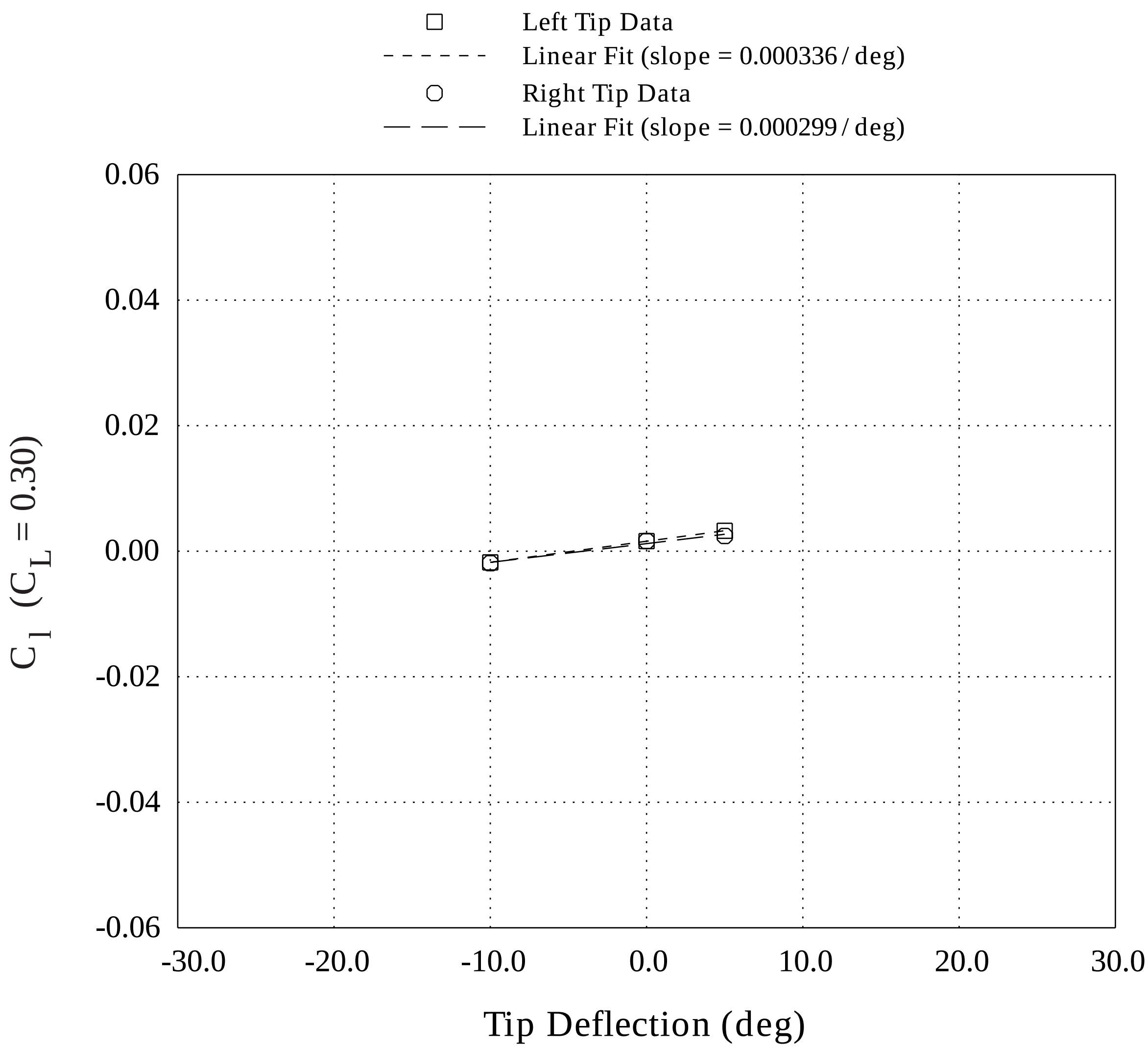

Figure 29(c). Tip deflection effectiveness for sweep = 65 deg, Mach = 1.20.

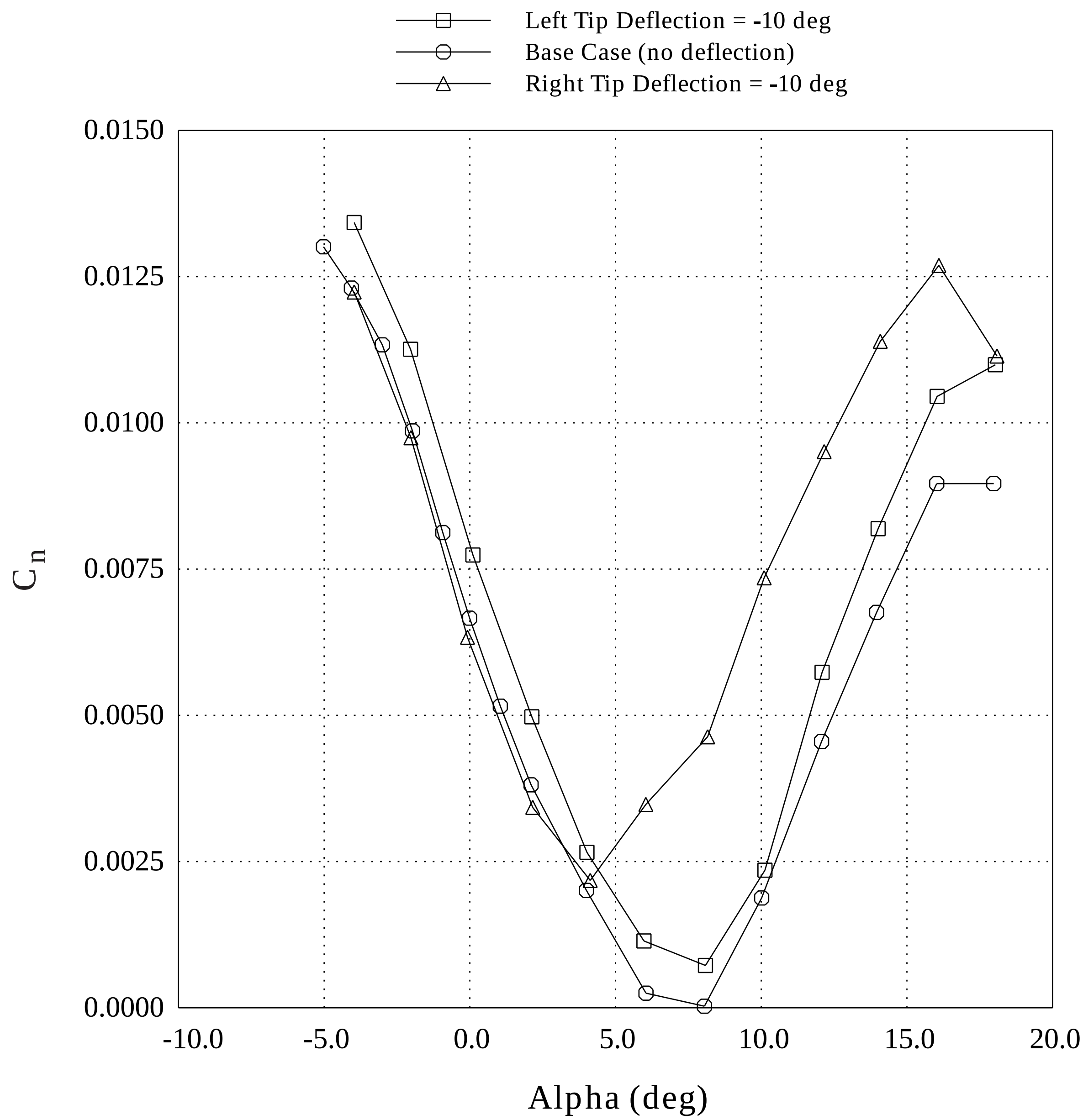

Figure 30. Right tip deflection provokes early break in yawing moment.

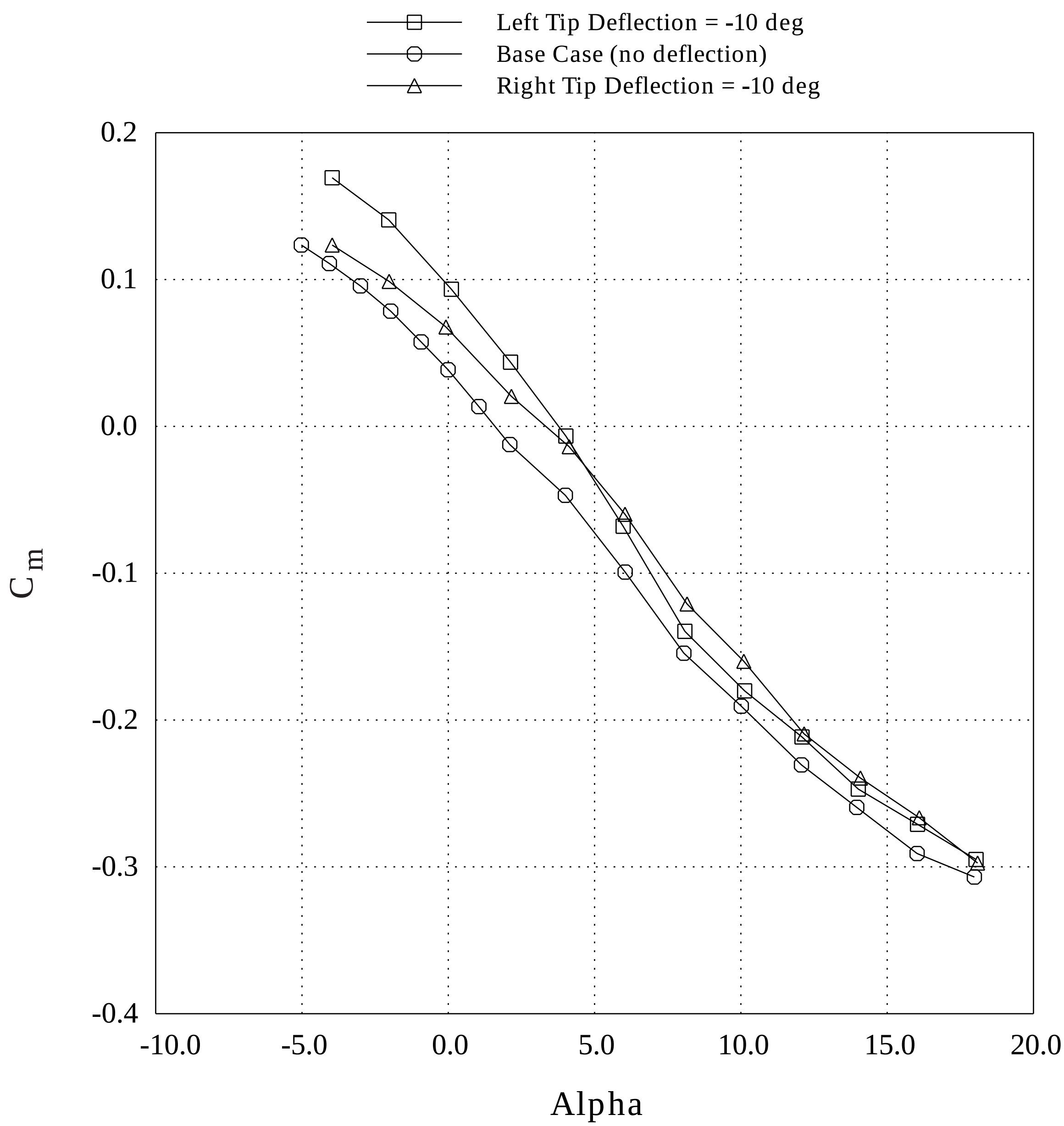

Figure 31. Effect of upward tip deflection on pitching moment is symmetrical.

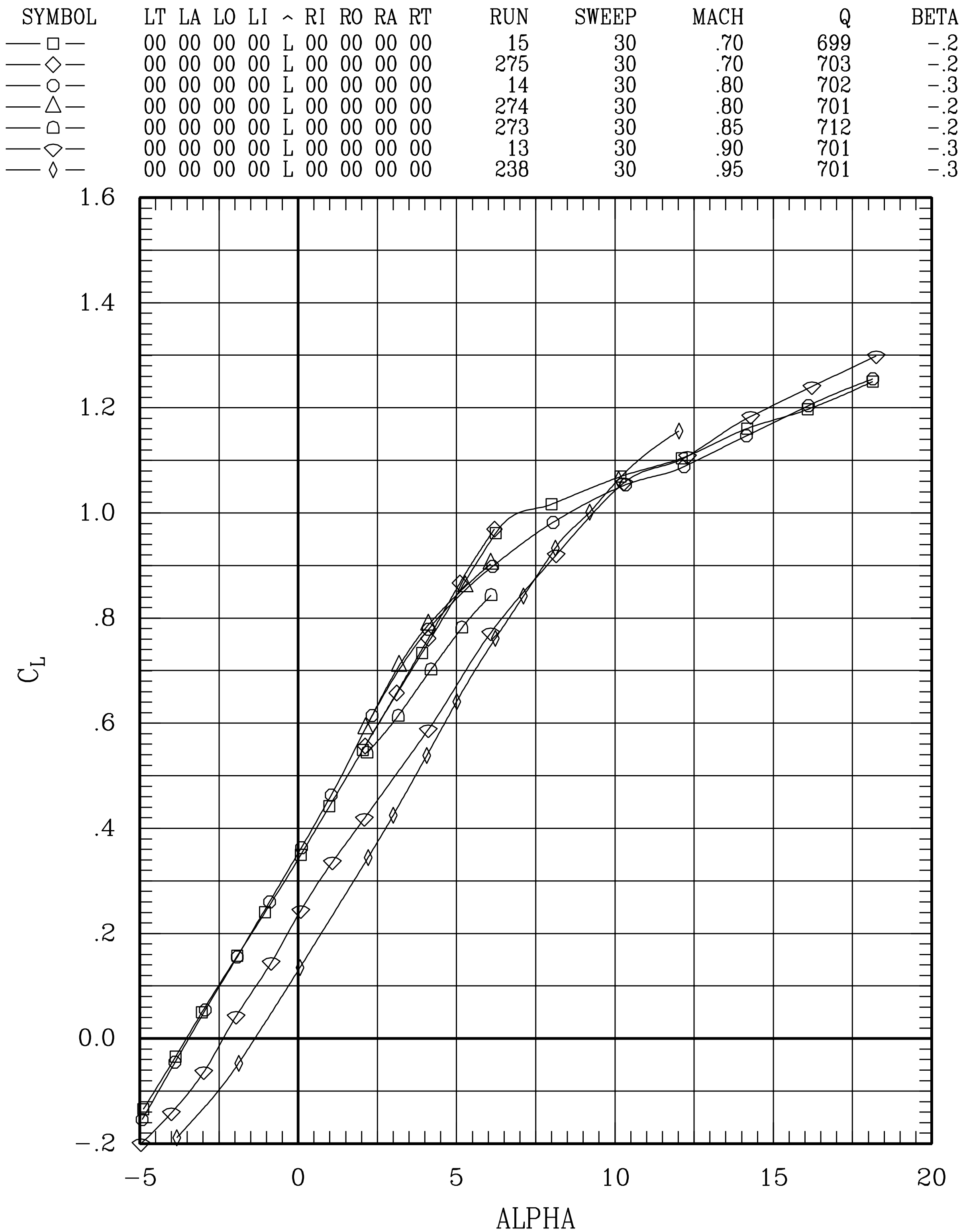

Figure 32(a). Transonic pitch-up for sweep = 30 deg.

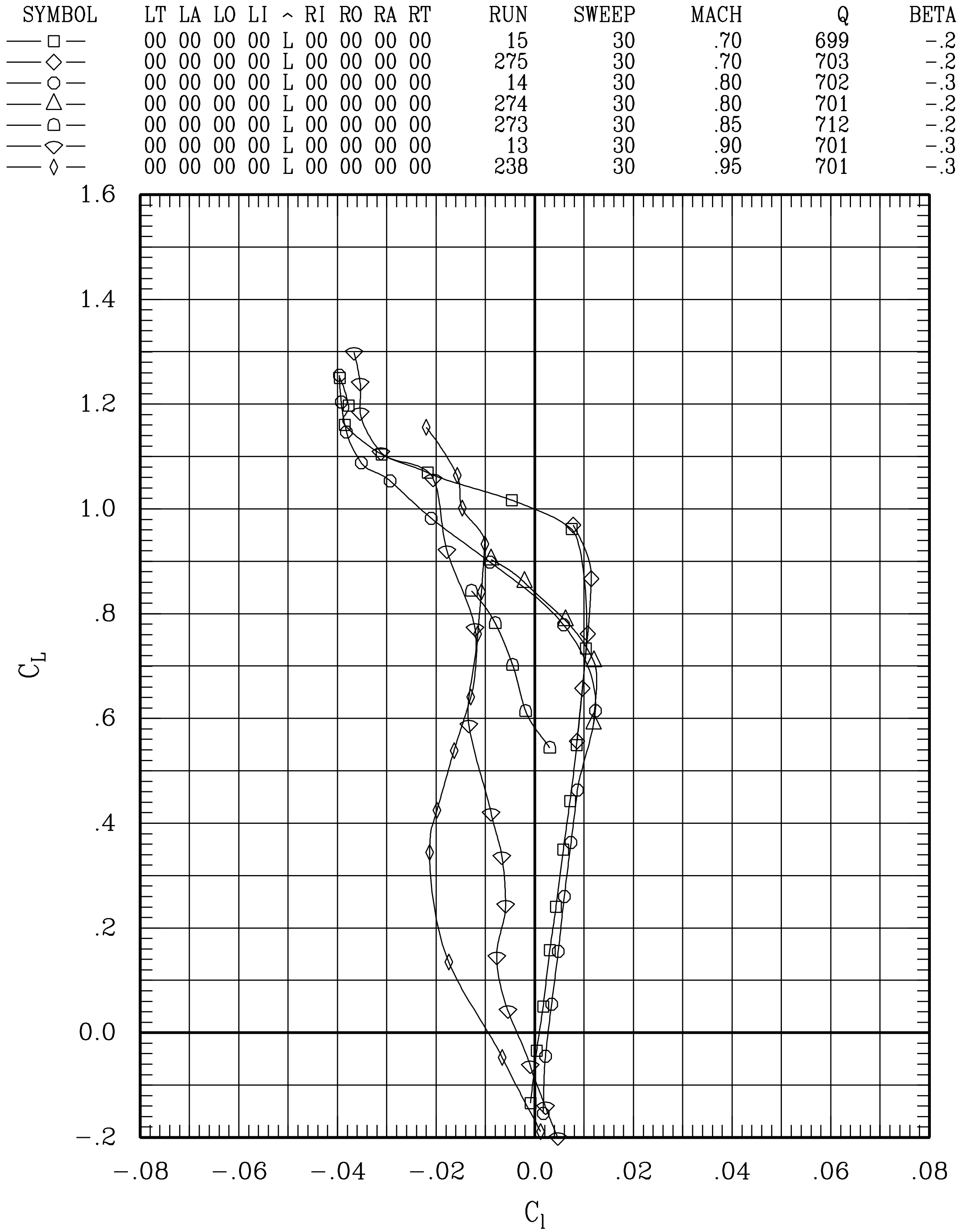

Figure 32(a). Transonic pitch-up for sweep = 30 deg.

SYMBOL	LT	LA	LO	LI	^	RI	RO	RA	RT	RUN	SWEEP	MACH	Q	BETA
—□—	00	00	00	00	L	00	00	00	00	15	30	.70	699	−.2
—◇—	00	00	00	00	L	00	00	00	00	275	30	.70	703	−.2
—○—	00	00	00	00	L	00	00	00	00	14	30	.80	702	−.3
—△—	00	00	00	00	L	00	00	00	00	274	30	.80	701	−.2
—⌓—	00	00	00	00	L	00	00	00	00	273	30	.85	712	−.2
—▽—	00	00	00	00	L	00	00	00	00	13	30	.90	701	−.3
—◊—	00	00	00	00	L	00	00	00	00	238	30	.95	701	−.3

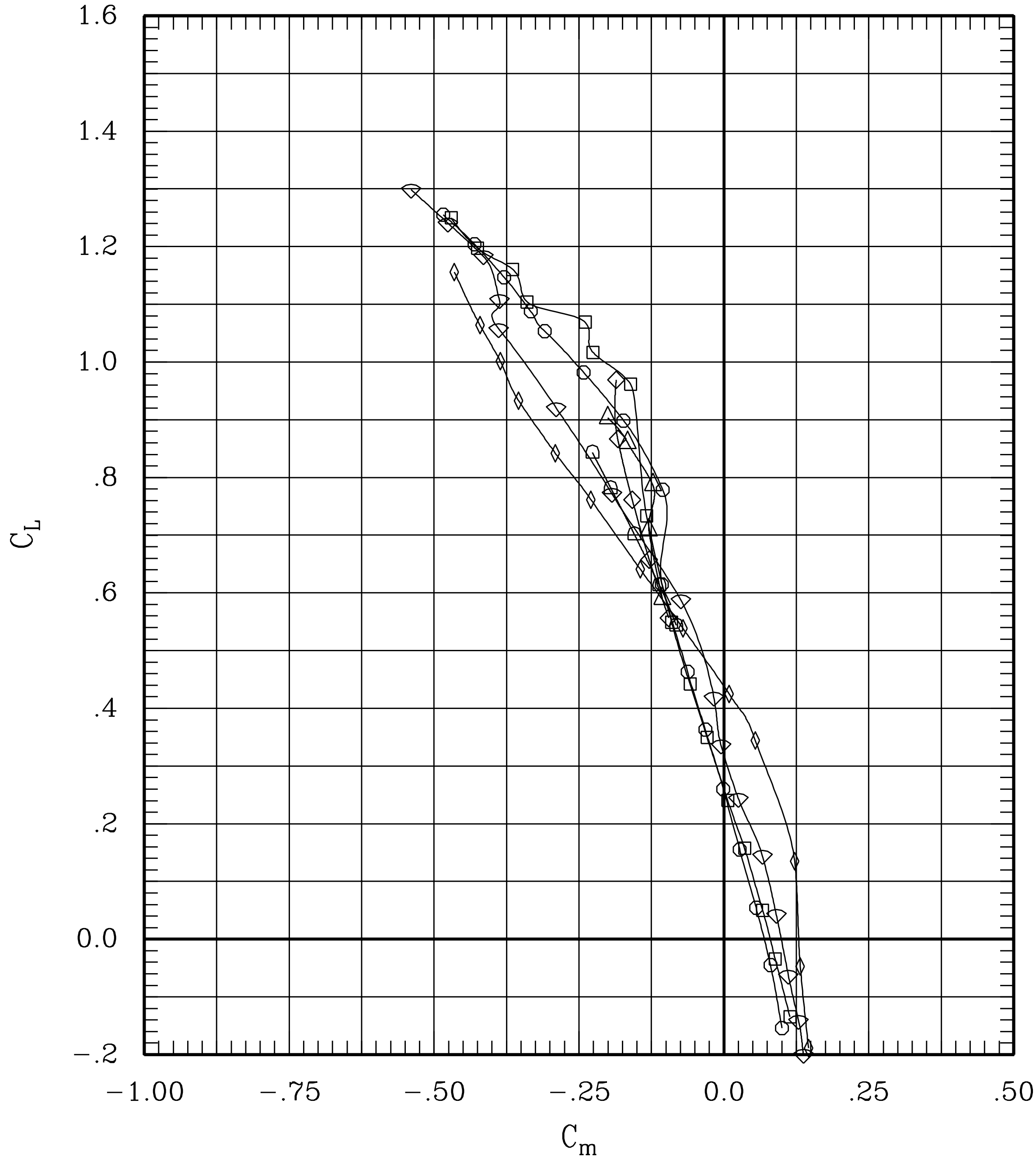

Figure 32(a). Transonic pitch-up for sweep = 30 deg.

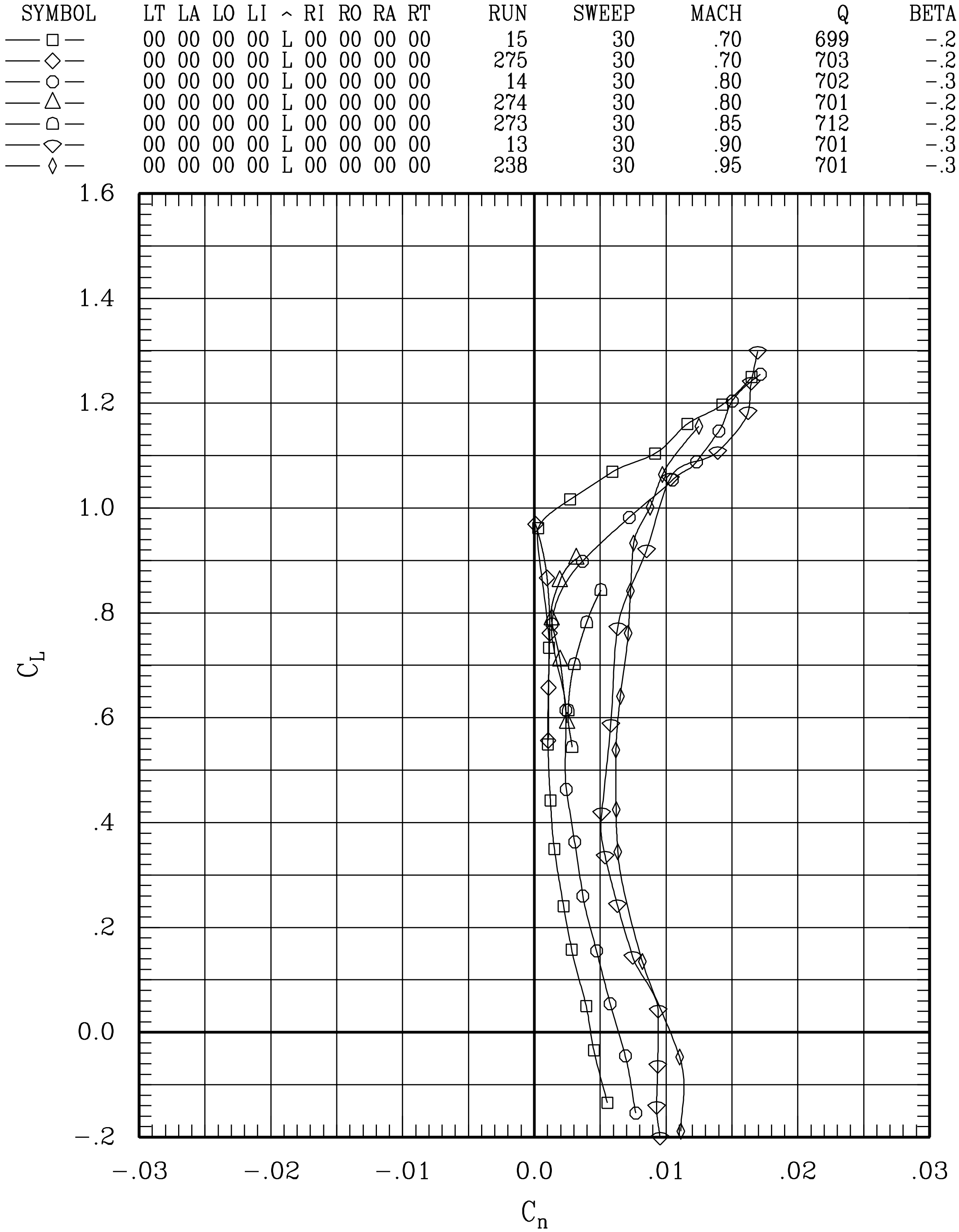

Figure 32(a). Transonic pitch-up for sweep = 30 deg.

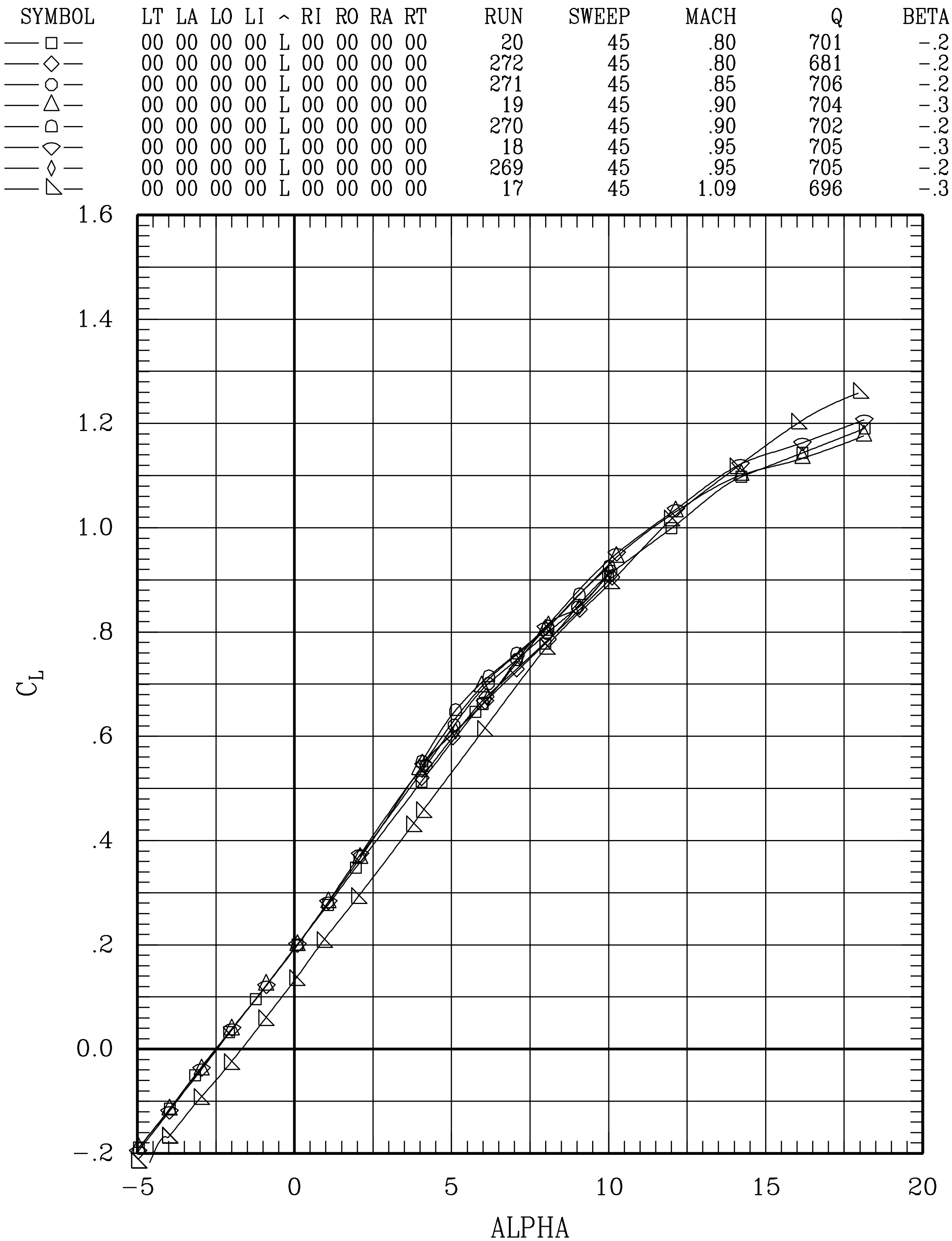

Figure 32(b). Transonic pitch-up for sweep = 45 deg.

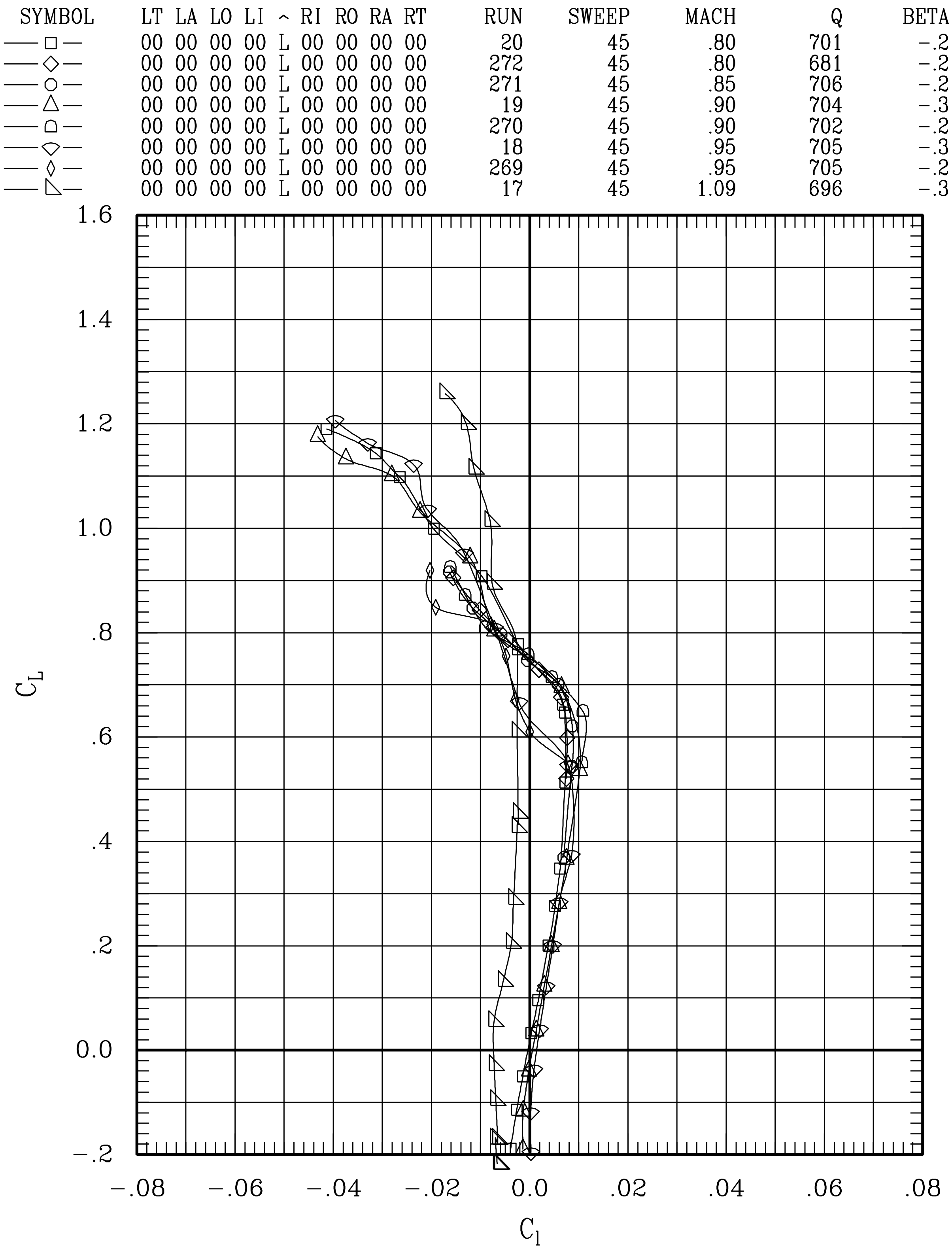

Figure 32(b). Transonic pitch-up for sweep = 45 deg.

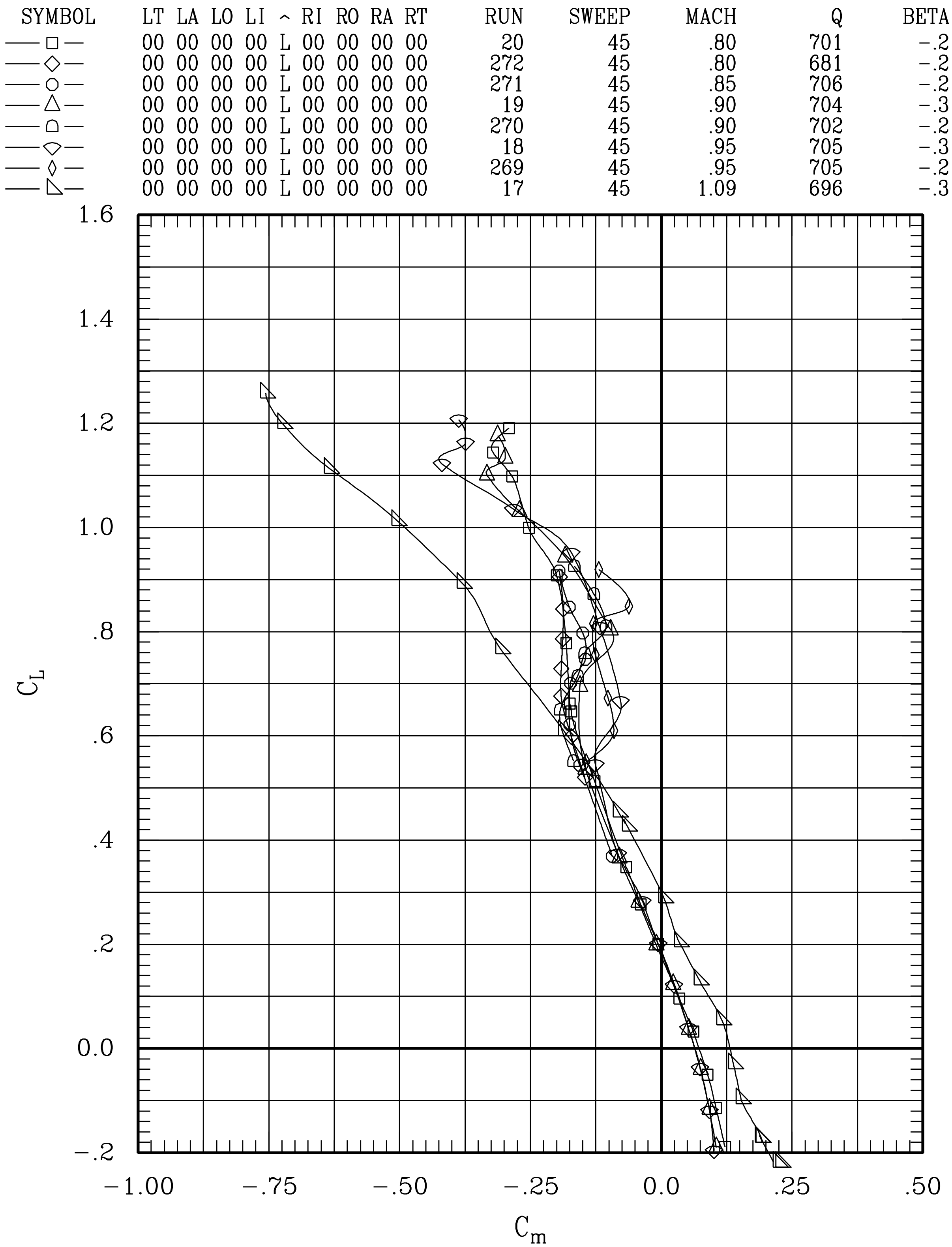

Figure 32(b). Transonic pitch−up for sweep = 45 deg.

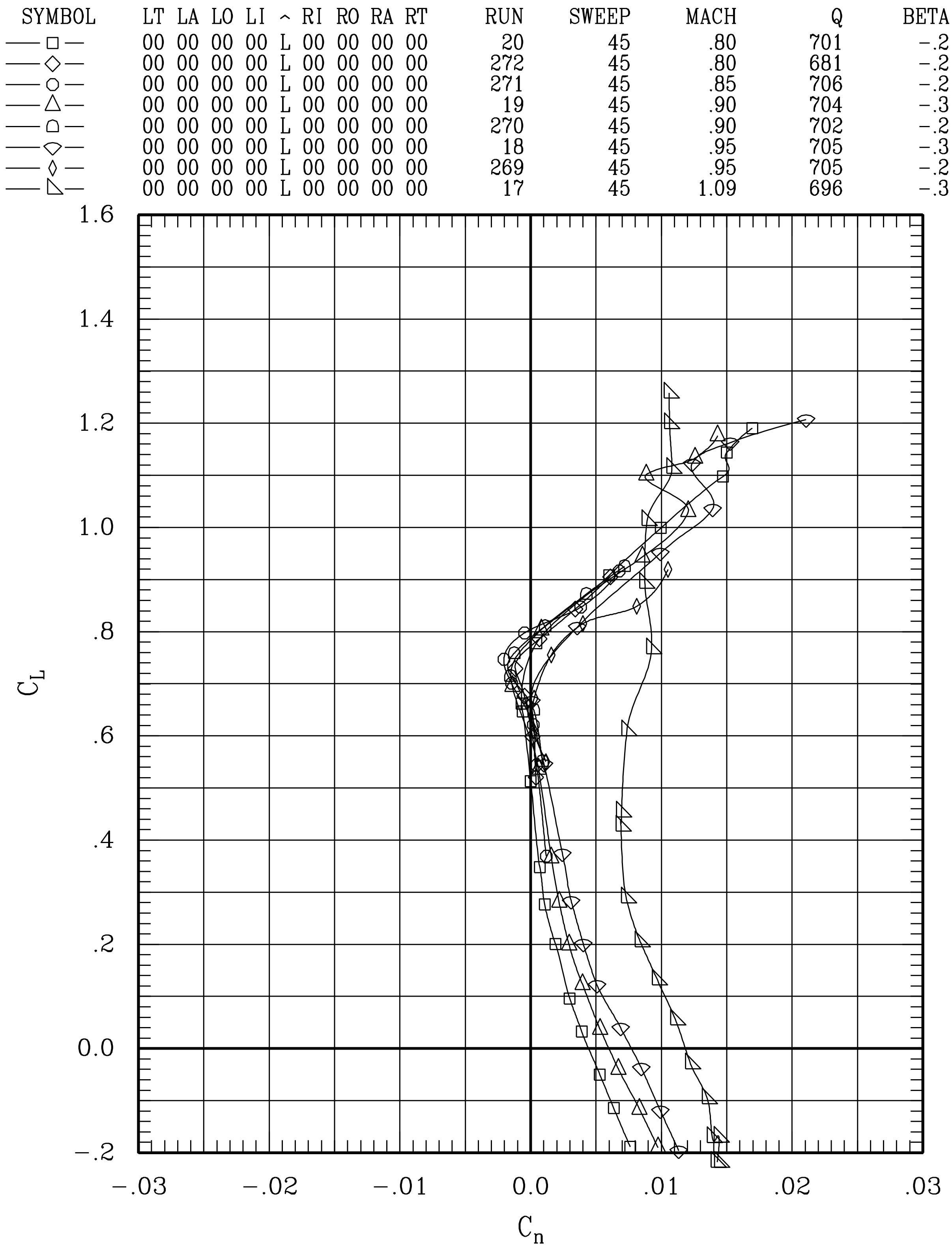

Figure 32(b). Transonic pitch-up for sweep = 45 deg.

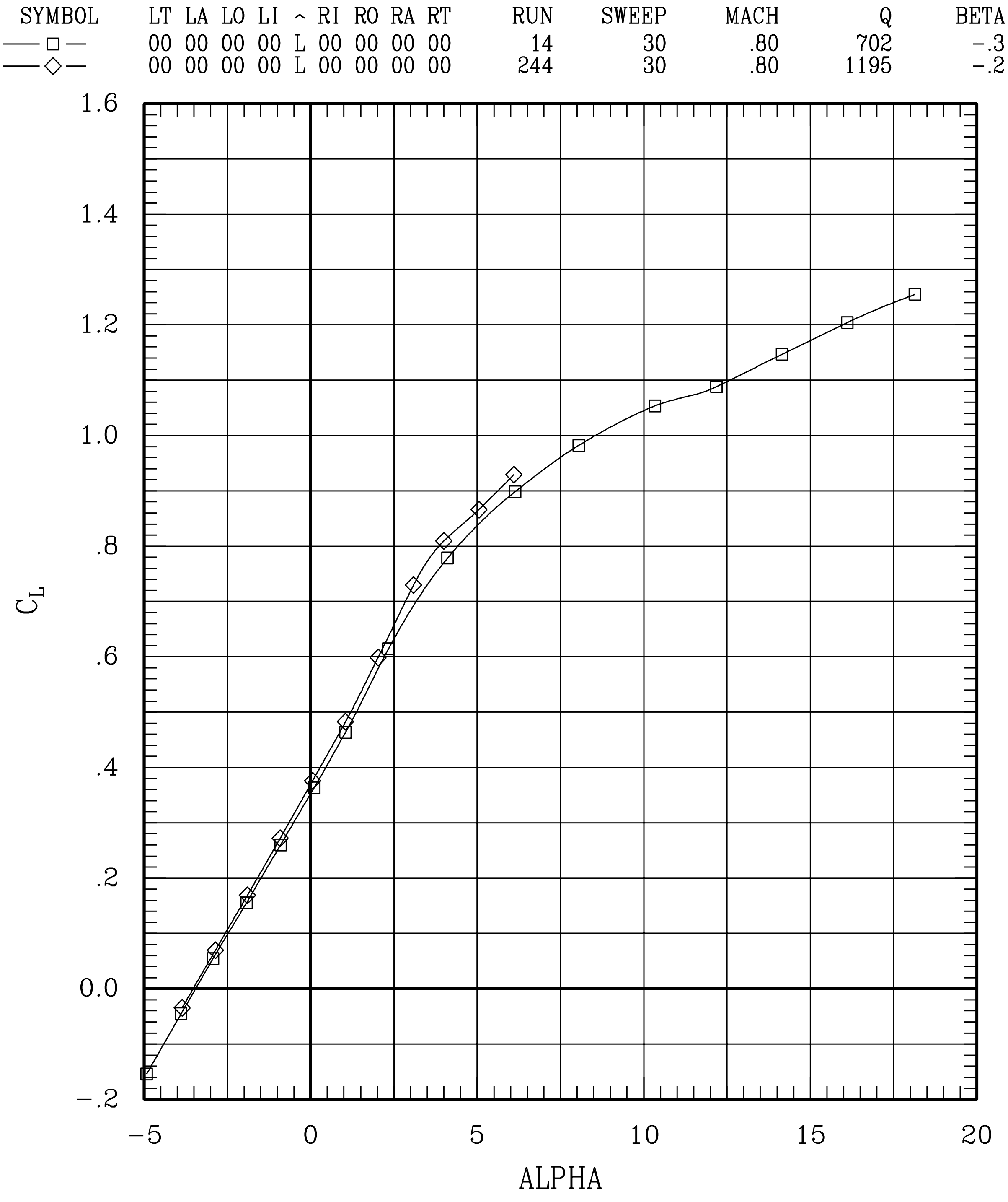

Figure 33(a). Effect of dynamic pressure for sweep = 30 deg, Mach = 0.80.

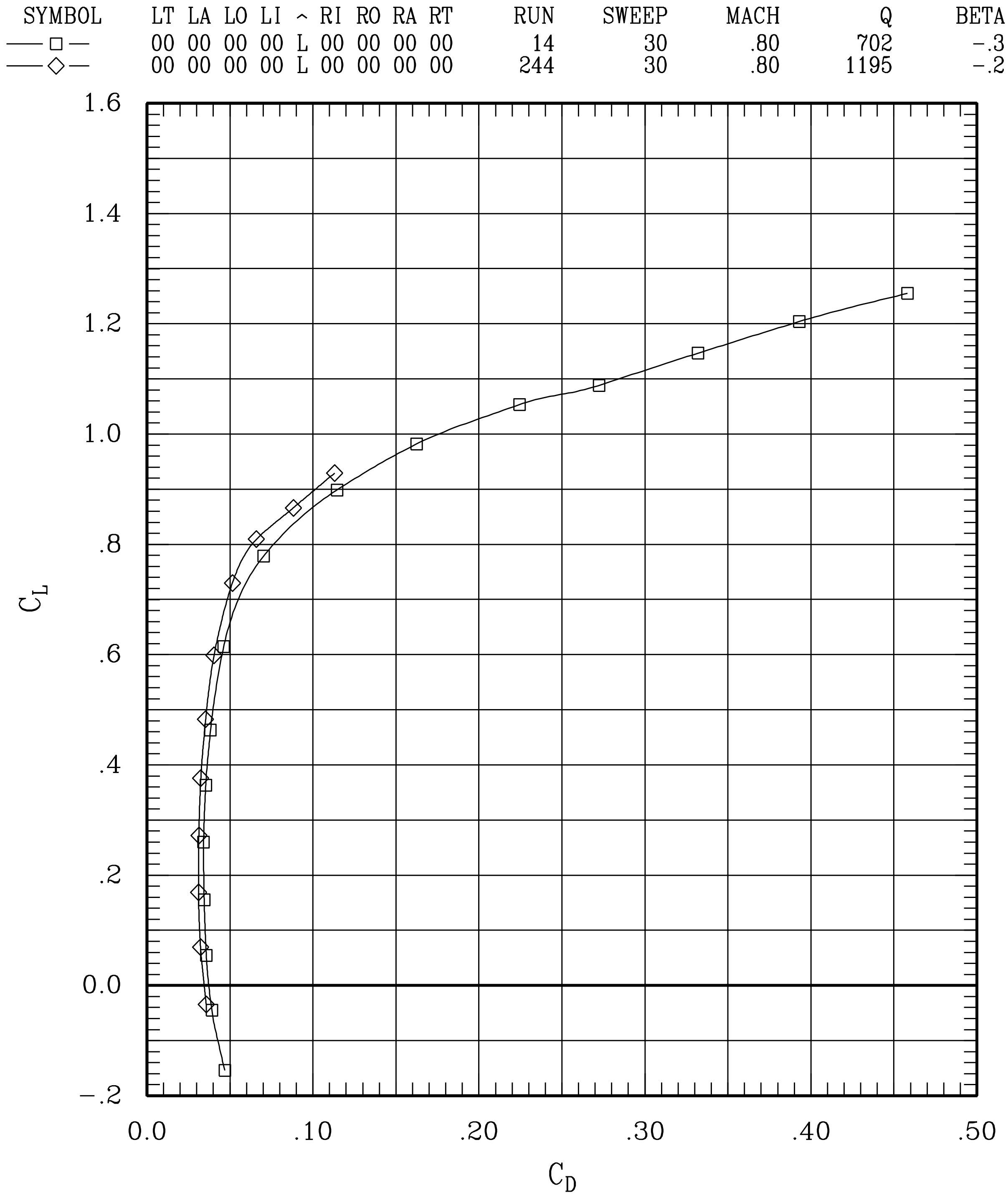

Figure 33(a). Effect of dynamic pressure for sweep = 30 deg, Mach = 0.80.

SYMBOL	LT LA LO LI ^ RI RO RA RT	RUN	SWEEP	MACH	Q	BETA
—□—	00 00 00 00 L 00 00 00 00	14	30	.80	702	−.3
—◇—	00 00 00 00 L 00 00 00 00	244	30	.80	1195	−.2

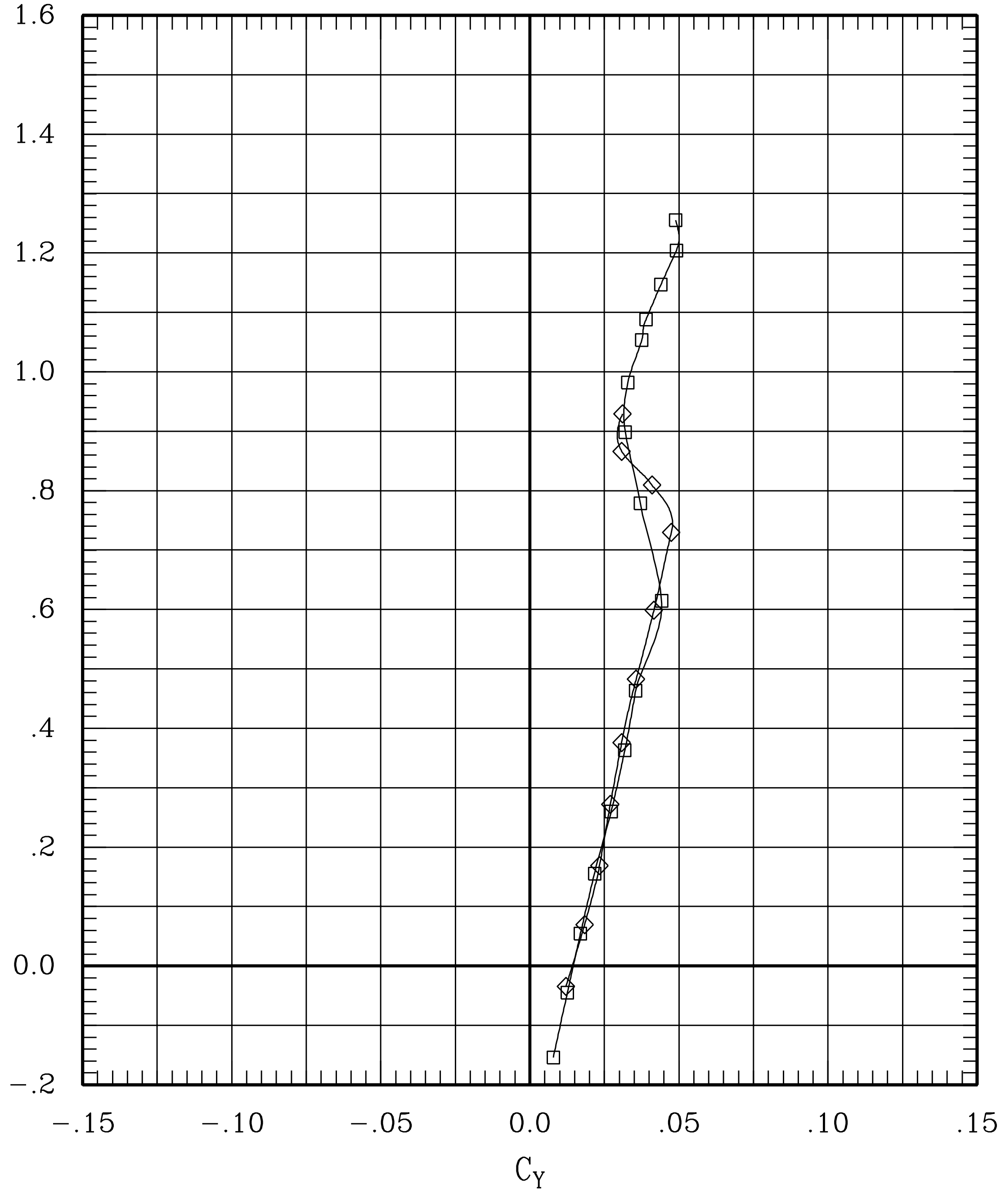

Figure 33(a). Effect of dynamic pressure for sweep = 30 deg, Mach = 0.80.

SYMBOL	LT LA LO LI ^ RI RO RA RT	RUN	SWEEP	MACH	Q	BETA
—□—	00 00 00 00 L 00 00 00 00	14	30	.80	702	−.3
—◇—	00 00 00 00 L 00 00 00 00	244	30	.80	1195	−.2

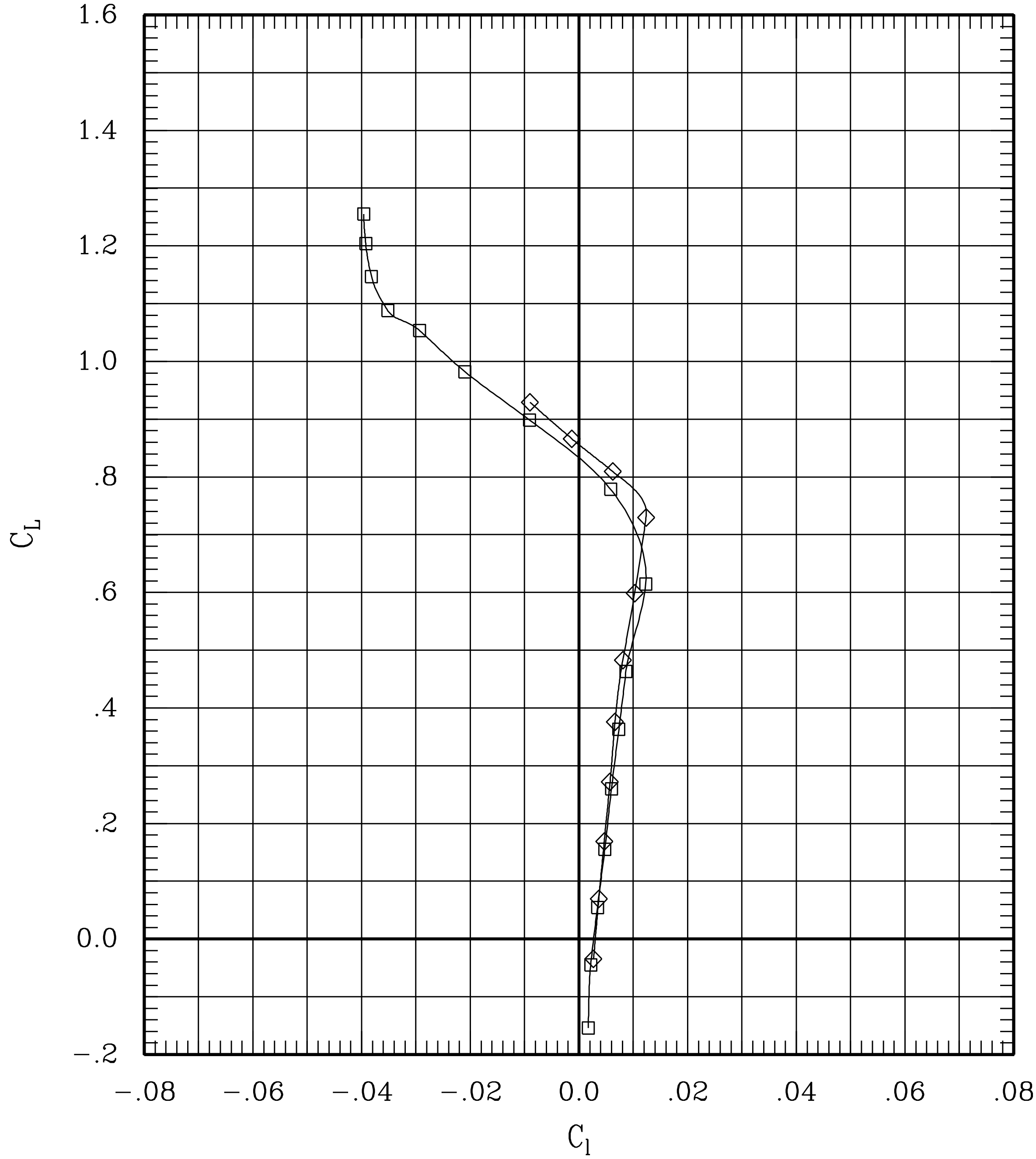

Figure 33(a). Effect of dynamic pressure for sweep = 30 deg, Mach = 0.80.

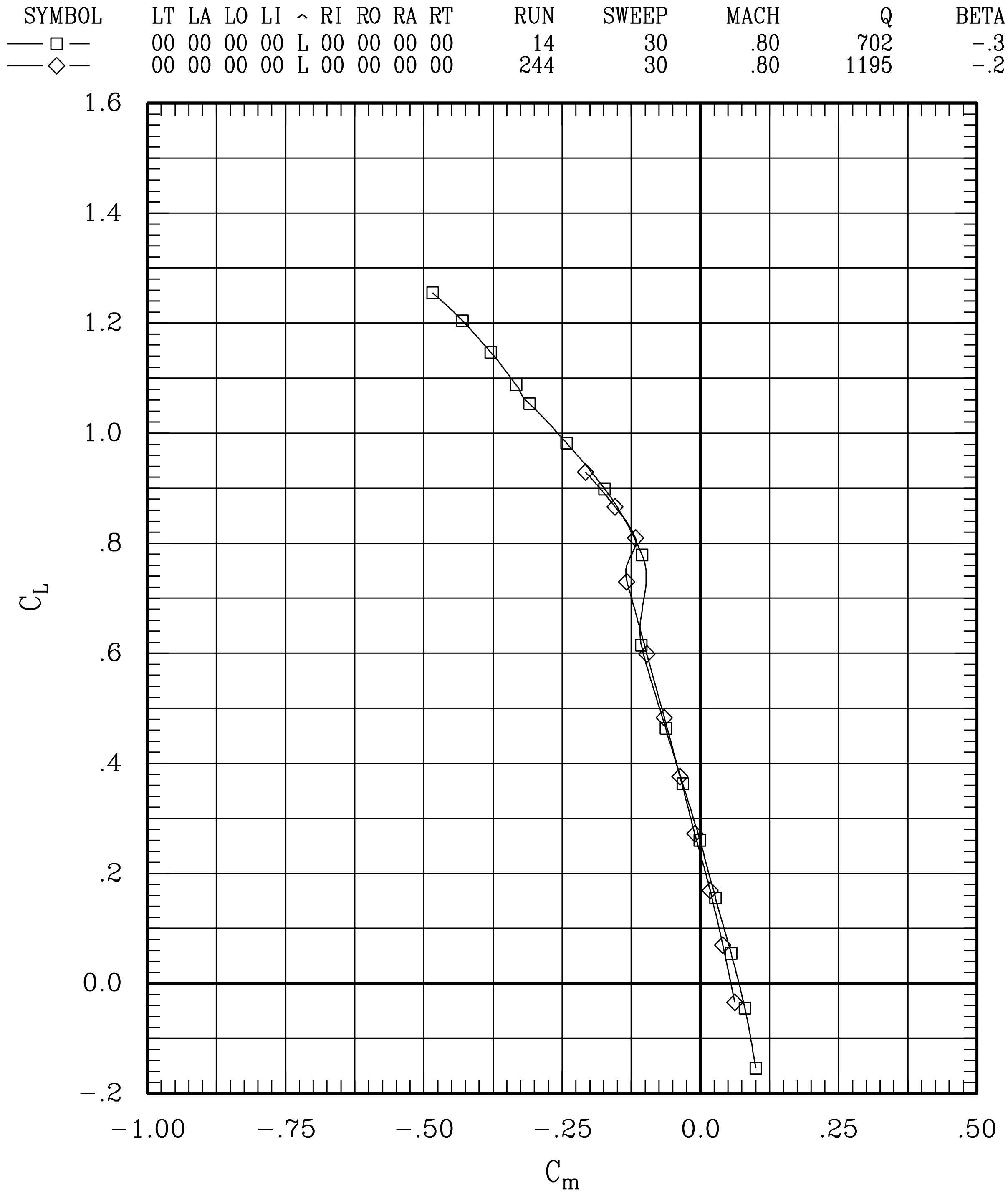

Figure 33(a). Effect of dynamic pressure for sweep = 30 deg, Mach = 0.80.

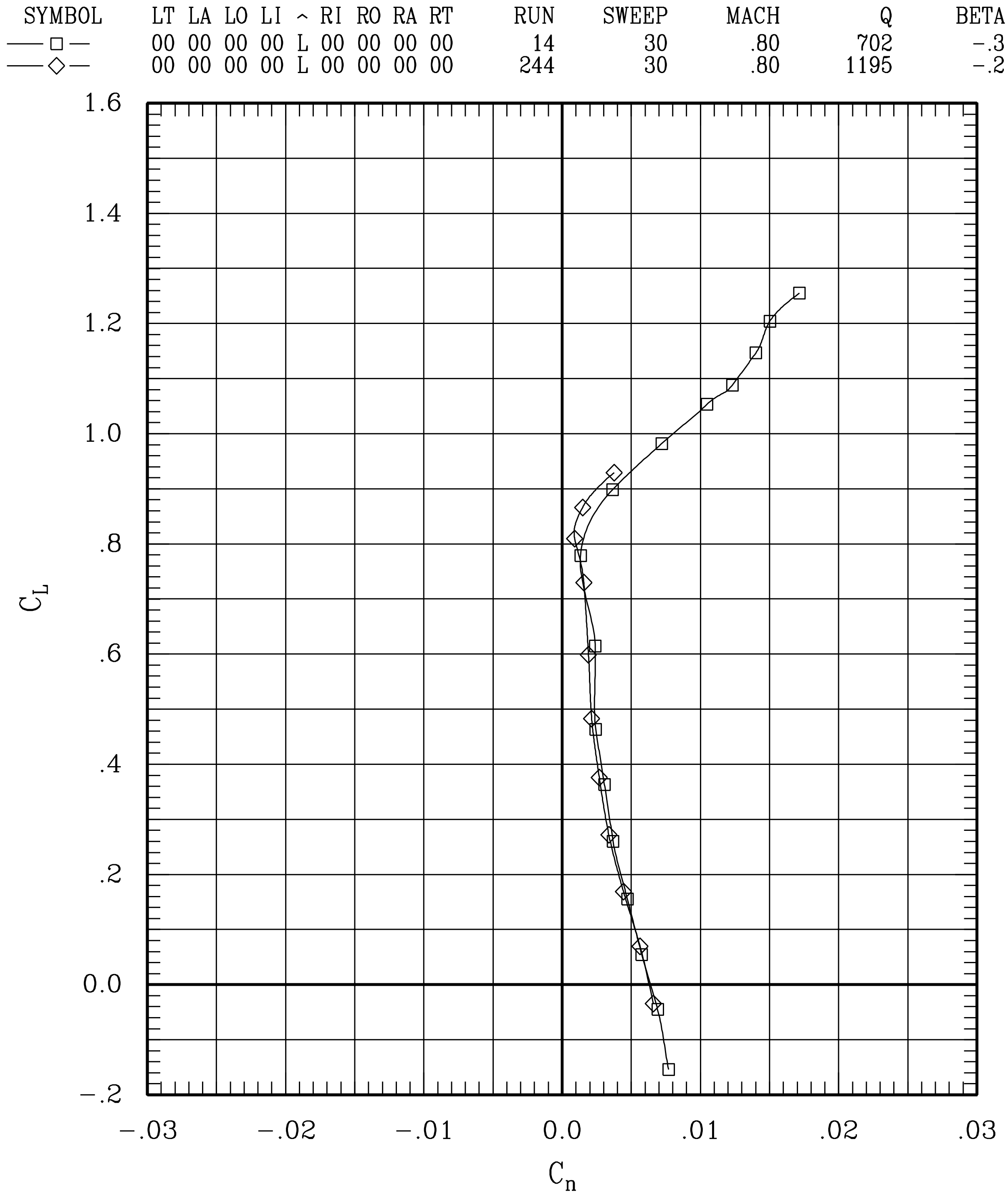

Figure 33(a). Effect of dynamic pressure for sweep = 30 deg, Mach = 0.80.

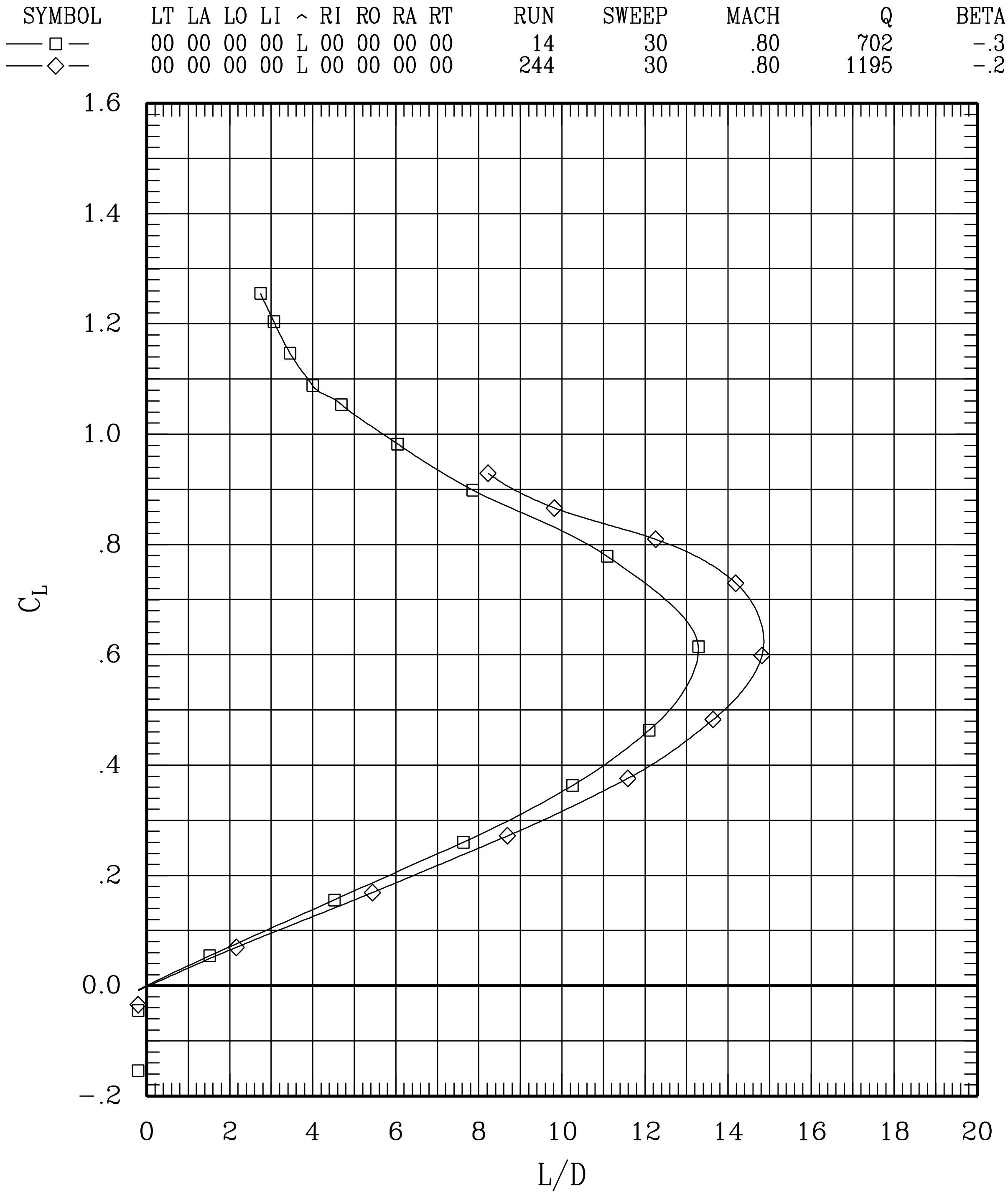

Figure 33(a). Effect of dynamic pressure for sweep = 30 deg, Mach = 0.80.

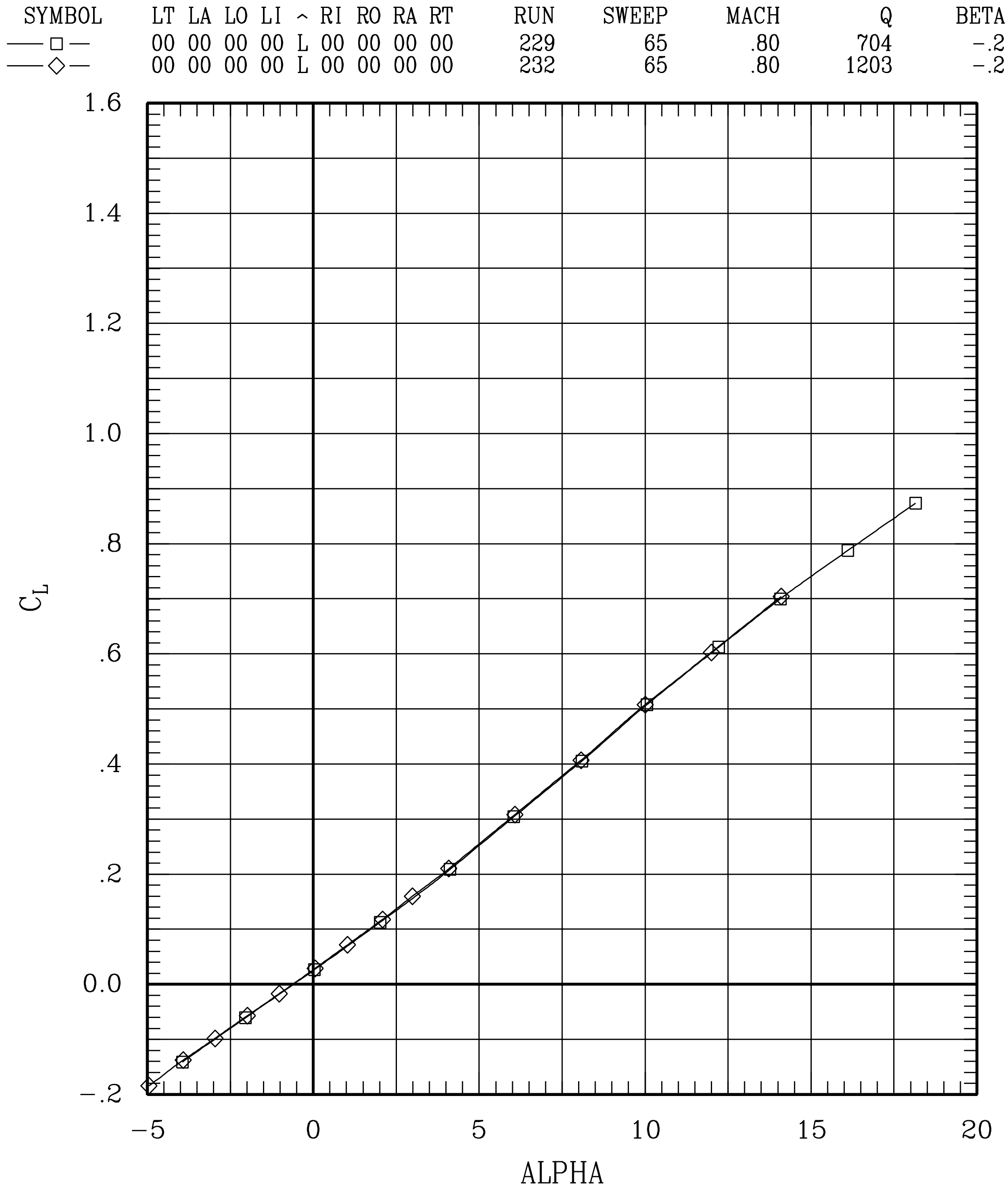

Figure 33(b). Effect of dynamic pressure for sweep = 65 deg, Mach = 0.80.

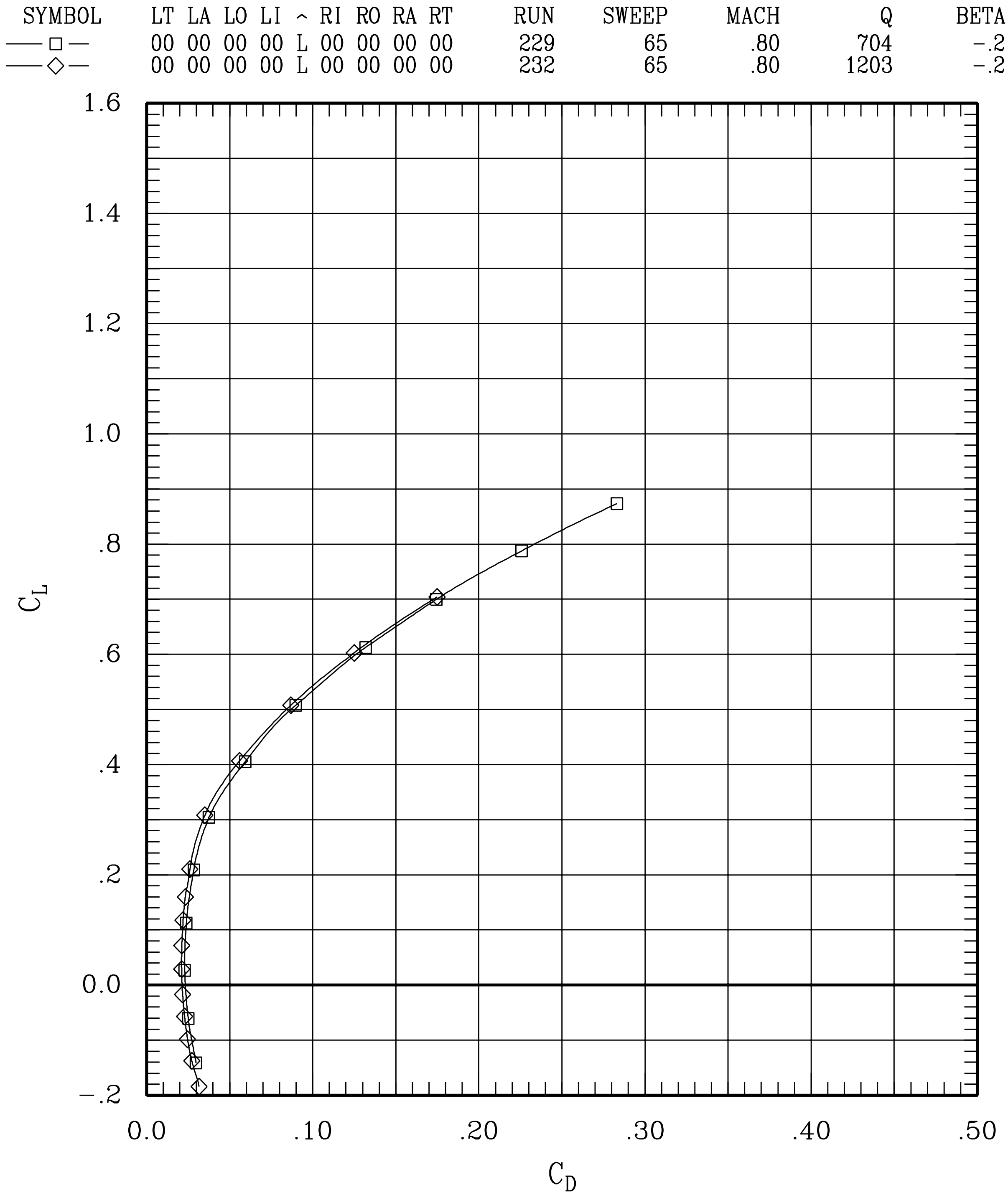

Figure 33(b). Effect of dynamic pressure for sweep = 65 deg, Mach = 0.80.

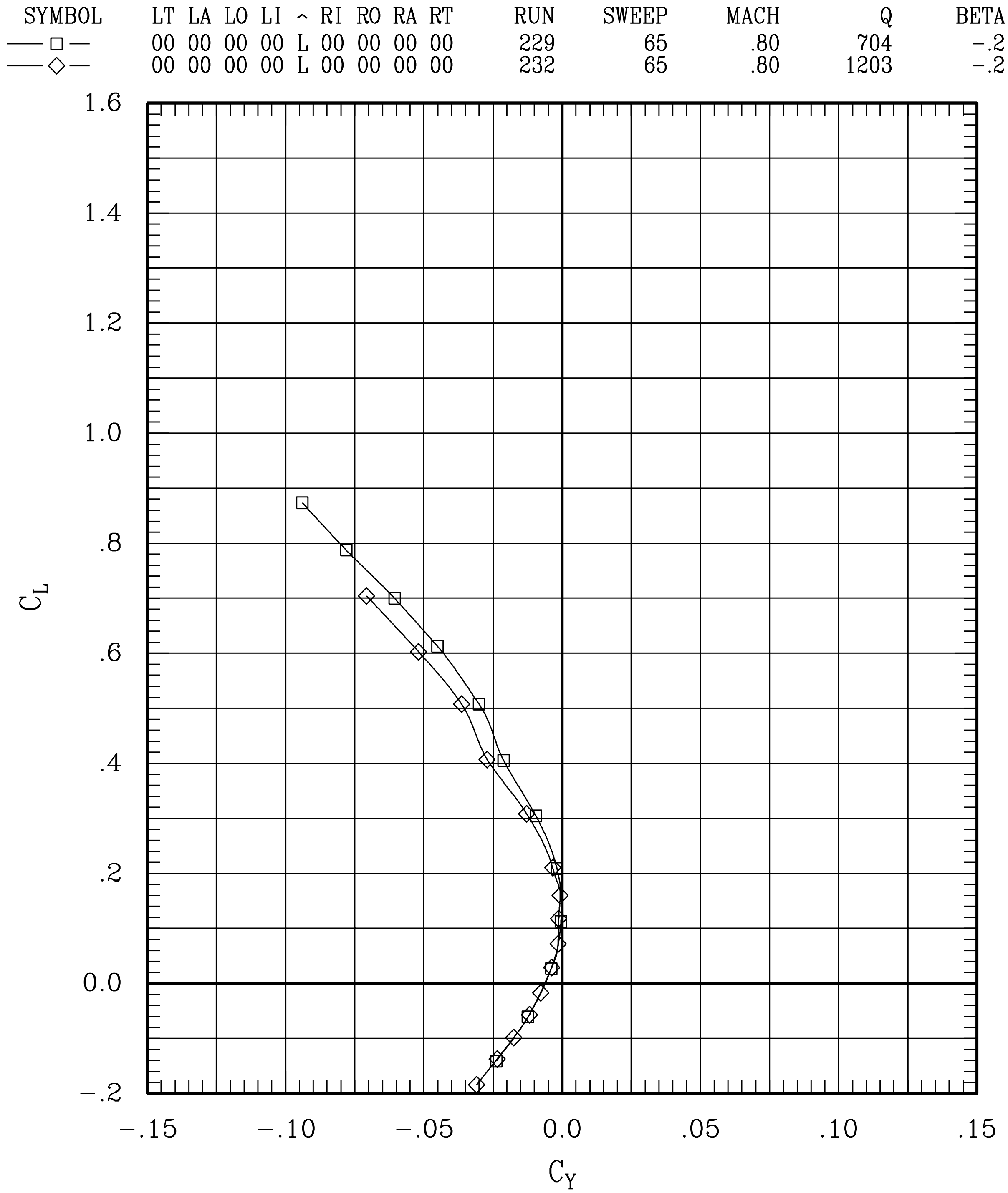

Figure 33(b). Effect of dynamic pressure for sweep = 65 deg, Mach = 0.80.

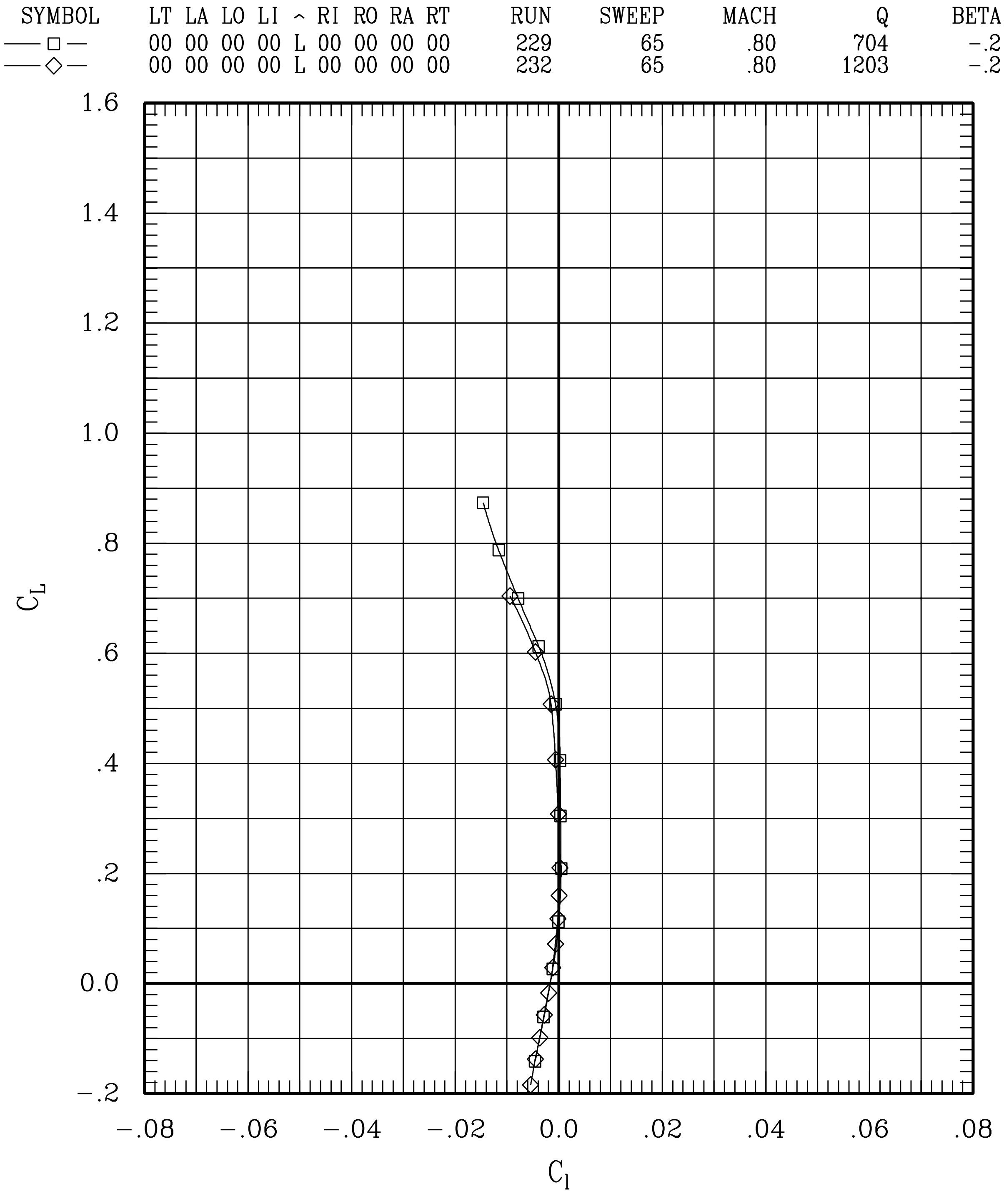

Figure 33(b). Effect of dynamic pressure for sweep = 65 deg, Mach = 0.80.

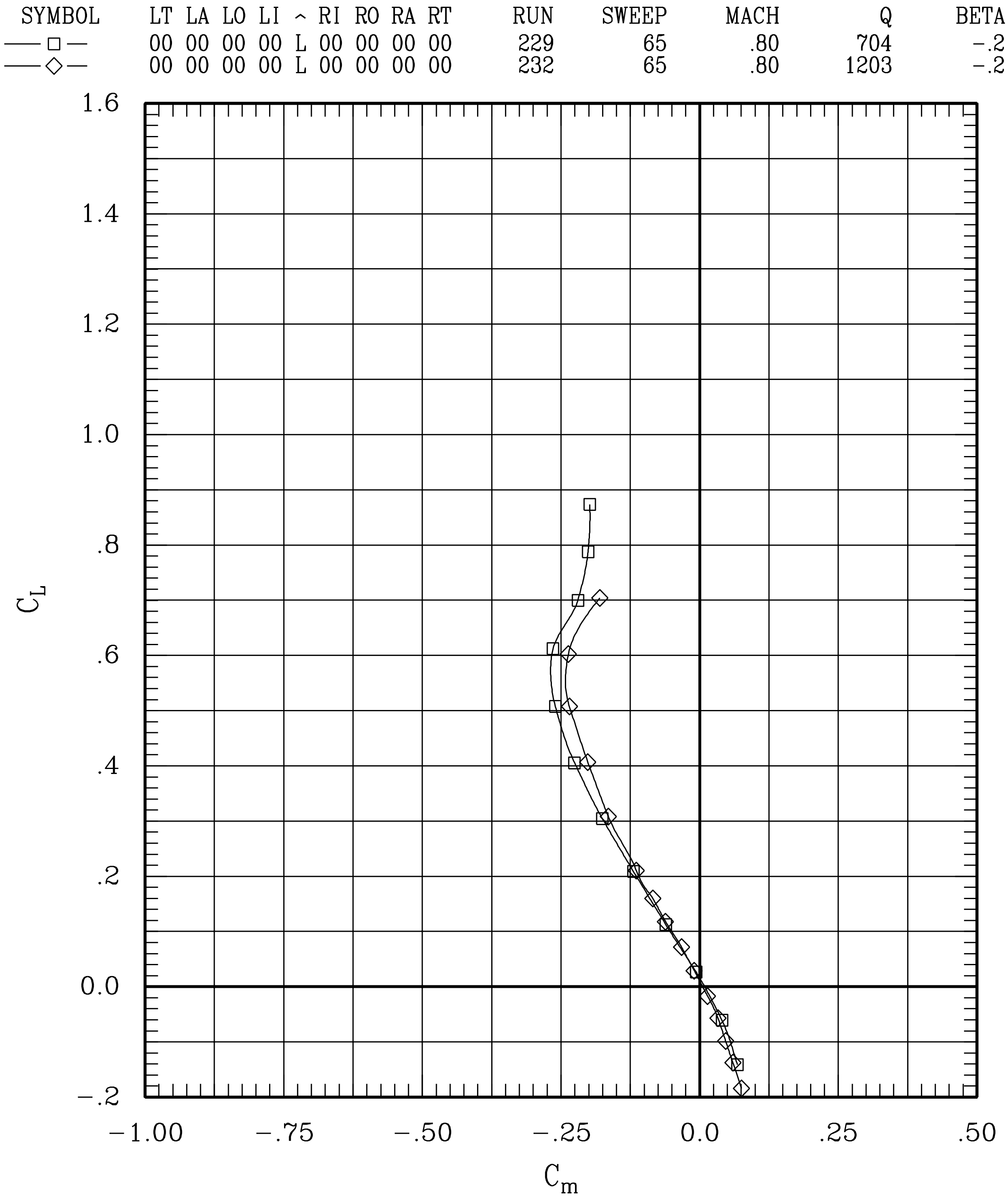

Figure 33(b). Effect of dynamic pressure for sweep = 65 deg, Mach = 0.80.

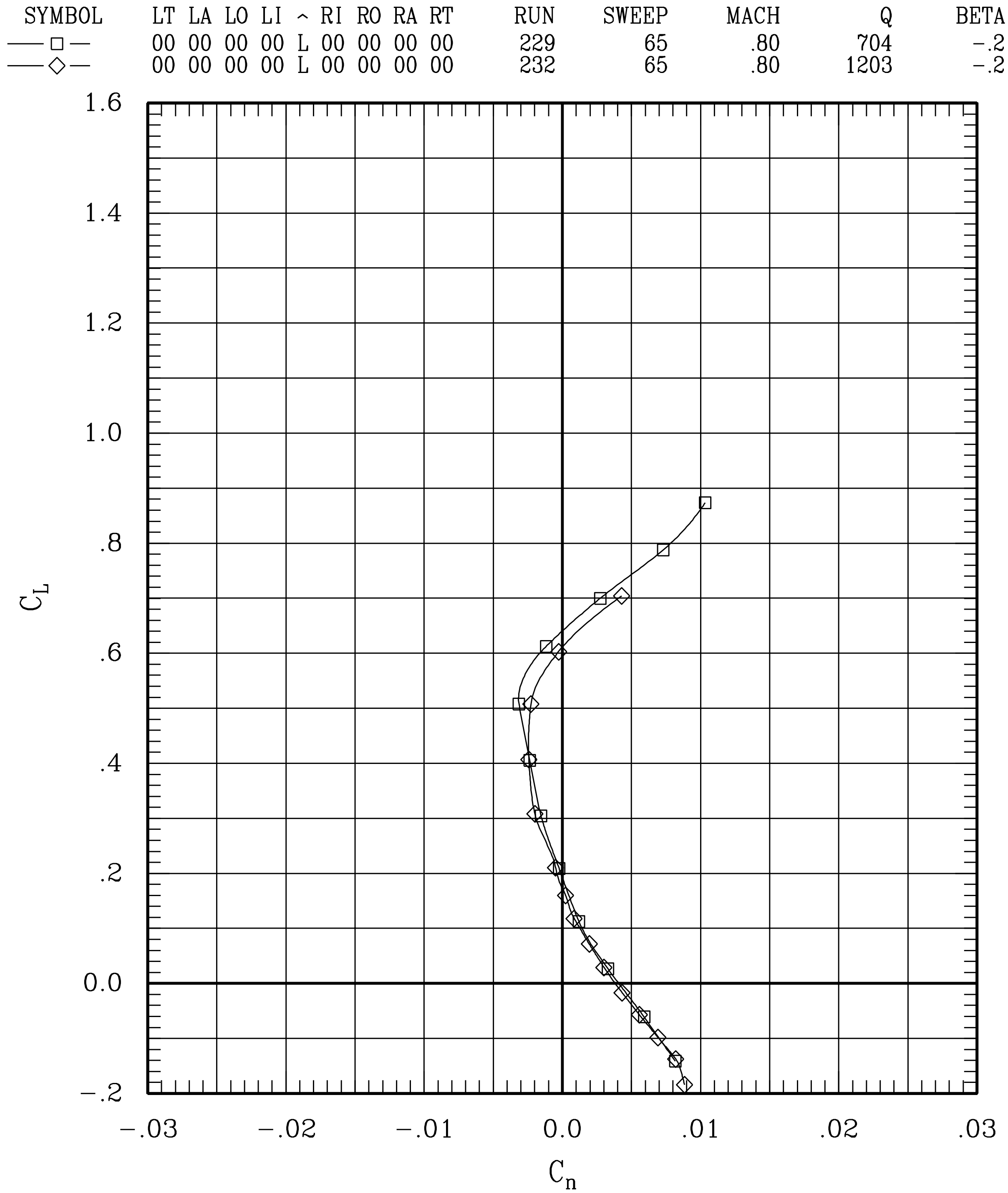

Figure 33(b). Effect of dynamic pressure for sweep = 65 deg, Mach = 0.80.

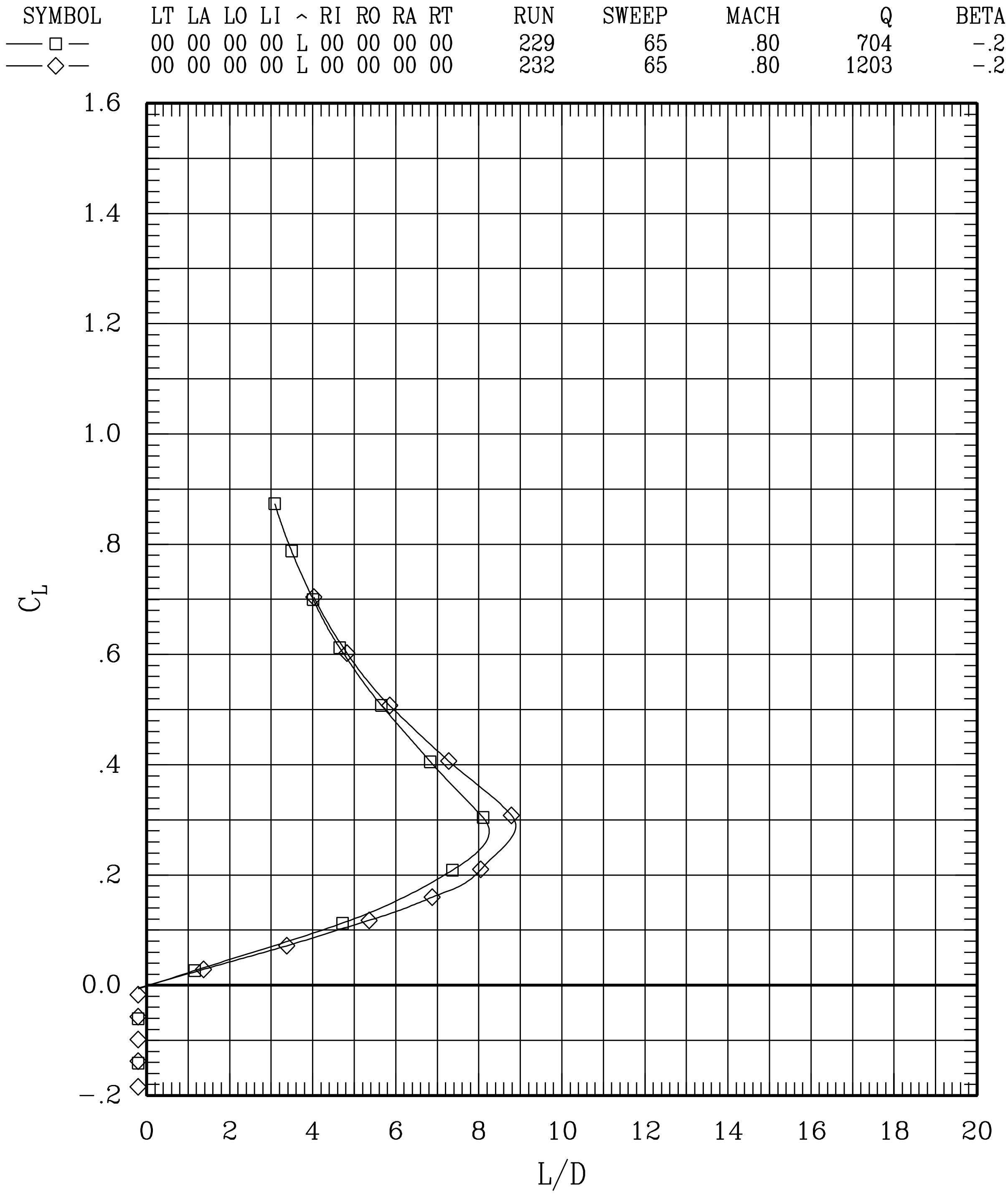

Figure 33(b). Effect of dynamic pressure for sweep = 65 deg, Mach = 0.80.

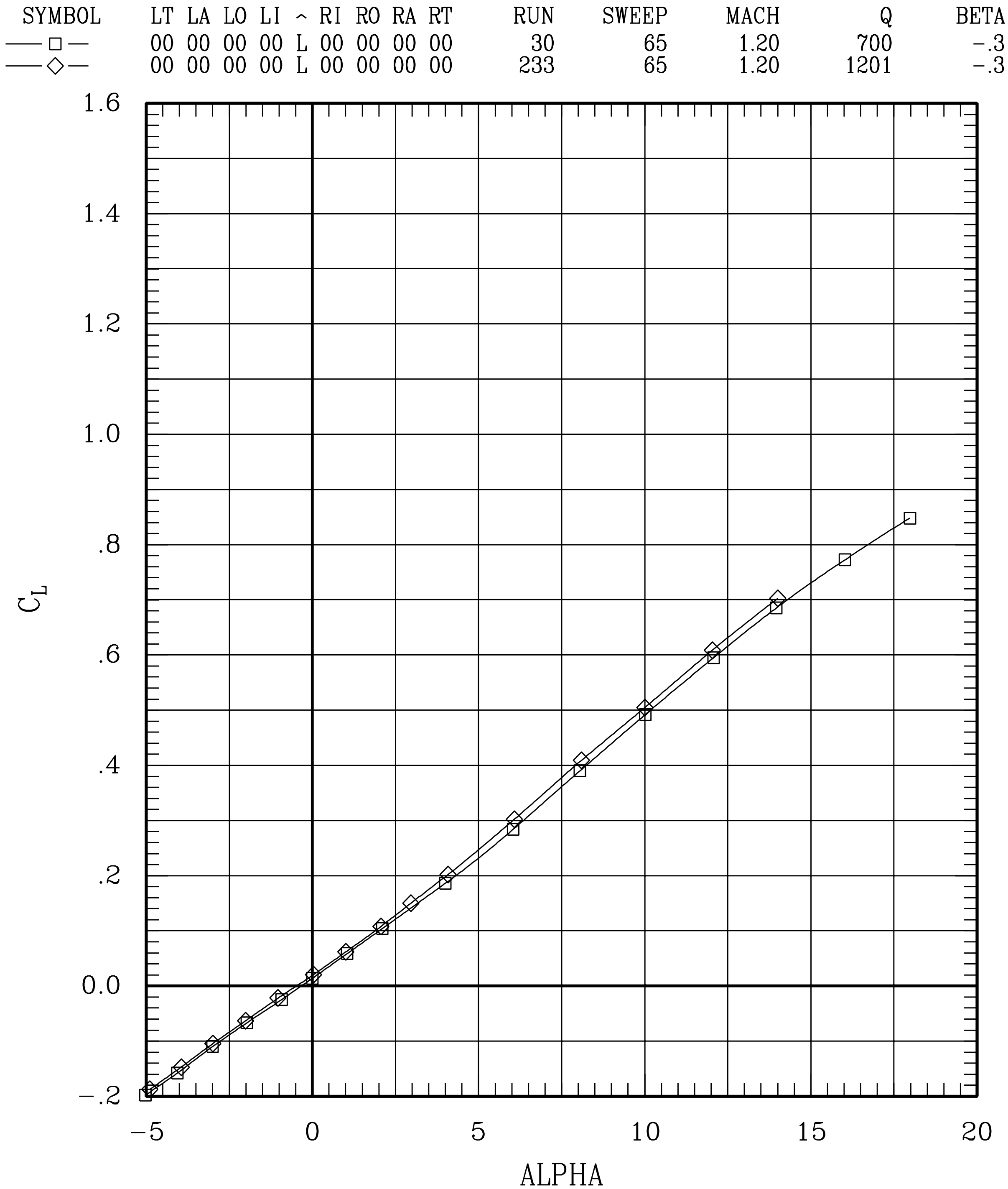

Figure 33(c). Effect of dynamic pressure for sweep = 65 deg, Mach = 1.20.

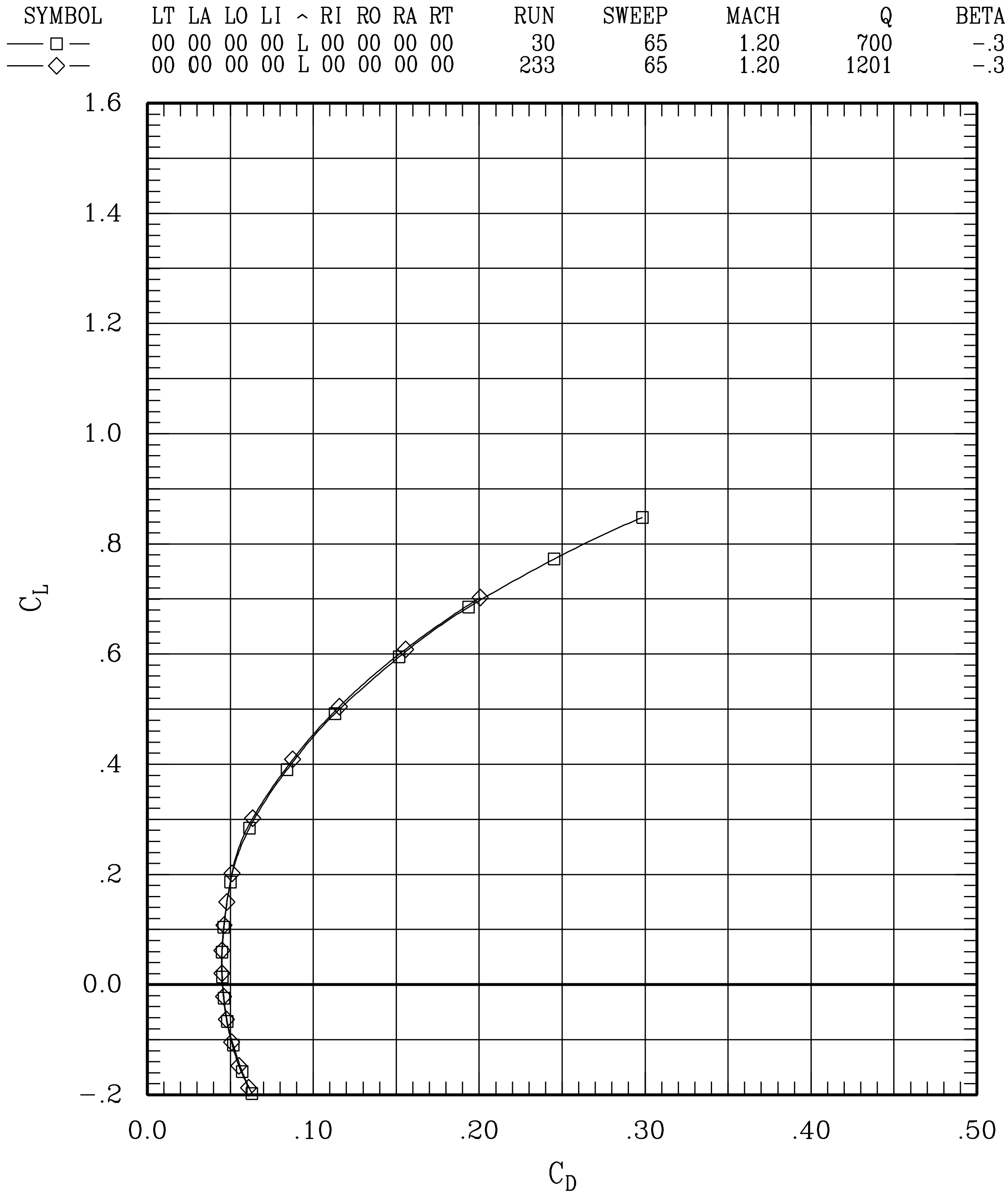

Figure 33(c). Effect of dynamic pressure for sweep = 65 deg, Mach = 1.20.

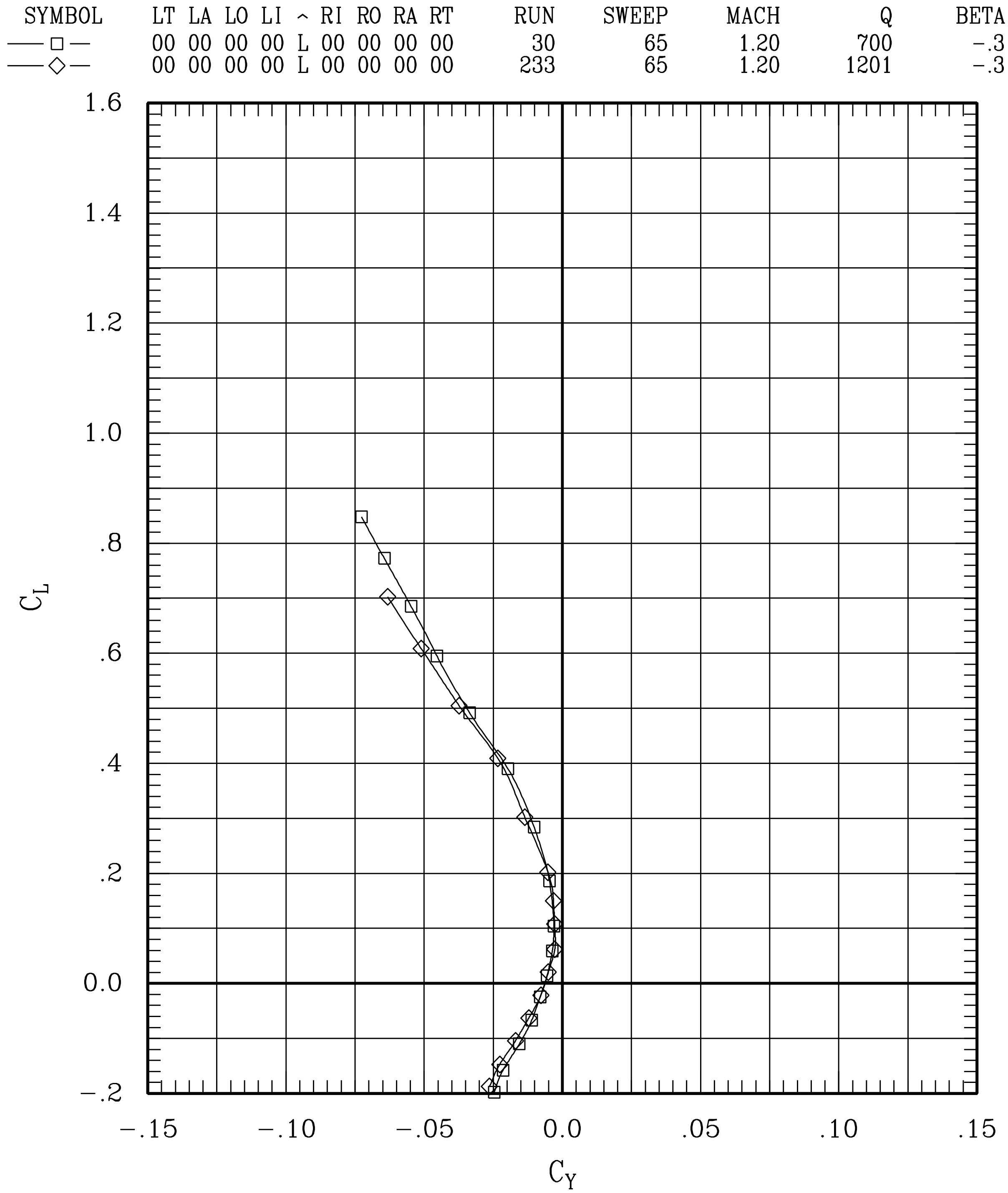

Figure 33(c). Effect of dynamic pressure for sweep = 65 deg, Mach = 1.20.

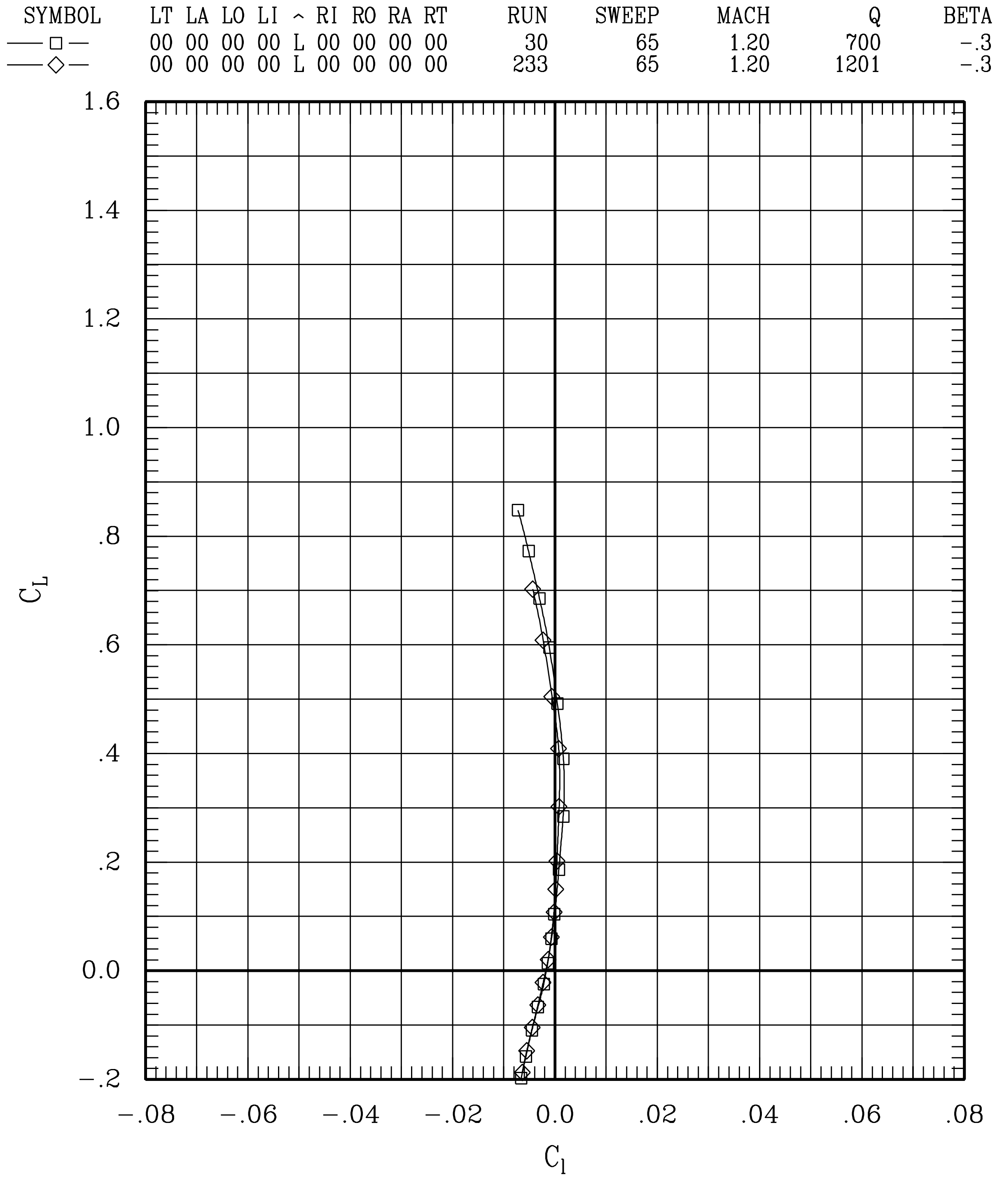

Figure 33(c). Effect of dynamic pressure for sweep = 65 deg, Mach = 1.20.

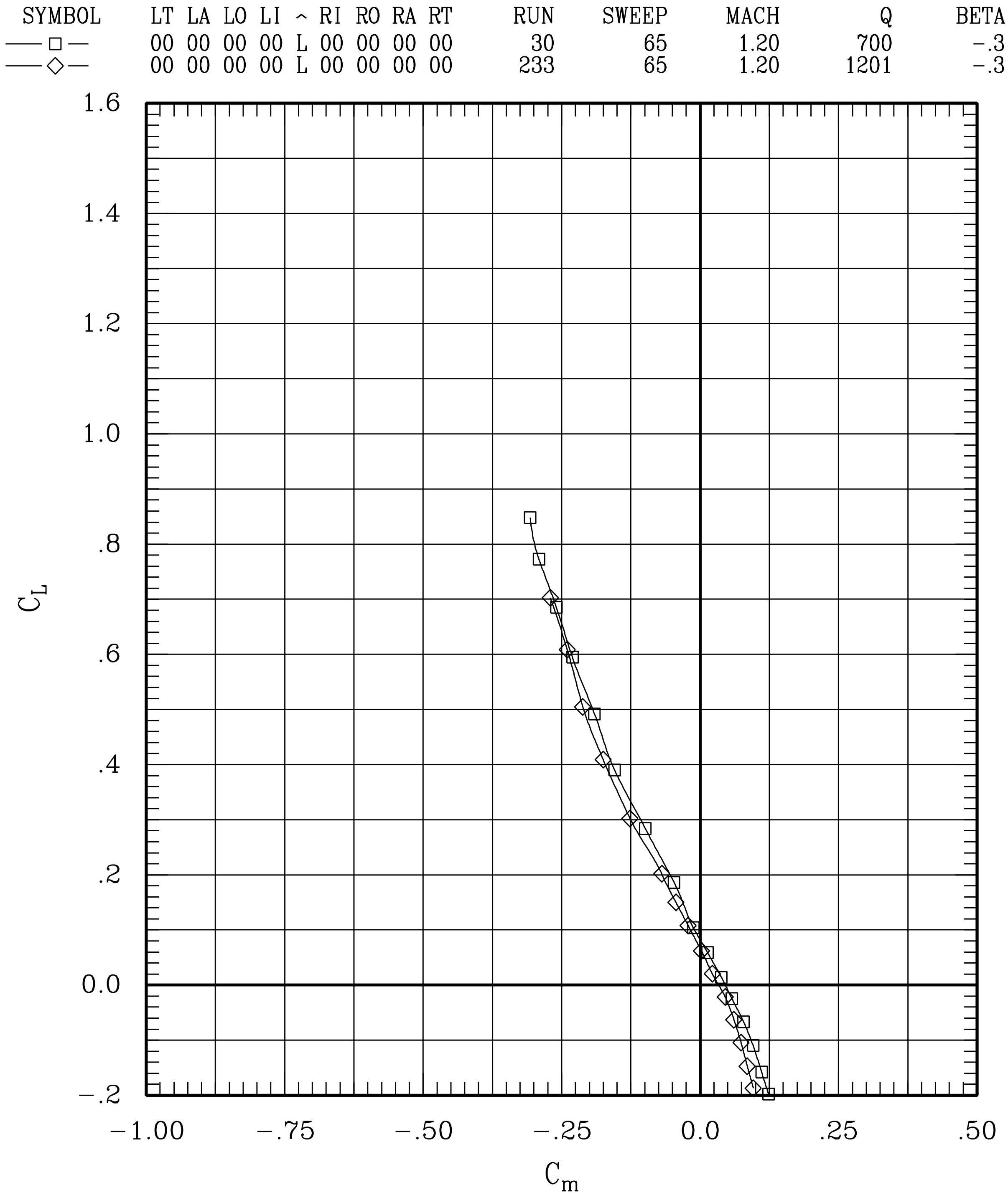

Figure 33(c). Effect of dynamic pressure for sweep = 65 deg, Mach = 1.20.

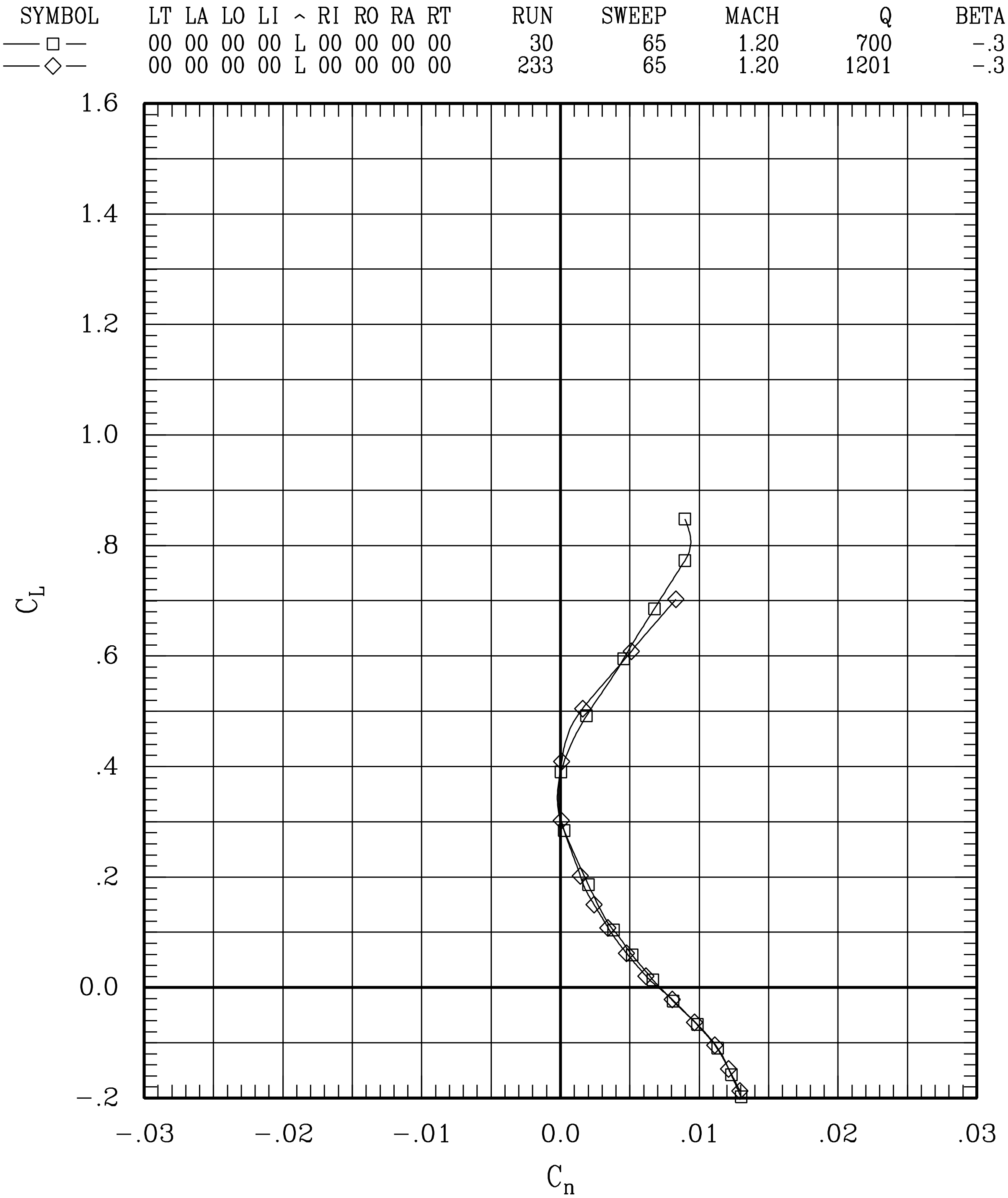

Figure 33(c). Effect of dynamic pressure for sweep = 65 deg, Mach = 1.20.

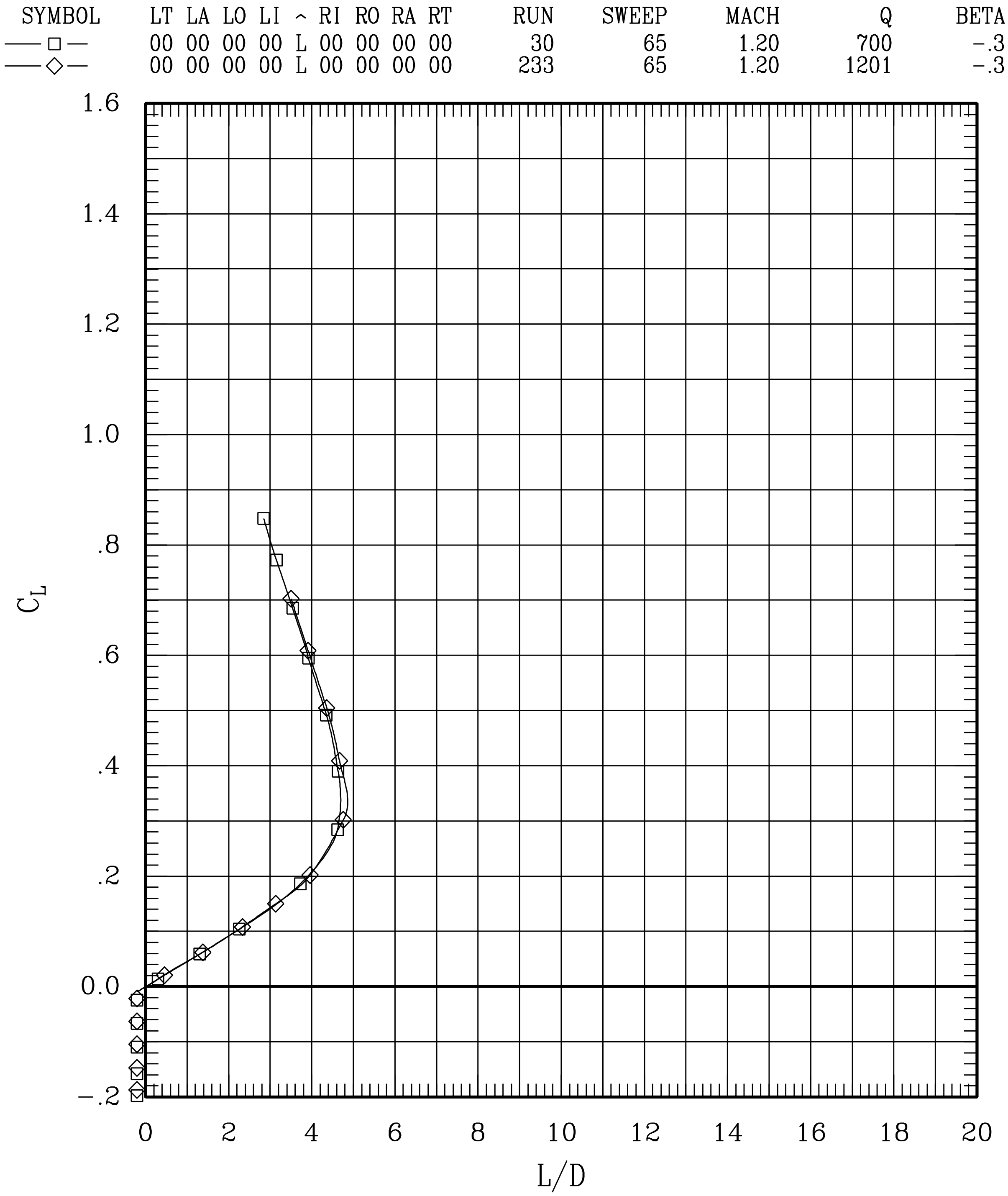

Figure 33(c). Effect of dynamic pressure for sweep = 65 deg, Mach = 1.20.

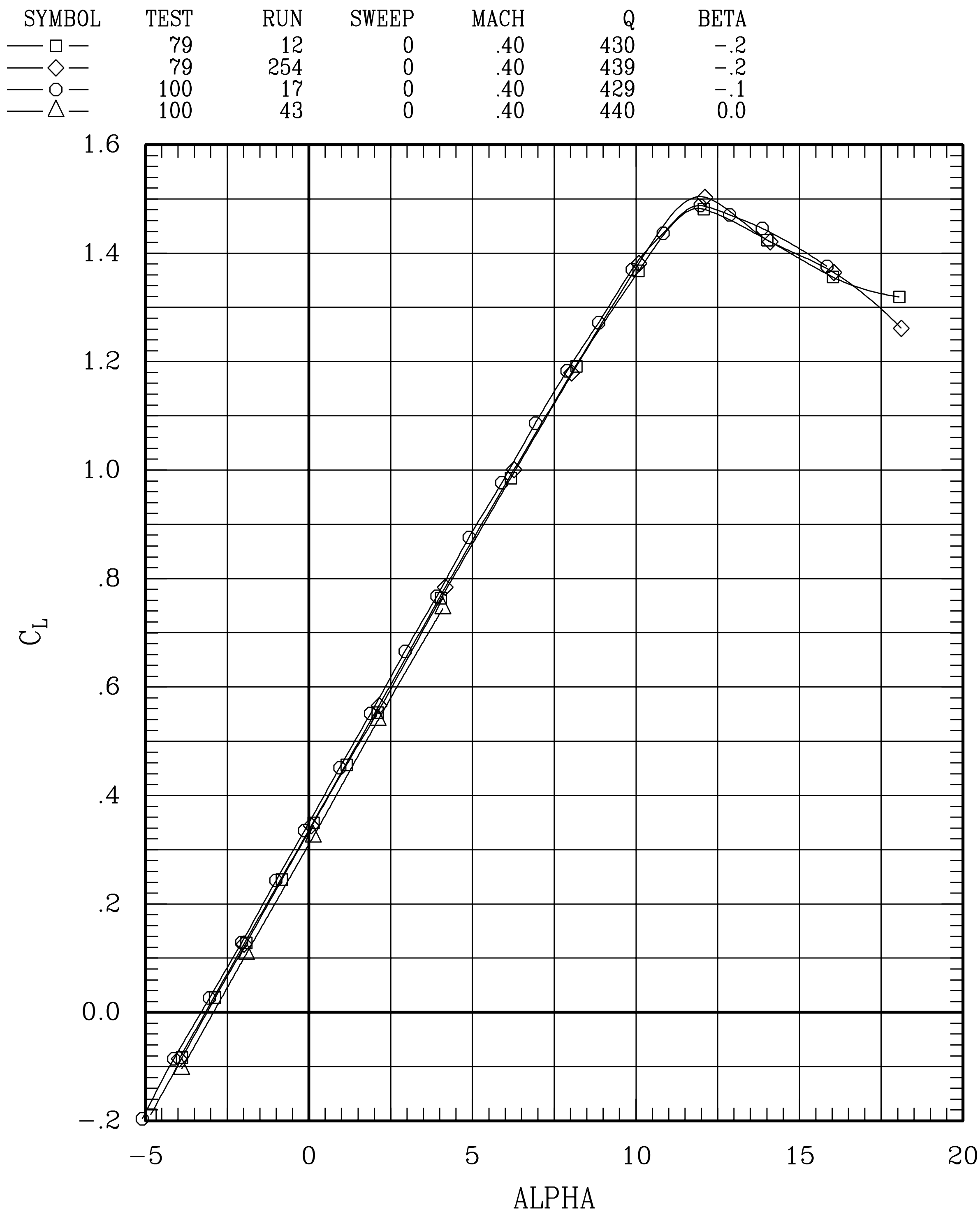

Figure 34(a). Repeat runs for sweep = 0 deg, Mach = 0.40.

SYMBOL	TEST	RUN	SWEEP	MACH	Q	BETA
—□—	79	12	0	.40	430	−.2
—◇—	79	254	0	.40	439	−.2
—○—	100	17	0	.40	429	−.1
—△—	100	43	0	.40	440	0.0

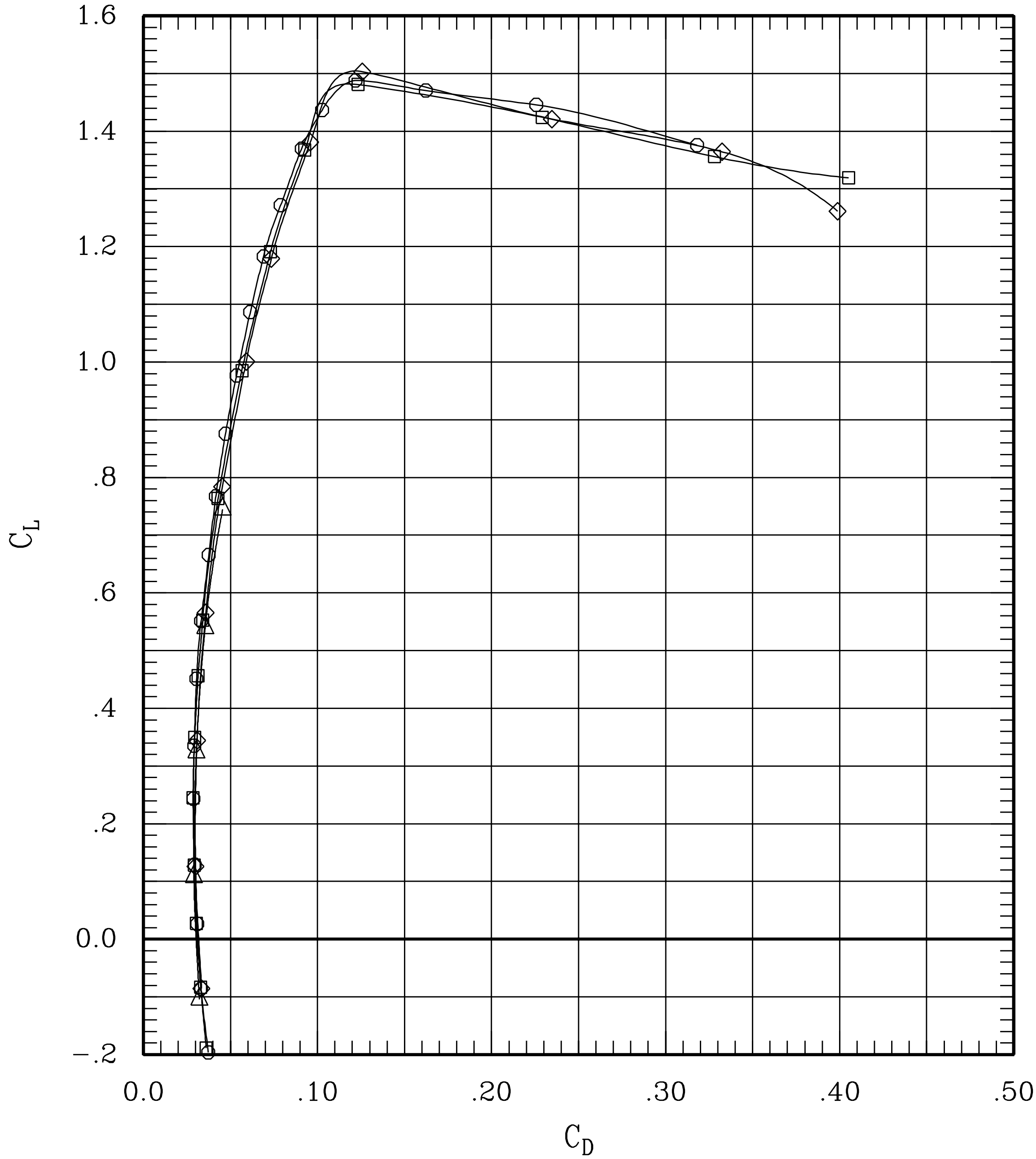

Figure 34(a). Repeat runs for sweep = 0 deg, Mach = 0.40.

SYMBOL	TEST	RUN	SWEEP	MACH	Q	BETA
—□—	79	12	0	.40	430	−.2
—◇—	79	254	0	.40	439	−.2
—○—	100	17	0	.40	429	−.1
—△—	100	43	0	.40	440	0.0

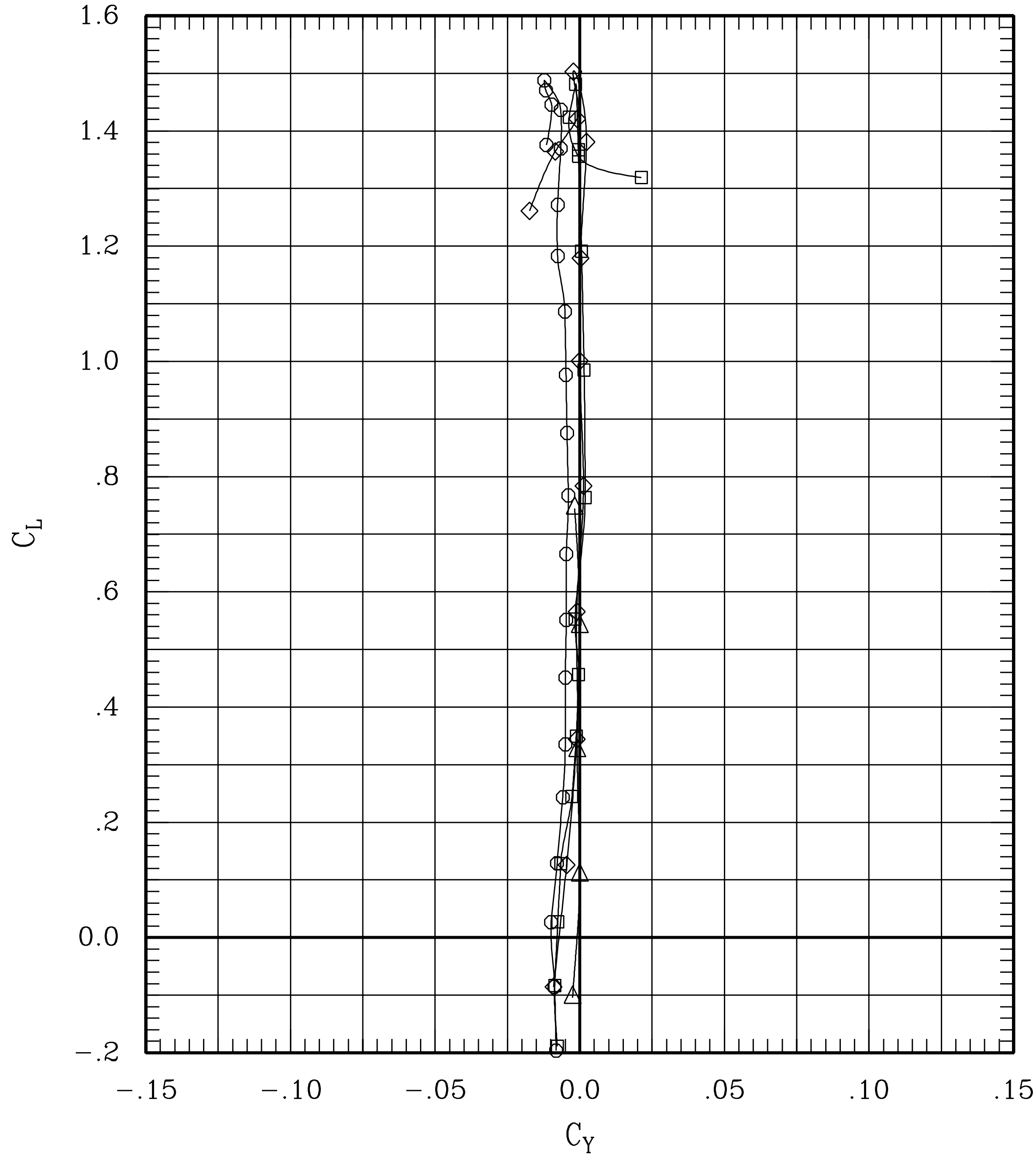

Figure 34(a). Repeat runs for sweep = 0 deg, Mach = 0.40.

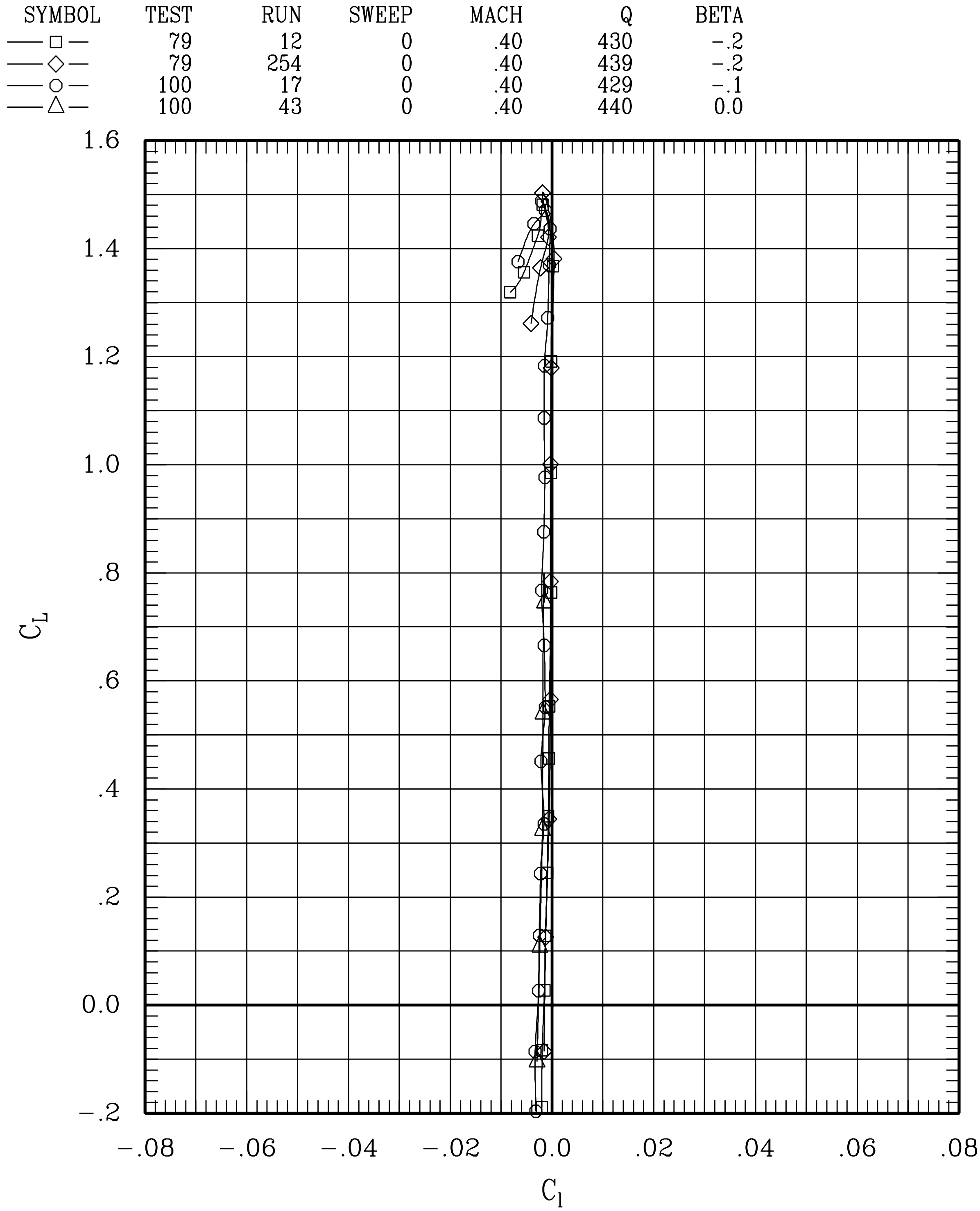

Figure 34(a). Repeat runs for sweep = 0 deg, Mach = 0.40.

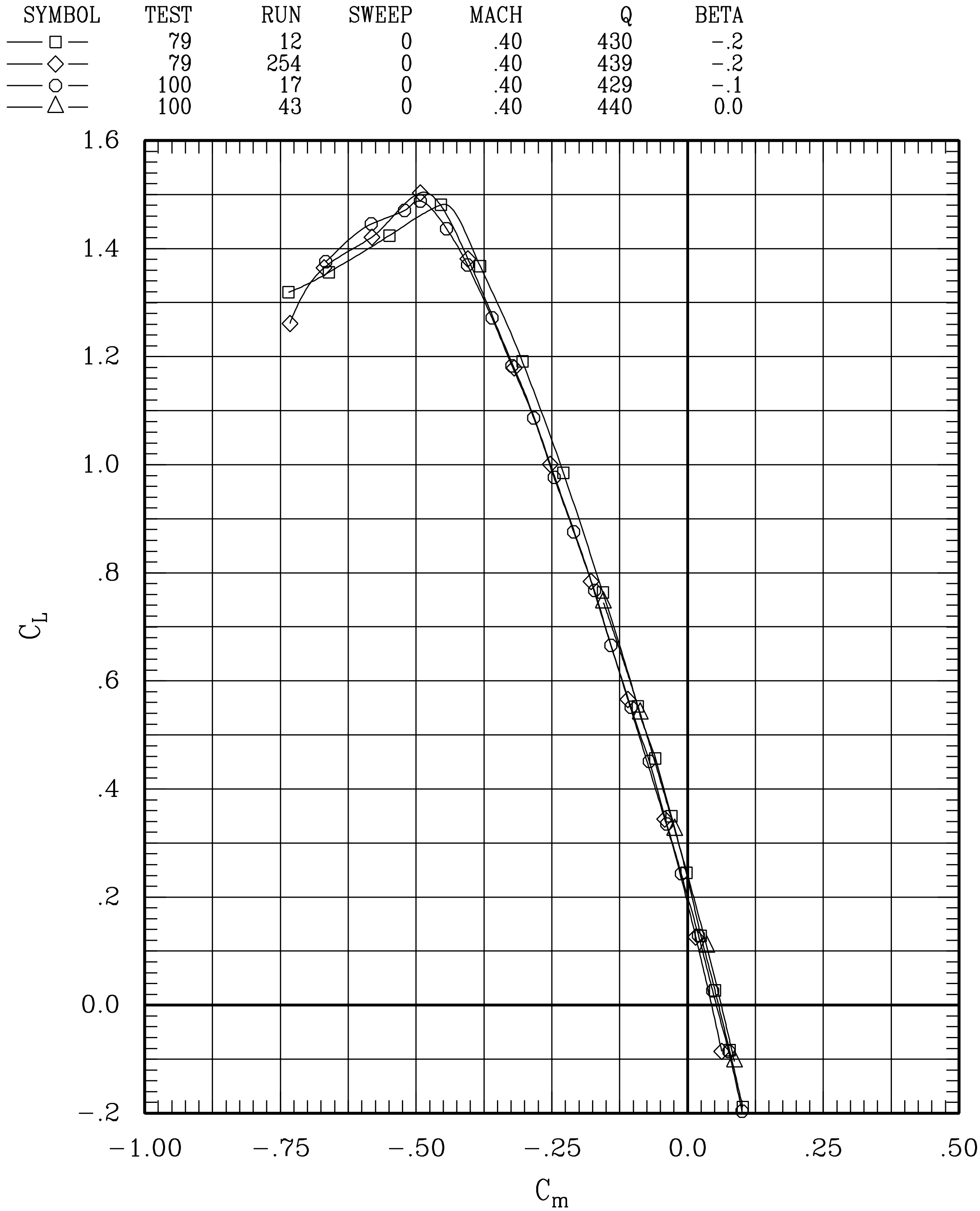

Figure 34(a). Repeat runs for sweep = 0 deg, Mach = 0.40.

SYMBOL	TEST	RUN	SWEEP	MACH	Q	BETA
—□—	79	12	0	.40	430	−.2
—◇—	79	254	0	.40	439	−.2
—○—	100	17	0	.40	429	−.1
—△—	100	43	0	.40	440	0.0

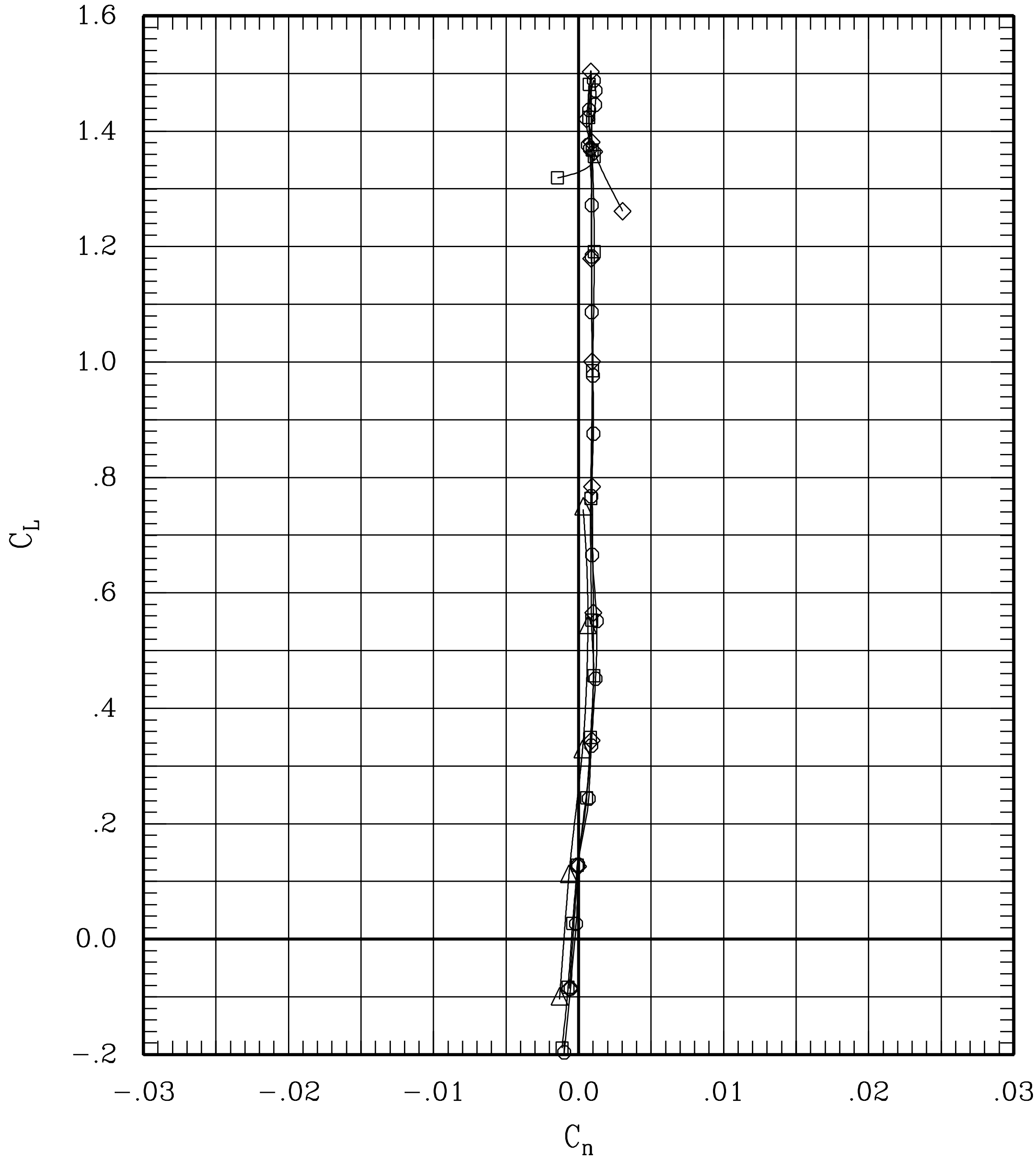

Figure 34(a). Repeat runs for sweep = 0 deg, Mach = 0.40.

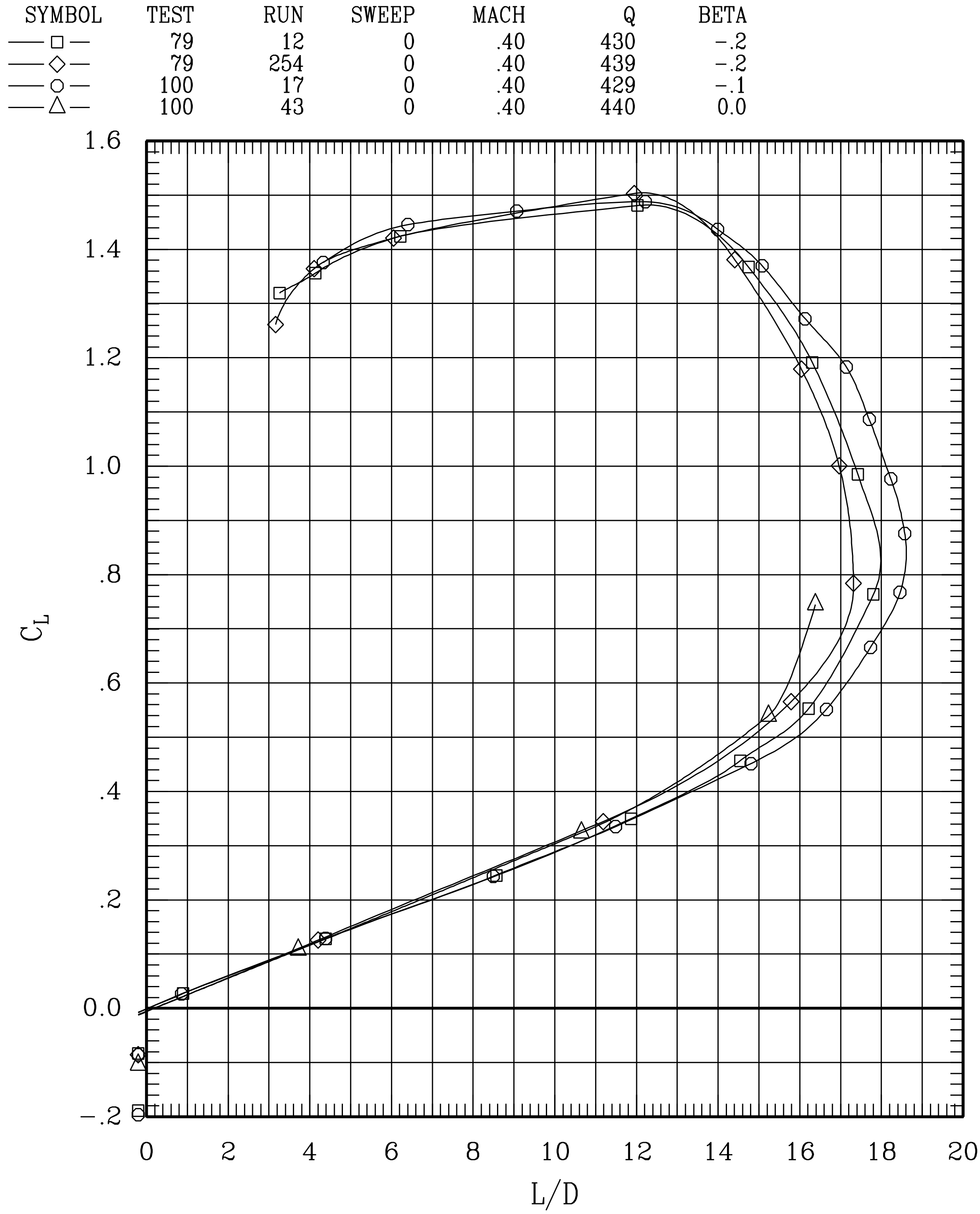

Figure 34(a). Repeat runs for sweep = 0 deg, Mach = 0.40.

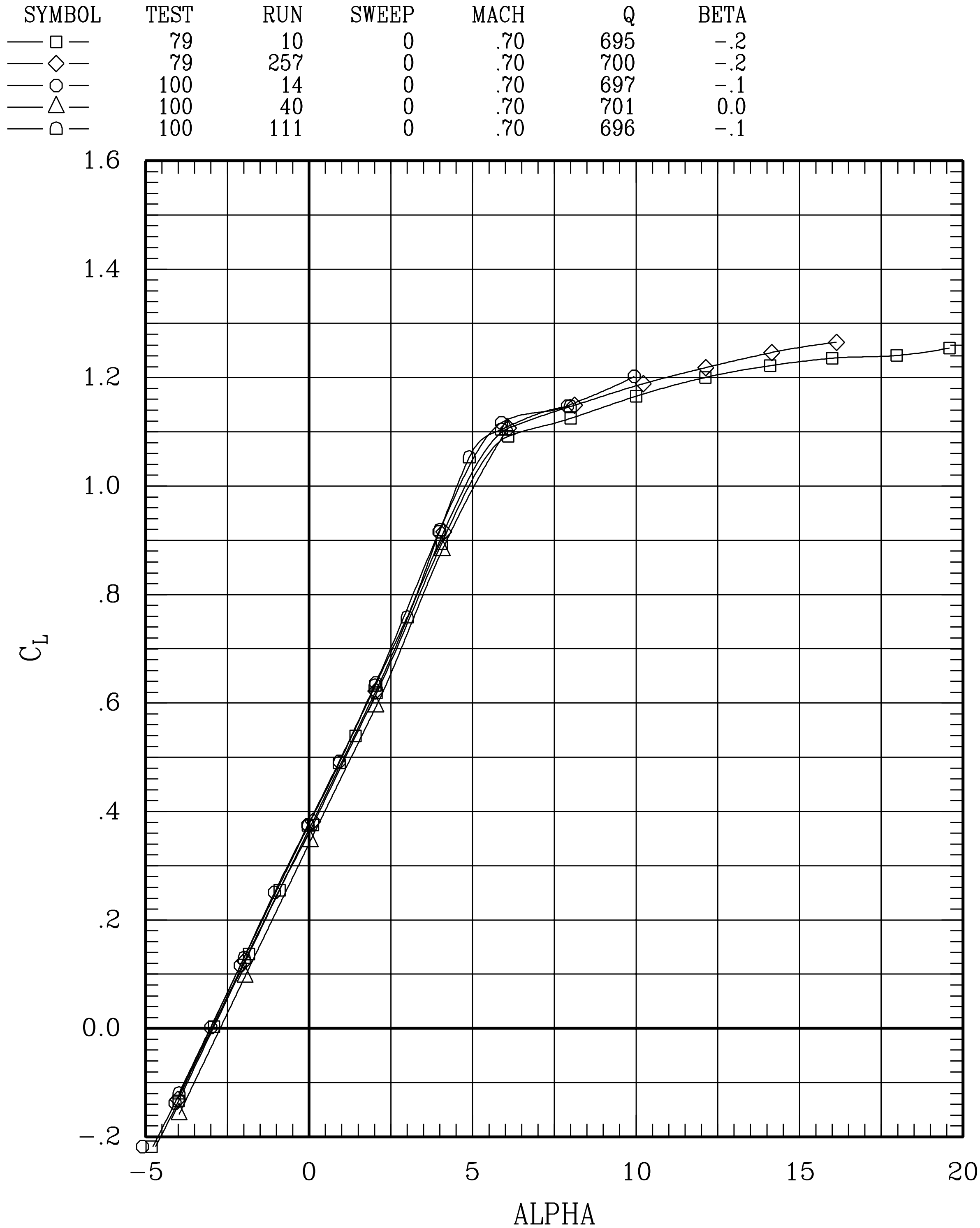

Figure 34(b). Repeat runs for sweep = 0 deg, Mach = 0.70.

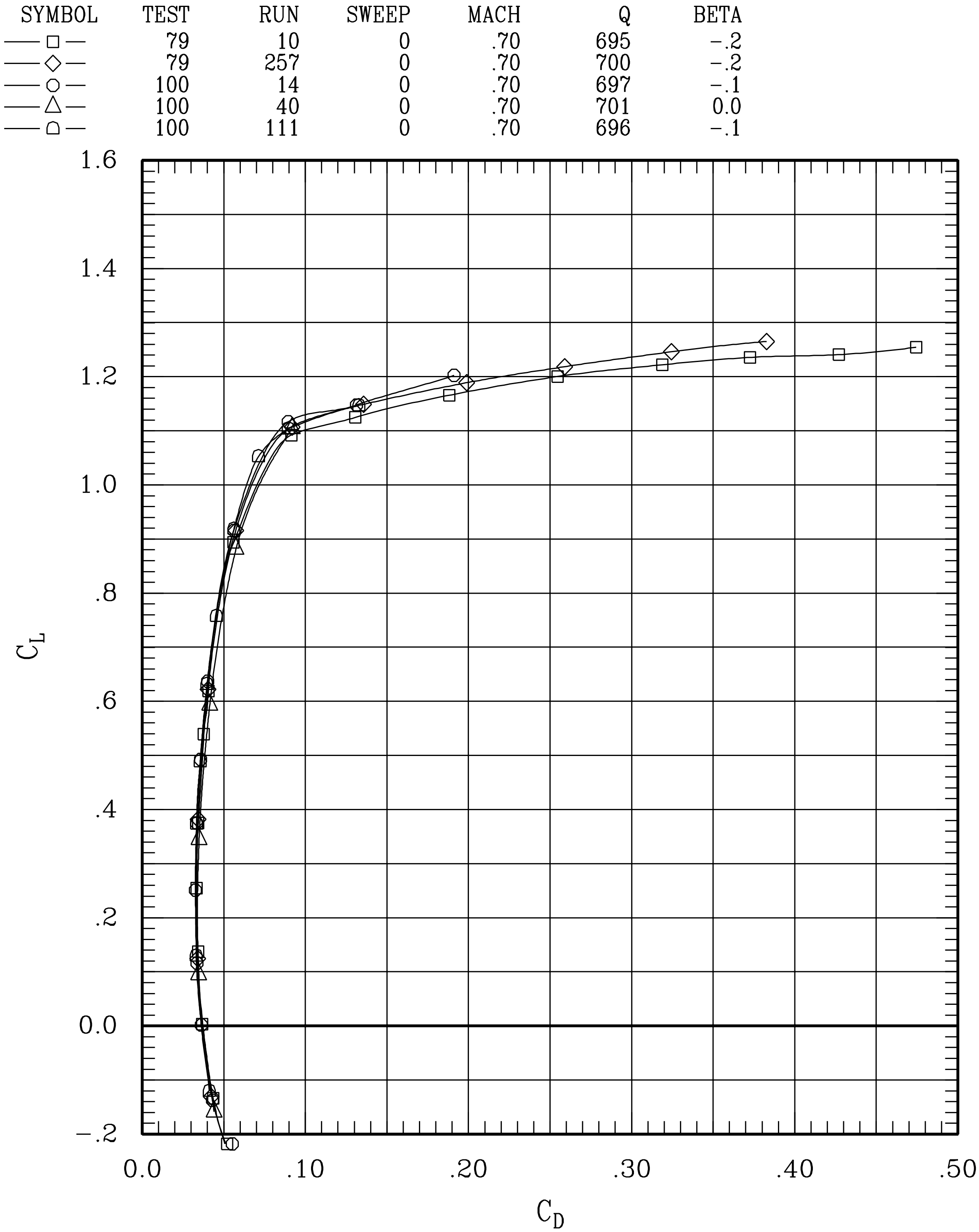

Figure 34(b). Repeat runs for sweep = 0 deg, Mach = 0.70.

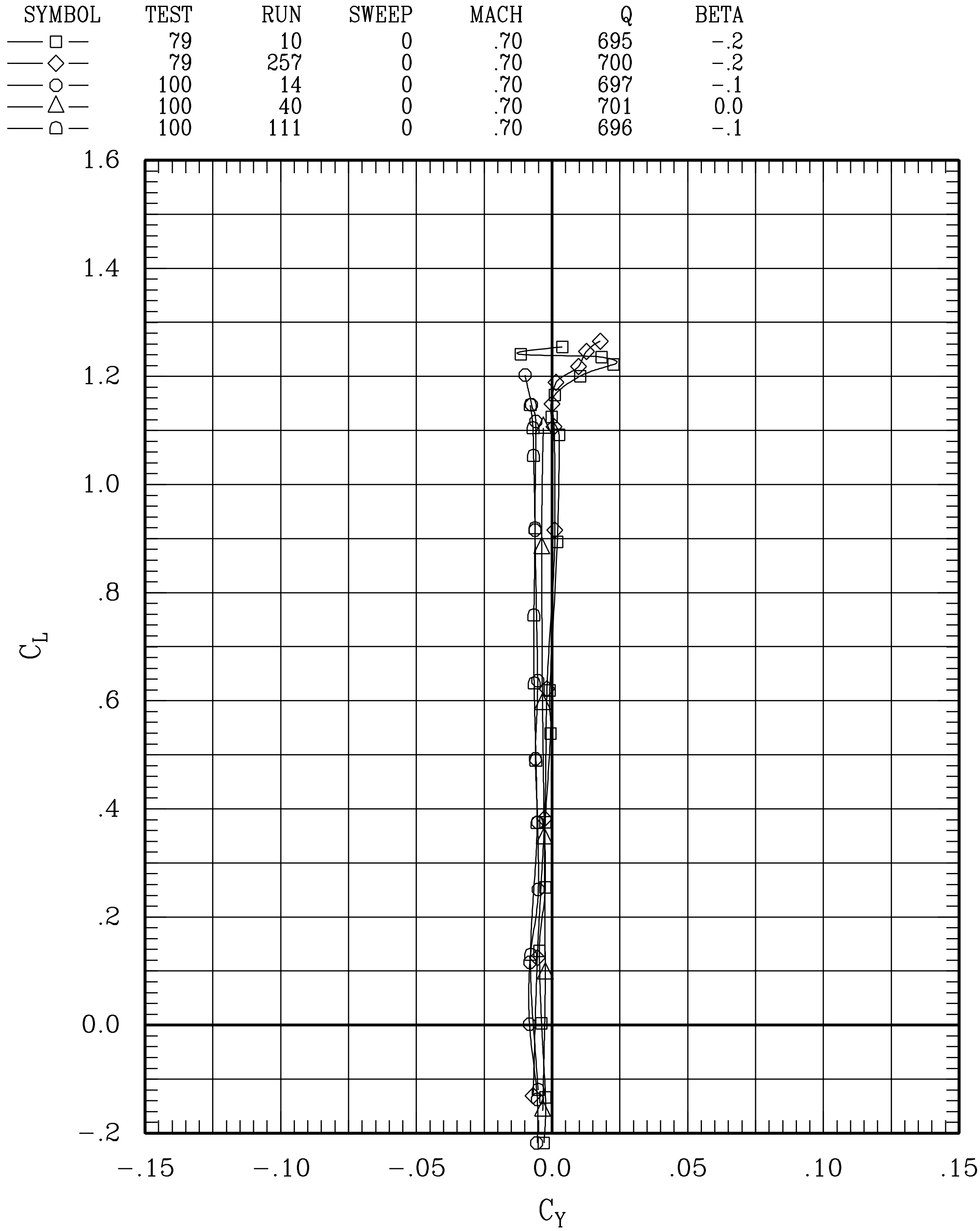

Figure 34(b). Repeat runs for sweep = 0 deg, Mach = 0.70.

SYMBOL	TEST	RUN	SWEEP	MACH	Q	BETA
□	79	10	0	.70	695	−.2
◇	79	257	0	.70	700	−.2
○	100	14	0	.70	697	−.1
△	100	40	0	.70	701	0.0
⌂	100	111	0	.70	696	−.1

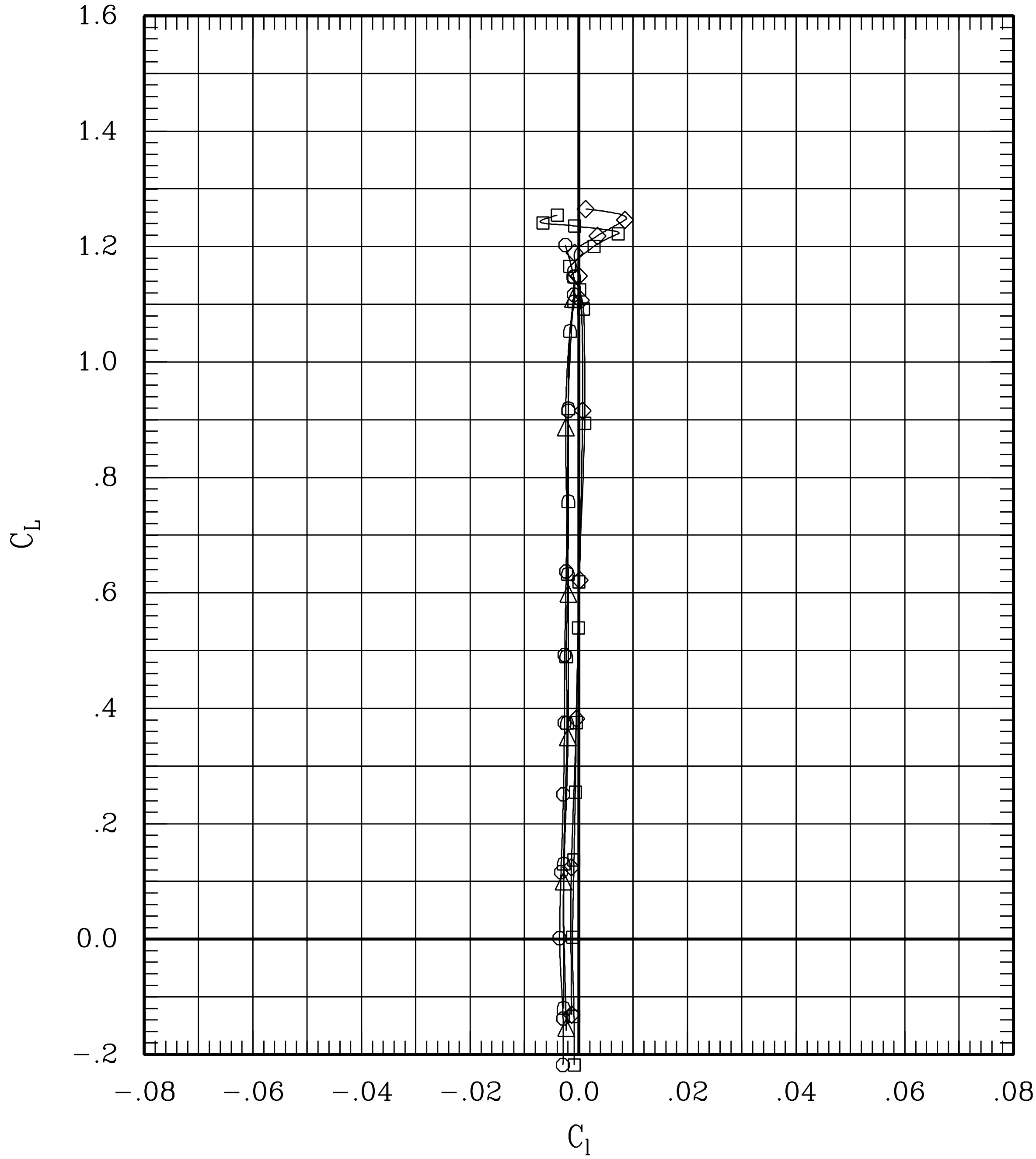

Figure 34(b). Repeat runs for sweep = 0 deg, Mach = 0.70.

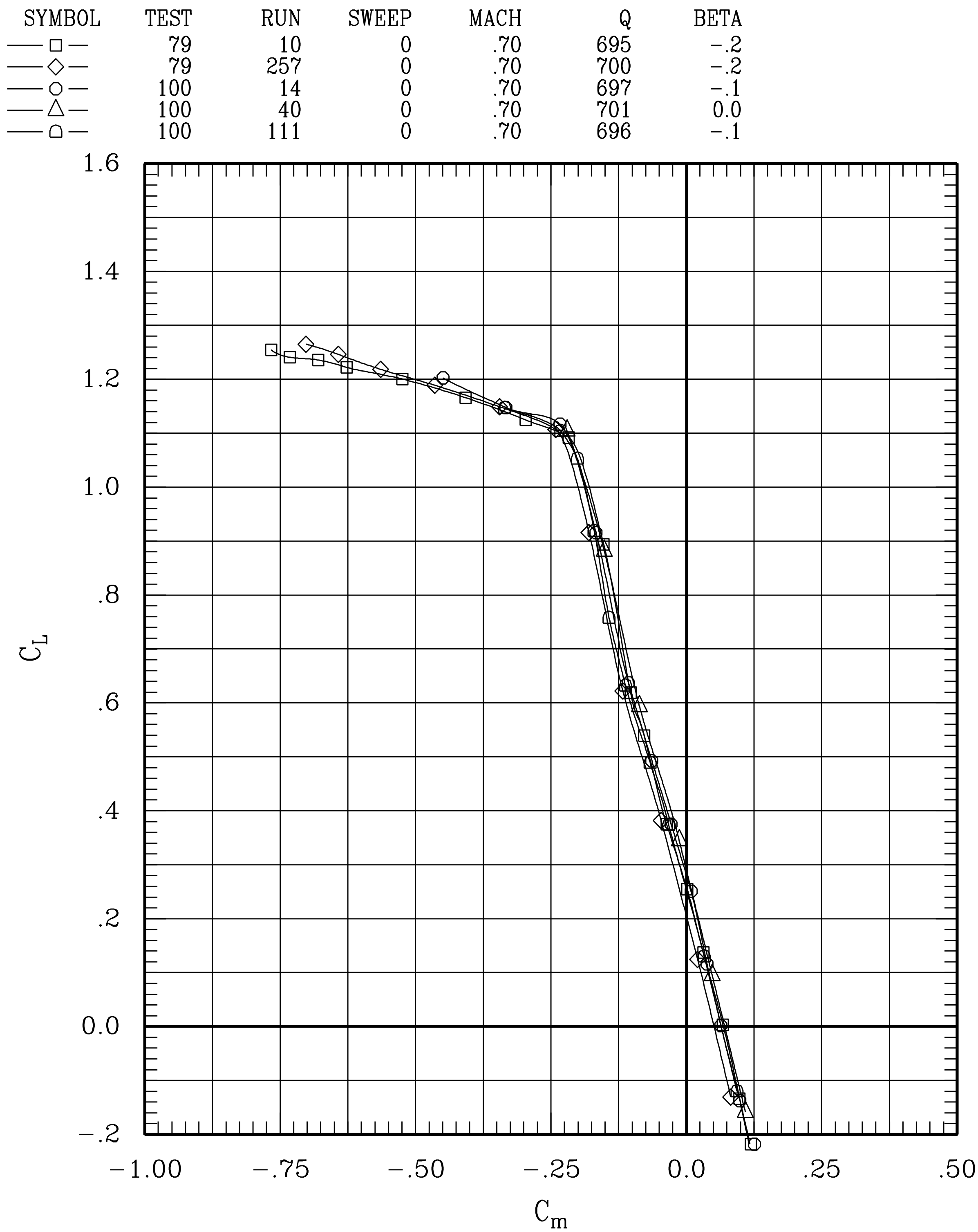

Figure 34(b). Repeat runs for sweep = 0 deg, Mach = 0.70.

SYMBOL	TEST	RUN	SWEEP	MACH	Q	BETA
—□—	79	10	0	.70	695	−.2
—◇—	79	257	0	.70	700	−.2
—○—	100	14	0	.70	697	−.1
—△—	100	40	0	.70	701	0.0
—⌂—	100	111	0	.70	696	−.1

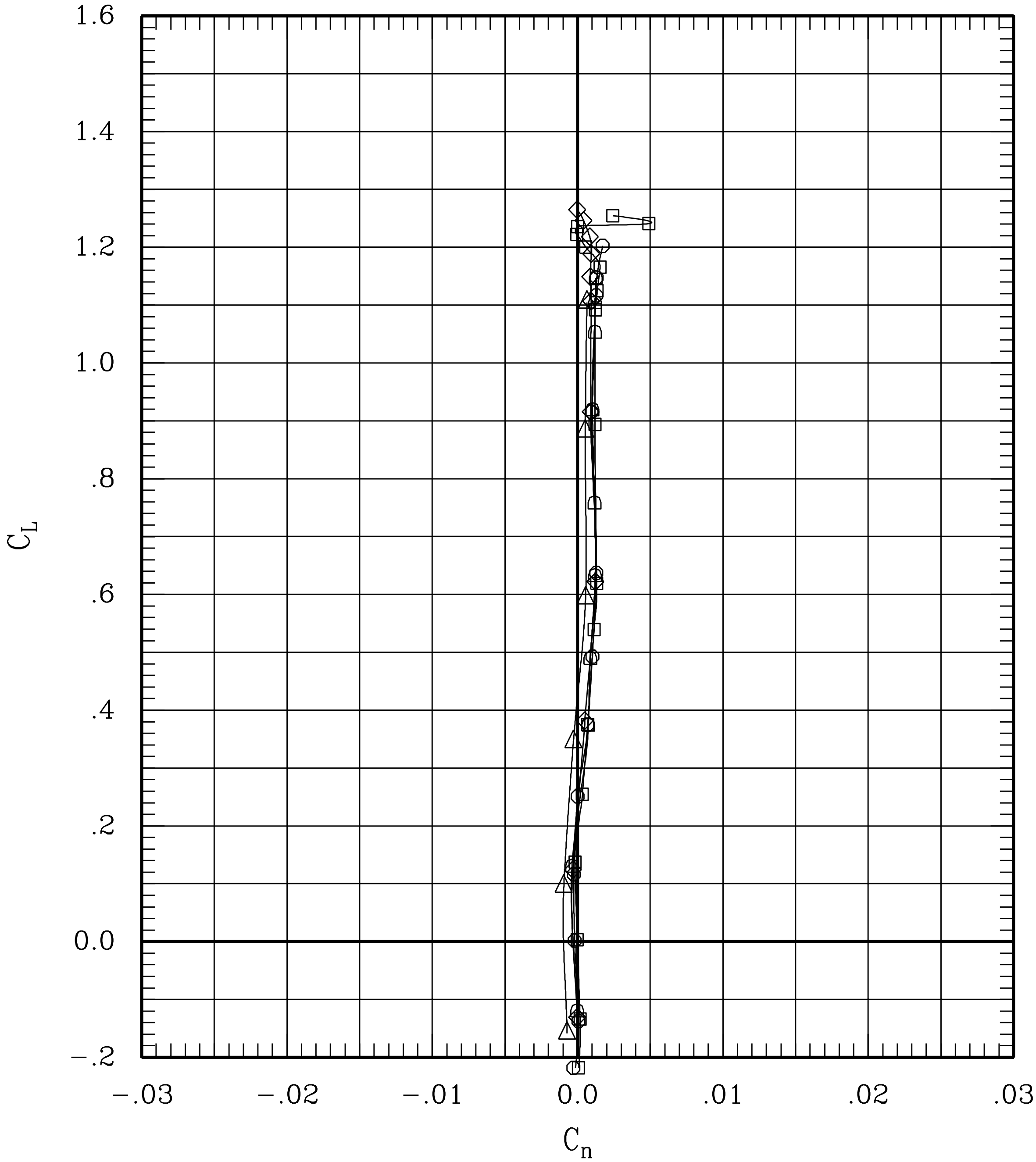

Figure 34(b). Repeat runs for sweep = 0 deg, Mach = 0.70.

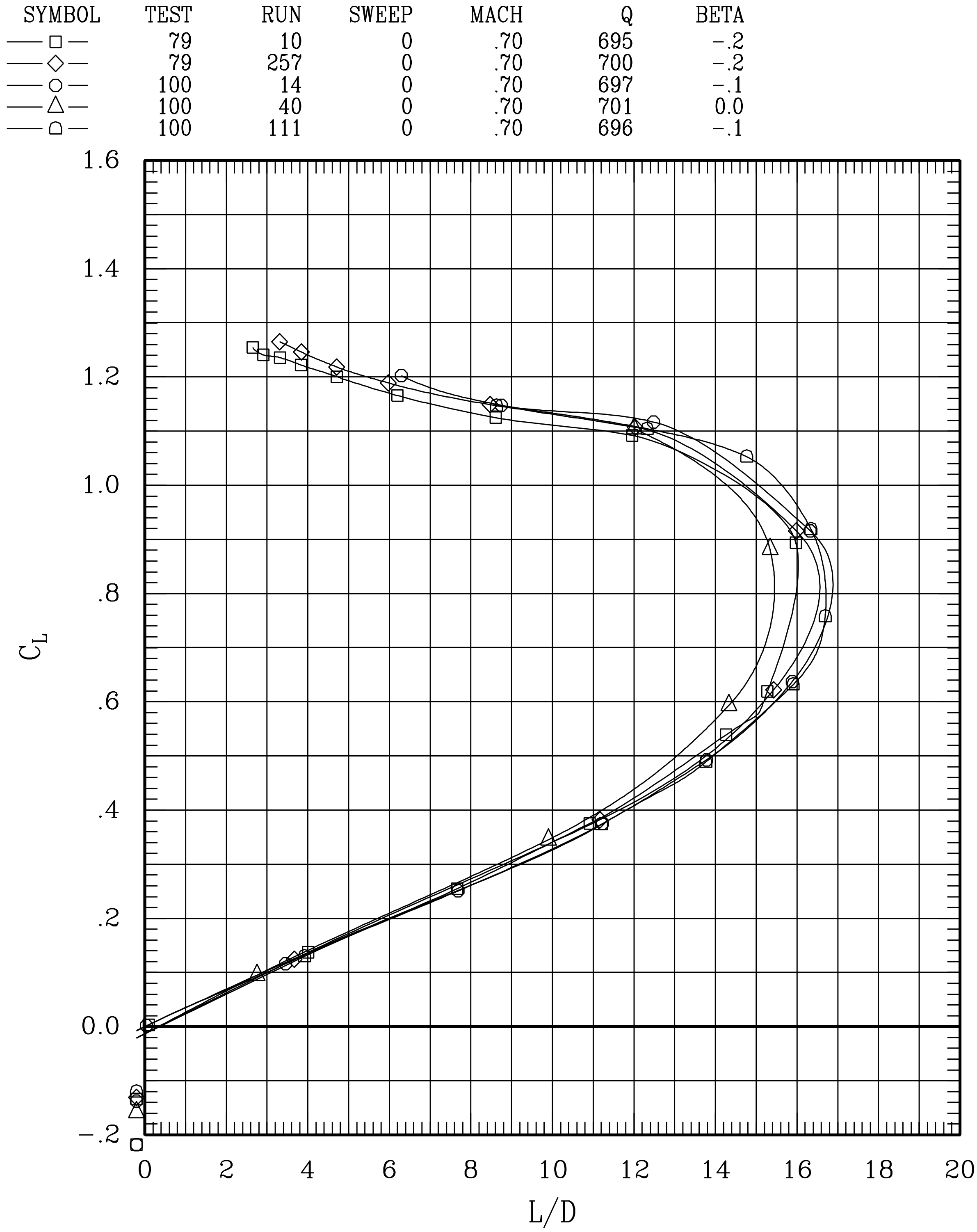

Figure 34(b). Repeat runs for sweep = 0 deg, Mach = 0.70.

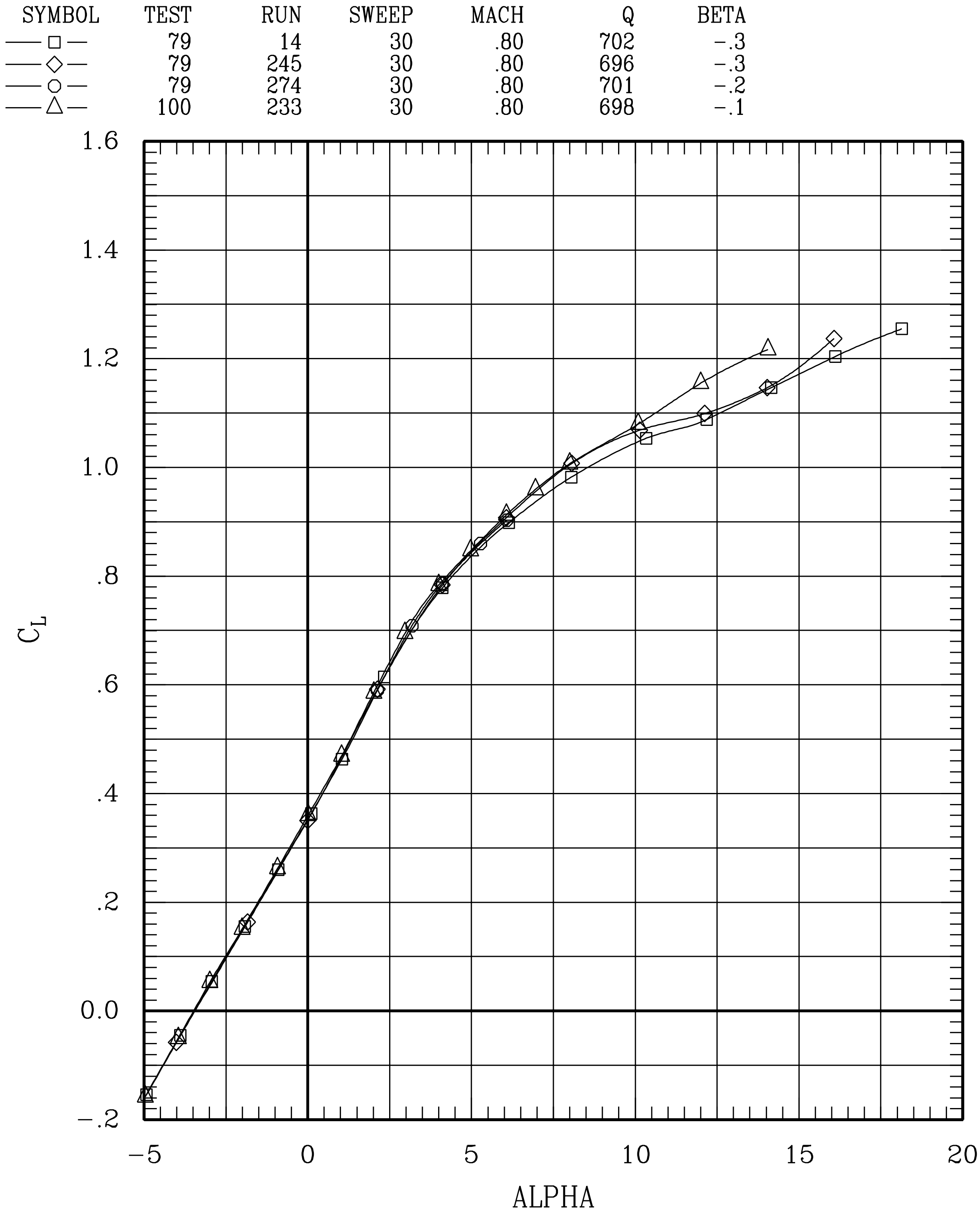

Figure 34(c). Repeat runs for sweep = 30 deg, Mach = 0.80.

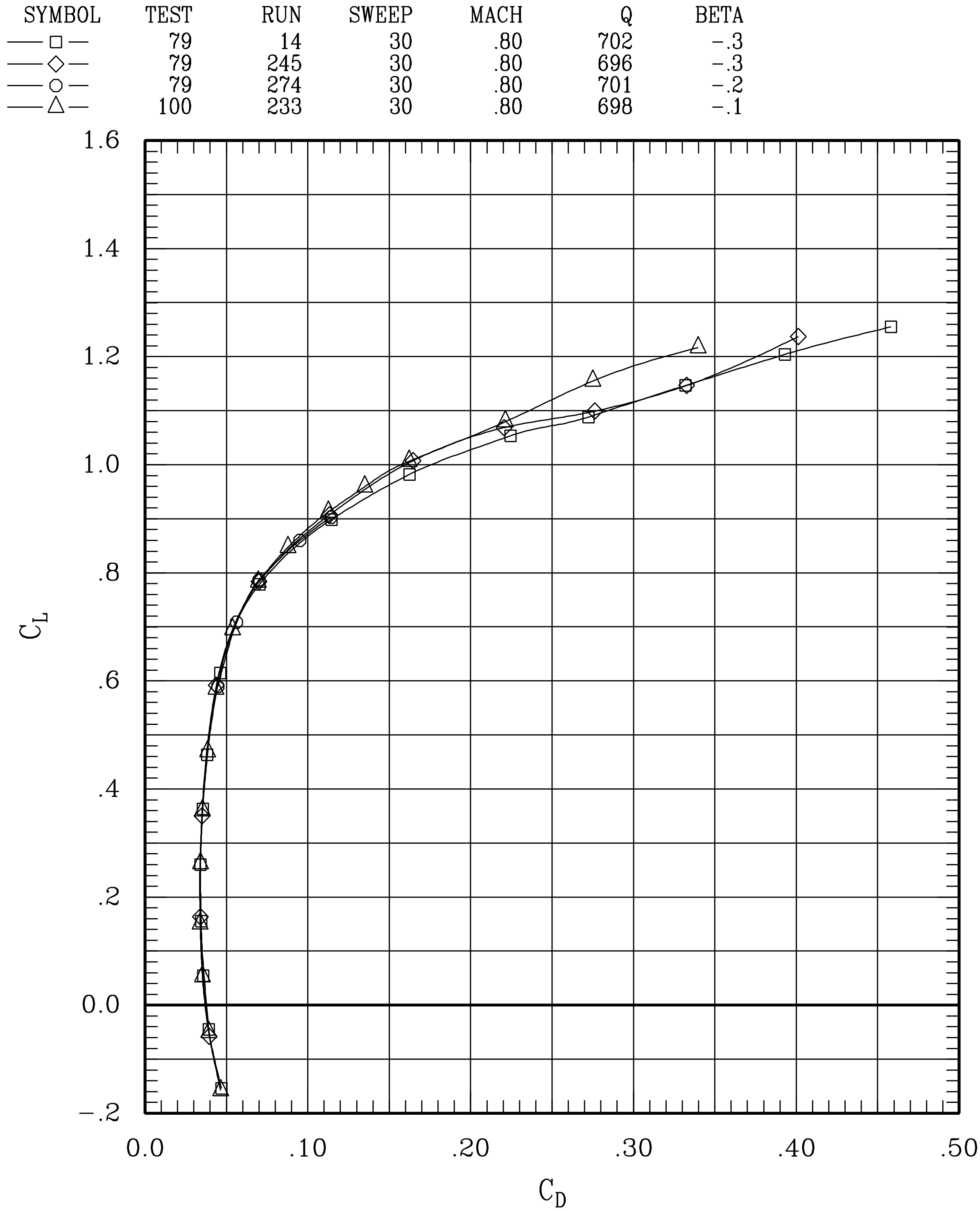

Figure 34(c). Repeat runs for sweep = 30 deg, Mach = 0.80.

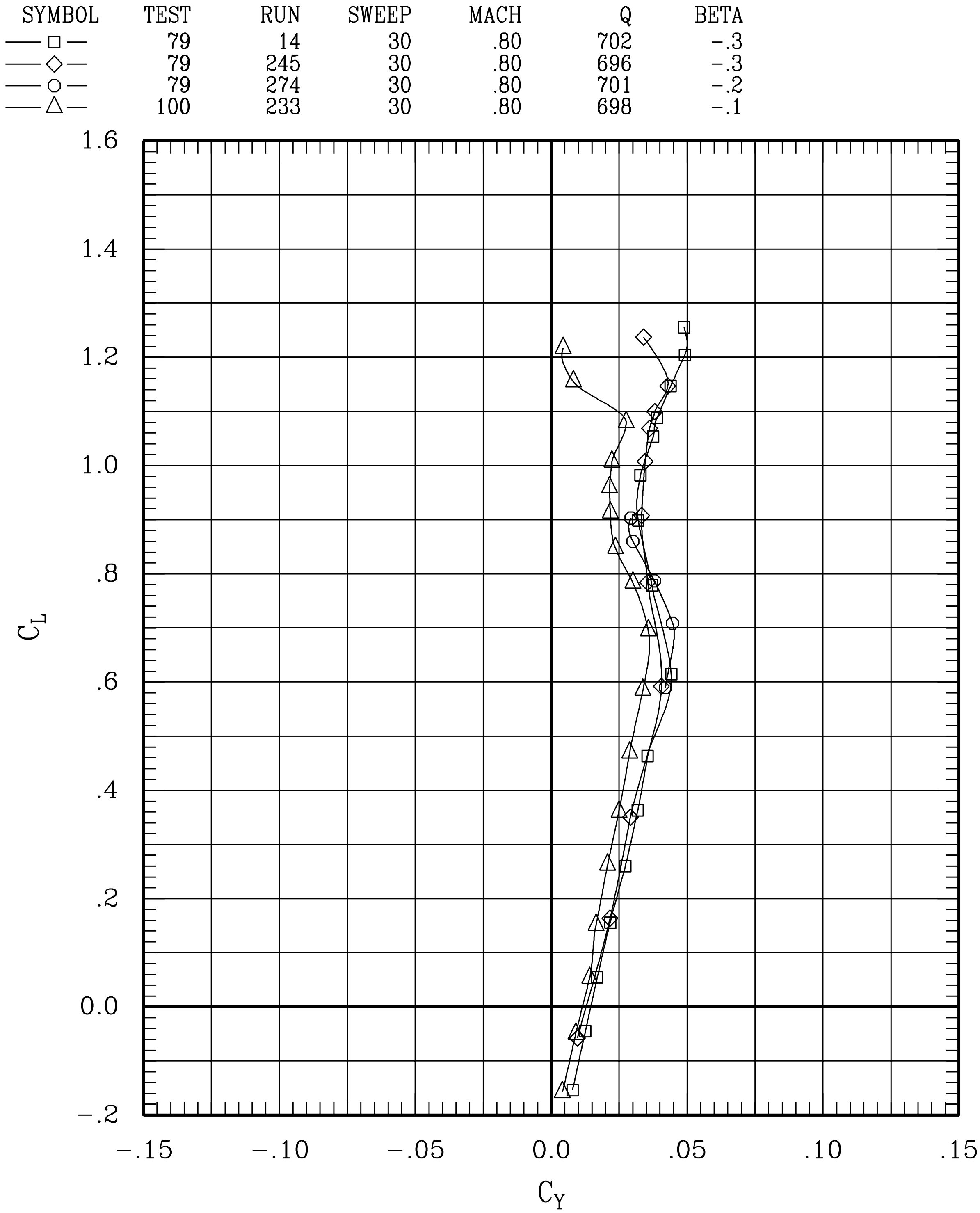

Figure 34(c). Repeat runs for sweep = 30 deg, Mach = 0.80.

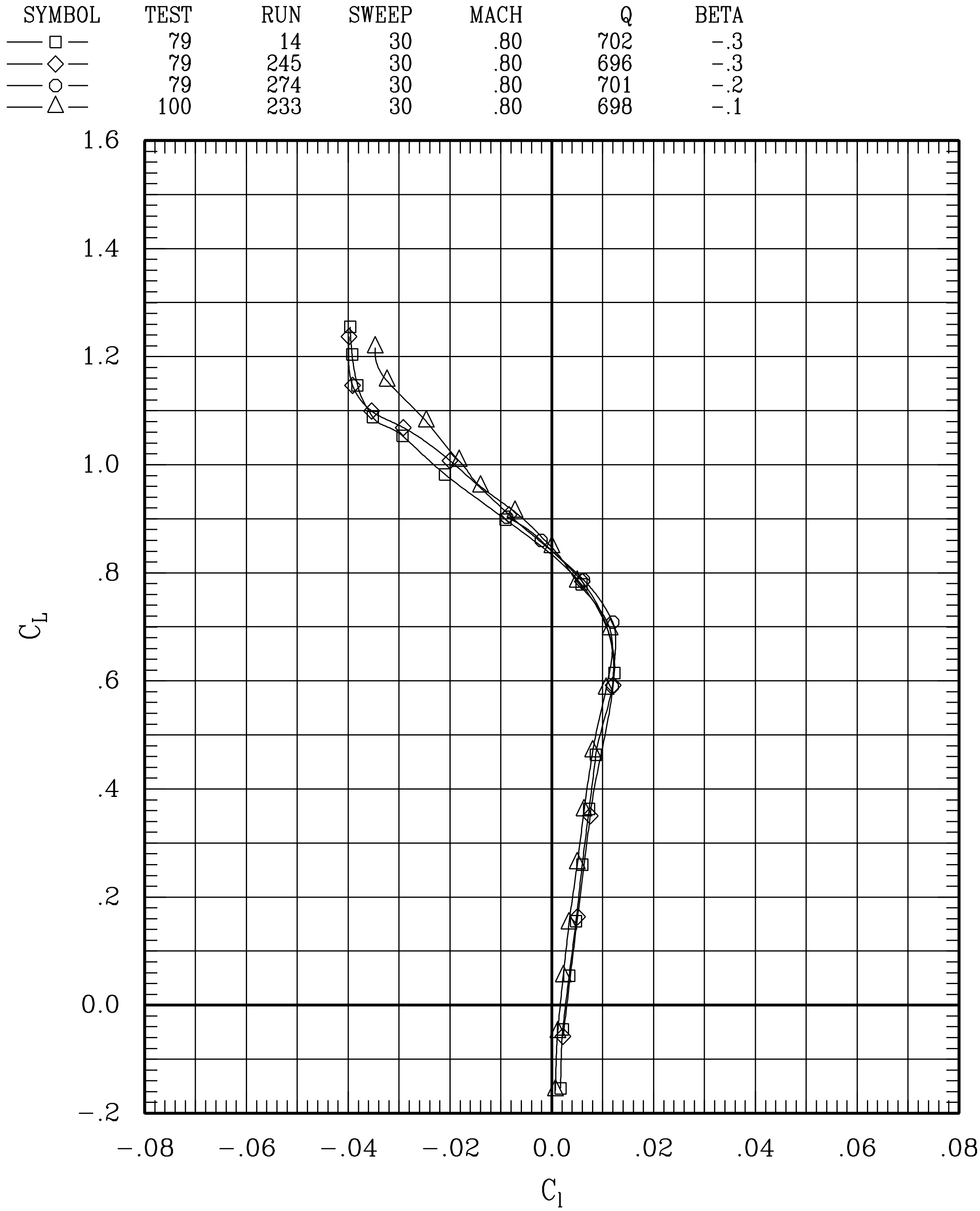

Figure 34(c). Repeat runs for sweep = 30 deg, Mach = 0.80.

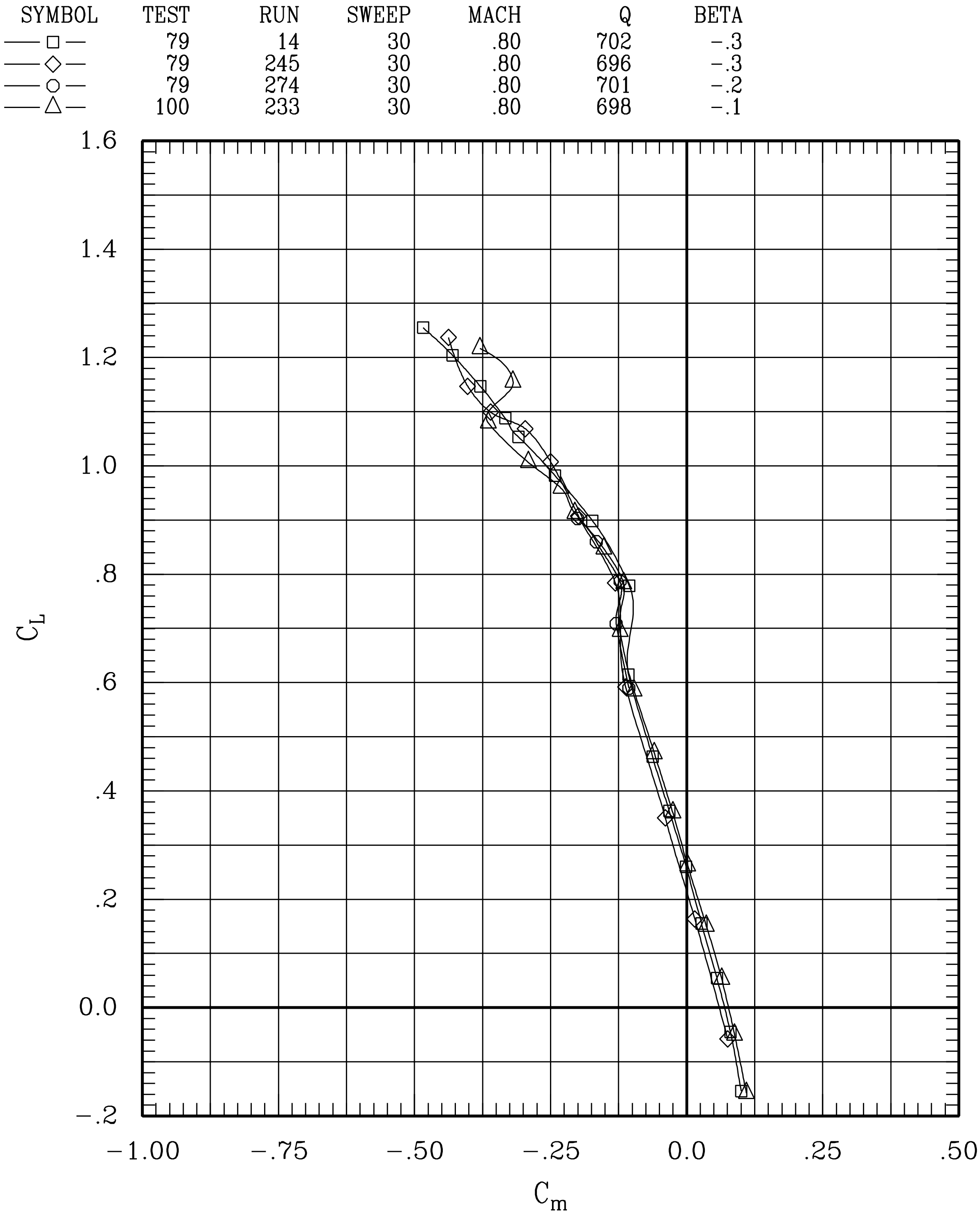

Figure 34(c). Repeat runs for sweep = 30 deg, Mach = 0.80.

SYMBOL	TEST	RUN	SWEEP	MACH	Q	BETA
—□—	79	14	30	.80	702	−.3
—◇—	79	245	30	.80	696	−.3
—○—	79	274	30	.80	701	−.2
—△—	100	233	30	.80	698	−.1

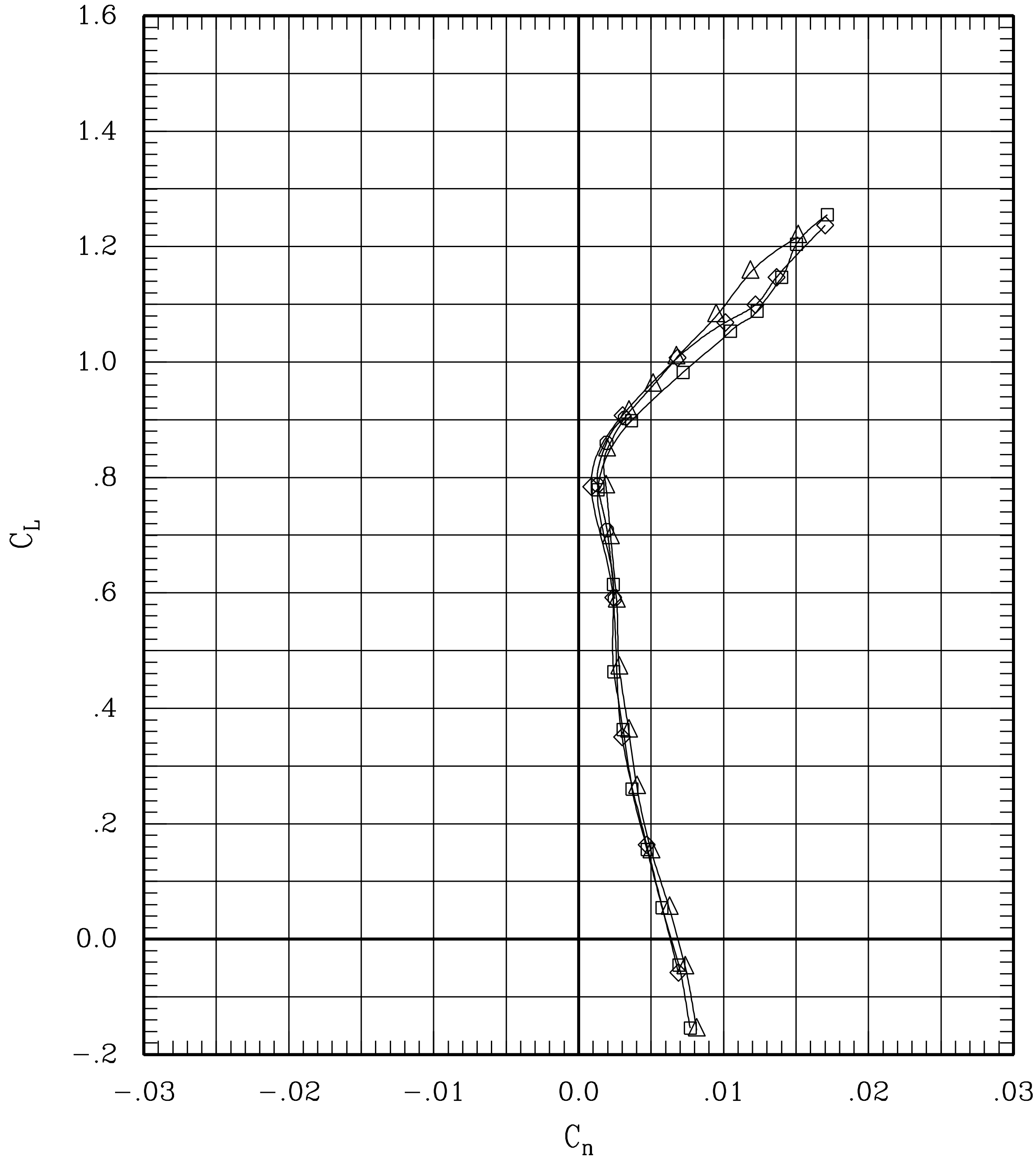

Figure 34(c). Repeat runs for sweep = 30 deg, Mach = 0.80.

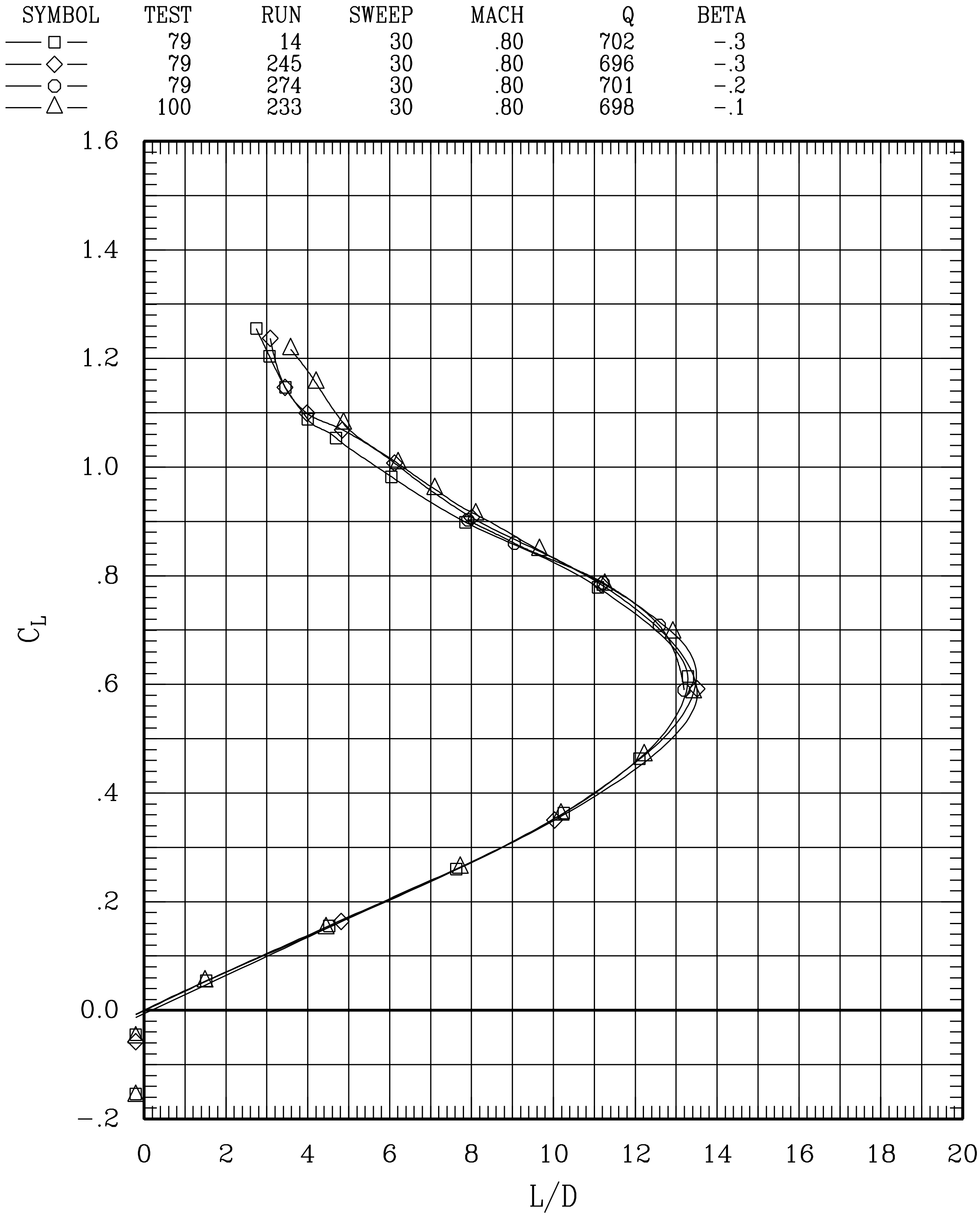

Figure 34(c). Repeat runs for sweep = 30 deg, Mach = 0.80.

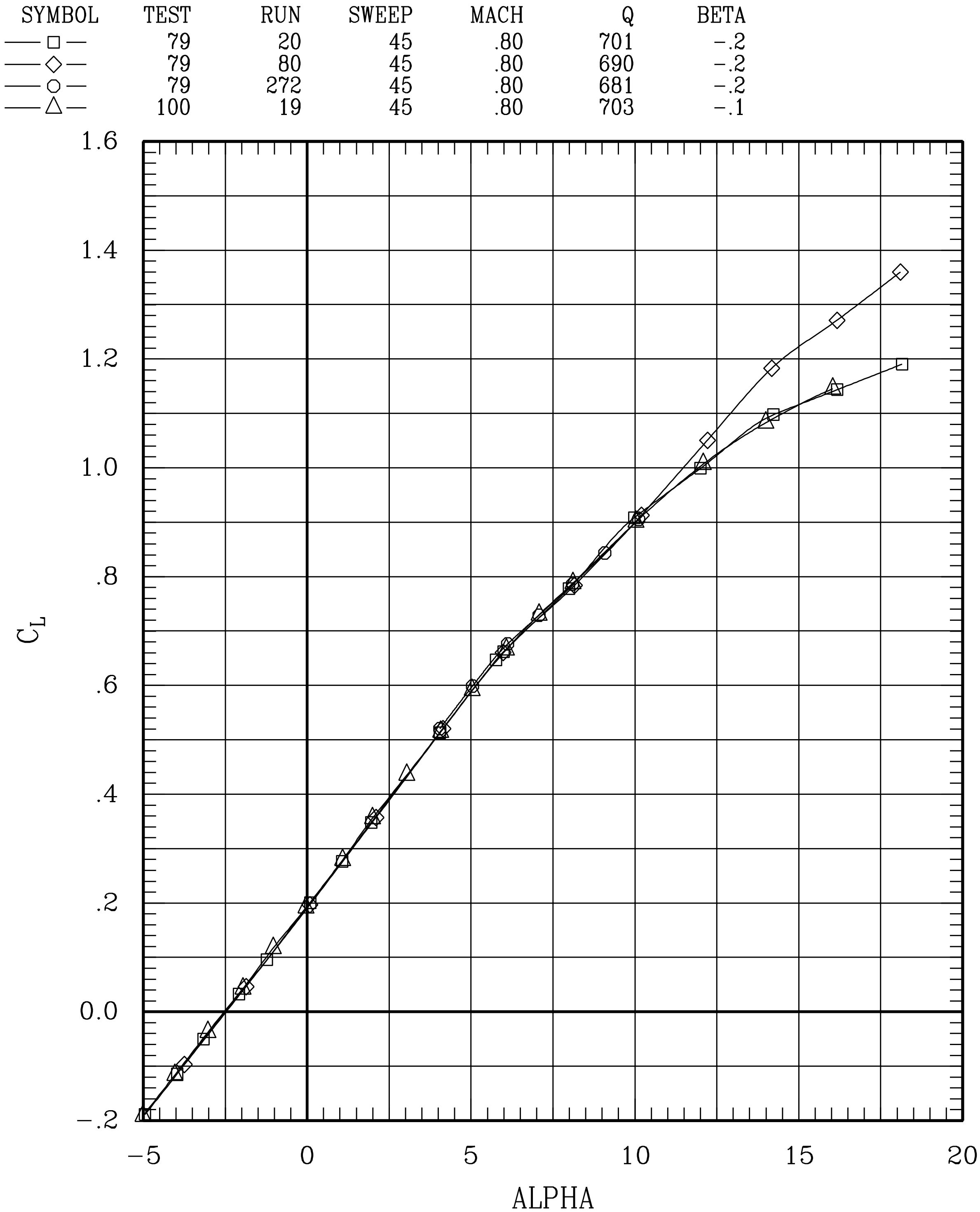

Figure 34(d). Repeat runs for sweep = 45 deg, Mach = 0.80.

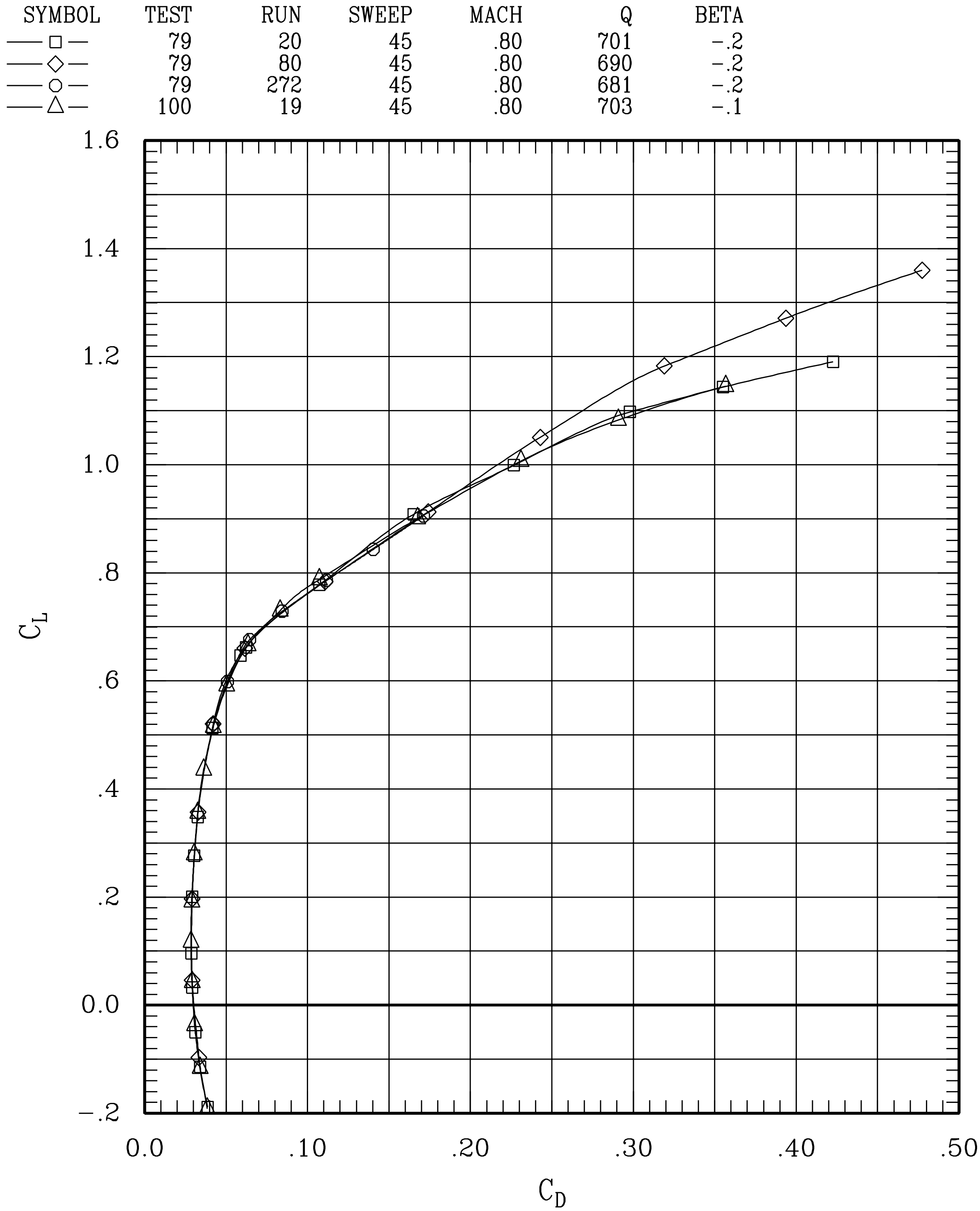

Figure 34(d). Repeat runs for sweep = 45 deg, Mach = 0.80.

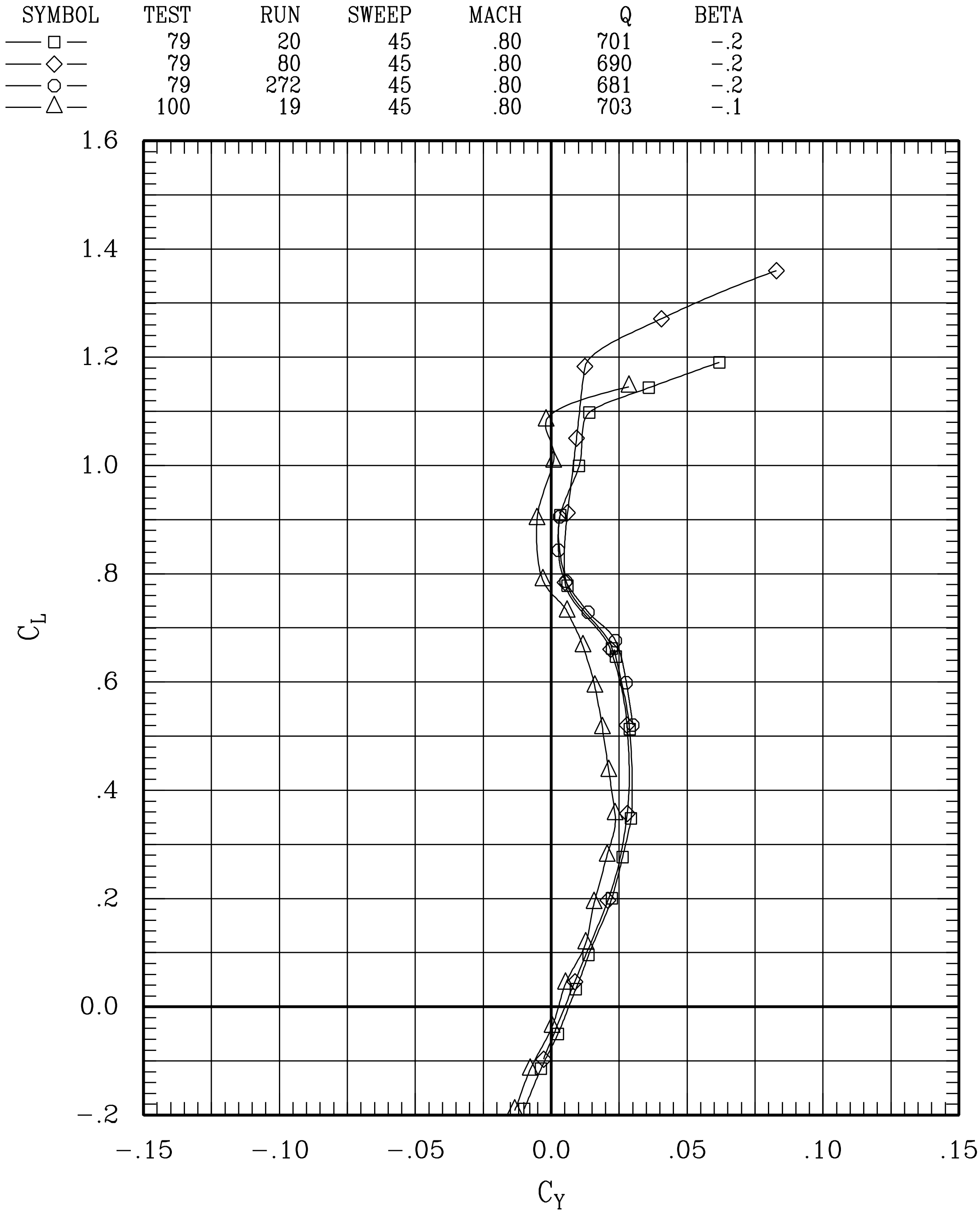

Figure 34(d). Repeat runs for sweep = 45 deg, Mach = 0.80.

SYMBOL	TEST	RUN	SWEEP	MACH	Q	BETA
—□—	79	20	45	.80	701	−.2
—◇—	79	80	45	.80	690	−.2
—○—	79	272	45	.80	681	−.2
—△—	100	19	45	.80	703	−.1

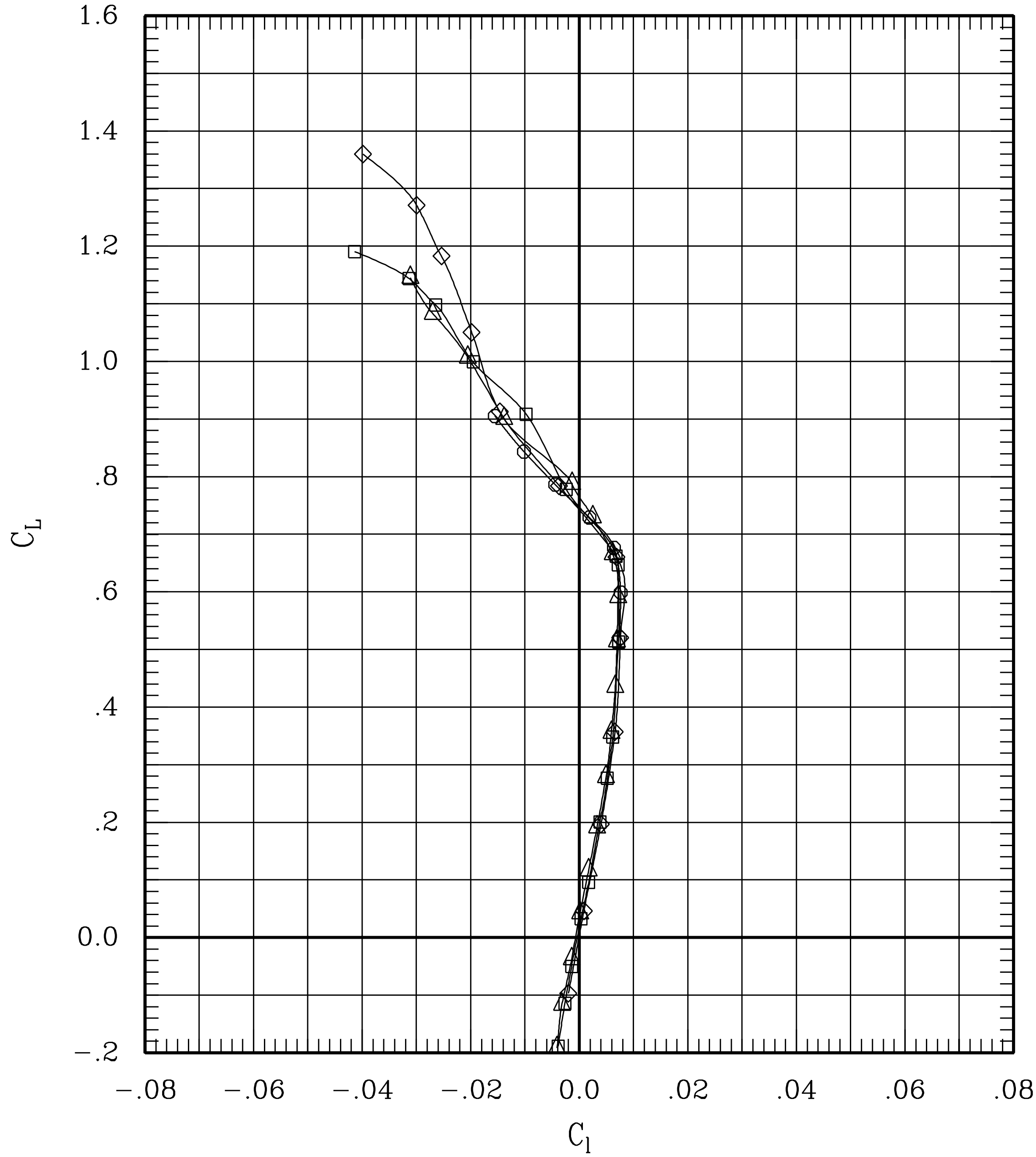

Figure 34(d). Repeat runs for sweep = 45 deg, Mach = 0.80.

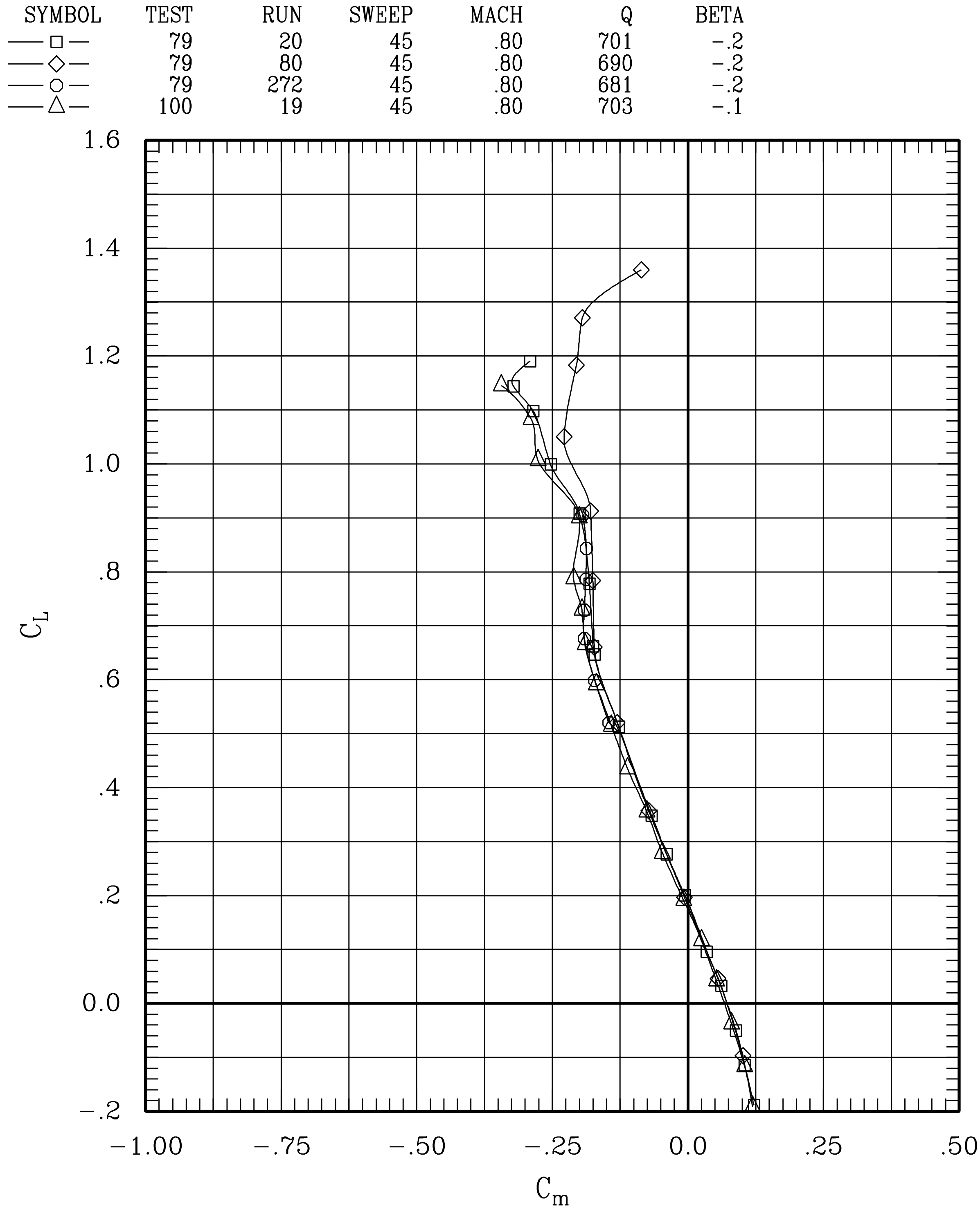

Figure 34(d). Repeat runs for sweep = 45 deg, Mach = 0.80.

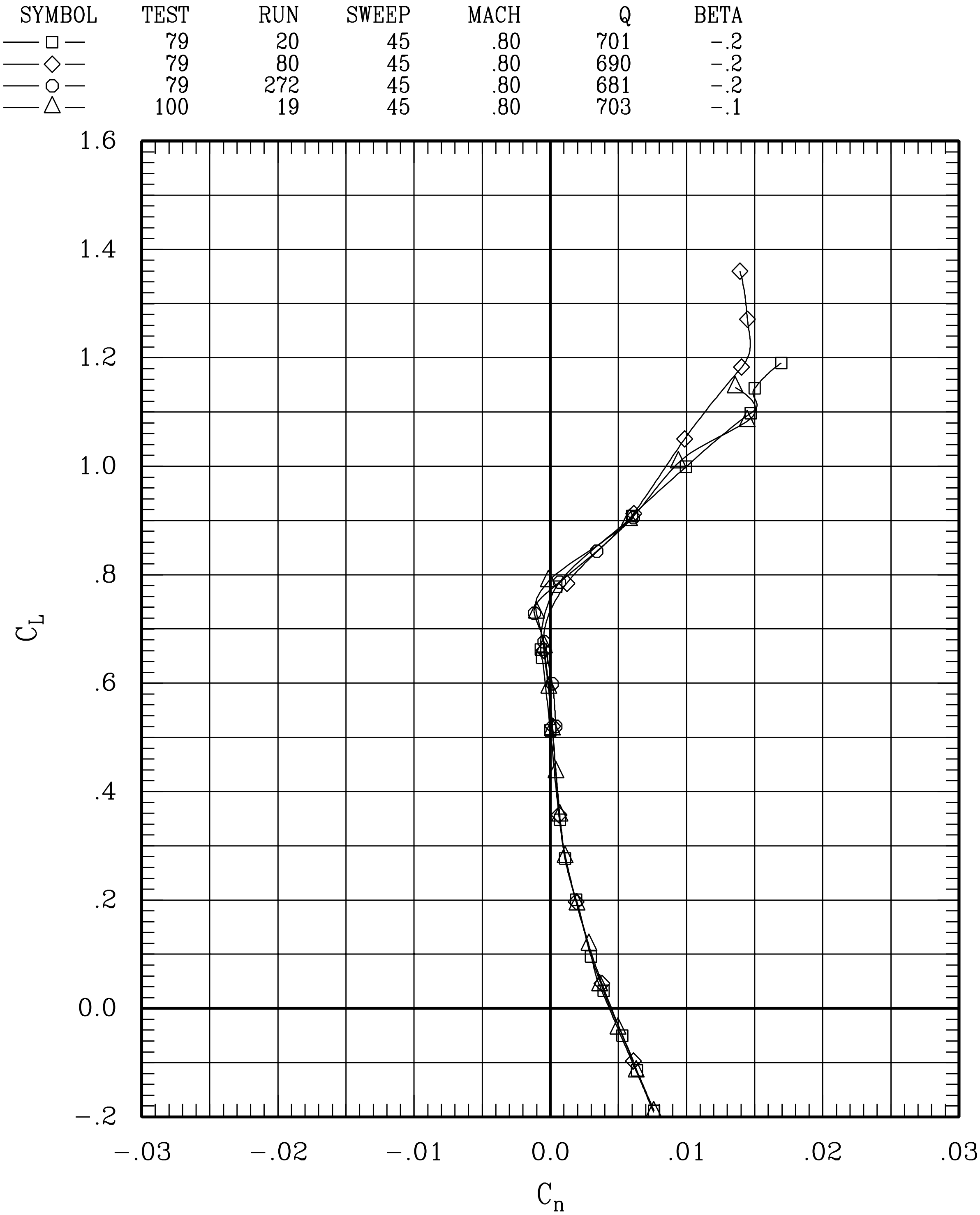

Figure 34(d). Repeat runs for sweep = 45 deg, Mach = 0.80.

SYMBOL	TEST	RUN	SWEEP	MACH	Q	BETA
—□—	79	20	45	.80	701	−.2
—◇—	79	80	45	.80	690	−.2
—○—	79	272	45	.80	681	−.2
—△—	100	19	45	.80	703	−.1

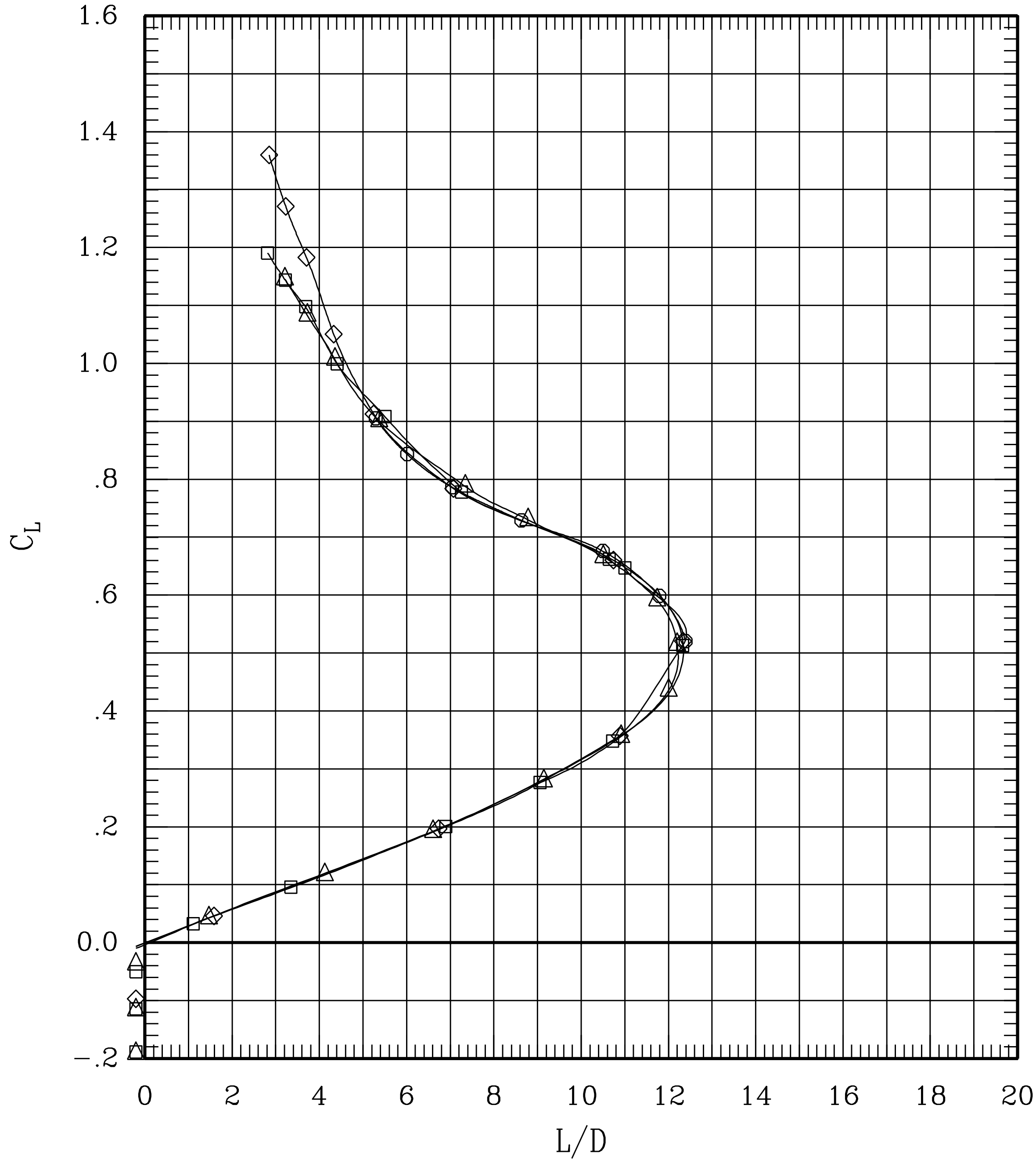

Figure 34(d). Repeat runs for sweep = 45 deg, Mach = 0.80.

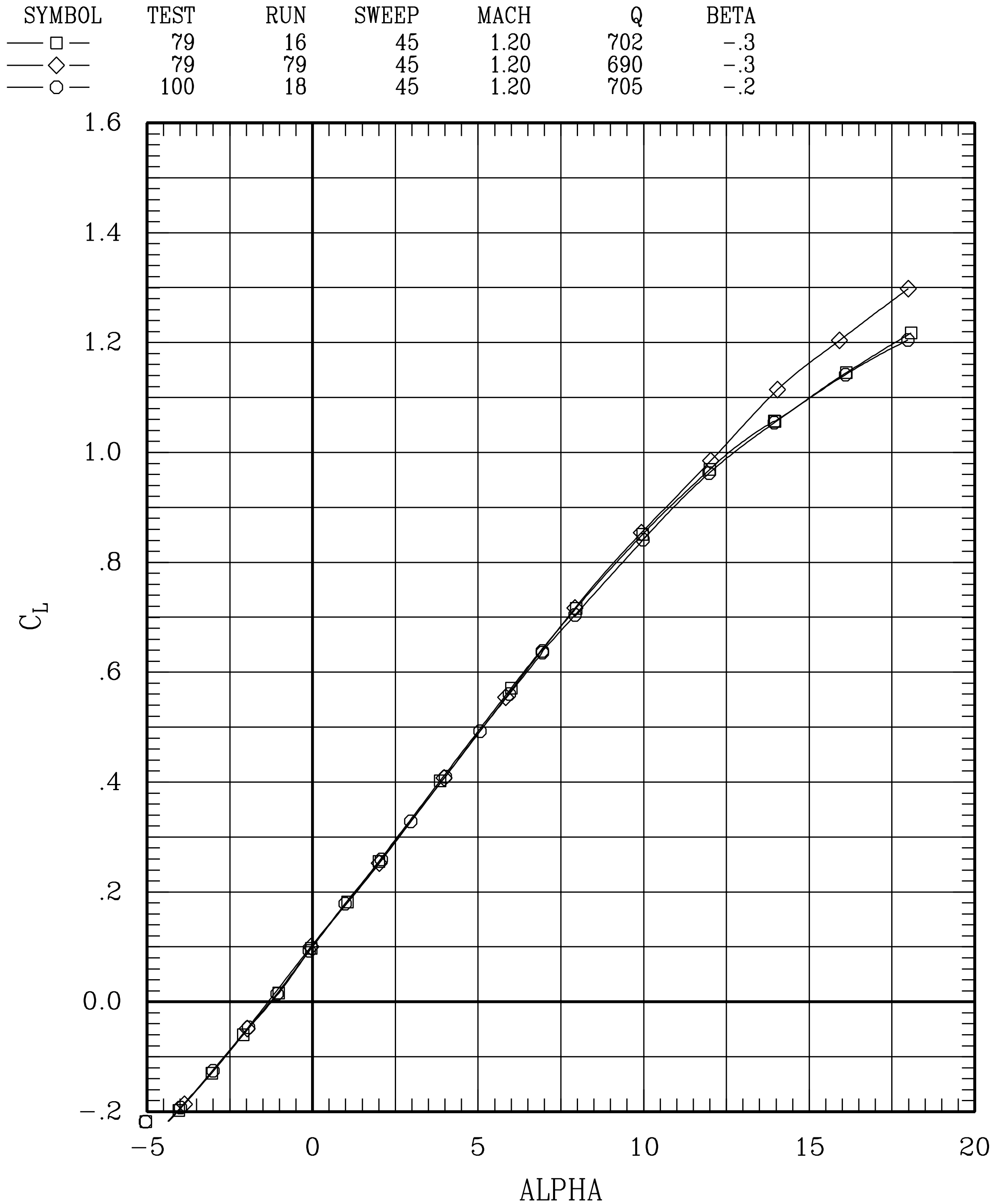

Figure 34(e). Repeat runs for sweep = 45 deg, Mach = 1.20.

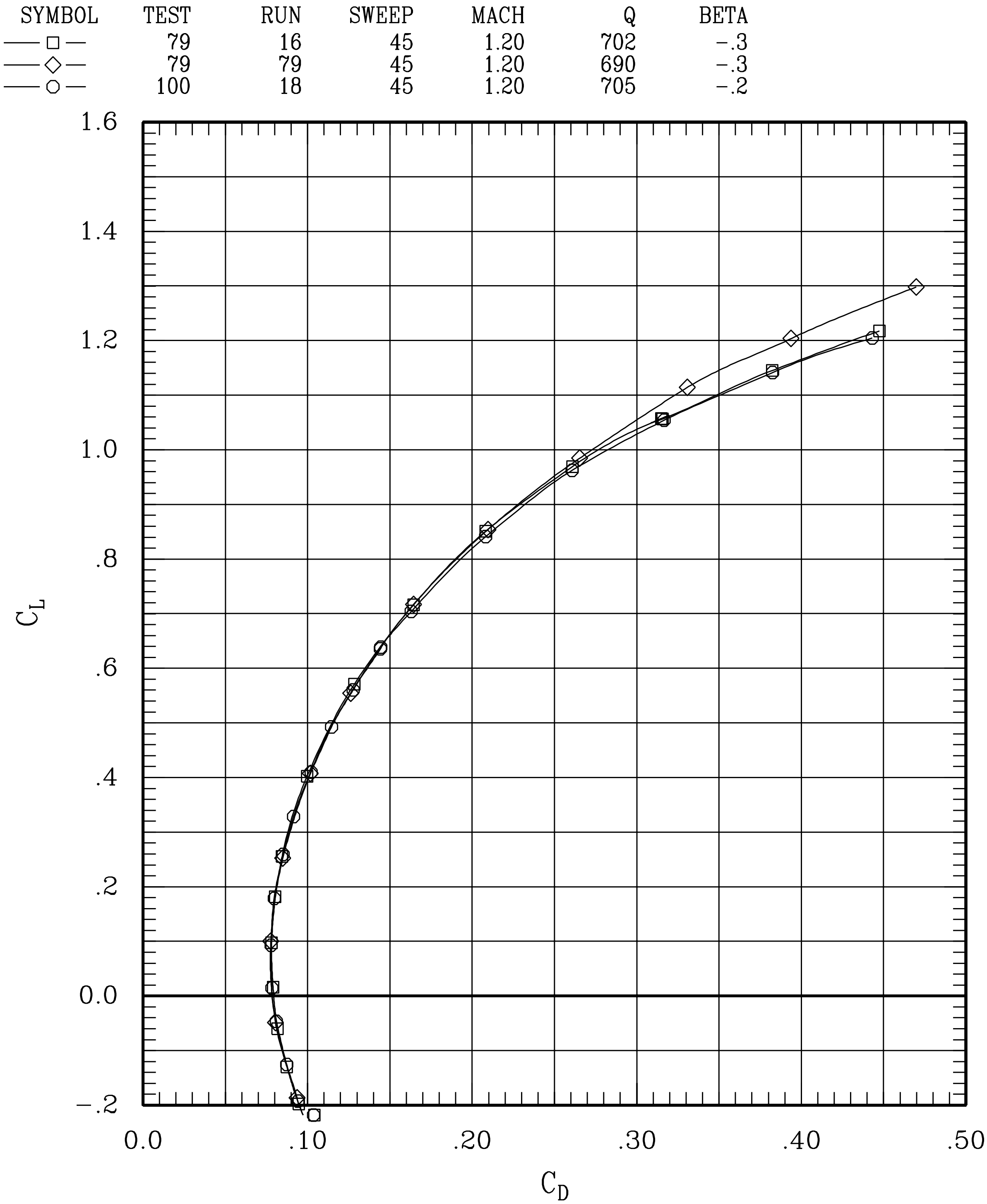

Figure 34(e). Repeat runs for sweep = 45 deg, Mach = 1.20.

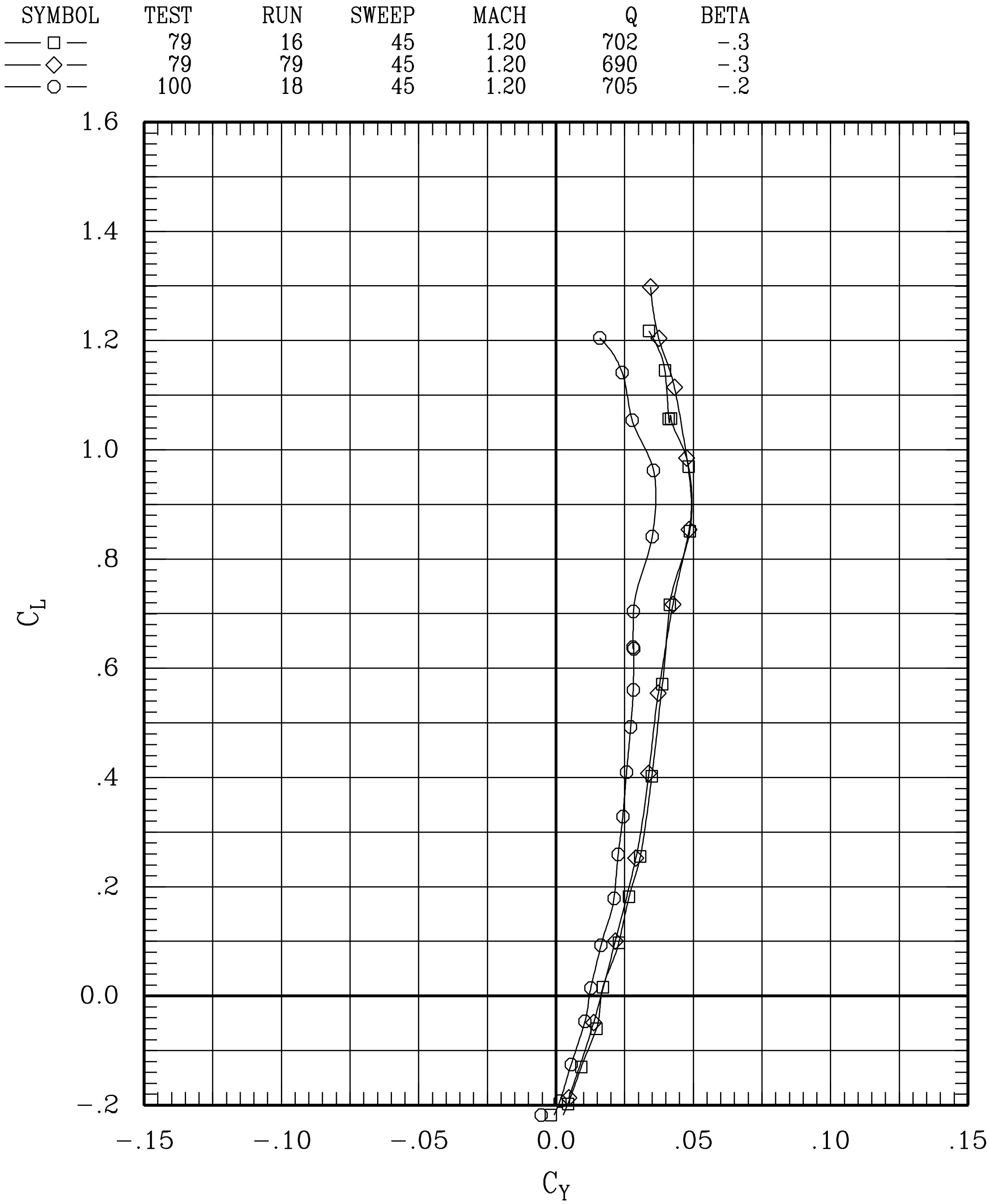

Figure 34(e). Repeat runs for sweep = 45 deg, Mach = 1.20.

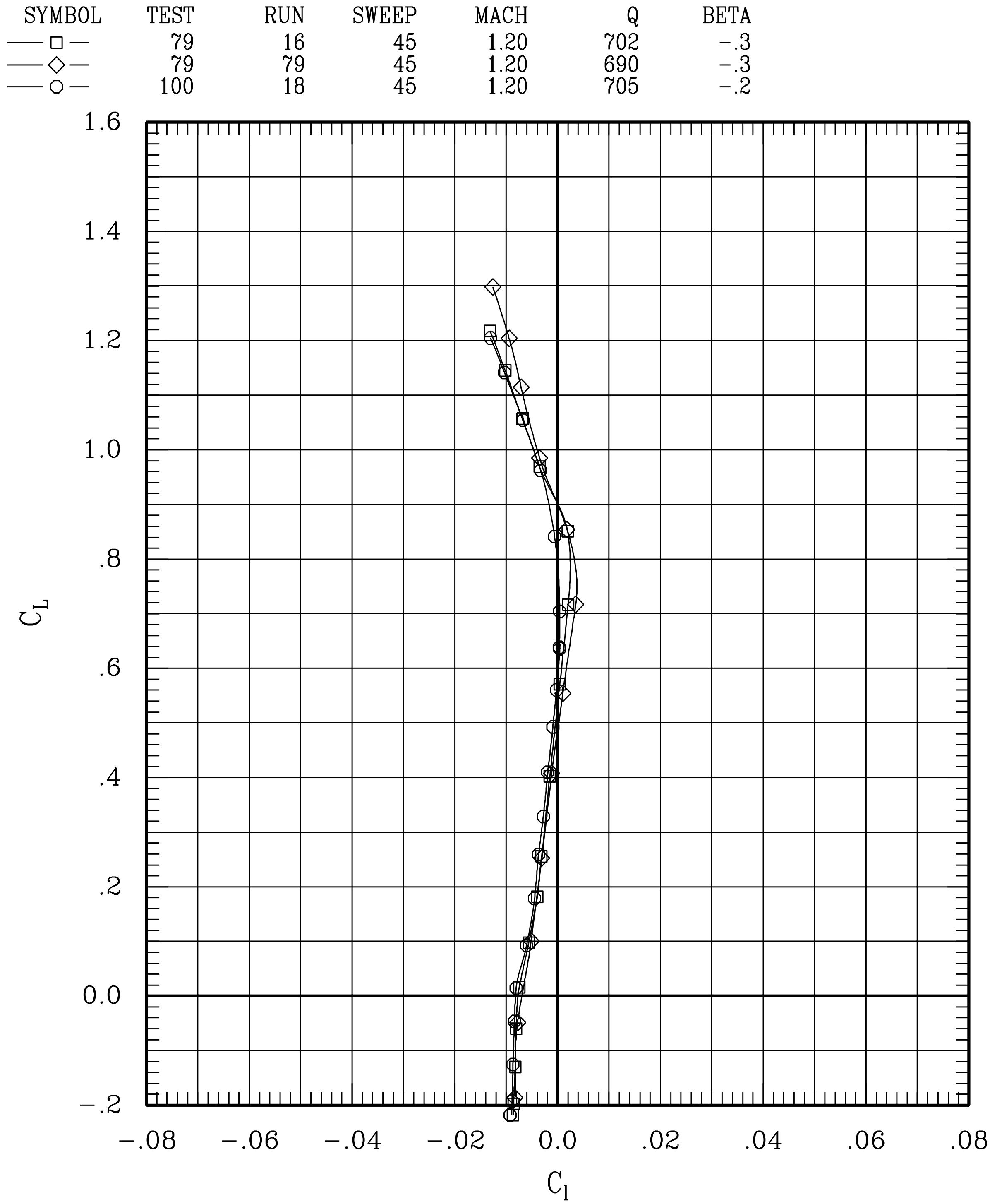

Figure 34(e). Repeat runs for sweep = 45 deg, Mach = 1.20.

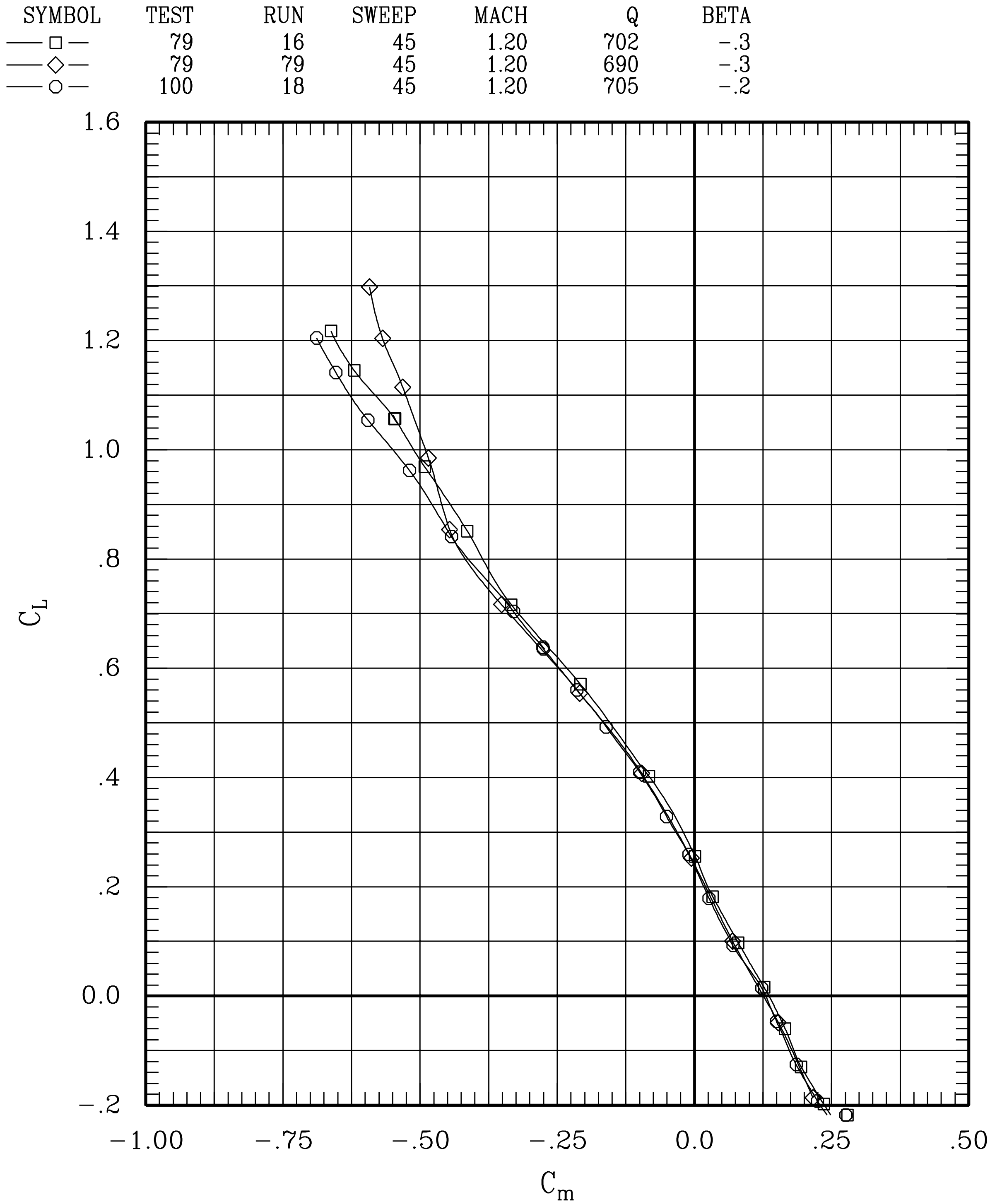

Figure 34(e). Repeat runs for sweep = 45 deg, Mach = 1.20.

SYMBOL	TEST	RUN	SWEEP	MACH	Q	BETA
—□—	79	16	45	1.20	702	−.3
—◇—	79	79	45	1.20	690	−.3
—○—	100	18	45	1.20	705	−.2

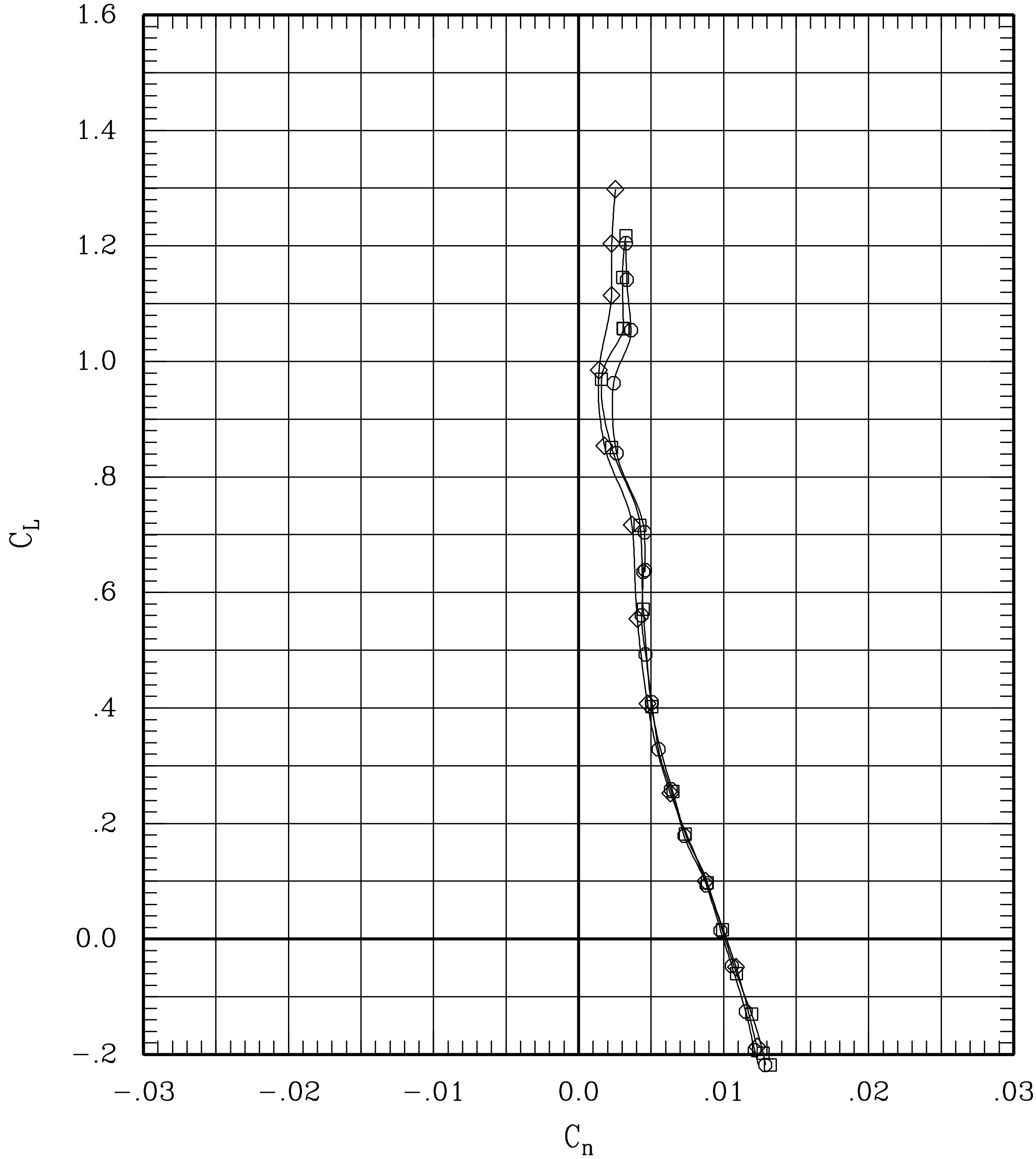

Figure 34(e). Repeat runs for sweep = 45 deg, Mach = 1.20.

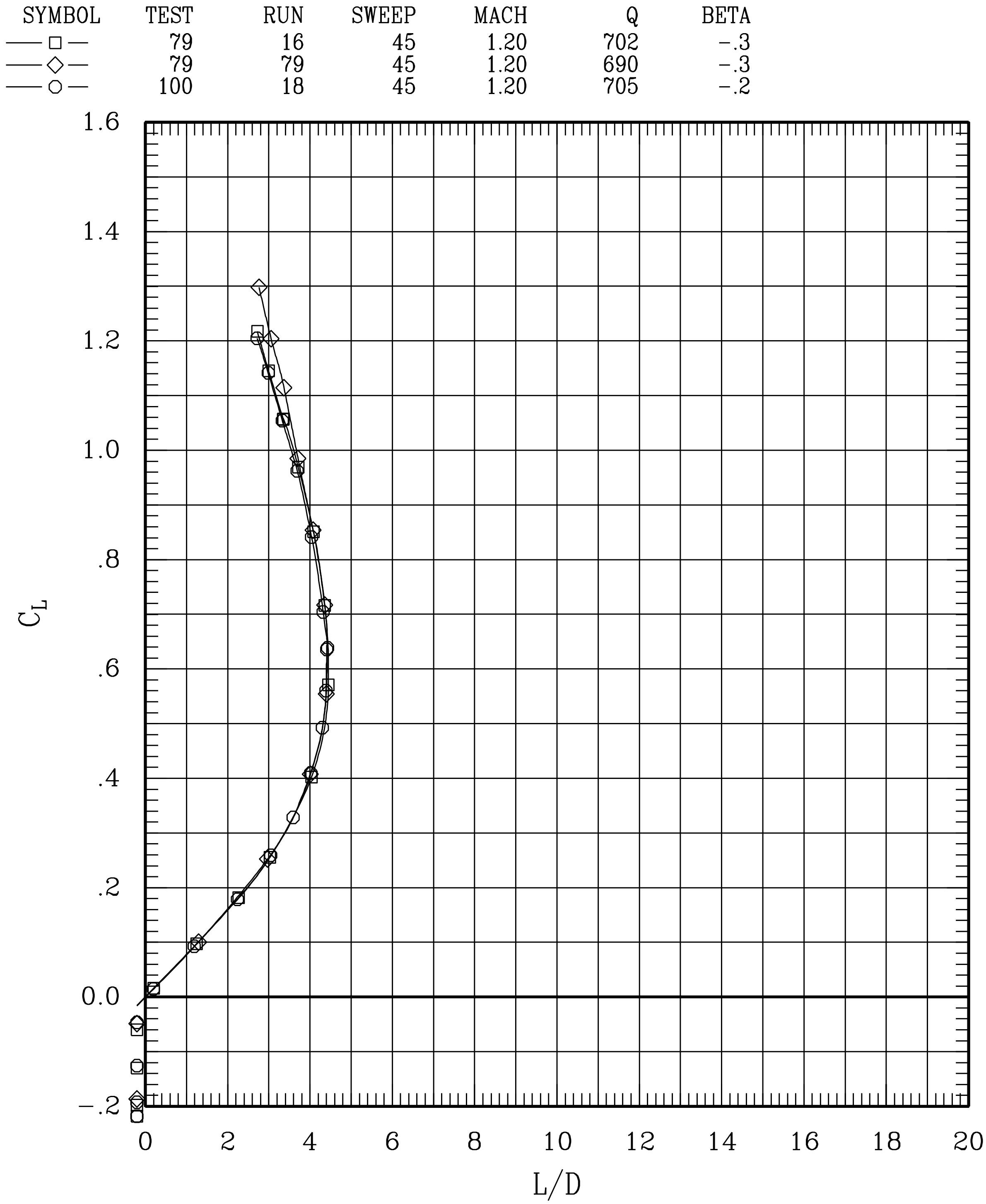

Figure 34(e). Repeat runs for sweep = 45 deg, Mach = 1.20.

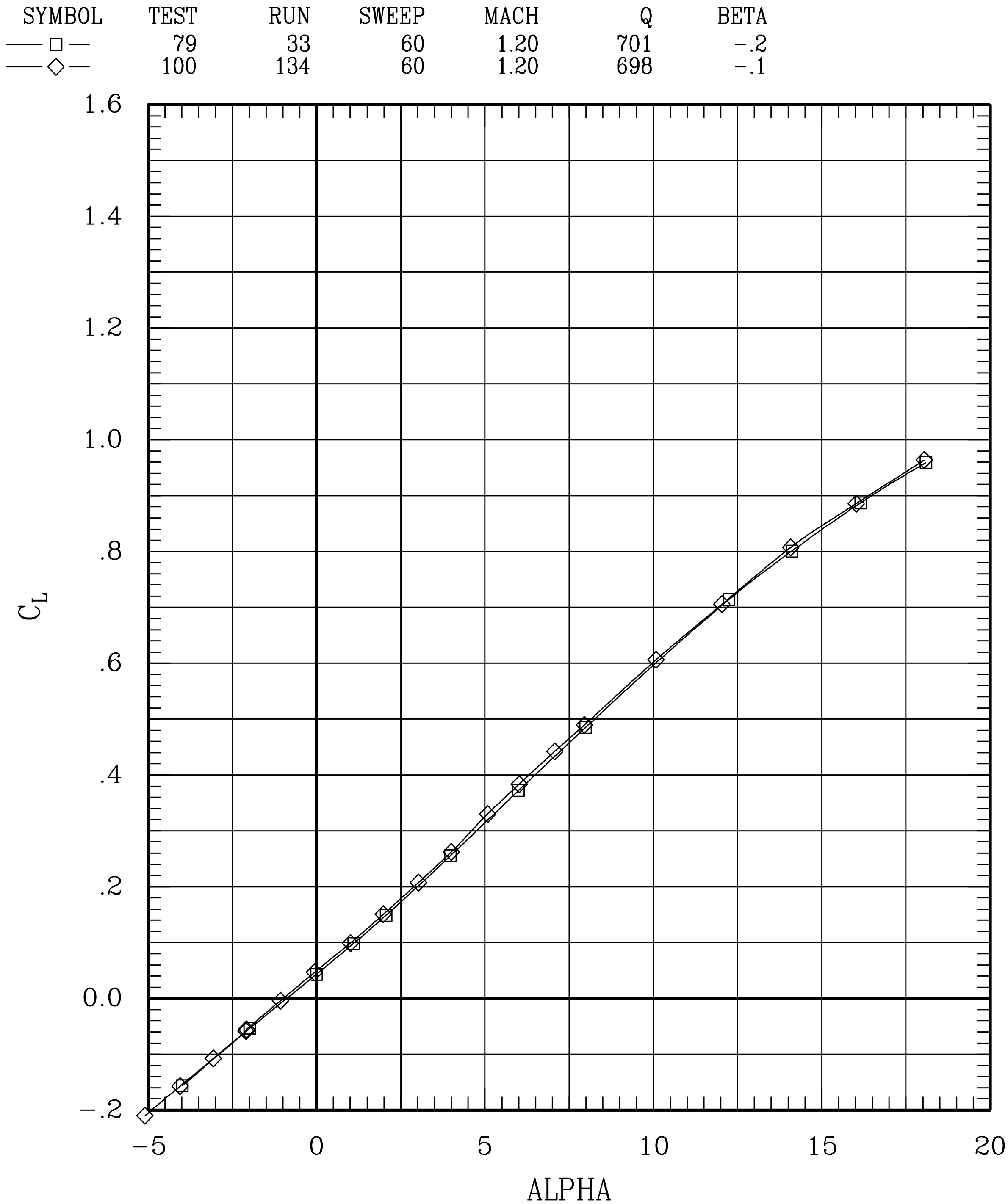

Figure 34(f). Repeat runs for sweep = 60 deg, Mach = 1.20.

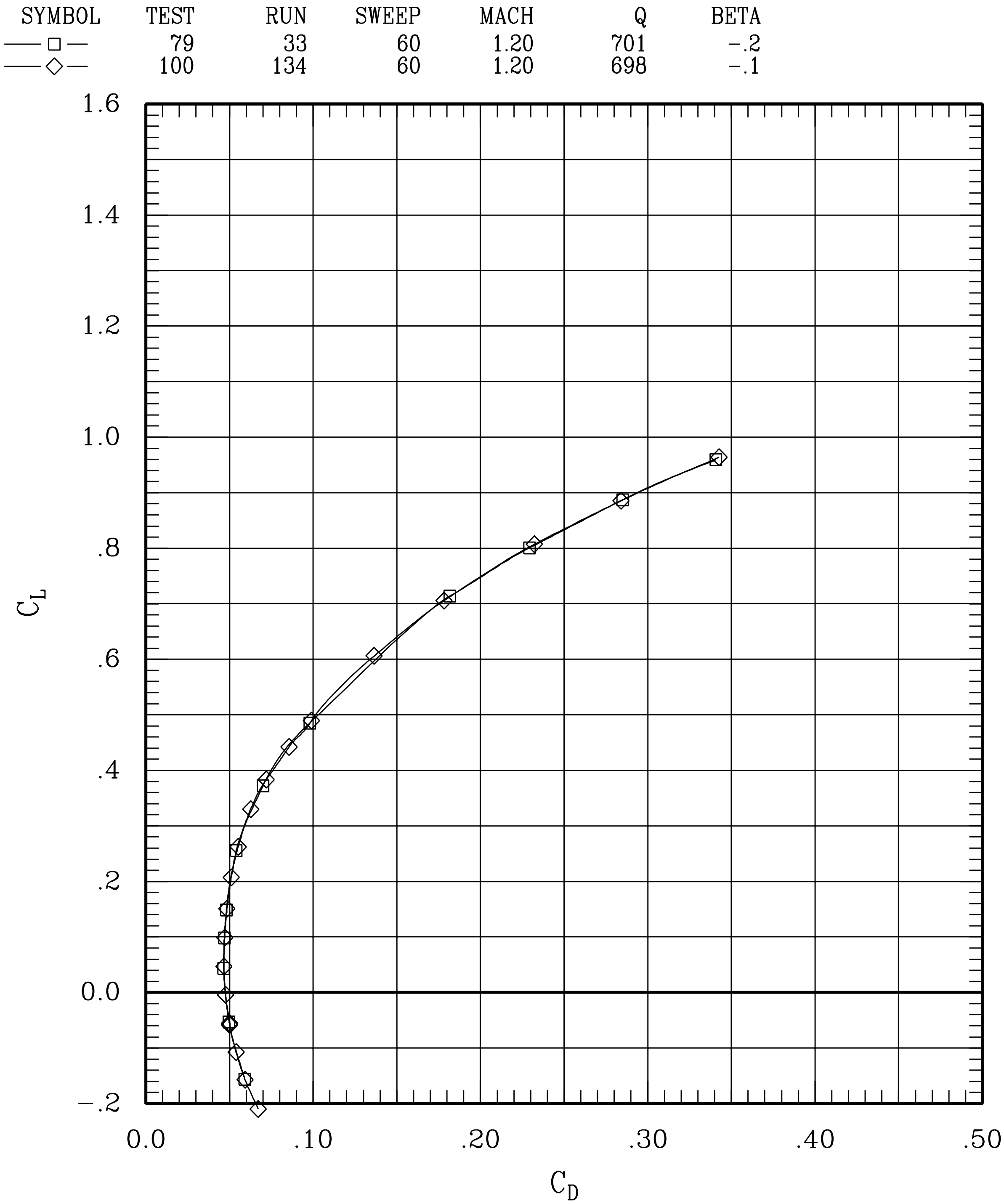

Figure 34(f). Repeat runs for sweep = 60 deg, Mach = 1.20.

SYMBOL	TEST	RUN	SWEEP	MACH	Q	BETA
—□—	79	33	60	1.20	701	−.2
—◇—	100	134	60	1.20	698	−.1

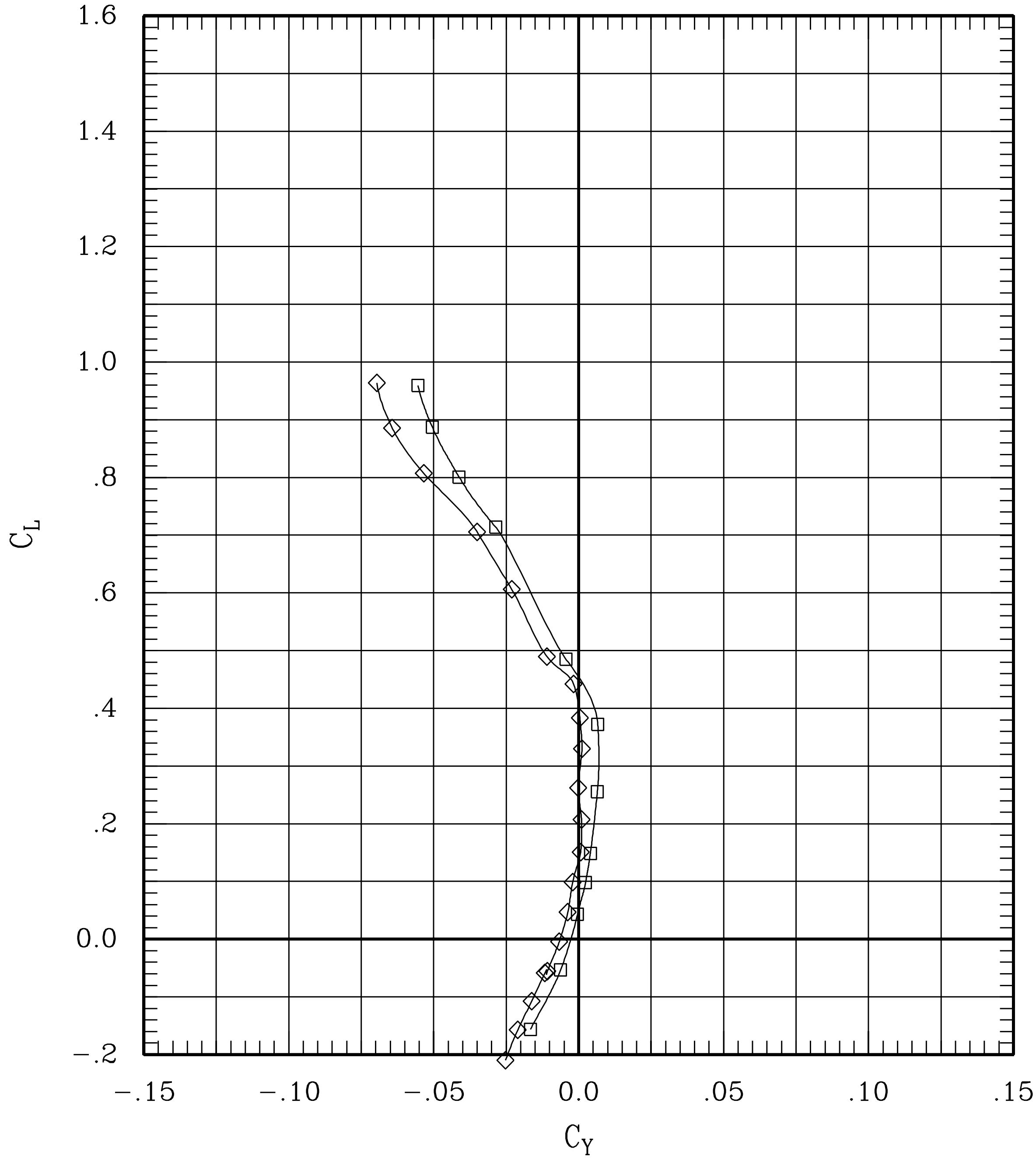

Figure 34(f). Repeat runs for sweep = 60 deg, Mach = 1.20.

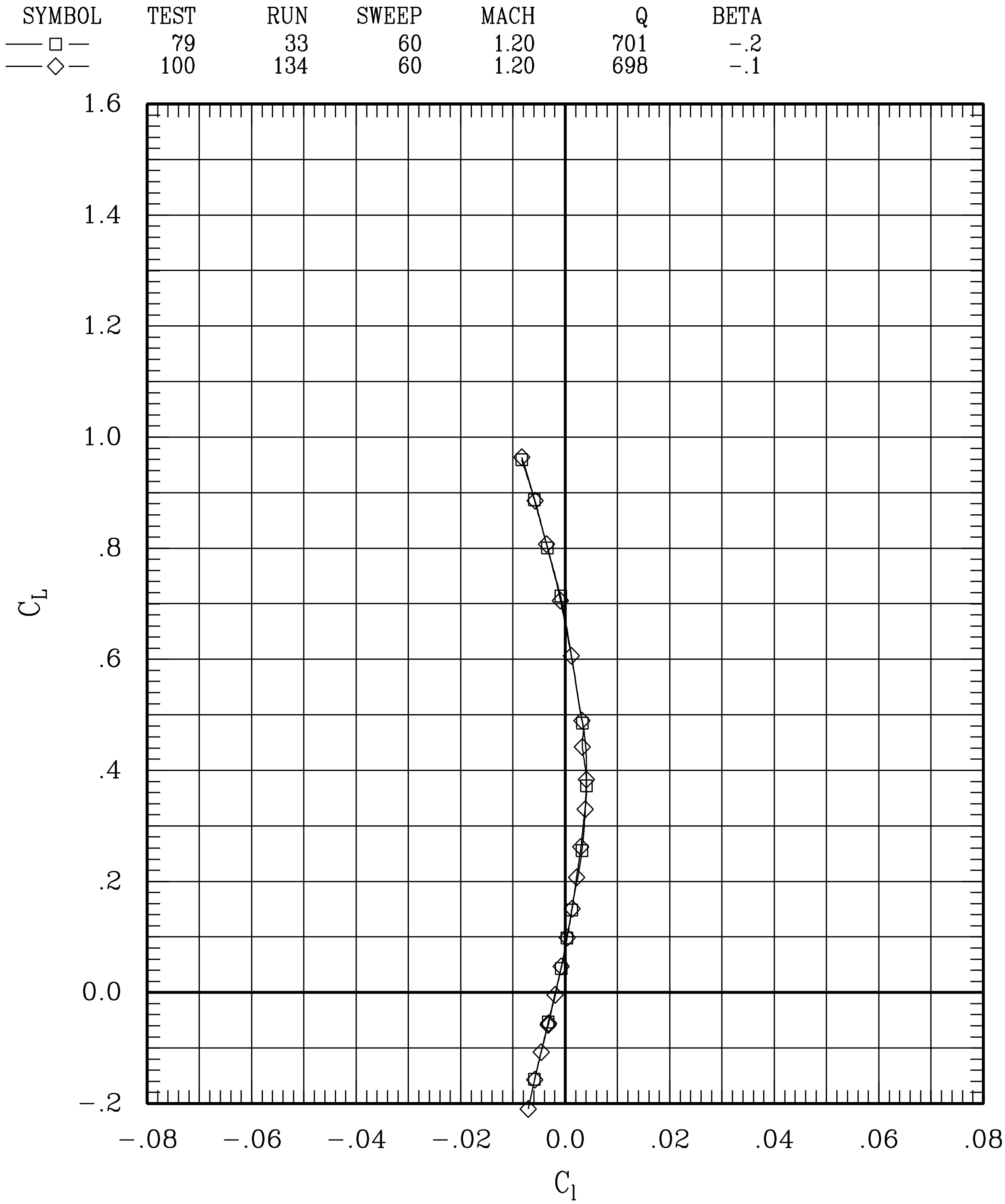

Figure 34(f). Repeat runs for sweep = 60 deg, Mach = 1.20.

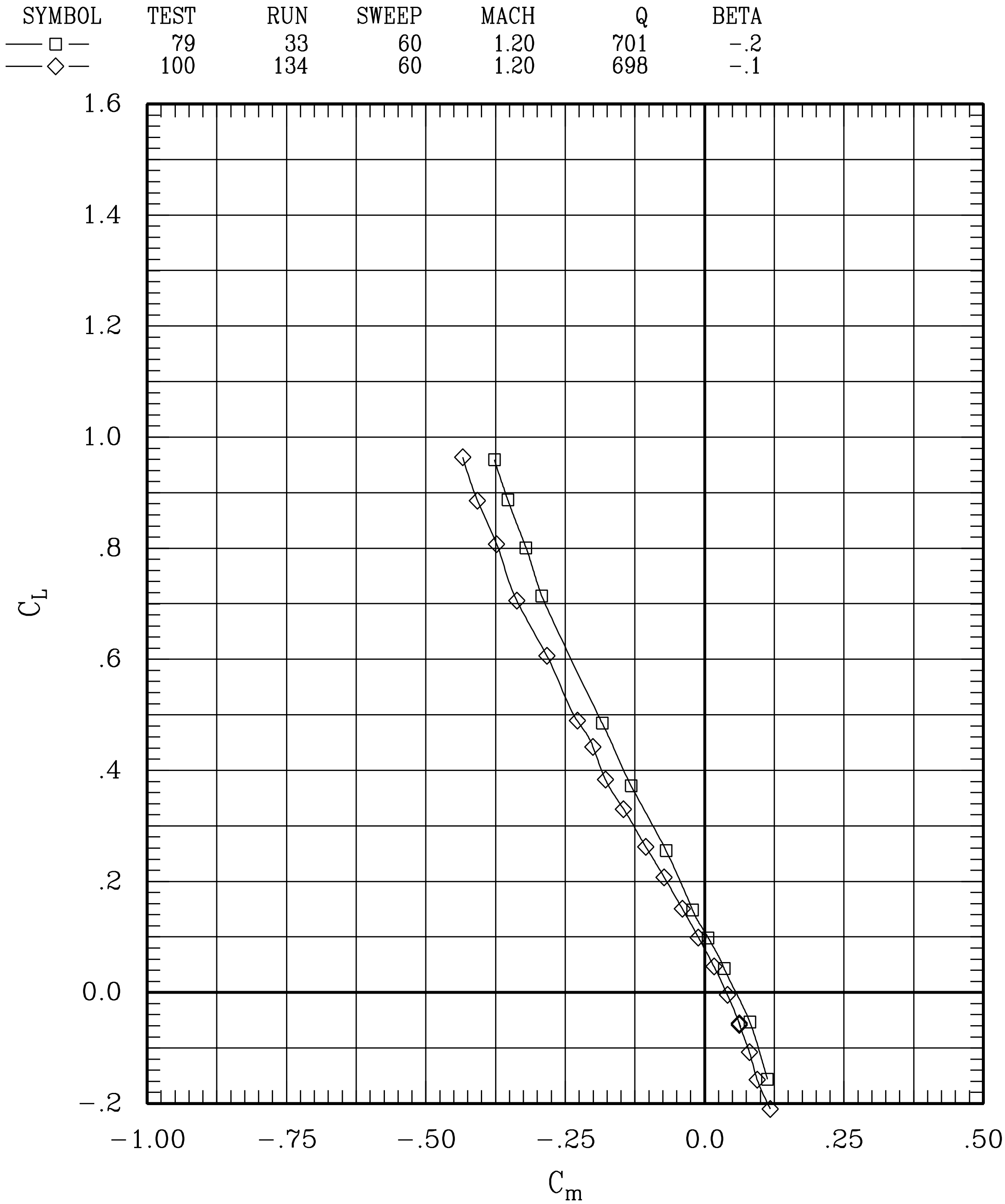

Figure 34(f). Repeat runs for sweep = 60 deg, Mach = 1.20.

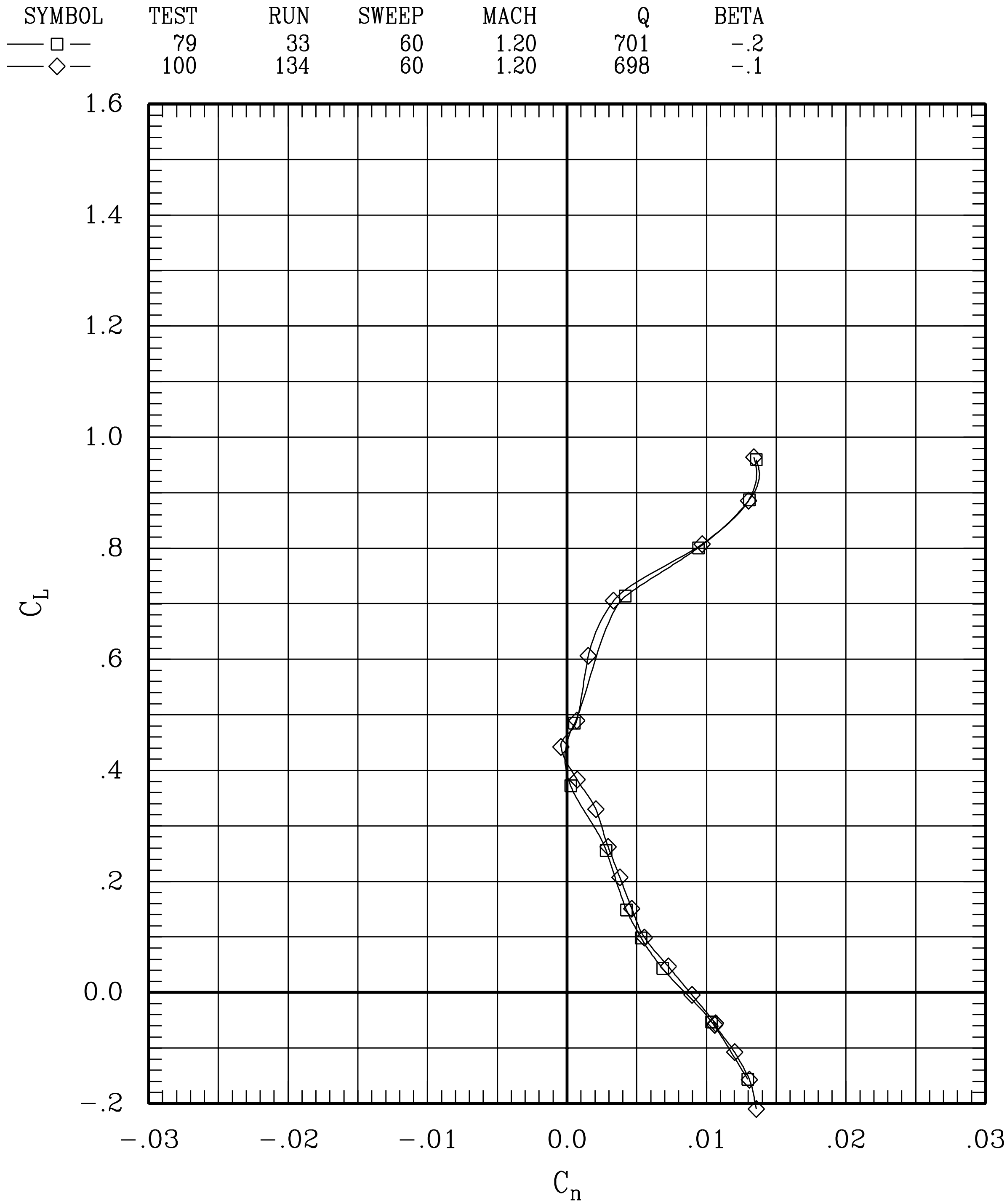

Figure 34(f). Repeat runs for sweep = 60 deg, Mach = 1.20.

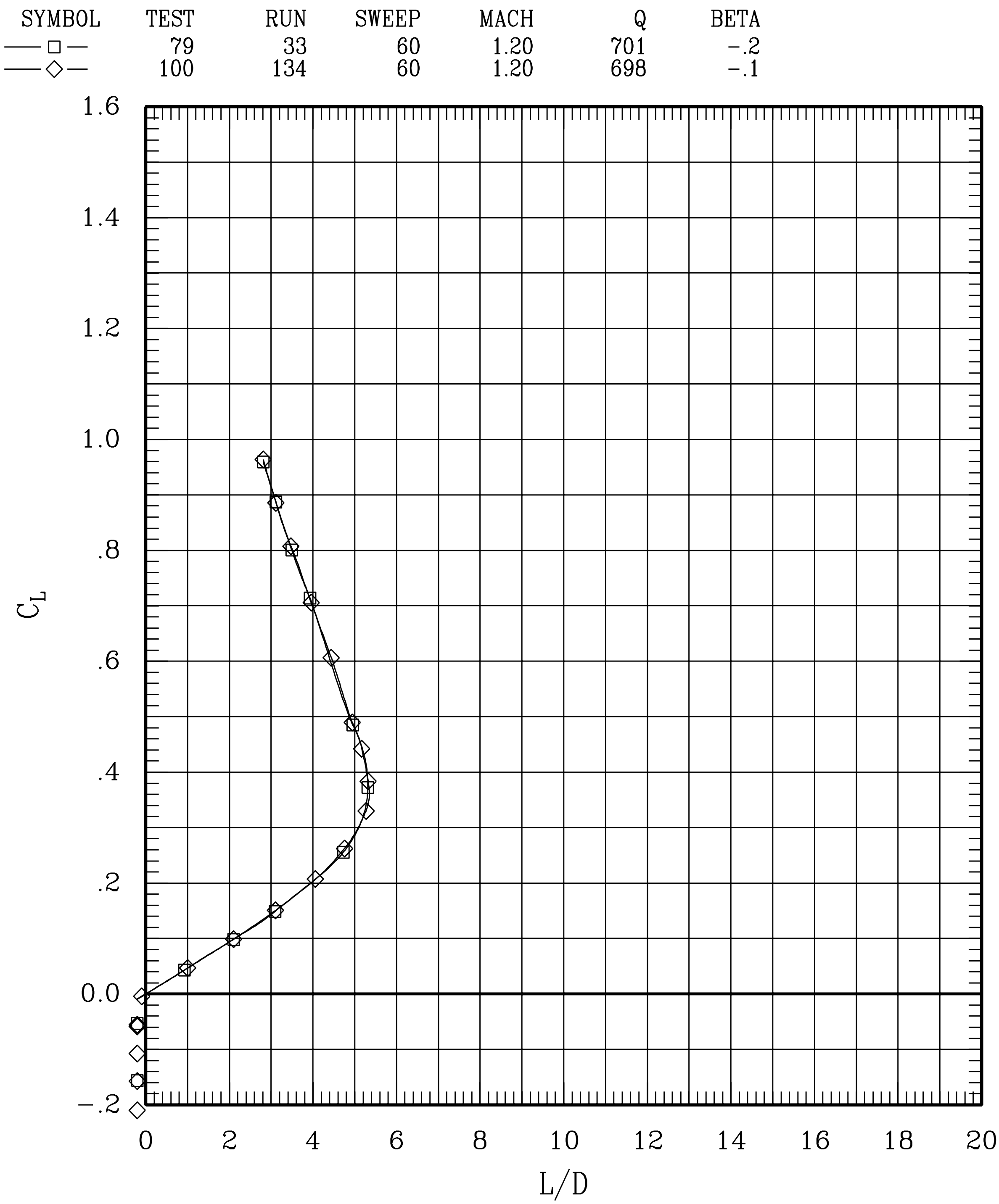

Figure 34(f). Repeat runs for sweep = 60 deg, Mach = 1.20.

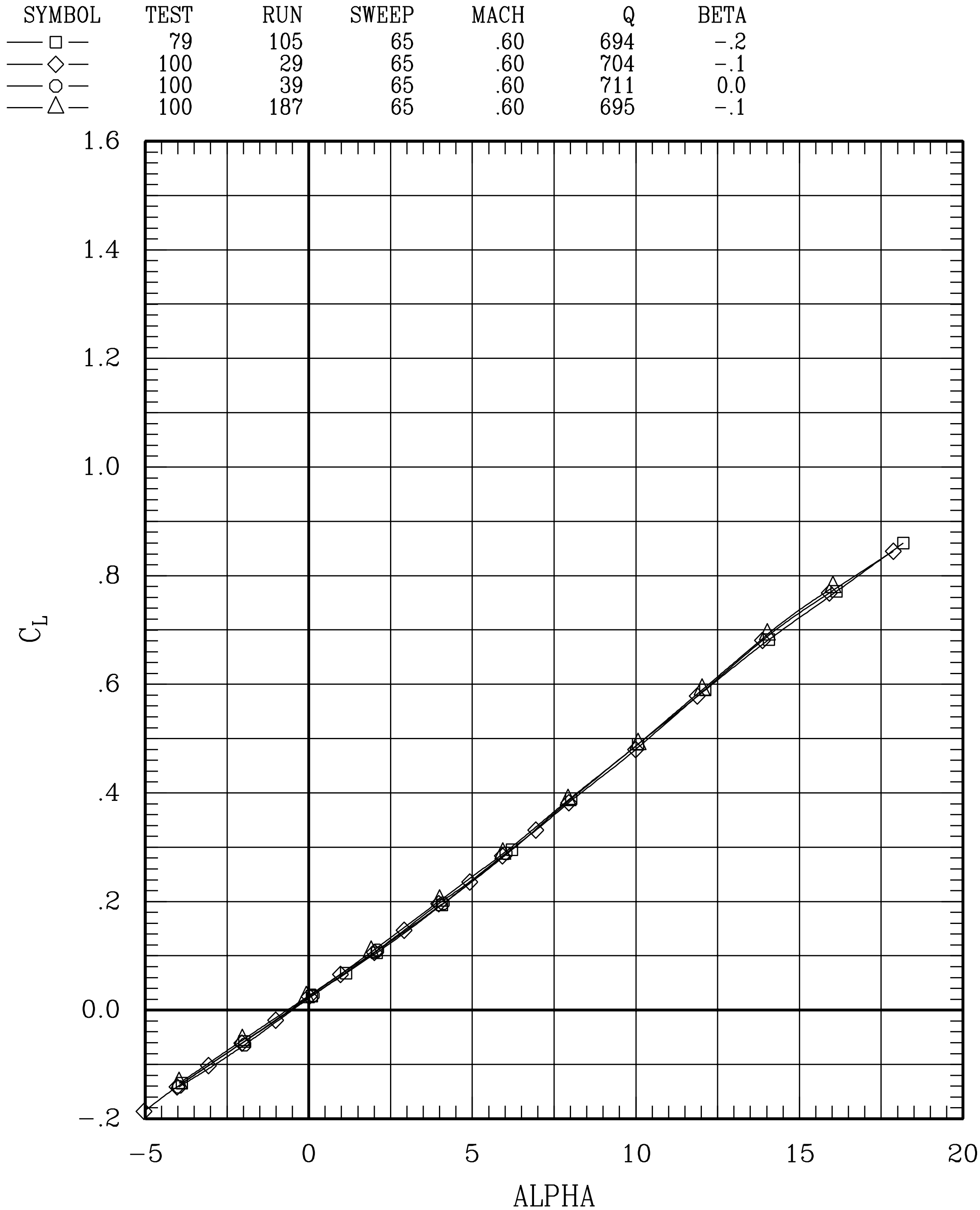

Figure 34(g). Repeat runs for sweep = 65 deg, Mach = 0.60.

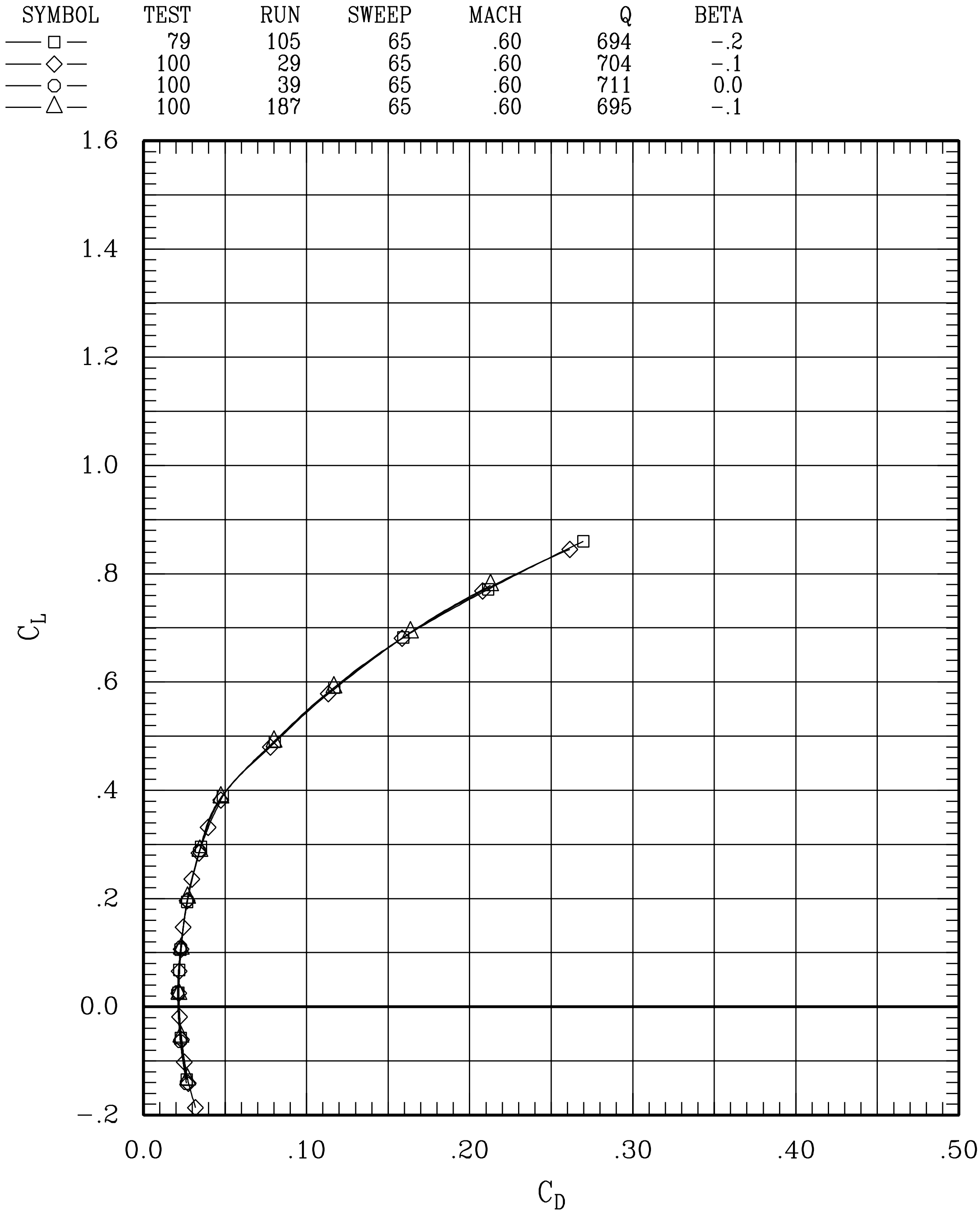

Figure 34(g). Repeat runs for sweep = 65 deg, Mach = 0.60.

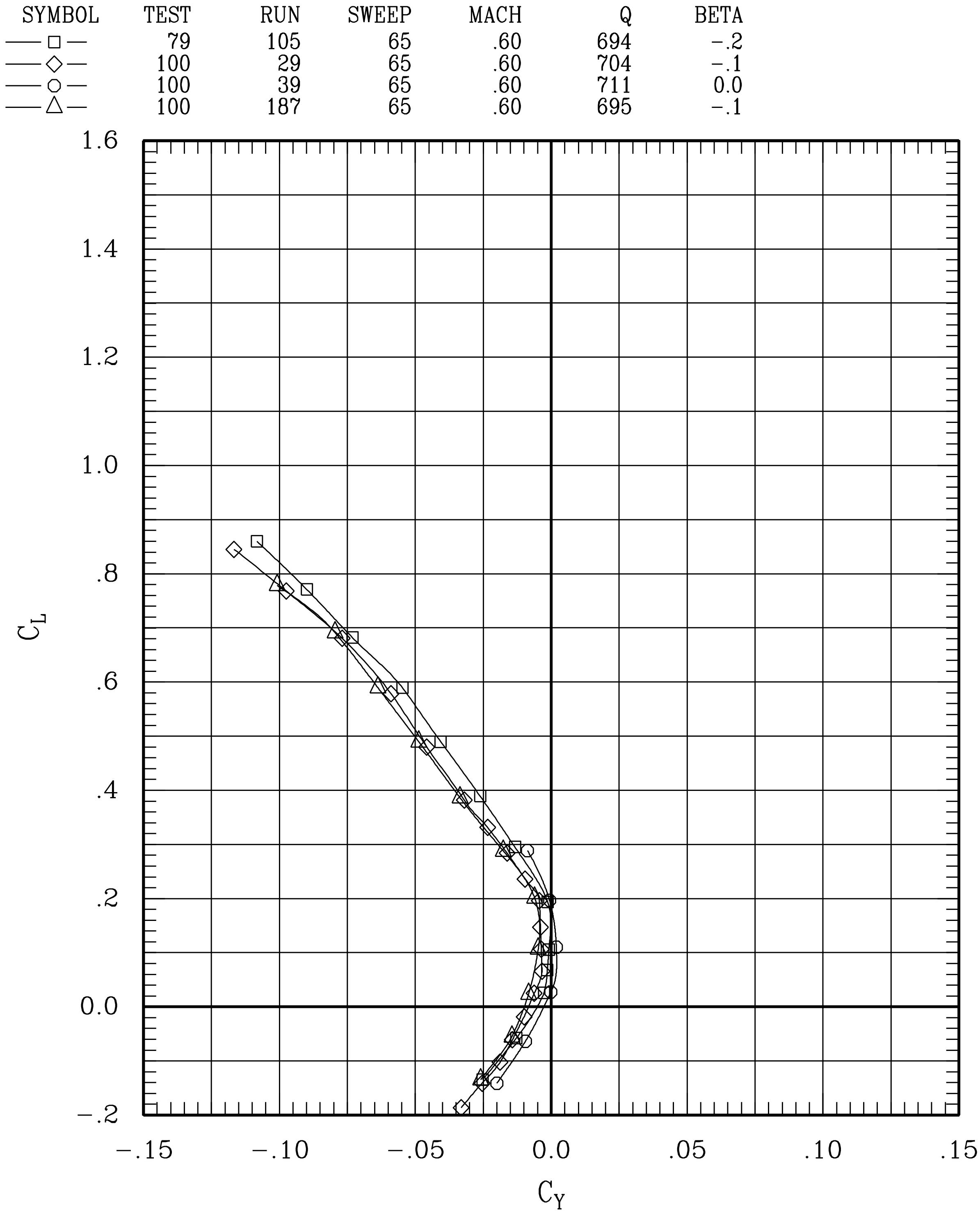

Figure 34(g). Repeat runs for sweep = 65 deg, Mach = 0.60.

SYMBOL	TEST	RUN	SWEEP	MACH	Q	BETA
—□—	79	105	65	.60	694	−.2
—◇—	100	29	65	.60	704	−.1
—○—	100	39	65	.60	711	0.0
—△—	100	187	65	.60	695	−.1

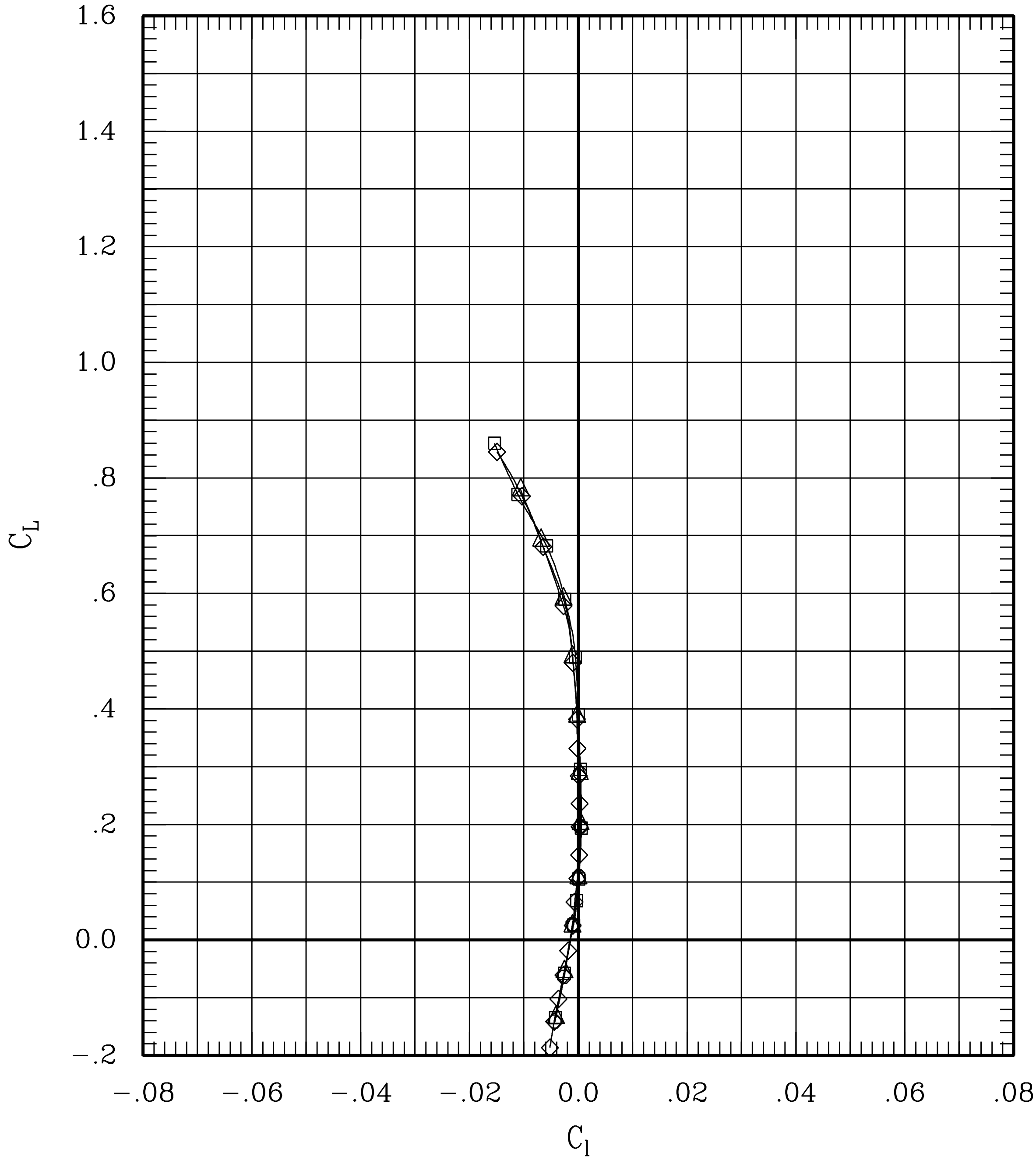

Figure 34(g). Repeat runs for sweep = 65 deg, Mach = 0.60.

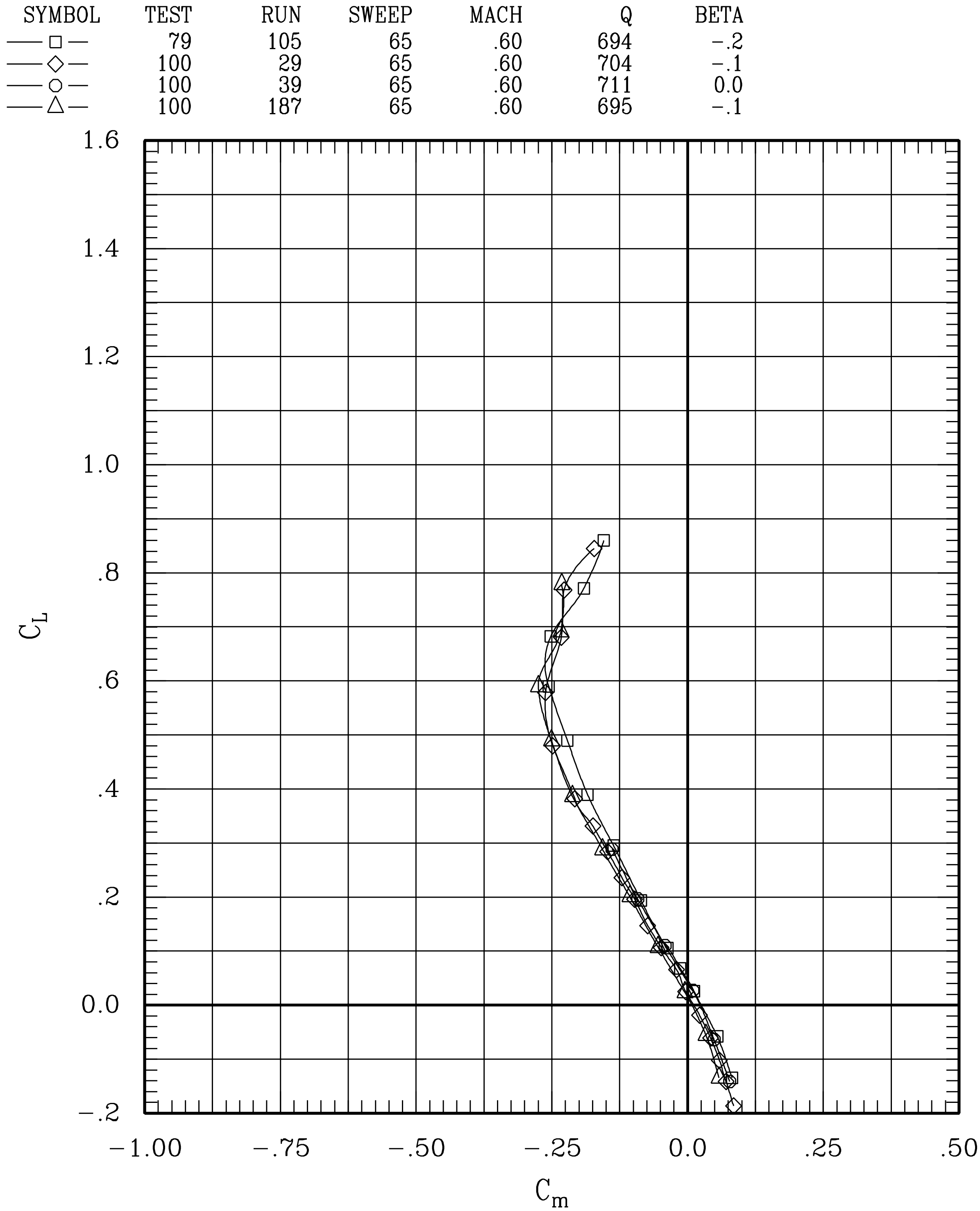

Figure 34(g). Repeat runs for sweep = 65 deg, Mach = 0.60.

SYMBOL	TEST	RUN	SWEEP	MACH	Q	BETA
—□—	79	105	65	.60	694	−.2
—◇—	100	29	65	.60	704	−.1
—○—	100	39	65	.60	711	0.0
—△—	100	187	65	.60	695	−.1

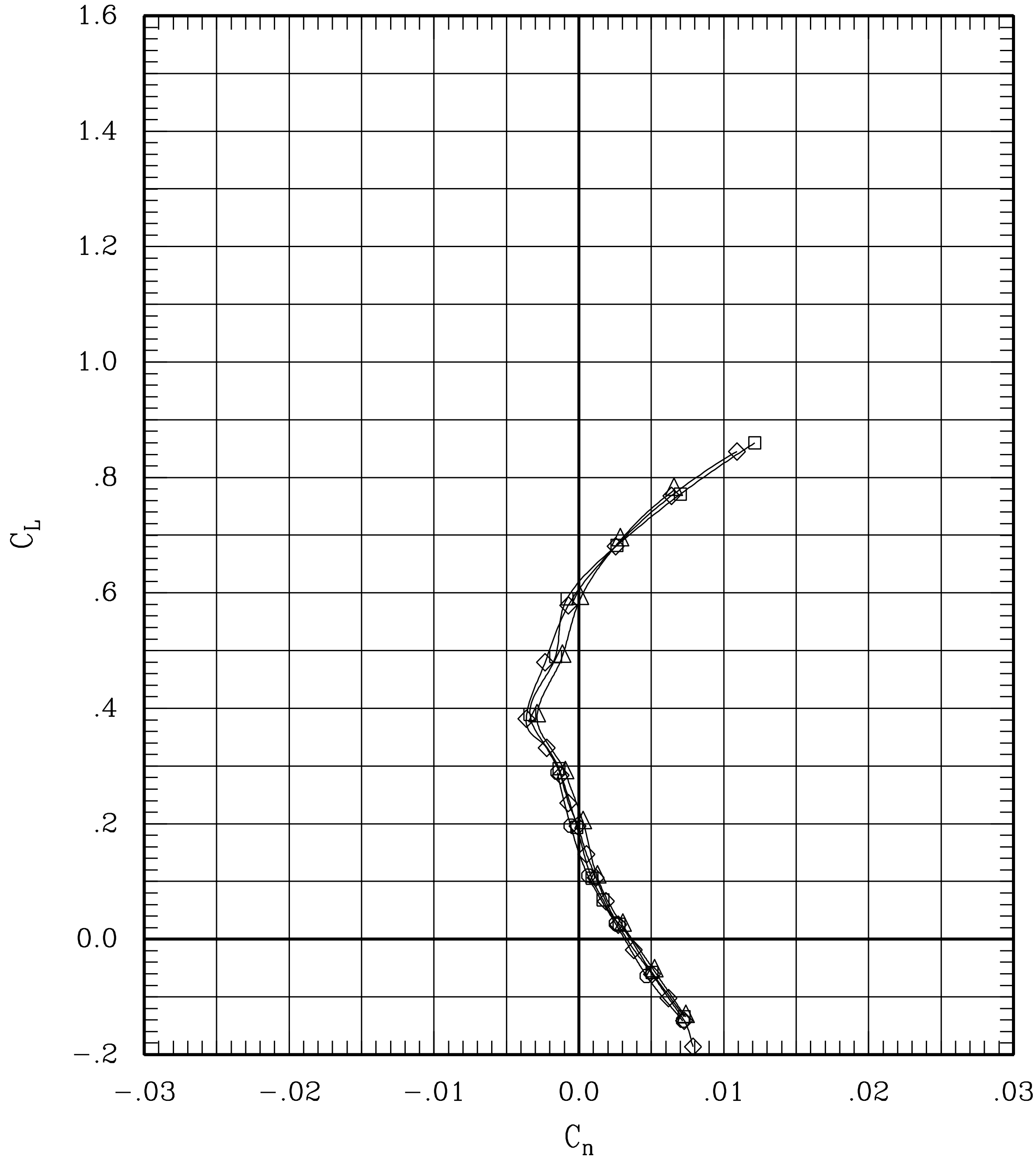

Figure 34(g). Repeat runs for sweep = 65 deg, Mach = 0.60.

SYMBOL	TEST	RUN	SWEEP	MACH	Q	BETA
—□—	79	105	65	.60	694	−.2
—◇—	100	29	65	.60	704	−.1
—○—	100	39	65	.60	711	0.0
—△—	100	187	65	.60	695	−.1

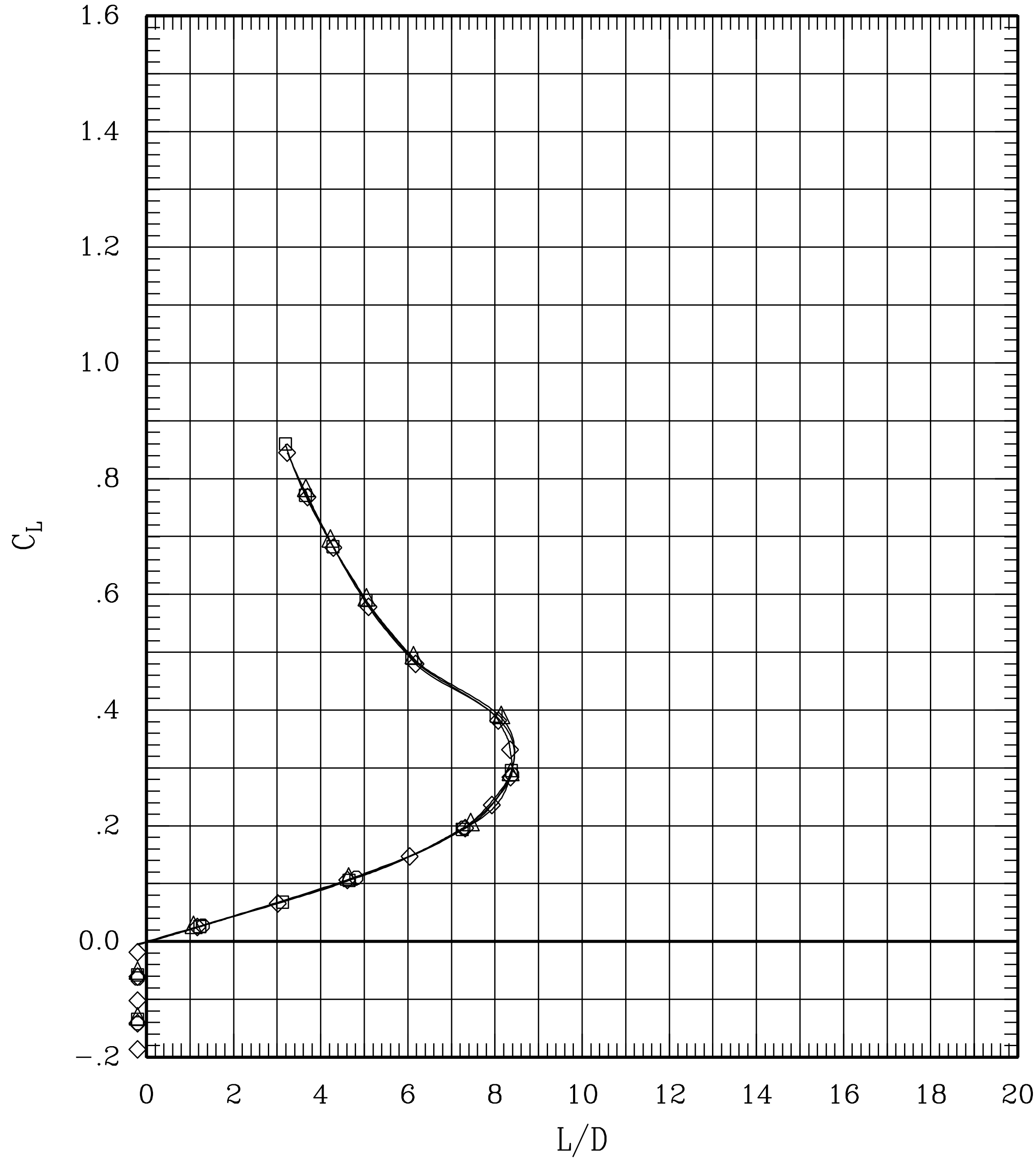

Figure 34(g). Repeat runs for sweep = 65 deg, Mach = 0.60.

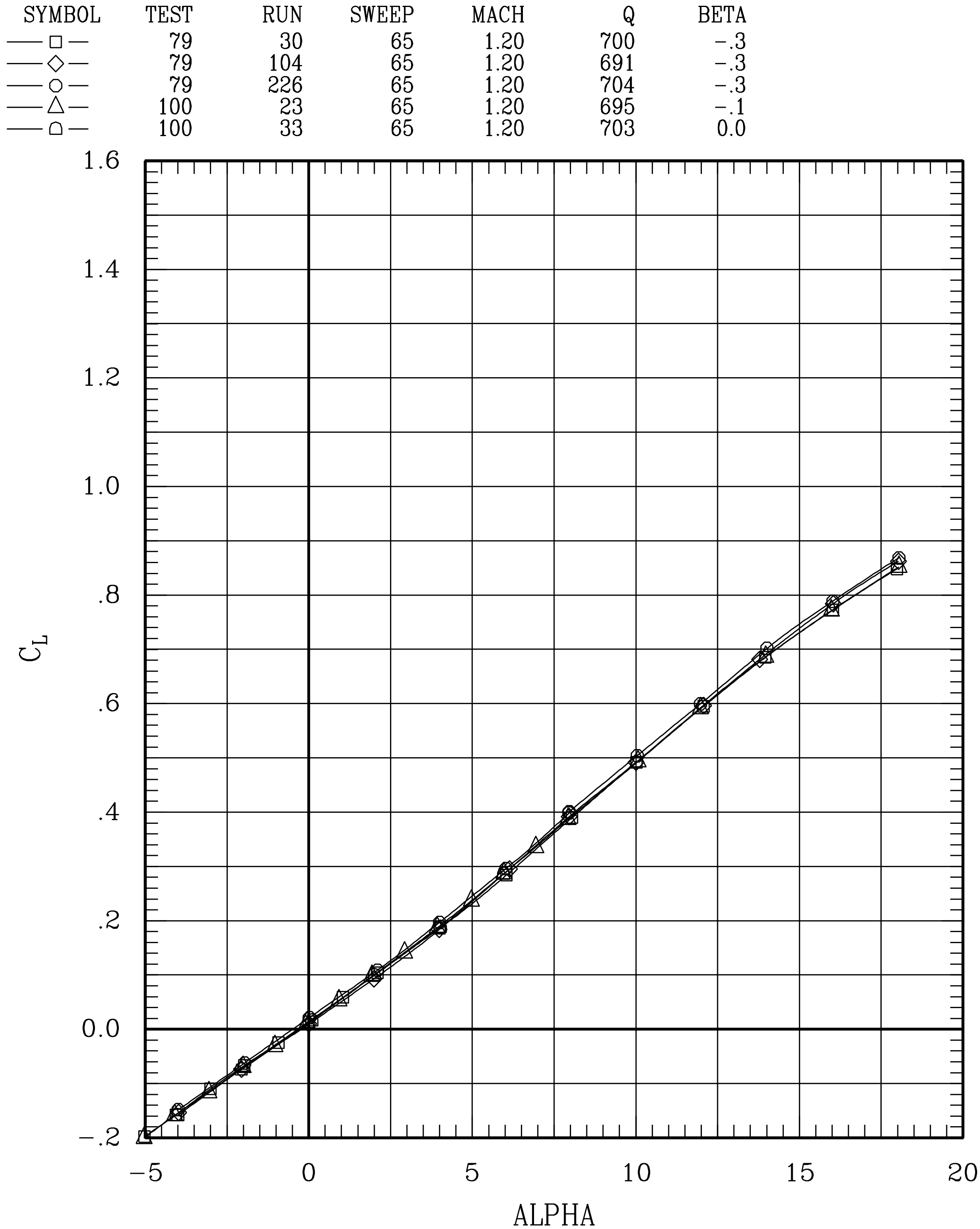

Figure 34(h). Repeat runs for sweep = 65 deg, Mach = 1.20.

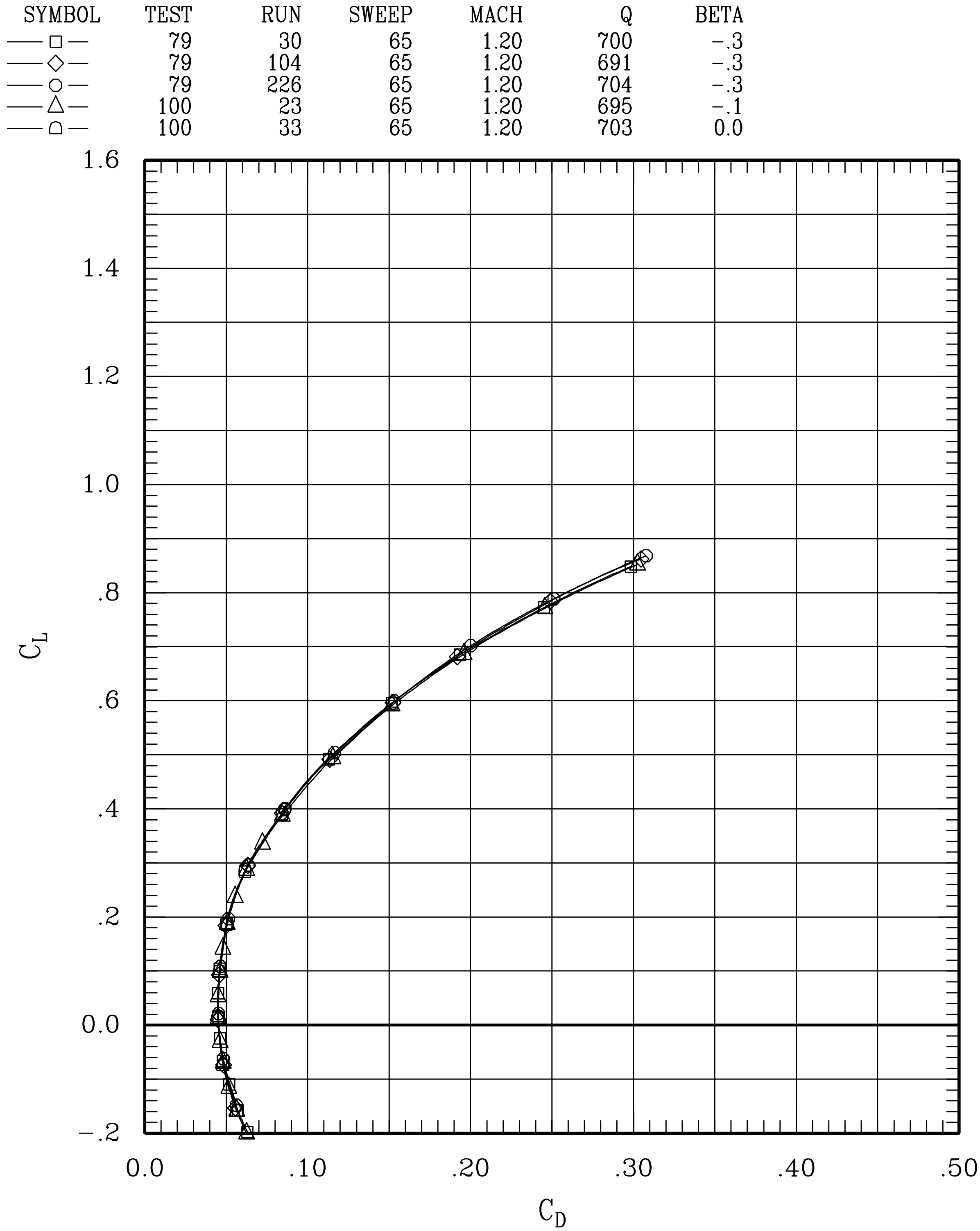

Figure 34(h). Repeat runs for sweep = 65 deg, Mach = 1.20.

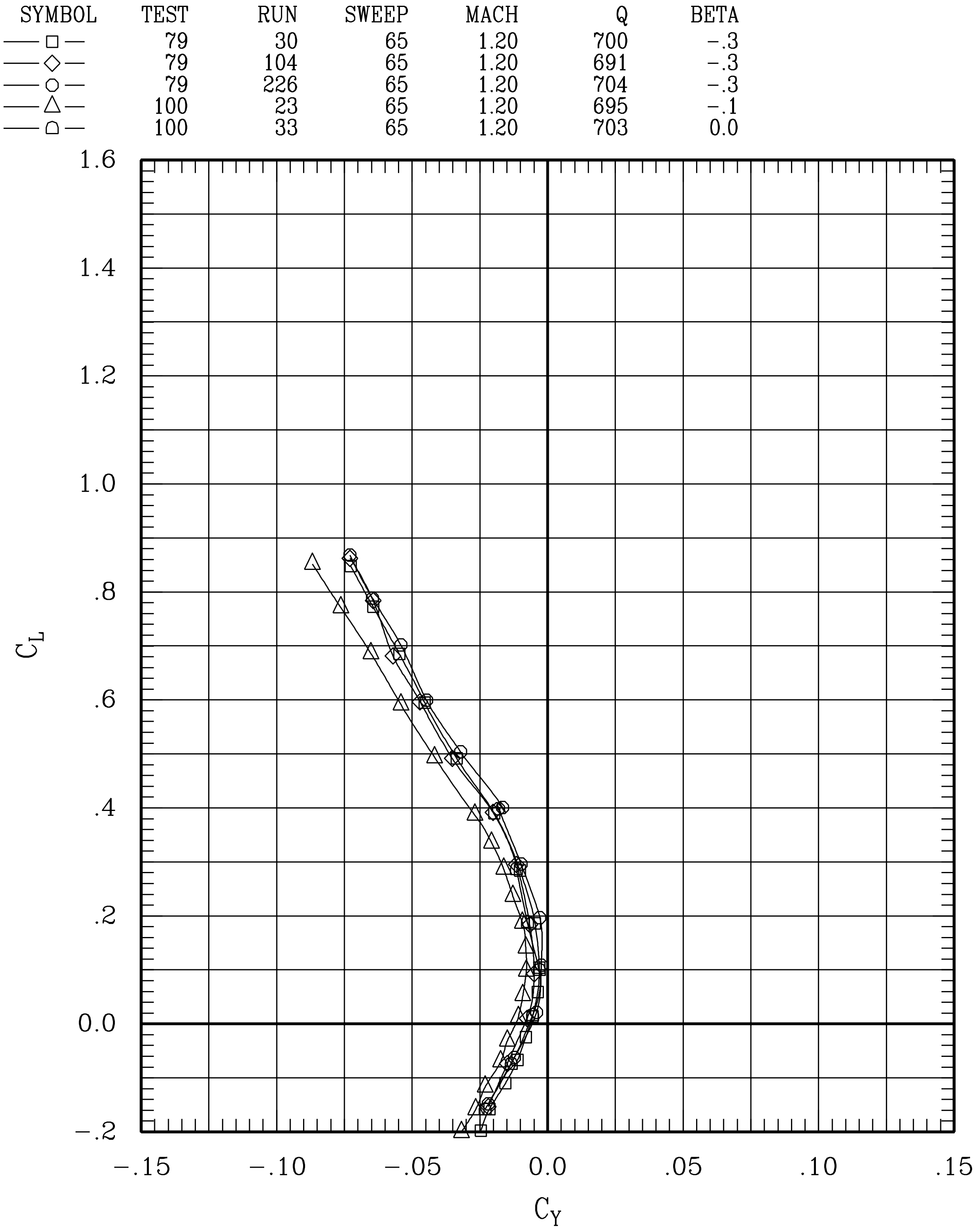

Figure 34(h). Repeat runs for sweep = 65 deg, Mach = 1.20.

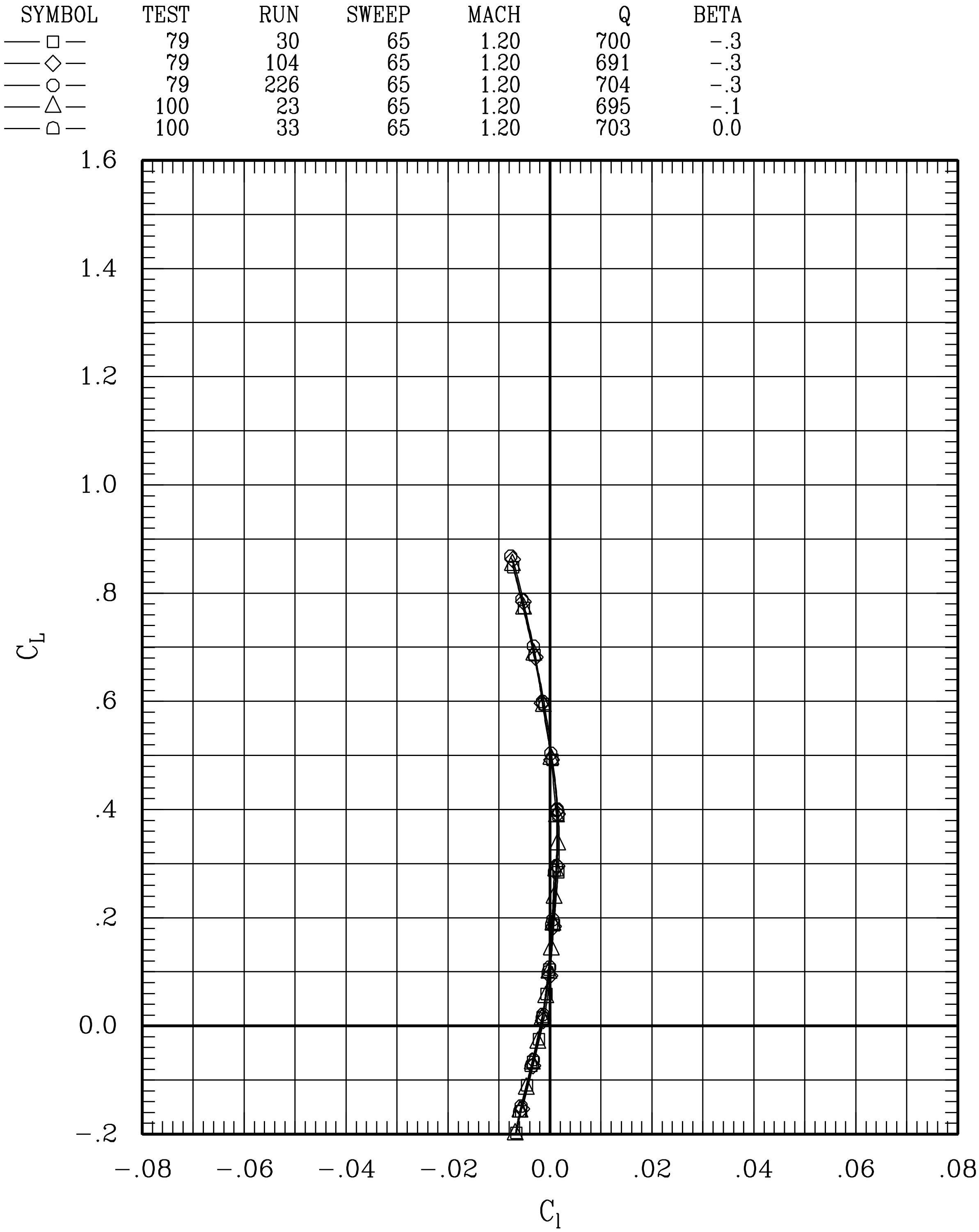

Figure 34(h). Repeat runs for sweep = 65 deg, Mach = 1.20.

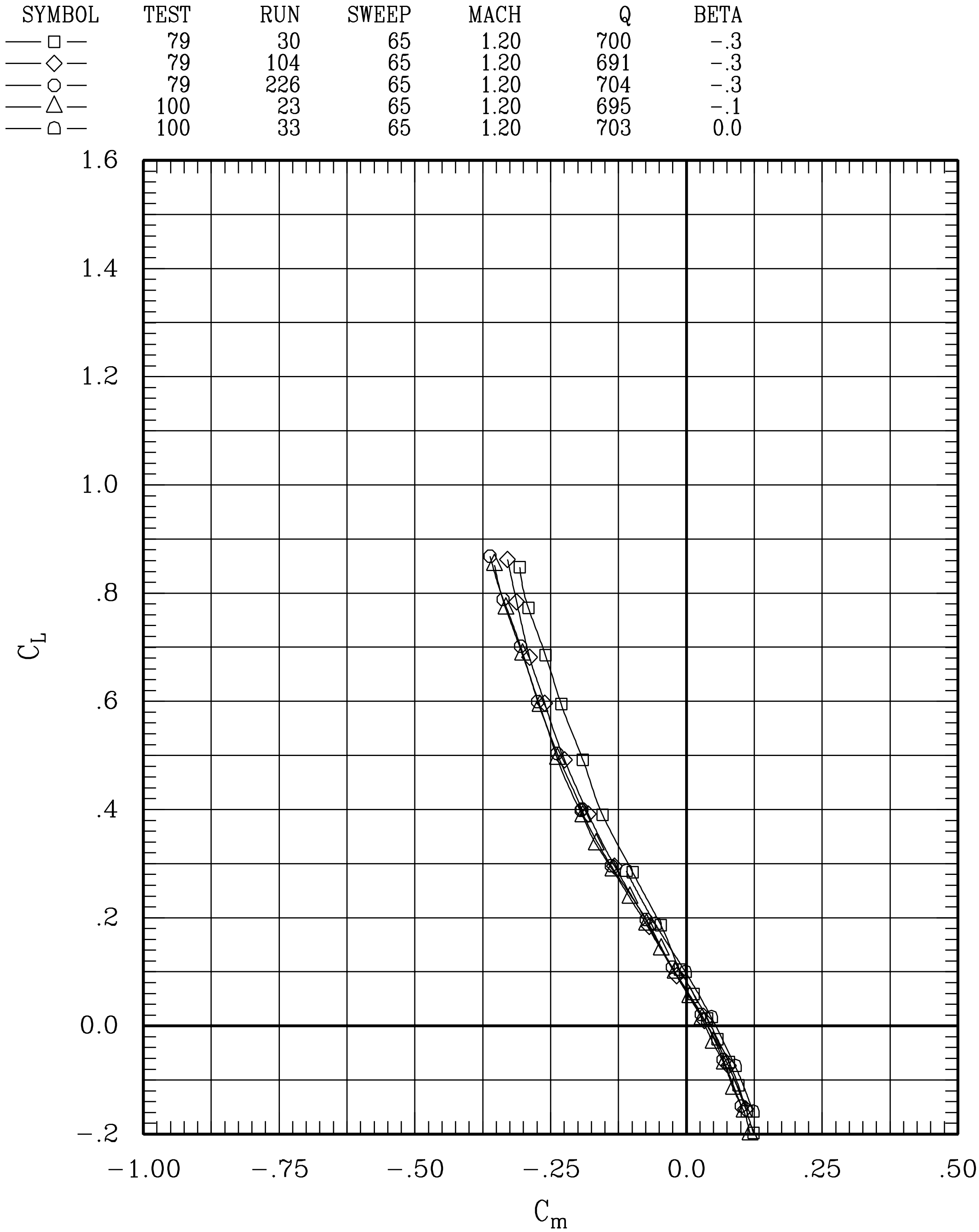

Figure 34(h). Repeat runs for sweep = 65 deg, Mach = 1.20.

SYMBOL	TEST	RUN	SWEEP	MACH	Q	BETA
—□—	79	30	65	1.20	700	−.3
—◇—	79	104	65	1.20	691	−.3
—○—	79	226	65	1.20	704	−.3
—△—	100	23	65	1.20	695	−.1
—⌂—	100	33	65	1.20	703	0.0

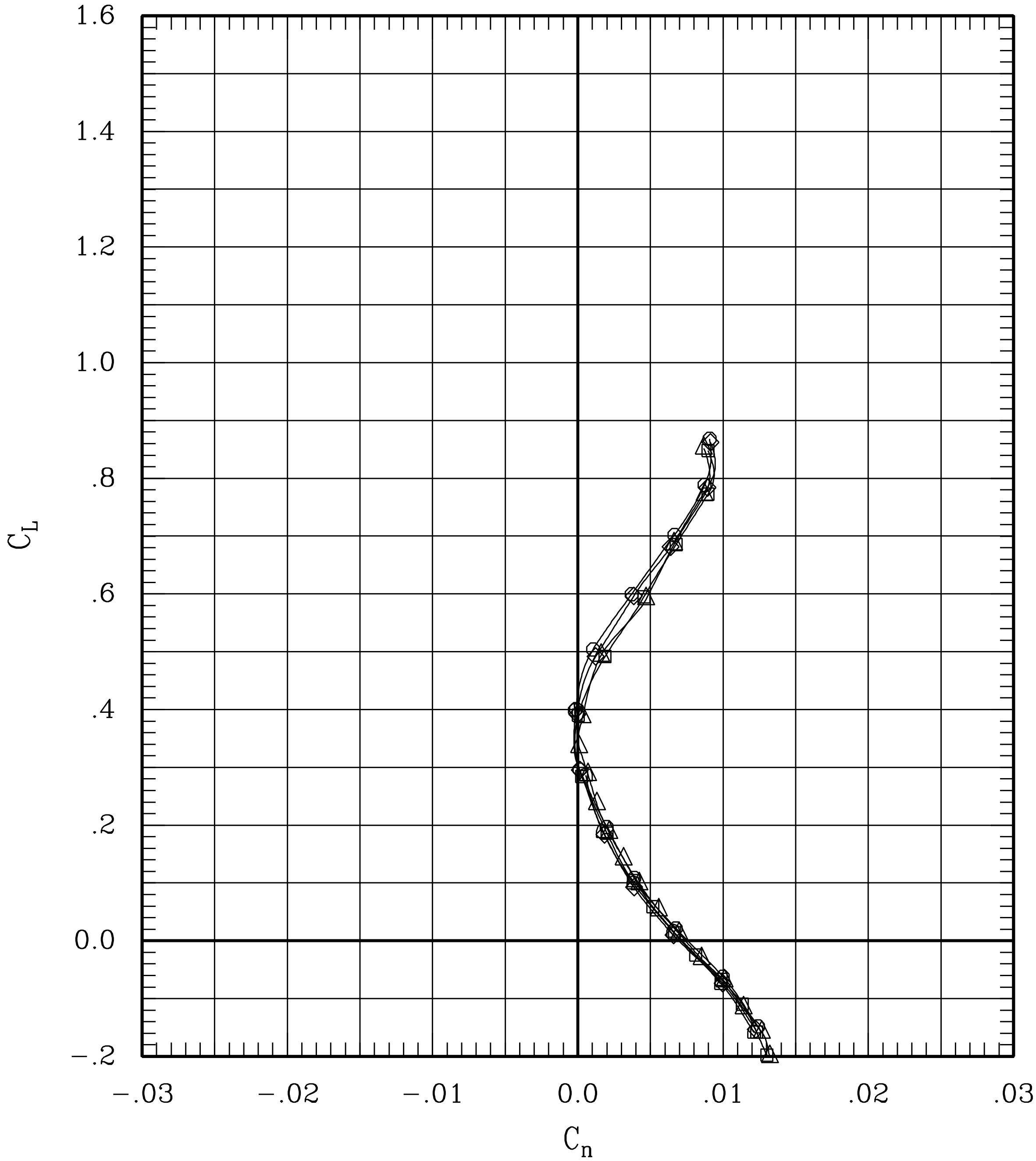

Figure 34(h). Repeat runs for sweep = 65 deg, Mach = 1.20.

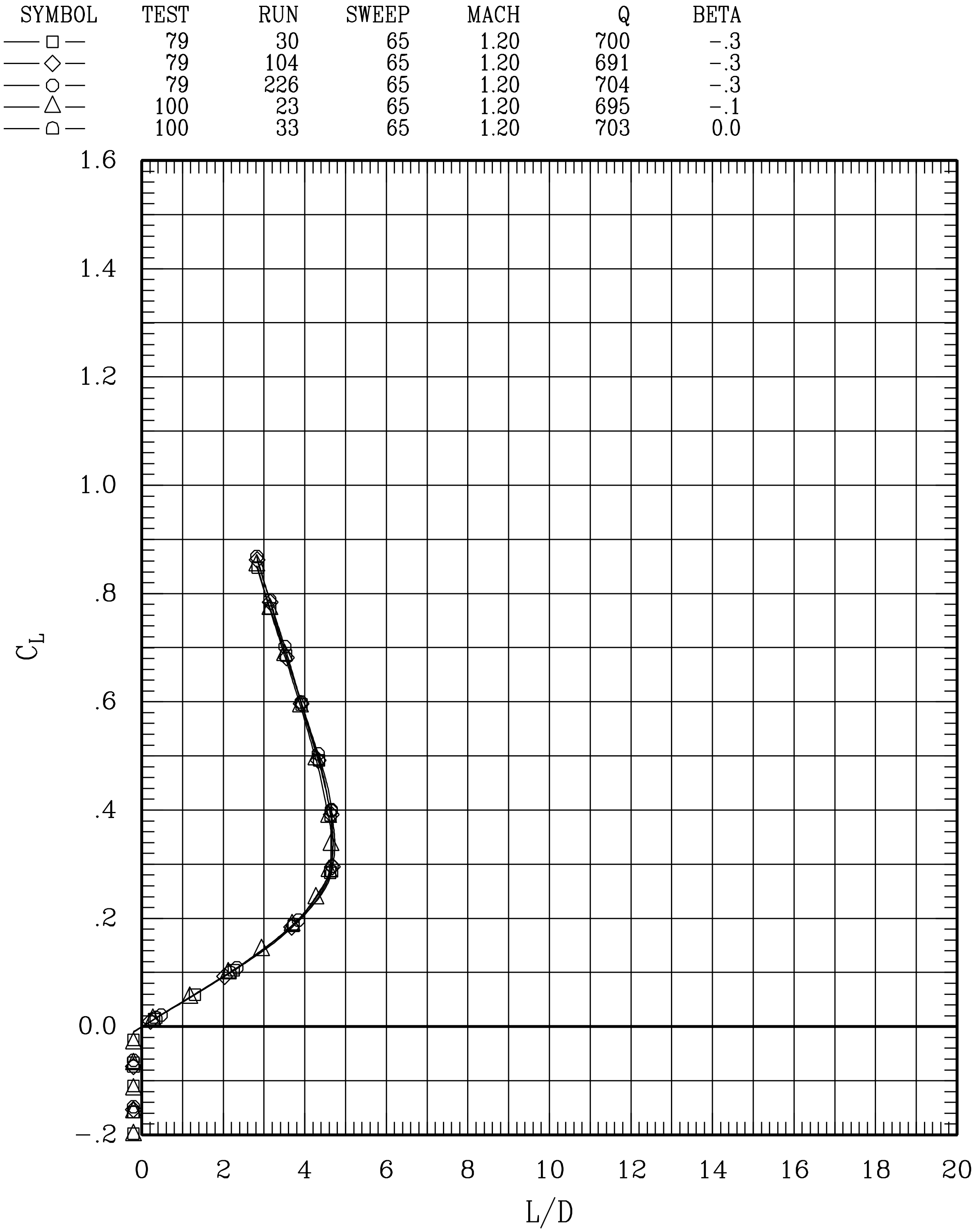

Figure 34(h). Repeat runs for sweep = 65 deg, Mach = 1.20.

REPORT DOCUMENTATION PAGE

Form Approved
OMB No. 0704-0188

1. AGENCY USE ONLY *(Leave blank)*	2. REPORT DATE	3. REPORT TYPE AND DATES COVERED
	September 1999	Technical Memorandum

4. TITLE AND SUBTITLE

Experimental Aerodynamic Characteristics of an Oblique Wing for the F-8 OWRA

5. FUNDING NUMBERS

533-06-01

6. AUTHOR(S)

Robert A. Kennelly, Jr., Ralph L. Carmichael, Stephen C. Smith, James M. Strong, and Ilan M. Kroo*

7. PERFORMING ORGANIZATION NAME(S) AND ADDRESS(ES)

Ames Research Center
Moffett Field, CA 94035-1000

8. PERFORMING ORGANIZATION REPORT NUMBER

A-99V0043

9. SPONSORING/MONITORING AGENCY NAME(S) AND ADDRESS(ES)

National Aeronautics and Space Administration
Washington, DC 20546-0001

10. SPONSORING/MONITORING AGENCY REPORT NUMBER

NASA/TM–1999-209579

11. SUPPLEMENTARY NOTES

Point of Contact: Robert A. Kennelly, Jr., Ames Research Center, MS 227-6, Moffett Field, CA 94035-1000
(650) 604-5860
*Department of Aeronautics and Astronautics, Stanford University, Stanford, CA

12a. DISTRIBUTION/AVAILABILITY STATEMENT

Unclassified — Unlimited
Subject Category 02 Distribution: Standard
Availability: NASA CASI (301) 621-0390

12b. DISTRIBUTION CODE

13. ABSTRACT ***(Maximum 200 words)***

An experimental investigation was conducted during June–July 1987 in the NASA Ames 11-Foot Transonic Wind Tunnel to study the aerodynamic performance and stability and control characteristics of a 0.087-scale model of an F-8 airplane fitted with an oblique wing. This effort was part of the Oblique Wing Research Aircraft (OWRA) program performed in conjunction with Rockwell International. The Ames-designed, aspect ratio 10.47, tapered wing used specially designed supercritical airfoils with 0.14 thickness/chord ratio at the root and 0.12 at the 85% span location. The wing was tested at two different mounting heights above the fuselage.

Performance and longitudinal stability data were obtained at sweep angles of 0°, 30°, 45°, 60°, and 65° at Mach numbers ranging from 0.30 to 1.40. Reynolds number varied from 3.1×10^6 to 5.2×10^6, based on the reference chord length. Angle of attack was varied from –5° to 18°. The performance of this wing is compared with that of another oblique wing, designed by Rockwell International, which was tested as part of the same development program. Lateral-directional stability data were obtained for a limited combination of sweep angles and Mach numbers. Sideslip angle was varied from –5° to +5°.

Landing flap performance was studied, as were the effects of cruise flap deflections to achieve roll trim and tailor wing camber for various flight conditions. Roll-control authority of the flaps and ailerons was measured. A novel, deflected wing tip was evaluated for roll-control authority at high sweep angles.

14. SUBJECT TERMS

Oblique wing, Transonic, Supersonic, Wind tunnel test, Skewed wing, Aerodynamics

15. NUMBER OF PAGES

580

16. PRICE CODE

A25

17. SECURITY CLASSIFICATION OF REPORT	18. SECURITY CLASSIFICATION OF THIS PAGE	19. SECURITY CLASSIFICATION OF ABSTRACT	20. LIMITATION OF ABSTRACT
Unclassified	Unclassified		

NSN 7540-01-280-5500

Standard Form 298 (Rev. 2-89)
Prescribed by ANSI Std. Z39-18
298-102